CANADIAN THESES ON MICROFICHE

THÈSES CANADIENNES SUR MICROFICHE

National Library of Canada
Collections Development Branch

Canadian Theses on
Microfiche Service

Ottawa, Canada
K1A 0N4

Bibliothèque nationale du Canada
Direction du développement des collections

Service des thèses canadiennes
sur microfiche

NOTICE

The quality of this microfiche is heavily dependent upon the quality of the original thesis submitted for microfilming. Every effort has been made to ensure the highest quality of reproduction possible.

If pages are missing, contact the university which granted the degree.

Some pages may have indistinct print especially if the original pages were typed with a poor typewriter ribbon or if the university sent us an inferior photocopy.

Previously copyrighted materials (journal articles, published tests, etc.) are not filmed.

Reproduction in full or in part of this film is governed by the Canadian Copyright Act, R.S.C. 1970, c. C-30. Please read the authorization forms which accompany this thesis.

AVIS

La qualité de cette microfiche dépend grandement de la qualité de la thèse soumise au microfilmage. Nous avons tout fait pour assurer une qualité supérieure de reproduction.

S'il manque des pages, veuillez communiquer avec l'université qui a conféré le grade.

La qualité d'impression de certaines pages peut laisser à désirer, surtout si les pages originales ont été dactylographiées à l'aide d'un ruban usé ou si l'université nous a fait parvenir une photocopie de qualité inférieure.

Les documents qui font déjà l'objet d'un droit d'auteur (articles de revue, examens publiés, etc.) ne sont pas microfilmés.

La reproduction, même partielle, de ce microfilm est soumise à la Loi canadienne sur le droit d'auteur, SRC 1970, c. C-30. Veuillez prendre connaissance des formules d'autorisation qui accompagnent cette thèse.

THIS DISSERTATION
HAS BEEN MICROFILMED
EXACTLY AS RECEIVED

LA THÈSE A ÉTÉ
MICROFILMÉE TELLE QUE
NOUS L'AVONS REÇUE

Canada

NL 339 (r. 86/09)

0-315-19592-4

National Library of Canada
Canadian Theses Division
Ottawa, Canada
K1A 0N4

Bibliothèque nationale du Canada
Division des thèses canadiennes

251

2 volumes enclosed.

67500

PERMISSION TO MICROFILM — AUTORISATION DE MICROFILMER

• Please print or type — Écrire en lettres moulées ou dactylographier

Full Name of Author — Nom complet de l'auteur

JOHN GORDON AGAR

Date of Birth — Date de naissance	Country of Birth — Lieu de naissance
FEBRUARY 18, 1950	INDIA

Permanent Address — Résidence fixe

108 SCENIC ACRES DRIVE N.W.
CALGARY, ALBERTA
T3L 1C7

Title of Thesis — Titre de la thèse

GEOTECHNICAL BEHAVIOUR OF OIL SANDS AT ELEVATED TEMPERATURES AND PRESSURES

University — Université

UNIVERSITY OF ALBERTA

Degree for which thesis was presented — Grade pour lequel cette thèse fut présentée

Ph D

Year this degree conferred — Année d'obtention de ce grade	Name of Supervisor — Nom du directeur de thèse
1984	DR. N.R. MORGENSTERN AND DR. J.D.

Permission is hereby granted to the NATIONAL LIBRARY OF CANADA to microfilm this thesis and to lend or sell copies of the film.

The author reserves other publication rights, and neither the thesis nor extensive extracts from it may be printed or otherwise reproduced without the author's written permission.

L'autorisation est, par la présente, accordée à la BIBLIOTHÈQUE NATIONALE DU CANADA de microfilmer cette thèse et de prêter ou de vendre des exemplaires du film.

L'auteur se réserve les autres droits de publication; ni la thèse ni de longs extraits de celle-ci ne doivent être imprimés ou autrement reproduits sans l'autorisation écrite de l'auteur.

Date	Signature
84/04/19	J Agar

NL-91 (4/77)

THE UNIVERSITY OF ALBERTA

GEOTECHNICAL BEHAVIOUR OF OIL SANDS AT ELEVATED TEMPERATURES AND PRESSURES

by

(C) JOHN GORDON AGAR

A THESIS

SUBMITTED TO THE FACULTY OF GRADUATE STUDIES AND RESEARCH

IN PARTIAL FULFILLMENT OF THE REQUIREMENTS FOR THE DEGREE

OF DOCTOR OF PHILOSOPHY

IN

GEOTECHNIQUE

DEPARTMENT OF CIVIL ENGINEERING

EDMONTON, ALBERTA

SPRING, 1984

THE UNIVERSITY OF ALBERTA

RELEASE FORM

NAME OF AUTHOR JOHN GORDON AGAR

TITLE OF THESIS GEOTECHNICAL BEHAVIOUR OF OIL SANDS AT ELEVATED TEMPERATURES AND PRESSURES

DEGREE FOR WHICH THESIS WAS PRESENTED DOCTOR OF PHILOSOPHY

YEAR THIS DEGREE GRANTED SPRING 1984

(Signed) .....J Agar.....

PERMANENT ADDRESS

108 Scenic Acres Drive N.W.
Calgary, Alberta
T3L 1C7

DATED April 12 1984

THE UNIVERSITY OF ALBERTA

FACULTY OF GRADUATE STUDIES AND RESEARCH

The undersigned certify that they have read, and recommend to the Faculty of Graduate Studies and Research, for acceptance, a thesis entitled Geotechnical Behaviour of Oil Sands at Elevated Temperatures and Pressures submitted by JOHN GORDON AGAR in partial fulfillment of the requirements for the degree of DOCTOR OF PHILOSOPHY.

N.R. Morgenstern
Supervisor

J.D. Scott
Co-Supervisor

Z. Eisenstein

J. Masliyah

K.Y. Lo
External Examiner

DATE March 28, 1984.

ABSTRACT

Thermally enhanced recovery of heavy hydrocarbons from oil sand introduces a number of difficult geotechnical engineering problems associated with ground heating. The pattern and magnitude of ground deformations resulting from *in situ* fluid injection and heating have a bearing on the stability of underground openings (e.g. shafts, tunnels, well casings) and on the efficiency of the oil recovery process. The following thesis documents geotechnical properties of oil sands required for analyses of ground heating problems. Properties of good quality oil sand samples were measured in an extensive laboratory investigation.

A review of relevant literature is presented. Modern development of energy and mineral resources has introduced a wide range of related problems involving heating of soils and rocks. These may be broadly classified as "Heat Consolidation" problems.

Results of numerical analyses of heat consolidation problems in oil sands are presented and discussed.

ACKNOWLEDGEMENTS

The research work documented in this thesis was performed over the period 1981 to 1983. Funding for the research was provided [illegible] by the Alberta Oil Sands Technology and Research Authority [illegible]. Research grants provided by AOSTRA were used to develop a high temperature/high pressure laboratory testing facility. I am particularly grateful for the AOSTRA scholarship which sustained myself and my family throughout the period of research. Operation of the laboratory testing facility was also supported in part by the National Sciences and Engineering Research Council (NSERC) and the Department of Civil Engineering.

The research was performed under the guidance of two highly reputable advisors: Professor N.R. Morgenstern and Professor J.D. Scott. The need for research in this area was identified by Professor Morgenstern who suggested the research topic. The learning experience resulting from this research was greatly enhanced because of the maturity and wisdom of both advisors who willingly provided key advice at critical stages yet encouraged independent research and personal development.

Denis Gagnon provided quality technical assistance during the experimental research. Denis was persistant and dedicated in obtaining the best possible test results.

Technical assistance was also provided by G. Cyre and other staff members. Ray Howells and Al Dunbar assisted with the computing work. Previous geotechnical studies of oil sands,

particularly that of Maurice Dusseault (1977), provided essential background for the work reported in this thesis.

M.J. O'Connor & Associates Ltd. generously prepared the manuscript and ably assisted with the drafting. My partners and friends, Mike O'Connor and Doug King, have been both technically and morally supportive throughout the research.

The learning experience at the University of Alberta was enriched by many friends among the staff and students in both geotechnical and petroleum engineering. I am grateful to Keith Koser for his assistance in submitting this thesis and guiding it through the final approval stage.

I wish to especially acknowledge the motivation, and loving support of my entire family. My parents passed on to me a sense of deep respect for education. My wife, Narda's sense of humour and confident support through "thick-and-thin" has enabled me to keep this phase of my life in perspective. Our children, Steven and Laura, both of whom were born during the research years, have brought unprecedented purpose and happiness into my life.

TABLE OF CONTENTS

VOLUME I

VOLUME II

LIST OF TABLES

LIST OF FIGURES

LIST OF PHOTOGRAPHIC PLATES

LIST OF SYMBOLS

The fundamentals of this research have been drawn from several disciplines. Consequently it has not been possible to maintain a completely unified system of symbols. The following list is included to assist the reader in interpretation of the equations. The meanings of many symbols are also identified within the text.

SYMBOL	MEANING
A, B	Parameters relating pore pressure response with undrained total stress changes
B_T	Parameters relating thermally generated pore pressure with undrained temperature change
C	Matrix of elastic stress-strain moduli
C_c	Drained isotropic compressibility
C_u	Uniformity coefficient ($C_u = D_{10}/D_{60}$)
c	Specific heat; or apparent cohesive strength
c_v	Coefficient of consolidation
D	Matrix of thermoelastic stress-temperature-strain moduli
D_n	Mean particle diameter greater than that of n percent by mass of the soil particles in a sample
d	Exact differential
E	Modulus of elasticity
e	Void ratio
G	Shear modulus of elasticity
h	Heat flow

SYMBOL	MEANING
I_D	Sample disturbance index for oil sand
I_1	First strain invariant
I	Hydraulic gradient
J_1	First stress invariant
K	Bulk modulus of elasticity
K_o	Coefficient of earth pressure at rest
k	Absolute permeability
k_o	Effective permeability of oil
k_w	Effective permeability to water
k_T	Thermal conductivity
m_v	One dimensional coefficient of volume compressibility
P	Absolute pore fluid pressure
R_T	Dimensionless heat consolidation ratio (the ratio of the coefficient of consolidation to the thermal diffusivity)
r	Radial distance
S	Pore fluid saturation
S_T	Coefficient of stress change with temperature
T	Absolute temperature
t	Time
u	Excess pore fluid pressure
V	Volume
v	Velocity
w_i	Displacement
w	Water content
X_i	Body forces
x,y,z	Cartesian coordinates

SYMBOL	MEANING
α	Coefficient of thermal expansion
β	Compressibility
γ	Weight density
Δ	Finite difference
∇	Differential operator
∂	Partial differential
η	Porosity
ϵ	Strain
χ	Soil-water interaction coefficient defined by Biot (1941)
λ	Lames elastic stress-strain constant
μ	Dynamic viscosity
ν	Poisson's ratio of normal to orthogonal linear strain
ξ	Dimensionless distance
ρ	Mass density
σ	Total stress
σ'	Effective stress
τ	Shear stress; dimensionless time
ϕ	Angle of internal shearing resistance

SUBSCRIPT	MEANING
o	Oil
B	Bitumen
w	Water
s	Solid
g	Gas

SUBSCRIPT	MEANING
DR	Drained
u	Undrained
L	Linear
v	Volumetric
l	Liquid
I	Initial, in situ
i	Initial
i,j,k	Spatial nodes corresponding with x,y,z Cartesian coordinates
n	Time level
T	Thermal
P	Pressure
1,2,3	Maximum, intermediate and minimum principal stresses and strains, respectively

1.0 INTRODUCTION

1.1 General

Oil sands are an important world energy resource by virtue of the magnitude of known reserves. Estimated in-place volumes of heavy hydrocarbons in oil sand deposits throughout the world approach 3000 billion barrels which is nearly equivalent to the total discovered conventional medium and light gravity oil reserves in-place in the world. More than 90 percent of known heavy hydrocarbon reserves occur in oil sand deposits in Alberta, Western Canada and in the Orinoco Heavy Oil Belt of Eastern Venezuela (Demaison, 1977).

Although abundant, the extremely high viscosity of the crude bitumen in oil sands makes conventional recovery by pumping impractical. Approximately 4 percent of Alberta oil sand reserves are buried at depths less than 50 m and are economically recoverable by surface mining techniques (Alberta Energy and Natural Resources, 1979). In situ extraction procedures are being developed for the remaining 96 percent of reserves buried at depths greater than 50 m.

In situ extraction methods generally involve heating the oil sand with super-heated steam or by in situ combustion. Both techniques are under active investigation at the pilot project stage. A hybrid method, Mine Assisted In Situ Processing (MAISP) is also under study. MAISP involves the development of an underground mine system of vertical shafts and tunnels in or adjacent to the

oil sand in order to provide access for horizontal steam injection and production wells (Devenny and Raisbeck, 1980). This layout is intended to provide a more cost-effective production facility through reduced heat losses and a higher density of wells within the formation. The concept has already been adopted in the USSR to recover heavy oil in north-eastern Siberia near Yarega. Figure 1.1 illustrates in a general manner some of the extraction processes.

A number of difficult geotechnical problems are introduced by thermally enhanced in situ extraction of heavy hydrocarbons from oil sands. The problems arise because of the elevated pressure-temperature conditions resulting from massive steam injection and/or combustion, the large scale of proposed recovery schemes, and the peculiar properties of oil sands. Stress changes and ground deformations are caused by: (i) excavation and support of underground openings to provide access to the formation, e.g. injection and production wells, shafts, tunnels and caverns; (ii) injection of water, condensed steam, air or other fluids into the formation to promote intraformational communication either by creating partings or improving fluid transmissibility, and (iii) ground heating and thermal expansion. The pattern and magnitude of ground deformations resulting from in situ extraction processes will have a bearing on the stability of underground openings and the efficiency of the oil recovery processes. Ground deformations associated with hydraulic fracturing are illustrated schematically in Figure 1.2. Since fractures may propagate by both parting and shear, knowledge of shear deformation and strength properties as well as in situ stresses is required, in order to develop rational

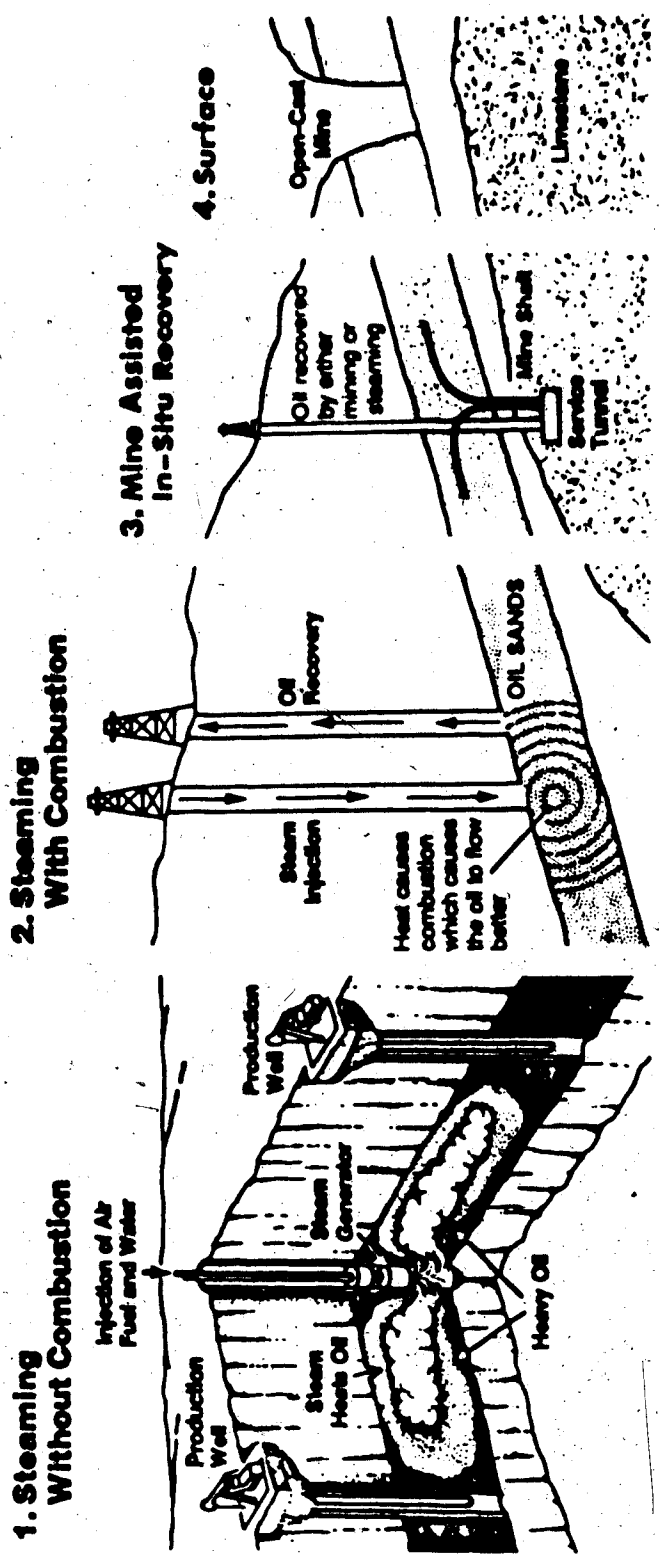

FIGURE 1.1 Extraction of Heavy Hydrocarbon Resources from Oil Sands

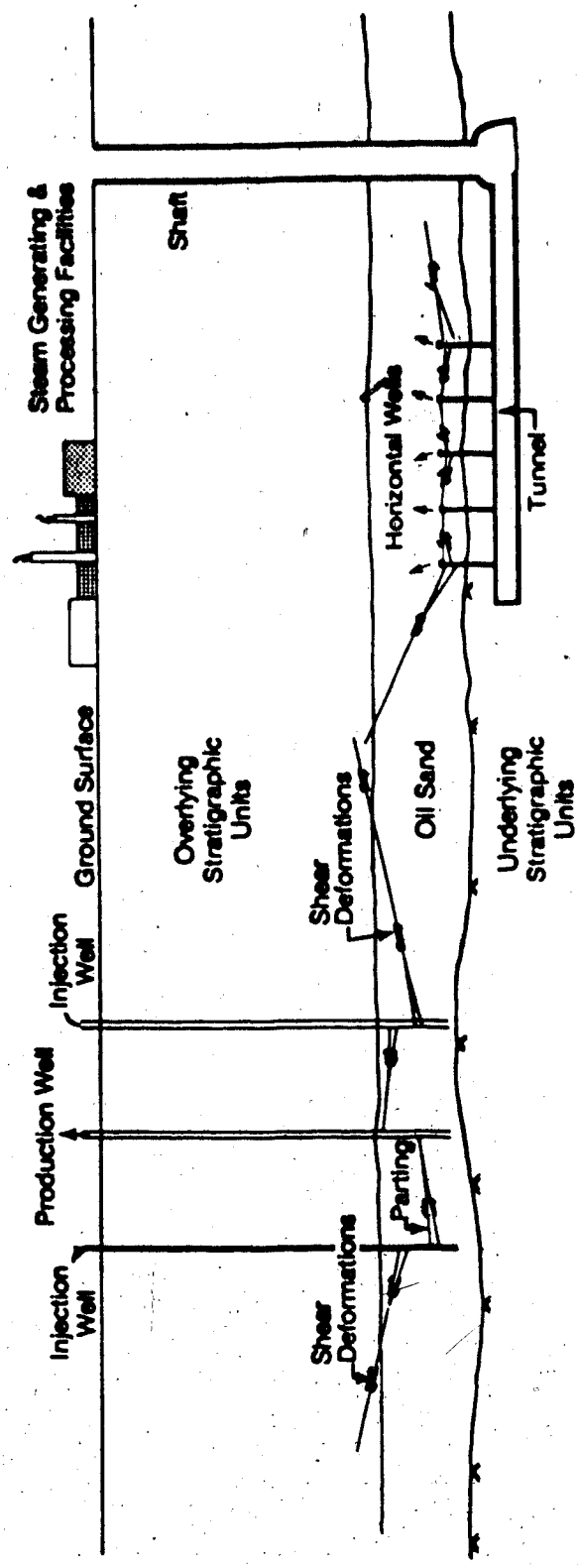

FIGURE 1.2 Parting and Shear Deformations Associated with Hydraulic Fracturing

analyses to predict orientation and extent of hydraulic fractures in cohesionless oil sands. The mechanics of fluid injection processes are further complicated when heated fluids are injected. In situ stresses may be altered by heating due to restraint of thermally induced strains and by thermal generation of pore fluid pressures. Ground deformations due to thermal expansion of heated oil sand are illustrated schematically in Figure 1.3. Prediction of thermally induced stress changes and ground deformations requires knowledge of thermal expansion and stress-deformation properties, in addition to permeability and heat transfer properties.

Recognition of the geotechnical complexities introduced by thermally enhanced oil recovery processes provided motivation for the study reported in this thesis. A laboratory testing facility has been developed to study the geotechnical behaviour of oil sands and other soils and rocks at elevated pressures and temperatures.

1.2 Heat Consolidation - A Class of Problems

Consolidation of porous soils and rocks is a transient process involving concommittant pore pressure variation and volumetric deformation, i.e. compression or swelling, in response to changes in the effective stresses.

Heat consolidation is an analogous process involving concurrent stress changes, pore pressure variation and volumetric deformation in response to heating (either transient or non-transient heating). Other "thermal consolidation" processes including frost heave and

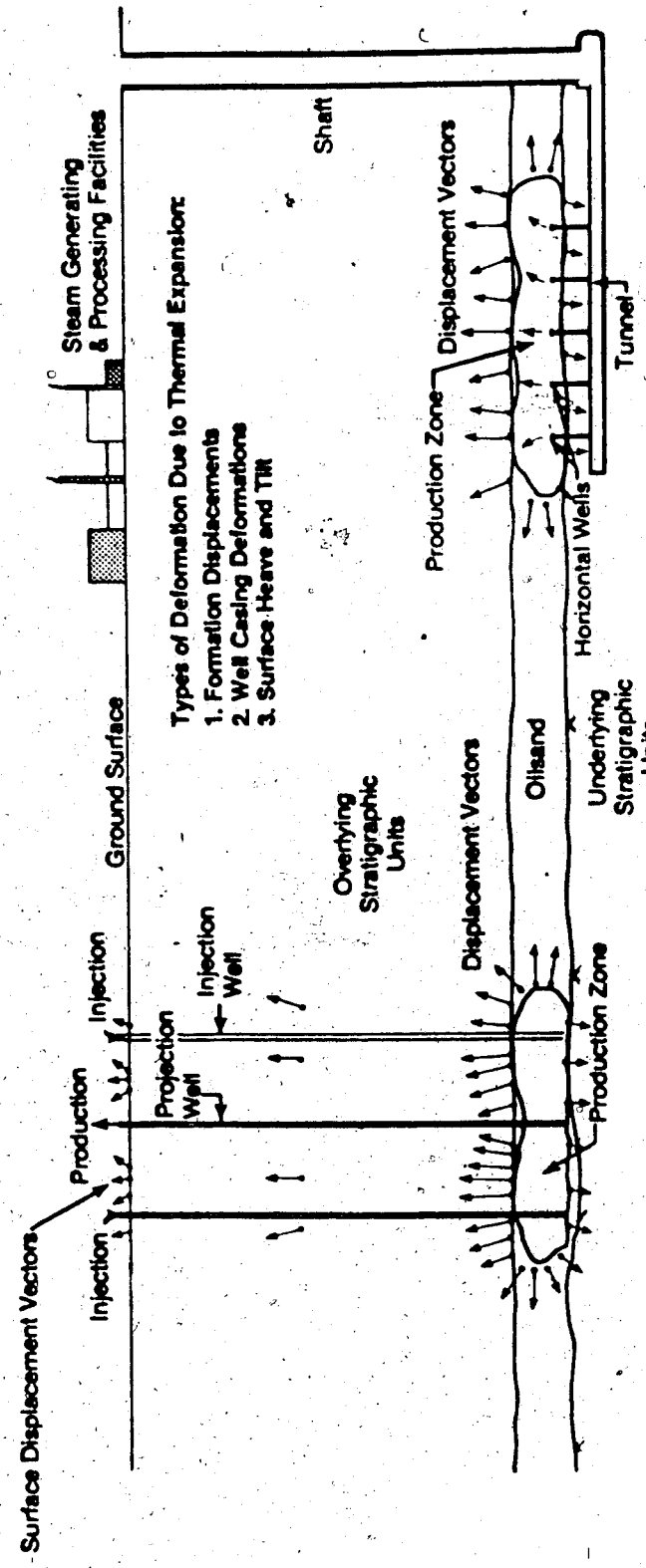

FIGURE 1.3 Deformations Due to Thermal Expansion of Oil Sand

thaw consolidation involve phase changes of the porewater in soils and rocks due to freezing and thawing. Consequently, the term "heat consolidation" is favoured for describing the class of problems involving heating above the freezing temperature of the pore fluids, whereas "thermal consolidation" is appropriate for describing thermally induced consolidation processes over the entire temperature range.

Formulation of the field equations governing all thermal condolidation processes involves coupling of heat transfer (energy balance) and appropriate consolidation relationships. The physics of heat consolidation are described in detail in Chapters 2 and 5 and numerical solutions for heat consolidation of oil sands are given in Chapters 5 and 6.

1.3 Nomenclature

Several terms are defined in this section to avoid confusion arising from multidisciplinary aspects of this research.

Stress and Pressure

The terms "stress" and "pressure" are often used interchangeably in both the soil and rock mechanics literature. It is possible to make systematic distinctions between these terms if it is understood that stress components are vector quantities with associated directional strains, whereas pressure is a scalar quantity. Accordingly, application of the term pressure to describe

stresses in the solid skeleton of porous soils and rocks is only correct for the condition in which stresses are isotropic. Stresses in the pore fluid phase of porous soils and rocks are correctly referred to as "pore pressures" since, by definition, a fluid cannot sustain shearing stresses. The term "pressure" therefore, is used exclusively with reference to fluid pressures in this thesis, and the term "stress" is used only for describing the vector quantities of effective and total stresses in oil sand or other soils and rocks.

Sign Conventions for Stresses and Deformations

The sign convention commonly used in geotechnical engineering defines compressive stresses and strains as positive quantities and tensile stresses and strains as negative quantities. This sign convention is adhered to throughout this thesis with one notable exception: volumetric strains due to thermal expansion measured in laboratory experiments are presented as positive strains. Coefficients of thermal expansion derived from the experimental results are also presented as positive quantities. This latter departure from the otherwise consistent geotechnical sign convention was adopted in order to conform with previously published thermal expansion data for other materials.

Drained, Undrained and Partially Drained Conditions

It is common in geotechnical engineering to bound the response of porous soils and rocks to loading in terms of the extreme

conditions of "drained" and "undrained" behaviour. Both conditions refer to non-transient response of pore fluid pressures.

Drained response refers to the condition in which the pore pressure in an element of soil or rock is constant during loading, i.e. mechanical or thermal loading. Drained behaviour of a porous continuum is approached when neither the porous medium nor the boundary conditions offer any resistance to the movement of pore fluids.

Undrained response refers to the condition in which the mass of an element of soil or rock remains constant during thermal or mechanical loading, although the volume of the element may change. This implies that there is neither any movement of pore fluid nor any diffusion of pore pressure from one point to another within the porous continuum. The undrained condition is only practically achievable in laboratory tests in which impervious boundary conditions are physically imposed around an element of soil or rock.

The term "partially drained" describes any condition intermediate between the drained and undrained extremes. Geotechnical laboratory compression tests and heating experiments are most conveniently performed and interpreted under drained or undrained conditions. Drained parameters are used to relate deformations of the solid skelton with mechanical and thermal loads in terms of effective stress changes. Transient experiments are also required to determine transient coupling parameters such as

permeability and thermal conductivity.

Effective Permeability and Pore Fluid Mobility

Some of the terms required to describe multiphase flow of fluids through porous media are not commonly used in traditional geotechnical engineering.

The concept of effective permeability is useful for describing fluid flow in porous media containing more than one continuous, immiscible fluid phase. Oil sand contains at least two immiscible fluids: oil and water, and under some pressure-temperature conditions a third gaseous phase may exist which may or may not be continuous. Effective permeability is a relative measure of the conductance of the porous medium for one fluid phase when the pore space is occupied by more than one fluid.

The mobility of pore fluid is defined as the ratio of effective permeability to dynamic viscosity. Dynamic viscosity of a fluid is a measure of the intermolecular shearing resistance of fluid flow. Dynamic viscosity, μ, is defined as a constant of proportionality relating shearing stress with the rate of shear strain according to Newtons's law of viscosity (Streeter and Wylie, 1979):

$$\tau = \mu \frac{dv}{dz} \qquad (1.1)$$

When the relationship given in equation 1.1 is linear for a given fluid, i.e. μ is constant for a range of shear stresses, the fluid

is described as a "Newtonian fluid". "Non-Newtonian fluids" have a nonlinear relationship between shear stress and rate of shear strain. The bitumen in Athabsca oil sands is a "non-Newtonian" fluid under some pressure-temperature conditions.

1.4 Scope of Thesis

The aim of the research documented in this thesis is to explore important aspects of the geotechnical behaviour of oil sands at elevated temperatures and pressures.

The necessary starting point for any research is a review of the relevant literature. An overview of the current state of elevated temperature geotechnics based on an extensive literature review is given in Chapter 2. Geoscience problems involving ground heating are categorized and discussed. General trends in the geotechnical response of soils and rocks to heating are outlined on the basis of references cited. Finally, theoretical concepts appropriate for the development of heat consolidation theory are presented.

A laboratory investigation to measure geotechnical properties of oil sand at elevated temperatures and pressure comprises a major proportion of the research work. Chapter 3 summarizes all aspects of the laboratory research including sampling, sample preparation techniques and testing procedures. In addition, the laboratory testing facility is described in some detail since it is unique. Also, procedures which were developed for properly calibrating

electronic measuring devices and determining correction factors required to isolate system response at elevated pressure and temperatures are outlined in Chapter 3. Detailed experimental results and procedures are documented in Appendices A to I, inclusive.

Geotechnical parameters and experimental results derived from the laboratory investigation are summarized and discussed in Chapter 4. The context in which each of the measured parameters may be applied in mathematical modelling of in situ processes is also presented, and the implications of sample disturbance on measured values of each parameter is quantified.

The heat consolidation process is described in Chapter 5. One dimensional heat consolidation theory is developed along with appropriate numerical modelling techniques. Techniques for modelling heat transfer by both diffusion and convection are included. Results of numerical analyses are presented which illustrate some of the implications of in situ heating in oil sands.

An uncoupled approach for modelling two or three dimensional heat consolidation problems is described in Chapter 6. Two and three dimensional numerical analyses of heat consolidation are required to evaluate in situ stress changes, i.e. to model stress paths. Results of analyses involving excavation and axisymmetric heating adjacent to a shaft and steam injection well in oil sand are presented in Chapter 6. Hyperbolic stress-strain parameters for

oil sand required for incremental elastic analyses using the hyperbolic model are also given in Chapter 6.

The thesis concludes with a summary of important findings of this research and recommendations for future research.

2.0 ELEVATED TEMPERATURE GEOTECHNICS: AN OVERVIEW

2.1 Introduction

The introduction of temperature as a state variable into the partial differential equations describing stresses and deformations in porous soils and rock requires consideration of a number of multidisciplinary concepts including:

a) fundamental thermodynamics (conservation of energy);
b) conservation of mass and fluid flow;
c) conservation of momentum (Newton's laws of motion) and stress equilibrium; and
d) thermoelasticity.

The presence of two or three pore fluid phases along with a solid phase introduces further complexity into the formulation and solution of engineering problems in some materials such as oil sands.

Theories coupling stress-temperature-strain response of solid bodies have been developed (e.g. thermoelastic and thermal viscoelastic theories). Thermoelastic theory has been widely applied (e.g. see Timoshenko and Goodier, 1934, and Boley and Weiner, 1960). Also, theories and analytical techniques have been developed for pressure-temperature-fluid flow in porous media (e.g. Mercer et al., 1982). The former "thermal solid mechanics" theories have been applied to problems involving heating of rocks, whereas the latter "thermal fluid flow" theories have been applied in

petroleum engineering and the hydrosciences. The need for a theory coupling stress-strain, pore fluid pressures and temperatures was recognized by Schiffman (1971) who developed a thermoelastic theory of consolidation. Further development and application of coupled theories to elevated temperature problems in the geosciences has been limited because of difficulties in applying the theory to obtain solutions to complex problems and because of inadequate representation of the thermomechanical behaviour of soils and rocks using a linear elastic stress-strain relationship. Heuze (1983b.) has discussed deficiencies in current state-of-the-art numerical modelling techniques for analyzing high level nuclear waste disposal problems.

No previous research has been directed toward determining geotechnical behaviour of oil sands at elevated temperatures and pressures. However, a range of similiar elevated temperature geoscience problems have been identified and studied. A review of relevant publications and theoretical concepts is outlined in following sections of this chapter to establish a framework for the oil sands research reported in this thesis.

Foregoing research on geotechnical behaviour of oil sands under isothermal conditions has provided essential background for developing the methodology for elevated temperature research (i.e. particularly the research work by Dusseault, 1977). A review of published strength and stress-strain properties of Alberta oil sands has been presented by Au (1983) and will not be repeated in this chapter.

2.2 Literature Review

2.2.1 Elevated Temperature Problems in the Geosciences

The relevant publications reviewed during this study can be broadly classified under two major categories:

1. Geoscience research; and
2. Energy and mineral resources development studies.

Many of the traditional areas of geoscience research have considered the implications of elevated temperatures and temperature changes within the earth's crust. By comparison, problems in the second category have been studied only recently. Modern development of energy and mineral resources has introduced a range of challenging engineering problems. The economics and feasibility of many energy and mineral resource development projects depend on utilization of underground space, often in an altered thermal regime. A range of research and engineering problems related to heating of soils and rocks is summarized in Table 2.1. Publications pertaining to the various problems listed in Table 2.1 generally address one or more of the following study aspects:

1. Problem identification and description;
2. Evaluation of material properties and techniques for laboratory or field measurement;
3. Description of theory and/or analytical procedures; or

GEOSCIENCES RESEARCH			ENERGY AND MINERAL RESOURCES DEVELOPMENT				
GEOLOGY	GEOPHYSICS AND ROCK MECHANICS	GEOTECHNICS	ENERGY GENERATION, TRANSPORTATION AND STORAGE	HYDROCARBON RESOURCES DEVELOPMENT	GEOTHERMAL ENERGY DEVELOPMENT	HIGH LEVEL NUCLEAR WASTE DISPOSAL	SOLUTION MINING
FORMATION OF ROCKS	EARTHQUAKE MECHANICS	THERMAL SAMPLE DISTURBANCE	POWER PLANTS AND NUCLEAR REACTOR FOUNDATIONS	HEAVY CRUDE AND OIL SANDS DEVELOPMENT	THERMAL ENERGY RECOVERY (HEAT EXCHANGE)	UNDERGROUND STORAGE REPOSITORIES	SULPHUR FRASCH PROCESS
ORIGINS OF PETROLEUM AND COAL	FRICTIONAL HEATING IN ROCK AVALANCHES	HEAT CONSOLIDATION	HOT OIL PIPELINES	OIL SHALE RETORTING	ELECTRICAL ENERGY USING STEAM TURBINES	DEEP SEABED DISPOSAL	URANIUM LEACHING
FORMATION OF INTRUSIVE STRUCTURES	PLATE TECTONICS AND STRESSES IN THE EARTH'S CRUST	HEATING AND SECONDARY CONSOLIDATION OF SEDIMENTS	BURIED ELECTRIC POWER CABLES	COAL GASIFICATION			SALT SOLUTION
FLUIDIZATION OF SEDIMENTS DUE TO MAGMA INTRUSION	THERMAL FRAGMENTATION OF ROCKS	FRICTIONAL HEATING IN RAPID LANDSLIDES	HOT OIL STORAGE TANKS	CONVENTIONAL PETROLEUM RECOVERY	NATURAL GAS PRODUCTION	SHALLOW LAND BURIAL OF LOW-LEVEL WASTES	POTASH SOLUTION
			UNDERGROUND OIL AND GAS STORAGE	ENHANCED SECONDARY OIL RECOVERY			DEEP INJECTION OF INDUSTRIAL AND MINERAL PROCESSING WASTEWATERS
			AQUIFER THERMAL ENERGY STORAGE (ATES)				

TABLE 2.1 ELEVATED TEMPERATURE PROBLEMS IN THE GEOSCIENCES

4. Characterization of material response based on results of analytical studies.

Theoretical and analytical developments, in general, depend upon the measurement of appropriate material properties and experimental characterization of material behaviour. Accordingly, much of the current research effort related to this class of problem has been directed toward experimental research, both in the laboratory and field.

Important material properties required for geotechnical analyses of this class of problems are:

1. Mechanical properties including shear strength, tensile strength, stress-strain moduli, viscosity and creep law parameters, and thermal expansion.
2. Physical properties including porosity, density, pore fluid saturations, fluid viscosities and permeability; and
3. Thermal properties including thermal diffusivity, thermal conductivity, specific heat, the melting temperature and heat of fusion of solids, and pressure-temperature relationships for phase change of pore fluids.

Elevated temperature problems listed in Table 2.1 are described under the following subheadings, and some of the relevant publications are noted.

Geological Research

Geological researchers have considered elevated temperatures and pressures in the earth's crust in a wide range of such complex geologic processes as folding, plate tectonics, diapirism and magma migration; e.g. Pollard and Johnson, 1973a. and 1973b., discuss the mechanics of growth of laccoliths. Theories to explain the origins of petroleum and coal, and thermal alteration of rocks require elevated temperature and pressure conditions. These subjects are discussed extensively in textbooks of geology and the geological literature. For example, Goetz (1971) has described high temperature rheology of granite. Shimamoto and Hara (1976), and Parrish et al. (1976) have studied the process of folding. Geological researchers have also measured and catalogued mechanical, physical and thermal properties of rocks and minerals (e.g. see Clark, 1966, and Burnham et al., 1969). Data for sands are particularly relevant to oil sand research. Maxwell (1960) studied the processes of compaction and cementation of deeply buried sands in experiments at temperatures to 350°C and confining stresses to about 300 MPa. Barnes and Dusseault (1980) studied diagenetic alteration of oil sands under moderate temperatures and pressures. The influence of thermally generated pore pressures has also been considered in geology. Reynolds (1954), Delaney (1982), and Kokelaar (1982) describe the process of "fluidization" of sediments during heating of rocks adjacent to intrusive magma.

Geophysical and Rock Mechanics Research

Traditional research in geophysics and rock mechanics has considered the role of heating in several areas including earthquake mechanics and fault movement, stresses in the earth's crust, frictional heating in rock avalanches, and thermal fragmentation of rocks. These research topics have stimulated extensive laboratory investigation of the influence of temperature on mechanical, thermal and physical properties of rocks. For example, Mogi (1972) studied the influence of elevated temperatures on the strength and ductility of intact rocks. Yamaguchi and Miyazaki (1970), Wingquist (1970), Lehnoff and Schellér (1975), and Finnie et al. (1979) have studied the influence of heating and cooling on rock strength in relation to the thermal rock fragmentation problem. Others have studied temperature-dependent changes of the mechanical properties (in particular shear strength) of fault gouge materials in relation to earthquake mechanics (e.g. Bonnet and Jouanna, 1980, and Moore et al., 1983).

Thermal expansion of various granitic rocks has been measured by Richter and Simmons (1974), Cooper and Simmons (1977), Wong and Brace (1979), Heard (1980) and Van der Molen (1981).

The influence of heating on permeability of various rocks has been measured in laboratory experiments by Summers et al. (1978), Brace (1980), Voegele and Brace (1983) and Morrow et

al. (1983). Voegele et al. (1981) measured rock joint permeability in an in situ "heated block" experiment.

The influence of thermally generated pore fluid pressures and effective stress changes on earthquake related fault movements was identified by Sibson (1973). More recently, Lachenbruch (1980) has analyzed in a comprehensive manner, the interaction between fault movement and pore pressure generated by frictional heating. Similarily Knapp and Knight (1977) have considered the role of thermally generated pore fluid pressures in fracture propagation and related microseismicity adjacent to hot magma. Knapp and Norton (1981) have carried out preliminary numerical analyses to predict stress changes in crustal rocks due to heating and cooling of pluton.

Geotechnics

Goetechnical researchers have studied the effects of temperature changes on soil behaviour, including such aspects as thermally induced moisture migration, heat consolidation and related strength changes. A moderate range of elevated temperatures up to about 60°C has traditionally been considered which is consistent with the maximum range of environmentally induced temperature changes which would be expected in soils.

The problem of thermal disturbance of soil samples when taken from the field to the laboratory has been studied by a number of researchers including Carter (1951), Finn (1951),

Hutcheon (1958), Paaswell (1967), Campanella and Mitchell (1968) and others.

Winterkorn (1954), Plum and Esrig (1969) and Mitchell (1976) have published data which illustrates that cyclic heating and cooling of soils can accelerate secondary consolidation and increase the apparent preconsolidation pressure of soils. In addition to common environmental sources of heat, biological researchers have recently been able to measure small amounts of heat produced by microorganisms present in recent sediments (e.g. see Pamatmat, 1982), which may also cause "micro-heat consolidation".

Voight and Faust (1982) have studied frictional heating and associated strength loss during rapid landslides in soils and rocks. These authors attribute increased mobility and travel distance of some rapid landslides to thermally induced pore pressures and strength reduction of materials within landslide masses.

Energy and Mineral Resources Development

Recent interest in the geotechnical behaviour of soils and rocks at elevated temperatures and pressures has evolved in conjunction with thermal geoscience and engineering problems associated with development of energy and mineral resources. Ground heating problems described in the literature are listed in Table 2.1.

Engineering implications of heat losses into the ground during generation, storage and transportation of energy resources must be considered during design studies. For example, thermally induced ground deformations and potential weakening of foundation soils and rocks must be considered during design of heated structures such as power plants, nuclear reactors, hot oil storage tanks, etc. Studies of such problems are discussed in Mitchell (1976) and Kosar (1983). Similarly heat consolidation of soils adjacent to buried electric power transmission cables and buried hot oil pipelines may result in ground deformations which will influence long term serviceability (e.g. see Radhakrishna, 1968). Storage of oil and liquified natural gas in underground cavities (e.g. Bawden and McCreath, 1979) may alter the thermal regime of surrounding rocks. A relatively new concept for underground storage of thermal energy by pumping heated water from various industrial and power generating sources is being studied in the hydrosciences. Mercer et al. (1982), Tsang and Hopkins (1982), Chen and Reddell (1983), and others have reported numerical modelling and field studies related to "Aquifer Thermal Energy Storage" (ATES). Sauty et al. (1982) have published results of a theoretical study of the ATES concept.

In situ development of heavy hydrocarbon resources often requires ground heating. Thermally enhanced recovery of heavy crude oil and bitumen from oil sands and oil shales, and even conventional recovery of geothermally heated oil from depth can

result in heating of ground adjacent to well casings. Thermally induced ground deformations adjacent to heated well casings have in fact resulted in irreparable damage; e.g. Mainland (1983), and Smith and Pattillo (1980) have described and analyzed thermally induced well casing deformations and failures. Mitchell and Goodman (1978), Ruedrich et al. (1978), and Lin and Wheeler (1978) have described casing deformations due to thawing of permafrost during oil recovery. Production of geothermally heated oil, often at temperatures exceeding 100°C, through a non-insulated well casing, may cause both thawing and subsequent heat consolidation around the casing.

Mine-assisted in situ processing (MAISP) of oil sands has been described by several authors including Haston (1978), Smith and Butler (1979), Devenny and Raisbeck (1980) and Charlwood et al. (1980). The study published by Smith and Butler (1979) includes comparative cost estimates which demonstrate the cost-effectiveness of being able to drill and install horizontal steam injection and recovery wells from access tunnels. The higher density of wells within the pay zone, improved "sweep efficiency" and reduced heat losses to the overburden make the MAISP scheme economically attractive when compared with the performance of vertical wells drilled from surface. Nevertheless, advocates of the MAISP concept have recognized that rational design and construction of shafts, tunnels and caverns for underground access depend upon development of appropriate analytical capabilities to predict stress changes and ground deformations induced by heating and

injection in production zones adjacent to these underground openings.

Other hydrocarbon resource recovery processes such as *in situ* coal gasification (Greg and Oleness, 1976; Maugh, 1977; Schrider and Fischer, 1976) and *in situ* retorting of oil shales (Smith and Atwood, 1976) also depend on maintenance of stable underground cavities in the heated formation rocks. Studies have been initiated to evaluate cavern stability and environmental problems related to thermally induced stress changes and ground deformations. For example, Greg (1977) has attempted to predict ground surface deformations resulting from *in situ* gasification of coal. Closmann and Phocas (1978) analyzed thermal stress changes near a heated fracture in transversely isotropic oil shale.

Economic recovery and use of energy resources from geothermally heated and pressurized strata within the earth's crust may be accomplished by several techniques including: (i) direct heating with geothermally heated steam or water through heat exchangers; (ii) conversion of the kinetic energy of the flowstream to electrical power using steam driven turbines; and (iii) recovery of natural hydrocarbon gases from geothermal reservoirs. Facca (1980) has given an historic summary of geothermal energy developments worldwide. Kern (1980) has analyzed recovery of heat from hot dry rocks using weighted brines as a mobile heat exchange medium. Garg et al. (1978) have developed software for numerical simulation of pressurized

geothermal reservoirs. Geothermal energy is commonly recovered from reservoirs ranging in depth from about 2 km to 16 km. Thermal stresses and ground deformations due to heating of shallower sediments adjacent to well casings and ancillary surface structures also constitute potential heat consolidation problems associated with geothermal energy development.

Underground disposal of partially consumed nuclear fuels and other radioactive waste by-products introduces ground heating problems which raise concerns about their safe long-term isolation. The magnitude and rate of heat generation depends on the level of radioactivity. Since radioactive decay of "low level" nuclear wastes is well advanced, the magnitude of heat generated is small (i.e. ground temperature increases less than about 100°C near the heat source). Disposal of "low level" nuclear wastes by shallow land burial schemes is therefore possible (e.g. see Daniel, 1983). Deep isolation schemes have had to be developed for "high level" nuclear wastes because of larger thermal loads and because of the more severe consequences of ineffective isolation. Ground temperatures may increase by several hundred to more than 1000°C depending upon the level of radioactivity of the waste. Extended exposure to high radiation levels is known to introduce carcinogenic and genetic health hazards. A wide range of disposal schemes have been proposed for high level nuclear wastes. Heuze (1981) has described very deep disposal, i.e. at depths of several kilometers or more, of high nuclear

wastes. The scheme would be applicable to very high level nuclear wastes which generate sufficient heat to melt rocks. Heuze (1983b.) has attempted to predict thermally induced stress changes and ground deformations due to heating and rock melting at depth. A significant research effort has been directed toward disposal of conventional high level nuclear wastes which have undergone primary radioactive decay and will only heat the surrounding rocks to maximum temperatures ranging from about 200°C to 400°C. Candidate repository rocks for these "conventional" high level nuclear wastes include granitic rocks, rock salt, and volcanic rocks such as basalt and tuff. Repository depths for conventional high level nuclear wastes are typically 500 m to 2000 m. Radhakrishna and Tsui (1981) have summarized engineering studies to evaulate the use of disposal vaults in granitic rocks of the Canadian Shield in southern Ontario. Wang et al. (1981) analyzed thermo-hydrologic aspects of nuclear waste disposal in granitic rocks. Cook (1983) has analyzed the influence of joints on thermally induced stresses and deformations in granitic repository rocks. Langer (1982) has outlined geotechnical investigation methods for nuclear waste repositories in rock salt. Cramer et al. (1983) have described an in situ heated block experiment in volcanic basalt related to high level nuclear waste disposal. Zimmerman (1983) has described in situ heater experiments in tuff at a candidate repository site.

Heard (1982) has outlined general requirements for geotechnical evaluation of a high level nuclear waste repository in hard rock. Pincus et al. (1982) have outlined

on-going research requirements for thermal rock mechanics problems. Thompson and Potts (1979) carried out analyses to predict the influence of thermal stresses on stability of underground storage cavities. Palciauskas and Domenica (1982) developed theoretical relationships to evaluate drained and undrained response of thermally loaded repository rocks.

Disposal of high level nuclear waste encased in protective cannisters and deposited in soft sediments on the seafloor has also been considered for the purpose of providing an international nuclear waste disposal site. Preferred deep sea disposal areas which have been identified are located where water depths exceed about 4000 m, mainly in the Pacific Ocean (Hinga et al., 1982). Many of the engineering problems associated with this concept are outlined in Anderson (1981) and Hinga (1982). The problem of predicting heat consolidation of the soft seabed clays after emplacement of the cannisters, is being studied experimentally and analytically by researchers in the Department of Civil Engineering at the University of California at Berkley (e.g. Williams, 1982; Green, 1983; and Lin, 1983).

Solution mining processes such as potash solution, salt solution, uranium leaching from sandstones and the sulphur frasch process involve the injection of heated water (up to several hundred degrees Celsius) or other solvents into deeply buried mineral deposits (e.g. see Cummins and Given, 1973, or Stout, 1980). Dissolved or melted minerals are often pumped

to the surface through the injection wells or through separate recovery wells. The implications of heating adjacent to injection and recovery well casings have not been addressed in the literature. Neither has there apparently been explicit study of the influence of heat on deep hydraulic fracturing for solution mining processes. Mineral processing and industrial waste waters also are often disposed of by deep injection in the form of brines and weighted solutions. Each of these deep injection processes alters the underground thermal regime and in situ stresses resulting in heat consolidation.

2.2.2 Geotechnical Behaviour of Soils, Rocks and Oil Sand at Elevated Temperatures

Thermal Expansion

Heating of porous soils and rocks to temperatures of several hundred degrees Celsius causes the constituent solids and pore fluids (liquid or gaseous) to expand. If thermal expansion is constrained pore fluid pressures increase and the magnitude of stresses in the solid continuum also increase. There are, however, limits to the range of temperatures over which thermal expansion is monotonic. For example, heating of water-saturated soils and rocks from temperatures below the freezing temperature of pore water (0°C) results in volumetric contraction during phase change of solid pore ice to liquid pore water. At elevated temperatures pore liquids may vapourize, depending on the pore pressure. Thermal expansion

properties of liquid water are summarized in Figure A-1 of Appendix A, for temperatures to 350°C and pressures to 35 MPa. Also, compressibility of liquid water at pressures to 35 MPa and temperatures to 350°C, is shown in Figure A-2, Appendix A. Note that the upper limit of compressibility, i.e. the "saturation curve", in Figure A-2 is close to the vapourization pressure-temperature condition for water. The increase in water pressure during heating when volumetric expansion is constrained is illustrated in Figure A-3, for a range of initial temperatures up to 350°C and constant liquid water densities above the saturation pressure. Pressures increase at approximately 1.0 - 1.5 MPa per °C in Figure A-3; the rate of thermal pressure increase declines at elevated temperatures and reduced water densities because of increasing compressibility of the heated water. Data plotted in Figures A-1 to A-3, inclusive, is taken from ASME, 1977 and JSME, 1968.

Petroleum fluids present in the pore space of oil sands and other oil bearing rocks exhibit more complex phase equilibrium behaviour than water because of their heterogeneous composition. Various constituent hydrocarbons in oil may change phase (liquid-gas) over a range of pressure-temperature conditions, leading to non-monotonic thermal expansion.

Thermal expansion and compression properties of several mineral solids including quartz, barite ($BaSo_4$), halite (NaCl), gypsum, and diamond are summarized in Table A-3 of Appendix A (based on data from Clark, 1966).

At very high temperatures, thermally induced volume change of mineral solids in soils and rocks becomes monotonic due to alteration of mineral crystal structures and subsequent melting. Volumetric expansion of quartz at atmospheric pressure is shown in Figure A-4, Appendix A, based on data published in Clark (1966). Alpha quartz crystals expand monotonically up to 573°C, the "alpha-beta transition" temperature. Beyond 573°C, alpha quartz crystals undergo inversion to a beta quartz crystal structure. Monotonic volumetric expansion is discontinued. In fact, volumetric contraction is observed beyond the "alpha-beta transition". Dry quartz will melt at about 1050°C, however, the presence of water lowers the onset of melting (Wyllie, 1971). Van der Molen (1981) measured thermal expansion of granite (dominantly quartzose) at confining pressures up to 300 MPa. Van der Molen observed a shift in "alpha-beta transition" temperature at elevated confining pressures. Figure 2.1 illustrates generalized trends in thermal volume change of quartz at several confining pressures and to elevated temperatures above the melting point. Figure 2.1 was developed on the basis of trends in data published by Clark (1966), Mysen (1981) and Van der Molen (1981).

Mechanical and Physical Properties

Mechanical and physical properties of cemented and crystalline rocks at elevated temperatures have been measured in a number of laboratory and field studies. Properties of

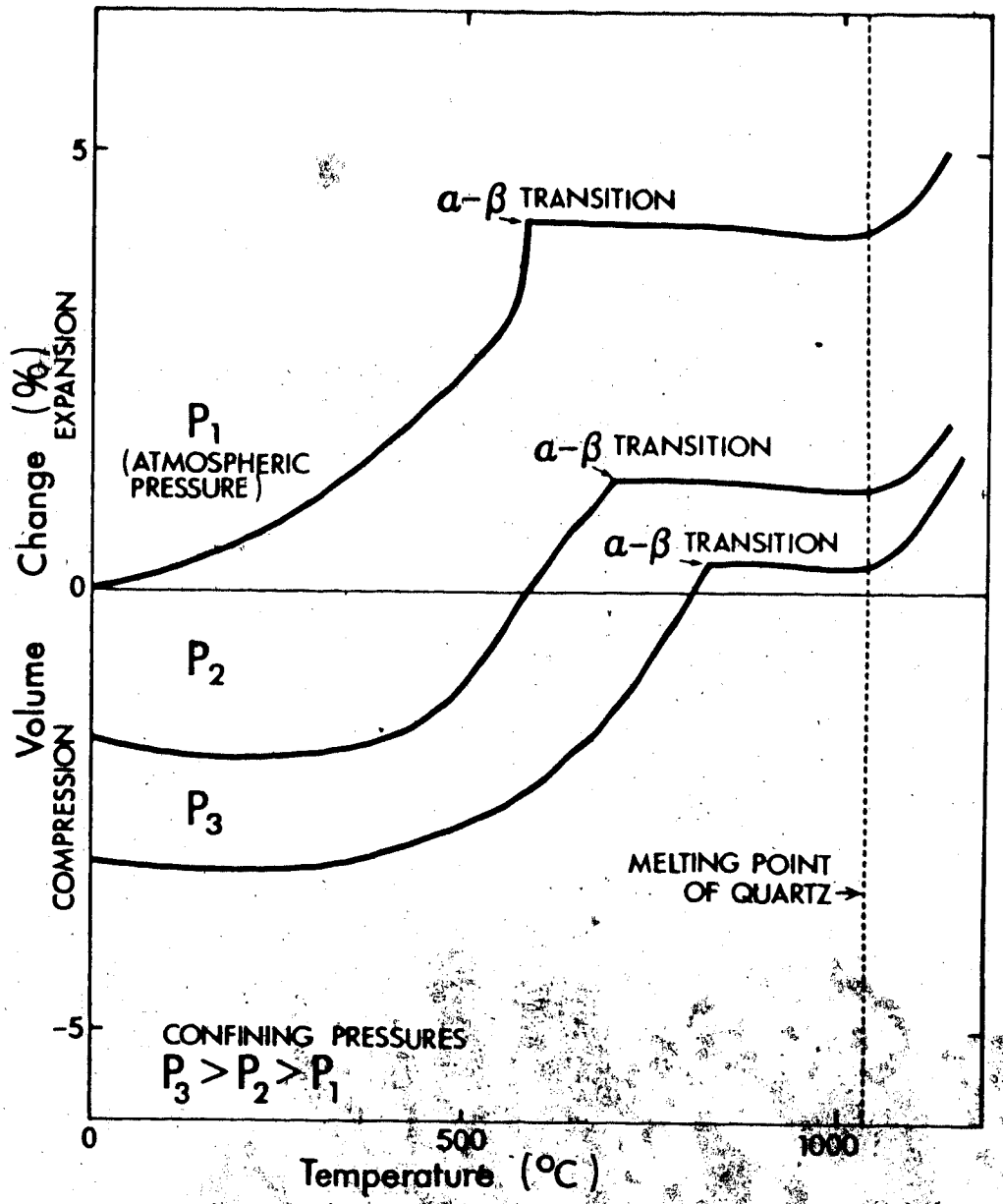

FIGURE 2.1 Trends in Thermal Volume Change of Quartzose Rocks at Atmospheric and Elevated Confining Pressures

granitic rocks have been widely published (e.g. Heard, 1982, and Heuze, 1983a, have summarized much of the recent work on granitic rocks). Experimental results have also been reported for limestones (e.g. Wai and Lo, 1981, and Olsson, 1974), cemented sandstones (e.g. Somerton, 1982) and oil bearing clay shales (e.g. Closmann and Bradley, 1979, and Zeuch, 1983).

Mechanical and physical properties of soils at elevated temperatures have not been studied as extensively as those of rocks. Limited data on Ottawa sand has been published by Gobran (1981) and Scott and Kosar (1982). Data for illite clays has been published by Campanella and Mitchell (1968) for moderate temperatures to 60°C. More recent testing of illite clays by Williams (1982) and Green (1983) has been performed at elevated temperatures to 200°C.

Moore et al. (1983) have measured stress-strain and strength properties of several "soil-like" fault gouge materials at temperatures to 600°C. Gouge materials tested by these authors included crushed granite, kaolinite, illite and serpentine.

Several trends in the mechanical and physical behaviour of rocks and soils at elevated temperatures have emerged from this literature review:

1. Intact rocks and jointed rock masses respond differently to increased temperatures. Intact rock

specimens have been used almost exclusively in laboratory studies while more recent large scale *in situ* experiments have identified some of the characteristic responses of jointed rock masses.

2. Intact rock specimens generally are damaged during heating by a process of "thermal cracking". Micro-cracks develop due to differential rates of heat transfer through the various mineral solids in the rock matrix with the resulting development of tensile and shearing stresses. Intact rock strength and stiffness, have been reported to decline with temperature while porosity increases due to thermal cracking. It has also been inferred that permeability of intact rock increases with temperature (e.g. Heard and Page, 1982). Actual permeability measurements on intact rock specimens have demonstrated that permeability is also strongly dependent on interaction between the rock and pore fluid. For example, Summers et al. (1978) reported a strong decrease in permeability of Westerly granite with increasing temperatures to 400°C due to deposition of precipitates in the pores. Morrow et al. (1983) have reported similar trends for Bullfrog Formation tuff.
3. Recent large-scale *in situ* testing of jointed rock masses has demonstrated that thermal expansion tends to close existing rock joints. Lundstrom and Stille (1978) reported a decrease in the rock mass permeability of Stripa granite at elevated

temperatures. Voegele et al. (1981) also observed a decrease in the in situ permeability of Idaho Springs granitic gneiss with increased temperature, Witherspoon et al. (1981) described in situ heater experiments at Stripa, Sweden in a jointed granite rock mass. Measured displacements during heating varied nonlinearly with temperature and were smaller than those predicted by calculations using linear thermoelasticity. Cook (1983) has developed a theoretical explanation for the observed effects of the rock joints at Stripa on thermally induced displacements and stresses. He concluded that thermally induced rock mass deformations depend more strongly on thermally induced effective stress changes normal to joints and shearing stresses along existing joints than on physical alteration of the rock during heating. Rock joints may either be opened or closed depending upon whether thermal stresses are tensile or compressive in a given region of the rock mass. Thermal stresses within the rock mass are therefore diminished due to opening and closure of the cracks.

4. Experimental research on soils indicates that, unlike intact rocks, soils undergo "thermal compaction" during heating. Work by Campenalla and Mitchell (1968) demonstrated that clays may be compressed substantially during heating under constant effective confining stress. Campanella and Mitchell attributed the "collapse" of the soil skeleton to development of

interparticle shearing stresses during heating which resulted in rearrangement of the skeletal configuration to enable it to support the same effective stress. Recent testing by Williams (1982) and Green (1983) has demonstrated that the compressive strength and stiffness of illite clays increase dramatically with temperature. Similar trends have been reported by Moore et al. (1983) for kaolinite and illite clay gouge materials.

5. Permeability of illite clays tested by Green (1983) and Lin (1983) was found to be essentially constant over the temperature range 4°C to 200°C despite the measured decrease in void ratio.

6. Physical and mechanical properties of dense oil sand were found to be essentially invariant over the temperature range 20°C to 300°C in the present research (see Agar et al., 1983). Gobran (1981) reported that absolute permeability of dense Ottawa sand also does not vary with temperature. Test results for crushed granite (similar to dense sand) reported by Moore et al., (1983) also showed no appreciable variation of strength or stiffness at elevated temperatures to 400°C. At 600°C, however, both stiffness and strength of the crushed granite decreased, apparently because the "alpha-beta transition" temperature of quartz had been exceeded.

Generalized trends in the mechanical and physical behaviour of clay soils, dense sands and intact rocks described above are illustrated schematically in Figure 2.2. Although changes in the mechanical and physical behaviour of soils and intact rocks with temperature are essentially opposite, it may be speculated that the macroscopic response of an intensely jointed rock mass to elevated temperatures is essentially similar to the smaller scale response of an assemblage of soil particles. This observation is supported by the work of Cook (1983).

One further important aspect of the geotechnical behaviour of oil sands at elevated temperatures relates to the viscosity of bitumen in the pore space. The dynamic viscosity of bitumen in Alberta oil sands is very high at reservoir temperatures, typically less than 20°C. Viscosity of bitumen decreases dramatically with increasing temperature. Hence, it is desirable to use thermally enhanced oil recovery techniques. The influence of temperature on the dynamic viscosities of Athabasca and Cold Lake bitumens is shown in Figure 2.3 for atmospheric pressure conditions. Figure 2.3 is based on data presented by Winestock (1974). Figure 2.3 presents a simplified picture since bitumen viscosities are also sensitive to the bitumen composition and pressure. Nevertheless it is apparent that both Athabasca and Cold Lake bitumen are essentially immobile at reservoir temperatures. The pore space of oil rich oil sands is typically 90 per cent saturated with bitumen while the remaining 10 per cent of the pore space is occupied by water. Hydraulic diffusivity of oil sands at

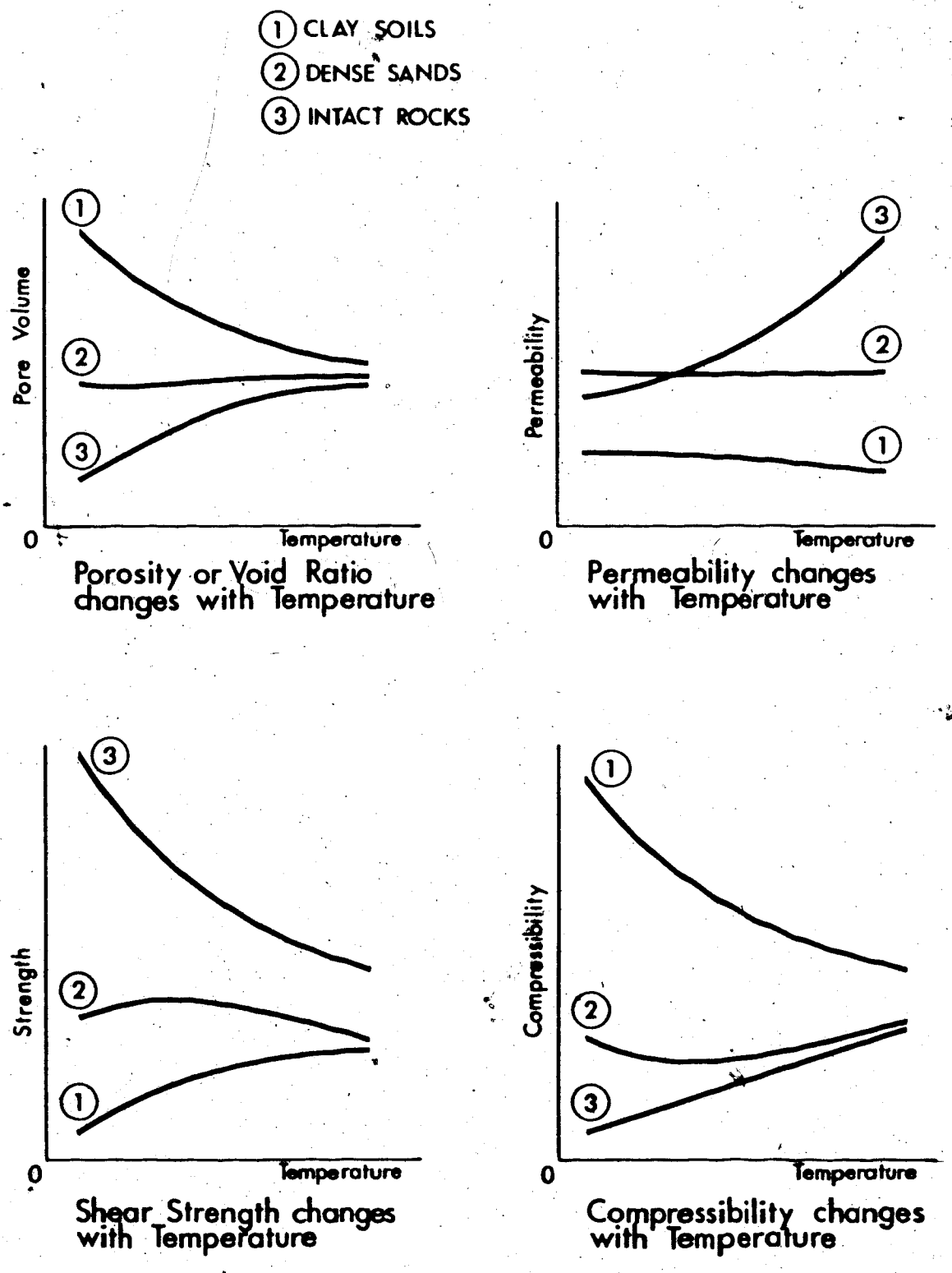

FIGURE 2.2 Generalized Trends in Physical and Mechanical Properties of Clay Soils, Dense Sands and Intact Rocks During Heating (below the melting point)

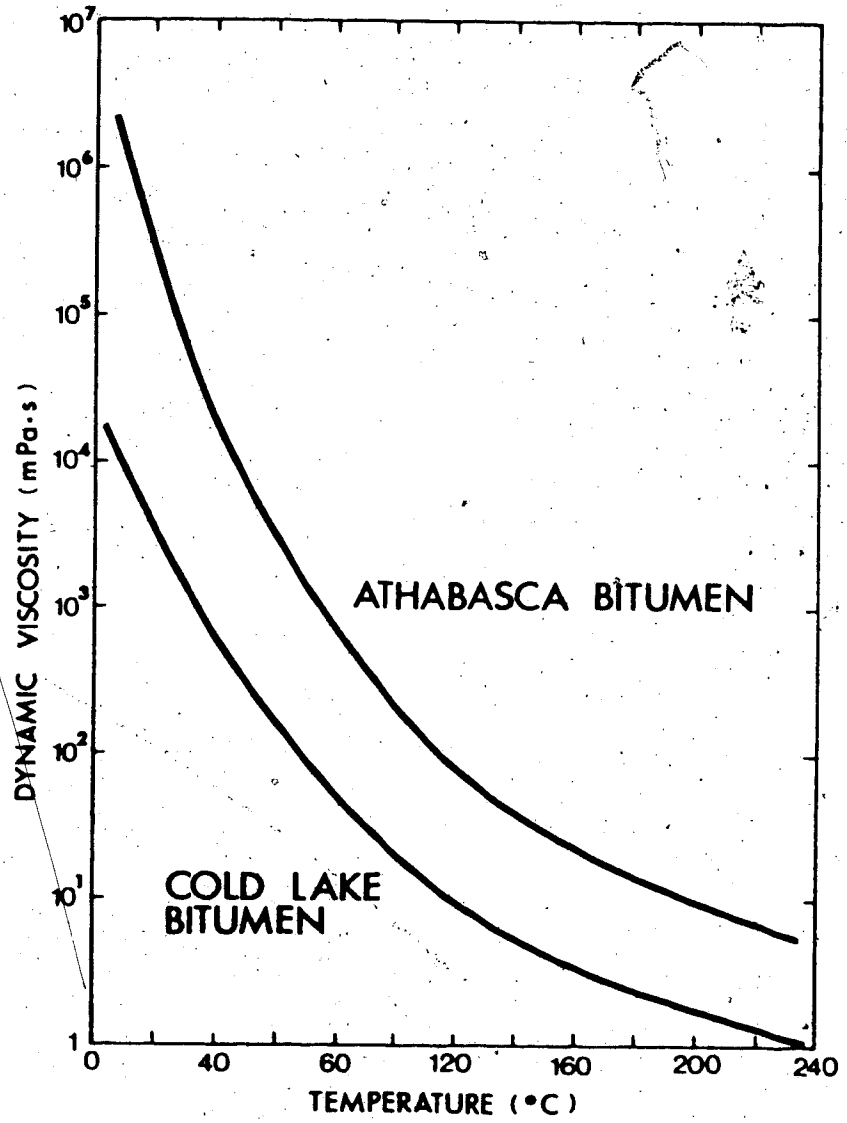

FIGURE 2.3 Viscosity Changes with Temperature for Athabasca and Cold Lake Bitumens at Atmospheric Pressure

reservoir temperatures is almost entirely dependent upon mobility of the water phase, i.e. the effective permeability to water. At elevated temperatures, excess pore pressures dissipate more readily because both the bitumen and water phases are mobile. The coefficient of consolidation of oil sand is therefore more strongly temperature dependent than that of other soils and rocks saturated with less viscous pore fluids such as water or gases.

2.3 Theoretical Concepts

The development of a self-consistent theory of heat consolidation requires consideration of the fundamental principals of thermodynamics in addition to traditional concepts of continuum mechanics. The classical consolidation theories apply specifically to multiphase porous media which include both solid and fluid continua. Application of mechanical and/or thermal energy changes to a multiphase porous medium causes deformation of both the solid and fluid phases. If deformation is restrained the state of stress in both the solid and fluid phases changes. Since fluids, by definition, cannot sustain shearing stresses, the viscous pore fluid continuum flows through the pore space of the solid phase in response to pore pressure gradients. The movement of fluid in response to thermal and mechanical perturbations relative to that of the solid phase involves a time-dependent process of mass transfer and pore stress change.

The basic equations for a heat consolidation theory include:

a) an energy equation;

b) a continuity equation; and

c) equations of motion.

A rigorous theory of heat consolidation requires that these field equations be fully coupled in terms of displacements and temperatures. The physical principals invoked to derive these equations are discussed briefly in the following subsections. Coupling of the heat consolidation equations through thermoelastic constitutive relationships is also described.

2.3.1 The Laws of Thermodynamics and the Energy Equation

The first and second laws of thermodynamics may be stated concisely as follows:

1. Energy may be tranformed from one form into another, but it can neither be created nor destroyed.
2. The entropy of an isolated system can never decrease.

It is generally assumed that a continuum is initially in a state of thermodynamic equilibrium, i.e. neither of the state variables, temperature or entropy, are varying with time. Upon application of mechanical or thermal perturbations, the entropy of the continuum increases. In general, the heat consolidation equations (i.e. the energy equation, continuity equation and equations of motion) must be coupled in terms of both temperature and strain because of the interconvertibility of

thermal and mechanical energy. For example, the temperature of a solid body is known to change when the state of strain of the body is altered adiabatically (Fung, 1965). The resultant energy equation for a porous medium would be of the form (e.g. Schiffmann, 1971):

$$\nabla(k_T \nabla T) + \rho q^* = \rho c \frac{\partial T}{\partial t} + TS_T \frac{\partial I_1}{\partial t} + TF_T \frac{\partial \epsilon_{vf}}{\partial t}, \qquad (2.1)$$

where: S_T denotes average stress variation with temperature in the solid phase, F_T denotes pore fluid pressure variation with temperature, I_1 denotes average strain in the solid continuum, ϵ_{vf} is the fluid volumetric strain, q^* is the heat supply per unit mass, k_T denotes thermal conductivity, ρ is mass density and c is the specific heat.

The second and third terms on the right hand side of equation 2.1 are mechanical energy terms accounting for straining of the solid and fluid phases. For some engineering applications the interaction between strain and temperature is ignored and the mechanical coupling terms are omitted. Equation 2.1 (the energy equation) then reduces to the differential equation for heat transfer by thermal diffusion. For problems involving forced convection, the third term is retained and the resulting form of the energy equation is described as the convective-diffusion equation.

2.3.2 Conservation of Mass and the Continuity Equation

A continuity equation is required to describe transient mass transfer of the fluid phases in porous media since pore fluids move with respect to the solid phase. Derivation of the continuity equation for heat consolidation problems is based on the principal of conservation of mass. It should be noted that the principal of mass conservation may violate the first law of thermodynamics for non-isothermal conditions. In fact, mass and energy are not conserved separately, but are inter-convertible. Molecular masses actually increase during heating, however the mass changes are generally so small that they are undectable, except in nuclear reactions. Consequently, the principal of conservation of mass is sufficiently rigorous for most heat consolidation problems in soils and rocks. It is often assumed that there are no physico-chemical interactions between the fluid and solid phases so that the mass of each phase is conserved separately. Where there are physico-chemical interactions such as precipitation or chemical dissolution of solids, derivation of the continuity equation must be based on combined mass conservation of the solid and fluid phases. When movement of the fluid phase relative to that of an inert solid phase is considered, the generalized continuity equation is of the form (e.g. see Mercer et al., 1982):

$$\frac{\partial(\rho\eta)}{\partial t} + \nabla(\nabla\rho v_i) = 0 \qquad (2.2)$$

Transient variation of the porosity, η, depends on mechanically and thermally induced variation of the principal effective stresses (i.e. σ_1', σ_2', and σ_3'). Also, if the solid particles (i.e mineral grains) are incompressible, porosity varies directly with the principal strains, i.e. the first invariant of strain $I_1 = \frac{1}{3}(\epsilon_1+\epsilon_2+\epsilon_3)$. Transient fluid flow velocity, v_i, is usually governed by Darcy's Law which states that the relative velocity is proportional to the pore pressure gradient.

2.3.3 Equations of Motion

The equations of motion of a porous solid continuum are governed by:

a) the law of conservation of mass;

b) Newton's laws of motion (conservation of momentum); and

c) the law of conservation of energy.

Conservation of energy and the energy equation have already been discussed in the foregoing section 2.3.1. Conservation of mass of the fluid phase was discussed in section 2.3.2. The requirement that the mass of the solid phase be conserved is satisfied in the derivation of the equations of motion of the porous solid continuum.

Newtons' laws of motion require that the rate of change of linear momentum of a body be equal to the resultant of the applied forces and that the rate of change of angular momentum be equal to the resultant momentum of the applied forces. Newton's laws are used in conjunction with the law of conservation of mass to derive the so-called "Eulerian equation of motion" (e.g. see Fung, 1965):

$$\rho \frac{Dv_i}{Dt} = \nabla \sigma_{ij} + X_i \qquad (2.3)$$

where X_i are body forces.

Consolidation of a porous medium is governed by effective stresses. Accordingly, the stress terms in equation 2.3 should be written in terms of effective stresses, e.g. see Schiffmann (1971).

In the absence of body forces equation 2.3 may be written in terms of effective stresses as follows:

$$\rho \frac{Dv_i}{Dt} = \nabla \sigma_{ij} - \chi \nabla P \qquad (2.4)$$

where χ is Biot's "soil-water interaction coefficient" (Biot, 1941); χ is a measure of the ratio of the volume of pore fluid drained to the volume change of the solid skeleton.

When non-transient, quasi-static conditions are assumed, the inertia term on the left-hand side of equation 2.3 goes to zero giving the equation of stress equilibrium.

2.3.4 Thermoelastic Consolidation

The simplest form of constitutive law relating stress and strain with temperature is a linear thermoelastic relationship. The Duhamel-Neumann law (see Fung, 1965) defines stress changes within a solid continuum during non-uniform heating due to suppression of thermal strains by boundary restraints, surface tractions, etc. The resulting constitutive equation is of the form:

$$\sigma_{ij} = C_{ijkl}\,\epsilon_{kl} - D_{ij}\,\Delta T \qquad (2.5)$$

where C_{ijkl} are the elastic moduli and D_{ij} are the thermoelastic moduli. For isotropic linear elastic material

$$D_{ii} = \left[\frac{\alpha E}{1-2\nu}\right] = \alpha(3\lambda + 2G)$$

Solution of boundary-value problems involving the foregoing fully-coupled heat consolidation equations is rather difficult, even when linear thermoelastic constitutive relationships are used. Accordingly, it is attractive to assume "quasi-static" conditions and ignore the interaction between strain and temperature. When these simplifying assumptions are introduced: (i) the inertia term may be

omitted from the equations of motion (equation 2.3 or 2.4) giving the stress equilibrium equations; and (ii) the mechanical coupling term in the energy equation (equation 2.1) may be omitted. The theory then degenerates to a quasi-static theory in which heat transfer (by diffusion or convective-diffusion) and thermoelastic consolidation are treated as two separate problems.

The equilibrium equations satisfying stress equilibrium and strain compatability of the porous elastic continuum may be derived by extension of Biot's poroelastic consolidation theory (Biot, 1941, 1955). The quasi-static thermoelastic equations of equilibrium may then be written in terms of displacements in the following form:

$$G'\nabla^2 w_i + (\lambda' + G')\nabla(\nabla - w_i) - \alpha(3\lambda' + 2G')\nabla T + \chi\nabla P = 0 \quad (2.6)$$

where λ' and G' are drained elastic moduli, and w_i are displacements.

Schiffmann (1971) has derived equilibrium equations of similar form. Analyses of transient heat consolidation problems using quasi-static thermoelastic theory, then require independent solution of: (i) the transient heat transfer equation, and (ii) the stress equilibrium equations (2.6).

Further decoupling is possible if it is assumed that total stresses remain constant during heating in the solution of the

continuity equation (2.2), and/or that pore pressures do not change with total stresses, i.e. ignore the fourth term on the left-hand side of equation 2.6 which links total stress and pore pressure changes through volumetric strain.

Numerical solutions for uncoupled thermoelastic consolidation are developed in Chapters 5 and 6 and implications of some of the foregoing assumptions on numerical predictions are explored.

2.4 Summary

This chapter gives a broad overview of the current state of elevated temperature geotechnics. A wide range of problems involving subterranean heating have been identified in the geosciences literature. The complexity of fully coupled three dimensional heat consolidation theory and solutions appropriate for many of these problems has not been addressed in a comprehensive manner to the present time. Simplified, uncoupled approaches have been adopted ranging from thermoelastic solid mechanics solutions for rock mechanics problems to thermal fluid flow solutions for petroleum engineering and hydroscience problems. The need for on-going experimental research to study geotechnical behaviour and to measure material properties at elevated temperatures is widely recognized. General aspects of the response of rocks and soils to heating have been outlined based on the literature review conducted during this research. Finally theoretical concepts required for development of heat consolidation theory drawn from thermodynamics

and continuum mechanics are summarized and discussed. Basic heat consolidation equations which may be derived from the theory are presented for illustration purposes.

3.0 LABORATORY TESTING

3.1 The Laboratory Testing Facility

3.1.1 General Description

Laboratory equipment was assembled to measure the influence of elevated temperatures and pressures on geotechnical properties of oil sands. The laboratory facility includes the following major components:

a) a one-dimensional consolidometer compression cell;
b) a triaxial compression cell and loading frame with servo-controlled axial loading;
c) two back pressure injection systems;
d) a confining pressure system;
e) heaters and temperature control systems; and
f) a data acquisition system.

The compression cells and pressure injection systems were designed and constructed primarily of grade 316 stainless steel to operate at confining stresses up to 30 MPa (4500 psi), pore pressures to 27 MPa (4000 psi) and temperatures to 300°C. Vertical compression loads up to 440 kN (100,000 lbs.) may be applied to triaxial samples. The laboratory facility also includes several innovative features. Heated reservoirs on line with the upstream and downstream back pressure systems permit injection of steam or hot water and experiments may be conducted with either liquid or vapour back pressures. Bitumen drainage and collection facilities allow flushing of oil from

samples during permeability tests at elevated temperatures. The servo controlled triaxial compression device may be used for stress or strain controlled testing. Pre-peak or post-peak behaviour may be investigated.

3.1.2 High Temperature Consolidometer

A schematic drawing of the consolidometer cell is shown in Figure 3.1.

Cylindrical samples 75 mm in diameter and 25 to 75 mm in height are laterally confined in a stiff stainless steel consolidometer ring mounted inside the cell. Vertical stress is applied to the sample through a hydraulic ram pushing a movable piston mounted above the sample. The hydraulic ram is driven by pressurized silicone oil (hydraulic fluid) from a constant pressure, air-actuated pump. A linear voltage displacement transducer (LVDT) is mounted vertically on top of the consolidometer cell and screw-connected to the loading piston. The LVDT monitors vertical deformation of the sample. Back pressure (or injection pressure) is applied to the top of the sample through a port in the consolidometer wall connected to a group of symmetrically located perforations in a circular pattern in the loading piston. Similarly, back pressure is applied at the base of the sample through a lower port in the consolidometer wall connected with a group of drainage conduits below the sample. Porous metal discs formed from pressed sintred stainless steel are mounted on the top and bottom of

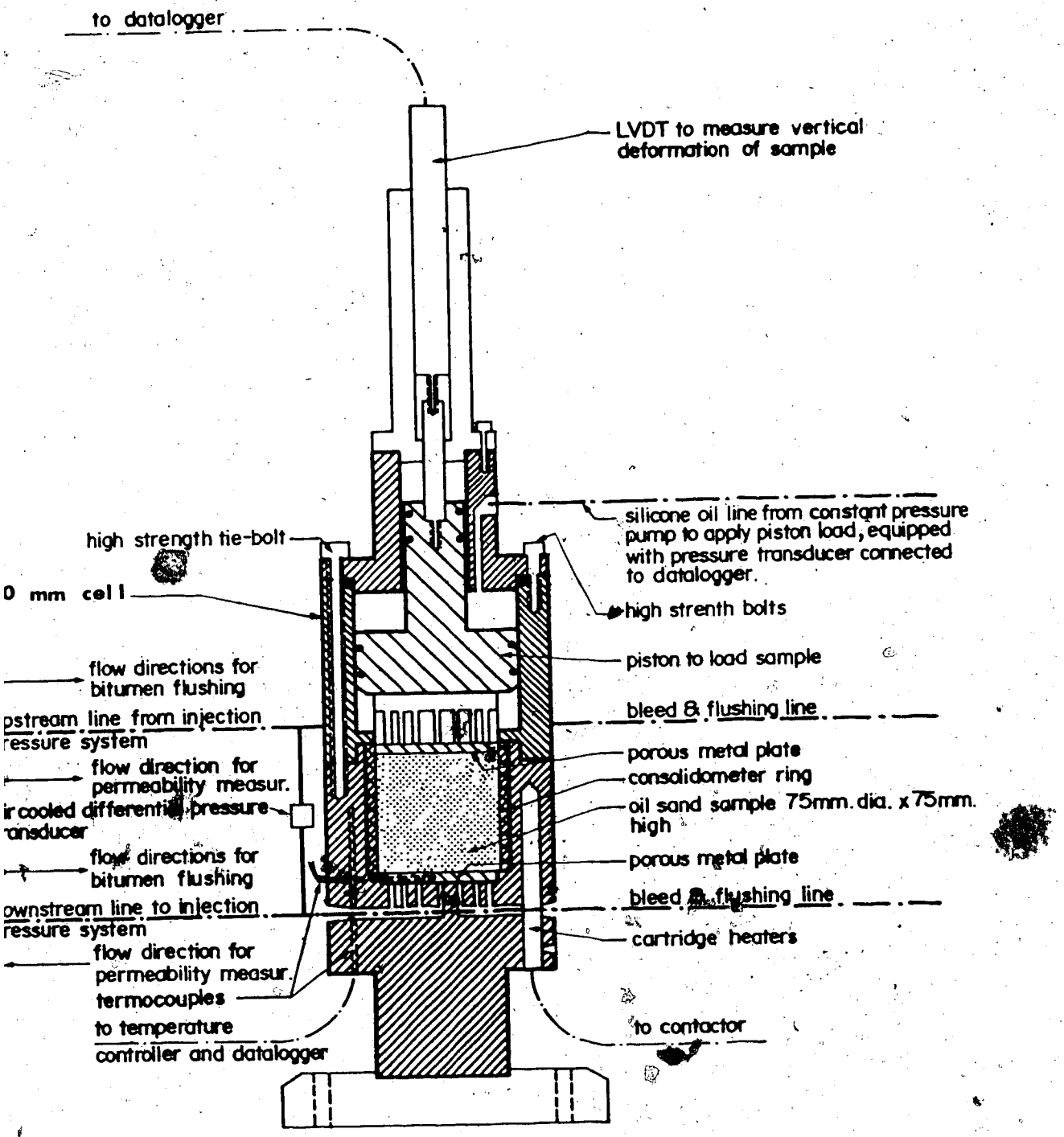

FIGURE 3.1 High Temperature Consolidometer

the sample uniformly, to act as filters to prevent erosion of sand grains from the sample into drainage conduits, and to generate relatively uniform distributions of back pressure at the top and bottom drainage interfaces. Porous metal discs were pre-compressed and preheated prior to apparatus calibration and testing. Two additional ports through the consolidometer walls are used for saturating, bleeding and flushing lines as well as for pressure monitoring access.

The sample is isolated from confining pressure fluid (silicone oil) by rubber O-ring seals mounted on the hydraulic ram. Leakage of pore fluid around the consolidometer ring is prevented by other O-ring seals on the piston and at the base of the consolidometer ring.

The consolidometer cell was constructed as two components seated together and connected with six high strength carbide steel tie-bolts extending through the wall of the top chamber and tapped into the lower chamber wall. Bolts are 0.5 inches in diameter by 6 inches long.

The consolidometer cell is heated by four 500 watt (at 240 volts) cartridge heaters (0.5 inches in diameter by 4 inches long) connected in series and embedded in the wall of the lower chamber around the perimeter of the sample. A J-type (iron/constantin) thermocouple embedded in the consolidometer wall monitors the temperature of the cartridge heaters as well as providing set-point feedback to the temperature controller.

The internal sample temperature is monitored by a thermocouple embedded in the bottom porous metal plate.

3.1.3 High Temperature Triaxial Compression Device

A schematic drawing of the triaxial cell is shown in Figure 3.2.

The triaxial cell was designed to test samples 75 mm in diameter by 150 mm high at confining pressures up to 27 MPa, back pressures up to 20 MPa and temperatures to 300°C. Other sample sizes ranging from NX core (50 mm dia.) to 125 mm diameter may also be tested if the appropriate size loading caps, internal strain gauge yoke and membrane are provided. The cell was constructed of grade 316 stainless steel with four components: (i) the cylindrical cell wall; (ii) a threaded and countersunk top plate; (iii) a loading piston; and (iv) a threaded base plate and pedestal. Back pressure and confining pressure drainage ports, strain gauge wires and thermocouples all access the interior of the triaxial cell through pressure sealed fittings in the base. Strain gauge wires are sealed in fusite (or glass-blown) fittings through the base of the cell.

The top plate and base plate screw into the cylindrical cell wall and each is pressure sealed with a single rubber O-ring. The loading piston is fitted through a hole in the top cap and is pressure sealed with a pair of rubber [illegible]ings.

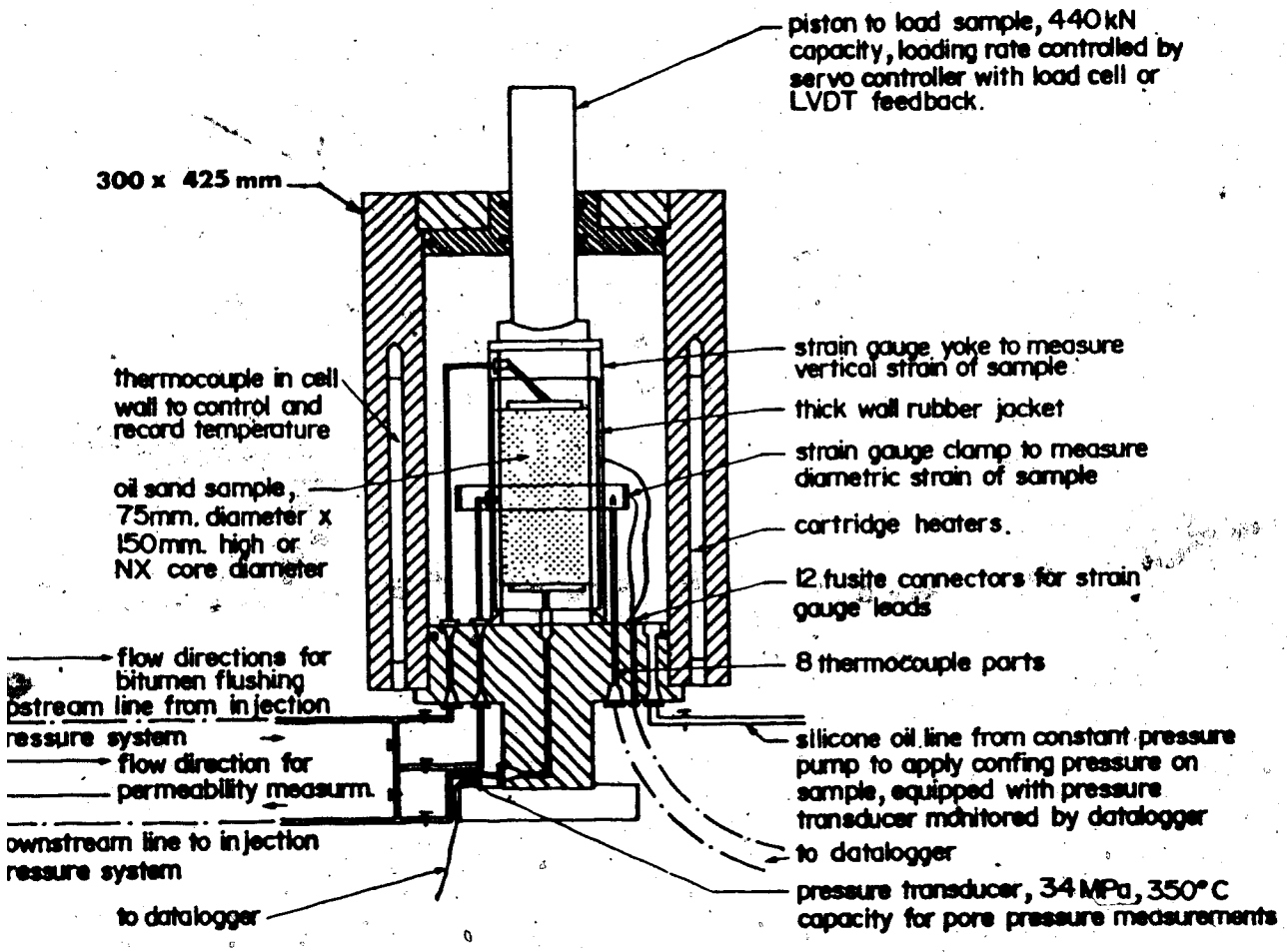

FIGURE 3.2 High Temperature Triaxial Compression Apparatus

The sample is mounted on the cell base with porous stainless steel discs, and top and bottom loading caps. The sample is enclosed in an impermeable membrane which is sealed with rubber O-rings to the top and bottom loading caps. Silicone rubber membranes were used for this research, however other membrane materials are available and are discussed in subsection 3.1.8. Back pressure drainage ports are connected through the top and bottom loading caps to the porous stainless steel plates. A third back pressure drainage port may also be optionally connected through the membrane at the mid-height of the sample. A steel strain-gauged yoke assembly is fastened to the top loading cap. The arms of the yoke are spread apart as vertical deformation proceeds, by a stainless steel cone attached to the bottom loading cap. The axial strain gauge yoke and loading cap are shown in Figure 3.2. Lateral deformations may be measured by a strain gauge clamp, with friction screws bearing against rigid stainless steel buttons embedded in the wall of the membrane (also shown in Figure 3.2).

Oil sand samples for triaxial testing are prepared and mounted on the cell base in a cold room (-20°C) separate from the testing laboratory. It was necessary to design and fabricate a trolley to transport the cell base and mounted sample from the cold room to the laboratory. The trolley consists of a rotating pedestal supported on a "hand-pump" hydraulic jack, all mounted on a base plate with three coaster wheels. Upon arrival in the laboratory, the cell base and

sample can be jacked up and screwed into the suspended triaxial cell wall. The cell and sample are then mounted in the loading frame using a 5000 lb. capacity, hand operated hydraulic crane, also on wheels.

The triaxial cell is filled with a temperature stable (i.e. high flash point and low vapourization pressure) hydraulic fluid; for this research, silicone oil with graphite additive was used. The cell fluid is pressurized by a constant pressure air-actuated diaphragm pump. The pressurized cell fluid applies confining stress to the sample through the flexible, impermeable membrane barrier.

The triaxial cell is heated by eight 1000 watt (at 240 volts) cartridge heaters 0.50 inches in diameter by 12 inches long embedded in the cylindrical wall of the triaxial cell. A J-type thermocouple is inserted in the triaxial cell wall to monitor wall temperatures and to provice set-point feedback to the temperature control unit. Internal cell temperatures are monitored by two thermocouples inside the cell: one located near the top, and the second located near the bottom of the sample.

The reaction loading frame for the triaxial apparatus is constructed entirely of grade 416 stainless steel. The loading frame consists of a bottom plate and a top plate each 56 cm by 56 cm by 7.5 cm thick and four threaded rods, each 5.0 cm in diameter by 140 cm long. The threaded rods are tapped into the

bottom plate while the top plate is positioned with eight hex head nuts (5.0 cm I.D.). A 440 kN capacity hydraulic jack is mounted in the base plate of the triaxial loading frame. The pedestal at the base of the triaxial cell is seated on the ram of this hydraulic jack. The hydraulic ram lifts the entire triaxial cell. Vertical stress is transmitted to the sample through the top loading piston which is forced to bear against the top plate of the reaction loading frame. The reaction loading frame was designed with a factor of safety not less than 2.5, for loads up to 440 kN. The rate of loading by the hydraulic ram is controlled by a servo-control unit with either load cell or LVDT feedback, i.e. for stress or strain controlled testing.

Since the entire triaxial cell moves up as axial shear loading proceeds, it was necessary to construct a flexible manifold [redacted] back pressure drainage lines connected to the base of th[redacted]. The manifold was assembled using a series of two-way swivel fittings in a configuration designed to eliminate bending stresses in the drainage tubing.

3.1.4 Pore Pressure Injection System

Figure 3.3 is a schematic diagram of the pore pressure injection system. The pressure injection system includes an upstream pressure supply (i.e. to the top of the sample) and a downstream pressure source to the bottom of the sample. The pressure injection system may be placed on-line with either the

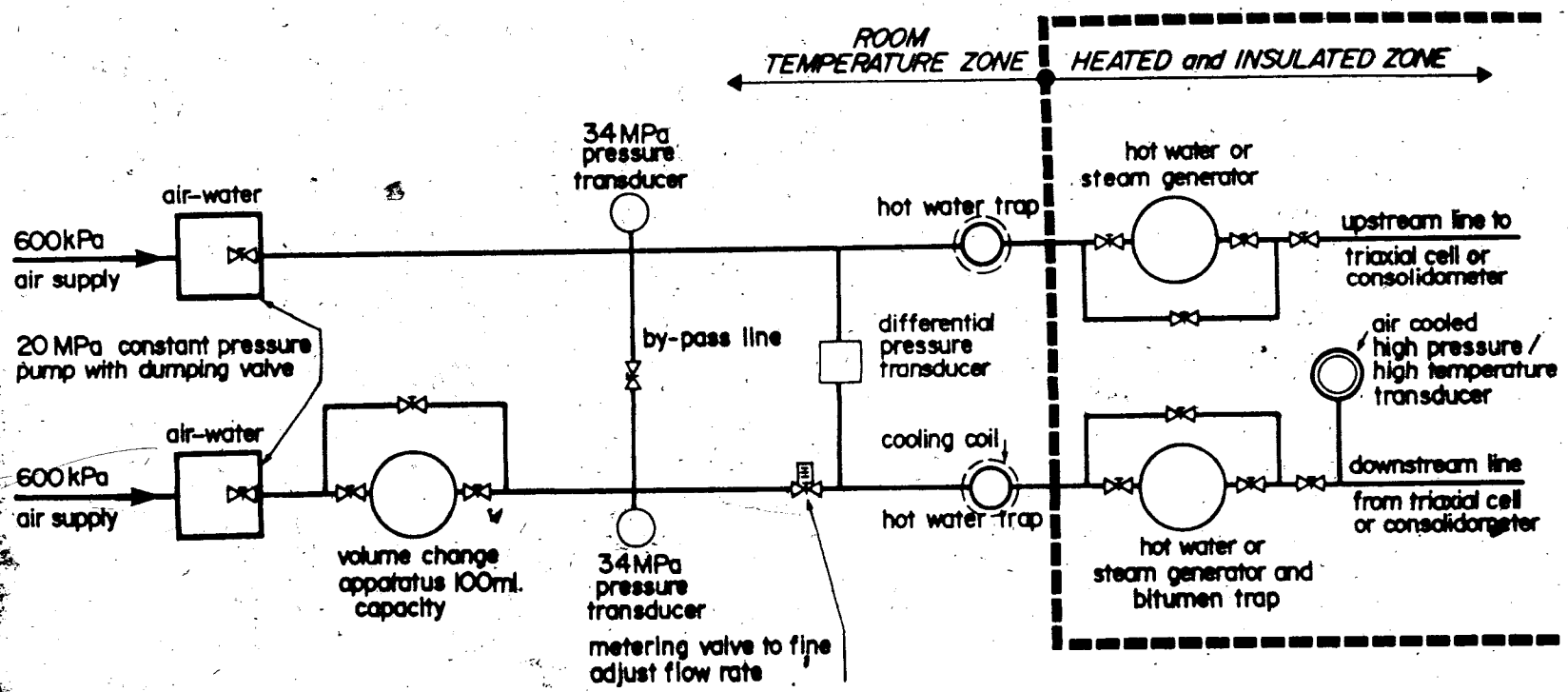

FIGURE 3.3 Pore Pressure Injection System

consolidometer or triaxial cell, or alternatively a single pressure source may be used with either cell for static compression or thermal expansion tests.

The upstream and downstream pressure sources are air actuated diaphragm pumps. The pumps are driven by a 600 kPa compressed air supply. A schematic diagram of the pump components and assembly is shown in Figure 3.4. For fluid pumping or static pressure applications, the pump diaphragm is activated by a slight reduction in the water pressure. Each time the diaphragm is activated, an instantaneous pressure decline of approximately 3% occurs before the set point pressure is restored. This tends to be disadvantageous in low pressure static testing and low differential pressure permeability testing. The system includes an accumulator which helps to maintain a constant pressure level during static tests in the high pressure range (i.e. 4 to 27 MPa). In order to permit better control in the low pressure range, a separate low pressure system (i.e. 0 to 4 MPa) was installed. Figure 3.5 is a schematic diagram of the low pressure system. The pressure source for the low pressure system is compressed nitrogen under 17 MPa pressure.

Tubing for the pore pressure injection system is 0.25 inch O.D., formed from grade 316 stainless steel and conforming to ASTM standard A-269. Tubing which is not subjected to heating has 0.035 inch wall thickness and is rated for pressures up to 5900 psi (40 MPa). Tubing in the heated and insulated zone has

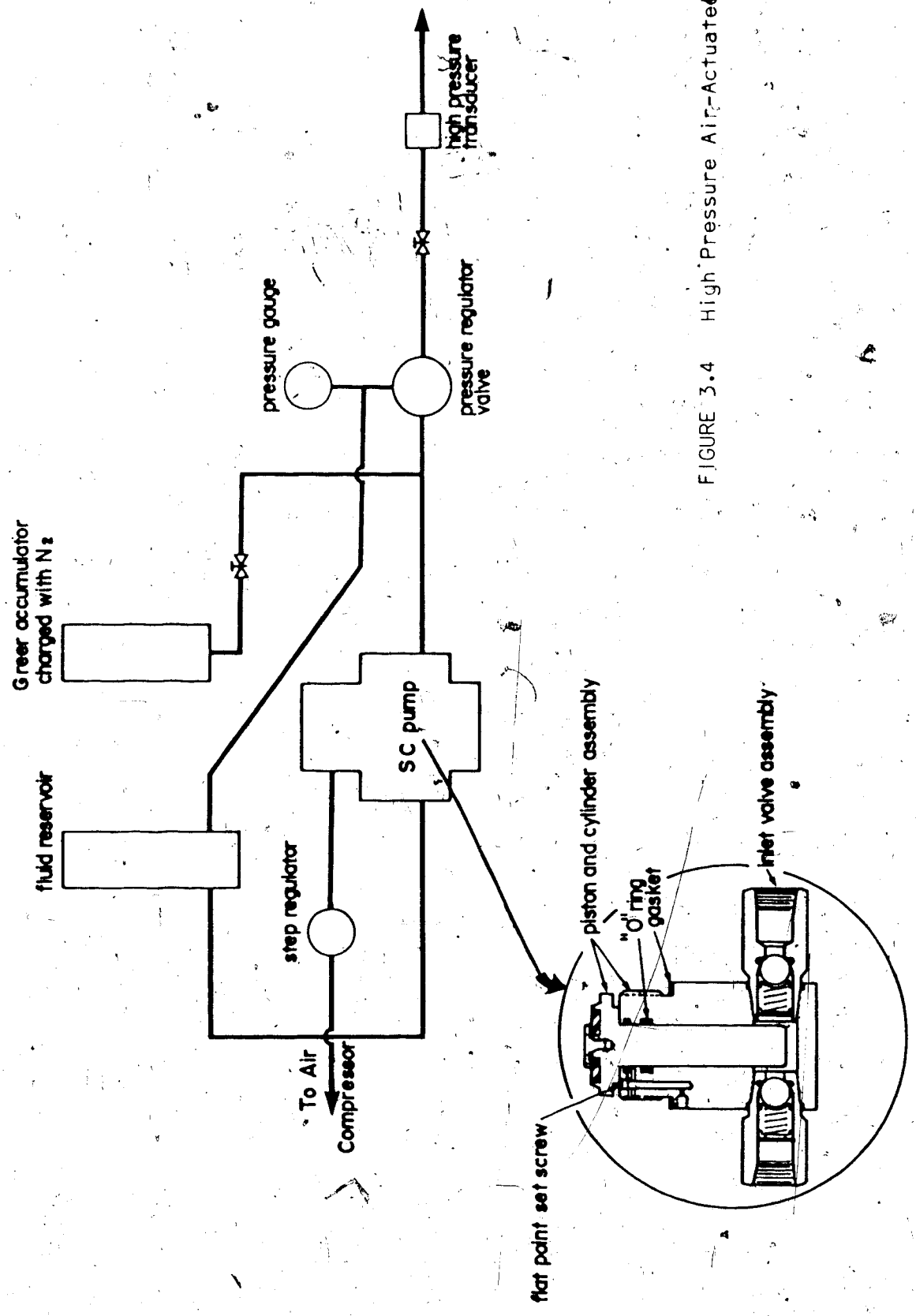

FIGURE 3.4 High Pressure Air-Actuated Pump

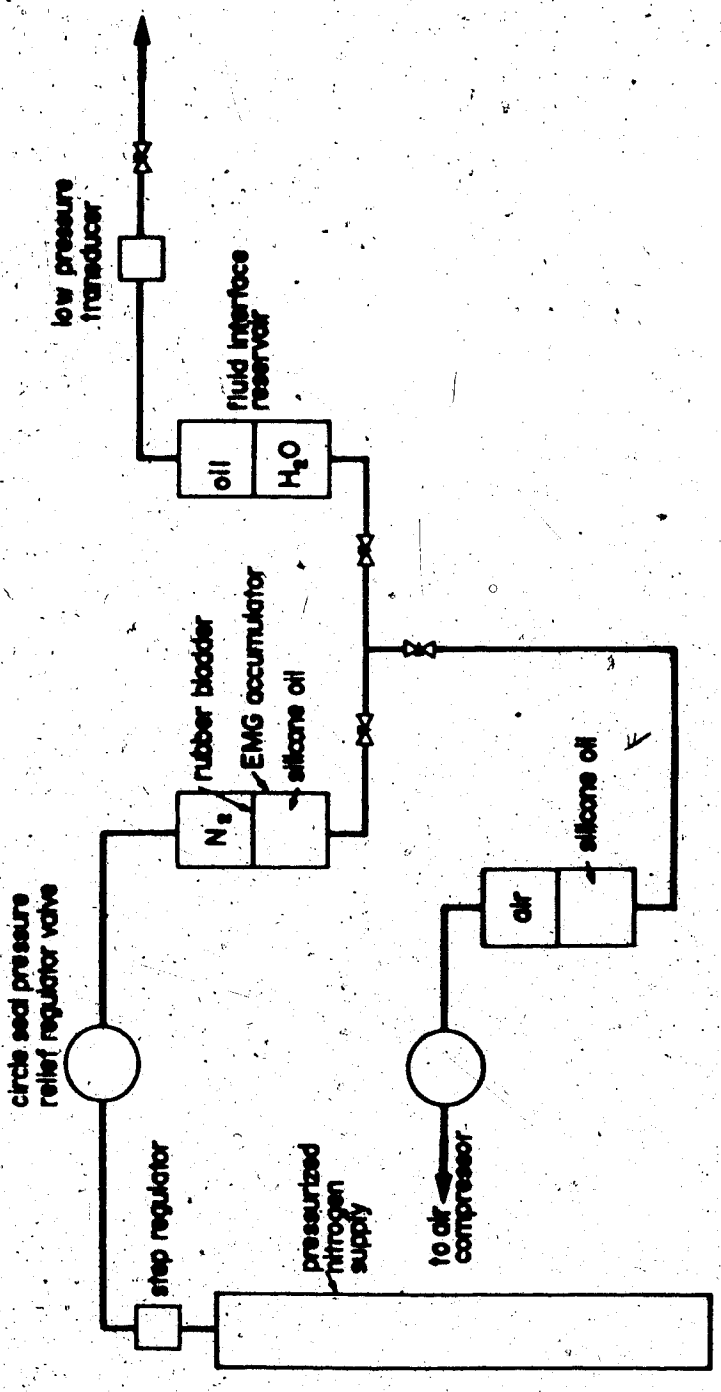

FIGURE 3.5 Schematic of Low Pressure System

0.049 inch wall thickness and is rated for pressures up to 8000 psi (55 MPa) at temperatures up to 300°C.

The pressure injection system is separated into two zones: (i) a room temperature zone away from the consolidometer and/or triaxial cells, and (ii) a heated and insulated zone adjacent to the test cells. As is shown in Figure 3.3, the room temperature and heated zones are separated by two 150 ml capacity heat exchange bottles, located adjacent to the upstream and downstream steam generators. The heat exchange bottles were fabricated from grade 316 stainless steel and are rated by the manufacturer for pressures up to 5000 psi (34 MPa) at temperatures up to 300°C. A cooling coil fabricated from 0.375 inch O.D. copper tubing was placed on the downstream heat exchange bottle. Cool tap water (5 to 10°C) is circulated through the copper coil during permeability experiments to prevent heat transfer beyond the heated zone.

Upstream and downstream hot water or steam generators each of 1900 ml volume capacity, are located in the heated pressure injection zone. The steam generators act as reservoirs of hot injection fluid and also serve as reservoirs for collection of bitumen drained (or flushed) from the sample during injection/permeability testing. Figure 3.6 is a schematic diagram of a steam generator. The steam generator cells were fabricated from grade 316 stainless steel with top and bottom plates connected to the cell with 0.5 inch diameter carbide steel bolts. The steam generators are heated by electrical steel

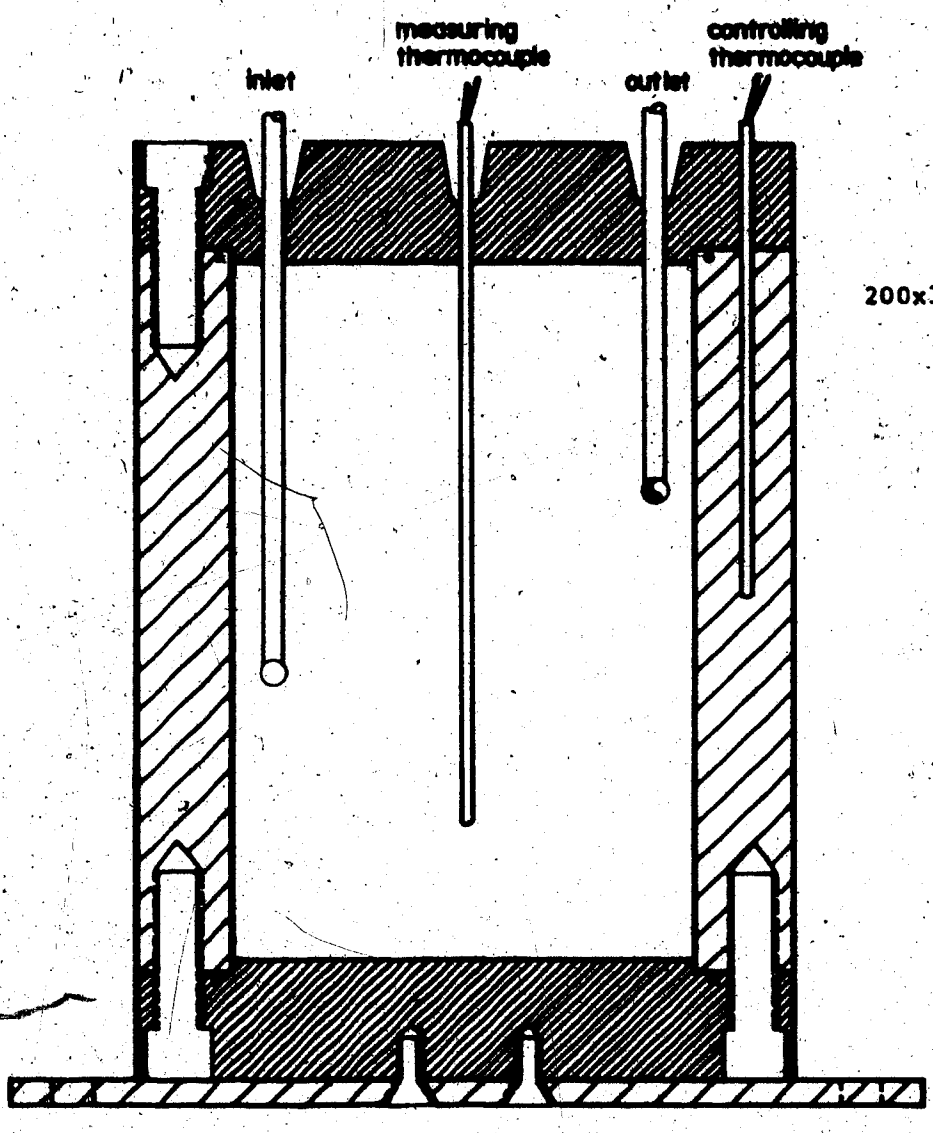

FIGURE 3.6 Hot Water or Steam Generator

heating jackets over the surface area of the steam generators is 2.5 watts/cm^2 at 240 volts.

Stainless steel tubing in the heated zone is heated with silicone rubber heat tracing. Silicone rubber strips are 1.5 mm thick by 20 mm wide and vary in length from 50 cm to 90 cm. The silicone rubber heat tracing supplies a wattage density of 2.2 watts/cm^2 at 120 volts.

The heat-traced tubing, steam generators and test cells (consolidometer and triaxial cell) are externally insulated. The insulation material used is produced from high strength ceramic fibres and inorganic bonding agents, brand name "Fiberfrax Moist-Pack D". This asbestos-free insulation material is supplied in 2.3 m^2 rolls of 6 mm or 12 mm thickness. When wetted the material is very flexible and may be cut and formed over the complex shapes of the laboratory equipment. The formed insulation then air dries to a hard, rigid structure which subsequently retains its form.

The volume change device measures the volume of fluid entering or leaving the test cells. The volume change device is located in the room temperature zone and may be placed on-line with either the upstream or downstream pressure injection pumps. It should be noted that the volume change cell is provided with an electrical heating jacket and may be placed in the heated zone. Figure 3.7 is a schematic drawing of the volume change device. The main chamber of the volume

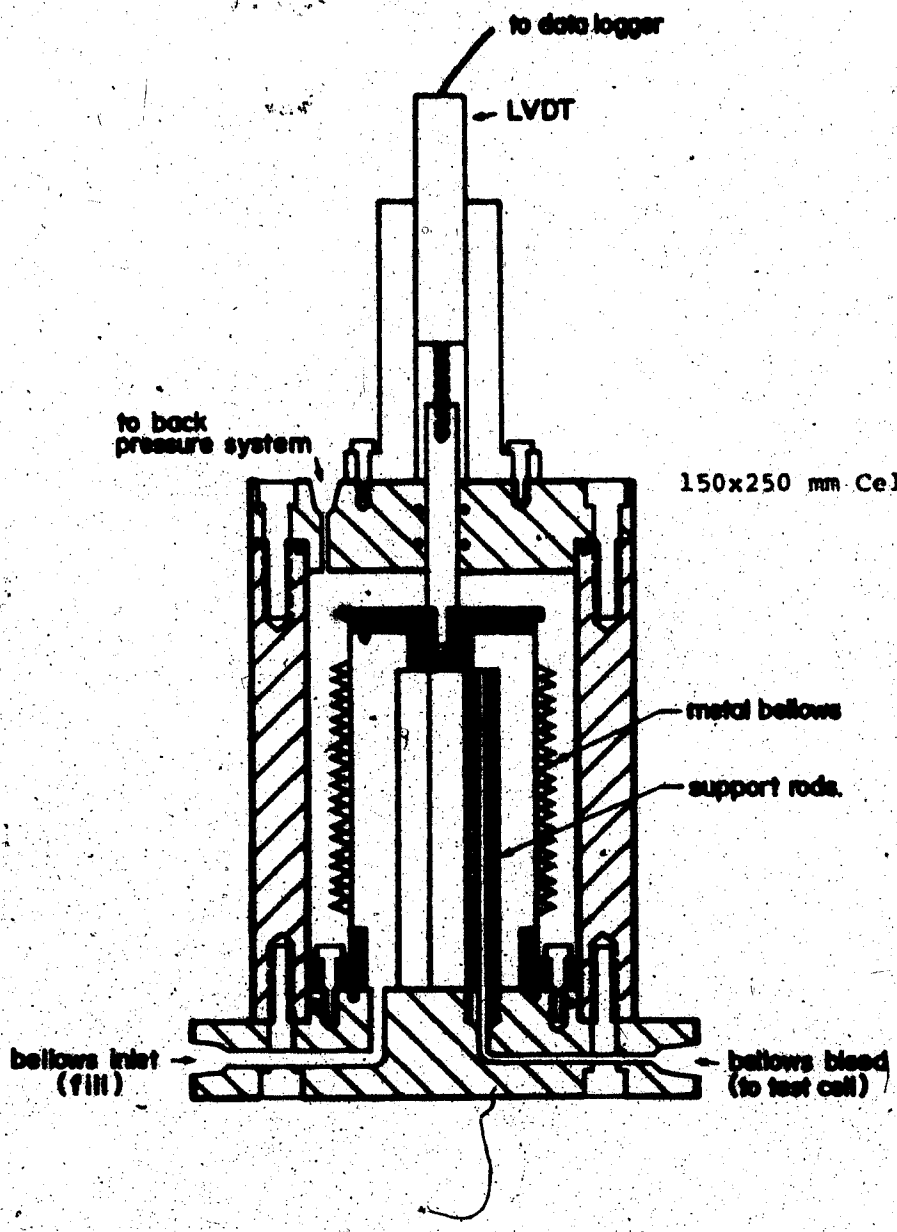

FIGURE 3.7 Volume Change Device

change device was constructed of grade 316 sheet stainless steel. Top and bottom plates are secured in place by 0.50 inch diameter carbide steel bolts. A metal bellows formed from grade 316 stainless steel of 0.020 inch wall thickness is mounted on the base of the chamber. The metal bellows is welded to stainless steel flanges top and bottom by means of a computer controlled cold wire feed heli-arc welding process. Alternatively, flanges may be silver soldered, however, great care is required to avoid damage to the thin sheet stainless steel and to ensure that a pressure seal is formed. The metal bellows is cylindrical in shape and expands or contracts vertically in response to small pressure gradients in the order of $\pm$ 0.50 kPa. Downward travel of the bellows is limited by three internal stainless steel rods 0.5 inches in diameter by 6.5 inches long which act as spreaders between the top flange and base plate to prevent buckling of the thin sheet stainless steel walls. An external LVDT mounted on the top plate of the chamber is connected to a stainless steel piston, 0.625 inches in diameter, which extends through an O-ring sealed port in the top plate and is tapped into the top flange of the metal bellows. The LVDT is calibrated against volume changes inside the metal bellows. The practical operating range of the metal bellows is 75 ml with an absolute maximum 100 ml capacity. The metal bellows may be damaged if subjected to differential pressures exceeding 450 kPa when it is either fully extended or contracted and supported by the spreader rods.

A flow metering valve with micrometer adjustment was placed on-line in the room temperature zone to fine adjust flow rate and thus control the pressure drop across a sample during permeability testing. Also, differential pressure transducers manufactured by Validyne Engineering Corporaton were used to measure differential pressures across the sample during permeability testing. Transducer diaphragms of varying sensitivity may be installed in these transducers.

Integral bonnet barstock "V-stem" valves (brand name "Whitey"), constructed from grade 316 stainless steel with teflon packing are used to control flow in the room temperature zone of the pressure injection system. The "V-stem" valves are rated for 40 MPa pressure at 25°C. Severe service union bonnet "ball tip" valves (brand name "Whitey"), constructed from grade 316 stainless steel with graphite packing are used to control flow in the heated pressure injection zone. The "ball tip" valves are rated for 40 MPa pressure at 25°C and 30 MPa pressure at 300°C.

All threaded fittings in the system are sealed with graphite tape (brand name "Grafoil") to prevent leaks over a wide range of temperatures.

Viton rubber O-ring seals have been used predominantly throughout the system to date. Viton rubber is rated for continuous service in oil up to 225°C, however, it deteriorates when exposed to water heated above 125°C. It has been

necessary to frequently replace the viton rubber O-rings exposed to extended hot water service; however, they have performed satisfactorily in tests at 250°C for durations up to five days. While the viton rubber O-rings are readily available and inexpensive, it will probably be necessary to use O-rings rated for hot water service in future tests of long duration. Silicone rubber O-rings are currently being used in the steam generators. Several other brands including "Parker" and "Kalrez" (by Dupont) are now available which are rated for hot water service. It should be noted here that several O-ring [redacted] the triaxial cell (on the top and bottom loading caps) ar[redacted]ected to both [redacted] water and hot silicone oil simultaneously.

3.1.5 Confining Pressure and Axial Loading Systems

Vertical confining stress in the consolidometer and lateral confining stress in the triaxial cell are transmitted through pressurized silicone oil. The pressure source at low pressures in the range 0 - 4 MPa, is a compressed nitrogen over silicone oil system identical to the back pressure injection system detailed in Figure 3.5. For higher confining pressures up to 30 MPa, a constant pressure air-actuated diaphragm pump, identical to the pore pressure injection pumps detailed in Figure 3.4, is used. The high pressure system includes a "bladder-type" accumulator for maintaining constant static confining stresses in the high pressure range.

Axial shear loading in the triaxial apparatus is powered by a servo-controlled, electric motor powered hydraulic pump driving a 440 kN capacity hydraulic ram. The hydraulic pump has manual valves for controlling flow. The electronic servo-control unit uses load cell transducer feedback to control the hydraulic pump loading rate between preset lower and upper load limits. Alternatively, LVDT feedback may be used to control the displacement rate of the hydraulic ram, i.e. for constant rate of strain testing. A block function diagram for the servo-controller is shown in Figure 3.8.

3.1.6 Temperature Control System

Temperatures of the consolidometer and triaxial cell cartridge heaters, and the steam generator heating jackets are controlled by three independent single set-point digital temperature controllers. The two cartridge heater controllers were manufactured by Omega Engineering, Inc. and the heating jacket controller for the steam generators was manufactured by Chromalox. The temperature control boxes have internal microprocessor based set-point delay time (SPDT) relays rated at 7 amps. resistive at 120 volts A.C. The relay is wired through an external 20 amp. circuit breaker. The microprocessor-based SPDT relay responds to feedback from a J-type thermocouple and alternatively switches the electric heating elements on and off at a fixed time interval to reach and maintain the set-point temperature.

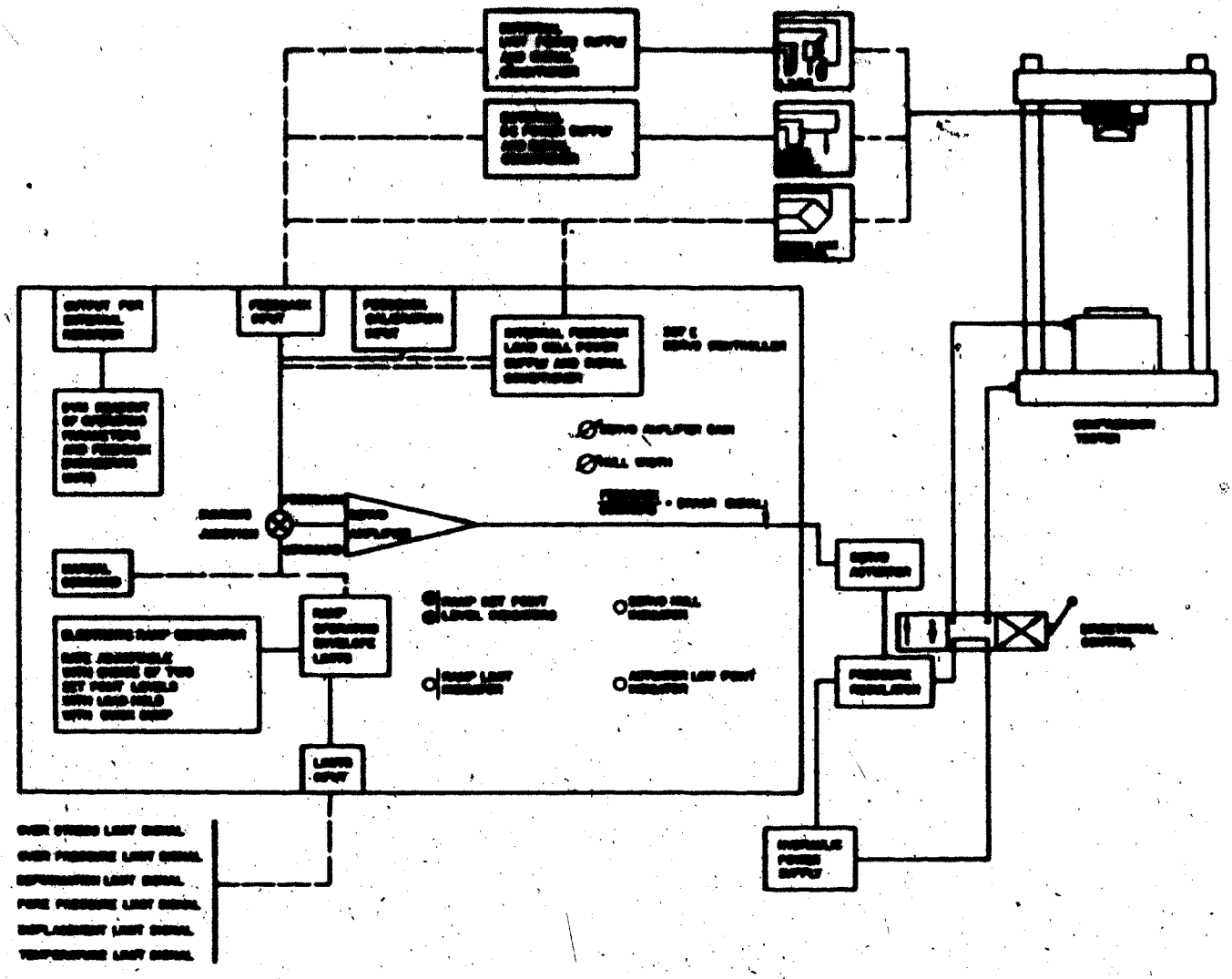

FIGURE 3.8 Servo-Controller: Block Function Diagram

Temperature control of silicone rubber heat tracing for stainless steel tubing in the system is essentially the same, i.e. single set point control. The microprocessor-based control box for the heat tracing, however, includes both a relay and an internal 15 ampere circuit breaker. This control box was manufactured by the Barber Colman Company.

3.1.7 Electronic Signal Conditioning and Data Acquisition Systems

The signal conditioning system includes three circuit boards each having ten channels. The signal conditioner transmits a constant excitation voltage from the power supply to each electronic transducer (i.e. LVDT's or strain gauge transducers). Most transducer circuits are wheatstone bridge configurations. The signal conditioner also picks up output voltage signals from the transducers and transmits these signals to the data acquisition system. The output voltage signals may be "conditioned" before transmission to the data acquisition system, i.e. corrected for electronic zero drift, by adjusting manual potentiometers which are mounted on the signal conditioner circuit boards (i.e. one per channel).

A Hewlett-Packard HP3054DL data logging system was used to scan, process and record output signals from electronic transducers and thermocouples. The data logging system includes a 100 channel HP3497A data acquisition unit and an HP85 microcomputer. The HP85 computer software is programmed

in BASIC command language to scan voltage signals from the electronic transducers at specified intervals and convert the voltage signals into engineering units of pressure, load, volume, displacement, etc. The HP85 is also programmed to record the converted voltage signals on cassette tape or floppy discs. A hard copy of the output in engineering units may be obtained on a paper tape printer as the experiment proceeds. Also, up to three key channels may be monitored on a CRT screen during the time interval between scans. EMF voltage signals from thermocouples are converted directly into °C and added to reference temperatures by calibrated linearized circuits in the data acquisition unit. Output temperatures are also recorded by the HP85 computer.

A "Gandolf" serial interface and telephone line have been installed to permit the HP85 microcomputer to be used as a remote terminal on the main frame AMDAHL computer at the University of Alberta. An interface program DATCOM was obtained from Hewlett Packard and modified to initiate communication and data transfer between the HP85 and AMDAHL systems.

3.1.8 Triaxial Sample Membranes and Cell Fluids

Rubber membrane jackets for triaxial samples were used for this research. An RTV silicone rubber produced both by Canadian General Electric and Dow Corning was selected because of its advertised stability at elevated temperatures.

The RTV silicone rubber is commercially available in liquid form (relatively high viscosity) with a companion catalyst. A catalytic reaction occurs gradually upon addition of 5 to 10% by mass of the catalyst forming a solid silicone rubber. A mould and injection system were designed and fabricated for forming 75 mm I.D. rubber membrane jackets. A schematic diagram of the membrane mould is shown in Figure 3.9.

During laboratory testing it was discovered that RTV silicone rubber tends to swell and depolymerize in the presence of silicone oil at elevated temperatures. The practical temperature limit for normal test durations less than five days is 200°C for this cell fluid - rubber jacket combination.

A range of other membrane materials and cell fluids was investigated in search of a non-reactive combination for testing above 200°C. Some of these materials and cell fluids are summarized in Tables 3.1 and 3.2. The most promising option apparent from this limited study is the use of copper membranes formed either from soft copper sheeting .001 to .003 inches in thickness or from copper tubing. Copper is non-reactive with silicone oil and stable at elevated temperatures less than 1000°C; however it may rupture at low strains in the order of 2% or less and preliminary trials indicate that it is very difficult to form a pressure seal around the loading caps unless mechanical seals are used.

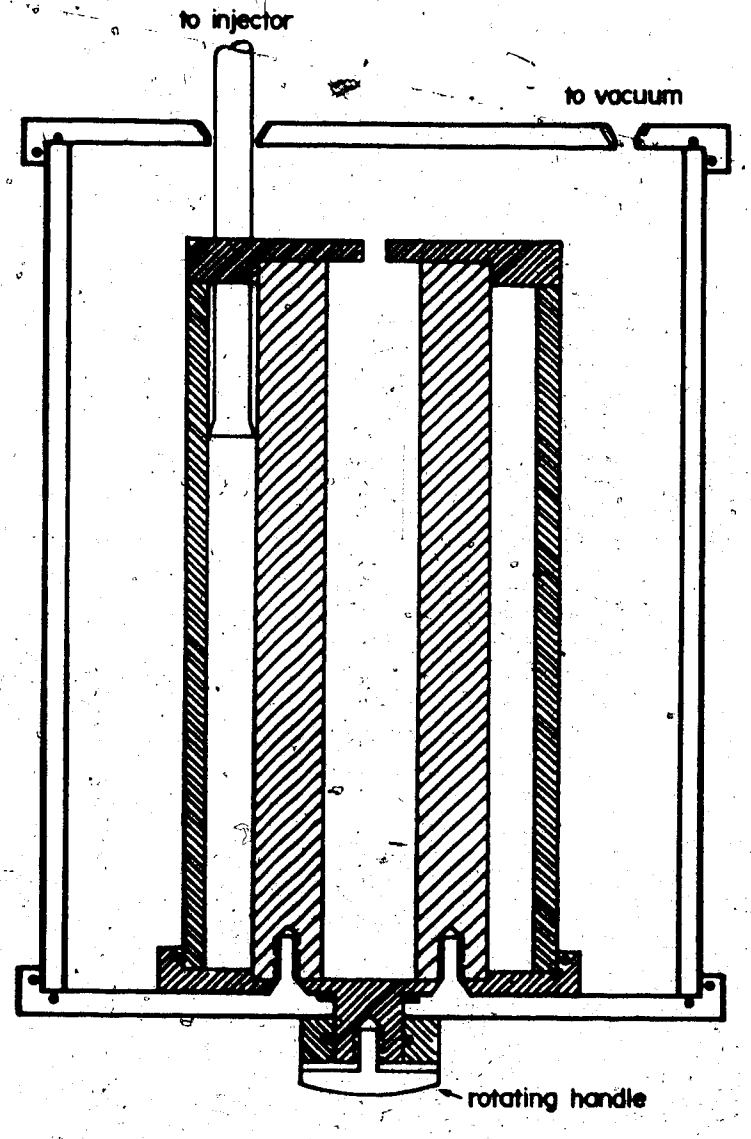

FIGURE 3.9 Mould for Forming Rubber Triaxial Membranes

TABLE 3.1

HIGH TEMPERATURE TRIAXIAL MEMBRANES

Membrane Material	Continuous Service Temperature Rating	Comments
1. Silicone Rubbers		
a) RTV (CGE & Dow Corning)	260°C	• Swell and Depolymerize in silicone oil above 200°C (Catalytic Cure)
b) Fluorosilicone (RTV730)	260°C	
c) Silicone Elastomers	260°C	• Cures by an addition reaction
2. Viton Rubber	>250°C in oil	• Deteriorates in contact with water
3. Teflon	230°C	• Stiff
4. Copper	>500°C (1083°C melting point)	• Difficult to seal • Limited axial strain (1.5%)

TABLE 3.2

HIGH TEMPERATURE TRIAXIAL CELL FLUIDS

Cell Fluids	Properties
1. Silicone Oil with Graphite	• Dow Corning 710.G Flash Pt. > 250°C
2. "Multitherm"	• Contains Silicone Oil
3. Fluorosilicone Oils	• Very Expensive
4. "Odourless Mineral Spirits"	• Pharmaceutical Grade Mineral Oils • Flash Point [illegible]0°C
5. Glycerine	• Flash Point 200°C
6. "Isomeric Dibenzyl Benzoil" BP OLEX WF0801	• Flash Point 220°C • Manufactured only in West Germany

Two other types of silicone rubber compound were tested: (i) fluorosilicone RTV rubber; and (ii) a silicone elastomer (brand name Sylgard) which cures by an addition reaction. Neither of these rubber compounds performed satisfactorily at temperatures in excess of 200°C.

3.2 Apparatus Compliance Testing

3.2.1 Introduction

Compliance testing may be separated into three general categories:

a) calibration of electronic monitoring devices including: pressure transducers, strain gauge load cells, LVDT's, strain gauge displacement devices, and thermocouples;

b) compliance measurements to isolate apparatus deformations and stresses which may be included with external measurements of sample behaviour, e.g. piston friction, apparatus thermal and stress expansion, and membrane stiffness, etc; and

c) compliance proof testing of the overall system on a sample of known properties (e.g. aluminium sample) in order to evaluate accuracy and precision.

The above three categories of compliance testing were completed prior to conducting tests on oil sand samples. In addition, calibration checks were repeated periodically during the testing program and a full suite of monitoring device

calibrations was again carried out upon completion of each major phase of the testing program.

3.2.2 Thermal Expansion and Compression Properties of the System Fluids, Mineral Solids and Metals

Volume change and external load and deformation measuring devices record the lumped response of both the sample and the testing apparatus to temperature and stress changes. Compliance testing categories (b) and (c) listed in subsection 3.2.1 are aimed at isolating the system response to thermal and stress changes. It was therefore, necessary to be cognisant of thermal expansion and compressibility properties of the metals from which the system is fabricated and the pressurizing fluids.

Properties of water were obtained from steam table publications (e.g. ASME Steam Tables, 1977 and Japanese Society of Mechanical Engineers Steam Tables, 1968). Thermal expansion and compressibility of water are presented graphically on Figures A-1 and A-2 in Appendix A. Figure A-3 illustrates the pressure response of water to heating at constant density, i.e. fully confined under conditions of zero volume change.

Silicone oil with graphite additive (Dow Corning 710G Oil) was used as the hydraulic fluid through which vertical confining stress was applied in the consolidometer and as the confining cell fluid in the triaxial cell. Selected properties

of the silicone oil cell fluid are listed along with properties of water and bitumen in Table A-1, Appendix A.

Properties of several metals are summarized in Table A-2. All components of the test apparatus subjected to heating were fabricated from stainless steel grade 316. The triaxial load frame was constructed of grade 416 stainless steel. Copper and brass were used to construct some elements of the low pressure systems. Kovar was used for glass blown pressure fittings in the base of the triaxial cell to permit access for strain gauge wires. Aluminium samples were used in the system compliance testing program. Silicone rubber was used for the triaxial membranes.

Volume change properties (published in Clark, 1966) of quartz and several other minerals are summarized in Table A-3.

Thermal expansion of quartz, the dominant mineral solid in Athabasca and Cold Lake oil sands, is plotted in Figure A-4 over the temperature range 20°C to 1000°C. Figure A-4 is a plot of data published in Clark, 1966.

3.2.3 Calibration of Electronic Monitoring Instruments

Calibrations were required for the following electronic monitoring devices:

a) 2 - 7000 kPa strain gauge pressure transducers

b) 4 - 35000 kPa strain gauge pressure transducers

c) 2 - 140 and 500 kPa differential pressure transducers (strain gauge type)

d) 1 - volume change device LVDT (500 HR)

e) 1 - consolidometer LVDT (1000 HR)

f) 1 - triaxial cell external LVDT (1000 HR)

g) 2 - internal axial strain gauge yoke arms for the triaxial cell

h) 1 - internal lateral strain gauge clamp for the triaxial cell

i) 1 - 220 kN load cell for the triaxial apparatus

j) 1 - 440 kN load cell for the triaxial apparatus

k) 13 - J-type thermocouples (iron/constantin).

Calibration of strain gauge pressure transducers was carried out using a dead weight table hydraulic pressure system. Transducer calibrations and electronic zero drift were checked during each test by connecting the dead weight pressure generator directly on line with the system transducers. Transducer calibrations were generally nonlinear in the lower 5 to 10 per cent of their operating range.

The volume change device LVDT was calibrated against a graduated burette for volume response and against a micrometer scale for linear displacement compliance. Similarly consolidometer and triaxial LVDT's were calibrated against a micrometer scale.

The internal axial strain device for the triaxial cell was calibrated using precision cut PVC plastic tube spacers. The internal lateral strain device for the triaxial cell was calibrated against a micrometer scale. Both internal strain device calibrations were checked at elevated temperatures, however, no significant deviation from room temperature calibration was measured. Strain gauges are mounted on these devices in pairs to provide temperature compensation.

External load cells, of 220 kN and 440kN capacities, for the triaxial test apparatus were calibrated against proving rings of compatible load capacity. Proving ring calibrations were checked against several other hydraulic loading system gauges at the University of Alberta which had been calibrated independently in order to verify the accuracy of the proving rings.

J-type thermocouples used for monitoring system temperatures were calibrated by the manufacturer, however, these calibrations were checked in constant temperature baths to ensure reliable performance.

Calibration for each of these devices used in the testing program are summarized in Table A-4.

3.2.4 Compliance of the Consolidometer Apparatus

Several aspects of the consolidometer response to thermal loading and stress changes were identified as follows:

a) The internal chamber of the consolidometer cell and the consolidometer ring expand during heating thus allowing the diameter of the sample to increase.

b) The consolidometer chamber expands laterally in response to increases in both back pressure and effective vertical confining stress.

c) Vertical thermal expansion of the apparatus and porous metal plates occurs due to heating causing an error in vertical LVDT readings.

d) The porous stainless steel plates ("porous stones") mounted on the top and bottom faces of the sample are compressible.

e) The volume change device measures thermal volume expansion of water in the consolidometer cell extraneous to the sample.

f) The volume change device measures volume change of extraneous water in the system due to pressure compressibility of the water and pressure expansion of the system (eg. tubing, cell, O-Rings, etc.).

g) Piston friction reduces the vertical stress being applied to the sample. Piston friction varies with confining stress, pressure and temperature.

It was necessary to quantify each of the above factors and apply the appropriate corrections to volume change, vertical LVDT deformation readings and confining stresses in order to isolate the sample response.

Item (a), lateral thermal expansion of the consolidometer cell was measured by connecting an external LVDT in a horizontal orientation to the consolidometer cell and measuring diameter changes during heating. The measured volume expansion is compared with predicted thermal expansion of a thick-walled stainless steel cylinder of 75 mm internal diameter in Figure A-5. The measured and predicted deformations shown in Figure A-5 are almost identical, with some minor divergence at high temperatures.

Lateral expansion of the consolidometer ring due to an increase in effective vertical confining stress depends upon the magnitude of Poisson's ratio of the sample. A lateral LVDT was again used to measure diametric expansion of the consolidometer due to vertical effective stress increase on an oil sand sample and due to internal pore pressure increase. Apparatus expansion measurements due to incremental pore pressure and effective vertical stress are presented in Figures A-6 and A-7 respectively.

The porous metal plates and consolidometer expand vertically due to thermal expansion causing an error in vertical LVDT measurements. The magnitude of apparatus expansion was measured during compliance testing on the aluminium sample. This correction factor is shown in Figure A-8.

The porous stainless steel plates were precompressed under

stress of 50 MPa and then the compressibility was measured up to 30 MPa, i.e. within the stress range of the consolidometer. Vertical compression versus compressive stress is shown in Figure A-9.

Correction of volume change measurments for thermal expansion and compressibility of extraneous water in the consolidometer cell and in the system was based on steam table data. System compressibility was also checked on several occasions by isolating the consolidometer cell, increasing the back pressure and recording the volume change. The measured volume of extraneous water inside the consolidometer was approximately 23 ml compared to sample volumes ranging from 125 to 275 ml. The volume of water in the system external to the consolidometer cell varies depending upon whether the steam generators are on or off-line. A typical correction curve for extraneous water in the consolidometer is shown in Figure A-10.

Piston friction was evaluated for the consolidometer in a series of undrained heating tests by balancing pore pressure and confining stress until the piston stabilized. The magnitude of piston friction at that particular temperature was then the difference between the confining stress anbd pore pressure. Figure A-11 is a synthesized plot of piston friction versus temperature.

3.2.5 Compliance of the Triaxial Apparatus

Compliance testing to isolate apparatus and sample responses to temperature and stress changes in the triaxial cell was conducted independent of the consolidometer compliance testing. Internal strain gauge deformation devices eliminated errors associated with apparatus thermal expansion. The following compliance corrections were quantified:

a) Compression of the porous stainless steel plates was as for the consolidometer.

b) The volume of extraneous water in the triaxial cell was determined to be 18 ml. Volume change correction for thermal expansion and compressibility of the extraneous water was determined from steam table data.

c) Volume change measurements were corrected for compressibility of apparatus and water external to the triaxial cell (i.e. the pressure injection system). This system compressibility was measured during each test at the test temperature by isolating the triaxial cell, increasing pressure and measuring volume change. System compressibility is dependent on heat tracing temperatures and whether or not the steam generators are on line (i.e. system temperature and volume). System compressibility typically ranged from 0.40 to 0.80 ml/MPa.

d) Piston friction reduces the magnitude of axial load applied to a triaxial sample, and is dependent upon

confining stress, temperature and axial stress. Internal load cells are generally preferred in geotechnical testing since they measure directly the axial load on the sample independent of piston friction. An external load cell was used in this experimental work and it was therefore necessary to quantify piston friction. Initially the influence of confining stress and temperature were measured simply by increasing the confining stress (cell pressure), which pushed the piston upward, and recording load cell readings over a range of temperatures from 20 to 245°C. Results of this calibration test are are summarized in Figure A-12. The magnitude of piston friction was found to be a linear function of confining stress and essentially independent of temperature. It was then discovered that lubrication of the piston "O-ring" seals with a molybdenum-based lubricant substantially reduced piston friction; furthermore piston friction was found to be nearly constant with confining stress. Calibration with the lubricated piston is presented in Figure A-13. A third test was conducted to determine the influence of axial stress on piston friction. This test was performed by mounting a 440 kN capacity strain gauge load cell inside the triaxial chamber and a 220 kN external load cell. Piston friction, the difference between internal and external load measurements was found to be approximately a linear function of axial stress with some minor hysteresis on unloading. Piston friction versus the external load cell reading is shown

In Figure A-14.

e) Deformation measurements in the triaxial cell include the combined response of sample and membrane to temperature and stress changes. It is therefore necessary to determine the stiffness of the sample membrane in order to isolate the deformation response of the sample. Corrections for rubber membrane stiffness may be determined provided several assumptions are made. Bishop and Henkel (1957) assumed (i) that the compression modulus of rubber is similar to the extension modulus; (ii) that the membrane is capable of taking compression when held against the sample by confining pressure; (iii) that the sample deforms as a right cylinder; and (iv) that hoop stresses are small since Poisson's Ratio is approximately 0.50 for rubber. Silicone rubber membranes 76.2 mm internal diameter by 170 mm high with an 8.3 mm wall thickness were used as a confining stress interface in this testing program. Membrane extension tests were carried out in an industrial oven over a range of temperature from 20°C to 205°C, to measure the extension modulus of the silicone rubber membranes. The membrane extension apparatus is shown schematically in Figure A-21. Load-deflection results from membrane extension tests are presented in Figure A-15. It is noted that the stiffness of silicone rubber in extension is approximately three orders of magnitude smaller than the compressive stiffness of oil sand.

It was observed during the testing that silicone rubber softens and depolymerizes in the presence of silicone oil cell fluid at elevated temperatures (i.e. a chemical reaction occurs). Delineation of this effect would have required design and construction of elaborate apparatus and procedures; and since this correction factor is already negligible it was decided to ignore the influence of further softening for this testing program.

f) Compliance proof testing on a cylindrical aluminium block sample in the triaxial cell was conducted to evaluate deformation and volume change measurements. Figure A-16 to A-20 inclusive summarize measured versus theoretical thermal expansion and stress induced deformations. The magnitudes of measured vertical and horizontal deformations were greater than those predicted assuming properties of aluminium listed in Table A-2. The difference between predicted and measured vertical deformations may be attributed in part to vertical compressibility of the loading caps and porous stainless steel plates. The back-calculated vertical compressibility of these components of the apparatus was 6.6×10^{-4} mm/kN (0.046 per cent strain per kN). This small correction factor was applied to test results for oil sand samples. The differences between measured and predicted lateral strains were small and are attributed to experimental error.

It should be noted that the lateral strain gauge clamp

was found to be too stiff to use on oil sand samples, which possess no true tensile strength. This problem is discussed further under triaxial testing.

3.3 Sampling and Sample Preparation

3.3.1 Sample Disturbance

Uncemented oil sand is highly susceptible to expansion and microstructure disturbance when in situ effective confining stresses are released rapidly, i.e. during sampling. Cohesionless sands possess no tensile resistance to expansion and very low resistance to torsional shear. Dissolved methane, carbon dioxide and light hydrocarbon gases in the bitumen and porewater phases begin to exsolve when confining stresses are released. The effective permeability of oil rich oil sand to gas is relatively low, i.e. less than $10^{-15} m^2$ or 1 millidarcy, at in situ temperatures because of the extremely high viscosity of bitumen. The dynamic viscosity of Athabasca bitumen at reservoir temperatures is in the range 1-5 x 10^6 mPa.s (1 mPa.s = 1 cp). Expansion of oil sand thus occurs as dissolved gases exsolve and expand but are prevented from draining. The rate and magnitude of expansion are increased due to the fact that exsolving gases expand rapidly and maintain elevated pore pressure even as volumetric expansion of the oil sand occurs. The relatively large volume expansion associated with gas exsolution disrupts the interlocking mineral grain structure. Hardy and Hemstock (1963) identified the mechanics of sample disturbance in oil sand. Dusseault (1980) has attempted to analytically quantify core expansion

due to the effects of solution gas. Core recovery in excess of 100 per cent is common when standard sampling techniques are employed. The gas exsolution and expansion processes are accelerated as unprotected core warms from in situ temperatures in the order of 4°C to 10°C, to warmer ambient air temperatures. This phenomenon is also visibly apparent in open pit mine slopes in oil sand where a "slabbing" mode of slope degradation commonly occurs (Brooker, 1975).

Sample disturbance can adversely influence geotechnical properties in laboratory tests. Petrophysical properties, pressure-volume-temperature (PVT) data for pore fluids and geological interpretation of core are also subject to incorrect interpretation as a result of sample disturbance. The influence of sample disturbance on the geotechnical properties: strength, compressibility and stress-strain behaviour has been quantified to some extent by Hardy and Hemstock (1963), Dusseault (1977), Barnes (1980), Dusseault (1980) and Sterne (1981).

In general, isothermal porosity or dry density change due to sampling is the best indicator of sample disturbance. Dusseault (1977) described the use of borehole geophysical data to determine in situ bulk density for comparison with sample densities.

Disturbance of the interlocking micro-structure of oil sand can dramatically decrease strength and increase

compressibility. For example, Tustin (1949) conducted some of the first triaxial compression tests on oil sand at the University of Alberta. Standard core sampling procedures were used and despite considerable care in handling and transporting his samples, he found very little difference between strength and compressibility properties for intact and remoulded samples of Athabasca oil sand.

More recent geotechnical laboratory studies and observations of natural slopes in oil sand indicate substantial differences in undisturbed and remoulded strength and compressibility.

Undrained thermal expansion and compression properties may be altered if the pore fluids (water, oil and gas) are changed. For example, if gross expansion of an oil sand sample is permitted, light hydrocarbon gases will exsolve and drain from the sample. A portion of the expanded pore volume will be occupied by air. If the sample is then saturated with water and trapped air driven into solution under pressure, the composition of the the pore fluids may be substantially altered and thus undrained parameters measured in laboratory tests will not be representative of in situ conditions.

3.3.2 Undisturbed Sampling Techniques

Hardy and Hemstock (1963) used a pressure coring procedure to obtain high quality core samples from depths up to 50 m.

The pressure core barrel, manufactured by Jersey Production Research, allowed oil sand core and drilling fluid to be sealed in the core barrel at bottom-hole pressure. Core samples were then frozen in the core barrel prior to releasing the confining pressure. Problems with handling, shipping and trimming this core cast some doubt on ultimate application of the measured geotechnical properties to in situ modelling.

Dusseault (1977) used a double tube Christensen core barrel with plastic inner liners and attempted to freeze oil sand core samples downhole by circulating chilled diesel fuel in the hole. This procedure worked with some degree of success for oil-poor and fine grained oil sands. However, oil rich sand samples expanded substantially and other operational problems such as sloughing of the hole limited the overall success of the operation. Dusseault (1977) described more ideal and costly techniques including pre-freezing the oil sand in situ prior to coring. This technique is known to have been employed with some degree of success in industry, however, the results have not been published. Recent proprietary development of pressure coring equipment has also resulted in successful high quality sampling in Alberta; again, however, details have not been published. Dusseault and Van Domselaar (1982) have described in a general manner some of the recent improvements in deep borehole core sampling technology.

Dusseault (1977) and Barnes (1980) obtained block samples of oil-free Athabasca sand from river valley outcrops in the

Fort McMurray region. Samples were used to measure shear strength and compressibility properties as well as for scanning electron microscope examination. Sterne (1981) used large block samples of oil rich sand from the Suncor open pit minesite near Fort McMurray. Test specimens obtained from the oil rich block samples were substantially disturbed (i.e. porosity in excess of 40 per cent).

Smith et al. (1978) obtained relatively high quality core samples from the walls of the Saline Creek tunnel. Reported bulk densities for these samples ranged from 2.10 to 2.12 Mg/m^3. Oil sand at this location near the valley wall has experienced gradual removal of confining stress and reduction of pore pressures due to erosion and formation of the Saline Creek valley (over a period of approximately 10,000 years, i.e. during Pleistocene).

Dusseault and Sterne (1980) attempted diamond coring on the Saline Creek valley wall outcrop during summer. Access problems and warm ambient temperatures caused sampling difficulties. Also, removal of unfrozen core samples from the bottom of the hole resulted in both tensile and torsional shear damage to samples.

Oil rich oil sand samples were obtained by diamond coring during late winter from the Saline Creek outcrop for the geotechnical testing reported herein. High quality samples with porosities ranging from 32.7 to 37 per cent were obtained.

Sampling difficulties experienced by Duseault and Sterne (1980) were alleviated due to the frozen condition of the outcrop and cold ambient temperatures.

Freezing prevents microfabric disturbance of oil sand during sampling by: (i) freezing the porewater to provide some true tensile resistance to expansion; (ii) increasing the bitumen viscosity to very high values; (iii) depressing the pore liquid pressures and the bubble point pressure by shrinkage; and (iv) increasing the solubility of gas in the bitumen and porewater thereby limiting the rate and amount of gas exsolution upon stress release.

3.3.3 Rationale for the Sampling Program

Oil sand core samples were taken from the Saline Creek valley wall, at a location approximately 1 km south of the town of Fort McMurray near the Saline Creek diversion tunnel. Coring and sampling were carried out in Late March of 1981. The rationale for obtaining samples at this location and time of year was fourfold.

1. Athabasca oil sand of fine to medium grain size and rich in bituminous oil is exposed near the surface, thus sample retrieval does not require costly deep coring techniques.
2. Overburden confining stresses and pore pressures have been reduced very gradually with erosion and

downcutting of the Saline Creek valley. The slow rate of stress release has allowed natural and light hydrocarbon gases (i.e. methane, carbon dioxide, hydrogen sulphide) exsolving from the pore liquids to drain without disturbance of the sand micro-structure.

3. A database for geotechnical properties of oil sands from this location already existed as a result of geotechnical investigation related to construction of the Saline Creek tunnel (eg. Smith et al., 1978).
4. The depth of freezing is near maximum, i.e. up to 2 m or more, in late winter.

Core samples 100 mm in diameter from the frozen depth interval 0.3 to 1.0 m below the slope face were immediatley sealed, packed on dry ice and transported to Edmonton. Samples were stored and trimmed for testing in a climate controlled room at -20°C. Samples remained frozen continuously during sampling and sample preparation, and were only allowed to thaw after being confined in the test cell.

The collection of core samples obtained were sufficiently uniform to conduct a comparative study of the effects of elevated temperature and pressure on the geotechnical properties of undisturbed oil sand. Also, it was possible to quantify for the first time, the influence of very subtle levels of disturbance on strength and stress deformation behaviour of Athabasca oil sand.

3.3.4 Outcrop Sampling Technique Used at Saline Creek

The coring rig used to obtain samples from the Saline Creek valley wall is constructed of aluminium and may be handled by one man. The support frame is supported in place on the slope by up to twelve 8 to 12 inch long rock anchors. The core barrel has diamond cutting teeth and is nominally 100 mm in internal diameter by 470 mm long, with a 2.5 mm nominal wall thickness. The core barrel is driven by an 8 horsepower gasoline engine side-mounted on the frame; rotary torque is transmitted through a chain drive and the gear driven "down-haul" force is applied manually. Chilled diesel fuel may be circulated through the drill string and core barrel to lubricate and cool the diamond cutting teeth. After coring the core barrel is removed from the hole. The down-hole end of the core sample is sheared off laterally using a long thin steel wedge. Specially designed wire hooks are used to lift the core out of the hole. This break-out operation becomes more difficult with increasing depth of sampling. Also, unfrozen oil sand core cannot be removed downhole by this technique without causing significant sample disturbance (Dusseault and Sterne, 1980). The maximum practical depth for outcrop sampling by this technique is less than 1.0 m.

After removal from the hole, frozen core samples were moisture sealed by coating in paraffin wax. Bulk densities of the waxed, frozen core samples were measured on site.

3.3.5 Sample Shipping and Storage

Frozen oil sand core samples, 100 mm in diameter were coated with paraffin wax, double wrapped in plastic, sealed and packed in heavy plywood shipping crates filled with dry ice and insulated with styrofoam. Samples were shipped to Edmonton, unpacked and stored in a climate controlled cold room at -20°C. Bulk densities of core samples were remeasured in the laboratory cold room for comparison with "on-site" bulk density measurements. The success of the shipping and handling procedure was confirmed by the fact that no measurable difference was detected between bulk density values measured "on-site" and in the laboratory cold room.

3.3.6 Undisturbed Sample Preparation

Sample preparation was carried out in a cold room at -20°C. Oil sand core samples, 100 mm in diameter, were prechilled on dry ice (-80°C) for twenty-four hours prior to trimming. Samples were then trimmed to the final 76 mm diameter on a four speed belt driven lathe using a diamond tipped trimming bit. Samples were notched using a carbide steel notching bit at the desired length, i.e. 25 mm for thermal expansion and compression testing, 50 mm for permeability tests or 150 mm for triaxial testing. Notched samples were then cut with a diamond saw. Samples were finally remounted in the lathe in a custom designed chuck, in which the ends were trimmed smooth at right angles to the cylindrical axis. Final diameter and end

trimming were performed with a square carbide-tipped finishing bit.

It should be noted that considerable care and patience were required to avoid sample disturbance during trimming. Initial trimming from 100 mm to 80 mm diameter was performed in 0.250 to 0.375 mm cuts. Final trimming and finishing were performed in 0.050 to 0.125 mm cuts. Several factors which were found to contribute to sample disturbance during sample preparation included:

a) Packing plastic wrapped samples on dry ice allowed carbon dioxide to diffuse through the plastic and permeate the sample. Samples were much more susceptible to swelling during sample preparation. Samples were subsequently stored in sealed paint cans to prevent permeation of carbon dioxide into the sample while chilling on dry ice.

b) Carbide tipped trimming bits were found to wear rapidly on the abrasive oil sand core. Considerable heat build-up resulted as the bits became worn. Also, bits had to be changed frequently during the trimming operation. A diamond tipped bit was found to be satisfactory for continuous trimming without resharpening.

c) Occasional delays are required during trimming, particularly during the final trimming stage to allow the bit to cool, in order to limit potential thermal disturbance of the sample.

3.3.7 Sample Mounting Procedures

Trimmed oil sand samples for testing in the consolidometer were mounted in a chilled stainless steel consolidometer ring in the cold room. The consolidometer ring and sample were then quickly mounted in the consolidometer test cell. Confining stress sufficient to prevent thermal expansion as the sample thawed and warmed to room temperature was applied immediately.

Triaxial oil sand samples were inserted into chilled rubber triaxial membranes. Rubber membranes were extended laterally either in a vacuum chamber or by axial compression in a steel mounting frame to facilitate insertion of the samples. The membrane and sample were then mounted on the triaxial cell base in the cold room. Strain gauge wires and drainage ports were also connected in the cold room. The trolley-mounted triaxial cell base and sample were then wheeled into the laboratory. The triaxial cell wall was lowered over the base; the base was then jacked up and screwed into the cell wall. The triaxial cell and sample were then hoisted by hydraulic crane and placed in the loading frame. The triaxial cell was filled with silicone oil cell fluid. The top cap of the triaxial cell was screwed into the threaded cell wall and the top loading piston inserted through the top cap. The top plate of the loading frame was then lowered into place by the hydraulic crane. The load cell and confining pressure system were connected and a confining stress applied to the sample to prevent expansion as the sample thawed and warmed to room temperature. The total

time required to transfer a triaxial sample from the cold room to the laboratory and apply confining stress ranged from 20 to 35 minutes. Vacuum confinement (100kPa) could be applied to samples during mounting in the laboratory, however, this was found to be cumbersome and of questionable value in preventing thermal sample disturbance.

The final stage of sample mounting involved connection of the back pressure system, thermo-couples and external LVDT's etc.

3.3.8 Quality of Undisturbed Samples

Dry density or porosity are the properties generally used in geotechnical engineering to evaluate disturbance of soil or rock samples for laboratory testing. Dusseault and Van Domeselaar (1982) have recommended that a disturbance index based on sample porosity and in situ porosity from borehole geophysical data, be used to evaluate the quality of oil snd samples. Disturbance index is defined as:

$$I_D = \frac{\eta_s - \eta_I}{\eta_I} \times 100 \qquad (3.1)$$

Table 3.3 summarizes bulk densities, porosities and disturbance indices for all samples tested. Since borehole geophysical data was not available, an average in situ porosity value of 0.33 was used to determine values of the disturbance index for Saline Creek oil sand. This is consistent with the

minimum porosity values reported for the Saline Creek tunnel project. A value of 0.35 was used for *in situ* porosity of Cold Lake oil sand (Mainland, 1983).

Several observations related to sample disturbance may be made based on the data presented in Table 3.3:

a) Samples are listed in chronological order in Table 3.3; it is apparent that sample quality improved with experience.

b) Disturbance of the first three samples for tests COS1, COS2 and COS3 resulted from exposure of these samples to gaseous carbon dioxide. A new mode of sample disturbance was identified.

c) Smaller samples, i.e. for thermal expansion, compression and permeability testing in the consolidometer (test series COS and CPERM in Table 3.1) are more susceptible to disturbance during trimming than larger triaxial samples.

d) Samples containing larger proportions of fine grained mineral solids, i.e. silt and clay particles, are less susceptible to sample disturbance. Dusseault (1977) also observed this phenomenon.

e) Saline Creek samples having porosities less than about 0.37 or disturbance index values less than about 10 per cent are considered to be sufficiently high quality for geotechnical testing. Only samples with porosities less than 0.36 were used for comparison of strength and stress-strain behaviour.

TABLE 3.3

SAMPLE DISTURBANCE

Test No.	Sample No.	Trimmed Bulk Density (Mg/m)	Porosity	Disturbance Index, I_D (%)	Comments
COS1	5	1.702	0.460	40.0	Disturbed
COS2	32	1,865	0.420	28.2	Disturbed
COS3	30	1.586	0.505	53.1	Disturbed
COS4	38	2.000	0.384	16.4	
COS5	18	1.994	0.375	13.6	
COS6	10A	1.968	0.388	17.6	
COS7	10B	1.990	0.381	15.5	
COS8	42	1.948	0.400	21.0	
COS9	41	2.073	0.350	6.0	
CPERM1	10C	2.046	0.364	10.3	
CPERM2	10C	2.046	0.364	10.3	
CPERM3	Remoulded	2.040	0.370	----	Compacted
CPERM4	36	2.026	0.371	12.4	
CPERM5	31A	2.045	0.366	10.9	
CPERM6	31B	2.033	0.361	9.4	
CPERM7	44	2.020	0.355	7.6	
CPERM8	16	2.058	0.327	0.0	
CPERM9	Remoulded	1.906	0.400	----	Compacted
TOS1	25	2.088	0.333	1.0	
TOS2	33	2.077	0.340	3.0	
TOS3	43	2.082	0.357	8.2	
TOS4	44	2.013	0.369	11.8	
TOS5	17	2.050	0.357	8.2	
TOS6	16	2.120	0.327	0.0	
TOS7	45	2.023	0.355	7.6	
TOS8	28	2.046	0.354	7.3	
TOS9	27	2.079	0.337	2.1	
TOS10	20	2.076	0.349	5.8	
TOS11	22	2.064	0.356	7.9	
TOS12	29	2.092	0.341	3.3	
TOS13	26	2.080	0.328	0.0	
TOS14	5,7,8	1.850	0.418	26.0	Remoulded
TOS15	Cold Lk.12B	1.965	0.383	9.4	
TOS16	13	2.053	0.358	8.5	
TOS17	23	2.054	0.360	9.1	
TOS18	24	2.080	0.334	1.2	
TOS19	19	2.084	-----	---	

3.3.9 New Modes of Sample Disturbance

Several causes of oil sand sample disturbance not previously identified were observed during this study in each of the following operational phases:

a) during core sampling;
b) during sample storage;
c) during sample preparation; and
d) during testing.

The downhole end of a core sample cannot readily be cut to allow removal of the sample from the borehole. The downhole end of a sample must either be sheared by lateral displacement or rotation causing torsional shear stresses. Frozen samples at shallow depth did not expand inside the core barrel, therefore, no diametral resistance was available to allow torsional shearing. Lateral displacement of the sample was possible after removal of the core barrel from the hole. Minor disturbance of the lower end of the frozen samples resulted during lateral shearing and removal from the hole. It was necessary to discard the disturbed ends of the frozen samples. Unfrozen core cannot be sheared downhole without substantial disturbance (Dusseault and Sterne, 1980).

During the initial stages of the laboratory research oil sand samples were double wrapped in plastic bags and chilled on dry ice for 24 hours prior to trimming on the lathe. It was

discovered that samples become more susceptible to expansion during trimming (even at very cold temperatures) with increased prechilling time. In fact, samples taken directly from storage at -20°C in the cold room were less susceptible to disturbance during sample preparation than samples prechilled on dry ice at -80°C. Continuous sublimation of the dry ice resulted in high concentration of carbon dioxide gas inside the insulated storage box. Also, it was known that gases permeate readily through thin plastic bags. Furthermore, carbon dioxide is highly soluble in heavy oils (Burcik, 1957; Amyx, Bass & Whiting, 1960) and solubility increases as the temperature decreases. It was, therefore, concluded that carbon dioxide had diffused through the plastic bag wrappers and into the sample at very cold storage temperatures, i.e. -20 to -80°C. As the sample was warmed to -20°C during trimming exsolution and expansion of the dissolved carbon dioxide gas resulted in significant sample disturbance. Thereafter, samples were isolated inside a sealed metal container prior to chilling on dry ice. The metal container was fabricated from two unused paint cans welded together. The first three samples (nos. 5, 32 and 30) in Table 3.3 were grossly disturbed due to contamination with solution of carbon dioxide in the bitumen phase during storage.

Carbide steel bits have been used by previous researchers for trimming oil sand samples on the belt-driven lathe in the cold room (eg. Dusseault, 1977; Sterne, 1981). Carbide steel tips on the bits were found to be susceptible to rapid abrasion by chilled oil sand. Typically, it was necessary to replace

bits five or six times during the course of trimming a single triaxial core sample from 100 mm diameter to 75 mm. Frictional heating of the carbide bits occurred more rapidly as the bits became dull and the contact area between bit and sample increased. A diamond tipped bit was acquired. The diamond tip was sufficiently resistant to abrasion that sharpening was not required during trimming of 12 triaxial samples. Heat build-up on the continuously sharp point is minimal and sample preparation time was reduced to about 40 minutes, i.e. approximately 10 to 15 per cent of the sample preparation time required using carbide steel tipped bits.

The larger triaxial samples (i.e. 150 mm long) were generally easier to trim in the cold room than were the smaller 25 mm to 50 mm long consolidometer samples. Final diameter of triaxial samples which are intended to fit in a flexible membrane, is less critical than that of consolidometer samples. Great care must be taken to trim the diameter of consolidometer samples to fit precisely in the rigid stainless steel consolidometer ring. Thermal shrinkage of the stainless steel ring due to prechilling in the cold room must also be accounted for in sizing the final sample diameter. Any over-trimming of the consolidometer sample diameter will result in lateral expansion within the stainless steel ring when thawing is permitted.

The strain gauge clamp device used for measuring lateral deformation of triaxial samples is a commonly used device in triaxial apparatus for compression testing of rocks. Accuracy

of the device depends on sufficient rigidity of the clamp arm to ensure intimate contact with the sample prior to and during testing. The device by necessity, therefore transmits small localized compressive stresses at the "metal button" contact points on the outer diameter of the sample. Furthermore, the contact stresses cause small tensile stresses at right angles to the contact radius when the sample is unconfined. The clamp device was found to cause preferential distortion of the oil sand samples and premature yielding when shear stress was applied. This disturbance effect is significant for oil sand since it is a cohesionless material, whereas, many rock materials possess sufficient tensile strength to resist these localized, tensile, diametral stresses. Lateral strain measurements were not perceptibly distorted during isotropic compression. The impact of the disturbance effect on stress-strain behaviour and strength of oil sand is quantified in Chapter 4, subsection 4.4.3.

The "B" test is commonly used in geotechnical testing to determine whether the triaxial apparatus and the pore space of a soil sample is completely saturated with liquid water prior to compression testing. When the compressibility of the mineral grain-skeleton of a soil is substantially greater than the compressibility of the pore water, an increase in total isotropic confining stress will cause a nearly equal increase in pore pressure for conditions of complete saturation with water (Bishop and Henkel, 1962); effective stress therefore remains nearly constant and no compression of the soil skeleton

results. For soils of low compressibility, Bishop (1966) and (1973), showed that effective stress does not remain constant when total isotropic confining stress is changed under undrained conditions. Isotropic compressibility of oil sand is of the same order of magnitude (10^{-6} to 10^{-7} kPa^{-1}) as that of water. Therefore, the pore pressure response is not equivalent to undrained stress change, even under saturated conditions for oil sand. It must be recognized that effective stresses increase and compression of an oil sand sample will result during undrained loading in a standard "B" test. Previous researchers in oil sand geotechnics at the University of Alberta have simply assumed that saturation was complete after applying back pressure for several hours. A procedure suggested by Wissa (1969) was adopted for the current research whereby effective stress is maintained constant. Details of the procedure are outlined in subsection 3.4.

3.3.10 Preparation of Remoulded Samples

Remoulded oil sand samples were tested to investigate microfabric changes and to study the implications of remoulded micro-structure on geotechnical behaviour.

Remoulded oil rich consolidometer samples were prepared by thoroughly mixing oil sand at its natural moisture content inside the consolidometer ring at room temperature. The remoulded sample was then compacted inside the consolidometer ring using a modified Proctor hammer. The mass of the modified

Proctor hammer is 10 lbs. (4.536 kg); the hammer was dropped from a height of 128 inches (457 mm), 50 times for each 25 mm (1 inch) thick layer. The level of compactive effort was more than twice that normally used for soils in the modified Proctor test procedure; every effort was made to recompact samples to undisturbed in situ density. Prior to testing samples were further compressed by "quick loading" in the consolidometer apparatus.

Oil free sand samples were prepared in the consolidometer by means of dry vibratory compaction; maximum vibration level was applied for at least 5 minutes. These samples were also compressed by quick loading in the consolidometer.

Remoulded oil rich triaxial samples were prepared by compacting oil sand at its natural moisture content in a steel split ring container. Compaction was again imparted using a modified Proctor compaction hammer in 25 mm (1 inch) lifts, and 50 blows per lift. The compacted sample and split ring container were then placed in the cold room. After the sample was completely frozen the split ring was removed and the sample mounted in the triaxial cell for testing.

It was found that oil rich remoulded samples could not be recompacted to densities equivalent to that of undisturbed samples. Recompacted dry densities ranged from 1.59 to 1.63 Mg/m^3 (i.e. porosity from 0.42 to 0.38), using the compaction method described above.

Dry oil free samples from which bitumen had been extracted, could be compacted consistently to dry densities of 1.69 to 1.70 Mg/m^3 (i.e. porosity of 0.37 to 0.36) by vibratory compaction. Several oil free samples were compacted to much higher densities by placing and vibrating the sand underwater. This technique is commonly used for preparing sand packs for permeability testing and in other geotechnical testing. Dry densities of approximately 1.80 Mg/m^3 (i.e. porosity of 0.32) were obtained using this technique, however, it was not convenient for preparing test samples since it would have been necessary to place the entire base of the test cell on the vibrating table.

3.4 Saturation of Oil Sand Test Specimens With Water

3.4.1 Rationale for Testing Under Conditions of Complete Saturation

In situ extraction of heavy hydrocarbon resources from oil sand by massive steam injection or combustion techniques has been proposed for deposits at depths exceeding about 250 m. Pore pressures are expected to be in the order of 2MPa or greater. Unsaturated conditions would not be anticipated in situ except at high temperatures approaching 200°C or more. At in situ temperatures, i.e. typically 5° to 10°C, pore fluids in deep oil sand deposits are expected to be liquid with dissolved natural gases.

Despite careful laboratory procedures for saturating test cells and drainage lines by displacing air in the system with water, a small amount of air, i.e. up to about 10 ml which is less than one per cent of the total system fluid volume, was found to be present in the apparatus after mounting each sample. Henry's coefficient of volume solubility of air in water is 0.026 (Fredlund, 1976), which implies that approximately one atmosphere (100 kPa) back pressure is required to dissolve each 2.6 per cent of initial air saturation. Natural hydrocarbon gases dissolve more readily than air in both water and oil (Amyx, Bass and Whiting, 1960). The solution of gas in a liquid may involve both physical and chemical solution processes. Air which is composed of about 60 per cent nitrogen does not undergo significant chemical solution in water or hydrocarbon liquids and is thus less soluble than most hydrocarbon gases (eg. carbon dioxide). It should be noted that although the mass of gas in solution increases with pressure, the relationship is generally not linear as suggested by Henry's Law. A common procedure for increasing the rate of gas sorption in laboratory samples is by applying an elevated back pressure.

For example, Dusseault (1977), applied back pressure of 200 to 300 kPa for periods up to three days. Sterne (1981) applied a back pressure of 1050 kPa for approximately 1.5 hours. Previous laboratory researchers in oil sand geotechnics at the University of Alberta have not conducted "B" tests to evaluate the degree of saturation of samples prior to compression testing.

Entrapped gas bubbles (air, methane, hydrocarbon gases) in the system can significantly influence volume change measurements during drained tests and pore pressure response in undrained tests because of the relatively high compressibility of gases. Despite the high pressure capability of the apparatus used in this research, it was deemed necessary to establish some quantitative evaluation of the degree of saturation achieved.

3.4.2 Influence of Isotropic Compressibility on the B Parameter

Bishop (1966, 1973) developed the following expression for pore pressure response of a saturated porous material to an undrained isotropic stress increment:

$$B = \frac{\Delta u}{\Delta \sigma} = \frac{1}{1 + \eta(\beta_w - \beta_s)/(\beta - \beta_s)} \qquad (3.2)$$

The compressibility of liquid water and oil fluids in the pore space of Athabasca oil sand are almost equal, i.e. $\beta_w = 4.5 \times 10^{-7}$ kPa^{-1} and $\beta_o = 4.1 \times 10^{-7}$ kPa^{-1}, at room temperature. Furthermore, the isotropic compressibility of Athabasca and Cold Lake oil sands is of similar magnitude, i.e. $\beta = 10^{-6}$ to 10^{-7} kPa^{-1}. Consequently, the value of the pore pressure parameter B given by equation 3.2, for saturated oil sand at room temperature may range from about 0.39 to 0.88. The common criterion used to test compressible soil samples for full saturation, i.e. a B value approaching

unity, is clearly not valid for low compressibility oil sand samples.

Black and Lee (1973) developed the following expression for calculating the initial degree of saturation of a sample based on the pore pressure parameter B:

$$S_i = \frac{1 - Z \times (1 - B)}{1 - Z \times Q} \qquad (3.3)$$

where: $Z = \left[\frac{B \Delta\sigma/\eta}{1 - P/(P + \Delta u)}\right]$

$Q = \left[\frac{B \eta \beta_w}{\beta}\right]$

P = absolute pore pressure

In deriving equation 3.3, Black and Lee (1973) assumed that Henry's coefficient, H = 0, since very little time is allowed for gas exsolution during a "B" test. Values of initial saturation calculated using equation 3.3 for seven triaxial samples are summarized in Table 3.4. Oil sand samples were saturated at back pressures of at least 2000 kPa for 20 hours or more throughout the laboratory investigation.

3.4.3 Test Procedures for Evaluating Degree of Saturation of Triaxial Oil Sand Samples

Procedure 1:

TABLE 3.4

Initial Saturation of Oli Sand Samples

TEST	SATURATION PRESSURE (MPa)	TEMPERATURE (°C)	B	STRESS RANGE (MPa)	INITIAL SATURATION SI(%)
TOS1	2	20	0.88	6 - 27	99.99
TOS2	2	20	0.77	6 - 26	99.85
TOS3	2	20	0.84	6 - 27	100.00
TOS4	2	20	0.81	6 - 28	99.99
TOS8	10	200	0.79	12 - 20	99.94
TOS10	10	20	0.77	6 - 14	100.00
TOS11	10	20	0.76	8 - 14	100.00

Typical Properties:

1. At 20°C and 2000 kPa:

   $\beta_w = 4.5 \times 10^{-7}$ kPa^{-1} (ASME Steam Tables, 1979)
   $\beta_o = 4.1 \times 10^{-7}$ kPa^{-1} (Robinson and Sims, 1981)
   $\beta_s = 2.7 \times 10^{-8}$ kPa^{-1} (Clarke, 1960)
   $\beta = 1.4 \times 10^{-6}$ to 5.6×10^{-7} kPa^{-1}

2. At 200°C and 10,000 kPa

   $\beta_w = 8.1 \times 10^{-7}$ kPa^{-1} (ASME Steam Tables, 1979)
   $\beta_o = 8.0 \times 10^{-7}$ kPa^{-1} (Robinson and Sims, 1979)
   $\beta = 1.1 \times 10^{-6}$ to 5.4×10^{-7} kPa^{-1}

The commonly used procedure for evaluation degree of saturation of triaxial soil samples and apparatus is summarized by Bishop and Henkel (1962). The procedure involves closing pore fluid drainage valves, then applying increments of isotropic confining stress (i.e. cell pressure) and measuring undrained pore pressure increase with each increment of confining stress. The ratio of pore pressure increase to confining stress increment (i.e. the B value) for fully saturated, compressible soil samples approaches a value of unity. As noted previously, the value of the B parameter for oil sand samples of lower compressibility may be substantially less than unity (i.e. in the range of 0.39 to 0.88). Nevertheless, degree of saturation may be evaluated using the approach of Black and Lee (1973).

The main disadvantage of using the standard B-test procedure is the fact that effective confining stress increases, thereby precompressing the oil sand microfabric prior to preforming other strength or compression tests. For example, in test, TOS2, isotropic confining stress was increased from 6 to 26 MPa; concurrently the pore pressure increased from 2 to 17.4 MPa. Effective stress on the sample therefore increased from 4 MPa to 8.6 MPa which would typically result in volumetric compression of about 0.25 per cent of initial sample volume. While this level of precompression may be quite acceptable where samples are significantly disturbed during sampling, it must be recognized as a potential source of microfabric disturbance in high quality test specimens.

Procedure 2:

Wissa (1969) described an alternate procedure for evaluating the B parameter and degree of saturation for soils of low compressibility. The method is based on the fact that pore pressure response in fully saturated soils is independent of the magnitude of the back pressure, whereas pore pressure response varies with back pressure in unsaturated soils. The procedure adopted in this program was as follows:

a) With pore pressure fluid drainage prevented, an increment of isotropic confining stress (usually 500 - 750 kPa) was applied and the pore pressure response was measured;

b) Pore fluid drainage valves were then opened and the back pressure increased to restore the initial effective stress level.

c) Steps (a) and (b) were then repeated at the new back pressure level. These incremental B-tests were conducted at about 12 different pressure levels to ensure that the pore pressure response was either constant or decreased slightly.

Effective stress on the sample was never increased by more than about 170 kPa using this procedure.

3.5 One Dimensional Thermal Expansion and Compression Testing

3.5.1 Introduction

A series of tests was performed in the high temperature consolidometer to investigate thermal volumetric expansion and compression behaviour of oil sand. A total of nine (9) tests were conducted including: five undrained thermal expansion tests at various back pressures, two gas exsolution tests and two drained thermal expansion tests. Thermal expansion tests are summarized in Table B-1, Appendix B.

Details of each thermal expansion test are summarized in Appendix B. The test procedure and plots of temperature history, back pressure history and sample height versus time are included in Appendix B for each test. Also, plots of volume expansion with temperature are included in Appendix B.

Table 3.5 is a summary of sample data for the thermal expansion test series. A number of problems were encountered during the first three tests, designated COS1, COS2 and COS3. Samples used in each of these tests were grossly disturbed due to infusion of carbon dioxide gas during the sample preparation, as described in subsection 3.3.9. Initial porosities ranged from 0.42 to 0.51 for these three samples, resulting in significant alteration of the proportions of water and bitumen in the pore space. Water saturation increased by as much as 45 percent after back saturation. Undrained thermal expansion behaviour is primarily dependent upon the porosity and pore fluid properties, therefore these test results cannot

TABLE 3.5

SAMPLE AND TEST DATA FOR THERMAL EXPANSION TESTS

Test No.	Saline Creek Sample No.	Maximum Test Temp. (°C)	Initial Sample Dimensions		Initial Bulk Density (Mg/m³)	Initial Porosity (%)	Initial Degree of Saturation (%)	Water Content (% Dry Mass)		Oil Content (% Dry Mass)		Pore Pressure (MPa)	Effective Confining Stress (MPa)	Grain Size Data			X-Ray Diffraction	Scanning Electron Microscope
			Height (cm)	Diameter (cm)				Initial	Final	Initial	Final			D_{50} (mm)	C_u	Fines Fraction (% <0.074 m)		
CDS1	5	200	2.530	7.620	1.702	46.2	60.2	1.7	14.6	17.9	17.9	2.0	0.5	—	—	—		
CDS2	32	200	2.545	7.615	1.865	42.3	79.5	3.0	8.7	19.0	19.0	2.5	0.5	—	—	—		
CDS3	30	250	2.619	7.610	1.586	50.5	54.5	2.5	20.0	18.5	18.5	0.2-3.7	0.5	—	—	—		
CDS4	38	300	2.540	7.623	2.000	38.4	95.7	4.6	5.6	17.9	17.9	2.0-15.0	0.5	—	—	—		
CDS5	18	300	2.490	7.623	1.994	37.5	90.2	1.6	3.8	18.9	18.9	5.0-17.0	0.5-6.0	—	—	—		
CDS6	10A	300	2.540	7.612	1.968	38.8	89.5	2.5	5.1	18.9	18.9	5.0-15.0	0.5-5.0	—	—	—		
CDS7	10B	300	2.616	7.620	1.990	38.1	92.1	2.5	4.3	18.9	18.9	5.0-15.0	0.5	—	—	—		
CDS8	42	399	2.586	7.620	1.948	40.0	90.7	4.0	6.4	19.0	19.0	0.5-9.1	0.5	—	—	—		
CDS9	41	300	2.400	7.633	2.073	35.0	100.0	6.0	6.0	14.4	14.4	10.0	0.5	0.20	1.4	2.1	✓	✓

be considered representative of confined *in situ* conditions.

Heat was applied in 25°C to 50°C temperature increments during tests COS1 and COS2. Large volume expansion associated with gas exsolution and/or phase change of pore fluids was observed during the tests in the temperature range 150°C to 200°C. Although the back pressure was maintained at 2000 to 2500 kPa and vertical confining stress was maintained slightly higher, the rate of heating was too fast. Local overheating adjacent to cartridge heaters in the consolidometer cell wall probably resulted in substantial temperature gradients within the sample. Subsequent thermal expansion tests at nominal effective confining stress were performed by heating very slowly, i.e. less than about 5°C per half hour. Test COS2 was terminated prematurely due to a system leak. Test COS3 was terminated at 240°C due to a power shut down. Tests COS4 to COS9 were heated to 300°C using sufficiently high quality oil sand samples to provide experimental results representative of *in situ* conditions.

3.5.2 Gas Exsolution Tests

Saline Creek oil sand has been substantially degassed during geologic unloading however, solution gases are present. Srajer and Barron (1978) detected measurable quantities of carbon dioxide, hydrogen sulphide and carbon monoxide gases during construction of the Saline Creek Tunnel. No methane was observed.

A small amount of dissolved air was introduced into the pore fluid phase during saturation of samples in the laboratory.

Gas exsolution tests were performed by increasing temperature very slowly under constant nominal effective confining stress and at a constant pore pressure. Volumetric expansion was monitored as the temperature was increased. Incidence of gas exsolution was identified by the rate of volumetric expansion. Rapid non-monotonic volumetric expansion associated with gas exsolution was reversed by decreasing the temperature slightly (i.e. 1°C or 2°C) until the loading piston re-established contact with the sample. An equilibrium pressure-temperature-volume change "critical point" was thus defined. The pore pressure and confining stress were then increased. Heating was then resumed up to a new gas exsolution temperature.

3.5.3 Undrained Thermal Expansion Tests

Undrained thermal expansion behaviour of oil sand at various pore pressures above gas exsolution pressure was investigated in tests COS4, COS5, COS8 and COS9. Vertical confining stress was maintained just slightly higher (i.e. approximately 50 kPa) than pore pressure to ensure contact was maintained between the loading piston and sample. Pore pressure was maintained constant by allowing thermal expansion under nominal effective confining stress. Undrained thermal expansion behaviour was investigated over the temperature range

22°C to 300°C and for back pressure ranging from 500 kPa to 15000 kPa.

In test COS5, pore pressure response to undrained heating was also investigated by subjecting the sample to an effective vertical confining stress of 6000 kPa, then heating undrained and monitoring pore pressure increase and volumetric expansion until pore pressure was nearly equal to confining stress. The pore pressure response to undrained heating was monitored in this manner over the temperature range 24°C to 50°C and from 150°C to 176°C. Undrained thermal expansion under nominal effective confining stress was monitored over the remainder of the temperature range from 50°C to 150°C and 176°C to 300°C.

3.5.4 Drained Thermal Expansion Tests

Drained thermal expansion behaviour of oil sand was investigated in tests COS6 and COS7. Test COS6 was conducted under constant vertical effective confining stress of 6 MPa. Test COS7 was carried out at nominal vertical effective confining stress. Temperature was increased slowly in both tests to ensure that constant uniform pore pressure was maintained throughout the samples. One dimensional drained volumetric expansion of the sand matrix was measured by the vertical LVDT as heating proceeded up to 300°C; the volume of pore fluid expelled from the samples during drained heating at constant pore pressure was also measured using the volume change device.

Plots of temperature and pressure history as well as sample height versus time are presented in Appendix C, for tests COS6 and COS7. Plots of undrained thermal expansion, volume of fluid expelled and the combined thermal expansion of the fluid plus sand matrix with temperature are also presented in Appendix B.

3.5.5 One Dimensional Drained Compression Tests

Drained compression tests were performed in the consolidometer on samples used for both thermal expansion and permeability testing. After heating to the test temperature, three cycles of compression and unloading were typically applied in each test at temperatures ranging from 20°C to 300°C, and for effective vertical stresses ranging from 2 MPa to as high as 26 MPa.

A summary of one dimensional drained compression tests is presented in Table C-1, Appendix C. Stress-volumetric strain plots for the cyclic compression tests are also presented in Appendix C. The coefficient of one dimensional volume compressibility m_v, is defined as the slope of the tangent to the stress-volumetric strain curves.

3.6 Permeability Testing

3.6.1 Permeability Testing Program

A series of permeability tests on oil sand was performed in the consolidometer test cell. The testing program was designed

to evaluate permeability properties of both remoulded and undisturbed oil sand samples over a range of temperatures from 20°C to 250°C, a range of bitumen (i.e. oil) saturations from 0 to 88 per cent, and at several different effective confining stress levels. Permeability tests are summarized in Table D-1, Appendix D.

Permeability tests essentially involved a water flooding process. Water was circulated through the sample by maintaining a pressure differential between upstream and downstream constant pressure air-actuated pumps. Flow rate was controlled by means of a flow metering valve.

The bitumen in Saline Creek oil sand was found to be immobile at room temperature (i.e. 20°C to 24°C) and small differential pressures (up to 50 kPa). At elevated test temperatures of 100°C, 150°C, 200°C and 250°C, bitumen was displaced from the sample as heated water was circulated. Huygen and Lowry (1983) also observed that Wabascaw bitumen, which has similar properties to Athabasca bitumen, begins to flow under gravitational stresses at tempertures in the range 93°C to 121°C, in scaled model experiments.

Elevated back pressures were maintained during all permeability tests to ensure that air and other gases in the system, remained in solution in the liquid water and oil phases; single phase flow properties for water permeability were measured in room temperature tests and on tests in oil-free sand, while two phase flow properties for oil and

water permeabilities were measured in elevated temperature tests on oil bearing oil sand samples.

Technical problems encountered during testing involved inaccurate measurement of differential pore pressure across the sample, maintenance of constant pressure gradient and maintenance of constant temperatures throughout the system.

Initial tests, CPERM1 and CPERM2, were performed using a pair of 34 MPa pressure transducers, one upstream and a second downstream of the sample. Low pressure differences (in the order of 0.5 to 5 kPa) across the sample could not be measured accurately because of the inherent low range inaccuracy of strain gauge transducers (i.e. errors of approximately $\pm$ 1 per cent or more of the rate capacity are common). This technical difficulty was overcome by installing a pair of differential pressure transducers with interchangeable diaphrams of 7 to 450 kPa rated capacity, to measure differential pressure across the sample.

Tests CPERM1 to CPERM6 were performed with insulated drainage lines, however, no heat tracing was installed. In order to heat the system, uniformly heated water was initially circulated rapidly through the lines, by-passing the sample. When uniform temperatures were monitored throughout the system, flow rates were reduced and the test started by placing the sample on-line. It was found, however, that stable system temperatures could only be maintained by using flow rates

greater than about 5 ml per minute. This was not a severe limitation, however, the installation of heat tracing greatly improved the flexibility and ease of testing in subsequent experiments.

Pump pressures declined by up to about 3 per cent of ambient pressure each time the pump diaphrams were activated without an accumulator on line. These fluctuations were damped out to some degree by compressible fluids in the system, nevertheless, small fluctuations in pressure drop across the sample did result. The small deviations in pressure drop were accounted for by taking frequent electronic readings and using statistical techniques to determine the average pressure difference during a number of larger segments of the total test duration. Installation of pressure accumulators improved the pressure control. Installation of dead weight constant pressure generators is recommended for future testing to further reduce this technical difficulty.

The testing program was designed to measure effective permeabilities of oil sand samples to water and oil. The general test procedure used was as follows: (i) measurement of room temperature effective permeability to water; (ii) drained heating of the sample and system to an elevated test temperature; (iii) measurement of fluid mobility and effective permeability as heated water was circulated through the sample; (iv) cooldown of the sample and system to room temperature and (v) remeasurement of room temperature effective permeability to water at a residual bitumen saturation.

Data describing permeability test samples are summarized in Table 3.6. Procedural details and test results for nine permeability tests are presented in Appendix D.

3.6.2 Permeability Tests on Oil Free Sand

Two permeability tests were performed on oil free oil sand samples. Test CPERM3 was performed on a remoulded and recompacted oil free sample of McMurray Formation oil sand taken from an outcrop on the High Hill River 40 km east of Fort McMurray. The recompacted dry density of the sample was 1.67 Mg/m^3 (i.e. initial porosity of 0.37). Effective permeability to water (or hydraulic conductivity) was measured only at room temperature for this sample. Laminar flow was observed for flow rates up to approximately 10 ml per minute (i.e. approximately 7.5 pore volumes per hour), and for effective vertical confining stresses of 2 MPa, 3 MPa and 4MPa as shown in Figure D-5. Room temperature effective permeability to water was in the range 3×10^{-12} m^2 (i.e. 3000 millidarcys) for this sample. This is equivalent to hydraulic conductivity of 3×10^{-3} cm/s which is typical for fine to medium clean sand; this provided some confidence in our pressure measuring capabilities since larger pressure drops were anticipated for oil rich samples.

Test CPERM7 was a permeability test on undisturbed oil free sand. An oil rich, undisturbed sample was prepared and mounted in the consolidometer ring by the standard procedures outlined

TABLE 3.6

SAMPLE AND TEST DATA FOR PERMEABILITY TESTS

Test No.	Saline Creek Sample No.	Maximum Test Temp. (°C)	Initial Sample Dimensions		Initial Bulk Density (Mg/m³)	Initial Porosity (%)	Initial Degree of Saturation (%)	Water Content (% Dry Mass)		Oil Content (% Dry Mass)		Pore Pressure (MPa)	Effective Confining Stress (MPa)	Grain Size Data			X-Ray Diffraction	Scanning Electron Microscope
			Height (cm)	Diameter (cm)				Initial	Final	Initial	Final			D_{50} (mm)	C_u	Fines Fraction (% <0.074 mm)		
OPERM1	10C	20	4.877	7.620	2.046	36.4	99.99	2.5	2.7	18.9	18.9	10.0	4.0	—	—	—		
OPERM2	10D	50	4.877	7.620	2.047	36.4	99.99	2.7	2.7	18.9	18.9	10.0	2.0-4.0	—	—	—		
OPERM3	M1	20	5.920	7.610	2.040	37.0	—	22.3	22.3	0.0	[illegible]	10.0	2.0-4.0	—	—	—		
OPERM4	36A	100	5.684	7.628	2.026	37.1	96.6	3.0	3.9	18.5	15.4	10.0	2.0-4.0	0.19	2.0	3.0		
OPERM5	31A	200	5.570	7.633	2.045	36.6	100.0	3.0	9.6	18.8	10.1	10.0	2.0-4.0	0.20	1.9	2.4	✓	
OPERM6	31B	250	5.540	7.633	2.033	36.1	94.3	4.0	11.6	16.1	7.0	10.0	2.0-4.0	0.20	1.9	2.4	✓	✓
OPERM7	44	150	5.120	7.600	2.02	35.5	98.1	3.2	20.0	17.1	0.3	10.0	2.0-18.0	—	—	—		
OPERM8	16	150	5.121	7.600	2.058	32.7	100.0	2.2	—	16.7	—	10.0	3.0	—	—	—		
OPERM9	36B	150	5.400	7.585	1.906	40.0	79.3	1.5	—	18.5	—	10.0	3.0	0.19	2.0	3.0		

in subsection 3.3.6. The sample was permitted to thaw under sufficient confining stress in the consolidometer to prevent volume expansion (i.e. 2 MPa). The consolidometer test cell was then flooded with liquid benzene to solvent extract bitumen from the sample. A cyclic procedure of alternate soaking and flushing was repeated numerous times over a ten day period until it was determined that all bitumen had been removed from the sample. The total volume of liquid benzene required to extract all of the bitumen from the sample by this procedure was 3600 ml or about 45 equivalent pore volumes. Confining stress and sample height (i.e. volume) were monitored throughout this process to ensure that the mineral grain structure remained undisturbed. After the extraction was completed the sample pore space was flushed with 200 ml of acetone, air dried, then back-saturated with water for 24 hours. Effective permeability to water was then measured at various flow rates and at several effective vertical confining stresses ranging from 2 MPa to 18 MPa. The sample and apparatus were heated under drained conditions to 150°C; the sample was then cooled due to a system leak and reheated to 150°C. Drained thermal expansion versus temperature is shown in Figure D15. Volume of fluid expelled during heating is plotted in Figure D16. Effective permeability to water at 150°C was again measured at constant stresses ranging from 2 MPa to 18 MPa. Flow velocity versus pressure gradient is plotted in Figure D17 for both room temperature and 150°C tests. Volumetric compression over the stress range 2 - 18 MPa at 150°C is plotted in Figure D18. Finally, the sample and

apparatus were cooled back down to room temperature and permeability measurements repeated.

Test CPERM7 was conducted with the objective of measuring the absolute (intrinsic) permeability of undisturbed oil sand and to determine the influence of heating and stress variations on absolute permeability.

3.6.3 Permeability Tests on Oil Rich Samples

A single test, CPERM9, was conducted on remoulded oil rich oil sand. The sample was remoulded and recompacted to an initial bulk density of 2.019 Mg/m^3 and an initial porosity of 0.383. Room temperature effective permeability to water was measured with an effective vertical confining stress of 3 MPa. The sample was subsequently heated to 150°C and heated water was circulated through the sample; fluid mobility and effective permeability were measured as bitumen saturation decreased from 80 per cent to a residual value of 52 per cent. The sample was subsequently recooled to room temperature (20°C) and the effective permeability to water remeasured at 52 per cent oil saturation.

Six permeability tests: CPERM1, CPERM2, CPERM4, CPERM5, CPERM6 and CPERM8 were performed on high quality undisturbed oil rich oil sand samples. As discussed in subsection 3.6.1, test data from tests CPERM1 and CPERM2 could not be interpreted because of inaccuracy of the pressure measuring system and

concomitant pump pressure fluctuations which were not fully transmitted to the sample. Figure D1 and D3 indicate that continuous uniform flow was passing through the sample, controlled by the flow metering valve. However, figures D2 and D4 are records of the measured pressures. It is clear that pressure differences could not be determined. A pair of differential pressure transducers of suitable sensitivity (i.e. 0 to 140 kPa pressure range) and accuracy were subsequently installed to measure pressure drop across the sample.

Initial bitumen saturations ranged from 81 to 88 per cent for all undisturbed oil rich samples. Room temperature effective water permeability was measured for all samples both at the initial bitumen saturation and after flushing some bitumen from samples at elevated temperatures. Elevated temperature tests were performed at 100°C, 150°C, 200°C and 250°C. Fluid mobility for combined flow of water and bitumen was monitored during each test as bitumen was displaced from the sample. End point oil saturations were measured by toluene extraction in a soxhlet extraction apparatus. Effective permeabilities were thus determined at various oil saturations and temperatures. Fluid saturations were measured separately for various sections of each permeability sample after testing at elevated temperature to determine whether preferred flow was occurring adjacent to the consolidometer ring. Summaries of water and bitumen saturations for each sample are presented in Appendix D. Although slightly more bitumen was generally displaced from the upper portion of the sample, no preferred flow paths were detected through the cross-section of the sample.

Flow rates through oil rich samples were generally maintained at approximately seven pore volumes per hour, or less. Plots of flow velocity versus pressure gradient in Appendix D indicate that Darcy's Law is valid for all room temperature tests, i.e. velocity versus pressure gradient yields as linear plot indicating Newtonian fluid flow behaviour for water flow only. However, bitumen apparently does not behave as a Newtonain fluid. Plots of fluid mobility (i.e. the ratio of absolute permeability to dynamic viscosity) versus flow volume at elevated temperatures are presented in Appendix D for tests CPERM4, CPERM5, CPERM6, CPERM8 and CPERM9. Values of fluid mobility corresponding to end point oil saturations and temperatures in these tests, were predicted using published dynamic viscosity values for Athabasca bitumen. In all cases, predicted values of fluid mobility are greater than the experimental values, particularly at the start of flow. The non-Newtonian fluid behaviour of heavy oils and bitumens in porous media is a topic of active research in both Petroleum and Chemical Engineering. The pattern of bitumen flow is often described as "viscous fingering" during immiscible displacement by water. Absolute permeability may also be lower than experimentally determined because of the presence of fines (i.e. clay and silt particles) in oil rich samples which are removed along with bitumen in solvent extraction processes.

3.7 Triaxial Testing

3.7.1 The Triaxial Testing Program

Triaxial compression tests were performed to measure

stress-strain behaviour and strength properties of oil sand over a range of temperatures from 20°C to 200°C and effective confining stresses to 8 MPa. Six triaxial stress paths were investigated typical of a range of anticipated in situ loading conditions. Stress paths investigated are shown in Figure 3.10. Triaxial tests were performed on both undisturbed and remoulded oil sand samples. A total of nineteen triaxial tests were conducted. In addition, a single unconfined compression test was performed on Saline Creek oil sand following unsaturated heating at 150°C. Sample and test data for the triaxial tests are summarized in Table 3.7. A summary of the types of triaxial tests performed is presented in Table E-1, Appendix E. Procedural details and test results for each of the nineteen triaxial tests and the unconfined test are presented in Appendix E.

Four of the nineteen triaxial tests were not successful due either to failure of rubber O-ring pressure seals or due to degradation and leakage of silicone rubber-jacket membranes at elevated temperatures. Rubber O-ring seals and membranes are most often the "weak links" in pressurized geotechnical testing systems. Elevated temperature further reduced the durability of these materials in the presence of both oil and water. As discussed in subsection 3.1.8, extended exposure of silicone rubber to silicone oil cell fluid at temperatures exceeding 200°C resulted in swelling, softening and ultimately depolymerization of the silicone rubber.

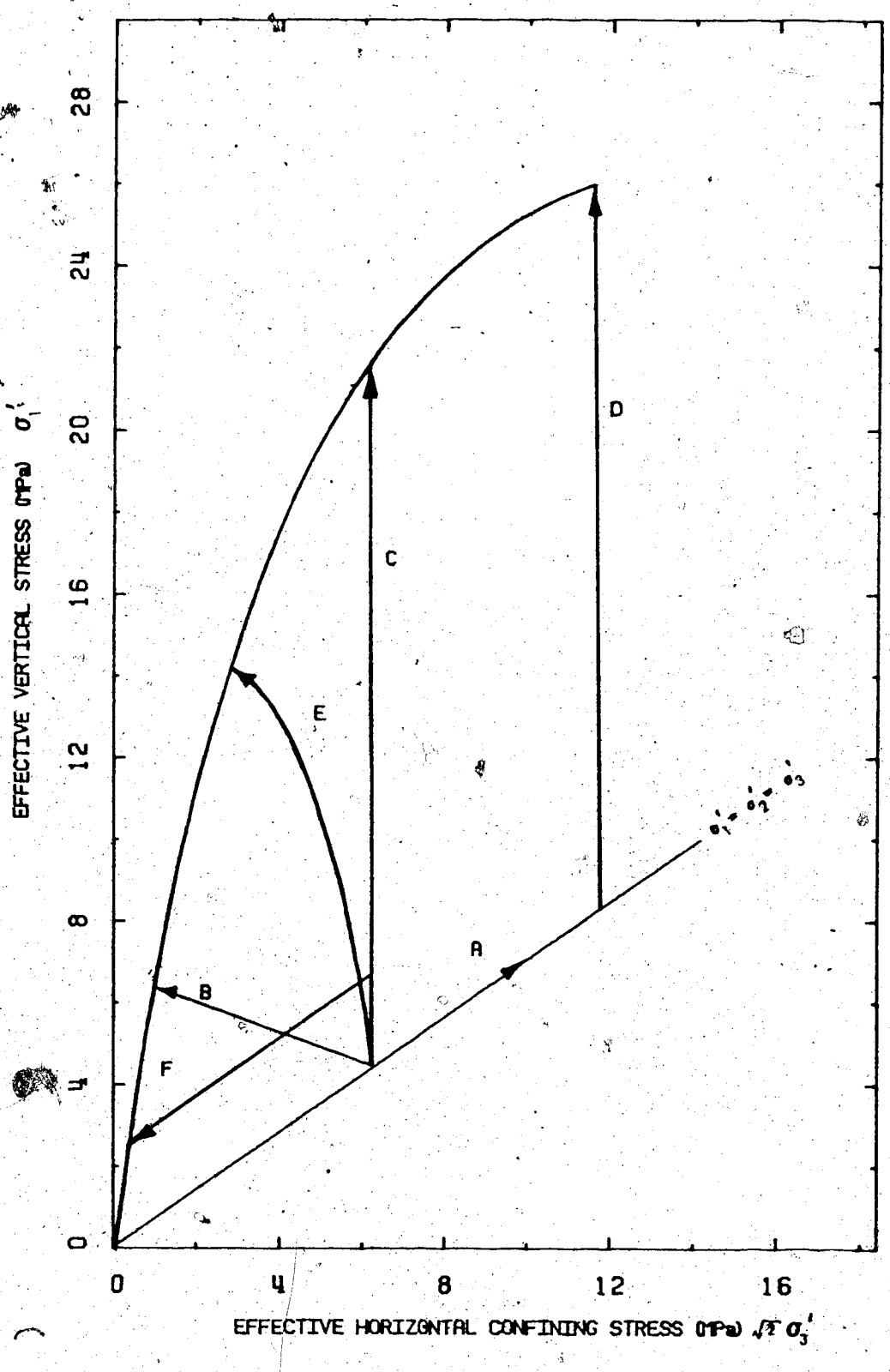

FIGURE 3.10 Stress Paths Investigated

TABLE 3.7

SAMPLE AND TEST DATA FOR TRIAXIAL TESTING

Test No.	Saline Creek Sample No.	Maximum Test Temp. (°C)	Initial Sample Dimensions		Initial Bulk Density (Mg/m³)	Initial Porosity (%)	Initial Degree of Saturation (%)	Water Content (% Dry Mass)		Oil Content (% Dry Mass)		Pore Pressure (MPa)	Effective Confining Stress (MPa)	Grain Size Data			X-Ray Diffraction	Scanning Electron Microscope
			Height (cm)	Diameter (cm)				Initial	Final	Initial	Final			D_{50} (mm)	C_u	Fines Fraction (% <0.074 mm)		
TOS1	25	20	15.316	7.604	2.088	33.3	99.98	3.0	3.7	15.2	15.2	2.0	4.0	0.17	2.2	5.4		
TOS2	33	20	15.240	7.600	2.077	34.0	99.96	2.5	3.2	16.3	16.3	2.0	4.0	0.17	2.1	4.0		
TOS3	43	20	15.408	7.600	2.082	35.1	100.0	3.0	3.0	18.0	18.0	0.0-2.0	0.9-4.0	0.17	2.3	6.5		
TOS4	44	20	15.100	7.597	2.013	36.9	97.0	3.2	4.4	17.1	17.1	2.0	8.0	0.18	2.0	1.8		
TOS5	17	20	15.300	7.590	2.050	35.7	95.5	3.5	4.9	16.8	16.8	2.0	8.0	0.19	1.8	3.7		
TOS6	16	125	15.107	7.600	2.120	32.7	100.0	2.2	2.2	16.7	16.7	10.0-12.0	0.6-4.0	0.19	2.0	0.5		
TOS7	45	125	15.430	7.610	2.023	35.4	90.0	2.2	7.7	16.0	16.0	10.0	4.0	0.19	2.0	2.1		
TOS8*	28	220	15.293	7.433	2.046	35.4	100.0	2.5	2.4	17.0	17.2	10.0	12.0-20.0	—	—	—		
TOS9*	27	240	15.110	7.610	2.079	33.7	95.4	1.2	3.6	17.1	17.1	10.0-14.5	0.0-4.5	—	—	—		
TOS10	20	200	15.170	7.610	2.076	34.9	100.0	2.6	2.6	17.8	17.8	10.0-12.0	4.0	0.18	2.4	6.3	✓	
TOS11	22	100	15.300	7.570	2.064	35.6	100.0	2.5	2.5	18.5	18.5	10.0-14.0	0.4-4.0	0.19	2.0	6.0		
TOS12	29	200	14.837	7.510	2.092	34.1	100.0	1.0	1.3	18.8	18.8	10.0	4.0-17.0	0.18	2.4	5.2		
TOS13*	26	240	15.300	7.620	2.080	32.8	100.0	3.6	3.6	13.2	13.2	10.0	4.0	—	—	—		
TOS14	5,7,8	20	15.238	7.576	1.850	41.8	92.2	1.7	8.4	18.7	18.7	2.0	2.0,4.0, 8.0	0.18	2.4	5.9		✓
TOS15	Cold Lk. SPL. No. 128	200	15.000	7.500	1.965	38.3	92.3	5.6	12.2	14.6	14.6	10.0	4.0	0.40	6.7	12.0	✓	✓
TOS16*	Saline Ck. 13	200	15.235	7.603	2.053	35.8	98.4	2.4	4.7	18.3	18.3	10.0	4.0	—	—	—		
TOS17	23	200	15.042	7.650	2.054	35.9	100.0	2.0	3.7	19.0	19.0	10.3	7.6	0.15	2.4	8.2	✓	✓
TOS18	24	200	15.143	7.590	2.080	33.4	95.2	3.5	7.8	14.5	14.5	10.0	0.6-4.0	0.19	2.0	2.6		
TOS19	19	125	15.055	7.500	2.084	33.4	96.3	2.1	4.8	16.2	16.2	10.0	4.0	0.19	1.7	2.8	✓	✓

*Tests terminated prematurely due to membrane failure or fluid leaked past O-ring seals.

Triaxial tests consequently were not performed successfully above 200°C.

3.7.2 Drained Triaxial Tests

Consolidated drained triaxial tests were performed to investigate strength and stress-strain behaviour at temperatures of 20°C, 125°C and 200°C, and following several stress paths. Stress paths A,B,C, and D shown in Figure 3.10 were investigated by drained compression testing.

Frozen oil sand samples were mounted in the triaxial cell, then thawed, back-saturated and consolidated, all under a constant isotropic effective confining stress (i.e. usually 4 MPa or occasionally 8 MPa). B-tests were performed as described in section 3.4 for tests TOS1, TOS2, TOS3, TOS4, TOS8, TOS10 and TOS11 to evaluate the degree of saturation attained in oil sand samples. In test TOS1 and TOS8 internal strain gauge deformation measurements permitted determination of undrained volume change and compressibility from B-tests. The sample and test cell were heated at very slow rates, typically less than 0.5°C per minute, to the test temperature under fully drained conditions, i.e. maintaining constant back pressure.

Drained isotropic compressibility, i.e. following stress path A, was determined in tests TOS1, TOS8, TOS12 and TOS19 for high quality undisturbed Saline Creek oil sand samples, and in

test TOS15 for a Cold Lake oil sand sample. Drained isotropic compressibility for a moderatley disturbed Cold Lake oil sand sample was also measured at 200°C in Test TOS 15. Three or four cycles of compression and unloading were applied over a range of effective confining stress from 4 MPa to 25 MPa during each of the isotropic compression tests.

Stress path B approximates a J1 constant stress path (i.e. J1 is the first stress invariant). Stress path B is applicable to stress changes in material adjacent to a shaft or deep tunnel during excavation. Stress path B was applied in Test TOS3, TOS6, and TOS18 at temperatures of 20°C, 125°C and 200°C, respectively.

Stress path C is a passive compression stress path; vertical effective stress, σ_1', was increased with the effective confining stress, σ_3', maintained constant at 4 MPa. Back pressure is maintained constant as shear stresses are applied in drained testing. Stress path C was investigated in tests TOS1, TOS2, TOS7, TOS12 and TOS19 for Saline Creek oil sand at temperature from 20°C to 200°C. Stress path C, i.e. passive triaxial compression at 4 MPa effective confining stress, was also followed for a Cold Lake oil sand sample in Test TOS15 at a temperture of 200°C.

Stress path D is a passive compression stress path, but with effective triaxial confining stress, σ_3', maintained constant at 8 MPa during vertical loading. Stress path D was

investigated in tests TOS4, TOS5 and TOS17 at temperatures of 20°C and 200°C for Saline Creek oil sand.

3.7.3 Drained Multistage Compression of Remoulded Oil Sand

A multistage loading test, test TOS14, was performed on a remoulded sample of Saline Creek oil sand in order to determine remoulded strength at several effective confining stress levels from a single test. A sample of oil sand was remoulded and recompacted to as high a density as possible using a Modified Proctor compaction hammer. The compacted sample was then frozen and mounted in the triaxial cell in the standard manner, and subsequently thawed, back saturated and consolidated under 2 MPa effective confining stress. The sample was then subjected to passive compression by increasing the vertical stress, σ_1', while maintaining the effective triaxial confining stress σ_3', constant at 2 MPa. As the deviator stress, $\sigma_1' - \sigma_3'$, reached a peak value, the effective confining stress, σ_3', was increased to 4 MPa. Passive compression was continued until a second peak deviator stress level was reached, then the effective confining stress was again increased to 8 MPa. Passive compression was continued and a third peak deviator stress defined by shearing the sample. Back pressure was maintained constant at 2 MPa throughout the three stages of passive compression. The temperatures of both the sample and the test cell were maintained constant at 20°C (i.e. room temperature) throughout the test.

3.7.4 Undrained Heating with Isotropic Effective Confining Stress Maintained Constant

The compressibility of the pore fluids in oil sand is an important parameter in numerical analyses of fluid flow. Compressibility of water, bitumen and gases is known to vary with temperature and pressure. A limited amount of published data exists for compressibility of solvent extracted Athabasca bitumen (i.e. Robinson and Sim, 1981); also extensive steam table data exists for pure distilled water (eg. ASME, 1977).

A test was designed to measure compressibility of the pore fluids in a high quality undisturbed triaxial specimen of Saline Creek oil sand. Test TOS10 was conducted as follows: a trimmed, frozen oil sand specimen was mounted in the triaxial cell, then thawed, back-saturated and consolidated under a constant isotropic effective confining stress of 2 MPa. Drainage valves were then closed and the sample was heated very slowly (i.e. at a heating rate of approximately 6°C per hour); the isotropic confining stress was increased concurrent with pore pressure build-up in order to maintain the effective confining stress on the sample nearly constant. By maintaining effective confining stress constant, no volume change or pore pressure changes result from compression of the mineral grain matrix. Pore pressure increase and volumetric strains result only from thermal expansion and pore pressure compression of the pore fluids (bitumen and water) and the individual mineral grains. Pore pressure and vertical axial deformation were

monitored as undrained heating proceeded. Lateral deformation of the sample was not measured during heating, since it was discovered that the lateral strain gauge clamp device imparted point stress concentrations to the sample. Future researchers may be able to overcome this problem by using temperature resistant LVDT's mounted inside the triaxial cell to measure lateral deformation or dilatometers to measure undrained volume expansion of the sample.

The condition of constant effective confining stress results in a very rapid build-up of pore pressure during heating (i.e. as much as 1 MPa per °C). The pressure limits of the triaxial cell and back pressure system were therefore reached with a temperature increase of between 25°C and 30°C, depending on the initial pore pressure. The undrained heating experiment was therefore conducted in eight heating cycles with temperature increments of between 20°C to 30°C. At the end of each heating cycle, the back pressure drainage valves were opened, and the confining stress and back pressure were decreased simultaneously in order to maintain a constant isotropic effective confining stress of 4 MPa on the sample. Volume change was measured at the end of each heating cycle by placing the external volume change device on line with the sample when pressures were being decreased.

After cyclic undrained heating to 200°C, the sample was subjected to undrained triaxial compression following stress path E shown in Figure 3.10. Starting with an effective

confining stress of 4 MPa, the back pressure drainage valve was closed and the vertical stress increased to a peak value corresponding with shear failure. Pore pressure response was also monitored during shearing.

3.7.5 Anisotropic Consolidation and Undrained Heating to Failure

Stress path F shown in Figure 3.10 was followed in test TOS11. A high quality undisturbed sample of Saline Creek oil sand was mounted in the triaxial cell, thawed, back saturated, and consolidated under an isotropic effective confining stress of 4 MPa. The vertical effective stress, σ_1', was then increased to 6 MPa and the sample was allowed to consolidate under a horizontal to vertical effective stress ratio, K_o, of 0.67. Drainage valves were then closed to prevent further drainage of pore fluid from the sample. The apparatus and sample were then heated very slowly, i.e. at approximately 6°C per hour. Total horizontal and vertical applied stresses were maintained constant during undrained heating; pore pressure and vertical deformation were monitored. Shear failure occurred as the sample temperature reached 100°C (i.e. heated from 20°C to 100°C) and the effective confining stress, σ_3', approached zero. Note that the deviator stress $\sigma_1' - \sigma_3'$, was maintained constant at 2 MPa throughout the test. Stress path F is considered to be illustrative of the mechanism by which shear deformations may extend in situ during steam injection and/or rapid heating.

3.7.6 Thermal Expansion Results for Triaxial Samples

No triaxial tests were performed with the specific intention of measuring thermal expansion behaviour of oil sand. However, thermal expansion measurements are reported in Appendix E for elevated temperature tests.

Volume change and vertical deformations were monitored during heating primarily as a means of controlling the rate of heating. Volumetric expansion reported for elevated temperature tests represents the volume of pore fluid expelled from the samples during heating, and not the total volumetric expansion of the sample. Lateral (horizontal) deformation of triaxial samples was not measured during heating because the lateral strain gauge clamp device was found to preferentially apply point loads at the outer perimeter of the sample during triaxial compression tests. It should be noted that the lateral strain gauge device performed very satisfactorily during compliance testing on a cylindrical aluminium block. However, lateral deformation measurements in tests TOS1 and TOS8 were found not to be reliable because of point loadings by the relatively stiff strain gauge clamp on the more deformable, cohesionless oil sand. Vertical (axial) deformation was monitored, however, drained volumetric thermal expansion of triaxial samples during heating could not be determined without some independent measurement of lateral deformation (e.g. dilatometer).

Temperature resistant linear voltage displacement

transducers (LVDT's) are currently available for temperatures up to 600°C. Dilatometer devices or LVDT's may be useful for measuring lateral deformations in future triaxial testing with this system without the problems inherent in a strain gauge clamp device.

3.8 Index Testing

3.8.1 Bitumen and Water Contents

Quantities of bitumen and water occupying the pore space in oil sand samples were determined using soxhlet refluxing. The laboratory procedure may be summarized as follows:

(a) An intact chunk of oil sand having a mass of approximately 200 - 400 g was placed in a cylindrical filter bag (or "thimble"). The mass of the sample was determined.

(b) The filter bag and sample were then placed inside the soxhlet extraction apparatus which consists of a closed system of glass chambers over a retort of solvent. Toluene was used as the solvent.

(c) The toluene was heated causing it to vapourize. Water in the sample also vapourized as the system was heated above 100°C. Toluene and water vapours were trapped in an upper cooling chamber which was cooled by continuously circulating tap water through an internal coil of glass tubing. Condensed toluene and water would then drip down into an accessory tube graduated

to measure the volume of water expelled from the sample. Toluene collected in the accessory tube was displaced by water (i.e. toluene has a lower density than water) through an overflow tube back into the main chamber containing the oil sand sample. As the main chamber filled with overflow toluene, the sample was soaked with toluene and bitumen was dissolved. When the liquid level in the main chamber reached a particular level, all of the toluene, dissolved bitumen and free water were drained back into the retort through an inverted U-tube siphon. Toluene and water were then reheated, vapourized and condensed, and the entire process repeated.

(d) The main chamber containing the oil sand sample was allowed to refill and drain repeatedly until the toluene was clear, indicating that all the bitumen had been extracted from sample. Some water would generally still remain in the system (i.e. either in the sample, in the retort or on the condenser) at this point in time, so the heating and condensing process was continued at least until the water level in the accessory tube had stabilized. Bitumen extraction was normally completed in about 6 - 8 hours, however the toluene was always circulated for a full 24 hours to ensure complete recovery of all of the pore water.

(e) The extracted oil sand sample and filter bag were removed from the apparatus and oven dried at 110°C to remove any residual toluene from the mineral grains and filter paper.

(f) The mass of the mineral solids was then determined by weighing the extracted sample and filter bag.

(g) The bitumen content was determined knowing the mass of solids and volume (or mass) of water.

Several special procedural considerations are worthy of note for future researchers. Correct determination of bitumen and water contents by soxhlet refluxing is very sensitive to accurate measurement of the water content. When sequential extractions are being carried out, it is important to ensure that the glass chambers and tubing are completely free of water and/or water vapour from the previous sample or from the atmosphere. This may be accomplished by circulating (i.e. heating and condensing) toluene through the system for one or two hours before placing a sample inside the apparatus. It is also important that all glass tube insert connections in the system be sealed with vacuum grease to prevent water vapour from entering or escaping the system. The thimble or filter bag should be oven-dried just prior to obtaining a tare mass and placing it in the extractor to remove any atmospheric water or water vapour from the filter paper. Toluene in the retort flask should be replaced frequently (i.e. about every third test). Cotton batting and water indicator pellets in the pressure vent at the top of the condenser should also be changed frequently (i.e. after about every third test).

Bitumen and water contents for all oil sand samples tested are summarized in Tables 3.5, 3.6 and 3.7 as a percent of the

dry mass (i.e. the mass of the solid mineral grains). Natural water contents of Saline Creek oil sand varied from 1.2 to 6.0%. Bitumen contents for the Saline Creek oil sand samples ranged from 13.2 to 19.0% of the mass of the mineral solids (i.e. 11.3 to 15.6% of the total mass of oil sand).

3.8.2 Density, Porosity and Fluid Saturations

Bulk density of 100 mm diameter frozen oil sand core samples was initially determined by the "wax, dip and weigh" technique. Frozen core samples were weighed, coated in paraffin wax, reweighed, dipped in water and the volume of water displaced was then measured. The mass and density (and therefore volume) of paraffin wax were known, thus allowing reasonably precise determination of the density of the frozen oil sand core.

Density of finished 76 mm diameter test samples was determined after sample preparation in the cold room by weighing and direct volume measurement. The diameter and height of finished cylindrical samples was determined by making multiple precise caliper measurements.

Dry density and porosity of the samples may be determined if the bulk density, water content, bitumen content and density of the mineral solids are known. A density of 2.65 Mg/m^3 was assumed for oil sand mineral solids which are primarily quartzose sand grains. Bitumen and water were both assumed to

have densities of 1.00 Mg/m^3 at room temperature and atmospheric pressure in determining pore fluid saturations.

Density, porosity and fluid saturations for core and test samples are summarized in Table 3.8.

Bulk densities of undisturbed core samples ranged from 2.02 to 2.10 Mg/m^3; corresponding porosities ranged from 0.33 to 0.37. Finished test samples no. 5, 32 and 30 used in Tests COS1, COS2 and COS3, respectively, were severely disturbed; these were the first three test samples prepared and as described in subsection 3.3.9, the samples were exposed to high concentrations of gaseous carbon dioxide. Bulk densities of the remaining test samples ranged from 1.95 to 2.12 Mg/m^3 with corresponding porosities ranging from 0.33 to 0.38.

The Saline Creek oil sand samples typically had bitumen saturations exceeding 80% and water saturation of less than 20% of the pore volume.

A single Cold Lake oil sand core sample was also tested. The Cold Lake sample was moderately disturbed; the bulk density of the test sample was 1.965 Mg/m^3 and the porosity was 0.383. Water and oil saturations were 25.6% and 66.7%, respectively.

3.8.3 Grain Size Distribution Analyses

A series of tests to determine grain size distributions of

TABLE 5.8

Density, Porosity and Fluid Saturation of Oil Sand Core Samples

Sample No.	Water Content (%)	Bitumen Content (%)	CORE SAMPLE				TEST SAMPLE			Comments
			γ (Mg/m^3)	η	Sw (%)	S_B (%)	γ (Mg/m^3)	η	Sw (%)	S_B (%)	
5	1.7	17.9	2.033	0.358	8.1	84.9	1.702	0.462	5.2	55.0	Disturbed
32	3.0	19.0	2.083	0.356	8.8	91.2	1.865	0.423	10.8	68.6	Disturbed
30	2.5	18.5	2.078	0.352	9.7	90.3	1.586	0.505	6.5	48.0	Disturbed
38	4.6	17.9	2.053	0.368	18.4	81.6	2.000	0.384	19.6	76.1	
18	1.6	18.9	2.080	0.349	6.9	93.6	1.994	0.375	7.0	83.3	
10	2.5	18.9	2.066	0.358	10.1	89.9	1.968	0.388	10.4	78.9	
42	4.0	19.0	2.046	0.372	15.1	84.9	1.948	0.400	15.7	74.8	
41	6.0	14.4	2.062	0.354	29.0	69.7	2.073	0.350	29.2	70.8	
36	3.0	18.5	2.086	0.352	9.8	90.2	2.026	0.371	13.5	83.2	
31	3.0	18.8	2.063	0.361	11.9	88.2	2.045	0.366	13.9	86.1	
44	3.2	17.1	2.016	0.368	14.6	78.0	2.013	0.369	14.5	77.6	
16	2.2	16.7	2.089	0.337	11.5	87.1	2.120	0.327	9.0	91.0	
25	3.0	15.2	2.084	0.335	15.8	80.1	2.088	0.333	15.9	80.5	
33	2.5	16.3	2.077	0.340	12.8	83.8	2.077	0.340	12.8	83.8	
43	3.0	18.0	2.026	0.368	13.6	81.9	2.082	0.351	11.7	88.3	
17	3.5	16.8	2.054	0.356	16.8	80.6	2.050	0.357	16.7	80.2	
45	2.2	16.0	2.042	0.348	10.9	79.4	2.023	0.354	10.6	77.3	
28	2.5	17.0	2.070	0.346	12.5	85.0	2.046	0.354	12.1	82.2	
27	1.2	17.1	2.068	0.340	6.2	87.5	2.079	0.336	6.3	88.9	
20	2.6	17.8	2.081	0.348	11.5	88.5	2.076	0.349	12.1	87.9	
22	2.5	18.5	2.072	0.354	10.5	89.5	2.064	0.356	11.4	88.6	
29	1.0	18.8	2.095	0.340	5.1	94.9	2.092	0.341	5.1	94.9	
26	3.6	13.2	2.077	0.329	19.5	71.4	2.080	0.328	19.5	71.7	
13	2.4	18.3	2.074	0.352	10.6	89.4	2.053	0.358	11.4	86.9	
23	2.0	19.0	2.045	0.362	9.3	88.6	2.054	0.359	9.4	89.7	
24	3.5	14.5	2.080	0.335	18.4	76.3	2.080	0.335	18.4	76.3	
19	2.1	16.2	2.086	0.335	11.1	85.4	2.084	0.335	11.5	85.5	

oil sand samples was performed before and after compression testing at elevated stresses and temperatures in the consolidometer and triaxial cell. The aim of the grain size analyses was to detect any mineral grain crushing due to high stresses and temperatures.

Mechanical sieve analyses were performed following the procedure outlined by the American Society for Testing and Materials in testing standard ASTM D422-72. Hydrometer analyses were also performed where applicable, on portions of samples having effective particle diameters smaller than 0.074 mm. The procedure for hydrometer analysis, also outlined in testing standard ASTM D422-72, was followed.

Bitumen was extracted from the oil sand samples by soxhlet refluxing with toluene prior to conducting grain size analyses. It should be noted that a small portion of the fine silt and clay size particles were absorbed by the filter bag during this process.

Data from the grain size analyses are summarized in Table 3.9. Grain size distribution curves for 20 test samples are included in Appendix F; grain size distributions before and after compression testing are included for 12 of the test samples.

The grain size analyses indicate that some crushing of mineral grains did occur at elevated temperature and stress

TABLE 3.9

Summary of Data From Grain Size Analyses

Sample No.	Test No.	Maximum Temperature (°C)	Maximum Effective Stress (MPa)	GRAIN SIZE (% FINER THAN) D_{10} (mm)	D_{50} (mm)	D_{60} (mm)	Uniformity Coefficient Cu	FINES CONTENT (%<0.074 mm) BEFORE	AFTER
41	COS9	300	18.0	0.16	0.20	0.22	1.4	2.1	2.2
36A	CPERM4	100	26.0	0.10	0.19	0.20	2.0	3.0	4.0
31A	CPERM5	200	19.5	0.11	0.20	0.21	2.0	2.5	2.8
31B	CPERM5	250	19.0	0.11	0.20	0.21	1.9	2.4	2.9
36B	CPERM9	150	3.0	0.10	0.19	0.20	2.0	4.5	4.6
25	TOS1	20	25.0	0.085	0.17	0.19	2.2	5.0	5.4
33	TOS2	20	21.0	0.09	0.17	0.19	2.1	4.0	-
43	TOS3	20	6.0	0.08	0.17	0.18	2.3	6.5	-
44	TOS4	20	21.5	0.095	0.18	0.19	2.0	1.8	-
17	TOS5	20	26.1	0.11	0.19	0.20	1.8	3.7	-
16	TOS6	125	6.7	0.10	0.19	0.20	2.0	0.5	-
45	TOS7	125	17.0	0.10	0.19	0.20	2.0	2.1	-
20	TOS10	200	13.5	0.08	0.18	0.19	2.4	4.2	6.3
22	TOS11	100	6.0	0.10	0.19	0.20	2.0	2.6	-
29	TOS12	200	19.0	0.08	0.18	0.19	2.4	5.2	6.7
5,7,8	TOS14	20	18.8	0.08	0.18	0.19	2.4	5.1	5.9
23	TOS17	200	24.9	0.07	0.15	0.17	2.4	7.2	8.2
24	TOS18	200	7.0	0.10	0.19	0.20	2.0	[illegible]	5.8
19	TOS19	125	21.5	0.12	0.19	0.20	1.7	[illegible]	-
Cold Lake 12B	TOS15	200	17.0	0.06	[illegible]	0.40	6.7	10.8	12.8

levels. However, the degree of alteration of the grain size distribution curves for Saline Creek oil sand is minimal even at stresses up to 25 MPa and temperatures up to 300°C. The grain size distribution of the single Cold Lake Oil sand test sample was altered more dramatically when subjected to effective confining stresses up to 17 MPa at 200°C. The mineral grains of oil sand from the Clearwater Formation at Cold Lake include substantial proportions of feldspar and volcanic clasts as well as quartz. The micaceous minerals are less resistant to shearing than quartz as evidenced by these grain size analyses.

Viscosity of Athabasca Bitumen

The dynamic viscosity of Athabasca bitumen was measured in a series of plate viscometer tests to illustrate the influence of unsaturated heating, i.e. "thermal aging", on bitumen viscosity. The test procedure followed is outlined in the American Society for Testing and Materials specification ASTM D3570-77, Procedure B.

A sample of Athabasca bitumen was extracted from an oil sand sample by soxhlet refluxing. The sample was then subjected to the following cycles of heating and testing:

1. The bitumen sample was heated at 135°C and atmospheric pressure in an oven for 24 hours. The bitumen was then mounted in a plate viscometer apparatus which was

subsequently submerged in a constant temperature water bath at 25°C. After temperatures had stabilized the plates were subjected to a range of shear displacement rates to determine dynamic viscosity of the bitumen.

2. The same bitumen sample was again heated in an oven for 24 hours at 150°C. A 25°C plate viscometer experiment was conducted.
3. The bitumen sample was heated a third time in the oven for 24 hours at 175°C. A third plate viscometer experiment was performed in the 25°C constant temperature bath.

Results of the three plate viscometer experiments are tabulated in Appendix I. Shear displacement rate versus shearing stress is plotted for each of the three experiments in Figure 3.11.

The dynamic viscosity of the bitumen decreased dramatically with time of heating and temperature. Dynamic viscosities corresponding to the three tests plotted in Figure 3.11 are:

a) 20×10^6 mPa.s after heating for 24 hours at 135°C;
b) 70×10^6 mPa.s after heating for a further 24 hours at 150°C; and
c) 450×10^6 mPa.s after heating for a further 24 hours at 175°C.

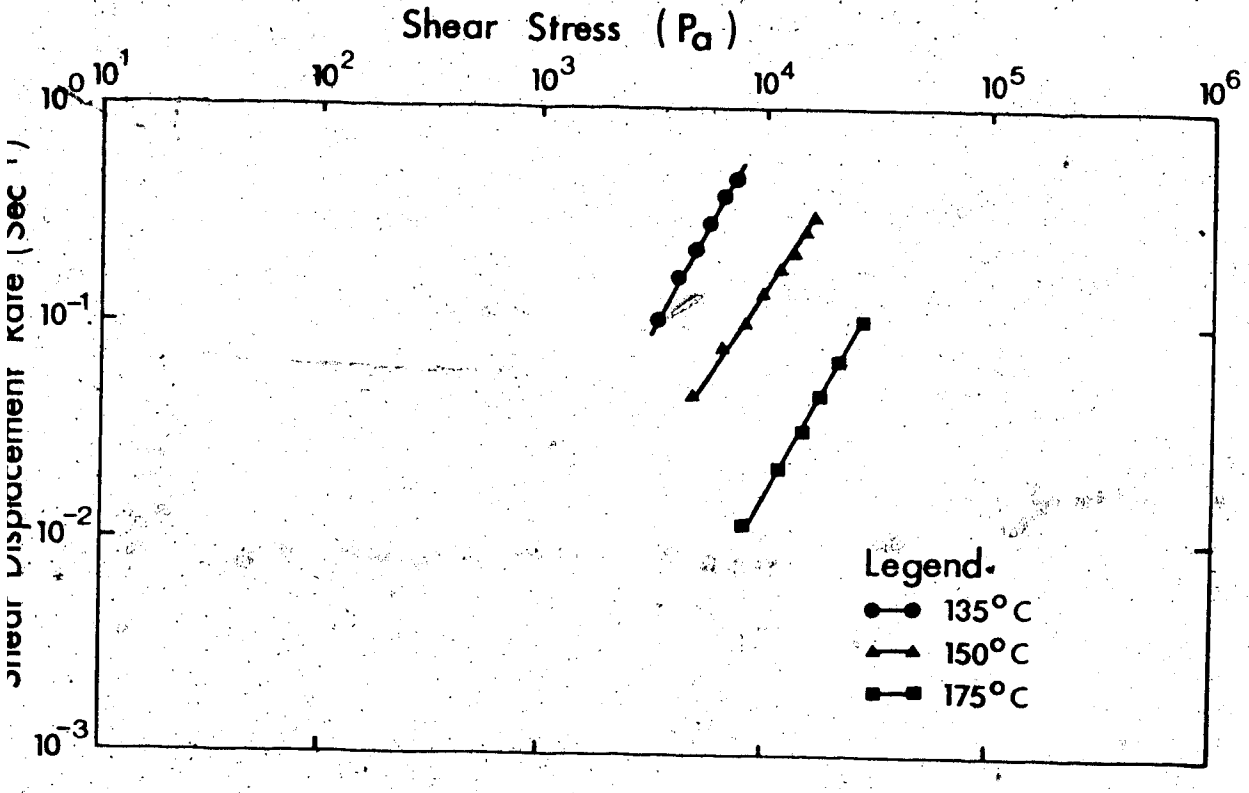

FIGURE 3.11 Viscosity Changes in Athabasca Bitumen Due to Thermal Aging

These plate viscometer test results illustrate that while heating is generally favourable for oil recovery, sustained heating unsaturated, i.e. at low pressures, may, in fact, cause "case hardening" of the bitumen. The geotechncial implications of "thermal aging" of bitumen are described in section 4.4.2 of Chapter 4.

3.9 Oil Sand Microfabric and Mineralogy Studies

3.9.1 Textural and Mineralogic Alteration at Elevated Temperature and Pressures

The University of Calgary Sedimentology Research Group (1981) have reported observed textural changes and mineralogic alterations in Cold Lake oil sand following high temperature steam injection. Injection of steam at temperatures up to 250°C was observed to cause mineral reactions which resulted in the formation of smectite minerals (<2 μm) from kaolinite and feldspar. Implications of textural changes due to grain crushing or smectite growth include reduction of total porosity and absolute permeability.

Scanning electron microscope study and X-ray diffraction analyses were conducted with the aim of identifying mineralogic or textural alterations resulting from compression and permeability testing of oil sand at elevated temperatures and stresses. The study was also useful in comparing the microfabric of intact and remoulded oil sand.

3.9.2 Scanning Electron Microscope Study

Mineral grain fabric and texture of seventeen oil sand specimens were studied and photographed by scanning electron microscope methods. Six samples were studied using a Cambridge Stereoscan (Model S-4) scanning electron microscope and the remaining eleven samples were studied using a Cambridge Stereoscan 100 model. Both models have similar capabilities.

Intact specimens of oil rich oil sand were carefully cut from larger samples using a sharp knife. Specimens were mounted on metallic stubs with heads 7.5 mm in diameter, using low-resistance contact cement. The mounted specimens were then placed in a vacuum dessicater jar for several hours to remove gaseous hydrocarbon components from the bitumen phase. Before viewing, specimens were coated in vacuo with a layer of carbon and two layers of gold, each approximately 50 to 75 Å thick. The gold coating provides conductive communication over the specimen surface and the metallic stub. Coated specimens were set up on a mounting frame inside the scanning electron microscope vacuum chamber. Up to 8 specimens may be placed on the mounting frame simultaneously for sequential viewing. Rotational, translational and tipping controls are provided on the mounting frame. An electron beam initiated by excitation voltages of 20 to 25 kV caused secondary electron emission from the coated specimens. Enhanced magnified images were viewed directly on a cathode ray screen and occasionally photographed on black and white film negatives.

A summary of specimens studied and photographed in the scanning electron microscope is listed in Table 3.10. Scanning electron microphotograph plates for these oil sand specimens are included with individual descriptive captions in Appendix G. Plates 3.1 to 3.6 inclusive show typical examples of microfabric and grain texture for both intact and remoulded oil sand samples from Saline Creek and Cold Lake. It is of interest to note that when oil sand is remoulded, the interpenetrative microstructure, characteristic of undisturbed oil sand in situ, is lost. Intact mineral grain arrangements for Saline Creek oil sand are shown in Plates 3.1, 3.2 and 3.3. A remoulded oil free sample (solvent extracted) is shown in Plate 3.4. Quartz sand grains with unclassified flucculated clay minerals adhering to their surfaces have lost their interpenetrative microstructural arrangement and are in "tangent-to-tangent" contact. By contrast, an oil rich remoulded oil sand sample is shown in Plate 3.5. Remoulding [redacted]gorous recompaction interestingly has not disrupted all individual grain contacts but has segregated clusters (or peds) of sand grains and bitumen. Plate 3.6 shows intact microfabric of a Cold Lake oil sand specimen. Sand grain size, shape and arrangement appear to be very similar to that of Saline Creek oil sand. The lower dynamic viscosity of Cold Lake bitumen is apparent since there is less smear than for oil rich Saline Creek specimens.

The scanning electron microscope is interfaced with a microprocessor and CRT screen for processing and plotting X-ray

TABLE 3.10

Scanning Electron Microscope Specimens

Sample No.	Test No.	Sample Description	Plate Nos.
SP1	-	Oven dried (110°C) sample from the Suncor minesite near Fort McMurray.	G1-G4
M1	CPERM3	Oil free McMurray oil sand from an outcrop on the High Hill River 40 km east of Fort McMurray.	G5-G6
33	-	Solvent extracted oil free Saline Creek oil sand.	G7 and 3.4
36	-	Intact Saline Creek oil sand.	G8-G11 and 3.1
36A	CPERM4	Saline Creek oil sand after removal of 10 per cent of the bitumen in a 100°C permeability test.	G12-G15
31B	CPERM6	Saline Creek oil sand after removal of 50 per cent of the bitumen in a 250°C permeability test.	G16 and 3.2
		Clay particles in sample 31B after 250°C permeability test.	G17-G18
10A	COS6	Saline Creek oil sand after 300°C drained thermal expansion and compression to 6 MPa effective confining stress.	G19-G20
5,7,8	TOS14	Remoulded Saline Creek oil sand after room temperature triaxial compression at 8 MPa effective confining stress.	G21 and 3.5
23	TOS17	Saline Creek oil sand sample after 200°C triaxial compression at 8 MPa effective confining stress.	G22-G23
24	TOS18	Saline Creek oil sand after 200°C triaxial compression at 4.0 to 0.6 MPa effective confining stress.	G24-G25
19	TOS19	Saline Creek oil sand sample after 125°C triaxial compression at 4 MPa effective confining stress.	G26 and 3.3
Cold Lake 12B	TOS15	Cold Lake oil sand sample after 200°C triaxial compression test at 4 MPa effective confining stress.	G27 and 3.6

PLATE 3.1 Intact fabric of oil-rich Saline Creek oil sand.

PLATE 3.2 Saline Creek oil sand fabric after removal of 50 percent of the bitumen during a 250°C permeability experiment.

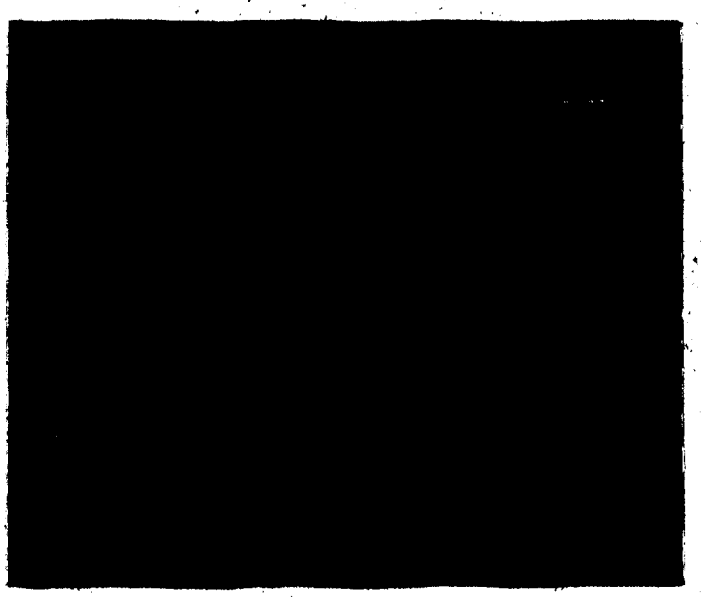

PLATE 3.3 Saline Creek oil sand after triaxial compression under 4 MPa effective confining stress and 125°C.

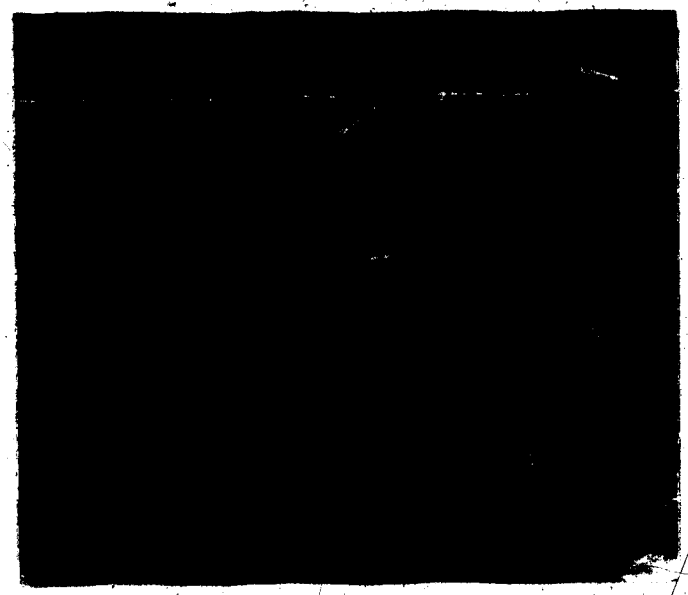

PLATE 3.4 Oil free Saline Creek sand following solvent extraction.

PLATE 3.5 Remoulded Saline Creek oil sand fabric (note clusters or peds of "oil-bonded" sand grains).

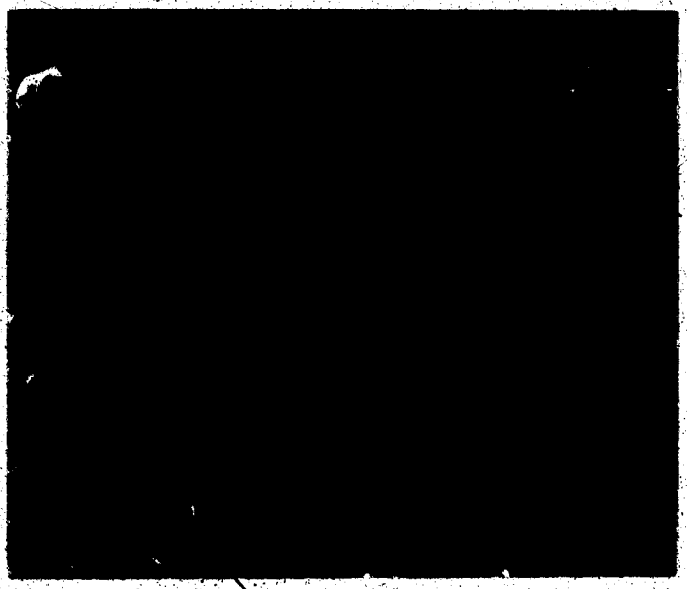

PLATE 3.6 Cold Lake oil sand fabric after triaxial compression under 4 MPa effective confining stress and at 200°C.

diffraction angles. The microprocessor has been programmed to identify minerals in the specimen on the basis of characteristic X-ray diffraction peaks. X-ray diffraction analyses were performed for one McMurray Formation sample, a Saline Creek sample and a Cold Lake sample. Plates 3.7 to 3.9 are photographs of X-ray diffraction peaks which were displayed on the CRT screen for these samples. Minerals in the McMurray and Saline Creek samples are predominantly silica (quartz). Traces of aluminium and nickel were also detected in the Saline Creek sample. Dominant minerals in the Cold Lake sample included both aluminium and silica with traces of potassium, calcium and iron. It should be noted that the peaks labelled AU in Plates 3.7 to 3.9 indicate the presence of artifically applied gold coatings on the samples.

3.9.3 X-Ray Diffraction Analyses

A series of X-ray diffraction analyses were performed and interpreted by staff of the Alberta Research Council with the aim of identifying any mineralogic alterations of Saline Creek samples tested at elevated temperatures and stresses.

Portions of samples not subjected to elevated temperature and stress conditions were analyzed for comparison with post test samples. Bitumen was first removed from the samples by soxhlet refluxing with toluene. Samples were then fractioned into coarse (>2 μm) and fine (<2 μm) fractions before X-ray analysis. The fractionating was performed in a centrifuge.

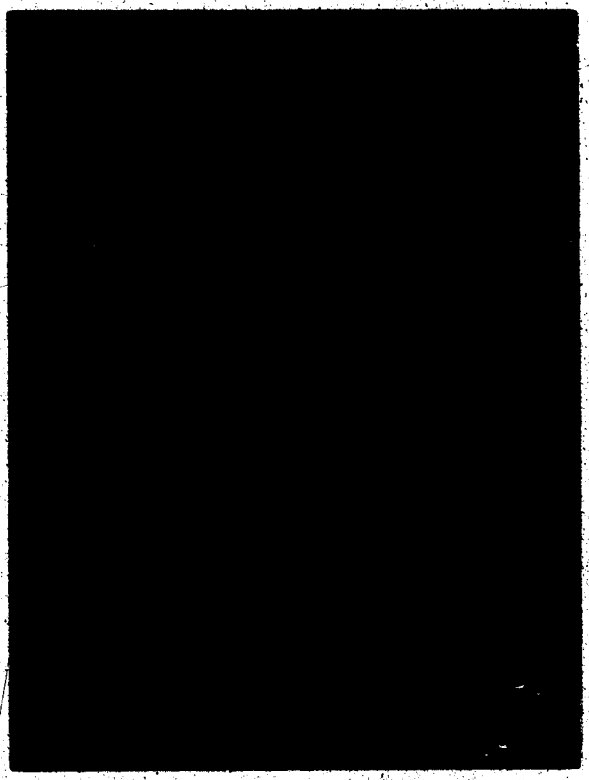

PLATE 3.7 X-ray diffraction angles for oil-free McMurray Formation sand (predominantly silica).

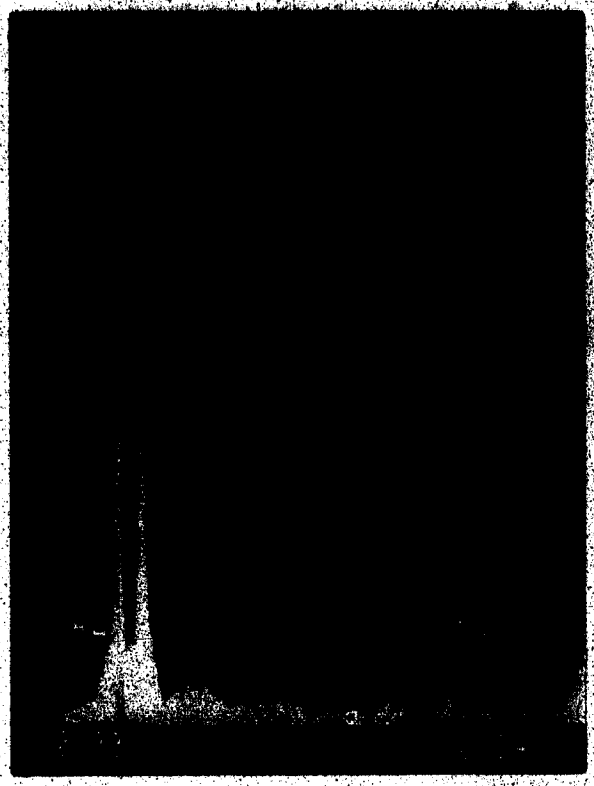

PLATE 3.8

X-ray diffraction angles for oil-rich Saline Creek oil sand. (Silica, Aluminium and Nickel peaks dominant).

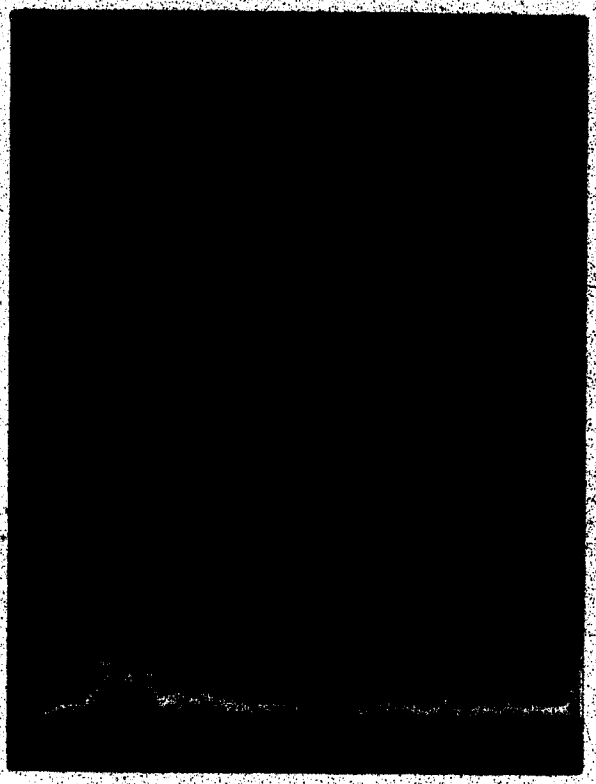

PLATE 3.9

X-ray diffraction angles for oil-rich Cold Lake oil sand. (Aluminium, Silica, Potassium, Calcium, Iron and Nickel peaks).

The coarse fractions of samples were ground into a fine powder and mounted on glass slides; fine fractions were wetted and smeared directly onto the glass slides.

X-ray diffraction traces for both coarse and fine fractions of the seven samples analyzed are presented in Appendix H. Results of the X-ray diffraction analyses are summarized in Table 3.11. No significant mineral alterations were detected for either the coarse or fine fractions of these samples. A small amount of the fine fraction of sample 41 (i.e. approximately 5%) was apparently converted from illite to montmorillonite under test temperatures up to 300°C. This is not considered to be of great practical significance since the fine fraction comprises less than 5% by mass of the total sample. This finding is, nevertheless, of academic interest.

3.10 Summary

This chapter describes testing equipment and procedures for determining geotechnical behaviour of oil sands at elevated temperatures and pressures. No attempt has been made to analyze or explain the engineering significance of test results.

The chapter includes:

(a) a detailed description of various components of the laboratory testing facility;

(b) compliance testing requirements, procedures and test results

TABLE 3.11

Summary of X-Ray Diffraction Analyses

Sample No.	Test	Maximum Temperature (°C)	Maximum Effective Stress (MPa)	Sample Fraction	MINERAL COMPONENTS	
					Before Testing	After Testing
20	TOS10	200	5.0	Coarse (>2μm)	Quartz, Feldspar, traces of pyrite (FeS_2) and brookite (TiO_2).	Quartz, Feldspar, traces of pyrite and brookite.
				Fine (<2μm)	Kaolinite - 80% Illite - 20%, trace quartz.	Kaolinite - 80% Illite - 20% trace quartz.
31A	CPER45	200	19.5	Coarse (>2μm)	Quartz, traces of pyrite and brookite.	Quartz, Feldspar, traces of pyrite and brookite.
				Fine (<2μm)	Kaolinite - 70% Illite - 30%.	Kaolinite - 80% Illite - 20%.
31B	CPER46	250	19.0	Coarse (>2μm)	Quartz, trace of pyrite and brookite.	Quartz, Feldspar, traces of pyrite and brookite.
				Fine (<2μm)	Kaolinite - 70% Illite - 30%.	Kaolinite - 75% Illite - 25%.
41	COS9	300	18.0	Coarse (>2μm)	Quartz, trace of pyrite (FeS_2).	Quartz, trace of pyrite (FeS_2).
				Fine (<2μm)	Kaolinite - 80% Illite - 20%.	Kaolinite - 80% Illite - 15% Montmorillonite - 5%.

(c) a description of sampling techniques and sample preparation procedures for obtaining high quality undisturbed oil sand samples;

(d) summaries of tests and testing procedures for thermal expansion and compression, permeability and triaxial testing;

(e) rationale and procedures for supplementary index tests, i.e. grain size, density, fluid saturations and bitumen viscosity measurement; and

(f) rationale and procedures for microfabric and mineralogy studies using scanning electron microscopy and X-ray diffraction analyses.

Many facets of the testing program involved development of testing procedures and techniques. A particular effort has been made to outline problems and suggested improvements for future research.

4.0 DISCUSSION OF EXPERIMENTAL RESULTS

4.1 Thermal Expansion

4.1.1 Thermal Expansion Parameters

Volumetric deformations resulting from temperature changes influence both stress and strain fields in-situ. In the theory of thermoelasticity linear thermal strain is given by:

$$\epsilon = -\alpha_L \Delta T \tag{4.1}$$

and the [illegible]ive stress required to suppress thermal strain in one dimension is given by:

$$\sigma = -\alpha_L E \Delta T \tag{4.2}$$

The coefficient of linear thermal expansion, α_L, is therefore required to determine thermal strains and stresses.

In a porous, multiphase geologic material such as oil sand the magnitude of α_L depends on whether fluid phases are mobile, i.e. whether or not mass transport occurs. A thermal stress analysis must therefore be coupled with both heat transfer and fluid flow analyses in order to correctly assess the magnitude of thermal stresses and strains. An upper bound for the magnitude of thermal expansion can be determined by conducting undrained heating experiments in which pore fluid drainage is prevented. The magnitude of undrained thermal expansion depends upon volumetric expansion of both the matrix of mineral solids and the pore fluids. The lower bound value

of the volumetric thermal expansion may be determined in drained heating experiments in which a constant pore pressure is maintained by heating sufficiently slowly to permit excess fluid pressures to dissipate by mass transport (i.e. fluid flow) out of the sample. The lower bound magnitude of drained thermal expansion depends only on volumetric expansion of the immobile solid phase. The volume of pore fluid expelled from a laboratory sample during drained heating is equivalent to the difference between undrained and drained volumetric thermal expansions at common pore pressure and effective stress.

The case of transient (time dependent) heating and transient drainage may result in a condition of partial drainage (i.e. partial dissipation of excess fluid pressure), depending upon the relative rates of heating and fluid pressure dissipation. For the case of partial drainage the magnitude of thermal expansion will include drained thermal expansion of the solid matrix plus a fraction of the difference between fully drained and undrained thermal expansions. Partially drained thermal volumetric expansion may be expressed by:

$$\left(\frac{\Delta V}{V}\right)_T = \left[\alpha_{DR} + f(\alpha_u - \alpha_{DR})\right]\Delta T \qquad (4.3)$$

where f is a fraction depending on the amount of pore fluid drainage at a given time.

It is clear then, that at least two coefficients of thermal expansion, α_u and α_{DR}, are required to evaluate thermal

stresses and strains for porous multiphase geologic materials. The appropriate value of α_L to be used in equations 4.1 and 4.2 must be expressed in terms of the parameters α_u, α_{DR} and f for transient drainage conditions.

As discussed in Chapter 2, Section 2.3, Campanella and Mitchell (1972) expressed drained and undrained thermal expansion in terms of thermal expansion and compressibility of the individual components of soils, i.e. mineral solids, pore fluids and the mineral grain matrix. Agar et al. (1983) and Kosar (1983) have extended the Campanella and Mitchell expressions to oil sand. These more fundamental expressions will be used in describing various features of the experimental results.

4.1.2 Drained Thermal Expansion

Drained thermal expansion of Saline Creek oil sand was measured in tests COS6 and COS7 at effective confining stresses of 6 MPa and 0.05 MPa respectively. Volumetric thermal expansion is plotted as a percentage of the original sample volume for these tests in Figure 4.1. The cubical volumetric expansion of an alpha quartz crystal (i.e. a sand grain) is also plotted for comparison. The pore pressure was maintained constant at 5 MPa up to 200°C, then increased and maintained at 15 MPa to 300°C in both tests. Several interesting observations concerning drained thermal expansion behaviour of oil sand may be derived from these test results:

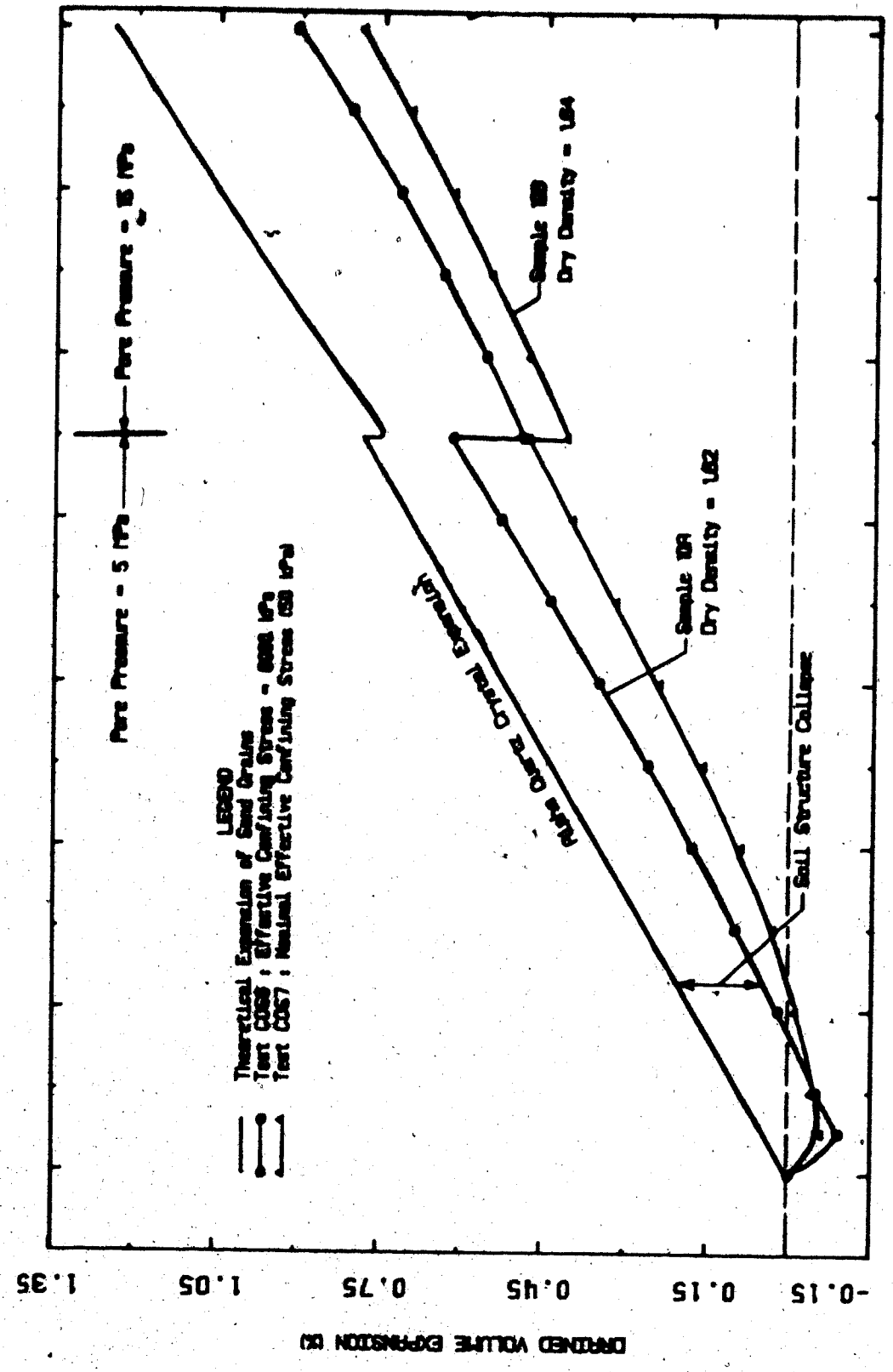

FIGURE 4.1 Drained Thermal Expansion of Saline Creek Oil Sand

a) There was a small volume decrease of both samples during the initial stage of heating. This may be attributed to rearrangement of the mineral grain structure as a consequence of decreased shearing strength of individual interparticle contacts combined with the development of thermally induced shear stresses as a result of lateral constraint in the consolidometer ring. This partial collapse of the grain structure enables the sand to carry the same vertical effective stress at a higher temperature. Campanella and Mitchell (1972) identified a similar but more dramatic phenomenon for illite clay samples. Kosar (1983) tested remoulded sand samples at various initial densities and found that the magnitude of the structural collapse was dependent upon initial density, i.e. the collapse component of volume change was larger for samples of lower dry density.

b) Subsequent volumetric thermal expansion after the initial grain structure collapse is almost parallel to the thermal expansion of individual sand grains for both tests.

c) The sample subjected to 6 MPa effective confining stress expanded more than the sample subjected to a nominal effective confining stress of about 50 kPa. This is probably due to higher interparticle shearing resistance at the higher effective stress level.

d) Further structural collapse was observed at 200°C in conjunction with cubical compression of the sand grains

when the pore pressure was increased from 5 MPa to 15 MPa despite the fact that effective confining stress was maintained constant. Also the sample under the higher 6 MPa effective confining stress collapsed slightly more at this stage than the sample under nominal effective stress.

While observed volume decreases due to structural collapse are of interest, the magnitude of this component of volume change is not considered to be of practical significance for dense oil sands in situ.

Drained thermal expansion was also measured in tests CPERM4, CPERM5, CPERM6, CPERM7, CPERM8 and CPERM9, at effective confining stresses of 2, 3 and 4 MPa. Thermal expansion plots for these tests are included in Appendix D. Drained thermal expansion behaviour observed in these tests was similar to the trends observed in Figure 4.1. The rate of heating was increased for tests CPERM4, CPERM5 and CPERM6 resulting in slightly more erratic thermal expansion behaviour; this is due to the fact that pore pressure within the samples tended to build up and fluctuate at the increased heating rates.

Figure 4.2 is a plot of pore volume changes with temperature for Saline Creek oil sand under constant effective confining stress. This plot was synthesized from results of several drained thermal expansion tests. The magnitude of pore volume change depends upon initial porosity and effective

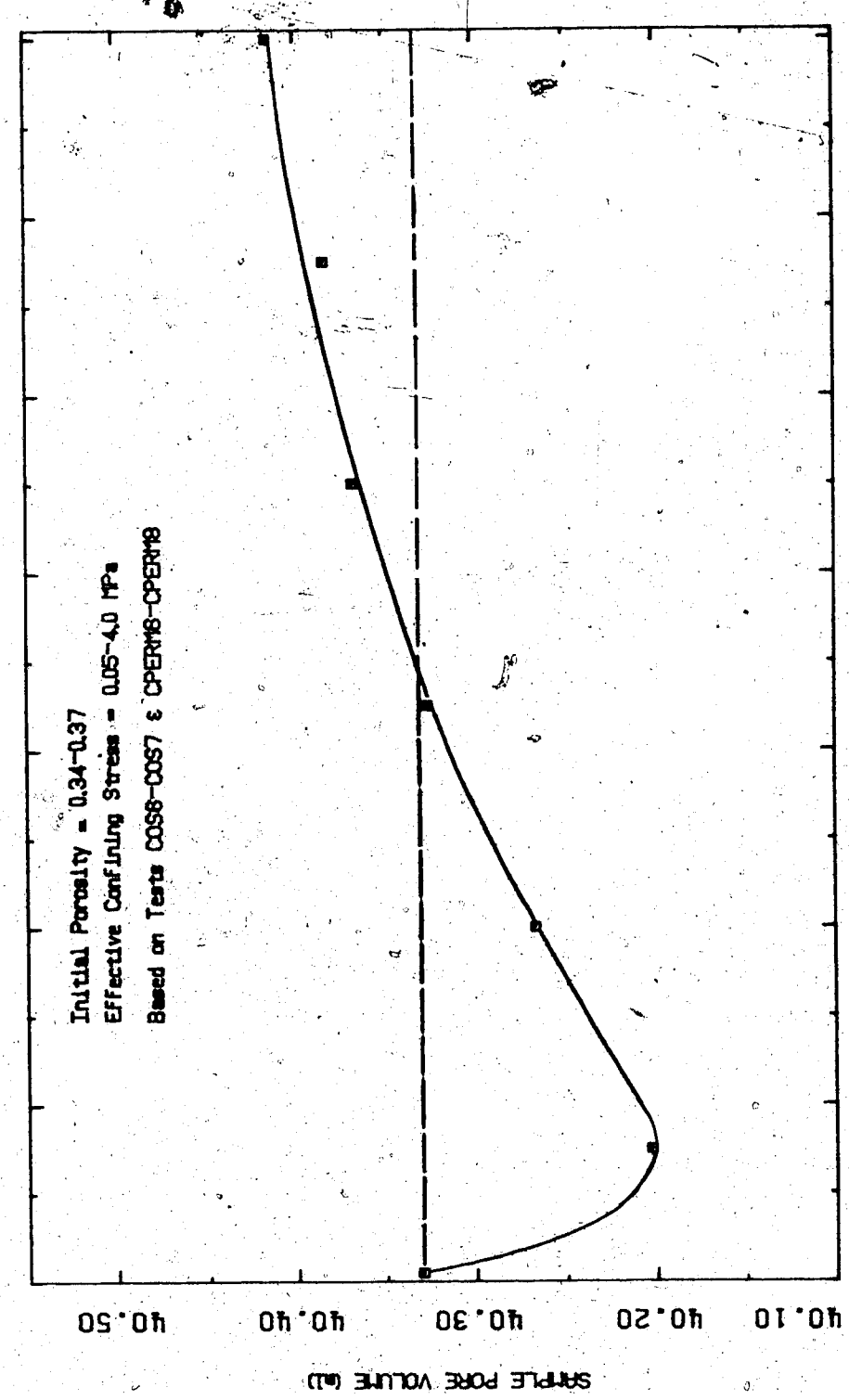

FIGURE 4.2 Pore Volume Changes with Temperature

stress. The commonly used parameters, porosity and void ratio, vary both as a result of pore volume changes and total volume changes during heating. For this reason it is considered more convenient to determine pore volume changes with temperature directly. Pore volume changes shown in Figure 4.2 are replotted in Figure 4.3 as percent of initial total volume at room temperature. Pore volume decreases initially due to partial grain structure collapse then increases. The magnitude of pore volume change is small, i.e. ± 0.1 percent.

Figure 4.4 is a plot of coefficient of cumulative drained thermal expansion, α_{DR}, with temperature for Saline Creek oil sand under constant effective confining stress.

It was not possible to accurately measure drained volumetric thermal expansion in the triaxial cell during this study because of incompatibility between the lateral deformation measuring device and oil sand. As discussed in Chapter 3, the lateral strain gauge-clamp device introduced diametral tensile stresses at right angles to the point contacts with the sample, which in turn caused significant distortion of lateral deformations. Strain gauge clamps are often used successfully for testing rocks however, since oil sand does not have any true tensile strength it cannot resist even the very small tensile stresses introduced by such a device. An alternative device for measuring volume change of triaxial samples is a dilatometer which measures volume changes of the cell fluid in a triaxial cell. Volume of pore fluids

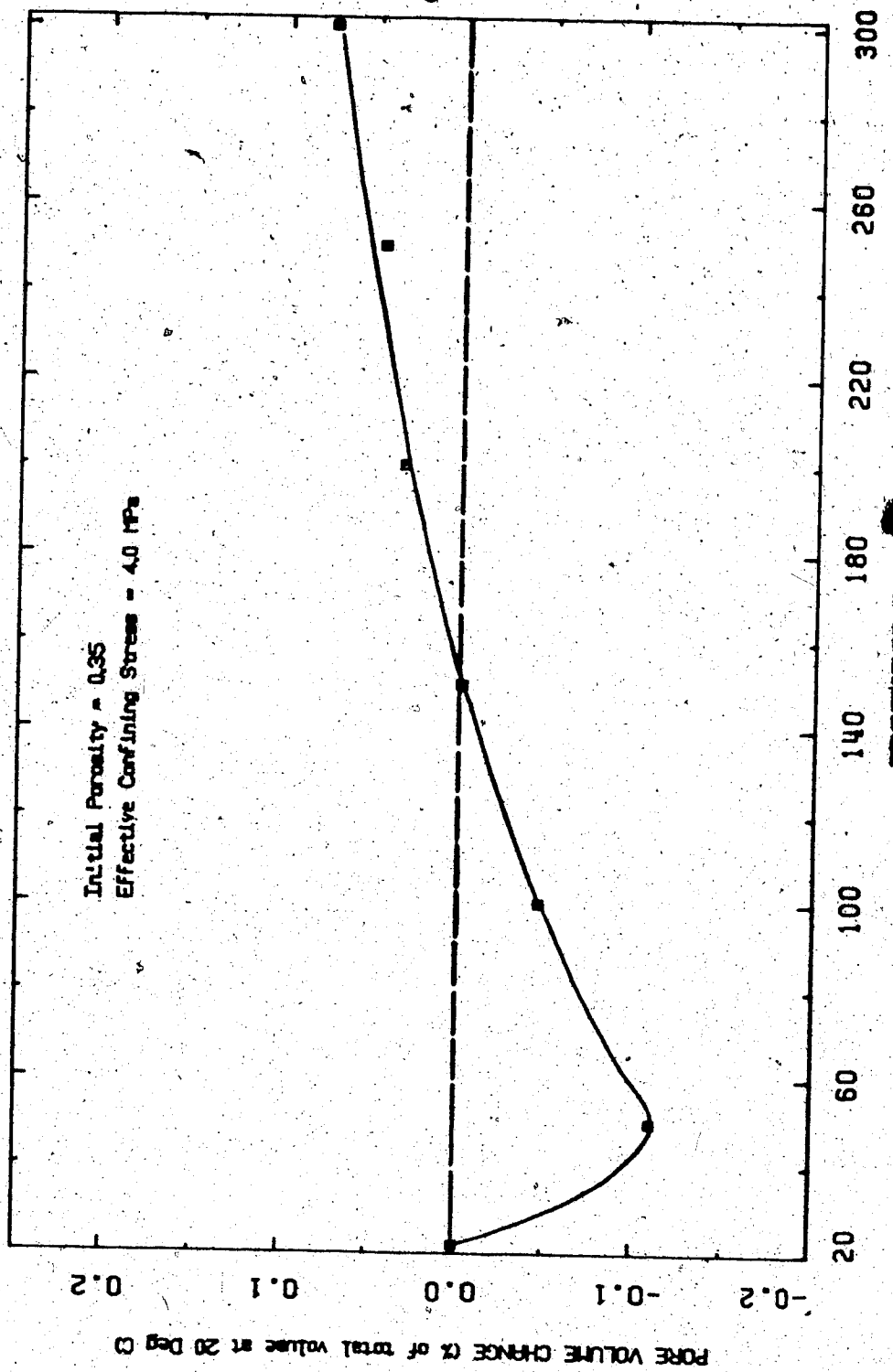

FIGURE 4.3 Thermal Pore Volume Strain

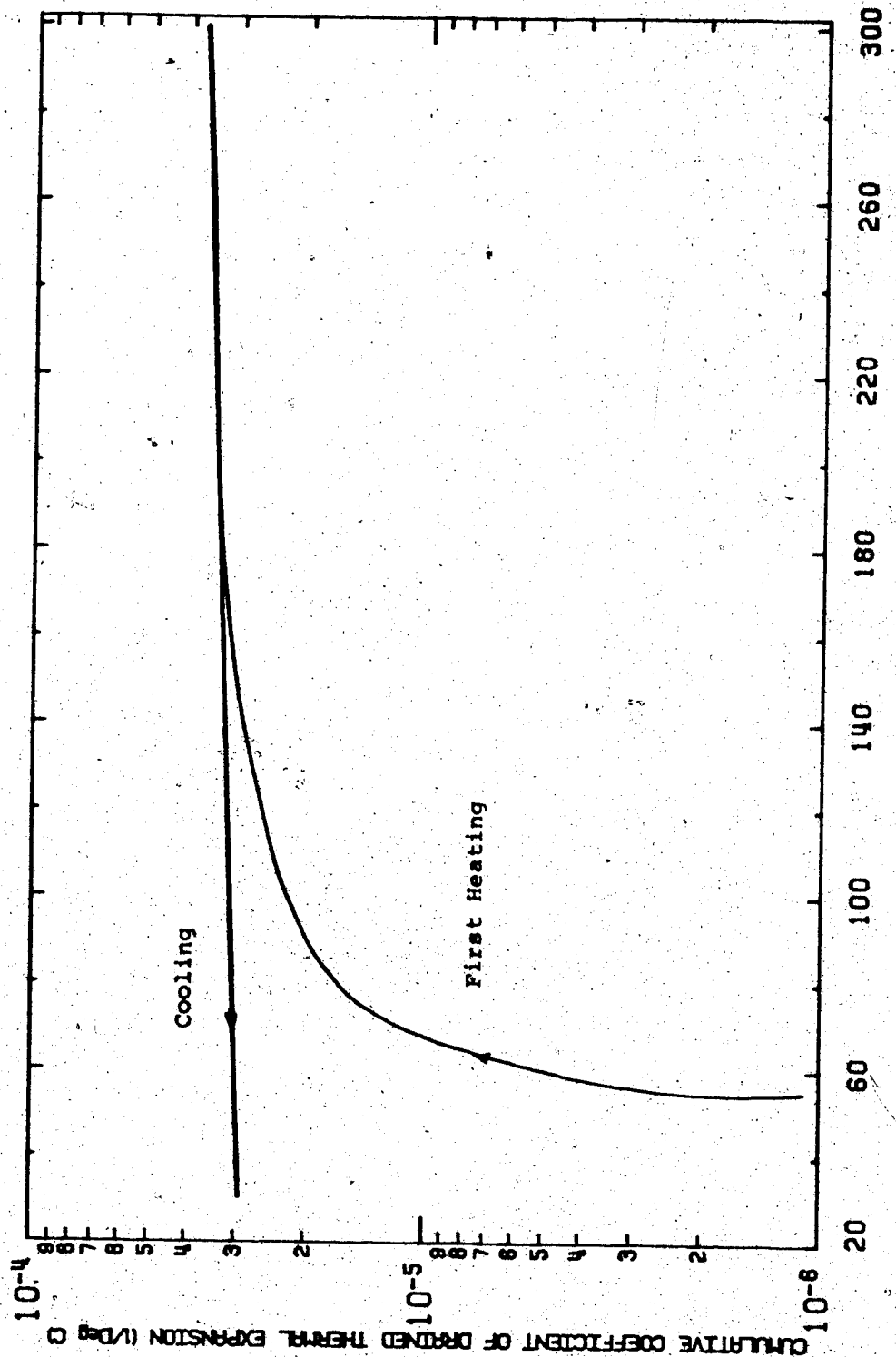

FIGURE 4.4 Drained Coefficient of Thermal Expansion

drained from triaxial samples during heating was measured; also vertical (axial) thermal expansion of triaxial samples was measured. This thermal expansion data is presented in Appendix E.

4.1.3 Undrained Thermal Expansion

Undrained thermal expansion of Saline Creek oil sand was determined in a series of tests at temperatures ranging from 20°C to 300°C at various pore pressures up to 15 MPa. All tests were performed at nominal effective confining stresses less than about 0.05 MPa. Pore fluid pressures and effective vertical confining stress were maintained constant during these undrained tests by heating very slowly and allowing volumetric expansion to occur so that pressures did not build up. A nominal effective confining stress was required to prevent uncontrolled expansion.

A gas exsolution pressure-temperature relationship for Saline Creek oil sand derived from undrained thermal expansion tests is compared with the saturation curve for water in Figure 4.5.

Undrained thermal expansion of Saline Creek oil sand at various pore fluid pressures ranging from 0.5 to 15 MPa up to the gas exsolution limit is summarized in Figure 4.6. Volumetric expansion is shown as a percent of the initial sample volume at room temperature in Figure 4.6. Gas exsolution pressures from Figure 4.5, corresponding to various

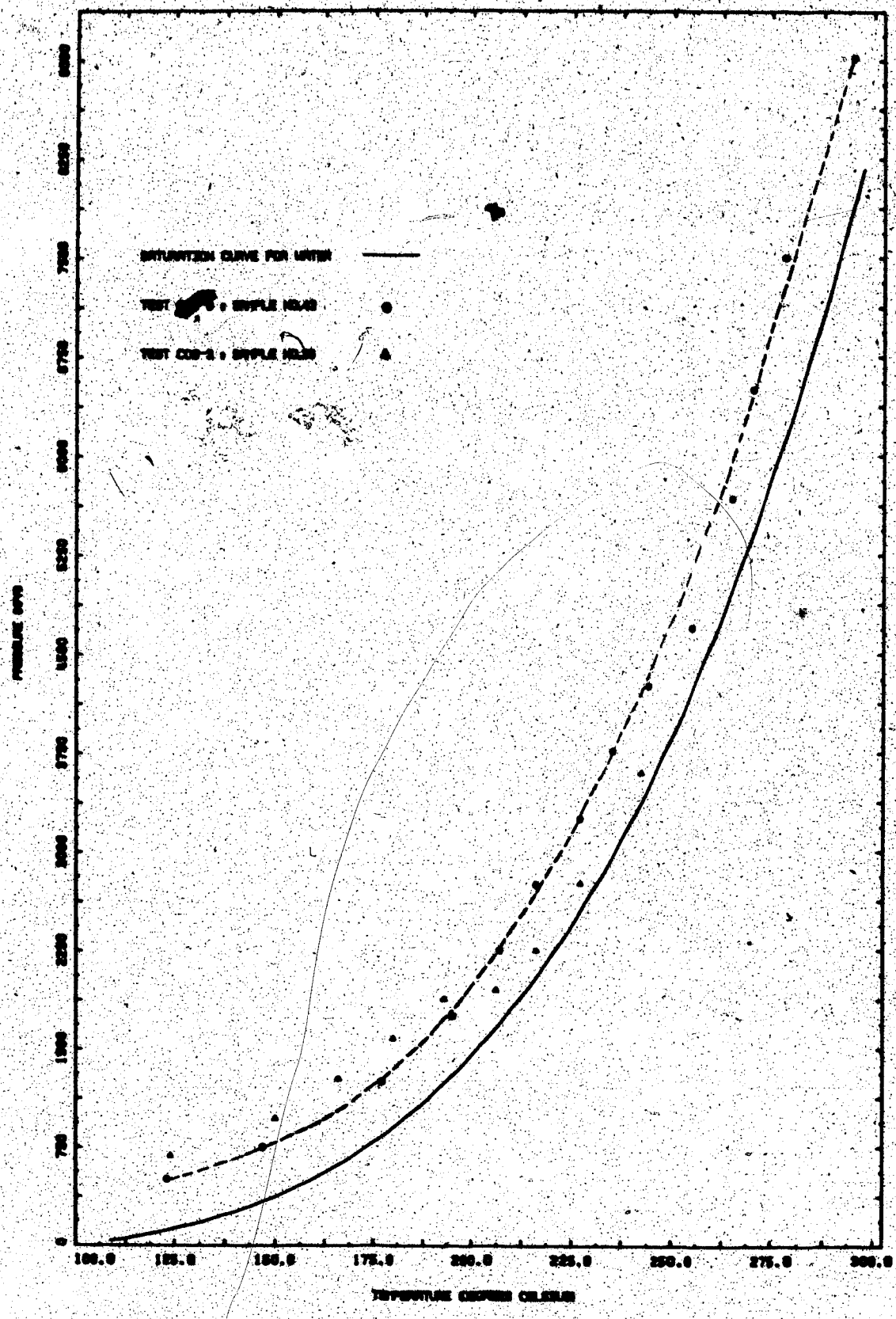

FIGURE 4.5 Gas Exsolution Pressure-Temperature Data for Saline Creek Oil Sand

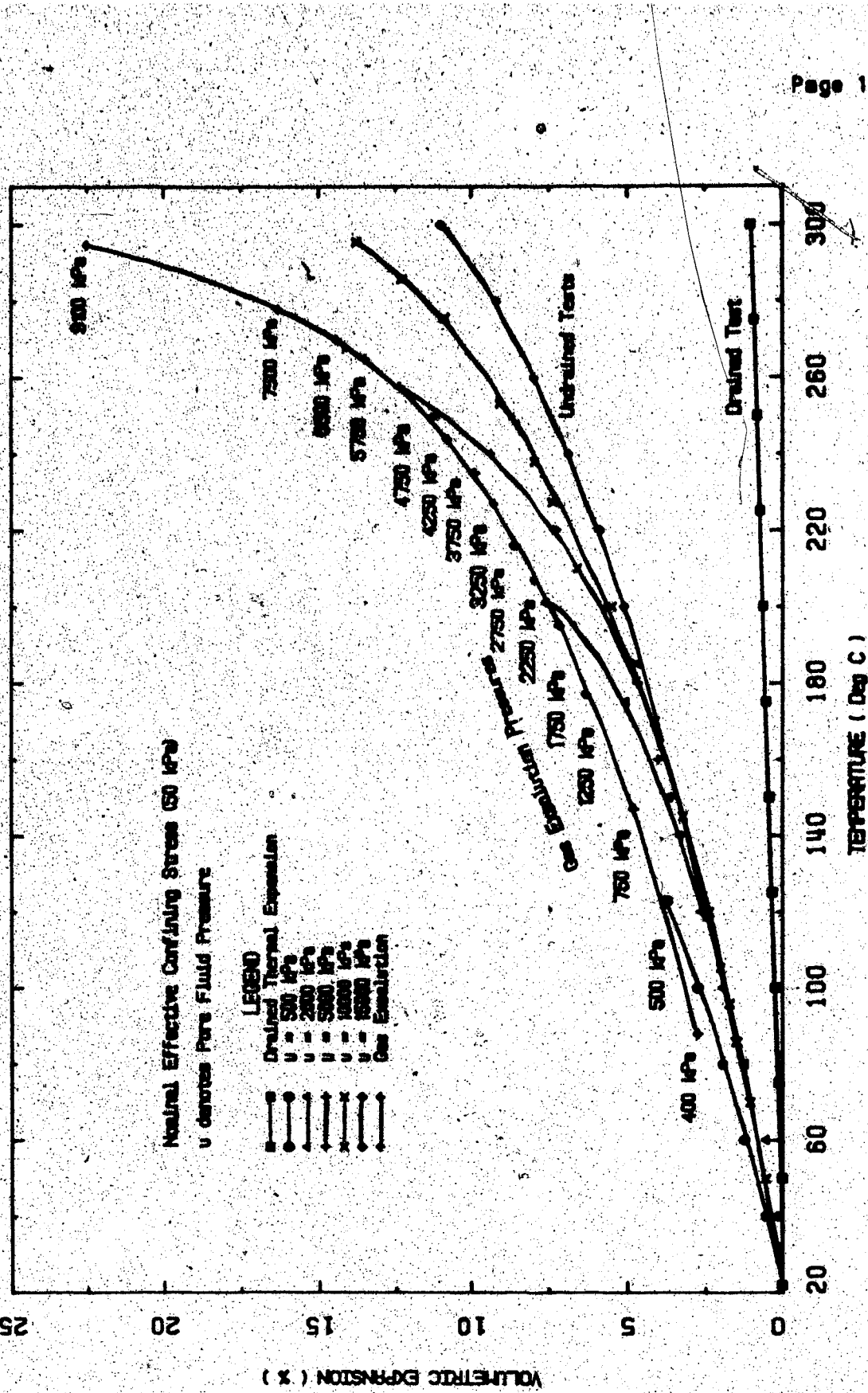

FIGURE 4.6 Thermal Expansion of Saline Ofeek Oil Sand

temperatures are shown on the gas exsolution volume change curve in Figure 4.6.

Also, a lower bound drained thermal expansion curve is plotted in Figure 4.6 to define the range of thermal expansion for Saline Creek oil sand for temperatures up to 300°C. It may be observed that undrained thermal expansion is suppressed at elevated temperatures when pore fluid pressure is increased due to compression of the pore fluids.

The undrained coefficient of thermal expansion, α_u, may be evaluated using thermal expansion data plotted in Figure 4.6. Variation of the cumulative undrained coefficient of thermal expansion, α_u, with temperature and pore pressure is shown in Figure 4.7. The logarithm of the drained and undrained thermal expansion coefficients are plotted against temperature in Figure 4.8.

4.1.4 Implications of Sample Disturbance

The magnitude of drained thermal expansion of laboratory samples of oil sand is reduced as a result of microfabric disturbance. Larger initial porosity permits individual sand grains to expand into the available pore space. Also, reduced frictional resistance at individual grain contacts in disturbed samples increases the potential magnitude of the structure collapse component of volume change. Reduction of the magnitude of drained thermal expansion of oil sand samples is not considered to be of practical significance for samples

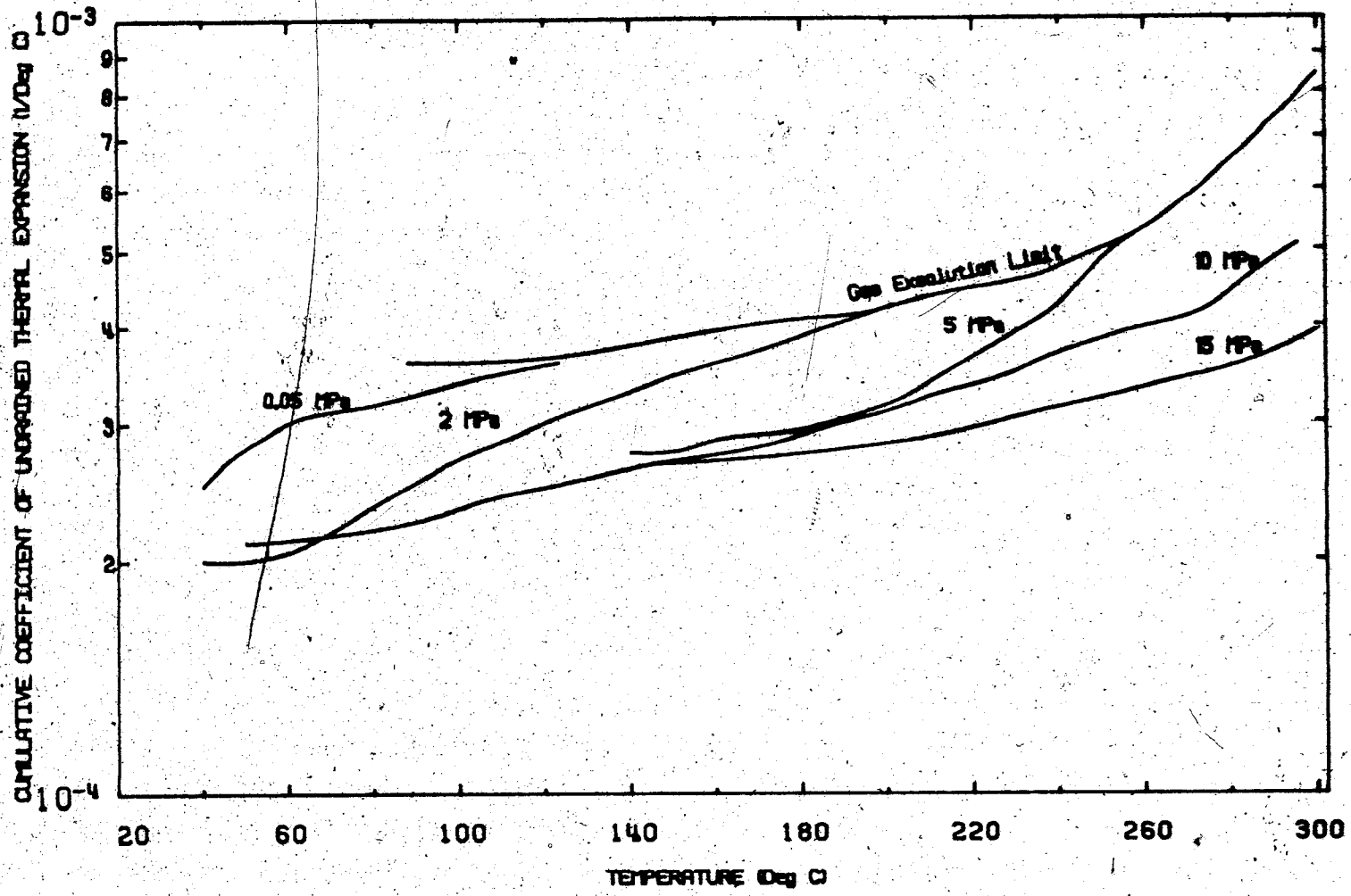

FIGURE 4.7 Undrained Coefficient of Thermal Expansion

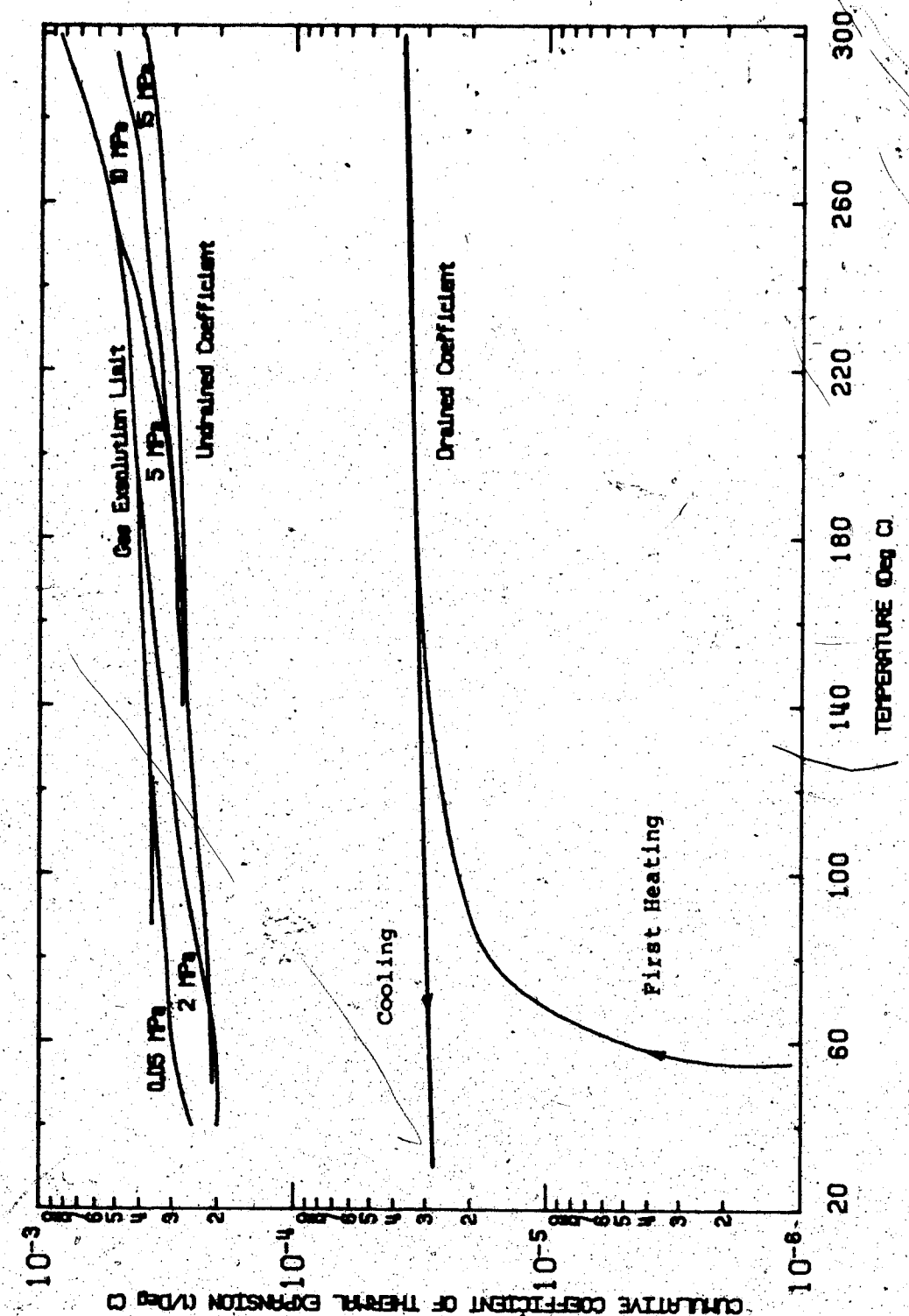

FIGURE 4.8 Coefficients of Thermal Expansion for Oil Sand

having disturbance indices, I_D, less than about 15%. Disturbance index was defined in section 3.3.8.

Increased pore volume resulting from sample disturbance is occupied by water in a back-saturated oil sand sample. Undrained thermal expansion of the sample is therefore increased by the magnitude of undrained thermal expansion of the extra pore water. For example, if the in situ porosity is 0.33 and a high quality oil sand sample having initial porosity 0.35 is tested, the corresponding increase in total volume is 2.0% and the pore volume increases by approximately 6.0%. If the sample is heated undrained to 200°C at constant pore pressure, thermal expansion of the additional water in the pore space will result in about 0.3% extra expansion of the sample, i.e. this represents an error in total expansion of about 4%. The magnitude of the error increases proportionally with the magnitude of temperature increase. The example cited here is typical for the test results presented. It is evident that undrained thermal expansion is very sensitive to sample disturbance. Samples having a disturbance index value, I_D, greater than about 8.0% are not considered suitable for undrained thermal expansion testing.

4.2 Drained Compressibility

4.2.1 Drained Compressibility Parameters

Volumetric compression or expansion of porous soils and rocks due to changes in effective stress depends on characteristics of the solid matrix such as porosity,

intergranular shear strength, mineralogy, etc. Compressibility of the solid grain structure is an important parameter for evaluating volumetric strains which may result from either a change in pore fluid pressure or a change in "all-round" confining stress.

Drained compressibility is commonly measured in two types of laboratory test: (i) one dimensional compression tests in which no lateral strain is permitted (eg. compression tests in the consolidometer, or Ko tests in a triaxial cell); and (ii) isotropic compression tests in a triaxial cell. Two different volume compressibility parameters have been defined for each of the above types of test: m_v is the coefficient of compressibility for one dimensional laterally constrained loading and C_c is the coefficient of compressibility under equal all-round stress changes. In general, C_c is greater than m_v (Skempton and Bishop, 1954). The difference is small for dense undisturbed oil sand. It should be emphasized that neither of the above compressibility parameters are generally applicable for determining dilatant volumetric strains resulting when the material is subjected to deviatoric or shear stresses. Dilatancy may be defined as the volume change consequent upon the application of shear stress, and will be discussed further in section 4.4.

A further important consideration in applying compressibility parameters in numerical modelling relates to the stress history of the material. Compressibility during first time loading (normal consolidation) is substantially

greater than for subsequent cycles of loading and unloading (i.e. overconsolidated behaviour).

4.2.2 One Dimensional Compressibility

One dimensional compressibility tests were performed in the high temperature consolidometer to evaluate the influence of elevated temperatures on m_v for Saline Creek oil sand. Stress-strain plots are presented in Appendix C. Three cycles of loading and unloading were typically applied to oil sand samples. Volumetric strain is a nonlinear function of vertical effective compressive stress; also cumulative non-recoverable (plastic) strain resulted with each cycle of loading and unloading. Nonlinearity and hysteresis are most pronounced for the first loading cycle after which one dimensional compressibility, m_v, approaches reversible linear elastic behaviour. The first cycle of loading corresponds to normal consolidation and, depending on the stress history of the sample, may be substantially greater than the cyclic compressibility.

Results of one dimensional compression tests at temperatures up to 300°C are summarized in Table 4.1. There is a modest decrease in the cyclic value of m_v from about 5×10^{-7} kPa^{-1} at room temperature to about 3×10^{-7} kPa^{-1} at elevated temperatures for oil sand. The observed decrease of m_v at elevated temperatures is consistent with observed porosity changes during drained heating. Values of Young's Modulus, E, which were calculated assuming Poisson's

TABLE 4.1

DRAINED ONE DIMENSIONAL COMPRESSIBILITY OF SALINE CREEK OIL SAND

Test	Sample	Initial Porosity	Temperature (°C)	Range of Effective Stress (MPa)	Coefficient of Compressibility m_v ($kPa^{-1} \times 10^{-17}$)				Young's Modulus E* (MPa)
					First Cycle		Third Cycle		
					Load	Unload	Load	Unload	
CPERM4	36A	0.37	22	0.5 - 4.0	9.2	8.8	9.0	8.0	930
CPERM4	36A	0.36	100	6.0 - 26.0	9.4	3.5	4.5	4.0	1860
CPERM7	44	0.36	22	2.0 - 18.0	14.0	5.9	-	-	1260
CPERM7	44	0.35	150	2.0 - 18.0	8.2	4.9	-	-	1520
CPERM5	31A	0.37	20	0.5 - 5.0	7.0	6.1	5.7	5.3	1400
CPERM5	31A	0.36	200	4.0 - 19.5	5.2	3.3	3.8	3.2	2320
CPERM6	31B	0.36	250	4.0 - 19.0	4.4	2.4	3.6	3.2	2320
COS9	41	0.35	20	2.0 - 18.0	12.0	4.9	5.8	5.2	1430
COS9	41	0.35	300	2.0 - 18.0	11.0	2.2	3.6	3.2	2320

* $E = \frac{(1+\nu)(1-2\nu)}{(1-\nu)\, m_v}$ where $\nu = 0.30$ assumed constant

ratio constant at 0.30, are listed in Table 4.1. Note that values of Young's Modulus derived in this manner are generally lower than those derived from triaxial compression tests.

4.2.3 Isotropic Compressibility

Isotropic compression tests were performed in the high temperature triaxial cell to determine C_c for Saline Creek and Cold Lake oil sand samples at various temperatures. Stress-strain plots are included with triaxial test data in Appendix E. Three cycles of drained isotropic compression and decompression were applied to samples. Characteristic hysteresis of the cyclic stress-strain curves was observed indicating inelastic behaviour. Nonlinear stress-strain behaviour was also observed. Both nonlinearity and hysteresis are reduced after the first compression cycle, as is typical for normal consolidation.

Results of isotropic compression tests at temperatures up to 200°C are summarized in Table 4.2. There is a modest decrease in the cyclic value of C_c from 5.6×10^{-7} kPa^{-1} at room temperature to 3.9×10^{-7} kPa^{-1} at elevated temperatures. This decrease is also consistent with observed porosity changes during drained heating. Compressibility of the Cold Lake oil sand sample at 200°C is somewhat greater than that of Saline Creek oil sand. This is due in part to the higher initial porosity and weaker mineralogy of the Clearwater Formation oil sand from Cold Lake. Young's modulus was calculated for each test assuming a

TABLE 4.2

DRAINED ISOTROPIC COMPRESSIBILITY OF OIL SAND

Test	Sample	Initial Porosity	Temperature (°C)	Range of Effective Stress (MPa)	Coefficient of Compressibility C_c ($kPa^{-1} \times 10^{-17}$)				Young's Modulus, E* (MPa)
					First Cycle		Third Cycle		
					Load	Unload	Load	Unload	
TOS1	Saline Creek 25	0.33	20	4.0 - 25.0	15.0	7.8	7.9	5.6	2140
TOS8	28	0.35	220	13.0 - 20.0	20.0	-	-	-	-
TOS12	29	0.34	200	4.0 - 17.0	11.8	3.9	5.4	3.9	3075
TOS19	19	0.33	125	4.0 - 17.0	5.5	3.6	4.1	3.8	3160
TOS15	Cold Lake 12B	0.38	200	4.0 - 17.0	34.0	4.4	6.8	5.4	2220

* $E = \frac{(1+\nu)\ (1-2\nu)}{(1-\nu)\ m_v}$ assuming $\nu = 0.30$

constant value of Poisson's Ratio of 0.30; modulus values are listed in Table 4.2. Note that these modulus values are greater than those determined using the lower m_v values in Table 4.1. In general, modulus values based on m_v are low because in situ horizontal stresses are not equivalent to those determined using linear elasticity.

Although values of C_c listed in Table 4.2 are generally greater than values of m_v listed in Table 4.1, the differences are not considered to be of practical significance in view of other more dominant factors such as sample disturbance, stress level, etc...

4.2.4 Implications of Sample Disturbance

Although no comprehensive study was conducted to evaluate quantitatively the influence of sample disturbance on drained compressibility, the following general conclusions may be cited:

a) Sample disturbance may significantly increase drained compressibility for first time loading. In fact, the effects of stress history and sample disturbance are often indistinguishable in compression test results.

b) Cyclic compressibility of oil sand samples in which the original structure has been preserved (i.e. disturbance index, I_D, less than about 10%), does not appear to be significantly affected.

4.3 Undrained Compressibility and Pore Pressure Response To Undrained Heating

4.3.1 Undrained Compressibility and Pore Pressure Response Parameters

Undrained compressibility, β_u, enters into undrained stress-deformation analyses. Also, compressibility of the pore fluids, β_f, is an important parameter in fluid flow and heat transfer analyses which are based on the principles of conservation of mass and energy, i.e. transient drainage of compressible fluids and convective heat transfer. For many geotechnical problems isothermal conditions prevail and water is the only pore fluid present. In oil sand where two or more pore fluid phases may exist simultaneously over a range of temperatures, evaluation of appropriate values of β_u and β_f is more complex. Compressibilities of oil sand pore fluids are often determined by "Pressure-Volume-Temperature" (PVT) testing of fluids extracted from the pore space of the oil sand (i.e. bitumen, water and gases). An alternate test method was devised during the course of this research in which an undisturbed oil sand sample was heated undrained in the triaxial cell under constant isotropic effective stress. Several parameters may be derived from such a test including β_u, β_f and the pore pressure response parameter, B_T, for undrained heating. A major advantage of this type of test over PVT testing is that pore fluids need not be altered by an extraction process.

Pore pressure response to undrained heating may be a factor in reducing effective confining stresses and available shear strength during rapid heating because of low effective permeability of oil sand at in situ temperatures. Just as an isothermal total stress change generates a pore pressure reaction expressed in terms of the parameter B, similarly an undrained temperature change induces a pore pressure response that can be expressed by an analogous parameter B_T (Morgenstern, 1981). The coefficient B_T may be expressed in terms of stress and temperature-dependent volume changes of the components of oil sand. Campanella and Mitchell (1968) developed a similar pore pressure parameter, F, based on undrained heating of illite clays in a consolidometer.

Provided that grain-to-grain contact is maintained during undrained heating (i.e. effective stresses are greater than zero), then thermal expansion and pore pressure compressibility of the individual components of oil sand may be equated with thermal expansion, effective stress compressibility and dilatancy of the mineral grain matrix as follows:

$$(\Delta V_w)_T + (\Delta V_B)_T + (\Delta V_S)_T - (\Delta V_w)_u - (\Delta V_B)_u - (\Delta V_S)_u = (\Delta V_m)_T - (\Delta V_m)_{\bar{\sigma}'} + (\Delta V_m)(\sigma_1 - \sigma_3) \quad (4.4)$$

where the subscripts:

w denoted water

B denotes bitumen

S denotes mineral solids

m denotes solids matrix

T denotes temperature change

u denotes pore pressure change

$\bar{\sigma}'$ denotes an ambient effective stress change

$(\sigma_1 - \sigma_3)$ denotes a deviatoric stress change

Equation 4.4 may be rewritten:

$$\left[\alpha_w \eta_w + \alpha_B \eta_B + \alpha_s \eta_s\right] \Delta T - \left[\beta_w \eta_w + \beta_B \eta_B + \beta_s \eta_s\right] \Delta u \qquad (4.5)$$

$$= (\alpha_S - \alpha_{ST}) \Delta T - C_c \left[\Delta \bar{\sigma}' + S_d \, (\sigma_1 - \sigma_3)\right]$$

where:

$\alpha_{ST} \Delta T$ denotes the structural collapse component of thermal volume change

S_d is a dimensionless "structural parameter accounting for dilatancy (Skempton and Bishop, 1954).

Skempton originally defined the parameter S_d to account for dilatant volume changes resulting when deviatoric stress changes were applied to a triaxial sample. The S_d parameter

is used here to account for dilatant volume changes during undrained heating of a sample under anisotropic stresses.

Equation 4.5 may be simplified by setting:

$$\alpha_u = \left[\alpha_w \eta_w + \alpha_B \eta_B + \alpha_s \eta_s\right]$$

$$\alpha_{DR} = (\alpha_s - \alpha_{ST})$$

$$\beta_u = \left[\beta_w \eta_w + \beta_B \eta_B + \beta_s \eta_s\right]$$

Then equation 4.5 may be written:

$$\alpha_u \Delta T - \beta_u \Delta u = \alpha_{DR} \Delta T - C_c \left[\Delta \bar{\sigma}' + S_d \Delta (\sigma_1 - \sigma_3)\right] \qquad (4.6)$$

For isotropic stress conditions:

$$\alpha_u \Delta T - \beta_u \Delta u = \alpha_{DR} \Delta T - C_c \Delta \bar{\sigma}' \qquad (4.7)$$

In general:

$$\Delta \bar{\sigma}' = \Delta \bar{\sigma} - \Delta u \qquad (4.8)$$

and:

$$B_T = \frac{\Delta u}{\Delta T} = \frac{\alpha_u - \alpha_{DR} + C_c\left(\frac{\Delta \bar{\sigma}}{\Delta T}\right)}{\beta_u + C_c} \qquad (4.9)$$

Laboratory heating experiments are generally either performed with constant total stresses or constant effective

stresses. For undrained heating and constant total stresses (i.e. $\Delta\bar{\sigma} = 0$):

$$B_T = \frac{\Delta u}{\Delta T} = \left[\frac{\alpha_u - \alpha_{DR}}{\beta_u + C_c}\right] \qquad (4.10)$$

and for undrained heating and constant effective stress:

$$B_T = \frac{\Delta u}{\Delta T} = \frac{\alpha_u - \alpha_{DR}}{\beta_u} \qquad (4.11)$$

It should be noted that dilatant volume changes resulting from shear stresses have not been considered in developing equations 4.7 to 4.11 inclusive. Undrained compressibility, βu, may be determined when B_T is measured in an undrained heating experiment using equation 4.11 and appropriate thermal expansion parameters.

Compressibility of the pore fluids, β_f, may also be determined, if porosity is known, as follows:

$$\beta_f = \frac{\beta_u - (1 - \eta)\,\beta_s}{\eta} \qquad (4.12)$$

Because of the presence of solution gases in oil sand pore fluids, β_f may vary from compressibilities of extracted bitumen and water determined by PVT methods.

4.3.2 Undrained Heating with Constant Effective Stress

Test TOS10 was conducted in the triaxial cell with near constant isotropic effective stress maintained on the sample during heating. No volume change results from compression of the mineral solids matrix when isotropic effective stress is maintained constant. Equations 4.11 and 4.12 therefore, may be used to determine β_u and β_f from this test. Heating was carried out in eight cycles, each about 20°- 30°C temperature increments, in order to avoid exceeding the limit of pressure capacity of the test cell. Detailed procedures and test results are presented in Appendix E. Pore pressure response B_T, undrained compressibility β_u and pore fluid compressibility β_f determined from results of test TOS10 are summarized in Table 4.3. Undrained compressibility, β_u, was measured in two other triaxial tests, TOS1 and TOS8, however, accuracy of the lateral deformation measurements was questionable, as discussed in section 3.7.

Undrained compressibility, β_u, determined in test TOS10 is plotted on Figure 4.9 over the temperature range of 20°-200°C. Drained isotropic compressibility of Saline Creek oil sand is also shown in Figure 4.9 for three tests at 20°C, 125°C and 200°C. Pore fluid compressibility, β_f, of bitumen and water determined in test TOS10, for temperatures up to 200°C is compared with published PVT data for water and solvent extracted Athabasca bitumen in Figure 4.10.

TABLE 4.3

Isotropic Undrained Compressibility of Oil Sand and Oil Sand Pore Fluids

Test	Sample Porosity	Temperature Range (°C)	B_T (kPa/°C)	Isotropic Undrained Compressibility β_u (kPa^{-1})	Compressibility of Pore Fluids β_f (kPa^{-1})
TOS1*	0.33	20	-	1.7×10^{-7}*	-
TOS8*	0.35	220	-	3.3×10^{-7}*	-
TOS10	0.35	20-30	980	1.6×10^{-7}	4.5×10^{-7}
TOS10	0.35	30-50	980	1.65×10^{-7}	4.6×10^{-7}
TOS10	0.35	50-70	880	2.0×10^{-7}	5.6×10^{-7}
TOS10	0.35	70-85	825	2.2×10^{-7}	6.2×10^{-7}
TOS10	0.35	85-105	790	2.9×10^{-7}	8.2×10^{-7}
TOS10	0.35	105-125	700	4.1×10^{-7}	1.16×10^{-6}
TOS10	0.35	125-150	590	5.1×10^{-7}	1.45×10^{-6}
TOS10	0.35	150-175	500	7.1×10^{-7}	2.02×10^{-6}
TOS10	0.35	175-200	450	9.1×10^{-7}	2.60×10^{-6}

* Volume change measurements inaccurate due to stiffness of the lateral strain gauge clamp for tests TOS1 and TOS8.

** Cubical compressibility of quartzose sand grains: $\beta_s = 5.0 \times 10^{-9} kPa^{-1}$

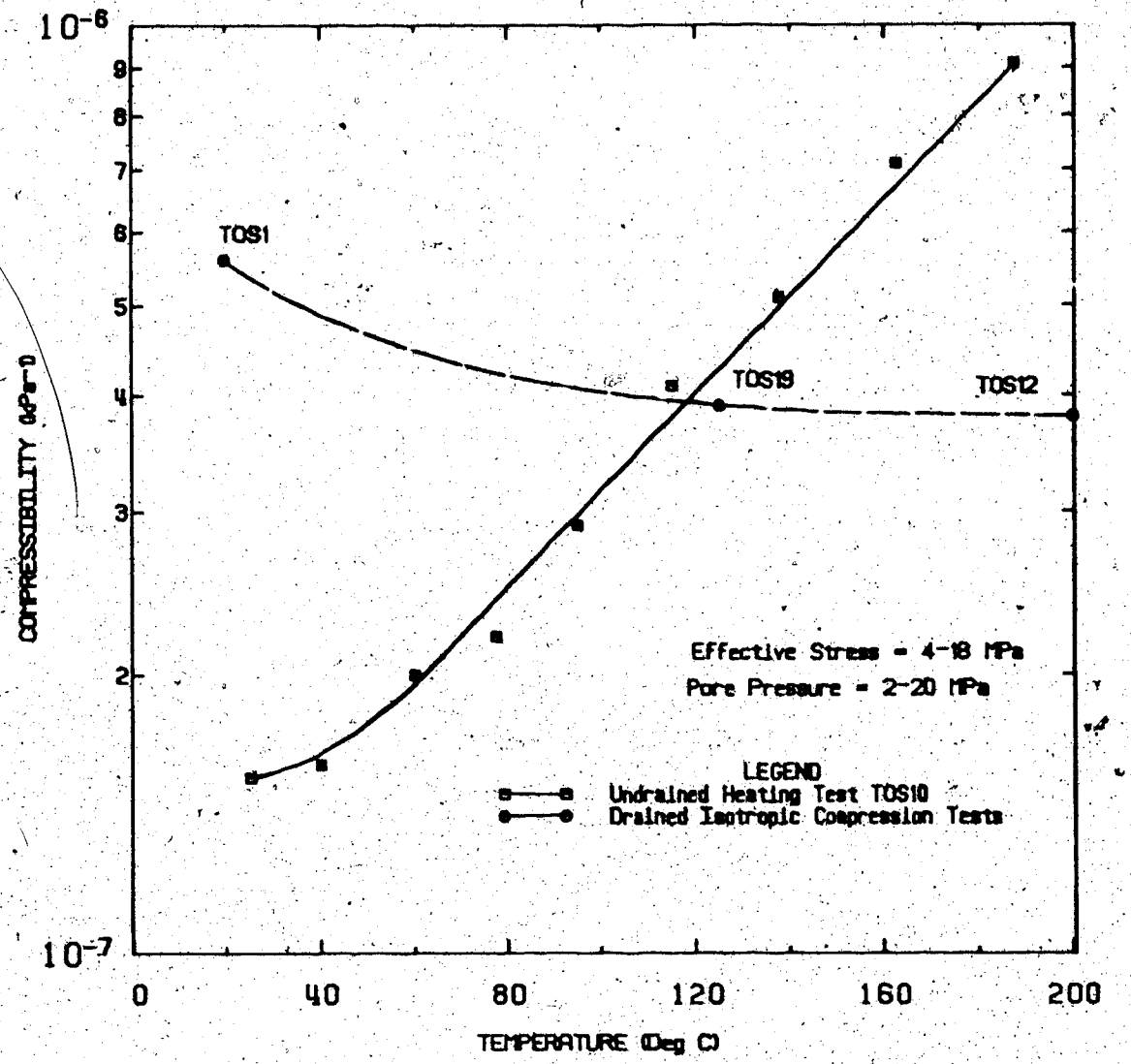

FIGURE 4.9 Isotropic Compressibility of Oil Sand

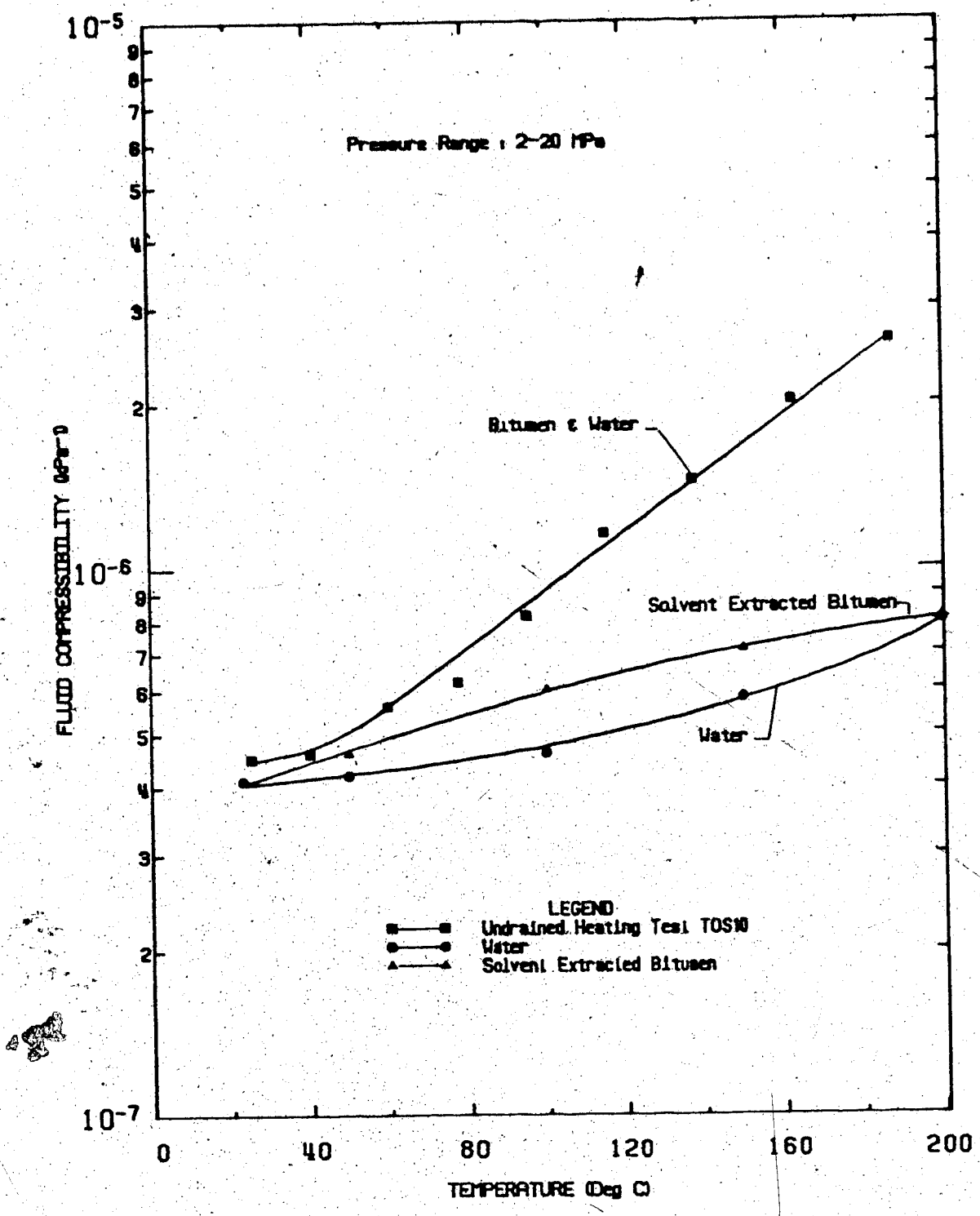

FIGURE 4.10 Compressibility of Oil Sand Pore Fluids

4.3.3 Undrained Heating with Constant Total Stresses

Undrained heating experiments with total stresses constant were performed both in the high temperature consolidometer and triaxial test cells. In test COS5 (see Appendix B), an oil sand sample was heated undrained in the consoliometer with the total vertical confining stress maintained constant at 11 MPa and initial pore pressure of 5 MPa. Pore pressure response was monitored over the temperature range 20° - 55°C (i.e. ΔT = 35°C). Undrained heating was repeated over the temperature range 150°C - 178°C with total vertical confining stress constant at 17 MPa and initial pore pressure 11 MPa. Nonlinear pore pressure increase with temperature was observed in both undrained heating cycles.

In test TOS11 (see Appendix E), an oil sand sample was heated undrained with constant anisotropic total stresses; horizontal stress was maintained at 14 MPa and the vertical stress at 16 MPa. The initial pore pressure was 10 MPa. Pore pressure increase with temperature was monitored over the temperature range 20°C to 100°C at which point the sample failed by shearing. Again pore pressure response due to undrained heating was nonlinear.

Figure 4.11 is a summary plot of pore pressure response to undrained heating in tests COS5 and TOS11. It should be noted that since deviatoric stresses were applied in test TOS11, dilatancy must be accounted for and pore pressure response is

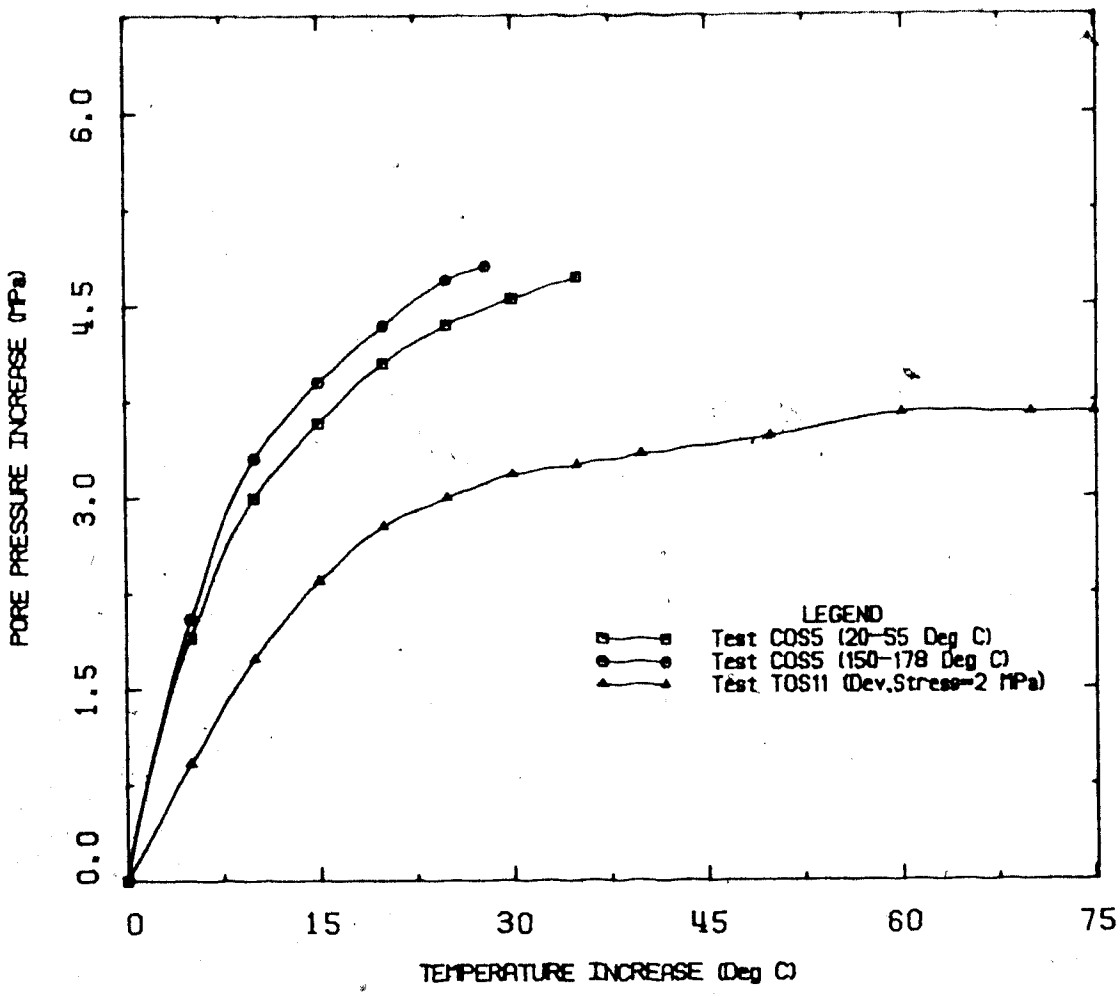

FIGURE 4.11 Undrained Heating with Constant Total Stresses

characterized by equation 4.4. Table 4.4 summarizes pore pressure response and back calculated values of the structural parameter, Sd, based on the results of test TOS11. Horizontal stresses were not measured in the consolidometer, however, the pore pressure response in test COS5 may be characterized by modifying equation 4.8 and substituting the one dimensional compressibility parameter m_v in place of isotropic compressibility, C_c, as follows:

$$B_T = \frac{\Delta u}{\Delta T} = \frac{\alpha_u - \alpha_{DR}}{\beta_u + m_v} \qquad (4.13)$$

This is similar to the expression developed by Campanella and Mitchell (1968).

It is of interest to note that the rate of pore pressure increase in test COS5 was slower during heating cycle 1 (from 20°C - 55°C) than during heating cycle 2 (from 150°C - 178°C); the initial effective stress was similar for both cycles, i.e. 5.8 MPa for cycle 1 and 6.0 MPa for cycle 2. Two factors contribute to this phenomenon:

a) the difference between undrained and drained coefficients of thermal expansion, $\alpha_u - \alpha_{DR}$, in equation 4.13 increases with temperature (see Figure 4.6); and

b) partial collapse of the mineral grain structure during the initial phase of heating (i.e. 24°C - 60°C) reduces

TABLE 4.4

TEST TOS11: DILATANCY DURING UNDRAINED HEATING

Temperature (°C)	Δu (MPa)	$B_T = \frac{\Delta U}{\Delta T}$ (MPa/°C)	α_u * ($°C^{-1}$)	α_{DR} * ($°C^{-1}$)	β_u * (MPa^{-1})	C_c * (MPa^{-1})	Sd *** (Dimensionless)
20	0.0	0.0	-	-	-	5×10^{-4}	-0.6 ***
30	1.80	0.180	1.8×10^{-4}	-5.0×10^{-5}	1.6×10^{-4}	5×10^{-4}	-2.9
40	2.80	0.140	1.9×10^{-4}	-4.0×10^{-5}	1.7×10^{-4}	5×10^{-4}	-4.8
60	3.30	0.083	2.1×10^{-4}	5.0×10^{-6}	2.0×10^{-4}	5×10^{-4}	-9.4
80	3.57	0.060	2.3×10^{-4}	1.7×10^{-5}	2.4×10^{-4}	5×10^{-4}	-13.7
100	3.70	0.046	2.4×10^{-4}	2.4×10^{-5}	3.0×10^{-4}	5×10^{-4}	-18.2

* Parameters determined from other tests

** Rearranging equation 4.4 gives: $S_d = \frac{(\beta_u - C_c)\Delta u - (\alpha_u - \alpha_{DR})\Delta T}{C_c(\Delta\sigma_1' - \Delta\sigma_3')}$

where $(\Delta\sigma_1' - \Delta\sigma_3') = 2$ MPa (constant)

*** Value based on volume change during anisotropic consolidation using Skempton's equation: $\frac{\Delta V}{V} = -C_c\left[\Delta\sigma_3' + S_d(\Delta\sigma_1' - \Delta\sigma_3')\right]$

compressibility of the mineral grain matrix, m_v, slightly at elevated temperatures, thereby increasing B_T.

Nonlinear pore pressure response curves shown in Figure 4.11 may be approximated reasonably accurately by a hyperbolic relationship of the form:

$$B_T = \frac{\Delta u}{\Delta T} = \frac{1}{\frac{1}{B_{Ti}} + \frac{\Delta T}{\sigma_o'}} \qquad (4.14)$$

where:

σ_o' denotes initial effective confining stress (i.e. in the consolidometer and in the triaxial cell)

and B_{Ti} denotes the initial pore pressure response parameter.

Values of hyperbolic parameters in equation 4.14 which best fit the results of tests COS5 and TOS11 are as follows:

TEST	TEMPERATURE RANGE (°C)	INITIAL EFFECTIVE CONFINING STRESS σ_o' (MPa)	B_{Ti} (MPa/°C)
COS5	24 - 60	5.8	0.40
COS5	150 - 176	6.0	0.60
TOS11	20 - 100	4.0	0.20

Test results are plotted with hyperbolic curves generated using equation 4.14 in Figure 4.12. Variation of the B_T parameter with temperature and stress based on the above relationship is discussed further in Chapter 5. The range of pore pressure response to undrained heating for constant total stress tests and constant effective stress tests is shown in Figure 4.13. The rate of pore pressure increase in constant total stress tests depends on the initial effective confining stress, σ_o'. The rate of pore pressure increase with temperature is substantially higher when total stress is increased to maintain constant effective stress as indicated by comparing equations 4.10 and 4.11.

4.3.4 Implications of Sample Disturbance

The effect of sample disturbance on undrained compressibility behaviour and pore pressure response to undrained heating is similar to that described for undrained thermal expansion since these properties are interrelated.

Sampling disturbance generally results in increased porosity of oil sand. The extra pore volume in laboratory samples initially is occupied by air and hydrocarbon gases evolved from the pore liquids. After back saturation, the extra pore volume is occupied by water introduced into the sample. The proportion of liquid to solid phases is thus increased, causing an increase in undrained compressibility since water is two orders of magnitude more compressible than

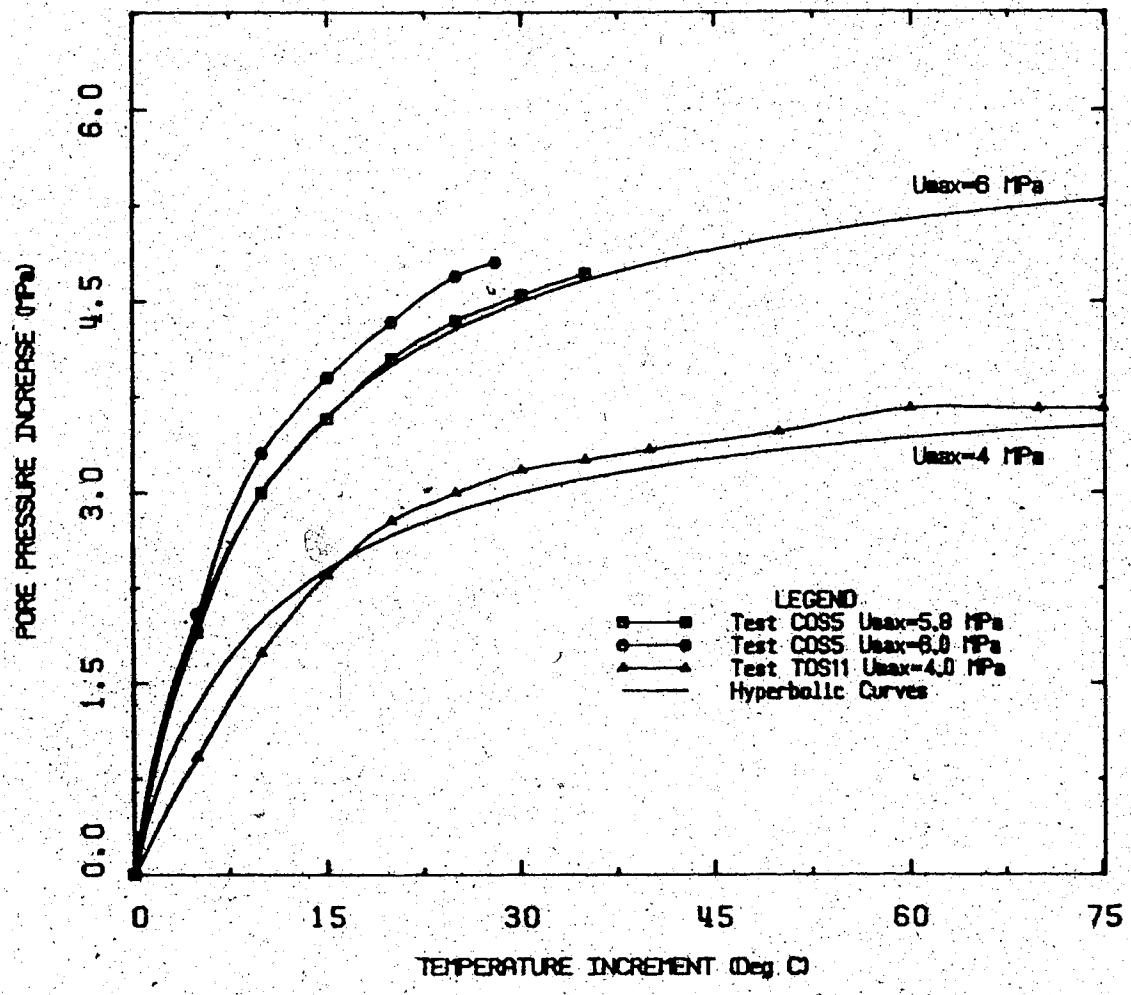

FIGURE 4.12 Pore Pressure Generation by Undrained Heating

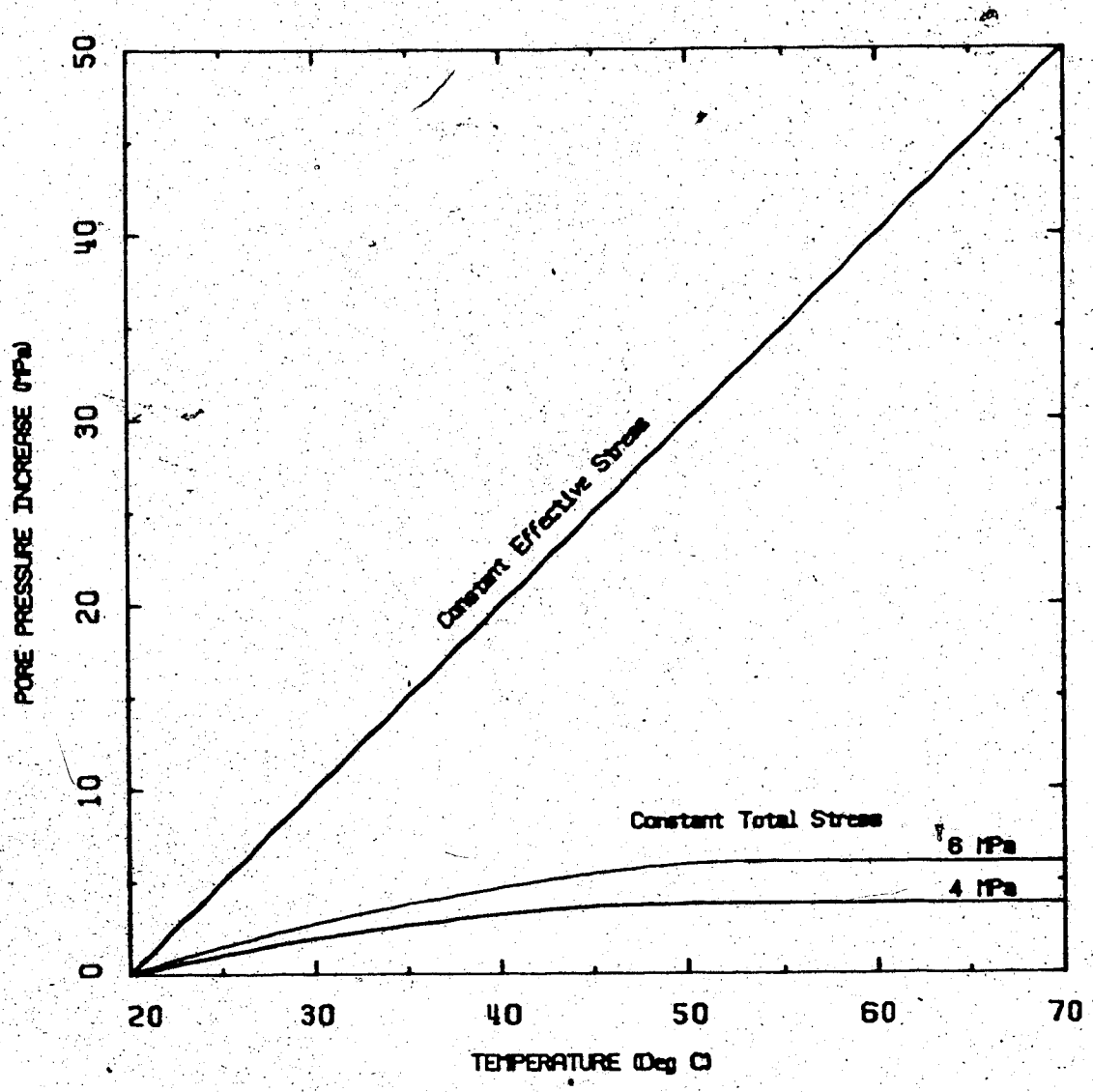

FIGURE 4.13 Pore Pressure Response to Undrained Heating Under Constant Total and Effective Stresses

the solid quartz sand grains, i.e. $\beta_w = 4.5 \times 10^{-7}$ kPa^{-1} and $\beta_s = 5 \times 10^{-9}$ kPa^{-1} at room temperature. For example, increasing porosity from 0.33 to 0.37 in a 690 ml triaxial sample will result in an increase in β_u from about 1.5×10^{-7} kPa^{-1} to 1.7×10^{-7} kPa^{-1}. The influence of sample disturbance on β_u, is somewhat more dramatic at elevated temperatures since the compressibility of water increases substantially more than that of solid quartz particles. Pore fluid compressibility, β_f is not altered appreciably by moderate sample disturbance. An increase in the proportion of liquid to solids in oil sand results in increased rate of pore pressure increase during undrained heating because of the increased propensity of the material to expand with temperature. This is identical to the influence of disturbance on undrained thermal expansion under conditions of elevated effective confining stress.

4.4 Strength and Stress-Strain Behaviour

4.4.1 Strength and Stress-Strain Parameters

Strength and stress-strain parameters are required to evaluate in situ stress changes and deformations resulting from:

a) lateral stress changes, i.e. by underground excavation or surface loading;

b) alteration of the thermal regime; and/or

c) pore pressure changes.

The shear strength of a specimen of oil sand may be broadly defined as the maximum shear stress which the specimen can withstand. Shear strength is defined in this study as the maximum shear stress which a cylindrical triaxial specimen, nominally 75 mm in diameter by 150 mm high can withstand following a specific triaxial compression stress path. Shear strength of oil sand may be characterized by the Mohr-Coulomb failure criterion as follows:

$$\tau_f = c' + \sigma' \tan \phi' \qquad (4.15)$$

where c' and ϕ' are the apparent cohesion and angle of shearing resistance with respect to effective stresses and σ' is the effective stress normal to the shear plane. The Mohr-Coulomb criterion like other failure criteria is empirical; for practical reasons it is by far the most widely used criterion for soils and rocks. Equation 4.15 may be written in terms of principal stresses:

$$\tfrac{1}{2}(\sigma_1' - \sigma_3')_f = \frac{c' \cos \phi' + \sigma_3' \sin \phi'}{1 - \sin \phi'} \qquad (4.16)$$

The Mohr-Coulomb relationship recognizes that neither shear stress nor normal stress on a plane can alone cause shear failure, but that failure develops under critical combinations of shear and normal stress.

Pre-failure stress-strain behaviour is also of interest for

In situ stress and deformation analyses. Stresses and strains are commonly related through stress-strain moduli. The simplest relationships drawn from the theory of elasticity assume that stress is a linear function of strain.

Several aspects of the stress-strain behaviour of oil sand require significant departures from linear elastic theory as follows:

a) strain is not a linear functions of stress;
b) stress path dependency (i.e. the magnitude of strain depends on the stress path followed during the history of loading and unloading);
c) shear stresses not only cause shear strains (i.e. angular distortion), but also volumetric strains, i.e. dilatancy.

These three features of the stress-strain behaviour of oil sand may be incorporated into numerical analyses by using concepts of incremental elasticity (eg. Duncan et al., 1980). Values of elastic moduli are varied with stress level to account for nonlinearity and in accordance with loading history to model stress path dependency; also elastic modulus values (i.e. Poisson's ratio or bulk modulus) may be varied with stress level to account for nonlinear volumetric strain. Stress dependent moduli are referred to as "tangent moduli" and separate modulus values are generally required for loading and unloading. Incremental elastic parameters are discussed in more detail in Chapter 6.

An extensive dissertation on elastic parameters and numerical modelling is given by Evgin (1981).

A second approach to modelling inelastic features of stress-strain behaviour of soils and rocks involves the development of elasto-plastic models. Two widely recognized models in geotechnique are the "Cam Clay Model" (Roscoe et al. 1958) and "Lade's Model" (Lade and Duncan, 1975). These models use separate stress-strain parameters for elastic and plastic (non-recoverable) components of strain. While this is a more fundamental approach, it is also extremely complex to handle numerically and therefore will not be discussed further here.

Other factors which often cause departure from linear elastic stress-strain behaviour include anisotropy and time dependency. Anisotropy of stress-strain parameters has not been studied for oil sand to date. Time dependency of stress-strain behaviour of Saline Creek oil sand is related primarily to pore pressure changes with time (i.e. consolidation and gas exsolution). Significant creep behaviour was not observed during this study, even in elevated temperature compression tests over durations up to seven days. Other oil sands comprised of weaker mineral solids may creep at elevated stresses and temperatures.

The influence of elevated temperatures to 200°C on shear strength and stress-strain behaviour of Saline Creek oil sand was evaluated in this study by conducting triaxial compression

tests. Vertical and horizontal stresses, pore pressure, vertical (axial) deformation and volume change were measured during triaxial compression testing to determine actual stress-strain behaviour and strength. Results of nineteen triaxial test are summarized in Table 4.5. Strength and stress-strain parameters for numerical modelling may be derived from results of triaxial compression tests discussed in the following sections.

4.4.2 Stress Path Dependency

Shear strength and stress-strain behaviour of oil sand are dependent upon the history of loading and unloading of triaxial test specimens during sampling and subsequent compression testing. Triaxial samples were consolidated under isotropic effective stresses of either 4 MPa or 8MPa in all tests prior to deviatoric or further compression in this study. Precompression to a stress level equal to or exceeding in situ stresses largely eliminates the influence of sampling history provided that the mineral grain structure of the oil sand was preserved.

Six triaxial stress paths were investigated during triaxial compression testing. The stress paths are illustrated in Figure 4.14 in triaxial stress space with an upper bound failure envelope for high quality "undisturbed" samples of Saline Creek oil sand. The stress paths may be described as follows:

TABLE 4.5

SUMMARY OF TRIAXIAL TEST RESULTS

Test	Maximum Temperature (°C)	Sample No.	Initial Bulk Density (Mg/m^3)	Initial Porosity	Disturbance Index I_D (%)	Stress Path	"B" Parameter	Initial Saturation (%)	Stresses at Failure σ_1'	σ_3'	μ_f	Strain at Failure (%)	Average Loading Rate (kPa/min)	Angle of Shearing Resistance ϕ'	Initial Tangent Modulus (MPa)	Remarks
T051	20	25	2.088	0.333	1.0	A/C	0.88	99.99	12880	3620	2010	3.0	80	-	-	- Sample disturbed by lateral strain gauge clamp.
T052	20	33	2.077	0.340	3.0	C	0.77	99.85	21000	4060	2005	1.2	80	43	2200.	
T053	20	43	2.082	0.357	8.2	B	0.84	100.00	6020	870	130	0.6	80	49	3100.	
T054	20	44	2.013	0.369	11.8	D	0.81	99.99	21450	8025	2000	1.0	80	27	3800.	
T055	20	17	2.090	0.357	8.2	D	-	-	26100	8200	1970	2.0	70	42	3600.	
T056	125	16	2.120	0.327	0.0	B	-	-	6700	650	9750	0.2	55	55	11000.	
T057	125	45	2.023	0.355	7.6	C	-	-	17000	4350	10040	1.0	70	36	6300.	
T058	220	28	2.046	0.354	7.3	A	0.79	99.94	-	-	-	-	-	-	-	- O-ring leak.
T059	240	27	2.079	0.337	2.1	A	-	-	0	0	14000	-	-	42-50	-	- Membrane meltdown.
T0510	200	20	2.076	0.349	5.8	E	0.77	100.00	13500	2650	11200	1.5	70	42	4400.	
T0511	100	22	2.064	0.356	7.6	F	0.76	100.00	2850	335	14050	0.4	-	50	9000.	
T0512	200	29	2.092	0.341	3.3	A/C	-	-	19050	4350	9790	1.6	70	39	3900.	
T0513	240	26	2.080	0.328	0.0	A	-	-	-	-	-	-	-	-	-	- Membrane meltdown.
T0514	20	5,7,8	1.850	0.418	26.0	3 stages of comp.	-	-	5000	2050	1950	1.5	50	25	3800.	
T0514	20	(Remoulded	-	-	-		-	-	9500	4000	1950	3.7	55	24	3700.	- Multistage compression of remoulded oil sand.
T0514	20	Sample)	-	-	-		-	-	18800	8000	2000	6.8	60	24	3600.	
T0515	200	Cold Lake #128	1.965	0.383	16.1	A/C	-	-	12400	4000	10070	2.0	75	30	3500.	- Cold Lake oil sand membrane leak.
T0516	200	13	2.053	0.358	8.5	A	-	-	-	-	-	-	-	-	-	
T0517	200	23	2.054	0.359	8.8	D	-	-	24875	7555	10275	1.5	65	32	3600.	
T0518	200	24	2.080	0.334	1.2	B	-	-	6980	840	9120	0.5	55	52	5300.	
T0519	125	19	2.084	0.334	1.2	A/C	-	-	21440	4390	10170	1.1	85	41	4500.	

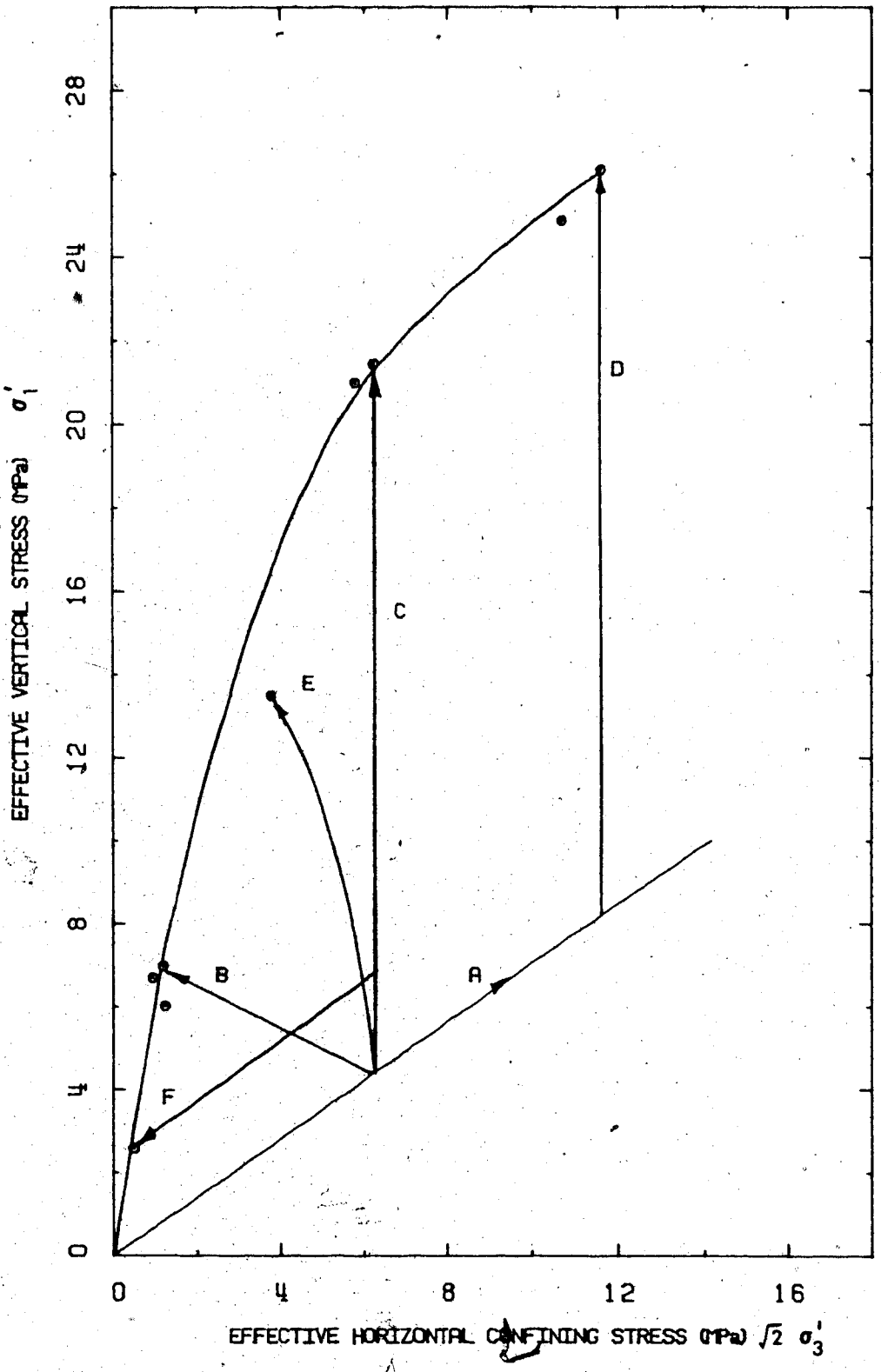

FIGURE 4.14 Strength of Oil Sand for Various Stress Paths

a) Stress path A is isotropic compression; results were discussed in section 4.2.

b) Stress path B is a proportional loading stress path in which the horizontal effective stress (i.e. $\sigma_2' = \sigma_3'$) is decreased while the vertical effective stress, σ_1', is simultaneously increased by reducing the pore pressure. The first stress invariant, J1 is nearly constant along this stress path. This stress path simulates stress changes resulting from excavation of a deep shaft or tunnel.

c) Stress path C is passive triaxial compression in which the horizontal effective stress (i.e. σ_3') is maintained constant at 4 MPa while effective vertical stress is increased. Pore pressure is maintained constant in drained passive compression tests.

d) Stress path D is passive traixial compression in which the horizontal effective stress is maintained constant at 8 MPa while vertical effective stress is increased, similar to stress path C.

e) Stress path E is undrained passive compression in which the horizontal total stress is maintained constant while the vertical total stress is increased. Pore fluid drainage is prevented in undrained tests, therefore pore pressure is observed to increase during passive compression.

f) Stress path F involves anistropic consolidation under an effective horizontal stress of 4 MPa and an effective vertical stress of 6 MPa (i.e. K_o=0.67).

The sample was then heated undrained to failure while monitoring vertical deformations and pore pressure. Pore pressure response during this test was discussed in section 4.3.3.

Saline Creek oil sand was tested following stress paths A, B, C and D at temperatures of 20°C, 125°C and 200°C. Stress path E was investigated only at 200°C. Stress path F was also investigated in a single test on Saline Creek oil sand.

The significant influence of stress path on shear strength of Saline Creek oil sand is illustrated in Figure 4.14. Shear strength increases nonlinearly with effective confining stress. Deviator stress and volumetric strain are plotted against axial strain for each of the six stress paths in Figure 4.15. The influence of stress path on peak deviator stress and stress-strain behaviour is again clearly illustrated. Dilatancy is more pronounced at lower effective confining stress (i.e. stress path B). The failure envelope plotted in triaxial stress space in Figure 4.14 is replotted in Figure 4.16 as shear stress versus effective normal stress. The nonlinear variation of strength with effective confining stress has been summarized in Figure 4.16.1, a plot of the angle of shearing resistance versus the logarithm of effective confining stress. Oil sand is a cohesionless material, i.e. oil sand has zero unconfined compressive strength. There are however, unsaturated heating processes by which oil sand may be altered such that it may acquire nominal cohesive strength. For example:

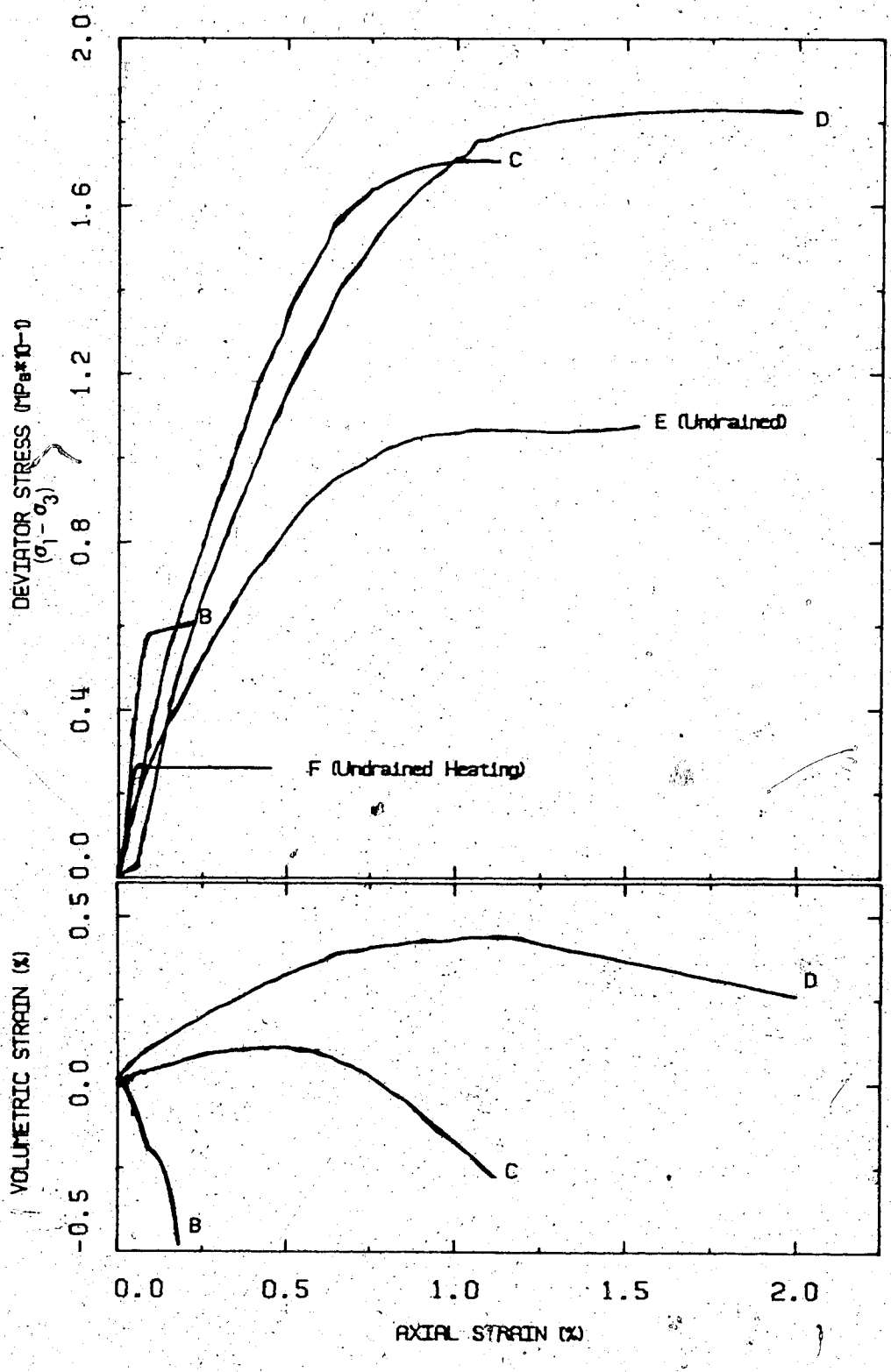

FIGURE 4.15 Stress-Strain Behaviour of Oil Sand for Various Stress Paths

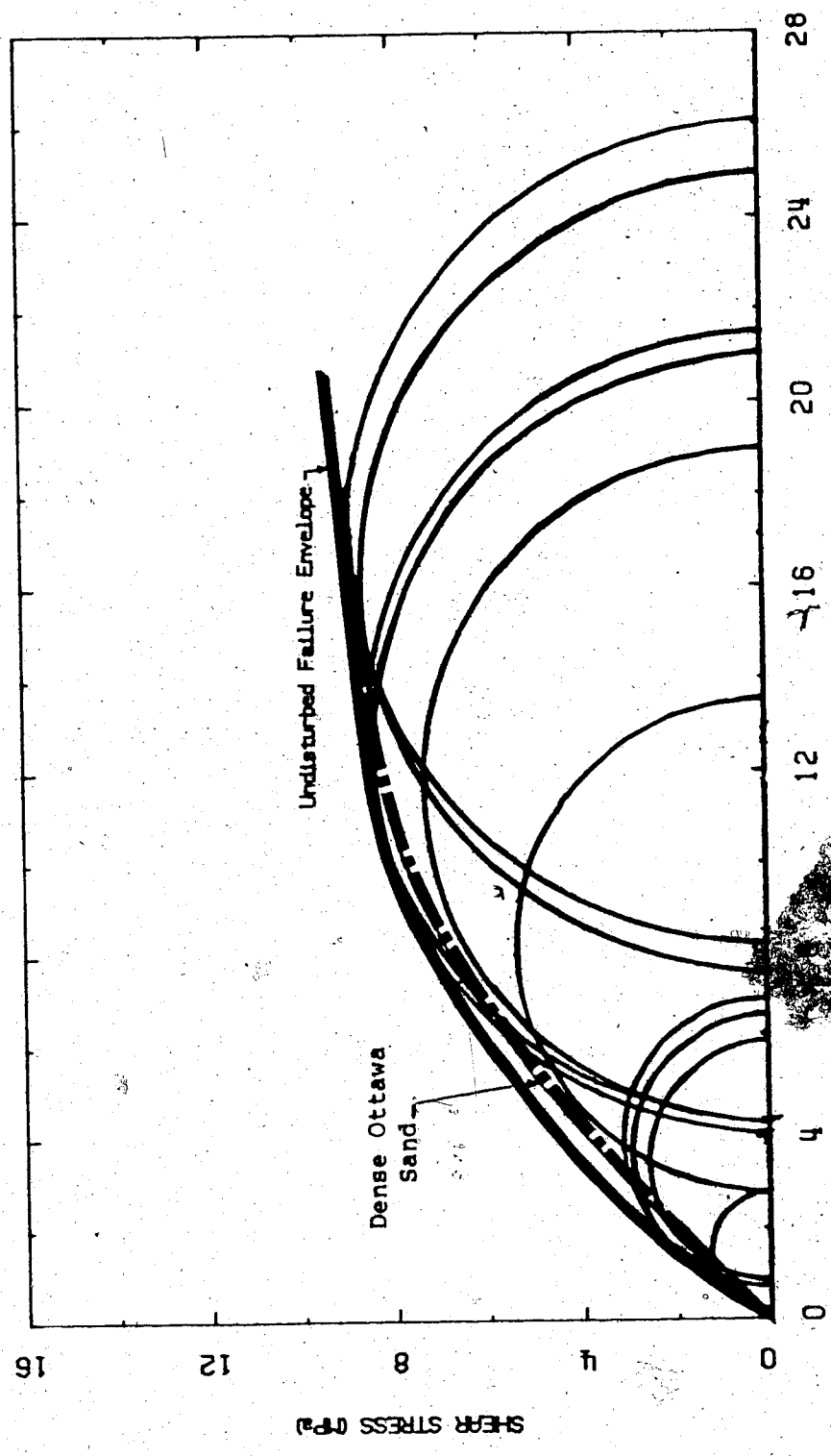

FIGURE 4.16 Strength of Undisturbed Saline Creek Oil Sand

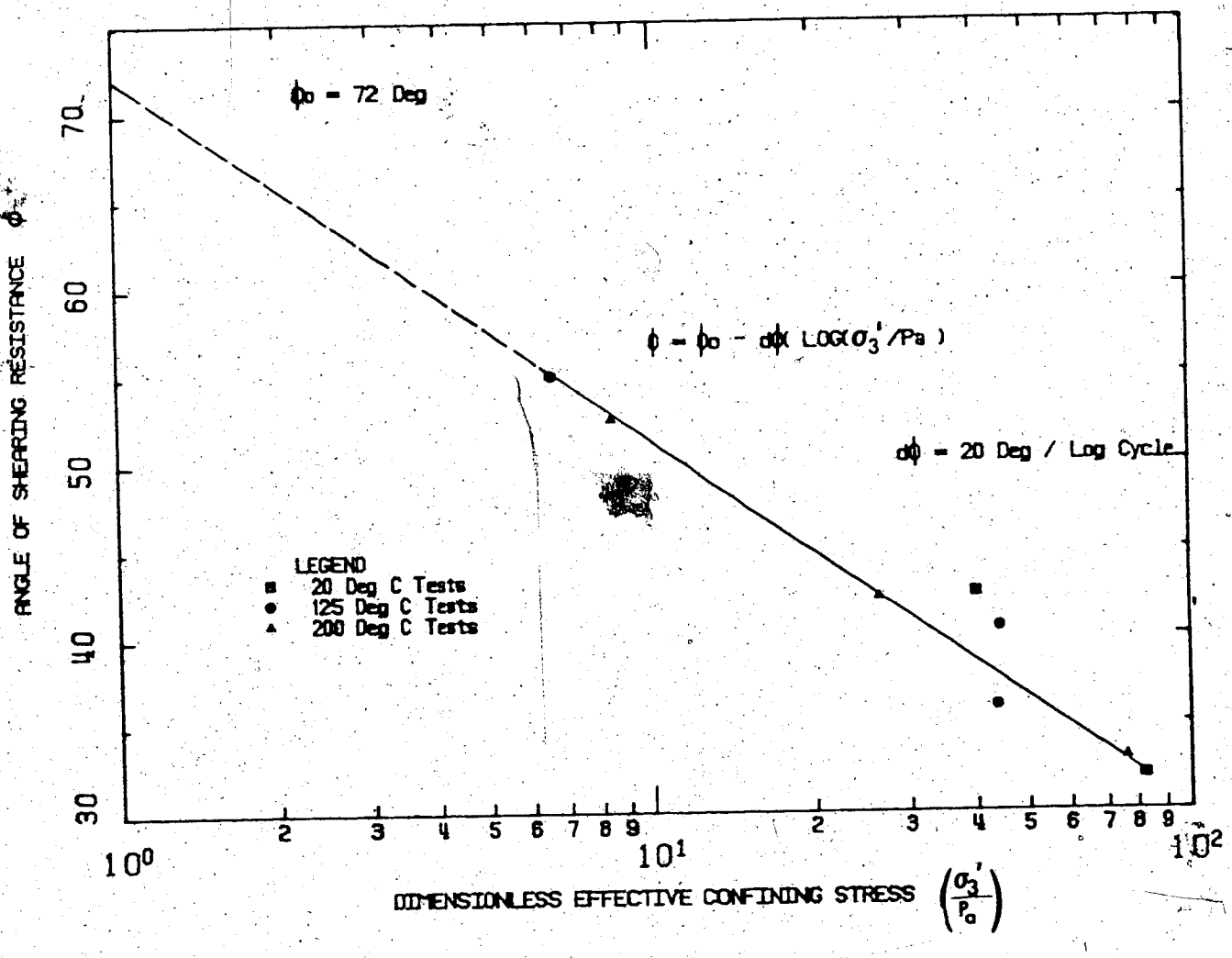

FIGURE 4.16.1 Variation of the Angle of Shearing Resistance for Saline Creek Oil Sand

1. Dusseault (1977) observed "case-hardened" talus bitumen in the basal scree and debris piles along outcrop slopes. Weathering had increased the viscosity of the bitumen, possibly through evaporation of volatiles and oxidation-polymerization of some bitumen components to such an extent that it behaved as a solid. Dusseault states "...at room temperature an inverted specimen displayed no movement after one year.".
2. Case hardening of Athabasca bitumen due to unsaturated heating was demonstrated in plate viscometer tests described in section 3.8.2 of Chapter 3 in this research.
3. A sample of Saline Creek oil sand which originally possessed no true cohesion, (i.e. it crumbled when pressed between the fingers), was oven heated at 150°C for 4 days. After cooldown, the sample was subjected to unconfined compression and found to have unconfined compressive strength of 540 kPa at room temperature, (i.e. unconfined shear strength of approximately 270 kPa). The deformation rate adopted during unconfined testing was 0.060 mm per minute (i.e. approximately 0.04% per minute). A stress-strain curve for this experiment is shown in Figure 4.17. Stress is plotted against time in Figure 4.17.1. Oven drying caused vapourization of pore water and evaporation of volatile hydrocarbons, thereby increasing viscosity of the bitumen. This is similar to the natural case hardening observed by Dusseault. Cohesion derived from highly

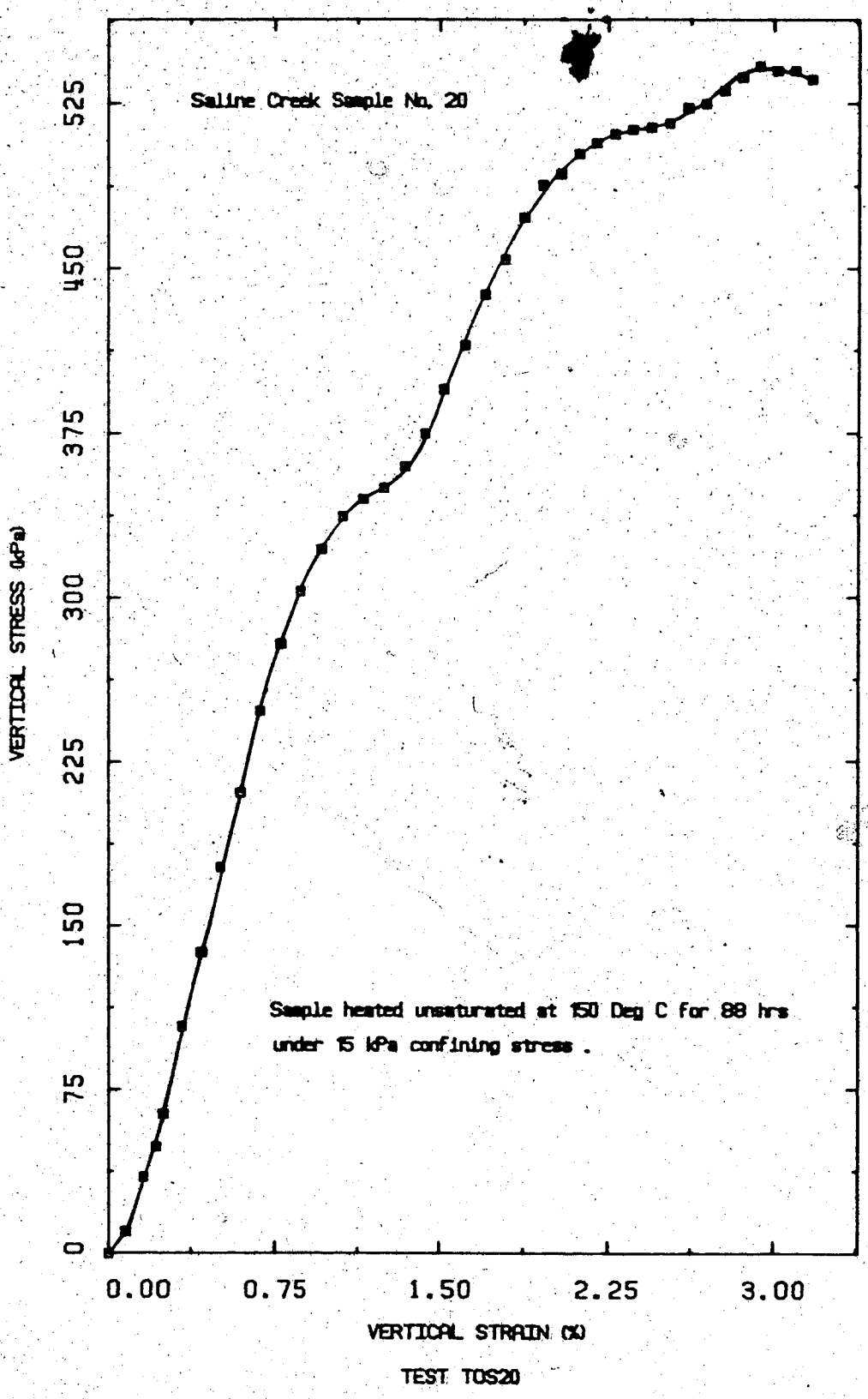

FIGURE 4.17 Unconfined Compression of Case Hardened Oil Sand

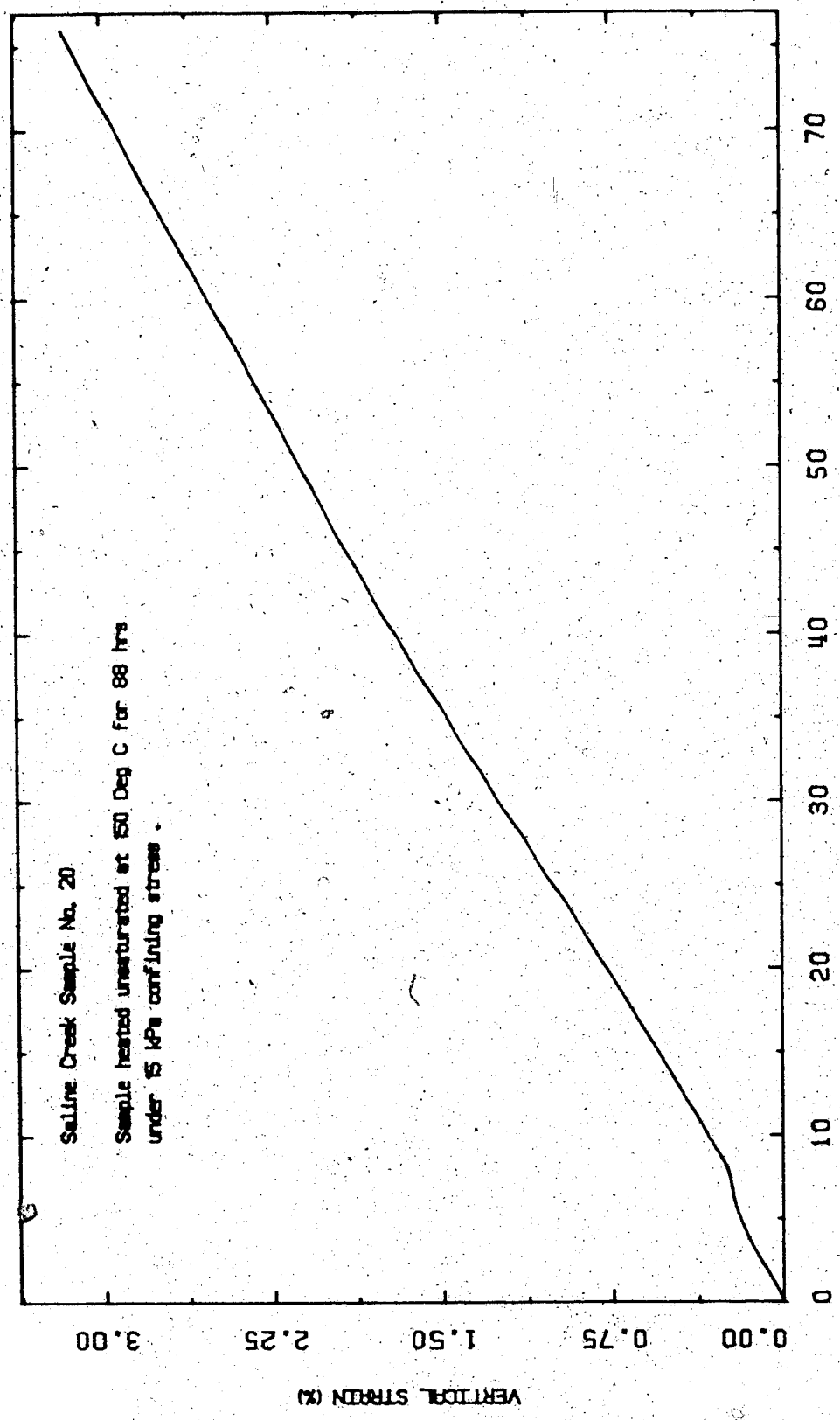

FIGURE 4.17.1 Rate of Strain During Confined Compression

viscous bitumen must be dependent upon strain rate. This simple experiment illustrates a process which may be active if unsaturated heating occurs *in situ*. Details and implications of this process deserve further attention.

4. The University of Calgary Sedimentology Research Group (1981) studied oil sand core from Cold Lake before and after *in situ* steaming. These researchers observed "... the unsteamed core has high oil saturations and is friable, whereas the steamed core is relatively clean and well indurated. The steam process, in addition to stripping the oil appears to have caused considerable *cementation* of the core". Here again unsaturated heating appears to have altered the oil sand and provided a component of cohesive strength. In this case, the researchers have attributed cementation to mineralogical alteration of kaolinite to smectite.

The above examples illustrate that unsaturated heating may give oil sand a component of cohesive strength, either through "case hardening" of the bitumen or due to mineralogic alteration. Saturated heating does *not* have a similar effect. In either case, dense *in situ* oil sand displays frictional behaviour. Both stiffness and strength of oil sand increase with increasing effective normal stress; also dilatancy is suppressed at elevated confining stresses.

4.4.3 Implications of Sample Disturbance

Microfabric disturbance can significantly reduce shear strength and stiffness of oil sand. Hardy and Hemstock (1963), Dusseault and Morgenstern (1978) and others have identified major causes and implications of sample disturbance. Data presented here is intended to quantify the influence of what may have previously been considered rather subtle degrees of disturbance on shear strength and stress-strain parameters for a relatively homogeneous set of oil sand samples from the Saline Creek outcrop.

The influence of sample disturbance on shear strength is summarized in Figure 4.18. A lower bound failure envelope was defined for remoulded Saline Creek oil sand. The remoulded failure envelope is also shown in Figure 4.19, plotted as shear stress versus normal stress. Despite vigorous recompaction, remoulded strength is very much lower than undisturbed strength. It may be noted that remoulded strength (i.e. $\emptyset$ = 25°) is somewhat lower than normally obtained for loose sands (i.e. typically $\emptyset$ = 30°). As discussed in section 3.9.2 and shown in Plate 3.5, remoulding of oil rich oil sand results in segregated clusters (peds) of sand grains. This remoulded fabric is very compressible. It is probable that peak deviatoric stress was not reached due to axial deformation limits of the apparatus in the test on compressible remoulded oil sand (see Figure E14.2, Appendix E). Remoulded porosity varied from 0.39 to 0.41 while the undisturbed strength

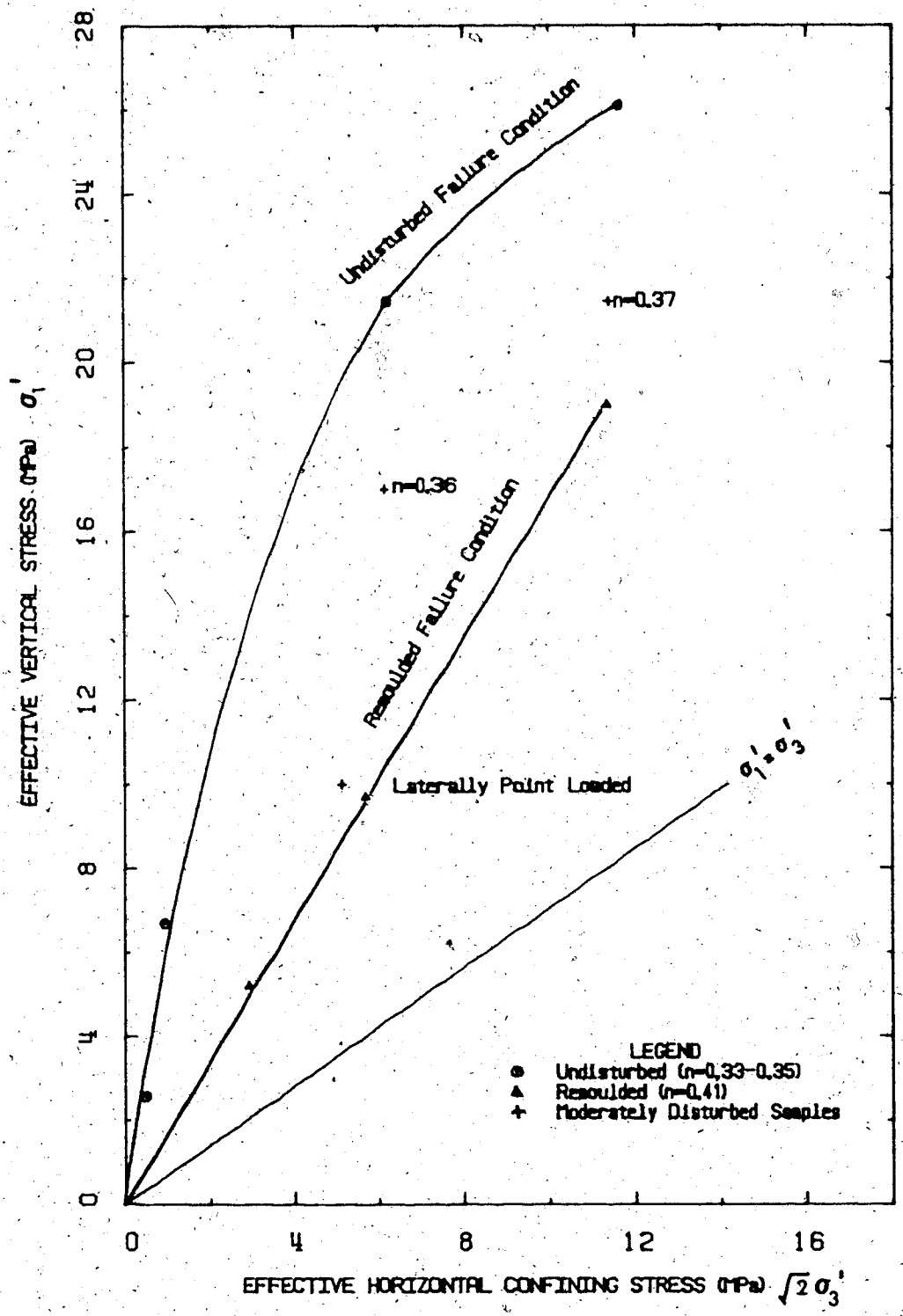

FIGURE 4.18 Effect of Sample Disturbance on Strength of Oil Sand

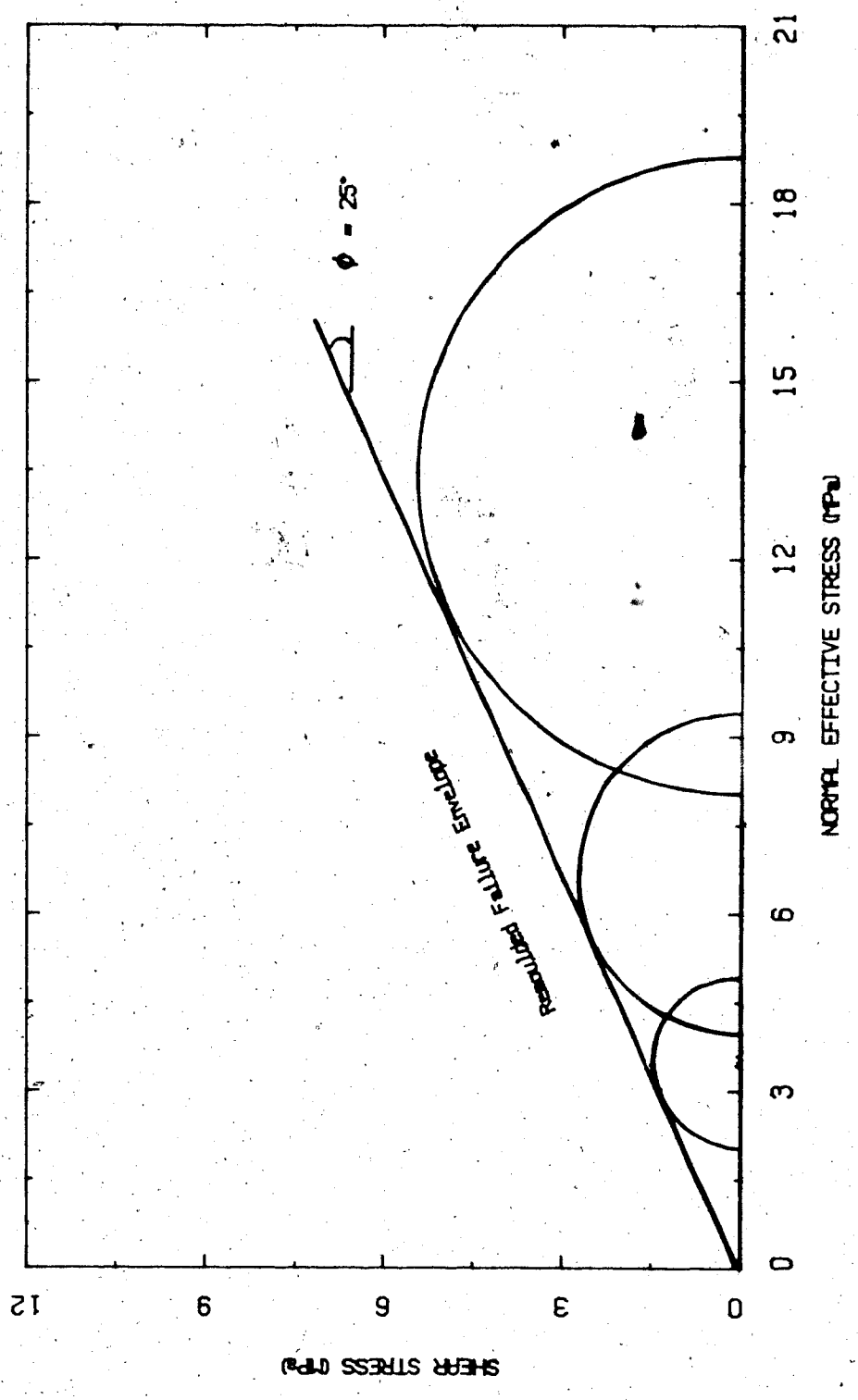

FIGURE 4.19 Strength of Remoulded Saline Creek Oil Sand

envelope was determined for intact samples with initial porosities varying from about 0.33 to 0.35. The dramatic influence of the "locked sand" structure is emphasized by the difference between these lower and upper bound strength envelopes. Intermediate strengths for three slightly disturbed samples are also shown on Figure 4.18. Stress-strain curves for these three slighlty disturbed samples are compared with those of higher quality samples tested under identical conditions in Figures 4.20 to 4.22 inclusive.

Figure 4.20 shows deviator stress and volumetric strain plotted against axial strain for two Saline Creek oil sand samples which were both subjected to passive compression (stress path D) with 8 MPa effective confining stress; both tests were conducted at room temperature (i.e. 20°C). No visible signs of weakness were observed in either sample, however, initial porosities were 0.369 and 0.357 for tests TOS4 and TOS5, respectively. Peak deviator stress in test TOS4 was 13.4 MPa as compared with 17.9 MPa in test TOS5. Despite the significant difference in shear strength of these two samples, initial stiffness and volume change did not differ appreciably. The difference in shear strength is attributed to very subtle (possibly localized) microfabric disturbance manifest by the small initial porosity difference.

Figure 4.21 is a stress-strain plot for two samples subjected to passive compression (stress path C) with 4 MPa effective confining stress and at 125°C. Initial porosities

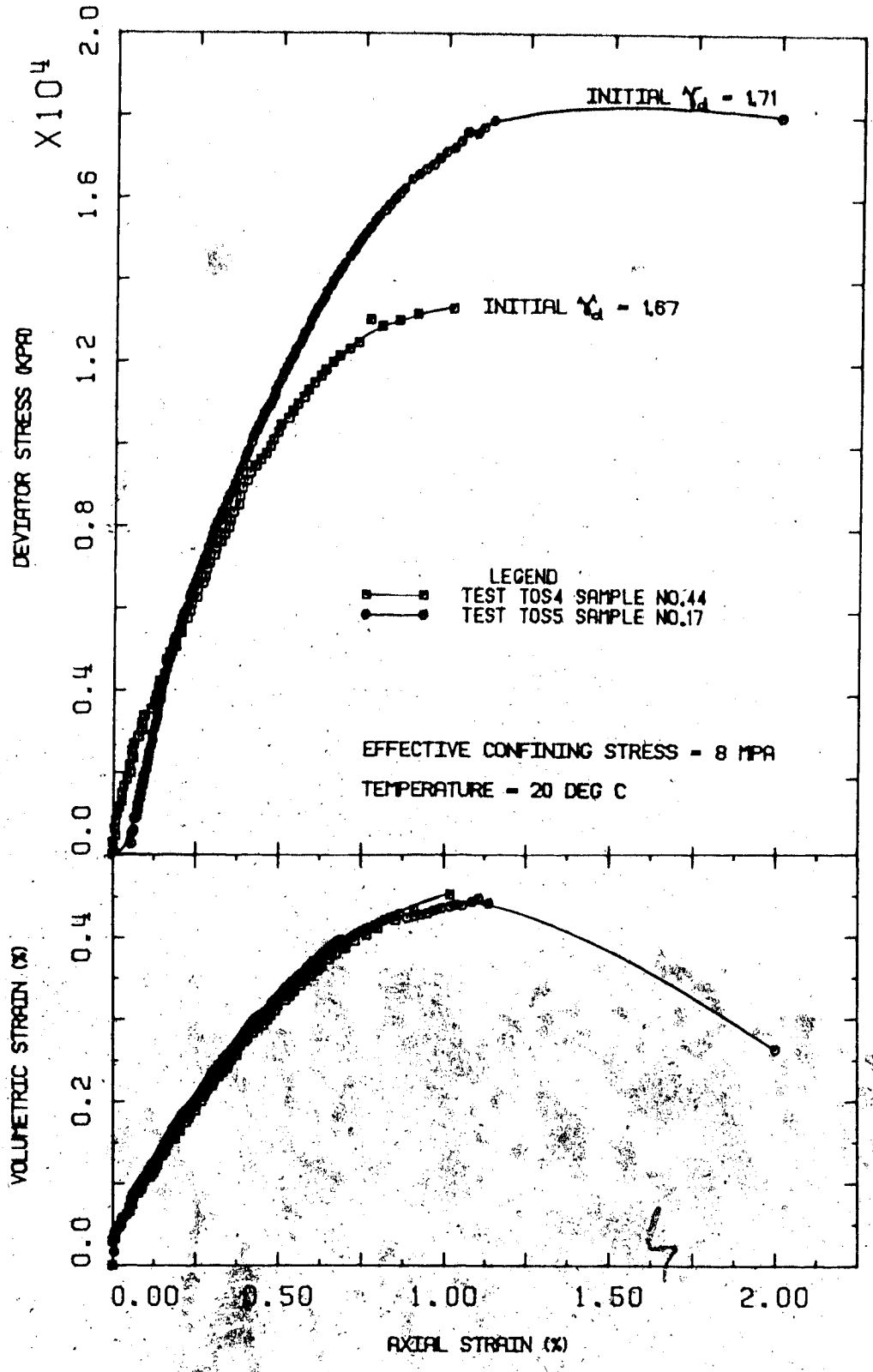

FIGURE 4.20 Effects of Sample Disturbance on Stress-Strain Behaviour of Oil Sand at 8 MPa Effective Confining Stress

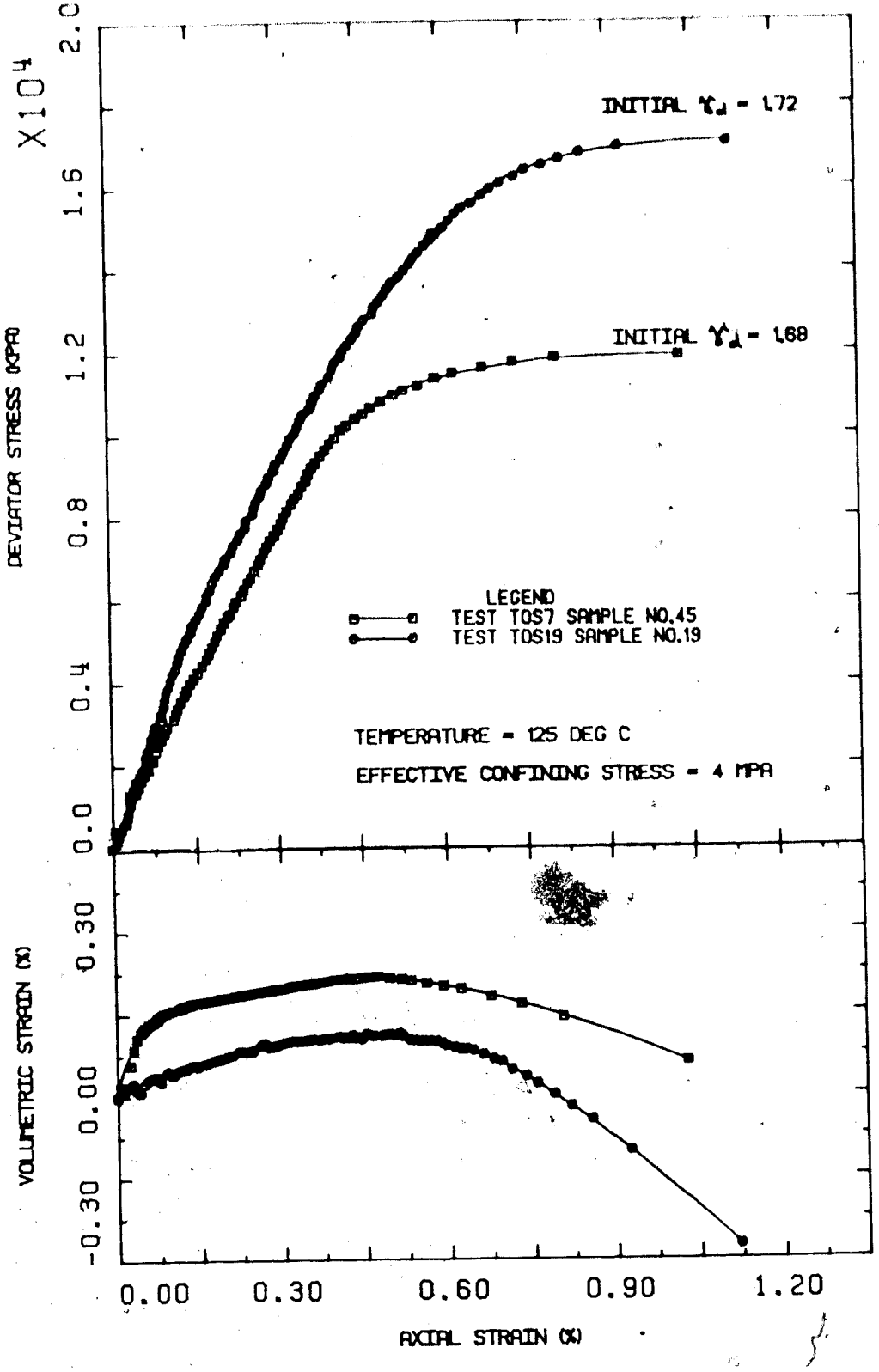

FIGURE 4.21 Effects of Sample Disturbance on Stress-Strain Behaviour of Oil Sand at 4 MPa Effective Confining Stress

were 0.355 and 0.334 for test TOS7 and TOS19, respectively. Peak deviator stresses were 12.7 MPa and 17.1 MPa in test TOS7 and TOS19, respectively. Again, the difference in shear strength of these two samples is attributed to rather subtle differing degrees of initial sample disturbance. The test TOS7 sample was also considerably more deformable (i.e. lower initial stiffness and greater volumetric compression) than the TOS19 sample, despite identical testing procedures.

Stress-strain behaviour in test TOS1 was altered because of horizontal point loading of the sample by the lateral strain gauge clamp. As previously discussed, this device is not considered to be suitable for oil sand. Figure 4.22 shows stress-strain plots for tests TOS1 and TOS2; initial porosities of these two samples were 0.334 and 0.340. Test conditions were identical for both samples: passive compression stress path C was followed with room temperature conditions (20°C), except that lateral deformation was constrained in one direction by the presence of a lateral strain gauge clamp in test TOS1. The lateral restraint resulted in the development of tensile stresses in a plane orthogonal to the plane of the strain gauge clamp (i.e. similar to boundary conditions in the Brazilian tensile strength test). The dramatic influence of this form of test-induced sample disturbance on both shear strength and stress-strain behaviour is clearly illustrated in Figure 4.22.

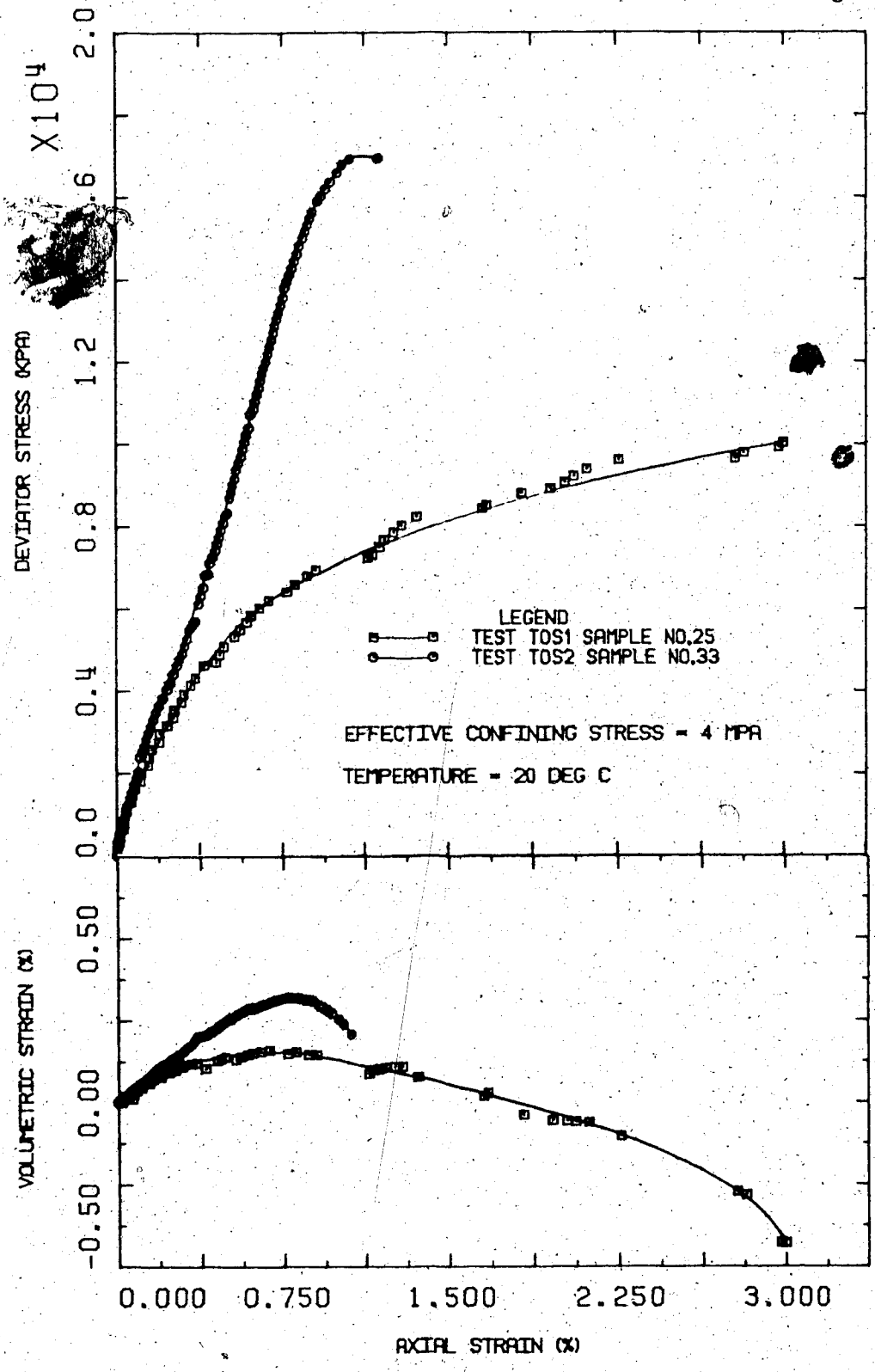

FIGURE 4.22 Effects of Lateral Point Loading on Stress-Strain Behaviour of Oil Sand

4.4.4 Influence of Elevated Temperatures

The influence of elevated temperatures on shear strength and stress-strain behaviour was studied by testing similar high quality undisturbed samples of Saline Creek oil sand at temperatures of 20°C, 125°C and 200°C. Figure 4.23 is a summary plot of effective stresses at failure for these tests. Failure envelopes are shown at 20°C and 200°C. It is evident that temperatures up to 200°C have little practical effect on shear strength. In fact, as illustrated in section 4.4.3, very subtle microfabric disturbance may account for greater scatter of test results than that shown in Figure 4.23. Operative pore pressure (including pore pressure increase and rate of dissipation) during heating is of far greater practical importance in determining available shear strength. Nevertheless, several interesting observations related to this influence of temperature on strength and stress-strain behaviour may be drawn from these test results.

Figure 4.24 is a plot of stress-strain curves comparing three triaxial compression tests following stress path B (i.e. constant) at temperatures of 20°C, 125°C and 200°C. Initial stiffness and strength are greater for the 125°C test than the 20°C test and intermediate at 200°C. Dilatant volumetric strain was observed prior to shear failure in all three tests, however dilatancy was maximum at 125°C and of intermediate magnitude at 200°C. Figure 4.25 is a stress-strain plot of three tests following stress path C (i.e.

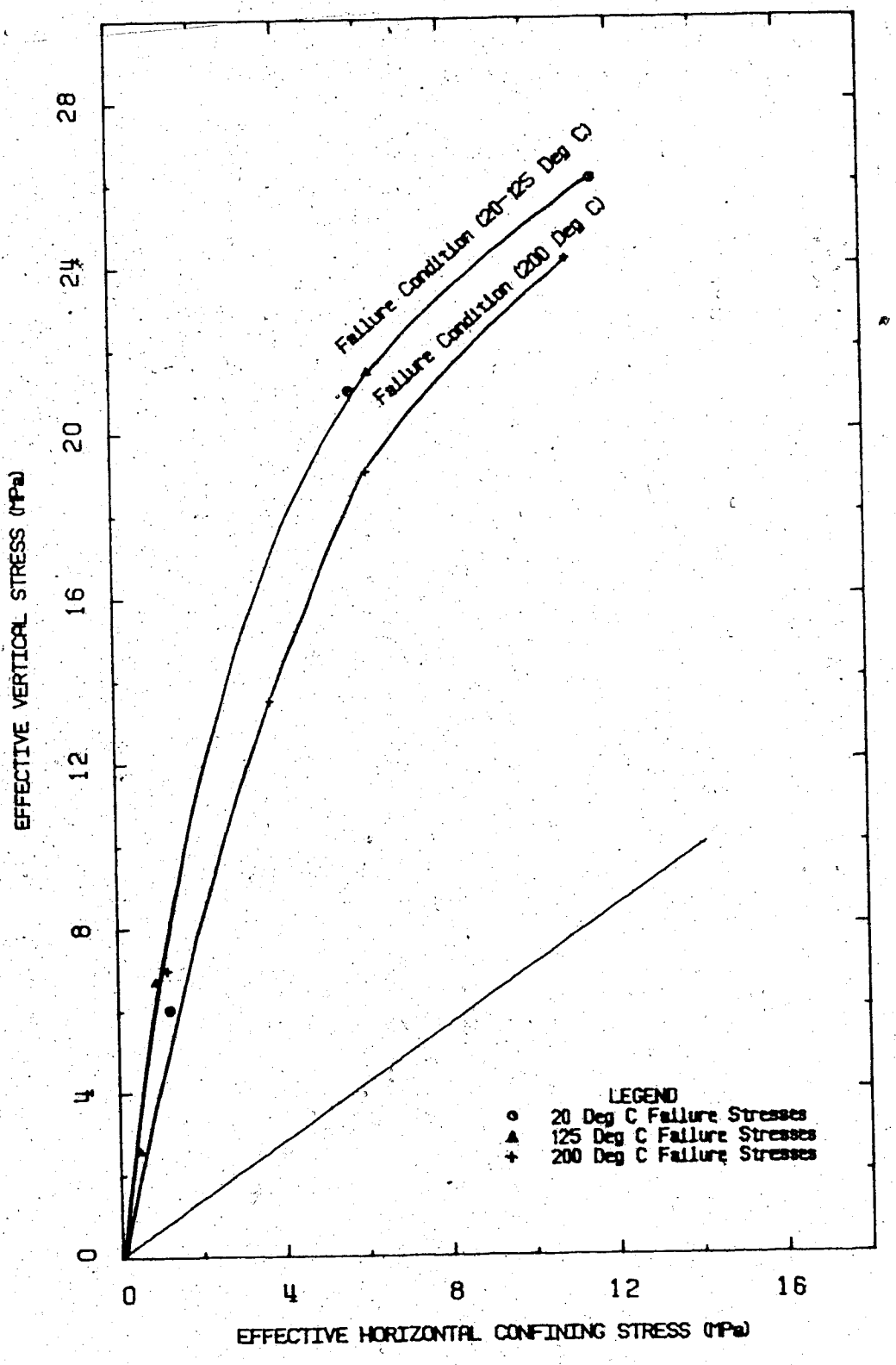

FIGURE 4.23 Effect of Temperature on Strength of Oil Sand

passive compression at 4 MPa effective confining stress). Again, the 125°C test resulted in greater initial stiffness, dilatancy and shear strength than the 20°C test. Shear strength (i.e peak deviator stress) was least at 200°C, however initial stiffness of the 200°C sample was slightly greater than the 20°C sample. Figure 4.26 is a stress-strain plot comparing two triaxial compression tests following stress path D (i.e passive compression at 8 MPa effective confining stress) at temperatures of 20°C and 200°C. Stress-strain behaviour is very similar in both tests. Initial stiffness of the 200°C sample is slightly greater than that of the 20°C sample. Interestingly, dilatant volumetric strain was observed prior to shear failure in both tests, despite the relatively large magnitude of effective confining stress.

Observed changes of stress-strain behaviour with temperature shown in Figures 4.24 to 4.26 are undoubtedly due in part, to material heterogeneities. Nevertheless several observed effects of elevated temperatures on stress-strain behaviour are consistent with pore volume changes observed during drained thermal expansion testing:

a) Figure 4.27 is a summary plot of the logarithm of initial tangent modulus versus the logarithm of effective confining stress. Figure 4.27 illustrates that the initial stiffness increases slightly at elevated temperatures; also stiffness is greater at 125°C than at 200°C.

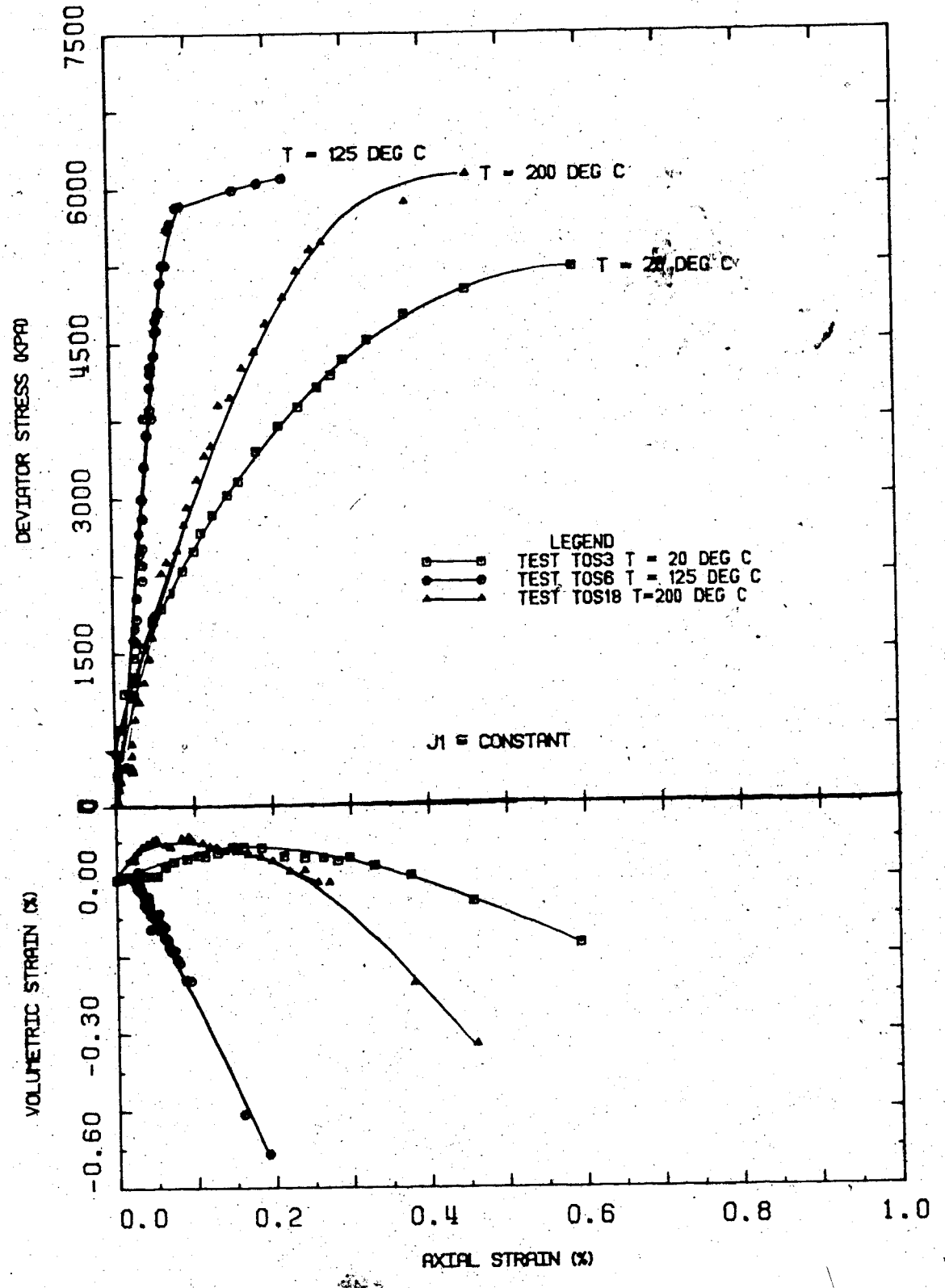

FIGURE 4.24 Effect of Temperature on Stress-Strain Behaviour for Stress Path B

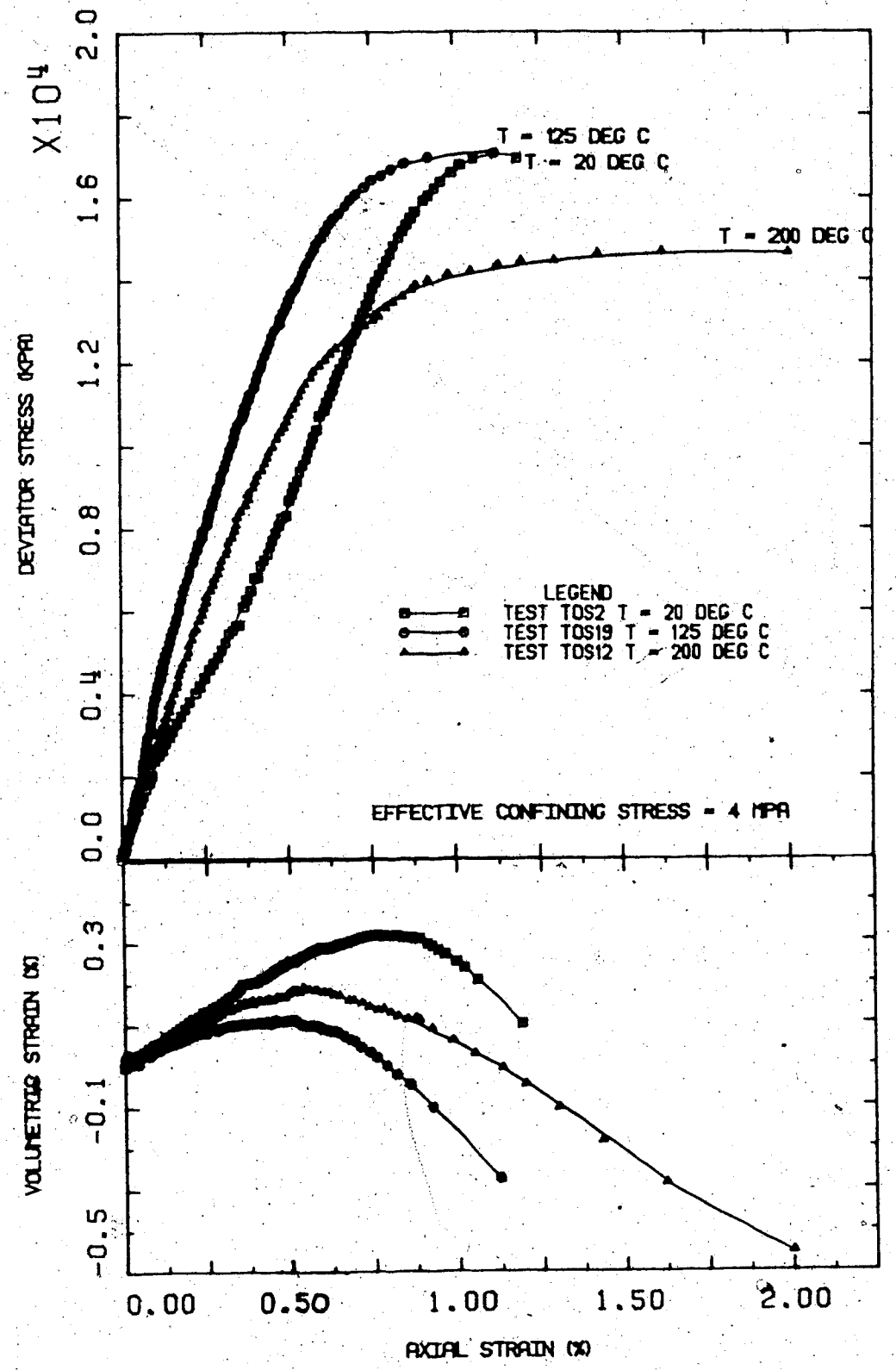

FIGURE 4.25 Effect of Temperature on Stress-Strain Behaviour for Stress Path C

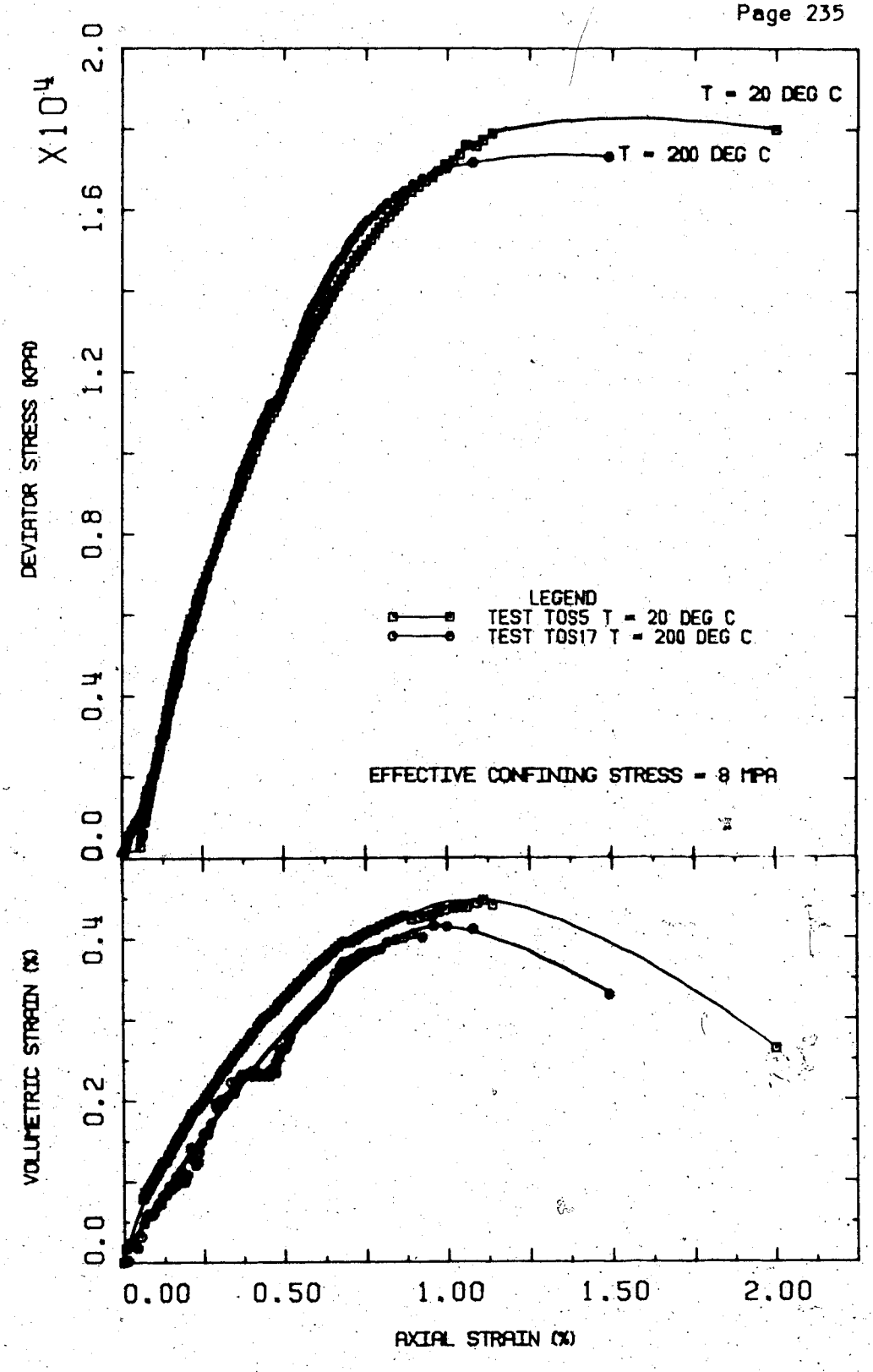

FIGURE 4.26 Effect of Temperature on Stress-Strain Behaviour for Stress Path D

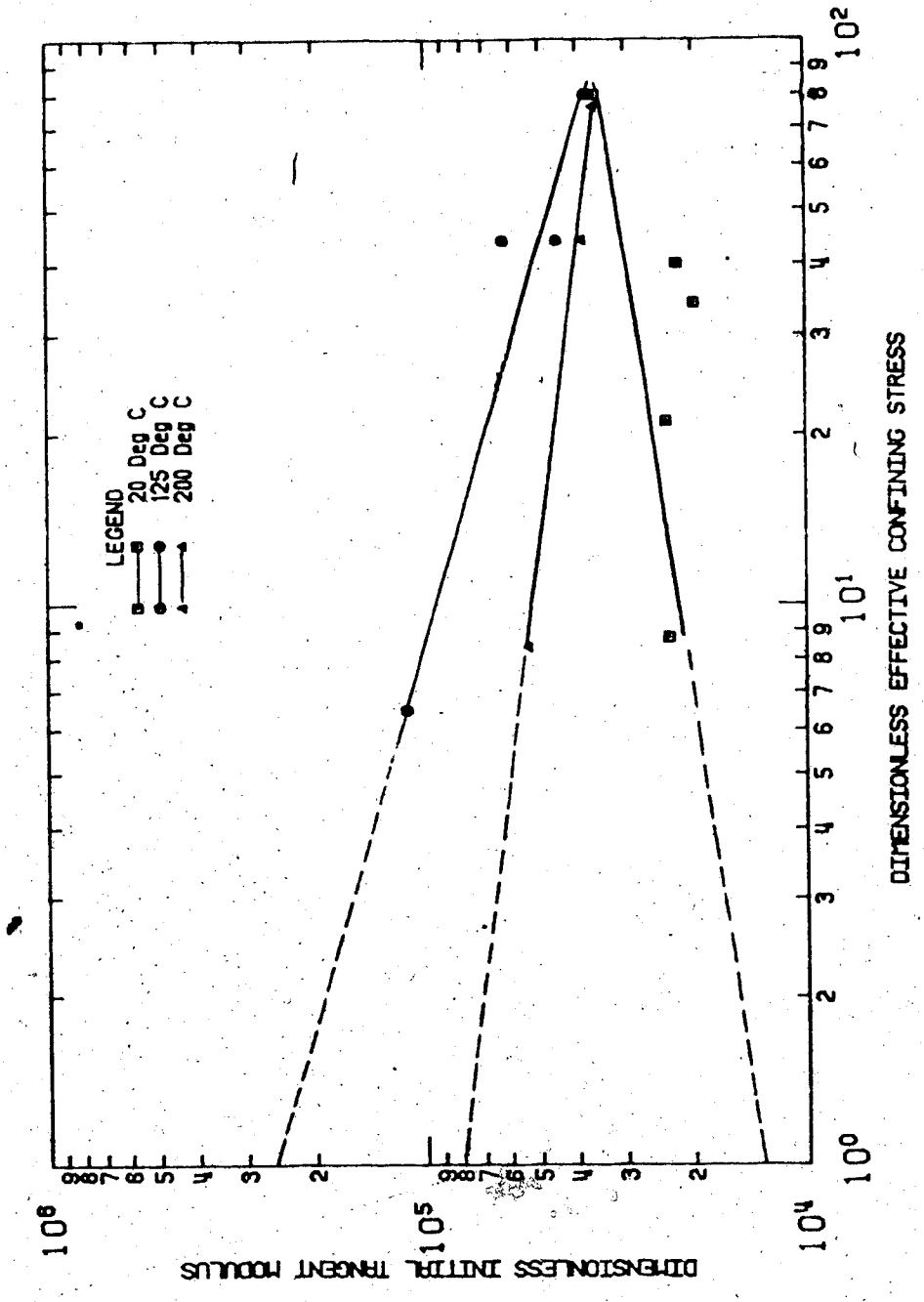

FIGURE 4.27 Variation of Initial Stiffness of Oil Sand with Effective Confining Stress

b) Volumetric compression during deviatoric loading is suppressed slightly at elevated temperatures.

c) Dilatant volume change (below the peak deviator stress) is increased at elevated temperatures; dilatancy is greater at 125°C than at 200°C.

4.4.5 Stress-Strain Behaviour of Cold Lake Oil Sand

A single sample of oil sand from the Clearwater Formation at Cold Lake was tested in triaxial compression for general comparison with Saline Creek oil sand. The test was performed at 200°C: three cycles of isotropic compression to 17 MPa (i.e. stress path A) were followed by passive triaxial compression along stress path C at 4 MPa effective confining stress. Stress-strain behaviour of the Cold Lake oil sand is compared with that of Saline Creek oil sand under identical test conditions in Figure 4.28. Stiffness and shear strength of the Cold Lake oil sand sample are much lower than stiffness and shear strength of the Saline Creek oil sand sample. The initial porosity of the Cold Lake sample was 0.383 while that of the Saline Creek sample was 0.341. Although the higher porosity of the Cold Lake sample is due in part to sample disturbance, average in situ porosity may in fact be higher in the Clearwater Formation at Cold lake. For example, Mainland (1983) reported that average in situ porosity of Clearwater Formation oil sand on Esso Resources Canada Limited leases at Cold Lake was 0.35. This suggests that the Clearwater Formation oil sands of Cold Lake may be more deformable in situ

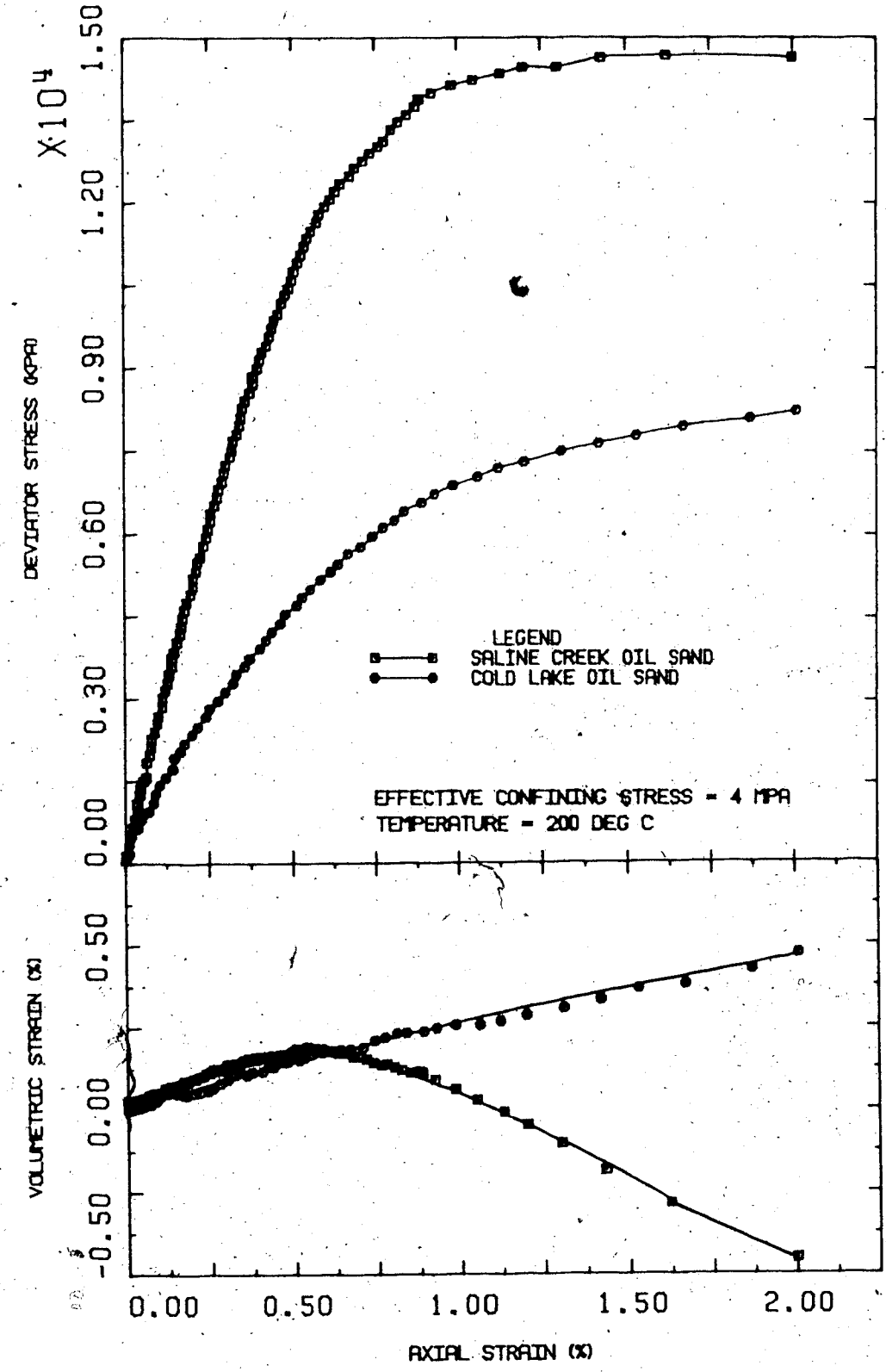

FIGURE 4.28 Comparison of Stress-Strain Behaviour and Strength of Saline Creek and Cold Lake Oil Sands at 4 MPa Effective Confining Stress and 200°C

than the McMurray Formation oil sands of the Athabasca region, in part, because of the higher natural porosity. Also, scanning electron microscope and x-ray diffraction analyses revealed that the Cold Lake material included a substantial portion (i.e. approximately 50%) of weaker minerals such as feldspar and siliceous volcanic particles along with quartz. Imperial Oil Limited (1978) published similar mineral compostion data in an application to the Energy Resources Conservation Board of Alberta for the Cold Lake Project. The presence of these weaker minerals also probably contributed to the lower shearing resistance observed in this test relative to that of the primarily quartzose Saline Creek oil sand.

4.5 Permeability

4.5.1 Permeability Parameters

Several proposed in situ extraction processes for oil sands involve hydraulic fracturing by injecting pressurized water at ambient temperatures (i.e. generally less than 20°C) to enhance fluid flow between injection and production wells. Subsequent heating by injection of condensed steam and/or by in situ combustion is intended to decrease viscosity of bitumen allowing recovery by pumping or gravity drainage. Some enhanced recovery schemes take advantage of a bottom layer of "water-bearing", oil free sand to establish interwell communication (eg. Huygen and Lowry, 1983) and a number of other variations have been employed depending upon local geologic conditions.

Permeability properties of oil sand over a wide range of temperatures (i.e. approximately 5°C to 250°C or more) and fluid saturations have a bearing on both reservoir production and in situ pore pressure response.

The term "permeability" is associated with the ability of a porous medium to conduct fluids. By analogy with electrical conductors, permeability represents the reciprocal of the resistance of the porous medium to fluid flow. Darcy (1856) established a relationship between average flow velocity and pressure gradient for water flow vertically downward through sand filters. Darcy's Law as commonly used in geotechnical engineering may be expressed by the following equation:

$$v = -k_h i \qquad (4.17)$$

where: v denotes average flow velocity

i denotes the hydraulic pressure gradient in the direction of flow; and

k_h is a constant of proportionality referred to as "hydraulic conductivity".

Darcy's Law as stated in equation 4.17 is only strictly valid for pure water under standard conditions of temperature and pressure, i.e. 60°F (15.6°C) and atmospheric pressure (101.3 kPa). Also, Darcy' Law is valid only for conditions of laminar flow, i.e. at very high pressure gradients flow becomes turbulent and average flow velocity is no longer a

linear function of pressure gradient. Despite these limitations Darcy's Law, in the form presented in equation 4.17, has been widely applied in geotechnical engineering and hydrogeology.

Later investigators (eg. Wyckoff and Botset, 1936) found that Darcy's Law could be restated in more fundamental terms to include both liquid and gaseous viscous fluids other than water, and for temperatures and pressures other than standard conditions. Laminar, one dimensional fluid flow through porous media may be described as follows:

$$v = -\frac{k}{\mu}\frac{\partial \Phi}{\partial s} \qquad (4.18)$$

where: k denotes absolute permeability of the porous medium.

μ denotes dynamic viscosity of the fluid phase.

Φ is a potential function (i.e. $\Phi = P + \rho gz$); and

s denotes distance in the direction of the flow.

The form of Darcy's Law described by equation 4.18 provides a useful conceptual framework for fluid flow in petroleum reservoirs where a range of pore fluid types, pressure and temperature conditions are commonly encountered.

Table 4.6 compares equivalent values of hydraulic conductivity and water permeability for room temperature water flow. Note that water permeability values refer either to effective or absolute permeability; also the reader is

TABLE 4.6

Comparison of Common Units of
Hydraulic Conductivity and Water Permeability
at 22°C assuming μ_w = 1 cp = 1 mPa.s

Hydraulic * Conductivity	EFFECTIVE PERMEABILITY TO WATER	
	k_w	k_w
(cm/s)	(m^2)	(millidarcys)
1	10^{-9}	10^6
10^{-1}	10^{-10}	10^5
10^{-2}	10^{-11}	10^4
10^{-3}	10^{-12}	10^3
10^{-4}	10^{-13}	10^2
10^{-5}	10^{-14}	10
10^{-6}	10^{-15}	1
10^{-7}	10^{-16}	10^{-1}
10^{-8}	10^{-17}	10^{-2}

* Hydraulic Conductivity: $k_h = \frac{k_w \gamma_w}{\mu_w}$

At Room Temperature: 1 Darcy = 10^{-3}cm/s

Note: Hydraulic Conductivity values are approximate

cautioned that these are not "hard conversions" i.e. values are approximate only.

The pore space of oil sand is generally occupied by two or three immiscible fluid phases including bitumen, water and/or gas. Where more than one fluid type is present and the fluids are immiscible, the concept of effective permeability is useful. In the definition of effective permeability each fluid phase is considered to be completely independent of other fluids in the pore network. Darcy's Law can be restated separately for one dimensional flow of each fluid phase as follows:

$$\left.\begin{aligned} V_o &= -\frac{k_o}{\mu_o}\frac{\partial \Phi_o}{\partial s} \\ V_w &= -\frac{k_w}{\mu_w}\frac{\partial \Phi_w}{\partial s} \\ V_g &= -\frac{k_g}{\mu_g}\frac{\partial \Phi_g}{\partial s} \end{aligned}\right\} \qquad (4.19)$$

The subscripts o, w, and g denote oil, water and gas, respectively.

The effective permeability is a relative measure of the conductance of the porous medium for one fluid phase when the medium is saturated with more than one fluid. Effective permeability then is a function of the prevailing fluid saturations. Experimental evidence has established that effective permeability is also a function of the "rock-wetting" characteristics (Amyx, Bass and Whiting, 1960), i.e. the

distribution of the various fluid phases in the porous medium. For example, when the solid mineral grains are preferentially water-wet, as is the case in some Alberta oil sands, the water phase loses its mobility at a higher value of water saturation than when the mineral grains are preferentially oil-wet. Conversely, in a water-wet oil sand medium the effective permeability to oil, k_o, is greater over a range of water saturation, than if the medium were oil-wet. Effective permeability then must be specified as a function of fluid saturations and in the context of "rock-wetting" characteristics.

Effective permeability data is often transformed into a dimensionless form referred to as relative permeability. Relative permeability is defined as the ratio of effective permeability of a fluid at a given saturation level to the effective permeability at 100 percent saturation. It is often assumed that the effective permeability is the same for all fluids at 100 percent saturation, this value being the absolute permeability of the medium. Relative permeability may be expressed symbolically as:

$$\left.\begin{aligned} k_{ro} &= \frac{k_o}{k} \\ k_{rw} &= \frac{k_w}{k} \\ k_{rg} &= \frac{k_g}{k} \end{aligned}\right\} \qquad (4.20)$$

which are relative permeabilities to oil, water and gas, respectively.

Important factors which affect relative permeability and effective permeabilty are: prevailing fluid saturations (S_o, S_w, S_g), "rock-wettability", pore geometry properties (i.e. rugosity, tortuosity) and saturation history; also effective stress level, temperature, clay mineralogy and physico-chemical interaction of the mineral grains and pore fluids influence absolute permeability. The presence of small amounts of clay minerals in oil sand is believed to be an important factor in interpreting permeability test results. Clay minerals which are present in undisturbed core samples are removed along with bitumen and water during solvent extraction processes (i.e. during soxhlet refluxing with toluene or benzene). Samples reconstituted using solvent extracted sand are therefore not entirely representative of in situ grain size distribution or absolute permeabilty. Mobility of clay minerals during hot water flooding may also influence pressure gradients and ultimate oil recovery.

Substantial research effort is on-going in a number of disciplines (eg. notably petroleum engineering, geotechnical engineering and chemical engineering) to evaluate the influence of these various factors on permeability properties of oil sand. A major contribution can be made by geotechnical engineering research in obtaining and testing high quality undisturbed core samples.

Results of a series of permeability experiments on both undisturbed and remoulded Saline Creek oil sand samples are presented in the following sections.

4.5.2 Absolute Permeability

Absolute permeability was determined for both a remoulded and an undisturbed sample of oil-free oil sand. An oil-free sample of McMurray Formation oil sand from the High Hill River near Fort McMurray was recompacted in the consolidometer test cell to a dry density of 1.67 Mg/m^3 (i.e. porosity of 0.37), then confined with a vertical effective confining stress of 3 MPa. Permeability of this sample to water measured at room temperature (20°C) was $3.0 \times 10^{-12} m^2$; i.e. this is equivalent to a value of hydraulic conductivity of approximately $3.0 \times 10^{-3} cm/s$. Detailed results of test CPERM3 are presented in Appendix D.

A second sample of undisturbed (frozen), oil-rich sand from Saline Creek was confined in the consolidometer under 2 MPa effective vertical confining stress. All of the bitumen was then removed from the sample by cyclic soaking and flushing with benzene over a ten day period. The initial porosity of the flushed sample was 0.35. Residual benzene was removed from the sample by flushing the oil-free sample with acetone and finally water. Absolute permeability to water was measured at room temperature (22°C) over a range of effective confining stresses from 2 MPa to 18 MPa. After the effective stress was cycled back to 2 MPa, the sample was heated to 150°C and permeability to water was again measured over a range of stresses from 2 MPa to 18 MPa. Results of this test are summarized in Figure 4.29. Measured permeability to water

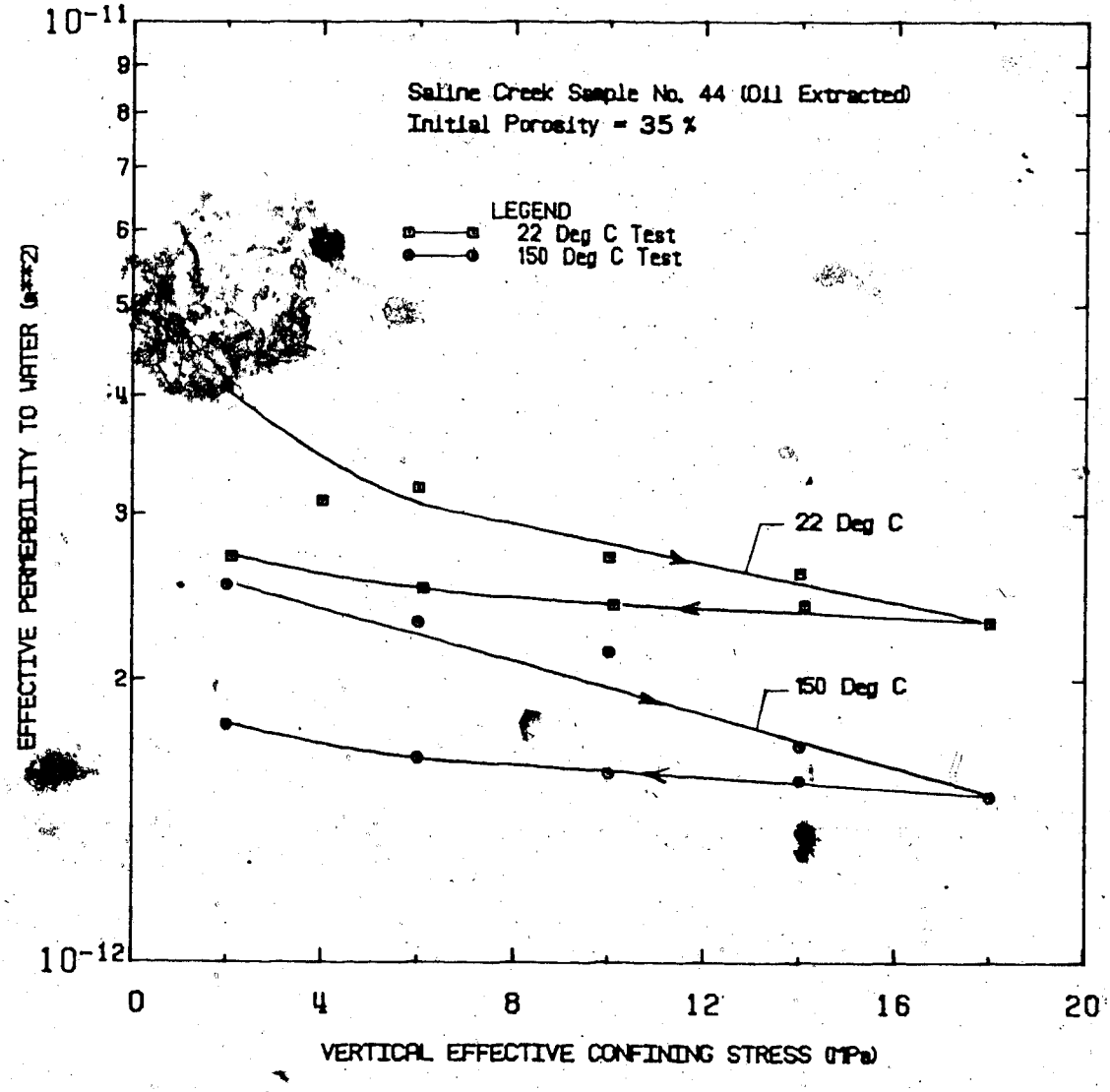

FIGURE 4.29 Absolute Permeability of Oil Sand with Confining Stress and Temperature

ranged from 4.2 x $10^{-12}m^2$ to 1.6 x $10^{-12}m^2$ (4200 to 1600 millidarcys) over the range of applied stresses and temperatures. Figure 4.29 indicates a trend of slight decrease in water permeability with effective confining stress and further small reduction after heating to 150°C and cycling the effective compressive stress between 2 MPa and 18 MPa.

It must be recognized, however, that experimental error (due to precision of monitoring devices) is approximately $\pm 0.4 \times 10^{-12}m^2$ ($\pm$400 millidarcys) in each of these permeability measurements. For practical purposes there is no appreciable influence of elevated temperature on absolute permeability and only a very small decrease in absolute permeability with effective stress cycling. These observations are consistent with the very small pore volume changes observed during drained heating and compression tests.

4.5.3 Permeability Changes with Temperature and Bitumen Saturation

A series of permeability experiments were performed on oil rich Saline Creek oil sand samples at temperatures from 20°C to 250°C. Effective vertical confining stress was maintained at 3 MPa in each of these tests. The dynamic viscosity of Saline Creek bitumen is approximately 300,000 mPa.s at 20°C (i.e. 1 mPa.s = 1 cp); it was determined that the bitumen was essentially immobile in room temperature permeability experiments. Initial bitumen (oil) saturation of the samples

tested varied from 81-88 percent of the sample pore volume. Room temperature effective permeability to water of these samples was approximately $1.0 \times 10^{-14} m^2$ (i.e. 10 millidarcys) on average.

At elevated temperatures of 100°C, 150°C, 200°C and 250°C, the bitumen viscosity decreased and bitumen was flushed out of the sample pore space during circulation of heated water. By measuring pressure drop across the sample and the combined flow rate of the water and bitumen a combined value of fluid mobility, k/ , for bitumen and water can be determined using equation 4.18 (Darcy's Law) as the experiment proceeds. Fluid mobility determined in this manner, is plotted against flow volume in Figure 4.30 for permeability tests on undisturbed Saline Creek oil sand samples at temperatures up to 250°C. The bitumen and water content were determined before and after each test. As shown in Figure 4.30 the logarithm of fluid mobility increases as heated water flows through the sample reducing the oil (bitumen) saturation. Bitumen saturation (S_o) was reduced from 81% to 73% at 100°C in test CPERM4. Bitumen saturation decreased from 88% to a residual saturation of 52% during the 150°C experiment, test CPERM6. Eleven pore volumes of 150°C water were injected into the sample during test CPERM8, however the fluid mobility did not increase after about 4.8 pore volumes of flow. None of the other elevated temperature flow tests were continued to a similar fluid mobility "plateau". It is believed that the fluid mobility remained constant beyond 4.8 pore volumes of flow since little

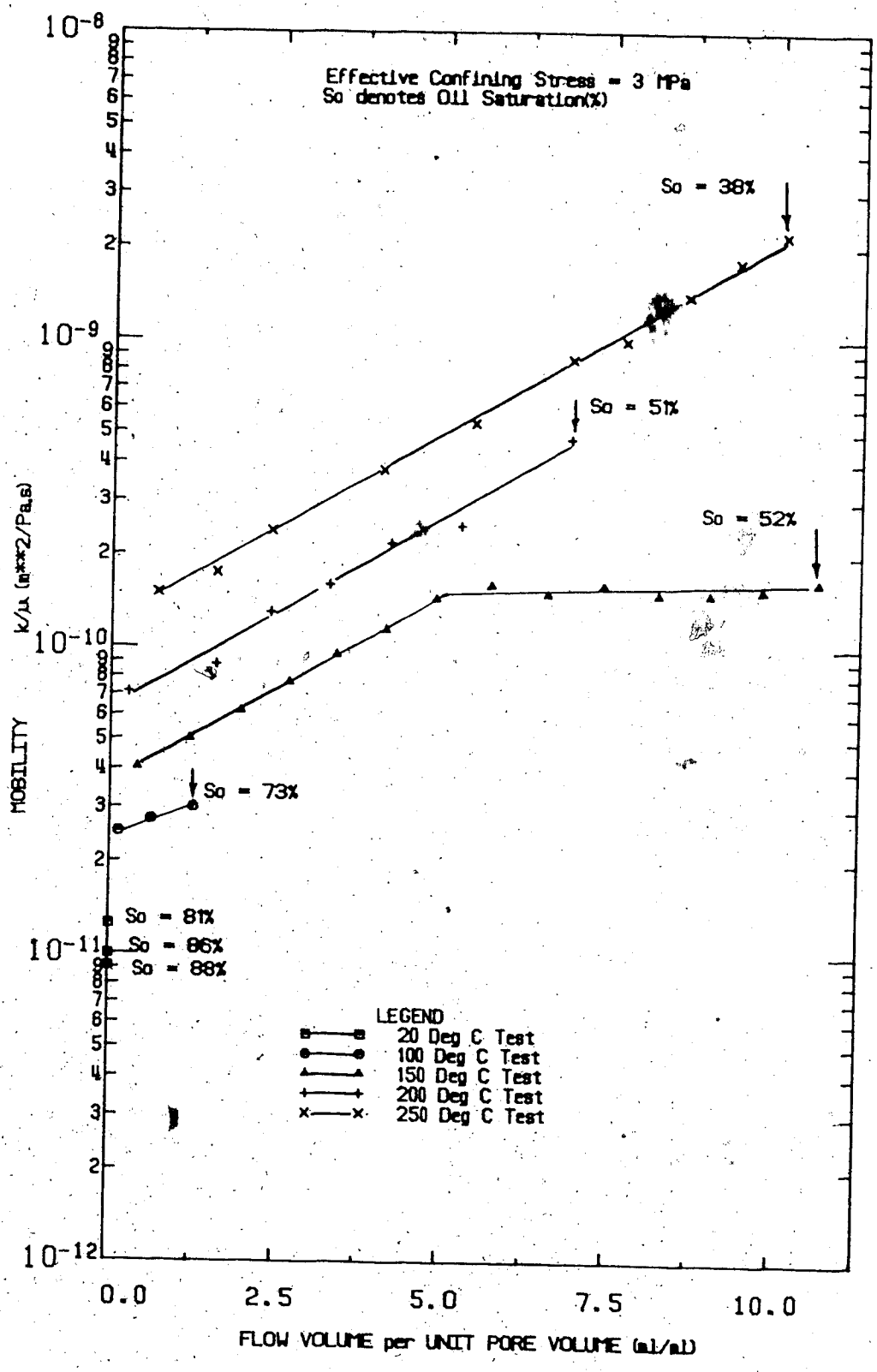

FIGURE 4.30 Fluid Mobility Variation in Saline Creek Oil Sand During Hot Water Flooding Experiments at Elevated Temperatures

or no more bitumen was being flushed out of the sample. Bitumen saturation decreased from 86% to 51% after 6.9 pore volumes of flow at 200°C in test CPERM5. Approximately 53% of the original bitumen was flushed out of a sample at 250°C during test CPERM6 reducing the bitumen saturation from 81% to 38% after 10.1 pore volumes of flow. Following each elevated temperature flow experiment the sample was cooled down to room temperature and effective permeability to water was measured at the residual bitumen saturation.

Fluid mobility values shown in Figure 4.30 corresponding to end point bitumen saturations have been plotted against temperature in Figure 4.31. Fluid mobility at constant oil saturation increases with temperature (i.e. the log of mobility increases in a quasi-linear manner with temperature). An upper limit of fluid mobility is shown in Figure 4.31 for zero oil saturation. This was determined assuming constant absolute permeability of $2 \times 10^{-12} m^2$ and published values of dynamic viscosity for water. A linear relationship has been assumed between logarithm of fluid mobility and temperature in Figure 4.30 where only two end point oil saturations were determined.

A single value of effective permeability to oil, k_o, and effective permeability to water, k_w, were determined for each of the experiments described in Figure 4.30. Effective permeabilities to oil and water were determined based on the volume of oil flushed from the sample during the experiment,

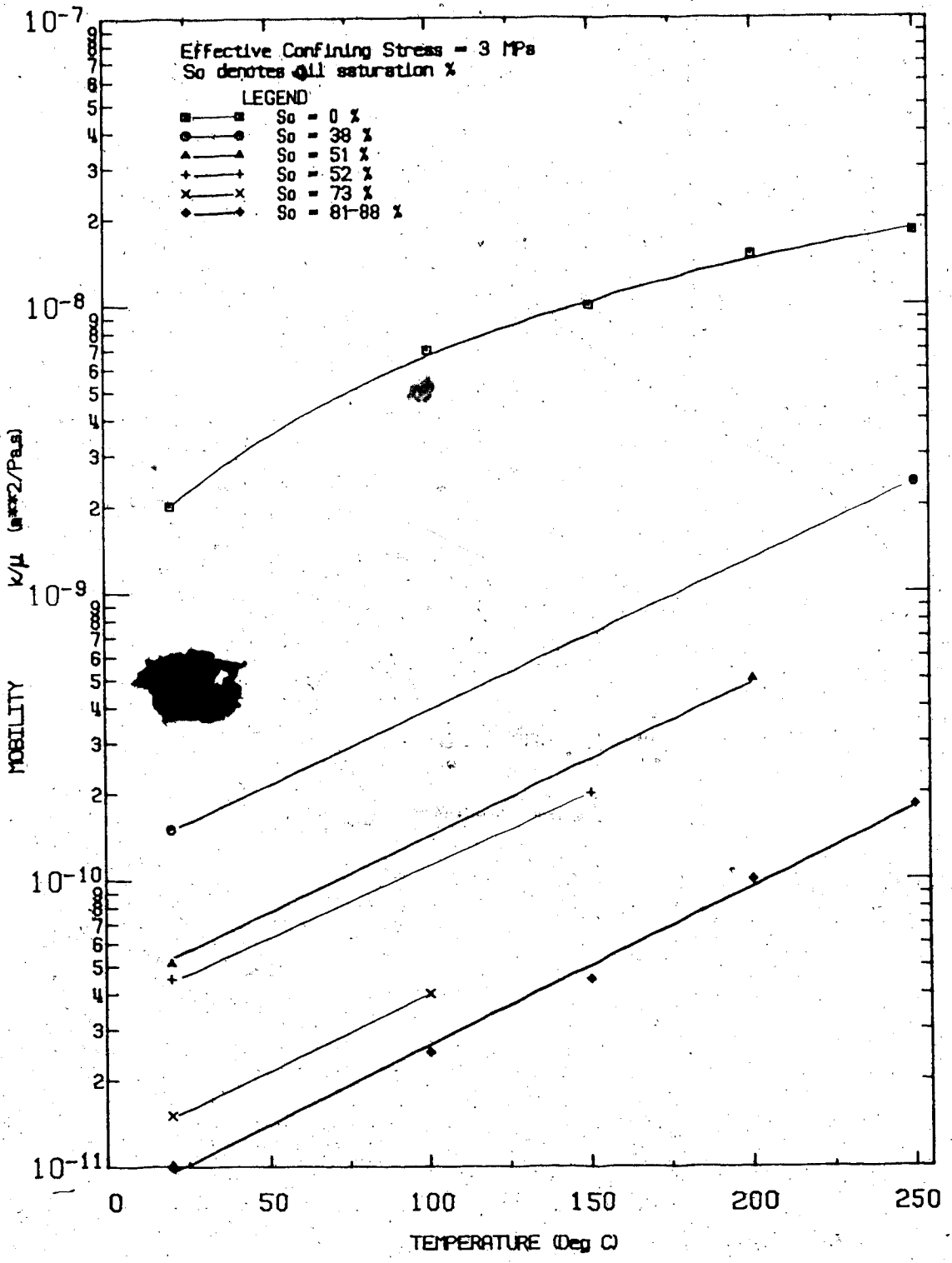

FIGURE 4.31 Variation of Fluid Mobility with Temperature and Oil Saturation

the remainder of the flow volume being water and on an average value of the pressure differential across the sample during the experiment. Effective permeabilities to oil and to water are plotted against water saturation (S_w%) in Figure 4.32. The effective permeability to water at room temperature increases with water saturation (i.e. decreasing oil saturation). Effective permeability to oil decreases with increasing water saturation in Figure 4.32. Effective permeabilities to oil, k_o, shown in Figure 4.31 were determined at elevated temperatures varying from 100°C to 250°C; k_o points have been connected on this plot by a dashed line to indicate the trend. In fact, effective permeability to oil would be expected to vary with temperature as well as water saturation. Fluid mobilities and effective permeabilities for all experiments are summarized in Table 4.7.

Relative permeabilities of undisturbed Saline Creek oil sand to oil and water (k_{ro} and k_{rw}) were determined based on effective permeability values presented in Figure 4.32 and assuming a constant value of absolute permeability of $2 \times 10^{-12} m^2$ (i.e. 2000 millidarcys). Relative permeabilities to oil and water are plotted against water saturation in Figure 4.33. Relative permeability to water increases while realtive permeability to oil decreases with water saturation. Again, values of relative permeability to oil at various tempertures have been connected with a dashed line to indicate trend. Relative permeability to oil is expected to vary with both temperature and water saturation.

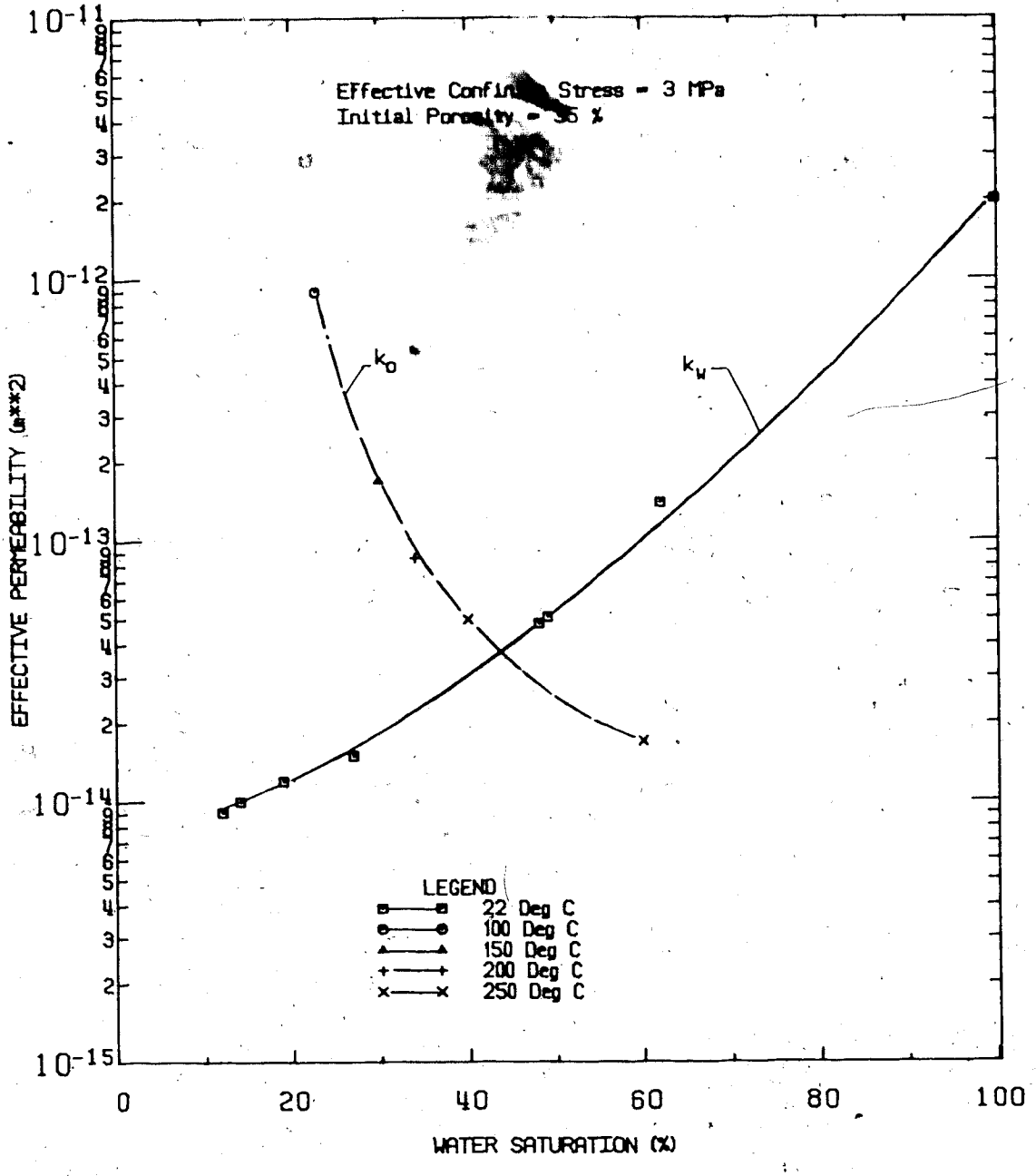

FIGURE 4.32 Variation of Effective Permeabilities to Oil and Water with Water Saturation

TABLE 4.7

SUMMARY OF PERMEABILITY TEST RESULTS

Test	Temperature (°C)	Initial Sample Porosity	Bitumen Saturation	Fluid Mobility k/μ (m^2/Pa.s)			Dynamic ** Viscosity (mPa.s)		Effective Permeability *** (m^2)	
				Combined	Oil	Water	Oil	Water	Oil (k_o)	Water (k_w)
CPERM3 *	20	0.37	0	-	-	3.0×10^{-9}	-	0.995	-	3.0×10^{-12}
CPERM7	20	0.35	0	-	-	$2.3 - 4.2 \times 10^{-9}$	-	0.995	-	$2.3 - 4.2 \times 10^{-12}$
CPERM7	150	0.35	0	-	-	$1.6 - 2.8 \times 10^{-9}$	-	0.995	-	$1.6 - 2.8 \times 10^{-12}$
CPERM4	20	0.36	81	-	-	1.2×10^{-11}	300,000	0.995	-	1.2×10^{-14}
CPERM4	100	0.36	81 - 73	$2.5 - 3 \times 10^{-11}$	2.3×10^{-12}	3.7×10^{-11}	400	0.284	9.1×10^{-13}	1.3×10^{-14}
CPERM4	20	0.35	73	-	-	1.5×10^{-11}	300,000	0.995	-	1.5×10^{-14}
CPERM8	20	0.35	88	-	-	9.1×10^{-12}	300,000	0.995	-	9.1×10^{-15}
CPERM8	150	0.35	88 - 52	$4.0 - 16 \times 10^{-11}$	7.2×10^{-12}	8.0×10^{-11}	30	0.200	1.7×10^{-13}	1.6×10^{-14}
CPERM8	20	0.34	52	-	-	4.5×10^{-11}	300,000	0.995	-	4.5×10^{-14}
CPERM9 *	20	0.383	80	-	-	1.3×10^{-11}	300,000	0.995	-	1.3×10^{-14}
CPERM9 *	150	0.385	80 - 52	$7.0 - 31 \times 10^{-11}$	1.4×10^{-11}	1.75×10^{-10}	30	0.200	4.2×10^{-13}	3.5×10^{-14}
CPERM9 *	20	0.375	52	-	-	6.0×10^{-11}	300,000	0.995	-	6.0×10^{-14}
CPERM5	20	0.360	86	-	-	1.0×10^{-11}	300,000	0.995	-	1.0×10^{-14}
CPERM5	200	0.365	86 - 51	$7.0 - 48 \times 10^{-11}$	8.6×10^{-12}	1.5×10^{-10}	10	0.136	8.6×10^{-14}	2.0×10^{-14}
CPERM5	20	0.355	51	-	-	5.1×10^{-11}	300,000	0.995	-	5.1×10^{-14}
CPERM6	20	0.36	81	-	-	1.1×10^{-11}	300,000	0.995	-	1.1×10^{-14}
CPERM6	250	0.365	81 - 38	$1.5 - 22 \times 10^{-10}$	1.3×10^{-11}	2.8×10^{-10}	4	0.110	5.0×10^{-14}	3.0×10^{-14}
CPERM6	20	0.355	38	-	-	1.5×10^{-10}	300,000	0.995	-	1.5×10^{-13}

4.5.4 Implications of Sample Disturbance

Laboratory permeability testing of oil sands and unconsolidated sands from heavy oil deposits is commonly performed with "packed sand cores" (Maini and Sayegh, 1983) or remoulded reservoir materials. Pore fluids (i.e. oil and water) are introduced into packed sand core samples under pressure and elevated temperature.

Remoulded oil sand samples are generally back saturated with water for permeability testing. Factors which may affect test results using remoulded and repacked samples include the following.

1. In situ porosity and mineral grain structure cannot be duplicated in packed or remoulded samples.
2. Clay minerals present in situ are not retained in packed core samples or solvent extracted sands.
3. Oil saturation is decreased and water saturation is increased in remoulded or disturbed oil sand samples when water is introduced into the expanded pore volume.

Permeability tests CPERM3 and CPERM9 were performed on remoulded oil sand samples in an effort to quantify the influence of sample disturbance.

Absolute permeability to water of a remoulded sample of oil-free McMurray Formation sand was determined in test CPERM3

at room temperature. Results of CPERM3 are compared with those for undisturbed solvent extracted Saline Creek oil sand of test CPERM7 in Table 4.7. Although initial porosities of the remoulded and undisturbed oil free samples are 0.37 and 0.35, respectively, there is no appreciable difference in measured values of absolute permeability to water.

Clay and silt particles were observed in all of the oil-rich samples used for permeability tests. Also, clay minerals were observed in some samples during the scanning electron microscope study when some of the bitumen coating was removed. However, it was observed that clay and silt fines were removed from oil sand samples during solvent extraction. Measurements of absolute permeability on both remoulded and undisturbed samples which were solvent extracted with toluene or benzene may in fact be in error because of the removal of fines. The magnitude of this possible source of error is unknown. Fluid mobility values predicted assuming a constant value of absolute permeability, $k = 3.0 \times 10^{-12} m^2$ and adopting typical published values of dynmaic viscosity for bitumen and water are summarized in Table 4.8. These values of fluid mobility are compared with actual permeability test results on plots in Appendix C. Predicted values consistently overestimate fluid mobility during the initial stages of water circulation in elevated temperature experiments. This may be due to the presence of fines (clay and silt particles) in oil-rich samples that are not present in solvent extracted samples, or to different values of bitumen viscosity than those assumed.

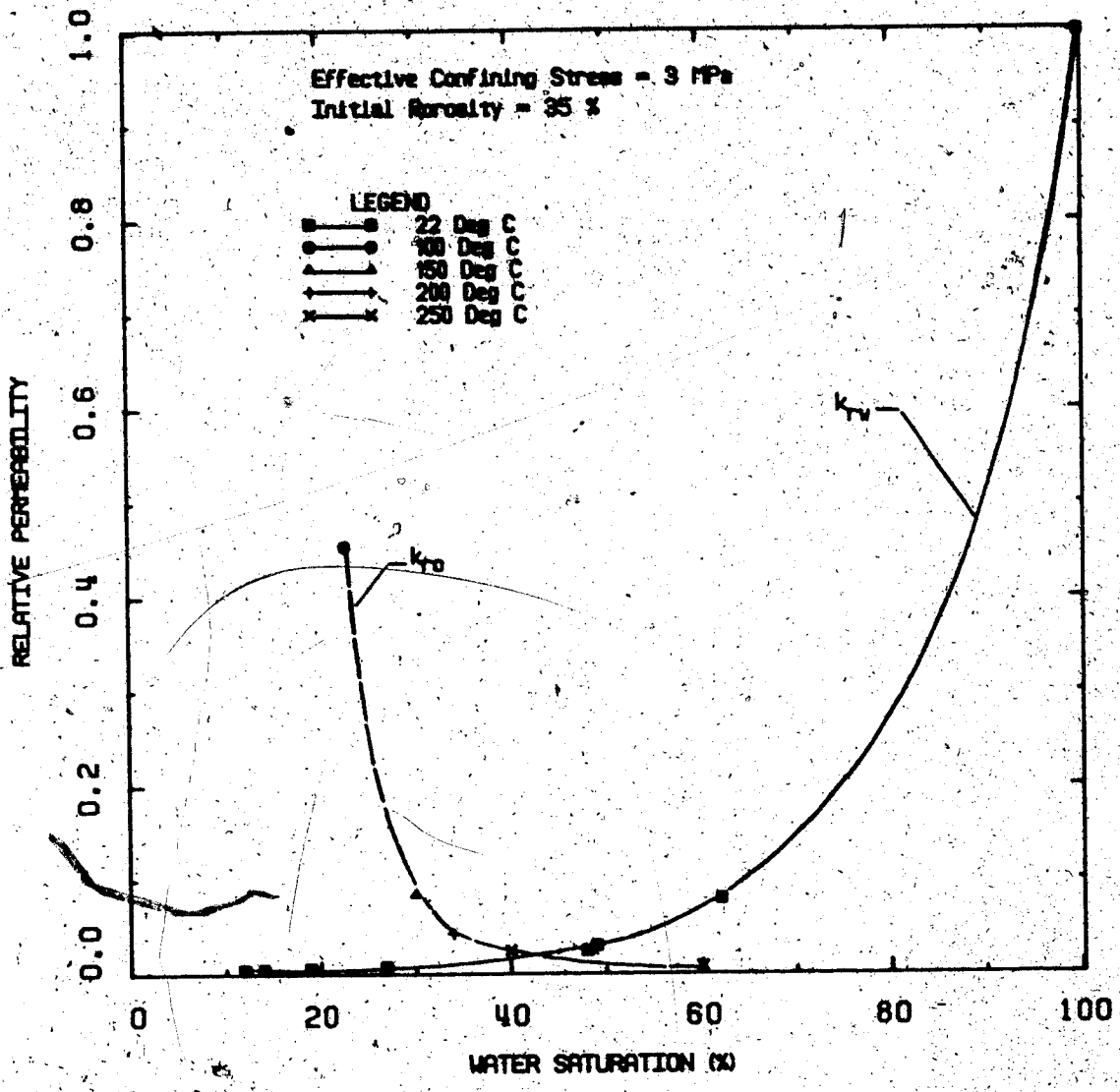

FIGURE 4.33 Variation of Relative Permeabilities to Oil and Water with Water Saturation

PREDICTED FLUID MOBILITY VALUES FOR SALINE CREEK OIL SAND AT TEST TEMPERATURES AND OIL SATURATIONS ASSUMING ABSOLUTE PERMEABILITY $k = 3 \times 10^{-12} m^2$

Test	Temperature (°C)	Dynamic Viscosity (Pa.s)		So (%)	Sw (%)	$\frac{k}{\mu}\left(\frac{m^2}{Pa.s}\right)$
		Water	Bitumen			
-	20	0.995×10^{-3}	300	100	0	1.00×10^{-14}
CPERM8	20	0.995×10^{-3}	300	88	12	1.14×10^{-14}
CPERM5	20	0.995×10^{-3}	300	86	14	1.16×10^{-14}
CPERM4	20	0.995×10^{-3}	300	81	19	1.23×10^{-14}
CPERM4	20	0.995×10^{-3}	300	73	27	1.37×10^{-14}
CPERM8	20	0.995×10^{-3}	300	52	48	1.92×10^{-14}
CPERM5	20	0.995×10^{-3}	300	51	49	1.96×10^{-14}
CPERM6	20	0.995×10^{-3}	300	38	62	2.63×10^{-14}
CPERM7	20	0.995×10^{-3}	300	0	100	3.02×10^{-9}
CPERM4	100	0.284×10^{-3}	.200	81	19	3.73×10^{-11}
CPERM4	100	0.284×10^{-3}	.200	73	17	4.10×10^{-11}
CPERM8	150	0.200×10^{-3}	.030	88	12	1.14×10^{-10}
CPERM8	150	0.200×10^{-3}	.030	52	48	1.91×10^{-10}
CPERM5	200	0.136×10^{-3}	.010	86	14	3.48×10^{-10}
CPERM5	200	0.136×10^{-3}	.010	51	49	5.81×10^{-10}
CPERM6	250	0.110×10^{-3}	.004	81	19	9.20×10^{-10}
CPERM6	250	0.100×10^{-3}	.004	38	62	1.89×10^{-9}

Identical test procedures were followed in tests CPERM8 and CPERM9 on undisturbed and remoulded samples of Saline Creek oil sand. Initial sample porosities were respectively 0.39 and 0.38 for the undisturbed and remoulded samples. Also, the initial undisturbed oil (bitumen) saturation was 88% whereas that of the remoulded sample was 80%. Room temperature effective permeability to water was measured in each of the tests, then samples were heated to 150°C and heated, 150°C water was circulated. The residual oil saturation in both tests was 52%. Finally, room temperature effective permeability to water was determined at the residual oil saturation following cooldown of the samples.

Results of CPERM8 and CPERM9 are compared in Table 4.7. Effective permeability to water was slightly higher for the remoulded sample both at initial and residual oil saturations. This difference is attributed to differing porosities of the two samples, however, it is <u>not</u> considered to be of much practical significance. Combined fluid mobility for bitumen and water versus flow volume at 150°C is compared for the two tests in Figure 4.34. Fluid mobility is greater for the remoulded sample than for the undisturbed sample throughout the test. Also, fluid mobility for the remoulded sample increased more rapidly than for the undisturbed sample indicating that bitumen was probably flushed more rapidly during the initial flow phase. The effect of remoulding Saline Creek oil sand resulted in over estimation of the fluid mobility and effective permeabilities by less than half an order of magnitude relative

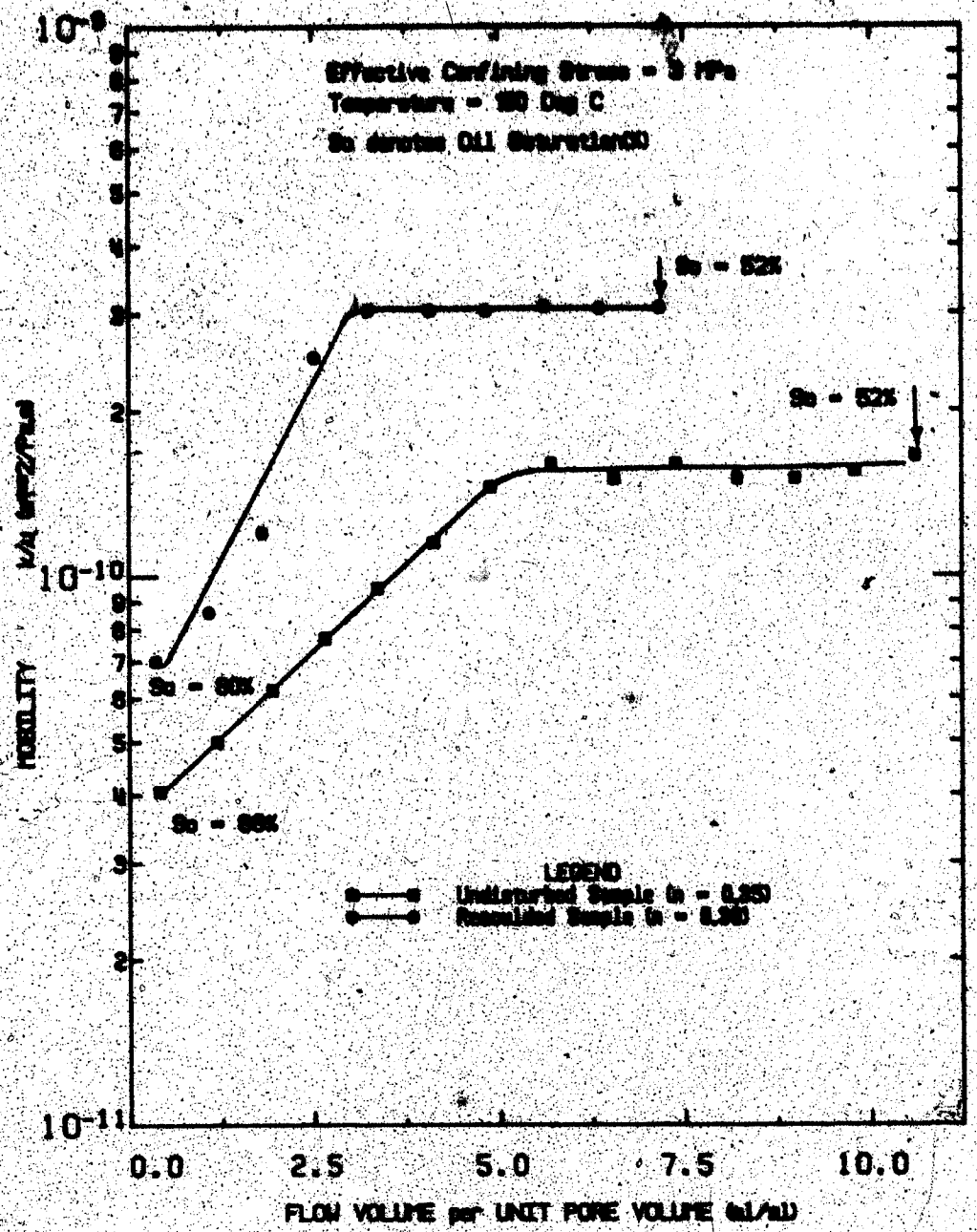

FIGURE 4.34 Influence of Sample Disturbance on Fluid Mobility in Saline Creek Oil Sand at 150°C

to comparable values for an undisturbed sample. This indicates that although tests on remoulded samples commonly used in industry may result in overestimation of permeability parameters, the magnitude of error is not excessive in view of other complexities in modelling multiphase fluid flow.

4.3.3 Comparison with Published Permeability Data

Field and laboratory measurements of permeability parameters published in the literature for Alberta oil sands vary considerably and in general, refer to isothermal conditions (i.e. either room temperature or *in situ* temperature). A summary of some of the published permeability data is presented in Table 4.9. References in Table 4.9 are listed in chronological order. Several published values of air permeability are listed in Table 4.9. Laboratory measurements of air permeability have been made to evaluate potential air injectivity requirements to support *in situ* combustion. It should be noted that effective permeability of oil sand to air is strongly dependent upon water and bitumen saturation. Direct comparisons between air and water permeabilities are therefore not meaningful. Hydraulic conductivity determined from regional *in situ* drawdown (pump) tests by Hackbarth and Nastasa (1969) for McMurray Formation oil sand in the Athabasca region agrees well with laboratory measurements of effective permability of undisturbed oil-rich Saline Creek oil sand to water at room temperature. The average value of hydraulic conductivity reported by Hackbarth and Nastasa was

TABLE 4.9

SUMMARY OF PERMEABILITY DATA REPORTED IN THE LITERATURE FOR ALBERTA OIL SANDS

AUTHORS	REPORTED PERMEABILITY VALUE	COMMENTS
1. Clark, K.A. (1960)	$5 \times 10^{-14} m^2$ (AVERAGE) (RANGE = 10^{-14} to $10^{-12} m^2$) (i.e. 10 to 1000 mD)	Air Permeability is a function of (Sw + Soi) % and fines content.
2. Carrigy and Kramers (1974)	up to $5 \times 10^{-12} m^2$ (5000 mD)	Air [illegible]bility.
3. Dusseault (1977)	3×10^{-6} to 5×10^{-6} cm/s (0.03 - 5 mD)	Hydr[illegible]conductivity based on consolidation of triaxial samples.
4. Camp (1970)	$5 \times 10^{-14} m^2$ for B > 10% $10^{-13} m^2$ for 4% < B < 10% $10^{-14} m^2$ for B < 4% (i.e. 10 to 1000 mD)	Air permeability for "undisturbed" samples. B = Bitumen content.
5. Starr, Prats and Messuiam (1979)	up to $5 \times 10^{-12} m^2$ (5000 mD)	Air permeability for clean sand.
6. Heckbarth and Nastasa (1979)	1×10^{-3} cm/s (AVERAGE) (RANGE = 10^{-6} to 10^{-3} cm/s) (or 1 to 1000 mD)	[illegible]raulic Conductivity based on pump tests.
7. Dusseault (1980)	10^{-10} to 10^{-8} cm/s (0.0001 to 0.01 mD)	[illegible]le" in-situ value of hydraulic c[illegible]ctivity at 40 m depth and in-situ temperature.
8. Parsons and Hemstock	120 to 1227 millidarcys Average = 440 millidarcys ($4.4 \times 10^{-13} m^2$)	P[illegible]ability of Peace River oil sand to brine.
9. Mainland (1983)	Average = 1500 millidarcys ($1.5 \times 10^{-12} m^2$)	Absolute Permeability of Cold Lake Oil Sand.
10. Ager (1983)	$0.9 - 1.2 \times 10^{-14} m^2$ (9 - 12 millidarcys) $1.6 - 4.2 \times 10^{-12} m^2$ (1600 to 4200 millidarcys)	Effective permeability of Saline Creek oil sand to water at room temperature (S_o = 81 - 88%). Absolute permeability of oil free Saline Creek oil sand to water.

10^{-5}cm/s. This is equivalent to a value of $10^{-14}m^2$ (i.e. 10 millidarcys) effective permeability to water, which was about the average value obtained for oil-rich Saline Creek samples. The average value of absolute permeability of $1.5 \times 10^{-12}m^2$ (1500 mD) published by Mainland (1983) for Clearwater Formation oil sand at the Esso Resources Canada Limited Cold Lake lease is at the lower limit of absolute permeability measurements in laboratory experiments on Saline Creek oil sand which ranged from $1.6 - 4.2 \times 10^{-12}m^2$ (1600-4200 mD).

Although substantial data has been published on the effects of temperature on dynamic viscosity of bitumen extracted from oil sands, no direct permeability measurements at elevated temperatures have yet been published to the writer's knowledge.

Gobran (1981) deals with the effects of temperature and effective confining stress on absolute permeability of repacked Ottawa sand. He concluded that temperature has no measurable effect on absolute permeability of Ottawa sand packs while increasing effective confining stress does reduce absolute permeability. Interestingly, absolute permeabilities reported by Gobran for Ottawa sand (100-200 mesh) over a wide range of temperatures and effective stresses were between about 2000 and 4000 millidarcys ($2 - 4 \times 10^{-12}m^2$). These measurements for Ottawa sand compare very closely with those reported for oil-free Saline Creek oil sand which typically has a slighlty

finer, though equally uniform grain size distribution (for example, see Appendix F).

4.6 Coefficient of Consolidation

One dimensional consolidation of soils resulting from a change in total stress or pore pressure is characterized by the following differential equation (Terzaghi, 1942):

$$\frac{\partial u}{\partial t} = c_v \frac{\partial^2 u}{\partial z^2} \qquad (4.21)$$

Equation 4.21 relates the spatial distribution of pore pressure with the time rate of pore pressure response (i.e. dissipation or increase). The coefficient of consolidation, c_v, is defined as a ratio of hydraulic diffusivity to compressibility of the soil skeleton as written in equation 4.22.

$$c_v = \frac{k_h}{m_v \gamma_w} \qquad (4.22)$$

As discussed in section 4.5, hydraulic conductivity, k_h, is not a convenient parameter for describing the flow of fluids other than water at standard temperature and pressure, through porous media. A more convenient definition of the coefficient of consolidation for oil sand is given in equation 4.23.

$$c_v = \frac{k}{\mu m_v} \qquad (4.23)$$

The fluid mobility k/μ, in equation 4.23 is the ratio of absolute permeability to dynamic viscosity. A combined value of fluid mobility for bitumen and water has been determined experimentally for oil sand. Mobility varies with both temperature and fluid saturations as discussed in section 4.5.

Pore pressure response to rapid (undrained) heating in situ and subsequent dissipation of thermally generated excess pore pressure is an example of heat consolidation. The definition of coefficient of consolidation given in equation 4.23 may be used in equation 4.21 for numerical evaluation of one dimensional heat consolidation.

The variation of fluid mobility with temperature and bitumen saturation shown in Figure 4.30 was used to evaluate coefficient of consolidation for oil sand over the corresponding range of temperatures (20°-250°C) and fluid saturations. A constant value of one dimensional volume compressibility (i.e. $m_v = 5 \times 10^{-7}$ kPa^{-1}) was used. As discussed in section 4.2.2, m_v for dense oil sand does not vary significantly for unloading-reloading with temperature. The inverse of m_v is commonly termed "the constrained modulus", D, and may also be determined in triaxial K_o consolidation tests, in which lateral deformations are restrained by increasing the confining stress as axial loading proceeds.

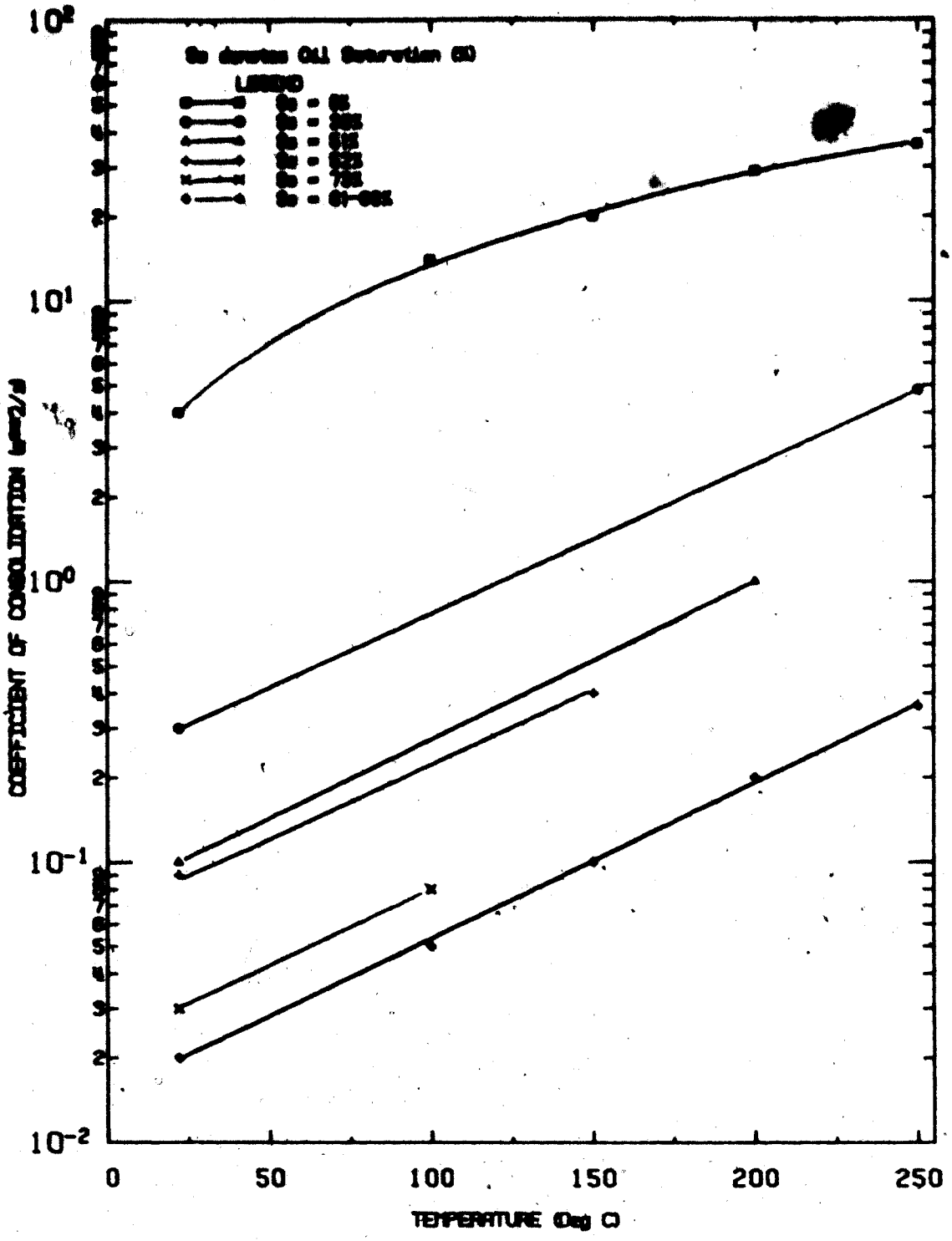

FIGURE 4.35 Variation of the Coefficient of Consolidation with Temperature and Oil Saturation

Variation of the coefficient of consolidation for Saline Creek oil sand with temperature and oil saturation is shown on Figure 4.35.

4.7 Summary

Geotechnical properties for undisturbed oil sand have been described for a range of temperatures, pressures and stresses. Geotechnical properties summarized and discussed in this chapter include thermal expansion and compressibility, shear strength and stress-strain behaviour, and permeability.

For each type of test, parameters required for numerical modelling have been described, the experimental results summarized and discussed, and the implications of sample disturbance have been evaluated. Highlights of the experimental research may be summarized as follows:

1. Test results from this experimental programme are unique. A suite of geotechnical properties was determined for high quality, "undisturbed" oil sand samples. Samples tested were sufficiently uniform and similar to permit quantitative comparison. Geotechnical properties of oil sand at elevated temperatures and pressure have not previously been measured. Furthermore, testing equipment was developed specifically for this research. Test procedures were developed during the course of the research since standardized procedures had not previously been established. The experimental results

provide insight into geotechnical behaviour of oil sand in situ.

2. Properties of quartzose sand grains and the densely packed solid skeleton of oil sand are not altered dramatically by elevated temperatures up to 300°C. Subtle changes in compressibility, shear strength, stress-strain behaviour and absolute permeability, which were detected are attributed to pore volume changes observed during heating and/or drained compression.
3. Physical properties of the pore fluids (water, bitumen and dissolved gases) in oil sand are subject to significant changes at elevated temperatures and pressures. Significant pore pressure increase and volumetric expansion result when the rate of heating or pressure injection is rapid relative to the rate of pore pressure dissipation (i.e. hydraulic diffusion).
4. Dynamic viscosity of the bitumen and pore water decrease with temperature resulting in increased mobility at elevated temperatures. Also, since the dynamic viscosity of bitumen is greater than that of water at all temperatures up to 300°C, the combined fluid mobility increases when bitumen is displaced from the oil sand pore space by water. The presence of fines, i.e. clay particles, in oil sand is known to reduce both absolute permeability and fluid mobility. It has been observed that some clay particles are removed during solvent extraction and may, in fact, be mobile during hot water flooding.

5. Although strength and compressibility of the solid skeleton are not substantially altered at elevated temperatures, significant reduction of available shear strength will result during heating if effective confining stresses are reduced by an increase in pore pressure (i.e. partially drained or undrained heating). The following simplified example will help to quantify the influence of pore pressures on available shear strength. If partially undrained heating were to generate a pore pressure increase of 700 kPa (i.e. 100 psi) in an oil sand deposit buried at typical depths ranging from about 200-400 m, the available shear strength would also be reduced by approximately 700 kPa which represents between about 12 and 25 percent of the total available shearing resistance (for cohesionless oil sand with $\phi = 45°$). Greater percentage reduction of shear strength would result at shallower depths (i.e. lower confining stresses). Stress-strain moduli are also strongly dependent upon effective confining stress. The implications of drained and undrained heating will be discussed further in following chapters.

5.0 HEAT CONSOLIDATION

5.1 The Heat Consolidation Process

Consolidation of porous soils and rocks, according to the classical theories, is a time dependent process of concurrent pore pressure change and volumetric deformation (i.e. compression or swelling) in response to a change in effective stress. Provided that the solid skeleton is immobile, volume change and pore pressure dissipation (or increase) are coupled through a fluid transport law, i.e. usually Darcy's Law.

Heat consolidation is an analogous process. Liquid and gaseous pore fluids and mineral solid constituents of soils and rocks typically expand when heated over a wide range of temperatures (i.e. approximately 0 - 500°C for oil sand). Undrained thermal expansion of constituent fluids and solids generates volumetric expansion and, provided that the effective stress is greater than zero, pore pressure increases. It should be noted that thermal expansion is not monotonic at all temperatures. For example, Alpha quartz crystals are physically altered at temperatures exceeding approximately 573°C and in fact, decrease in volume at temperatures above this "Alpha-Beta" transition temperature as shown in Figure A-4, Appendix A. Also pore water freezes at temperatures below 0°C causing volumetric expansion associated with phase change. Frost heave and thaw consolidation theories have been developed to describe "thermal consolidation" processes associated with freezing and thawing of pore fluids. The term "thermal consolidation" may be used to describe consolidation processes over the entire range of

temperatures, whereas "heat consolidation" is favoured for describing the response of soils and rocks to heating (or cooling) at elevated temperatures above the freezing point.

Heat consolidation includes the following concommittant processes:

(a) Thermal expansion and thermal pore pressure generation occur in response to temperature increase, and are dependent on the current effective confining stresses.

(b) Time-dependent dissipation of excess pore pressure is governed by the coefficient of consolidation which is also temperature dependent.

(c) The solid skeleton is compressed during dissipation of excess pore pressure and ultimately must carry the same effective stresses which existed prior to heating. If the original effective stresses are not restored, the process is not purely one of "heat consolidation", but also includes some mechanical consolidation. Total stresses may be altered in situ due to density changes during heating; also thermal stresses may alter local in situ stresses.

(d) When the preheating effective stresses are restored (e.g. in laboratory samples), there is a net volume change. This net volume change is attributed to thermal expansion

of the solid mineral grains and volume change of the solid skeleton. A net volume change will also result if heating proceeds very slowly, under fully drained conditions.

Volume change of the solid skeleton in soils results from temperature-induced shearing at interparticle contacts and physico-chemical changes with temperature. Increasing the temperature of soils generally causes a decrease of pore volume, i.e. "thermal compaction". Williams (1982) has reported significant volumetric compression of illitic clays after heating up to 200°C. This component of thermal volume compression is small for dense oil sand.

The solid skeleton of intact crystalline and cemented rocks is altered during heating by a process often described as "thermal cracking". Differential thermal expansion during heating of the various mineral grains and cementing materials is believed to cause tensile stresses within the solid matrix. Temperature-induced micro-cracking has been widely observed to cause dilation of rocks, i.e. the pore volume increases, (e.g. Heard and Page, 1982, and Lo and Wai, 1982).

In fact, a technique for breaking rocks which goes back to antiquity, involves thermal cycling by heating the rock and then suddenly cooling it with water (Finnie et al., 1979).

It is important to recognize that the influence of heating and thermal history on volume change and mechanical properties varies dramatically for various soil and rock materials. Observed volumetric responses to heating range from "thermal compaction" of some soils to "thermal cracking" (and expansion) of intact rocks. At very high temperatures, mineralogic alteration prior to melting may result in volume decrease.

5.2 Coupling Heat Transfer, Mass Transfer and Stress-Strain Analyses

The development of a heat consolidation theory involves coupling heat and mass transfer relationships with a stress-strain-temperature model for porous materials that may be subjected to both mechanical and thermal perturbations. As described in the foregoing section, stress-strain-temperature relationships are likely to vary widely for different soil and rock materials.

The simplest stress-strain models commonly used to predict the behaviour of earth masses assume that deformations of the solid skeleton occur uniaxially in response to uniaxial stress changes according to linear-elastic or elastic-perfectly plastic constitutive relationships. The original theory of mechanical consolidation developed by Terzaghi in 1923 (see Terzaghi, 1943) coupled a one-dimensional linear stress-strain relationship with uniaxial fluid flow (i.e. mass transfer) for porous soils saturated with incompressible water. The condition of reversibility inherent in elastic theory was <u>not</u> required in Terzaghi's formulation, since

he recognized that in general, the coefficient of compressibility differed for conditions of: (I) virgin compression and (II) unloading-reloading. Rendulic (1936) (see also Terzaghi, 1943) extended the Terzaghi consolidation theory to three dimensions in a non-rigourous manner by assuming constant total stresses throughout the medium and volumetric strains due only to effective stress changes. Biot (1941) developed a rigorous theory of three-dimensional consolidation for perfectly linear elastic porous media. The Biot theory has been criticized on the grounds that the stress-strain behaviour of real soils is not well approximated by linear elastic constitutive relationships. Implementation of an extended Biot theory incorporating more complex nonlinear and non-elastic models of mechanical behaviour have been discouraged by the complexity of solving other than very simple problems (see Gibson et al., 1963).

The development of a rigorous and self-consistent three-dimensional theory of heat consolidation involves the further complexities resulting from the introduction of temperature as a state variable. Schiffman (1971) has developed a three-dimensional thermoelastic theory of consolidation. The theory developed by Schiffman is an extension of the three-dimensional consolidation theory developed by Biot (1941) and was derived by analogy with the theory of mixtures (see Atkin, 1967). Schiffman's complete theory consists of five field equations including a continuity equation, three displacement equations of equilibrium, and an energy equation. These equations are coupled in terms of both temperature and displacement. Application of the Schiffman theory to soils, or for

that matter to oil sand, is subject to the same limitations for which the Biot theory has been criticized, i.e. the inadequate representation of mechanical behaviour using a linear elastic stress-strain relationship and difficulties in applying the theory to obtain solutions to complex problems.

Campanella and Mitchell (1968) developed theoretical temperature-volume-stress relationships for soils based on laboratory experiments on illite clay samples heated to moderate temperatures up to about 60°C. One-dimensional heat consolidation theory outlined in subsequent sections of this chapter, is an extension of the Campanella-Mitchell theory based on the experimental research summarized in Chapters 3 and 4. Solutions of one-dimensional heat consolidation problems in cartesian and radial coordinates for oil sand are presented in following sections of this chapter. Solutions are presented in Chapter 6 for two dimensional axisymmetric problems related to heating and injection around a shaft and/or borehole. The assumption that total stresses remain constant during heating and consolidation has been used to determine thermally generated, transient pore pressures and volumetric strains. Transient volumetric strains determined in the heat consolidation analyses are used as input for thermoelastic stress analyses. This approach is analogous to that adopted in developing the Terzaghi-Rendulic three dimensional theory for mechanical consolidation. This type of analysis is not rigorous since the dependence of pore pressure on thermally induced total stress changes is ignored. Nevertheless, solutions of this type are believed to provide insight into problems of practical interest,

and delineate requirements for development of solutions of a rigorous three dimensional heat consolidation theory.

5.3 Practical Applications of One Dimensional Heat Consolidation Theory

A number of problems of practical interest in oil sands development as well as other areas of resource development may be studied initially using a simplified one-dimensional theory of heat consolidation. Several examples related to oil sands development include:

(a) In situ heating using long electrical strip heaters, e.g. Towson (1979) has described pilot In situ experiments conducted by Petro Canada Ltd.;

(b) steam flooding through a bottom water-bearing sand zone, e.g. (i) Huygen and Lowry (1983) described results of scaled model laboratory experiments to model this process for Wabasca oil sand. Results of the laboratory simulation indicate that conditions of one dimensional heat transfer are valid at substantial distance from the steam injection well(s); (ii) Parsons and Hemstock (1983) have also described implementation of this technique at the Shell Canada Resources Ltd., Peace River In-Situ Project site;

(c) pore pressure development and heave of hot oil storage tanks, e.g. Koser (1983) has studied this problem using two-dimensional numerical analyses, however in principal, the problem may also be studied in a piece-wise manner using one-dimensional heat consolidation theory; an advantage of one dimensional solutions is the reduced computational effort;

(d) in situ heating by injection of condensed steam into a large planar hydraulic fracture;

(e) radially symmetric heating and/or steam injection through a well casing, or steam injection through a point source in a semi-infinite medium (i.e. spherically symmetric); or

(f) concentric radial heating inward toward a central shaft from a peripheral production zone.

One dimensional modelling of any of the above examples is a gross simplification of reality. Ultimately, it will be both desirable and necessary to undertake two and three dimensional analyses. Nevertheless it is considered prudent to initially incorporate the physics of heat consolidation in one dimensional analyses which may later be extended to multi-dimensional modelling.

5.4 One-Dimensional Heat Consolidation Theory

A one dimensional heat consolidation theory analogous to the isothermal Terzaghi theory of one-dimensional consolidation (see Terzaghi, 1943) is developed in this section. Assumptions invoked in the Terzaghi theory are also used here. Several important assumptions common to both isothermal consolidation and heat consolidation theories include:

1. Strains in the solid skeleton and pore fluid phase are one-dimensional, i.e. vertical.
2. The vertical total stress is constant.
3. Fluid flow is adequately described by Darcy's Law.

Strains in the solid skeleton during heat consolidation are due to changes in both the effective stresses and the temperature. Heat consolidation theory therefore requires coupling of effective stress and strain with temperature and time.

5.4.1 Development of an Uncoupled One-Dimensional Heat Consolidation Theory.

Consider a control element of soil or rock of volume, V, and height, dz. The control element is saturated with liquid pore fluids at an initial absolute pore pressure, P_o. The initial temperature of the control element is To and the total vertical confining stress is σ_v.

When the temperature of the control element is increased by an amount, ΔT, the element expands and the pore pressure increases. The initial undrained pore pressure increase is given by:

$$\Delta u_T = B_T \Delta T \tag{5.1}$$

where B_T is the coefficient of thermal pore pressure generation defined previously by equations 4.11 and 4.12. The initial undrained volumetric expansion of the element is given by:

$$\left(\frac{\Delta V}{V}\right)_u = \alpha_u \Delta T - \beta_u \Delta T = \alpha_{DR} \Delta T + m_v \Delta u \tag{5.2}$$

where α_u, β_u, α_{DR} and m_v are undrained and drained coefficients of thermal expansion and compressibility previously defined in Chapter 4.

The thermally generated excess pore pressure, u_T, dissipates with time. The fluid flow rate out of the element is governed by Darcy's Law and is equivalent to the volume change of the element with time:

$$\frac{\partial V}{\partial t} = \frac{\partial}{\partial z}\left(-\frac{k}{\mu}\frac{\partial u}{\partial z}\right) dz\, dA \tag{5.3}$$

Eventually, $u = 0$ and the initial effective confining stress is restored. The ultimate volume change of the control element at the new steady temperature, $T_o + \Delta T$, after the thermally

generated excess pore pressure has dissipated is given by:

$$\left(\frac{\Delta V}{V}\right)_{DR} = \alpha_{DR}\Delta T \qquad (5.4)$$

The volume of pore fluid drained from the element is the difference between the undrained and drained volumetric strains given by equations 5.2 and 5.4:

$$\left(\frac{\Delta V}{V}\right)_{EX} = \left(\frac{\Delta V}{V}\right)_{u} - \left(\frac{\Delta V}{V}\right)_{DR} = m_v B_T \Delta T \qquad (5.5)$$

The rate of change of volume of the control element during consolidation at the constant elevated temperature, $T_o + \Delta T$, is:

$$\frac{\partial V}{\partial t} = - m_v \frac{\partial u}{\partial t} dz\, dA \qquad (5.6)$$

The standard form of the one-dimensional consolidation equation is recovered by equating the expressions for rate of volume change given in equations 5.3 and 5.6:

$$\frac{\partial u}{\partial t} = \frac{k}{\mu m_v} \frac{\partial^2 u}{\partial z^2} \qquad (5.7)$$

where $k/\mu m_v = c_v$, the coefficient of consolidation described in section 4.6 of Chapter 4.

As discussed in Chapter 4, section 4.6, c_v varies nonlinearly with temperature, and also with the relative saturations of water and bitumen in oil sands. The coefficent

of consolidation, c_v, varies only with temperature and pressure in porous materials having a single, continuous pore fluid phase.

In general, total stresses are not constant during heating. Total stresses may be altered by: (I) restraint of thermally induced strains, and (II) bulk density changes. Thermal expansion of the solid and pore fluid phases causes density to decrease. During consolidation time dependent mass transfer proceeds as thermally generated excess pore pressures dissipate and pore fluids drain. The dominant upward pressure gradient resulting from thermal density changes is often described as "thermal buoyancy".

Bulk density may be defined in terms of the relative proportions of the solid and fluid phases as follows:

$$\gamma = (1 - \eta)\,\gamma_s + \eta\gamma_f \tag{5.8}$$

Porosity, η, and the densities of the solids and pore fluids vary with temperature, pore pressure and effective stresses:

$$\eta = \eta_o \left(1 + m_v \Delta\sigma' - (\alpha_{DR} - \alpha_s)\,\Delta T \right. \tag{5.8.1}$$

$$\gamma_s = \frac{\gamma_{so}}{1 + \alpha_s \Delta T + \beta_s \Delta\sigma'} \tag{5.8.2}$$

$$\gamma_f = \frac{\gamma_{fo}}{1 + \alpha_f \Delta T + \beta_f \Delta\sigma'} \tag{5.8.3}$$

During undrained heating, porosity and densities vary directly with temperature since pore pressure and effective stress changes are related to temperature change through the B_T parameter.

It is useful then to introduce a coefficient linking bulk density variation with undrained temperature change as follows:

$$M_T = -\left(\frac{\Delta\gamma}{\Delta T}\right) \qquad (5.9.1)$$

The total stress change within a control thickness, dz, due to density decrease resulting from an undrained temperature increase, ΔT, is:

$$\Delta\sigma_T = M_T \Delta T \, dz \, dA \qquad (5.9.2)$$

The total stress change given by equation 5.14.2 results in a nearly equivalent change in pore pressure, depending on the value of Skempton's B parameter.

$$\Delta u_T = B\Delta\sigma = B M_T \Delta T \, dz \, dA \qquad (5.9.3)$$

It should be noted that the magnitude of B also varies with temperature and pressure. For example, undrained heating of a high quality sample of dense Saline Creek oil sand over the temperature range 20°C to 200°C at ambient pore pressure of 5 MPa, would result in approximately 5.4 percent volumetric

expansion (see Figure 4.6). Since the mass of the sample remains constant during undrained heating, the bulk density decreases from 21.5 to 20.4 kN/m^3 over the 180°C temperature increment; the corresponding value of M_T is 6.0×10^{-3} kPa/m-°C.

Since bulk density varies with effective stress, total stress must also increase as excess pore pressures dissipate during heat consolidation. A second coefficient relating bulk density to changes with effective stress change may therefore be defined as follows:

$$M_p = \left(\frac{\Delta\gamma}{\Delta\sigma'}\right) \tag{5.9.4}$$

Total stress change within a control thickness dz due to bulk density variation with pore pressure is given by:

$$\Delta\sigma_p = M_p \, \Delta\sigma' \, dz \, dA \tag{5.9.5}$$

The resulting pore pressure change is given by:

$$\Delta u_p = B\Delta\sigma_p = B \, M_p \, \Delta\sigma' \, dz \, dA \tag{5.9.6}$$

The magnitude of pore pressure change due to bulk density variation is, in general, very small. Also, heating decreases density while consolidiation causes density to increase.

Total stress changes due to restraint of thermally induced

strains is considered to be of greater practical importance in the heat consolidation process. Solutions presented in this chapter were developed assuming that total stresses remain constant during heating and consolidation, however in many problems lateral stresses increase during heating due to conditions of lateral restraint in situ.

5.4.2 Numerical Example of Uncoupled One-Dimensional Heat Consolidation of Oil Sand

The following example illustrates the process of heat consolidation under non-transient heating for a laterally confined, deeply buried layer of oil sand. Total vertical stress is constant in this example. Boundary and initial conditions are illustrated in Figure 5.1 as follows:

a) σ_v = 9 MPa;

b) P_o = 3 MPa;

c) H = 15 m;

d) at z = o, u = o, t = o to∞;

e) at z = o, u = o, t = o to∞;

The initial pore pressure response to the temperature increment, ΔT, is determined using equation 4.12 with $B^*T_i = \sigma_{vo}'/10$. One dimensional volume change of the oil sand layer, i.e. vertical expansion, is determined by equation 5.2 assuming a constant value of $m_v = 5 \times 10^{-7}$ kPa^{-1}. The coefficient of consolidation, c_v, varies nonlinearly with temperature from 0.01 m^2/s at 5°C to 0.1

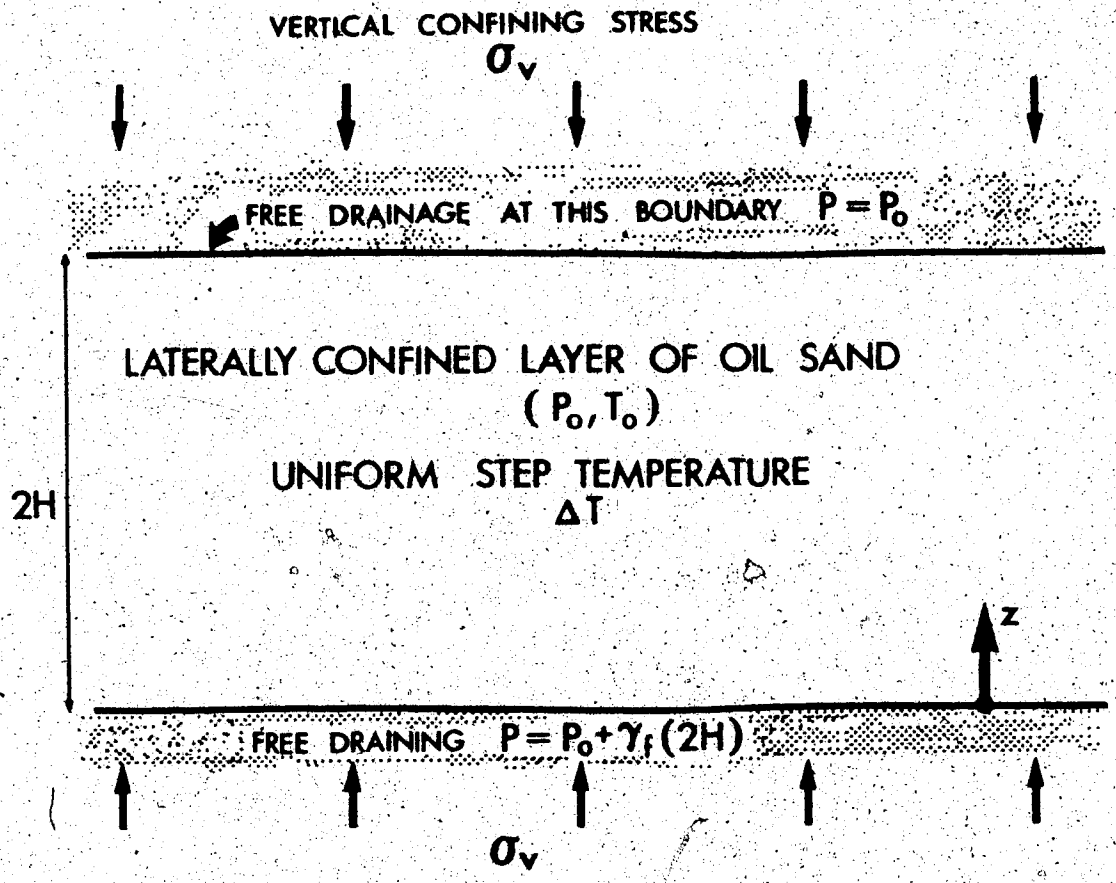

FIGURE 5.1 Analytical Model for One-Dimensional Heat Consolidation Following Non-Transient Heating

m^2/s at 205°C according to the following relationship:

$$\Delta \log c_v = \frac{\Delta T}{200}$$

The drained coefficient of thermal expansion, α_{DR}, was assumed to be constant at $3 \times 10^{-4} °C^{-1}$. Dissipation of excess pore pressure throughout the layer with time following heating is determined by solving equation 5.7, the one dimensional consolidation equation. The mathematical solution for equation 5.7 used here was developed by Taylor (1948). Carslaw and Jaeger (1959) also give analytical solutions applicable to the consolidation equation. Pore pressure isochrones within the consolidating layer are characterized as sine wave segments.

A computer program "HC" was coded in Fortran language to solve the above example. The program code is included in Appendix J. Results of the analysis are summarized in Figures 5.2.1 to 5.2.5, inclusive.

Isochrones of pore pressure with depth at various times following heating are plotted in Figures 5.2.1 to 5.2.4 for temperature increments, ΔT, of 1°C, 10°C, 100°C and 200°C. Although the initial pore pressure increase, u_o, is greater for larger temperature increments, the coefficient of consolidation, c_v, for oil sand also increases with temperature. Excess pore pressures dissipate very rapidly at 100°C and 200°C.

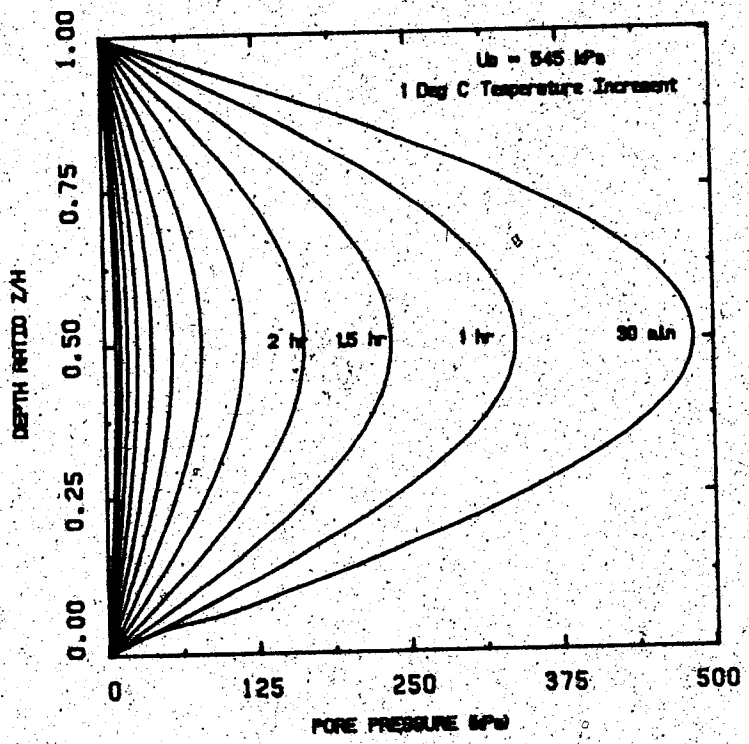

FIGURE 5.2.1 Pore Pressure Dissipation Following a 1°C Temperature Increase in a Confined Oil Sand Layer

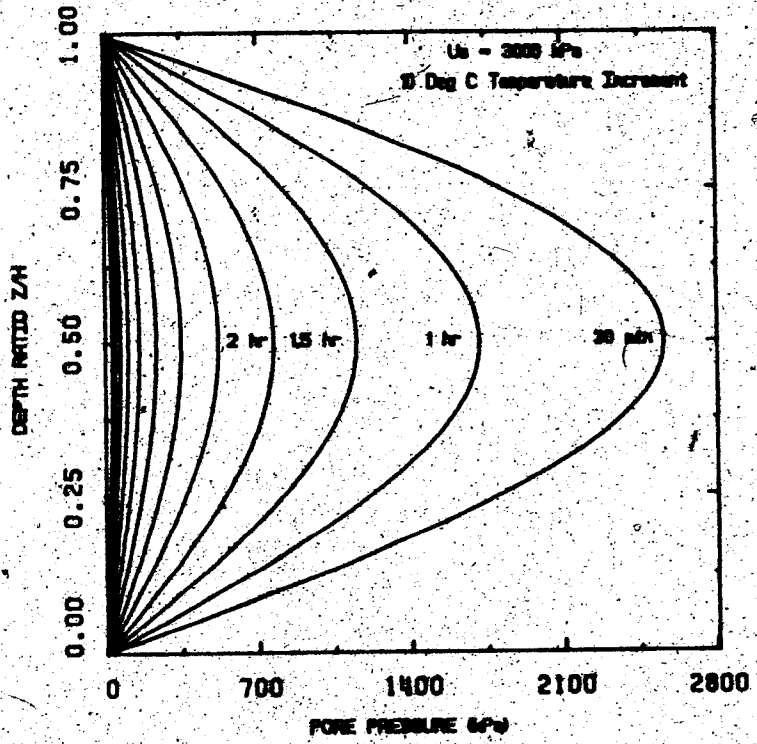

FIGURE 5.2.2 Pore Pressure Dissipation Following a 10°C Temperature Increase in a Confined Oil Sand Layer

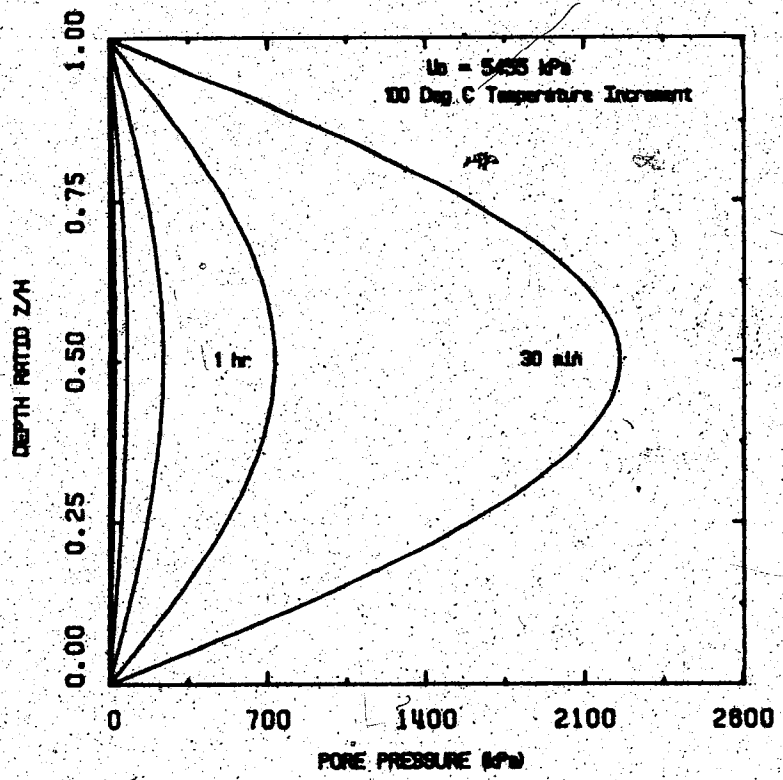

FIGURE 5.2.3 Pore Pressure Dissipation Following a 100°C Temperature Increase in a Confined Oil Sand Layer

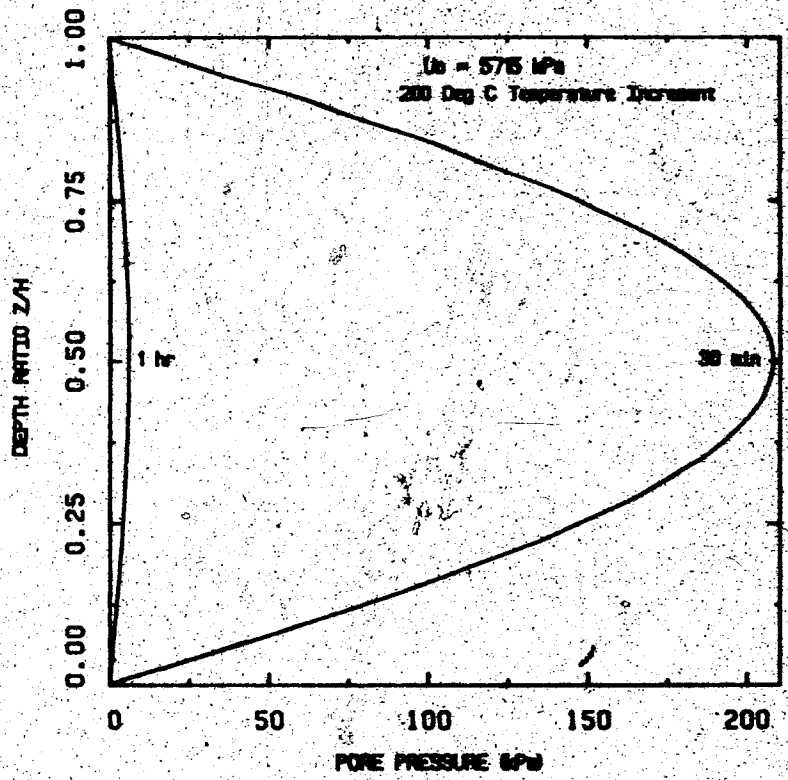

FIGURE 5.2.4 Pore Pressure Dissipation Following a 200°C Temperature Increase in a Confined Oil Sand Layer

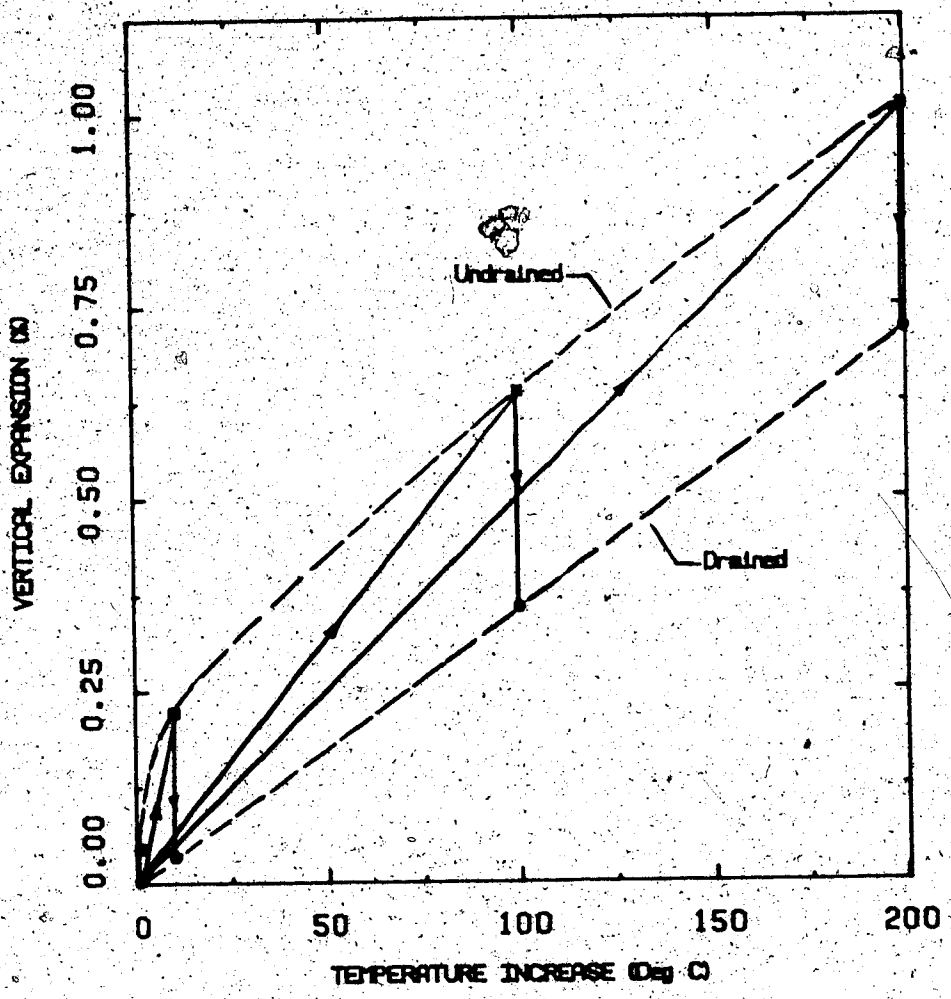

FIGURE 5.2.5 Undrained and Drained Thermal Expansion of a Confined Oil Sand Layer for Various Step Temperatures

The initial (undrained) and long-term (drained) vertical expansion of the oil sand layer are plotted for each temperature increment in Figure 5.2.5. Undrained vertical expansion occurs simultaneously with the initial (undrained) temperature increase. Drained vertical expansion represents the long-term thermal expansion after all excess pore pressure has dissipated.

5.4.3 One Dimensional Heat Consolidation During Transient Heating

In general heat transfer in porous materials is a transient process. Important modes of heat transfer include both diffusion and convection. Heat flow by diffusion is described by Fourier's Law which relates the time rate of heat transfer to a temperature gradient through a proportionality factor called the thermal conductivity. Fourier's Law is analogous to Darcy's Law and for one dimensional conduction may be expressed mathematically as:

$$\frac{\partial h}{\partial t} = k_T \frac{\partial T}{\partial z} \qquad (5.10)$$

The thermal conductivities of the solid and liquid phases of porous soils and rocks are often combined or measured experimentally to give a single value of thermal conductivity for the medium. Cervenan et al (1980) have measured thermal conductivity of Athabasca oil sand. At the microscopic level in multiphase media conductive heat transfer is enhanced by a form of convection due to temperature and velocity gradients within the pore space. Bear (1972) describes this combined conduction-convection mode of heat

transfer macroscopically as "thermal dispersion", and the constant of proportionality is termed the medium "conduction-dispersion coefficient".

Convection is defined as transfer of heat by fluid flow. If the pore fluid is forced to move by the action of a pump, the phenomenon is called "forced convection", whereas the term "advection" has been used to describe convection associated with regional groundwater flow (Mercer et al., 1982).

A third parameter which enters into the differential equation describing heat transfer is the heat capacity. Heat capacity per unit mass of the system is called specific heat and is a measure of the heat storage capacity of a material. The specific heat of mineral solids in soils and rocks is typically only 25% of that of water.

The differential equation describing heat transfer by thermal diffusion may be derived using the principle of thermal energy conservation. The equation describing one dimensional thermal diffusion in cartesian coordinates is of the form:

$$\rho c \frac{\partial T}{\partial t} = k_T \frac{\partial^2 T}{\partial z^2} \qquad (5.11)$$

For some boundary value problems in which k_T, ρ and c are all constants in space and time, a single parameter, the thermal diffusivity, α_T, may be used and equation 5.11 becomes:

$$\frac{\partial T}{\partial t} = \alpha_T \frac{\partial^2 T}{\partial z^2} \qquad (5.11.1)$$

When fluid flow and heating occur simultaneously, heat transfer involves both thermal diffusion and convection. Both mass conservation and thermal energy conservation must be considered in derivation of the convective-diffusion equation. The one dimensional convective-diffusion equation is of the form:

$$\left[(1-\eta)\,\rho_s c_s + \eta_f \rho_f c_f\right]\frac{\partial T}{\partial t} = k_T\,\frac{\partial^2 T}{\partial z^2} - \rho_f c_f v\,\frac{\partial T}{\partial z} \qquad (5.12)$$

where the flow velocity, v, is given by Darcy's Law and is constant over the flow path under consideration.

The problem of one dimensional heat consolidation during transient heating involves simultaneous solution of at least two differential equations.

1. Heat transfer by thermal diffusion alone given by equation 5.17, may be solved uncoupled from the heat consolidation equation. Consideration of heat transfer by convective-diffusion given in equation 5.12 requires coupling of the heat transfer and consolidation equations.
2. Thermal pore pressure generation during transient undrained heating is given by:

$$\left(\frac{\partial u}{\partial t}\right)_T = B_T\,\frac{\partial T}{\partial t} \qquad (5.13)$$

Transient heat consolidation may be characterized by summation of simultaneous pore pressure responses to transient undrained heating (equation 5.13) and

consolidation as given in equation 5.7.

The heat consolidation equation describing simultaneous thermal pore pressure generation and dissipation of excess pore pressures then, is:

$$\frac{\partial u}{\partial t} = B_T\,(u,T)\,\frac{\partial T}{\partial t} + c_v\,(u,T)\,\frac{\partial^2 u}{\partial z^2} \qquad (5.14.1)$$

For transient heating by diffusion equation 5.14.1 becomes:

$$\frac{\partial u}{\partial t} = B_T \alpha_T \frac{\partial^2 T}{\partial z^2} + c_v \frac{\partial^2 u}{\partial z^2} \qquad (5.14.2)$$

Lachenbruch (1980) has also developed a similar expression which includes a term for frictional heat generation within a fault or shear zone.

Equations 5.14.1 and 5.14.2 are nonlinear because of the dependence of the coefficients B_T and c_v on excess pore pressure, u, the primary variable. Because of nonlinearity of equations 5.14.1 and 5.14.2, solutions for different boundary conditions are not superposable. In general, there are no exact solutions for the partial differential equations describing heat consolidation.

The possibility of assuming constant values for the coefficients B_T, α_T and c_v in equation 5.20.2 was considered as a means of obtaining an exact solution for comparison with and verification of numerical solutions.

Carslaw and Jaeger (1959) give exact solutions for a similar differential equation describing simultaneous heat generation and diffusion within a slab. Assigning constant values for α_T and c_v in equation 5.14.2 does not violate physical principles. However, assuming that B_T is constant can result in the unrealistic prediction that excess pore pressure increases continuously with temperature and time and may even exceed the initial effective confining stresses. Hence, the exact solution of equation 5.14.2 with B_T constant and time, $t > 0$, is only physically correct if the rate of thermal pore pressure generation is less than or equal to the rate of pore pressure diffusion. Satisfying this constraint yields trivial solutions of no practical interest, even for verifying numerical solution techniques, since no excess pore pressures are generated during heating.

Exact solution of the general case in which B_T is a function of u, the primary variable in equations 5.14.1 and 5.14.2, is intractable (see for example, Carslaw and Jaeger, 1959, p. 12 and p. 130).

Analytical solutions for thaw consolidation (another thermal consolidation problem) given by Nixon (1973) yield a dimensionless "thaw consolidation ratio". By inference, a similar and useful dimensionless "heat consolidation ratio" may be defined as follows:

$$R_T = \left(\frac{c_v}{\alpha_T}\right) \qquad (5.15)$$

Numerical solutions for one dimensional heat consolidation during transient heating by both diffusion and convective-diffusion are developed in following subsections of this chapter.

Numerical solutions for two and three dimensional heat consolidation problems are described in Chapter 6. An uncoupled numerical modelling procedure may be used if pore pressure response to total stress changes is assumed to be small.

As discussed in section 4.1 of Chapter 4, volumetric expansion during transient heating and consolidation may be characterized using a "partially drained" coefficient of thermal expansion. Transient temperatures and excess pore pressures calculated in an uncoupled heat consolidation analysis may be used to determine resultant transient volumetric strains throughout the porous medium. The distribution of volumetric strains corresponding to a given period of heating may be used to determine the spatial distribution of an "equivalent" coefficient of transient thermal expansion. Transient volumetric expansion due to heating and consolidation accordingly may be input into thermoelastic stress analyses using corresponding transient temperatures and the "equivalent" thermal expansion coefficients.

For the more general case in which the total stresses are not constant in space and time, a stress-induced pore pressure term may be added to the heat consolidation equation as follows:

$$\frac{\partial u}{\partial t} = B_T \frac{\partial T}{\partial t} + c_v \nabla^2 u + \left[B \frac{\partial \sigma_3}{\partial t} + AB \frac{\partial (\sigma_1 - \sigma_3)}{\partial t} \right] \qquad (5.16)$$

where A and B are Skempton's pore pressure parameters.

Development of solutions for equation 5.16 are beyond the scope of this study.

5.4.4 Heat Transfer Properties of Oil Sand

Heat transfer properties of oil sand were not investigated during the present laboratory investigation. A limited amount of data exists in the literature pertaining to heat transfer properties of oil sand. Cervenan et al. (1980) measured thermal conductivity of reconstituted Athabasca oil sand samples at moderate temperatures (i.e. 25 to 40°C). No measurement of thermal conductivity of oil sands has been made at elevated temperatures to the present time. However, thermal conductivity data has been published for quartz (Clarke, 1966) and for water in numerous steam table publications (e.g. ASME, 1977), at elevated temperature and pressures. Thermal conductivities of quartz, water and oil sand are plotted in Figure 5.3 for temperatures ranging from 0 to 300°C. The thermal conductivity of solid quartz increases linearly with temperature, whereas thermal conductivity of water is nearly constant with temperature over a range of pressures from 0.1 to 15 MPa. The range of thermal conductivity values reported by Cervenan et al. (1980) for Athabasca oil sand is also shown in

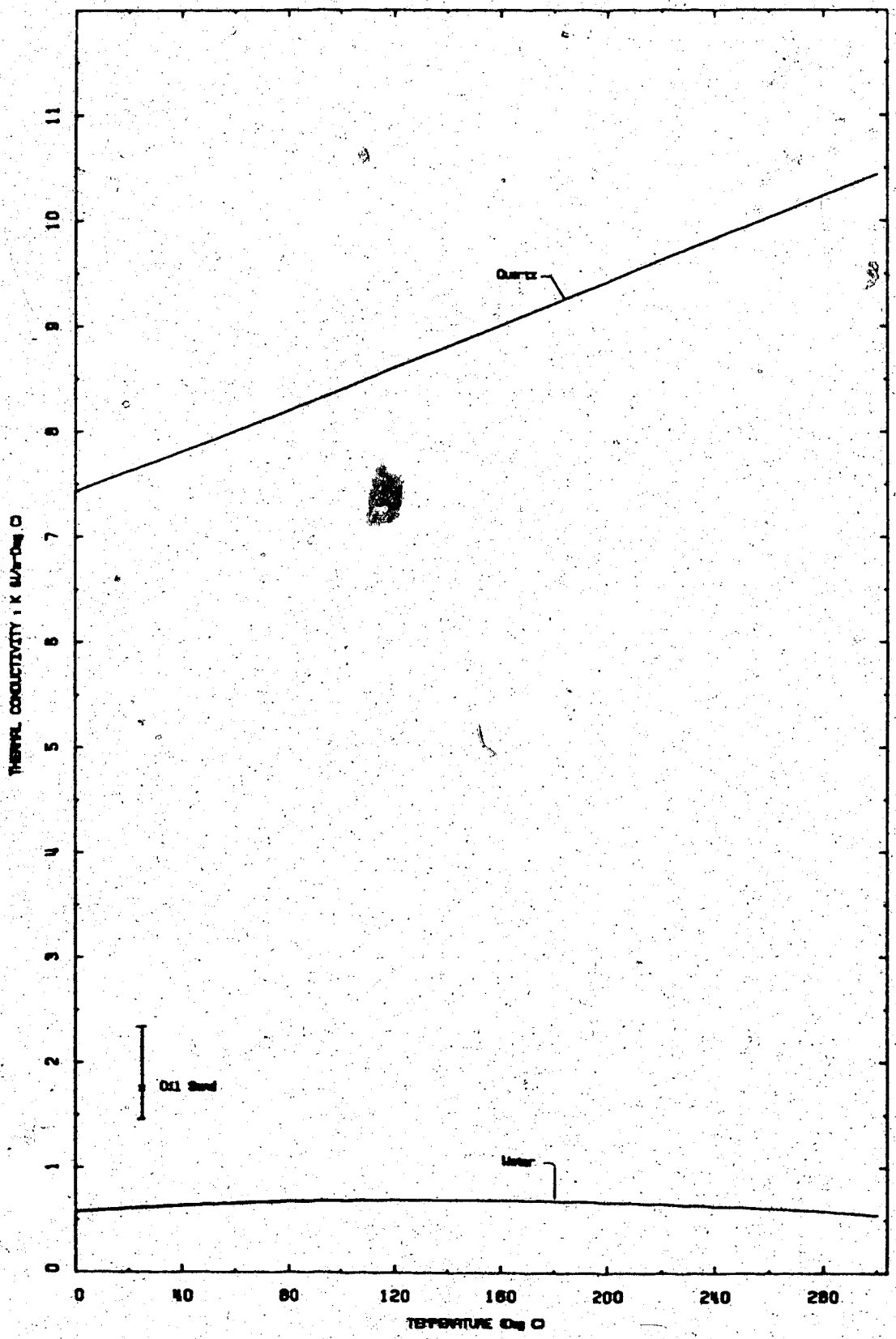

FIGURE 5.3 Thermal Conductivities of Quartz, Water and Oil Sand With Temperature

Figure 5.3; these researchers concluded that the mixture laws presented by Somerton et al. (1974) for heat transfer properties of unconsolidated sands do not apply to Athabasca oil sand. This conclusion must be viewed with caution, however, since the samples tested by Cervenan et al. probably contained a substantial proportion of air due to remoulding and disturbance.

Smith-Magowan, Skauge and Hepler (1982) measured specific heat of Athabasca oil sands and components over the temperature range 50-300°C using calorimetry. Specific heat was found to increase nonlinearly from about 0.9 to 1.2 J/g°C (Joules per gram per degree Celsius) over the above temperature range.

Thermal diffusivity also depends on density of the material as indicated in equations 5.11 and 5.12. In particular, the densities of the pore fluids in oil sand decrease significantly at elevated temperatures. Density of the solid particles decreases to a lesser extent. Variation of density with temperature for Athabasca bitumen and water are shown in Figure 5.4. Data for Athabasca bitumen was taken from Camp (1970) and the data for water was obtained from the ASME Steam Tables (1977). Corresponding changes in the bulk density of undisturbed oil sand would produce a typical decrease in mass density from about 2.15 to 2.02 Mg/m^3 over the temperature range 5°C to 300°C.

Based on the above published information, possible variation of the coefficient of thermal diffusivity, α_T, for

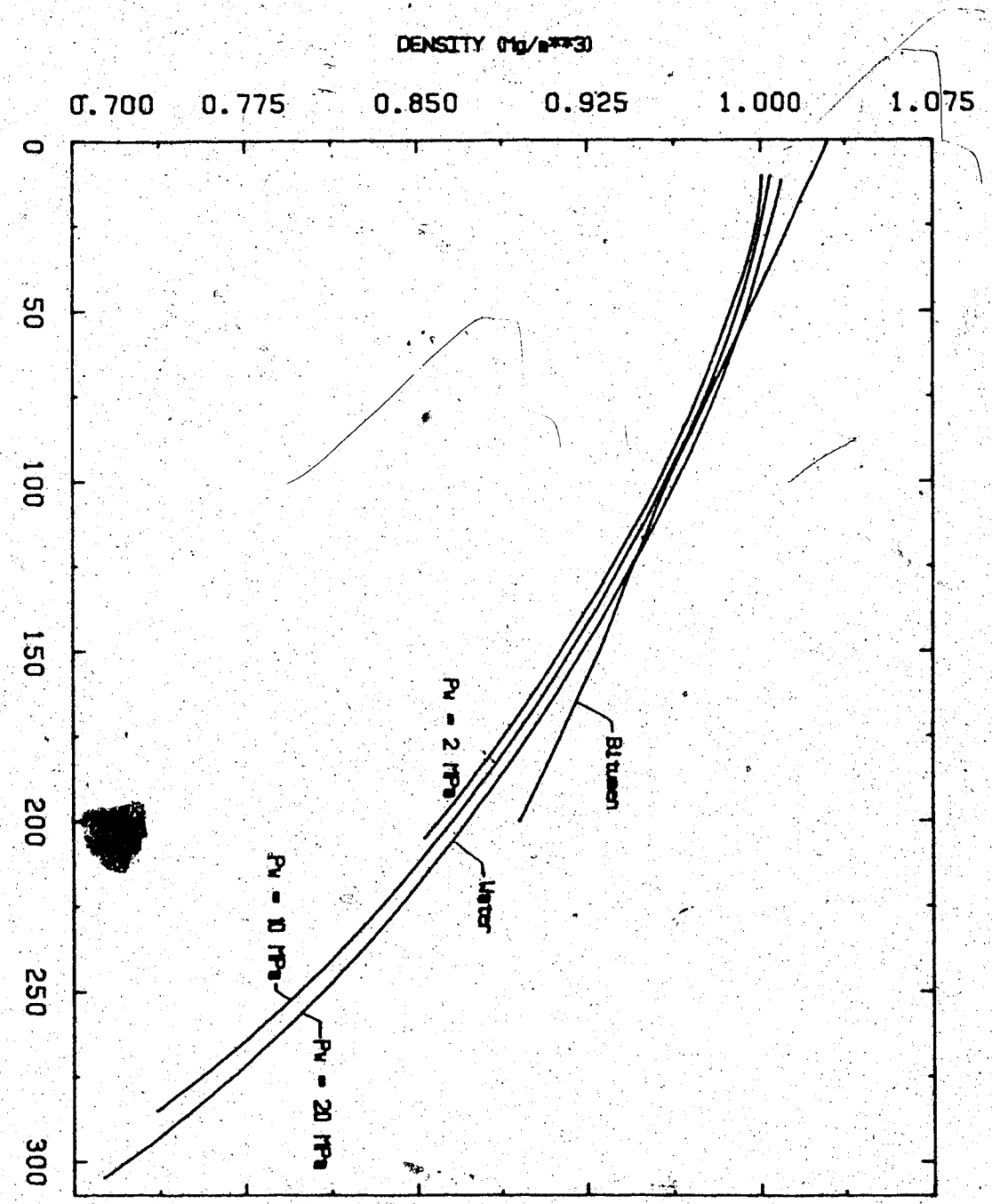

FIGURE 5.4 Variation of the Densities of Water and Athabasca Bitumen with Temperature

oil sand may range from about 8×10^{-7} to 1.1×10^{-6} m^2/s, over the temperature range 5°C to 300°C. This range of variation is rather modest. Thermal diffusivity, α_T, for oil sand is accordingly assumed to have a constant value of 1.0×10^{-6} m^2/s independent of temperature and pressure for numerical modelling studies presented in the following sections. Definitive experimental research should be initiated to determine thermal conductivity and thermal diffusivity of oils sands at elevated temperatures and pressures.

5.5 Numerical Solutions for One Dimensional Heat Consolidation Coupled with Heat Transfer by Thermal Diffusion

Numerical solution techniques are required for solving equations 5.14.1 and 5.14.2, the partial differential equation describing one dimensional heat consolidation. As previously noted, the parameters c_v and B_T vary nonlinearly with temperature and excess pore pressure.

Equation 5.11.1, the partial differential equation describing heat transfer by thermal diffusion may be solved analytically for boundary value problems assuming that the coefficient of thermal diffusion, α_T, is constant. Equation 5.11.1 has been solved numerically in the following examples for reasons of convenience in coupling the heat transfer and heat consolidation solutions.

Implicit finite difference solutions are generally preferrable to explicit schemes because of the very restrictive discretization constraints on both spatial and time derivations inherent in

explicit schemes. Instability of finite difference solutions results when truncation errors, arising from truncation of infinite series approximations of derivatives, become large. It can be shown that if only three-point spatial approximations are used, there is a maximum order of accuracy that may be achieved in approximating the individual terms of a partial differential equation (Laumbach, 1975).

The approach adopted here was to solve each pore pressure term in equation 5.14.2 separately for a single time step. Pore pressure variation resulting from bulk density changes was also included in the solution. Implicit finite difference solutions for heat transfer by diffusion and for pore pressure dissipation, together with explicit approximations for thermal pore pressure generation and total stress change were summed after each time step. Equation 5.11 may be approximated by the implicit finite difference equation:

$$T_{i,j} = T_{i,\,j+1} - \frac{\alpha_T \Delta t}{\Delta z^2}\left[T_{i+1,\,j+1} - 2T_{i,\,j+1} + T_{i-1,\,j+1}\right] \qquad (5.17)$$

where Δt and ΔZ are the time step and grid spacing, respectively; the subscript i refers to spatial nodes; and the subscript j refers to time level. Three-point central difference approximations have been used for the spatial derivatives and the time derivative has been approximated by a forward difference approximation in equation 5.17.

The discretization results in a set of linear equations having a tridagonal structure. The system of equations may be solved at each time level by inverting the tridiagonal matrix using techniques such

as Gaussian elimination or the Thomas Algorithm (Ames, 1965). Thomas's Algorithm has been used in this study for reasons of efficiency and minimal storage requirements.

Similarly, the consolidation equation 5.7 may be approximated by the implicit finite difference equation:

$$u_{i,j} = u_{i,\,j+1} - \frac{c_v \Delta t}{\Delta z^2}\left[u_{i+1,\,j+1} - 2u_{i,\,j+1} + u_{i-1,\,j+1}\right] \qquad (5.18)$$

This system of linear difference equations also has a tridiagonal structure. The system of equations may be solved simultaneously by the Thomas Algorithm at each time level.

The implicit finite difference solutions given in equations 5.17 and 5.18 are unconditionally stable. The thermal pore pressure generation term in equation 5.14.2 is a function of temperature and effective stress. Consequently, this contribution to the transient pore pressure distribution, must be determined explicitly at each time level.

A computer program "HCD" was coded in Fortran language to solve the one dimensional heat consolidation problem coupled with transient heating by thermal diffusion. The computer code for HCD is included in Appendix J. Figure 5.5 is a flow chart of the programming logic and step-by-step operation of HCD. The program accesses two subroutines TEMPD and CONSOL during execution to calculate the temperature distribution and spatial dissipation of excess pore pressure at each time level.

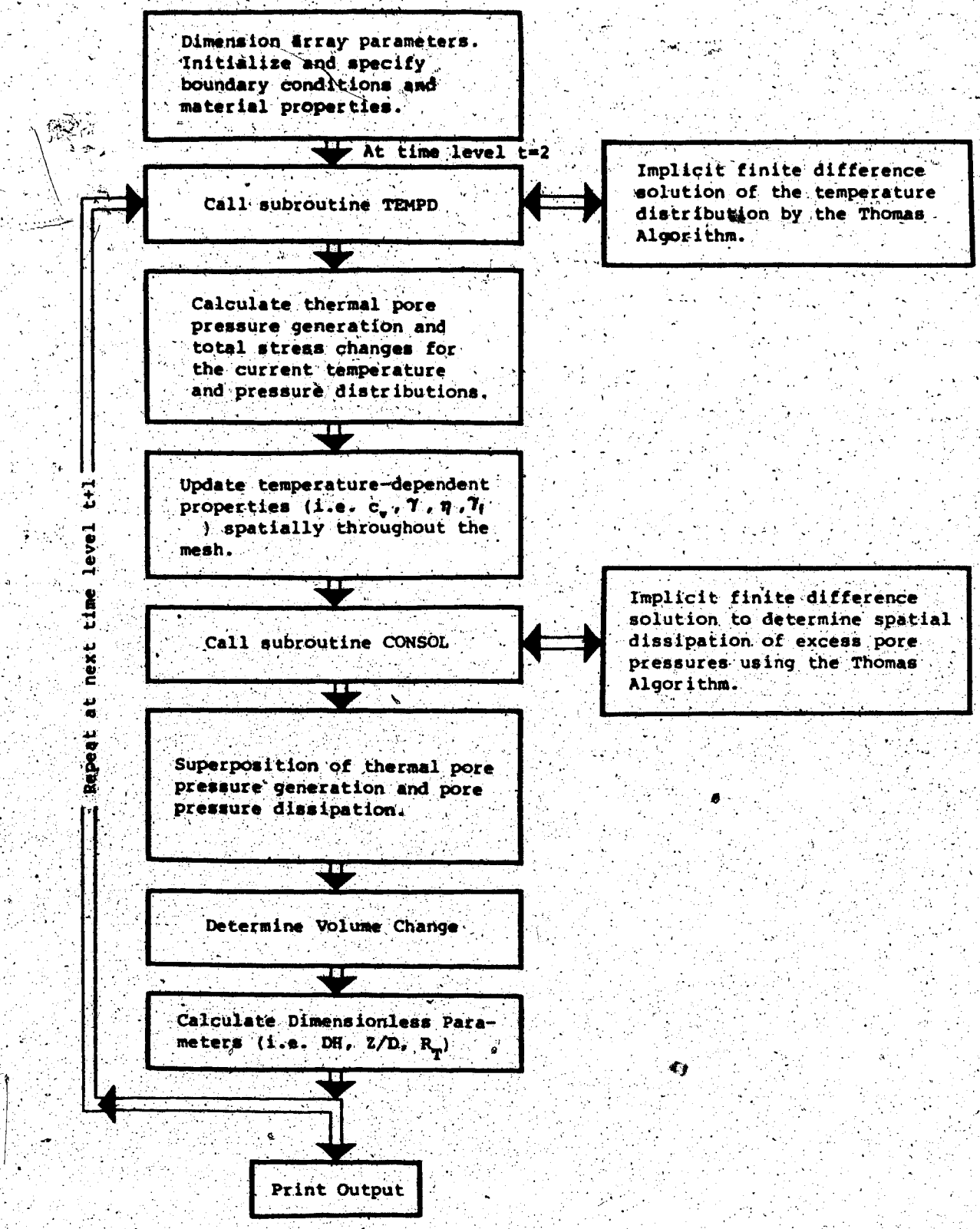

FIGURE 5.5 Flow Diagram for Numerical Analysis of Heat Consolidation

Two analytical models of heat consolidation were analyzed with the program HCD. The analytical models are illustrated in Figures 5.6 and 5.7. Model No. 1 in Figure 5.6 has a step temperature applied at the base of a semi-infinite oil sand layer. The bottom boundary is a free-draining constant pressure/constant temperature boundary while no flow of heat or fluid is permitted at the top boundary. Model No. 1 is a "one-way drainage" model. Model No. 2 illustrated in Figure 5.7 is a "two-way drainage" model, i.e. both top and bottom boundaries are free-draining constant pressure/ constant temperature boundaries. In Model No. 2 the bottom boundary is the heat source while the top boundary is a heat sink. The computer code of Program HCD was modified for 2-way drainage boundary conditions, for this analysis.

The implicit solutions for heat transfer in subroutine TEMPD and for pore pressure dissipation in subroutine CONSOL are unconditionally stable. Also, since the coefficient of thermal diffusion, α_T, remains constant, the prediction of temperature distribution with time is independent of the magnitude of time step used in the analysis. However, the coefficient of consolidation, c_v, varies nonlinearly with temperature, and therefore prediction of pore pressure dissipation with time is dependent on the magnitude of time increment selected for the analysis. The time step dependence of pore pressure predictions in the finite difference solution is further complicated by the fact that the thermal pore pressure generation parameter, B_T, varies nonlinearly with temperature increment which depends on the time step size.

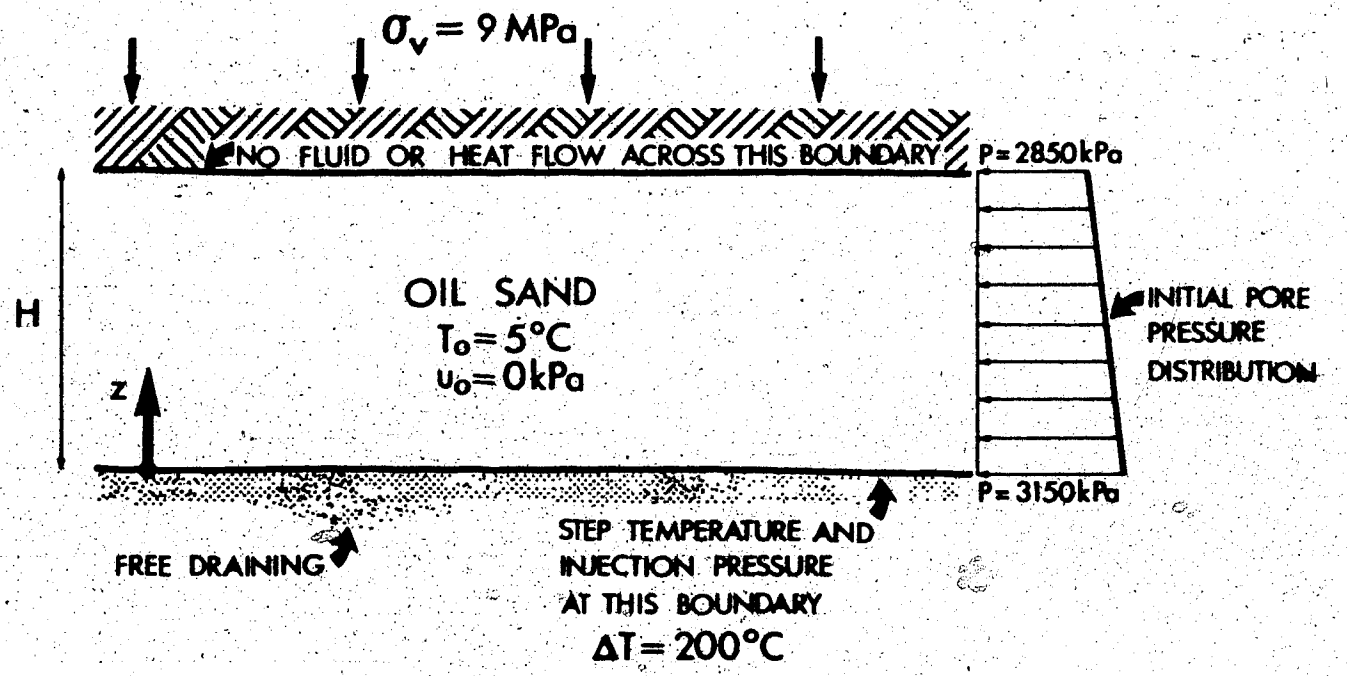

FIGURE 5.6 Analytical Model No. 1 - One-Way Drainage

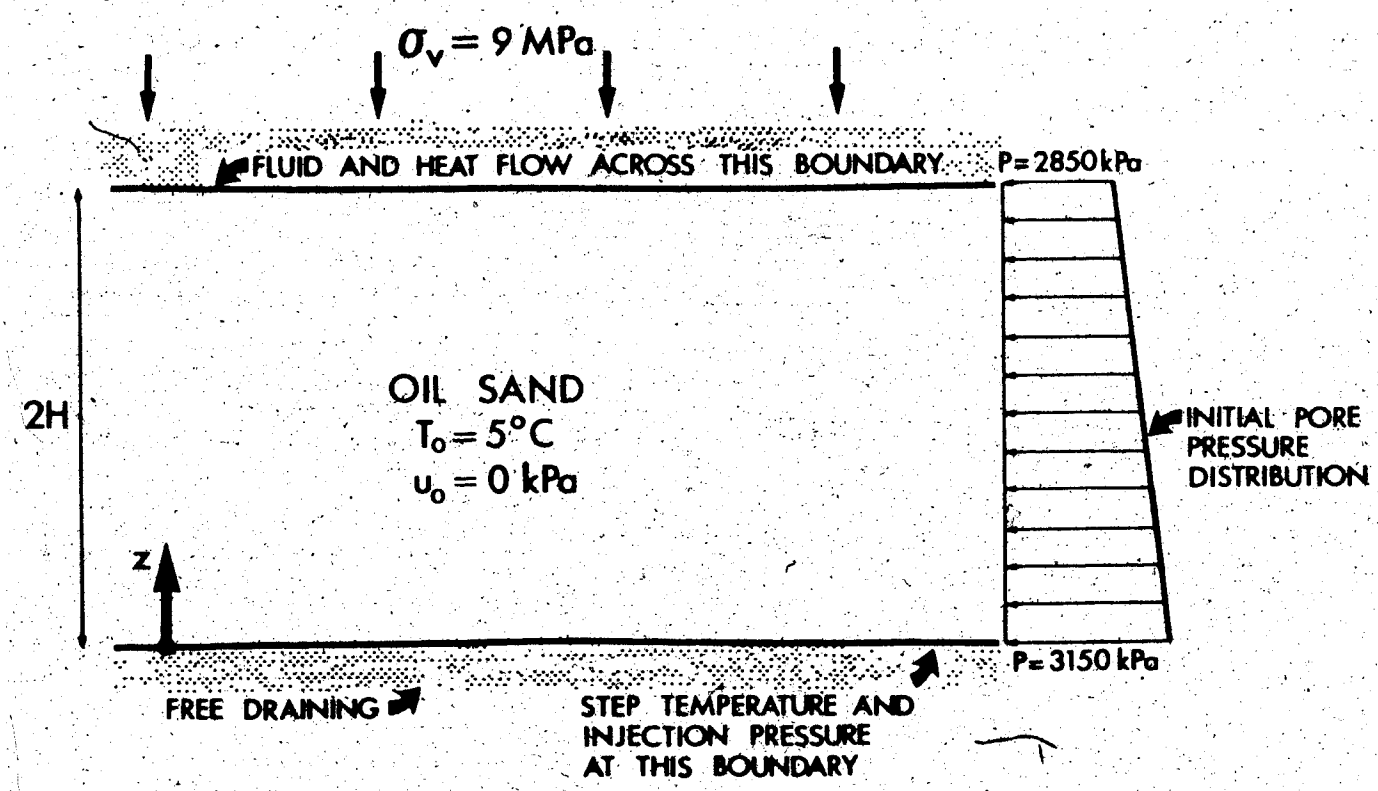

FIGURE 5.7 Analytical Model No. 2 - Two-Way Drainage

5.5.1 Influence of Temporal Discretization on Numerical Solutions

Requirements for selecting a suitable time step in order to ensure a stable, convergent solution were not readily apparent for the coupled numerical analyses. In general, smaller time increments yield closer approximations to analytical solutions of partial differential equations. Criteria for temporal discretization of purely explicit finite difference approximations such as the Neumann Criterion (see Desai and Christian, 1977), or the Karplus Criterion (see Farouq Ali, 1981) are not directly applicable to the numerical scheme presented here. A "trial-and-error" approach was adopted to test stability and convergence of the heat consolidation numerical analyses.

1. <u>One-Way Drainage Analyses</u>

The configuration described in Figure 5.6, i.e. analytical model no. 1, was analyzed using the following time steps:

a) 1 month;
b) 1 day;
c) 1 hour;
d) 10 minutes;
e) 1 minute;
f) 30 seconds; and
g) 15 seconds.

The analyses involved introduction of a 200°C step temperature at the base of a 30 m thick oil sand layer. The base, i.e. Z=0, was maintained at constant pressure and temperature while no flow of heat or fluid was permitted across the top boundary.

Temperature and excess pore pressure distributions within the oil sand layer determined using a 1 month time step are shown in Figures 5.8.1 and 5.8.2, respectively. Distributions of the heat consolidation ratio, R_T, within the oil sand layer are shown in Figure 5.8.3. Vertical expansion of the oil sand layer with time predicted in this analysis (i.e. using a one month time step) is shown in Figure 5.8.4.

Results of a second similar analysis predicted using a 1 day time step are presented in Figures 5.9.1 to 5.9.4, inclusive. Comparison of Figures 5.8.2 and 5.9.2 clearly demonstrates that the magnitude and distribution of excess pore pressures predicted are very much influenced by the size of time step selected. Deformations predicted in the two analyses are also influenced by the temporal discretization, as may be seen by comparing Figures 5.8.4 and 5.9.4.

Results of similar analyses using shorter time steps of 1 hour, 10 minutes, 1 minute, 30 seconds and 15 seconds are presented in Appendix K, Figures K1.1 to K5.3,

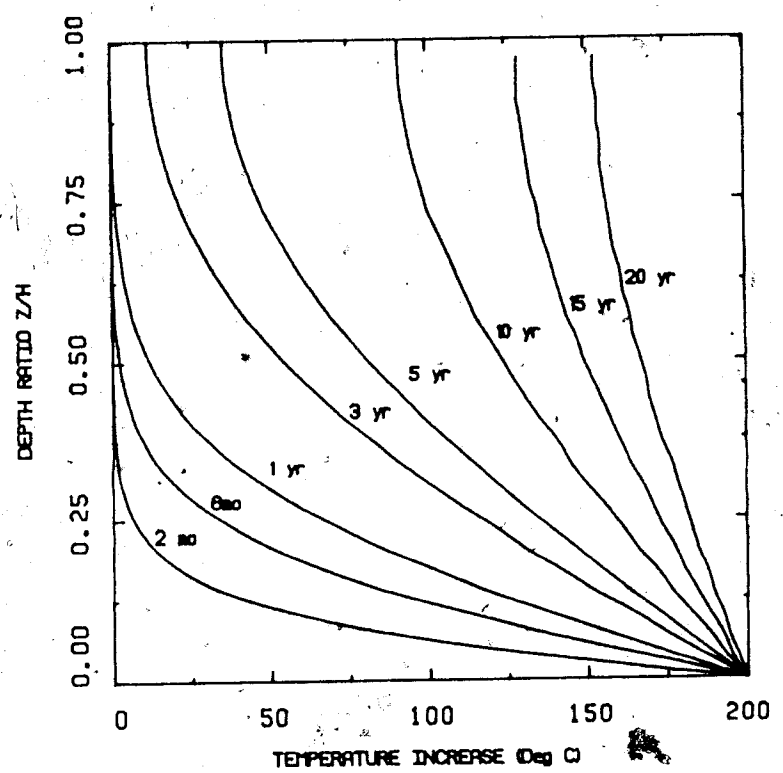

FIGURE 5.8.1 Transient Temperatures - One-Way Drainage (1 Month Time Step)

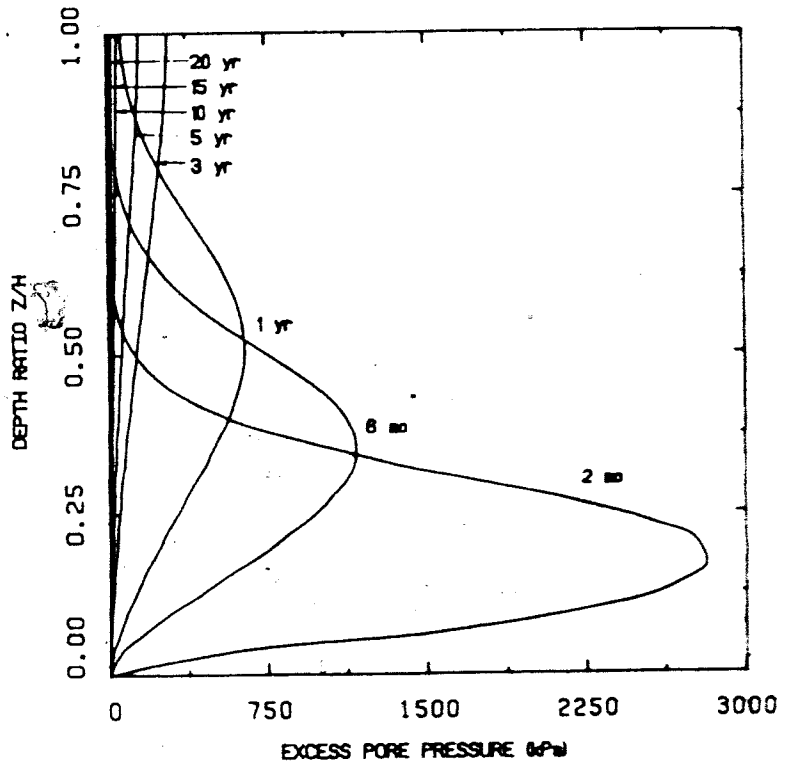

FIGURE 5.8.2 Transient Excess Pore Pressures - One-Way Drainage (1 Month Time Step)

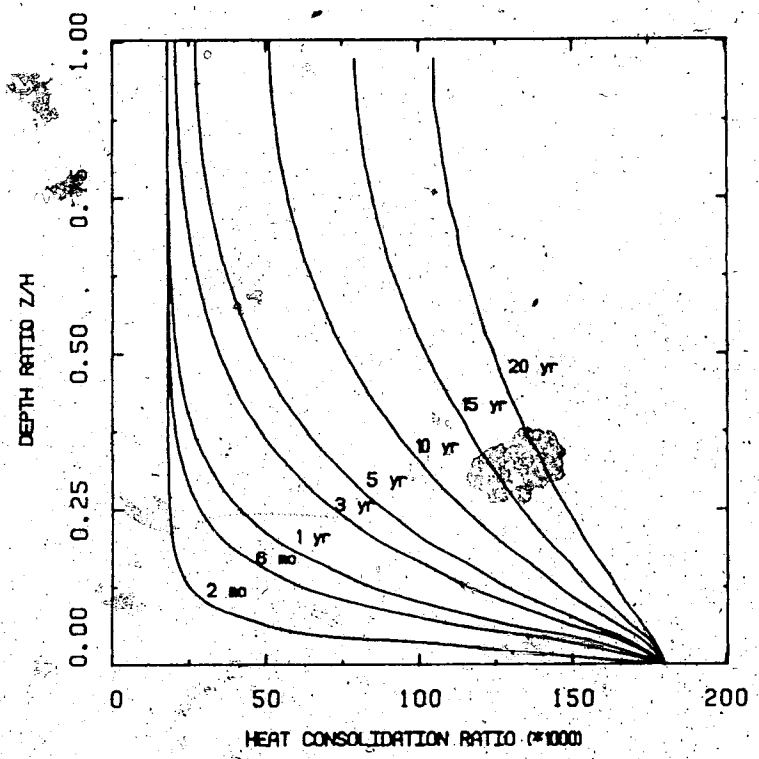

IGURE 5.8.3 Transient Vertical Expansion - One-Way Drainage (1 Month Time Step)

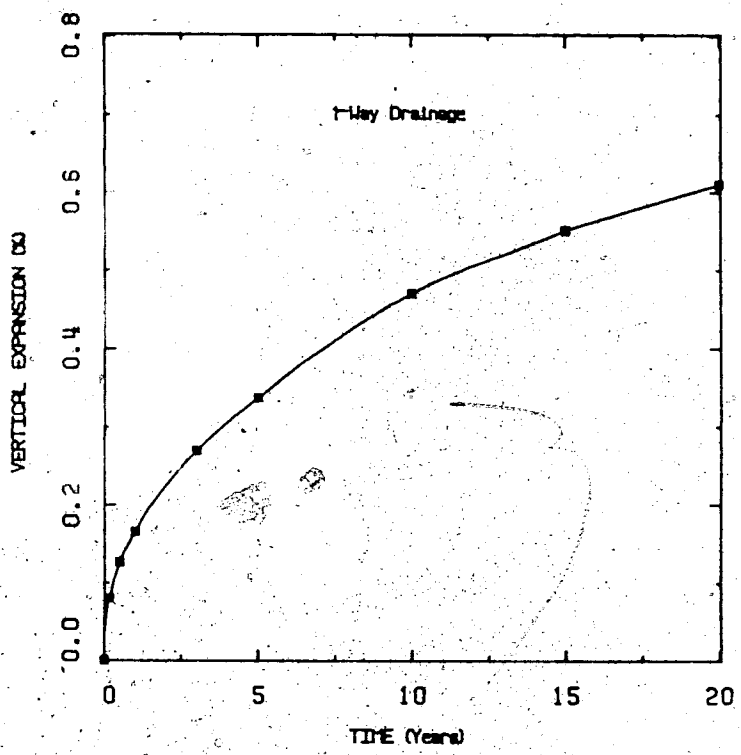

FIGURE 5.8.4 Transient Heat Consolidation Ratio One-Way Drainage (1 Month Time Ste

Pag

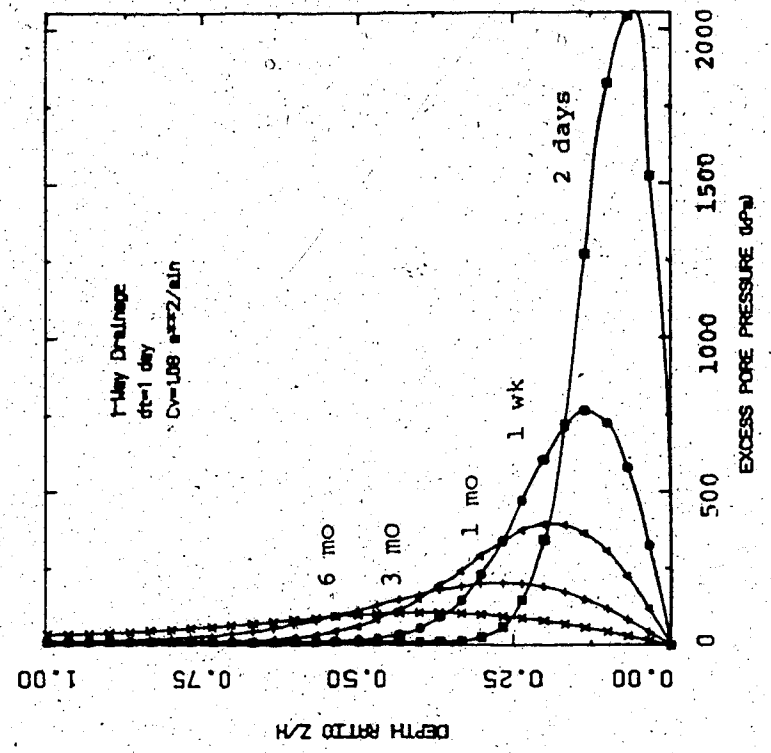

FIGURE 5.9.2 Transient Excess Pore Pressures - One-Way Drainage (1 Day Time Step)

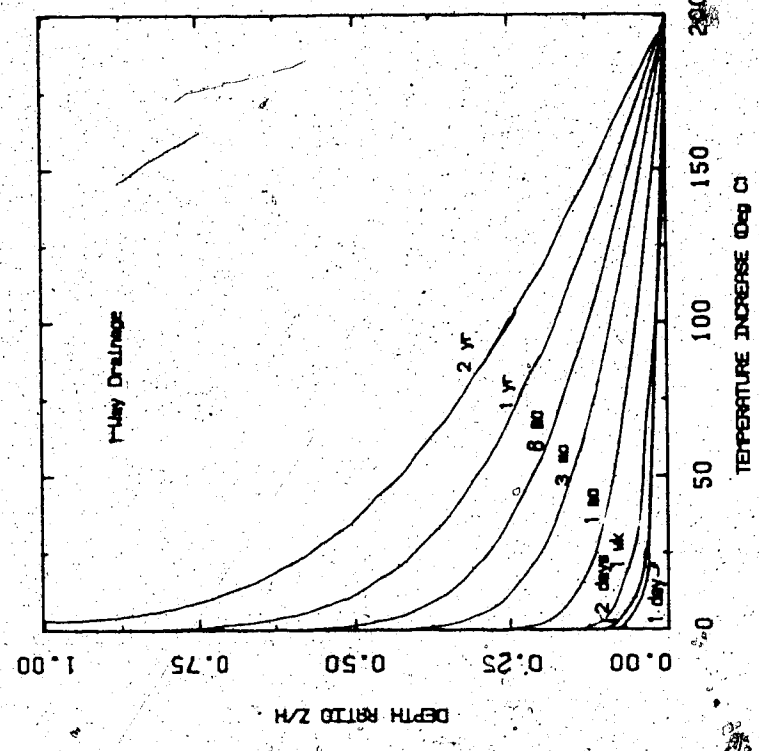

FIGURE 5.9.1 Transient Temperatures - One-Way Drainage (1 Day Time Step)

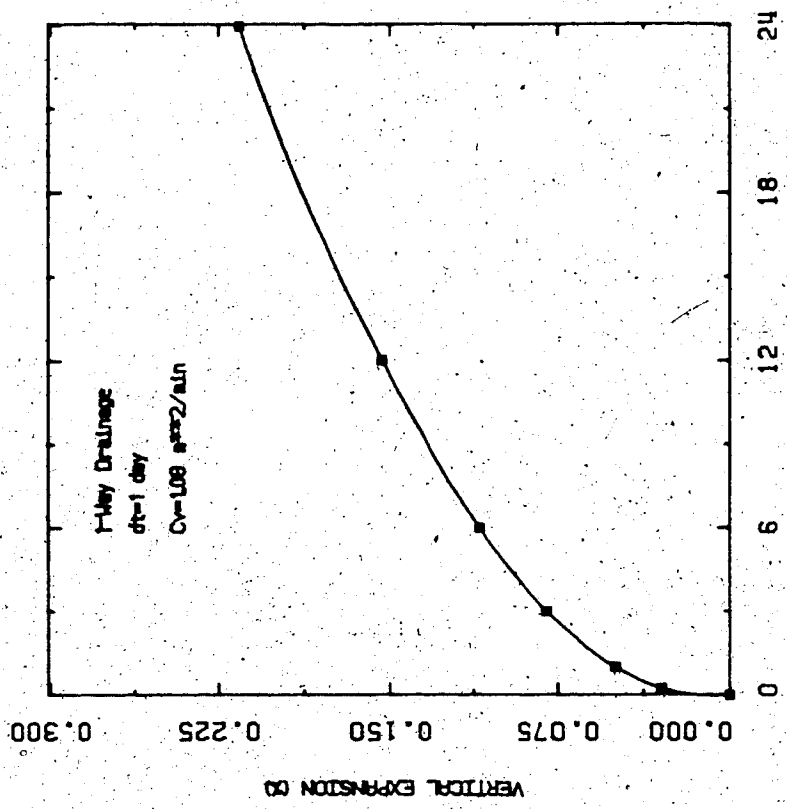

FIGURE 5.9.4 Transient Heat Consolidation Ratio - One-Way Drainage (1 Day Time Step)

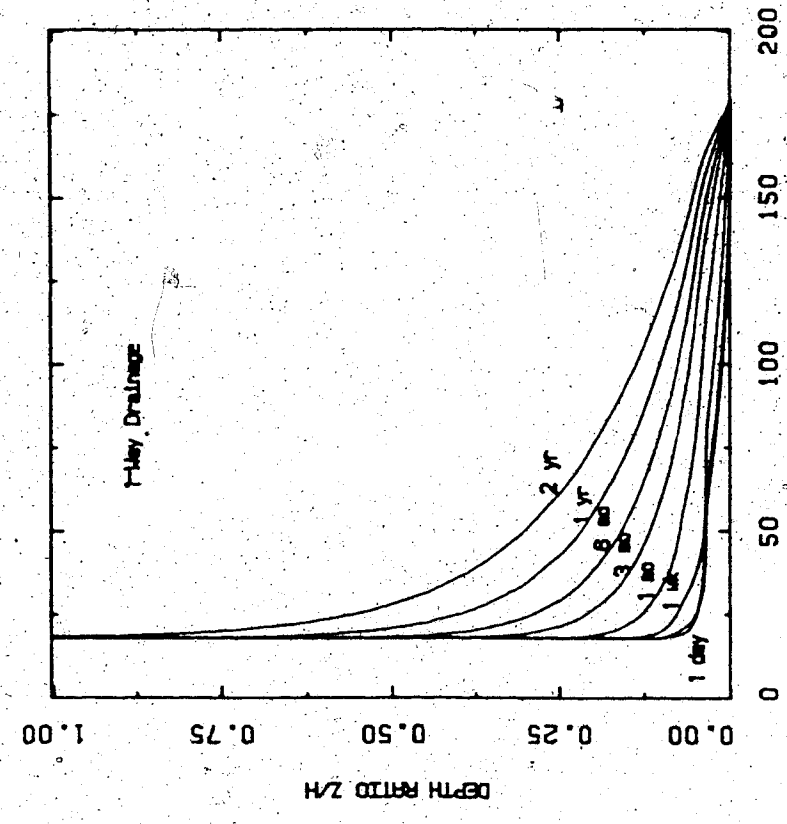

FIGURE 5.9.3 Transient Vertical Expansion - One-Way Drainage (1 Day Time Step)

inclusive. These analytical results also illustrate that pore pressures and deformations are overpredicted if very large time steps are used in the analysis.

Similar, although not quite identical, predictions of pore pressure and vertical deformation were obtained using time step durations of 1 minute, 30 seconds and 15 seconds. For practical purposes, a 1 minute time step appears to be adequate, although small instabilities persist near the constant temperature boundary. Pore pressure spikes near the heat source are present during early time steps because of the very high temperature gradient which is applied instantaneously in these analyses. The instability represented by these spikes is eliminated when sufficiently small time steps are used or after some elapsed time when the temperature gradient is reduced.

2. Two-Way Drainage Analyses

Two-way drainage boundary conditions for heat and fluid drainage (see Figure 5.7) were also analyzed using one month and one day time steps. Results are presented in Figures 5.10.1 to 5.10.4 for the 1 month step and 5.11.1 to 5.11.4 for the 1 day time step. Long term temperature and pore pressure distributions are altered by introducing a top drainage boundary, however short term predictions are very similar to those of the one-way drainage analyses.

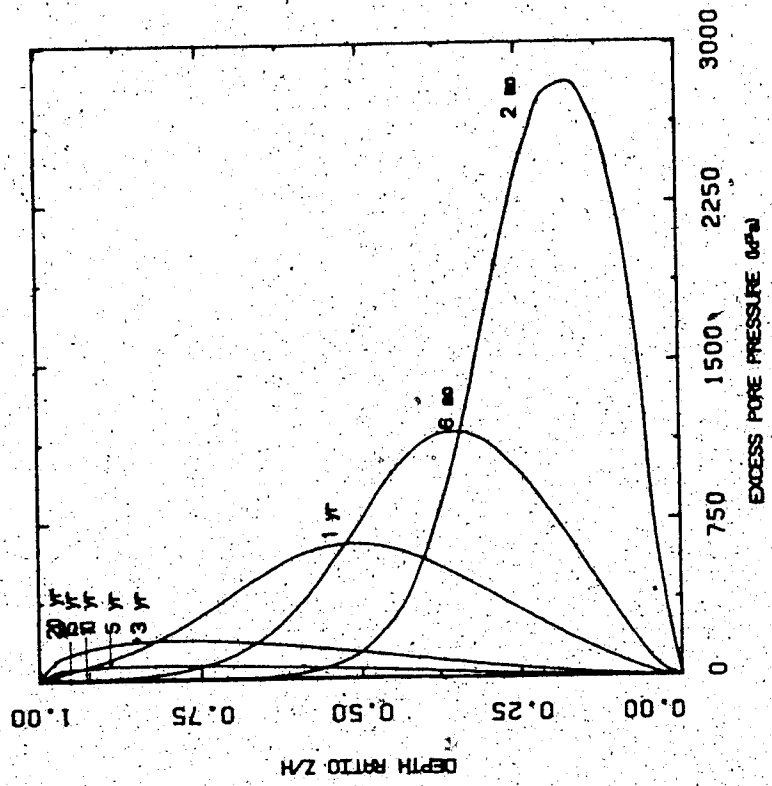

FIGURE 5.10.2 Transient Excess Pore Pressures-Two-Way Drainage (1 Month Time Step)

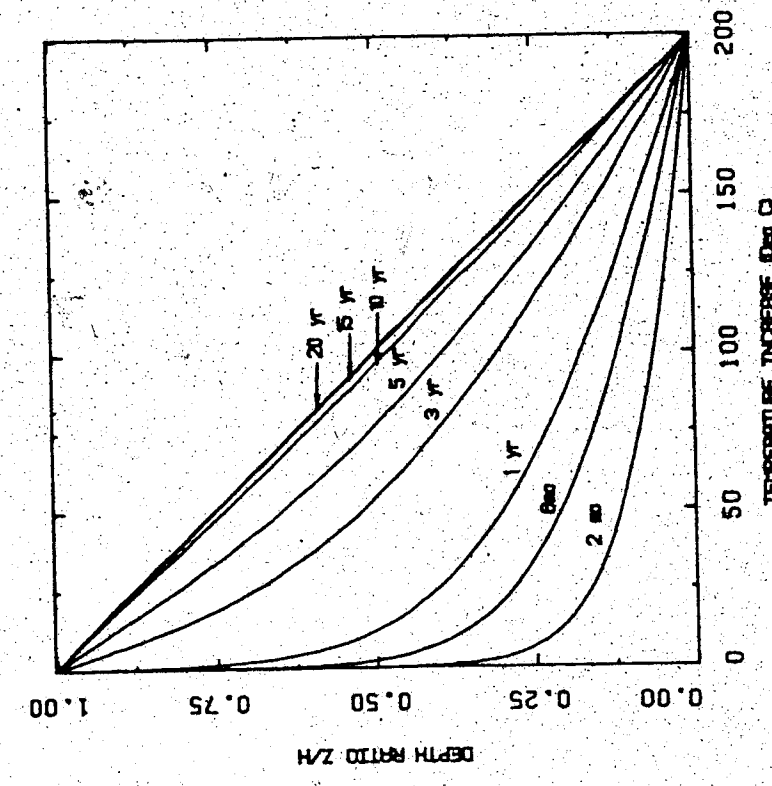

FIGURE 5.10.1 Transient Temperatures - Two-Way Drainage (1 Month Time Step)

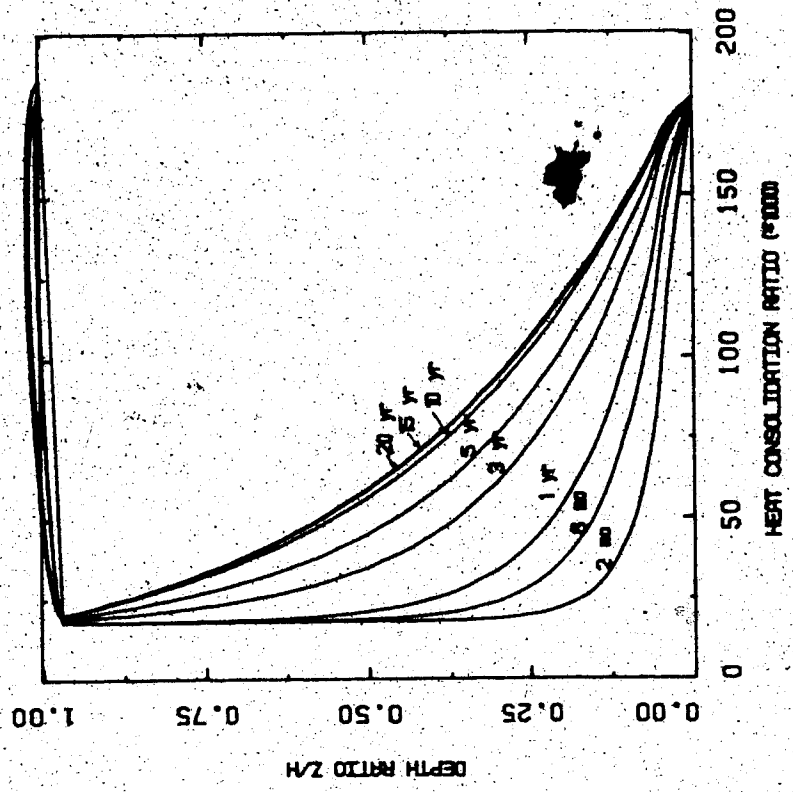

FIGURE 5.10.4 Transient Vertical Expansion - Two-Way Drainage (1 Month Time Step)

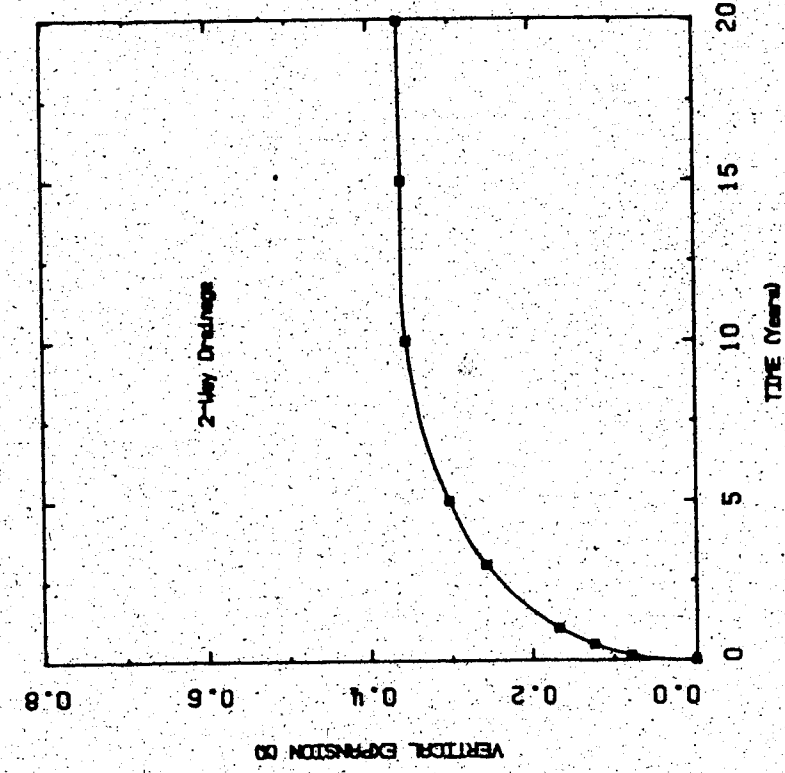

FIGURE 5.10.3 Transient Heat Consolidation Ratio Two-Way Drainage (1 Month Time Step)

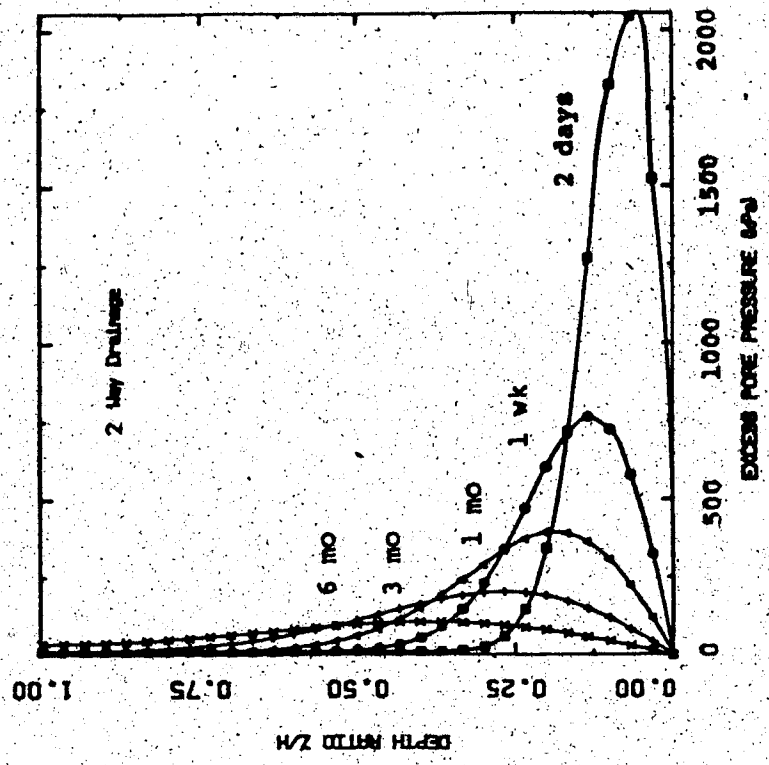

FIGURE 5.11.2 Transient Excess Pore Pressures-Two-Way Drainage (1 Day Time Step)

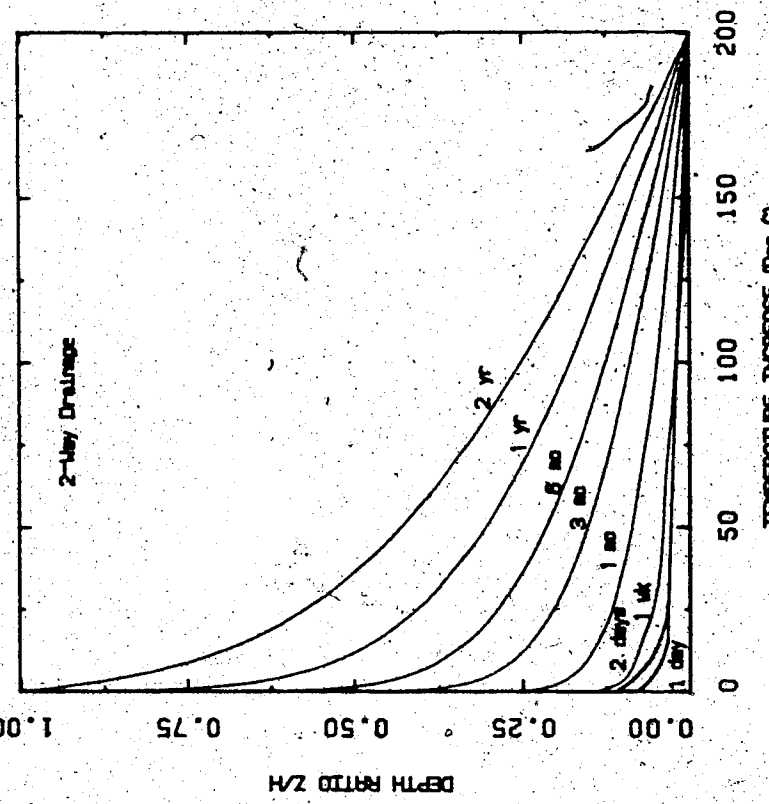

FIGURE 5.11.1 Transient Temperatures - Two-Way Drainage (1 Day Time Step)

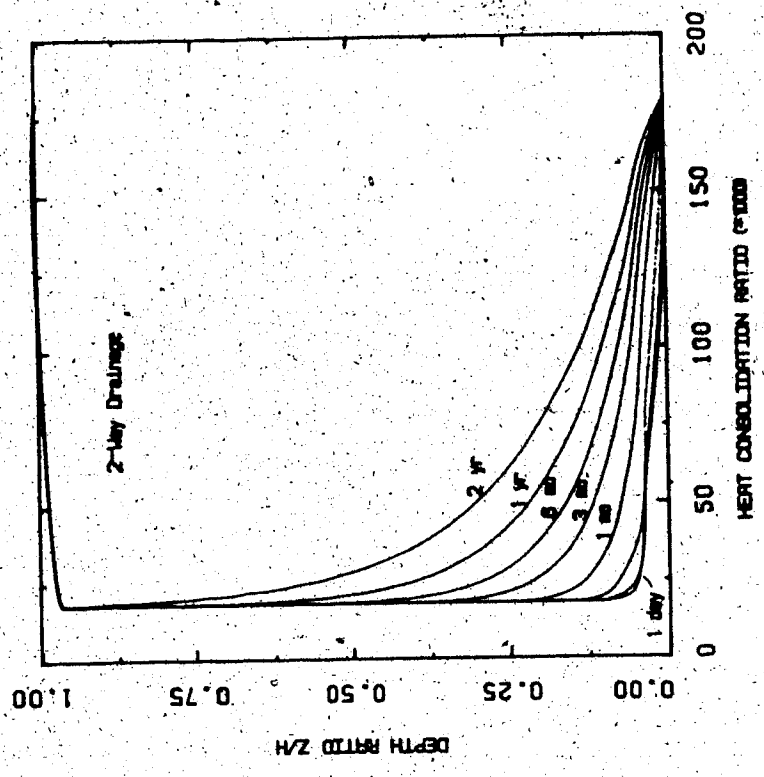

FIGURE 5.11.4 Transient Vertical Expansion - Two-Way Drainage (1 Day Time Step)

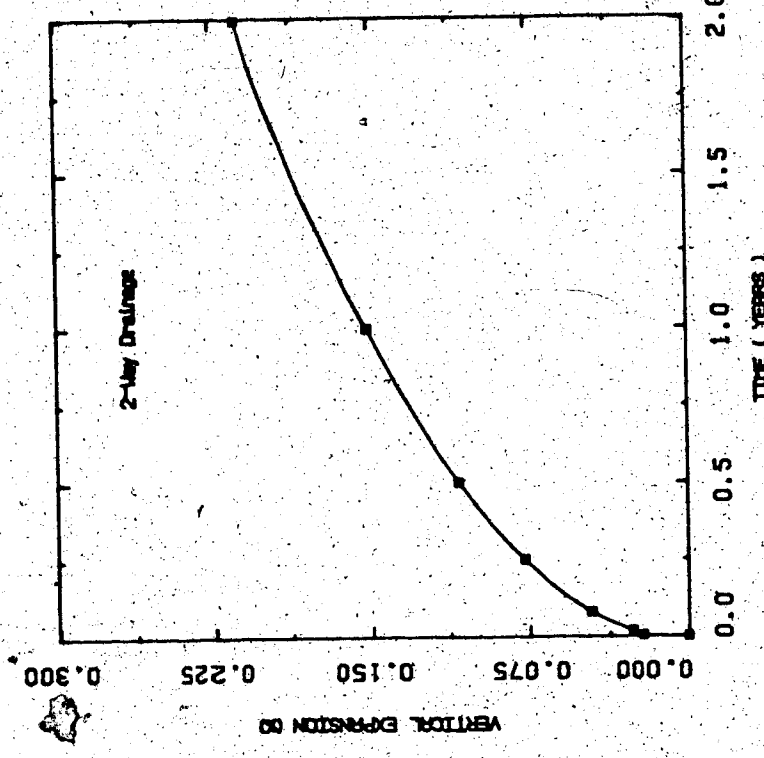

FIGURE 5.11.3 Transient Heat Consolidation Ratio - Two-Way Drainage (1 Day Time Step)

It is of interest to note that the pore pressures generated in Saline Creek oil sand due to heating at relatively slow rates by thermal diffusion, are not large, i.e. less than one percent of the effective confining stress (see Appendix K - Figures K1.1 to K5.3, inclusive). This is due to the greatly differing magnitudes of hydraulic and thermal diffusivity for Saline Creek oil sand. The heat consolidation ratio, R_T, varies from about 2.0×10^4 at 5°C to 2.0×10^5 at 200°C, i.e. the coefficient of consolidation is 4 to 5 orders of magnitude larger than the coefficient of thermal diffusivity over the temperature range of interest. The rate of heat transfer and thermal generation of pore pressures is thus much slower than the rate of dissipation of excess pore pressure.

5.5.2 Influence of Oil Sand Permeability on Heat Consolidation

Saline Creek oil sand is very clean, i.e. it generally contains less than 3 percent by mass of fine grained silt and clay sized particles. For this reason it is not typical of other areas of the Athabasca deposit or other deposits. It has been observed that the introduction of fine grained silt and clay particles into a matrix of sand grains has the influence of significantly reducing permeability and the coefficient of consolidation (Cedergren, 1977). For example, the presence of 20 percent by mass of fine particles, less than 0.074 mm effective particle diameter, in Saline Creek oil sand would

reduce the value of the coefficient of consolidation, c_v, by 2 to 3 orders of magnitude.

Although the samples of Saline Creek oil sand tested in this research program consisted of fairly uniform clean sand typically containing 0 to 3 percent fines, other oil sand deposits typically are more geologically complex and heterogeneous. Mossop (1978), Carrigy and Kramers (1974) and others have decribed geologic complexities of Alberta oil sand facies.

In order to illustrate the implications of reducing the coefficient of consolidation on the heat consolidation process, Analytical model no. 1 was reanalyzed with reduced c_v values of 0.108, 1.08×10^{-2} and 3×10^{-4} m^2/minute, using a 1 minutes time step in each case. The corresponding values of heat consolidation ratio, R_T are 1800, 180, 18 and 5, respectively, assuming a constant value of thermal diffusivity. Predicted temperature distributions with time are identical for each of the above four analyses. The spatial variation of temperature with time in the lower 10 percent of the oil sand layer is shown in Figure K6 in Appendix K. Pore pressure distributions and vertical deformations at common time levels are shown in Figures K7.1 to K10.2 inclusive, for the above cases. The foregoing analyses were repeated using a smaller 30 second time step; essentially identical results were obtained for predicted pore pressure distribution and volumetric

expansion at comparable time levels. It is of interest to note that large peak pore pressures are generated as the coefficient of consolidation is reduced and coincidentally, that the rate at which elevated pore pressures are transmitted ahead of the heating front is reduced. Therefore reduced values of c_v have the effect of both increasing the magnitude of thermal pore pressure generation by undrained heating while limiting the rate at which the zone of elevated pore pressures diffuse beyond the heated zone. Peak pore pressures generated in these analyses are shown in Figure 5.12, plotted as a pore pressure ratio, i.e. the ratio of maximum pore pressure generated to the maximum possible pore pressure if heated undrained (i.e. σ_o'), versus the heat consolidation ratio, R_T^*. The magnitude of thermal diffusivity, α_T, was assumed to remain constant at 6.0×10^{-5} m^2/minute in each of the above analyses.

Excess pore pressures generated during heating of oil sand strata containing more than about 8 to 10 percent fines, by mass, are seen to be significant in Figure 5.12. Excess pore pressures due to combined undrained heating and pressurized injection may substantially reduce available shear strength and initiate shear deformations in a non-uniform stress field. Understanding the mechanism by which such shearing events are initiated and the dependence of thermal pore pressure generation on geologic detail is of paramount importance in preventing damage to well casings, shaft and tunnel liners during thermally enhanced oil recovery operations.

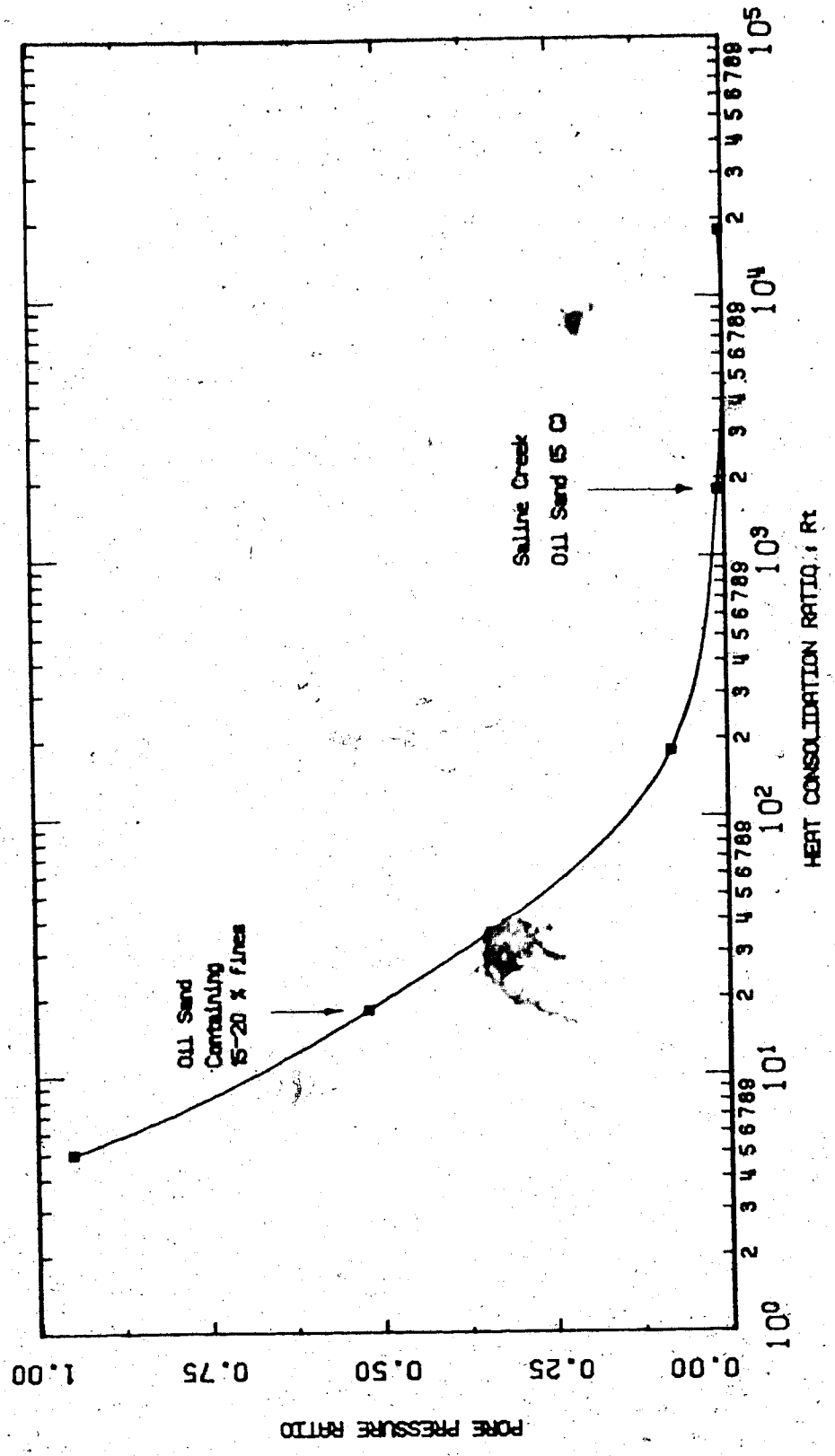

FIGURE 5.12 Maximum Pore Pressures Generated by Transient Heating of Oil Sands Varying Permeability

5.6 Numerical Solutions for One Dimensional Heat Consolidation Coupled with Heat Transfer by Convection and Diffusion

Numerical solution of equation 5.12, the convective-diffusion equation is very difficult, particularly when the flow velocity is large causing convective transport to dominate the heat transfer process. Peaceman and Rachford (1962) noted that when convection predominates the equation assumes a hyperbolic form. When three-point central difference approximations of the spatial derivatives are used, the truncation error on the convection term is first order ($O(\Delta Z)$ while that on the diffusion term is only second order (i.e. $O(\Delta Z^2)$. The key to obtaining a good numerical approximation to equation 5.12 lies in reducing the truncation error in the approximation to the convection term. Laumbach (1975) developed an improved finite difference formulation for treating the convective-diffusion equation which is referred to as the "Truncation Cancellation Procedure" (TCP). This finite difference formulation reduces the truncation error in the convection term by cancelling it with an "artificial" first order error in the accumulation term (i.e. the approximation of the time derivative). A weighting parameter, ω, is included with the accumulation term to artificially introduce a spatial truncation error associated with the time derivative approximation which, in turn, cancels a portion of the convection term error. It should be noted that the time derivative approximation in implicit formulations normally has no spatial truncation error.

The TCP discretization for the convective-diffusion equation is of

of the Crank-Nicolson (semi-implicity) type. In one dimension the TCP discretization developed by Laumbach (1975) is as follows:

$$(1-\omega)\left(\frac{T_{i,j+1}-T_{i,j}}{\Delta\tau}\right)+\frac{\omega}{2}\left[\frac{(T_{i+1,j+1}-T_{i+1,j})+(T_{i-1,j+1}-T_{i-1,j})}{\Delta\tau}\right]$$
$$=\frac{1}{2N_{pe}\Delta\xi^2}\left[(T_{i+1,j+1}-2T_{i,j+1}+T_{i-1,j+1})+(T_{i+1,j}-2T_{i,j}+T_{i-1,j})\right]$$
$$-\frac{1}{4\Delta\xi}\left[(T_{i+1,j+1}-T_{i-1,j+1})+(T_{i+1,j}-T_{i-1,j})\right]$$

(5.19)

where: τ = dimensionless time = $\dfrac{vt}{H\,(1-\eta\rho_s c_s/\rho_f c_f+\eta)}$

ξ = dimensionless distance = $\dfrac{Z}{H}$

$r = \Delta\tau/\Delta\xi$

ω = weighting parameter = $\dfrac{1}{3}+\dfrac{r^2}{6}$

N_{pe} = the Peclet Number = $\dfrac{\rho_f c_f VH}{k_T}$

The Peclet Number is a dimensionless ratio of the characteristic convection rate to the characteristic diffusion rate. When the Peclet Number is large convection dominates, and when it is small diffusion dominates. Laumbach (1975) has tested the stability and convergence of the TCP solution against analytical solutions for heat transfer by one dimensional convective diffusion.

A modified version of the program HCD was developed to solve the one dimensionless heat consolidation problem coupled with heat transfer by convective-diffusion. The program HCCD includes a subroutine TEMPC which solves the tridiagonal matrix for a set of equations corresponding to the difference equation 5.23 at each time level. Flow velocity, v, is determined using Darcy's Law. The differential pressure term in Darcy's equation was approximated by a three point, spatial central difference approximation at the preceding time level. The resulting velocity distribution thus lags behind the temperature distribution by one time step.

A restriction of the solution technique is that the pressure difference, and thus velocity may not equal zero. A listing of the code for "HCCD" is included in Appendix J. A modified version "HCCD2" was written to solve the case of two-way fluid drainage and heat flow.

Analytical Model No. 1 illustrated in Figure 5.6 was reanalyzed using the convective-diffusion heat transfer solution.

Similar temporal discretization restrictions to those discussed for the one dimensional heat consolidation problem coupled with heat transfer by thermal diffusion also apply to the convective-diffusion analysis.

Temperature, pore pressure and vertical expansion for the TCP analysis are shown in Figures 5.13.1 to 5.13.3, inclusive, at time

levels up to 24 hours after introduction of boundary step temperatures. It was observed that heat transfer was accelerated slightly by convection for the first few time steps following introduction of the step temperature, however the rate of heat transfer was later retarded because of fluid drainage back toward the heat source in this "one-way drainage" analysis.

Although convective heat transfer does not have a dominant influence on the "predicted temperature and pressure distributions in the above example, it is known to be important when large pressure gradients are induced by simultaneous operation of neighboring injection and production wells during enhanced oil recovery or aquifer thermal energy storage and recovery (see for example Mercer et al., 1982, or Peaceman and Rachford, 1962).

Heat consolidation solutions presented in the remainder of Chapter 5 and in Chapter 6 include boundary conditions similar to the "one-way drainage" example presented here. The assumption that the dominant heat transfer mechanism is conduction will accordingly be applied hereafter.

5.7 One Dimensional Heat Consolidation in Radial Coordinates

Formulation of the one-dimensional heat consolidation equations in radial coordinates (i.e. assuming conditions of radial symmetry) is of practical interest for modelling a number of problems outlined in Section 5.2. Pore pressure and temperature distributions generated in the heat consolidation analysis may be combined with

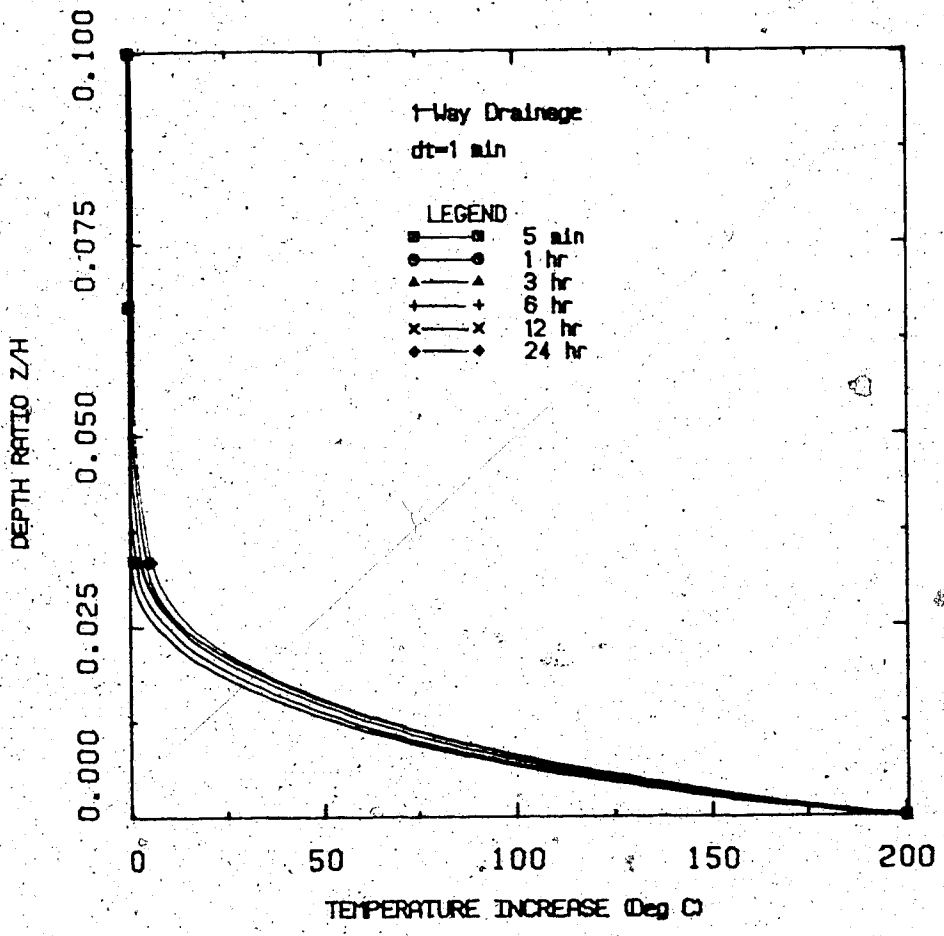

FIGURE 5.13.1 Transient Temperatures - Heating by Convective-Diffusion

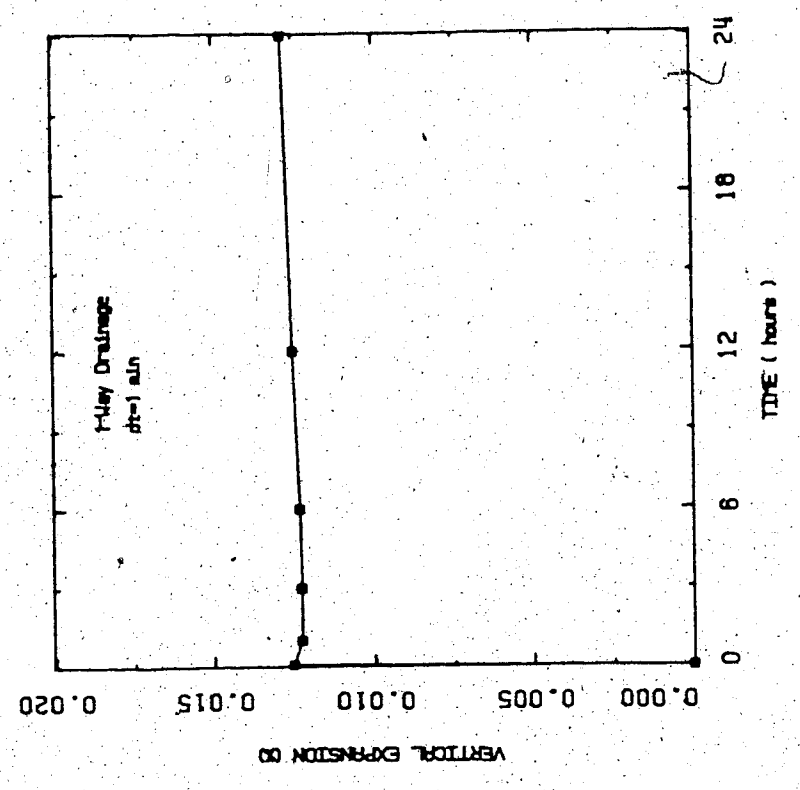

FIGURE 5.13.3 Transient Vertical Expansion - Heating by Convective-Diffusion

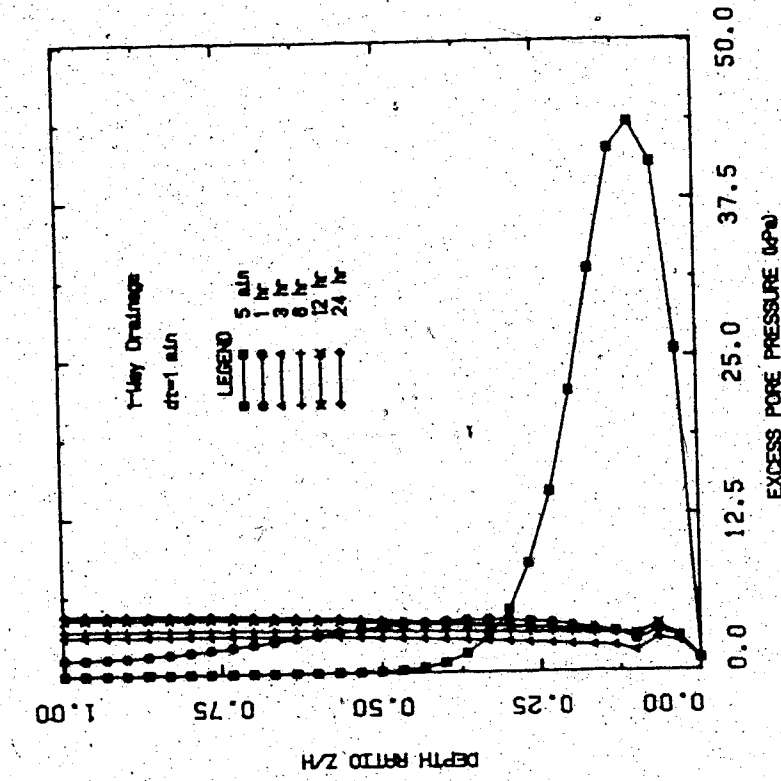

FIGURE 5.13.2 Transient Excess Pore Pressures - Heating by Convective-Diffusion

axisymmetric thermo-mechanical models to analyze deep borehole, shaft or tunnel configurations with a hydrostatic vertical distribution of pressure so that $\frac{\partial u}{\partial z} = 0$.

Following is the thermal diffusion equation, transformed into radial coordinates:

$$\frac{\partial T}{\partial t} = \alpha_T \left[\frac{\partial T}{\partial r} + \frac{1}{r}\frac{T}{r}\right] \tag{5.20}$$

Similarly the one dimensional radial consolidation equation may be written:

$$\frac{\partial u}{\partial t} = c_v \left[\frac{\partial^2 u}{\partial r^2} + \frac{1}{r}\frac{\partial u}{\partial r}\right] \tag{5.21}$$

Thermal pore pressure generation is coupled spatially with temperature and pore pressure in time as previously detailed in equation 5.14.

Implicit finite difference approximation of equation 5.20 yields the following difference equation:

$$T_{i,j} = \left[\frac{\alpha_T \Delta t}{2r_i \Delta r} - \frac{\alpha_T \Delta t}{(\Delta r)^2}\right] T_{i-1,\, j+1} + \left[1 + \frac{2\,\alpha_T \Delta t}{(\Delta r)^2}\right] T_{i,\, j+1} - \left[\frac{\alpha_T \Delta t}{2r_i \Delta r} + \frac{\alpha_T \Delta t}{(\Delta r)^2}\right] T_{i+1,\, j+1} \tag{5.22}$$

Similarly equation 5.25 may be exprssed in algebraic finite difference form using an implicit scheme as follows:

$$u_{i,j} = \left[\frac{c_v \Delta t}{2r_i \Delta r} - \frac{c_v \Delta t}{(\Delta r)^2}\right] u_{i-1,\, j+1} + \left[1 + \frac{2c_v \Delta t}{(\Delta r)^2}\right] \qquad (5.23)$$

$$u_{i,\, j+1} - \left[\frac{c_v \Delta t}{2r_i \Delta r} + \frac{c_v \Delta t}{(\ r)^2}\right] u_{i+1,\, j+1}$$

Equations 5.22 and 5.23 may be solved numerically by techniques described in Section 5.5.

A computer code for heat consolidation in radial coordinates, HCDR, is included in Appendix J. Temperature and pore pressure distributions predicted for the "one-way drainage" case are shown in Figures 5.14.1 and 5.14.2 plotted against dimensionless radius, r/R, where r is the radius from a "line source" of heat and R is the radius to the external boundary. Five minute time steps were used in the analysis and again some instability is apparent near the step temperature boundary. Nevertheless, the magnitude of pore pressures generated is very small relative to effective confining stress.

The partial differential equation describing heat transfer by convective-diffusion in radial coordinates is as follows:

$$\frac{\partial T}{\partial t} = \alpha_T \left[\frac{\partial^2 T}{\partial r^2} + \frac{1}{r}\frac{\partial T}{\partial r}\right] - \frac{\rho_f c_f}{\rho c} v_r \frac{\partial T}{\partial r} \qquad (5.24)$$

where radial flow velocity v is given by Darcy's Law.

Laumbach (1975) has transformed the convective-diffusion equation into dimensionless form as follows:

$$\frac{\partial T}{\partial \tau} = \xi \frac{\partial^2 T}{\partial \xi^2} + (1 - N_{pe_r}) \frac{\partial T}{\partial \xi} \qquad (5.25)$$

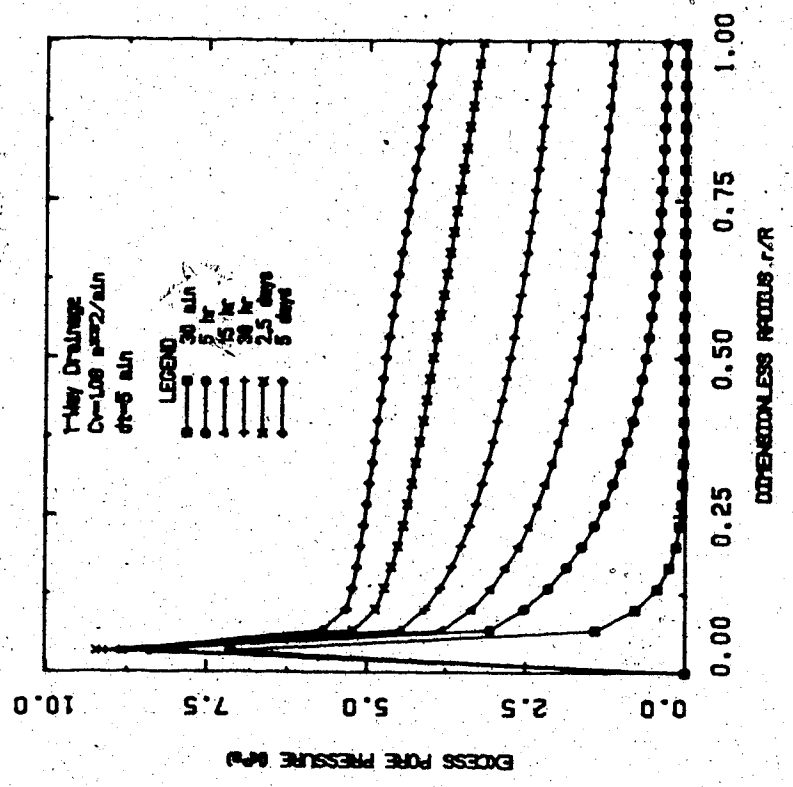

FIGURE 5.14.2 Transient Radial Excess Pore Pressures (One-Way Drainage)

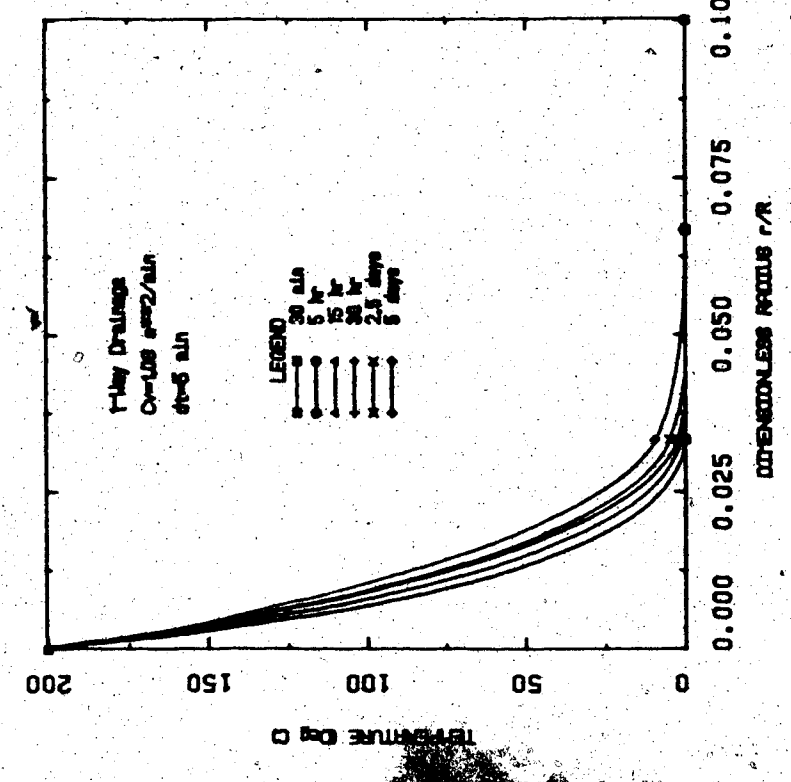

FIGURE 5.14.1 Transient Radial Temperatures: Diffusion (One-Way Drainage)

where $\xi = (r/R)^2$

$$T = \frac{vt}{4R\left[(1-\eta)\frac{\rho_s c_s}{\rho_c} + \eta\right]} \quad \text{(dimensionless time)}$$

$$N_{per} = \frac{\rho_f c_f v r^2}{2k_T h} \quad \text{(the Peclet Number in radial coordinates)}$$

The "TCP" finite difference approximation for equation 5.25 developed by Laumbach (1975) is as follows:

$$(1-\omega)\left[\frac{T_{i,j+1} - T_{i,j}}{\Delta T}\right] + \frac{\omega}{2}\left[\frac{(T_{i+1,j+1} - T_{i+1,j}) + (T_{i-1,j+1} - T_{i-1,j})}{\Delta T}\right]$$

$$= \frac{\xi}{2\Delta\xi^2}\left[(T_{i+1,j+1} - 2T_{i,j+1} + T_{i-1,j+1}) + (T_{i+1,j} - 2T_{i,j} + T_{i-1,j})\right]$$

$$+ \left(\frac{1 - N_{per}}{4\Delta\xi}\right)\left[(T_{i+1,j+1} - T_{i-1,j+1}) + (T_{i+1,j} - T_{i-1,j})\right] \quad (5.26)$$

where $\omega = \frac{1}{3} + \frac{r_D}{6}$

$$r_D = \frac{\Delta T}{\Delta \xi} \leq \frac{1}{2}$$

Time step limitations for stability and convergence of radial heat consolidation coupled with heat transfer by convective-diffusion are very restrictive for reasons described in section 5.5.

5.8 Summary

The heat consolidation process has been described and a one dimensional heat consolidation theory developed. Numerical solution techniques and solutions for one dimensional heat consolidation of oil sand in cartesian and radial coordinates were presented.

Major conclusions evolving from numerical heat consolidation analyses in Chapter 5 may be summarized as follows:

1. Numerical solutions of heat consolidation using standard finite difference techniques are very sensitive to temporal discretization due to nonlinear variation of the coefficient of consolidation, and since thermal pore pressure generation and total stress change terms must be included explicitly in the analysis.

2. The absence of fines (i.e. clay and silt sized particles) and the uniform grain size distribution of Saline Creek oil sand result in relatively high permeability. Pore pressures generated during transient heating of Saline Creek oil sand are very small relative to effective confining stress. Very large thermally generated pore pressures may however, be expected when 10 - 20 percent by mass of fines are introduced into the oil sand matrix. The magnitudes of thermally generated pore pressures, thermal stress changes and ground deformations depend largely on geologic detail within the oil sand formation.

3. Permeability of oil sand may be reduced by 2 to 3 orders of magnitude when the fines content of oil sand is increased to 20% by mass. The reduction in permeability results in a reduction of the coefficient of consolidation, c_v. As noted above, significant excess pore pressures, i.e. greater than 50% of the effective confining stress, may be generated

when 10-20% by mass of silt and clay size particles are present in oil sands. Also, the rate at which pore pressures migrate ahead of the heating front and dissipate is reduced. The shear strength of oil sand decreases in proportion with effective stress decline and pore pressure increase. Also, stress-strain moduli are proportional to effective stresses.

4. Heat transfer by convection was found to have little influence on predicted temperature and pore pressure distributions when the primary direction of drainage is toward the heat source. Convective heat transfer must be considered, however, when large pressure gradients associated with "forced convection" are introduced.

5. Excess pore pressures resulting from high pressure injection are transmitted rapidly through clean quartzose oil sands. In lower permeability oil sands, thermally-induced excess pore pressures are also significant. This is particularly important for enhanced oil recovery schemes in which large injection pressures are applied since it would be difficult to isolate adjacent shafts or tunnels from the injection pressure.

6. Numerical solutions of one dimensional heat consolidation may be applied to a number of problems of practical interest. Nevertheless, development of rigorous and self-consistent theory of three-dimensional heat consolidation

with accompanying solutions which are in reasonable accord with the known mechanical behaviour of "real" soils and rocks, is required. The development of a rigorous three-dimensional theory and solutions is beyond the scope of this research. However, a practical non-rigorous approach for analyzing multi-dimensional heat consolidation problems is developed and illustrated in Chapter 6.

6.0 NUMERICAL ANALYSES PREDICTING STRESS CHANGES AND DEFORMATIONS DUE TO UNDERGROUND EXCAVATION, HEATING AND INJECTION

6.1 The Analytical Approach

Two problems of practical interest related to thermally enhanced in situ recovery of oil from oil sands involve the prediction of stress changes and ground deformations resulting from:

1. excavation and construction of a shaft or deep tunnel followed by steam injection and oil recovery in a peripheral production zone; and
2. drilling and installation of a well casing followed by injection of pressurized, condensed steam through the well casing.

These two problems are illustrated schematically in Figures 6.1.1 and 6.1.2. Solutions to the above problems require incremental analytical procedures, including concomittant solutions of the differential equations of heat transfer, mass transfer and stress-temperature-strain response.

The above three-dimensional problems may be solved using two-dimensional axisymmetric formulations by assuming conditions of radial symmetry. Furthermore, the differential equations describing

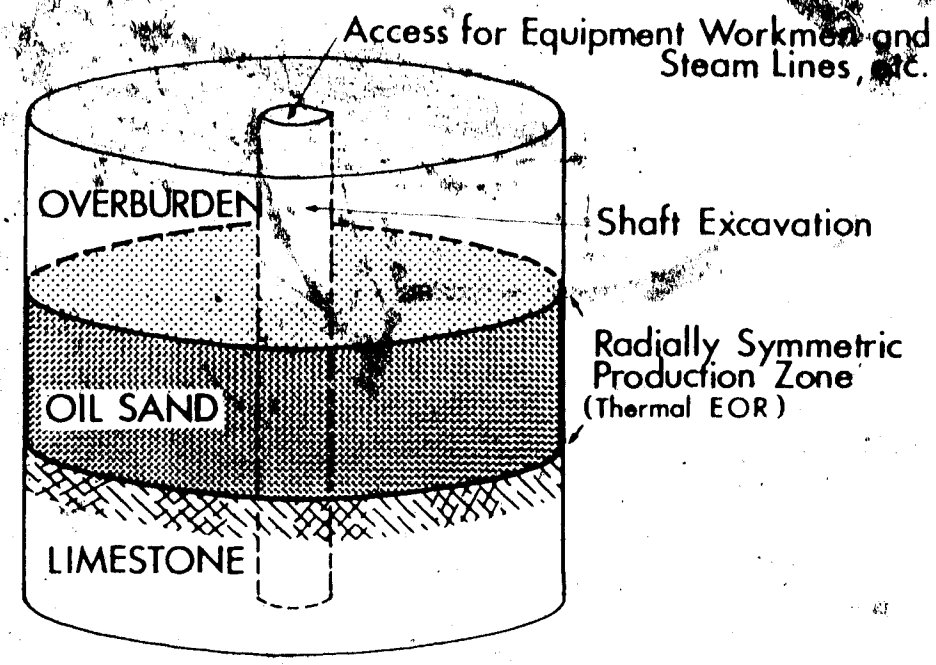

FIGURE 6.1.1 Schematic Illustration of a Shaft and Peripheral Production Zone for Thermally Enhanced Oil Recovery

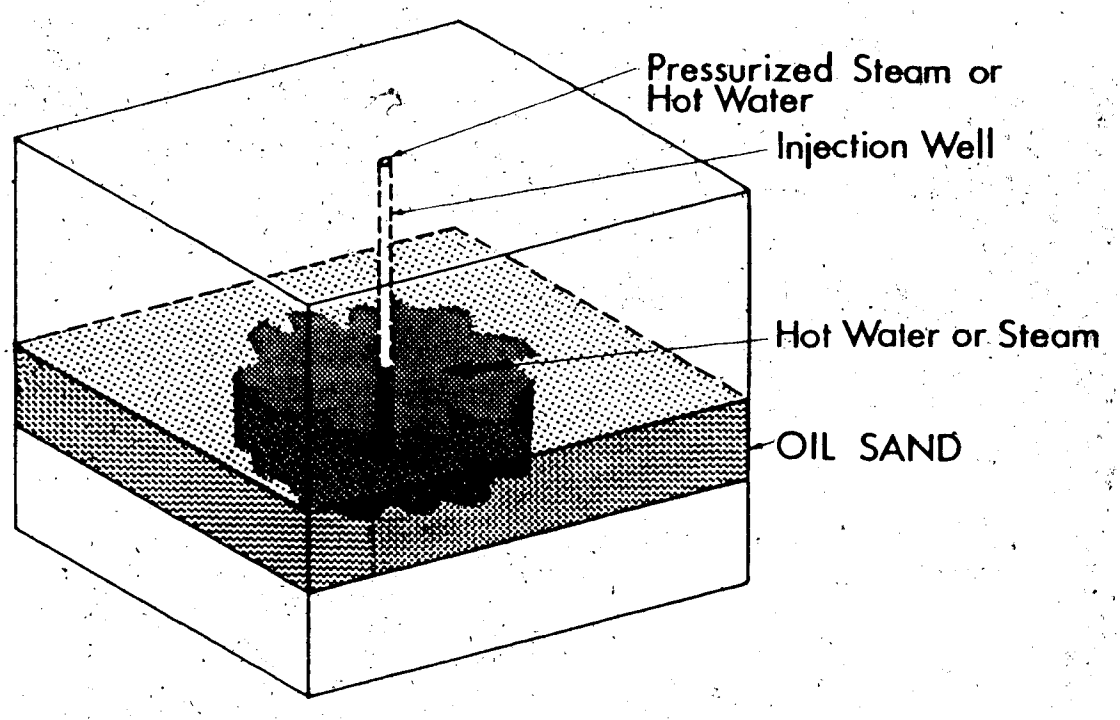

FIGURE 6.1.2 Schematic Illustration of Pressurized Steam Injection Through a Single Cased Well

heat transfer and consolidation may be reduced to one-dimensional radial form if it is assumed that the shaft or injection well within the pay zone is relatively long, or that there is no fluid "leak-off" or heat transfer to the overburden and underburden.

Experimental results presented in Chapters 3 and 4 demonstrated that the mechanical properties (i.e. shear strength and stress-strain properties) of oil sand are dominated by effective confining stresses. Excess pore pressures are generated during thermally enhanced oil recovery by elevated injection pressures and by heating. Accordingly, it is important to analyze the above problems in terms of effective stresses rather than total stresses.

The analytical approach adopted here involves a non-rigorous coupling of the heat consolidation solutions developed in Chapter 5 and existing stress-strain solutions using finite element analyses. The numerical modelling procedure may be summarized as follows:

1. Stress changes and deformations resulting from excavation of the shaft or injection well are predicted using a nonlinear axisymmetric finite element solution. Axisymmetric finite element discretization is illustrated in Figure 6.1.3.
2. Transient temperature changes, excess pore pressures and associated volumetric strains are determined using the finite difference solutions for radial heat consolidation developed in Chapter 5. Pore pressures in excess of the initial <u>in situ</u> pressure due to excess injection pressure

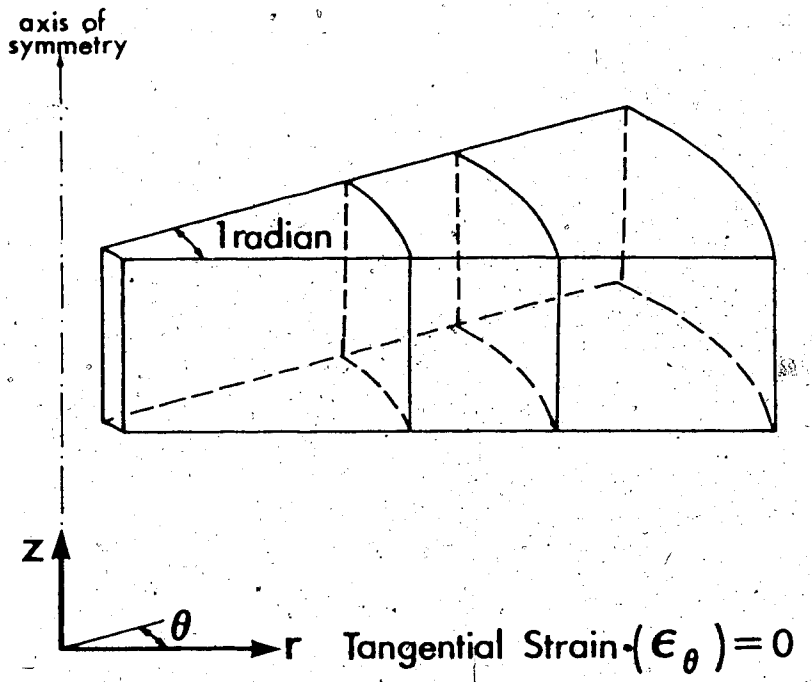

FIGURE 6.1.3 Axisymmetric Finite Element Discretization

and thermal pore pressure generation are calculated assuming that the total confining stresses remain constant during heating. Thus, pore pressure changes resulting from thermally induced total stress changes are neglected. An equivalent coefficient of volumetric thermal expansion which varies both spatially and temporally, with temperature and effective confining stress is determined for input into the thermal stress analysis. Variations of stress-strain moduli with effective confining stress (in space and in time) are also determined at this stage.

3. Total stress changes and deformations due to injection and heating are predicted using an axisymmetric thermoelastic, finite element analysis. Volumetric strains induced by injection and heating are input using appropriate distributions of temperature increase and the "equivalent" coefficient of volumetric expansion determined in the foregoing heat consolidation analysis.

The numerical modelling procedure is summarized in Figure 6.1.4. Although pore pressure changes due to total stress changes may, in principle, be calculated in an uncoupled manner as described in step 5 of Figure 6.1.4, this procedure becomes very cumbersome and accordingly was omitted from analyses in the following sections.

Effective stresses are determined in the foregoing analytical procedure by superposition of the original effective stresses with: (i) stress changes during excavation; (ii) excess pore pressure due to injection; (iii) thermally generated excess pore pressure; (iv) total stress changes induced by heating and injection. In general,

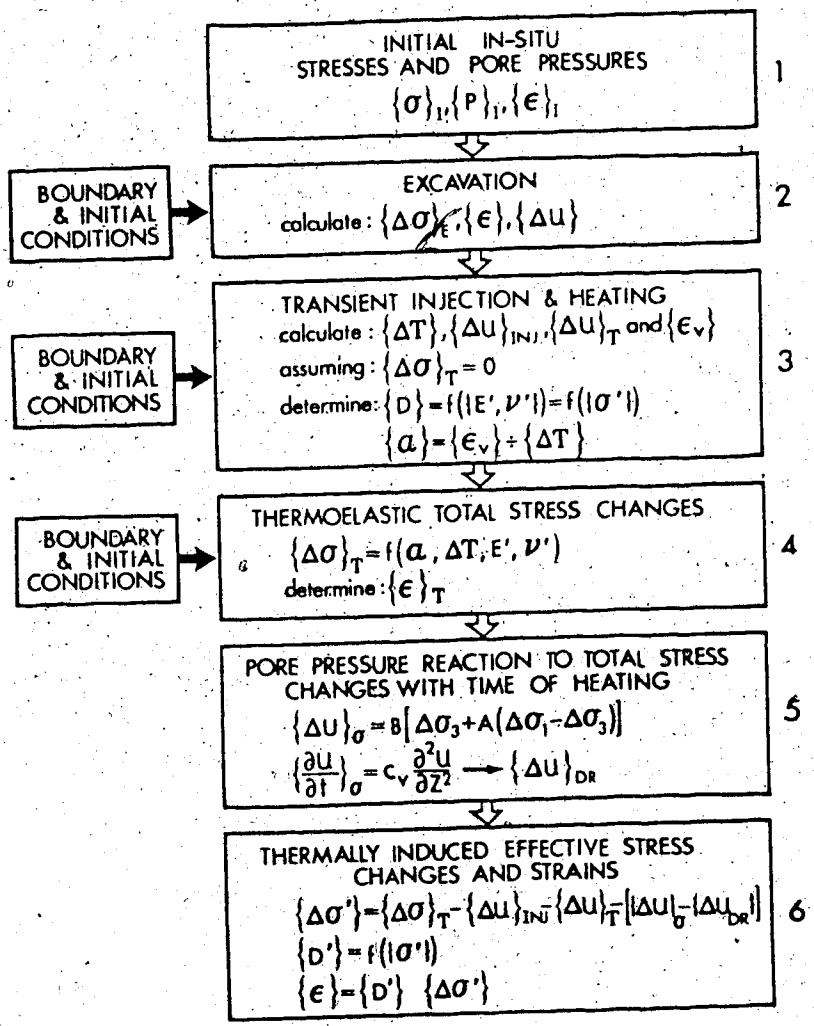

FIGURE 6.1.4 Flow Chart of Recommended Procedures for Uncoupled Numerical Analyses of Heat Consolidation

there is also a pore pressure reaction to thermally induced total stress changes according to equation 5.16. This component of pore pressure response has been neglected here.

Some limitations of the above analytical procedure are as follows:

1. Standard finite element algorithms for thermoelastic stress-strain modelling do not include coupling of total stresses and pore pressures, nevertheless some recent developmental progress has been made toward this requirement by Zienkiewicz et al (1982). Although the requirement for performing effective stress analyses of heat consolidation problems in saturated soils and rocks has been identified, rigorous solution procedures have not yet been developed. Total stress changes during heating result from: (i) material density changes associated with thermal expansion and mass transfer; and (ii) restraint of thermally induced strains. Pore pressure changes resulting from the former may be included in the heat consolidation solutions developed in Chapter 5. Pore pressure (and effective stress) changes resulting from the latter are not included in solutions presented in this chapter. Implications of this simplifying assumption are discussed further in following subsections.
2. It is known that the temperature of a solid body changes when the state of strain of the body is altered adiabatically. Kelvin's theory may be used to calculate the temperature change of an insulated elastic body due to

uniform straining. It has been shown that the temperature change in elastic materials due to adiabatic straining is small for most engineering applications (Fung, 1965). The interaction of strain and temperature has been ignored in the analytical procedure outlined above.

3. The radial (one-dimensional) heat consolidation analysis does not account for fluid "leak-off" or heat dissipation to formations above or beneath the oil sand layer.
4. It has been assumed throughout that the thermal, physical and mechanical properties of oil sand are isotropic since anisotropy of the material properties has not yet been evaluated for oil sands. Nevertheless, it is well known that permeability and stress-strain properties are often anisotropic in other sedimentary rocks and soils.
5. Material properties used in the analyses were derived from laboratory tests on disturbed, albeit good quality samples of Saline Creek oil sand. The degree of sample disturbance and implications were discussed extensively in Chapters and
6. Stress changes and deformations due to heating and injection were predicted using a linear thermoelastic solution technique. The stress-strain behaviour of oil sand is neither linear nor elastic, particularly over large strain increments. There is a need to develop a thermal stress algorithm which accounts for non-recoverable strains, i.e. either by extending an incremental elastic procedure such as the hyperbolic model or within the framework of plasticity theory.

Stress-strain analyses of the shaft and injection well problems were performed using the general purpose finite element program ADINA (Automatic Dynamic Incremental Nonlinear Analysis) developed by Bathe (1975). A hyperbolic material model for soils has been implemented in the University of Alberta version of ADINA. The hyperbolic model in ADINA was used to calculate stress changes and deformations due to excavation of a vertical shaft or borehole through oil sand. Hyperbolic stress-strain parameters for oil sand are presented in section 6.2. An isotropic thermoelastic material model in ADINA was used to calculate total stress changes and deformations due to heating and injection.

Comparative analyses of the shaft problem illustrated in Figure 6.1.1 were carried out to illustrate the numerical modelling procedure and to explore implications of varying material properties and boundary conditions. Analytical results using properties of Saline Creek oil sand are compared for a range of boundary conditions at the production zone boundary. Analyses of the shaft problem were also performed assuming fully "drained" and "undrained" conditions during transient heating and injection, in an effort to compare lower bound and upper bound solutions. Since the transient analyses using properties of Saline Creek oil sand were close to the "drained" case, a transient heat consolidation analysis was also carried out using consolidation properties typical of a low permeability oil sand or shale material. The importance of varying elastic stress-strain moduli in space and time with effective confining stresses for analyses other than "drained" analyses is demonstrated in these numerical results.

The injection well problem illustrated in Figure 6.1.2 was analyzed using properties of Saline Creek oil sand and a single set of boundary conditions.

6.1.1 Stress Paths During Heating

A range of potential effective stress changes, i.e. stress paths, which may result during drained and undrained heating under various deformational constraints are illustrated in Figure 6.2. In general, stress paths followed during transient heating and consolidation in situ under the influence of moving and variable boundary conditions would be much more complex. The simplified stress paths shown in Figure 6.2 illustrate however, that effective stress changes during heating depend on both the heat consolidation characteristics of the soil or rock, and on the boundary conditions. Stress paths in Figure 6.2 also illustrate the need to analyze many heat consolidation problems in terms of effective stresses.

6.2 Hyperbolic Stress-Strain Parameters for Oil Sand

Algebraic relationships of hyperbolic form have been used to approximate the nonlinear relationships between stress and strain for a range of geotechnical materials (Kondner, 1963; Duncan and Chang, 1970). The hyperbolic model presented by Duncan and Chang (1970) is a technique for modelling the nonlinear stress-strain behaviour of soils within the framework of incremental elasticity. Procedures suggested by Duncan et al. (1980), were used to derive hyperbolic stress-strain parameters for Saline Creek oil sand from

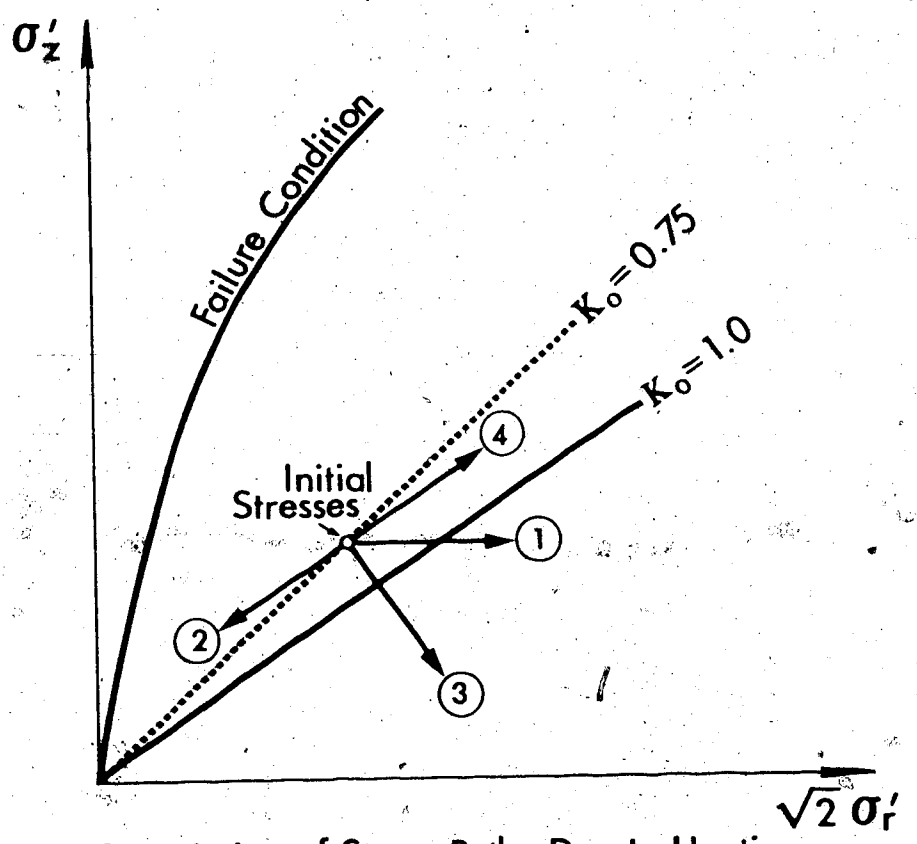

Description of Stress Paths Due to Heating

(1) Drained / Radially Constrained Heating
(2) Undrained / Unconstrained Heating
(3) Undrained / Radially Constrained Heating
(4) Drained / Fully Constrained Heating

FIGURE 6.2 Stress Paths Due to Ground Heating

the experimental data. Experimental data from drained triaxial tests are plotted along with "best-fit" hyperbolic curves in Figures 6.3 to 6.6, inclusive. Triaxial compression test data derived from the tests shown in Figures 6.3 to 6.6, inclusive, are also summarized in Table 6.1. The fundamental form of the hyperbolic relationship between deviatoric stress and axial strain is as follows (Kondner, 1963):

$$\frac{1}{(\sigma_1 - \sigma_3)} = \left[\frac{1}{E_i} + \frac{\epsilon}{(\sigma_1 - \sigma_3)_{ULT}}\right] \qquad (6.1)$$

Duncan et al. (1980) suggested that the nonlinear relationship between volumetric strain and axial strain for a conventional triaxial test may be represented by the following equation:

$$K_B = \left(\frac{\sigma_1 - \sigma_3}{\epsilon_v}\right) \qquad (6.2)$$

where K_B is the bulk modulus of the soil. The relationship given in equation 6.2 is based on the assumption that the bulk modulus, K_B, is independent of the deviatoric stress level and that it varies with confining stress.

Figures 6.3.1, 6.3.2 and 6.3.3 show test data for tests following stress path B (see Figure 4.14) at temperatures of 20°C, 125°C and 200°C along with "best-fit" hyperbolic curves. Figures 6.4.1 and 6.4.2 show test results and hyperbolic curves for two room temperature passive compression tests on Saline Creek oil sand at effective confining stresses of 2.1 MPa and 3.4 MPa conducted by Au (1983). Figures 6.5.1 to 6.5.4, inclusive are plots of test results

TABLE 6.1

SUMMARY OF DRAINED TRIAXIAL COMPRESSION TEST DATA FOR SALINE CREEK OIL SAND

TEST	TEMPERATURE (°C)	σ_3' (MPa)	E_i (MPa)	K_b (MPa)	ε_f (%)	$(\sigma_1-\sigma_3)_f$ (MPa)	$(\sigma_1-\sigma_3)_{ult}$ (MPa)	FAILURE RATIO (R_f)	ANGLE OF SHEARING RESISTANCE (Ø)
1*	20	2.1	2340	1436.	0.7	8.0	16.9	0.48	41
2*	20	3.4	1985	1136.	1.4	10.7	22.2	0.48	38
J1 Constant Tests									
TOS3	20	0.870	2310	1895.	0.6	5.2	9.3	0.56	49
TOS6	125	0.650	11320	785.	0.2	6.1	15.0	0.40	55
TOS18	200	0.840	5330	2867.	0.5	6.1	8.2	0.75	53
Passive Compression Tests									
TOS2	20	4.0	2200	1318.	1.2	16.9	71.4	0.24	43
TOS7	125	4.4	6270	1496.	1.0	12.7	14.7	0.86	36
TOS12	200	4.4	3870	2044.	1.6	14.7	23.0	0.64	39
TOS19	125	4.4	4540	3755.	1.1	17.1	31.4	0.54	45
TOS4	20	8.0	3790	1119.	1.0	13.4	23.1	0.58	27
TOS5	20	8.0	3600	1193.	2.0	17.9	33.1	0.54	32
TOS17	200	7.6	3610	1418.	1.5	17.3	34.7	0.50	36

* Passive compression tests performed by Au (1983).

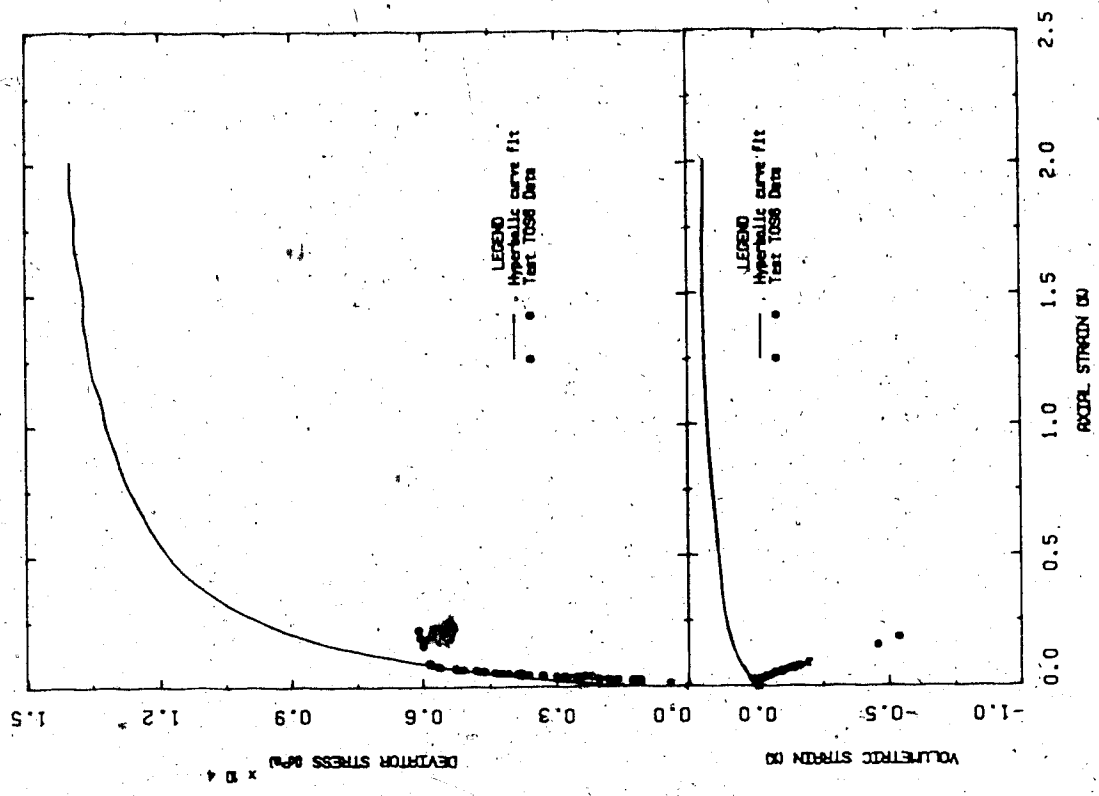

FIGURE 6.3.2 - Hyperbolic Curve-Fit for Triaxial Compression of Oil Sand (Stress Path B at 125°C)

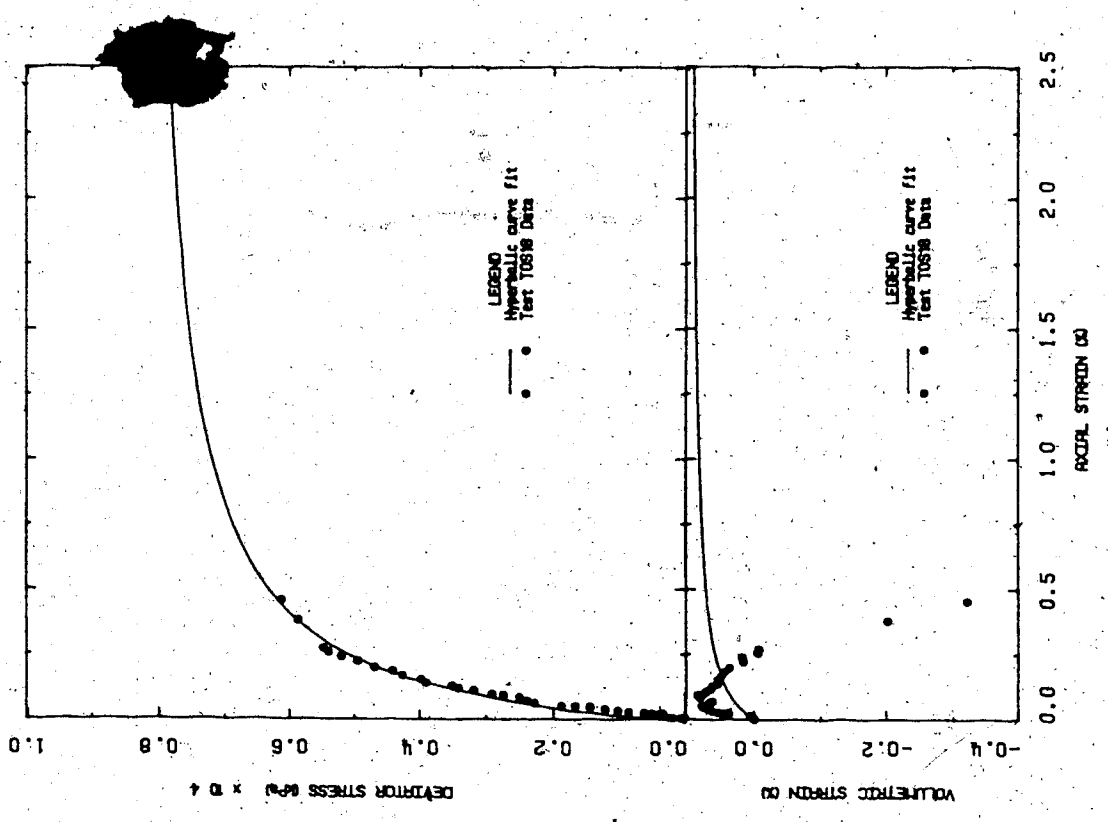

FIGURE 6.3.1 - Hyperbolic Curve-Fit for Triaxial Compression of Oil Sand (Stress Path B at 20°C)

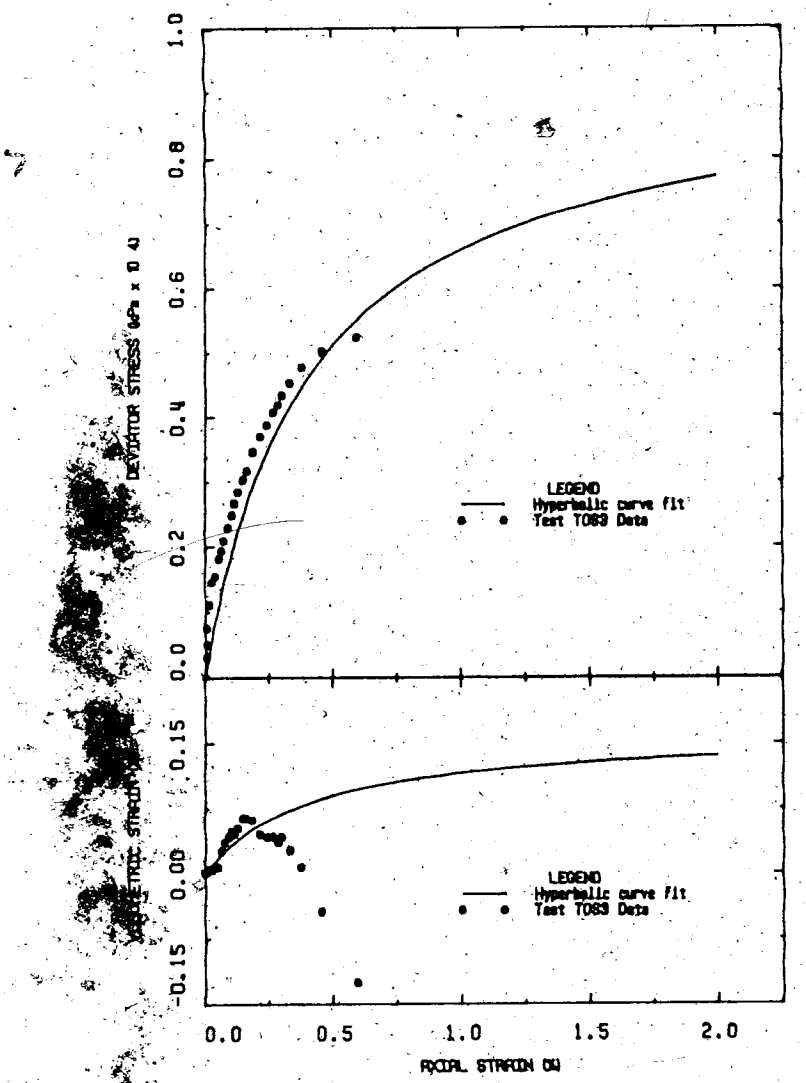

FIGURE 6.3.3 Hyperbolic Curve-Fit for Triaxial Compression of Oil Sand (Stress Path B at 200°C)

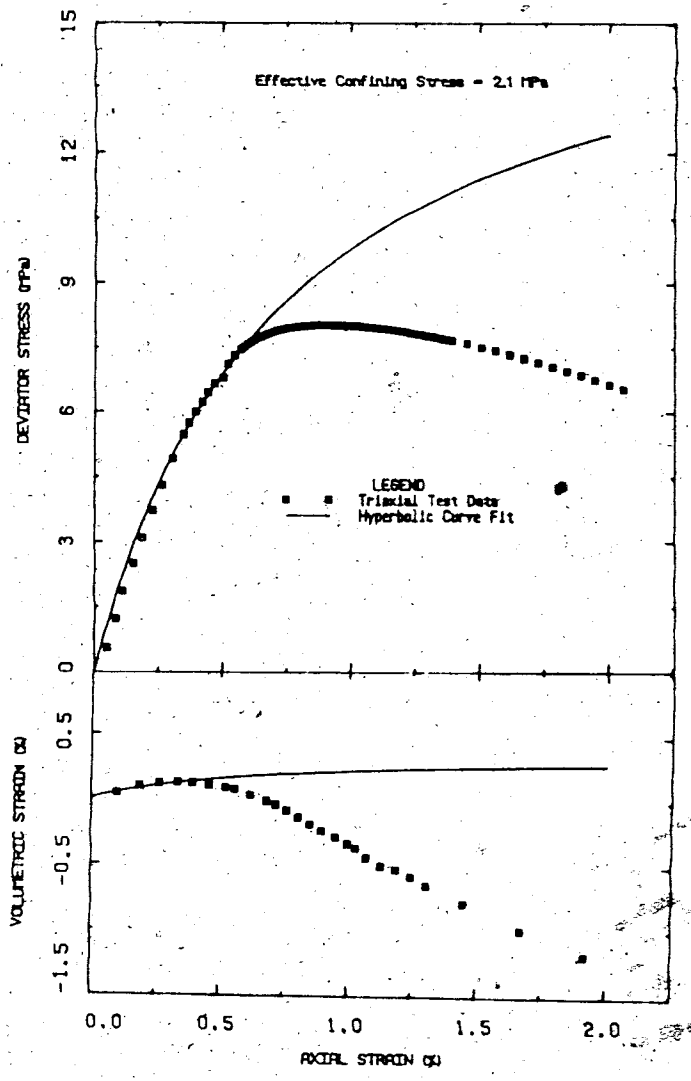

FIGURE 6.4.1 Hyperbolic Curve-Fit for Passive Triaxial Compression of Oil Sand at 2.1 MPa Effective Confining Stress

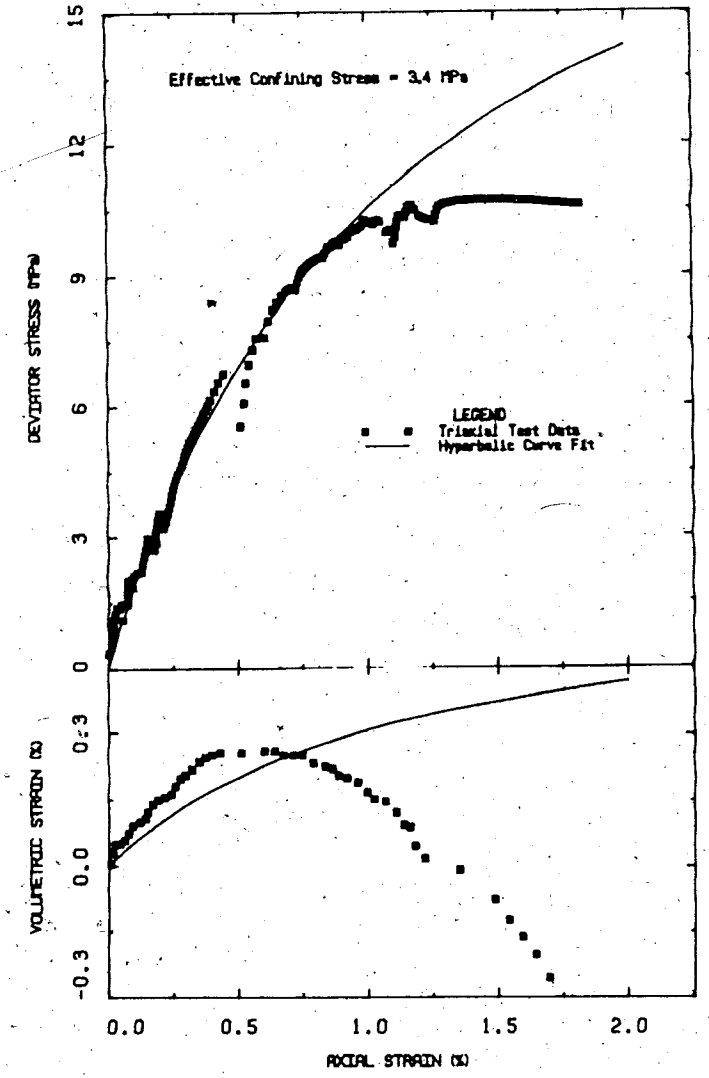

FIGURE 6.4.2 Hyperbolic Curve-Fit for Passive Triaxial Compression of Oil Sand at 3.4 MPa Effective Confining Stress

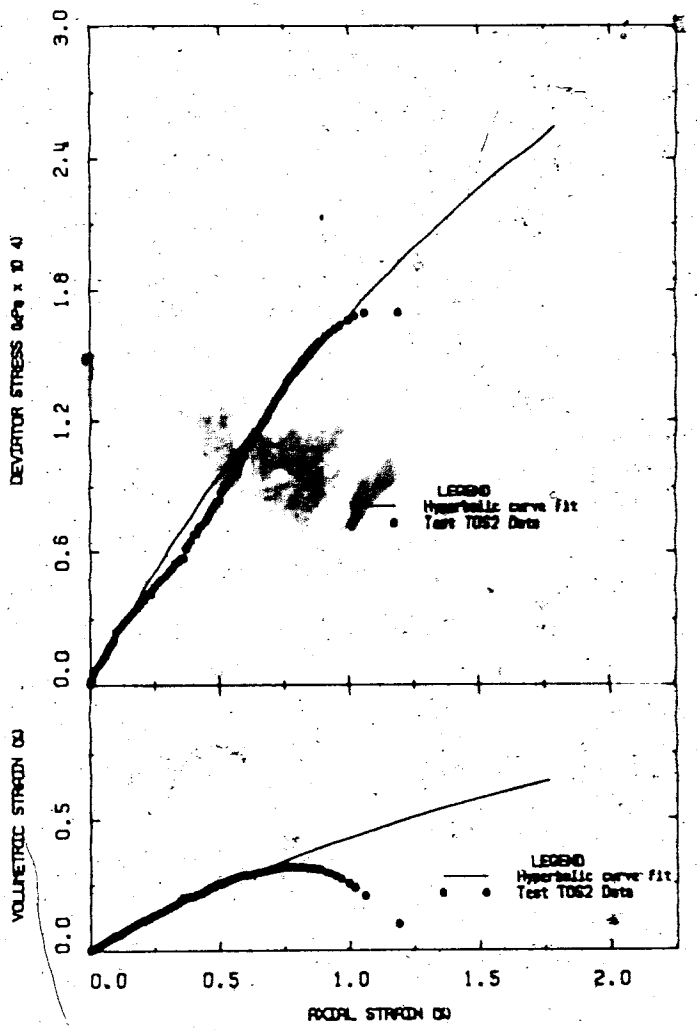

FIGURE 6.5.1 Hyperbolic Curve-Fit for Triaxial Compression of Oil Sand (Stress Path C at 20°C)

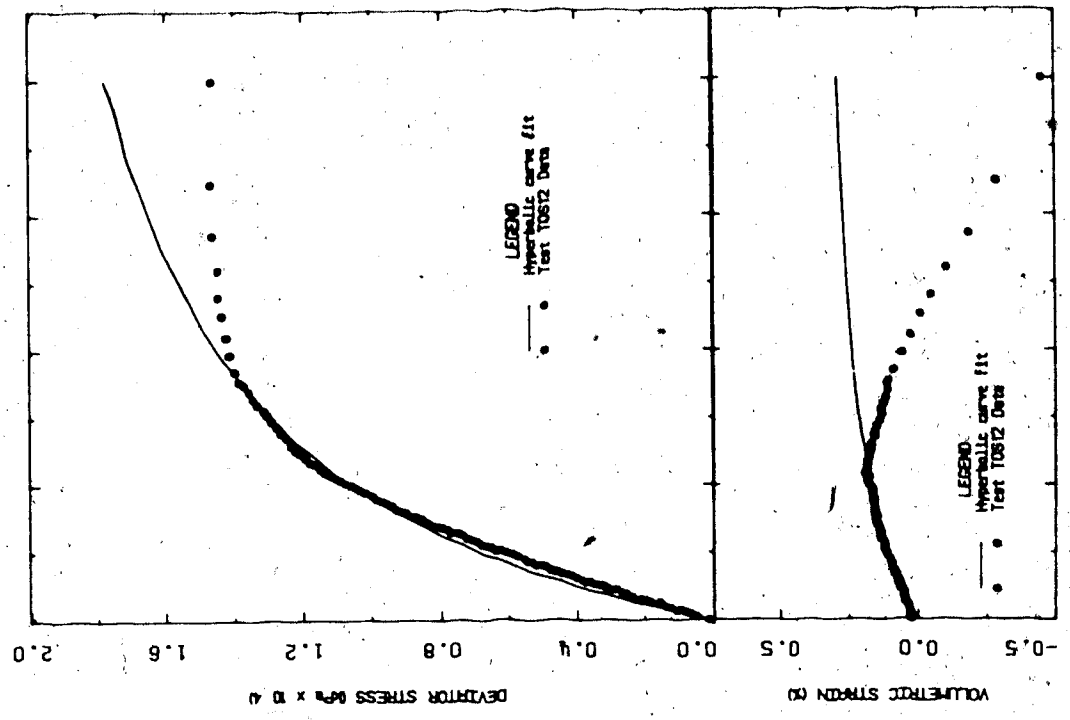

FIGURE 6.5.3 Hyperbolic Curve-Fit for Triaxial Compression of Oil Sand (Stress Path C at 200°C)

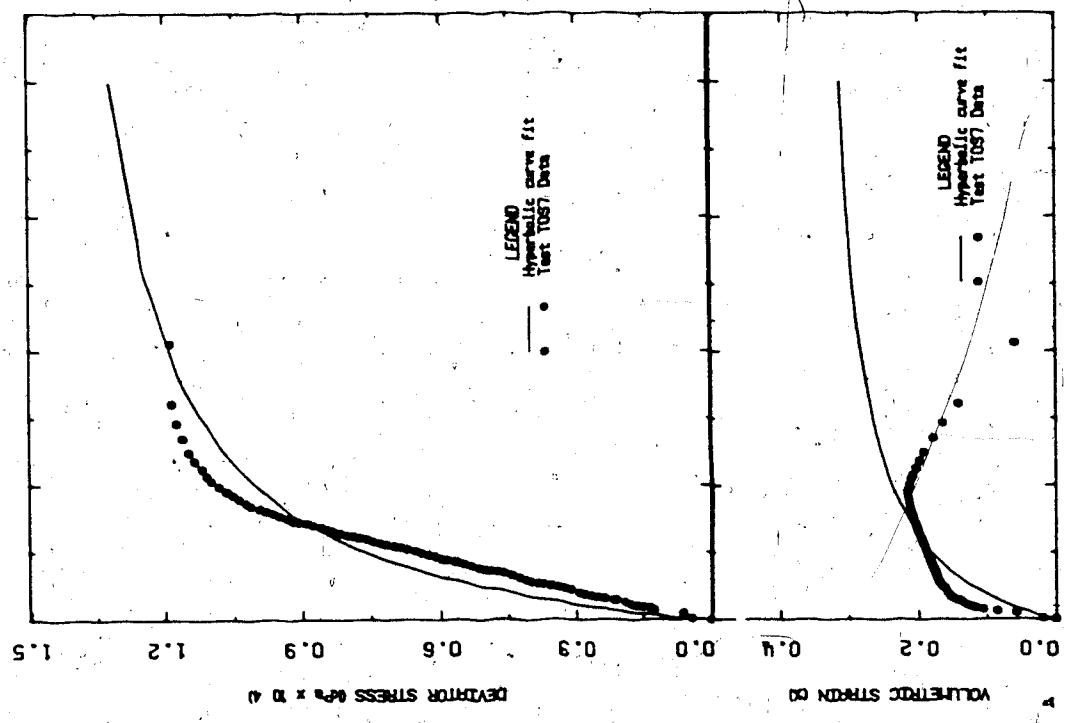

FIGURE 6.5.2 Hyperbolic Curve-Fit for Triaxial Compression of Oil Sand (Stress Path C at 125°C)

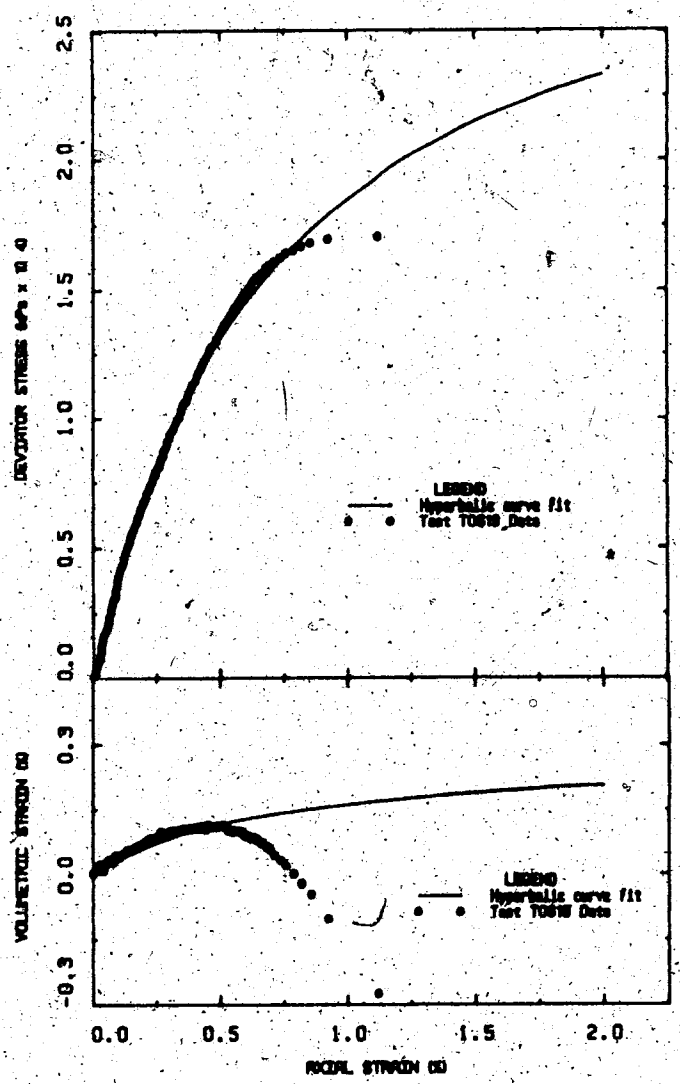

FIGURE 6.5.4 Hyperbolic Curve-Fit for Triaxial Compression of Oil Sand (Stress Path C at 125°C)

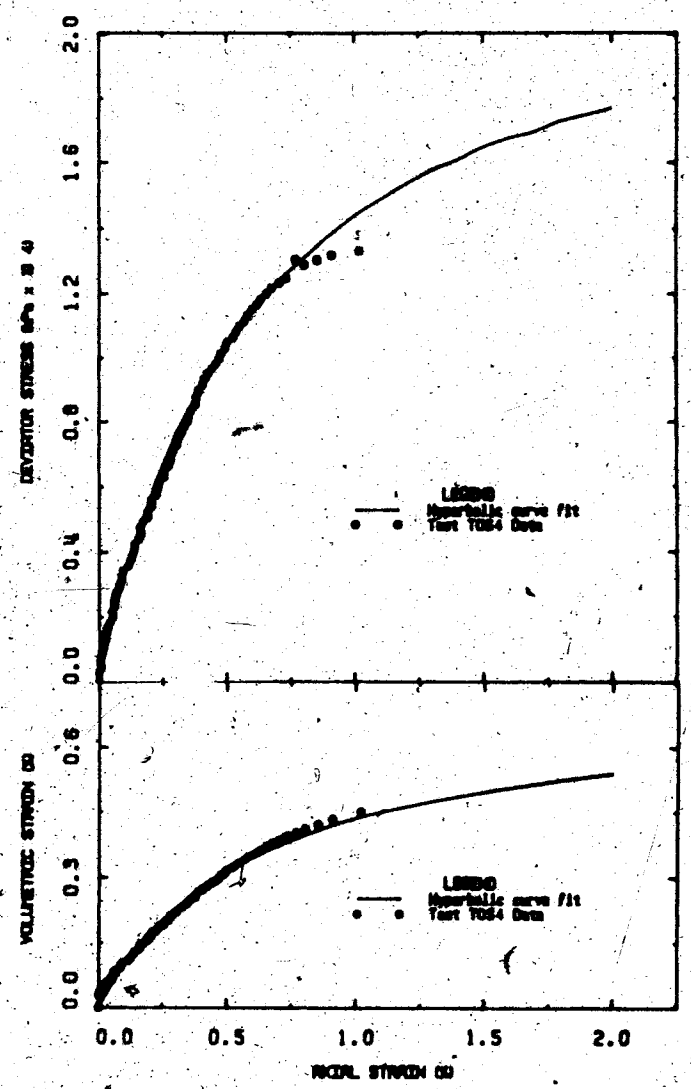

FIGURE 6.6.1 Hyperbolic Curve-Fit for Triaxial Compression of Oil Sand (Stress Path D at 20°C)

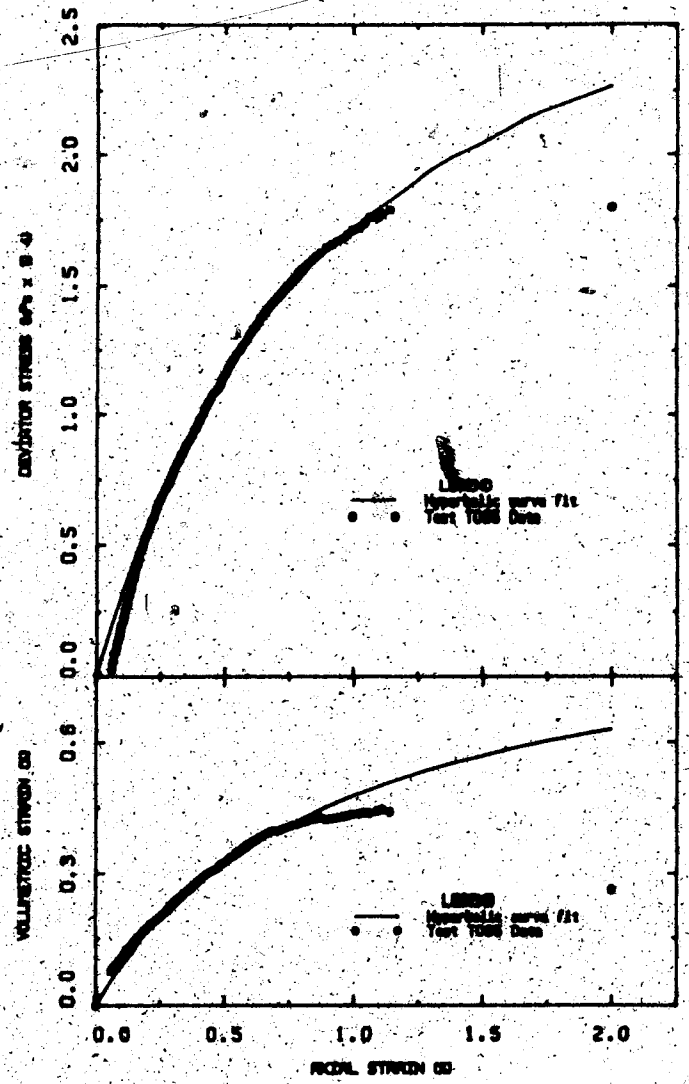

FIGURE 6.6.2 Hyperbolic Curve-Fit for Triaxial Compression of Oil Sand (Stress Path D at 20°C)

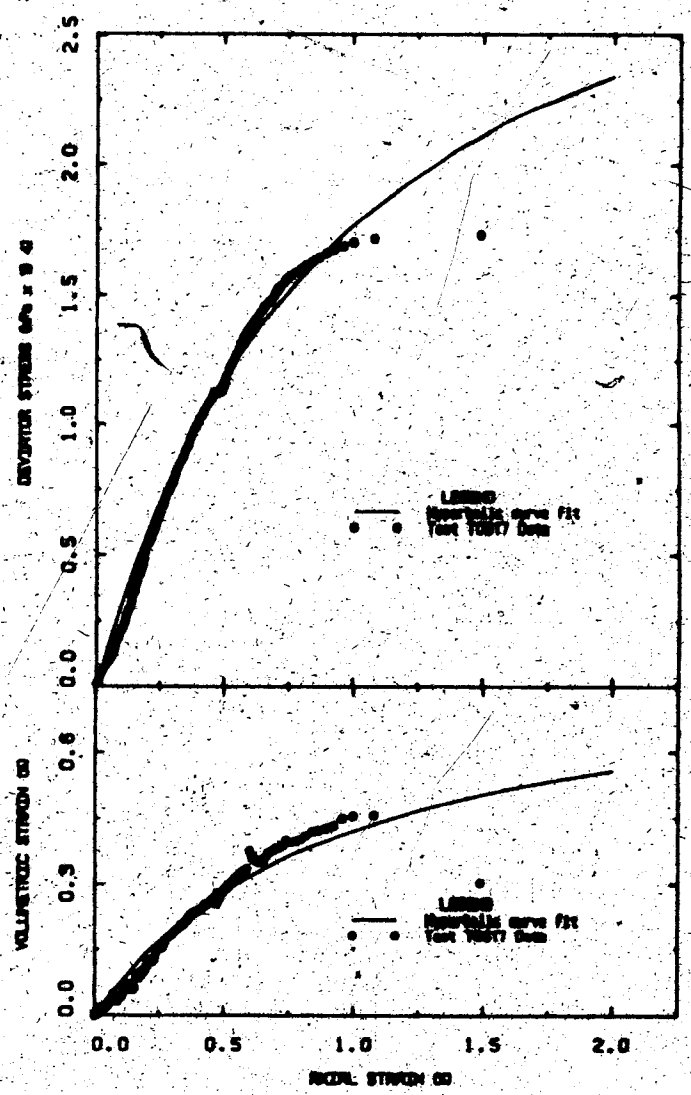

FIGURE 6.6.3 Hyperbolic Curve-Fit for Triaxial Compression of Oil Sand (Stress Path D at 200°C)

and hyperbolic curves for passive compression (stress path C) at 4 MPa and at temperatures of 20°C, 125°C , 200°C and 125°C, respectively. Figures 6.6.1, 6.6.2 and 6.6.3 show test results and "best-fit" hyperbolic curves for passive compression (stress path D) at 8 MPa effective confining stress and temperatures of 20°C, 125°C and 200°C, respectively.

Figures 6.3 to 6.6, inclusive, illustrate that the stress-strain behaviour of Saline Creek oil sand up to about 80% of peak deviator stress may be approximated reasonably accurately by the hyperbolic model. Although the hyperbolic model was developed exclusively for conventional passive triaxial compression, the results shown in Figures 6.3.1, 6.3.2 and 6.3.3 for stress path B (J1 constant) in which both σ_1' and σ_3' are varied, indicate that these stress-strain curves are also of hyperbolic form. It should be noted that the volume change relationship given in equation 6.2 does not predict dilatant volume changes, characteristic of the triaxial test data for Saline Creek oil sand. Byrne and Eldridge (1982) have modified equation 6.2 within the framework of incremental elasticity to account for dilatant volumetric strain. The modified relationship of Byrne and Eldridge may be expressed as follows:

$$\epsilon_v = \left[\frac{(\sigma_1 - \sigma_3)}{3K_B} + D_t \gamma_s\right] \qquad (6.3)$$

where D_t is a tangential dilitancy parameter;

$D_t = -\sin \nu_D$, and

ν_D is the dilation angle after Rowe (1971), and

γ_s is shear strain.

Equation 6.1 may be transformed into the following more convenient linear form:

$$\left(\frac{\epsilon}{\sigma_1 - \sigma_3}\right) = \left[\frac{1}{E_i} + \frac{\epsilon}{(\sigma_1 - \sigma_3)_{ULT}}\right] \qquad (6.4)$$

Experimental data presented in Figures 6.4 to 6.6 inclusive are summarized in Figure 6.7, a plot of $\epsilon/(\sigma_1-\sigma_3)$ versus ϵ according to equation 6.4. Data points shown on Figure 6.7 are at 70 per cent and 95 per cent of the peak deviator stress, as recommended by Duncan et al. (1980). Transformed stress-strain curves for the stress path B tests ($J1 \approx$ constant) are plotted in Figure 6.8. There is a very distinct variation of the stress-strain behaviour with temperature in Figure 6.8. The sample tested at 20°C along stress path B had the least stiffness and strength, while the 125°C test sample had greater stiffness; the 200°C test sample had intermediate stiffness and strength. As discussed in Chapter 4 these differences are small for clean quartzose Saline Creek oil sand.

The variation of stiffness with temperature is further illustrated in Figure 6.9, a plot of the logarithm of initial tangent modulus versus the logarithmn of effective confining stress, i.e. log E_i versus log σ_3'. Similarly Figure 6.10 is a plot of log K_B versus log σ_3'. While there is a clear trend of decreasing bulk modulus with effective confining stress at poth 20°C and 200°C, there is considerable scatter in bulk modulus values for the three 125°C tests. Again the data in Figure 6.10 generally indicate an increase in bulk modulus, K_B, i.e. stiffness, at elevated temperatures.

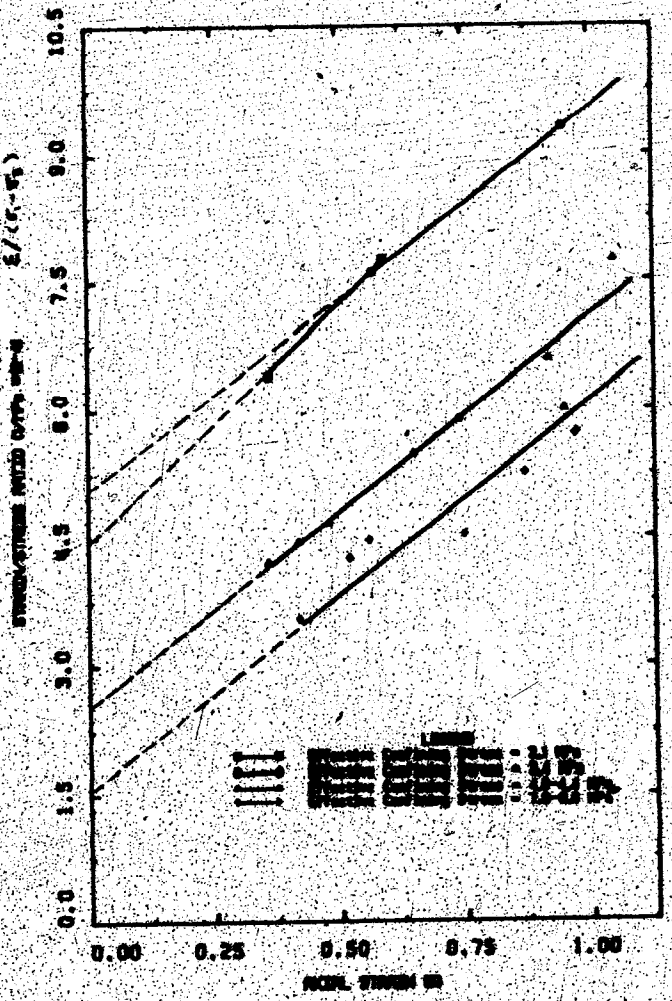

FIGURE 6.7 Transformed Hyperbolic Stress-Strain Curves for Passive Triaxial Compression

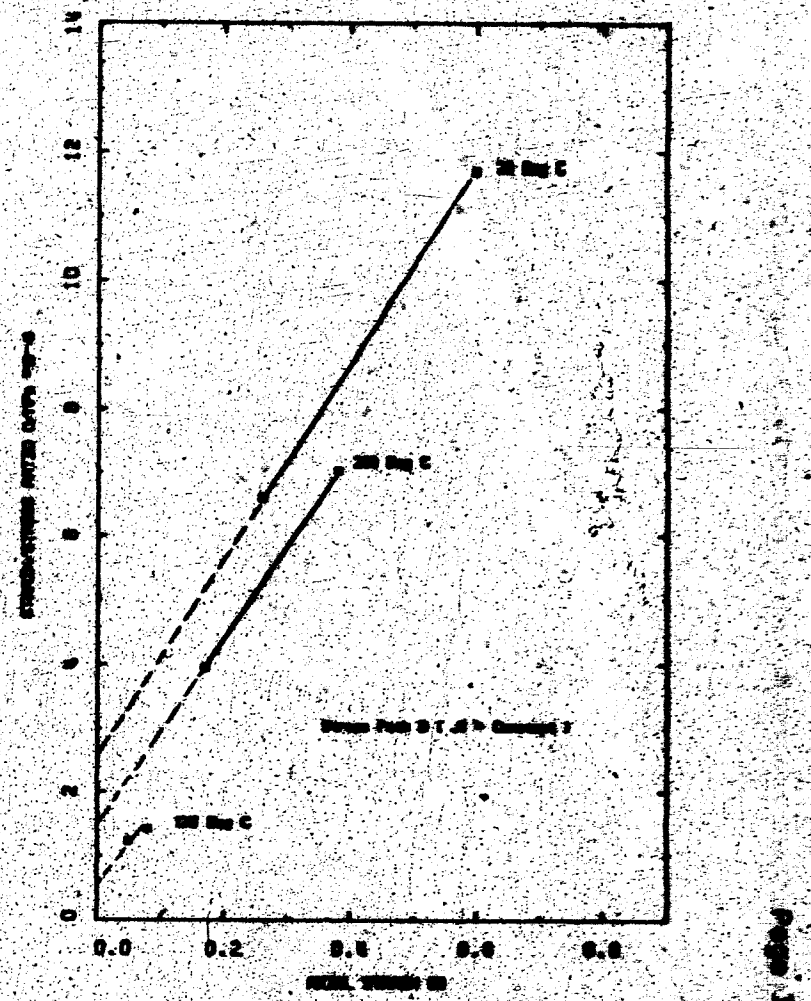

FIGURE 6.8 Transformed Hyperbolic Stress-Strain Curves for Stress Path B

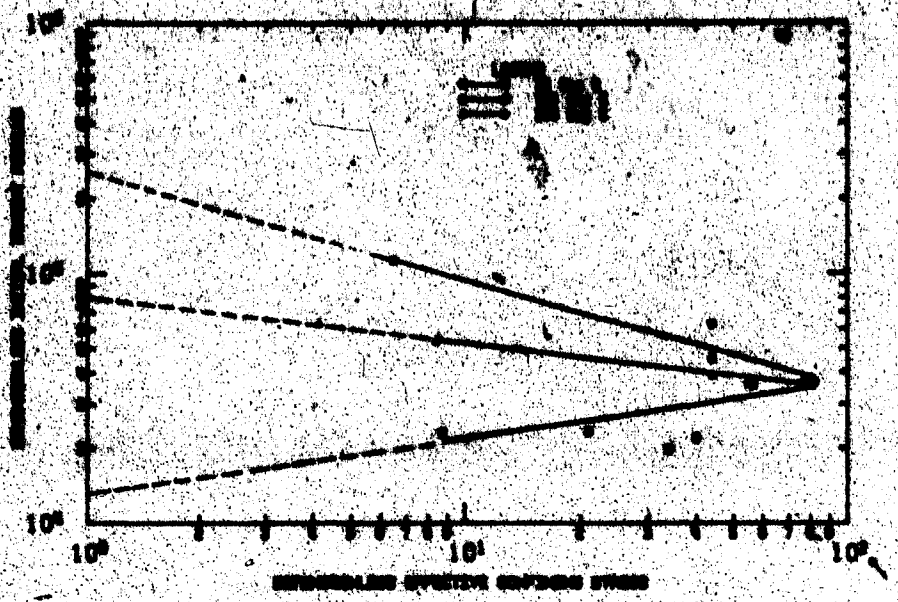

FIGURE 6.9 Variation of Initial Tangent Modulus with Effective Confining Stress

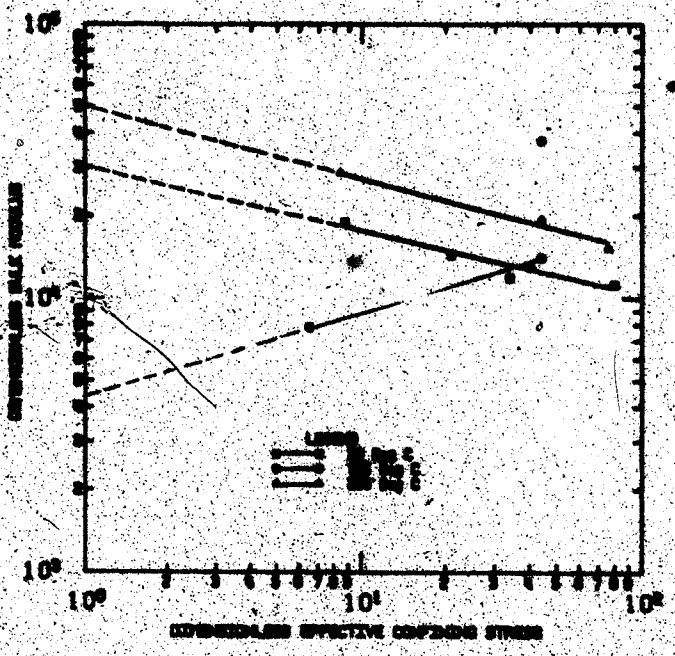

FIGURE 6.10 Variation of Bulk Modulus with Effective Confining Stress

The fundamental equations used in an incremental elastic stress-strain analysis employing the hyperbolic model are as follows (Duncan et al., 1980):

$$E_t = K P_a \left(\frac{\sigma_3}{P_a}\right)^n \left[1 - \frac{R_f(1-\sin\phi)(\sigma_1-\sigma_3)}{2c\cos\phi + 2\sigma_3\sin\phi}\right] \quad (6.5)$$

$$E_{ur} = K_{ur} P_a \left(\frac{\sigma_3}{P_a}\right)^n \quad (6.6)$$

$$\varepsilon_v = \left[\frac{(\sigma_1-\sigma_3)}{3 K_B P_a \left(\frac{\sigma_3}{P_a}\right)^m}\right] \quad (6.7)$$

$$\phi = \phi_o - \Delta\phi \log\left(\frac{\sigma_3}{P_a}\right) \quad (6.8)$$

Values of the eight experimentally determined parameters for Saline Creek oil sand required in equations 6.5 to 6.8 are summarized in Table 6.2 for temperatures of 20°C, 125°C and 200°C. A ninth parameter, the tangential dilatancy parameter, D_t, proposed by Byrne and Eldridge (1982) has not been determined here but should be included in future analyses to correctly model dilatant volumetric straining of dense oil sands.

The version of the hyperbolic model currently in use in the general purpose finite element program, ADINA, at the University of Alberta uses equations 6.5 and 6.6, and assumes constant values of Poisson's ratio, ν, and friction angle, ϕ. Thus volumetric strain is assumed to vary linearly with axial strain according to the following relationship from linear elastic theory:

TABLE 6.2

SUMMARY OF HYPERBOLIC PARAMETERS FOR S[redacted]REEK OIL SAND

TEMPERATURE (°C)	MODULUS NUMBER (k)	MODULUS EXPONENT (n)	UNLOAD-RELOAD MODULUS NO. (k_{ur})*	BULK MODULUS NUMBER (k_b)	BULK MODULUS EXPONENT (m)	AVERAGE FAILURE RATIO (R_f)	FRICTION ANGLE PARAMETERS (ϕ_o)	($\Delta\phi$)
20	25000.	+0.09	30000.	30000	-0.2	0.53	72	20
125	30000.	-0.47	36000.	3000	+0.5	0.60	72	20
200	80000.	-0.19	96000.	47500	-0.2	0.63	72	20

* Estimated values assuming $k_{ur} = 1.2\ k$

$$\varepsilon_v = \varepsilon / (1 - 2\nu) \qquad (6.9)$$

A family of stress-strain curves generated for effective confining stresses, σ_3', ranging from 2 to 10 MPa, and assuming $\phi = 40°$ and $\nu = 0.43$ is presented in Figure 6.11. The stress-strain relationships given in Figure 6.11 were used in the numerical analyses of shaft excavation described in the following section.

6.3 Stress Changes and Deformation During Excavation of a Vertical Shaft or Borehole in Oil Sand

Stress changes and deformations due to unloading during excavation of a cylindrical shaft or borehole depend on the excavation technique, and in particular, on the method used to provide temporary support for the floor and walls of the advancing shaft excavation prior to installing a permanent support system. Boreholes drilled for the purpose of installing well casings for fluid injection or hydrocarbon recovery are generally supported temporarily with a bentonite slurry or drilling mud. This technology, i.e. so-called "blind drilling", has recently been extended to larger diameter shaft excavations up to 6.0 m in diameter (Stephenson and Owens, 1983). A second temporary support technique commonly used in the mining industry involves artifical freezing of a pillar of soil and/or rock adjacent to the shaft excavation. Freezing the porewater in soil and rock materials provides temporary tensile resistance and enhanced compressive strength when lateral and vertical confining stresses are reduced during excavation.

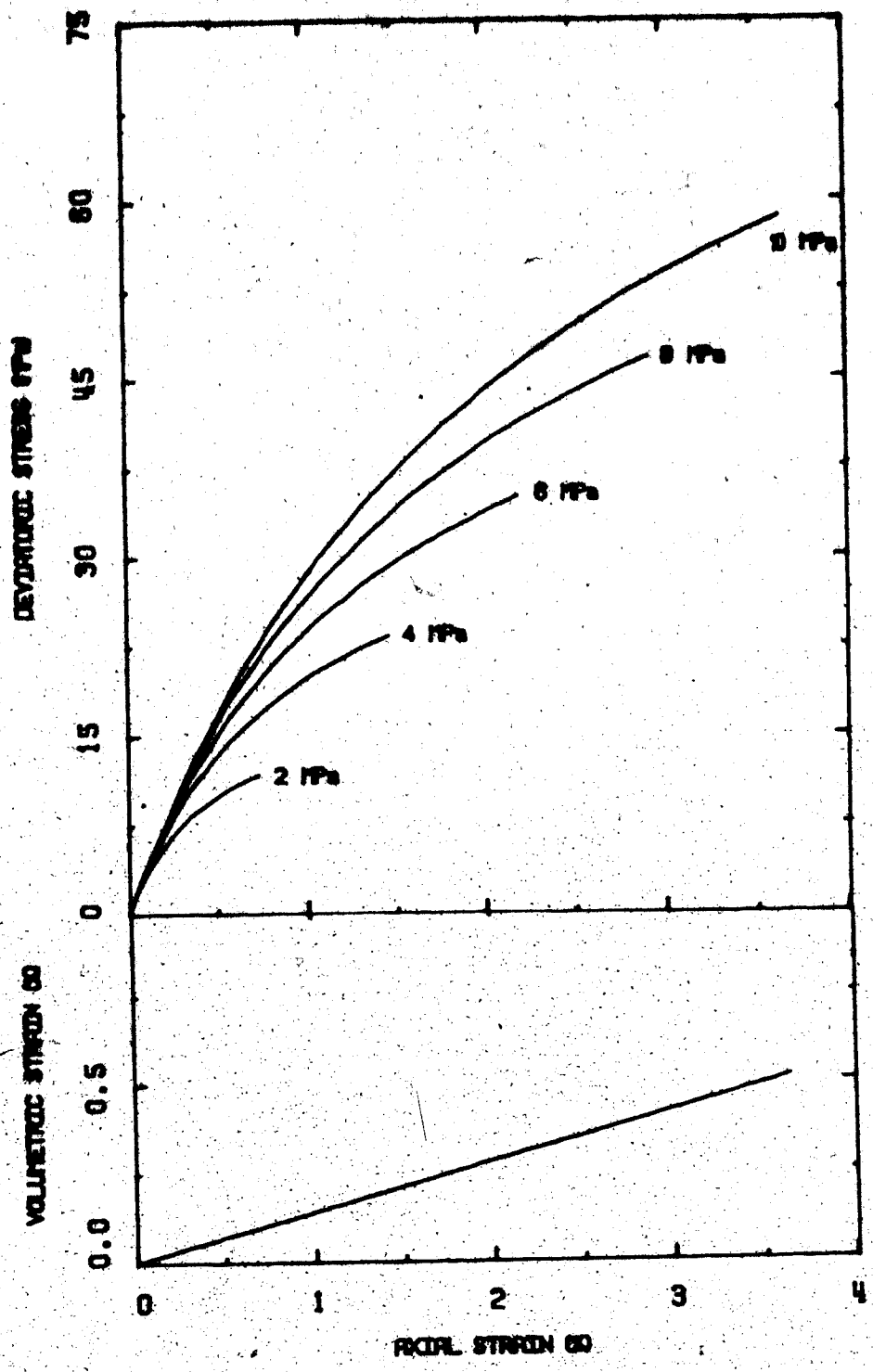

FIGURE 6.11 Family of Hyperbolic Stress-Strain Curves for $\phi = 40°$ and $\nu = 0.43$

Stress changes and deformations during excavation by "blind drilling" were analyzed here since the technique has application to both well boring and shaft sinking. The finite element program ADINA was used to model stress changes and deformations in an oil sand deposit during excavation. A two-dimensional axisymmetric finite element mesh was used to model a 20 m thick layer of oil sand at a depth of 400 m below ground surface. The hyperbolic material model was used in a nonlinear incremental stress-strain analysis, using parameters summarized in section 6.2. The finite element mesh is shown in Figure 6.12. Vertical effective confining stress (overburden) and gravity (mass proportional) stresses were applied to the layer in 20 increments. The element stiffness matrix was updated according to the hyperbolic model before each loading increment. Fully drained conditions were assumed (i.e. pore pressures were assumed to remain constant during both the loading and subsequent shaft excavation stages). Ambient pore pressures are sufficiently large to prevent gas exsolution at the 400 m depth.

Applied stresses were non-uniform resulting in an initial ratio of horizontal to vertical effective stresses of 0.75, (i.e. K_o=0.75). Stress ratio (K_o) values less than unity are believed to be fairly representative of conditions at the 400 m depth being analyzed here.

Vertical confining stress overlying the first column of elements on the left-hand side of the mesh in Figure 6.12, was removed in 10 equal increments in order to model excavation of the shaft through the overburden. The element stiffness matrix was updated before each excavation step. Radial, tangential and

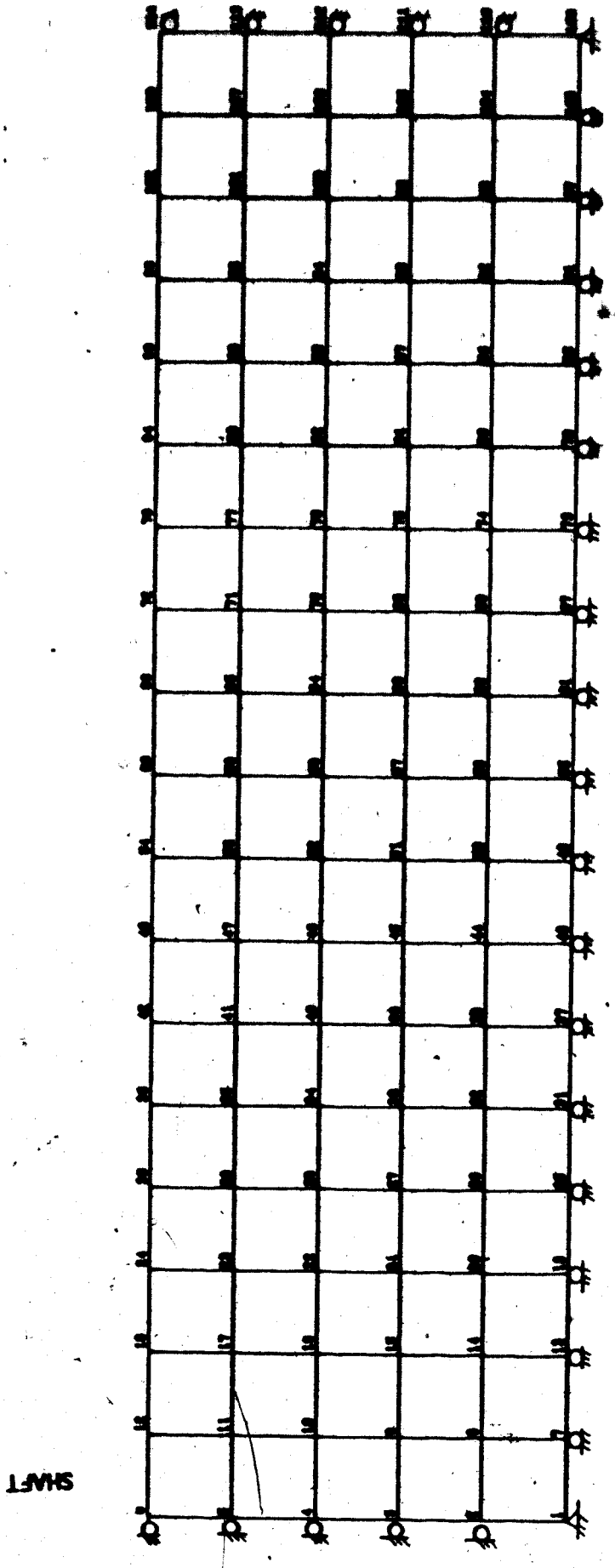

FIGURE 6.12 Finite Element Mesh for Axisymmetric Analysis of the Shaft Excavation Problem

vertical stresses at mid-depth in the oil sand layer following this excavation stage, i.e. excavation stage 1, are shown in Figure 6.13.1. Deformation vectors throughout the mesh resulting from the 10 step excavation stage 1 are summarized in Figure 6.13.2.

Shaft excavation through the oil sand was modelled in five sequential excavation steps, i.e. excavation stages 2 to 6, inclusive. The "element death option" available in ADINA was used to excavate shaft elements within the 5 discretized layers of oil sand shown in Figure 6.12. At the instant that each shaft element was "killed", a support pressure equivalent to hydrostatic drilling mud pressure was applied along the side and bottom boundaries of the shaft excavation. The element stiffness was updated before each excavation stage. Stresses at mid-depth in the oil sand, i.e. σ_r, σ_θ and σ_z, and deformation vectors after each of excavation stages 2 to 6, are shown in Figures 6.14.1 to 6.18.2, inclusive.

Figures 6.13.1 to 6.18.2, inclusive, illustrate that stress changes and deformations resulting from the excavation are very small. This is due to the relatively large support pressure which is continuously provided by the "drilling mud" used in the "blind drilling" excavation technique. It is also apparent that vertical deformations and stress changes near the shaft are greater than horizontal stress changes and deformations during excavation stages 1 to 4. This is due to the initial state of stress, in which vertical stresses were greater than horizontal stresses (i.e. $K_o = 0.75$).

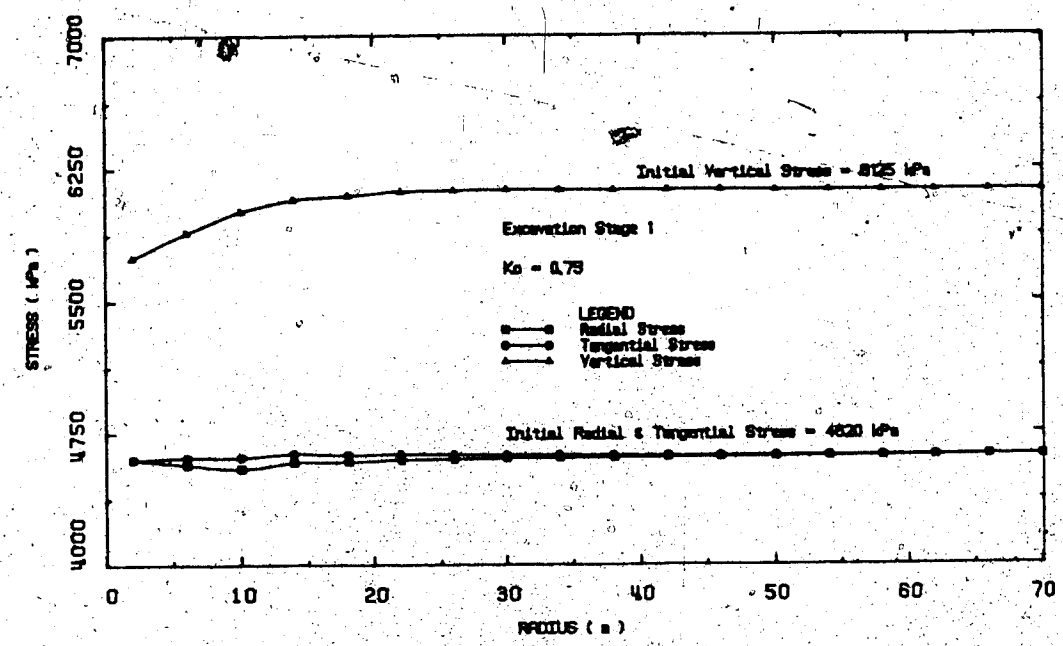

FIGURE 6.13.1 Stresses Following Shaft Excavation Stage 1

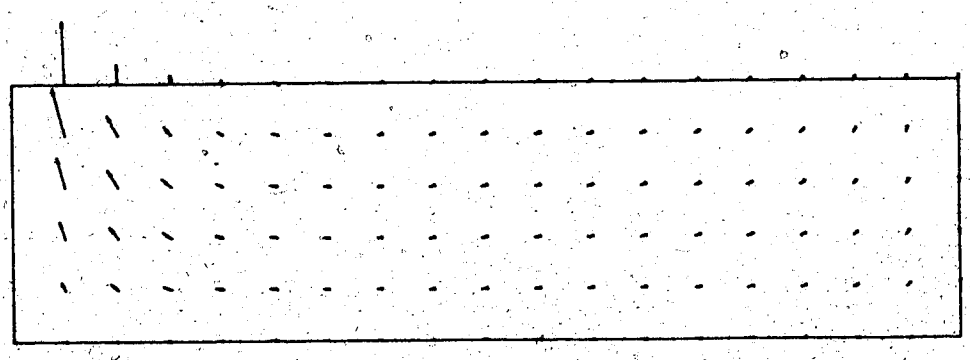

FIGURE 6.13.2 Displacements Following Shaft Excavation Stage 1

DISPLACEMENT SCALE 10:1

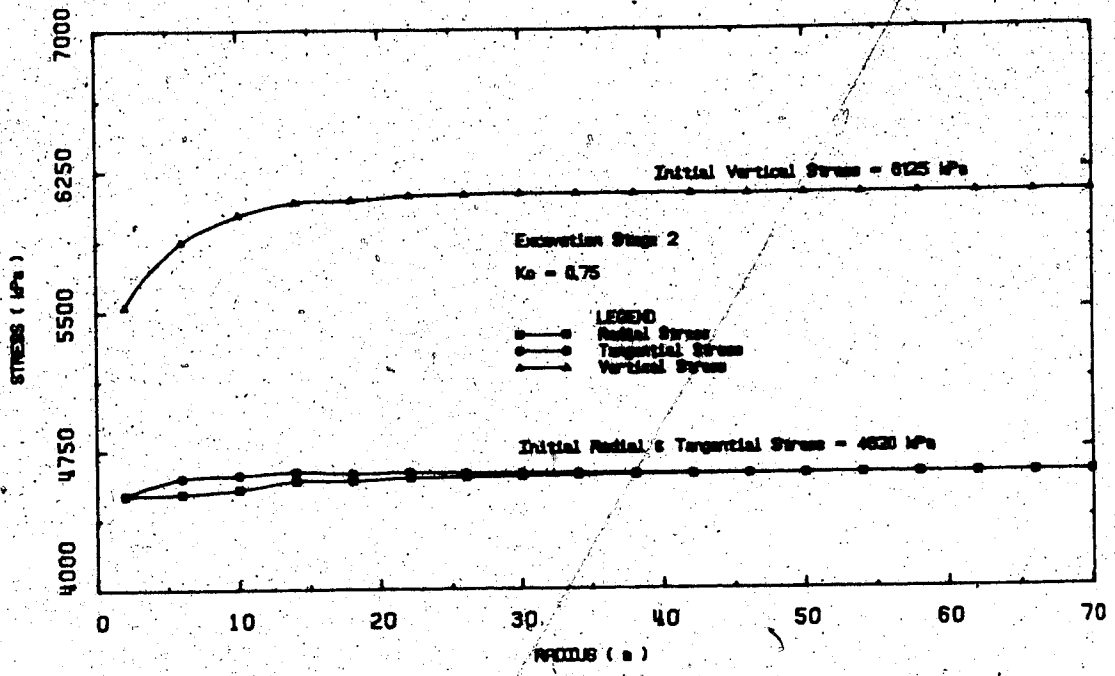

FIGURE 6.14.1 Stresses Following Shaft Excavation Stage 2

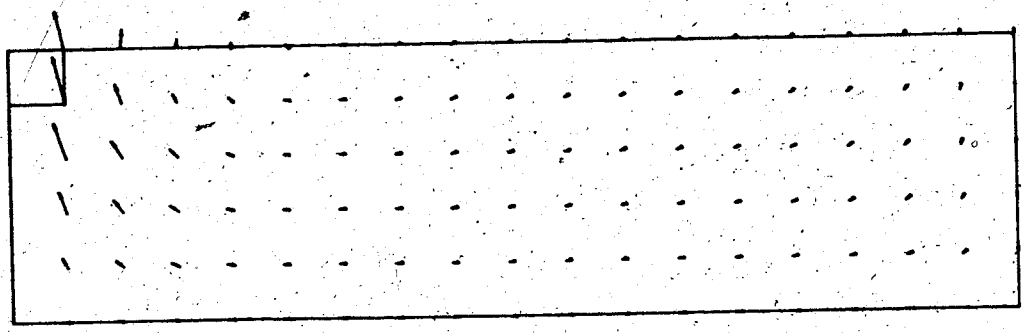

FIGURE 6.14.2 Displacements Following Shaft Excavation Stage 2

DISPLACEMENT SCALE 10:1

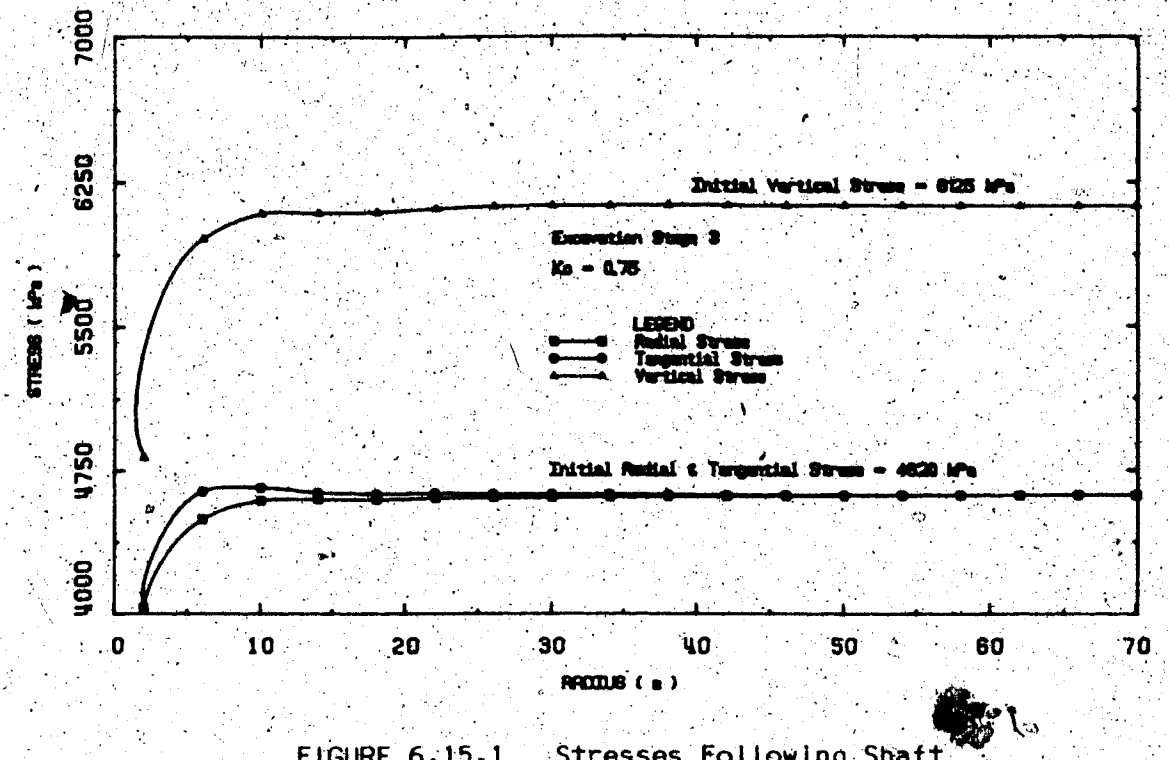

FIGURE 6.15.1 Stresses Following Shaft Excavation Stage 3

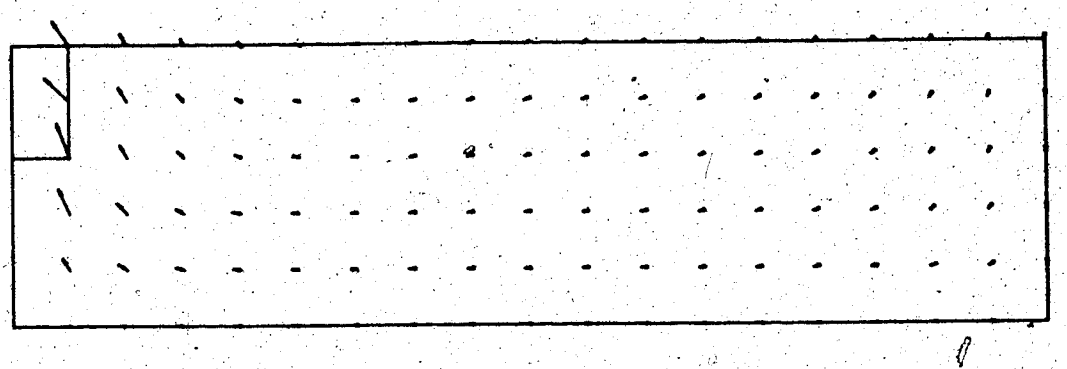

FIGURE 6.15.2 Displacements Following Shaft Excavation Stage 3

DISPLACEMENT SCALE 10:1

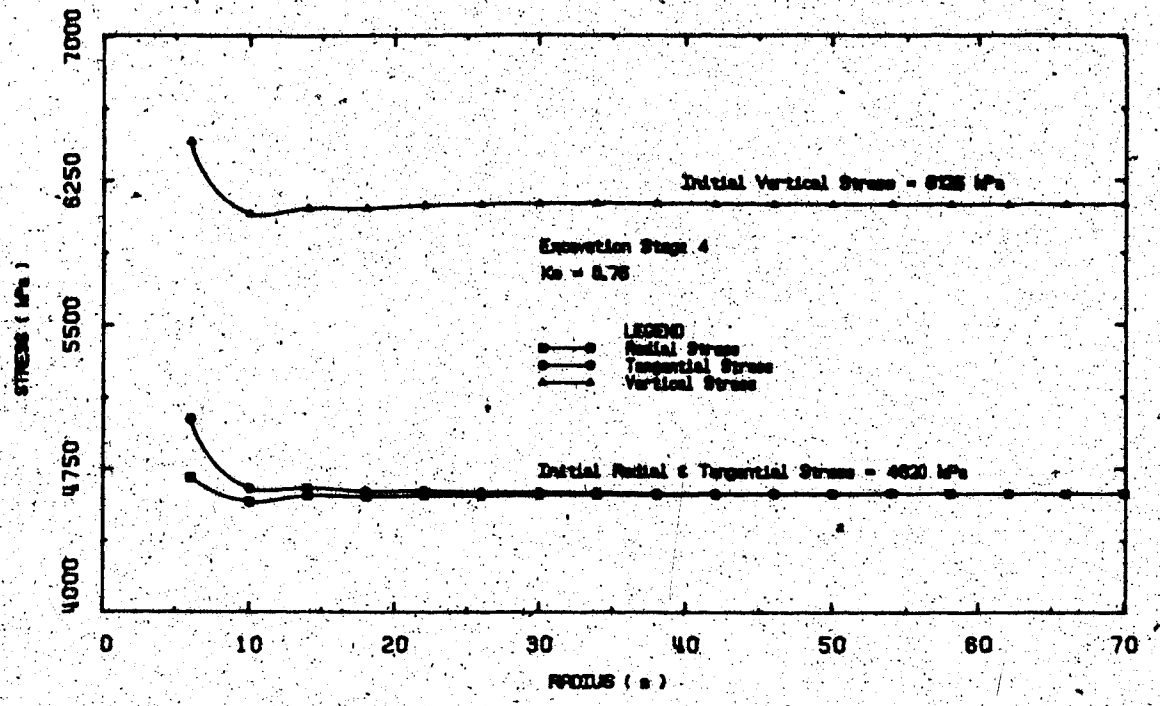

FIGURE 6.16.1 Stresses Following Shaft Excavation Stage 4

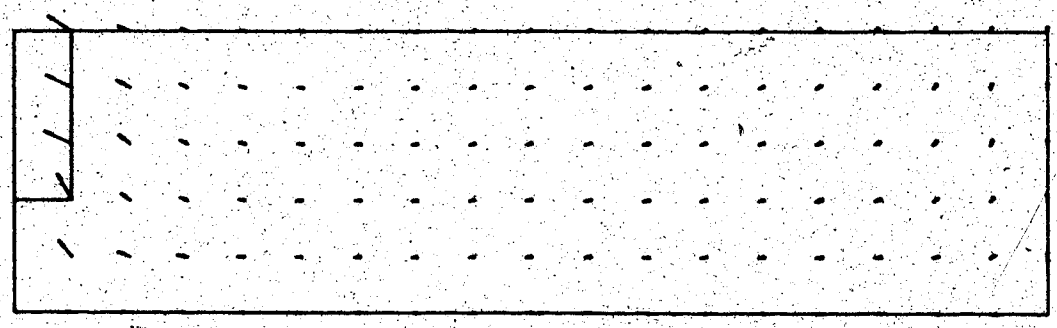

FIGURE 6.16.2 Displacements Following Shaft Excavation Stage 4

DISPLACEMENT SCALE 10:1

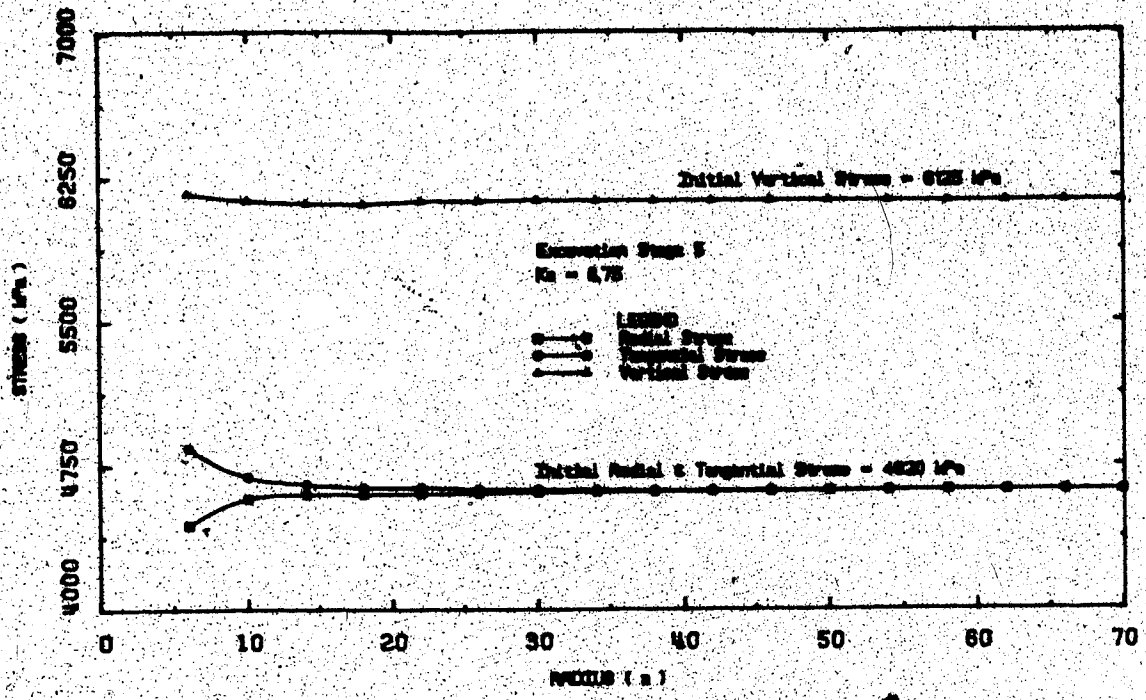

FIGURE 6.17.1 Stresses Following Shaft Excavation Stage 5

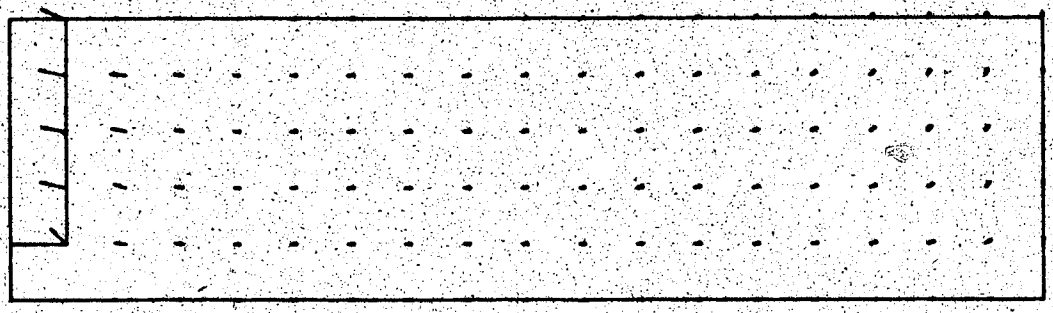

FIGURE 6.17.2 Displacements Following Shaft Excavation Stage 5

DISPLACEMENT SCALE 10:1

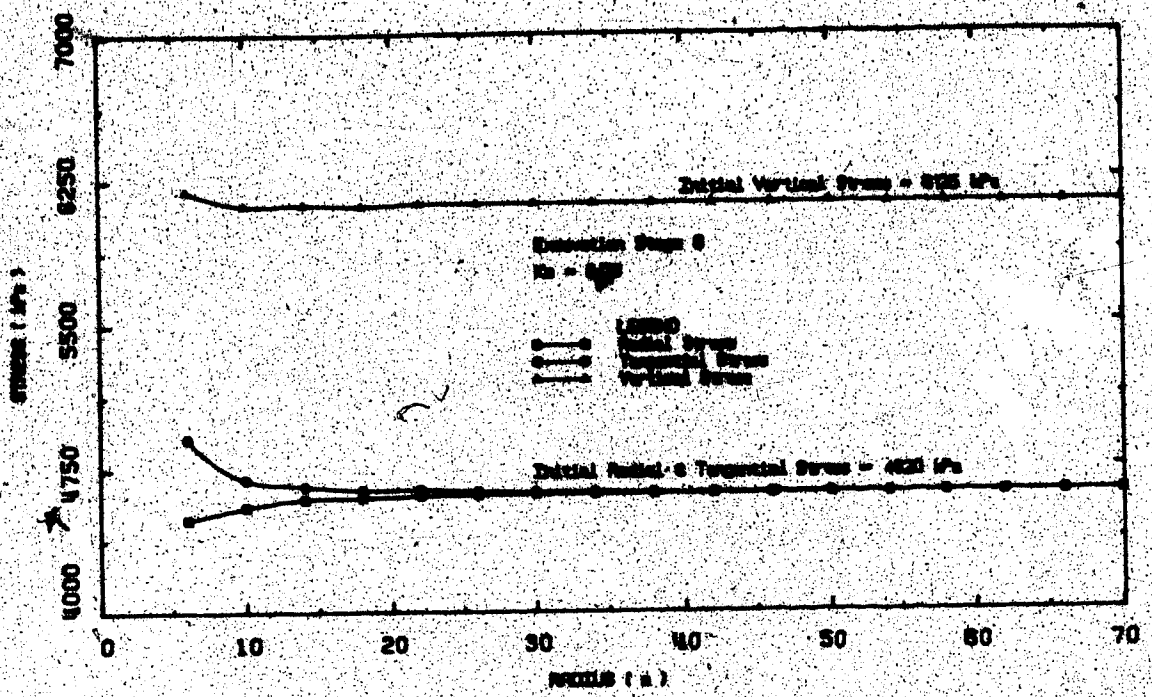

FIGURE 6.18.1 Stresses Following Shaft Excavation Stage 6

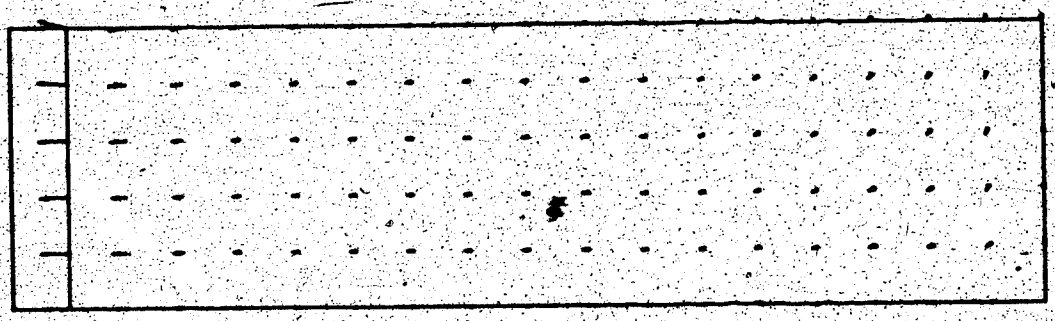

FIGURE 6.18.2 Displacements Following Shaft Excavation Stage 6

DISPLACEMENT SCALE 10:1

Radial convergence of the shaft wall is plotted as a function of horizontal support pressure in Figure 6.19, a ground response curve. It is interesting to note that the horizontal stress (or support pressure) in the oil sand actually increased slightly during removal of vertical overburden stresses above the oil sand deposit in excavation stage 1. Stress changes in an element of oil sand immediately adjacent to the shaft excavation during the six excavation stages are illustrated in the stress path plot shown in Figure 6.20. Although the stress path in the element of oil sand during excavation is complex, the stress changes are very small and do not increase the shear stress level substantially.

Larger stress changes would be predicted for other shaft excavation techniques using other temporary support systems such as artifical freezing and/or shotcrete (NATM) because of the lower support pressures provided during excavation when using these techniques.

6.4 Stress Changes and Deformations Adjacent to a Shaft During Thermally Enhanced Oil Recovery

6.4.1 Problem Description

Figure 6.21 illustrates the problem to be analyzed in this section. The shaft excavation described in section 6.3 penetrates a 20 m thick layer of oil sand buried at a depth of 400 m. It was assumed that thermally enhanced oil recovery processes are being carried out in a production zone, radially symmetric about the shaft. It was also assumed that steam injection and production in this zone cause a step temperature

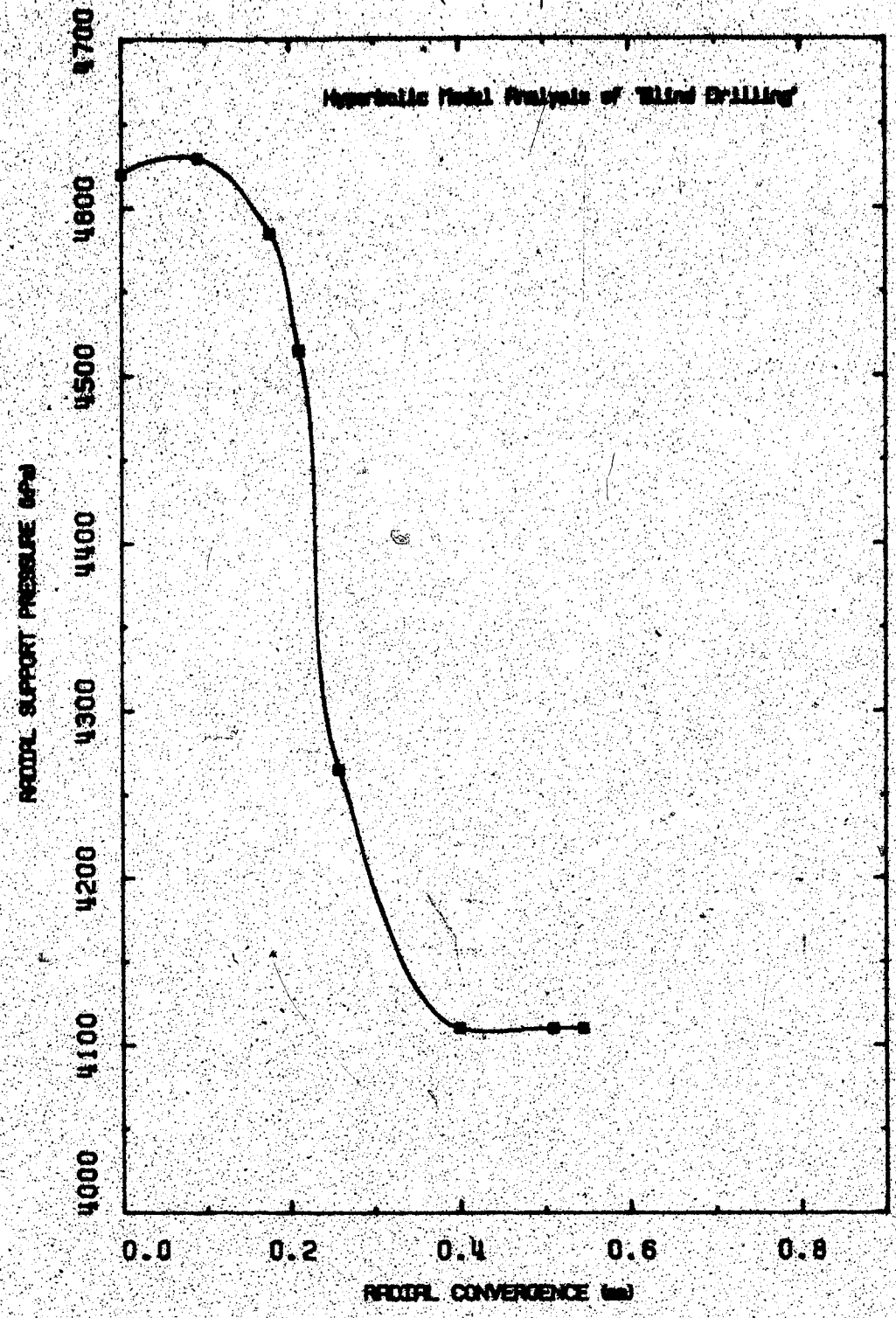

FIGURE 6.19 Ground Response Curve for Shaft Excavation

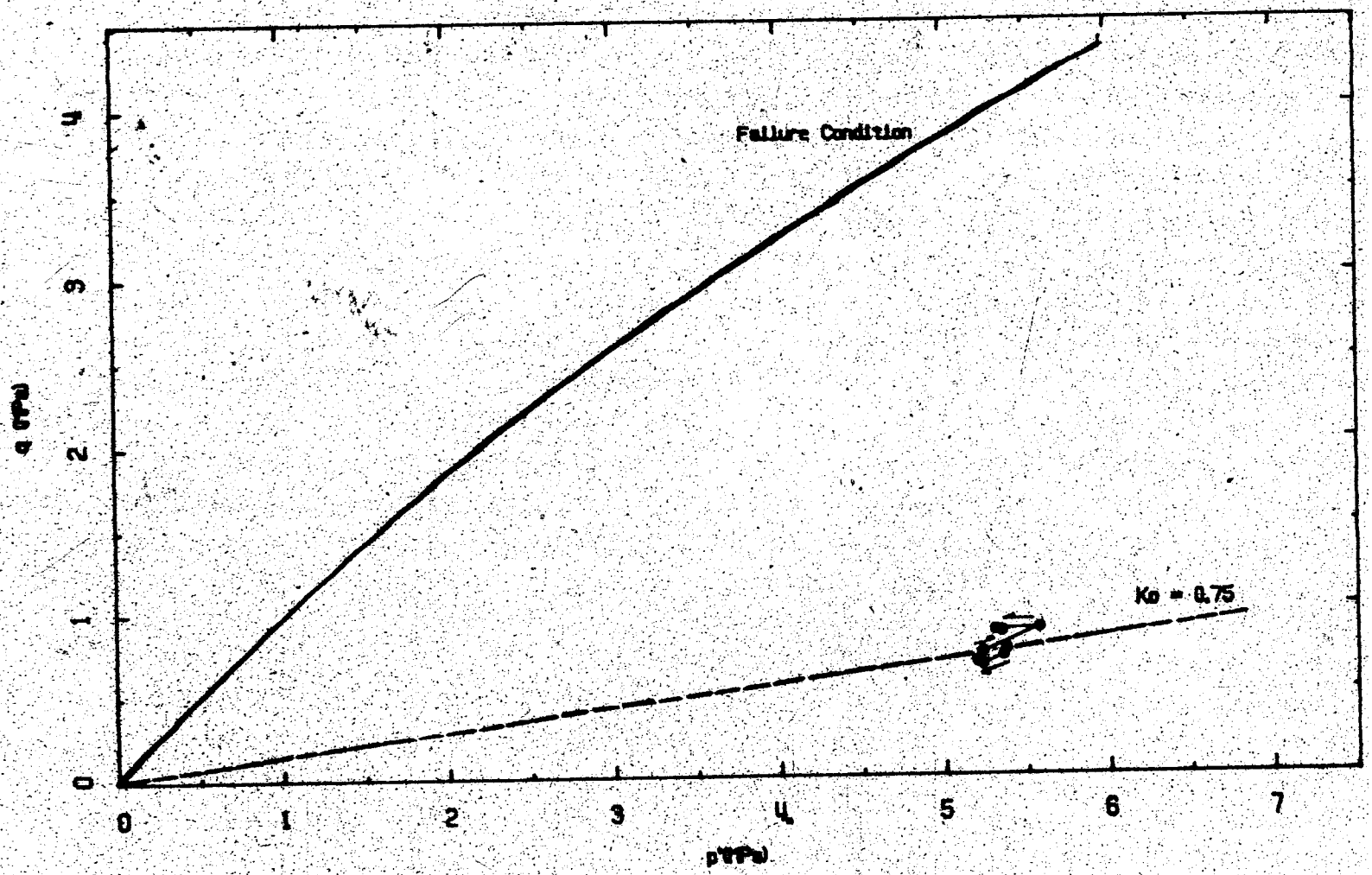

FIGURE 6.20 Stress Path in Oil Sand During Blind Drilling

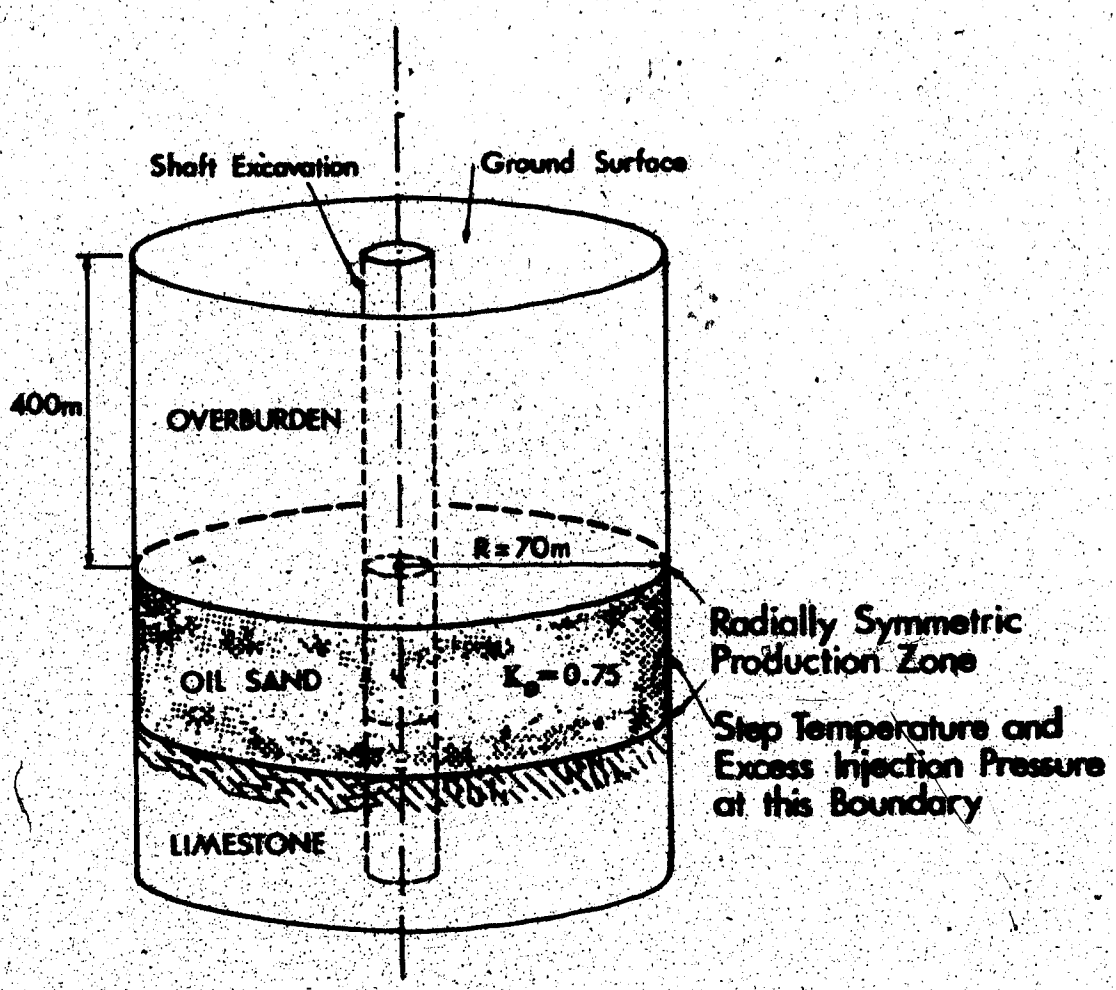

FIGURE 6.21 The Shaft Problem

of 200°C and initial excess injection pressure of 2 MPa at a radially symmetric boundary located 70 m from the centre of the shaft. This configuration introduces the concept of leaving a "protective pillar" of oil sand around a shaft or deep tunnel as a buffer against dynamic injection and heating activities in the production zone. Dimensioning such a pillar requires evaluation of stress changes and deformations adjacent to the shaft with time.

Initial stresses and pore pressures at mid-depth in the oil sand layer prior to shaft excavation, heating and injection were assumed to be:

(1) Initial Vertical Stress, σ_{vo}, of 9225 kPa
(2) Initial Pore Pressure, p_o, of 3100 kPa
(3) Initial Vertical Effective Stress, σ_{vo}', of 6125 kPa
(4) Ratio of Horizontal to Vertical Effective Stresses, K_o of 0.75 (i.e. initial horizontal effective stress, σ_H', of 4600 kPa).

Stresses and pore pressures may be altered from the initial conditions outlined above by:

(1) Shaft excavation and installation of a permanent ground support system;
(2) Development of the production zone including well drilling, hydraulic fracturing etc.;

(3) High pressure injection and heating within the production zone; and

(4) Transmission of excess pore pressure and heat transfer beyond the zone of enhanced oil recovery (the production zone), toward the shaft.

Stress changes and deformations resulting from development of the production zone as described in items (2) and (3) of the proceeding paragraph are not predicted specifically in finite element analyses in this chapter for several reasons:

(1) Proposed schemes for developing inter-well communication and promoting sweep efficiency in oil sand reservoirs vary widely depending upon such factors as geologic facies and the cost-effectiveness of various well completion configurations.

(2) Production zone development concepts, i.e. "production scenarios", are typically complex involving multiple injection cycles; and finally

(3) The primary purpose of the following analysis is to illustrate important aspects of the numerical modelling procedure, rather than to provide site-specific numerical results.

Detailed analyses required for practical applications must include evaluation of the stress changes and deformations resulting from a specific production zone "development scenario". This phase of oil sands project planning and design obviously requires close liaison between reservoir and geotechnical engineering specialists.

Heat transfer from the specified production zone boundary, i.e. from the 70 m radius, toward the shaft, is assumed to involve thermal diffusion only, in the following analyses. This assumption is consistent with specified boundary conditions. Convective heat transfer would be important if drainage or depressurization facilities were provided near the shaft causing flow toward the shaft.

6.4.2 Influence of Injection Pressure

The development of excess pore pressure in situ is influenced by injection pressure as well as by heating.

It may reasonably be assumed that massive injection at pressures exceeding the minimum principal total stress, will cause the magnitude of horizontal total compressive stresses to increase under conditions of lateral constraint. Vertical stress would not be expected to exceed the total overburden stress since increases may be relieved by vertical heave. The pore pressure response to undrained total stress changes (in terms of principal stresses) is given by the following relationship (after Skempton, 1954):

$$\Delta u = [B\ \Delta\sigma_3 + A\ (\Delta\sigma_1 - \Delta\sigma_3)] \qquad (6.10)$$

If it is assumed that the major and minor principal stress orientations are vertical and horizontal, and that horizontal stress change is equivalent to the magnitude of the injection

pressure in excess of the original horizontal stress, then:

$$\Delta\sigma_1 = \Delta\sigma_v = 0$$

$$\Delta\sigma_3 = \Delta\sigma_H = (P_{INJ} - \sigma_{HO}) \qquad (6.11)$$

$$\Delta u = B(1 + A)(P_{INJ} - \sigma_{HO})$$

Typical values of the coefficients B and A for dense oil sand saturated with liquid pore fluids of low compressibility are 0.7 to 0.8 and 0.2 to 0.4, respectively. Massive injection into liquid saturated oil sand would result in pore pressure increase:

$$\Delta u = 0.84\ (P_{INJ} - \sigma_{HO}) \text{ to } 1.12\ (P_{INJ} - \sigma_{HO})$$

$$\text{or } \Delta u \simeq P_{INJ} - \sigma_{HO}$$

Therefore, injection pressure in excess of the original horizontal total stress would cause a rapid increase in pore pressure approximately equivalent to the excess amount of the injection pressure.

In cohesionless oil sands, a parting, i.e. hydraulic fracture, is created when the injection pressure exceeds the minimum principal total stress. The difference between injection pressure and minimum principal stress, i.e. $(P_{INJ} - \sigma_{HO})$, required to extend a parting in oil sand is not large. Although oil sands injection mechanics is not well understood, it is postulated that at distances remote from the parting, the pore pressure increase due to total stress increase during injection is generally not large because of pressure decline as the parting extends.

The magnitude of the B parameter for oil sands may be less than 0.7 - 0.8 if the compressibility of the constituent pore fluids is increased by such factors as temperature increase or the presence of undissolved gaseous pore fluids. As discussed in Chapters 3 and 4, the compressibility of water and bitumen at ambient temperatures less than 20°C is low, i.e. approximately 4.0×10^{-7} kPa^{-1} over a range of pressures from 0.1 to 15 MPa. Increasing the temperature of oil sand to 300°C has the effect of reducing compressibility of the pore fluids to the extent that the magnitude of the B parameter is reduced to 0.2 - 0.3 at pressures above the saturation pressure. The presence of undissolved gaseous pore fluids has the effect of reducing the initial pore pressure response to total stress change because of the large compressibility of gases, i.e. the B parameter is reduced. The pore pressure response following a total stress change is time-dependent due to gas exsolution/ sorbtion processes (see Sobkowitcz, 1982).

Sustained injection at pressures less than the minimum principal total stress may also result in shear failure and/or hydraulic parting if the magnitude of the minimum effective principal stress, σ_3', approaches zero.

Ishijima and Roegiers (1983) and Horsrud et al. (1982) have recognized that hydraulic fracture initiation depends on formation pressures and injection fluid viscosity. They observed that fractures are initiated at pressures below the "breakdown pressure", particularly in materials of high

permeability. When heated water or condensed steam is being injected the magnitude of excess pore pressure (i.e. pore pressure exceeding the initial in situ pore pressure) is the algebraic sum of excess injection pressure and thermally generated excess pore pressure. Transmission of injection pressure greater than the initial in situ pore pressure Po, but less than the minimum effective principal stress, σ_3', through the medium is governed by the consolidation process, i.e. hydraulic diffusion.

Injection at intermediate pressures, between the minimum effective and minimum total principal stresses, i.e. $\sigma_3' \leq P_{INJ} < \sigma_3$, will also cause shear failure and/or hydraulic parting. The rate of extension of the fracture or parting, in this case, depends upon hydraulic diffusivity of the porous medium. Partings may be expected to extend more rapidly in high permeability materials than in low permeability materials.

Injection at pressures less than the minimum total principal stress, σ_3, is generally not considered to be an efficient hydraulic fracturing process. However, injection of heated fluids at lower pressures, in many circumstances, has been found to improve the "sweep efficiency" of thermally enhanced oil recovery processes in oil sands.

The injection pressure applied at the production zone boundary in analyses of the shaft problem was 2 MPa. This

injection pressure is less than the minimum effective principal stress, i.e. σ_H' = 4.6 MPa, and therefore does not cause parting of the formation.

6.4.3 Boundary Conditions

Boundary conditions applied in the heat transfer analysis of the shaft problem illustrated in Figure 6.21, included:

1. Free heat flow at the ventilated shaft wall with no temperature increase; and
2. Constant 200°C temperature at the production zone boundary (R=70 m).

Consolidation analysis boundary conditions included:

1. A "no-flow" or reflection boundary at the impervious shaft wall; and
2. Free drainage and constant pore pressure equivalent to the initial pressure plus excess injection pressure of 2 MPa at the production zone boundary.

A range of boundary conditions were considered in thermo-elastic stress-strain analyses:

1. The shaft wall was assumed to be supported by a constant horizontal pressure equivalent to the hydrostatic drilling mud support pressure applied in

the excavation analysis in section 6.4.3. This boundary condition has obvious limitations when compared with the deformational resistance provided by a compressible steel or concrete shaft lining system. The bottom of the shaft wall at the base of the oil sand layer was fixed vertically by a "roller" support.

2. A constant effective overburden pressure was applied over the surface of the oil sand layer.
3. A rigid boundary condition ("rollers and pin") was applied along the base of the oil sand layer.
4. Three different boundary conditions applied at the production zone (R=70 m) are illustrated in Figure 6.22. The rigid boundary (i.e. "roller") and the constant pressure boundary are extremes while the compressible boundary is an intermediate condition.

The question arises concerning which of the three boundary conditions illustrated in Figure 6.22 is appropriate. Oil sand adjacent to the production zone boundary is subjected to large temperature gradients and therefore thermal stress changes and deformations are greatest near this boundary, particularly during the early stages of heating. Numerical modelling results presented later in this section illustrate that vastly differing stresses and deformations are predicted depending upon which boundary condition is used. Clearly, oil sand in the production zone is compressible. If effective confining stresses in the production zone are very low because of

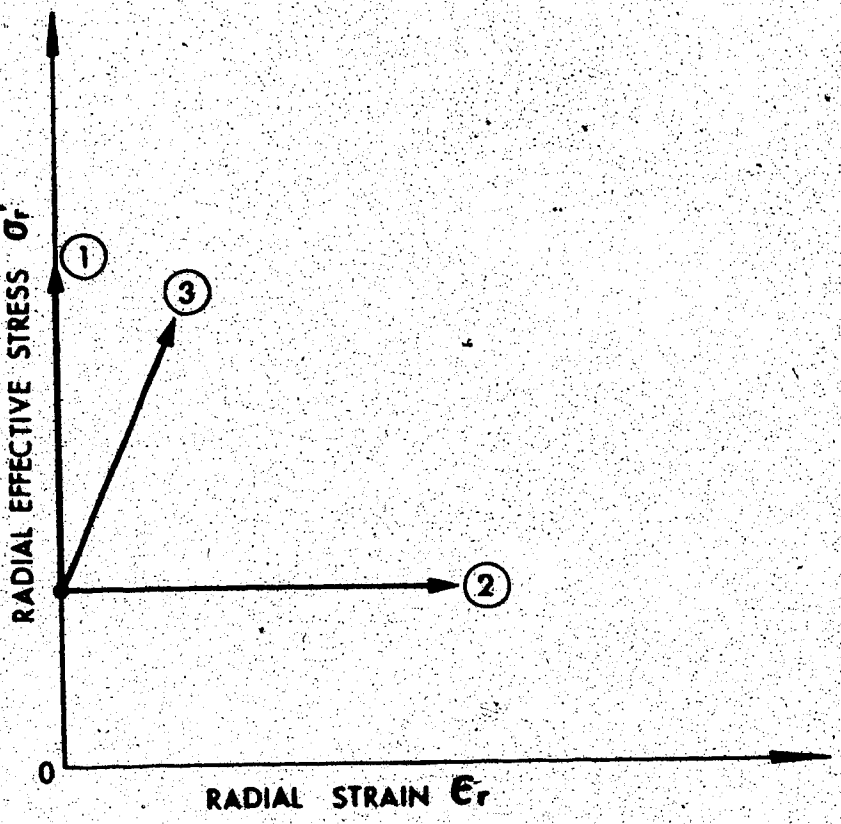

(1) Rigid Boundary Condition

(2) Constant Pressure / Free Displacement Boundary Condition

(3) Stiff, Compressible Boundary Condition

FIGURE 6.22 Stress/Displacement Boundary Conditions at the Production Zone

elevated injection pressures and thermally generated excess pore pressures, then the oil sand within the production zone could be very compressible (i.e. E is a function of effective stress), and the constant pressure boundary condition is approached. Conversely, if effective confining stresses in the the production zone are large and the production zone is expanding (due to drained heating), then the rigid boundary condition may be more appropriate. It is most important to recognize that the appropriate boundary condition within or adjacent to the production zone is controlled to a large extent, by the "production scenario". In fact, compressibility of oil sand within the production zone is likely to vary dramatically both spatially and with time as the injection, heating and production processes proceed.

6.4.4 Transient Heating and Consolidation of Saline Creek Oil Sand

Numerical analyses of the shaft problem described in this section were carried out using material properties of Saline Creek oil sand. It is recognized that the nearly pure quartzose minerology and limited content of fine clay and silt size particles in Saline Creek oil sand are not typical of other oil sand deposits. As discussed in Chapter 5, the minerology and grain size distribution of Saline Creek oil sand result in much greater permeability than might be observed in other oil sand or shale materials. Transient heating of Saline Creek oil sand consequently does not result in large thermally

generated excess pore pressures, and is thus closer to the "drained" heating condition.

A numerical modelling procedure for transient heat consolidation problems is described and the influence of boundary conditions imposed adjacent to the high temperature gradients at the production zone are illustrated in three thermoelastic stress analyses.

6.4.4.1 Transient Temperatures, Pore Pressures and Volumetric Expansion

Transient temperatures, pore pressures and volumetric expansion were predicted using the radial heat consolidation theory and analytical methods outlined in Chapter 5. This analytical approach assumes constant, equal total stresses, i.e. $K_o = 1.0$, during heating. Pore pressure changes resulting from total stress changes during heating are therefore, not calculated in this analysis. Further analytical development is required before the precise influence of this assumption can be evaluated.

Predicted radial distributions of temperature between the shaft and production zone for various heating periods up to 4 years are plotted in Figure 6.23.1. Transient excess pore pressures resulting from injection during the first month are shown in Figure 6.23.2. It is apparent

that the effective injection pressure in the production zone is transmitted rapidly through the oil sand layer toward the shaft. Transient thermally generated excess pore pressures are plotted separately in Figure 6.23.3 for heating periods up to 4 years. Thermally generated pore pressures are relatively small. Volumetric strains due to transient heating, injection and consolidation may be predicted using theory developed in Chapter 5 by the following equation:

$$\frac{\Delta V}{V} = \alpha_{DR} \Delta T + C_c \Delta \bar{\sigma}' \qquad (6.12)$$

For the assumed condition of constant , equal total stresses (K_o = 1.0), the total stresses, $\Delta\sigma$ = 0. Excess pore pressure change, Δu, is due to both injection and heating. Volumetric strains due to injection and heating are introduced into thermoelastic stress-strain calculations through a coefficient of thermal expansion, α_v. The appropriate value of the thermal expansion coefficient for a finite volume of the oil sand medium is determined by dividing the volumetric strain calculated using equation 6.12 by the temperature increase of the element of oil sand:

$$\alpha_v = (\alpha_{DR} \Delta T + C_c \Delta u) / \Delta T \qquad (6.13)$$

Radial distributions of the coefficient of volumetric thermal expansion, , calculated using equation 6.11

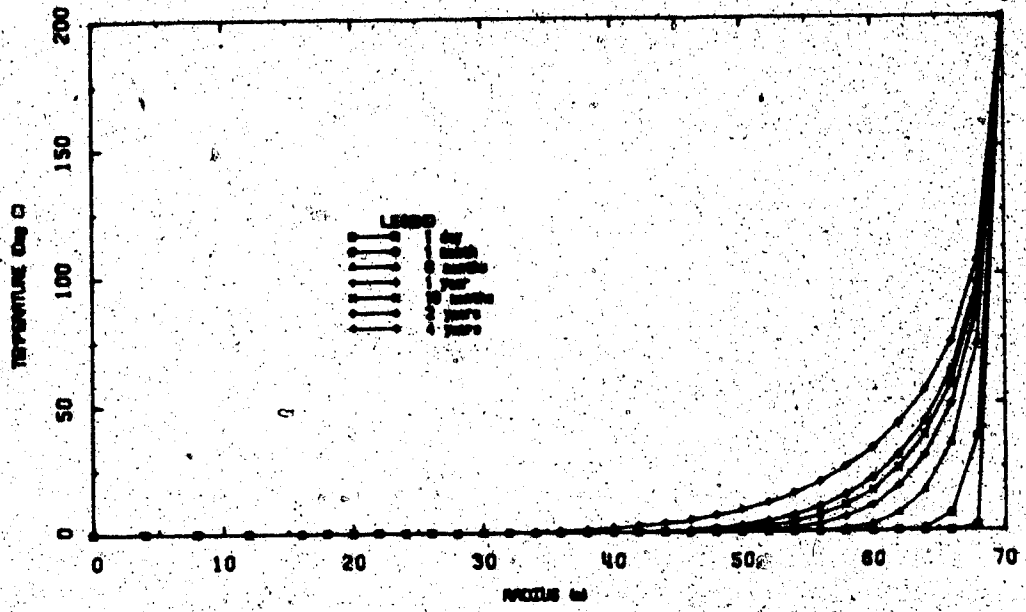

FIGURE 6.23.1 Transient Temperatures Around the Shaft

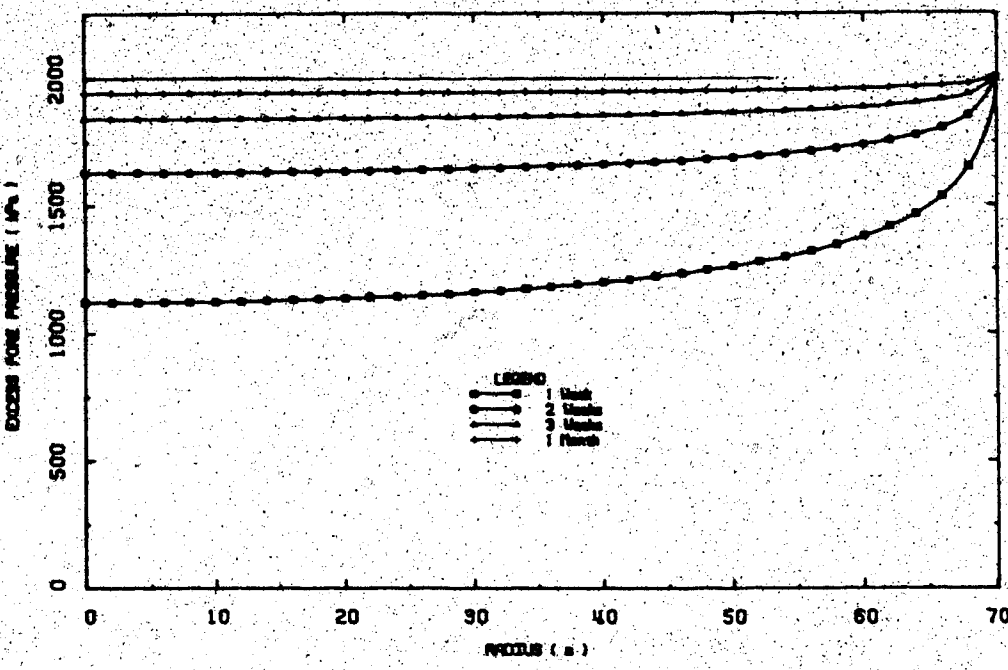

FIGURE 6.23.2 Transient Excess Pore Pressures Due to Injection Around the Shaft

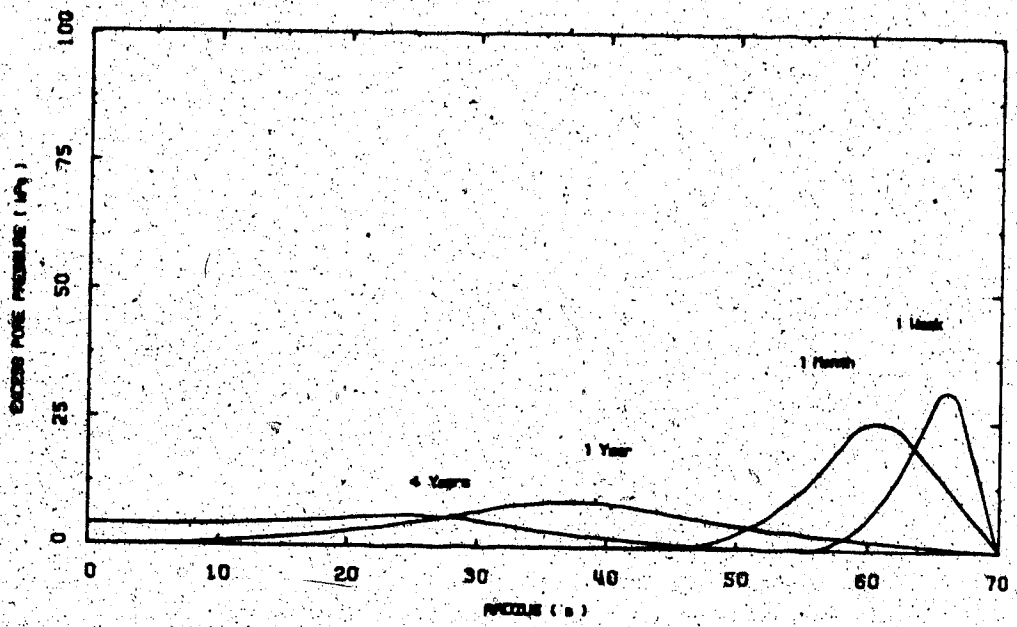

FIGURE 6.23.3 Thermally Generated Excess Pore Pressures Around the Shaft

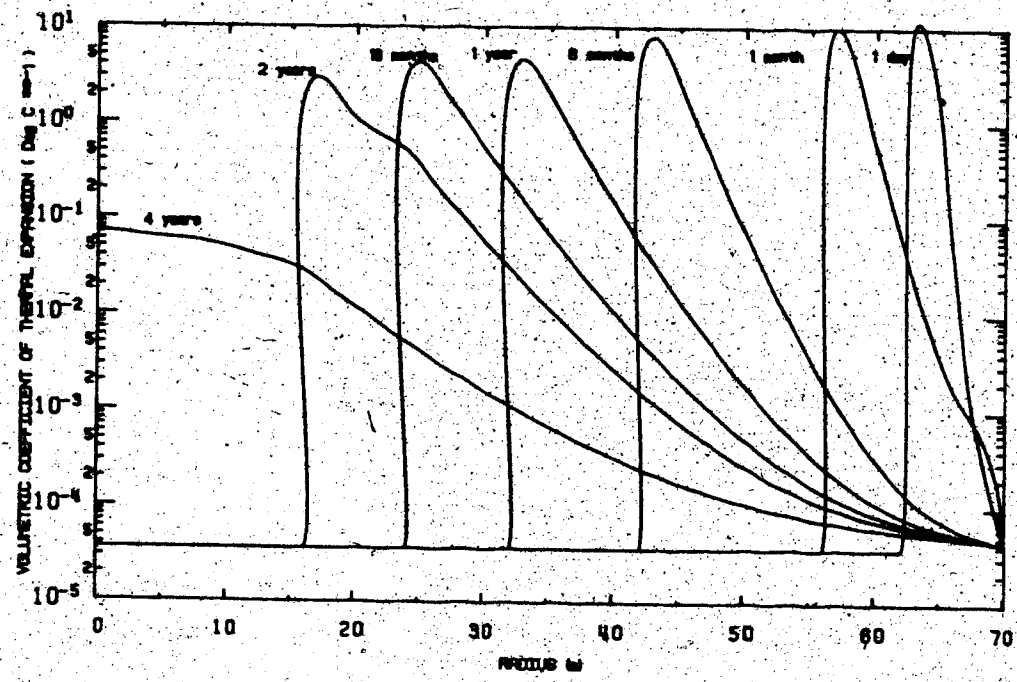

FIGURE 6.23.4 Transient Volumetric Expansion Around the Shaft

for heating periods up to 4 years are plotted in Figure 6.23.4. Transient distributions of temperature shown in Figure 6.23.1, and the equivalent thermal expansion coefficient shown in Figure 6.23.4 may now be input into a thermoelastic stress-strain analysis to determine induced stress changes and deformations under appropriate boundary stress and displacement conditions.

Elastic stress-strain moduli, in general, would vary throughout the medium with time in response to changes in effective confining stresses during injection and transient heating.

6.4.4.2 Rigid Boundary at the Production Zone

The spatial distributions of temperature and coefficient of thermal expansion described in the preceding section (6.4.4.1) were input into a series of thermoelastic analyses at times corresponding to various heating periods up to 4 years. The axisymmetric finite element mesh and boundary conditions used in the analyses are shown in Figure 6.24. Total stress changes are calculated in the thermoelastic analyses. Since the heat consolidation ratio, R_t, for Saline Creek oil sand is relatively high, i.e. due to the relatively large value of c_v, thermally induced pore pressure changes shown in Figure 6.23.2 are small. Effective confining stresses, therefore, are expected to remain reasonably constant

FIGURE 6.24 Finite Element Mesh for Thermoelastic Analysis of Stresses and Deformations Around the Shaft with a Rigid Boundary Condition at the Production Zone

during transient heating of the oil sand. The stiffness of the oil sand accordingly, would not be reduced substantially due to reduction of effective confining stresses, however, stiffness does decrease with deviatoric stress level as discussed in section 6.2. Since elastic moduli cannot be varied with stress level in linear thermoelastic solutions, a constant "average" value of 2000 MPa was used for the modulus of the elasticity, E.

Thermally induced stress changes and deformations within the oil sand layer adjacent to the shaft were calculated at the following heating periods:

a) 1 month;
b) 6 months;
c) 1 year;
d) 2 years; and
e) 4 years.

Total stress changes, deformations and effective stresses following 1 month are shown in Figures 6.25.1, 6.25.2 and 6.25.3, respectively. Total stress changes, deformations and effective stresses following 1 year are also presented in Figures 6.25.4, 6.25.5 and 6.25.6, and following 4 years in Figures 6.25.7 to 6.25.9.

Results of analyses following 6 months and 2 years of heating and injection are included in Appendix L, Figures

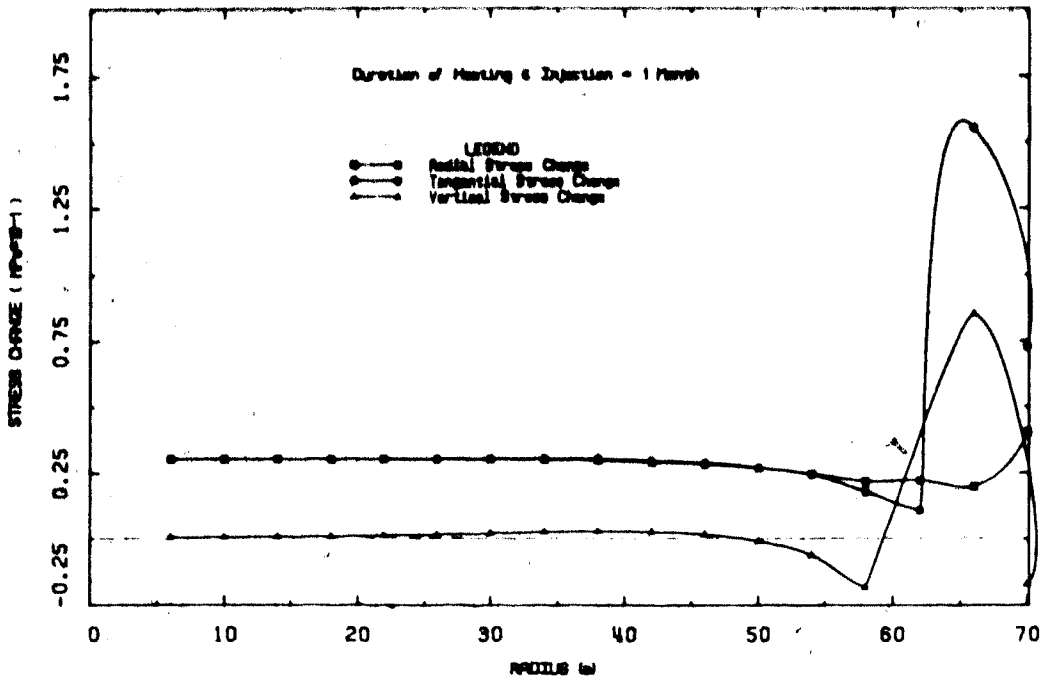

FIGURE 6.25.1 Stress Changes Around the Shaft After 1 Month of Steam Injection

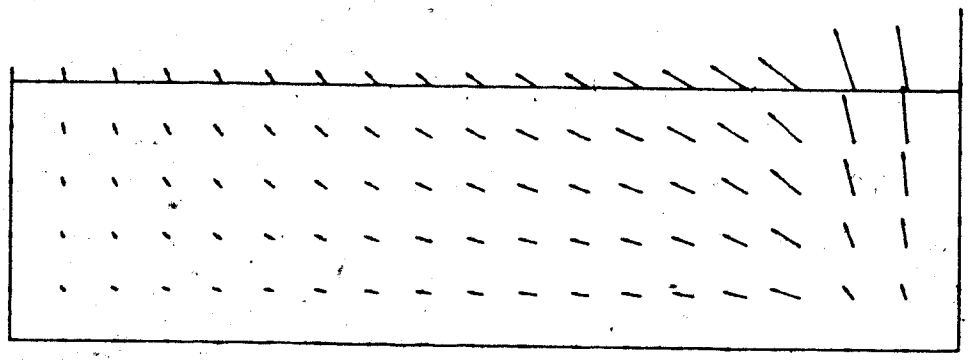

FIGURE 6.25.2 Deformations Around the Shaft After 1 Month of Steam Injection

DISPLACEMENT SCALE 1:100

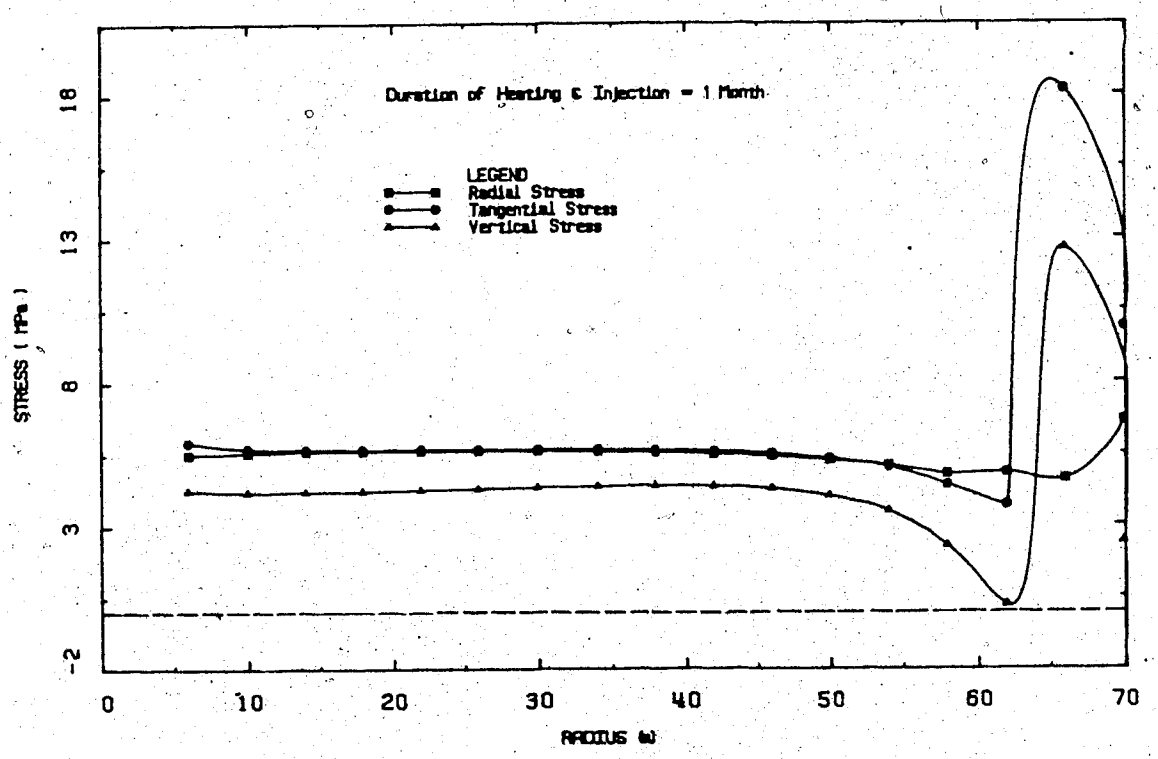

FIGURE 6.25.3 Effective Stresses Around the Shaft After 1 Month of Steam Injection

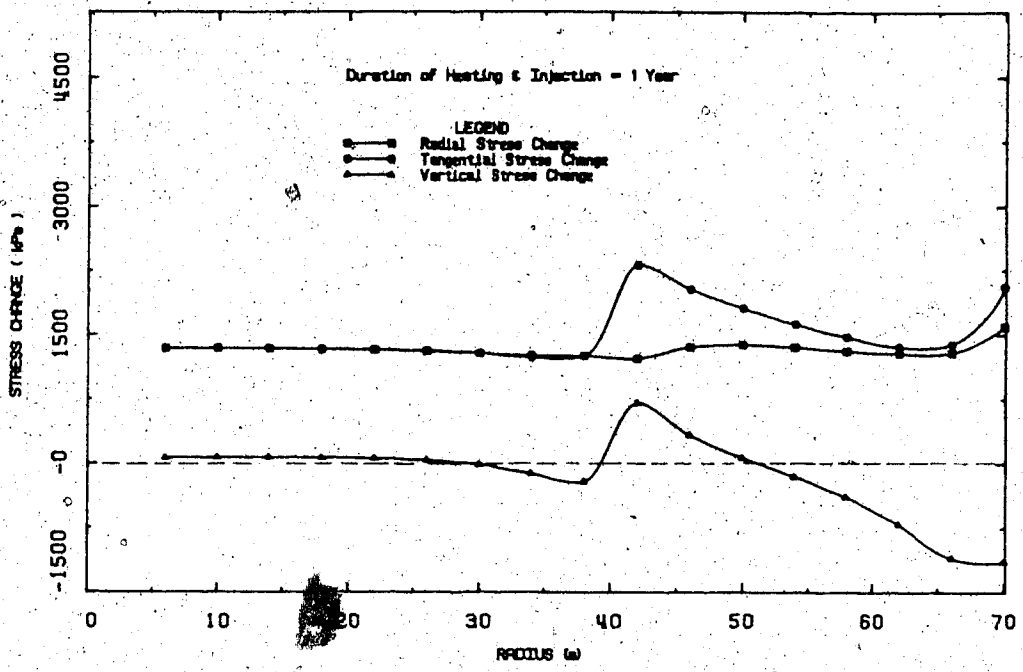

FIGURE 6.25.4 Stress Changes Around the Shaft After 1 Year of Steam Injection

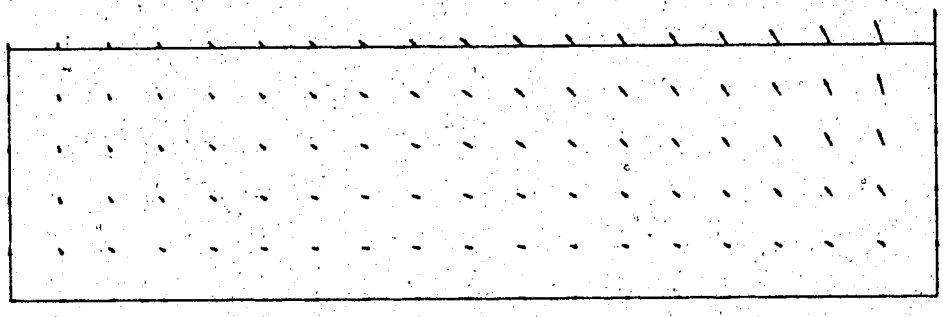

FIGURE 6.25.5 Deformations Around the Shaft After 1 Year of Steam Injection

DISPLACEMENT SCALE 1:100

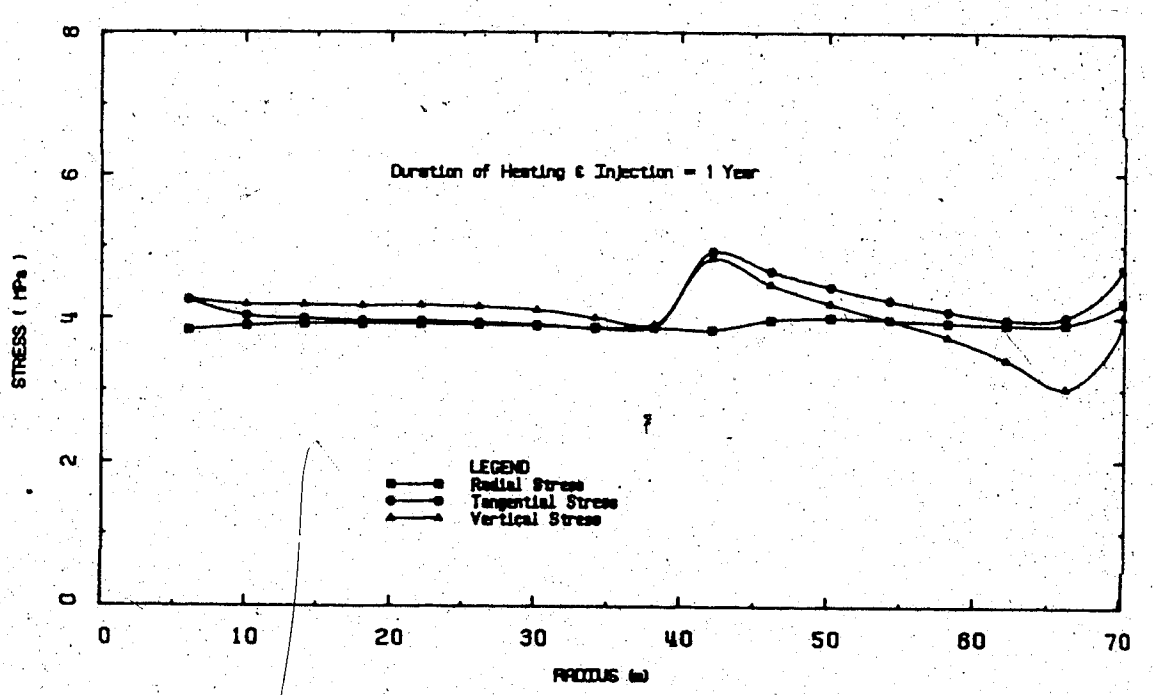

FIGURE 6.25.6 Effective Stresses Around the Shaft After 1 Year of Steam Injection

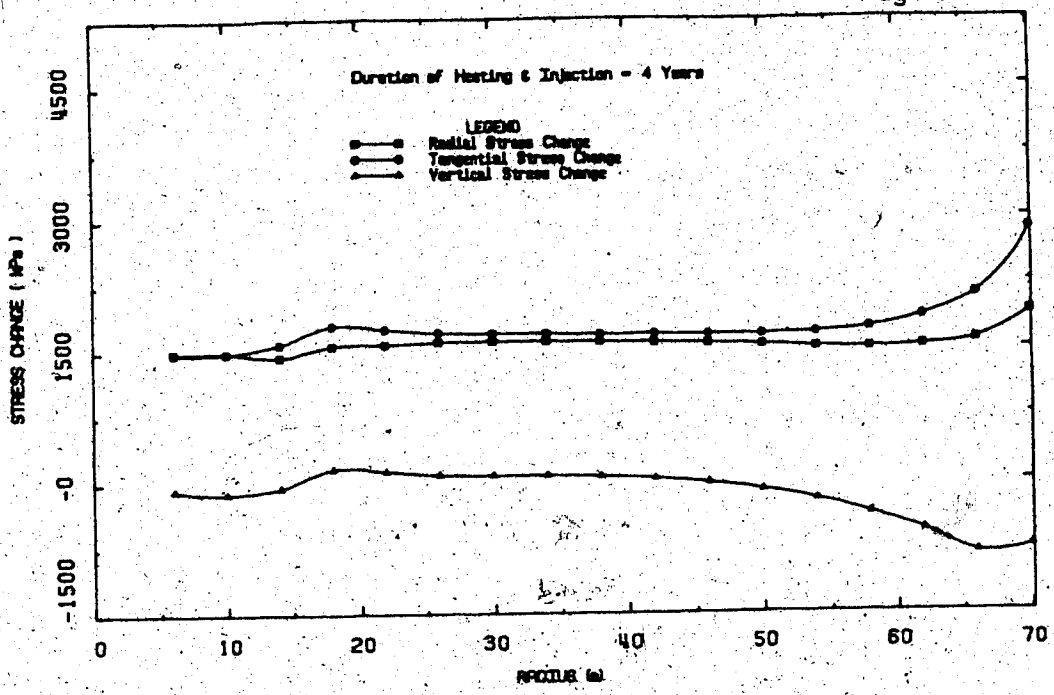

FIGURE 6.25.7 Stress Changes Around the Shaft After 4 Years of Steam Injection

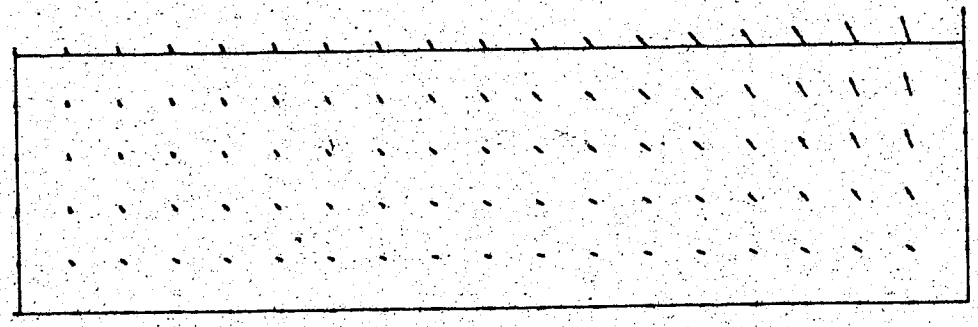

FIGURE 6.25.8 Deformations Around the Shaft After 4 Years of Steam Injection

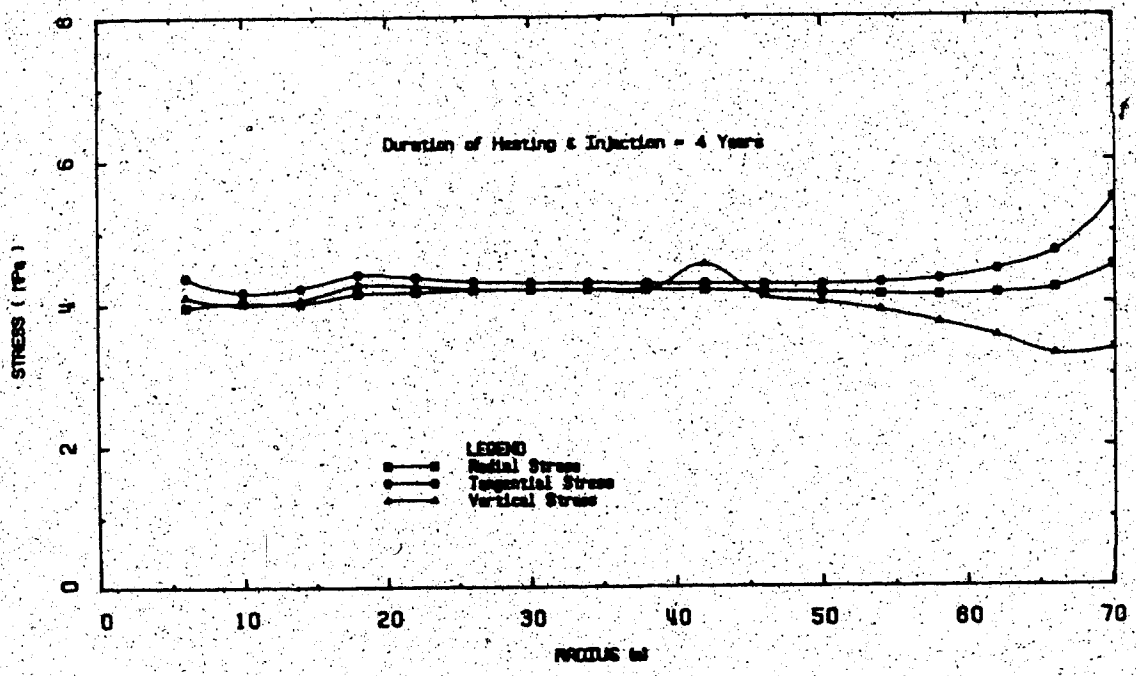

FIGURE 6.25.9 Effective Stresses Around the Shaft After 4 Years of Steam Injection

L1.1 to L2.2, inclusive The three plots presented for each analysis show:

a) thermally induced radial, tangential and vertical stress changes at mid-depth in the oil sand layer;

b) thermally induced deformation vectors; and

c) current radial, tangential and vertical effective stresses at mid-depth. Effective stresses were determined by superposition of (i) initial effective stresses, (ii) stress changes due to excavation, (iii) excess pore pressures due to injection and heating, and (iv) thermally induced total stress changes.

Several interesting observations are forthcoming from this series of analyses:

1. Thermal loading has the effect of increasing radial and tangential stresses without substantial increase in the vertical stress. This is due to the condition of lateral constraint applied at the production zone boundary. The original effective stress condition described by K_o of 0.75 was altered throughout the mesh causing the stress ratio K_o to increase. Effective stresses (i.e. σ_r', σ_θ' and σ_z') have been reduced by excess pore pressure due to injection and heating.

2. There is a zone of stress and displacement perturbation which migrates away from the production zone boundary and attentuates with time of heating. The location of the stress perturbation corresponds with the maximum thermal loading which is governed by the product $\alpha\Delta T$; both α and ΔT vary spatially and with time in these analyses as described in sub-section 6.4.3.1.

3. A severe limitation of linear elastic theory for thermal stress-strain modelling is introduced by these numerical results. The magnitude of predicted deformations is greater during the early stages of heating than at later times. This is illustrated in Figure 6.26 in which the radial convergence of the shaft wall actually decreases during the early heating period. This paradox arises from the fact that stress perturbation is greatest near the rigid, high temperature gradient, production zone boundary during the early stages of heating before thermally generated excess pore pressures dissipate. The deformations predicted during the early stages of heating and injection would be largely non-recoverable in oil sand. The introduction of the rather severe rigid boundary condition at the high temperature gradient production zone boundary and the use of linear elastic theory thus yield questionable numerical results.

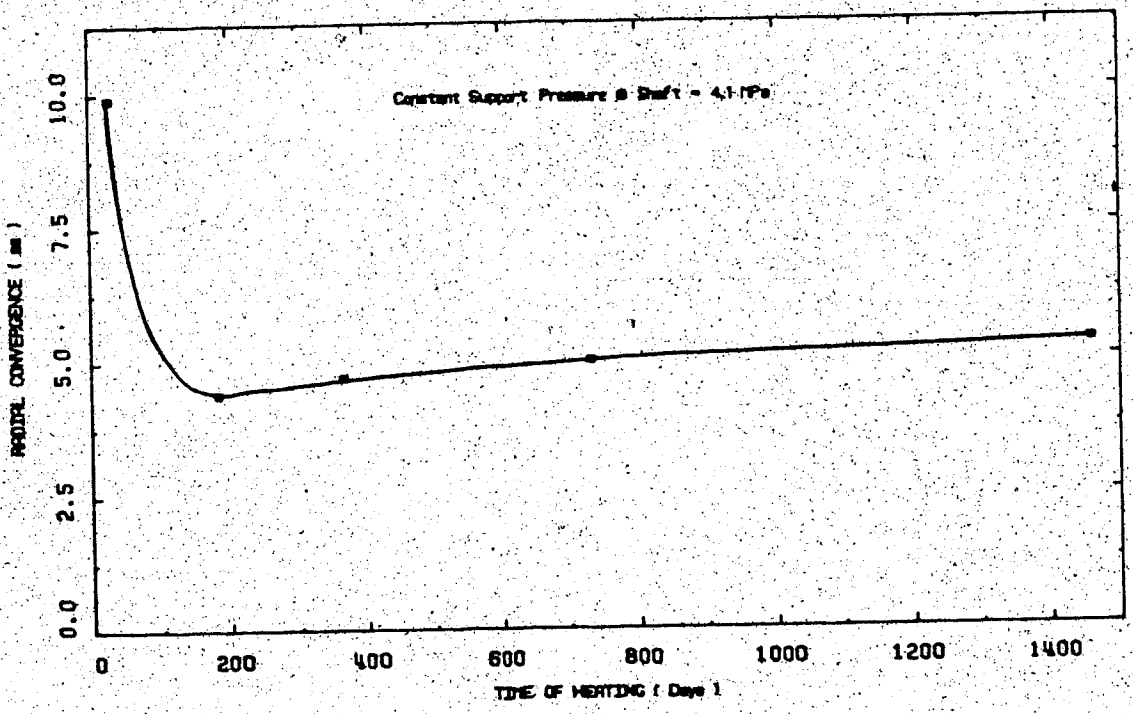

FIGURE 6.26 Predicted Radial Convergence of the Shaft: Rigid Boundary Condition

6.4.4.3 Constant Pressure Boundary Condition at the Production Zone

The same axisymmetric finite mesh used in the previous section was used in a second series of analyses with a constant pressure/free displacement boundary condition at the production zone. The mesh and boundary condition are shown in Figure 6.27. The horizontal pressure applied at the production zone boundary was equivalent to the initial horizontal effective stress.

Transient temperatures and volumetric strains determined in section 6.4.4.1 were again applied; thermoelastic stress-strain analyses were carried out for injection and thermal loading conditions corresponding to heating periods of:

a) 1 month;
b) 1 year; and
c) 4 years.

Stresss changes, ground deformations and current effective stresses predicted for the above periods of heating and injection are shown in Figures L3.1 to L3.9, inclusive, in Appendix L.

Application of the constant pressure boundary condition resulted in stress reduction and horizontal components of deformation of opposite signs (i.e. tension)

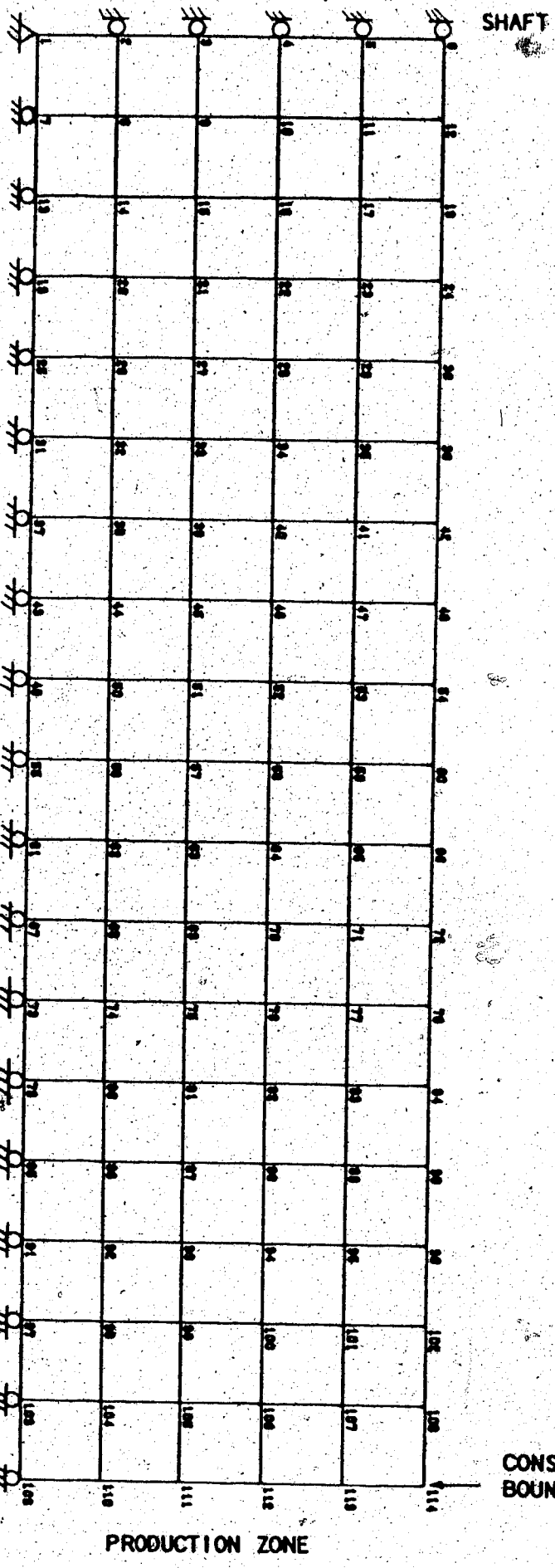

FIGURE 6.27 Finite Element Mesh for Thermoelastic Analysis of Stresses and Deformations Around the Shaft with a Constant Pressure Boundary Condition at the Production Zone

compared with results of the rigid boundary analysis described in section 6.4.4.2.

The dramatic differing stress-deformation predictions obtained by altering the boundary condition at the production zone illustrates that the selection of appropriate boundary conditions for this class of thermal stress analyses is not trivial. Predicted negative convergence (i.e. divergence) of the shaft wall with time shown in Figure 6.28 results in development of tensile stresses. Again, the magnitudes of predicted deformations during the initial phases of heating were greater than those at later times for similar reasons to those discussed in section 6.4.4.2.

6.4.4.4 Compressible Boundary Condition at the Production Zone Boundary

In order to introduce a compressible boundary condition at the production zone, the finite element mesh was extended as illustrated in Figure 6.29. Oil sand within the production zone was maintained at 200°C and constant excess pore pressure of 2 MPa throughout the analyses. The stiffness of the production zone oil sand was accordingly assumed to be equal to that of the adjacent oil sand, as characterized by a constant value of Young's Modulus, E, of 2000 MPa. Transient injection and thermal loading described in subsection 6.4.4.1 was applied in oil sand adjacent to the production zone at times corresponding to heating periods of:

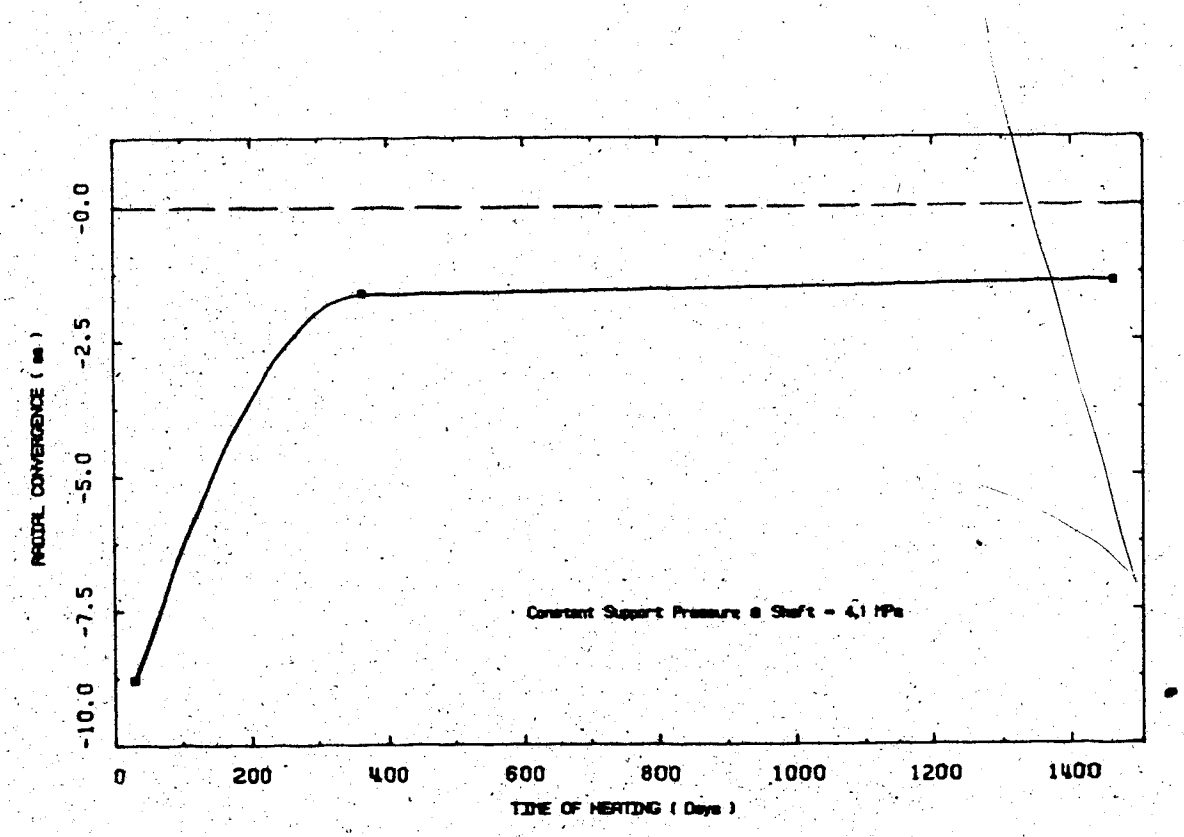

FIGURE 6.28 Predicted Radial Convergence of the Shaft: Constant Pressure Boundary Condition

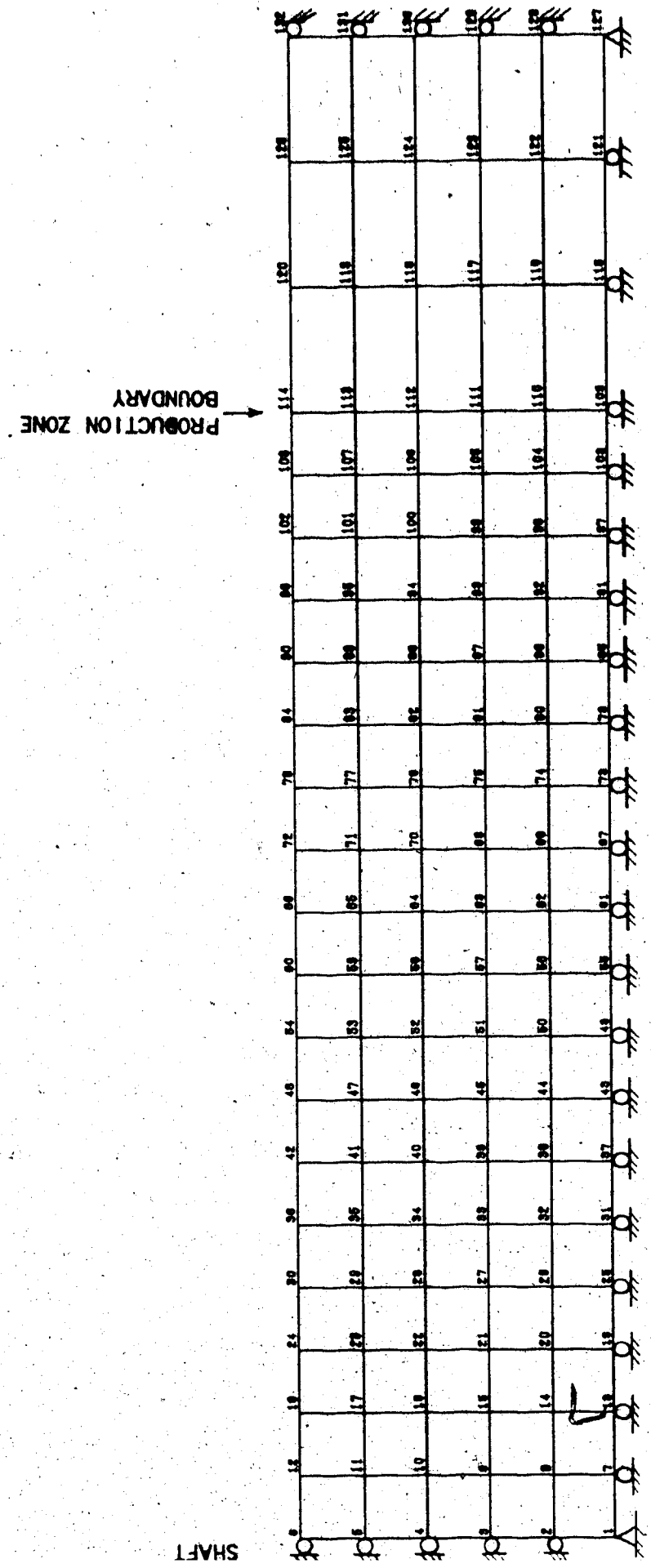

FIGURE 6.29 Finite Element Mesh for Thermoelastic Analysis of Stresses and Deformations Around the Shaft with a Compressible Boundary Condition at the Production Zone

a) 1 month;

b) 6 months;

c) 1 year; and

d) 4 years.

Distribution of stress changes, ground deformations and current effective stresses corresponding to the above time levels are plotted in Figures L4.1 to L4.12, inclusive, in Appendix L. Numerical results presented in this subsection are intermediate between the two extreme cases summarized in subsections 6.4.4.2 and 6.4.4.3.

A zone of stress-displacement perturbation is again observed migrating toward the shaft and attentuating with time. Horizontal components of the displacement vectors are bi-directional. Predicted radial convergence of the shaft wall with time is shown in Figure 6.30. Although these analyses predict that the shaft wall will converge monotonically with time, it should be noted that the magnitude of predicted deformations throughout the mesh does not increase monotonically. The foregoing observation is again due to limitations inherent in using a linear elastic constitutive relationship. A substantial proportion of deformation of oil sand is non-recoverable.

6.4.4.5 Disscusion of Thermoelastic Stress-Deformation Analyses in Saline Creek Oil Sand

Several difficulties in numerical analysis of stress

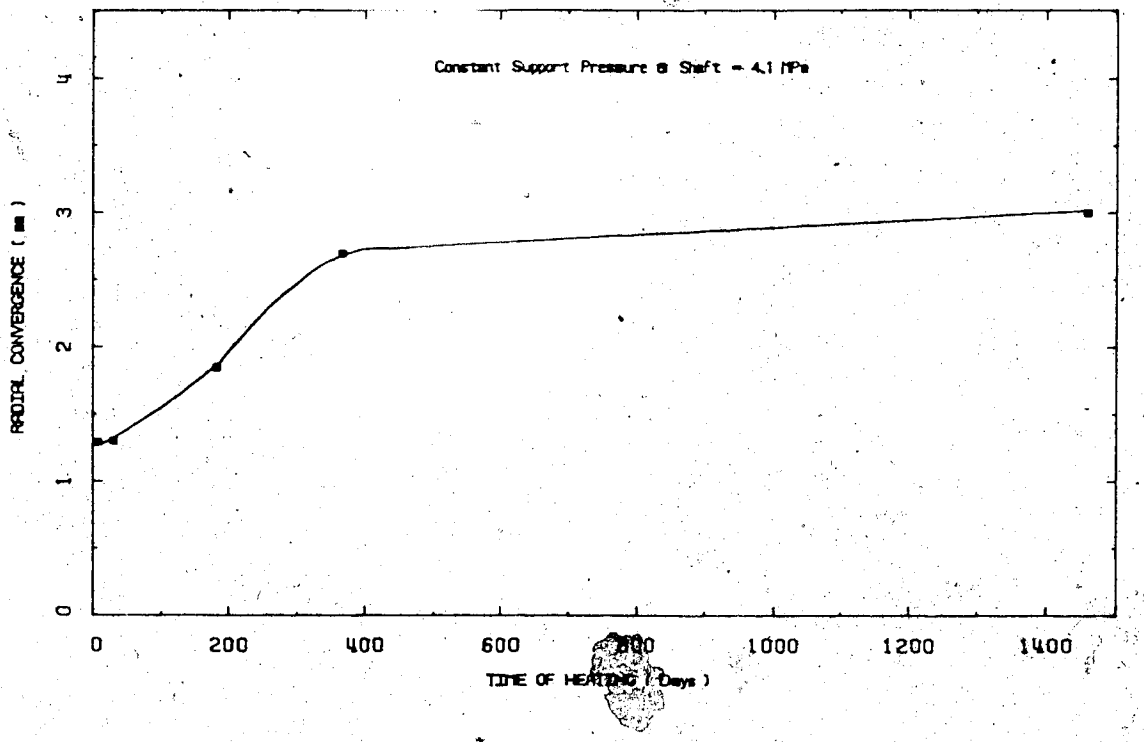

FIGURE 6.30 Predicted Radial Convergence of the Shaft: Compressible Boundary Condition

changes and deformation induced by injection and heating have been identified:

1. Material properties used in thermoelastic stress-strain analyses such as the coefficient of thermal expansion, α, and the modulus of elasticity, E, vary both spatially and temporally, with changes in effective confining stress. It was considered reasonable to assume a constant value of E in relatively free-draining Saline Creek oil sand for the preceding analyses. In general, it is necessary to vary E in space and time with effective confining stresses.
2. Volumetric expansion results from elevated injection pressures, thermally induced pore pressures and thermal expansion of the solid skeleton. Thermal stresses must therefore be calculated using values of the coefficient of thermal expansion and temperature which generate the appropriate volumetric strains.
3. Linear elastic stress-strain relationships are inadequate for modelling thermally induced effective stress changes and deformations because a substantial proportion of the deformations in oil sands, and many other soils and rocks, is non-recoverable. Also, yielding and stress redistribution cannot be modelled numerically using a linear elastic constitutive relationship, unless different elastic moduli are applied

for loading and unloading in terms of effective stress, and a load shedding algorithm is incorporated in the analysis.

4. Predicted patterns and magnitudes of thermal stresses and deformations are very sensitive to boundary conditions in the vicinity of a high temperature gradient. The selection of an appropriate boundary condition is very much dependent upon "the heating and injection scenario" as well as the heat consolidation characteristics of the reservoir materials. Figure 6.31 summarizes radial convergence predictions for the shaft problem in Saline Creek oil sand. Deformation predictions in Figure 6.31 correspond to radial stress/displacement boundary conditions illustrated in Figure 6.22, applied at the production zone boundary. Not only are the magnitudes of predicted deformations influenced by this boundary condition, but the predicted direction of radial displacement can actually be reversed, in elastic materials. Nevertheless, the magnitudes of deformations predicted in these analyses are relatively small because of the free-draining characteristics of Saline Creek oil sand.

5. The magnitudes of predicted stress changes and deformation are larger during the early stages of heating and injection than in the long term. Also stress perturbations move away from the

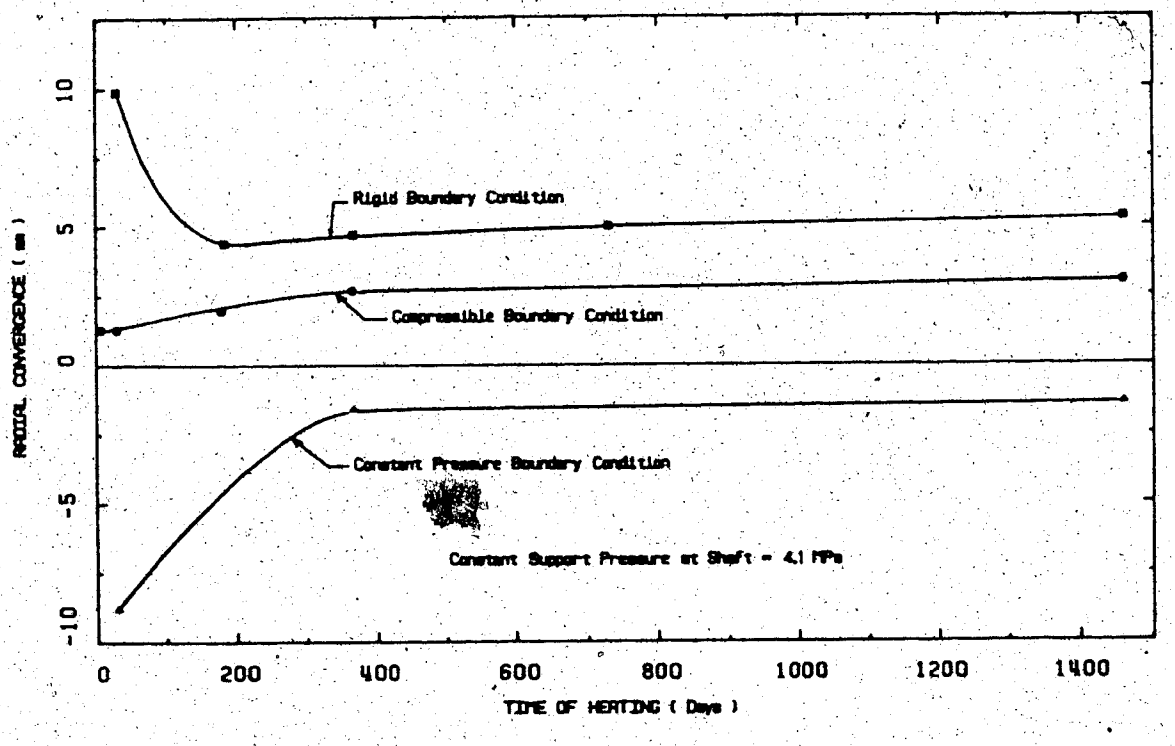

FIGURE 6.31 Comparison of Shaft Wall Convergence Predictions Using Various Boundary Conditions at the Production Zone

production zone boundary and attenuate with time. This is due to: (i) reduction of the temperature gradient at the production zone with time, (ii) migration of thermally generated excess pore pressures away from the production zone boundary and (iii) attentuation of pore pressures with time. Yielding of overstressed material and associated stress redistribution during the early stages of heating cannot be modelled using linear thermoelastic relationships.

6.4.5 Drained and Undrained Analyses

Thermoelastic stress-strain analyses require knowledge of appropriate material properties including elastic stress-strain moduli (i.e. E, ν) and coefficients of thermal expansion. It is recognized that these material properties vary with temperature for many soils and rocks. The experimental research described in Chapters 3 and 4 indicated that these material properties, in fact, vary to a greater degree with effective confining stresses than with temperature, for quartzose oil sands. This observation implies that the appropriate values of stress-strain moduli and thermal expansion coefficients vary both in space and time with effective stresses and/or pore pressures, and to a lesser extent with temperature during transient heating and consolidation. The influence of thermal pore pressure generation during transient heating of porous soils and rocks in general, must be considered in stress-strain analyses,

particulary for materials having relatively low values of the heat consolidation ratio.

Material properties, i.e. elastic moduli and thermal expansion coefficients, generally are assumed to have constant values independent of space and time, or to vary with temperature. Neither of these assumptions account for material property variations due to injection or thermally induced effective stress changes. Accordingly, it would seem attractive to invoke the assumptions of fully drained or undrained pore pressure response in order to link effective stresses with temperature only, and to determine lower and upper bound solutions. Based on experimental and analytical results for Saline Creek oil sand, drained analysis is considered prudent for oil rich oil sands.

Drained Conditions:

The assumption of fully drained conditions implies that no excess pore pressure will be generated by total stress changes or thermal loading. Accordingly, material properties are not altered by transient effective stress changes and soil or rock properties will vary directly with temperature when fully drained conditions are assumed.

It is reasonable to assume constant material properties (α, E) for quartzose oil sands subjected to temperatures up to 200°C - 300°C, when fully drained conditions are assumed.

The shaft problem analyzed in section 6.4.4.4 was reanalyzed assuming fully drained conditions and constant material properties (i.e. E, ν, α). The compressible boundary condition was applied at the "production zone" boundary. An effective excess injection pressure of 2 MPa was again applied at the production zone boundary. Transient temperature changes presented in subsection 6.4.4.1 were applied in the sands adjacent to the "production zone" at times corresponding to heating periods of:

a) 1 month;
b) 1 year; and
c) 4 years.

Thermal stress changes, ground deformations and current effective stresses predicted for the above heating time periods are plotted in Figures L5.1 to L5.9, inclusive. Predicted stress changes and ground deformations are relatively small, however, they do increase monotonically with the time of heating. Radial convergence of the shaft wall with time is plotted in Figure 6.32 for the drained heating analysis.

Undrained Conditions:

a) Undrained Analysis #1:

The simplest approach for modelling thermoelastic stresses and deformations during undrained heating is to assume that the coefficient of thermal expansion is constant in time and space,

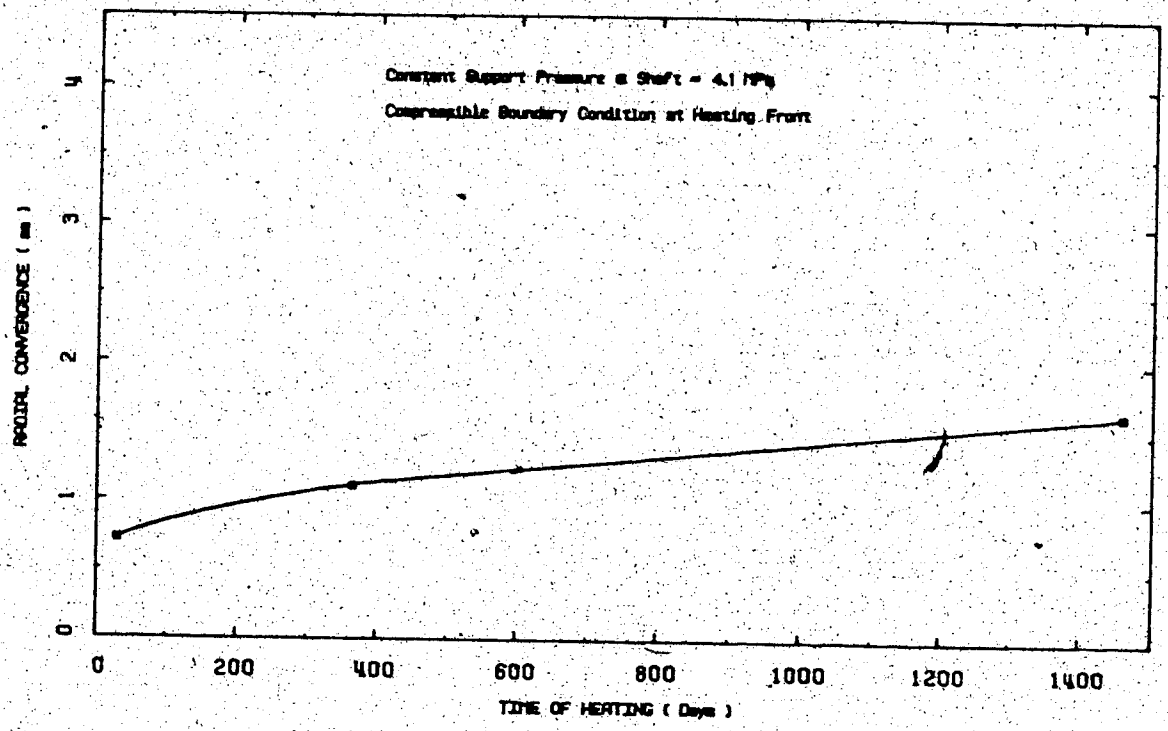

FIGURE 6.32 Predicted Radial Convergence of the Shaft During Drained Heating

and that elastic moduli are either constant or vary only with temperature. The shaft problem was analyzed using a constant value for the undrained volumetric coefficient of thermal expansion, α_u, of 3.0×10^{-4} $°C^{-1}$ and a constant value of Young's Modulus, E, of 2000 MPa. Calculated thermal stress changes and deformations are presented in Figures L6.1 to L6.6, inclusive of Appendix L, corresponding to transient heating periods of 1 month, 1 year and 4 years. Effective stresses could not be determined since pore pressures were not calculated. Thermal stress changes and deformations increase monotonically with time of heating and are larger than comparable stress changes and deformations calculated in the drained heating analysis by an amount proportional to the difference between α_u, and α_{DR}. Although straightforward, the foregoing analytical approach does not correctly model the physics of undrained heating. Undrained heating of a porous material, by definition, results in generation of excess pressures and effective stress changes. Material properties including elastic moduli and thermal expansion coefficients vary proportionally with effective stress and pore pressure changes. In fact, the shear strength and modulus of elasticity for oil sand and other soils and rocks approach zero as the effective stress approaches zero. Effective stress changes must therefore be evaluated in order to model even the simplified case of undrained heating.

b) Undrained Analysis #2 (TRANSIENT UNDRAINED HEATING):

The assumption that undrained conditions prevail implies

that pore fluids within the porous medium are immobile. The distribution of undrained, thermally generated excess pore pressures is therefore, strictly a function of the temperature distribution, assuming that total stresses remain constant. Since pore pressures (and effective confining stresses) vary with temperature, the stress-strain moduli and shear strength also vary in space and time with temperature.

The shaft problem was reanalyzed assuming transient undrained heating conditions. Calculated radial distributions of temperature increase, excess pore pressure and volumetric expansion are shown in Figures 6.33.1. to 6.33.3, inclusive. Excess pore pressure due to injection is constant at 2 MPa for reasons discussed in section 5.7. Radial distributions of the equivalent coefficient of volumetric thermal expansion for transient undrained heating corresponding to several heating periods are shown in Figure 6.33.4. The modulus of elasticity, E, was varied with effective confining stress according to the following relationship:

$$\frac{E\ (r,t)}{E_i} = \left[1 - \frac{u\ (r,t)}{\sigma_o'}\right] \qquad (6.14)$$

Radial distributions of the modulus ratio in equation 6.14, corresponding to several undrained heating periods up to 4 years are shown in Figure 6.33.5. Variation of the coefficient of thermal expansion and modulus of elasticity with temperature are plotted in Figures 6.33.6 and 6.33.7, respectively.

Radial distribution of temperature increase, coefficient

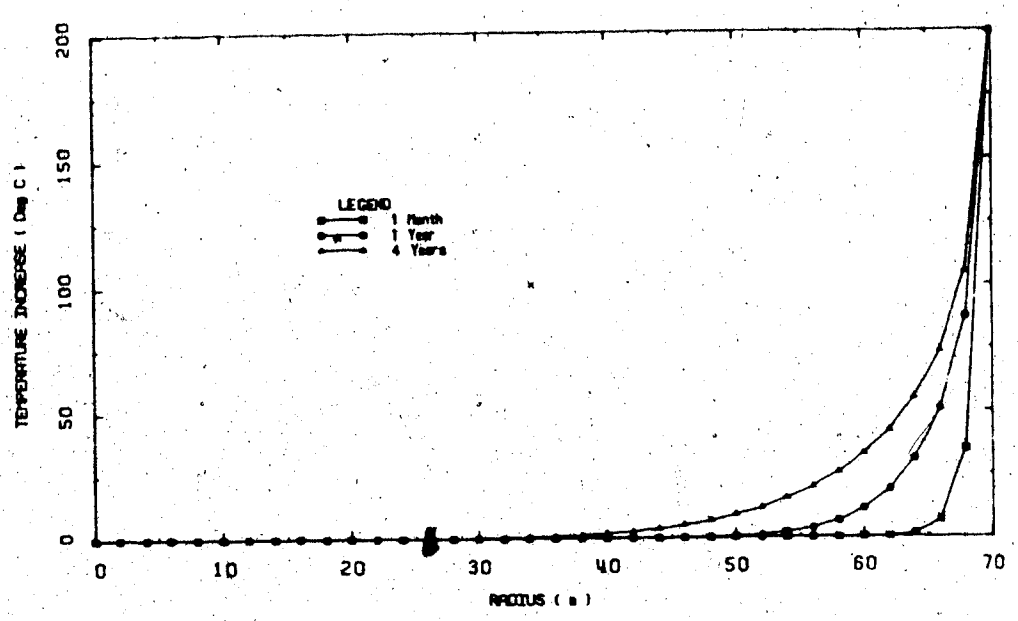

FIGURE 6.33.1 Transient Temperatures Around the Shaft

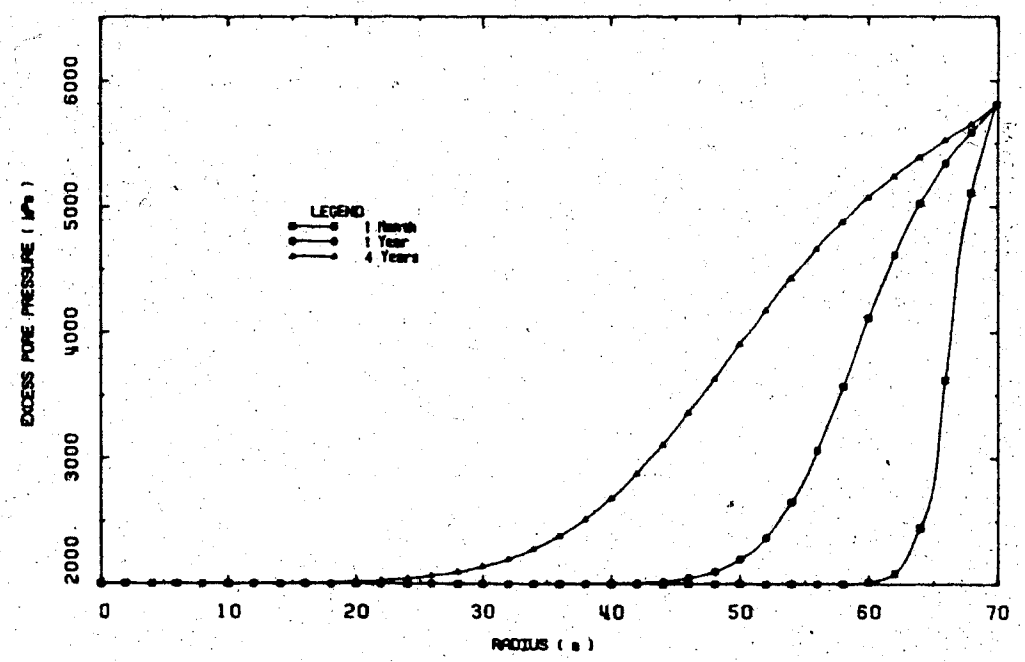

FIGURE 6.33.2 Transient Excess Pore Pressures Due to Undrained Heating and Injection Around the Shaft

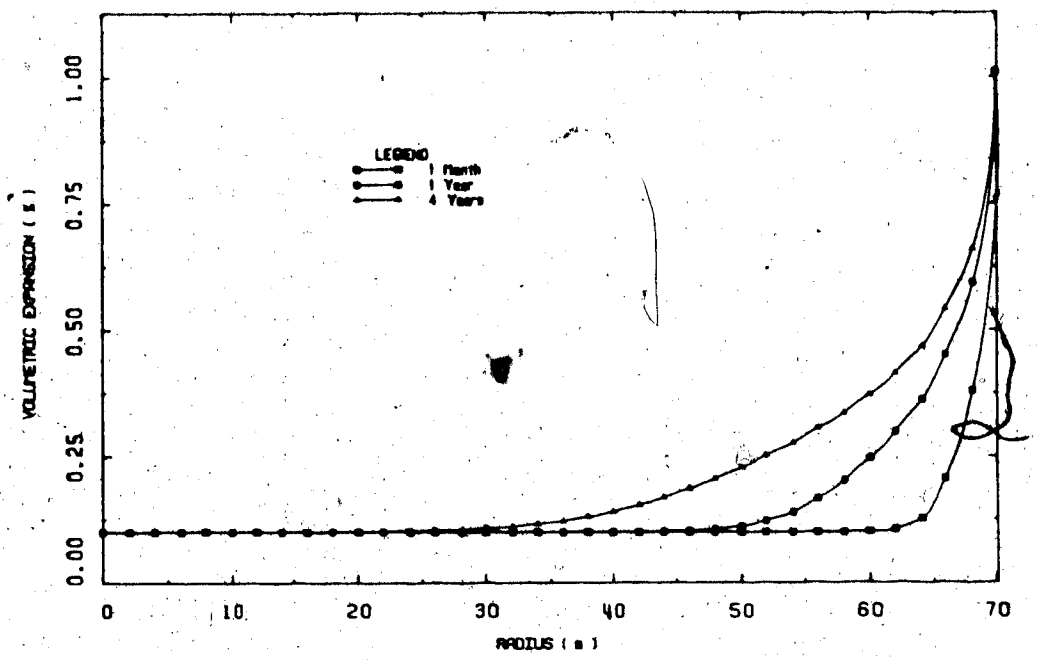

FIGURE 6.33.3 Transient Undrained Volumetric Expansion Around the Shaft

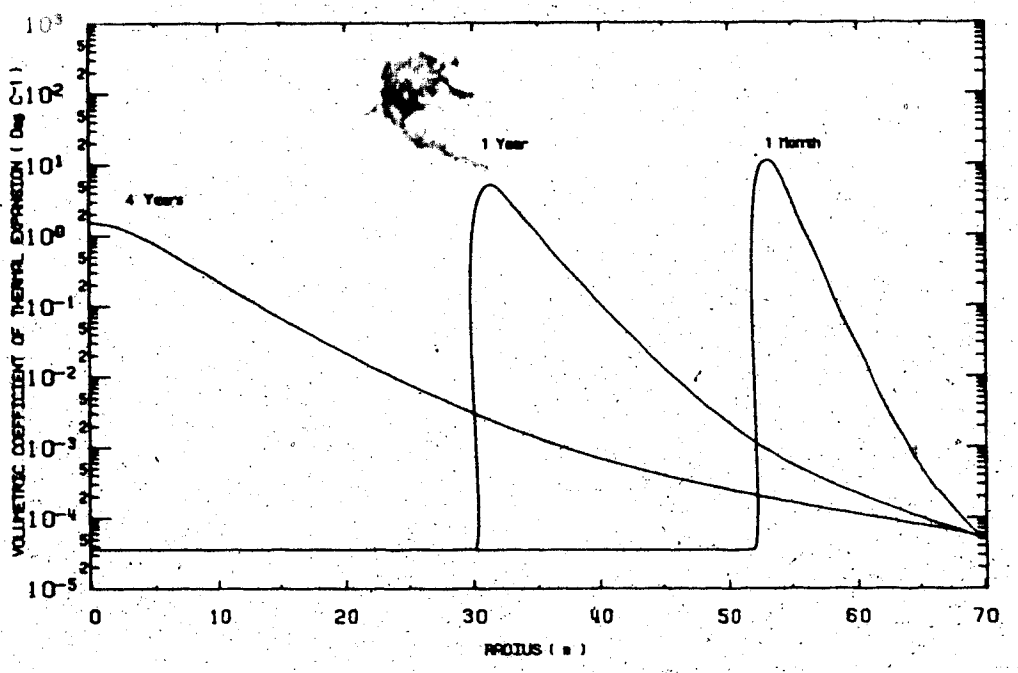

FIGURE 6.33.4 Transient Undrained Coefficient of Volumetric Expansion

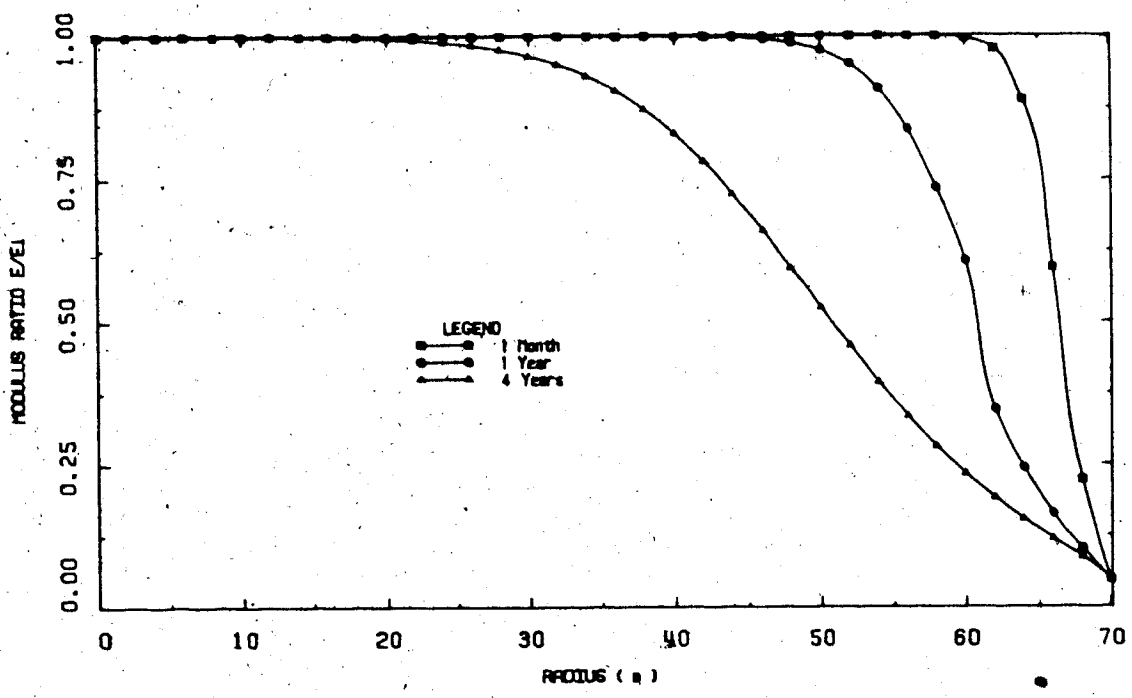

FIGURE 6.33.5 Variation of the Modulus of Elasticity During Transient Undrained Heating

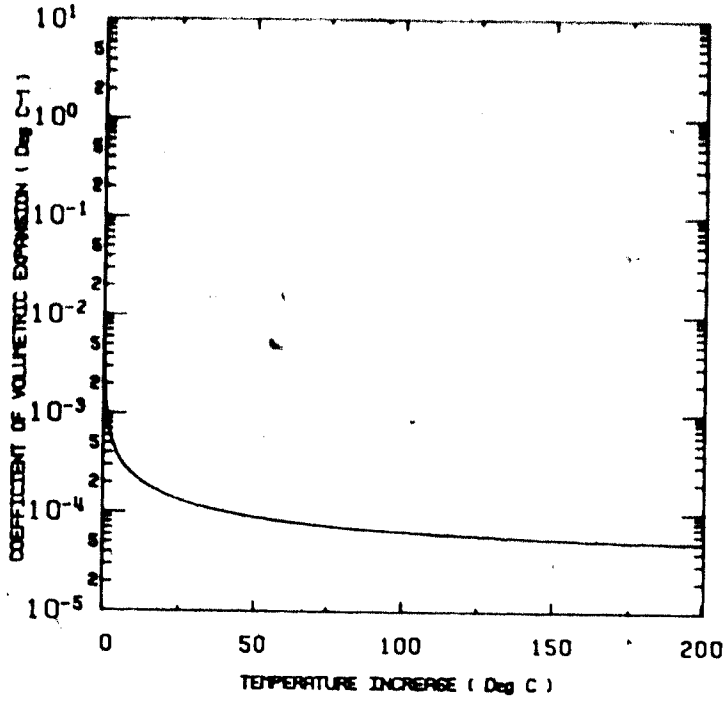

FIGURE 6.33.6 Undrained Coefficient of Volumetric Expansion Versus Temperature

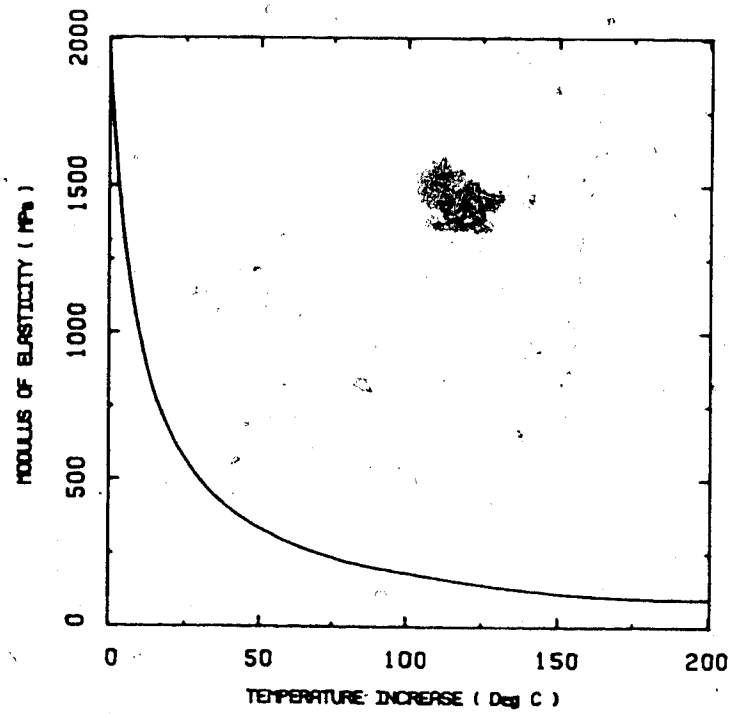

FIGURE 6.33.7 Variation of the Modulus of Elasticity with Temperature During Undrained Heating

of thermal expansion and modulus of elasticity determined in the foregoing undrained heating analysis were input into thermoelastic stress analyses at times corresponding to heating periods of:

a) 1 month;

b) 1 year; and

c) 4 years.

It should be noted again, that since variation of material stiffness with deviatoric stress level cannot be accounted for explicitly in linear thermoelastic solutions, an "average" value of 2000 MPa was used for the initial modulus of elasticity, E_i, in equation 6.14. Thermal stress changes, deformations and current effective stresses around the shaft are plotted in Figure L7.1 to L7.9, inclusive, at times corresponding to the above heating periods. Effective stresses near the production zone are reduced because of thermally generated excess pore pressures. In fact effective stresses approach zero near the production zone. Spatial variations of the modulus of elasticity and coefficient of thermal expansion with time alter the pattern and magnitudes of predicted stress changes and deformations. Stress changes and deformations do not increase monotonically throughout the mesh during transient undrained heating as predicted in the foregoing simplified undrained heating analysis (i.e. using constant material properties).

Radial convergence of the shaft wall with time predicted in each of the two preceding undrained heating analyses is plotted (for comparison) in Figure 6.34. The limitations of linear thermoelastic stress-strain modelling for this class of problems are again illustrated. Predicted radial convergence of the shaft wall actually decreases with time for the second analysis using variable material properties. This is due to the increasing size of the "softened" zone adjacent to the production zone with time, which has the effect of damping radial deformations at the shaft. In fact, these deformations are predominantly non-recoverable (inelastic) and therefore would not be expected to decrease with time.

One further unsettling complexity arises from the observation that the undrained heating condition is <u>not</u> necessarily an upper bound prediction of thermally induced stress changes and deformations. Rock and soil materials of very low permeability impede dissipation of excess pore pressures, however, when excess pore pressures are transmitted spatially within the medium, the zone of elevated pore pressure may be substantially larger than the heated zone, particularly during the early stages of transient heating. The transient consolidation condition may result in a more extensive zone of softened and swelling material due to thermally generated pore pressure spreading, than predicted assuming undrained conditions in which thermally generated excess pressures are assumed to vary directly with the temperature increase. Analytical results presented in the following section

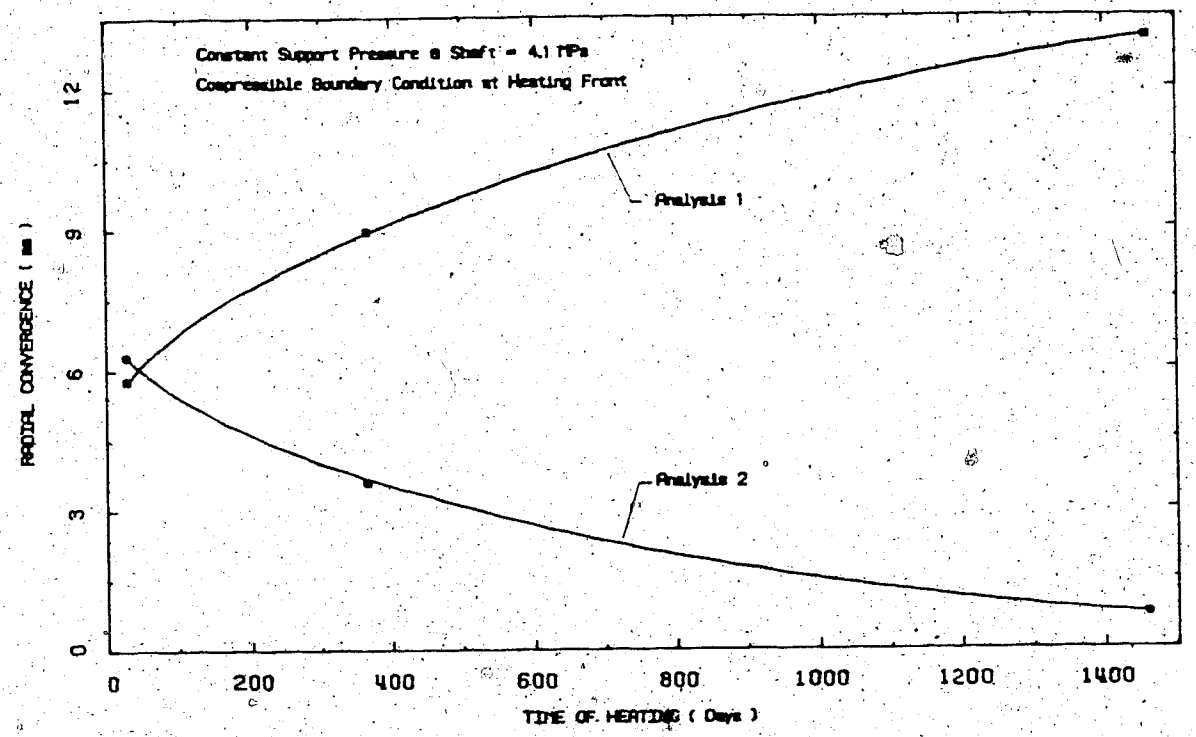

FIGURE 6.34 Radial Convergence of the Shaft During Undrained Heating

illustrate thermal stress changes and deformations assuming transient consolidation in a low permeability material.

6.4.6 Transient Heat Consolidation of Low Permeability Oil Sand or Shale

Transient heat consolidation analyses were carried out using material properties typical of low permeability materials such as oil sand containing more than about 15-20 percent by mass of clay size particles, or shale. The following consolidation properties were used in the analysis:

1. Average mass permeability of 0.01 mD (hydraulic conductivity of 10^{-8} cm/s);
2. Average volumetric compressibility of 10^{-6} kPa^{-1};
3. Coefficient of consolidation of 6.0×10^{-4} m^2/min; and
4. Heat consolidation ratio (R_T) of 10.

Transient radial distributions of temperature increase, excess pore pressures and volumetric expansion at times corresponding to heating periods of 1 month, 1 year and 4 years are plotted in Figures 6.35.1 to 6.35.4 inclusive. It is noteworthy that despite the limited extent of the zone of elevated temperatures even after 4 years, thermally generated excess pore pressures and volumetric expansion have spread through a more extensive zone around the shaft. Excess pore

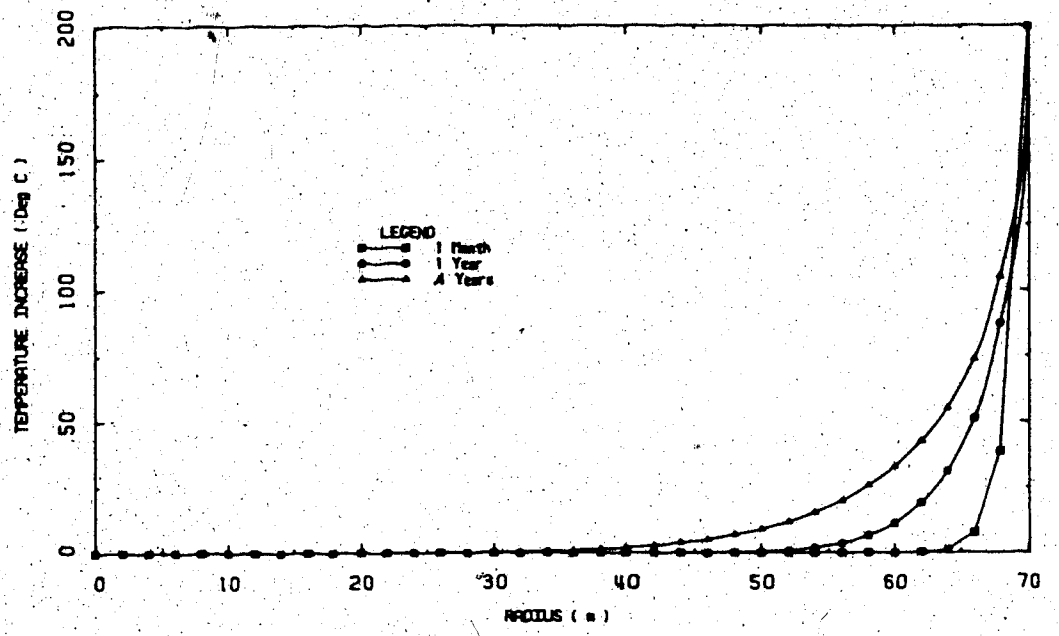

FIGURE 6.35.1 Transient Temperatures Around the Shaft

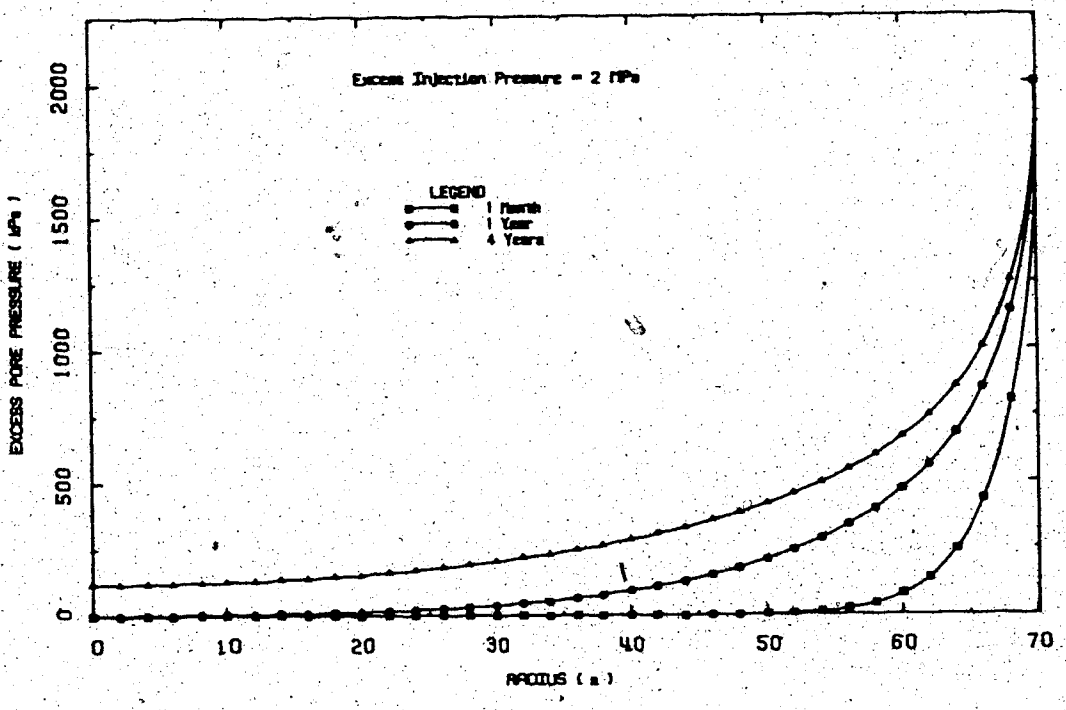

FIGURE 6.35.2 Transient Excess Pore Pressures Due to Injection

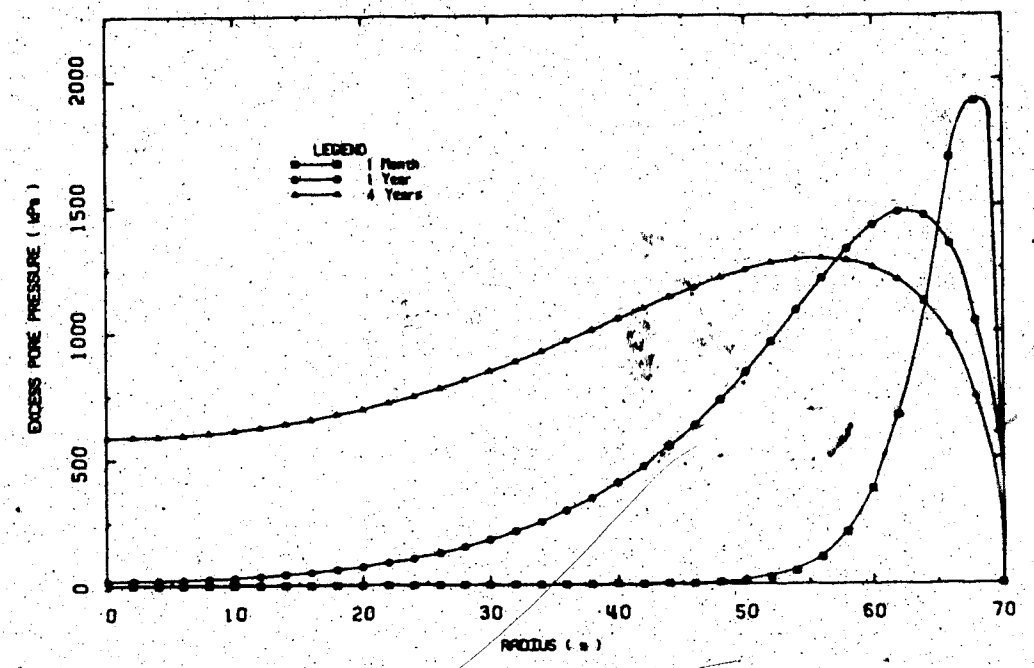

FIGURE 6.35.3 Thermally Generated Excess Pore Pressures

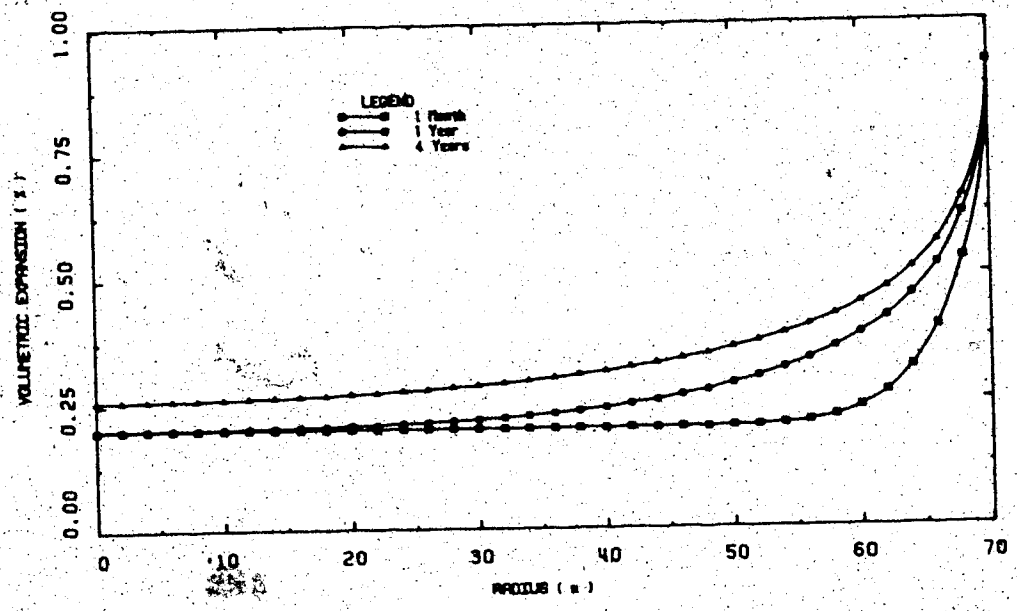

FIGURE 6.35.4 Transient Volumetric Expansion

pressures shown in Figure 6.35.2 are due to diffusion of excess injection pressure while those shown in Figure 6.35.3 are due to spreading of thermally generated excess pore pressures. The production zone boundary is assumed to be a constant pore pressure boundary. Radial distributions of the equivalent coefficient of volumetric thermal expansion (partially drained) at heating periods up to 4 years are plotted in Figure 6.35.5. Radial distributions of the modulus ratio (based on equation 6.14) and reduced modulus of elasticity (i.e. due to effective stress reduction) are plotted in Figures 6.35.6 and 6.35.7, respectively. Although the magnitudes of modulus reduction are less than corresponding values determined in the preceding undrained heating analysis #2, the extent of zones of reduced elastic modulus are much larger here because of pore pressure spreading.

Radial distributions of temperature increase, and equivalent coefficients of thermal expansion and modulus of elasticity determined in the foregoing transient radial heat consolidation analysis were input into thermoelastic finite element analyses of the shaft problem. Thermal stress changes, deformations and current effective stress distributions around the shaft at 1 month, 1 year and 4 years are shown in Figures L8.1 to L8.9, inclusive, in Appendix L.

Thermal stress changes and deformations predicted in this transient heating and consolidation analysis are generally larger than comparable stress changes and deformations

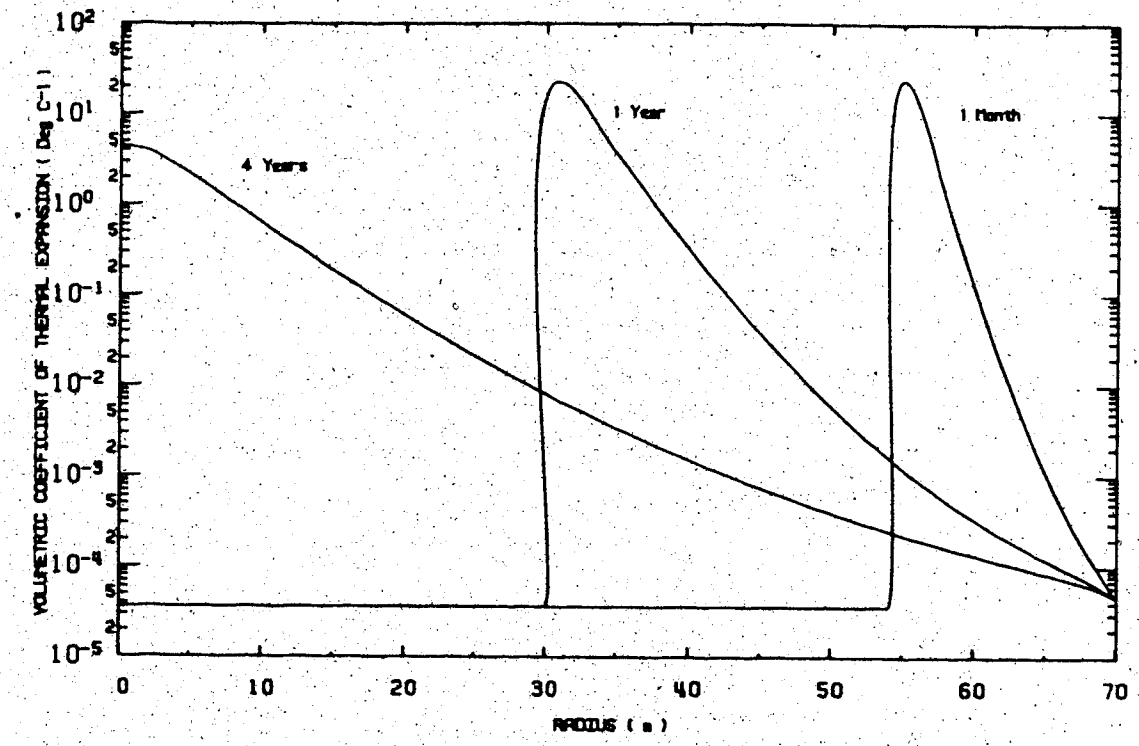

FIGURE 6.35.5 Transient Coefficient of Volumetric Expansion

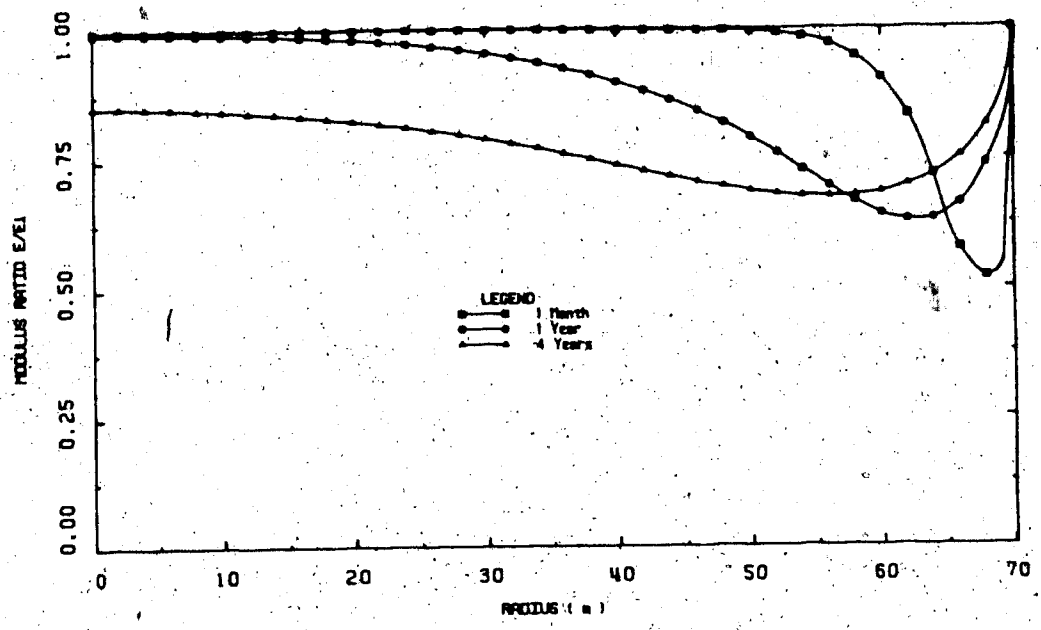

FIGURE 6.35.6 Transient Modulus Ratio Around the Shaft

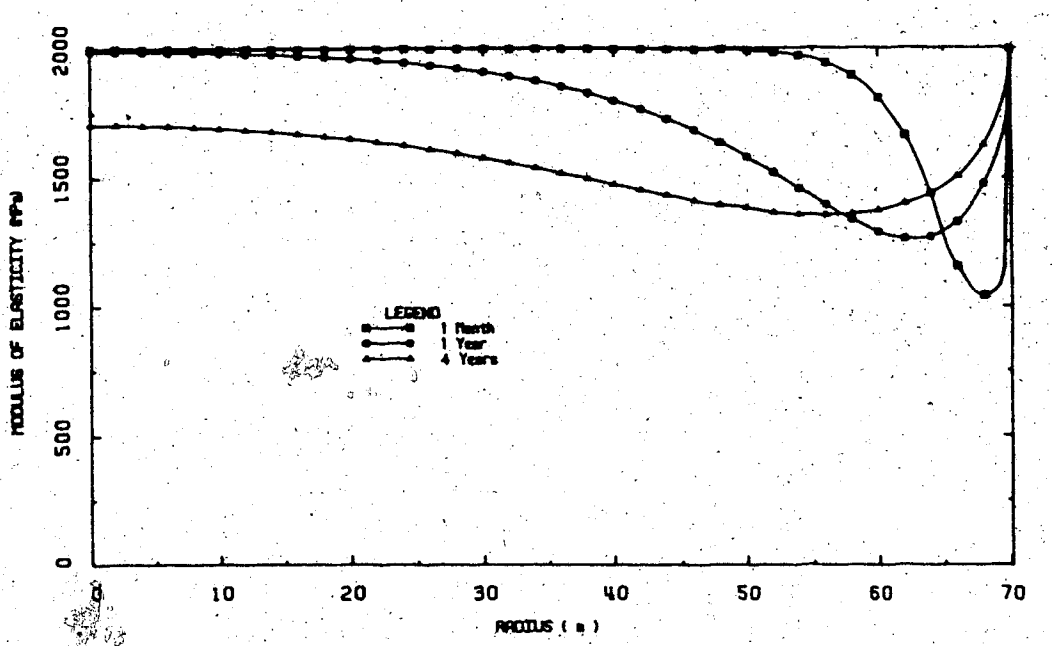

FIGURE 6.35.7 Transient Modulus of Elasticity Around the Shaft

predicted in the transient undrained heating analysis #2. The undrained condition is not necessarily an upper bound solution for predicting deformations during transient heating of low permeability rocks or soils.

Radial convergence of the shaft wall predicted in these analyses is plotted against time in Figure 6.36. The shaft wall again does not converge monotonically as would be predicted using an analytical model which determines non-recoverable (plastic) strains.

6.4.7 Comparison of Analyses of the Shaft Problem

Maximum principal effective stress ratios and maximum radial and vertical deformations calculated in each of the seven preceding analyses of the shaft problem are summarized in Table 6.3. Values of the principal effective stress ratio at failure for cohesionless materials having angles of internal shearing resistance ranging from 30° to 50° are listed in Table 6.4 for comparison with stress ratios tabulated in Table 6.3. The angle of shearing resistance of Saline Creek oil sand at effective confining stresses appropriate for the shaft problem (i.e. 2 MPa to 6 MPa) ranges from about 35° to 50°. Accordingly, shear failure may be expected for principal effective stress ratios greater than about 4.0 to 6.0, or if tensile stresses develop. Note that total principal stress ratios are listed for undrained heating analysis #1 since effective stresses were not predicted in this simplified

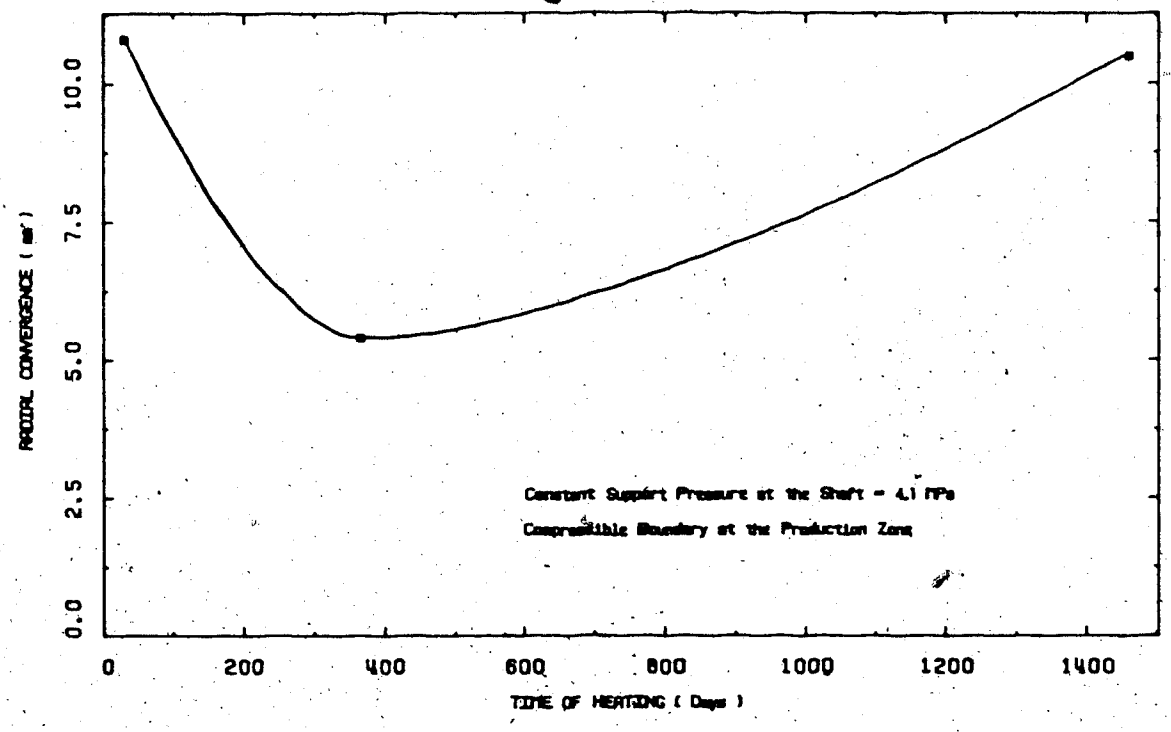

FIGURE 6.36 Predicted Radial Convergence of the Shaft Due to Steam Injection in Low Permeability Oil Sand or Shale

TABLE 6.3

SUMMARY OF MAXIMUM PRINCIPAL STRESS RATIOS AND MAXIMUM DEFORMATIONS PREDICTED USING VARIOUS THERMOELASTIC ANALYSES OF THE SHAFT PROBLEM

ANALYSIS	PRODUCTION ZONE BOUNDARY CONDITION	MAXIMUM PRINCIPAL STRESS RATIO (σ_1'/σ_3')			MAXIMUM DEFORMATIONS (mm)					
					1 Month		1 Year		4 Years	
		1 Month	1 Year	4 Years	δ_r	δ_z	δ_r	δ_z	δ_r	δ_z
1. Transient heat consolidation of Saline Creek Oil Sand	a) Rigid	6.0	1.5	1.7	210.	288.	53.	129.	63.	136.
	b) Constant Pressure	Tension	2.5	2.0	461.	509.	132.	120.	147.	120.
	c) Compressible	Tension	1.5	1.2	140.	169.	62.	56.	58.	40.
2. Drained	Compressible	1.4	1.5	1.6	20.	49.	29.	57.	40.	53.
3. Undrained #1 (Constant Material Properties , E)	Compressible	3.0*	3.5*	4.0*	156.	285.	234.	363.	330.	444.
4. Undrained #2 (Properties varied with effective stress)	Compressible	6.5	3.8	3.6	108.	123.	60.	63.	68.	116.
5. Transient heat consolidation of low permeability oil sand or shale	Compressible	7.0	1.5	3.0	83.	178.	39.	56.	44.	61.

* Maximum total stress ratios are listed for Undrained Analysis # 1 since pore pressures and effective stress were not calculated in this analysis.

TABLE 6.4

PRINCIPAL STRESS RATIO AT FAILURE FOR COHESIONLESS SANDS BASED ON THE MOHR-COULOMB FAILURE CRITERION

ANGLE OF SHEARING RESISTENCE (Ø°)	PRINCIPAL EFFECTIVE STRESS RATIO AT FAILURE (σ_1'/σ_3')
30	3.0
35	3.7
40	4.6
45	5.8
50	7.55

analysis. Shear failure could not be predicted rationally on the basis of this total stress analysis.

Several comparative observations may be summarized based on the data tabulated in Table 6.3:

1. Shear failure of oil sand adjacent to the production zone boundary was predicted during the early stage of heating and injection (i.e. 1 month) in each of the transient analyses except the drained heating analysis. Stress redistribution (i.e. "load shedding") during yielding of material adjacent to the production zone cannot be incorporated in linear thermoelastic analyses.
2. Smaller maximum principal effective stress ratios were predicted for long term heating periods (1 year and 4 years). Thermally generated excess pore pressures and associated thermal stress perturbations move away from the production zone boundary and attenuate with time in transient heat consolidation analyses. Also, the temperature gradient at the production zone boundary decreases with time reducing the magnitudes of the thermally induced stress differences.
3. Maximum predicted radial and vertical deformations listed in Table 6.3 are also larger during the early stages of transient heating, injection and consolidation (1 month) than at later times (1 year, 4 years), for reasons discussed above. However,

deformations predicted in the drained anal and undrained analysis #1 using constant material properties (α, E, ν), increase monotonically with time. The drained analysis provides a reasonable "lower bound" estimate of stress changes and deformations for this class of problems. The simplified undrained analysis however, does not provide an "upper bound" estimate of stress change and deformations since pore pressure spreading and variation of material stiffness with effective stress are not taken into account.

The original horizontal to vertical effective stress ratio, K_o, prior to shaft excavation heating and injection was 0.75. Values of K_o adjacent to the shaft, and adjacent to the production zone, predicted in the foregoing analyses are summarized in Table 6.5. Predicted values of K_o following injection and heating are consistently greater than 0.75, except for the analysis using a constant pressure boundary condition at the production zone. Horizontal effective stresses increase more than vertical effective stresses because of constraint of horizontal deformations, and free vertical displacement when vertical stresses exceed overburden pressure. Calculated values of K_o are also larger during the early stages of heating (1 month) than for long term heating and injection (1 year, 4 years) for the same reason that the maximum principal stress ratio and predicted maximum deformations were larger in Table 6.3.

TABLE 6.5

SUMMARY OF CALCULATED STRESS CHANGES ADJACENT TO THE SHAFT AND THE PRODUCTION ZONE FOR VARIOUS THERMOELASTIC ANALYSES

ANALYSIS	PRODUCTION ZONE BOUNDARY CONDITION	HORIZONTAL TO VERTICAL EFFECTIVE STRESS RATIO (K_o) ADJACENT TO THE SHAFT			HORIZONTAL TO VERTICAL EFFECTIVE STRESS RATIO (K_o) ADJACENT TO THE PRODUCTION ZONE		
		1 Month	1 Year	4 Years	1 Month	1 Year	4 Years
1. Transient heat consolidation of Saline Creek Oil Sand	a) Rigid	1.4	1.0	1.0	2.7	1.3	1.3
	b) Constant Pressure	Tension	0.5	0.5	Tension	0.5	0.6
	c) Compressible	1.0	0.8	0.8	Tension	0.8	0.9
2. Drained	Compressible	0.8	0.8	0.8	0.8	0.8	0.8
3. Undrained #1 (Constant Material Properties , E)	Compressible	-	-	-	-	-	-
4. Undrained #2 (Properties varied with effective stress)	Compressible	1.1	0.8	0.8	4.2	0.9	0.8
5. Transient heat consolidation of low permeability oil sand or shale	Compressible	1.5	1.0	2.2	5.0	1.2	1.5

Tensile stresses and reduced K_o values are predicted in Analysis 1 b), in which a constant pressure/displacement free boundary condition was applied at the production zone. Linear elastic analyses are clearly not applicable for this rather severe boundary condition, particularly in a cohesionless (no tension) material.

Predicted radial and vertical deformations adjacent to the shaft wall are summarized for various heating periods for each of the seven analyses in Table 6.6. Deformations calculated in the drained analysis and simplified undrained analysis #1 (assuming constant stress-temperature-strain material parameters) increase monotonically with time. The magnitudes of deformations predicted in the transient consolidation analyses are greater during the early stages of heating and injection than for long-term heating periods. As previously discussed this departure from reality arises from the use of a linear thermoelastic constitutive relationship, which is inappropriate for modelling this class of problems.

6.5 Stress Changes and Deformations Adjacent to a Single Steam Injection Well in Oil Sand

The steam injection well problem described in section 6.1 is analyzed in this section using analytical procedures described in the preceding sections of the chapter. Properties of Saline Creek oil sand are assumed in the analysis. Initial stresses in the oil sand layer are identical to those assumed for the shaft problem:

TABLE 6.6

SUMMARY OF PREDICTED SHAFT WALL DEFORMATIONS WITH TIME
FOR VARIOUS THERMOELASTIC ANALYSES

ANALYSIS	PRODUCTION ZONE BOUNDARY CONDITION	PREDICTED DEFORMATIONS OF THE SHAFT WALL					
		RADIAL CONVERGENCE (mm)			VERTICAL DISPLACEMENT (mm)		
		1 Month	1 Year	4 Years	1 Month	1 Year	4 Years
1. Transient heat consolidation of Saline Creek Oil Sand	a) Rigid	9.8	4.7	5.3	18.9	1.5	3.6
	b) Constant Pressure*	-8.5	-1.6	-1.4	-35.	-12.1	-17.0
	c) Compressible	1.3	2.7	3.0	6.8	7.9	9.5
2. Drained	Compressible	0.8	1.0	1.7	2.7	2.9	3.0
3. Undrained #1 (Constant Material Properties α, E)	Compressible	5.8	9.0	13.2	1.0	14.4	28.2
4. Undrained #2 (Properties varied with effective stress)	Compressible	6.3	3.6	0.8	23.4	11.1	31.8
5. Transient heat consolidation of low permeability oil sand or shale	Compressible	10.8	5.4	10.5	29.2	17.1	82.2

* Note: (1) Negative radial deformation denotes divergence of the shaft wall.
(2) Negative vertical deformation denotes downward displacement.

1. Effective vertical stress of 6125 kPa;
2. Effective horizontal stress of 4600 kPa;
3. Initial pore pressure of 3100 kPa.

It is also assumed that 200°C steam is being injected at a pressure 2000 kPa in excess of the initial pore pressure, as in the shaft problem.

The injection well is assumed to be a free draining rigid (no radial displacement) boundary. A "far-field" boundary radially symmetric about the well and located at a radius of 70 m from the centre of the well is assumed to be a "no-flow" (or reflection) boundary which is also rigid (i.e. no radial displacement). These boundary conditions might be considered representative of a single well within a field of equally spaced, identical injection wells.

Predicted radial distributions of temperature increase and excess pore pressures due to diffusion of excess injection pressure are plotted in Figures 6.37.1 and 6.37.2, respectively. Thermally generated excess pore pressures are plotted separately in Figure 6.37.3 at times corresponding to heating periods up to 4 years. Radial distributions of an equivalent coefficient of volumetric expansion, also for heating periods up to 4 years are plotted in Figure 6.37.4.

The finite element mesh used for the thermoelastic stress analyses is shown in Figure 6.38 with boundary restraints. Thermoelastic stress analyses were carried out using temperature distributions and radial distributions of the equivalent coefficient

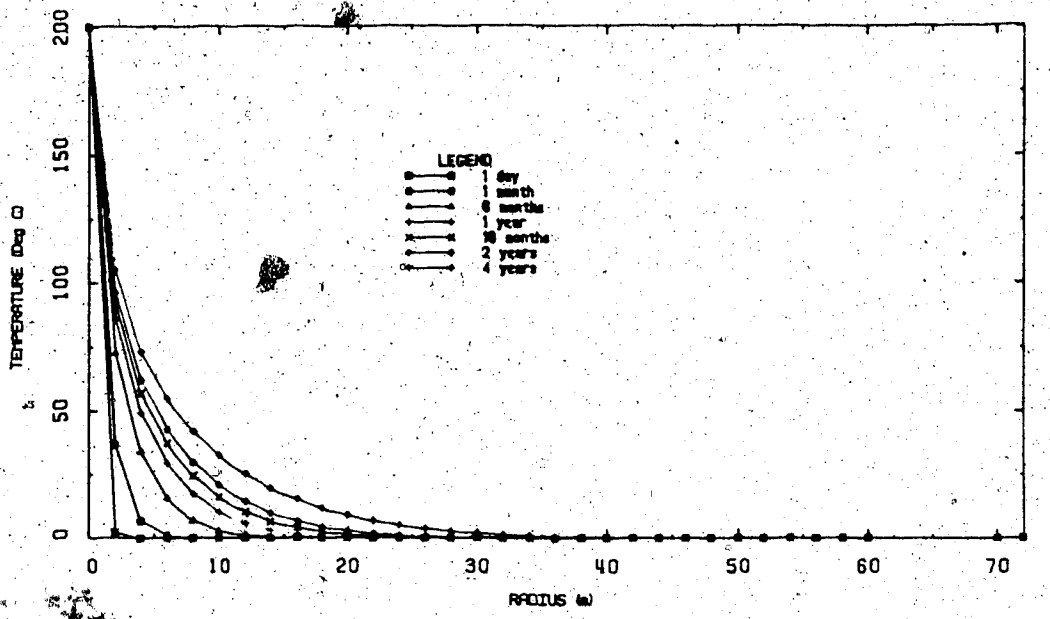

FIGURE 6.37.1 Transient Temperatures Around a Steam Injection Well

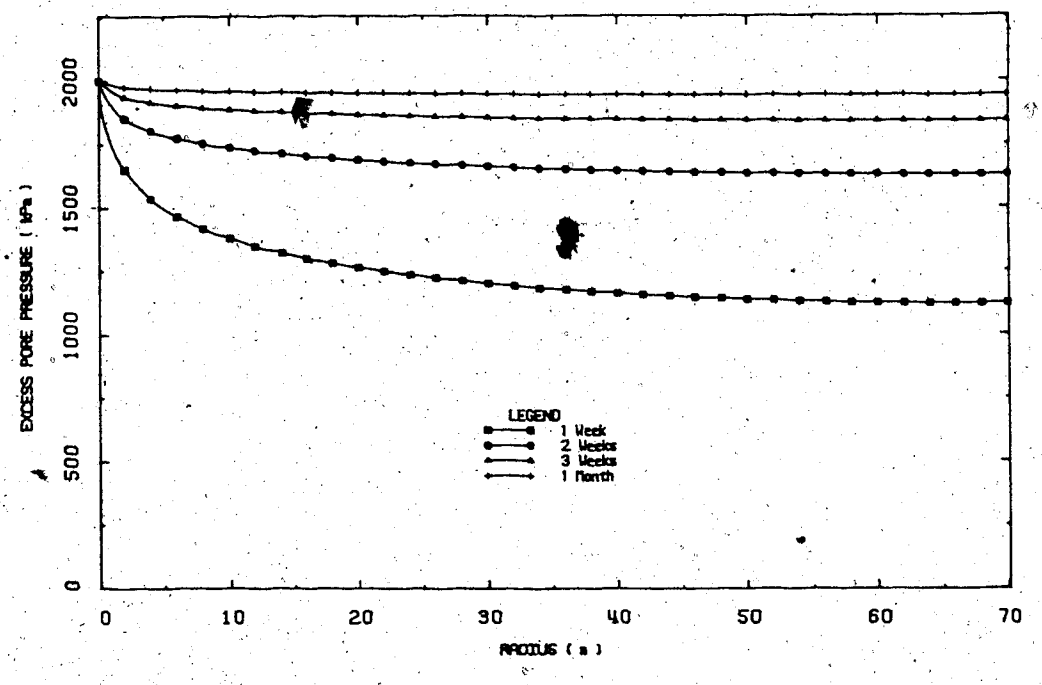

FIGURE 6.37.2 Transient Excess Pore Pressure Due to Injection

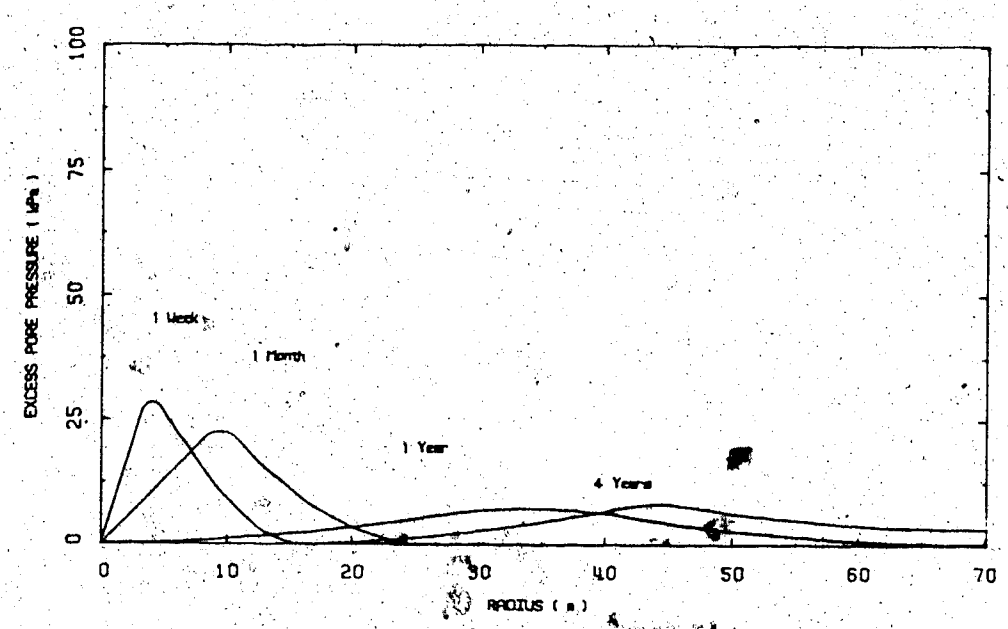

FIGURE 6.37.3 Thermally Generated Excess Pore Pressures Around the Well

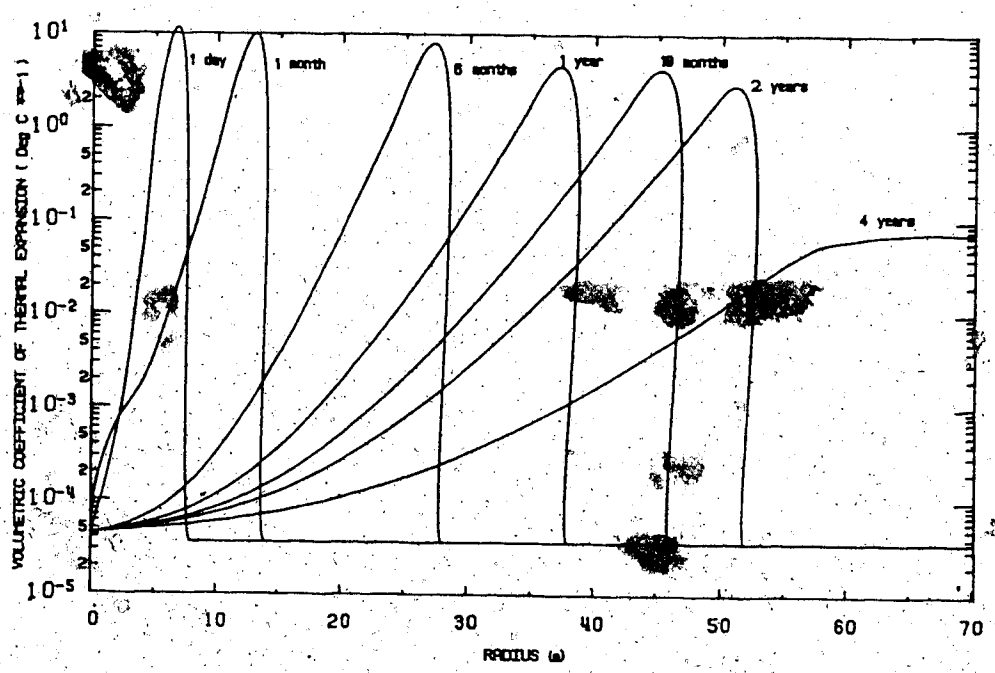

FIGURE 6.37.4 Transient Coefficient of Volumetric Expansion Around the Well

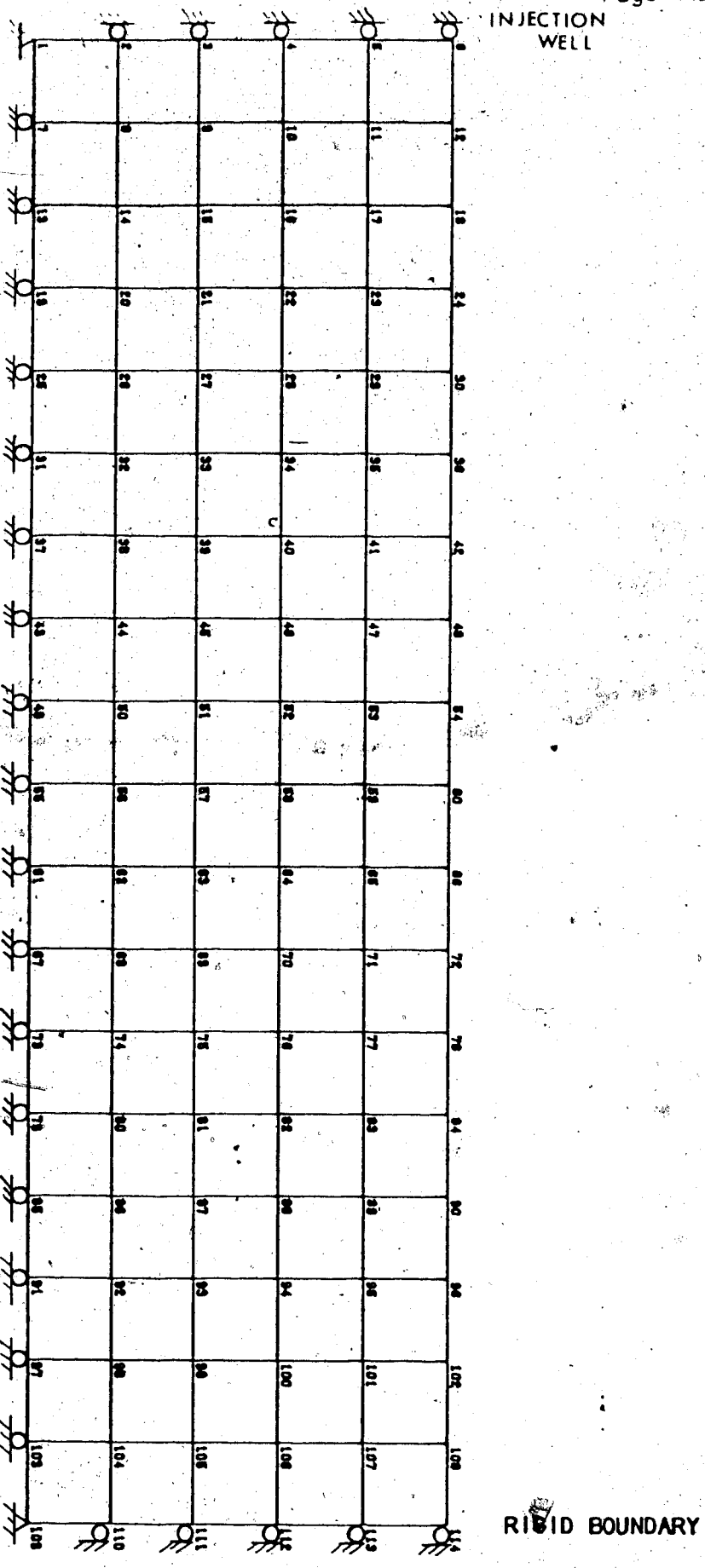

FIGURE 6.38 Finite Element Mesh for Thermoelastic Analyses of Stresses and Deformations Around the Steam Injection Well

of volumetric expansion at heating periods of:

a) 1 month;
b) 6 months;
c) 1 year;
d) 2 years; and
e) 4 years.

Since the thermally generated excess pore pressures were small (see Figure 6.37.3) and the excess injection pressure was assumed to be constant, effective confining stresses did not change after 1 month of injection and heating. Accordingly, a constant average value of 2000 MPa was used for the modulus of elasticity, E. Poisson's ratio was assumed to have a constant value of 0.43.

Stress changes, ground deformations and effective stresses (radial, tangential and vertical) at mid-depth in the oil sand layer are shown in Figures 6.39.1 to 6.39.9, inclusive, for heating periods of 1 month, 1 year and 4 years. Effective stresses were again calculated by superposition of: (i) initial effective stresses; (ii) stress changes due to excavation of the borehole (as determined in section 6.3); (iii) excess pore pressures due to injection and heating; and (iv) total stress changes due to injection and heating. Pore pressure changes due to horizontal total stress increase are expected to be small in this case, because of the large hydraulic diffusivity of Saline Creek oil sand.

Because of the rigid boundary condition at the well two zones

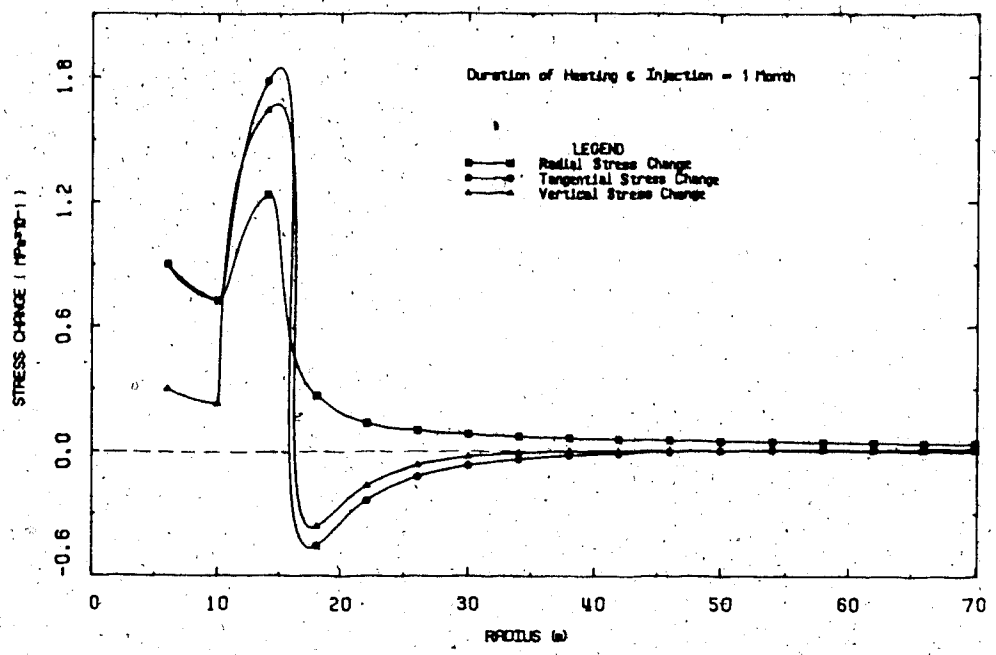

FIGURE 6.39.1 Stress Changes Around the Well After 1 Month of Steam Injection

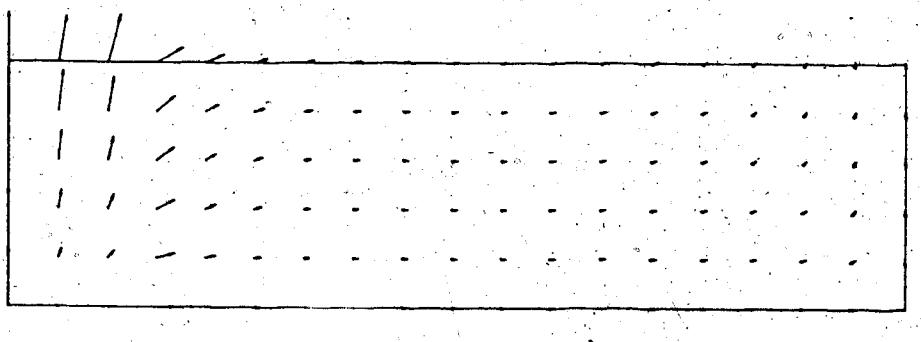

FIGURE 6.39.2 Deformations Around the Well After 1 Month of Steam Injection

DISPLACEMENT SCALE 1:100

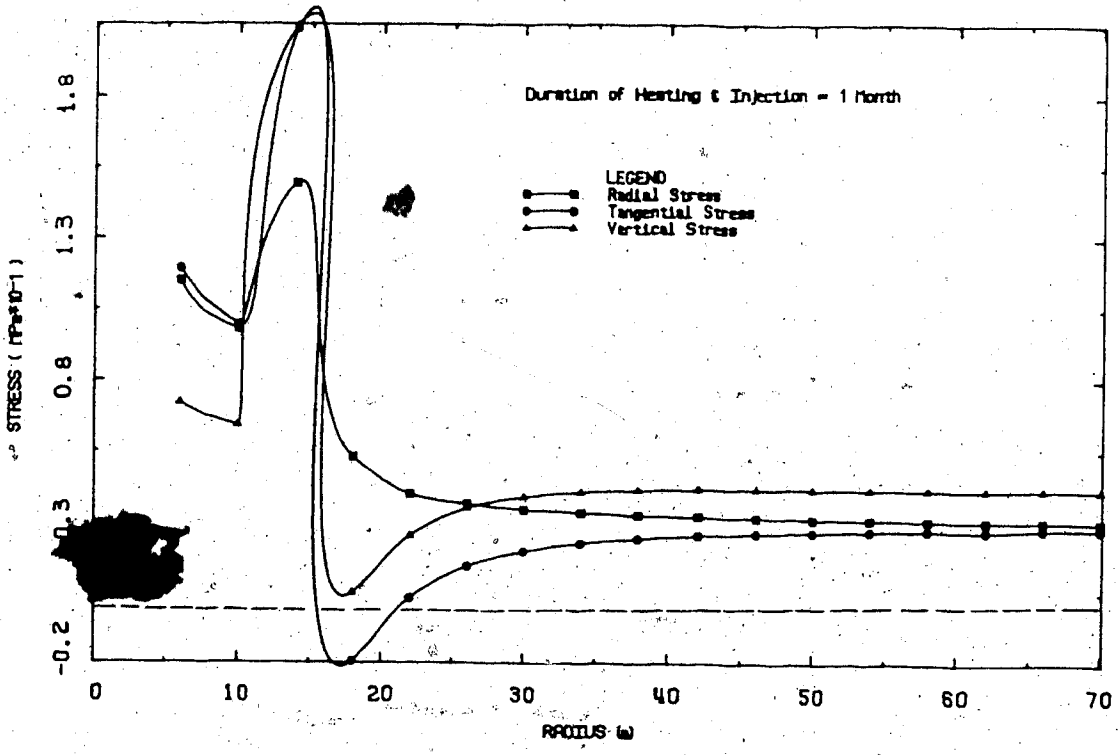

FIGURE 6.39.3 Effective Stresses Around the Well After 1 Month of Steam Injection

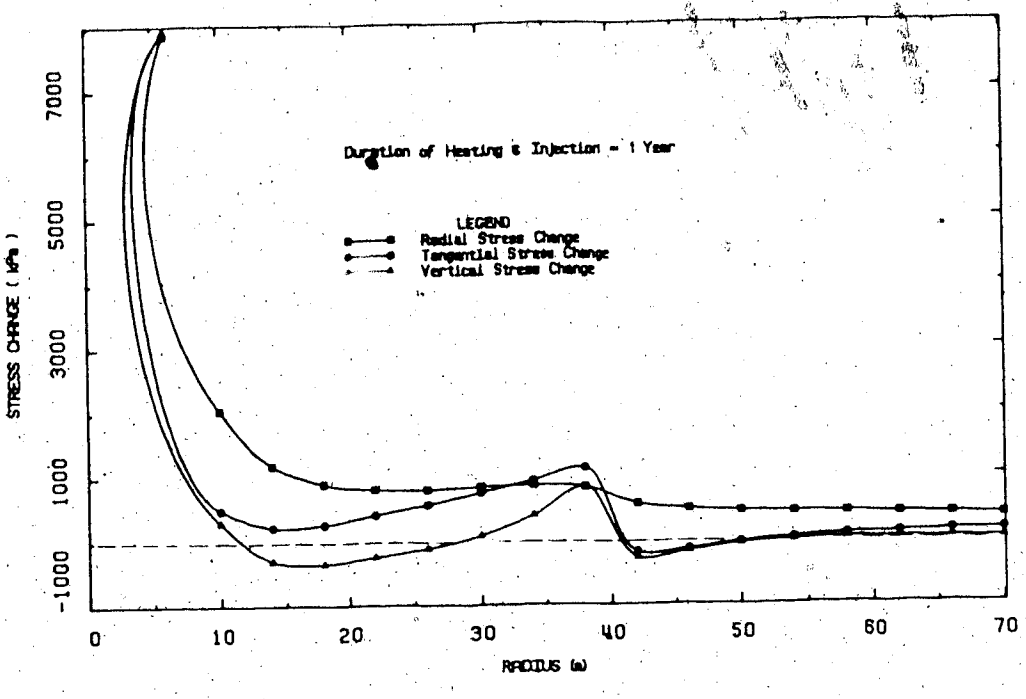

FIGURE 6.39.4 Stress Changes Around the Well After 1 Year of Steam Injection

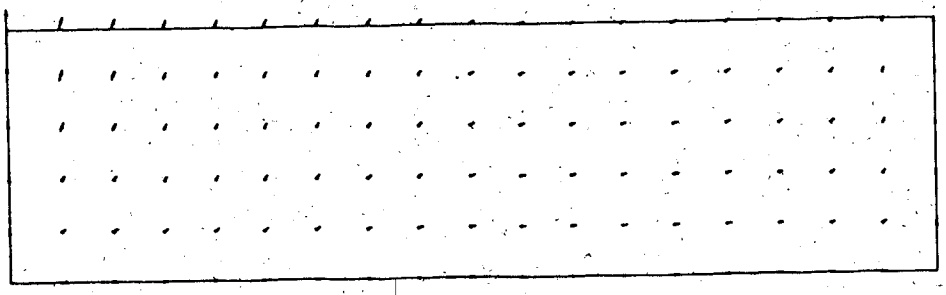

FIGURE 6.39.5 Deformations Around the Well After 1 Year of Steam Injection

DISPLACEMENT SCALE 1:100

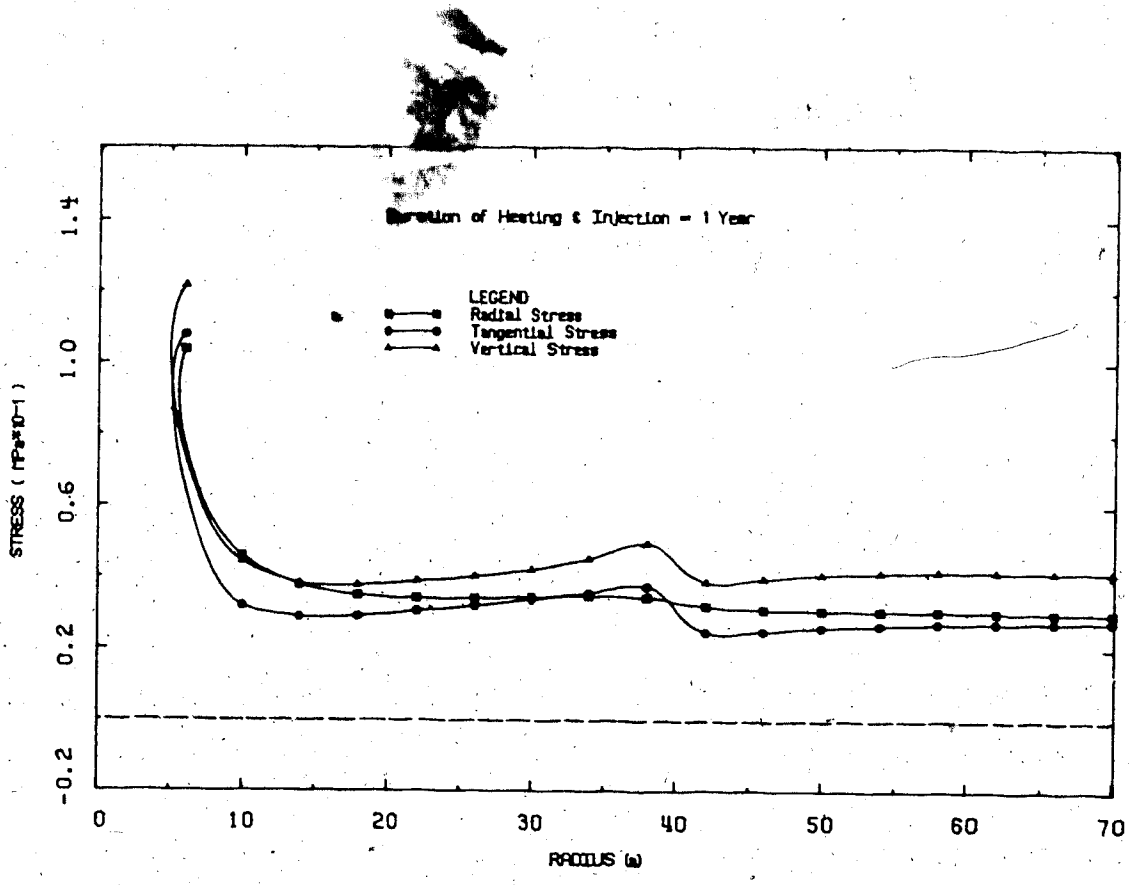

FIGURE 6.39.6 Effective Stresses Around the Well After 1 Year of Steam Injection

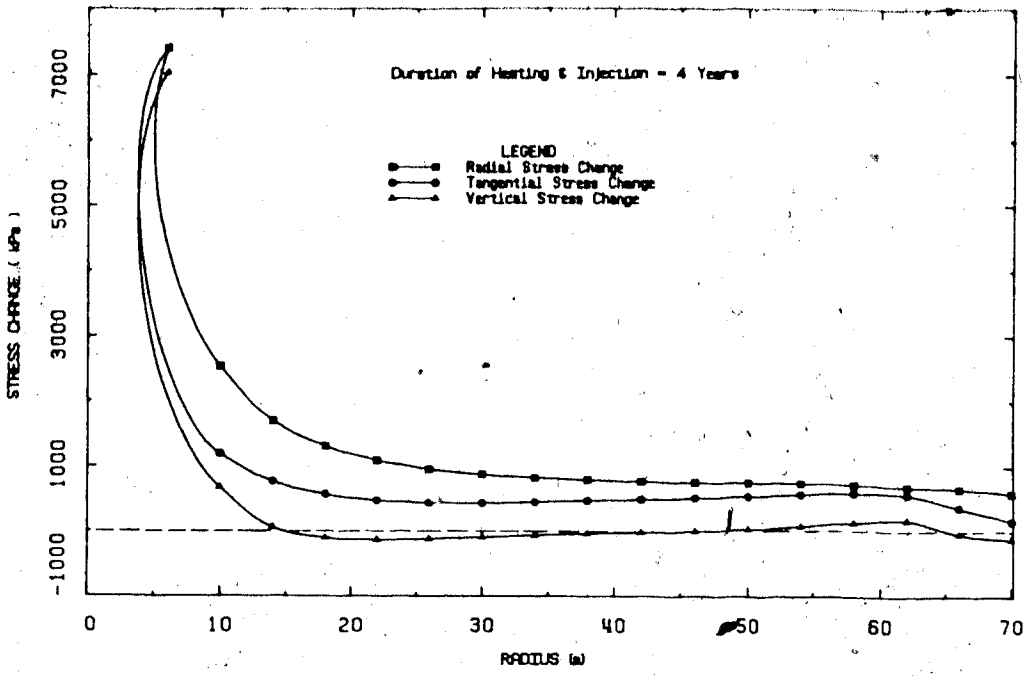

FIGURE 6.39.7 Stress Changes Around the Well After 4 Years of Steam Injection

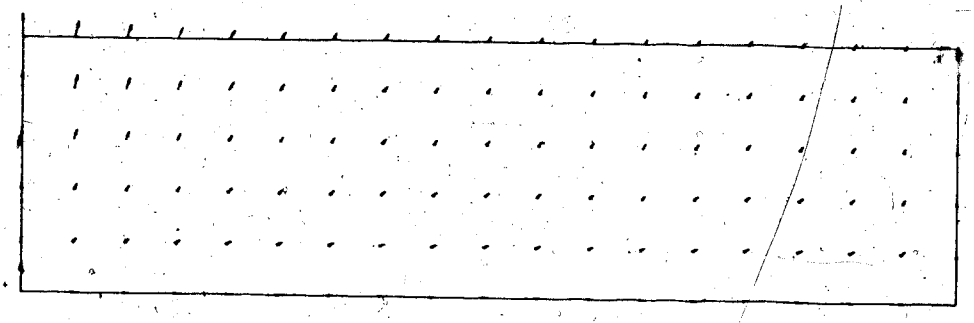

FIGURE 6.39.8 Deformations Around the Well After 4 Years of Steam Injection

DISPLACEMENT SCALE 1:100

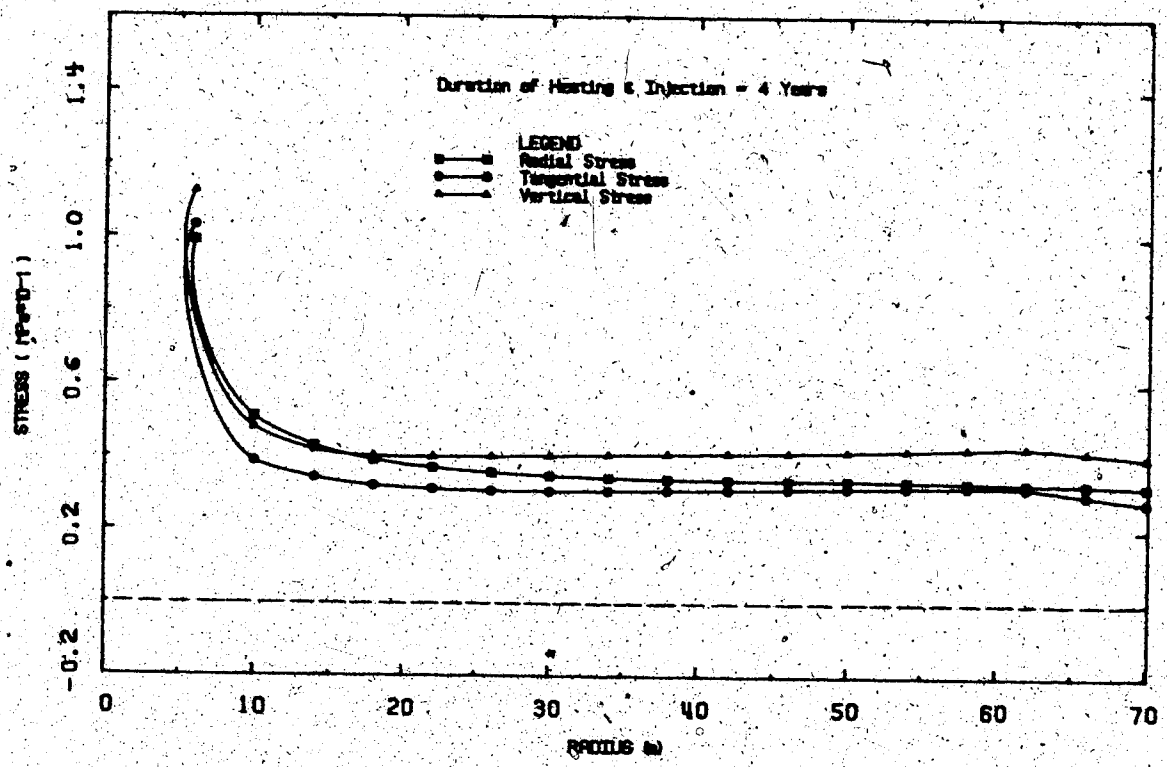

FIGURE 6.39.9 Effective Stresses Around the Well After 4 Years of Steam Injection

of stress perturbation result: (i) a zone immediately adjacent to the well, and (ii) a second zone moving away from the well and attenuating with time.

Maximum principal effective stress ratios and deformations predicted in the analyses are summarized in Table 6.7. Failure of oil sand adjacent to the well, in tension (i.e. by parting) is predicted during the first month of heating and injection. Again, larger stress changes and deformations are predicted during the early stages of heating than in the long-term because of limitations inherent in linear thermoelastic analyses discussed in preceding sections of the chapter.

Predicted values of K_o adjacent to the well casing and remote from the well are summarized in Table 6.8. Horizontal (i.e. radial and tangential) effective stresses increased more than vertical effective stresses throughout the 4 year heating period resulting in values of K_o greater than the initial value of 0.75. Rotation of the principal stresses is actually predicted adjacent to the well casing due to the conditions of radial constraint at the boundaries.

These analytical results illustrate the potential for manipulation of the stress field by controlled heating and/or injection. This concept was previously described by others including Mathews et al. (1969), and Closmann and Phocas (1978). Since the orientation of hydraulically induced "fractures" or partings, is controlled primarily by the orientation of the

TABLE 6.7

SUMMARY OF MAXIMUM PRINCIPAL EFFECTIVE STRESS RATIOS AND DEFORMATIONS PREDICTED ADJACENT TO A STEAM INJECTION WELL IN OIL SAND

TIME OF HEATING AND INJECTION	MAXIMUM PRINICPAL EFFECTIVE STRESS RATIO (σ_1'/σ_3')	MAXIMUM DEFORMATIONS (mm)	
		RADIAL (δr)	VERTICAL (δz)
1 month	2.1 (tension)	156	239
6 months	1.7	45	66
1 year	1.5	32	58
2 years	1.5	34	64
4 years	1.5	30	66

TABLE 6.8

PREDICTED STRESS CHANGES ADJACENT TO A SINGLE STEAM INJECTION WELL IN OIL SAND

TIME OF HEATING AND INJECTION	HORIZONTAL TO VERTICAL STRESS RATIO (K_o)	
	ADJACENT TO THE STEAM INJECTION WELL	REMOTE FROM THE STEAM INJECTION WELL
1 Month	1.6	0.80
6 Months	1.3	0.80
1 Year	1.1	0.85
2 Years	1.1	0.90
4 Years	1.1	0.95

principal stresses, it may in certain instances be desirable to alter the local stress field by preheating and/or controlled injection, prior to inducing fractures or partings by rapid water injection.

Numerical analyses may be improved by introducing concepts of nonlinear incremental elasticity or plasticity, and rigorously coupling total stress changes due to heating and injection with pore pressure changes, as discussed in preceding sections of the chapter.

Analyses predicting stress changes and ground deformations around well casings may also be used to identify risks of shearing and buckling of well casings during pressurized steam injection.

6.6 Summary

An analytical approach for solving two or three dimensional heat consolidation problems was introduced in this chapter. The analytical approach is non-rigorous since pore pressure changes during heating are not directly coupled with thermally induced total stress changes as outlined in equation 5.16 of Chapter 5. Thermally generated pore pressures are calculated using the simplifying assumption that total stresses remain constant during heating. The magnitude of error introduced by this assumption is dependent upon the thermal loading and the degree of restraint of thermal strains, i.e. the temperature increase, the boundary conditions and geometry of the problem. This analytical approach is analogous to the

three-dimensional theory of consolidation (isothermal) developed by Rendulic (1936), who extended Terzaghi's one-dimensional consolidation theory. The assumption that total stresses remain constant during consolidation may be reasonable for vertical (overburden) stress, but ignores total stress changes due to horizontal restraint of deformations.

The analytical approach to three-dimensional heat consolidation problems presented here, provides a practical first step for solving this class of problems using existing numerical modelling techniques. Nevertheless, there is a need for a more rigorous formulation of the theory together with appropriate solution techniques.

Analyses of two similar problems were carried out to illustrate application of the proposed analytical method. The problems analyzed involved: (i) heating and injection near a vertical shaft in oil sand; and (ii) pressurized steam injection through a well casing in oil sand. The shaft problem was analyzed extensively to illustrate the influence of boundary conditions and consolidation characteristics of the heated material on numerical results. Simplified drained and undrained heating analyses of the shaft problem were also presented and discussed. It was illustrated that a drained heating analysis provides a reasonable "lower bound" solution. The assumption that undrained conditions prevail during heating does not necessarily provide an "upper bound" solution for stresses and deformations because of effective stress reduction due to pore pressure "spreading" during transient heat consolidation in low permeability materials.

The selection of appropriate boundary conditions at various stages of the shaft problem requires detailed consideration of the "production scenario" including procedures for development of inter-well communication (i.e. hydraulic fracturing), injection pressures and temperatures, proposed durations of injection and production cycles, etc. Analyses for oil sands project planning also require evaluation of stress changes and deformations resulting from activities within the production zone. It is evident that analysis of this class of problem requires input from reservoir planners and specialists in other disciplines.

Several difficulties related to the use of standard numerical modelling methods were identified during analyses of the shaft problem. These difficulties are believed to be common to boundary value problems involving large temperature gradients and are summarized below:

1. Stress redistribution (i.e. "load shedding") following yielding or shear failure of soil/rock elements cannot be modelled within the framework of linear thermoelastic theory.
2. Non-recoverable (i.e. plastic) deformation of oil sand cannot be accounted for using linear thermoelastic solution methods.
3. The preceding deficiencies inherent in linear elastic formulations yield paradoxical numerical results. Predicted stress changes and deformations decrease with time, as the temperature gradient decreases and thermally

generated pore pressures dissipate. Development of a thermal stress algorithm, which accounts for nonlinear stress-strain behaviour and non-recoverable deformations is required in order to correctly model problems involving large temperature gradients. Extension of the hyperbolic model to calculate thermal stresses and deformations would be useful for heat consolidation analyses in oil sand.

4. If total stress changes are large due to constraint of thermally induced strains, resultant pore pressure changes may also be large in low permeability materials. Stress- and strength properties of soils and rocks are very [redacted] ive to effect[redacted]tress changes. The error introduced by ignori[redacted]rous coupling between total stress and pore pressure changes may be substantial, particularly for large thermal stress changes in low permeability materials.

Hyperbolic stress-strain parameters for Saline Creek oil sand were summarized and used in an analysis to determine stress changes and deformations during excavation of a shaft through oil sand.

7.0 CONCLUSIONS AND RECOMMENDATIONS

7.1 General

It is the purpose of this chapter to summarize significant findings of this research and to outline areas which warrant further investigation. Major aspects of the research summarized here include: (I) development of capabilities for elevated temperature experimental research; (II) geotechnical implications of ground heating based on both experimental and analytical studies, and literature review; and (III) analyses of heat-consolidation problems.

7.2 Experimental Research at Elevated Temperatures

Meaningful laboratory measurement of geotechnical properties is contingent upon our ability to obtain high quality undisturbed samples. Cohesionless sands have traditionally been difficult to sample. High quality oil sand samples were obtained for this research programme during late winter months from a frozen outcrop along Saline Creek near Fort McMurray, Alberta.

A specialized laboratory facility was assembled at the University of Alberta for geotechnical testing of oil sand at elevated temperatures and pressures. The facility includes both one-dimensional and triaxial compression equipment along with compatible system components for conducting permeability experiments, all at temperatures to 300°C and pressures to 30 MPa.

It is particularly important to isolate system responses at elevated temperatures and pressures from the sample response for correct interpretation of test results. Compliance testing procedures were developed to achieve this end.

Experimental procedures were developed and laboratory experiments were performed over a range of temperatures to measure:

a) drained and undrained thermal expansion;
b) drained and undrained compressibility;
c) pore pressure generation during undrained heating;
d) shear strength and stress-strain parameters; and
e) permeability properties.

Supplementary index testing of oil sand samples was performed to evaluate: density, grain size, pore fluid saturations and bitumen viscosity. The microfabric and mineralogy of oil sand samples were also studied using scanning electron microscopy and x-ray diffraction analyses.

The experimental programme has provided a wide range of information which has enabled geotechnical characterization of Saline Creek oil sand. The oil sand samples studied were sufficiently uniform to permit quantitative comparison of geotechnical behaviour at different temperatures, pressures and confining stresses. Heat transfer properties (i.e. thermal conductivity, thermal diffusivity, etc.) were not measured, however some published data was available for input into heat consolidation analyses.

Limited testing of Cold Lake oil sand was also performed which has permitted limited comparison of Athabasca and Cold Lake oil sand materials.

7.3 Geotechnical Implications of Ground Heating

Significant geotechnical implications of ground heating which have been identified in this research are summarized in this section.

1. Thermal Alteration of Mechanical and Physical Properties

Heating to temperatures approaching 300°C has little influence on the properties of quartzose sand grains or on the densely packed solid skeleton of Saline Creek oil sand. Changes detected in compressibility, shear strength, stress-strain behaviour, and absolute permeability of Saline Creek oil sand due to temperature changes were small in comparision with other factors such as sample disturbance and effective stress changes.

A review of the literature indicates that heating may cause much more dramatic changes in the geotechnical behaviour of other oil sands, soils and rocks. Cold Lake oil sand, for example, is mineralogically weaker than Saline Creek oil sand and therefore is apparently more sensitive to strength reduction at elevated temperatures. Mineralogical alteration of Cold Lake oil sand due to *in situ* steaming has been identified by the Sedimentology

Group at the University of Calgary (1981). A review of experimental research on other materials published in the literature was described in Chapter 2.

The literature review revealed that the stiffness and strength of intact cemented and crystalline rocks generally decrease at elevated temperatures due to "thermal cracking". Conversely, the strength and stiffness of clay soils increase with temperature due to "thermally induced compaction".

The mobility of bitumen in the pore space of oil sands increases dramatically at elevated temperatures because of decreasing viscosity. The coefficient of consolidation of oil sand, therefore, also increases with temperature. The mobility of other liquid pore fluids in soils and rocks, such as water, also increases with temperature, though to a lesser extent than bitumens or heavy oils. The rate of consolidation of oil sand increases at elevated temperatures.

2. Thermal Pore Pressure Generation and Shear Strength Reduction

Transient heating in situ results in simultaneous thermal pore pressure generation and dissipation of excess pore pressures. The rate and magnitude of thermal pore pressure generation are dependent upon the rate of heating, the ambient pore pressure and the effective confining stresses, while the rate of excess pore pressure

dissipation is dependent upon the consolidation characteristics of the porous medium and the boundary conditions. The propensity for thermal pore pressure generation during transient heating by diffusion may be characterized by the dimensionless "heat consolidation ratio", R_T, described in Chapter 5.

The shearing resistance of cohesionless oil sands and many other essentially cohesionless soil and rock masses is entirely frictional. Shear strength is directly proportional to effective normal stresses acting across all potential planes of shear deformation within a soil or rock mass. Therefore, an increase in pore pressure due to ground heating causes a proportional decrease in the available shearing resistance. Since the principal effective stresses in situ are generally not equal, i.e. $\sigma_1' > \sigma_2' > \sigma_3'$, excess pore pressures generated during heating may, in fact, cause shear failure. Figure 7.1 illustrates the mechanism by which a frictional soil or rock material may fail by shearing during undrained heating in a non-uniform stress field.

Excess pore pressures generated during transient heating and consolidation of Saline Creek oil sand are small (i.e. generally less than 1 percent of effective confining stress) due to the large value of R_T which is characteristic of Saline Creek oil sand.

Although thermally generated excess pore pressures are likely small in oil rich oil sands, it is important to

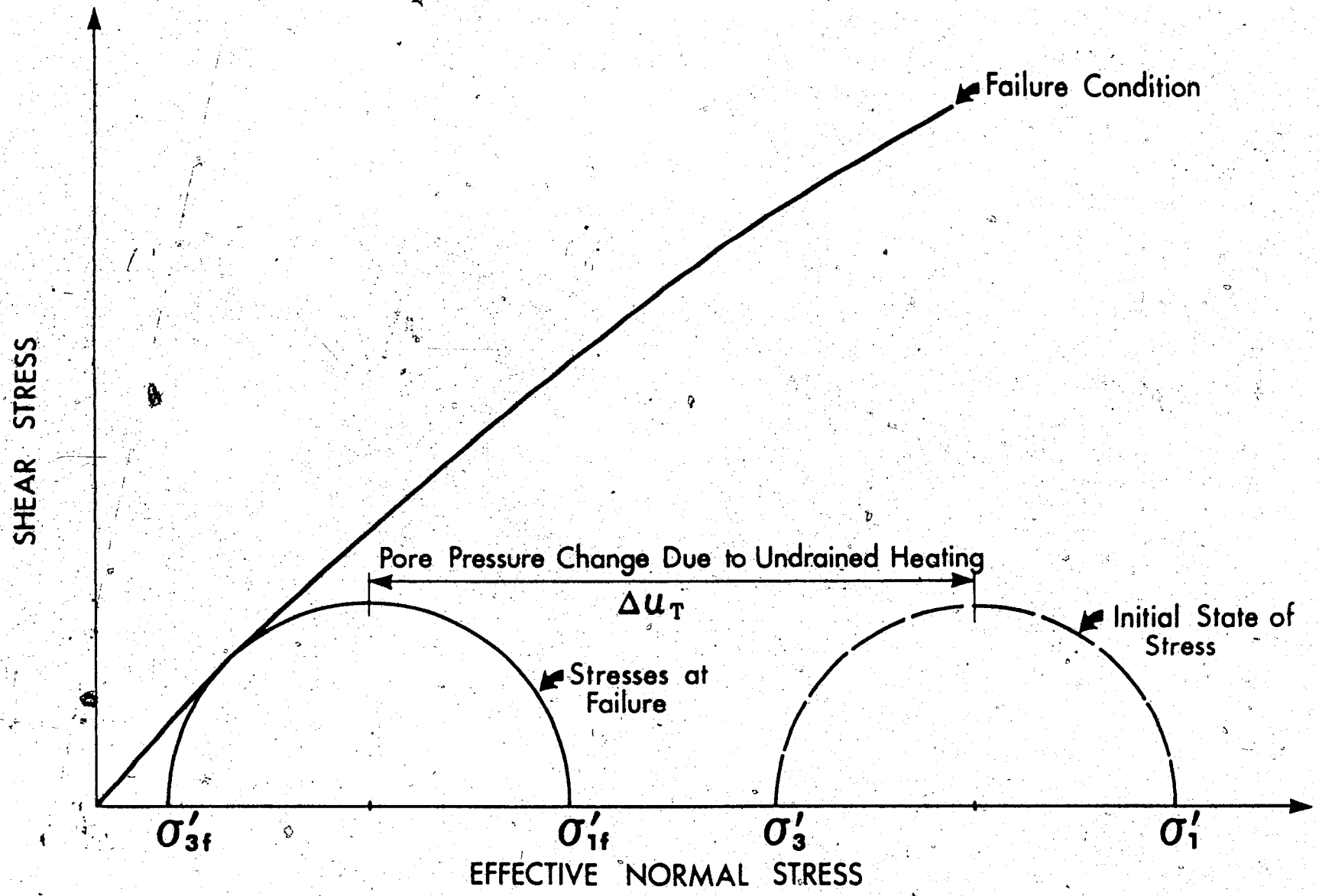

FIGURE 7.1 Shear Failure By Undrained Heating

recognize that excess injection pressures may be expected to diffuse readily through these materials. This has imporant implications for shaft and tunnel design since it is likely to be very difficult to isolate shaft and tunnel lining systems from the influence of excess injection pressures. Other oil sands may be less permeable if they contain larger proportions of fine-grained clay and silt sized particles. Oil sand containing 10-20 percent fine grained particles by mass (or more) are more highly susceptible to thermal pore pressure generation and shear strength reduction. There is considerable potential for shear failure by undrained heating in low permeability materials such as clay shales.

3. Thermally Induced Stress Changes

Heating causes thermal expansion of the constituent solids and pore fluids in soils and rocks. Restraint of vertical deformations due to in situ heating and thermal expansion is limited since vertical overburden stresses remain nearly constant. Conditions of horizontal continuity which are prevalent in the earth's crust result in restraint of thermally induced horizontal deformations. Consequently horizontal stresses increase more than vertical stresses during in situ heating and thermally induced vertical deformations are larger than horizontal deformations. It is possible to cause local rotation of the principal stresses in some instances, depending upon

the initial stresses, the magnitude of temperature changes, stress-strain properties of the medium and the degree of restraint of horizontal strains (i.e. boundary conditions). This observation introduces the possibility of manipulating the in situ stress field by heating (e.g. see Mathews et al, 1969). This is of particular interest since the orientation of hydraulic fractures is controlled to a large extent by the orientation of the principal stresses.

Non-uniform increase of the principal stresses due to in situ heating may also, in some circumstances, lead to shear failure. Hydraulic fractures may propagate both by parting and shear deformation. The potential for thermally induced shear failure is enhanced in low permeability materials because of the potential for thermal generation of excess pore pressures and the larger strains associated with undrained thermal expansion.

7.4 Analyses of Heat Consolidation Problems

Procedures for numerical analyses of heat consolidation problems were presented in Chapters 5 and 6. The theory and numerical modelling procedure developed in Chapter 5 coupling heat transfer with consolidation was based on the assumption that total stresses are constant. Although not rigorous there are circumstances in which this assumption is reasonable:

a) The vertical overburden stress in situ does not increase substantially due to heating since vertical displacements

are unrestrained, although conditions of horizontal restraint are common.

b) Thermally induced total stress changes in very compressible soils such as clays are small. Larger thermal stress changes develop in stiffer materials such as rocks when thermally induced strains are suppressed.

c) Heating of highly permeable materials such as clean water-bearing sands or gravels does not result in very large values of thermally generated pore pressures because the "drained" heating condition is approached.

d) During the early stages of heating in porous soils and rocks which are saturated with relatively incompressible pore fluids, the pore pressure response to thermally induced total stress changes may be nearly equivalent to the magnitude of the total stress changes, i.e. based on Skempton's pore pressure equation (Skempton, 1954). This condition results in very small effective stress changes initially, however, as the material consolidates and excess pore pressures dissipate, a net change in the effective stresses does develop.

In materials of low permeability, thermally generated pore pressures are much larger than those due to total stress changes.

An uncoupled numerical modelling procedure for two and three dimensional heat consolidation problems was presented in Chapter 6. Thermally generated excess pore pressure and volumetric strains were again calculated assuming constant total stresses. Transient

volumetric strains, temperatures and appropriate stress-strain moduli were then input into a finite element thermoelastic analsyis to calculate thermally induced stress changes and deformations. The procedure was summarized in flow chart form in Figure 6.1.4. In principal, pore pressures resulting from total stress changes may also be calculated in an uncoupled manner as outlined in step 5 of Figure 6.1.4. However, this becomes very cumbersome since it is necessary to proceed incrementally allowing for continuous pore pressure generation due to injection, heating and total stress changes, and also transient dissipation of these excess pore pressures. Accordingly, step 5 was omitted from uncoupled analyses presented in Chapter 6. Rigorous formulation of the problem including coupling between total stress changes and pore pressures is required to treat this class of problems more systematically.

Important findings arising from numerical analyses of heat consolidation around a shaft and injection well in oil sand include:

1. Thermally generated pore pressures are relatively small in oil rich oil sands. Consequently deformations due to transient heating are also relatively small. However, large deformations may result if injection pressures are large (i.e. if injection pressures approach the magnitude of confining stresses). Rapid diffusion of injection pressure is expected in oil rich oil sands, consequently it is considered difficult to isolate shaft and tunnel liners (or well casings) from the influence of elevated injection pressures i.e. increased earth pressures at reduced effective confining stresses.

2. It was demonstrated that the patterns and magnitudes of thermal stresses and deformations predicted in thermo-elastic analyses are very sensitive to boundary conditions applied in the vicinity of a high temperature gradient. The selection of appropriate boundary conditions adjacent to large temperature gradients is very much dependent upon the "heating and injection scenario" as well as the heat consolidation characteristics of the reservoir materials.

3. Correct modelling of incremental stress changes and defogmations due to transient heating and consolidation of oil sand requires the ability to predict non-recoverable plastic deformations. This may be accomplished using an incremental thermoelastic formulation or by developing a thermal stress algorithm based on the theory of plasticity.

7.5 Recommended Future Research

Analytical Research:

1. There is merit in implementing the hyperbolic model in conjunction with thermoelasticity in a finite element program such as ADINA. The suitability of the hyperbolic model for oil sand and the need for the capability of predicting non-recoverable strains in heat consolidation problems were demonstrated in Chapter 6.

2. Development of a finite element program capable of analyzing three dimensional heat consolidation with rigorous coupling of transient excess pore pressures and total stresses is required. Implementation of the hyperbolic model in conjunction with thermoelasticity is also strongly recommended for coupled three dimensional heat consolidation in order to permit sensible modelling of the transient thermomechanical response of soil and rocks.

Experimental Research

1. There is a need to study the influence of elevated temperatures and pressures on heat transfer properties of undisturbed oil sands. The limited thermal conductivity data which has been published for Athabasca oil sand is based on testing of remoulded oil sand samples at low ambient temperatures and pressures. Since transient heat consolidation is directly influenced by the rate of heat transfer, further analyses of convection and/or dispersion processes are warranted to evaluate their potential influence on the magnitudes of thermally generated excess pore pressures.
2. A range of geotechnical tests on Saline Creek oil sand are worth performing in order to fill inevitable gaps in the testing performed to date:

    a) Standard passive triaxial compression tests including unloading-reloading cycles and straining beyond the peak deviatoric stress may be performed using strain-

controlled testing procedures and a stiffer compression testing frame than that used in this research. Typical stress-strain test results for this type of testing are illustrated in Figure 7.2.

b) Triaxial compression testing between 200°C and 300°C is of both academic and practical interest.

c) Undrained passive triaxial compression tests may be worth performing over a range of temperatures to evaluate the influence of temperature on Skempton's pore pressure parameters, A and B.

d) A range of stress paths may be investigated which are appropriate for various heating and loading conditions of interest (e.g. "active compression", "active extension", "proportional loading" and "proportional unloading" stress paths).

3. Geotechnical testing of other Alberta oil sands such as Cold Lake oil sand, Peace River oil sand or oil sands from other areas of the Athabasca deposit is of interest since some of these oil sands are believed to include minerals which are weaker than quartz, e.g. feldspar and mica. Such materials are believed to be more susceptible to physical alteration at elevated tempertures and stresses. Experience with Saline Creek oil sand indicates that a full suite of geotechnical tests should be performed on any other oil sand materials investigated in order to gain reasonably comprehensive information about geotechnical behaviour of the material. Investigation of these other oil sands is contingent upon developing techniques for obtaining high quality undisturbed samples.

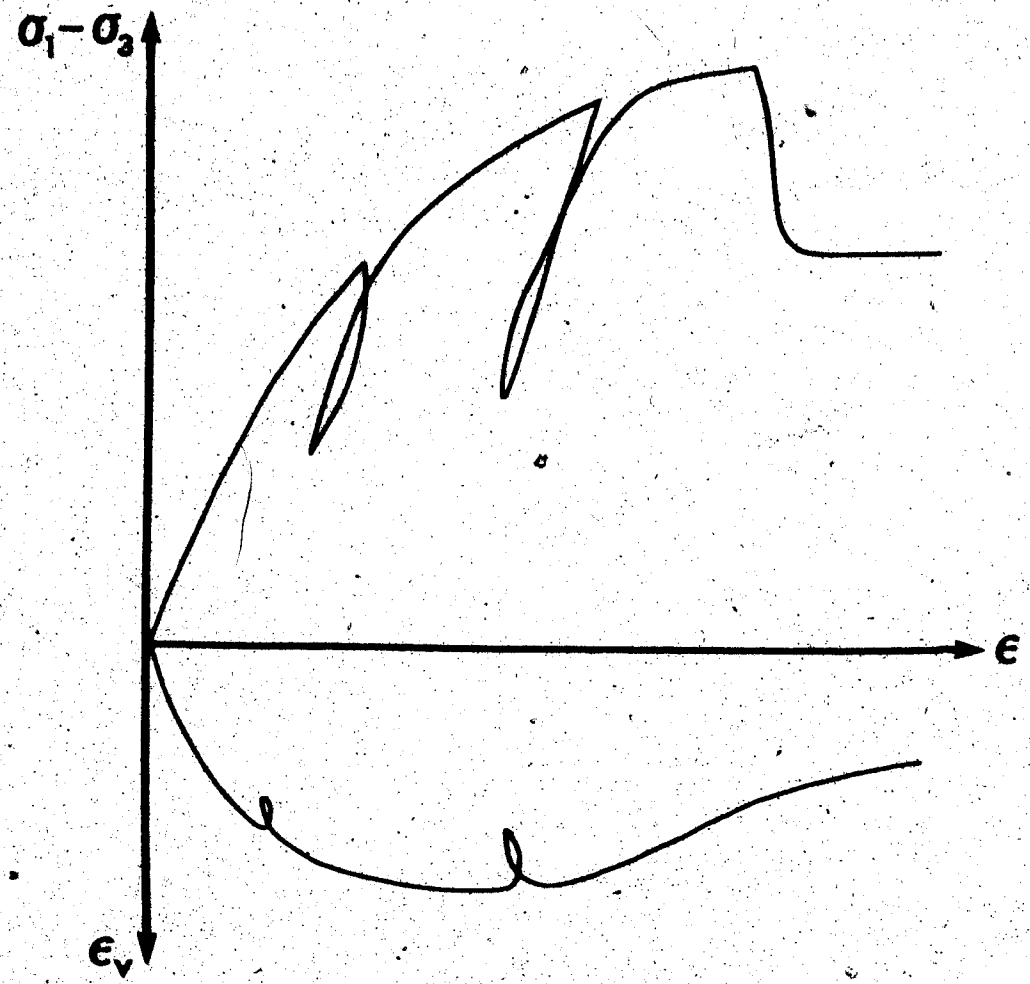

FIGURE 7.2 Typical Stress-Strain Test Results for Strain-Controlled Triaxial Compression Including Unload-Reload Cycles and Post-Peak Straining

4. The influence of heating on geotechnical behaviour of shales and limestones which are interbedded with and adjacent to most oil sands is of considerable interest for *in situ* development of oil sands. Some of the possible implications of heating these lower permeability rocks have been discussed elsewhere in the thesis. Investigation of the geotechnical behaviour of these materials is also contingent upon obtaining and testing samples which are representative of the *in situ* rock fabric.

5. There is a definite need for geotechnical field studies which could be carried out in conjunction with *in situ* pilot or commerical developments to provide information which is complementary to that obtained in laboratory and analytical studies, and to enable verification of numerical modelling results. There is considerable scope for development of geotechnical instrumentation and *in situ* testing equipment suitable for conditions of elevated ground temperatures and pressures.

BIBLIOGRAPHY

ABOUSTIT, B. L., ADVANI, S. H., LEE, J. K. and SANDHU, R. S. 1982. Finite element evaluations of thermoelastic consolidation. In Proceedings of the Twenty-Third Symposium on Rock Mechanics, Berkeley, California, Society of Mining Engineers of AIME, New York, pp. 587-595.

ABRAMOWITZ, M. and STEGUN, I. A. 1970. Handbook of mathematical functions. Dover Publications, Inc., New York, 1046 p.

ABRAMS, A. 1975. The influence of fluid viscosity, interfacial tension and flow velocity on residual oil saturation left by waterflood. Society of Petroleum Engineers of AIME, Vol. 15, pp. 437-447.

AFINOGENOV, Y. A. 1970. How the liquid permeability of rocks is affected by pressure and temperature. Consultants Bureau, Plenum Publishing Corporation, New York, translated from Russian publication SNIIGIMS, No. 6, pp. 34-42.

AGAR, J. G., MORGENSTERN, N. R. and SCOTT, J. D. 1983. Geotechnical testing of Alberta oil sands at elevated temperatures and pressures. Proceedings of the 24th U.S. Symposium on Rock Mechanics, Texas A & M University, pp. 795-806.

ALBERTA ENERGY AND NATURAL RESOURCES, 1979. Alberta oil sands facts and figures. ENR Report No. 110, 67 p.

ALHEID, H.-J., MOEHRING-ERDMANN, G. and RUMMEL, F. 1983. Experimental and theoretical approach to friction in rocks at high pressure and temperature. In Proceedings of the 24th U.S. Symposium on Rock Mechanics, Texas A & M University, pp. 481-488.

AMERICAN SOCIETY OF MECHANICAL ENGINEERS 1977. ASME steam tables - thermodynamic and transport properties of steam. ASME, New York, 3rd Edition, 1977, 329 p.

AMERICAN SOCIETY FOR TESTING AND MATERIALS 1963. Symposium on X-ray and electron probe analysis. Sixty-sixth annual meeting of ASTM, Atlantic City, N. J., June 27, 1963. ASTM Special Technical Publication No. 349, 209 p.

AMYX, J. A., BASS, D. M. Jr. and WHITING, R. L. 1960. Petroleum reservoir engineering. McGraw-Hill Book Company, New York, 610 p.

ANDERSON, D. R. (ed.) 1981. Proceedings of the Sixth Annual NEA-Seabed Working Group Meeting, Paris, France, published by Scandia National Laboratories, Albuquerque, New Mexico, 220 p.

ANNOR, A., MILES, P., KAPELLER, F. and LAROCQUE G. 1981. High temperature and pressure triaxial compression tests on rock samples from Pinawa and the Creighton Mine. Atomic Energy of Canada Limited, Technical Record TR-158, 32 p.

ATKIN, R. J. 1967. Constitutive theory for a mixture of an elastic isotropic solid and a non-Newtonian fluid. Zeitschrift for Angewandte Mathematik und Physik (ZAMP), 18, pp. 803-825.

AU, K. S. 1983. The strength-deformation properties of Alberta oil sands. M. Eng. Report, University of Alberta, 135 p.

AUSTIN, R. S. and DROULLARD, R. F. 1979. Effects of heating on Radon-222 emanation from domestic uranium ores. U.S. Department of the Interior, Bureau of Mines, Report of Investigations, #RI 8361, 46 p.

BARNES, D. J. 1980. Micro-fabric and strength studies of oil sands. M.Sc. Thesis, University of Alberta, Edmonton, Alberta, 244 p.

BARNES, D. J. and DUSSEAULT, M. B. 1980. The influence of diagenesis on the behaviour of oil sands. In Proceedings of Applied Oilsands Geoscince, edited by M. B. Dusseault, Edmonton, Alberta, 32 p.

BATHE, K. J. 1978. ADINA: A finite element program for automatic dynamic incremental nonlinear analysis. Report 82448-1, Massachusetts Institute of Technology, Cambridge, Massachusetts, 385 p.

BATHE, K. J. and WILSON, E. L. 1976. Numerical methods in finite element analysis. Prentice-Hall, Inc., Englewood Cliffs, New Jersey, 528 p.

BAUER, S. J. and JOHNSON, B. 1979. Effects of slow uniform heating in the physical properties of the Westerly and Charcoal granites. Proceedings of the 20th Symposium on Rock Mechanics, pp. 7-18.

BAWDEN, W. F. and McCREATH, D. R. 1979. Geotechnical study for an abandoned limestone mine for crude oil storage. Canadian Geotechnical Journal, Volume 16, No. 3, pp. 577-590.

BEAR, J. 1972. Dynamics of fluids in porous media. American Elsevier, New York, 562 p.

BEISER, A. 1975. The origin of rocks, In theory and problems of the earth sciences. McGraw-Hill Book Company, New York, 1975, 129 p.

BELL, M. L. and NUR, A. 1978. Strength changes due to reservoir-induced pore pressure and stresses with application to Lake Oroville. Journal of Geophysical Research, Vol. 83, No. B9, pp. 4469-4483.

BENNION, D. W., VORNDRAN, L., DONNELLY, J. K. and MOORE, R. G. 1977. Fire flooding changes in Athabasca bitumen. Oil Sand and Oil Shale Chemistry. Edited by Otto P. Strausz and Elizabeth M. Lown. Montreal, Canada, pp. 186-197.

BIOT, M. A. 1941. General theory of three-dimensional consolidation. Journal of Applied Physics, Vol. 12, February 1941, pp. 155-164.

BIOT, M. A. 1941. Consolidation settlement under a rectangular load distribution. Journal of Applied Physics, Vol. 12, May 1941, pp. 426-431.

BIOT, M. A. 1941. Consolidation settlement of a soil with an impervious top surface. Journal of Applied Physics, Vol. 12, July 1941, pp. 578-581.

BIOT, M. A. 1955. Theory of elasticity and consolidation for a porous anisotropic solid. Journal of Applied Physics, Vol. 25, No. 2, February 1955, pp. 182-185.

BIOT, M. A. 1959. Stability problems of inhomogeneous viscoelastic media. Non-Homogeneity in Elasticity and Plasticity. Proceedings of IUTAM, New York, Pergamon Press, 26 p.

BISHOP, A. W. 1959. The principle of effective stress. Teknisk Ukeblad, 106: No. 39, pp. 859-863.

BISHOP, A. W. 1966. Soils and soft rocks as engineering materials. Inaugural Lecture, Imperial College of Science and Technology, 6, pp. 289-313.

BISHOP, A. W. 1973. The influence of an undrained change in stress on the pore pressure in porous media of low compressibility. Geotechnique, Vol. 23, No. 3, pp. 435-442.

BISHOP, A. W. and HENKEL, D.J. 1962. The measurement of soil properties in the triaxial test. Second Edition, Edward Arnold (Publishers) Ltd., London, U. K., 227 p.

BLACK, D. K. and LEE, K. L. 1973. Saturating laboratory samples by back pressure. ASCE JSMFD SM1, Vol. 99, 75 p.

BOGA, S. K., HWANG, C. T. and KRISHNAYYA, A. V. G. 1980. Thermal foundation design for Syncrude's hot-bitumen tanks. Applied Oilsands Geoscience, Edmonton, Alberta, 41 p.

BOLEY, B. A. and WEINER, J. H. 1960. Theory of thermal stresses. John Wiley & Sons, Inc., New York, 470 p.

BONNET, G. and JOUANNA, P. 1980. Thermomechanical friction tests on artificial joints. International Journal of Rock Mechanics. Mineral Science and Geomechanics Abstract; Vol. 17, pp. 209-217.

BOON, J. A., HAMILTON, T., HOLLOWAY, L. and WIWCHAR, B. 1982. Reaction between rock matrix and injected fluids in Cold Lake oil sands - potential for formation damage. Petroleum Society of CIM, 6th Symposium on Engineering Applications of Mechanics, Calgary, Alberta, June 6-9, 1982. CIM Paper No. 82-33-37.

BRACE, W. F. 1980. Permeability of crystalline and argillaceous rocks. International Journal of Rock Mechanics, Mining Sciences and Geomechanical Abstracts, 17, pp. 241-251.

BRAUN, R. L. and CHIN, R. C. Y. 1977. Research and development on rubble in situ extraction of oil shale (RISE) at Lawrence Livermore Laboratory. In Proceedings of the 10th oil shale symposium. Edited by J. H. Gary. Colorado School of Mines, 166 p.

BRESCIA, F. ARENTS, J., MEISLICH, H. and TURK, A. 1980. Fundamentals of chemistry. Academic Press, Inc., New York, 782 p.

BROOKER, E. W. 1975. Tarsand mechanics and slope evaluation. 10th Canadian Rock Mechanics Symposium, Kingston, Ontario, September 1975, Vol. 1, pp. 409-446.

BROOKER, E. W., DEVENNY, D. W. and McRAE, A. M. 1978. Deep excavation in oil sand - why, where, how?. AOSTRA Seminar on Underground Excavation in Oil Sands, Edmonton, Alberta, Paper No. 12, 27 p.

BROOKER, E. W. and FARRUKH KHAN 1980. Design and performance of oil sand surface mine slopes. Applied Oil Sands Geoscience 1980. Edited by M. B. Dusseault. University of Alberta, Edmonton, 18 p.

BROWN, E. T., BRAY, J. W., LADANYI, B. and HOCK, E. 1983. Ground response curves for rock tunnels. American Society of Civil Engineers, Journal of Geotechnical Engineering, Vol. 109, No. 1, January, 1983, pp. 15-39.

BURCIK, E. J., 1957. Properties of petroleum reservoir fluids. International Human Resources Development Corporation, Boston, Ma., 190 p.

BURNHAM, C. W., HOLLOWAY, J. R. and DAVIS, N. F. 1969. Thermodynamic properties of water to 1000°C and 10,000 bars. Geological Society of America, Spec. Paper 132, Boulder, Colorado, 96 p.

BUTLER, R. M. and STEPHENS, D. J. 1981. The gravity drainage of steam-heated heavy oil to parallel horizontal wells. Journal of Canadian Petroleum Technology, April-June 1981, pp. 90-96.

BYRNE, P. M. and ELDRIDGE, T. L. 1982. A three parameter dilatant elastic stress-strain model for sand. International Symposium on Numerical Methods in Geomechanics, Zurich, Switzerland, September 13-17, 1982, pp. 73-80.

CAMP, F. W. 1970. The tar sands of Alberta, Canada. Manuscript published by Cameron Eng. Inc., Denver, Colorado, 82 p.

CAMPANELLA, R. G. and MITCHELL, J. K. 1968. Influence of temperature variations on soil behaviour. Journal of Geotechnical Engineering, ASCE, Vol. 94, SM3, May 1968, pp. 709-734.

CAMPBELL, J. H. and BURNHAM, A. K. 1980. Reaction kinetics for modelling oil shale retoring. In Situ, 4(1), pp. 1-37.

CANADIAN INSTITUTE OF STEEL CONSTRUCTION, 1970. Handbook of steel construction. Second Edition, Published by the Canadian Institute of Steel Construction, Toronto, Ontario, 720 p.

CARPENTER, H. C., JENSEN, H. B. and DECORA, A. W. 1977. Potential shale oil production processes. Symposium on Oil Sand and Oil Shale, Montreal, CIM, pp. 48-65.

CARRIGY, M. A. and KRAMERS, J. W. 1973. Guide to the Athabasca oil sands area. Published by Alberta Research Council, Information Series 65, 215 p.

CARRIGY, M. A. and KRAMERS, J. W. 1974. Geology of the Alberta oil sands. In Athabasca Oil Sands. Conference Proceedings, 1974, EIC, Western Region, pp. 13-24.

CARSLAW, H. S. and JAEGER, J. C. 1959. Conduction of heat in solids. 2nd Edition, Oxford University Press, London, 1959, 510 p.

CARTER, C. 1951. Soil temperature, moisture content and thermal properties. University of Tennessee, Engineering Experiment Station, Bulletin 15, 32 p.

CASSE, F. J. and RAMEY, H. J. 1979. The effect of temperature and confining pressure on single-phase flow in consolidated rocks. Journal of Petroleum Technology, August, 1979, pp. 1051-1059.

CEDERGREN, H. R. 1977. Seepage, drainage and flow nets. John Wiley & Sons, Inc., New York, 534 p.

CERVENAN, M. R., VERMEULEN, F. E. and CHUTE, F. S. 1980. Thermal conductivity and specific heat of oil sand samples. Applied Oilsands Geoscience 1980. Edited by M. B. Dusseault. University of Alberta, Edmonton, Alberta, 26 p.

CHAN, T. and JEFFREY, J. A. 1983. Scale and water saturation effects for thermal properties of low-porosity rock. Proceedings of the 24th U.S. Symposium on Rock Mechanics, Texas A & M University, pp. 287-302.

CHARLWOOD, R. G. 1981. Thermal-geomechanical analyses for the design of a mine assisted heavy oil recovery facility. AOSTRA Workshop on Computer Modelling. University of Alberta, January, 1981.

CHARLWOOD, R. G., BYRNE, P. M., MCKINLAY, D. W. and VAROGLU, E. 1980. Thermal geomechanical analyses and criteria for the design of a mine assisted heavy oil recovery facility. In Applied Oilsands Geoscience. M. Dusseault (editor). University of Alberta, Edmonton

CHEN, CHIA-SHYUM and REDDELL, D. L. 1983. Temperature distribution around a well during thermal injection and a graphical technique for evaluating aquifer thermal properties. Water Resources Research, Vol. 19, No. 2, pp. 351-363.

CHU, M. S. and CHANG, N. Y. 1980. Uniaxial creep of oil shale under elevated temperatures. In Rock Mechanics, A State of the Art. Proceedings of the 21st Symposium on Rock Mechanics, University of Missouri, Rolla, pp. 207-216.

CHUTE, F. S., VERMEULEN, F. E., CERVENAN, M. R. and McVEA, F. J. 1979. Electrical properties of Athabasca oil sands. Canadian Journal of Earth Sciences, Vol. 16, No. 10, pp. 2009-2021.

CLARK, K. A. 1957. Bulk densities, porosities and liquid saturations of good grade Athabasca oil sands. Edmonton: Research Council of Alberta, Mimeo., Circ. 22, 22 p.

CLARK, K. A. 1960. Permeabilities of the Athabasca oil sands. Transactions, Canadian Institute of Mining and Metallurgy (CIM), Vol. 63, pp. 151-156.

CLARK, S. P. 1966. Handbook of physical constants. The Geological Society of America, Memoir 97, 175 p.

CLOSMANN, P. J. and BRADLEY, W. B. 1979. The effect of temperature on tensile and compressive strengths and Young's modulus of oil shale. Society of Petroleum Engineers, Journal, 19, pp. 301-312.

CLOSMANN, P. J. and PHOCAS, D. M. 1978. Thermal stresses near a heated fracture in transversely isotropic oil shale. Society of Petroleum Engineers Journal, AIME, February, 1978, pp. 59-74.

COOK, N. G. W. 1983. Effects of joints on thermally induced displacements and stresses. Proceedings of the 24th U.S. Symposium on Rock Mechanics, Texas A & M University, pp. 303-308.

COOPER, H. W. and SIMMONS, G. 1977. The effects of cracks on thermal expansion of rocks. Earth Planetary and Scientific Letters, 36, pp. 404-413.

COX, D. O. 1978. Generalizations of the heat balance for thermal recovery projects. Proceedings of the Fifth Symposium on Improved Methods for Oil Recovery. Society of Petroleum Engineers of AIME, Tulsa, Oklahoma, pp. 451-458.

CRAMER, M. L., CUNNINGHAM, J. P. and KIM, K. 1983. Rock mass deformational properties from a large scale block test. Proceedings of the 24th U.S. Symposium on Rock Mechanics, Texas A & M University, pp. 267-270.

CRYER, C. W. 1963. A comparison of the three-dimensional consolidation theories of Biot and Terzaghi. Quarterly Journal of Mechanics and Applied Mathematics, Vol. 16, No. 4, pp. 401-412.

CULLITY, B. D. 1956. Elements of X-Ray diffraction. Addison-Wesley Publishing Co., Inc., Reading, Massachusetts, 1956, 514 p.

CUMMINS, A. B. and GIVEN, I. A. (editors), 1973. SME mining engineering handbook (Volumes I and II). Society of Mining Engineers of the American Institute of Mining, Metallurgical, and Petroleum Engineers, Inc., New York, 2615 p.

CURRY, D. M. and COX, J. E. 1971. Two-dimensional analysis of heat and mass transfer in porous media. Environmental and Geophysical Heat Transfer, Vol. 4, American Society of Mechanical Engineers (ASME), Heat Transfer Division, pp. 9-19.

DANIEL, D. E. 1983. Shallow land burial of low-level radioactive waste. American Society of Civil Engineers, Journal of Geotechnical Engineering, Vol. 109, No. 1, January 1983, pp. 40-55.

DAVIDSON, L. B. 1969. The effect of temperature on the permeability ratio of different fluid pairs in two-phase systems. Journal of Petroleum Technology, August 1969, pp. 1037-1046.

DAVIS, S. N. 1982. Hydrogeology of radioactive waste isolation. Geological Society of America, Special Paper 189, 1982, pp. 389-395.

DEALY, J. M. 1979. Viscosity of oil sands liquids. Progress Report to AOSTRA, 1979, Department of Chemical Engineerings, McGill University, Montreal, Quebec.

DEALY, J. M. 1979. Rheological properties of oil sand bitumens. Canadian Journal of Chemical Engineering, Vol. 57(6), 677 p.

DELANEY, P. T. 1982. Rapid intrusion of magma into wet rock: groundwater flow due to pore pressure increases. Journal of Geophysical Research, Vol. 87, No. B9, September 10, 1982, pp. 7739-7756.

DEMAISON, G. J. 1977. Tar sands and supergiant oil fields. In The Oil Sands of Canada-Venezuala. Edited by D. A. Redford and A. G. Winestock. CIM Special Volume 17, pp. 9-16.

DESAI, C. S. and CHRISTIAN, J. T. 1977. Numerical methods in geotechnical engineering. McGraw-Hill Book Company, New York, 1977, 783 p.

DEVENNY, D. W. and RAISBECK, J. M. 1980. Rock mechanics considerations for in-situ development of oil sands. In CIM Special Volume 22, Underground Rock Engineering, 13th Canadian Rock Mechanics Symposium, Toronto, 1980.

DUNCAN, J. M., BYRNE, P., WONG, K. S. and MABRY, P. 1980. Strength, stress-strain and bulk modulus parameters for finite element analyses of stresses and movements in soil masses. Report No. UCB/GT/80-01, College of Engineering, Office of Research Services, University of California, Berkeley, 80 p.

DUNCAN, J. M. and CHANG, C. Y. 1970. Nonlinear analysis of stress and strain in soils. Proceedings, Journal of Geotechnical Engineers, American Society of Civil Engineers, Vol. 96, pp. 1629-1654.

DUSSEAULT, M. B. 1977. The geotechnical characteristics of Athabasca oil sands. Ph. D. Thesis, University of Alberta, Edmonton, 1977.

DUSSEAULT, M. B. 1980. Sample disturbance in Athabasca oil sands. Journal of Canadian Petroleum Technology, Vol. 19, No. 2.

DUSSEAULT, M. B. and MORGENSTERN, N. R. 1978a. Characteristics of natural slopes in the Athabasca oil sands. Canadian Geotechnical Journal, Vol. 15, pp. 202-215.

DUSSEAULT, M. B. and MORGENSTERN, N. R. 1978b. Shear strength of Athabasca oil sands. Canadian Geotechnical Journal, Vol. 15, pp. 216-238.

DUSSEAULT, M. B. and MORGENSTERN, N. R. 1978c. Locked sands. University of Alberta, Department of Civil Engineering, Internal Memorandum.

DUSSEAULT, M. B. and NYLAND, E. 1982. Fireflood microseismic monitoring: rock mechanics implications. In Proceedings of the Twenty-third Symposium on Rock Mechanics, Berkeley, California, published by the Society of Mining Engineers of AIME, pp. 1065-1076.

DUSSEAULT, M. B. and SIMMONS, J. V. 1982. Injection induced stress and fracture orientation changes. Canadian Geotechnical Journal, Vol. 19, No. 4, November, 1982, pp. 483-498.

DUSSEAULT, M. B. and STERNE, K. B. 1980. University of Alberta, Department of Civil Engineering, Edmonton, Alberta, Personal Communication.

DUSSEAULT, M. B. and VAN DOMSELAAR, H. R. 1982. Unconsolidated sand sampling in Canadian and Venezualan oil sands. Second Unitar Conference on the Future of Heavy Crudes and Tar Sands, Caracas, Venezuala.

EDMONSON, T. A. 1965. Effect of temperature on waterflooding. Petroleum Society of CIM, Heavy Oil Seminar, Calgary, Alberta, May 5, 1965, pp. 236-242.

EISENSTEIN, Z. and LAW, S. T. C. 1979. The role of constitutive laws in analysis of embankments. Third International Conference on Numerical Methods in Geomechanics. Edited by W. Wittke, Aachen, April 2-6, 1979, pp. 1413-1430.

EISENSTEIN, Z. and MEDEIROS, L. V. 1983. Deep retaining structure in till and sand. Canadian Geotechnical Journal, Vol. 20, No. 1, pp. 131-140.

ENERGY RESOURCES CONSERVATION BOARD OF ALBERTA 1973. Geology and proved in-place reserves of the Cold Lake oil sands deposits. Calgary, Alberta, September, 1973.

ENERGY RESOURCES CONSERVATION BOARD OF ALBERTA 1974. Geology and proved in-place reserves of the Peace River oil sands deposits. Calgary, Alberta, October, 1974.

ENERGY RESOURCES CONSERVATION BOARD OF ALBERTA 1976. Geology and proved in-place reserves of the Wabasca oil sands deposits. Calgary, Alberta, May, 1976.

ENNISS, D. O., BUTTERS, S. W., McFARLAND, C. B. JR. and JONES, A. H. 1979. Capabilities to determine rock properties at simulated geothermal conditions. Transactions of the American Society of Mechanical Engineers, Journal of Energy Resources Technology, Volume 101, No. 117, pp. 117-123.

EVGIN, E. 1981. Evaluation of an elasto-plastic model. Ph. D. Thesis, University of Alberta, Edmonton, Alberta, 197 p.

FACCA, G. 1980. Geothermal energy development: an historic summary. Geothermal Energy, Vol. 8, No. 10 & 11, October-November, 1980, 12 p.

FAROUQ-ALI, S. M. 1967. Fluid viscosity, its estimation, measurement and role in thermal recovery. Producers Monthly, pp. 20-25.

FAROUQ-ALI, S. M. 1974. Application of in situ methods of oil recovery from tar sands. In Oil Sands Fuel of the Future, Canadian Society of Petroleum Geologists, Calgary, pp.199-212.

FAROUQ-ALI, S. M. 1981. Elements of reservoir modelling. Department of Mineral Engineering, University of Alberta, Edmonton, Alberta, 64 p.

FAROUQ-ALI, S. M. 1982. Integrated simulation of oil and gas production and the accompanying rock deformations. Proceedings of the Fourth International Conference on Numerical Methods in Geomechanics, Edmonton, Alberta, Volume 3, pp. 1081-1090.

FINN, F. N. 1951. The effect of temperature on consolidation characteristics of remoulded clay. ASTM, STP No. 120, pp. 65-71.

FINNIE, I., COOPER, G. A. and BERLIE, J. 1979. Fracture propagation in rock by transient cooling. International Journal of Rock Mechanics, Mining Science and Geomechanics Abstract, Vol. 16, pp. 11-21.

FREDLUND, D. G. 1976. Density and compressibility characteristics of air-water mixtures. Canadian Geotechnical Journal, Vol. 13, pp. 386-396.

FREEZE, R. A. and CHERRY, J. A. 1979. Groundwater. Prentice-Hall International, Inc., London, 604 p.

FRYDMAN, S. 1968. The effect of stress history on the stress deformation behaviour of sand. M.Sc. Thesis, Technion-Israel Institute of Technology, Haifa, 170 p.

FRYDMAN, S. 1972. An Inquiry into the stress-strain behaviour of particulate media. D.Sc. Thesis, Technion-Israel Institute of Technology, Haifa, April, 1972, 240 p.

FUNG, Y. C. 1965. Foundations of solid mechanics. Prentice-Hall, Inc., Englewood Cliffs, New Jersey, 1965, 525 p.

GARG, S. K., PRITCHETT, J. W., RICE, M. H. and RINEY, T. D. 1977. U.S. Gulf coast geopressured geothermal reservoir simulation. Systems, Science and Software Report No. SSS-R-77-3147, University of Texas at Austin and U. S. Energy Research and Development Adminstration Contract E (40-1)-5040, February, 1977, 113 p.

GATES, E. M. and GILPIN, R. R. 1978. Jet cutting of oil sand. In AOSTRA Seminar on Underground Excavation in Oil Sand, University of Alberta, Edmonton, Alberta, Paper No. 10, 14 p.

GEERTSMA, J. 1973a. Survey of rock mechanics problems associated with the extraction of mineral fluids from underground formations. Proceedings of the Third Congress of the International Society for Rock Mechanics, Vol. 1, Part B, May, 1973, pp. 1471-1481.

GEERTSMA, J. 1973b. Land subsidence above compacting oil and gas reservoirs. Transactions of the American Institute of Mining Engineers, Vol. 255, 1973, pp. 734-744.

GEERTSMA, J. 1974. Estimating the coefficient of inertial resistance in fluid flow through porous media. Society of Petroleum Engineers of American Institute of Mining Engineers Journal, Vol. 14, pp. 445-451.

GHABOUSSI, J. and WILSON, E. L. 1972. Variational formulation of dynamics of fluid saturated porous elastic solids. Journal of Engineering Mechanics Division of ASCE, Vol. 98, No. EM4, pp. 947-963.

GIBSON, R. E., KNIGHT, K. and TAYLOR, P. W. 1963. A critical experiment to examine theories of three-dimensional consolidation. Proceedings of the European Conference on Soil Mechanics and Foundation Engineering, Weisbaden, Vol. 1, pp. 69-76.

GIGUERE, R. J. 1976. An *in situ* recovery process for the oil sands of Alberta. 26th Chemical Engineering Conference, Symposium on Tar Sands, Toronto, Ontario, 1976.

GOBRAN, B. D. 1981. Permeability of unconsolidated sands and sandstone with temperature, pore pressure and confining pressure. Ph.D. Dissertation, Stanford University, 210 p.

GOBRAN, B. D., BRIGHAM, W. E. and RAMEY, H. J. 1981. Absolute permeability as a function of confining pressure, pore pressure and temperature. Society of Petroleum Engineers of the American Institute of Mining Engineers. Proceedings, 56th Annual Fall Technical Conference, San Antonio, Texas, October 5-7, 1981.

GOETZE, C. 1971. High temperature rheology of Westerly granite. Journal of Geophysical Research, 76, pp. 1223-1230.

GOLDSTEIN, J. I. and YAKOWITZ, H. 1975. Practical scanning electron miscroscopy. Plenum Press, New York, 1975, 582 p.

GRANDONE, P. and HOLLEYMAN, J. B. 1949. Injection rates and pressures for water flooding mid-continent oil sands. U.S. Department of the Interior, Bureau of Mines, Report of Investigations 4600, 31 p.

GREEN, G. E. 1969. Strength and compressibility of granular materials under generalized strain conditions. Ph. D., University of London.

GREEN, S. 1983. Personal communication on heat consolidation and strength of Pacific illite clays (to 200°C). Ph. D. research in progress, Department of Civil Engineering, University of California, Berkley.

GREG, D. W. 1977. Ground subsidence resulting from underground gasification of coal. Lawrence Livermore Laboratory, Report UCRL-52255, 42 p.

GREG, D. W. 1980. Relative merits of alternate linking techniques for underground coal gasification and their system design implications. *In Situ*, 4(3), pp. 207-236.

GREG, D. W., HILL, R. W. and OLNESS, D. U. 1976. An overview of the Soviet effort in underground gasification of coal. Lawrence Livermore Laboratory, Report UCRL-52004, 66 p.

GREG, D. W. and OLNESS, D. U. 1976. Basic principles of underground coal gasification. Lawrence Livermore Laboratory, Report UCRL-52107, 36 p.

GRIM, R. E. 1968. Clay mineralogy. McGraw-Hill, Toronto, Ontario, 1968, 596 p.

HACKBARTH, D. A. 1978. Hydrogeological concerns in underground excavation, Athabasca oil sands area. In AOSTRA Seminar on Underground Excavation in Oil Sands, University of Alberta, Edmonton, Paper No. 2, 28 p.

HANLEY, E. J., DEWITT, D. P. and ROY, R. F. 1978. The thermal diffusivity of eight well characterized rocks for the temperature range 300-1000 K. Engineering Geology, 12, pp. 31-47.

HARDIN, E. L., VOEGELE, M. D., BOARD, M. P. and PRATT, H. R. 1983. Development of a test series to determine in situ thermomechanical and transport properties. Symposium on Measurement of Rock Properties At Elevated Pressures and Temperatures, College Station, Texas, American Society for Testing and Materials, pp.?

HARDY, R. M. 1980. Implications of the peculiar geotechnical characteristics of tar sand to the design of viable open pit mining plants. Oil Sands Geoscience Conference. Edited by M. B. Dusseault, Edmonton, Alberta, 16 p.

HARDY, R. M. and HEMSTOCK, R. A. 1963. Shearing strength characteristics of Athabasca oil sands. In The K. A. Clark Volume on the Athabasca Oil Sands. Edited by M. A. Carrigy, published by The Research Council of Alberta, Information Series No. 45, pp. 109-122.

HARDY, R. M. and SCOTT, J. D. 1978. The 1963 G.C.O.S. test shaft. In AOSTRA Seminar on Underground Excavation in Oil Sand, University of Alberta, Edmonton, Paper No. 13, 22 p.

HARR, M. E. 1962. Groundwater and seepage. McGraw-Hill Book Company, New York, 315 p.

HARRIS, M. C. and SOBKOWICZ, J. C. 1977. Engineering behaviour of oil sand. The Oil Sands of Canada-Venezuala, CIM Special Volume 17. Edited by D. A. Redford and A. G. Winestock, pp. 270-282.

HARRIS, M. C. and SOBKOWICZ, J. C. 1978. Feasibility study of underground mining of oil sand. In AOSTRA Seminar on Underground Excavation in Oil Sands, 1978, University of Alberta, Edmonton, Paper No. 5, 23 p.

HARRISON, D. B., GLAISTE, R. P. and NELSON, H. W. 1979. Reservoir description of the clearwater oil sand, Cold Lake, Alberta, Canada. In First International Conference on the Future of Heavy Crude Oils and Tar Sands. UNITAR, Edited by R. F. Meyer and C. T. Steele, Chapter 30, pp. 264-280.

HART, R. D. 1980. A fully coupled thermal-hydraulic-mechanical model for nonlinear geologic systems. Ph.D. Dissertation, University of Minnesota, 327 p.

HASTON, J. A 1978. Mine assisted *in situ* processing. *In* AOSTRA Seminar on Underground Excavation In Oil Sands, May 19, 1978, University of Alberta, Edmonton, Paper No. 4, 23 p.

HAY, R. S. and EVANS, J. B. 1983. Grain boundary grooving of calcite bicrystals. Proceedings of the 24th U.S. Symposium on Rock Mechanics, Texas A & M University, pp. 469-472.

HEARD, H. C. 1980. Thermal expansion and inferred permeability of Climax quartz monzonite to 300°C and 27.6 MPa. International Journal of Rock Mechanics, Mining Sciences and Geomechanics Abstracts, 17, pp. 289-296.

HEARD, H. C. 1982. Mechanical, thermal and fluid transport properties of rock at depth. *In* Proceedings of the Twenty-Third Symposium on Rock Mechanics, Berkeley, California. Published by the Society of Mining Engineers of the American Institute of Mining, Metallurgical and Petroleum Engineers, Inc., New York, pp. 249-260.

HEARD, H. C. and PAGE, L. 1982. Elastic moduli, thermal expansion and inferred permeability of two granites to 350°C and 55 Megapascals. Journal of Geophysical Research, Vol. 87, No. B11, pp. 9340-9348.

HEARD, H. C. and RALEIGH, C. B. 1971. Steady-state flow in marble at 500°C to 800°C. Geological Society of America Bulletin.

HENNIG-MICHAELI, C. and SIEMES, H. 1982. Compression experiments on natural magnetite crystals at 200°C and 400°C at 400 MPa confining pressure. *In* Proceedings of the Twenty-third Symposium on Rock Mechanics, Berkeley, California. Published by the Society of Mining Engineers of the American Institute of Mining Engineers, New York, pp. 380-388.

HEUZE, F. E. 1981. On the geotechnical modelling of high level nuclear waste disposal by rock melting. Lawrence Livermore Laboratory, University of California, Manuscript UCRL-53183, 53 p., published by National Technical Information Service, U.S. Department of Commerce, Springfield, VA 22161.

HEUZE, F. E. 1983a. High temperature mechanical, physical and thermal properties of granitic rocks-a review. International Journal of Rock Mechanics, Mining Sciences and Geomechanical Abstracts, Volume 20, No. 1, pp. 3-10.

HEUZE, F. E. 1983b. Thermal and thermomechanical calculations of deep-rock nuclear waste disposal with the enhanced SANGRE code. Lawrence Livermore Laboratory, University of California, Manuscript UCRL-53394, 42 p., published by National Technical Information Service, U.S. Department of Commerce, Springfield, Va 22161.

HIGHWAY RESEARCH BOARD 1969. Effects of temperature and heat on the engineering behavior of soil. Special Report 103, 225 p.

HINGA, K. R., 1982. Ocean research conducted for the subseabed disposal program. EOS, Transactions, American Geophysical Union, Vol. 63, No. 40, October 5, 1982, pp. 802-803.

HINGA, K. R., HEATH, G. R., ANDERSON, D. R. and HOLLISTER, C. D. 1982. Disposal of high-level radioactive wastes by burial in the sea floor. Environment Science Technology, No. 16, pp. 28A-37A.

HOEK, E. and BROWN, E. T. 1980. Underground excavations in rock. Published by the Institute of Mining and Metallurgy, London, 527 p.

HOLMAN, J. P. 1976. Heat transfer. McGraw-Hill Book Company, New York, 4th Edition, 1976, 528 p.

HOLZHAUSEN, G. R., WOOD, M. D., RAISBECK, J. M. and CARD, C. C. 1980. Results of deformation monitoring during steam injection in a single well test. Applied Oilsands Geoscience, Edmonton, Alberta, June 1980.

HOLZHAUSEN, G. R., WOOD, M. D., RAISBECK, J. M. and CARD, C. C. 1980. Results of deformation monitoring during steam stimulation in a single well test. Applied Oilsands Geoscience. Edited by M. B. Dusseault. University of Alberta, Edmonton, Alberta, June 1980.

HORNBECK, R. W. 1975. Numerical methods. Quantum Publishers Inc., New York, New York, 310 p.

HORSRUD, P., RISNES, R. and BRATLI, R. K. 1982. Fracture initiation pressures in permeable poorly consolidated sands. International Journal of Rock Mechanics. Mineral Science and Geomechanics Abstract; Vol. 19, pp. 255-266, December 1982.

HOSKINS, W. N., UPADHYAY, R. P., BILLS, J. B. and SANBERG, C. R. 1977. A technical and economic study of candidate underground mining systems for deep, thick oil shale deposits. Quarterly of the Colorado School of Mines, pp. 199-234.

HUNGR, O. and MORGENSTERN, N. R. 1980. A numerical approach to predicting stresses and displacements around a three-dimensional pressurized fracture. Internal Report, Department of Civil Engineering, University of Alberta, Edmonton, Alberta, April 1980.

HUTCHEON, W. L. 1958. Moisture flow induced by thermal gradients within soils. Special Report No. 40, Highway Research Board, National Research Council, Washington, D.C., pp. 113-133, 1958.

HUYGEN, H. A. and LOWRY, W. E. 1983. Steamflooding Wabasca tar sand through the bottomwater zone-scaled model tests. Society of Petroleum Engineers Journal, Vol. 23, No. 1.

HWANG, C. T., MORGENSTERN, N. R. and MURRAY, D. T. 1971. On solutions of plane strain consolidation probelms by finite element methods. Canadian Geotechnical Journal, Vol. 8, No. 1, pp. 109-118.

IMPERIAL OIL LIMITED 1978. The Cold Lake Project: A report to the Energy Resources Conservation Board. Calgary, Alberta, 3 Volumes.

ISHIJIMA, Y. and ROGIERS, J.-C. 1983. Fracture initiation and breakdown pressure-are they similar? Proceedings of the 24th U.S. Symposium on Rock Mechanics, Texas A & M University, pp. 761-772.

JAEGER, J. C. and COOK, N. G. W. 1979. Fundamentals of rock mechanics. Chapman and Hall, London, England, 3rd Edition, 593 p.

JAPANESE SOCIETY OF MECHANICAL ENGINEERS 1968. JSME Steam Tables, 3rd Edition, JSME, Tokyo, Japan, 1968, 116 p.

KNAPP, R. B. and KNIGHT, J. E. 1977. Differential thermal expansion of pore fluids: fracture propogation and microearthquake production in a hot pluton environment. Journal of Geophysical Research, 82, pp. 2515-2522.

KNAPP, R. B. and NORTON, D. 1981. Preliminary numerical analysis of processes related to magma crystallization and stress evolution in cooling pluton environments, American Journal of Science, 281, pp. 35-68.

KOSAR, K. M. 1983. The effect of heated foundations on oil sand. M.Sc. Thesis, University of Alberta, 248 p.

KERN, L.R. 1980. Use of weighted brines in recovery of geothermal energy from hot dry rock. Geothermal Energy, Vol. 8, No. 2, 12 p.

KERSTEN, M. 1949. Thermal properties of soils. Bulletin No. 28, Engineering Experiment Station, University of Minnesota Institute of Technology, Vol. 52, No. 21, 262 p.

KOKELAAR, B. P. 1982. Fluidization of wet sediments during the emplacement and cooling of various igneous bodies. Journal of the Geological Society, Vol. 139, Part 1, pp. 21-33.

KONDNER, R. L. 1963. Hyperbolic stress-strain response: cohesive soils. Proceedings of the American Society of Civil Engineers, Journal of the Soil Mechanics and Foundations Division, SM1, February 1963, pp. 115-143.

KULHAWY, F. H. and DUNCAN, J.M. 1972. Stresses and movements in Oroville Dam. Proceedings of the American Society of Civil Engineers, Journal of the Soil Mechanics and Foundations Division, SM7, July 1972, pp. 653-665.

LACHENBRUCH, A. H. 1980. Frictional heating, fluid pressure and the resistance to fault motion. Journal of Geophysical Research, Vol. 85, No. B11, pp. 6097-6112.

LADE, P. V. and DUNCAN, J. M. 1975. Elastoplastic stress-strain theory for cohesionless soils. Journal of the Geotechnical Engineering Division, ASCE, Vol. 101, No. GT10.

LAMBE, T. W. and WHITMAN, R. V. 1969. Soil mechanics. John Wiley & Sons, Inc., New York, 553 p.

LANGER, M. 1982. Geotechnical investigation methods for rock salt. Bulletin of the International Association of Engineering Geologists, No. 25, June 1982, pp. 155-164.

LAUMBACH, D. D. 1975. A high-accuracy finite-difference technique for testing the convective-diffusion equation. Society of Petroleum Engineers Journal, AIME, December 1975, pp. 517-531.

LAURIELLO, P. J. 1974. Application of a convective heat source to the thermal fracturing of rock. International Journal of Rock Mechanics, Mining Sciences and Geomechanics Abstracts; Vol. 11, pp. 75-81.

LEE, C. F. and SIMMONS, G. R. 1981. Thermal effects on rock and fluid flow. Proceedings of the 9th Waste Management Information Meeting, AECL, Toronto, Ontario, January 1981.

LEE, K. L., MORRISON, R. A. and HALEY, S. C. 1969. A note on the pore pressure parameter B. Proceedings of the 7th International Conference on Soil Mechanics and Foundation Engineering, pp. 231-237.

LEHNOFF, T. F. and SCHELLER, J. D. 1975. The influence of temperature dependent properties on thermal rock fragmentation. International Journal of Rock Mechanic, Mining Sciences and Geomechanics Abstracts; Vol. 12, pp. 255-260.

LEWIS, A. E. and ROTHMAN, A. J. 1975. Rubble in situ extraction (RISE): a proposed program for recovery of oil from oil shale. National Technical Information Service, U.S. Department of Commerce, 32 p.

LIN, C. J. and WHEELER, J. D. 1978. Simulation of permafrost thaw behaviour at Prudhoe Bay. Journal of Petroleum Technology, Vol. 30, March 1978, pp. 461-467.

LIN, HORN-DA 1983. Personal communication on heat consolidation and strength of Pacific illite clays (4°C-40°C). Ph.D. research in progress, Department of Civil Engineering, University of California, Berkley.

LINDROTH, D. P. 1974. Thermal diffusivity of six igneous rocks at elevated temperatures and reduced pressures. U.S. Bureau of Mines, Report of Investigations, RI7954, 21 p.

LO, H. Y. and MUNGAN, N. 1973. Temperature effect on relative permeabilities and residual saturations. Petroleum Recovery Research Institute, Calgary, Alberta, Research Report RR-19, April 1973, 36 p.

LO, K. Y. and WAI, R. S. C. 1982. Thermal expansion, diffusivity and cracking of rock cores from Darlington, Ontario. Canadian Geotechnical Journal, Vol. 19, No. 2, May 1982, pp. 154-166.

LOCKNER, D. A., SUMMERS, R., MOORE, D. and BYERLEE, J. D. 1982. Laboratory measurements of reservoir rock from the Geysers Geothermal Field, California. International Journal of Rock Mechanic, Mining Sciences and Geomechanical Abstracts; Vol. 19, pp. 65-80, 1982.

LUNDSTROM, L. and STILLE, H. 1978. Large scale permeability tests in the granite of the Stripa Mine (Sweden). Lawrence Berkeley Laboratory, Research Report #LBL-7052.

MAINI, B. and SAYEGH, S. 1983. Laboratory techniques for investigating recovery in heavy oil reservoirs. Alberta Oil Sands Technology and Research Authority, Proceedings of the 4th Annual Conference on Advances in Petroleum Recovery Technology, Calgary, Alberta, 31 p.

MAINLAND, G. G. 1983. The development of in-situ recovery technology at Cold Lake. Alberta Oil Sands Technology and Research Authority, Proceedings of the 4th Annual Conference on Advances in Petroleum Recovery Technology, Calgary, Alberta, 13 p.

MANDEL, J. 1957. Consolidation des sols. Geotechnique, Volume 3, pp. 287-299.

MATHEWS, C. S. , VAN MEURS, P. and VOLEK, C. W. 1969. Process for horizontally fracturing subterranean earth formations. U.S. Patent No. 3, 455, 391; July 15, 1969.

MATHEWS, K. E. 1980. Potential of the underground mining of oil sands in Canada. Rockstore '80, Proceedings of the International Symposium on Subsurface Space for Environmental Protection, Low-Cost Storage and Energy Savings, Stockholm, Sweden, June 1980.

MATHEWS, K. E. , RAWLINGS, G.E. and BHARTI, S. 1980. Investigation of the geotechnical and mining characteristics of the Devonian Limestones Athabasca Oil Sands area. Applied Oilsands Geoscience Conference. Edited by M. Dusseault. University of Alberta, Edmonton, Alberta, 1980.

MAUGH, T. H. 1977. Underground gasification: an alternate way to exploit coal. Science, Vol. 198, December 16, 1977, pp. 1132-1134.

MAXWELL, J. C. 1960. Experiments on compaction and cementation of sand. In Rock Deformation. Edited by Griggs and Handin, pp. 105-132.

McCLAIN, W. C. 1969. The mechanics of hydraulic fractures in shales. The Northern Ohio Geological Society Inc. Proceedings of the 3rd Symposium on Salt, Vol. 2, pp. 410-420. The Northern Ohio Geological Society Inc.

MEDEIROS, L. V. and EISENSTEIN, Z. 1982. Stress path effects in till and sand. Canadian Geotechnical Journal, Vol. 20, No. 1, pp. 120-130.

MERCER, J. W. , FAUST, C. R., MILLER, W. J. and PEARSON, F. J., JR. 1982. Review of simulation techniques for aquifer thermal energy storage (ATES). In Advances in Hydroscience, Volume 13, edited by Ven Te Chow, pp. 1-129.

MESRI, G., ADACHI, K. and ULRICH, C.R. 1976. Pore pressure response in rock to undrained change in all round stress. Geotechnique 26, No. 2, June 1976, pp. 317-330.

MILNE, W. E. 1970. Numerical solution of differential equations. Dover Publications, Inc., New York, 360 p.

MINKEN, D. F. 1974. The Cold Lake Oil Sands: Geology and a reserves estimate. In Oil Sands, Fuel of the Future. Edited by L.V. Hills. CSPG, Memoir 3, pp. 84-99.

MITCHELL, J. K. 1969. Temperature effects on the engineering properties and behavior of soils. NRC Highway Research Board, Special Report 103, pp. 3-32.

MITCHELL, J. K. 1976. Fundamentals of soil behaviour. John Wiley and Sons Inc., 422 p.

MITCHELL, R. F. and GOODMAN, M. A. 1978. Permafrost thaw-subsidence casing design. Journal of Petroleum Technology, Vol. 30, March 1978, pp. 455-460.

MOGI, K. 1972. Fracture and flow of rocks. In The Upper Mantle. Edited by A. R. Ritsema. Tectonophysics, 13 (1-4), pp. 541-568.

MOORE, D. E., SUMMERS, R. and BYERLEE, J. D. 1983. Strengths of clay and non-clay fault gauges at elevated temperatures and pressures. Proceedings of the 24th U.S. Symposium on Rock Mechancis, Texas A & M University, pp. 489-500.

MORGENSTERN, N. R. 1962. A relation between hydraulic fracture pressure and tectonic stresses. Geofisca Pura E Applicate, Volume 52, pp. 104-114.

MORGENSTERN, N. R. 1981. Geotechnical engineering and frontier resource development. 21st Rankine Lecture, March 1981, Geotechnique 31, pp. 303-365.

MORROW, C., MOORE, D. and BYERLEE, J. 1983. Permeability and pore-fluid chemistry of the Bullfrog tuff in a temperature gradient. Proceedings of the 24th U.S. Symposium on Rock Mechanics, Texas A & M University, pp. 819-828.

MOSSOP, G. D. 1978a. Geological controls on reservoir heterogeneity in Athabasca oil sands. In AOSTRA seminar on Underground Excavation in Oil Sands, University of Alberta, Edmonton, Alberta, Paper No. 1, 27 p.

MOSSOP, G. D. 1978b. Facies control on bitumen saturation in the Athabasca oil sands. Canadian Society of Petroleum Geologists, Calgary, Alberta, Memoir 6, June 1978.

MOSSOP, G. D. 1980. Geology of the Athabasca Oil Sands. Science, Vol. 207, No. 11, January 1980, pp. 145-152.

MOSSOP, G. D., KRAMERS, J. W., FLACH, P. D. and ROTTENFUSSER, B. A. 1979. Geology of Alberta's oil sands and heavy oil deposits. In Proceedings of the 1st International Conference on the Future of Heavy Crude and Tar Sands, June 4-12, 1979, McGraw-Hill, New York, pp. 197-207.

MUSKAT, M. 1946. The flow of homogeneous fluids through porous media. J.W. Edwards Inc, 1st Edition, Ann Arbor, Michigan, 1946, 755 p.

MYSEN, B. O. 1981. Melting curves and viscosity of rock forming melts. In Physical Properties of Rocks and Minerals, Chapter 11, edited by Touloukian & Ho, McGraw-Hill, New York, pp. 361-407.

NAKORNTHAP, K. and EVANS, R. D. 1982. Temperature dependent relative permeability and its effect upon oil displacement by thermal methods. Society of Petroleum Engineering of AIME, 57th Annual Fall Technical Conference, New Orleans, LA., September 26-29, 1982.

NUR, A. and BYERLEE, J. D. 1971. An exact effective stress law for elastic deformation of rock with fluids. Journal of Geophysical Research, Vol. 76, No. 26, September 1971.

NYLAND, E. and DUSSEAULT, M. B. 1983. Fireflood microseismic monitoring: results and potential for process control. Journal of Canadian Petrolum Technology, March-April 1983, pp. 62-68.

OIL AND GAS CONSERVATION BOARD OF THE PROVINCE OF ALBERTA 1963. A description and reserve estimate of the oil sands of Alberta. Calgary, Alberta, 1963, 124 p.

OLSSON, J. T. 1974. Effects of temperature, pressure and displacement on the frictional characteristics of a limestone. International Journal of Rock Mechanics, Mining Sciences and Geomechanical Abstracts, Volume 11, pp. 267-281.

PAASWELL, R. E. 1967. Temperature effects on clay soil consolidation. ASCE, JSMFD, Vol. 93, SM3, pp. 9-22, May 1967.

PAGE L. and HEARD, H. C. 1981. Elastic moduli, thermal expansion and inferred permeability of climax quartz monzonite and Sudbury glabbro to 500°C and 55 MPa. Journal of Geophysical Research, Vol. 4, 1981, pp. 97-103.

PALCIAUSKAS, V. V. and DOMENICA, P. A. 1982. Characterization of drained and undrained response of thermally loaded repository rocks. Water Resources Research, Vol. 18. No. 2, pp. 281-290, April 1982.

PAMATMAT, M .M. 1982. Heat production by sediment: ecological significance. Science, Vol. 215, pp. 395-397, January 22, 1982.

PAQUET, J. and FRANCOIS, P. 1980. Experimental deformation of partially melted granitic rocks at 600-900°C and 250 MPa confining pressures. Tectonophysics, 68, pp. 131-146.

PARRISH, D. K., KRIVZ, A. L. and CARTER, N. L. 1976. Finite element folds of similar geometry. Tectonophysics, 32, pp. 183-207.

PARSONS, L. J. and HEMSTOCK, J. D. 1983. Peace River in-situ project: current operations and future outlook. Alberta Oil Sands Technology and Research Authority, 4th Annual Conference on Advances in Petroleum Recovery Technology, Calgary, Alberta, 22 p.

PATCHING, T., JEREMIC, M. and STIMPSON, B. 1978. On the possibility of mining oil sand by underground methods. In AOSTRA Seminar on Underground Excavation in Oil Sands, University of Alberta, Edmonton, Alberta, Paper No. 3, 17 p.

PATTON, F. D. and SCOTT, J. D. 1980. Subsurface monitoring for deep in-situ oil sand production. Oilsands Geoscience '80. Edited by M. B. Dusseault. University of Alberta, Edmonton, Alberta, June 1980.

PEACEMAN, D. W. and RACHFORD, H. H. 1962. Numerical calculation of multidimensional miscible displacement. Society Petroleum Engineers Journal, December 1962, Trans. AIME, Vol. 225, pp. 327-339.

PEARSON, C. 1981. The relationship between microseismicity and high pore pressures during hydraulic stimulation experiments in low permeability granitic rocks. Journal of Geophysical Research, 86, pp. 7855-7864.

PERRY, C. and GILLOTT, J. E. 1982. Mineralogical transformations as indicators of combustion zone temperatures during in-situ combustion. Bulletin of Canadian Petroleum Geology, Vol. 30, No. 1, March 1982, pp. 34-42.

PINCUS, H. J., HANDIN, J., JUDD, W. R. and ENGELDER, T. 1982. Rock mechanics research requirements for resource recovery, construction and earthquake hazard reduction. EOS, Transactions, American Geophysical Union, Vol. 23, No. 25, June 22, 1982, pp. 545-547.

PLUM, R. L. and ESRIG, M. I. 1969. Some temperature effects on soil compressibility and pore water pressure. HRB Special Report 103, pp. 231-242.

POLLARD, D. P. and JOHNSON, A. M. 1973a. Mechanics of growth of some laccolith intrusions in the Henry Mountains, Utah, I: Field observations, Gilbert's model, physical properties and flow of the magma. Tectonophysics, 18, pp. 261-309.

POLLARD, D. P. and JOHNSON, A. M. 1973b. Mechanics of growth of some laccolith structures in the Henry Mountains, Utah, II: Bending and failure of overburden layers and sill formation. Tectonophysics, 18, p. 311-354.

POLLARD, D. P. and MULLER, O. H. 1976. The effect of gradients in regional stress and magma pressure on the form of stress intrusions in cross sections. Journal of Geophysical Research, Vol. 81, No. 5, pp. 975-984.

POULOS, H. G. and DAVIS, E. H. 1974. Elastic solutions for soil and rock mechanics. John Wiley & Sons, New York, 411 p.

POULOS, S. J. 1981. The steady state of deformation. JGED, Proceedings ASCE, Vol. 107, No. GT5, May 1981, pp. 553-561.

RADHAKRISHNA, H. S. 1968. Heat flow and moisture migration in cable backfills. Ontario Hydro Research Quarterly, 20, No. 2, 16 p.

RADHAKRISHNA, H. S. and TSUI, K. K. 1981. Thermal properties of buffer/backfill materials and their effects on the near-field thermal regime in a nuclear fuel waste disposal vault. Proceedings of the 9th Waste Management Meeting, AECL, 18 p.

RAISBECK, J. M. and CARD, C. C. 1978. Recovery of heavy oil from oil sands. Proceedings of the 28th Canadian Chemical Engineering Conference, Halifax, Nova Scotia.

RAISBECK, J. M. and CURRIE, J. B. 1981. A laboratory investigation of hydraulic fracturing in oil sands. In Situ, 5 (1), pp. 1-24.

REYNOLDS, D. L. 1954. Fluidization as a geological process, and its bearing on the problem of intrusive granites. American Journal of Science, Volume 252, pp. 577-614.

RICHTER, D. and SIMMONS, G. 1974. Thermal expansion behaviour of igneous rocks. International Journal of Rock Mechanics. Mineral Science and Geomechanic Abstract; Vol. 11, pp. 403-411, 1974.

ROBINSON, D. B. and SIM, S. K. 1981. The behavior of bitumen mixtures during in-situ recovery. A Progress Report to Alberta Oil Sands Technology and Research Authority on AOSTRA Agreement 184, 32 p.

ROESNER, E. K. and POPPEN, S. A. 1978. Shaft sinking and tunnelling in the oil sands. In AOSTRA Seminar on Underground Excavation in Oil Sands, University of Alberta, Edmonton, Alberta, Paper No. 11, 36 p.

ROGERS, G. 1978. Geological aspects of Saline Creek tunnel. In AOSTRA Seminar on Underground Excavation in Oil Sands, University of Alberta, Edmonton, Alberta, Paper No. 8, 42 p.

ROSCOE, K. H., SCHOFIELD, A. N. and WROTH, C. P. 1958. On the yielding of soils. Geotechnique, Vol. 8, No. 1, pp. 22-52.

ROSS, C. T. F. 1982. Computational methods in soil and continimum mechanics. Ellis Horwood Ltd., Chichester, 288 p.

ROWE, P. W. 1971. Theoretical meaning and observed values of deformation parameters for soil, stress-strain behavior of soils. Proceedings of the Roscoe Memorial Symposium, Cambridge University, pp. 143-194.

ROWE, R. K., LO, K. Y. and THAM, L. G. 1982. The analysis of tunnels and shaft in dense (oil) sand. Proceedings of the Fourth International Conference on Numerical Methods in Geomechanics, Edmonton, Alberta, edited by Z. Eisenstein, Volume 2, pp. 587-596.

RUEDRICH, R. A., PERKINS, T. K., ROCHAN, J. A. and CHRISTMAN, S. A. 1978. Casing strain resulting from thawing of Prudhoe Bay permafrost. Journal of Petroleum Technology, March 1978, Vol. 30, pp. 468-474.

SASS, J. H., KENNELLY, J. P., WENDT, W. E., MOSES, T. H. and ZIAGOS, J. P. 1981. In-situ determination of heat flow in unconsolidated sediments. Geophysics, Vol. 46, No. 1, January, 1981, pp. 76-81.

SAUTY, J. P., GRINGARTEN, A. C., MENJOZ, A. and LANDELL, P. A. 1982. Sensible energy storage in aquifers 1. Theoretical study. Water Resources Research, Vol. 18, No. 2, April, 1982, pp. 245-252.

SCHIFFMAN, R. L. 1971. A thermoelastic theory of consolidation. Environmental and Geophysical Heat Transfer, American Society of Mechanical Engineers (ASME), Heat Transfer Division, Volume 4, pp. 78-84.

SCHORA, F. C., TARMAN, P. B. and FELDKIRCHNER, H. L. 1977. In situ shale processing: state-of-the-art. Hydrocarbon Processing, Volume 56, No. 3[redacted]rch, 1977, pp. 127-129.

SCHRIDER, L. A. and FISCHER, D. D. 1976. In-situ coal gasification, a unique means of energy recovery. Mechanical Engineering, March 1976.

SCHRODT, J. K. and HOLDER, J. T. 1983. Temperature and strain rate effects on micromechanical behaviour in triaxially compressed marbles. Proceedings of the 24th U.S. Symposium on Rock Mechanics, Texas A & M University, pp. 449-468.

SCOTT, J. D. 1978. General report on the AOSTRA seminar on underground excavation in oil sands. In Proceedings of the AOSTRA Seminar on Underground Excavation in Oil Sands, Edmonton, Alberta, 27 p.

SCOTT, J. D. and KOSAR, K. M. 1982. Thermal expansion of oil sands. Forum on Subsidence due to Fluid Withdrawal, U.S. Department of Energy and Republic of Venezuala Ministry of Energy and Mines, Oklahoma, U.S.A., 28 p.

SEDIMENTOLOGY RESEARCH GROUP, UNIVERSITY OF CALGARY 1981. The effects of in-situ steam injection on Cold Lake oil sands. Bulletin of Canadian Petroleum Geology, Vol. 29, No. 4, December 1981, pp. 447-478.

SENSEY, P. E. 1983. Determination of a constitutive law for salt at elevated temperature and pressure. Symposium on Measurement of Rock Properties at Elevated Pressures and Temperatures, College Station, Texas, American Society for Testing and Materials, pp.?

SETTARI, A. and RAISBECK, J. M. 1979. Fracture mechanics analysis in in-situ oil sands recovery. Journal of Canadian Petroleum Technology, 18, pp. 85-94.

SHIMAMOTO, T. and HARA, I. 1976. Geometry and strain distribution of single-layer folds. Tectonophysics, 30, pp. 1-34.

SHUSTER, J. A. 1972. Controlled freezing for temporary ground support. RETC Proceedings, Vol. 2, Chapter 49, pp. 863-895.

SIBSON, R. H. 1973. Interactions between temperature and pore fluid pressure during earthquake faulting and a mechanism for partial and total stress relief. NATURE Physical Science, Vol. 243, pp. 66-68.

SIMMONS, G. and COOPER, H. W. 1978. Thermal cycling cracks in three igneous rocks. International Journal of Rock Mechanics. Mineral Science and Geomechanics Abstract; Vol. 15, pp. 145-148.

SIMMOKROT, A. A., RAMEY, H. J. and MARSDEN, S. S. 1971. Effect of temperature level upon capillary pressure curves. Society of Petroleum Engineers Journal, March 1971, pp. 13-22.

SISCO, F. T. 1947. Modern metallurgy for engineers. Second Edition, Pitman Publishing Corporation, New York, 499 p.

SKEMPTON, A. W. 1954. The pore pressure coefficients A and B. Geotechnique, Volume 13, No. 4, pp. 143-147.

SKEMPTON, A. W. 1960. Effective stress in soils, concrete and rocks. Proceedings of the Conference on Pore Pressure and Suction in Soils, Butterworths, London, England, pp. 4-16.

SKEMPTON, A. W. and BISHOP, A.W. 1954. Soils. Chapter X of Building materials, their elasticity and inelasticity. North Holland Publishing Company, Amsterdam, pp. 418-482.

SKINNER, B. J. 1966. Thermal expansion. In Handbook of Physical Constants, Geological Society of America, New York, Memoir 37, Section 6, pp. 75-96.

SMITH, G. W. and BUTLER, R. M. 1979. Studies on the use of tunnels and horizontal wells for the recovery of heavy crudes, First International Conference on the Future of Heavy Crude Oils and Tar Sands, edited by R. F. Meyer and C. T. Steele, United Nations for Training and Research, AOSTRA, and the U.S. Department of Energy, Edmonton, Alberta, Chapter 49, pp. 455-459.

SMITH, J. W. and ATWOOD, M. T. (editors) 1976. Oil shale and tar sands. American Institute of Chemical Engineers, Symposium series, Volume 72, No. 55, 84 p.

SMITH, L. B. and CHAPMAN, D. S. 1983. On the effects of groundwater flow. Regional scale systems. Journal of Geophysical Research, Vol. 88, No. B1, pp. 593-608.

SMITH, L. B., CHATTERJI, P. K., INSLEY, A. E. and SHARMA, L. 1978. Construction of Saline Creek tunnel in Athabasca oil sand. In AOSTRA Seminar on Underground Excavation in Oil Sand, University of Alberta, Edmonton, Alberta, Paper No. 7, 58 p.

SMITH M. B. and PATTILLO, P. D. 1980. Analysis of casing deformations due to formation flow. Oil Sands Geoscience, Edmonton, Alberta, June, 1980, 15 p.

SMITH-MacGOWAN, D., SKAUGE, A. and HEPLER, L.G. 1982. Specific heats of Athabasca oil sands and components. Journal of Canadian Petroleum Technology, May-June 1982, pp. 28-32.

SNEDDON, I. N. 1946. The distribution of stress in the neighborhood of a crack in an elastic solid. Proceedings of the Royal Society of London, A, 187, pp. 229-260.

SOBKOWICZ, J. C. 1982. The mechanics of gassy sediments. Ph.D. Thesis, University of Alberta, Edmonton, Alberta, 531 p.

SOLBERG, P., LOCKNER, D. and BYERLEE, J. D. 1980. Hydraulic fracturing in granite under geothermal conditions. International Journal of Rock Mechanics. Mineral Science and Geomechanics Abstract; Vol. 17, pp. 25-33.

SOMERTON, W. H. 1982. Porous rock-fluid systems at elevated temperatures and pressures. Geological Society of America, Special Paper 189, 1982, pp. 183-197.

SOMERTON, W. H. and GUPTA, V. S. 1965. Role of fluxing agents in thermal alteration of sandstones. Journal of Petroleum Technology, May 1965, pp. 585-593.

SOMERTON, J. H., KEESE, J. A. and CHU, S. L. 1974. Thermal behavior of unconsolidated oil sands. Scolety of Petroleum Engineering Journal, Vol. 14, pp. 513-521, 1974.

SOMERTON, W. H. and UDELL, K. S. (1981). Thermal and high temperature properties of rock-fluid systems. Department of Mechanical Engineering, University of California, Berkley Internal Research Report UCB/ME/81-01, College of Engineering, Office of Research Services, 12 p.

SOMERTON, W. H., ZIMMERMAN, R. W. and HARADEN, J. L. 1983. The effects of pore pressure, confining pressure and temperature on pore and bulk volume compressibilities of consolidated sandstones. Symposium on Measurement of Rock Properties at Elevated Pressures and Temperatures, College Station, Texas, American Society for Testing and Materials, pp.?

SPEIGHT, J. G. and MOSCHOPEDIS, S. E. 1979. The influence of crude oil composition on the nature of the upgrading process: Athabasca bitumen. Chapter 67 In the First International Conference on the Future of Heavy Crude Oils and Tar Sands. Edited by R. F. Meyers and C. T. Steele, Edmonton, Alberta, June 4-12, 1979, pp. 603-611.

SRAJER, V. and BARRON, K. 1978. Gas observations in the Saline Creek tunnel. In AOSTRA Seminar on Underground Excavation in Oil Sand, University of Alberta, Edmonton, Alberta, Paper No. 9, 20 p.

STARR, J. and PRATS, J. M. 1979. Chemcial properties and reservoir characteristics of bitumen and heavy oil from Canada and Venezuala. Chapter 21 in the First International Conference on the Future of Heavy Crude Oil and Tar Sands. Edited by R. F. Mewyers and C. T. Steele, Edmonton, Alberta, pp. 168-173.

STEPHENS, G. and VOIGHT, B. 1982. Hydraulic fracturing theory for conditions of thermal stress. International Journal of Rock Mechanics, Mineral Science and Geomechanics Abstract, Vol. 19, pp. 279-284.

STEPHENSON, H. G. 1978. An evaluation of the underground approach to oil sand development. In AOSTRA Seminar on Underground Excavation in Oil Sands, University of Alberta, Edmonton, Alberta, Paper No. 6, 18 p.

STERNBERG, E. 1958. On transient thermal stresses in linear viscoelasticity. Proceedings of third U.S. National Congress of Applied Mechanics, pp. 96-102.

STERNE, K. B. 1981. Hollow cylinder testing of oil sands. M.Sc. Thesis, University of Alberta, Edmonton, Alberta, 228 p.

STEWART, G.A. and MacCALLUM, G. T. 1978. Athabasca oil sands guide book. Canadian Society of Petroleum Geologists, Calgary, Alberta, 33 p.

STONE, H. L. and BRIAN, P. L. T. 1963. Numerical solution of convective transport problems. AICHE Journal, September 1963, Vol. 9, No. 5, pp. 681-688.

STONE, R. B. 1977. Technical and economic study of an underground mining, rubblization and in situ retorting system for deep oil shale deposits. Quarterly of the Colorado School of Mines, pp. 235-258.

STOUT, K. S. 1980. Mining methods and equipment. McGraw-Hill, Inc., New York, 218 p.

STREETER, V. L. and WYLIE, E. B. 1979. Fluid mechanics. Seventh Edition, McGraw-Hill Book Company, New York, 570 p.

SUFI, A. H., RAMEY, H. J. and BRIGHAM, W. E 1982. Temperature effects on relative permeabilites of oil-water systems. Society of Petroleum Engineers of AIME, 57th Annual Fall Technical Conference, New Orleans, LA., SPE 11071, 12 p.

SUMMERS, R., WINKLER, K. and BYERLEE, J. D. 1978. Permeability changes during the flow of water through Westerly granite at temperatures of 100-400°C. Journal of Geophysical Research, Volume 83, pp. 339-344.

SYDANSK, R. D. 1980. Discussion of the effect of temperature and confining pressure on single-phase flow in consolidated rocks. Journal of Petroleum Technology, August 1980, pp. 1329-1330.

TAYLOR, D. W. 1948. Fundamentals of soil mechanics. John Wiley and Sons Inc., New York, 425 p.

TERZAGHI, K. 1943. Theoretical soil mechanics. John Wiley and Sons, Inc., New York, New York, 510 p.

TERZAGHI, K. and RICHART, F. E. 1952. Stress in rock about cavities. Geotechnique, Vol. 3, 1952, pp. 57-90.

THOMPSON, T. W. and POTTS, E. L. J. 1979. The influence of thermal stresses on the stability of underground storage cavities. International Journal of Rock Mechanics, Mineral Science and Geomechanics Abstract, Vol. 16, pp. 117-125.

TIMOSHENKO, S. P. and GOODIER, J. N. 1934. Theory of Elasticity. McGraw-Hill Book Company, third Edition, Engineering Societies Monographs, 567 p.

TOWSON, D. 1979. The electrical preheat recovery process. Chapter 45 in the First International Conference on the Future of Heavy Crude Oil and Tar Sands. Edited by R. F. Meyers and C. T. Steele, Edmonton, Alberta, pp. 410-412.

TSANG, C. F. and HOPKINS, D. L. 1982. Aquifer thermal energy storage: a survey. Geological Society of America, Special Paper 189, 1982, pp. 427-441.

TSUI, K. K., LEE, C. F., TSAI, A. and HARRIS, N. L. 1982. Thermo-mechanical modelling of a nuclear waste disposal vault in crystalline hard rock. Proceedings of the Fourth International Conference on Numerical Methods in Geomechanics, Edmonton, Alberta, edited by Z. Eisenstein, Volume 2, pp. 503-512.

TUSTIN, T. G. 1949. The shear and consolidation characteristics of the McMurray tar sands. M.Sc. Thesis, University of Alberta, Edmonton, Alberta, 102 p.

U.S.S.R. NAVAL MINISTRY 1975. Recommendations for thermal consolidation of weak clayey soils. Draft Translation 630, translated by U.S. Foreign Sciences and Technology Centre for the U.S. Army Cold Regions Research and Engineering Laboratory, Hanover, New Hamspire, 36 p.

VAN BUSKIRK, R., ENNISS, J. and SCHATZ, J. 1983. Measurement of thermal conductivity and thermal expansion at elevated temperatures and pressures. Symposium on Measurement of Rock Properties at Elevated Pressures and Temperatures, College Station, Texas, American Society for Testing and Materials, pp.?

VAN DER MOLEN, I. 1981. The shift of the alpha-beta transition temperature of quartz associated with the thermal expansion of granite at high pressures. Tectonophysics 73, pp. 323-342.

VICKERS, B. 1978. Laboratory work in soil mechanics. Second Edition, Granada Publishing Limited, London, 170 p.

VIGRASS, L. W. 1968. Geology of Canadian heavy oil sands. American Association of Petroleum Geologists, Bulletin, Vol. 52, No. 10, 1968, pp. 1984-1999.

VOEGELE, M. D. and BRACE, W. F. 1983. Measurement of permeability at elevated pressures and temperatures. Symposium on Measurement of Rock Properties at Elevated Pressures and Temperatures, College Station, Texas, American Society for Testing and Materials, pp.?

VOEGELE, M., HARDIN, E., LINGLE, D., BOARD, M. and BARTON, N. 1981. Site characterization of joint permeability using the heated block test. Proceedings of the 22nd U.S. Symposium on Rock Mechanics, pp. 120-128.

VOIGHT, B. and FAUST, C. 1982. Frictional heat and strength loss in some rapid landslides. Geotechnique 32, No. 1, pp. 43-54.

WAI, R. S. C. and LO, K. Y. 1981. Temperature effects on strength and deformation behavior of rocks in Southern Ontario. Research Report GEOT-6-81, University of Western Ontario, London, Ontario, 31 p.

WANG, J. S. Y., TSANG, C. F., COOK, N. G. W. and WITHERSPOON, P. A. 1981. A study of regional temperature and thermohydrologic effects of an underground repository for nuclear wastes in hard rock. Journal of Geophysical Research, Vol. 86, No. B5, pp. 3759-3770.

WEINBRANT, R. M., RAMEY, H. J. and CASSE, F. J. 1975. The effect of temperature on relative and absolute permeability of sandstones. Society of Petroleum Engineers Journal, October 1975, pp. 376-384.

WILLIAMS, K. A., STIMPSON, B., PATCHING, T.H. AND JEREMIC, M.L. 1980. Rock mechanics properties of the Waterways formation. Applied Oilsands Geoscience Conference. Edited by M.B. Dusseault, University of Alberta, Edmonton, Alberta, 24 p.

WILLIAMS, N. 1982. High Temperature Triaxial Testing of Clays. Ph.D. Dissertation, University of California, Berkley, Department of Civil Engineering, 368 p.

WILSON, J. W. 1956. Determination of relative permeability under simulated reservoir conditions. A.I.Ch.E. Journal, March 1956, pp. 94-100.

WINESTOCK, A. G. 1974. Developing a steam recovery process. In Oil Sands Fuel of the Future, Canadian Society of Petroleum Geologists, Calgary, Alberta, pp. 186-198.

WINGQUIST, C. F. 1970. Elastic moduli of rock at elevated temperatures. United States Department of the Interior, Bureau of Mines, Report of Investigations #7269, 18 p.

WINTERKORN, H. 1954. Fundmental similarities between electro-osmotic and thermo-osmotic phenomena. Highway Research Board Proceedings, Volume 27, National Research Council, Washington, D.C.

WITHERSPOON, P. A., COOK, N. G. W. and GALE, J. E. 1981. Geologic storage of radioactive waste: field studies in Sweden. Science, Volume 211, pp. 894-900.

WISSA, A. E. Z. 1969. Pore pressure measurement in saturated stiff soils. ASCE, JSMFD, SM4, July 1969, pp. 1063-1073.

WONG, T. F. and BRACE, W. F. 1979. Thermal expansion of rocks: some measurements at high pressure. Tectonophysics, 57, pp. 95-117.

WYCKOFF, R. D. and BOTSET, H. G. 1936. Flow of gas-liquid mixtures through sands. Physics, 1936, 325 p.

WYLLIE, P. J. 1971. The dynamic earth. John Wiley and Sons, Inc., New York, 416 p.

YAMAGUCHI, U. and MIYAZAKI, M. 1970. A study of the strength at failure of rocks heated to high temperatures. Journal of the Mining and Metallurgical Institute of Japan, 86, (986), pp. 346-351.

ZEUCH, D. H. 1983. The mechanical behavior of Anvil Points oil shale at elevated temperatures and confining pressures. Canadian Geotechnical Journal, Vol. 20, No. 2, pp. 344-352.

ZIENKIEWICZ, O. C. 1977. The finite element method. McGraw-Hill Book Company, third edition, London, England, 787 p.

ZIENKIEWICZ, O. C., LEUNG, K. H. and HINTON, E. 1982. Earthquake response behaviour of soils with drainage. In Proceedings of the Fourth International Conference on Numerical Methods in Geomechanics, edited by Z. Eisenstein, Edmonton, Alberta.

ZIMMERMAN, R. M. 1983. First phase of small diameter heater experiments in tuff. Proceedings of the 24th U.S. Symposium on Rock Mechanics, Texas A & M University, pp. 271-282.

ZOBACH, M. D. 1978. A simple hydraulic fracturing technique for determining fracture toughness. In Proceedings of the 19th U.S. Rock Mechanics Symposium, pp. 83-85.

ZOBACH, M. D., HEALY, J. H., ROLLER, J. C., GOHN, G. S. and HIGGINS, B. B. 1978. Normal faulting and in-situ stress in the South Carolina coastal plain near Charleston. Geology, Vol. 6, pp. 147-152.

Vol 2

THE UNIVERSITY OF ALBERTA

GEOTECHNICAL BEHAVIOUR OF OIL SANDS AT ELEVATED TEMPERATURES AND PRESSURES

VOLUME II

APPENDICES

by

JOHN GORDON AGAR

A THESIS

SUBMITTED TO THE FACULTY OF GRADUATE STUDIES AND RESEARCH

IN PARTIAL FULFILLMENT OF THE REQUIREMENTS FOR THE DEGREE

DOCTOR OF PHILOSOPHY

IN

GEOTECHNIQUE

DEPARTMENT OF CIVIL ENGINEERING

EDMONTON, ALBERTA

SPRING, 1984

VOLUME II

LIST OF FIGURES IN APPENDIX A

LIST OF TABLES IN APPENDIX A

LIST OF FIGURES IN APPENDIX B

LIST OF FIGURES IN APPENDIX C

LIST OF FIGURES IN APPENDIX D

LIST OF FIGURES IN APPENDIX E

LIST OF FIGURES IN APPENDIX F

LIST OF PHOTOGRAPHIC PLATES IN APPENDIX G

LIST OF FIGURES IN APPENDIX H

LIST OF FIGURES IN APPENDIX K

LIST OF FIGURES IN APPENDIX L

APPENDIX A

APPARATUS COMPLIANCE TESTING AND CALIBRATIONS

TABLE A-1

PROPERTIES OF SYSTEM FLUIDS

FLUID	DENSITY AT 25°C AND ATMOSPHERIC PRESSURE (Mg/m^3)	FREEZE POINT (°C)	BOILING POINT (°C)	FLASH POINT (°C)	DYNAMIC VISCOSITY AT 25°C AND ATMOSPHERIC PRESSURE (mPa.s)
Distilled Water	1.000	0°C	100°C	10°C	1.0
Athabasca Bitumen	1.03 - 1.05	-	-	-	$2 - 3 \times 10^6$
Silicone Oil Cell Fluid (Dow Corning 710G)	1.10 - 1.12	-22°C	230°C	301°C	550.0

TABLE A-2

THERMAL EXPANSION AND COMPRESSION PROPERTIES OF APPARATUS MATERIALS

MATERIAL	LINEAR COEFFICIENT OF THERMAL EXPANSION ($°C^{-1}$)	VOLUME COEFFICIENT OF THERMAL EXPANSION ($°C^{-1}$)	YOUNG'S MODULUS (kPa)	POISSON'S RATIO
Aluminium	$23.0 * 10^{-6}$	$69.0 * 10^{-6}$	$67 * 10^{6}$ @ 25°C $44 * 10^{6}$ @ 250°C	0.25
Stainless Steel	$17.8 * 10^{-6}$	$53.4 * 10^{-6}$	$193 * 10^{6}$ @ 25°C $130 * 10^{6}$ @ 250°C	0.25
Copper	$16.7 * 10^{-6}$	$50.1 * 10^{-6}$	-	-
Brass	$18.7 * 10^{-6}$	$56.1 * 10^{-6}$	-	-
Silicone Rubber	$1.7 * 10^{-4}$	$5.2 * 10^{-4}$	36 kPa (extension @ 25°C)	0.50

TABLE A-3

VOLUME CHANGE PROPERTIES OF SOME MINERALS

MINERAL SOLID	TEMPERATURE RANGE (°C)	COEFFICIENT OF VOLUME THERMAL EXPANSION ($°C^{-1}$)	ISOTROPIC COMPRESSIBILITY (MPa^{-1})	MELTING POINT TEMPERATURE (°C)
Alpha Quartz Crystal	20	$3.4 * 10^{-6}$	$27 * 10^{-6}$	
Alpha Quartz Crystal	400	$69.0 * 10^{-6}$	-	Inversion @ 573°C
Beta Quartz Crtsyal	575 - 1000	$-3.0 * 10^{-6}$	$18 * 10^{-6}$	1050°C
Barite ($BaSO_4$)	20 - 200	$57.0 * 10^{-6}$	$17 * 10^{-6}$	-
Hailte (NaCl)	-80 - 20	$107.0 * 10^{-6}$	$43 * 10^{-6}$	804°C
Gypsum ($CaSO_4 \cdot 2H_2O$)	20 - 100	$73.0 * 10^{-6}$	$25 * 10^{-6}$	-
Diamond (C)	20 - 1200	$10.0 * 10^{-6}$	$2 * 10^{-6}$	-

TABLE A-4

SUMMARY OF CALIBRATIONS FOR ELECTRONIC MEASURING DEVICES

Electronic Measuring Device	Calibration	Precision
1. Consolidometer LVDT (1000 HR)	1.965 mm/V	±.001 mm/V
2. Volume change LVDT (500 HR)	10.0 ml/V	±.10 ml to ±.001 m
3. Triaxial External LVDT (1000 HR)	1.559 mm/V	±.005 mm
4. 7 MPa Strain Gauge Back Pressure Transducer	190.50 kPa/mV	±.10 kPa
5. 7 MPa S.G. Confining Pressure Transducer	185.36 kPa/mV	±.10 kPa
6. 35 MPa S.G. (Air Cooled) Back Pressure Transducer	1262.80 kPa/mV	±.50 kPa
7. 35 MPa Strain Gauge Confining Pressure Transducer	1145.60 kPa/mV	±.50 kPa
8. 35 MPa S.G. Upstream Back Pressure Transducer	1167.40 kPa/mV	±.50 kPa
9. 35 MPa S.G. Downstream Back Pressure Transducer	1080.00 kPa/mV	±.50 kPa
10. 500 kPa Validyne Differential Pressure Transducer	37.10 kPa/mV	±.10 kPa
11. 140 kPa Validyne Differential Pressure Transducer	10.748 kPa/mV	±.01 kPa
12. 220 kN Strain Gauge Load Cell	31.207 kN/mV	±.01 kN
13. 440 kN Strain Gauge Load Cell	35.063 kN/mV	±.01 kN
14. Internal Axial Strain Gauge Yoke		
a) Axial Arm #1	4.610 mm/V	±.01 mm
b) Axial Arm #2	4.075 mm/V	±.01 mm
15. Lateral Strain Gauge Clamp Device	0.500 mm/V	±.01 mm
16. J Type Thermocouples (Iron/Constantin)	°C (Linearized Circuit)	±.5 °C

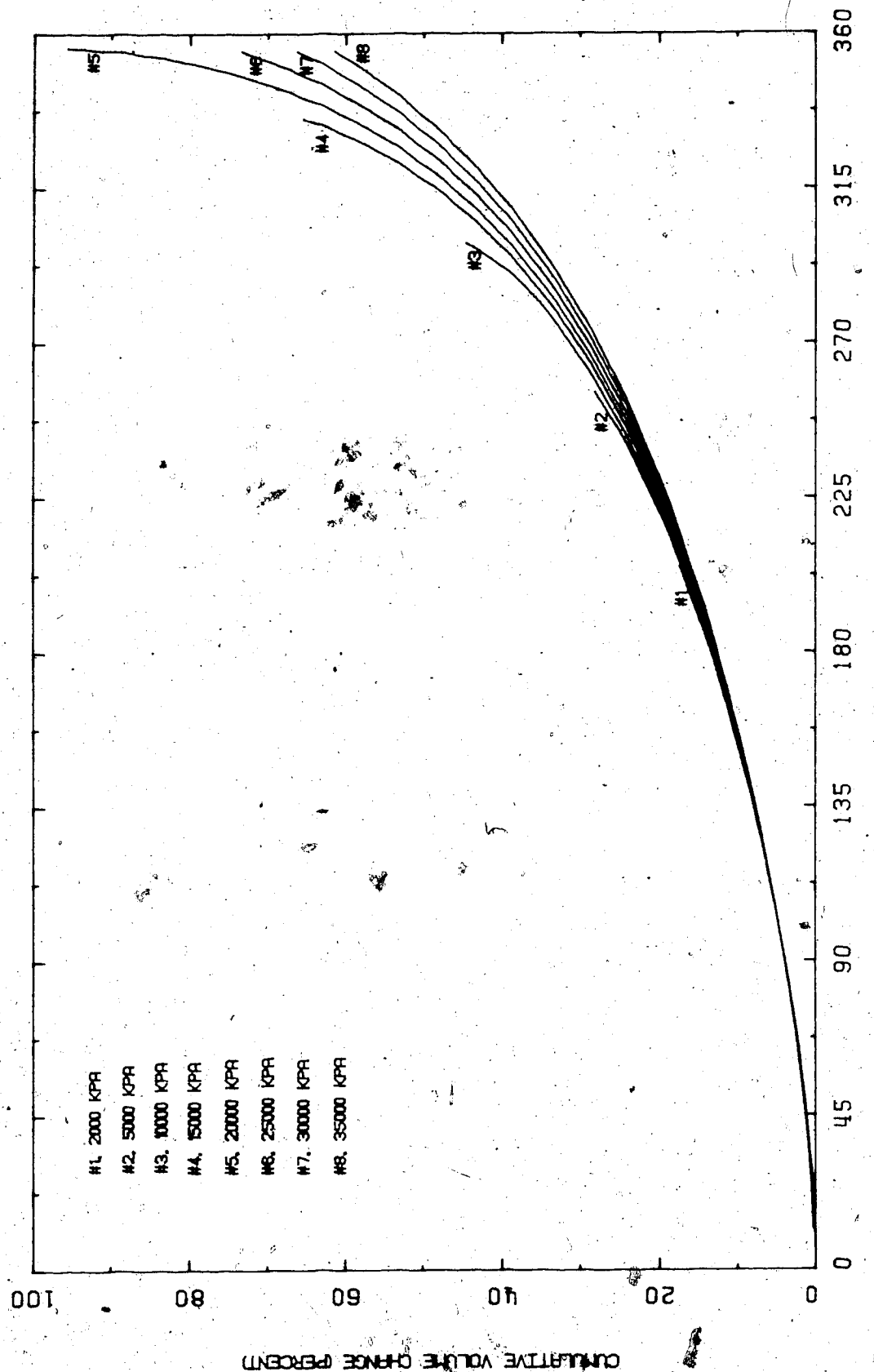

FIGURE A1 Thermal Expanison of Water

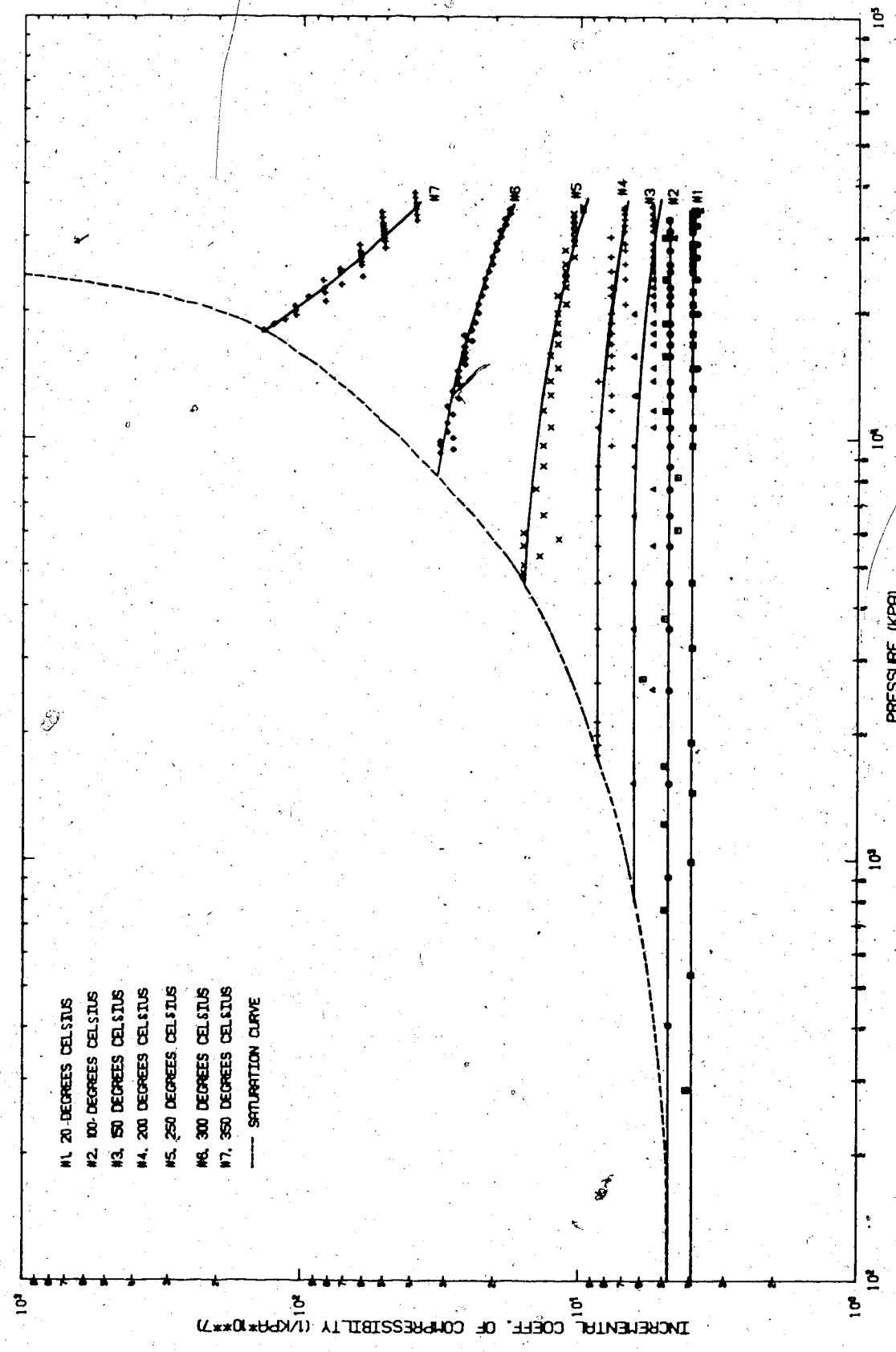

FIGURE A2 Compressibility of Water at Elevated Temperatures

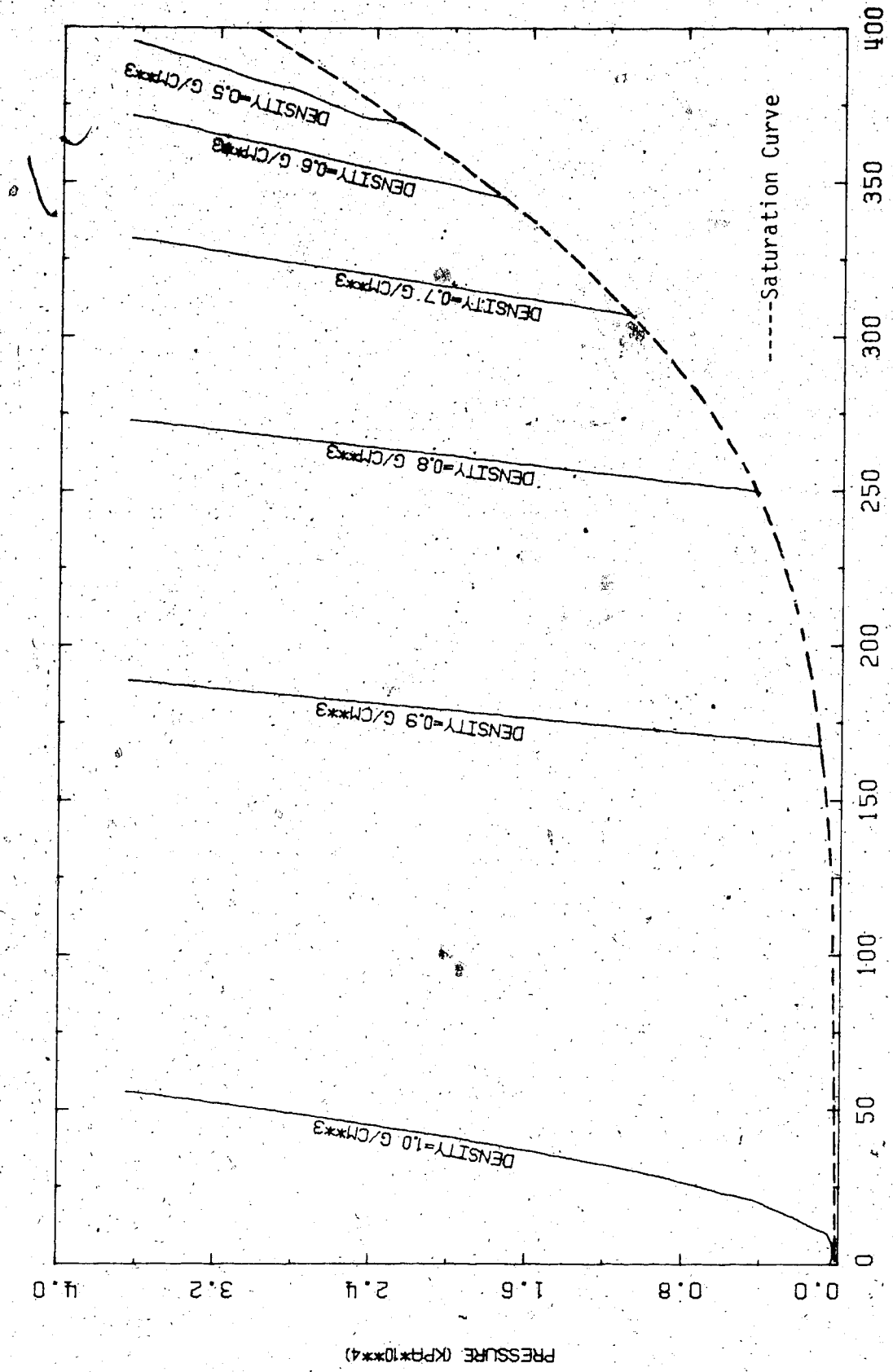

FIGURE A3 Pressure Increase During Constant Volume Heating

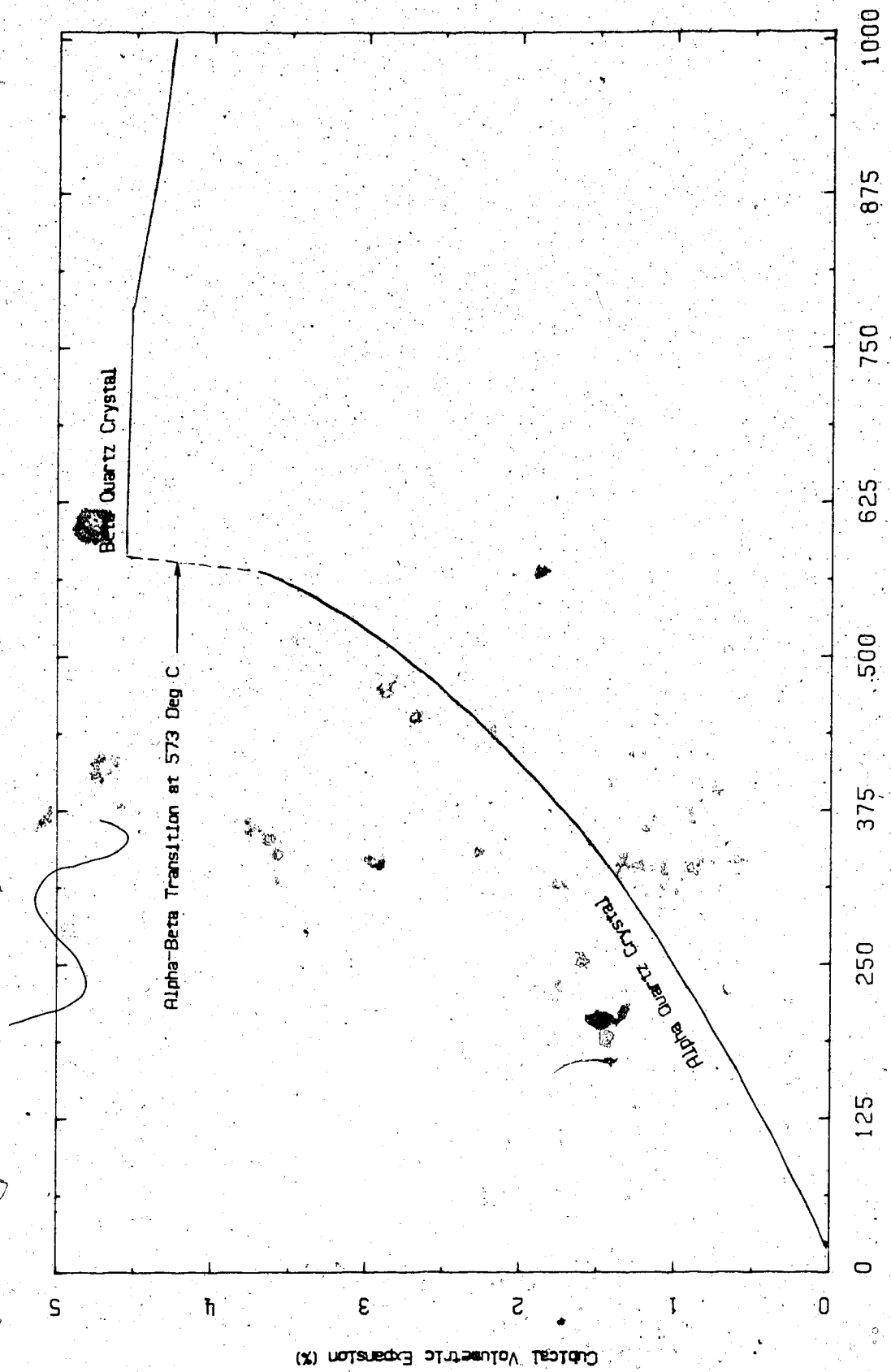

FIGURE A4 Thermal Expansion of Quartz

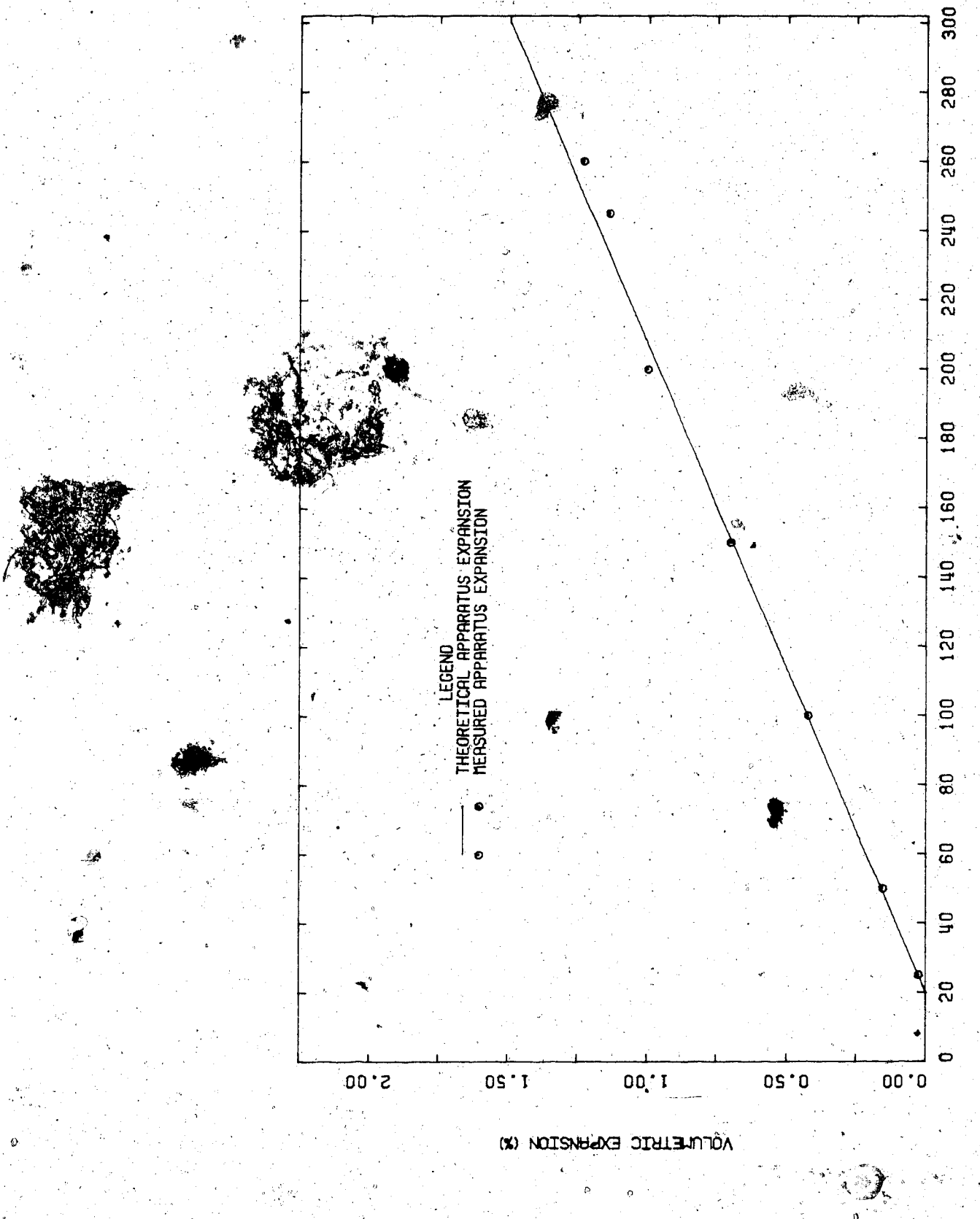

FIGURE A5 Consolidometer: Correction for Apparatus Thermal Expansion

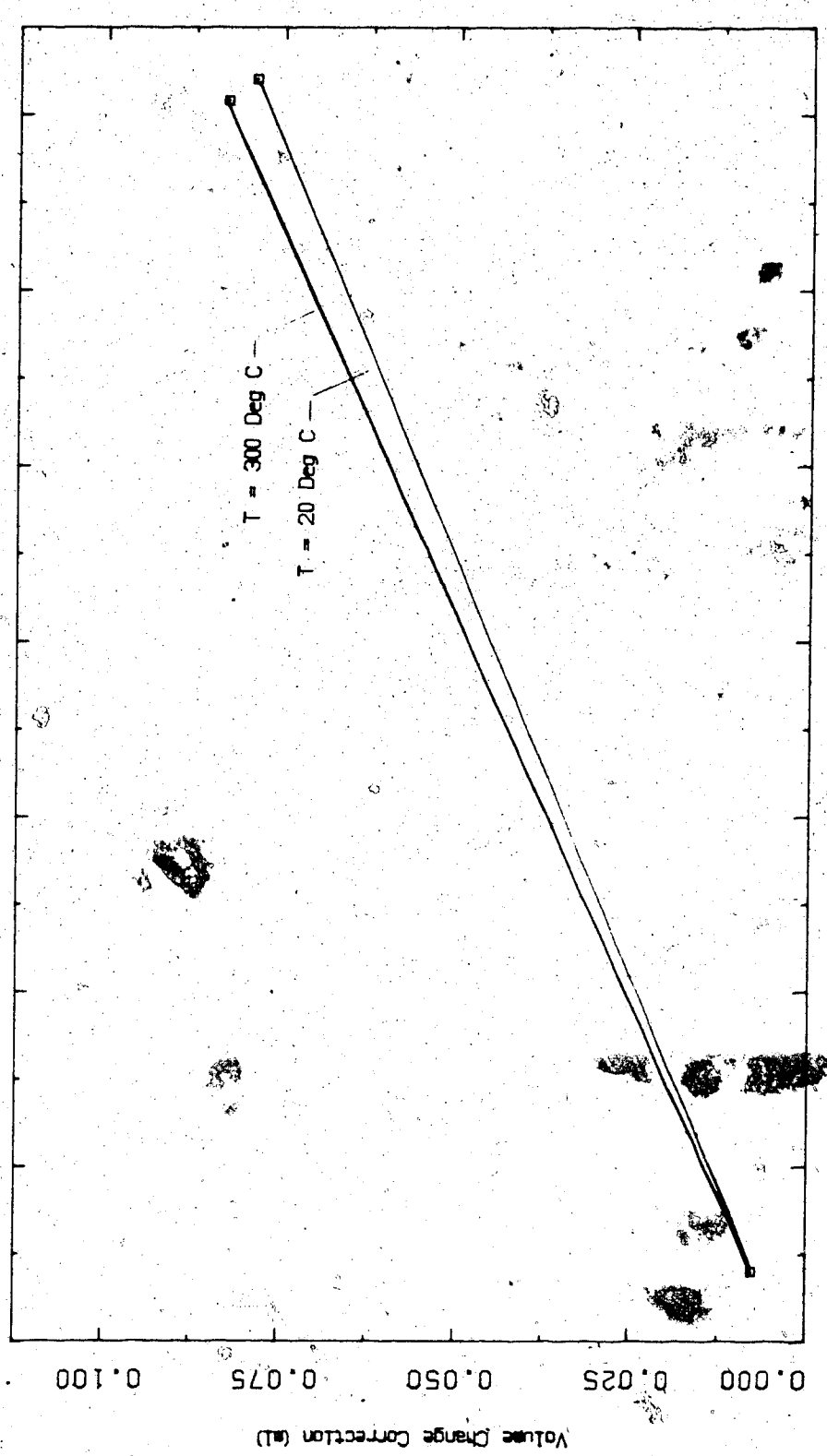

FIGURE A6 Consolidometer: Correction for Stress Induced Apparatus Expansion

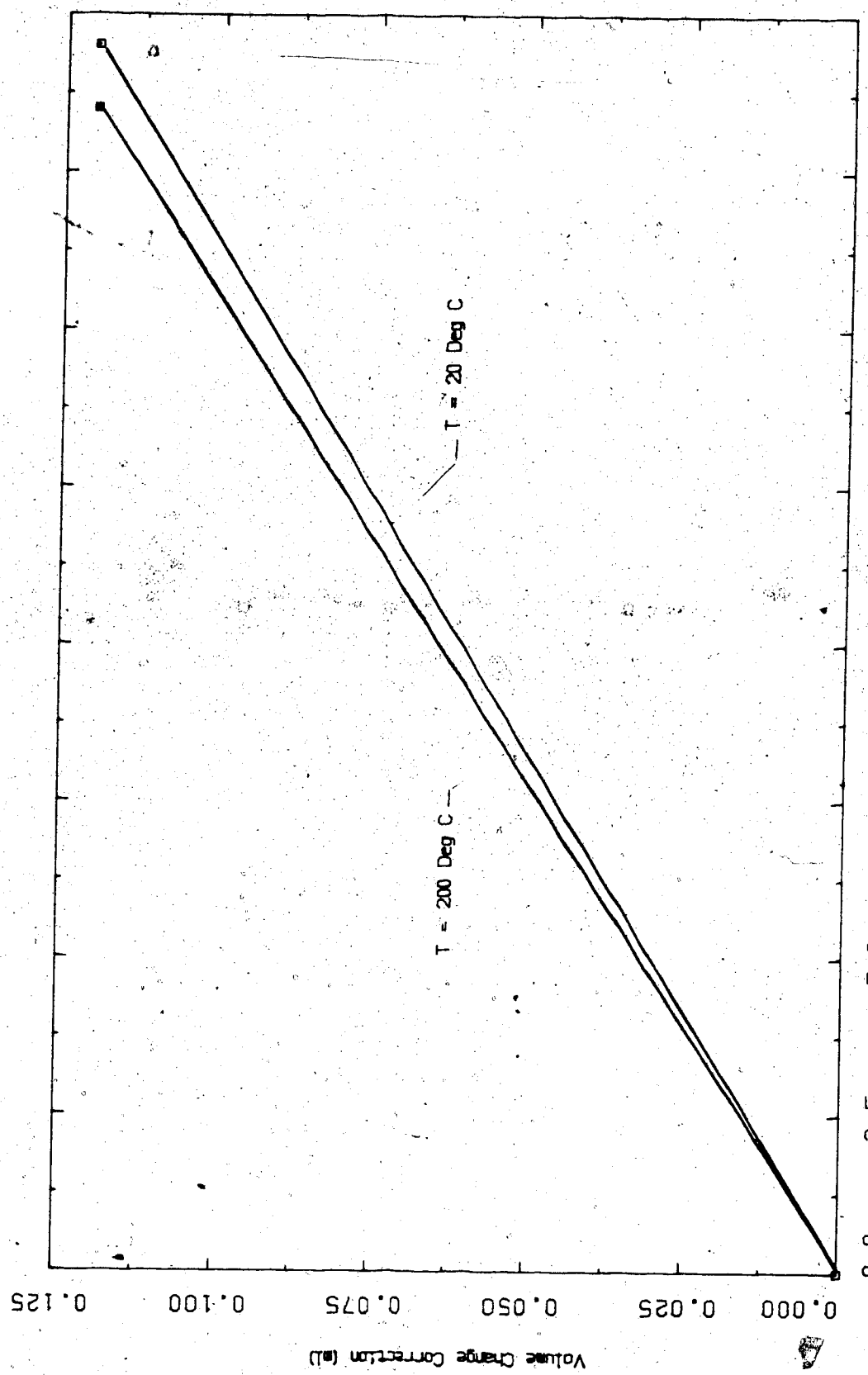

FIGURE A7 Consolidometer: Correction for Back Pressure Induced Apparatus Expansion

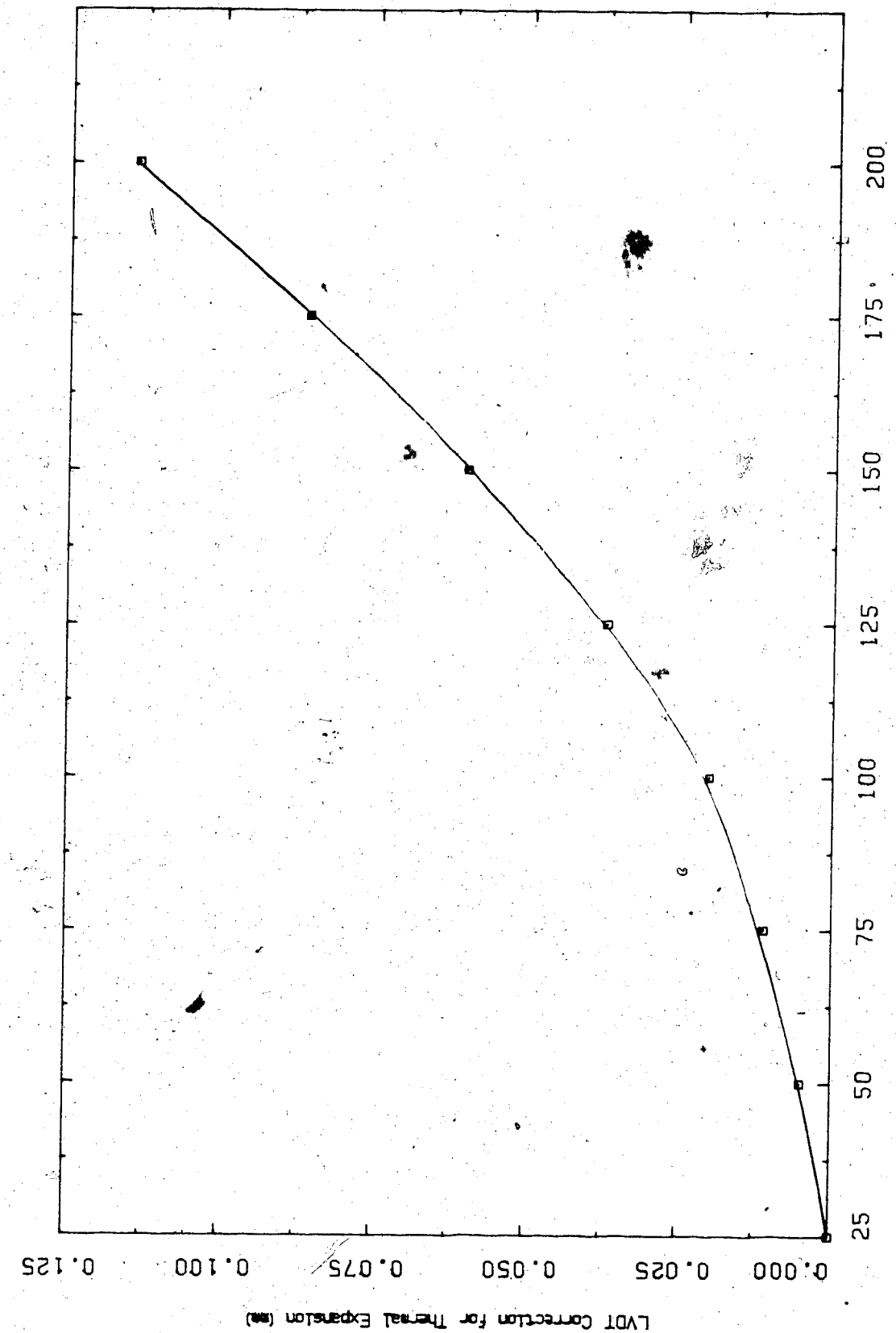

FIGURE A8 Consolidometer: LVDT Correction for Vertical Thermal Expansion of the Apparatus

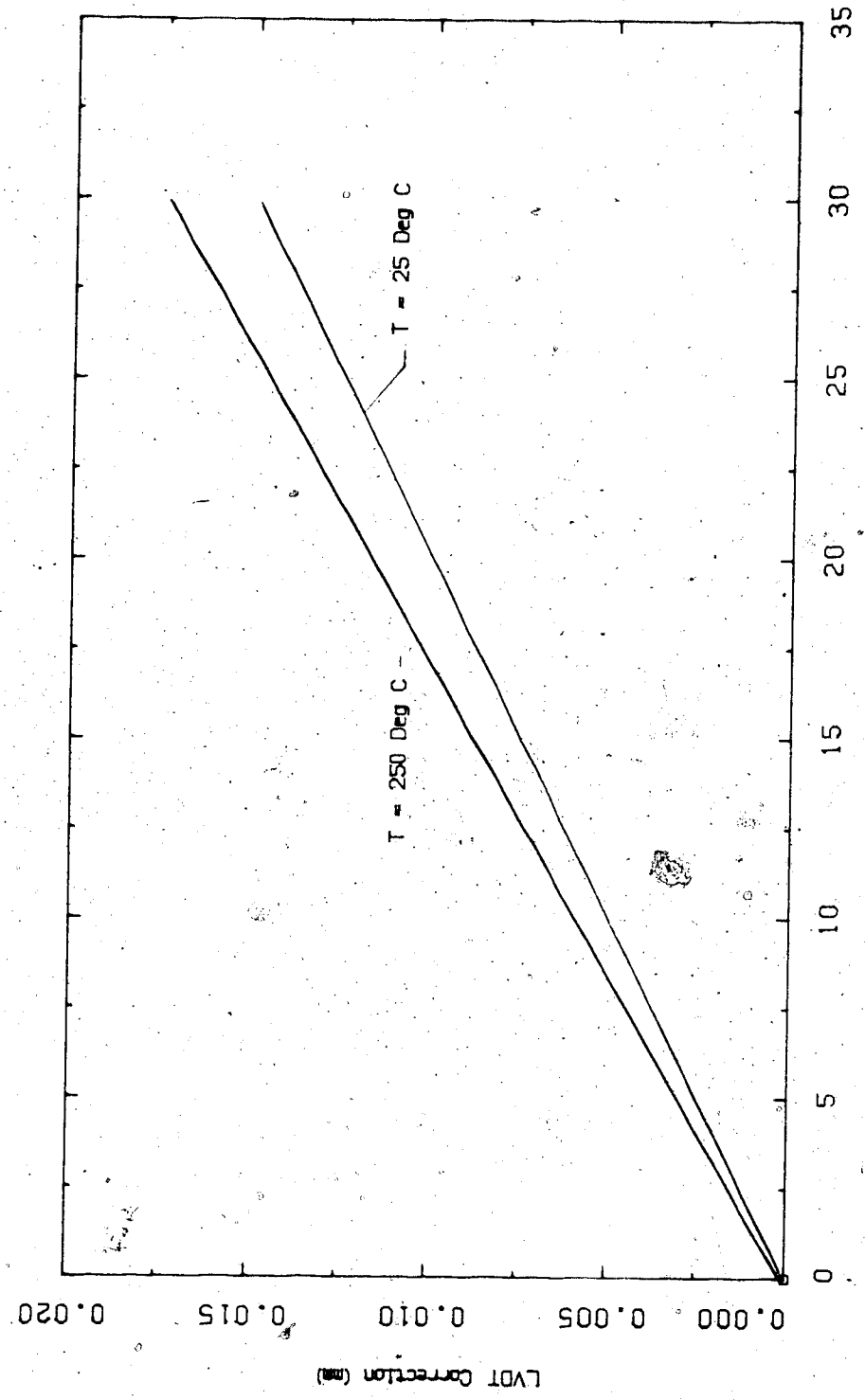

FIGURE A9 Consolidometer: LVDT Correction for Vertical Apparatus Compression

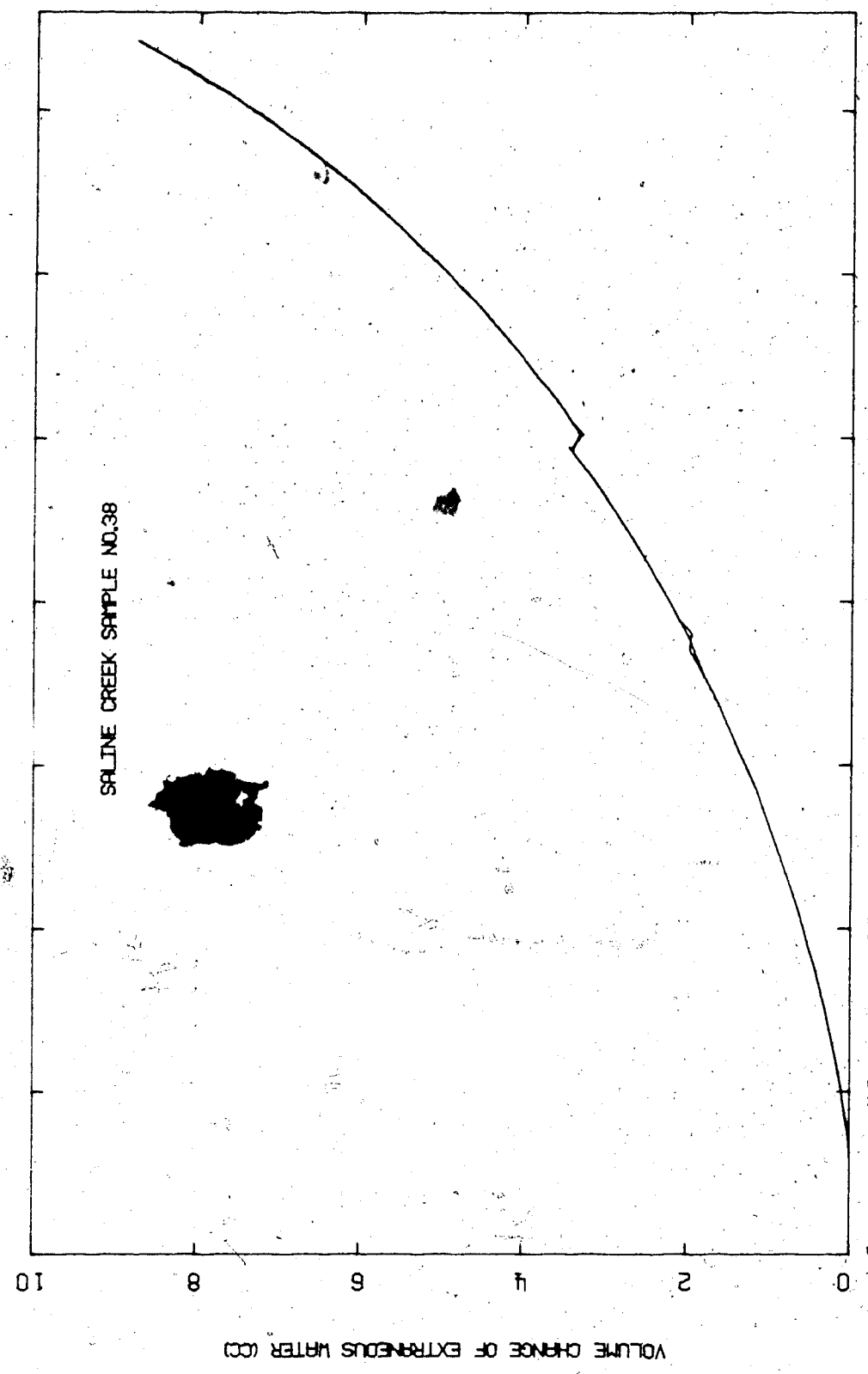

FIGURE A10 Consolidometer: Volume Change Correction for Thermal Expansion of Extraneous Water

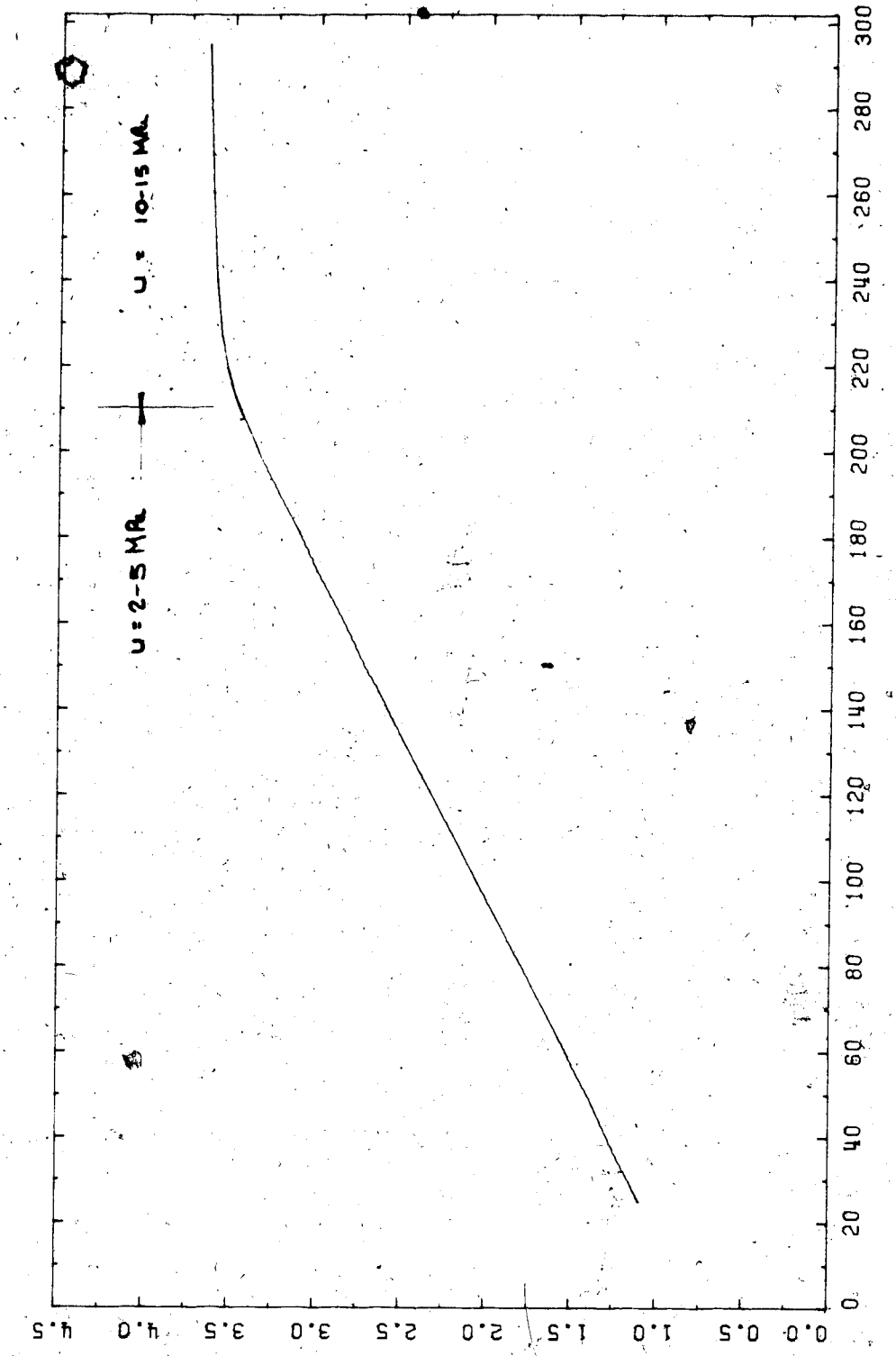

FIGURE A11 Consolidometer: Piston Friction at Elevated Temperatures and Back Pressures

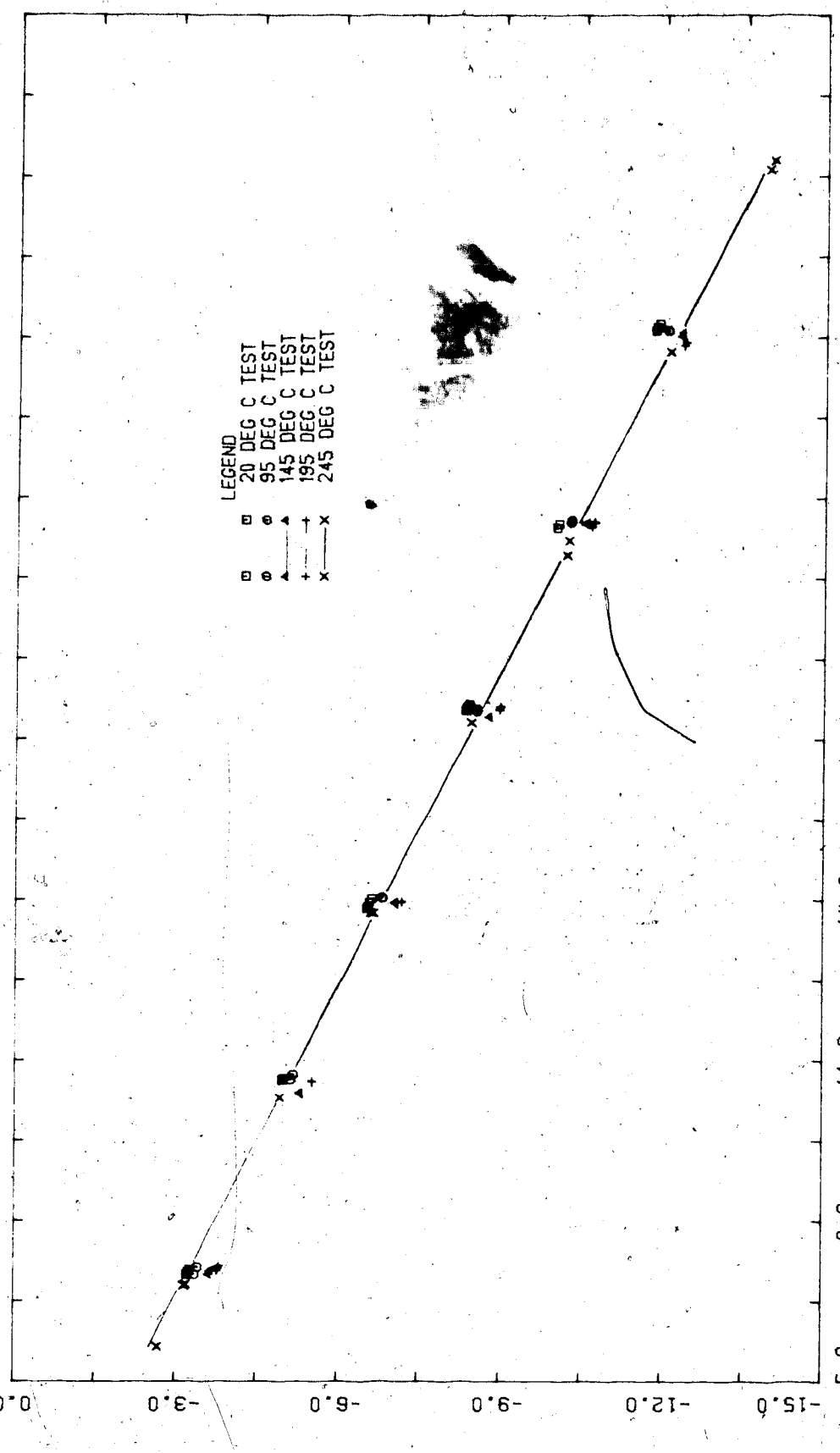

FIGURE A12 Triaxial Apparatus: Piston Friction at Elevated Confining Stresses and Temperatures Using a Non-Lubricated Piston

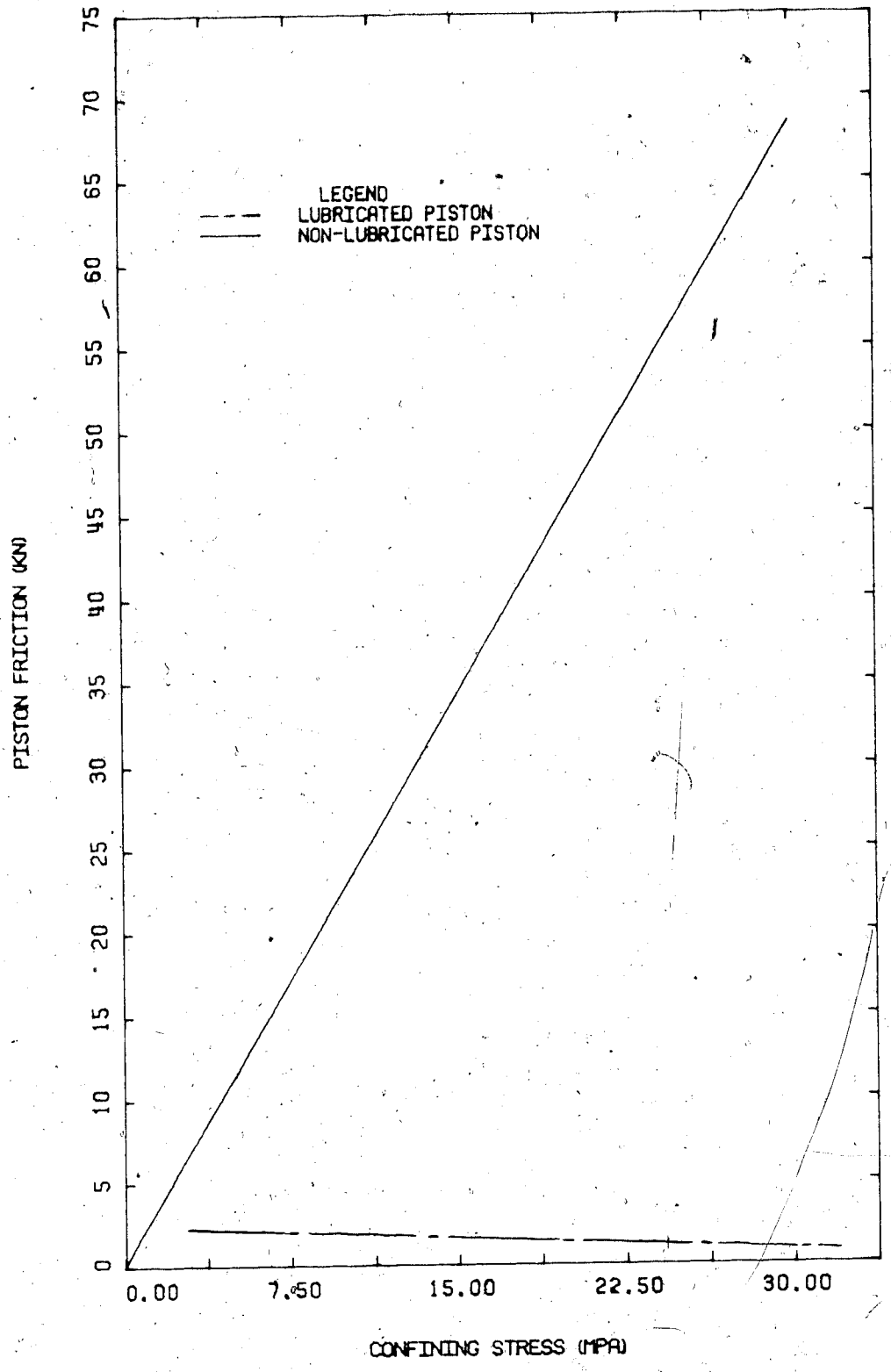

FIGURE A13 Triaxial Apparatus: Influence of Lubrication on Measured Piston Friction

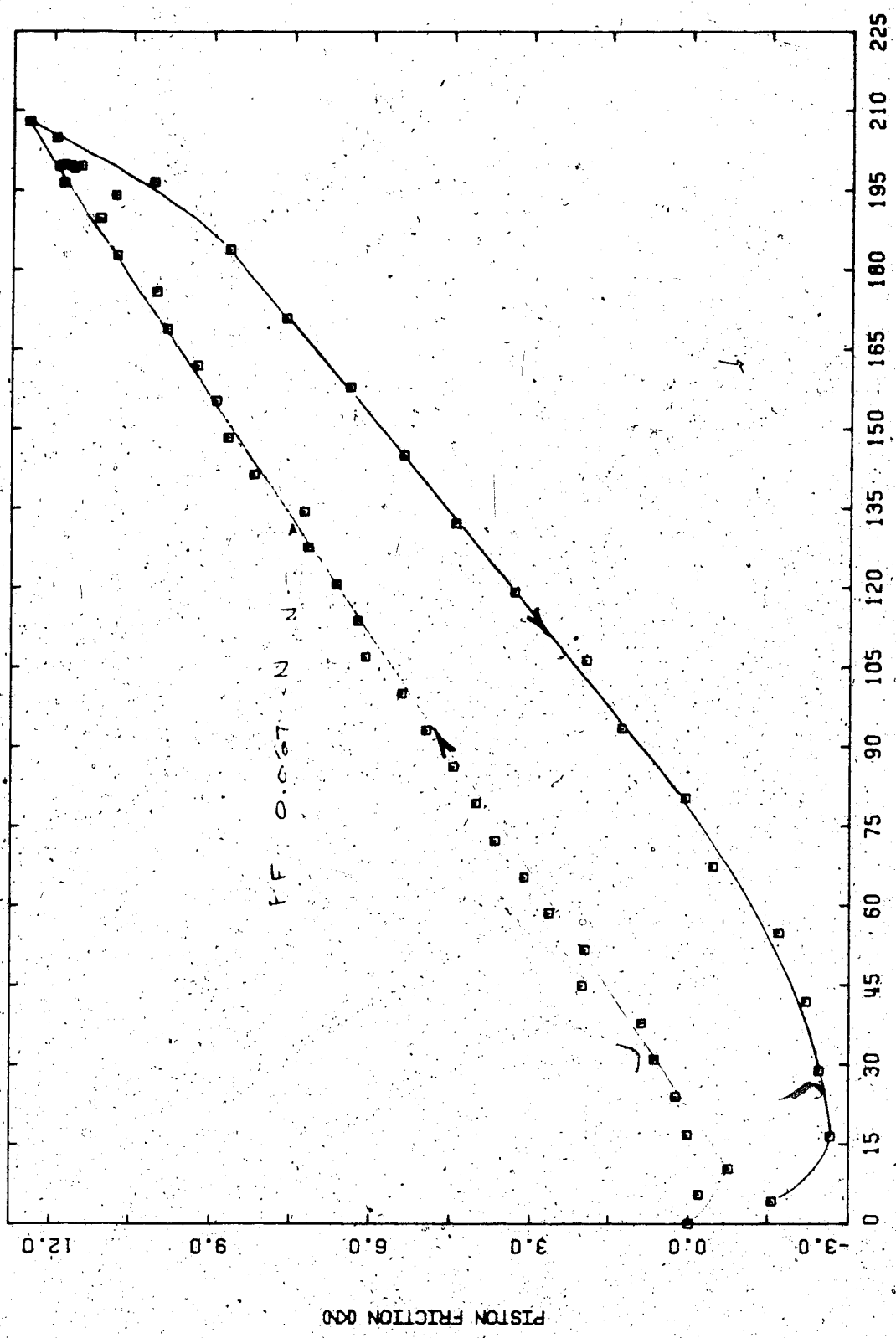

FIGURE A14 Triaxial Apparatus: Correction for Piston Friction with Applied Vertical Load

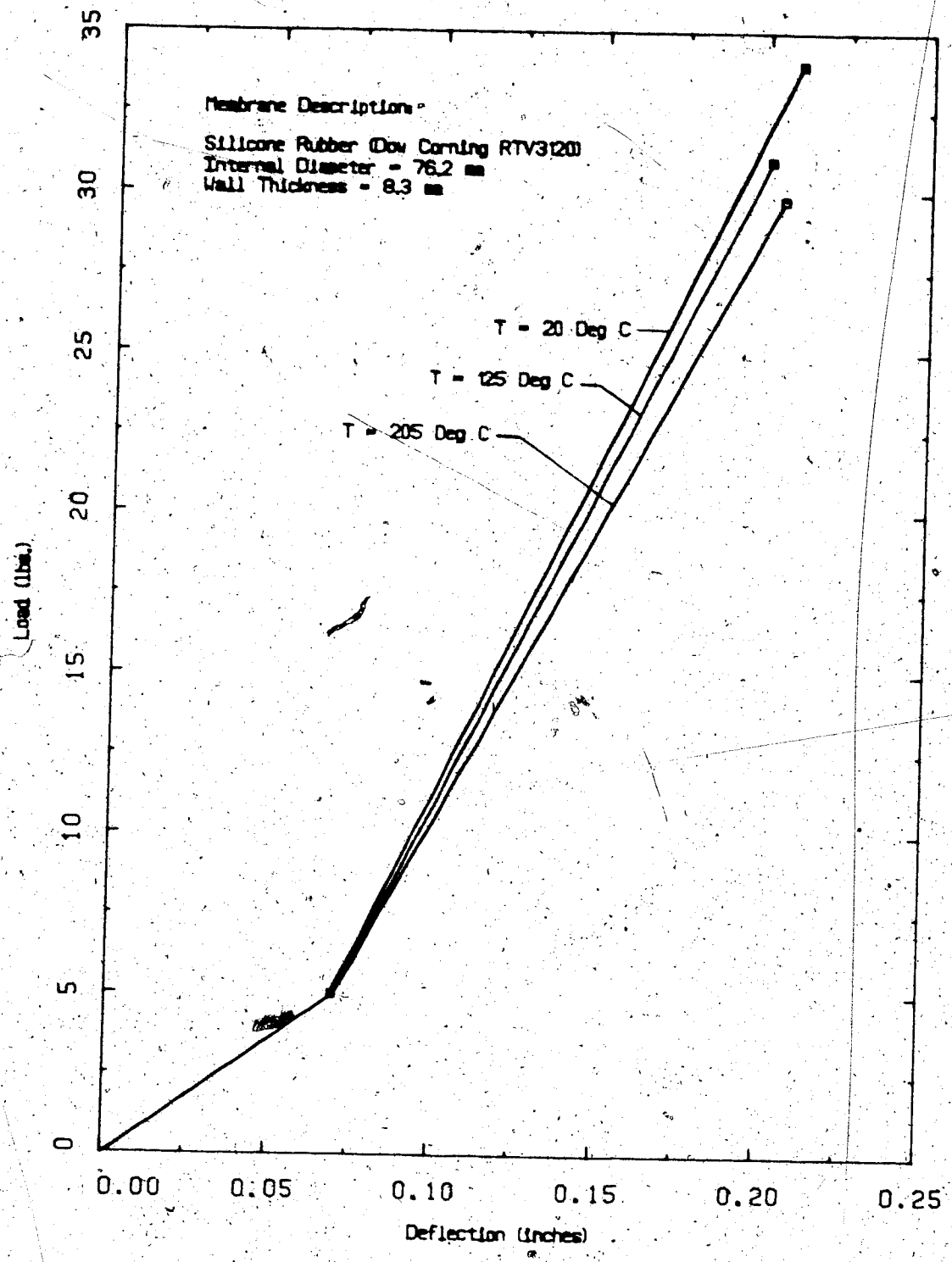

FIGURE A15 Triaxial Rubber Membrane Compliance at Elevated Temperatures

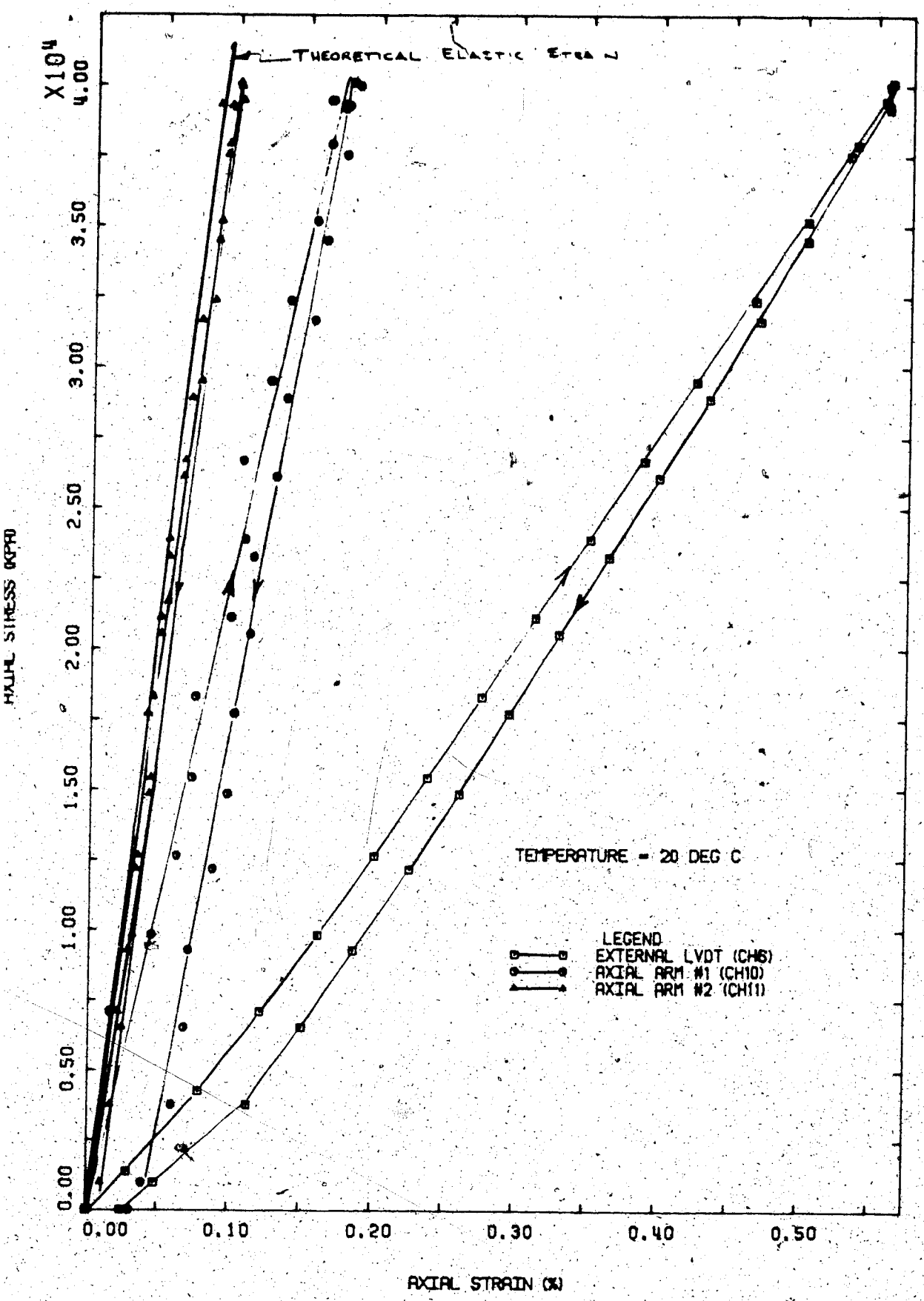

FIGURE A16 Triaxial Apparatus: Accuracy of Internal and External Axial Strain Measuring Devices During Compression of an Aluminium Sample at 20°C

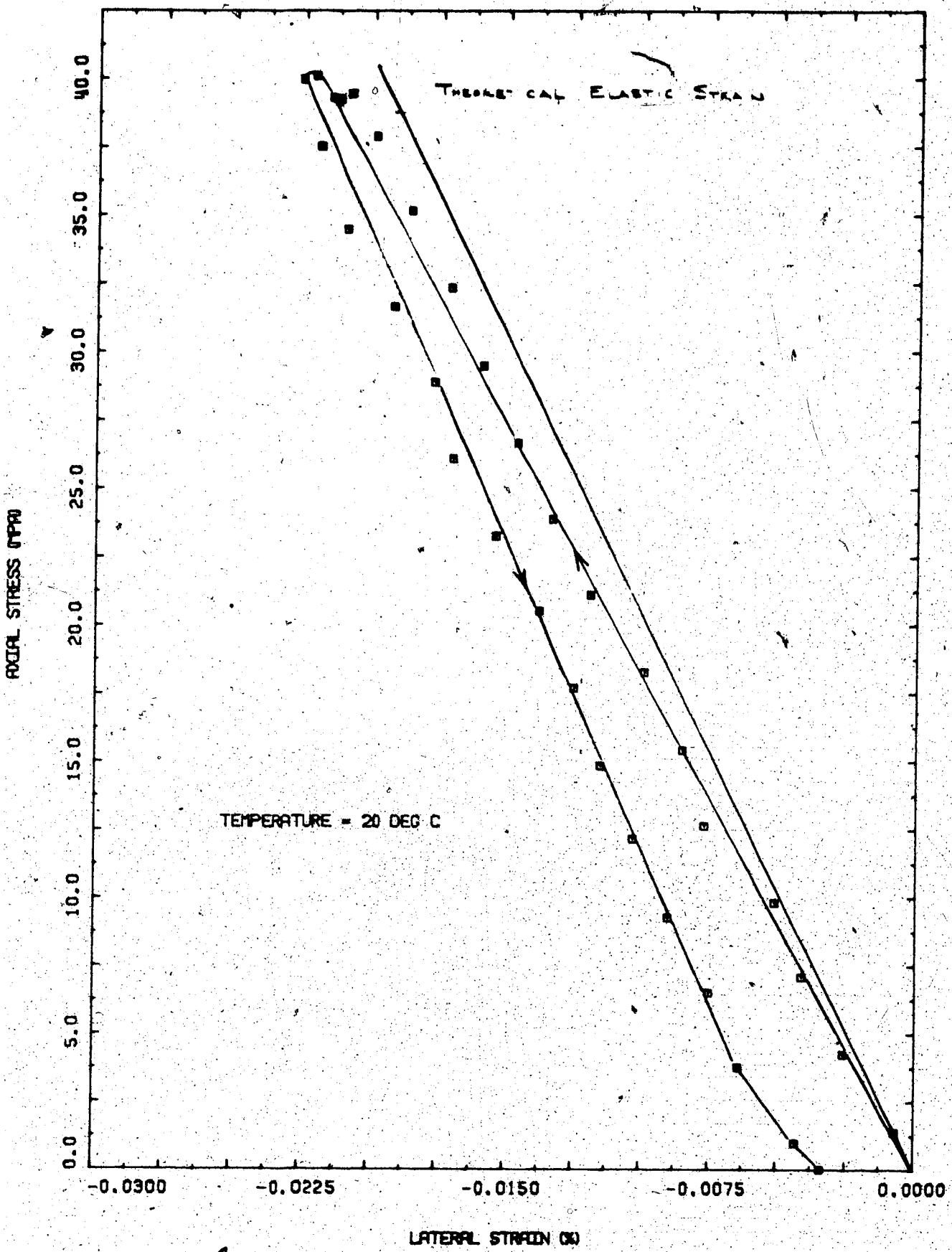

FIGURE A17 Triaxial Apparatus: Accuracy of an Internal Lateral Strain Measuring Device During Compression of an Aluminium Sample at 20°C

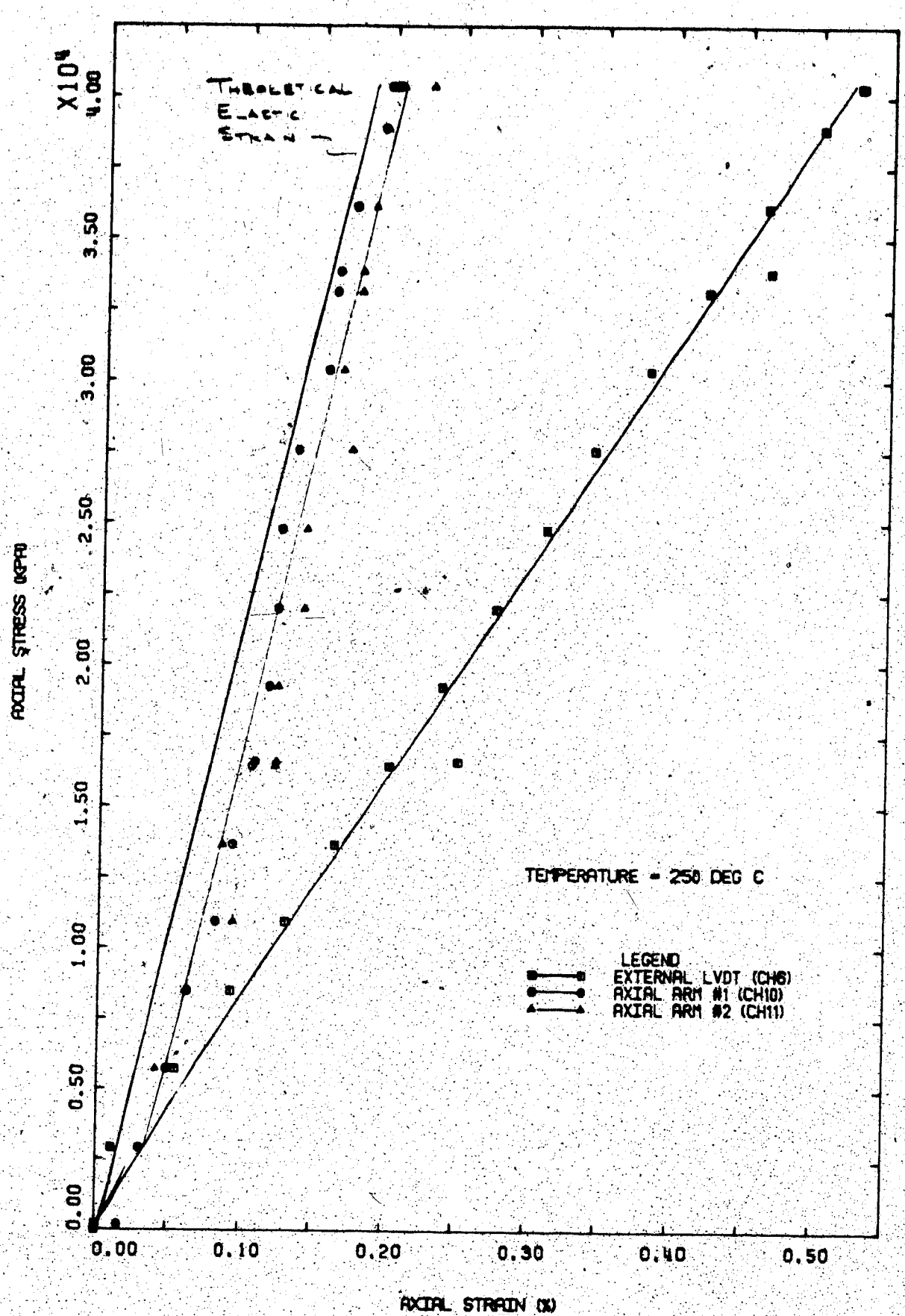

FIGURE A18 Triaxial Apparatus: Accuracy of Internal and External Axial Strain Measuring Devices During Compression of an Aluminium Sample at 250°C

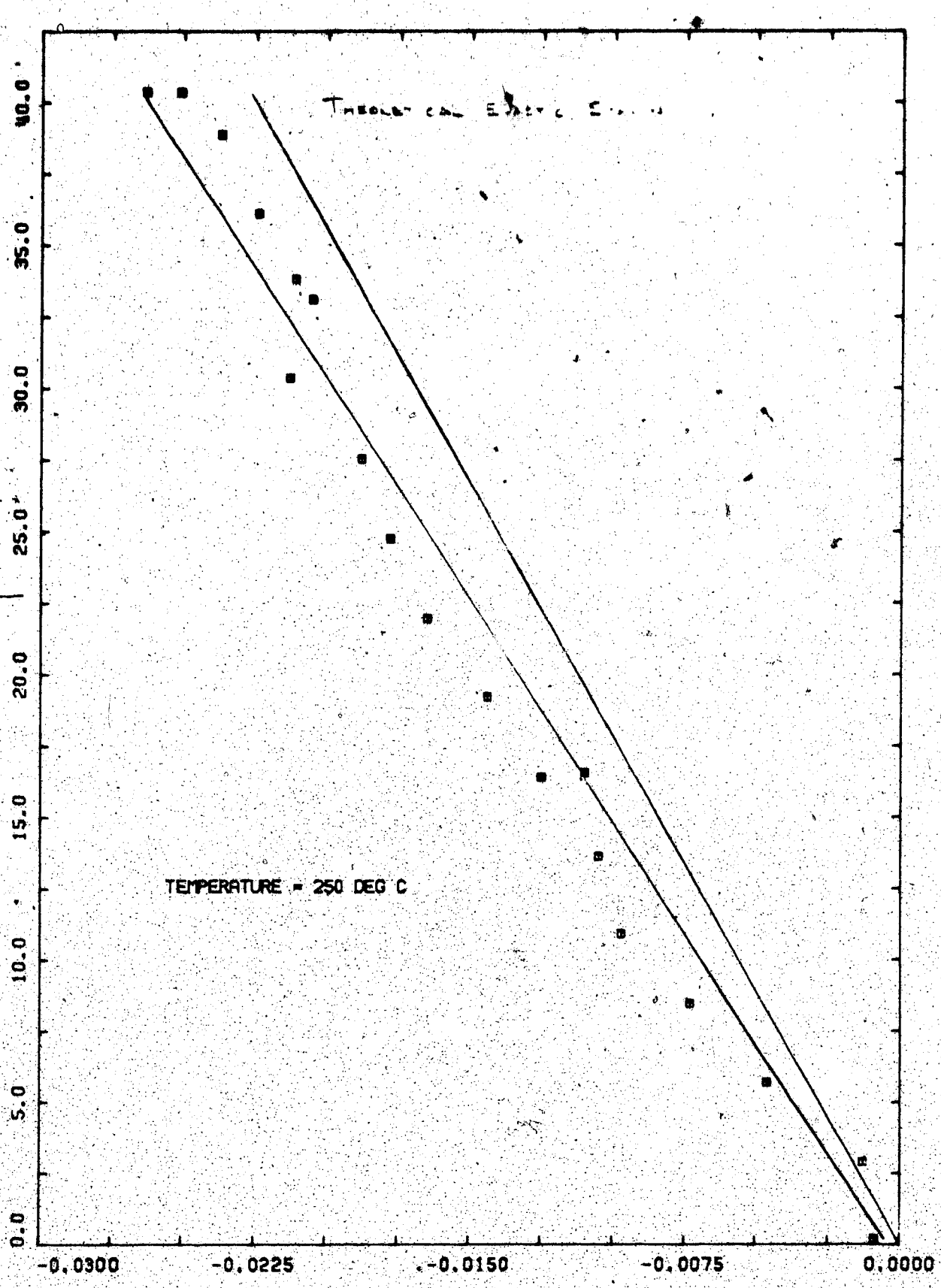

FIGURE A19 Triaxial Apparatus: Accuracy of an Internal Lateral Strain Measuring Device During Compression of an Aluminium Sample at 250°C

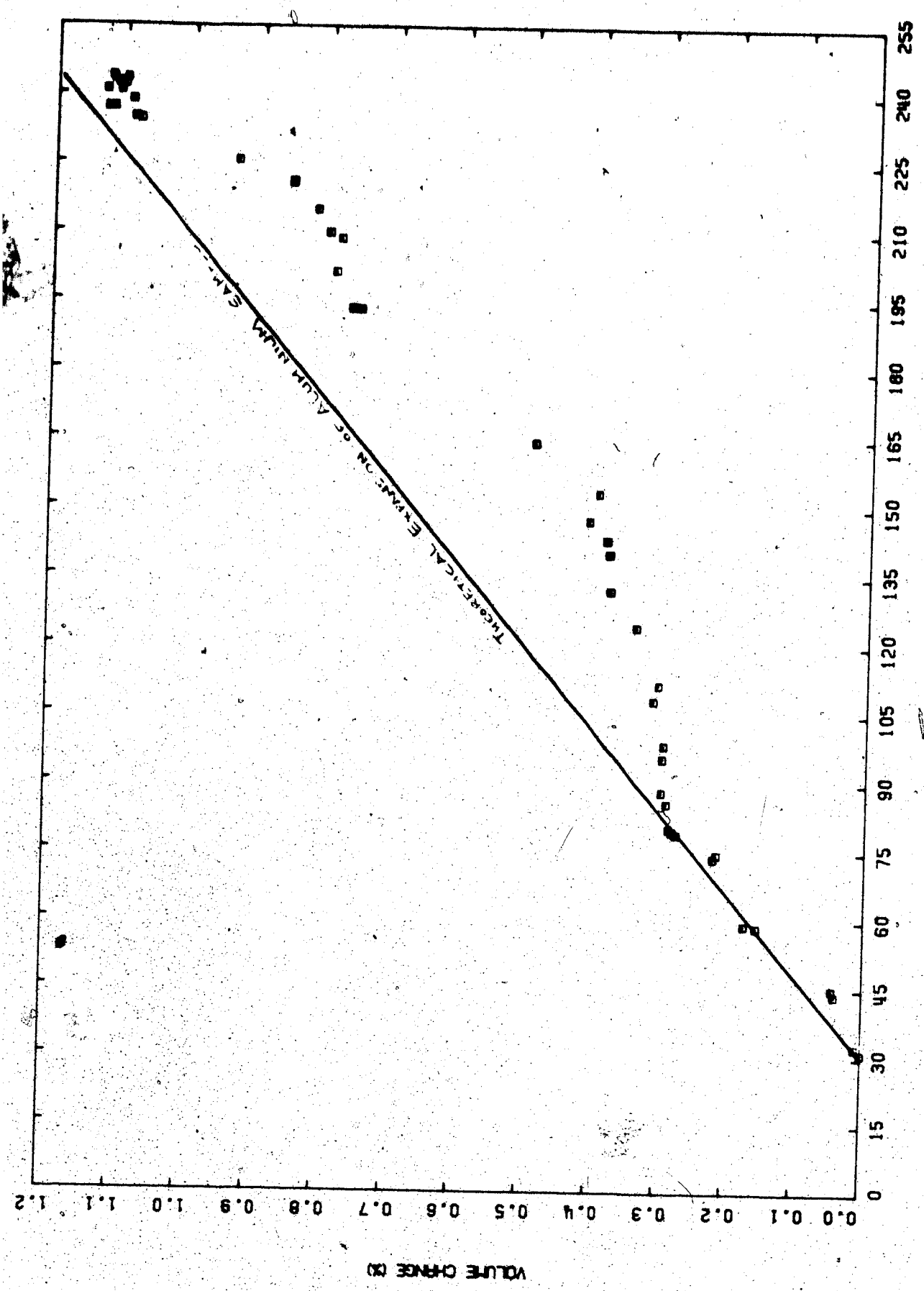

FIGURE A20 Triaxial Apparatus: Compliance of Volume Change Measurements During Thermal

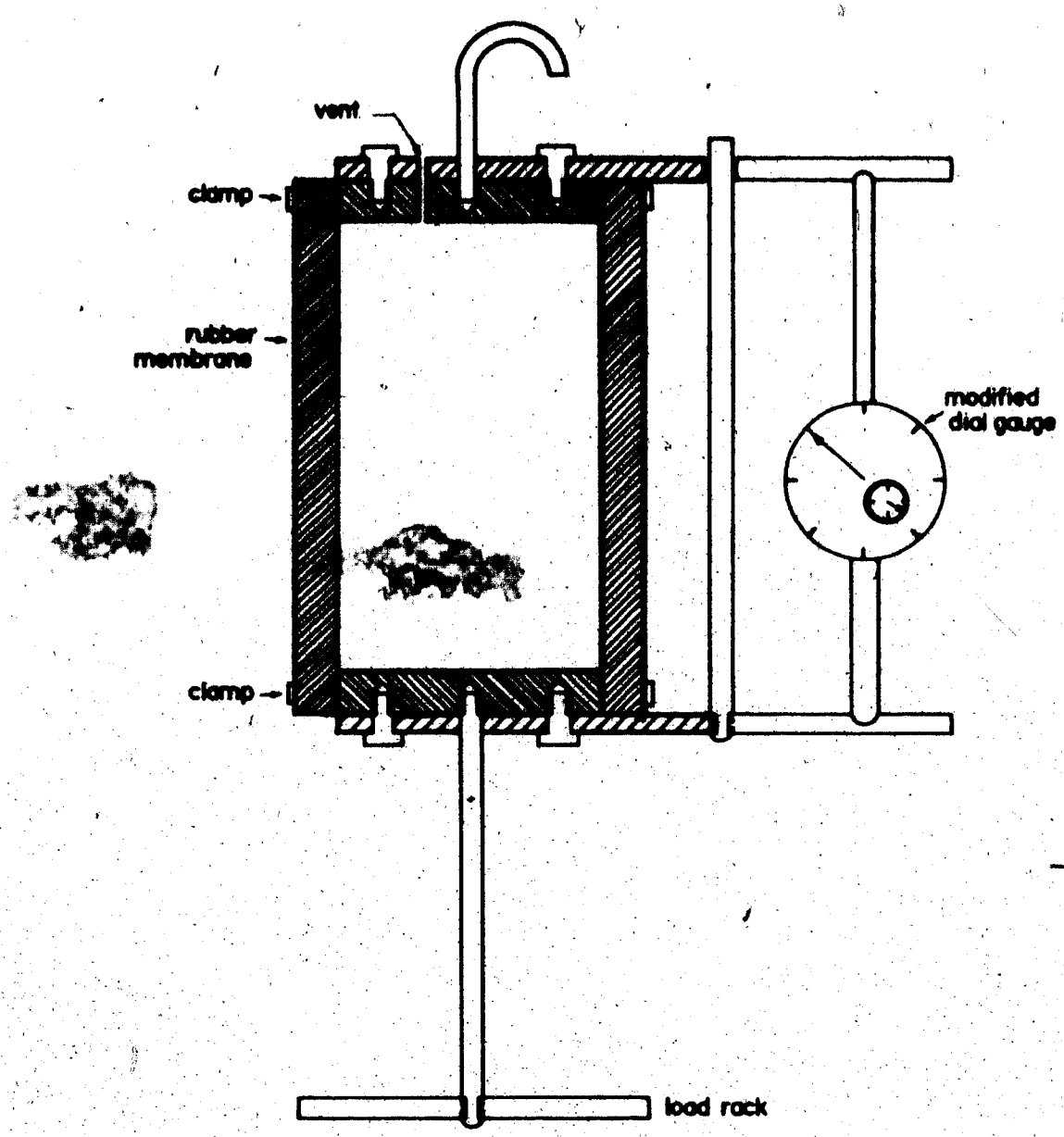

FIGURE A21 Schematic Cross Section of a Membrane Extension Testing Apparatus Used at Elevated Temperatures in an Oven

APPENDIX B

THERMAL EXPANSION TESTS

TABLE B-1

SUMMARY OF TEST DATA FOR THERMAL EXPANSION TESTS

Test Number	Sample Number	Type of Test	Maximum Temperature (°C)	Maximum Back Pressure (MPa)	Effective Confining Stress (MPa)	Total Sample Expansion (%)	Volume of Pore Fluid Expelled (%)
COS 1	5	Undrained	200	2.4	0.05	73.0	-
COS 2	32	Undrained	200	2.5	0.05	10.0	-
COS 3	30	Gas Exsolution	242	4.0	0.05	9.5	-
COS 4	38	Undrained	300	15.0	0.05	11.3	-
COS 5	18	Undrained	[illegible]	17.0	0.05-6.0	9.2	-
COS 6	10A	Drained	300	15.0	6.0	0.9	6.6
COS 7	10B	Drained	300	15.0	0.05	0.8	8.1
COS 8	42	Gas Exsolution	300	10.0	0.05	24.0	-
COS 9	41	Undrained	300	10.0	0.05	15.2	-

TEST COS1

Undrained Thermal Expansion of Saline Creek
Oil Sand Sample No. 5 Under Nominal
Effective Confining Stress from 24 - 200°C

Procedural Details: Test COS 1

1. Saline Creek sample no. 5 was warmed to room temperature (approximately 24°C) under a nominal vertical confining stress of sufficient magnitude to prevent expansion of the sample.
2. The vertical stress and back pressure were increased simultaneously to approximately 2000 kPa (290 psi) in 200 kPa increments. The sample was left to saturate under this 2000 kpa back pressure for a period exceeding 24 hours.
3. The back pressure valve was closed isolating the 2000 kPa back pressure in the cell.
4. Cell temperatures were elevated in stages as follows: 24°C, 60°C, 100°C, 150°C, 200°C.
5. The applied vertical stress was adjusted continuously to maintain approximately zero effective vertical stress in the sample as temperature increased.
6. The sample height (i.e. piston postion) was monitored throughout the test.
7. A significant volume change in the order of 60 percent was observed when the temperature was raised from 150°C to 200°C. This volume change is believed to have been due to

gas exsolution and/or phase change of pore fluids adjacent to heating rods in the test cell. It is believed that local overheating may have occurred when such a large temperature increment (50°C) was applied.

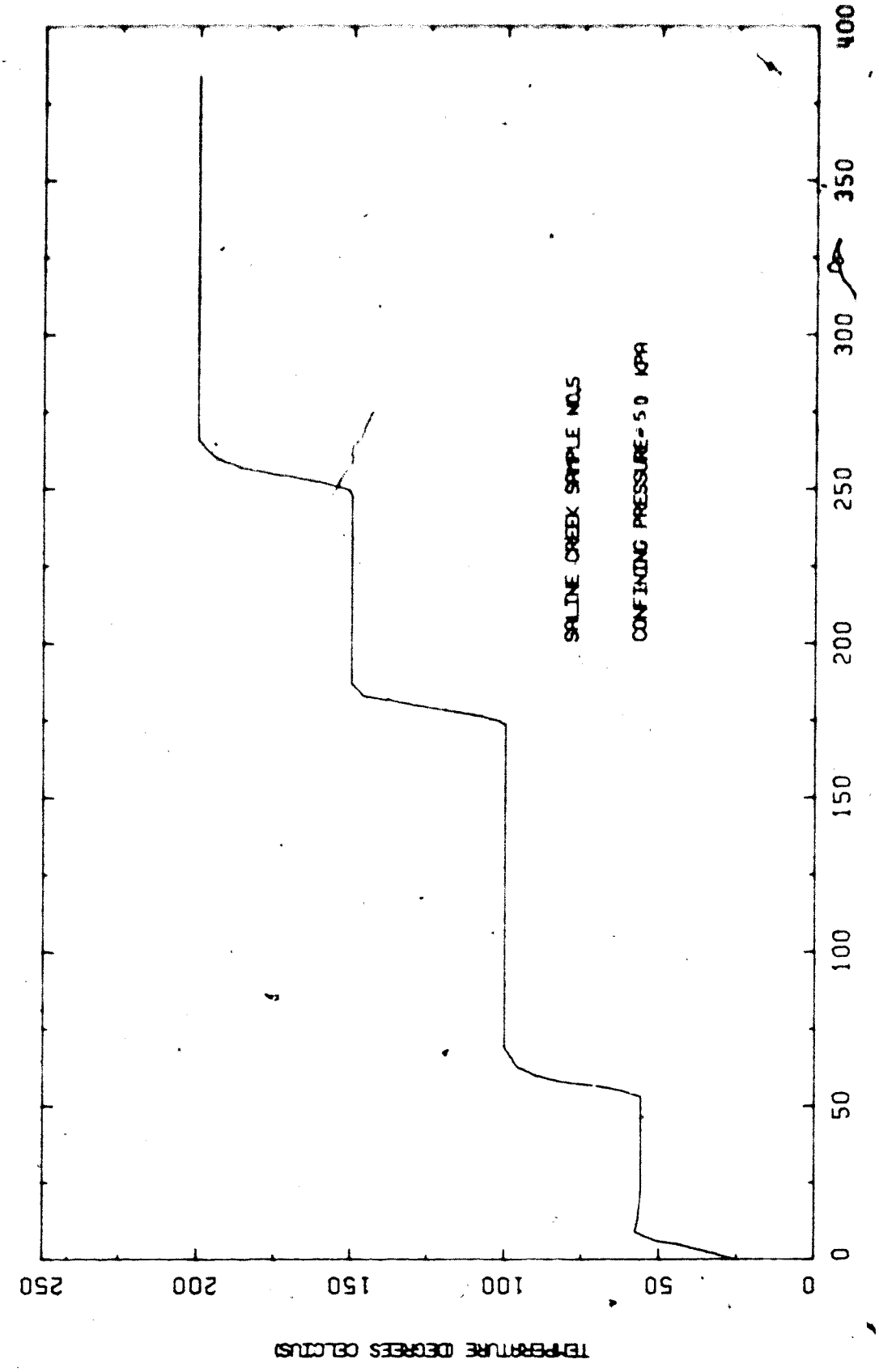

FIGURE B1 Temperature Versus Time: Test C091

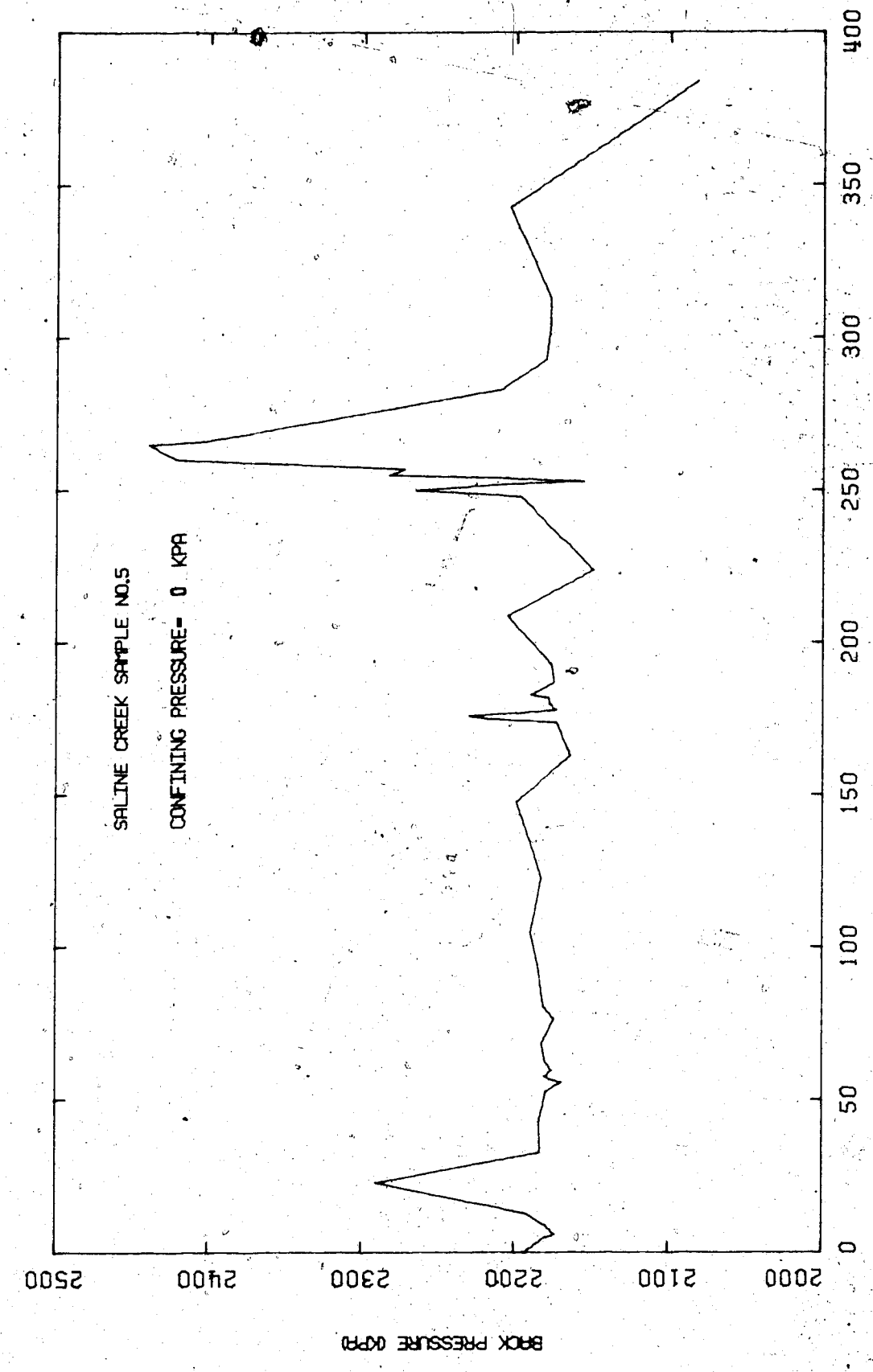

FIGURE B2 Back Pressure Versus Time: Test COS1

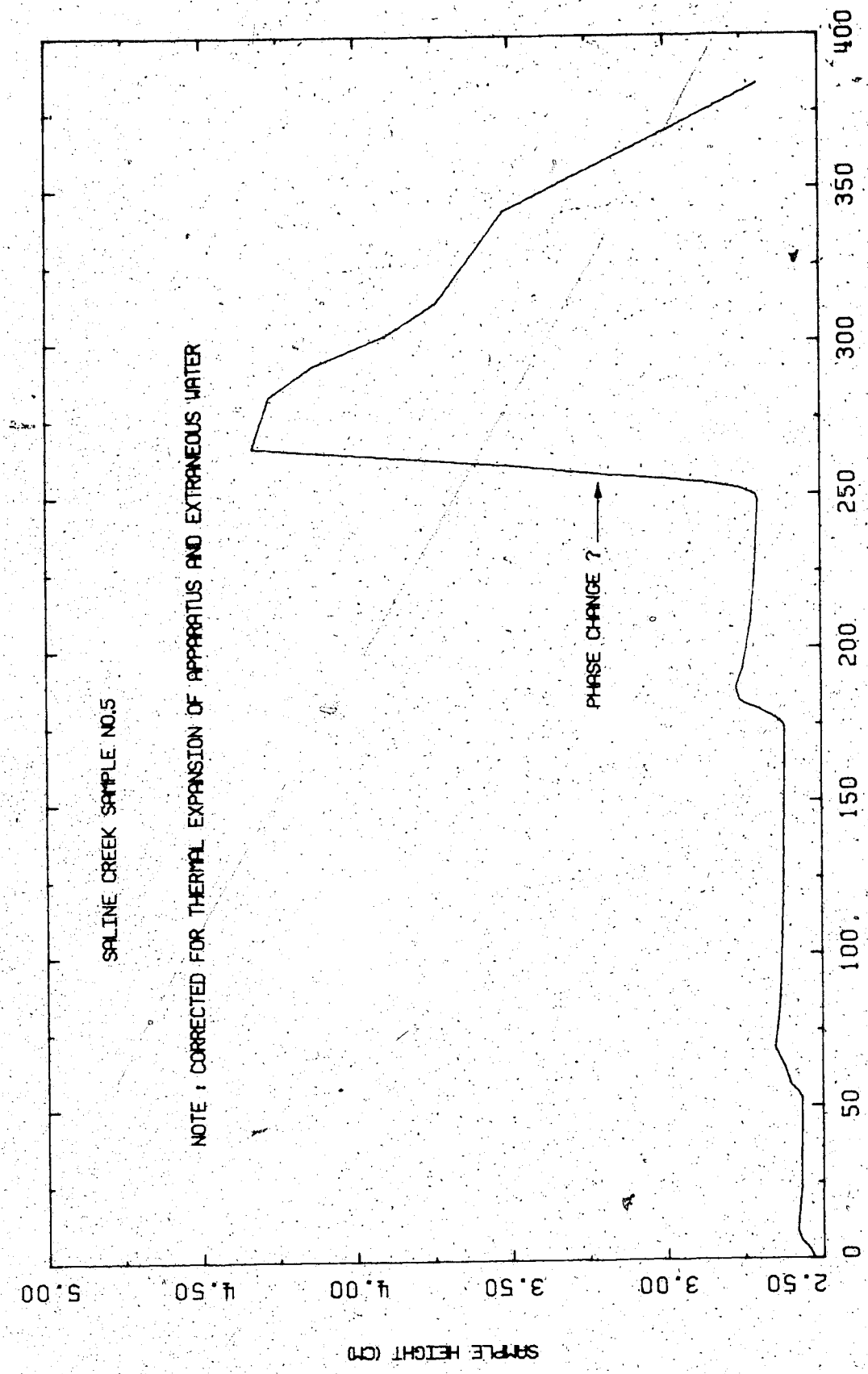

FIGURE B3 Sample Height Versus Time: Test COS1

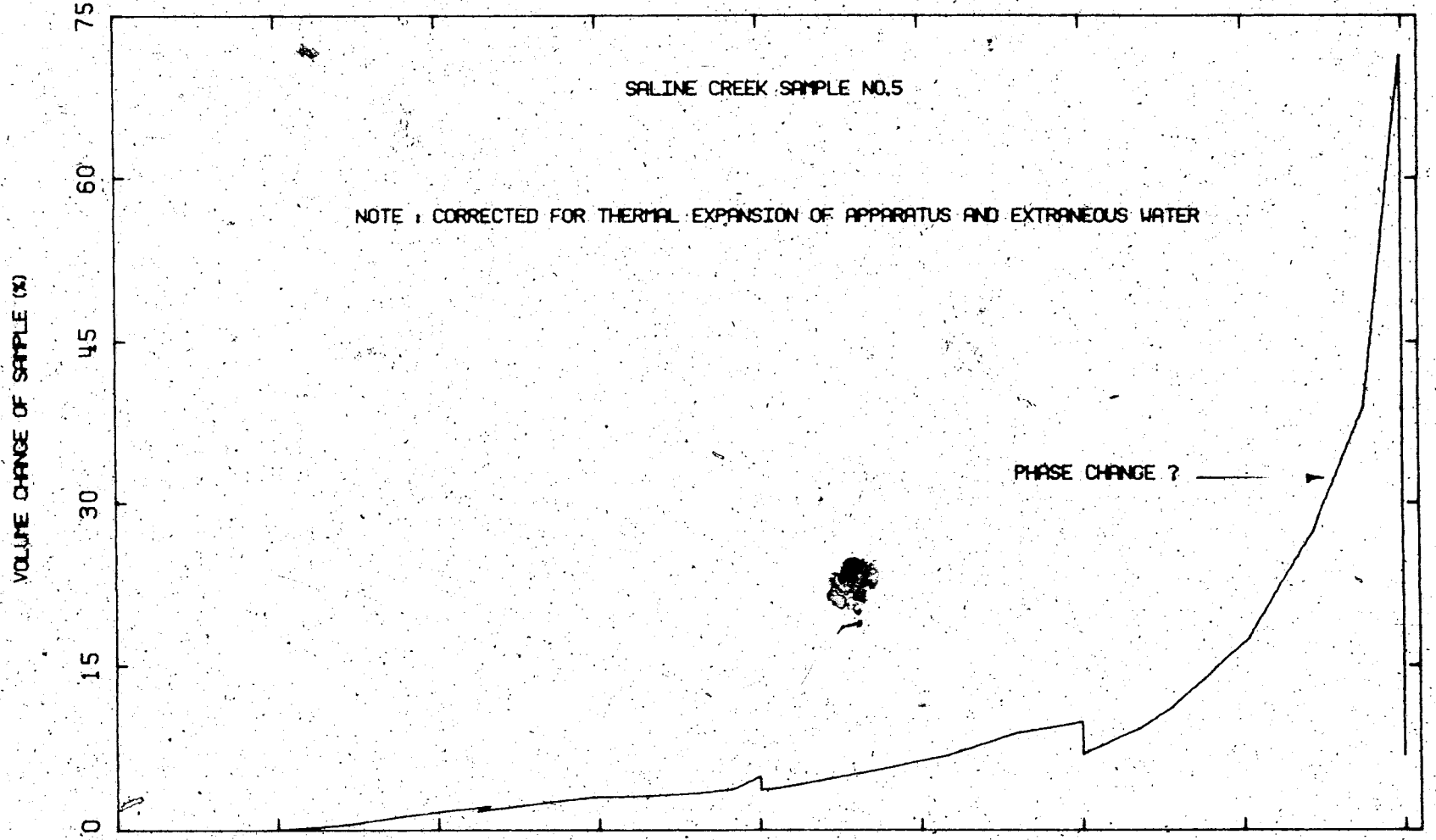

FIGURE B4 Undrained Volumetric Thermal Expansion:

TEST COS2

Undrained Thermal Expansion of Saline Creek Oil Sand Sample No. 32 under Nominal Effective Confining Stress (50 kPa) from 20-200°C

Procedural Details: Test COS 2

1. Sample No. 32 was warmed to room temperature under confined conditions to prevent thermal expansion of the sample.
2. The sample was saturated under confining and back pressures of approximately 2000 kPa for a period exceeding 24 hours. The 2000 kPa back pressure was then shut in and drainage prevented.
3. Cell temperatures were increased in 10°C increments up to 200°C.
4. The confining pressure was adjusted continuously to maintain approximately 50 kPa effective vertical stress in the sample as heating proceeded.
5. At 180°C the back pressure and confining pressure were increased to 2500 kPa to prevent large volume changes associated with phase change and/or gas exsolution.
6. The test was terminated at 200°C after the development of a leak in the back pressure system.

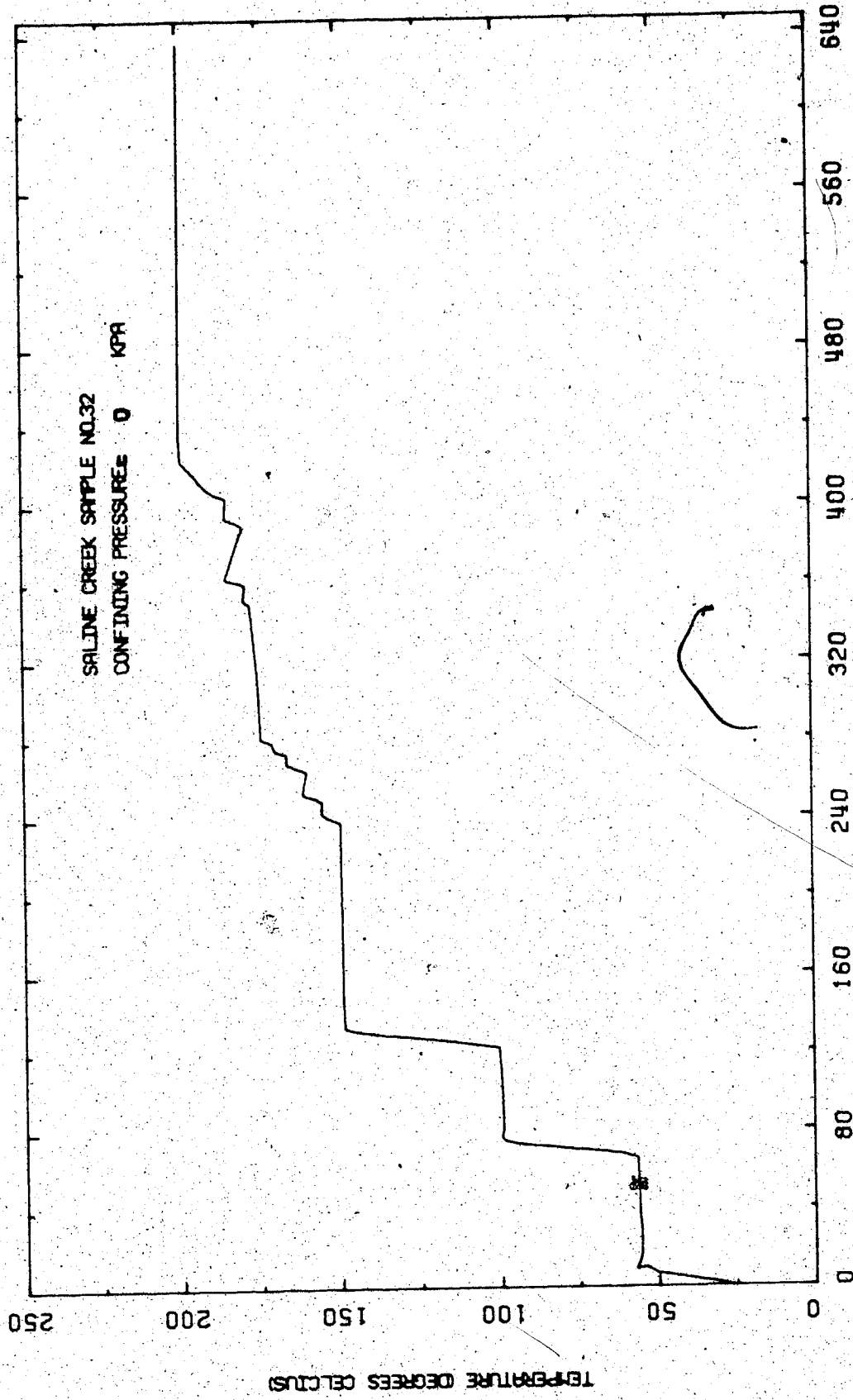

FIGURE B5 Temperature Versus Time: Test COS2

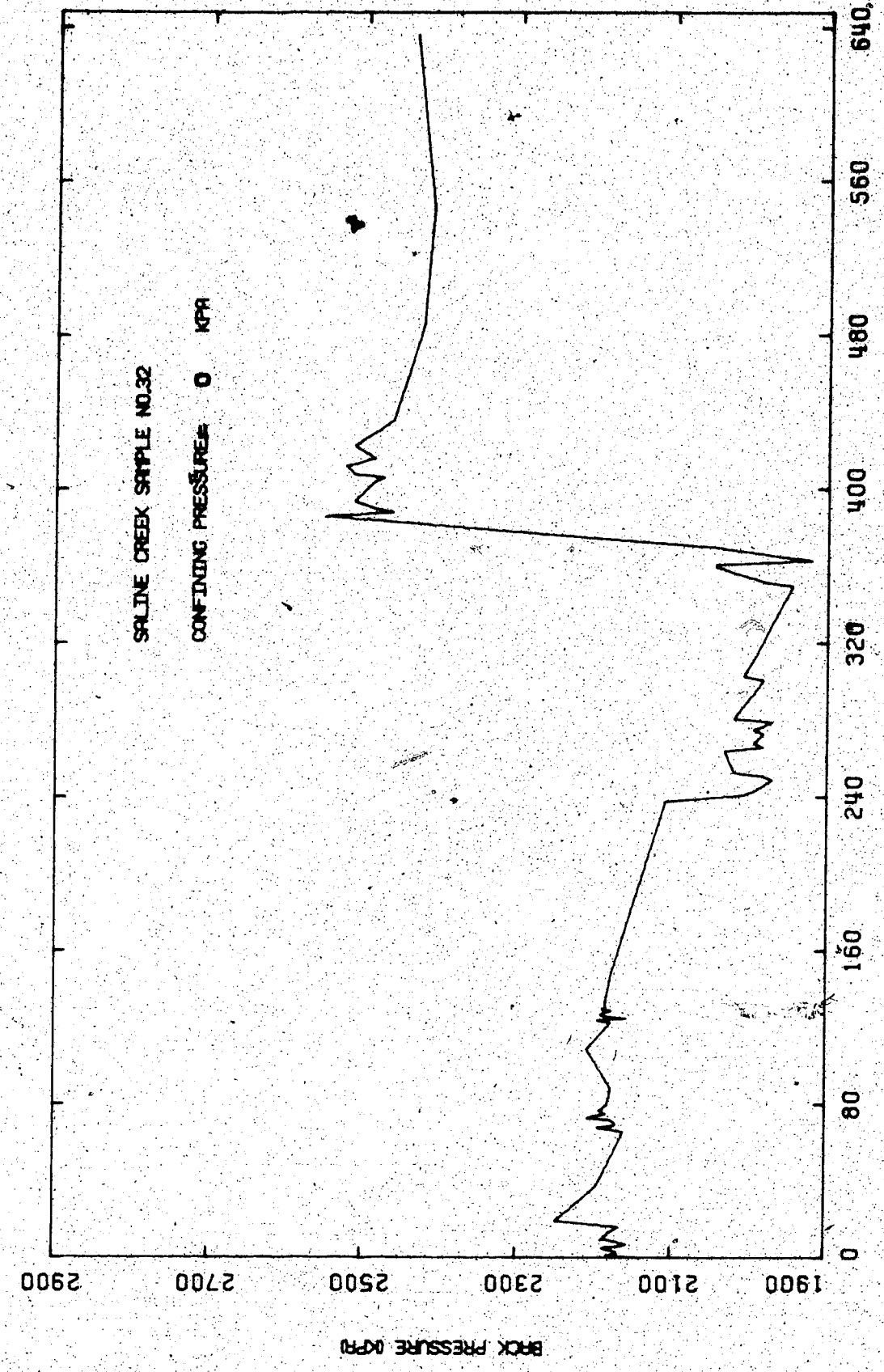

FIGURE B6 Back Pressure Versus Time - Test CDS2

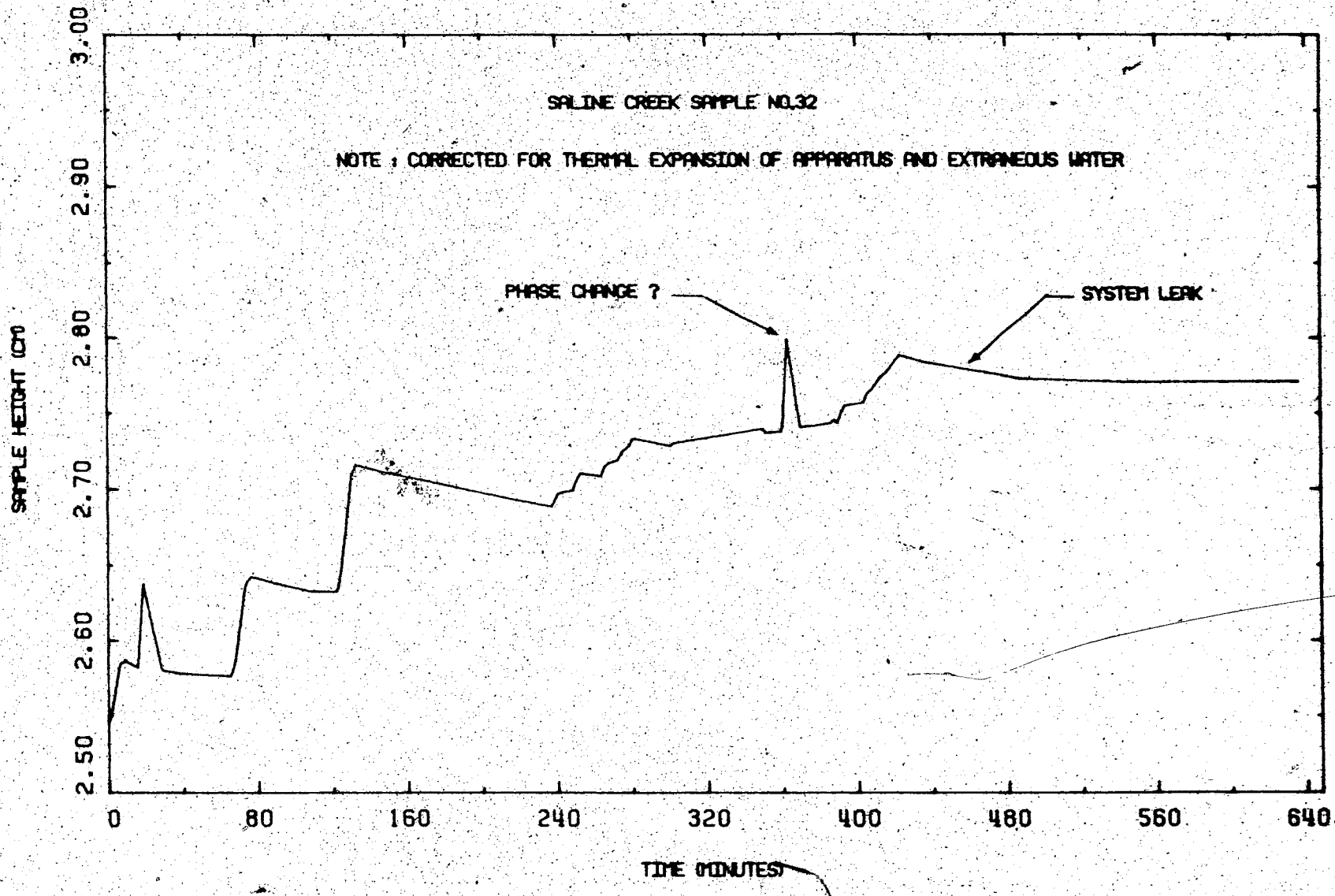

FIGURE B7 Sample Height Versus Time: Test COS2

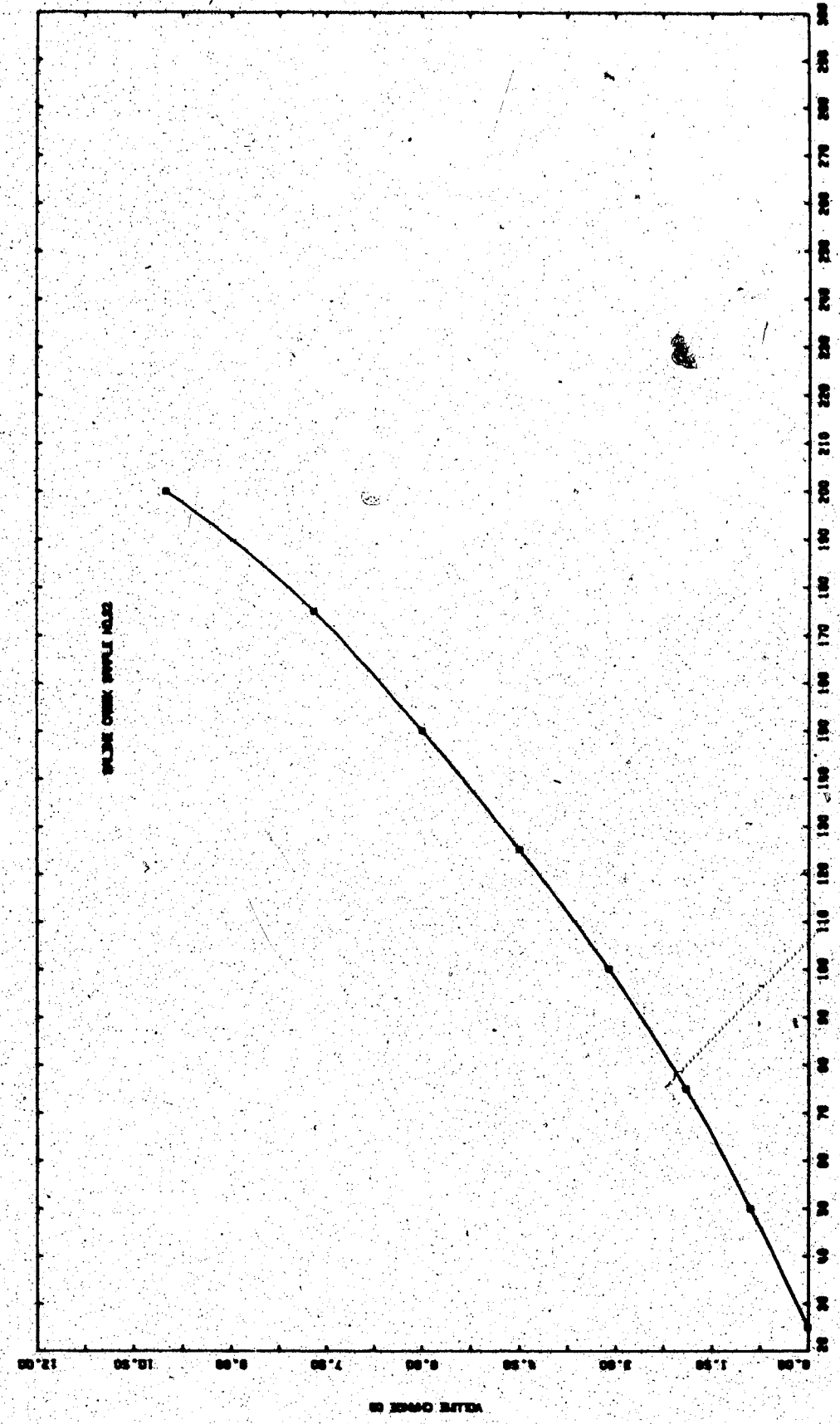

FIGURE B8 Undrained Volumetric Thermal Expansion: Test COS2

TEST COS3

Undrained Thermal Expansion under Nominal Effective Confining Stress (50 kPa) and Gas Exsolution Test For Saline Creek Oil Sample No. 32 at Temperatures from 25-242°C

Procedural Details: Test COS 3

1. Saline Creek Sample No. 32 was confined under a nominal confining pressure to prevent thermal expansion as it warmed to room temperature.
2. The sample was saturated under confining and back pressures of approximately 2000 kPa for a period exceeding 24 hours.
3. The vertical confining pressure and back pressure were initially reduced to 200 kPa. The back pressure valves were then shut in.
4. The cell temperature was raised in 5°C increments.
5. Confining and back pressure were increased only when required to prevent phase change/or gas exsolution of the pore fluids.
6. Each time that large volumetric expansion was observed which was believed to be due to phase change/gas exsolution, the cell temperature was immediately decreased to the previous temperature increment. The confining pressure was increased gradually during these mini cool-down phases to maintain near-constant back pressure and to re-establish the previous sample volume.
7. The confining and back pressures were then increased.

simultaneously prior to applying the next temperature increment.

8. The purpose of the above procedure was to attempt to define a pressure-temperature relationship corresponding to gas exsolution and/or phase change of the pore fluids.
9. The test was terminated at 242°C due to an electrical power shut-down at the University of Alberta.

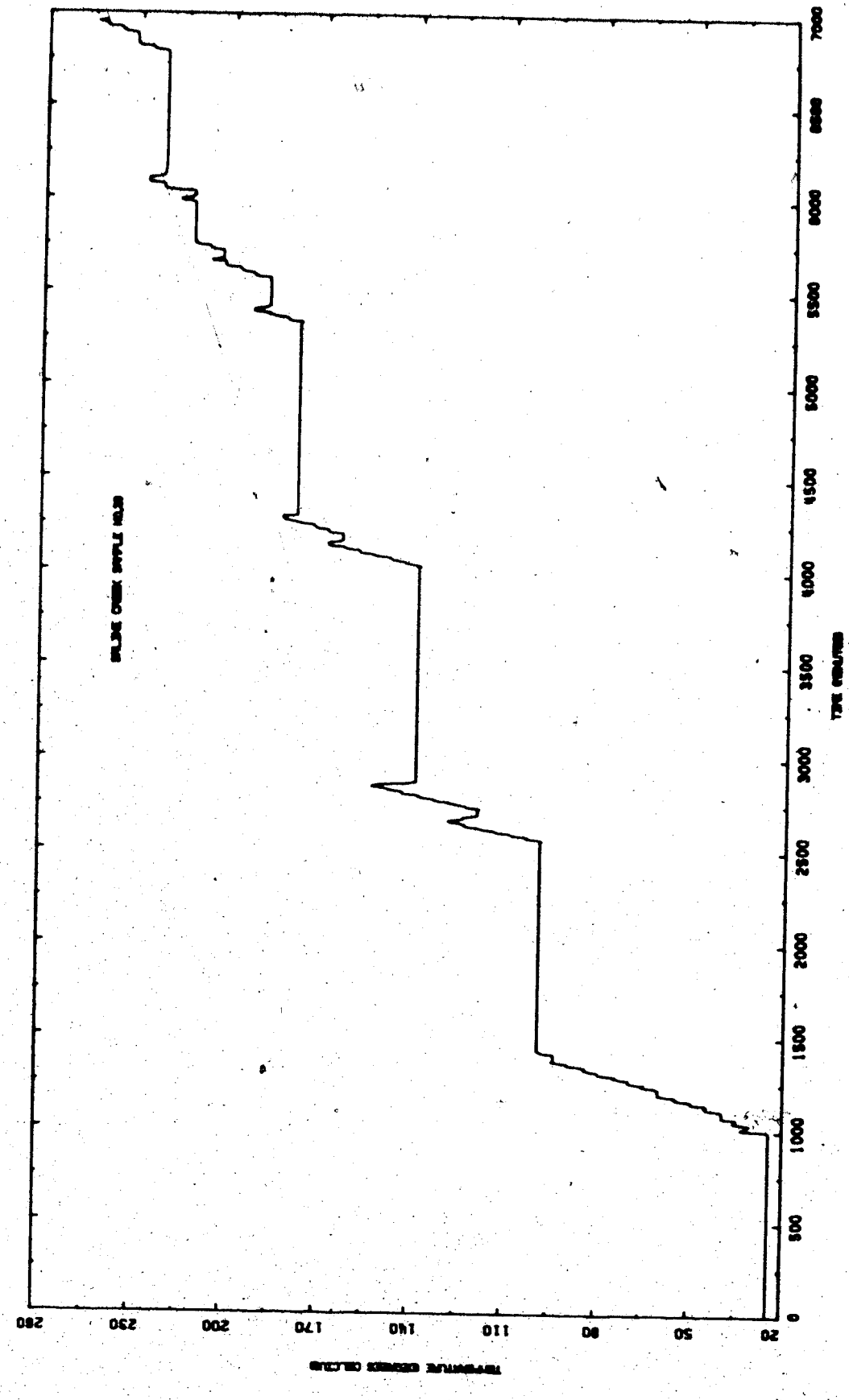

FIGURE B9 Temperature Versus Time: Test COS3

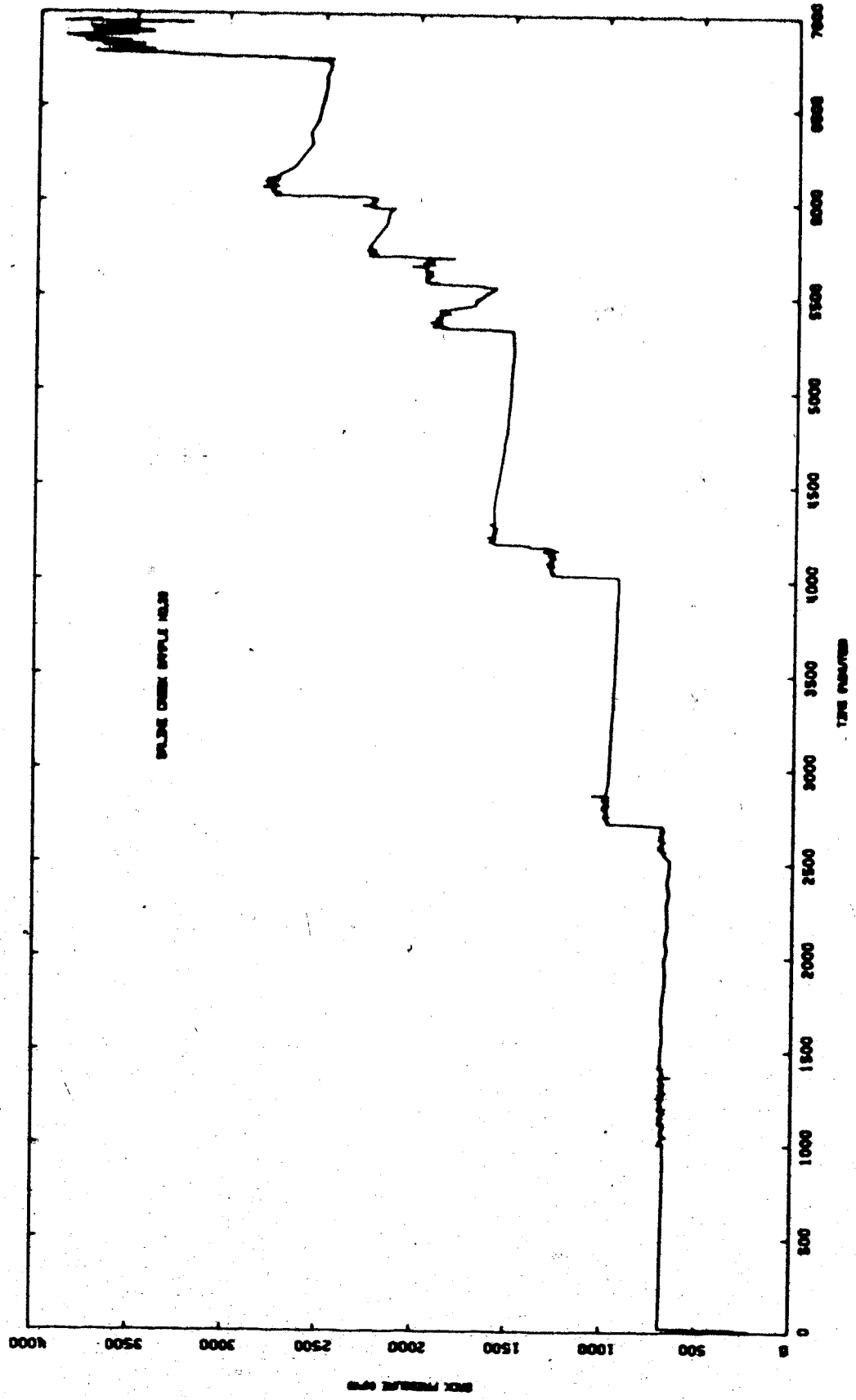

FIGURE B10 Back Pressure Versus Time: Test COS3

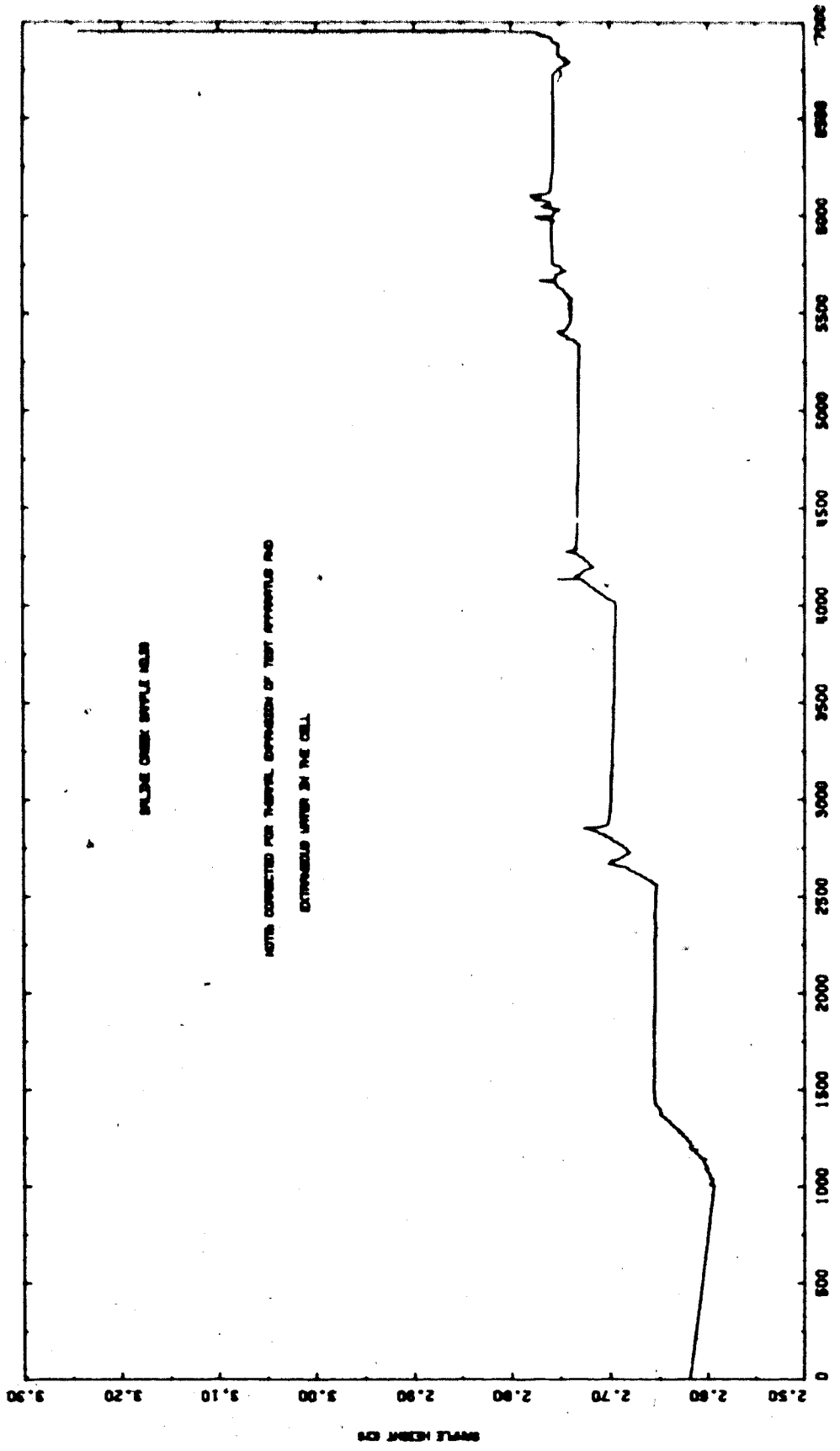

FIGURE B11 Sample Height Versus Time: Test COS3

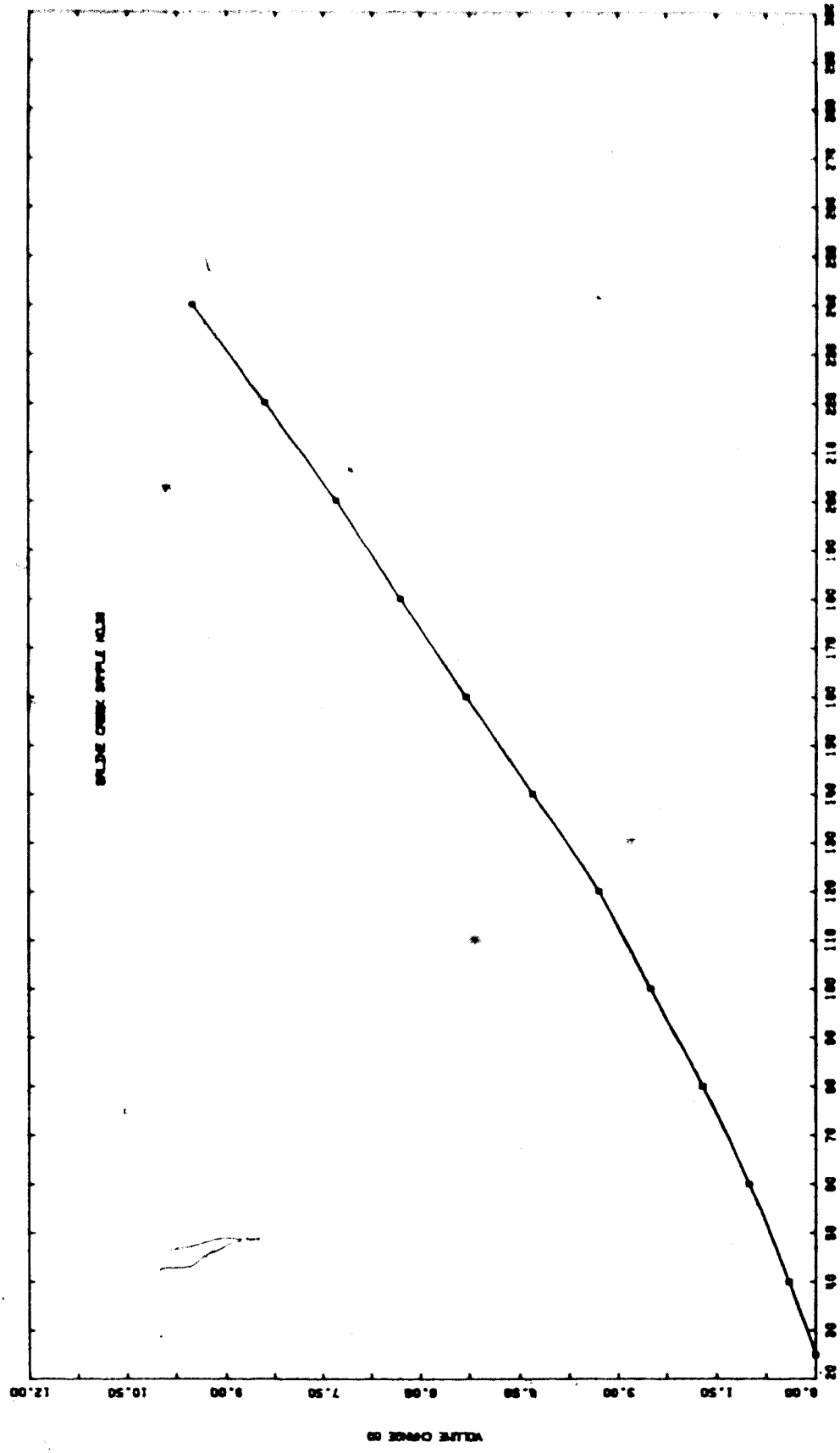

FIGURE B12 Undrained Volumetric Thermal Expansion: Test COS3

TEST C0S4

Undrained Thermal Expansion of Saline Creek Oil Sand Sample No. 38 under Nominal Effective Confining Stress (50 kPa) and over the Temperature Range 25-300°C

Procedural Details: Test C0S4

1. Sample no. 38 was warmed to room temperature under nominal confining pressure to prevent thermal expansion.
2. The sample was saturated under back and confining pressures of 2000 kPa for a period exceeding 24 hours. The 2000 kPa back pressure was then shut in.
3. The cell temperature was raised in 5°C increments.
4. The confining pressure was adjusted continuously during heating to maintain approximately zero effective vertical stress on the sample.
5. Back pressures and confining pressures of sufficient magnitude to prevent phase change and/or gas exsolution were applied as follows:

Temperature Range	Back Pressure
25 - 150°C	2000 kPa
151 - 200°C	5000 kPa
201 - 300°C	15000 kPa
300 - 25°C (cool down)	15000 kPa

6. Sample height was monitored during the test.

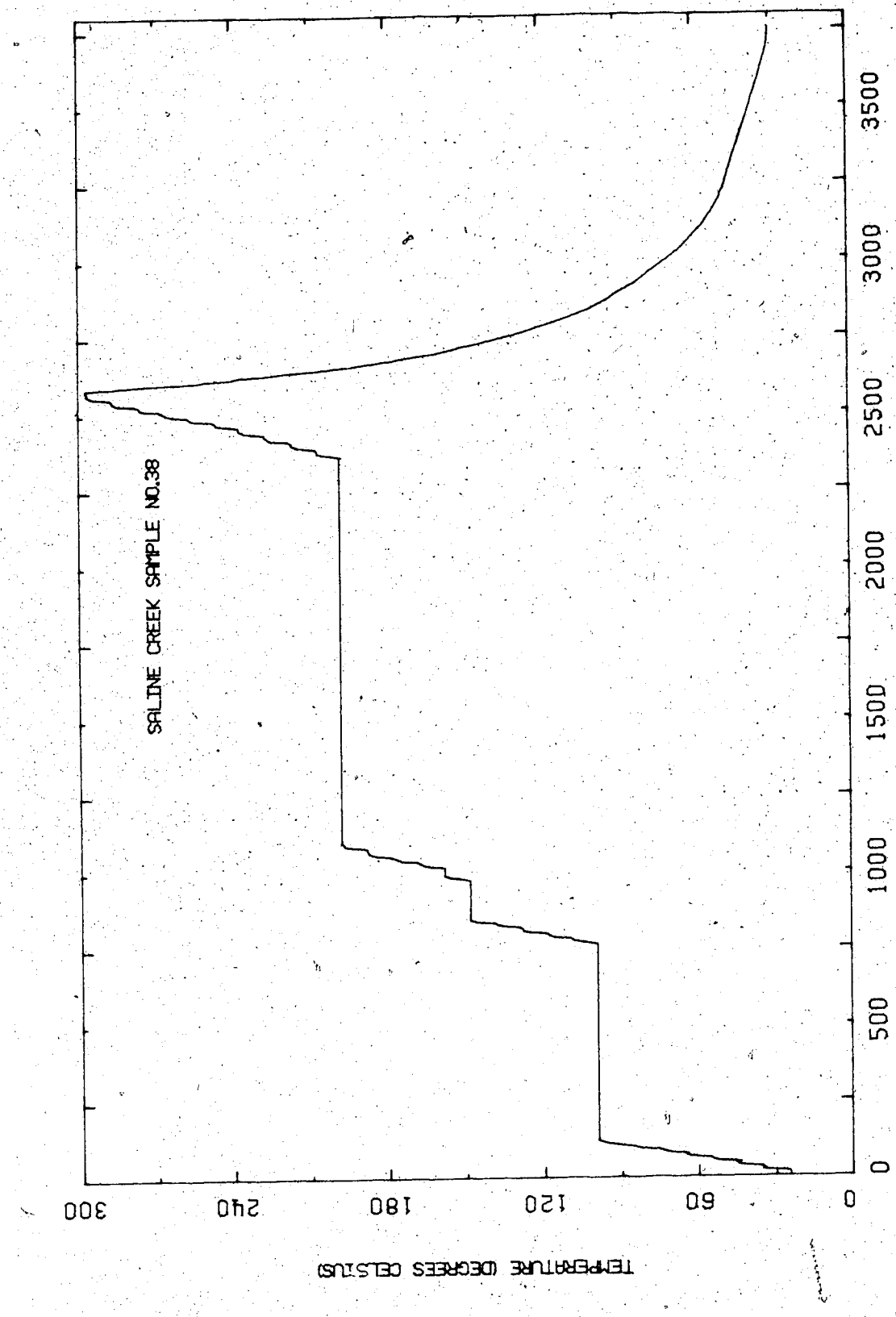

FIGURE B13. Temperature Versus Time: Test COS4

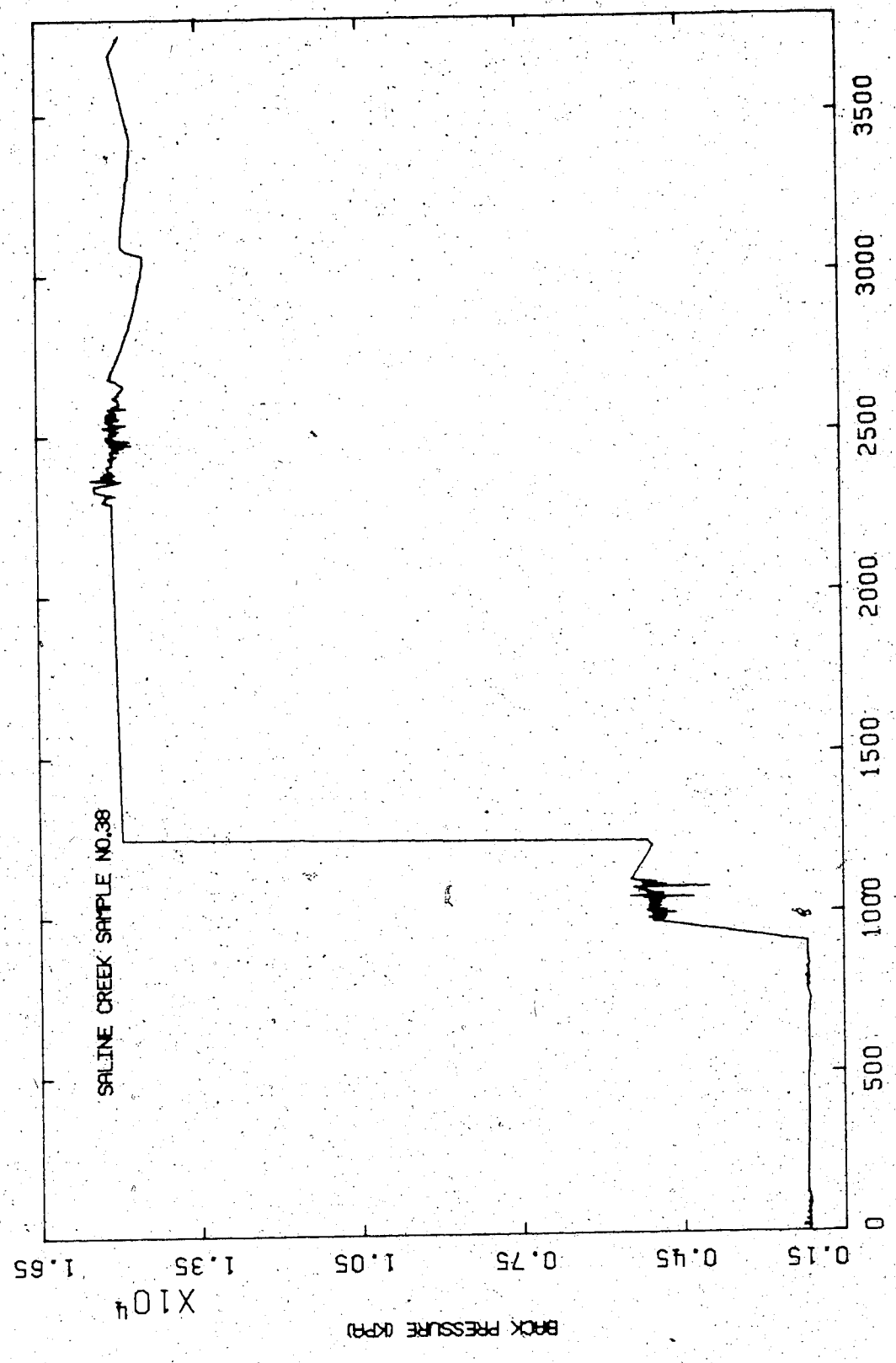

FIGURE B14 Back Pressure Versus Time: Test COS4

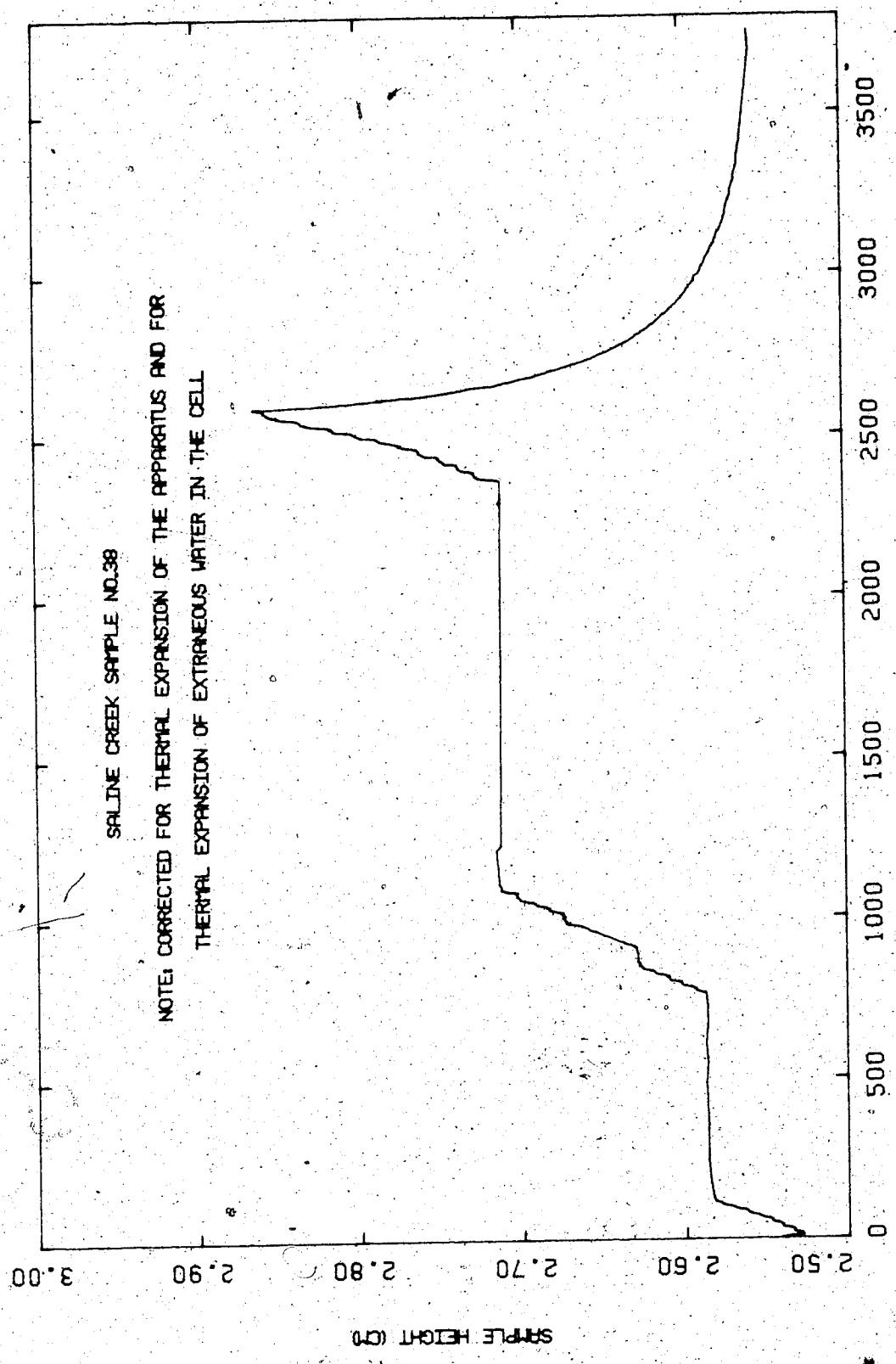

FIGURE B15 Sample Height Versus Time: Test COS4

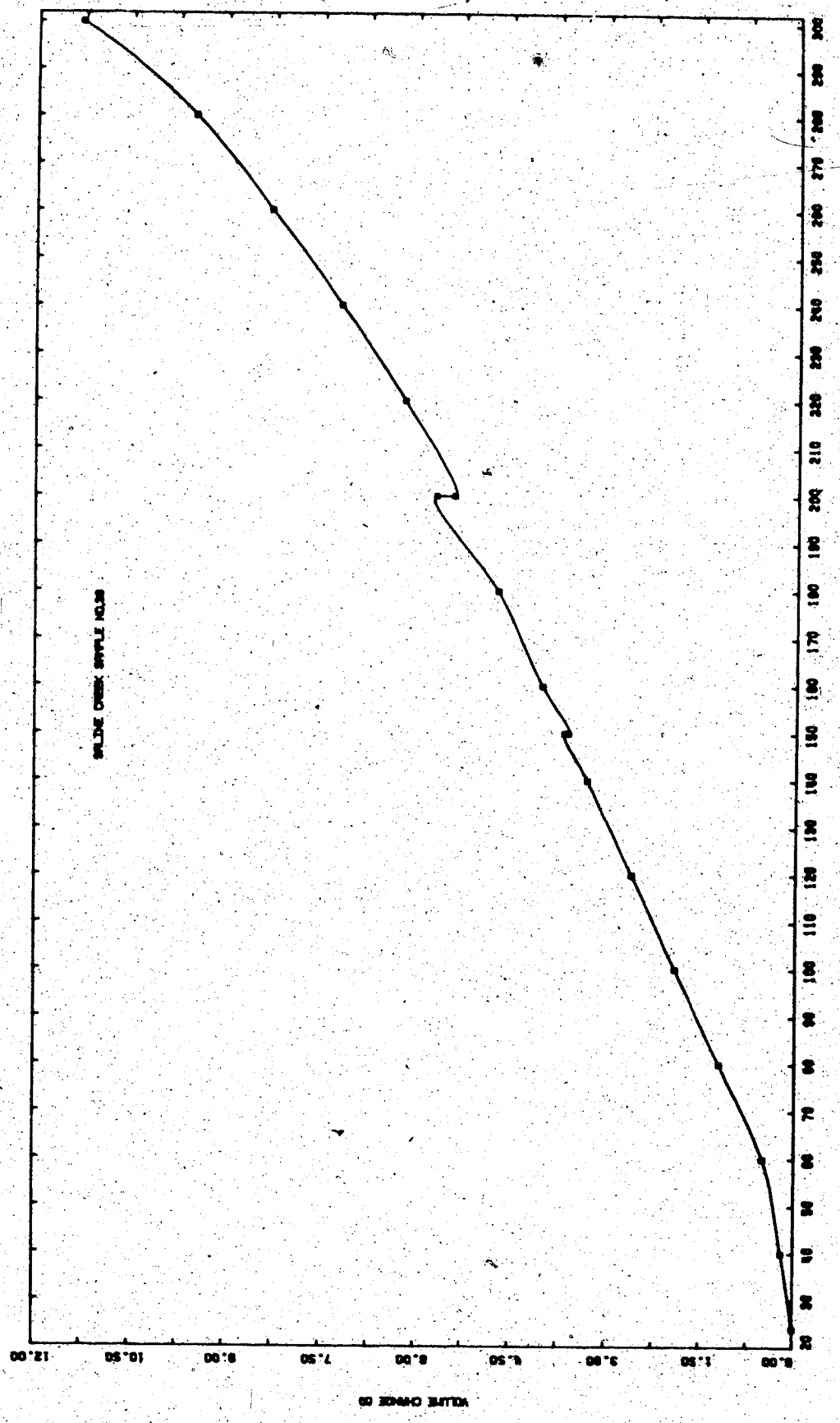

FIGURE B16 Undrained Volumetric Thermal Expansion: Test COS4

TEST COS5

Undrained Thermal Expansion and Pore Pressure Response to the Undrained Heating of Saline Creek Oil Sand Sample No. 18 at Effective Confining Stresses 0.05 - 6.0 MPa and Over the Temperature Range 20 - 292°C

Procedural Details: Test COS5

1. Sample No. 18 was saturated at approximately 2000 kPa (290 psi) back pressure for 24 hours +.
2. Confining pressure and back pressure were increased simultaneously to approximately 5000 kPa (725 psi).
3. Confining pressure was then increased to approximately 11,000 kPa (1600 psi) in 200 kPa increments.
4. The sample drainage valves were closed and a back pressure of 5000 kPa (725 psi) was shut in.
5. The sample was heated incrementally with the confinihg pressure held constant and the increase in pore fluid pressure (back pressure) was monitored during undrained heating. After the back pressure had increased to equal the confining pressure (ram pressure + piston friction), heating was continued up to 150°C with approximately zero vertical effective stress on the sample.
6. The confining pressure was then increased to approximately 17,000 kPa while the back pressure was maintained at approximately 11,000 kPa. Drainage of pore fluid from the

sample was permitted under this effective stress level (approximately 6000 kPa).

7. The back pressure of approximately 11,000 kPa was shut in and further drainage prevented.

8. Heating of the sample above 150°C was continued and the undrained pore pressure increase was monitored until it equalized with the confining pressure. This pore pressure build-up occurred very rapidly, as anticipated.

9. Heating of the sample under approximately zero effective vertical stress was continued up to 292°C when leakage pas the O-ring seal occurred causing a sudden drop in the back pressure and allowing sudden uncontrolled pore fluid drainage. The test was terminated at this point.

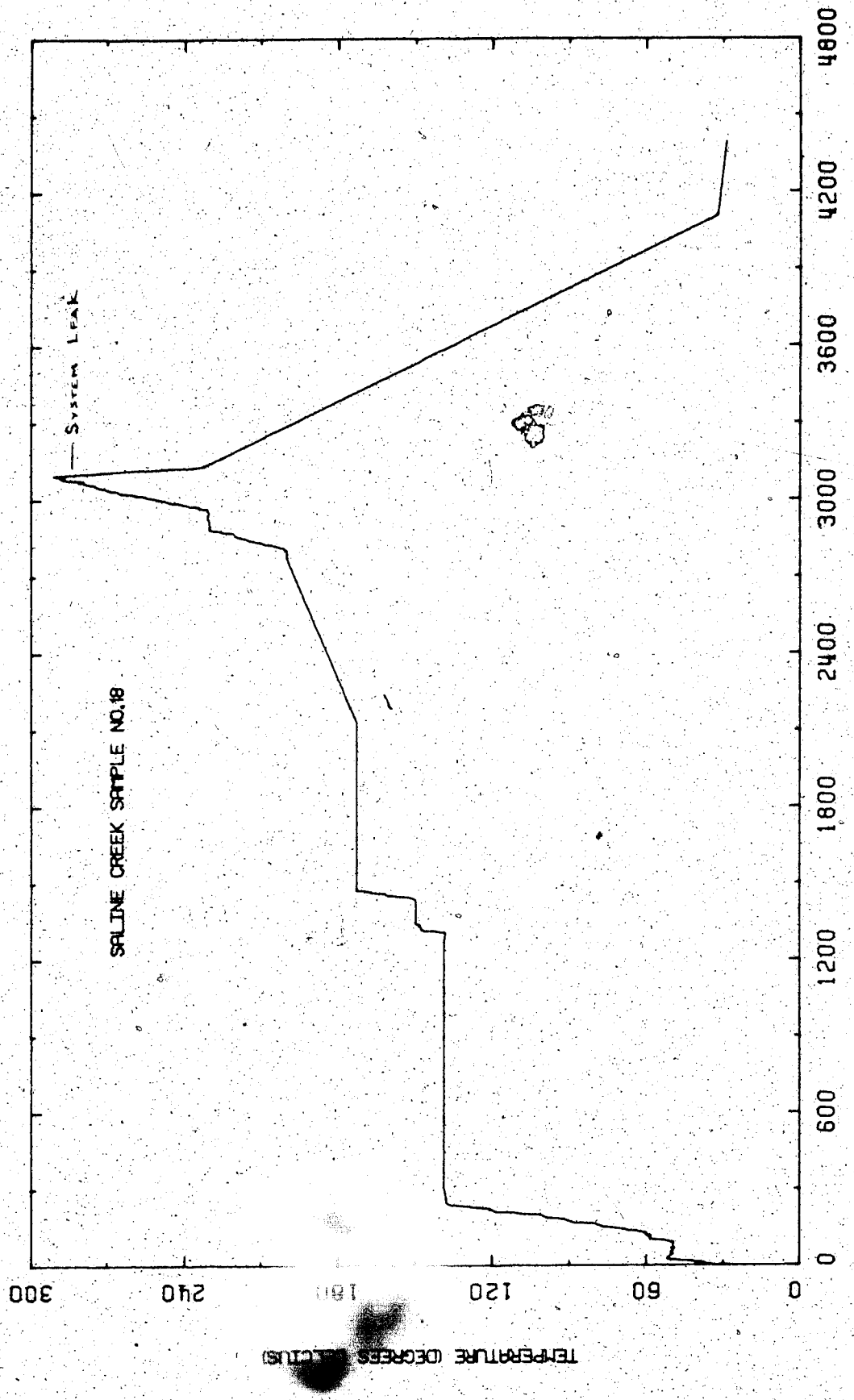

FIGURE B17 - Temperature Versus Time: Test COS5

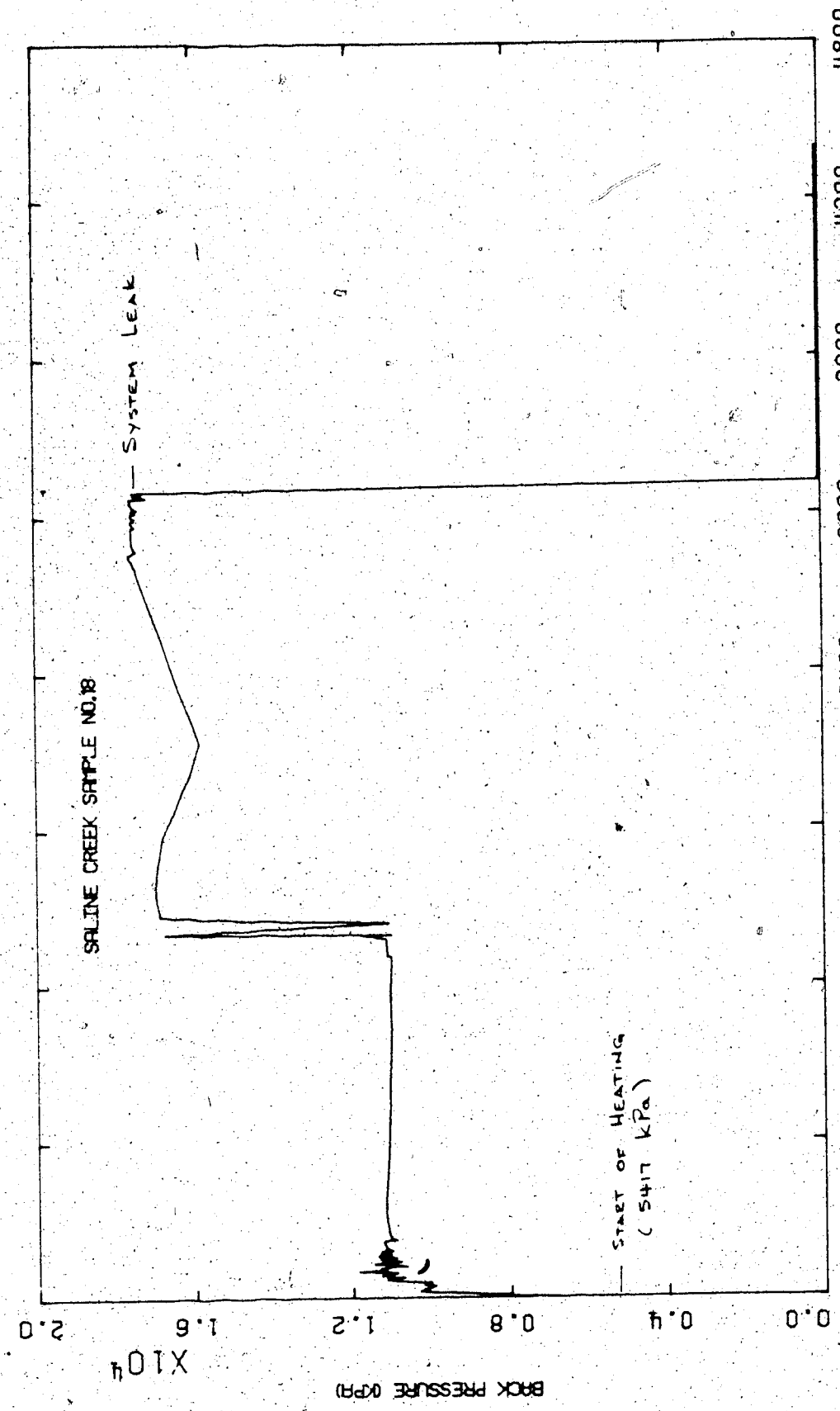

FIGURE B18. Back Pressure Versus Time: Test COS5

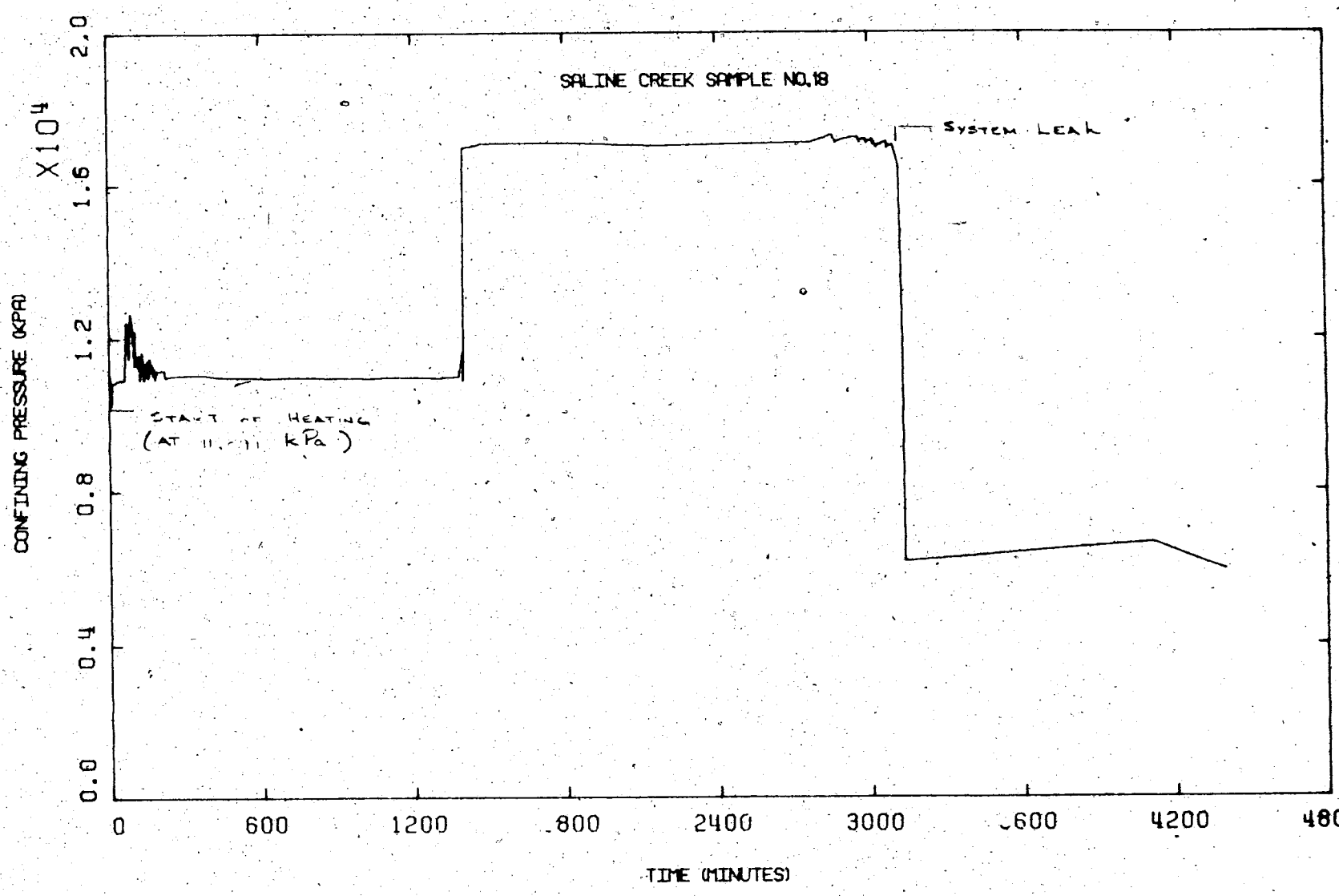

FIGURE B19 , Confining Pressure Versus Time: Test COS5

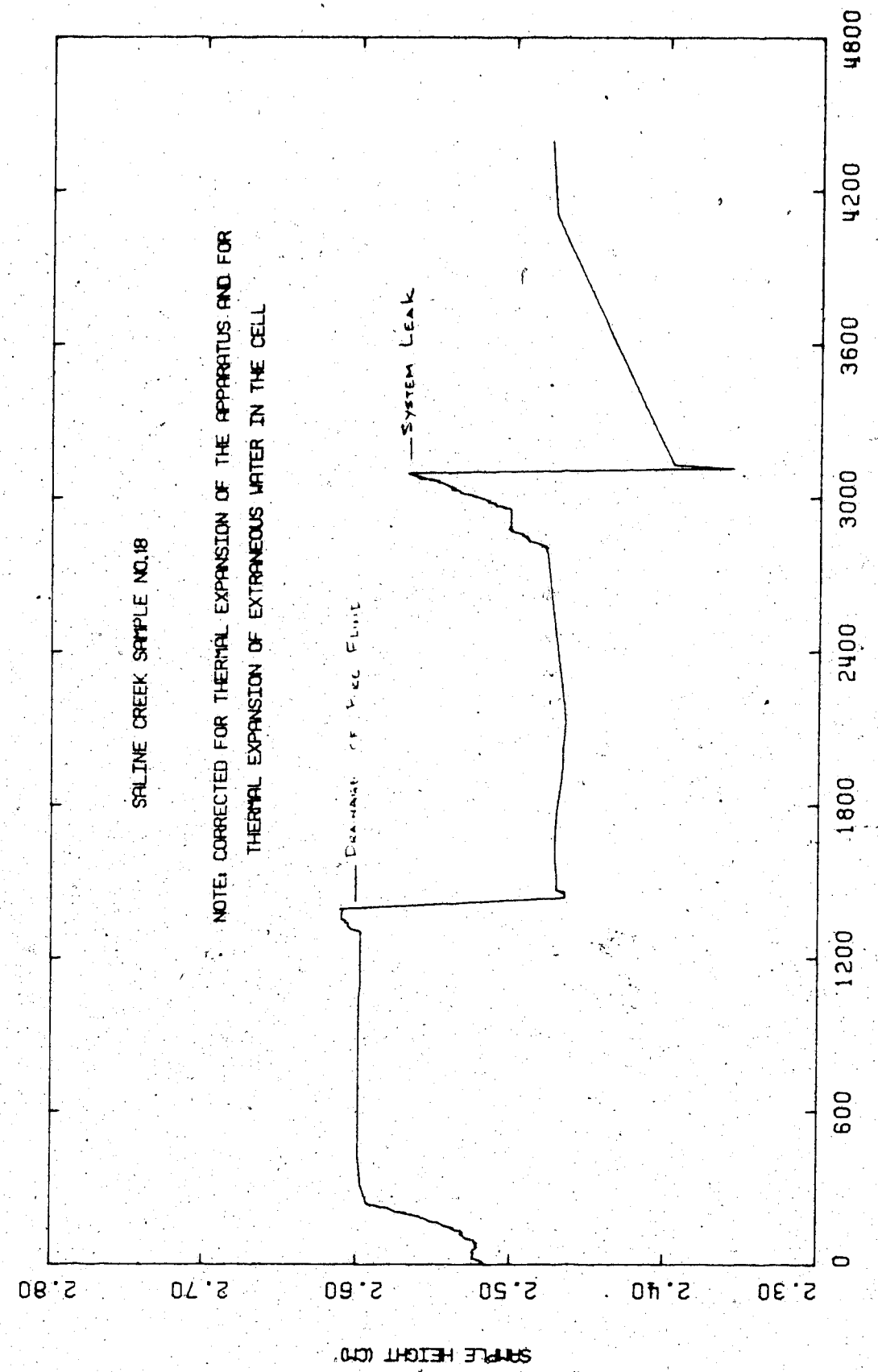

FIGURE B20 Sample Height Versus Time: Test COS5

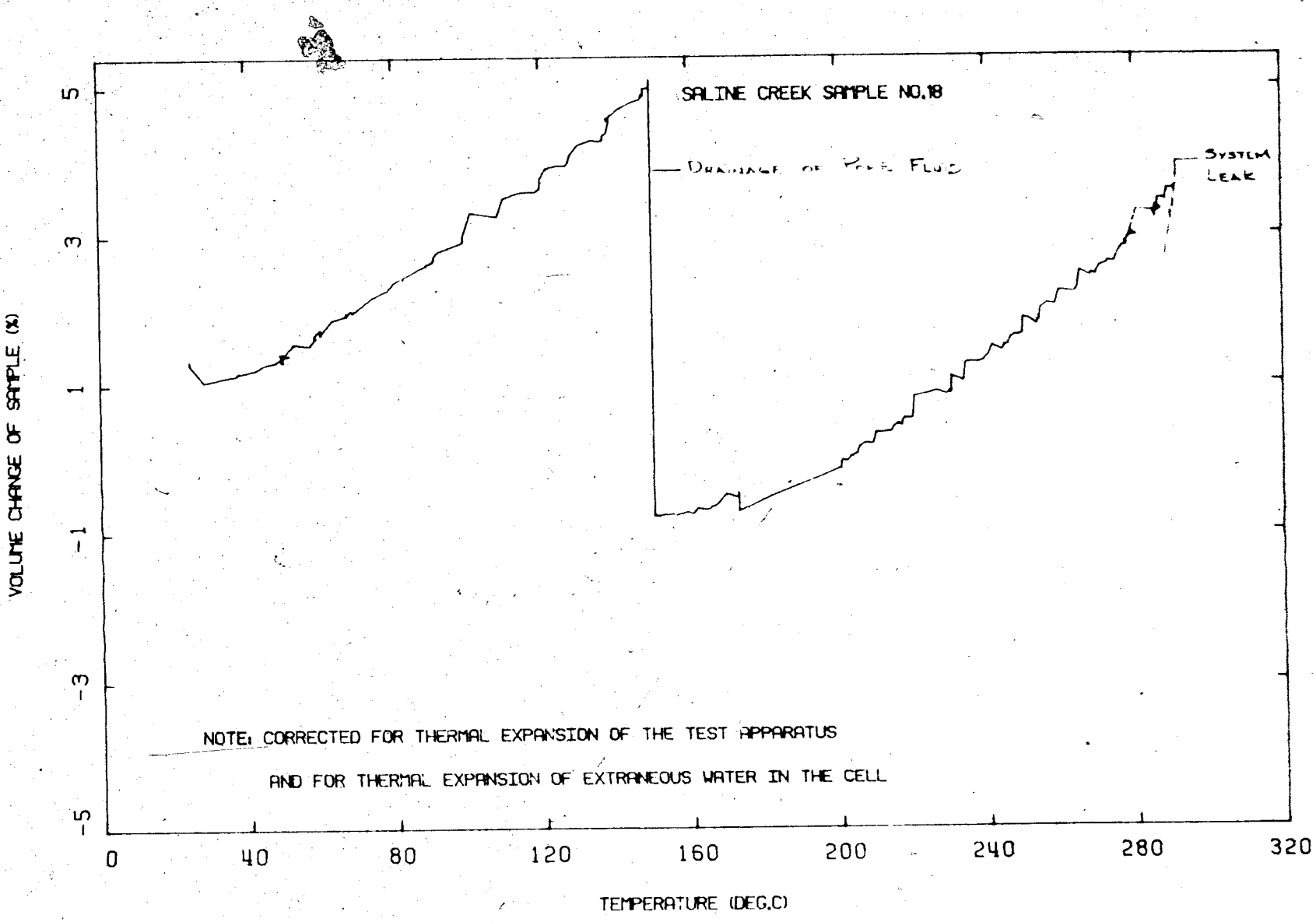

FIGURE B21 Undrained Volumetric Thermal Expansion: Test C055

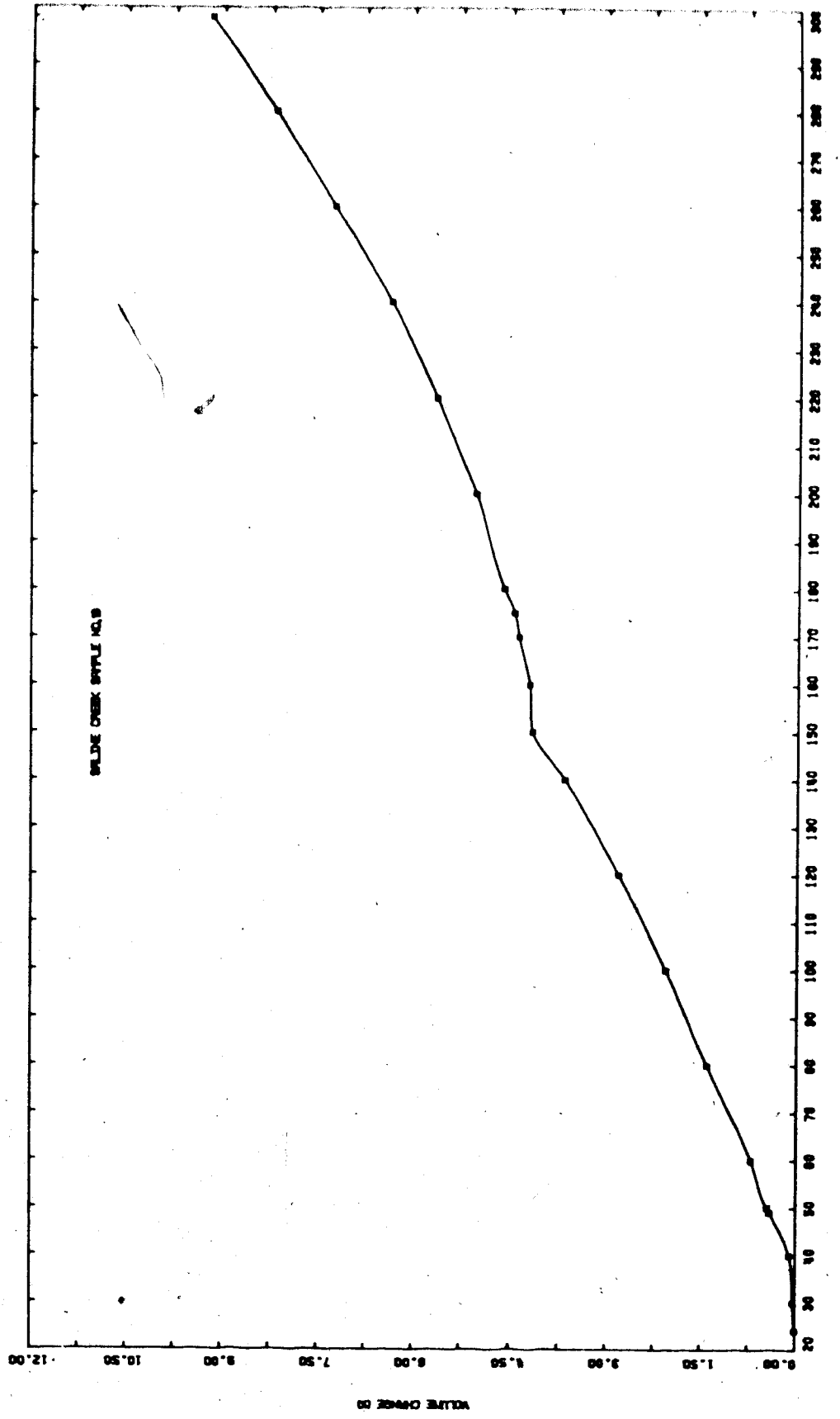

FIGURE B22 Undrained Volumetric Thermal Expansion: Test COS5

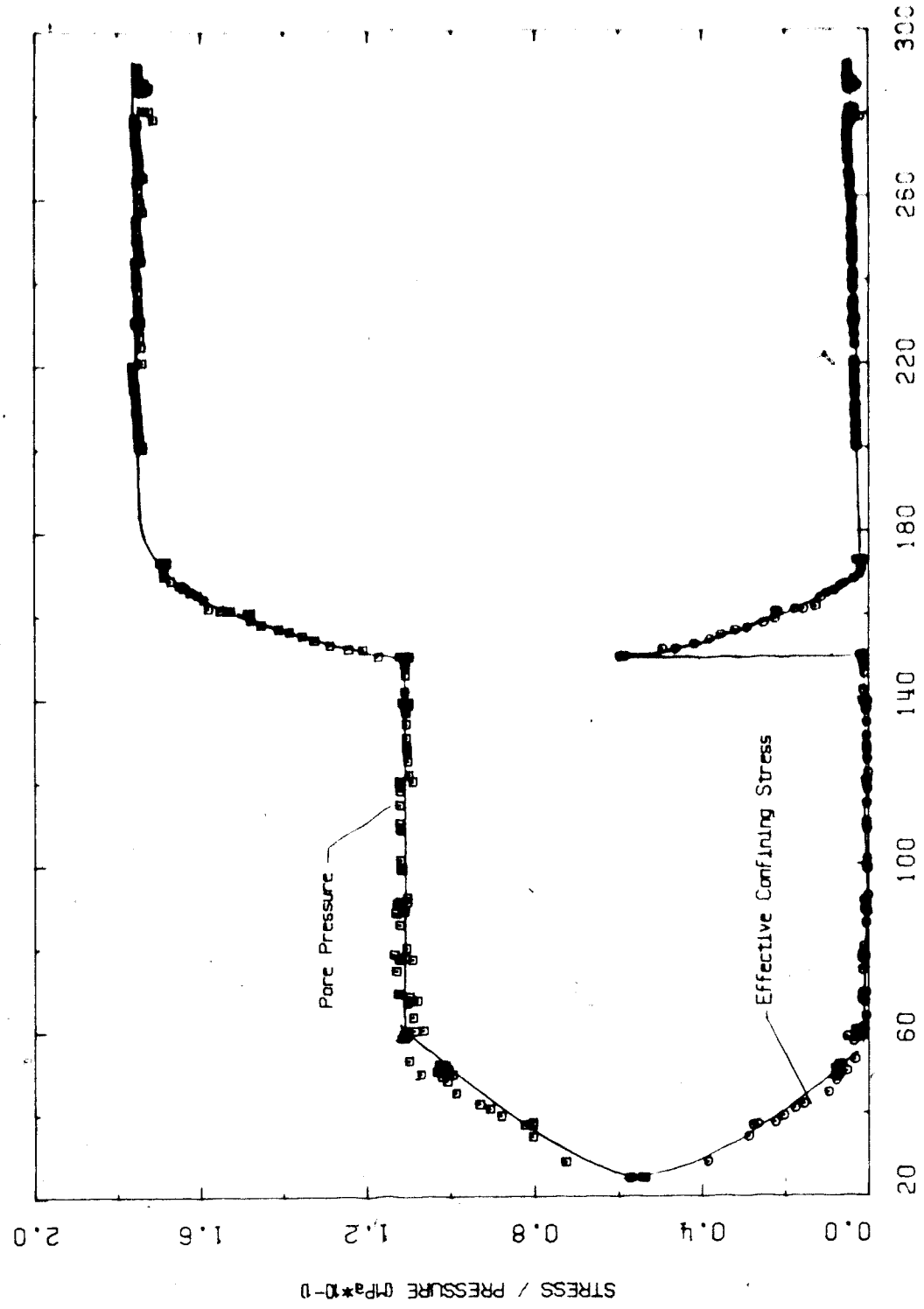

FIGURE B23 Pore Pressure Response to Undrained Heating: Test C055

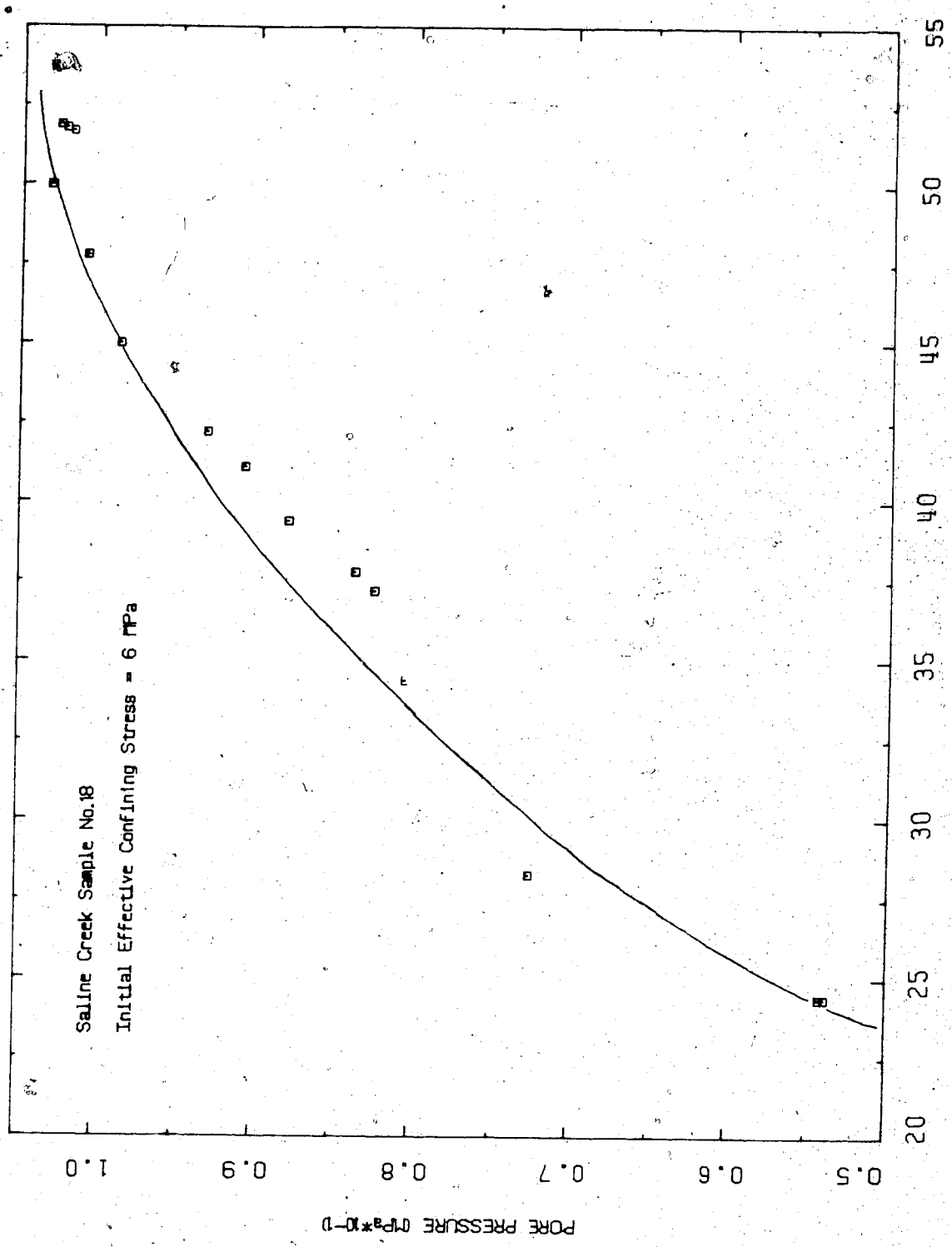

FIGURE B24 Pore Pressure Response to Undrained Heating: Test COS5

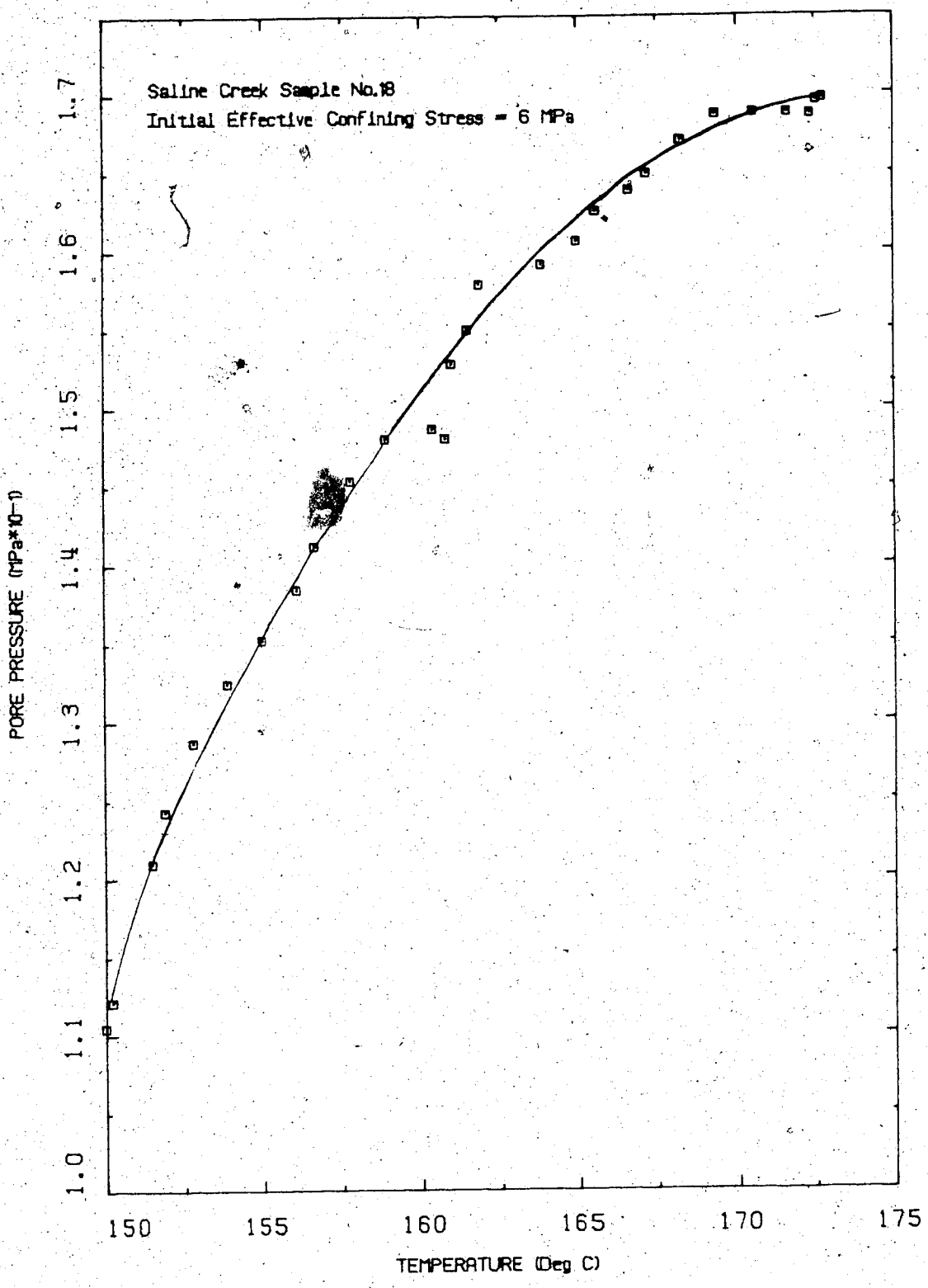

FIGURE B25 Pore Pressure Response to Undrained Heating: Test C0S5

TEST COS6

Drained Thermal Expansion of Saline Creek Oil Sand Sample No. 10A at 6 MPa Effective Confining Stress and Temperatures from 20 - 300°C

Procedural Details: Test COS6

1. Sample no. 10A was warmed to room temperature under confining pressure of sufficient magnitude to prevent thermal expansion of the sample.
2. The sample was saturated over a period exceeding 24 hours under confining and back pressures of 2000 kPa.
3. The back pressure and confining pressures were increased simultaneously in increments of 200 kPa to approximately 5000 kPa.
4. The confining pressure was then increased to 11,000 kPa and the 5000 kPa back pressure was maintained. The back pressure line was left open to permit drainage of fluid from the sample and communication of fluid pressure with the volume change cell.
5. The cell temperature was increased in 5°C to 10°C increments to 200°C and sample height was monitored along with the volume change of the pore fluids.
6. The confining pressure was then increased step-wise to 21,000 kPa while the back pressure was increased to 15,000 kPa maintaining a constant 6000 kPa difference between the confining and back pressures.

7. The cell temperature was then raised in 10°C increments from 200°C to 300°C. The sample height and volume of pore fluid drained from the sample were monitored continuously.

8. It should be noted that a small system leak developed between temperatures 108°C and 140°C. It is estimated that approximately 1 to 2 ml of pore fluid escaped from the cell prior to repairing this leak. Accordingly, the volume change data presented may be in error by as much as 2 percent for this test.

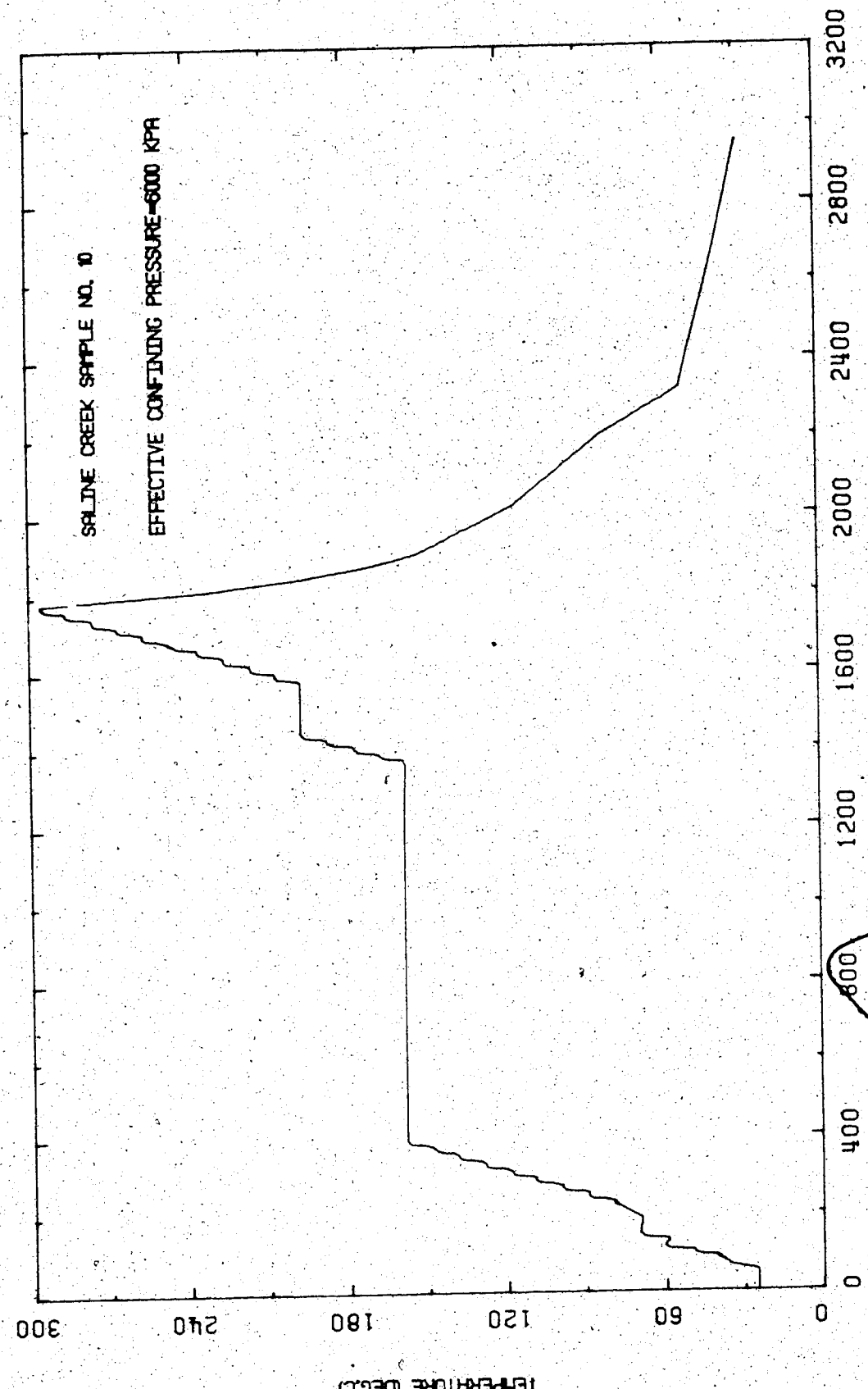

FIGURE B26 Temperature Versus Time: Test COS6

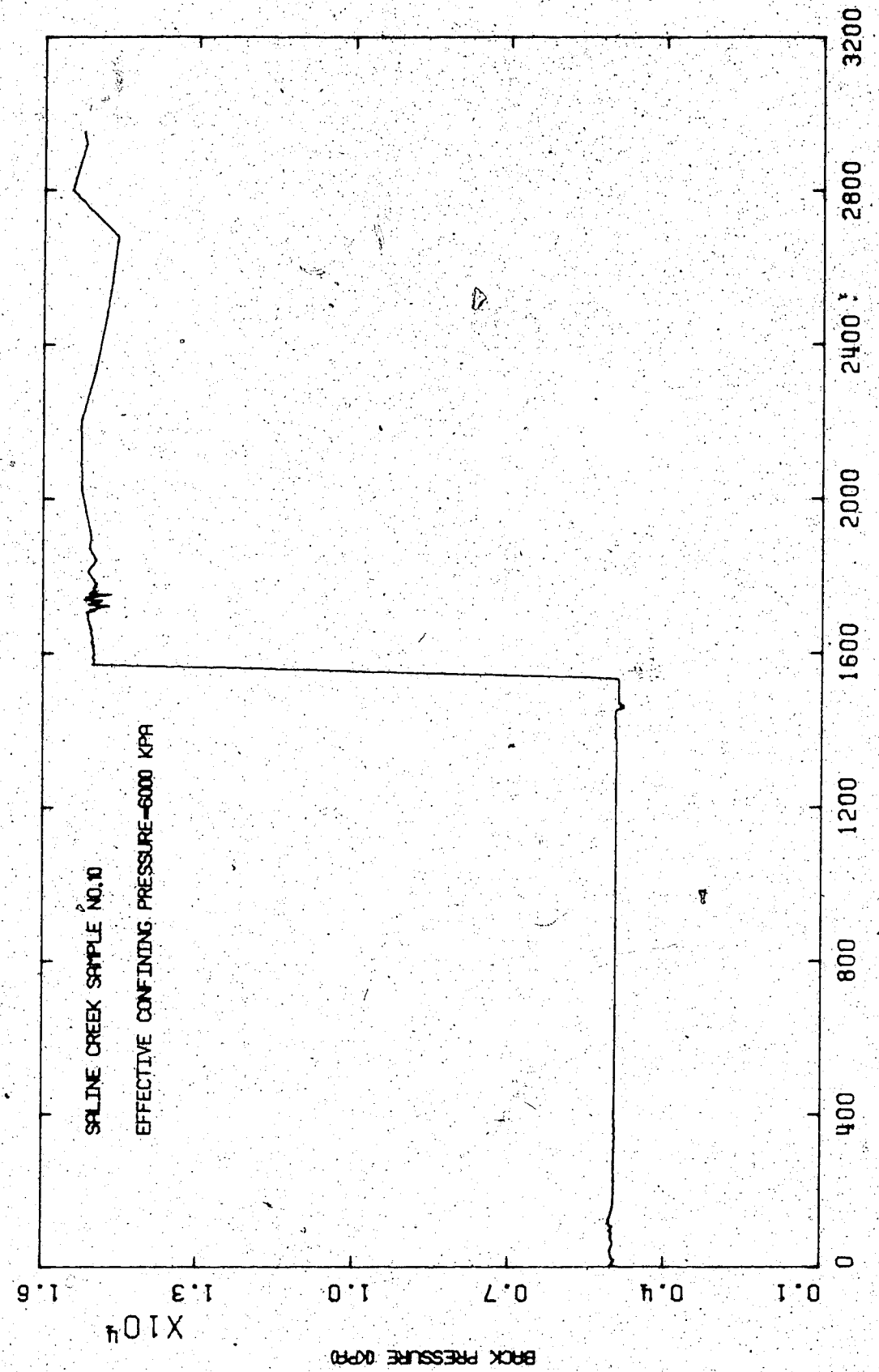

FIGURE B27 Back Pressure Versus Time: Test COS6

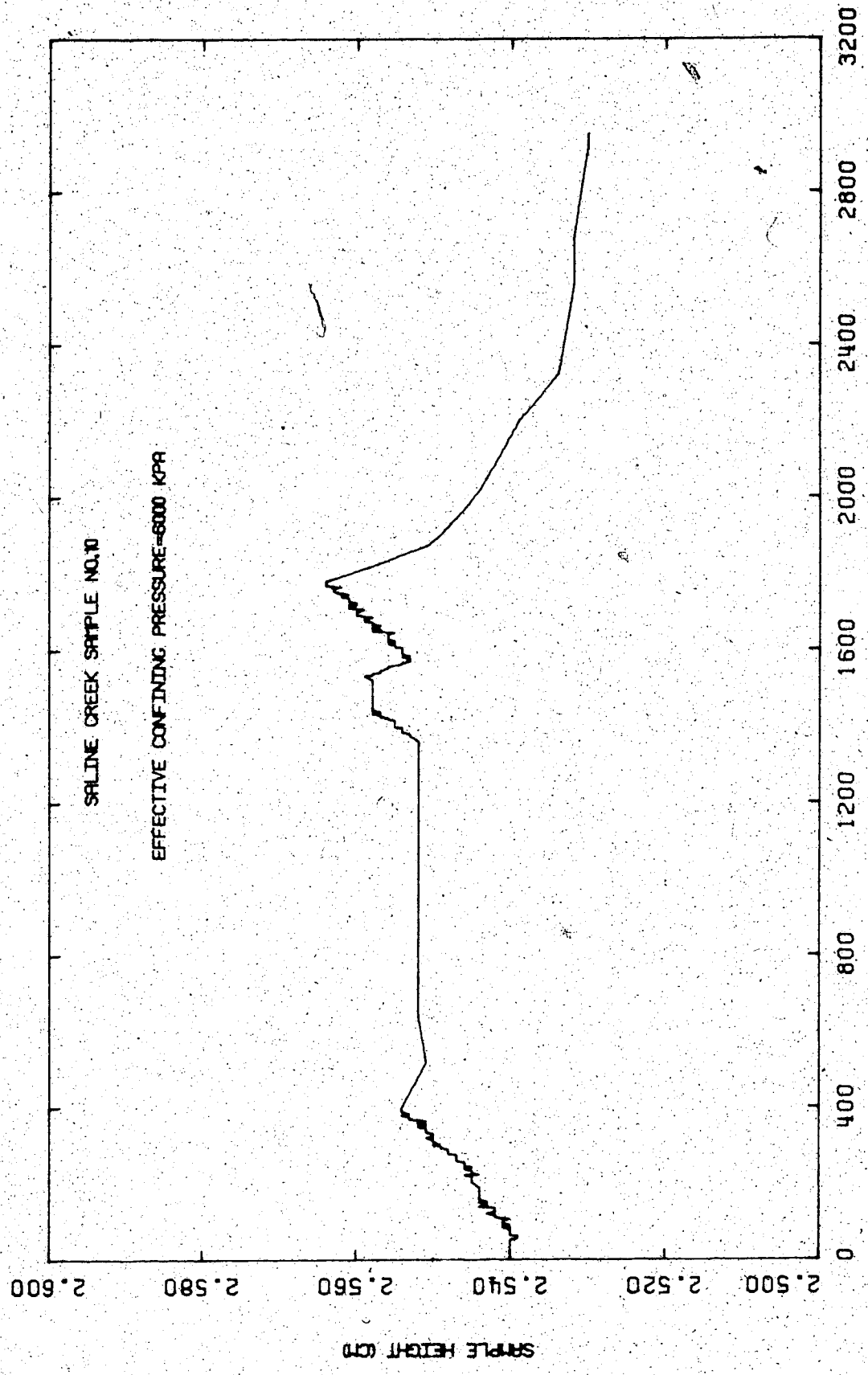

FIGURE B28 Sample Height Versus Time: Test COS6

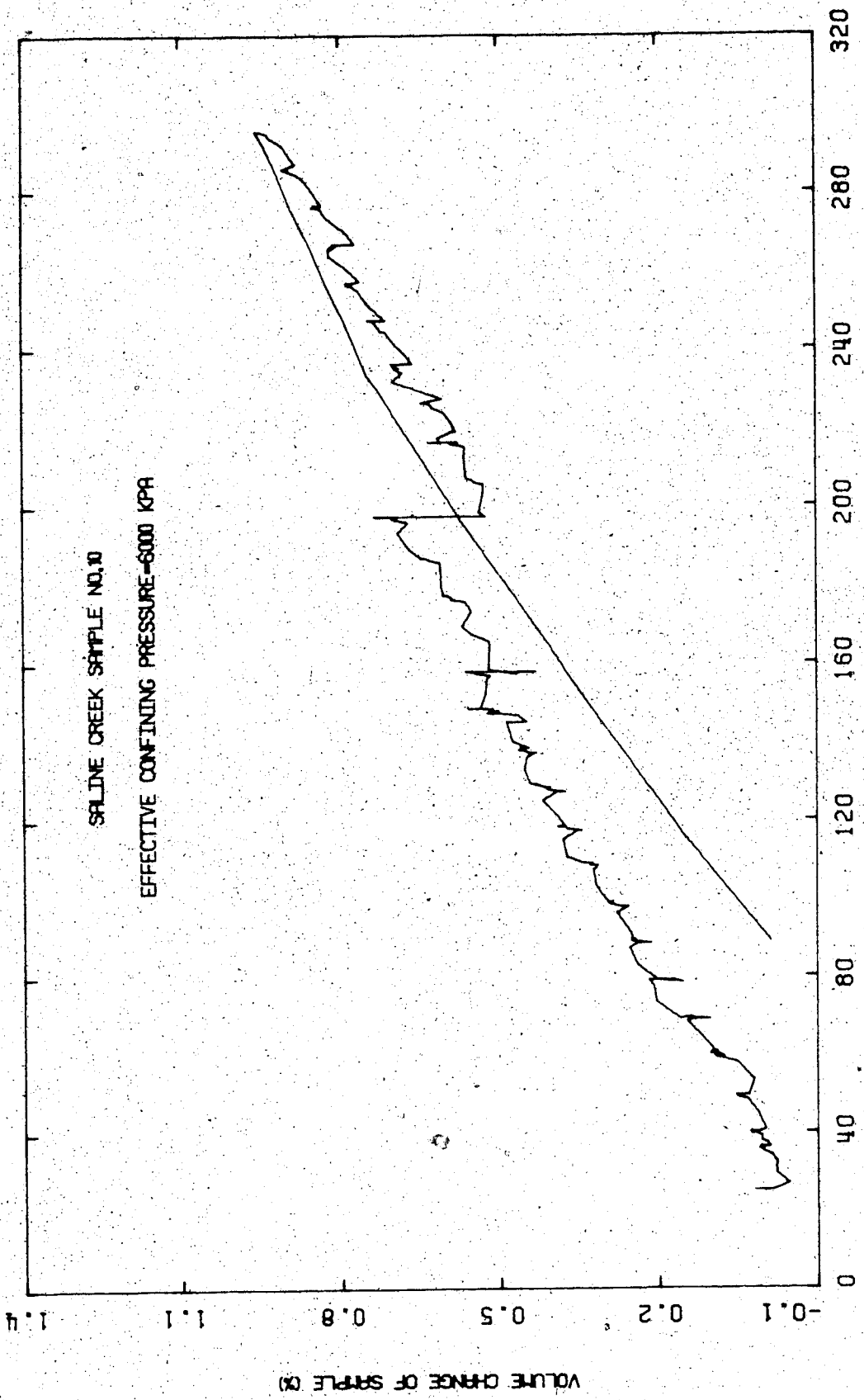

FIGURE B29 Drained Volumetric Thermal Expansion: Test COS6

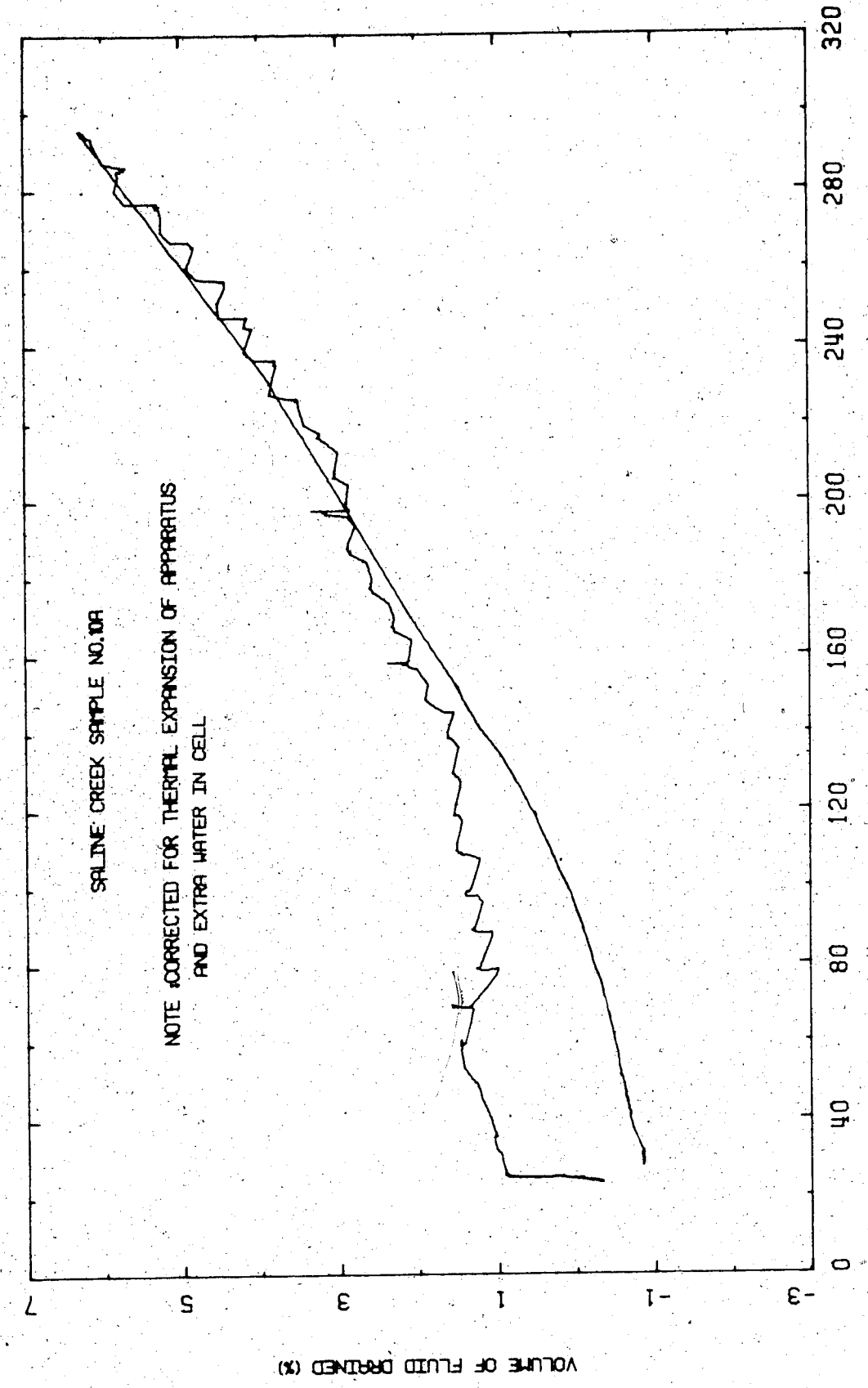

FIGURE B30 Volume of Pore Fluid Drained During Heating: Test COS6

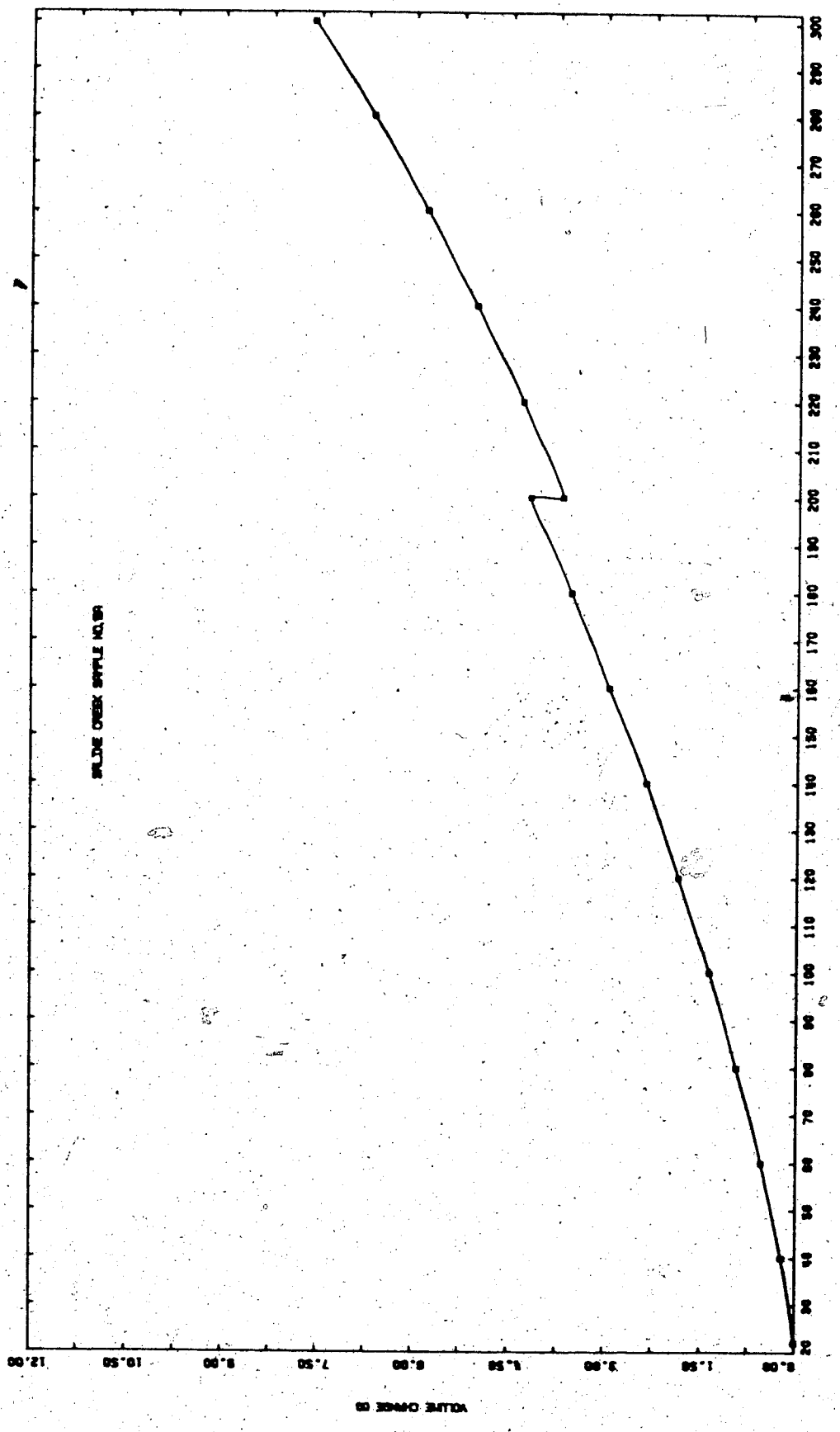

FIGURE B31 Equivalent Undrained Thermal Expansion: Test COS6

TEST COS7

Drained Thermal Expansion of Saline Creek Oil Sand Sample No. 10B at Nominal Effective Confining Stress and Temperatures from 20 - 300°C

Procedural Details: Test COS7

1. Sample 10B was warmed to room temperature under a nominal confining pressure of sufficient magnitude to prevent thermal expansion of the sample.
2. The sample was saturated for a period of 24 hours under a back pressure of 2000 kPa.
3. Confining pressure and back pressure were increased simultaneously, step-wise to 5000 kPa. The back pressure line was left open to permit communication of pore fluid drainage with the volume change measuring apparatus.
4. Cell temperatures were increased in 5°C to 10°C increments up to 200°C.
5. Confining pressure and back pressure were increased simultaneously, step-wise from 5000 kPa to 15,000 kPa.
6. Cell temperatures were then increased in 5°C to 10°C increments from 200°C to 300°C.
7. Sample height and pore fluid drainage volume were monitored continuously throughout the test.

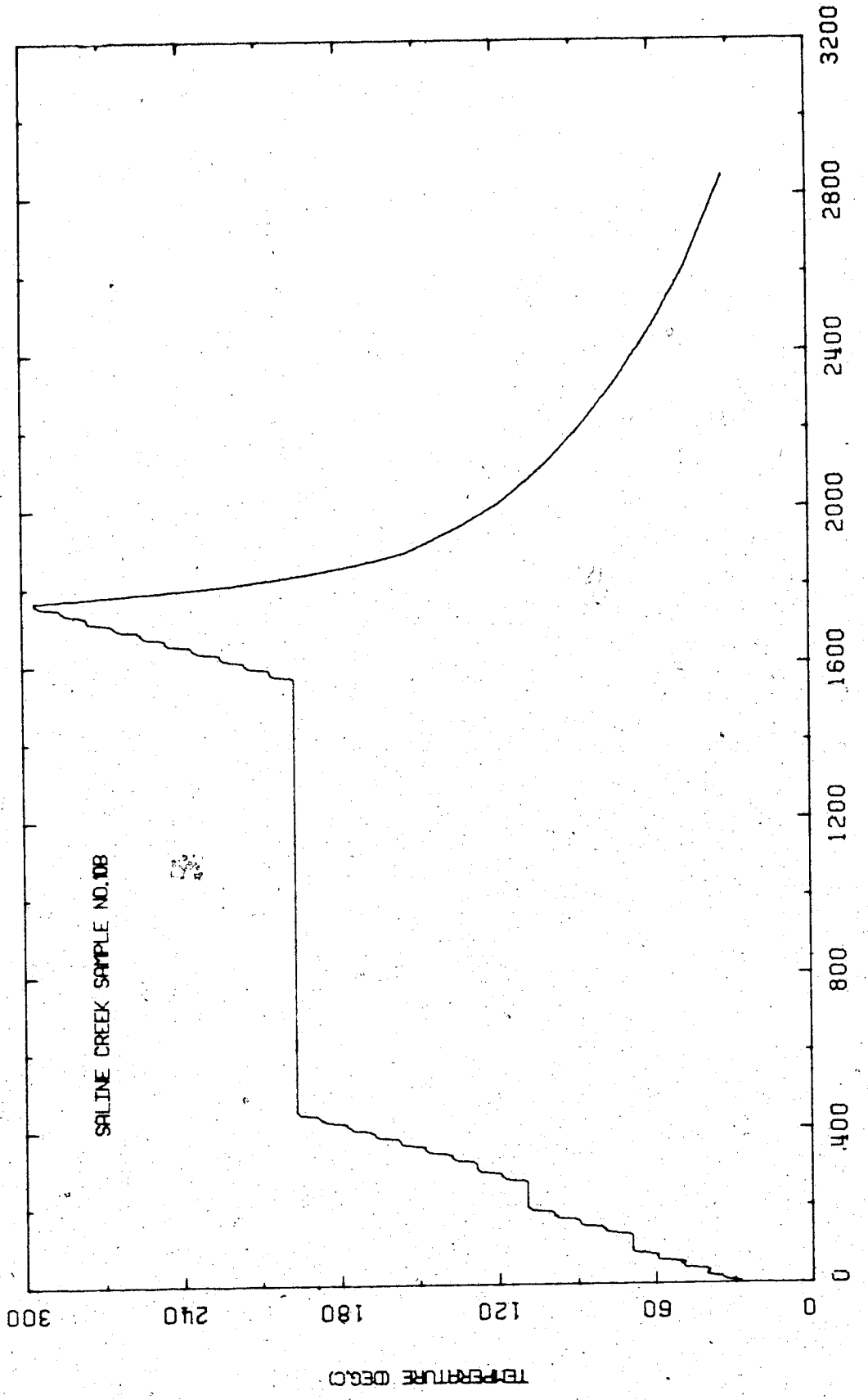

FIGURE B32 Temperature Versus Time: Test COS7

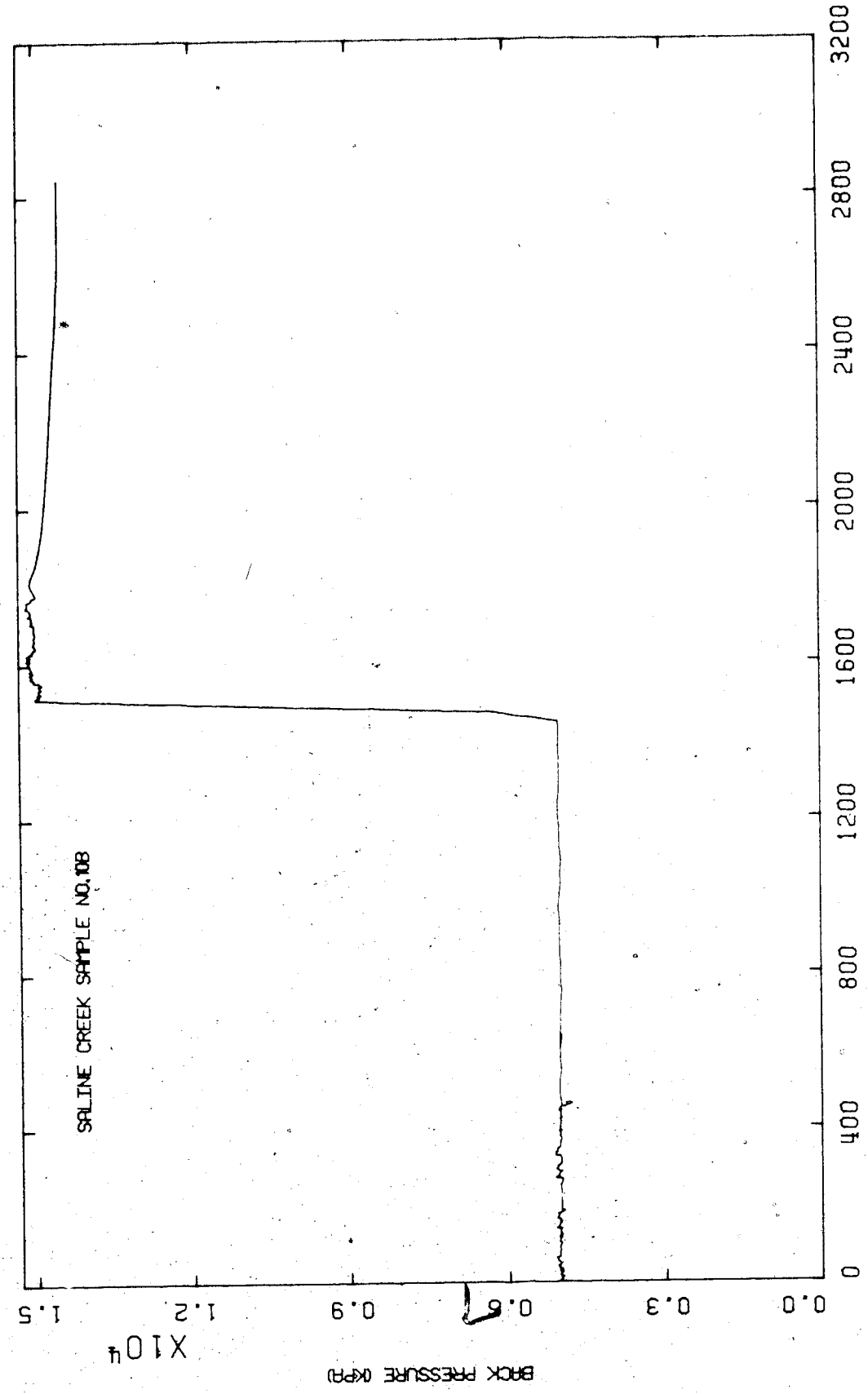

FIGURE B53 Back Pressure Versus Time: Test COS7

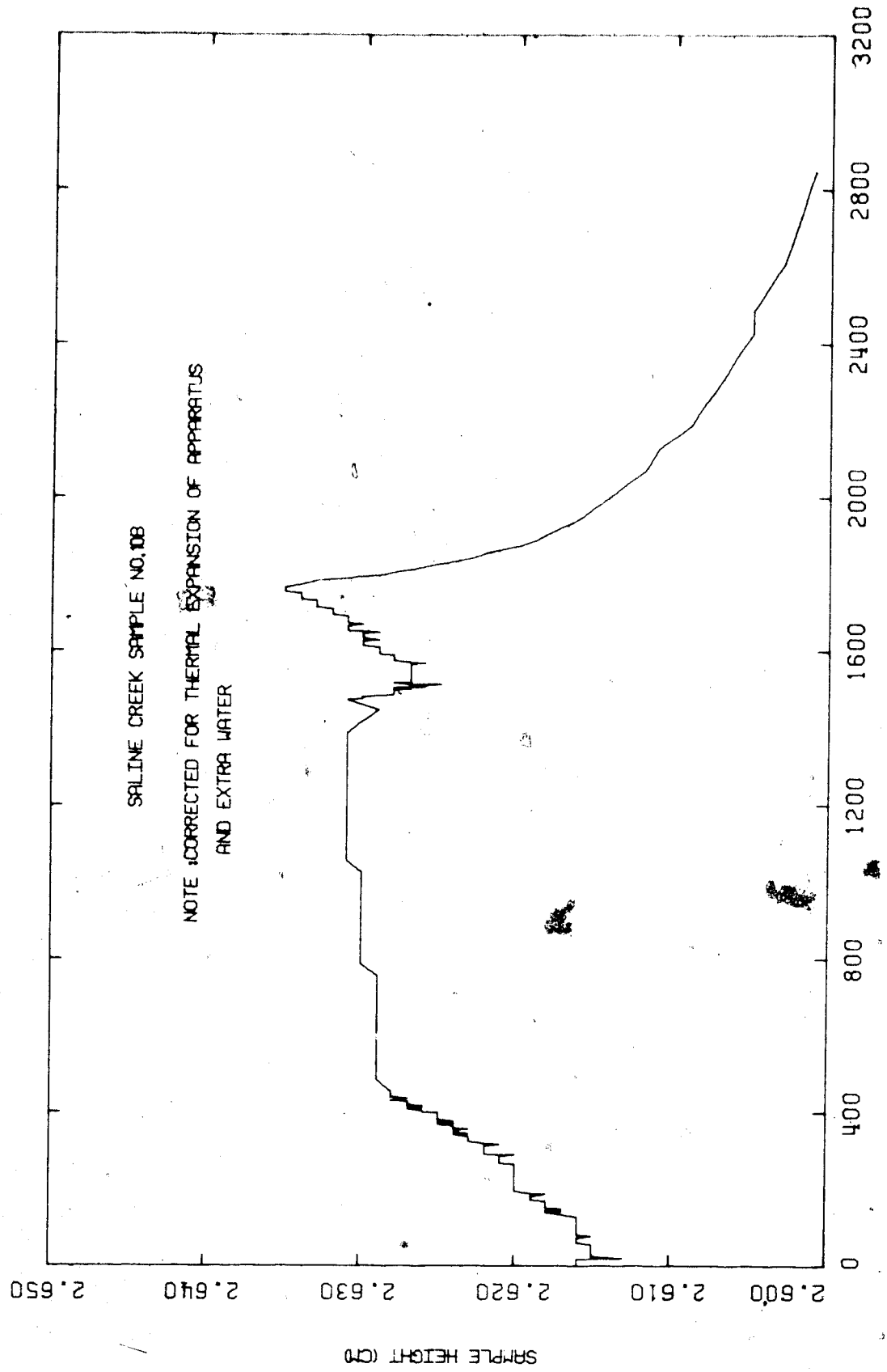

FIGURE B-[illegible] Sample Height Versus Time: Test C057

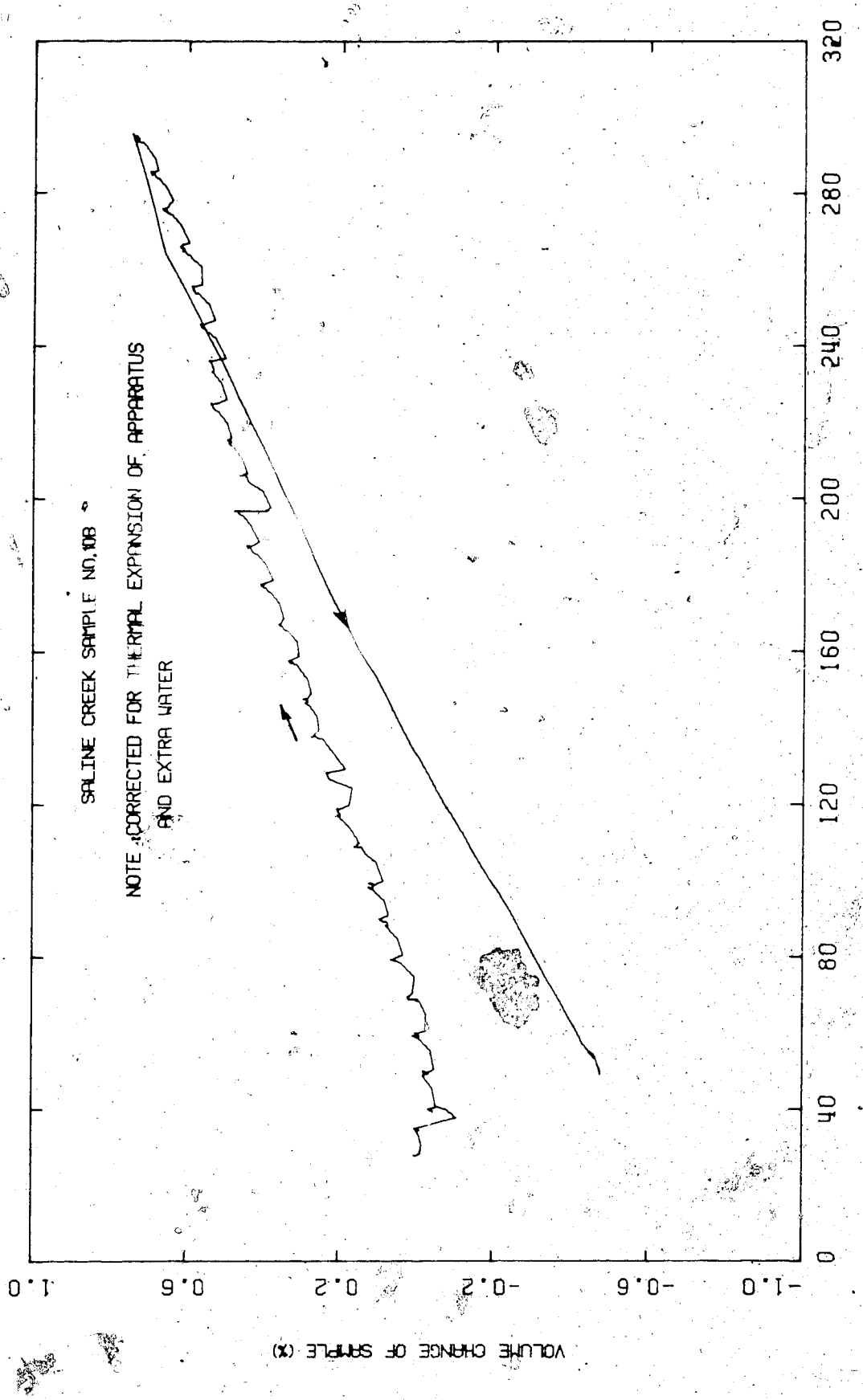

FIGURE B35 Drained Thermal Expansion: Test COS7

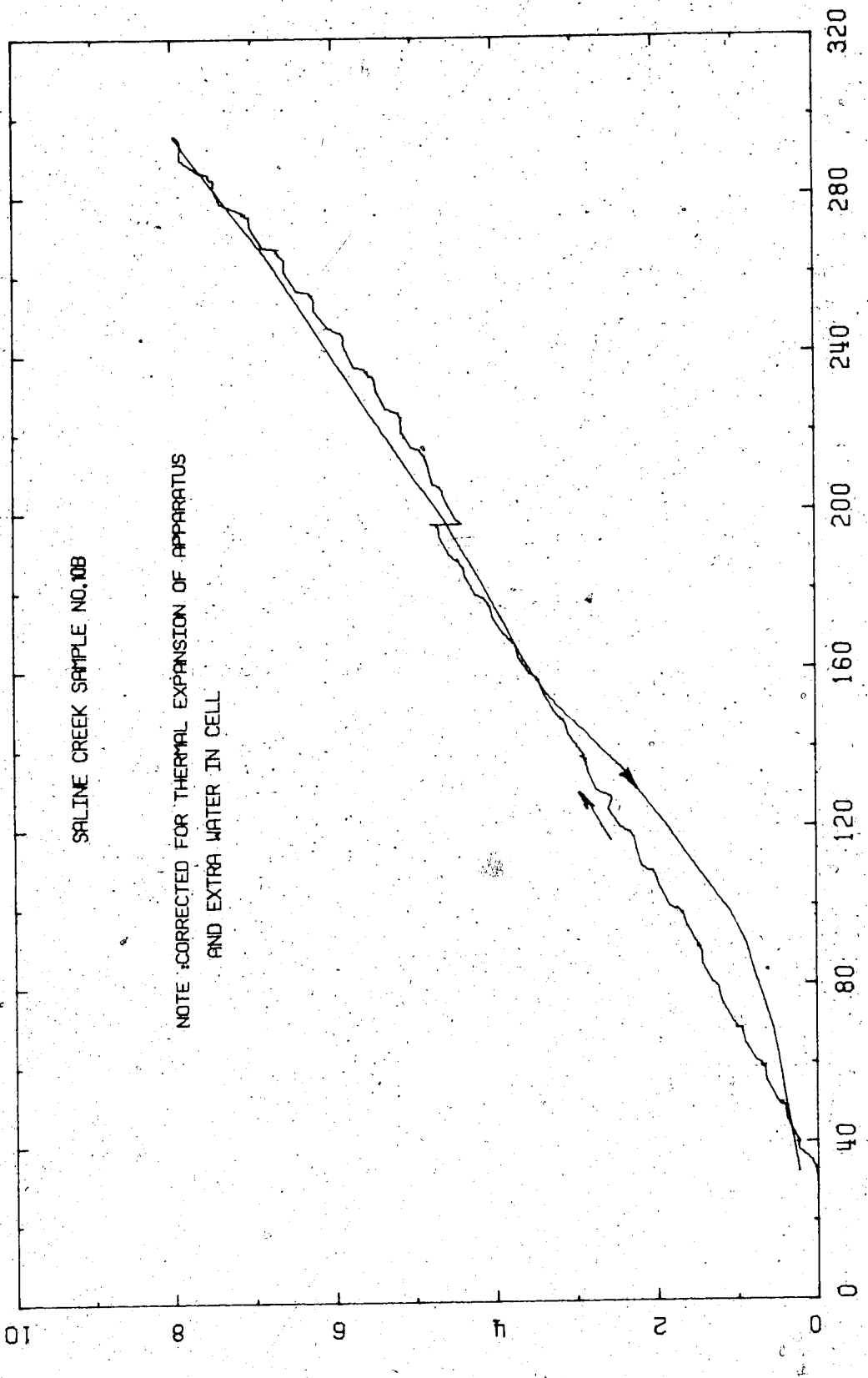

FIGURE B36. Volume of Pore Fluid Drained During Heating: Test COS7

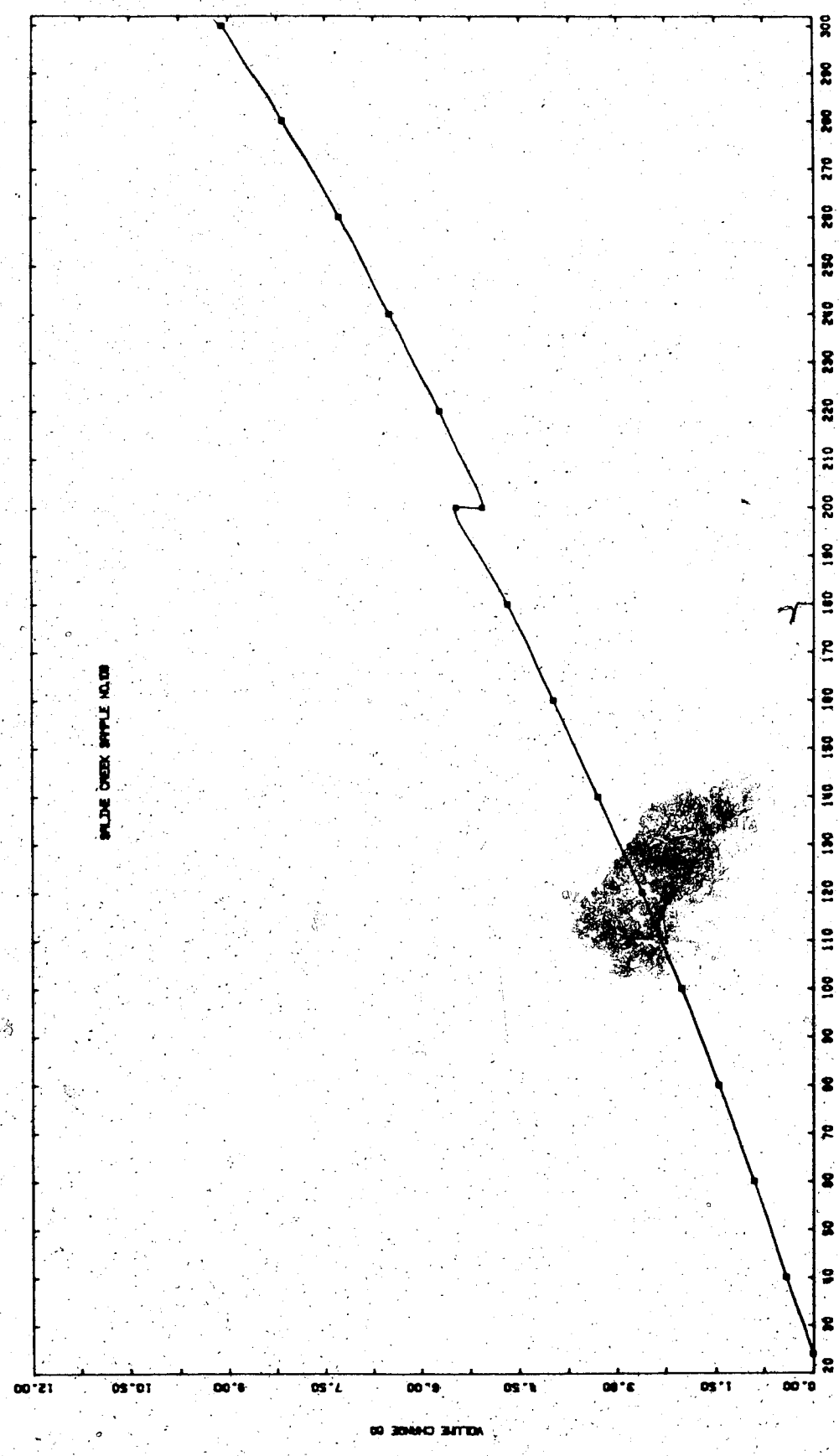

FIGURE B37 Equivalent Undrained Thermal Expansion: Test COS7

TEST COS8

Undrained Thermal Expansion at Nominal
Effective Confining Stress and Gas Exsolution Test
for Saline Creek Sample No. 42 from 20 - 300°C

Procedural Details: COS8

1. Saline Creek Sample No. 42 was confined under a nominal pressure to prevent thermal expansion and fabric disturbance as it warmed to room temperature.
2. The sample was saturated under confining and back pressures of approximately 2000 kPa for a period exceeding 24 hours.
3. The vertical confining pressure and back pressure were initially reduced to 200 kPa. The back pressure was then shut in.
4. The cell temperature was raised in 5°C increments.
5. Confining and back pressures were increased only when required to prevent phase change/or gas exsolution of the pore fluids.
6. Each time significant volumetric expansion was observed which was believed to be due to phase change/gas exsolution, the cell temperature was immediately decreased to the previous incremental temperature level. The confining pressure was increased gradually during these mini cool-down phases to maintain near-constant back pressure and to re-establish the previous sample volume.

7. The confining and back pressures were then increased simultaneously prior to applying the next temperature increment.
8. The purpose of the above procedure was to attempt to define a pressure-temperature relationship corresponding to gas exsolution and/or phase change of the pore fluids.
9. The test was terminated at 300°C. Sample volume change was monitored during cool-down.

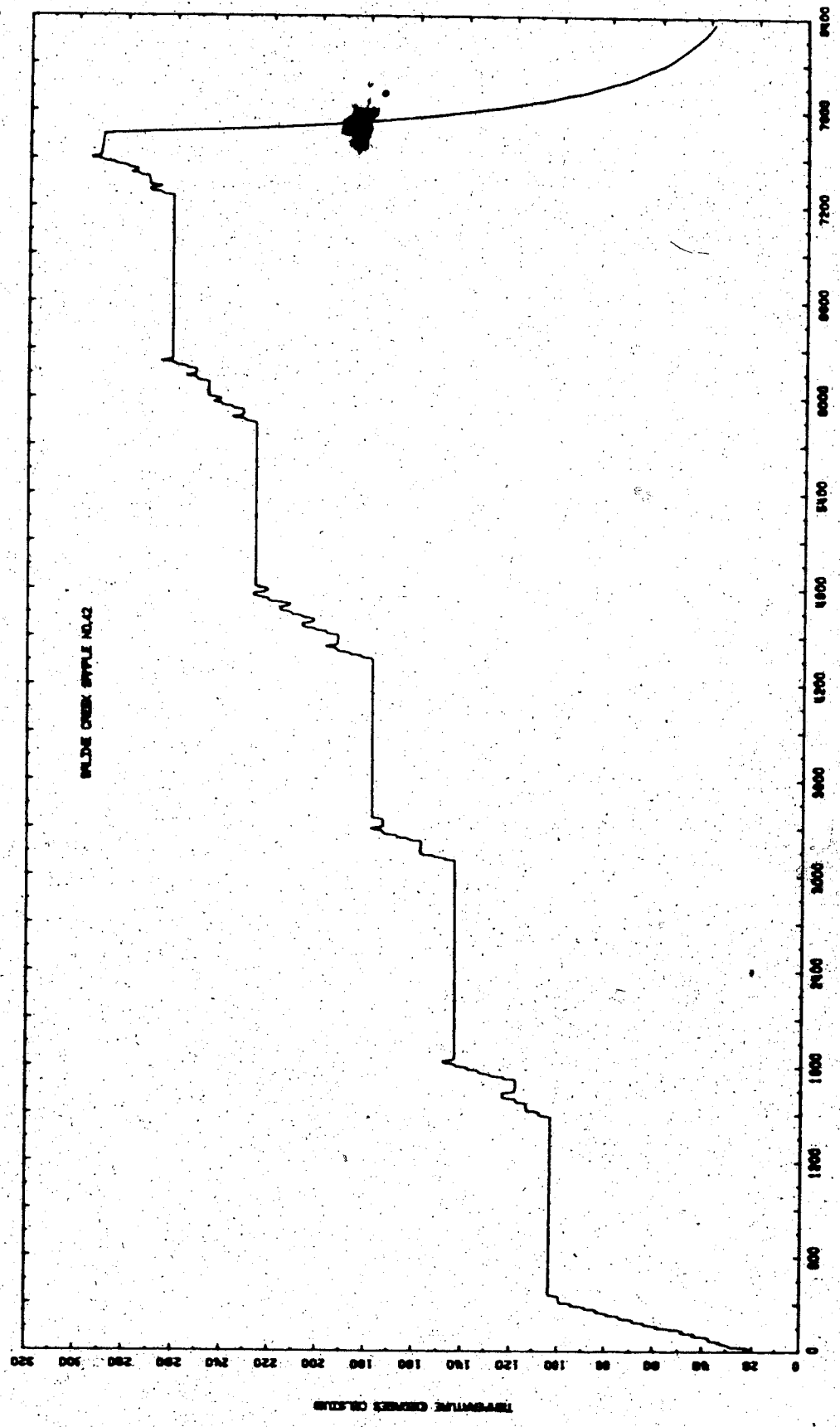

FIGURE B38 Temperature Versus Time: TEST COS8

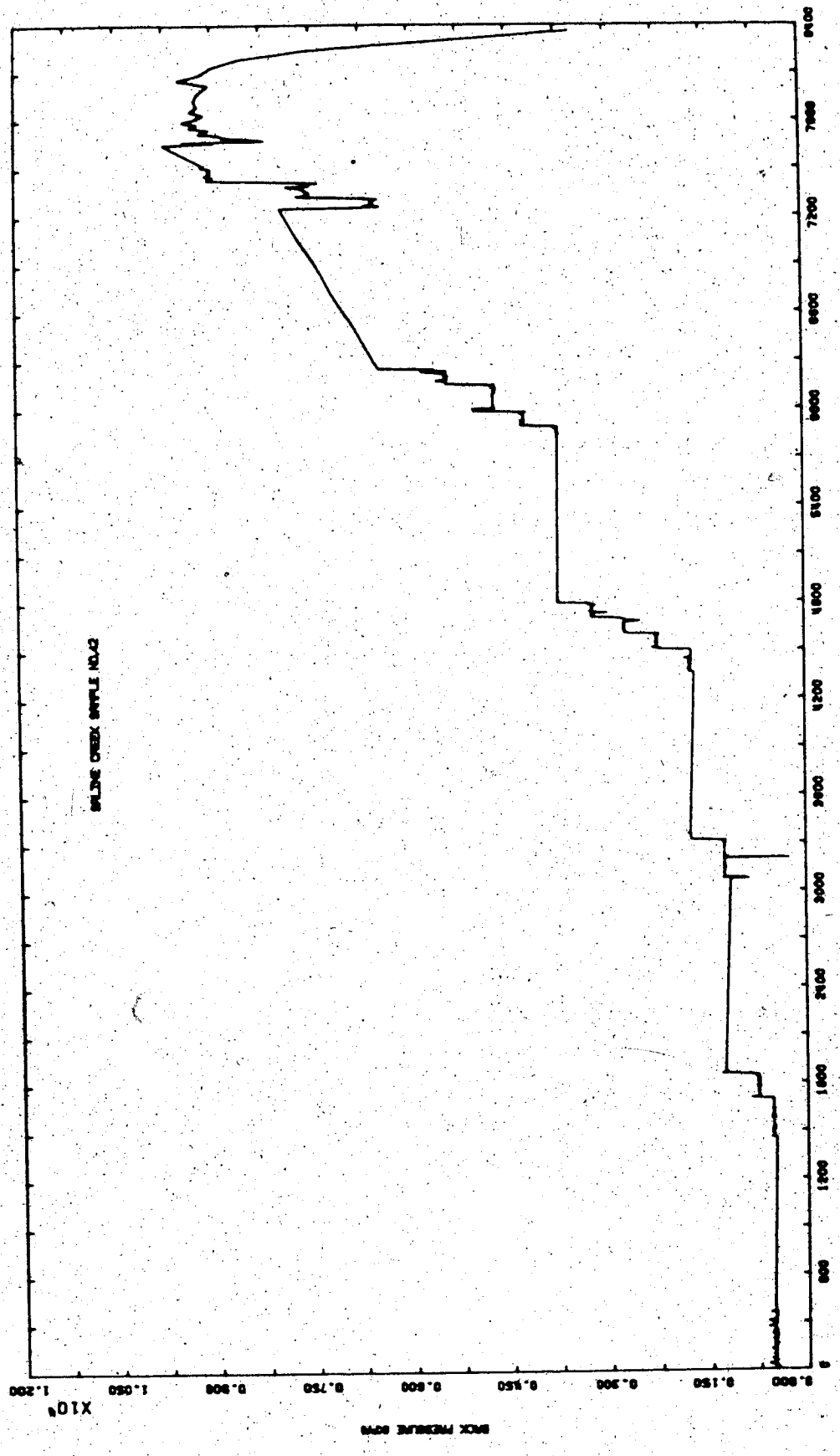

FIGURE B39 Back Pressue Versus Time: Test COS8

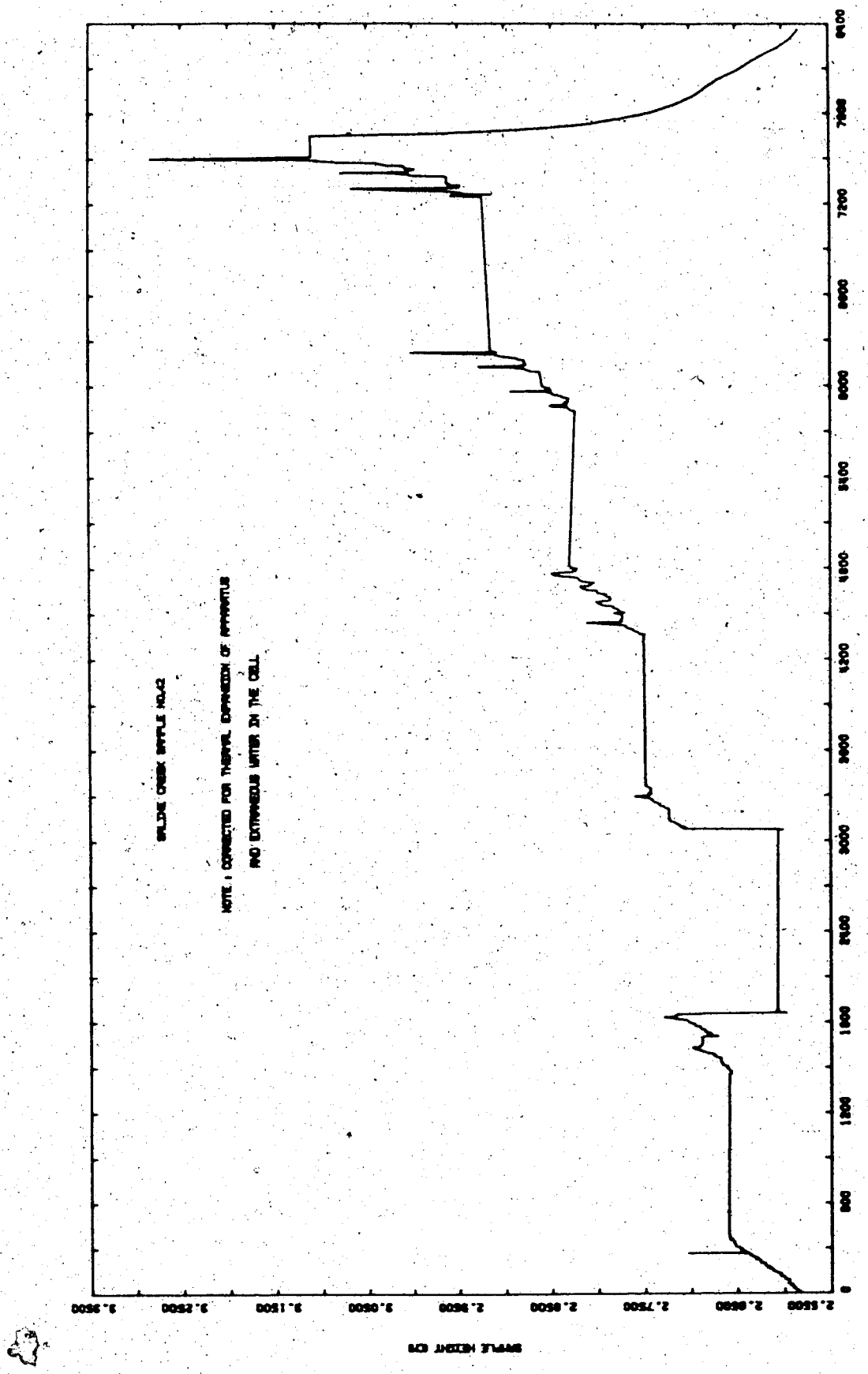

FIGURE B40 Sample Height Versus Time: Test COS8

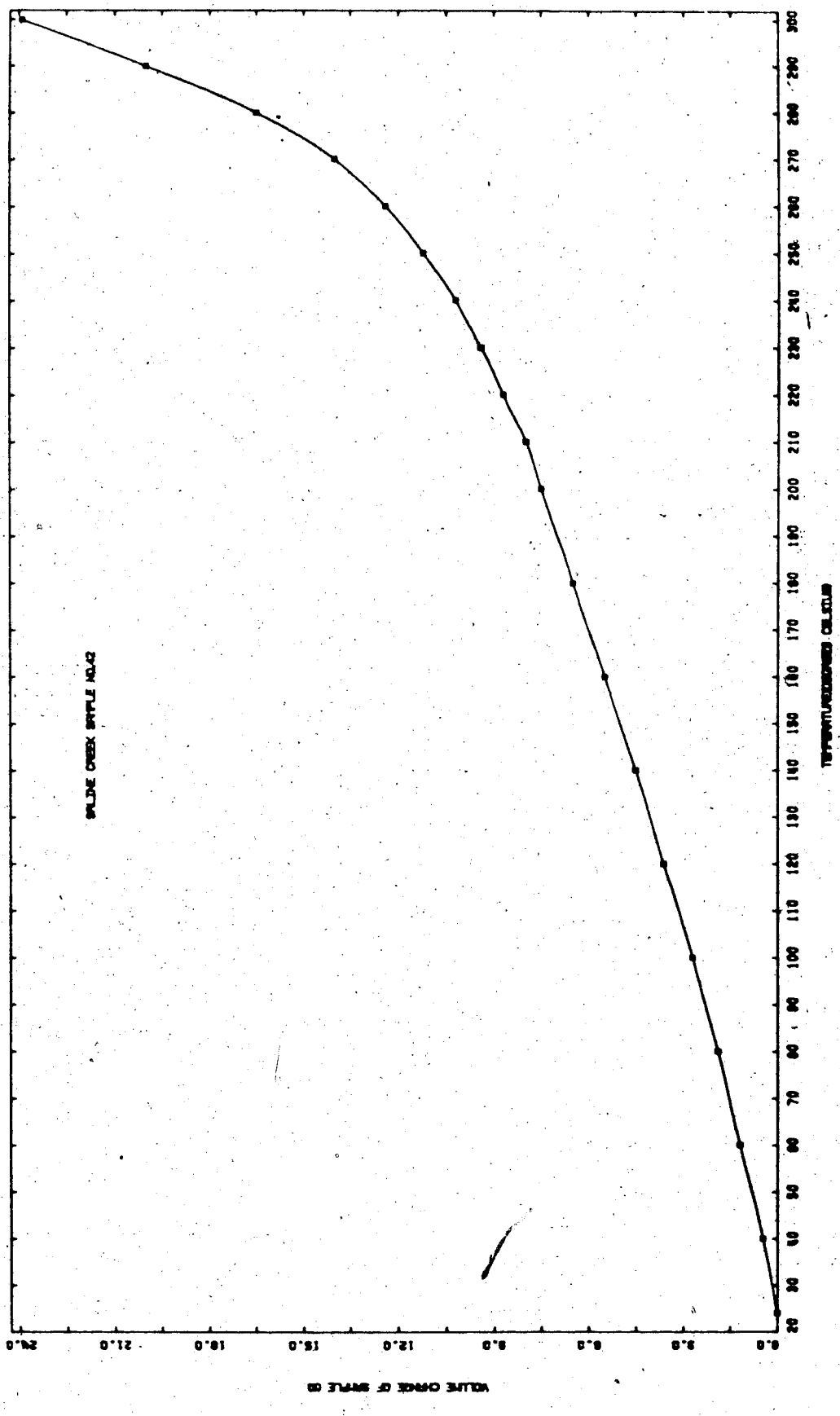

FIGURE B41 Undrained Volumetric Thermal Expansion: Test COS8

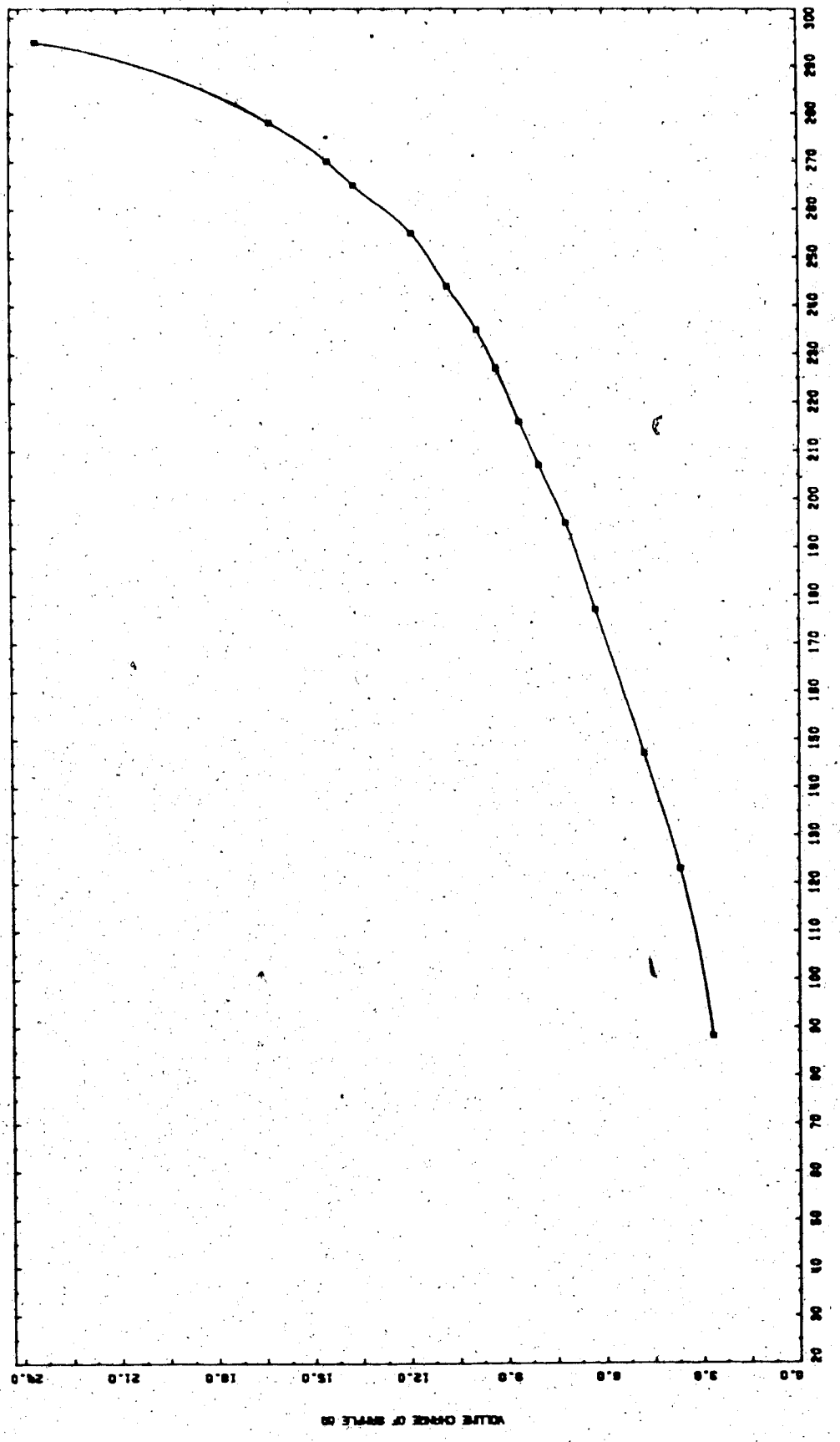

FIGURE B42 Undrained Thermal Expansion at Initiation of Gas Exsolution: Test COS8

TEST COS9

Undrained Thermal Expansion of Saline
Creek Sample No. 41 at 10 MPa
Back Pressure from 20 - 300°C

Procedural Details: COS9

1. Sample no. 41 was warmed to room temperature under a nominal confining pressure of sufficient magnitude to prevent thermal expansion of the sample.
2. The sample was saturated for a period of 24 hours under confining and back pressures of 2000 kPa.
3. Confining pressure and back pressure were increased simultaneously, step-wise to 10,000 kPa. The back pressure line was shut in.
4. A room temperature compressibility test was performed over the effective stress range - 18 MPa.
5. Cell temperatures were increased in 5°C to 10°C increments up to 300°C.
6. Sample height and undrained volumetric expansion were monitored continuously as heating proceeded.
7. The thermal expansion test was terminated at a temperature of 300°C. The gas exsolution pressure was checked at 300°C for comparison with Test COS8.
8. A compressibility test was performed at 300°C over the effective vertical stress range 4 - 18 MPa.
9. Sample volume was monitored during cool-down.

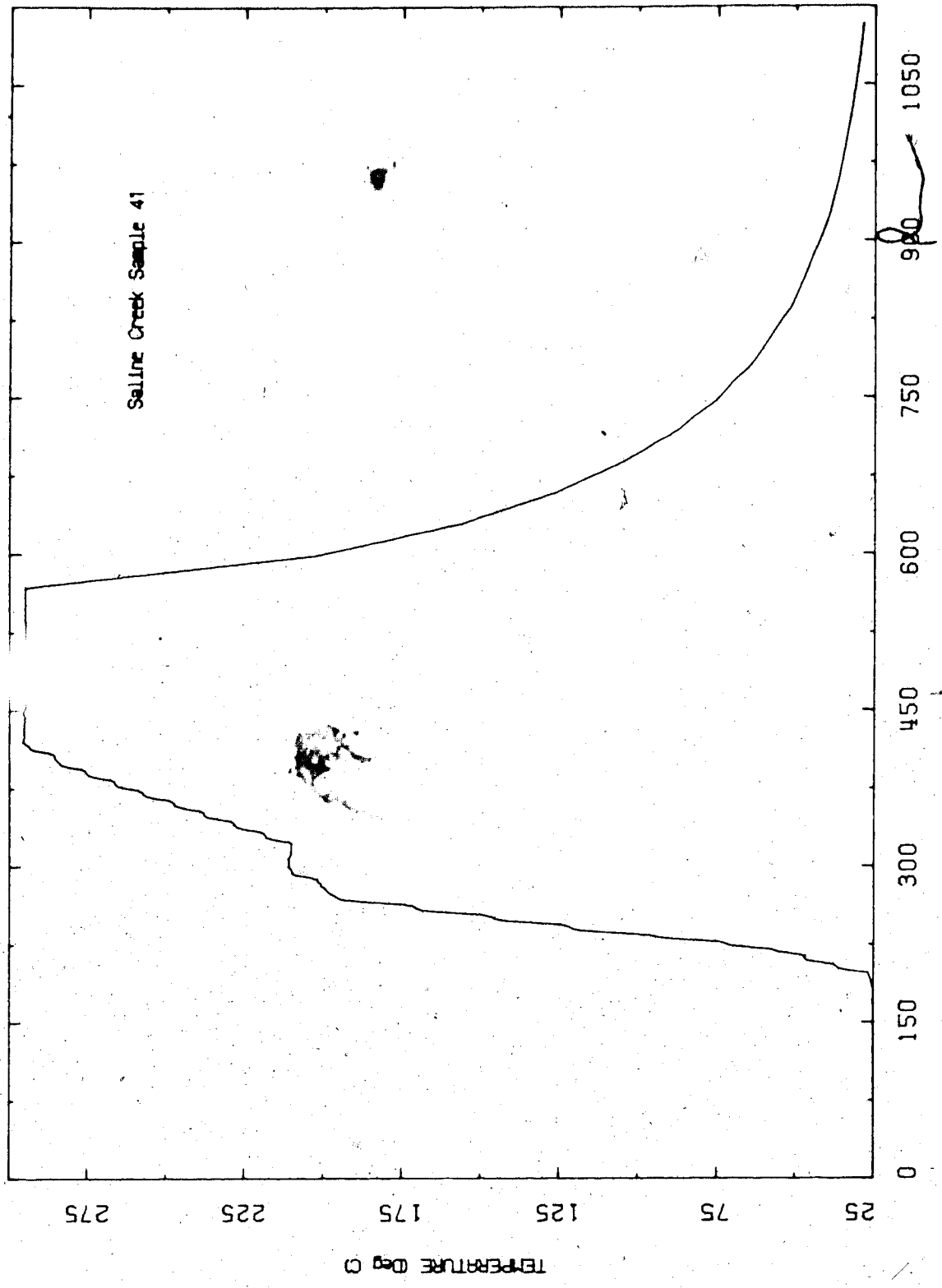

FIGURE B43 Temperature Versus Time: Test COS9

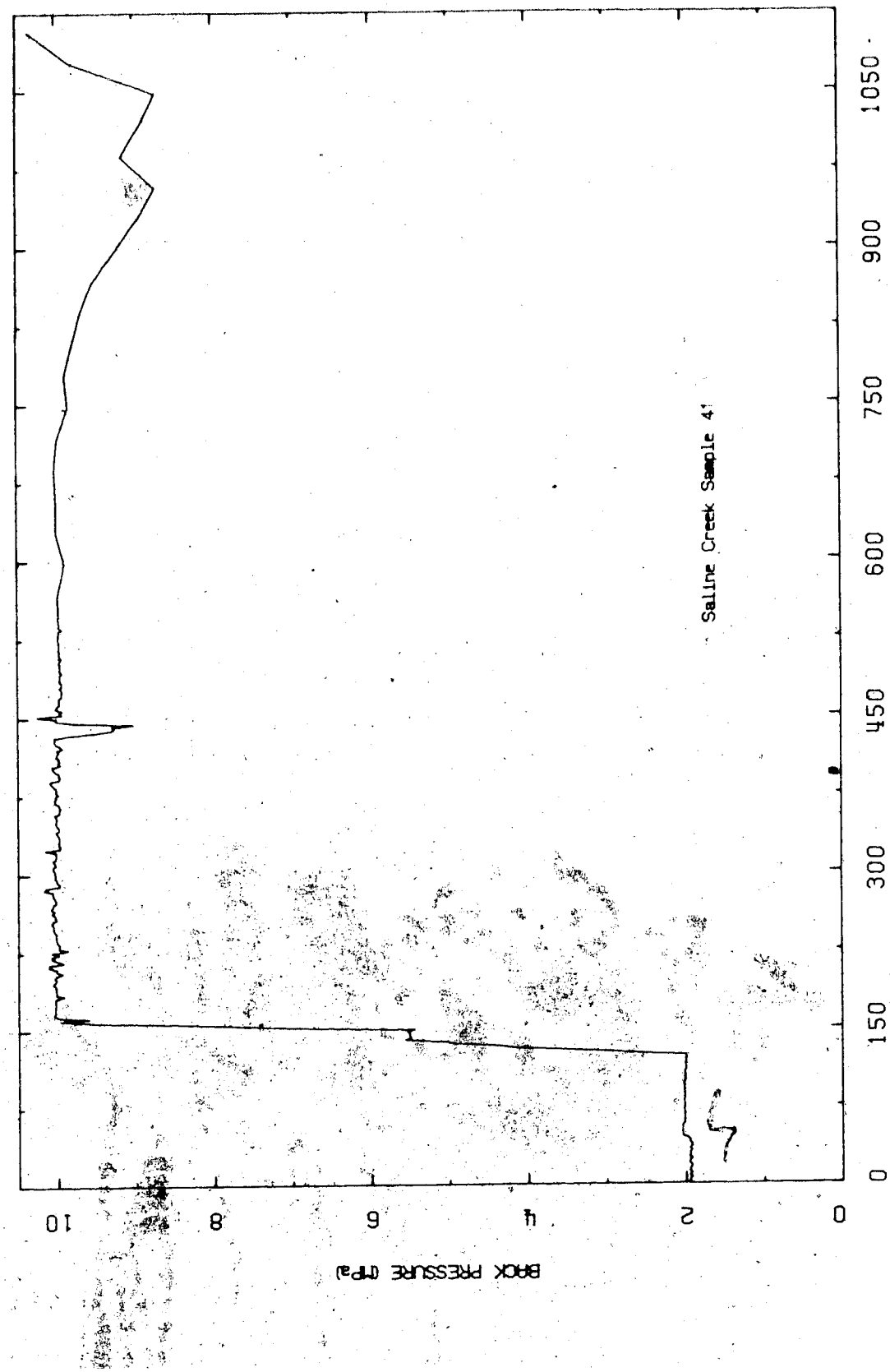

FIGURE B44 Back Pressure Versus Time: Test COS9

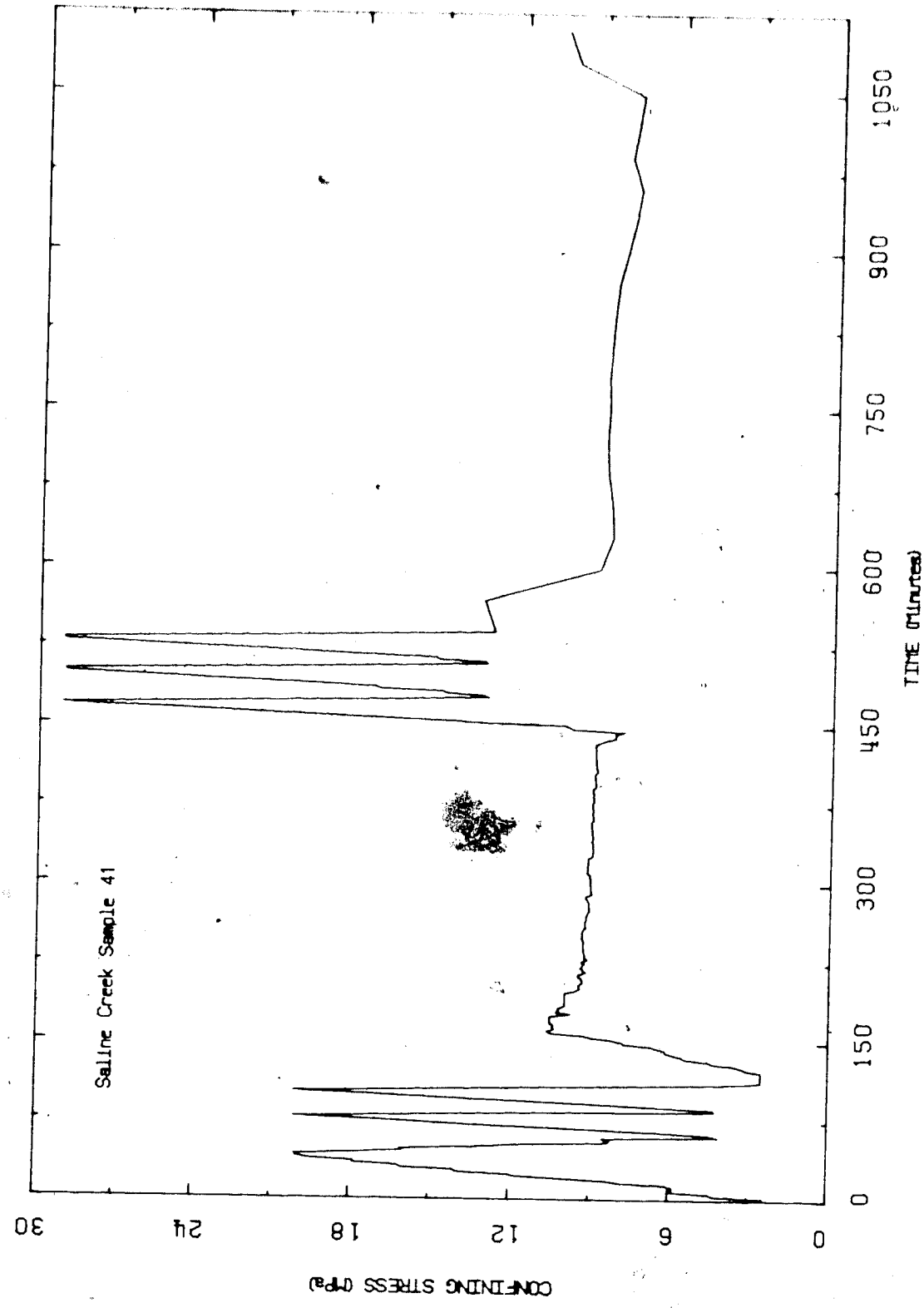

FIGURE B45 Confining Stress Versus Time: Test 0039

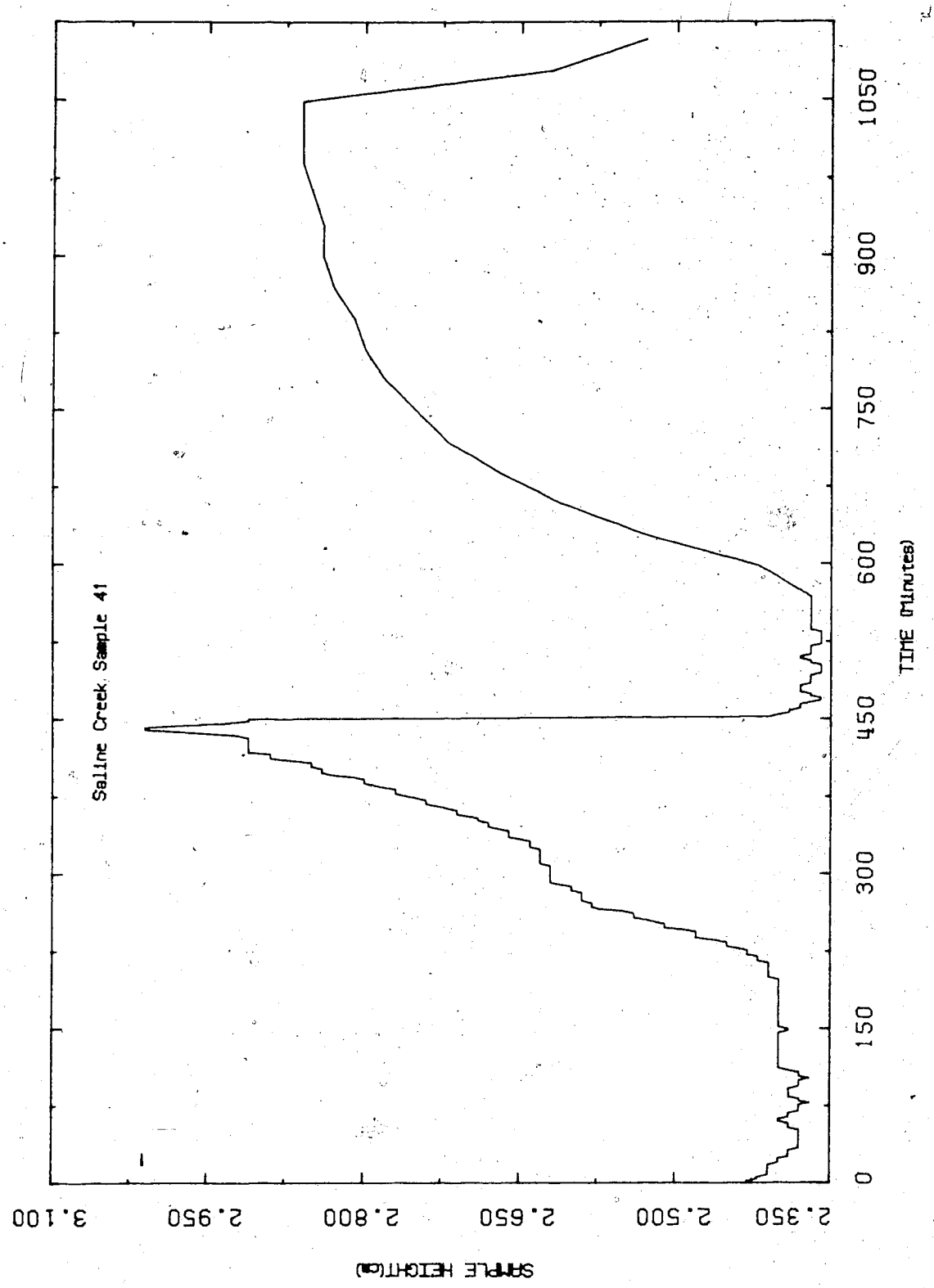

FIGURE B46 Sample Height Versus Time: Test COS9

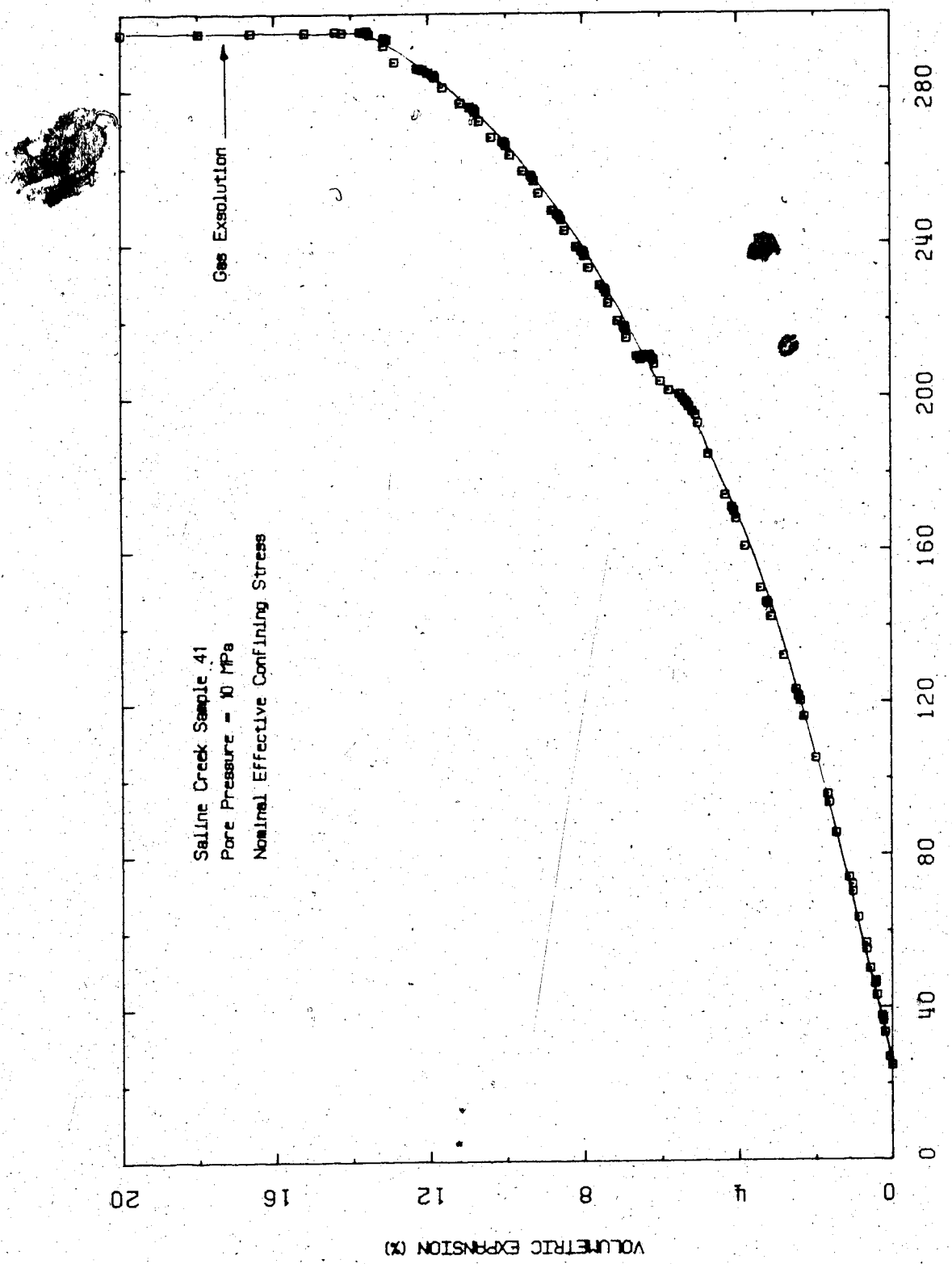

FIGURE B47 Undrained Volumetric Thermal Expansion: Test COS9

APPENDIX C

ONE DIMENSIONAL COMPRESSION TESTS

TABLE C-1

DRAINED ONE DIMENSIONAL COMPRESSION TESTS

Test	Temperature (°C)	Sample No.	Initial Bulk Density (Mg/m^3)	Initial Porosity	Range of Vertical Effective Stress (MPa)
CPERM 5	20	31A	2.04	0.37	0.5 - 5.0
CPERM 7	22	44	2.06	0.35	2.0 - 18.0
COS 9	22	41	2.07	0.35	2.0 - 18.0
CPERM 4	22	36	2.03	0.37	0.5 - 4.0
CPERM 4	100	36	2.03	0.36	4.0 - 26.0
CPERM 7	150	44	2.06	0.34	2.0 - 18.0
CPERM 5	200	31A	2.05	0.35	4.0 - 19.5
CPERM 6	250	31B	2.04	0.35	4.0 - 19.0
COS 9	300	41	2.00	0.34	4.0 - 18.0

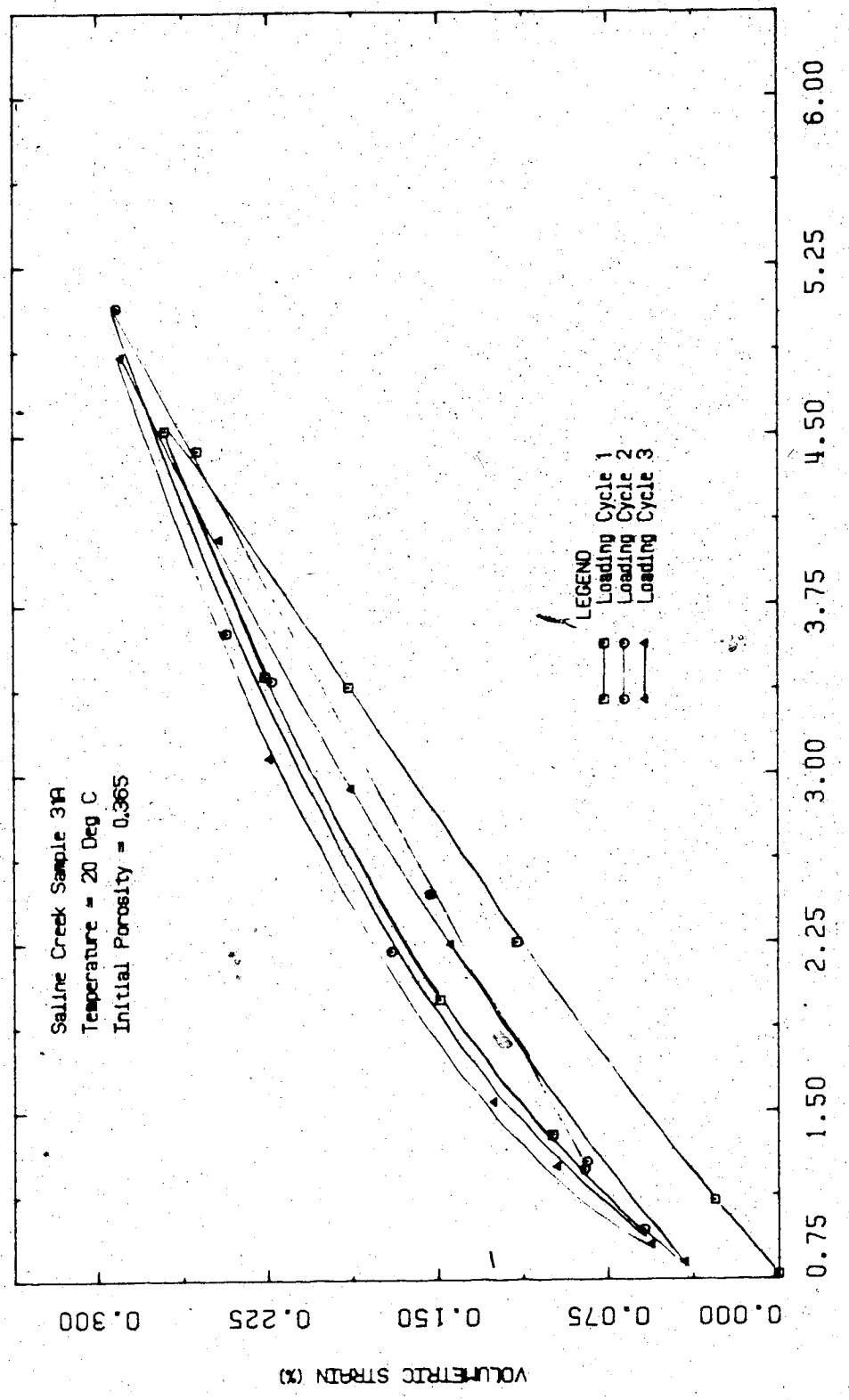

FIGURE C1 One Dimensional Compression at 20°C:
Test CPERM5

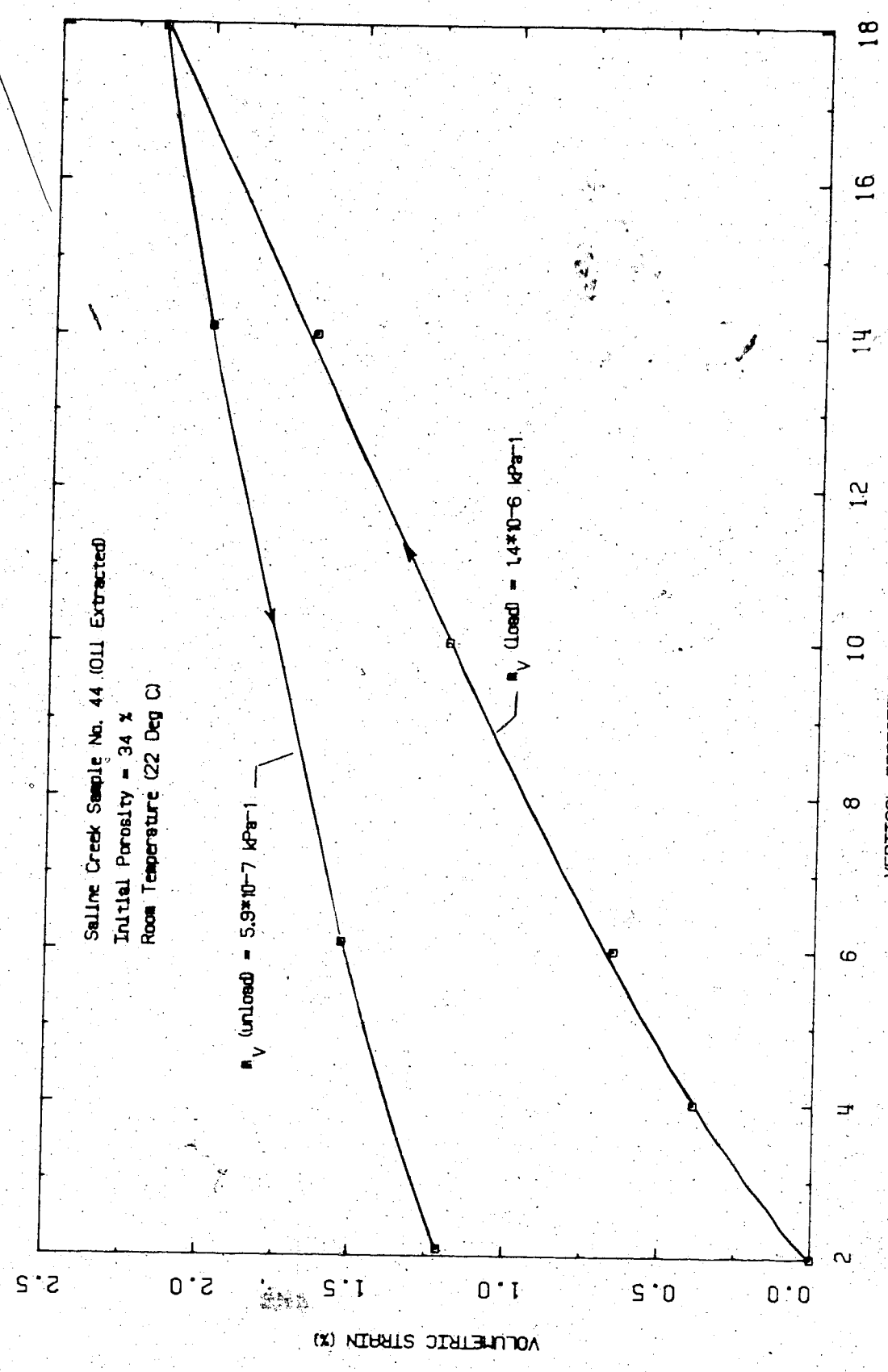

FIGURE C2 One Dimensional Compression at 22°C: Test CPERM7

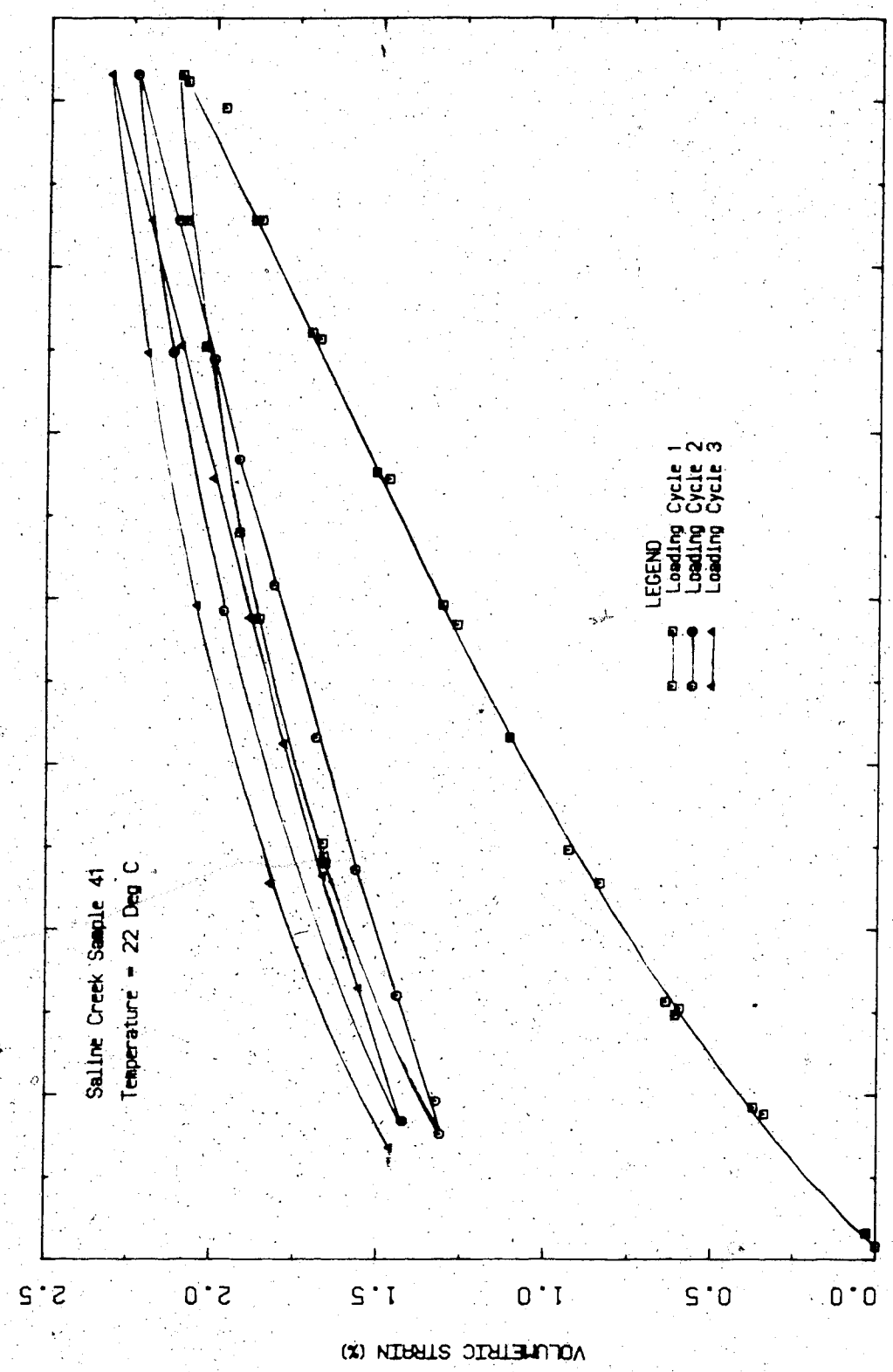

FIGURE C3 One Dimensional Compression at 22°C.
Test COS9

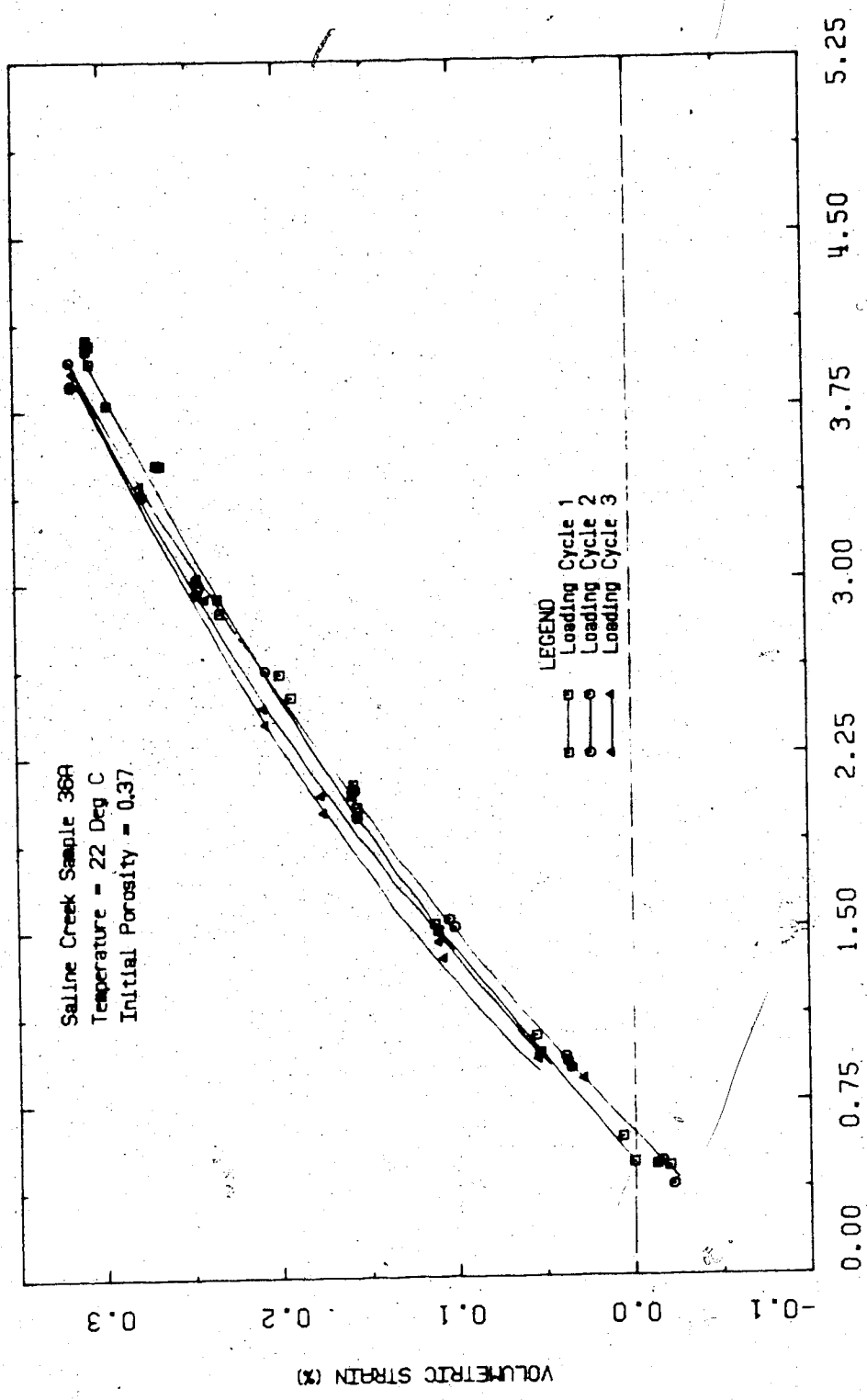

FIGURE C4 One Dimensional Compression at 22°C:
Test CPERM4

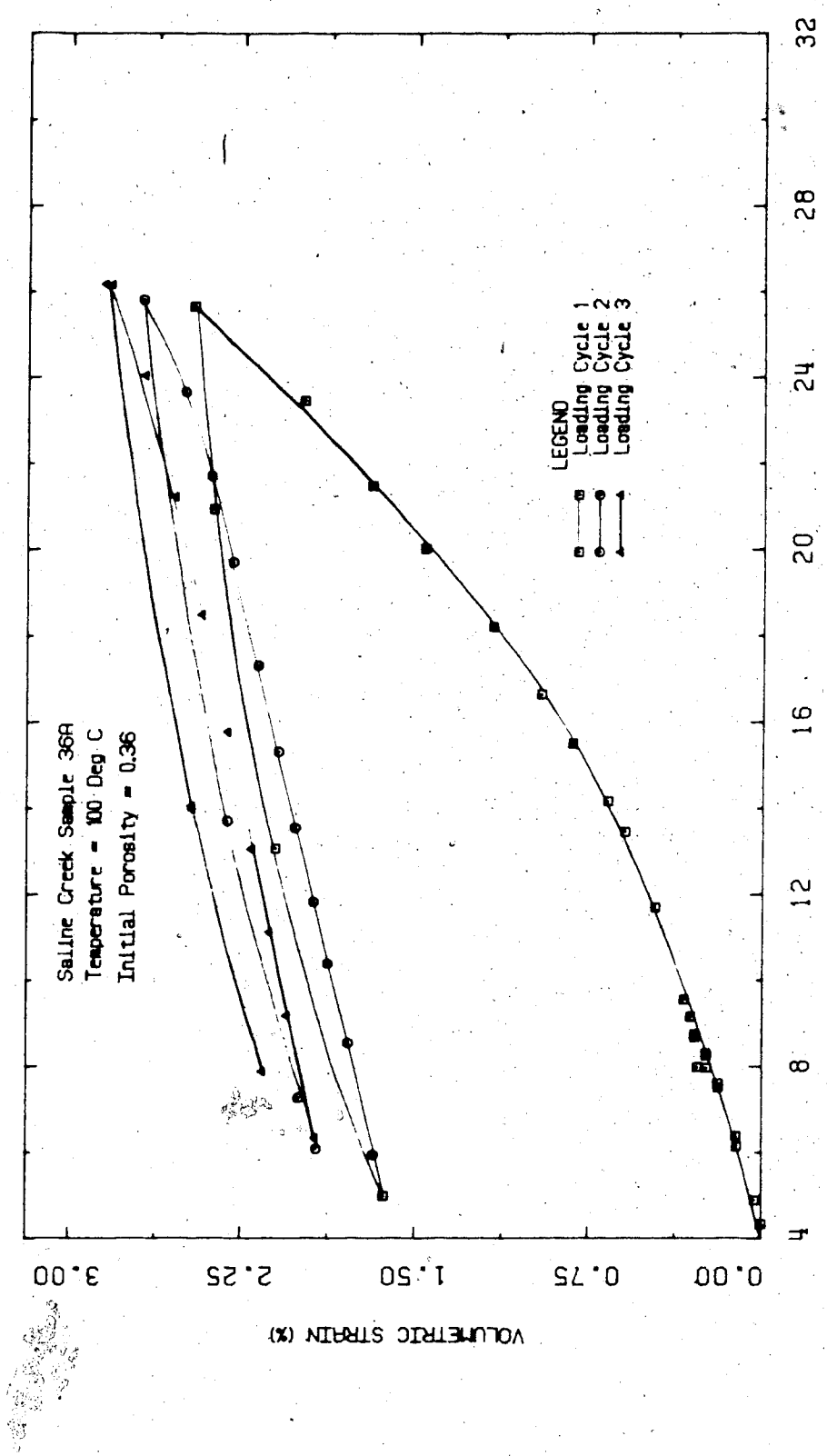

FIGURE C5 One Dimensional Compression at 100°C:
Test CPERM4

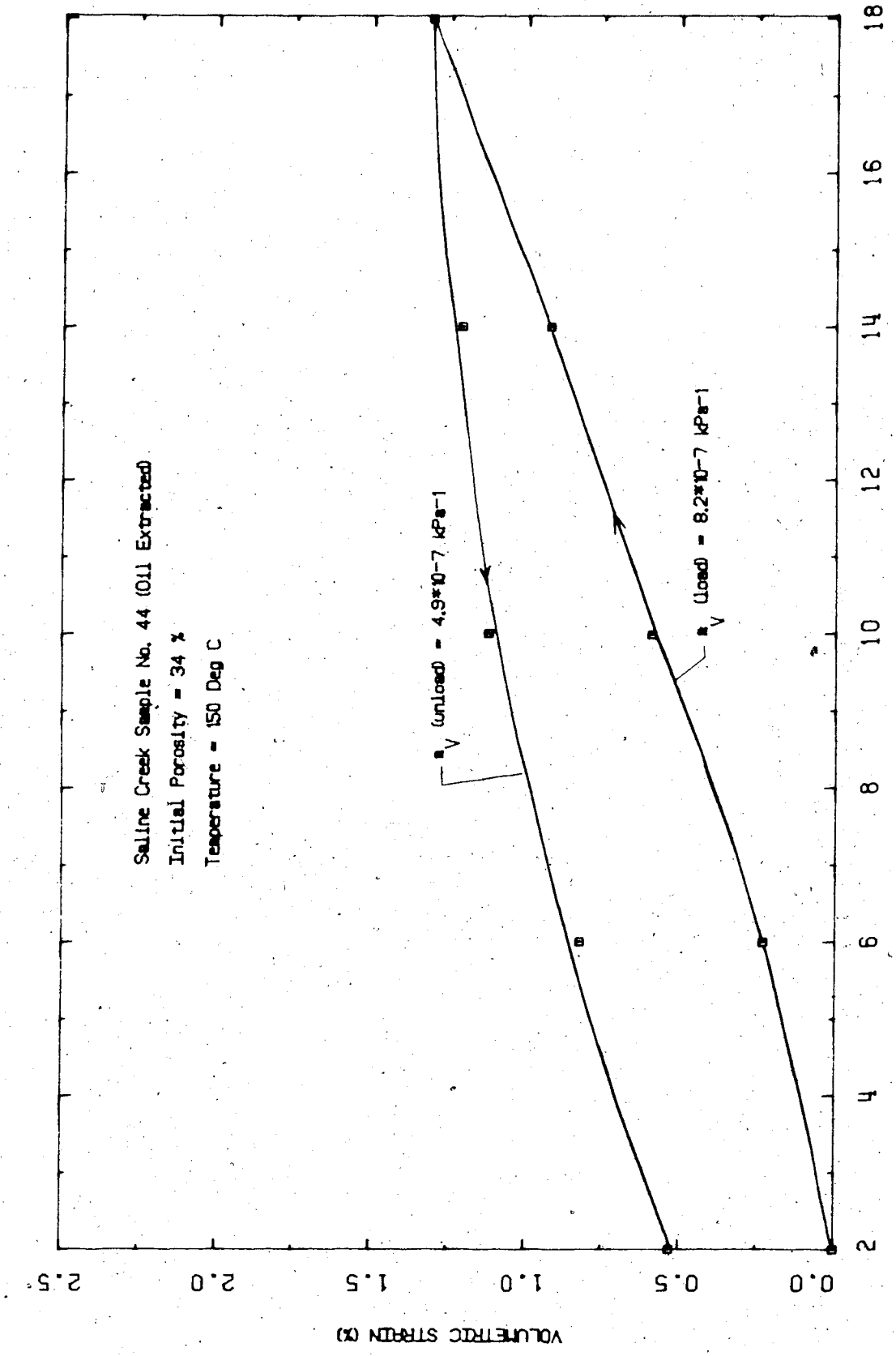

FIGURE C6 One Dimensional Compression at 150°C:
Test CPERM7

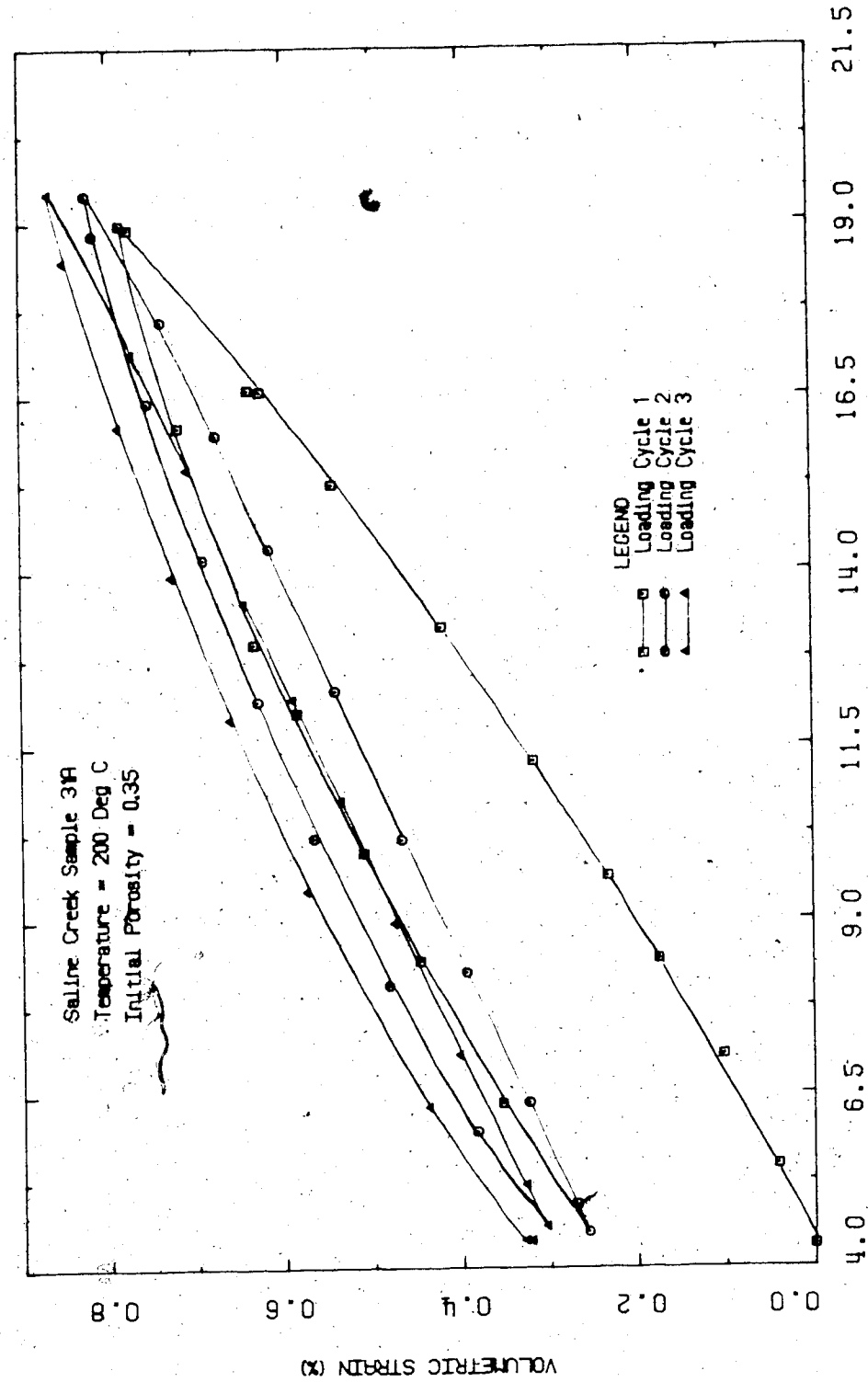

FIGURE C7 One Dimensional Compression at 200°C: Test CPERM5

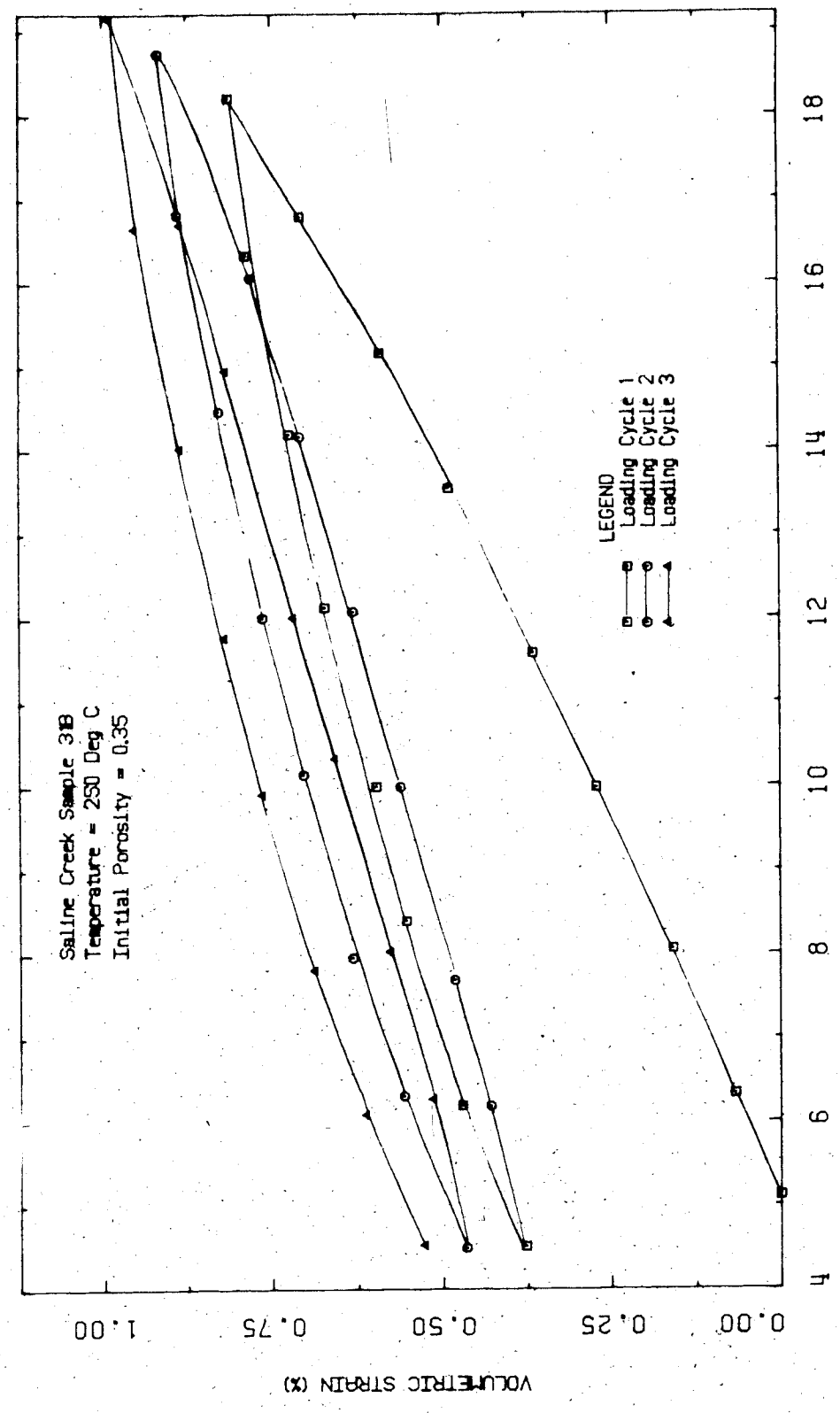

FIGURE C8 One Dimensional Compression at 250°C: Test CPERM6

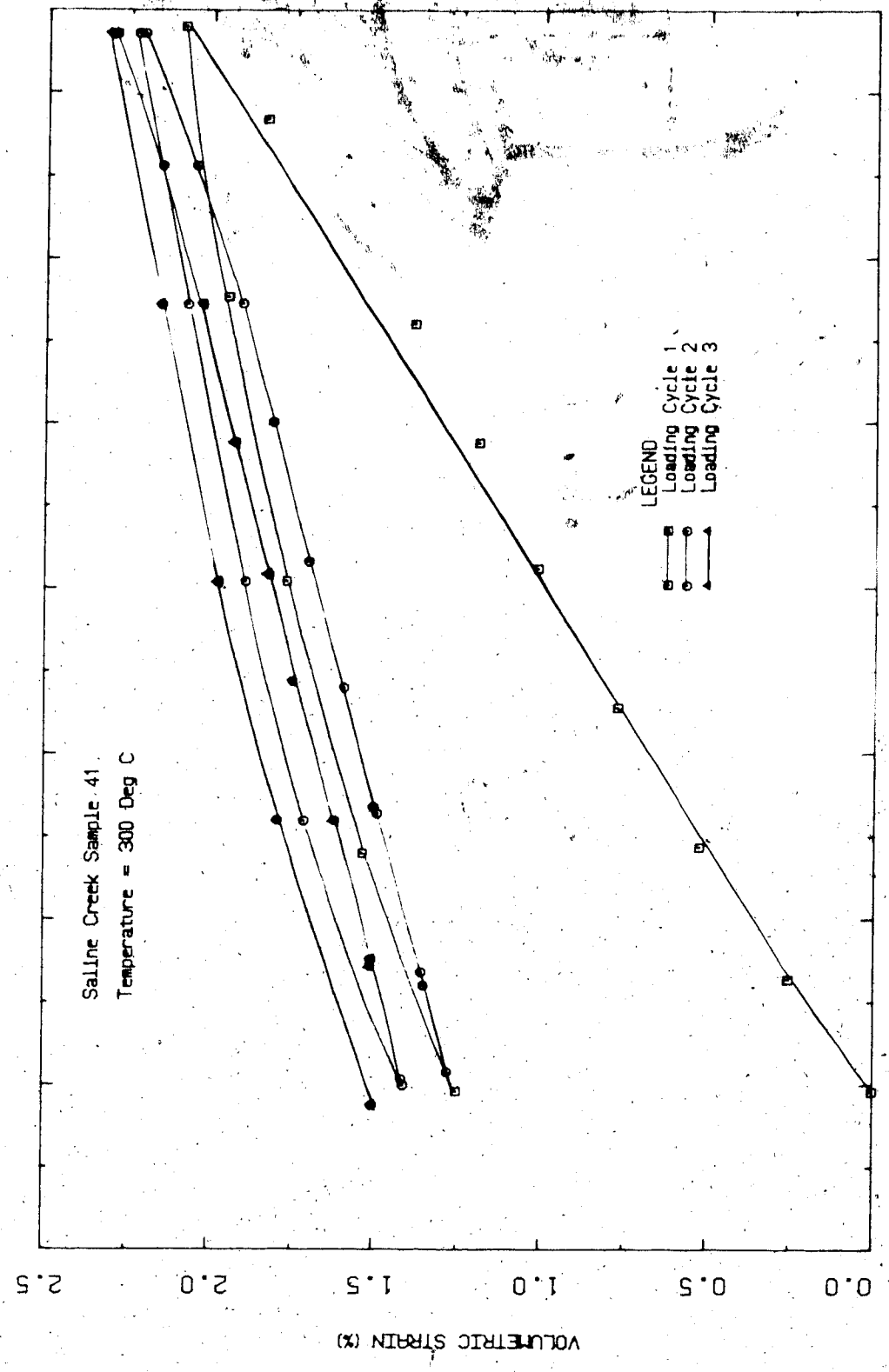

FIGURE C9 One Dimensional Compression at 300°C: Test C059

APPENDIX D

PERMEABILTY TESTS

TABLE D-1

SUMMARY OF PERMEABILITY TESTS

Test	Sample No.	Temperature Range (°C)	Effective Confining Stress (MPa)	Test Description
CPERM 1	10C	20	4	Inaccurate Differential Pressure Measurement.
CPERM 2	10D	50	2 - 4	Inaccurate Differential Pressure Measurement.
CPERM 3	M1	20	2 - 4	Absolute Permeability of remoulded oil free McMurray Formation Sand.
CPERM 4	36A	20 - 100	2 - 4	Permeability of undisturbed Saline Creek oil sand at room temperature and 100°C.
CPERM 5	31A	20 - 200	2 - 4	Permeability of undisturbed Saline Creek oil sand at room temperature and 200°C.
CPERM 6	31B	20 - 250	2 - 4	Permeability of undisturbed Saline Creek oil sand at room temperature and 250°C.
CPERM 7	44	20 - 150	2 - 18	Absolute permeability of undisturbed oil free Saline Creek oil sand at 20°C and 150°C over a range of effective confining stresses from 2 - 18 MPa.
CPERM 8	16	20 - 150	3	Permeability of undisturbed Saline Creek oi sand at 20°C and 150°C.
CPERM 9	36B	20 - 150	3	Permeability of remoulded Saline Creek oil sand at room temperature and 150°C.

TEST CPERM 1

Room Temperature Permeability Test on Saline Creek
Sample No. 10C Under 4 MPa Effective Confining Stress

TEST CPERM 1: SAMPLE DATA

Sample No. 10C

H = 4.877 cm

Dia. = 7.620 cm

c/s Area = 45.604 cm^2

V = 222.41 ml

Mass = 455.0 g

DENSITY: = 2.046 Mg/m^3

W = 2.5 % of M_S

B = 18.9% of M_S

M_S = 374.8 g

V_S = 141.45 ml

V_V = 80.96 ml

Initial Porosity

n = 0.364

S_W = 11.6%

S_B = 87.5%

S_G = 0.9%

Note: Differential pressure across the sample could not be measured with sufficient accuracy to determine permeability using twin 34 MPa pressure transducers as illustrated in Figure D2.

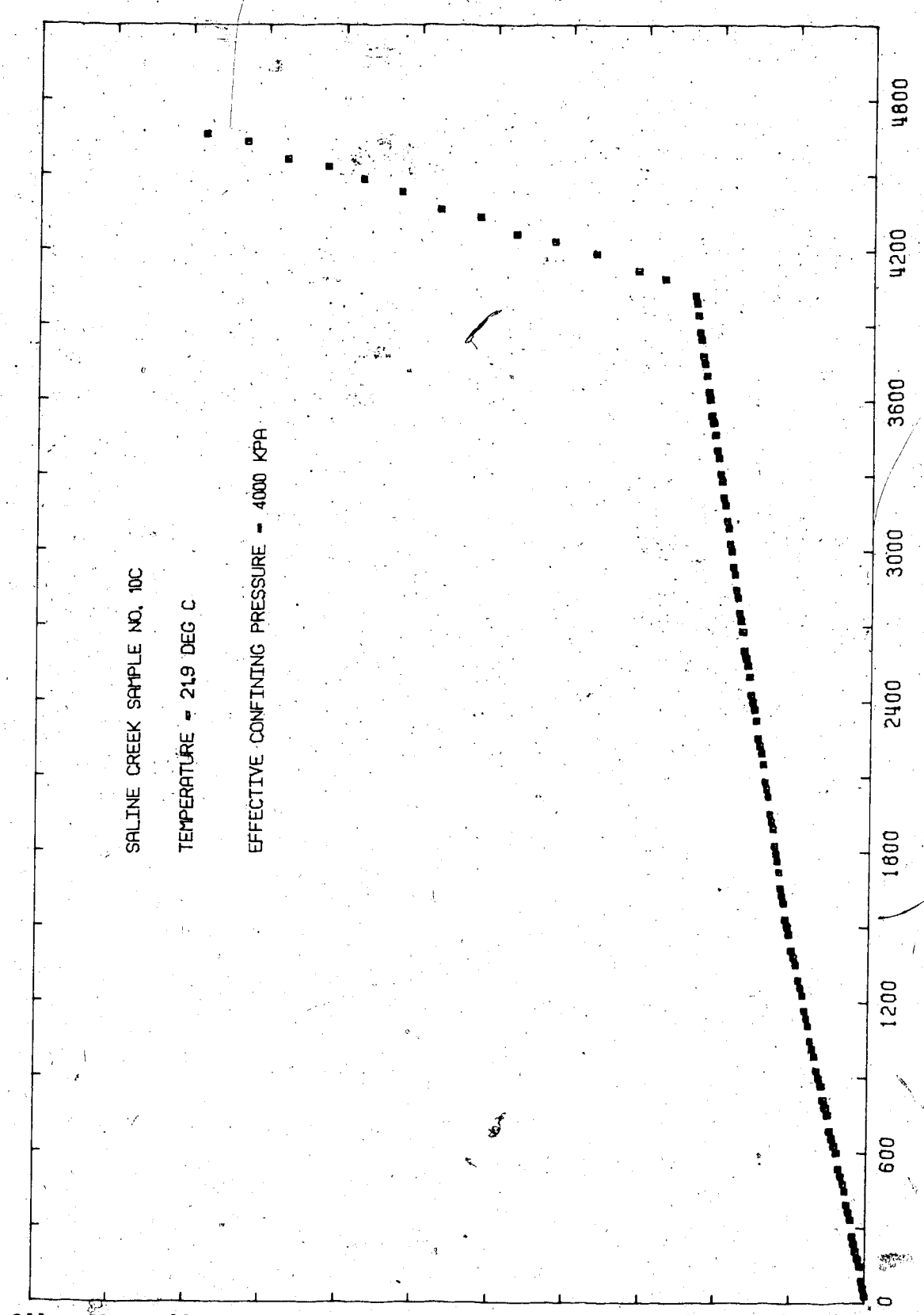

FIGURE D1 Flow Rate: Test CPLRM1 (20°C)

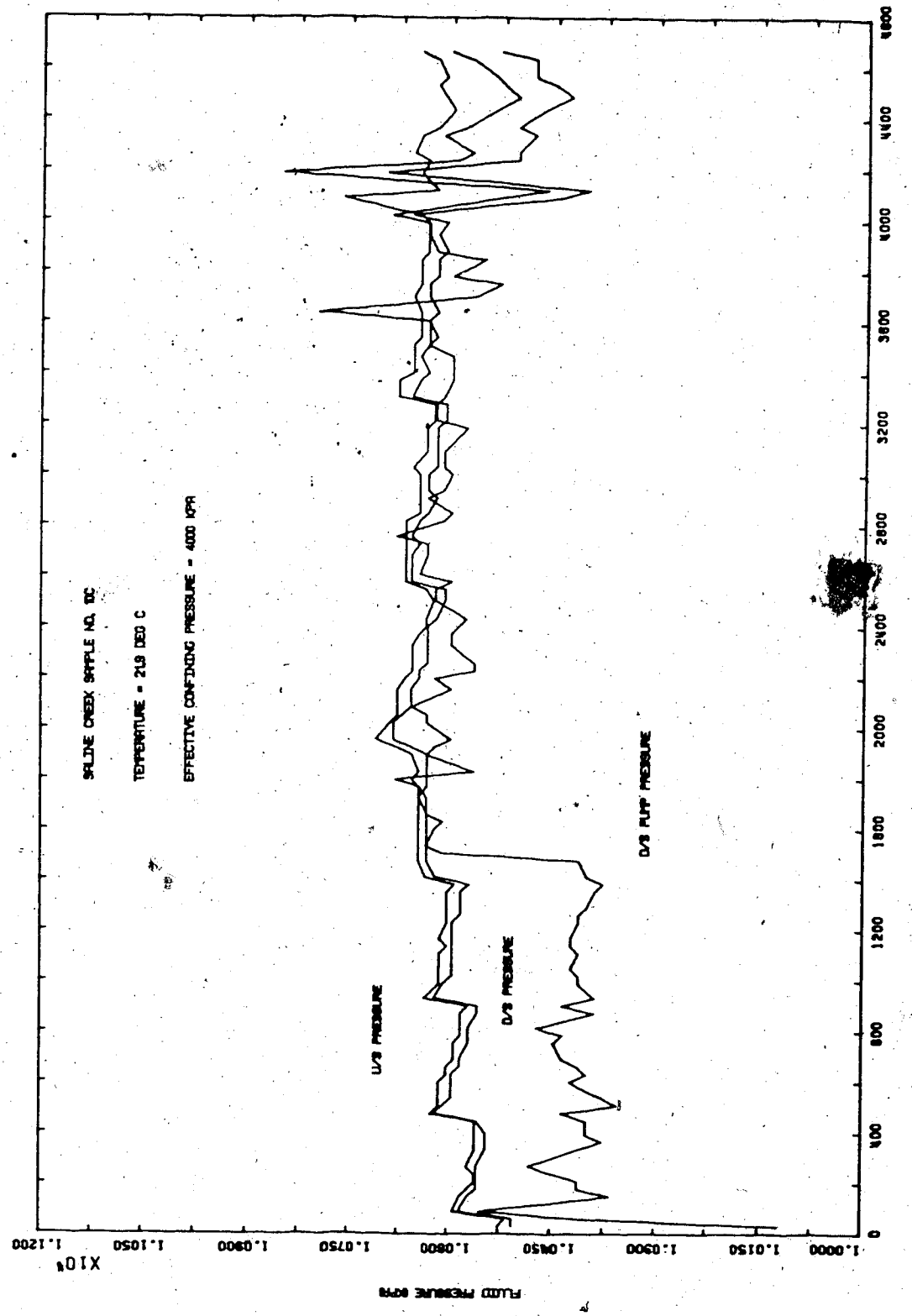

FIGURE D2 Pressure Variation With Time: Test CPERM1

TEST CPERM 2

Permeability Test on Saline Creek Sample No. 10 C
at 48°C and 4MPa Effective Confining Stress

TEST CPERM 2: SAMPLE DATA

Pretest Sample No. 10C

H	=	4.877 cm
Dia.	=	7.620 cm
c/s Area	=	45.604 cm^2
V	=	222.41 ml
Mass	=	455.25 g
Density	=	2.047 Mg/m^3

w	=	2.7 % of M_S
B	=	18.9% of M_S
M	=	374.8 g
V	=	141.45 ml
V	=	80.96 ml

Initial Porosity

n	=	0.364
S_W	=	12.5%
S_B	=	87.5%

Note: Differential pressure across the sample could not be measured with sufficient accuracy to determine permeability using twin 34 MPa pressure transducers as illustrated in Figure D4.

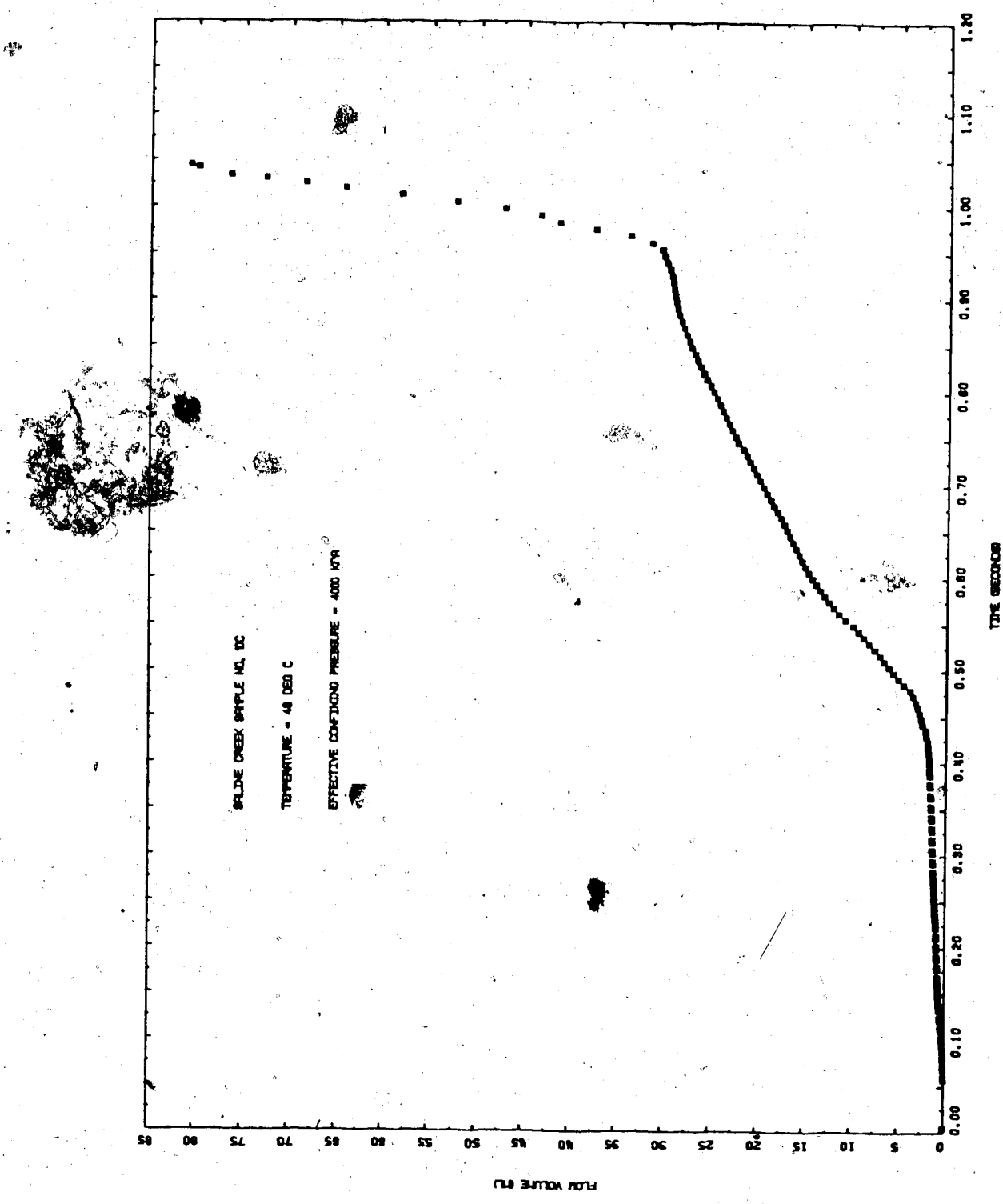

FIGURE D3 Flow Rate: Test CPERM2 (48°C)

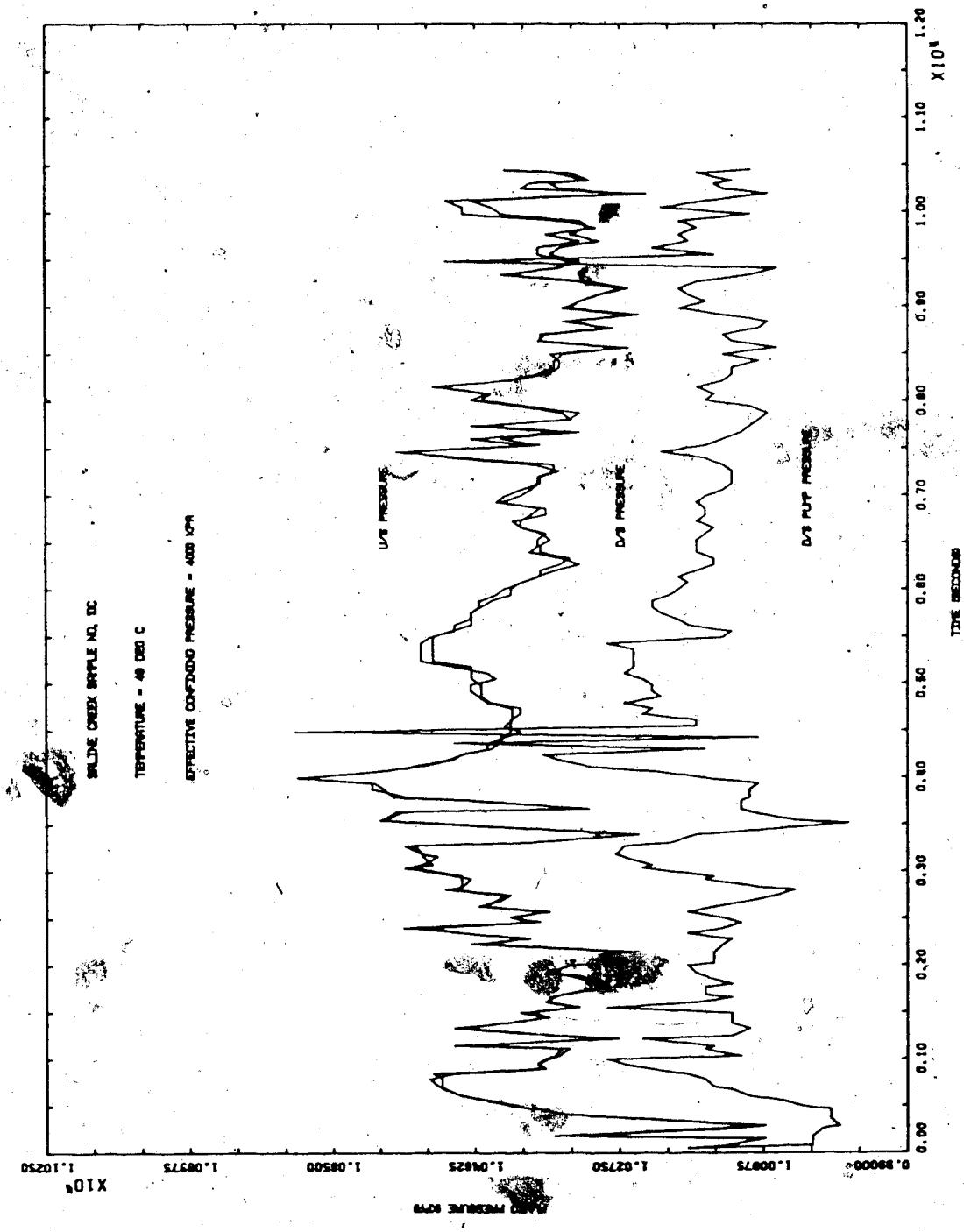

FIGURE D4 Pressure Variation With Time: Test CPERM2

TEST CPERM 3

Room Temperature Permeability of Remoulded Oil Free McMurray Sand Sample M1 at 2, 3 and 4 MPa Effective Confining Stresses

Procedural Details: Test CPERM 3

1. A sample of oil free McMurray Formation sand obtained from an outcrop along the High Hill River 40 km east of Fort McMurray in a remoulded state was compacted in 5 layers in the consolidometer cell.
2. The system and sample were back saturated under 2 MPa pore pressure for 24 hours and at 6 MPa confining stress.
3. Flow rate (i.e. volume change with time) and pressure drop across the sample were monitored simultaneously at room temperature and under effective confining stresses of 2, 3 and 4 MPa.
4. Pressure difference was measured at flow rates ranging up to 10 ml/minute at each effective confining stress level.

TEST CPERM 3: SAMPLE DATA

Remoulded "Oil-Free" McMurray Formation Sand Sample

Sample: Diameter: $\emptyset$ = 7.610 cm

Height: H = 5.920 cm

Area: A = 45.480 cm^2

Volume: V = 269.24 cm^3

Dry Mass: M = 448.8 g

Dry Density: $= \frac{448.8}{269.24}$ 1.670 Mg/m^3

Void Ratio: = 0.587

Porosity: = 0.370

Water Saturated Bulk Density: = 2.040 Mg/m^3

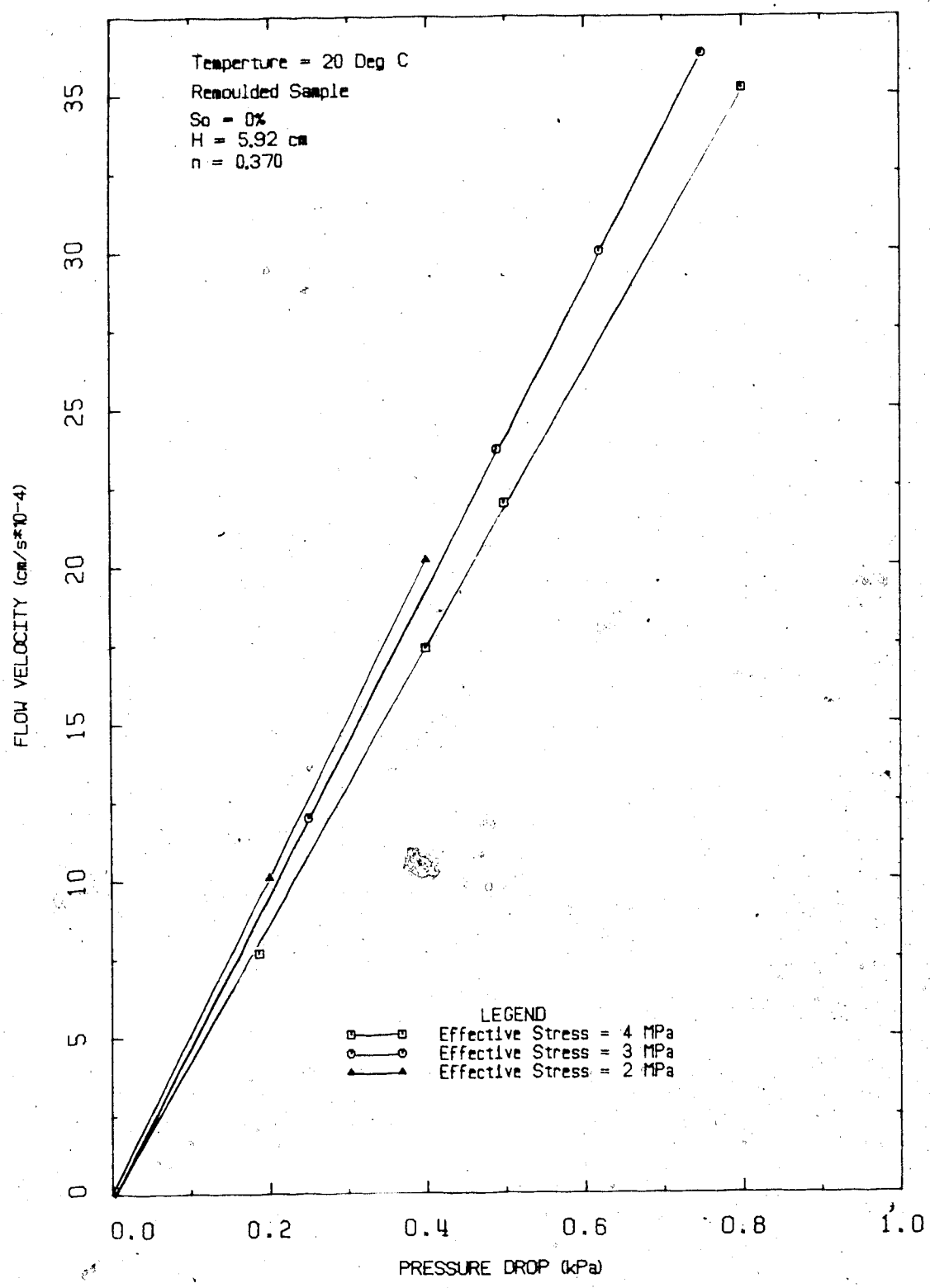

FIGURE D5 Flow Velocity Vs. Pressure Difference: Test CPERM3

TEST CPERM 4

Permeability Tests on Saline Creek Oil Sand
Sample No. 36A at 22°C and 100°C

Procedural Details: Test CPERM 4

1. Sample 36A was mounted in the consolidometer under frozen conditions.
2. The sample was thawed and back saturated for 24 hours under 2 MPa back pressure and 6 MPa confining stress.
3. Compressibility of the sample was measured at room temperature (22°C) over a range of effective stress from 0.5 - 4.0 MPa. The compressbility test included three cycles of loading and unloading.
4. A room temperature permeability test was performed by circulating water through the sample at flow rates varying up to about 4 ml/minute. Effective confining stress was maintained constant at 3 MPa.
5. Back pressure and confining stress were increased simultaneously in increments to 10 MPa and 13 MPa respectively.
6. The system and sample were heated slowly up to 100°C. Drained thermal expansion and the volume of fluid expelled from the sample during heating were measured.
7. A permeability test was conducted at 100°C in which 100°C water was circulated through the sample. Bitumen was flushed from the sample reducing the bitumen saturation from 81 percent to 73 percent.

8. Compressibility was measured at 100°C for a range of effective confining stresses from 4 - 26 MPa. The test included 3 cycles of loading and unloading.

9. The sample was cooled down to room temperature and a room temperature permeability test was performed at the residual oil saturation of 73% and for flow rates varying up to about 5 ml/minute.

TEST CPERM 4: SAMPLE DATA

Original Sample No. 36A at 22°C

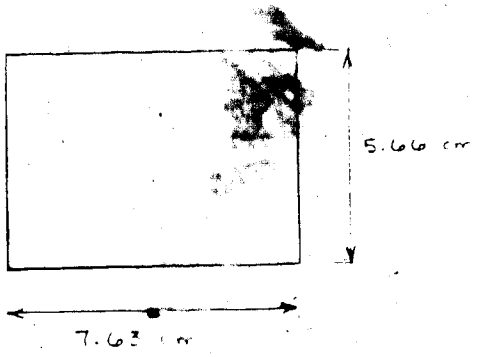

Total Mass = 526.1 g

Total Volume = 256.54 cm^3

Mass Sand = $\frac{526.1}{1+w+B}$ = 436.24

w = 2.8%

Bo = 17.6%

Mass Bitumen = 77.65 g

Volume Sand = $\frac{436.24}{2.65}$ = 164.62 cc

Volume Voids = $V_T - V_S$ = 93.92 cc = 36%

$V_B = \frac{77.65}{1.027}$ = 75.61 cc S_B = 80.5%

V_W = 18.31 cc S_W = 19.5%

Sample No. 36A After 100°C Permeability Test

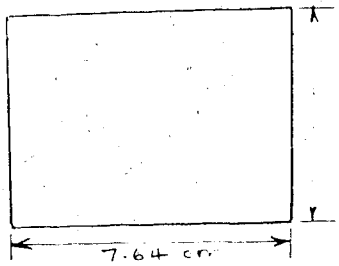

V_T = 259.00
V_S = 165.00
V_V = 94.0 cc
Mass Bitumen = 67.2 g
= 15.4%

DISTRIBUTION OF WATER AND BITUMEN:

Top	V_B = 62.8	S_B = 66.8%
	V_W = 31.2	S_W = 33.2%
Middle	V_B = 68.5	S_B = 72.9%
	V_W = 25.5	S_W = 27.1%
Bottom	V_B = 70.2	S_B = 74.7%
	V_W = 23.8	S_W = 25.3%

AVERAGE SATURATIONS:

V_B = 67.0 cc
S_B = 71.3%
V_W = 27.0 cc
S_B = 28.7%

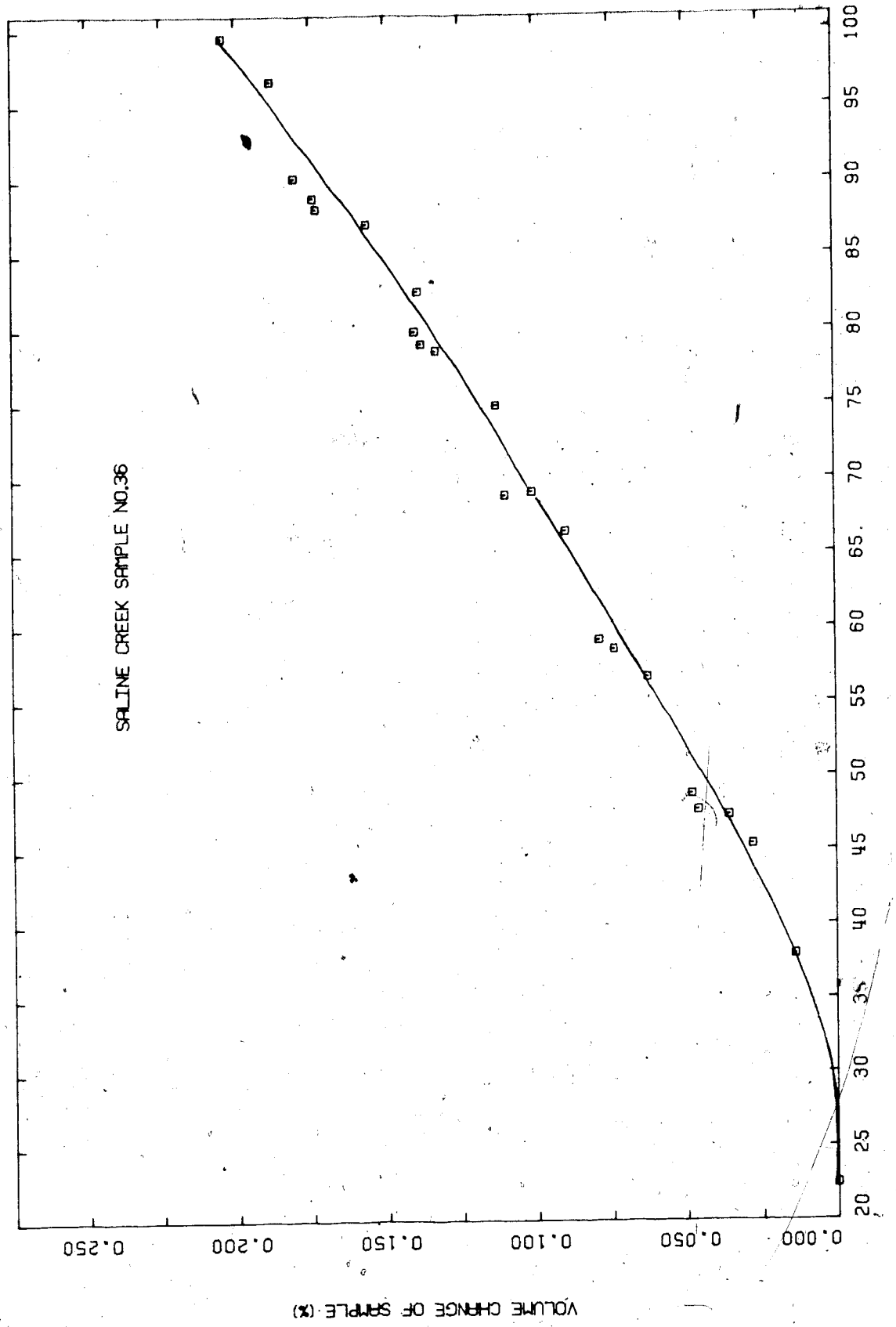

FIGURE D6 Drained Thermal Expansion: Test CPERM4

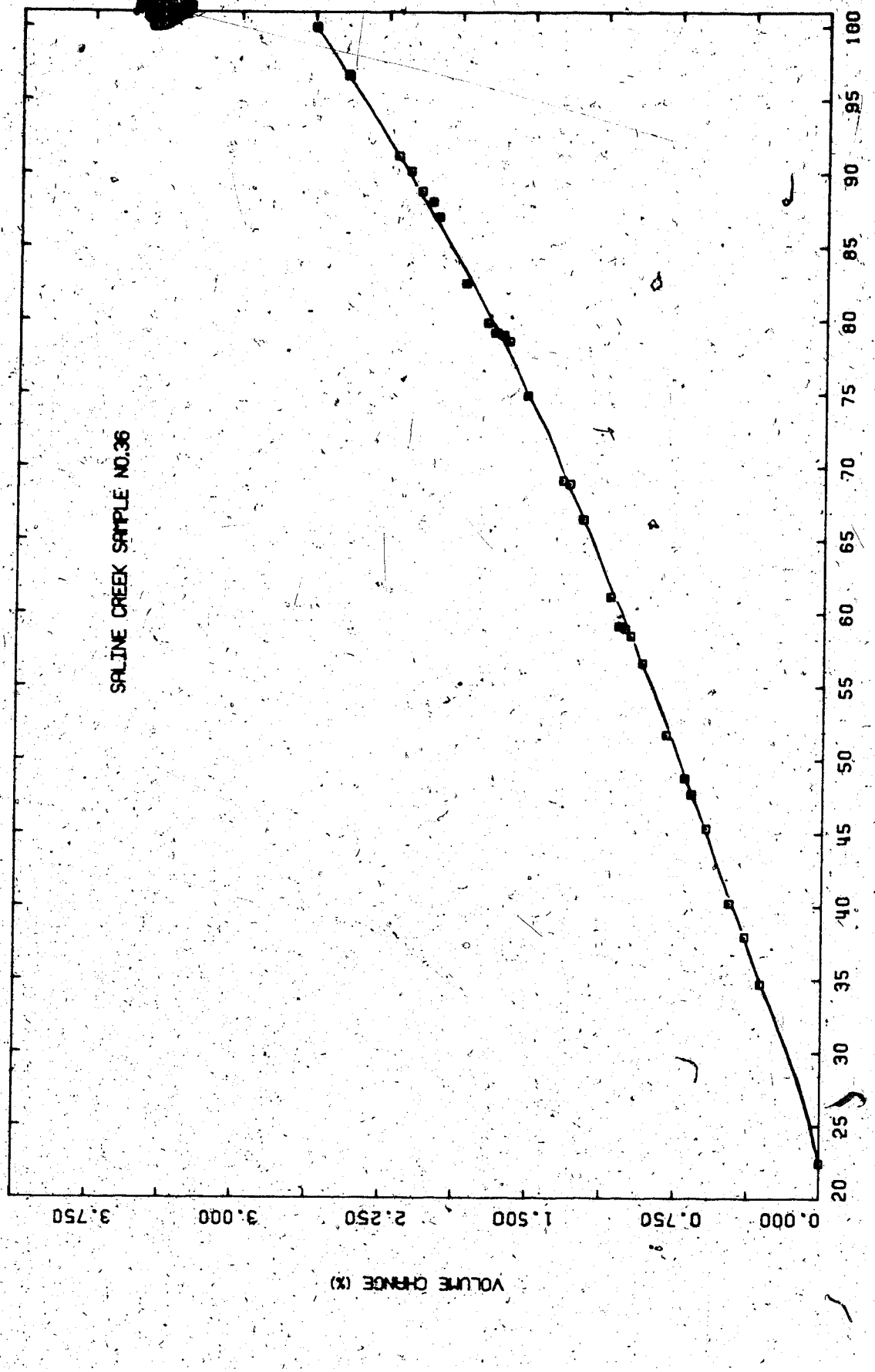

FIGURE D7 Undrained Thermal Expansion: Test CPERM4

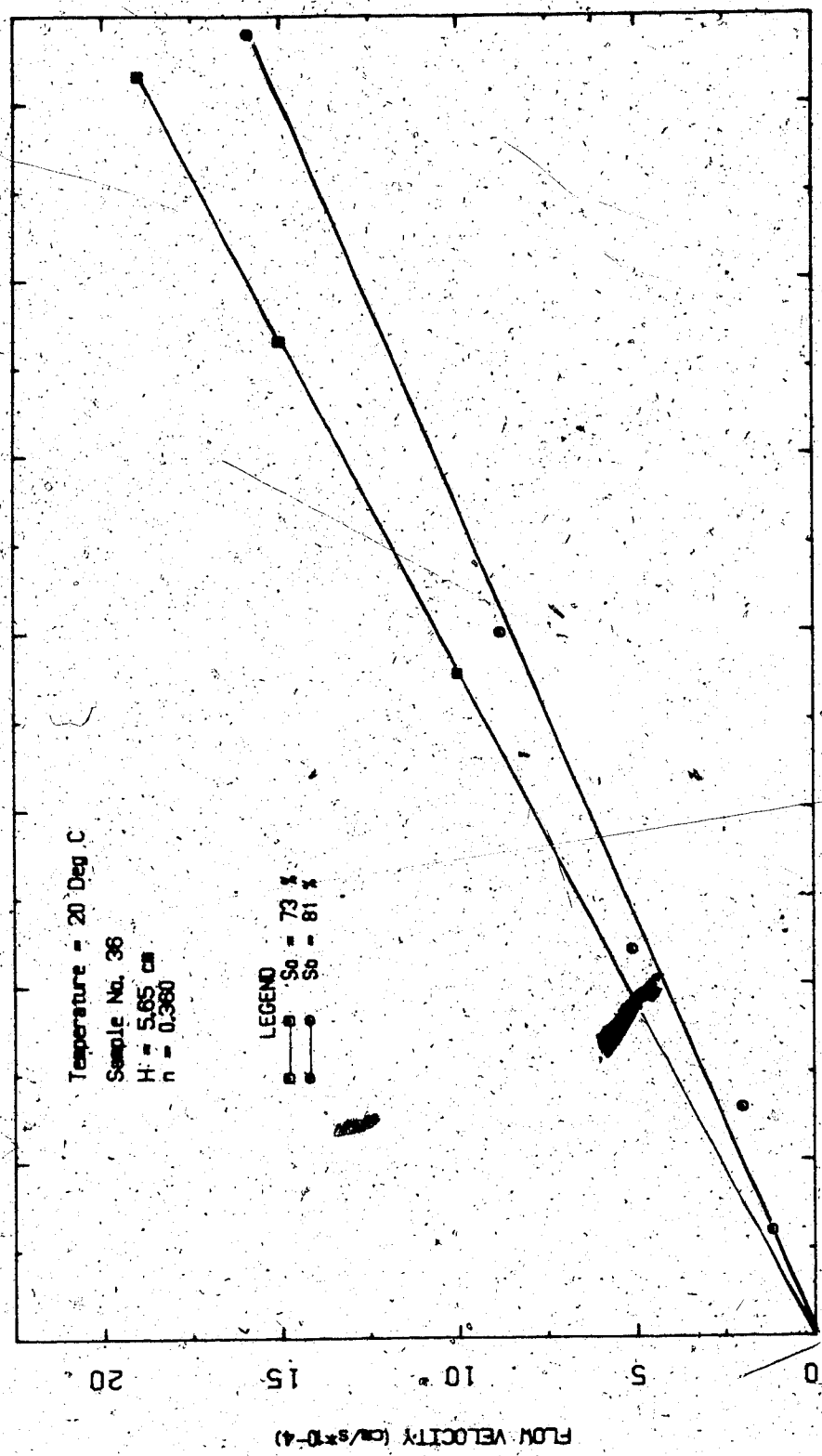

FIGURE D8 Flow Velocity Vs. Pressure Difference: Test CPERM4

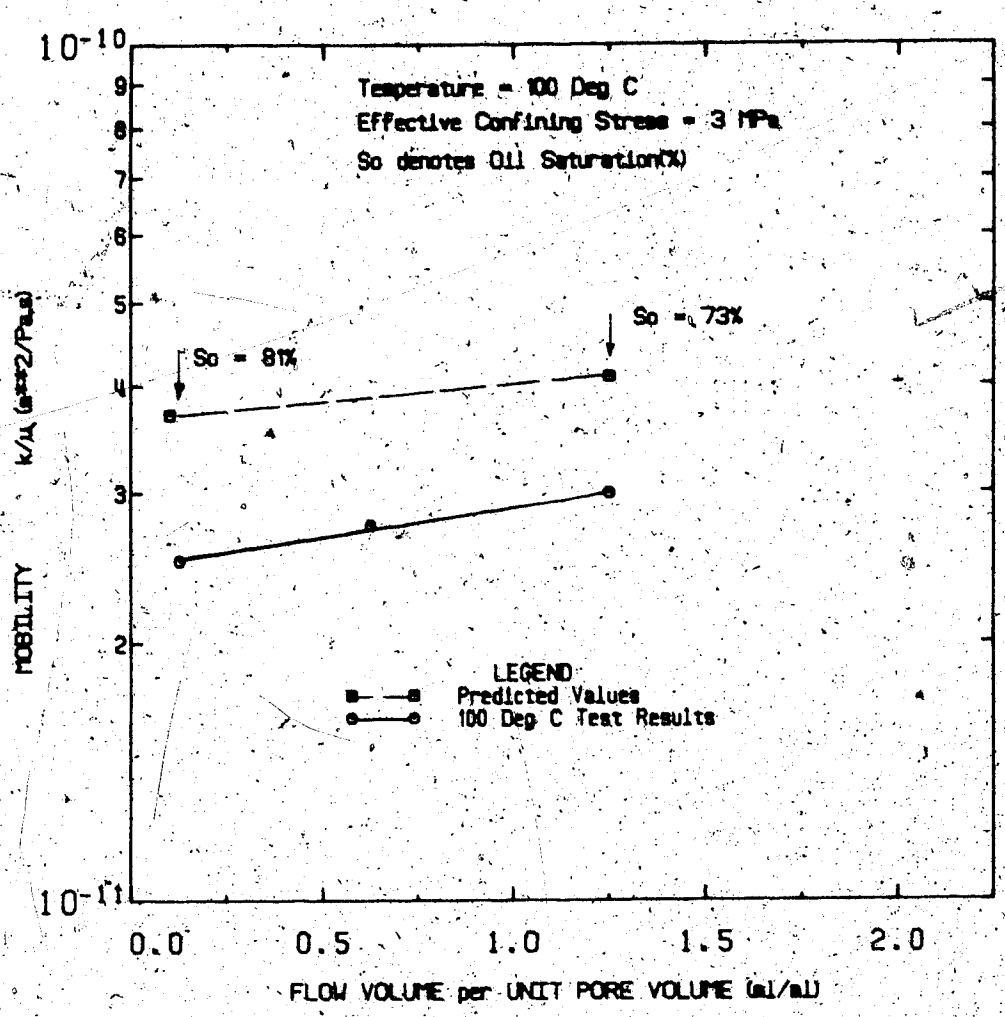

FIGURE D9 Fluid Mobility Vs. Normalized Flow Volume: Test CPERM4

TEST CPERM 5

Permeability Tests on Saline Creek Sample No. 31A at 20°C and 200°C

Procedural Details: Test CPERM 5

1. Saline Creek Sample No. 31A was thawed and back saturated for 24 hours under 2 MPa back pressure and 6 MPa confining stress.
2. Cyclic room temperature compressibility was measured over a range of effective stress from 0.5 - 5.0 MPa.
3. Room temperature permeability was measured by circulating water through the sample at flow rates varying up to 2.5 ml/minute. Effective confining stress was maintained constant at 3 MPa.
4. The back pressure and confining pressure were increased simultaneaously in increments to 10 MPa and 14 MPa, respectively.
5. The apparatus and sample were heated to 200°C. Drained thermal expansion of the sample was monitored.
6. A permeability test was performed at 20°C by circulating heated water and measuring pressure drop across the sample. Bitumen was flushed from the sample reducing the bitumen saturation from 86% to 51%. Effective confining stress was maintained at 3 MPa.

7. Cyclic compressibility was measured at 200°C over the effective stress range 4 - 19.3 MPa.
8. Room temperature permeability as measured at the residual bitumen saturation of 31% for flow rates up to about 7.5 ml/minute.

TEST OPERM-3: SAMPLE DATA

Original Sample No. 31A at 22°C:

Dia.: ϕ = 7.633 cm
Area: A = 45.756 cm^2
Height: H = 5.570 cm
Volume: V = 254.86 cm^3
Mass: M = 521.3 g

w = 3% = 12.85 g B = 18.75% = 80.28 g $W_S = \frac{521.3}{1+w+B}$ = 428.17 g

$V_S = \frac{W_S}{2.65}$ = 61.57 cm^3

V_V = 254.86 − V_S = 93.29 cm^3 = 36%

Initial Fluid Saturations: S_W = 13.8% S_O = 86.2%

After Permeability Test at 200°C

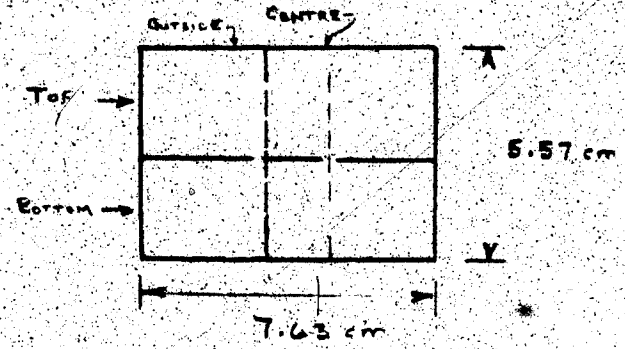

Distribution of Pore Fluids:

Top Centre:	w	= 9.8%
	B	= 9.1%
	S_O	= 48.4%
	S_W	= 51.6%
Bottom Centre:	w	= 9.3%
	B	= 10.6%
	S_O	= 53.4%
	S_W	= 46.6%
Top Outside:	w	= 9.9%
	B	= 10.1%
	S_O	= 50.6%
	S_W	= 49.4%
Bottom Outside:	w	= 9.3%
	B	= 10.6%
	S_O	= 53.3%
	S_W	= 46.7%

Final Fluid Saturations:

Average Top Half:	S_O	= 49.5%	S_W	= 50.5%
Average Bottom Half:	S_O	= 53.4%	S_W	= 46.6%
Average For Sample:	S_O	= 51.4%	S_W	= 48.6%

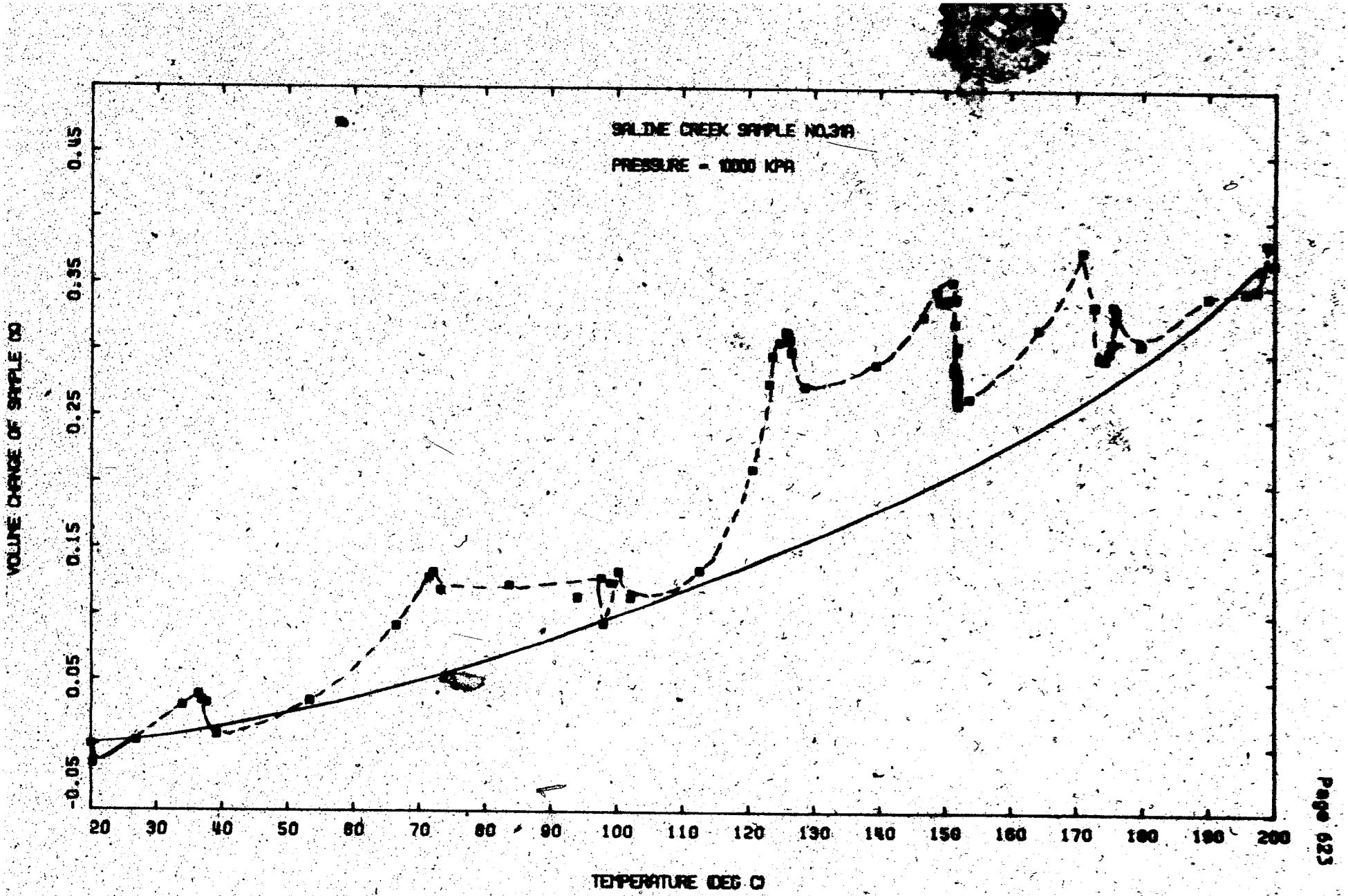

FIGURE D10 Drained Thermal Expansion: Test CPERM3

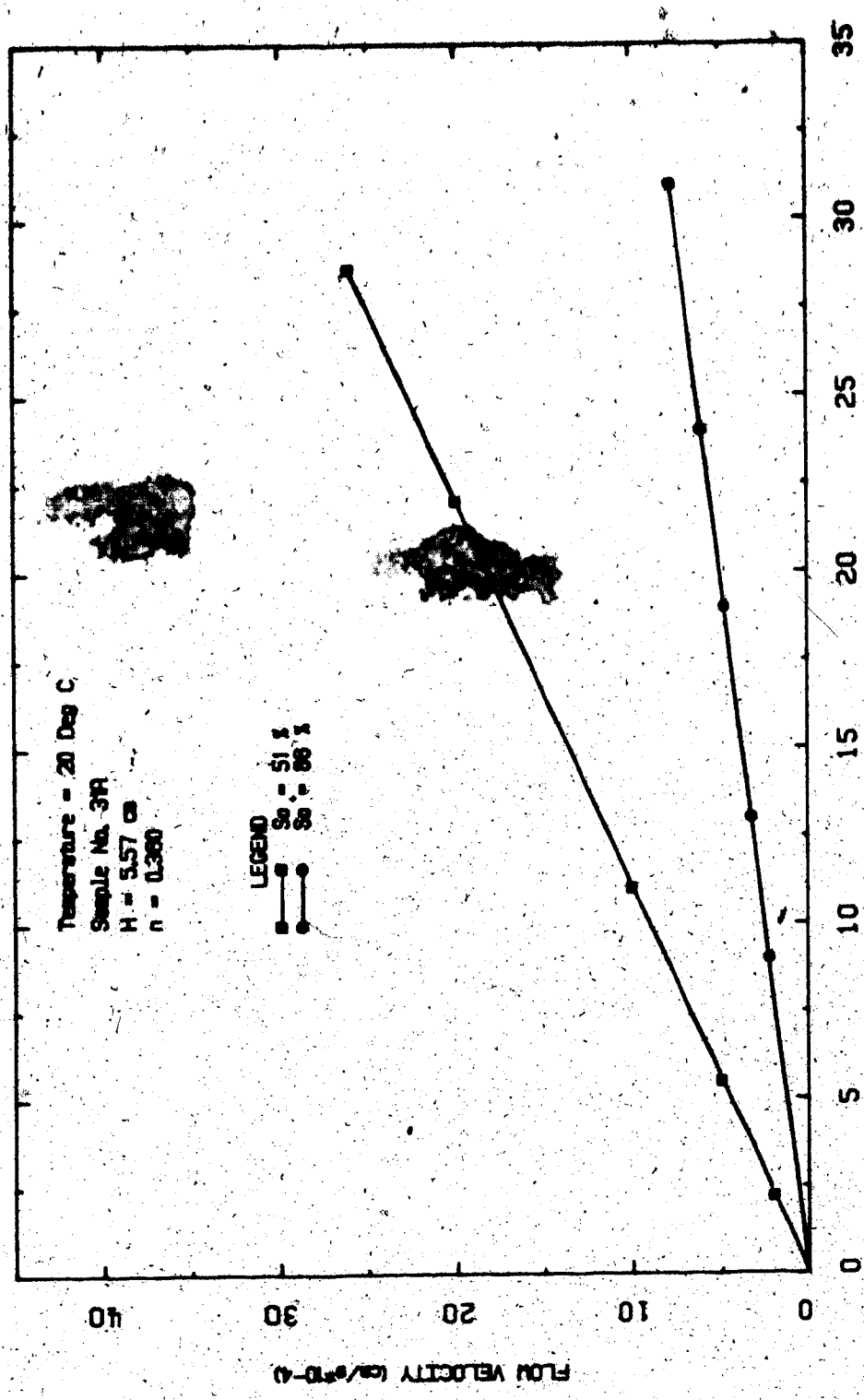

FIGURE D11 Flow Velocity Vs. Pressure Difference: Test CPERM5

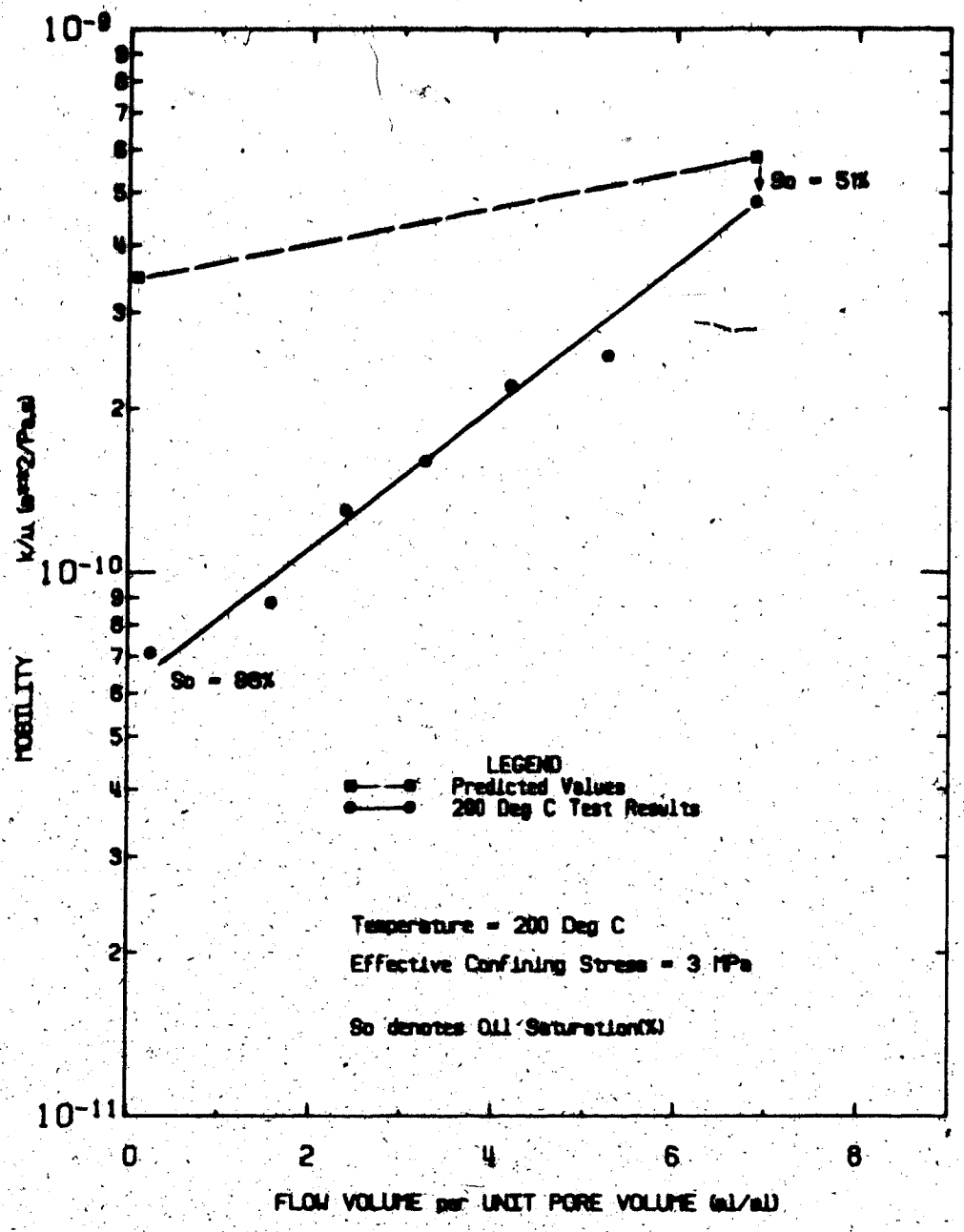

FIGURE D12 Fluid Mobility Vs. Normalized Flow Volume; Test CPERM5

TEST CPERM 6

Permeability of Saline Creek Oil Sand Sample No. 31B at Room Temperature and 250°C

Procedural Details: Test CPERM 6

1. Sample No. 31B was thawed and back saturated for 24 hours under 2 MPa back pressure and 6 MPa confining stress.
2. Room temperature permeability was measured by circulating water through the sample and measuring pressure difference at flow rates up to about 4 ml/minute. Effective confining stress was maintained at 3 MPa.
3. Back pressure and confining stress were increased simultaneously in increments up to 10 MPa and 13 MPa.
4. The apparatus and sample were heated to 250°C. Drained thermal expansion of the sample was monitored during heating.
5. A permeability test was performed at 250°C by circulating heated water and monitoring pressure drop across the sample. Bitumen was flushed from the sample pore space reducing the bitumen saturation from 81% to 38%.
6. Cyclic compressibility was measured at 250°C over a range of effective stresses from 4 - 19 MPa.
7. The sample was cooled down to room temperature and a permeability test performed at the residual bitumen saturation of 38 percent.

TEST CPERM 6: SAMPLE DATA

Original Sample No. 31B at 20°C:

Dia.: $\emptyset$ = 7.633 cm
Area: A = 45.756 cm^2
Height: H = 5.540 cm
Volume: V = 253.488 cm^3
Mass: M = 515.40 g

w = 4% B = 16.1

$W_S = \frac{515.4}{1+W+B} = 429.14$ g

$V_S = \frac{W_S}{2.65} = 161.94$ ml

$V_V = V - V_S = 91.55$ ml

$S_W = 19\%$ $S_O = 81.\%$

After 250°C Permeability Test

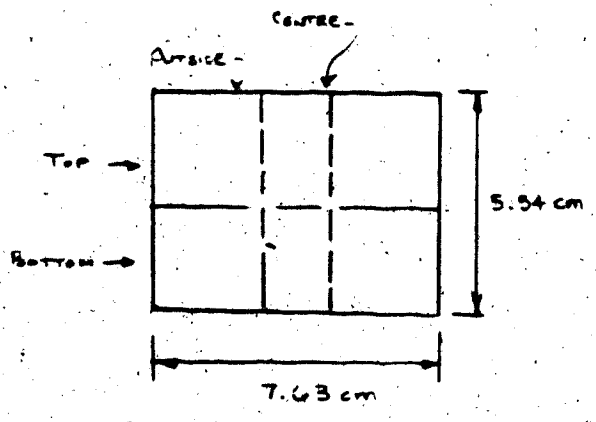

Distribution of Pore Fluids:

Top Centre:	w	=	12.72%
	B	=	5.27%
	S_O	=	29.3%
	S_W	=	70.7%
Bottom Centre:	w	=	12.86%
	B	=	7.64%
	S_O	=	37.3%
	S_W	=	62.7%
Top Outside:	w	=	11.65%
	B	=	6.24%
	S_O	=	34.9%
	S_W	=	65.1%
Bottom Outside:	w	=	10.74%
	B	=	7.93%
	S_O	=	42.5%
	S_W	=	57.5%

Final Fluid Saturations:

Average for Sample after 250°C test:

Wet Mass = 450.87 Dry Mass = 380.18

w = 44.0 ml B = 26.69 ml

= 11.57% = 7.02%

S_W = 62.2% S_W = 37.8%

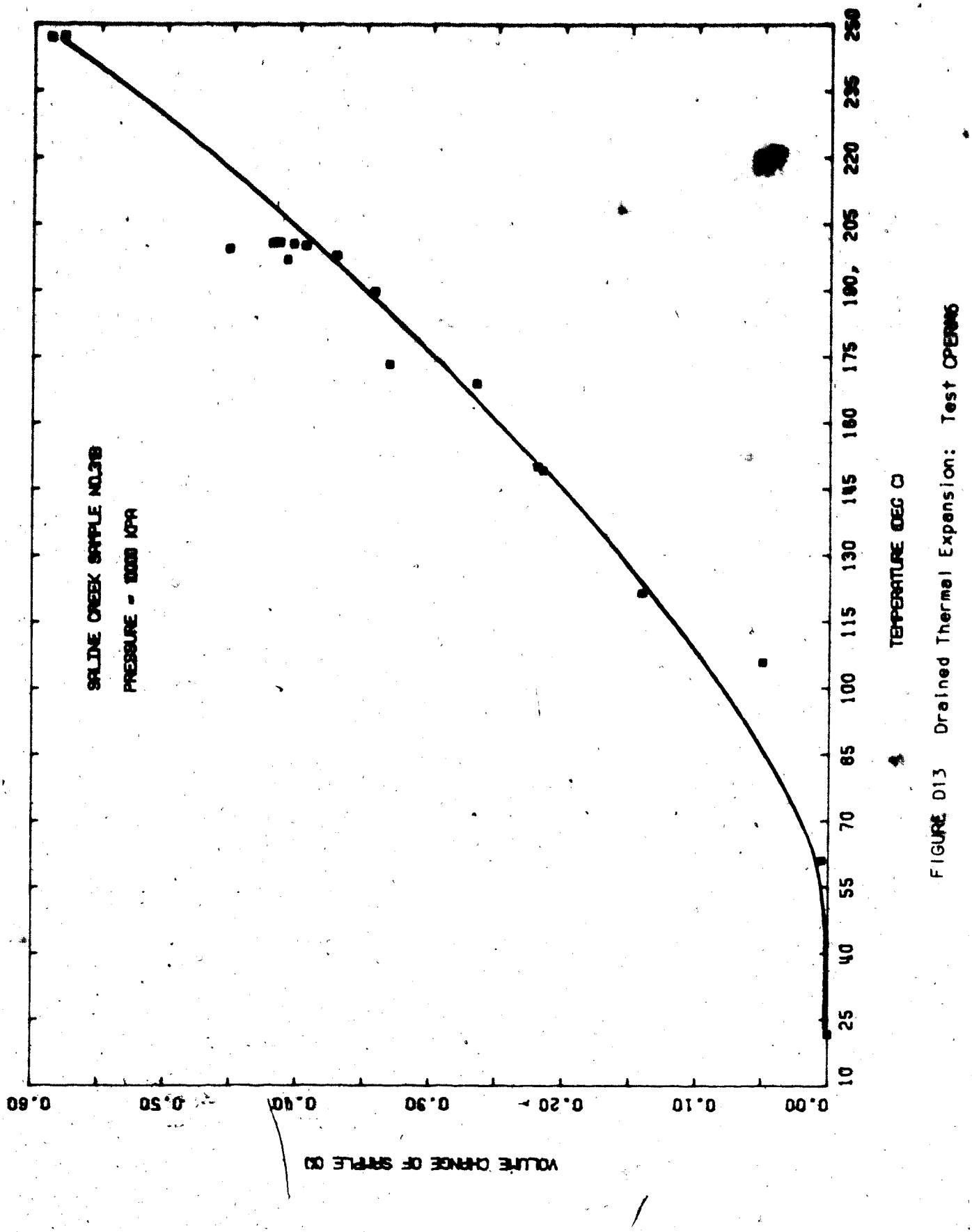

FIGURE D13 Drained Thermal Expansion: Test OPENING

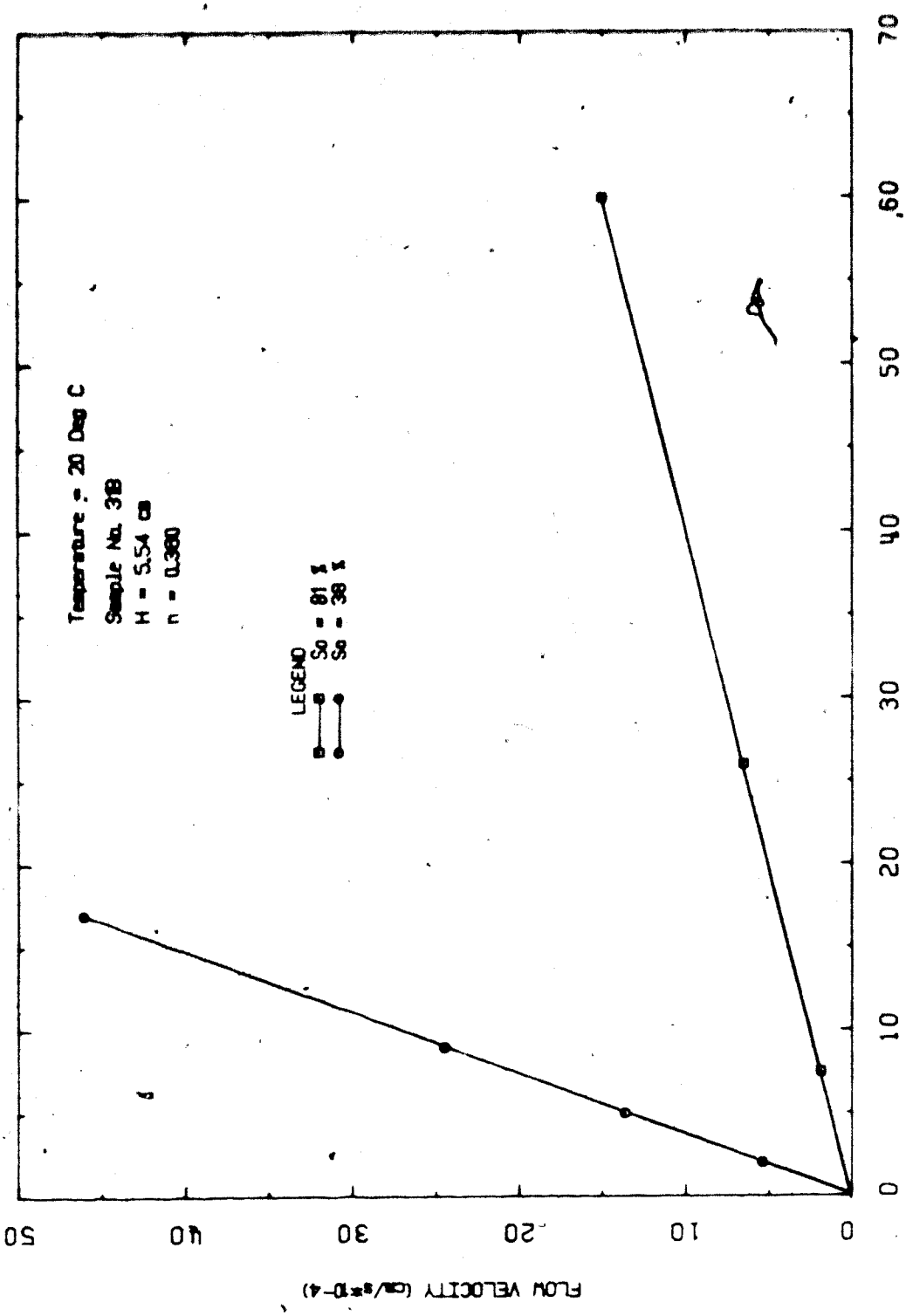

FIGURE D14 Flow Velocity Vs. Pressure Difference: Test CPERM6

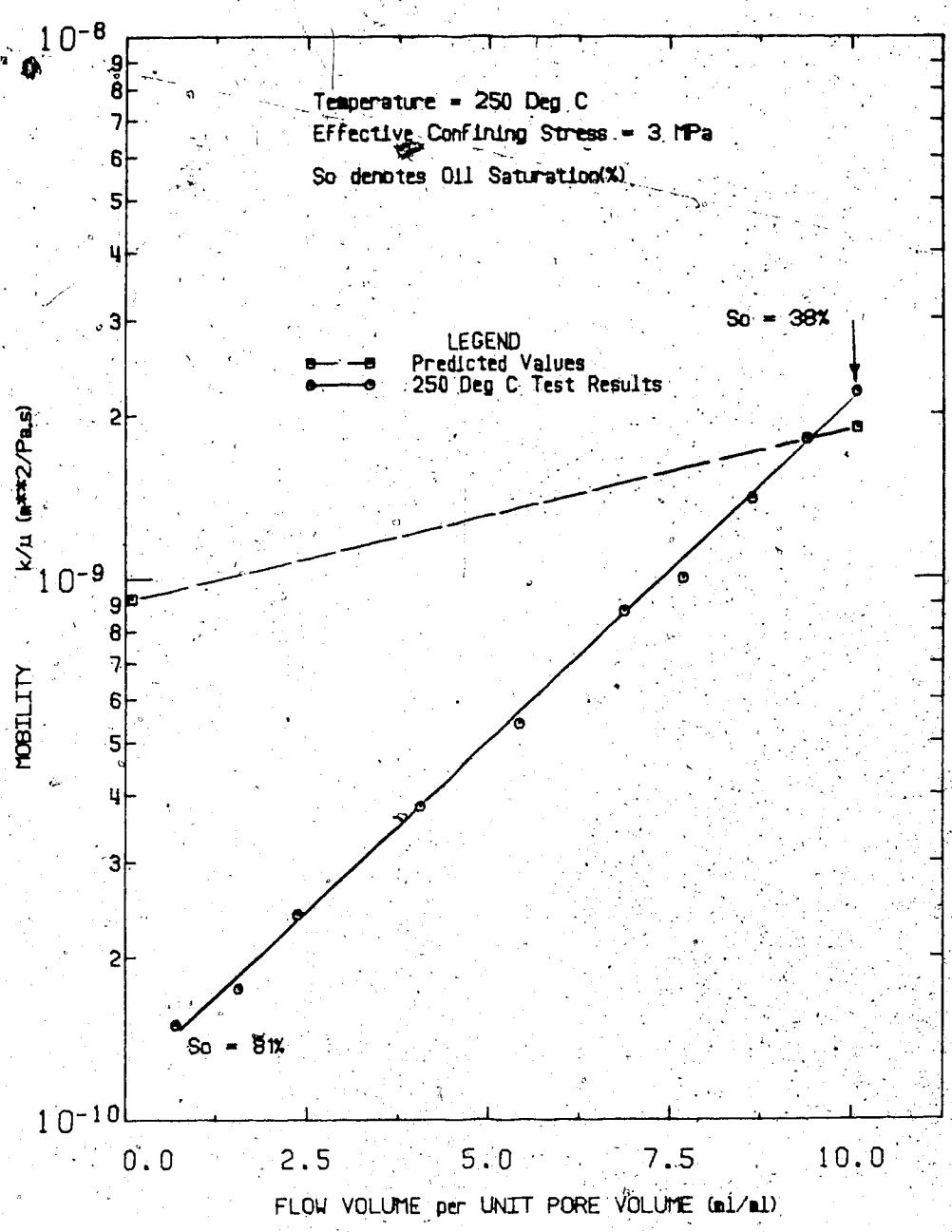

FIGURE D15 Fluid Mobility Vs. Normalized Flow Volume: Test CPERM6

TEST CPERM 7

Absolute Permeability of Saline Creek Oil Sand Sample No. 44 (at 20°C and 150°C) and over a Range of Effective Stress from 2 to 18 MPa

Procedural Details: Test CPERM 7

1. Sample No. 44 was mounted and allowed to thaw under 2 MPa effective confining stress.
2. Bitumen was extracted from the pore space of the sample by alternate soaking and flushing; 3600 ml of benzene was circulated through the sample over a 10 day period to completely remove all the bitumen. Residual benzene was removed by flushing with 200 ml of acetone and finally with 500 ml of water.
3. The sample was back saturated for 24 hours under 10 MPa back pressure and 12 MPa confining stress.
4. Absolute permeability was measured at room temperature by circulating water through the sample at flow rates up to 10 ml/minute and measuring the pressure drop across the sample. Absolute permeability was measured at effective confining stresses of 2, 3, 4, 6, 10, 14 and 18 MPa. Compressibility of the sample was also measured as the effective stress was varied.
5. The system and sample were heated slowly to 150°C. Drained thermal expansion and the volume of pore fluid expelled from the sample were monitored during heating.

6. Absolute permeability was measured at 150°C by circulating heated water at flow rates up to 9 ml/minute and measuring pressure drop across the sample. Permeability was measured at effective confining stresses of 2, 6, 10, 14, 18, 14, 10 and 2 MPa. Compressibility of the sample was also measured as the effective confining stress was varied.

TEST CPERM 7: SAMPLE DATA

Original Sample No. 44 at 20°C:

Height: H = 5.120 cm
Dia.: Ø = 7.600 cm
Area: A = 45.36 cm^2
Volume: V = 232.27 cm^3
Mass: M = 470 g

M_S = 390.4 g V_S = 147.3 ml

Initial Water Content: w = 3.0%
Initial Bitumen Content: B = 17.1%

Initial Bulk Density: = 2.024
Initial Dry Density: = 1.681

Initial Void Ratio: = 0.577
Initial Porosity: = 0.366

Bitumen extraction by alternate "Soak and Flush" Process; 3600 ml of benzene (i.e. 45 pore volume circulated over a period of 10 days).

After 150°C Permeability Test:

Height: H = 5.012 cm
Dia.: Ø = 7.600
Volume: V = 227.5 ml
Mass: M = 470.6 Density = 2.069

w = 22.5% B = 0.00%

Porosity: n = 0.353
Void Ratio: e = 0.544
So: = 0%

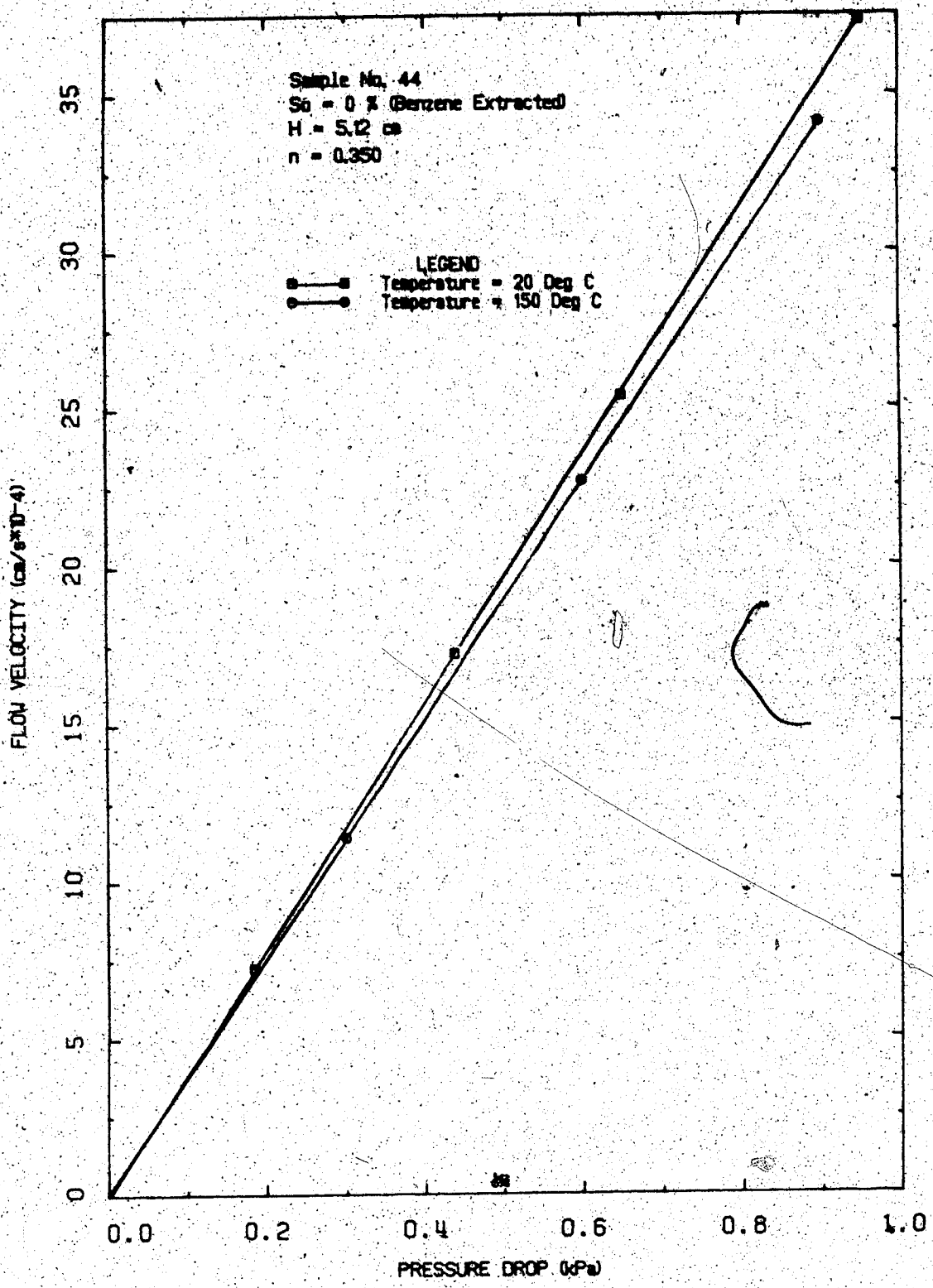

FIGURE D16 Flow Velocity Vs. Pressure Difference: Test CPERM7

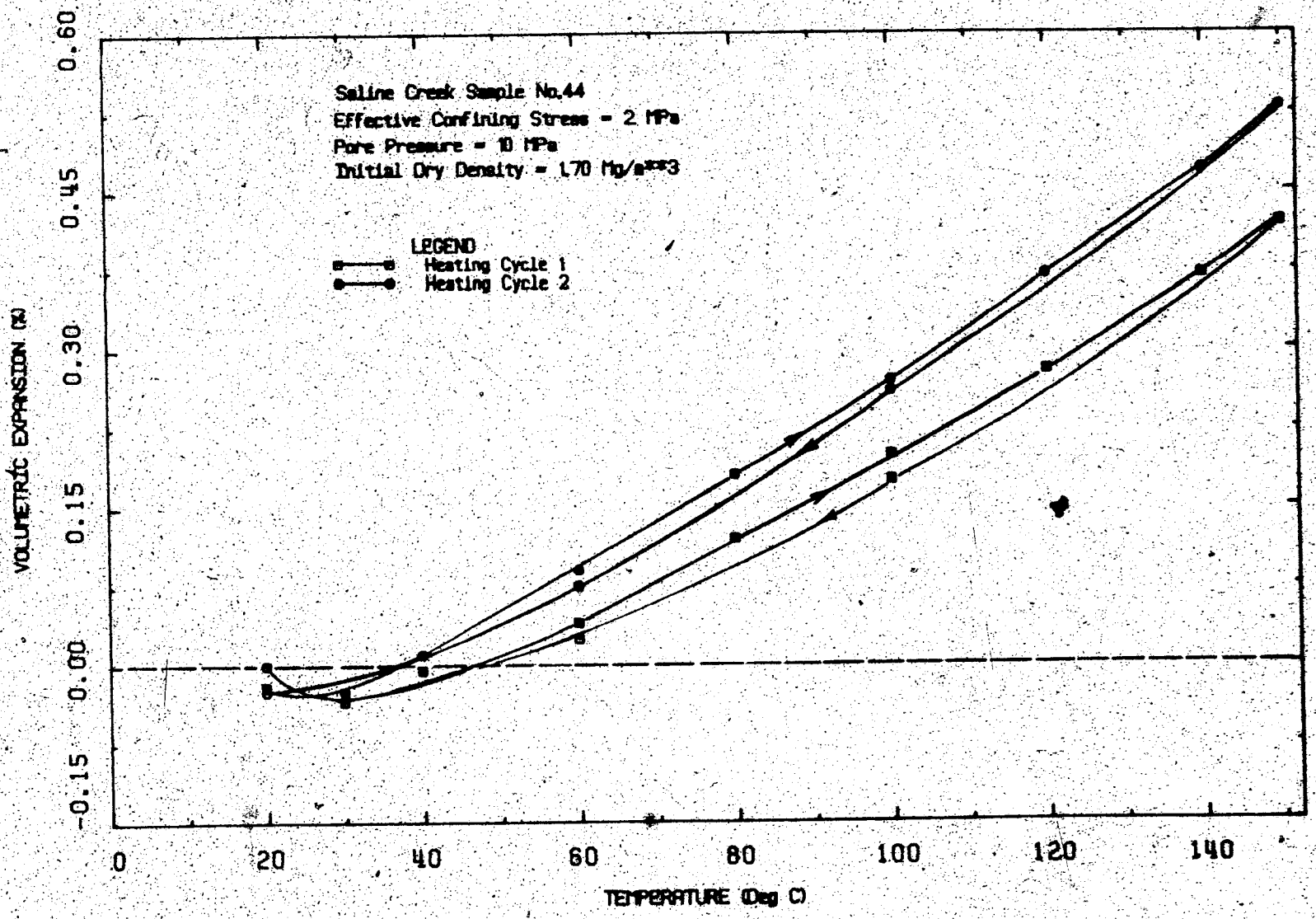

FIGURE D17 Drained Thermal Expansion: Test CPERM7

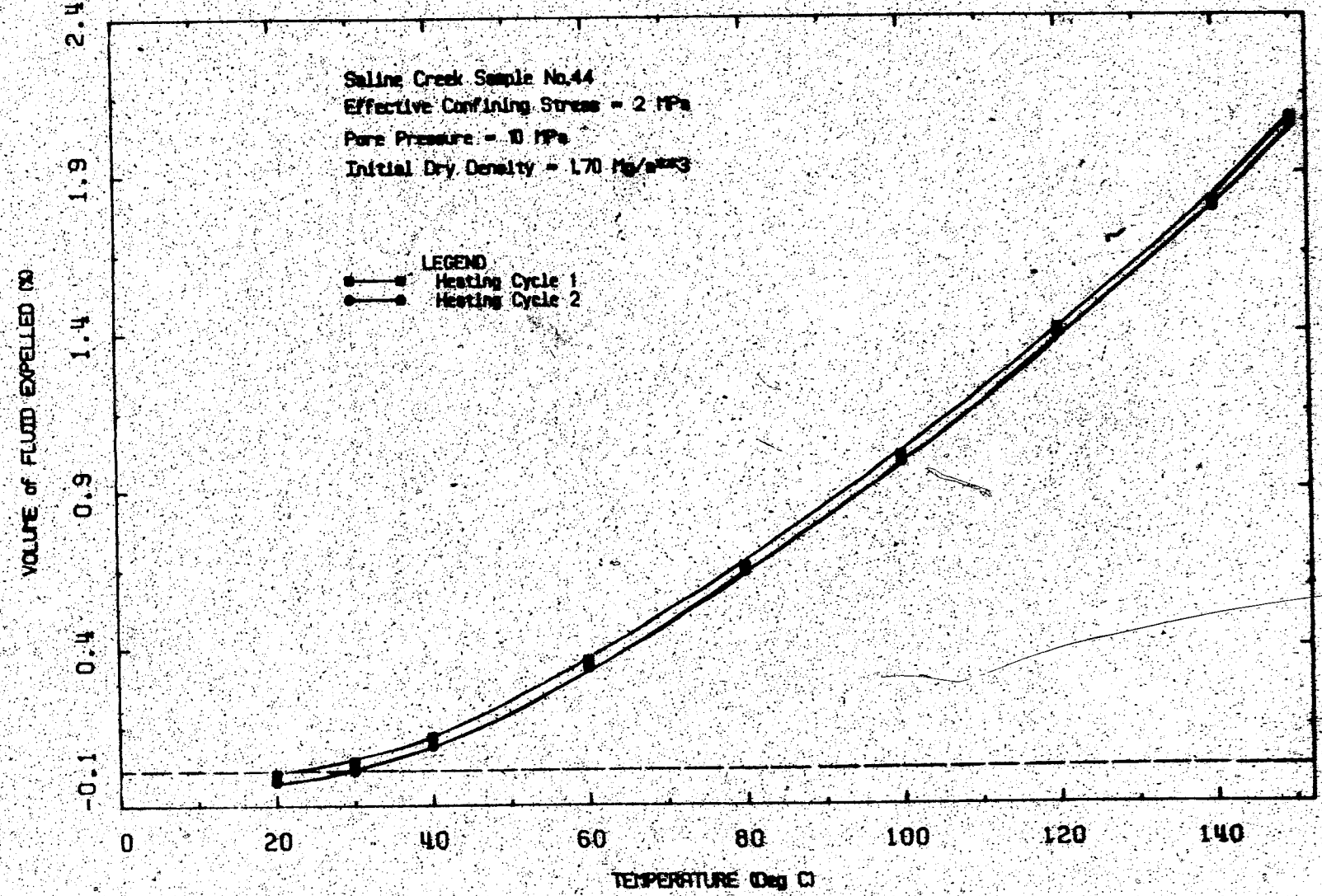

FIGURE D18 Volume of Fluid Drained During Heating: Test CPERM7

TEST CPERM 8

Permeability of Saline Creek Oil Sand
Sample No. 16 at 20°C and 150°C

Procedural Details: Test CPERM 8

1. Sample No. 16 was allowed to thaw and then back saturated for 24 hours under 10 MPa back pressure and 13 MPa confining stress.
2. A room temperature permeability test was performed at flow rates varying up to 4 ml/minute. Effective confining stress was maintained constant at 3 MPa.
3. The system and sample were then heated slowly to 150°C. Drained thermal expansion of the sample was monitored during heating.
4. A permeability test was performed at 150°C by circulating heated water through the sample. Bitumen was flushed from the sample reducing the bitumen saturation from 65% to 52%.
5. The sample was then cooled down to room temperature and a room temperature permeability test was performed at the residual bitumen saturation of 52 percent.

TEST CPERM 8: SAMPLE DATA

Original Sample No. 16:

Dia.: $\emptyset$ = 7.600 cm
c/s Area: A = 45.36 cm^2
Height: H = 5.121 cm
Volume: V = 232.31 cm^3
Mass: M = 478 g Density: = 2.058

w = 2.2% B = 16.7%

M_S = 402
V_S = 151.71 cm^3
V_V = V - V_S = 80.60 cm^3
= 0.347
S_W = 11.6% So = 88.4%

After 150°C Permeability Test

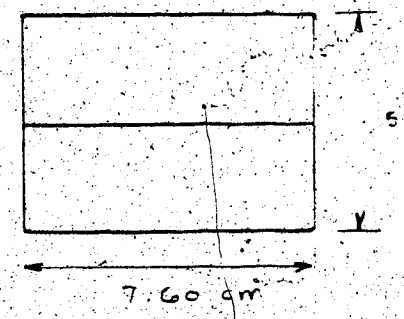

Top: w = 9.43%
B = 8.70%
So = 49.0%
S_W = 51.0%

Bottom: w = 8.70%
B = 10.21%
So = 55.0%
S_W = 46.0%

Average Fluid Saturations for Sample: So = 52.0%
S_W = 48.0%

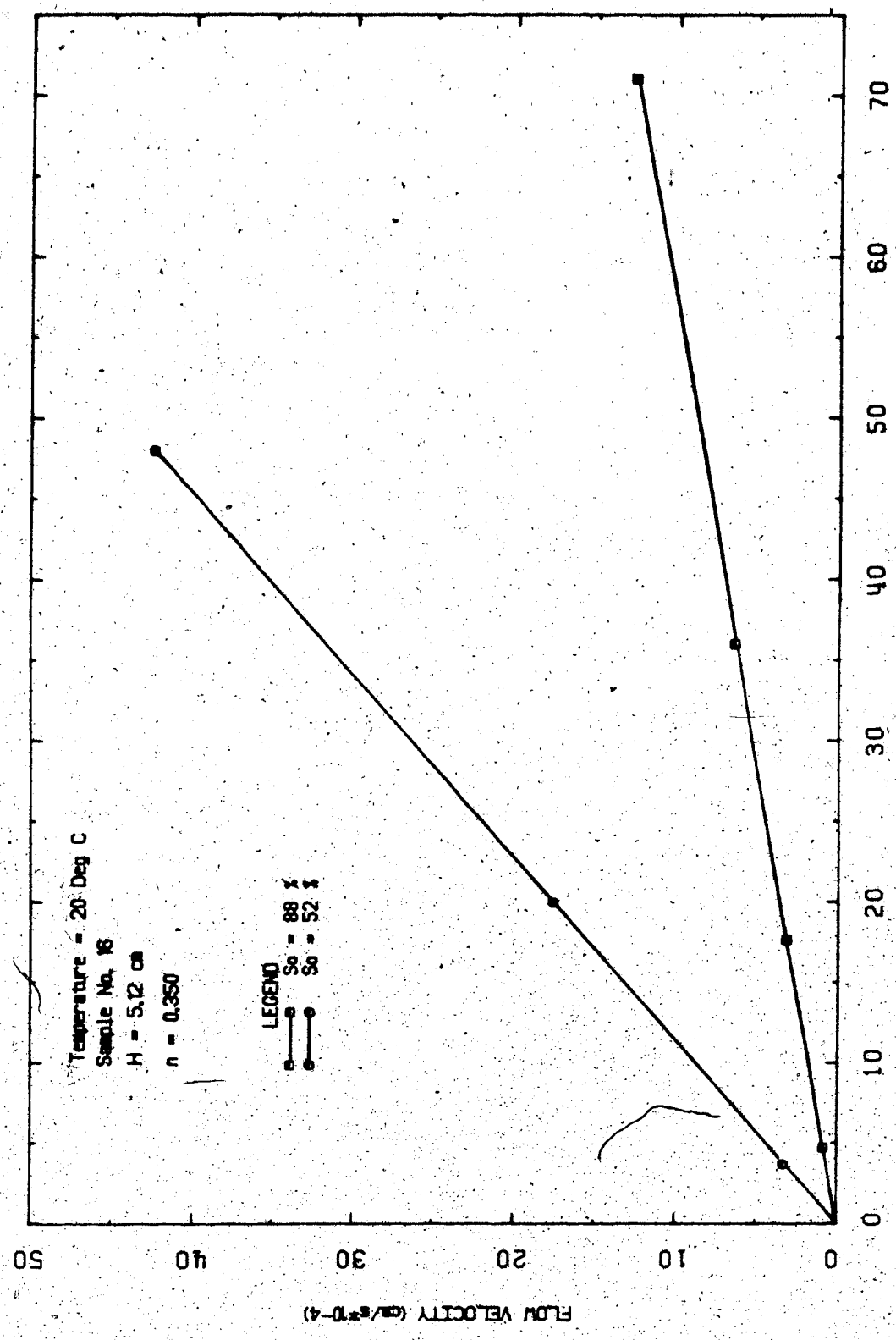

FIGURE D19 Flow Velocity Vs. Pressure Difference: Test CPI RMA

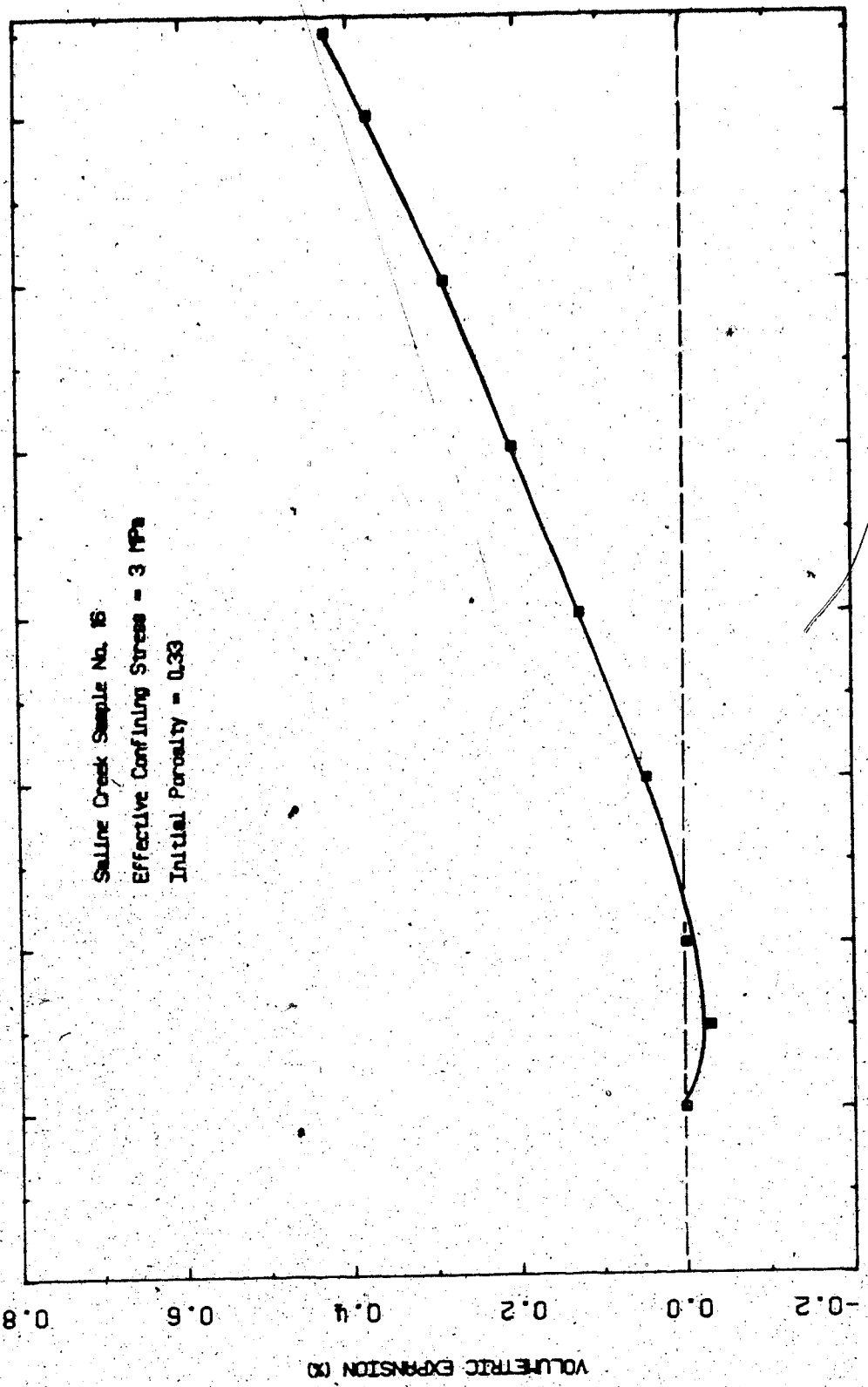

FIGURE D20 Drained Thermal Expansion: Test CPERM6

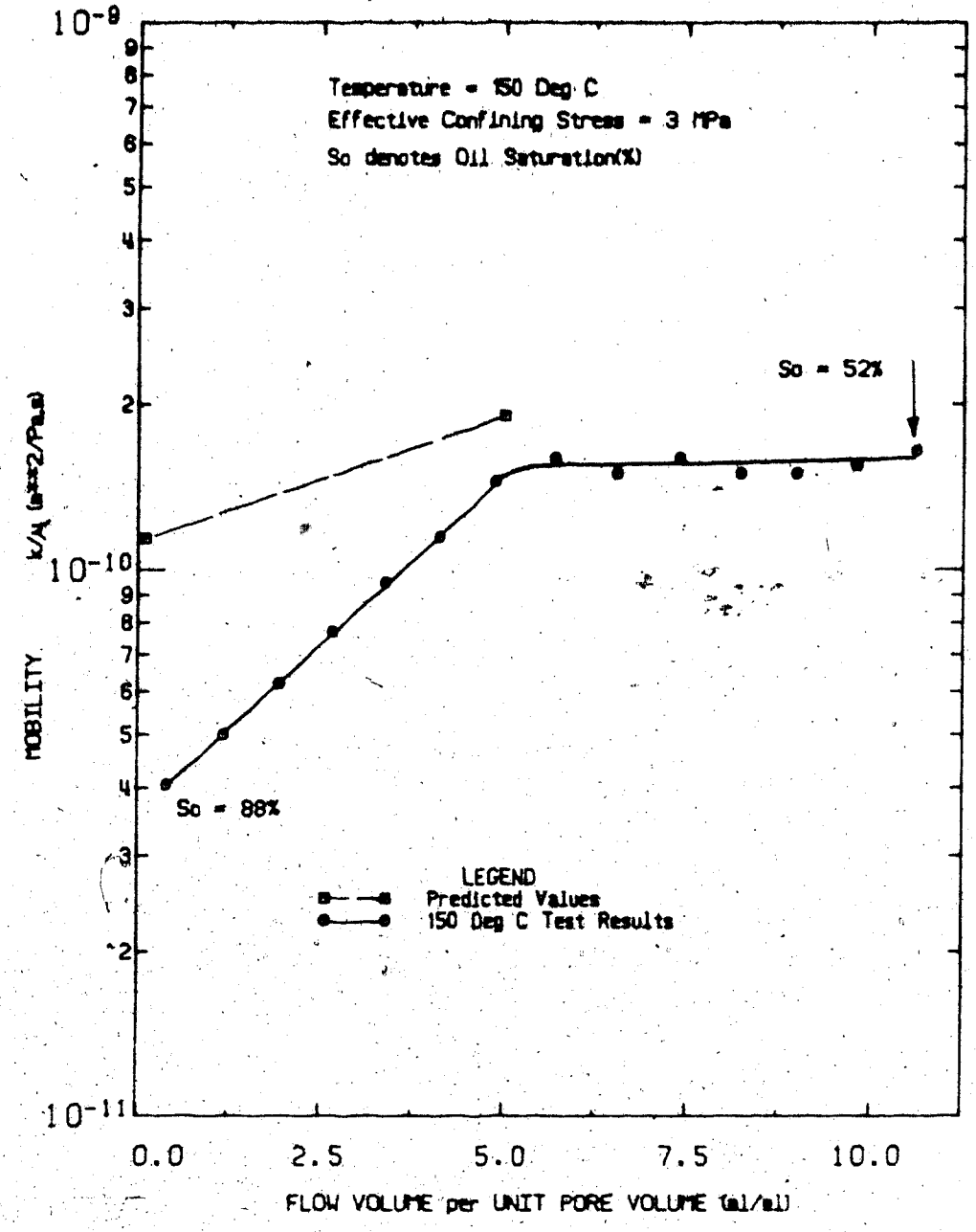

FIGURE D21 Fluid Mobility Vs. Normalized Flow Volume: Test CPERM8

TEST CPERM 9

Permeability of Remoulded Saline Creek Sample No. 36B at 20°C and 150°C

Procedural Details: Test CPERM 9

1. Saline Creek oil sample No. 36B was thawed, then remoulded by kneading. The sample was compacted in 5 layers in the consolidometer cell using a modified Proctor drop hammer. Compactive effort consisted of at least 30 hammer blows per layer.
2. The sample was further compacted by quick loading it under an effective confining stress of 10 MPa.
3. The sample was then back saturated for 24 hours with an applied back pressure of 10 MPa and a confining stress of 13 MPa.
4. Room temperature effective permeability to water was measured by circulating water through the sample at varying flow rates up to 4 ml/minute and measuring differential pressure difference across the sample and flow rate.
5. The apparatus and sample were slowly heated to 150°C under 10 MPa back pressure and 13 MPa confining stress. Drained thermal expansion was monitored during heating.
6. A permeability test was performed at 150°C by circulating heated water through the sample. Bitumen was flushed from the sample reducing the bitumen saturation from 80% to a residual value of 52% of the sample pore volume. Pressure drop and flow rate were monitored during the test.

7. The apparatus and sample were cooled down to room temperature. Room temperature water permeability was measured at a residual oil saturation of 0%.

TEST CPERM 9: SAMPLE DATA

Original Remoulded and Recompacted Sample No. 36B:

Dia.: Ø = 7.600 cm
c/s Area: A = 45.36 cm^2
Height: H = 5.22 cm
Volume: V = 236.8 ml
Mass: M = 478 g Density: = 2.019

w = 4.9%
B = 18.5%
M_S = 367.5 g
V_S = 146.2 ml
V_V = V - V_S = 90.6 ml
n = 0.383
S_W = 20.9%
So = 79.1%

After 150°C Permeability Test

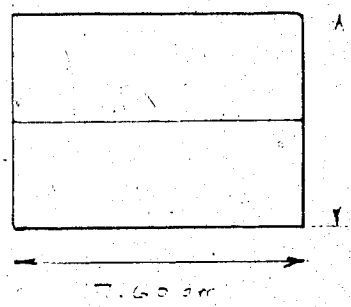

Top: w = 11.9%
B = 12.0%
So = 51.1%
S_W = 48.9%

Bottom: w = 11.5%
B = 12.3%
So = 52.7%
S_W = 47.3%

Average Fluid Saturations For Sample: So = 51.9%
S_W = 48.1%

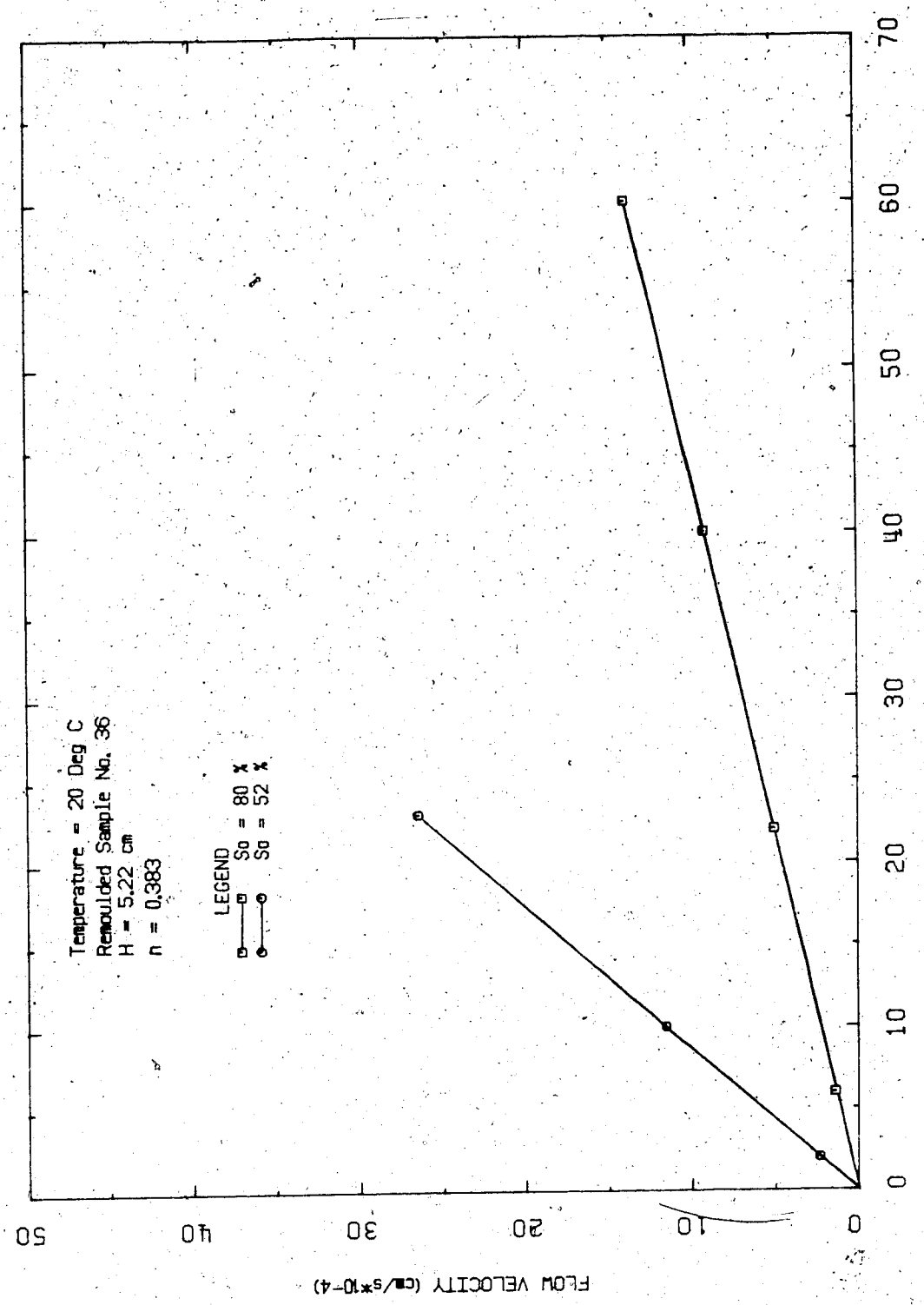

FIGURE D22 Flow Velocity Vs. Pressure Difference: Test CPFRM9

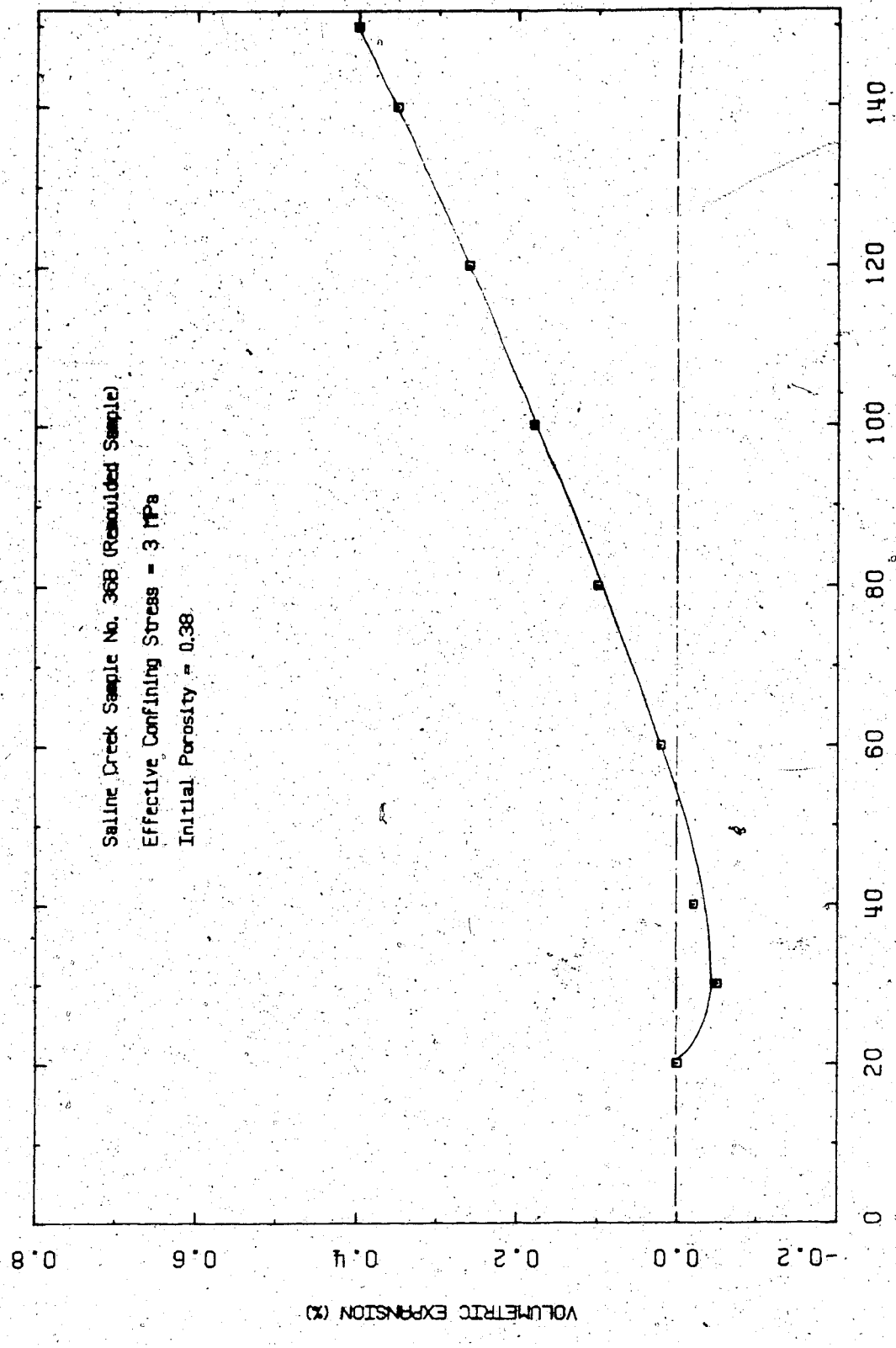

FIGURE D23 Drained Thermal Expansion: Test CPERM9

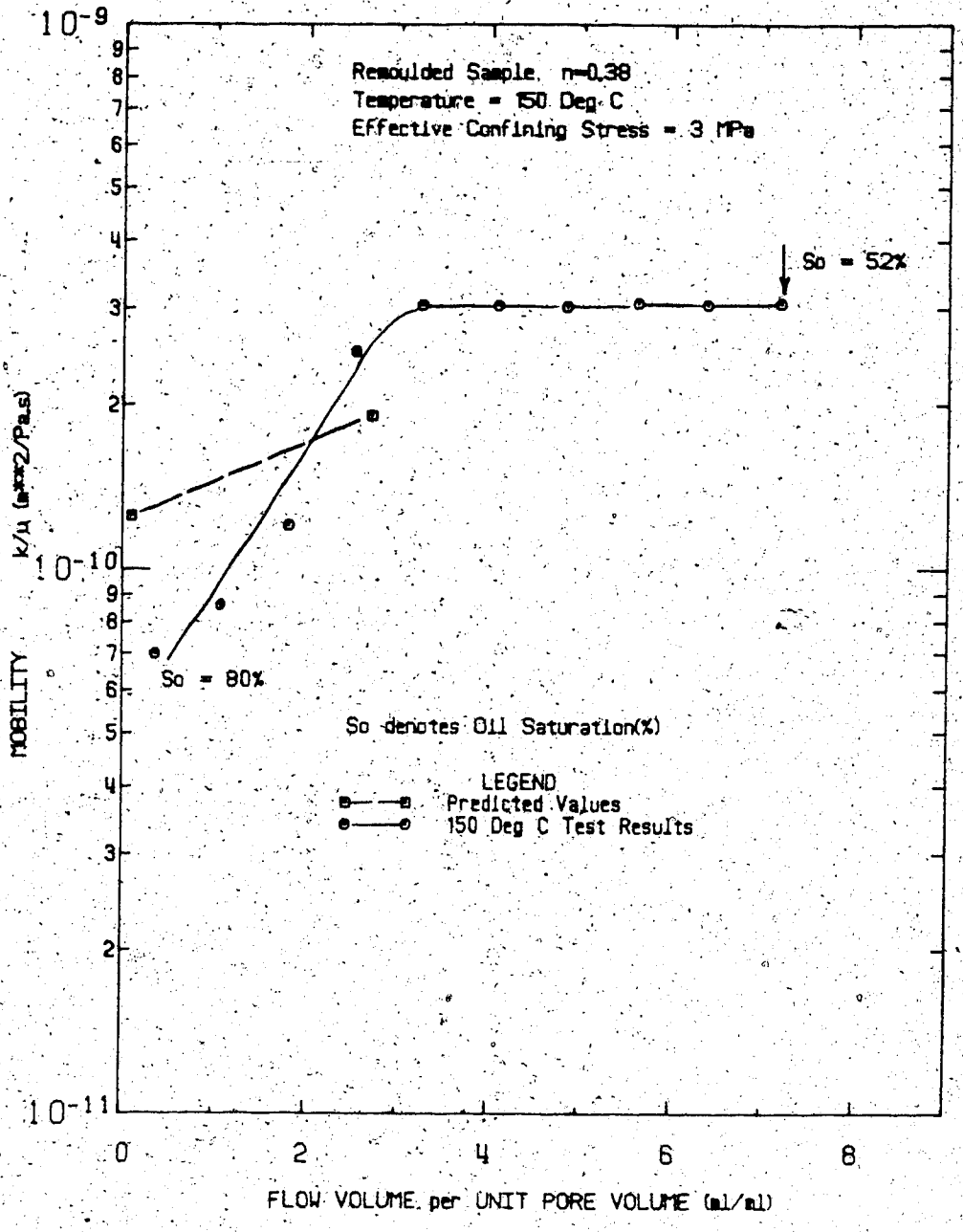

FIGURE D24 Fluid Mobility Vs. Normalized Flow Volume: Test CPERM9

APPENDIX E

TRIAXIAL TESTS

TABLE E-1

Summary of Triaxial Tests

Test No.	Temperature (°C)	Effective Confining Stress (MPa)	Test Description
TOS 1	20	4 - 26	Isotropic Compression
TOS 2	20	4	Passive Compression
TOS 3	20	4 - 0.87	J1 ≅ Constant
TOS 4	20	8	Passive Compression
TOS 5	20	8	Passive Compression
TOS 6	125	4 - 0.6	J1 ≅ Constant
TOS 7	125	4	Passive Compression
TOS 8	220	12 - 20	Isotropic Compression
TOS 9	240	4 - 0	Membrane Meltdown
TOS 10	200	4 4 - 0.25	Undrained Heating with Constant and Undrained Passive Compression
TOS 11	100	4 - 0.25	Amistropic Consolidation and Undrained Heating to Failure
TOS 12	200	4 - 17 4	Isotropic Compression and Passive Compression
TOS 13	240	4	Membrane Meltdown
TOS 14	20	2, 4, 8	Multistage Passive Compression of Remoulded Oil Sand
TOS 15	200	4 - 17 4	Isotropic Compression and Passive Compression of Cold Lake Oil Sand
TOS 16	200	4	Membrane Meltdown
TOS 17	200	8	Passive Compression
TOS 18	200	4 - 0.6	J1 ≅ Constant
TOS 19	125	4 - 17 4	Isotropic Compresson and Passive Compression
TOS 20	20	0	Unconfined Compression of Case Hardened Sample

TEST TOS 1

Isotropic Compression of Saline Creek Oil Sand Sample No. 25 at 20°C: Drained and Undrained Isotropic Compressibility

Procedural Details: Test TOS 1

1. Saline Creek sample No. 25 was thawed, then back saturated for 24 hours at an applied back pressure of 2 MPa and isotropic confining stress of 6 MPa.
2. Back pressure drainage valves were closed and a B-test was performed to check the degree of saturation of the sample. Volumetric strains determined from internal strain gauge measurements were used to determine isotropic compressibility over a range of confining stress from 6 - 26 MPa.
3. Back pressure drainage valves were opened and a drained isotropic compression test was performed. Four cycles of compression and unloading were applied over a range of isotropic effective stress from 4 - 26 MPa. Volumetric strain determined from internal strain gauge device measurements (i.e. vertical and lateral deformations) was compared with volumetric strain determined using the volume change device. Volumetric strains varied by approximately $\pm$ 1.6 x 10^{-4} per MPa; internal strain measurements being rather more erratic. It was found that this rather substantial error resulted from inaccurate lateral (horizontal) deformation measurements.

The stiff lateral strain gauge clamp was found to distort lateral deformation of cohesionless oil sand samples.

4. A drained triaxial compression test was performed. The lateral strain guage clamp, however, impeded lateral deformation and caused tensile stresses to develop in the orthogonal plane as vertical deformation proceeded. The sample was weakened and yielded prematurely.
Effective lateral confining stress was maintained constant at 4 MPa and back pressure was maintained constant at 2 MPa during laoding. Vertical effective stress was increased to a constant rate of 80 kPa/minute.

TEST TOS 1: SAMPLE DATA

Pretest Saline Creek Sample No. 25:

Dia.:	Ø	=	7.604 cm	w	=	0.30
Height:	H	=	15.316	B	=	0.152
Area:	A	=	45.412 cm^2			
Volume:	V	=	695.54	V_S	=	463.5 ml
Mass:	M	=	1452 g	V_V	=	232.0 ml
M_S:		=	1228 g	Dry Density	=	1.766 Mg/m^3

Density: = 2.088 Mg/m^3
Porosity: = 0.333
Void Ratio: = 0.49914 g

Failed Sample No. 25 After Test TOS 1

Diameter in plane parallel to lateral strain gauge clamp:

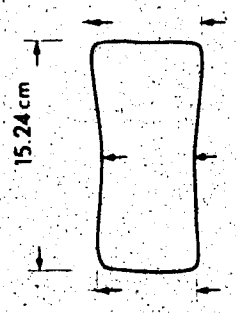

Top = 7.70cm

Middle=7.58cm

Bottom=7.59cm

Diameter in plane perpendicular to lateral strain gauge clamp:

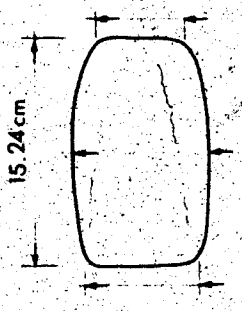

Top = 7.77cm

Middle = 8.16cm

Bottom = 7.82cm

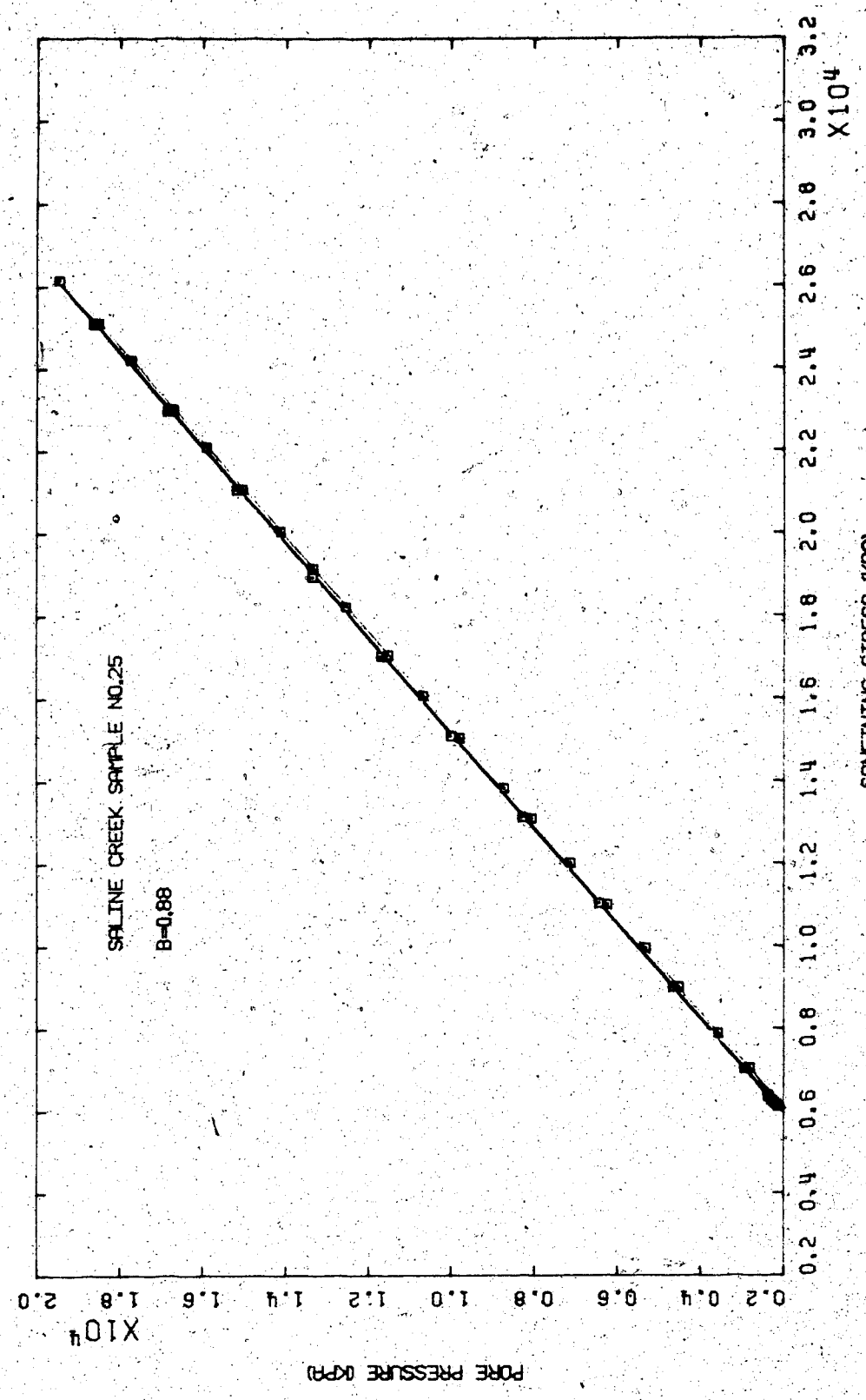

FIGURE E1.1 Triaxial Test TOS1: B Test

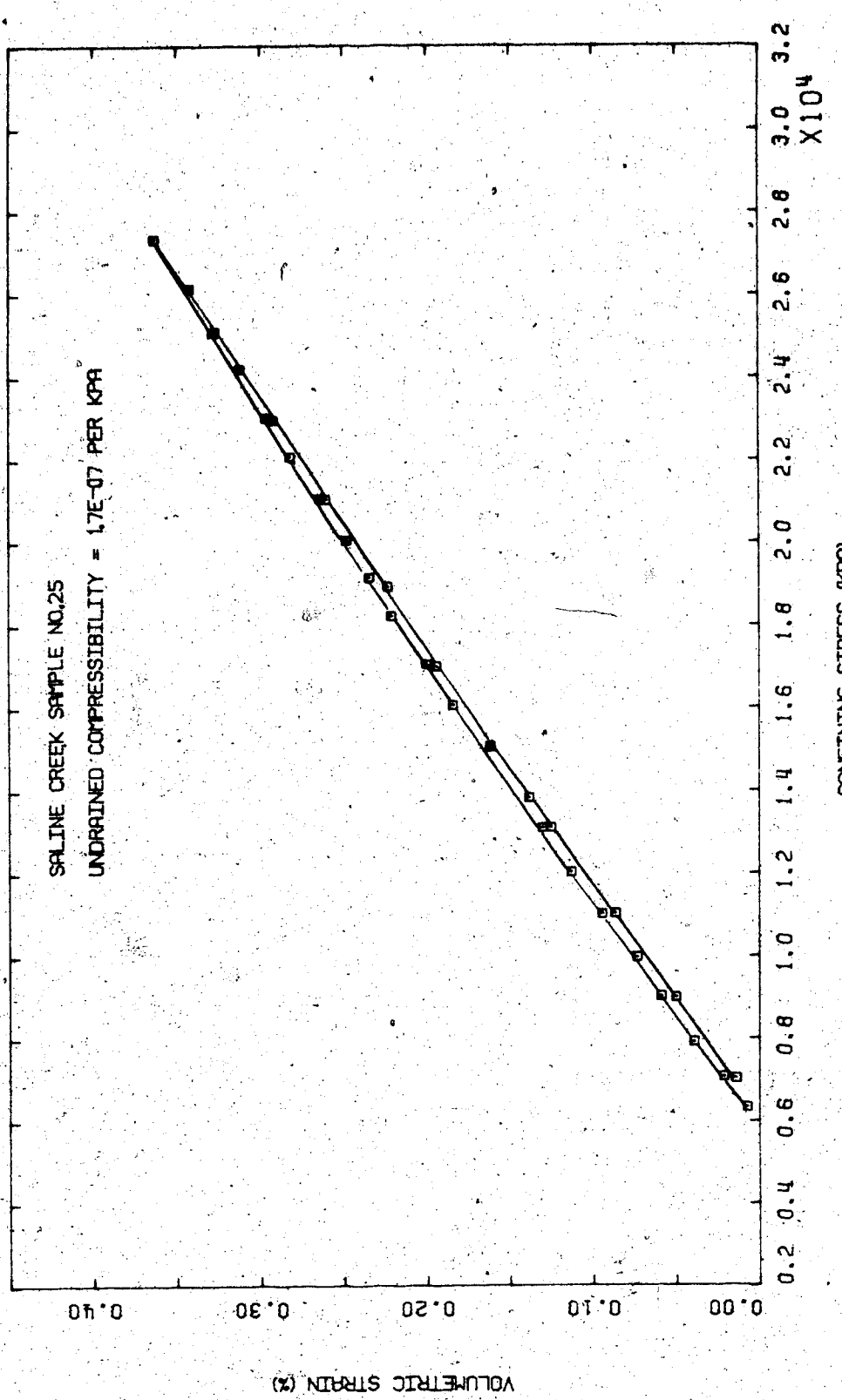

FIGURE F1.2 Triaxial Test T051: Undrained Compressibility

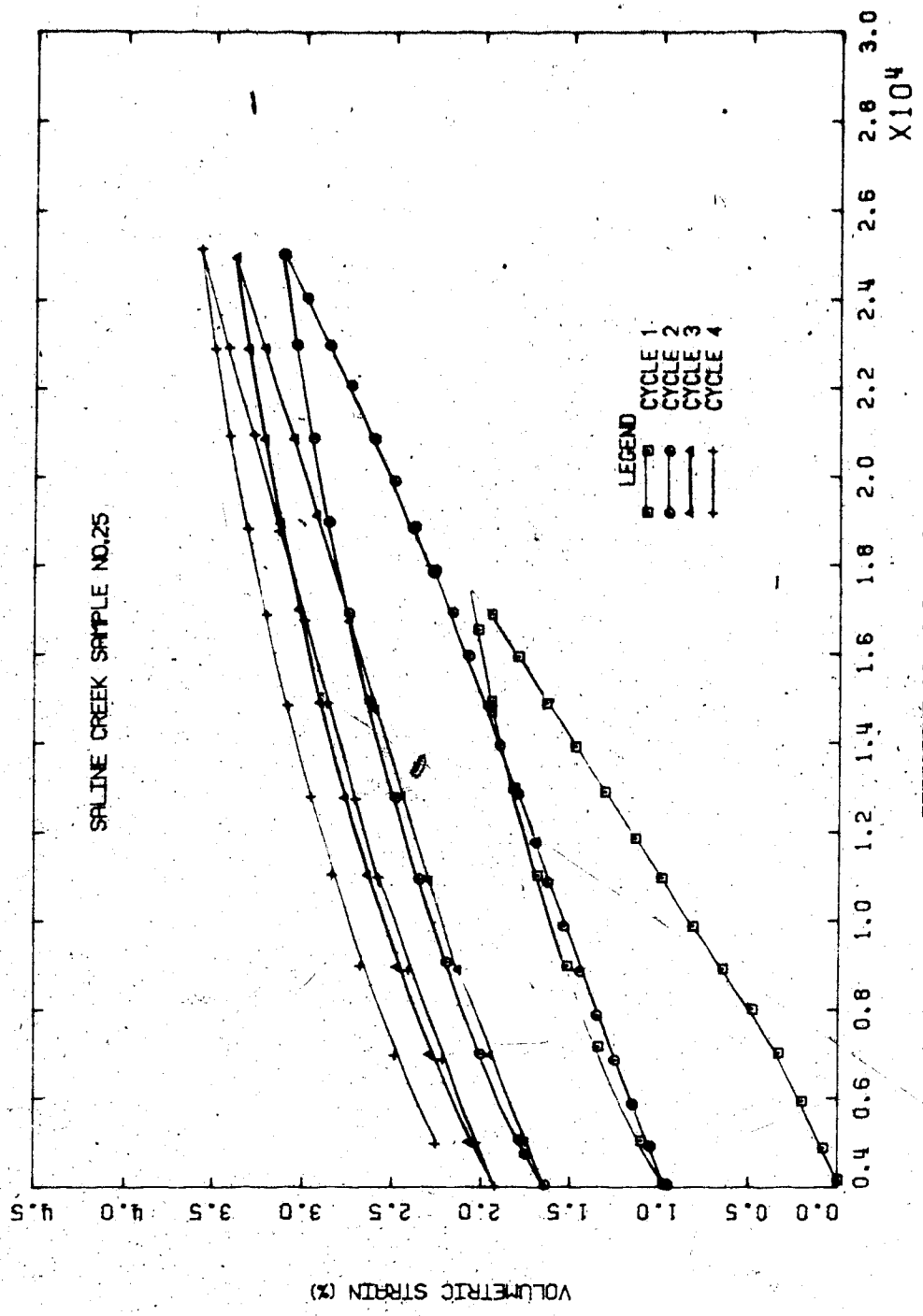

FIGURE E1.3 Triaxial Test TOS1: Drained Isotropic Compressibility

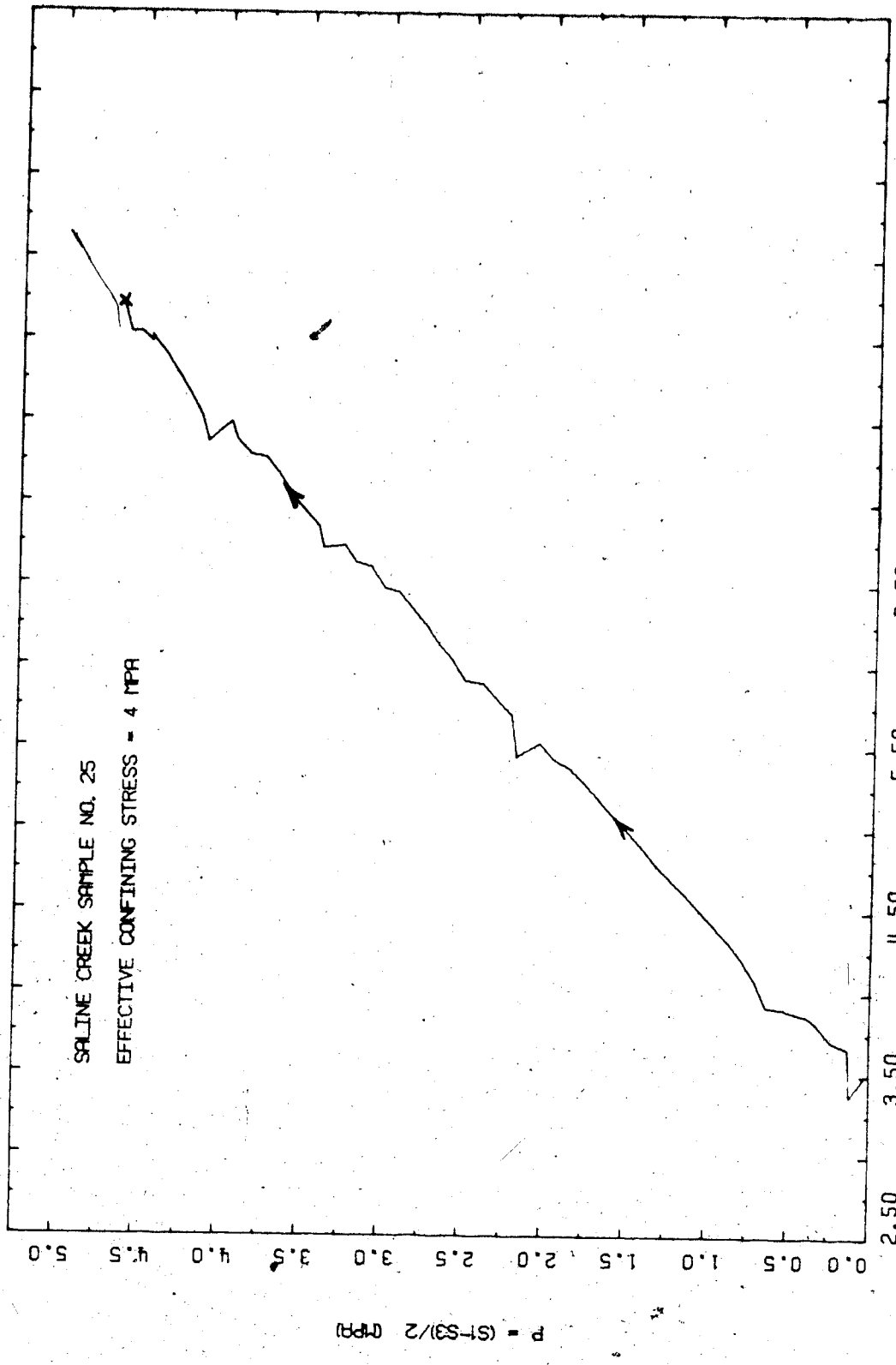

FIGURE E1.4 Triaxial Test TOS1: Stress Path

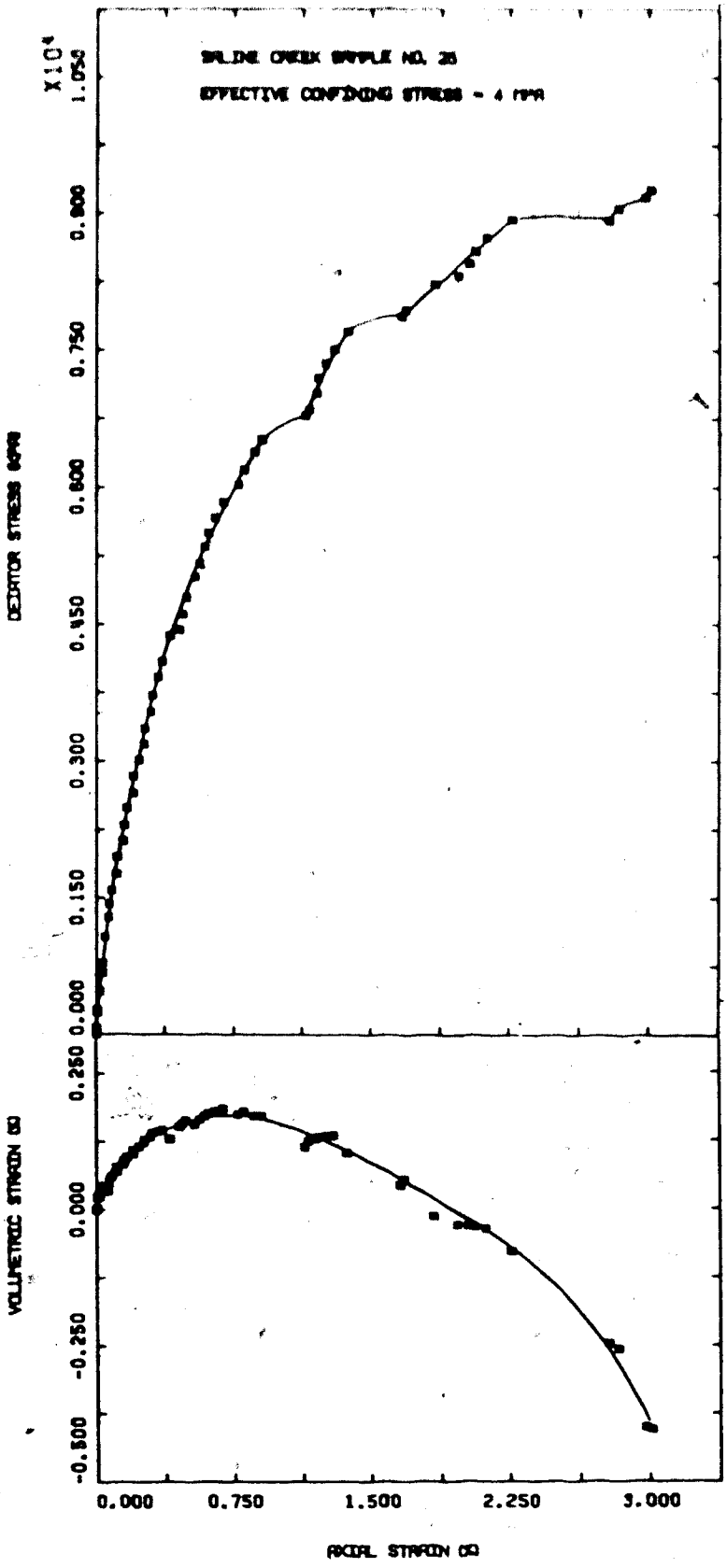

FIGURE E1.5 Triaxial Test TOS1: Deviator Stress Vs. Strain

TEST TOS 2

Drained Triaxial Compression of Saline Creek Sample No. 33 at 4 MPa Effective Confining Stress and at 20°C

Procedural Details: Test TOS 2

1. Sample No. 33 was thawed and back saturated for 24 hours under 2 MPa back pressure and 6 MPa isotropic confining stress.
2. A B-test was performed to ensure that gases in the system had dissolved in the liquid phase (i.e. complete saturation).
3. A drained triaxial compression test was performed at room temperature (20°C) maintaining the effective lateral confining stress constant at 4 MPa and the back pressure constant at 2 MPa while vertical effective stress was increased at a near constant rate of 80 kPa per minute. Vertical (axial) and volumetric deformations were monitored during loading.

TEST TOS 2: SAMPLE DATA

Pretest Saline Creek Sample No. 33:

Dia.:	Ø	=	7.600 cm	w	= 0.025
Height:	H	=	15.240 cm	B	= 0.163
Area:	A	=	45.365 cm^2		
Volume:	V	=	691.36 ml	V_S	= 456.2 ml
Mass:	M	=	1436 g	V_V	= 235.16 ml
M_S:		=	1209 g	Dry Density	= 1.748 Mg/m^3

Density: = 2.077 Mg/m^3
Porosity: = 0.340
Void Ratio: = 0.515 g

Failed Sample No. 33 After Test TOS 2

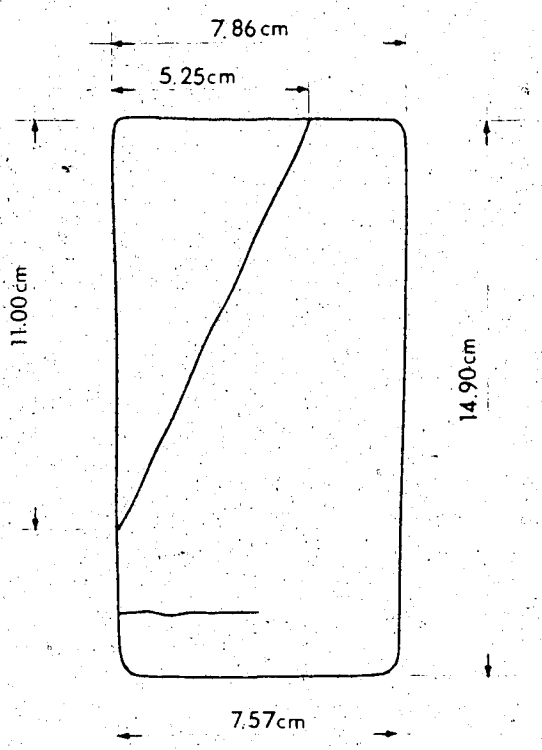

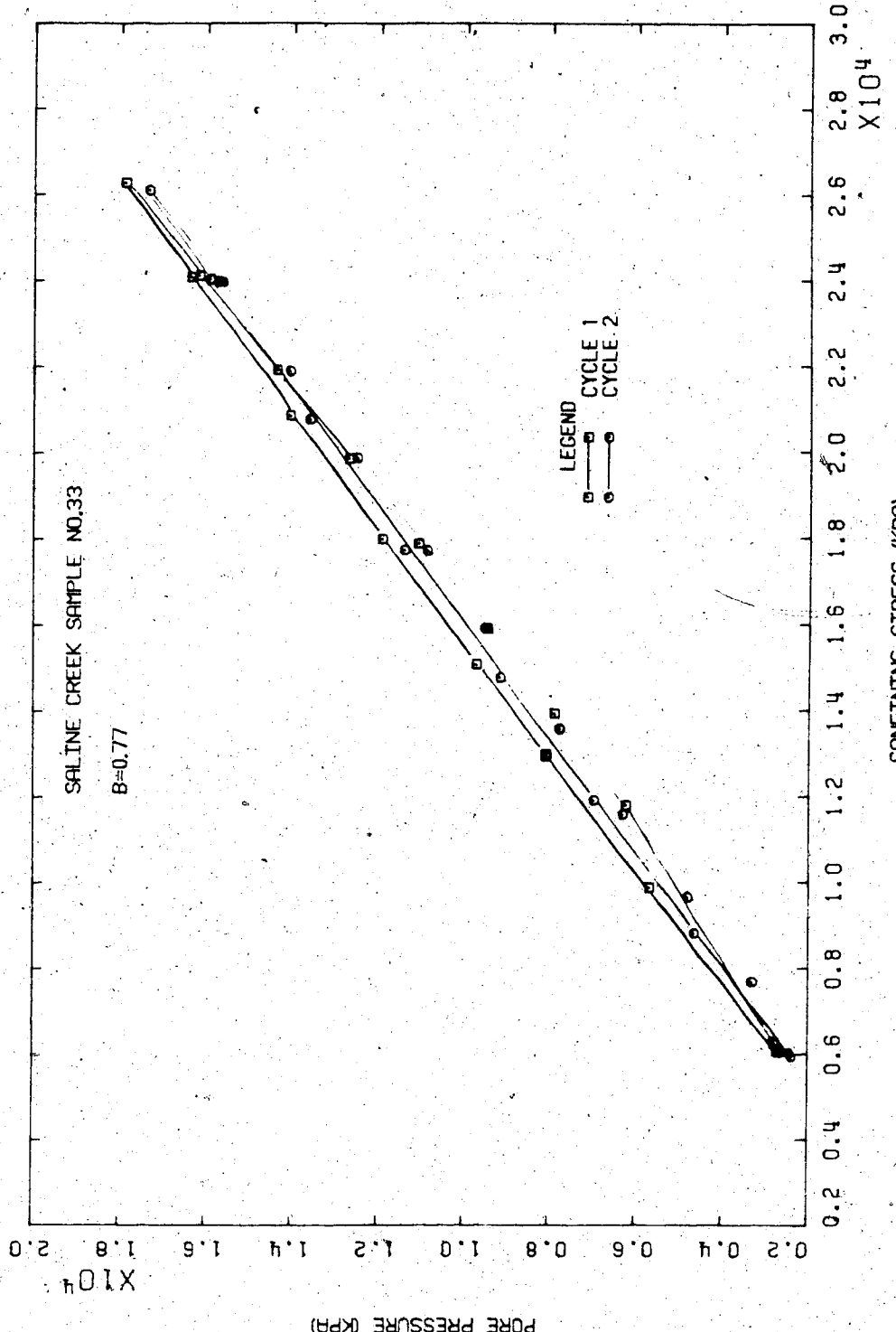

FIGURE 12.1 Triaxial Test TOS2: B Test

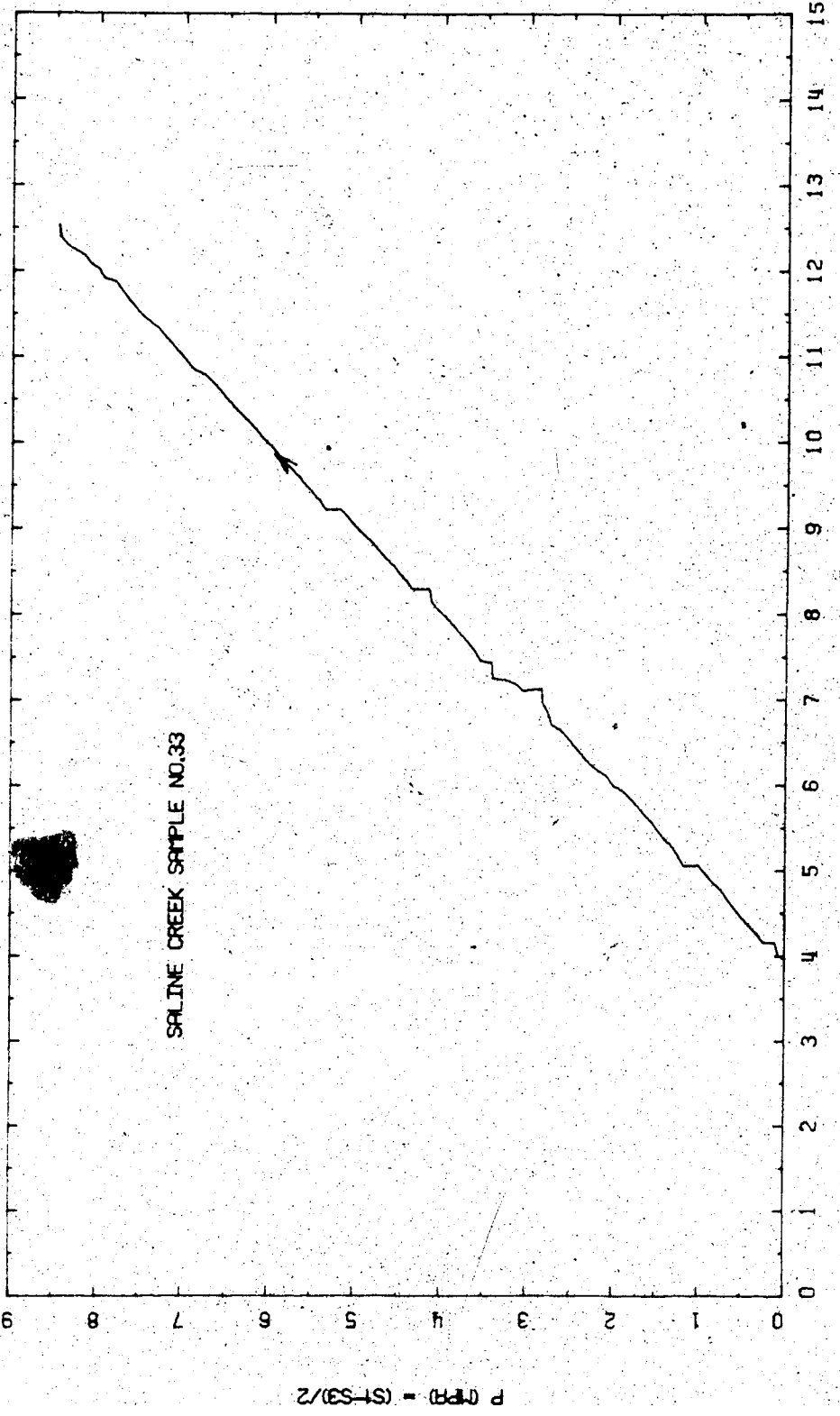

FIGURE E2.2 Triaxial Test TOS2: Stress Path

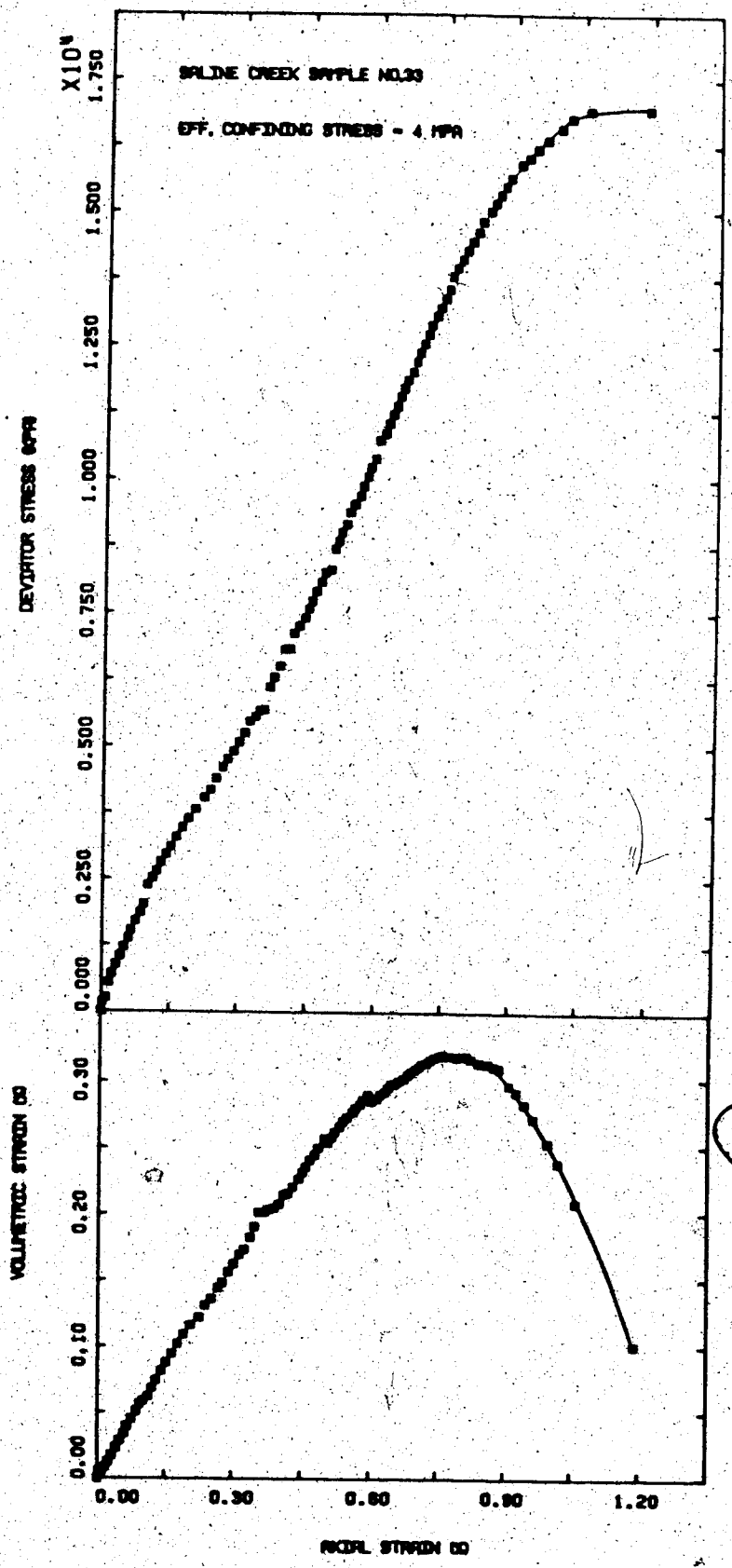

FIGURE E2.3 Triaxial Test TOS2: Deviator Stress Vs. Strain

TEST TOS 3

Drained Triaxial Compression of Saline Creek Sample No. 43
at 20°C Following Stress Path "F" (J1 Constant)

Procedural Details: Test TOS 3

1. Saline Creek sample No. 43 was thawed and back saturated for 24 hours under 2 MPa back pressure and 6 MPa isotropic confining stress.
2. A B-test was performed over a range of confining stresses from 6 - 27 MPa to evaluate the degree of saturation of the pore fluid phase.
3. A drained triaxial compression test was performed following stress path "F", i.e. close to a J1 constant path:
   a) Vertical stress was maintained constant at 6 MPa throughout the test.
   b) Lateral confining stress was decreased in 250 kPa increments fom 6 MPa to 1 MPa. Back pressure was decreased simultaneously in 50 - 75 kPa increments from 2 MPa to 870 kPa.
   c) Vertical (axial) deformation and volume change were monitored during loading.

TEST TOS 3: SAMPLE DATA

Pretest Saline Creek Sample No. 43:

Dia.:	Ø	=	7.600 cm		w	=	0.030
Height:	H	=	15.408 cm		B	=	0.180
Area:	A	=	45.365 cm^2				
Volume:	V	=	698.98 ml		V_S	=	453.86 ml
Mass:	M	=	1455 g		V_V	=	245.12 ml
M_S:		=	1203 g	Dry Density	=		1.721 Mg/m^3

Density: = 2.082 Mg/m^3
Porosity: = 0.351
Void Ratio: = 0.541 g

Failed Sample No. 43 After Test TOS 3

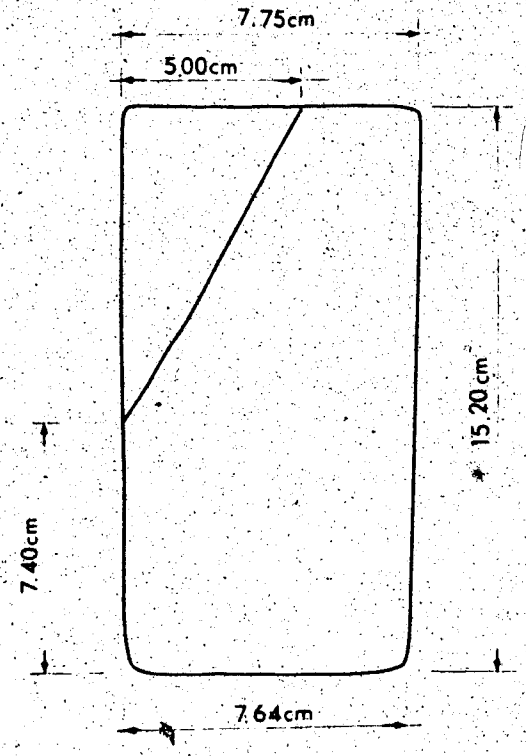

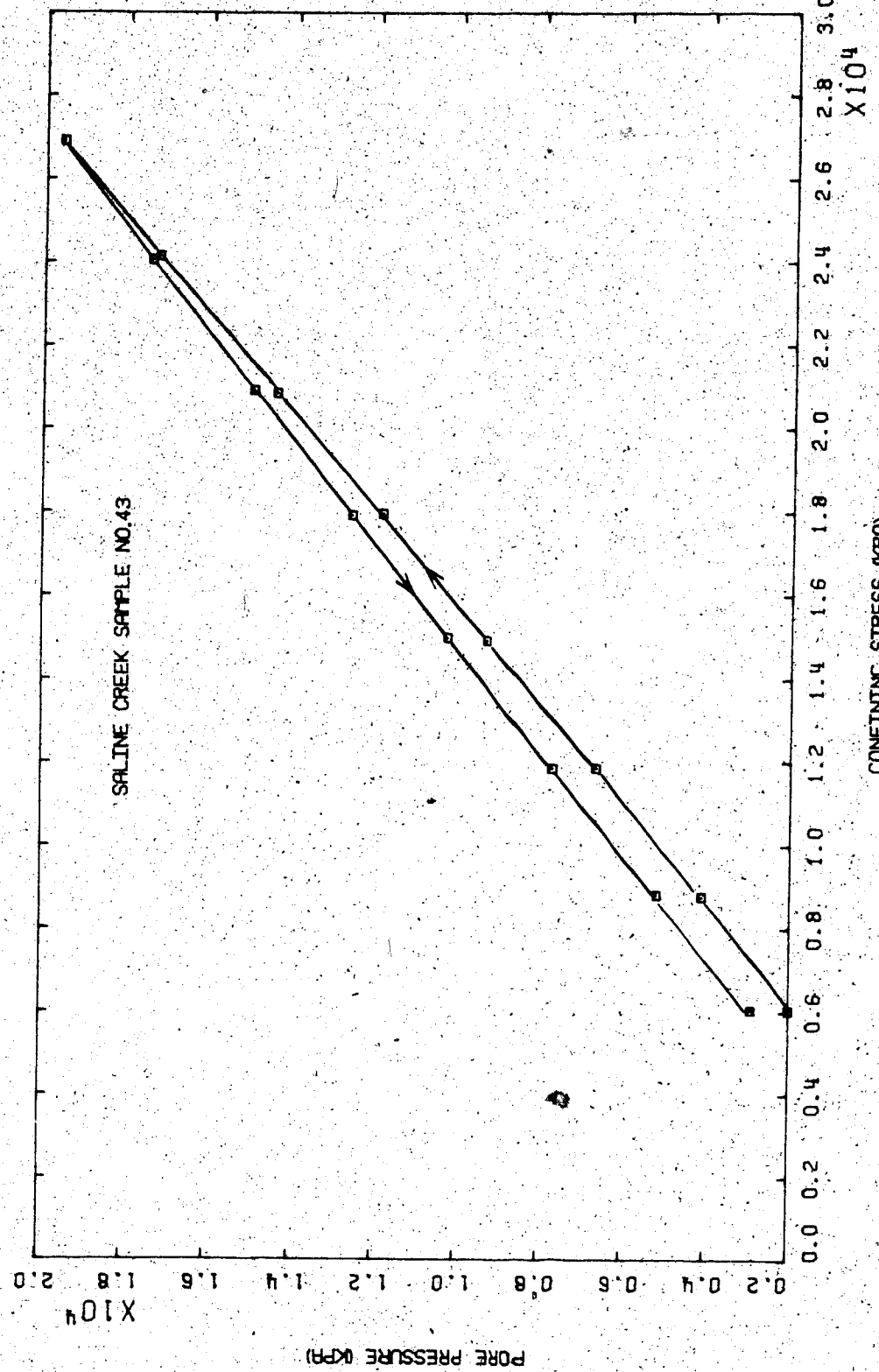

FIGURE E3.1 Triaxial Test TOS3: B Test

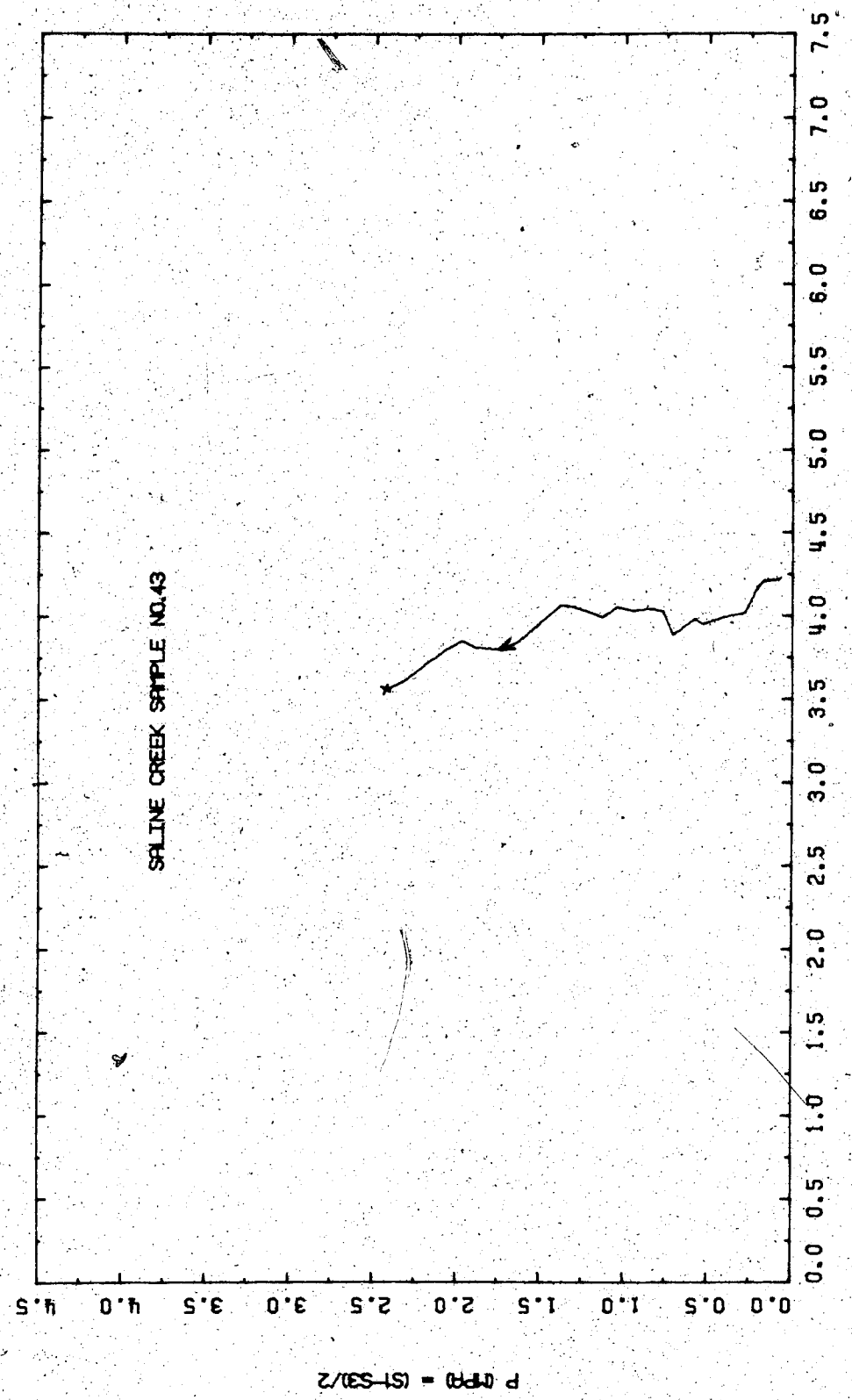

FIGURE E3.2 Triaxial Test TOS3: Stress Path

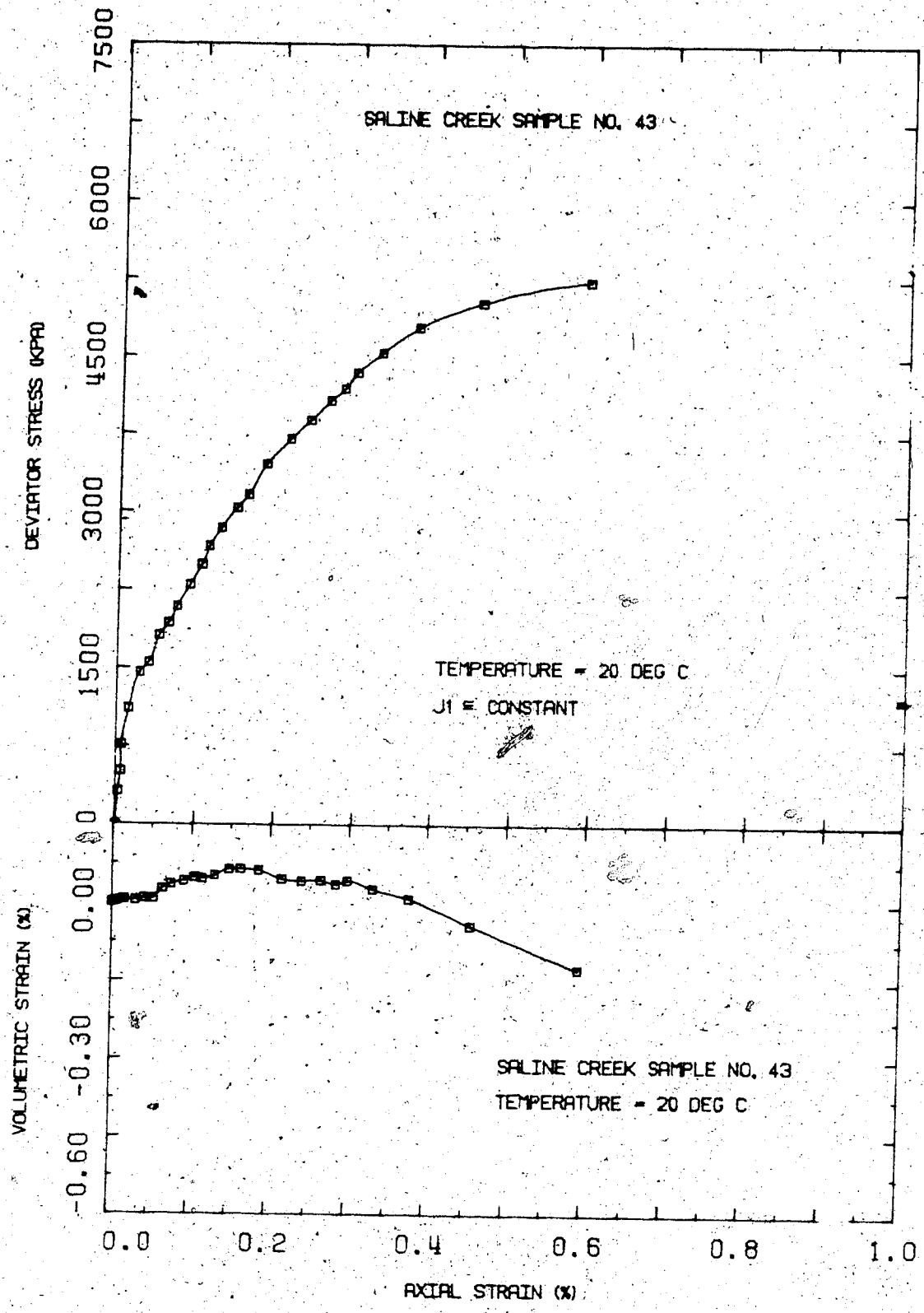

FIGURE E3.3 Triaxial Test TOS3: Deviator Stress Vs. Strain

TEST TOS 4

Drained Triaxial Compression of Saline Creek Sample No. 44
at 20°C and 8 MPa Effective Confining Stress

Procedural Details: Test TOS 4

1. Sample 44 was thawed and back saturated for 24 hours under 2 MPa back pressure and 6 MPa isotropic confining stress.
2. A B-Test was performed to evaluate degree of saturation.
3. Isotropic confining stress was increased to 10 MPa and the sample was allowed to consolidate.
4. A drained triaxial compression test was performed increasing vertical stress with the lateral stress maintained constant at 10 MPa and back pressure constant at 2 MPa. The average loading rate was 65 kPa/minute.
5. The sample was slightly disturbed (i.e. initial porosity of 0.37) and failed along what appeared to have been a pre-formed plane of weakness.

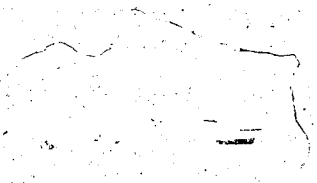

TEST TOS 4: SAMPLE DATA

Pretest Saline Creek Sample No. 44:

Dia.:	Ø	=	7.590 cm	w	=	0.032
Height:	H	=	15.100 cm	B	=	0.171
Area:	A	=	45.245 cm^2			
Volume:	V	=	683.20 ml	V_S	=	431.4 ml
Mass:	M	=	1375 g	V_V	=	251.8 ml
M_S:		=	1143 g	Dry Density	=	1.673 Mg/m^3

Density: = 2.013 Mg/m^3
Porosity: = 0.369
Void Ratio: = 0.585 g

Failed Sample No. 44 After Test TOS 4

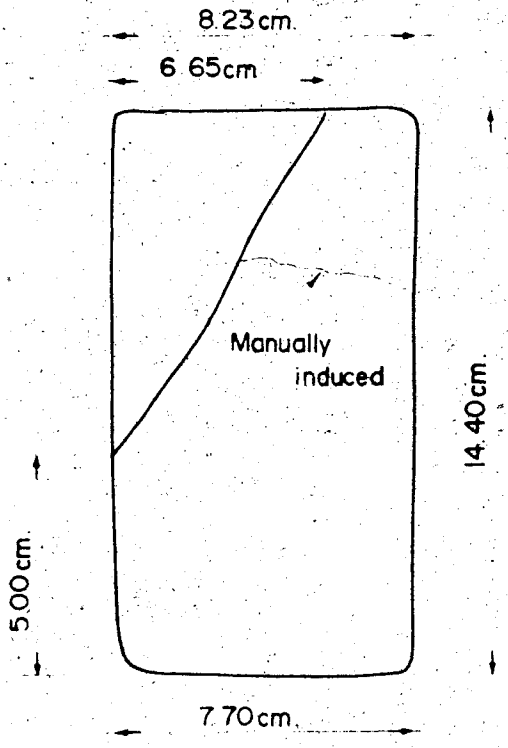

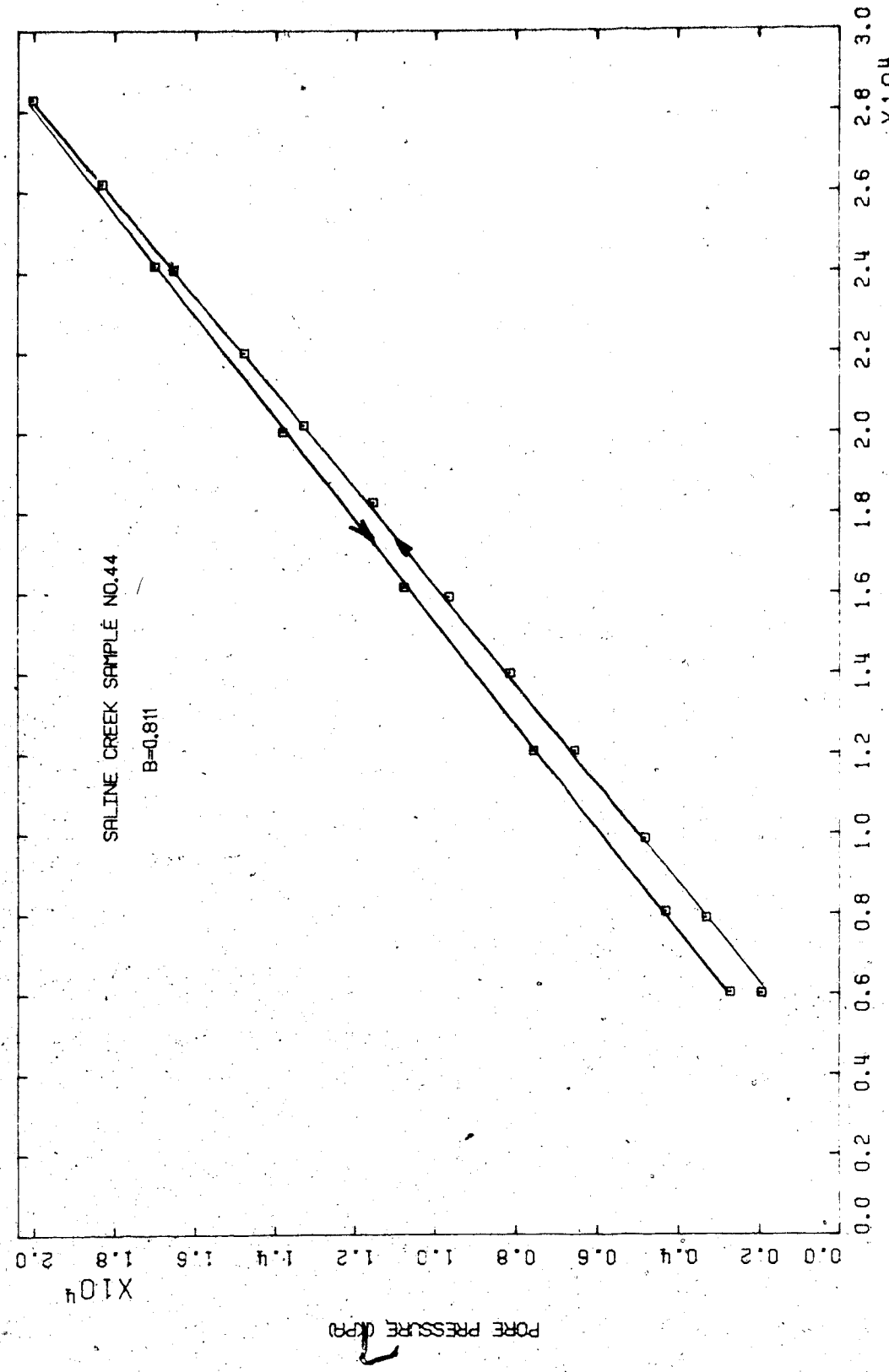

FIGURE 14.1 Triaxial Test TOS4: B Test

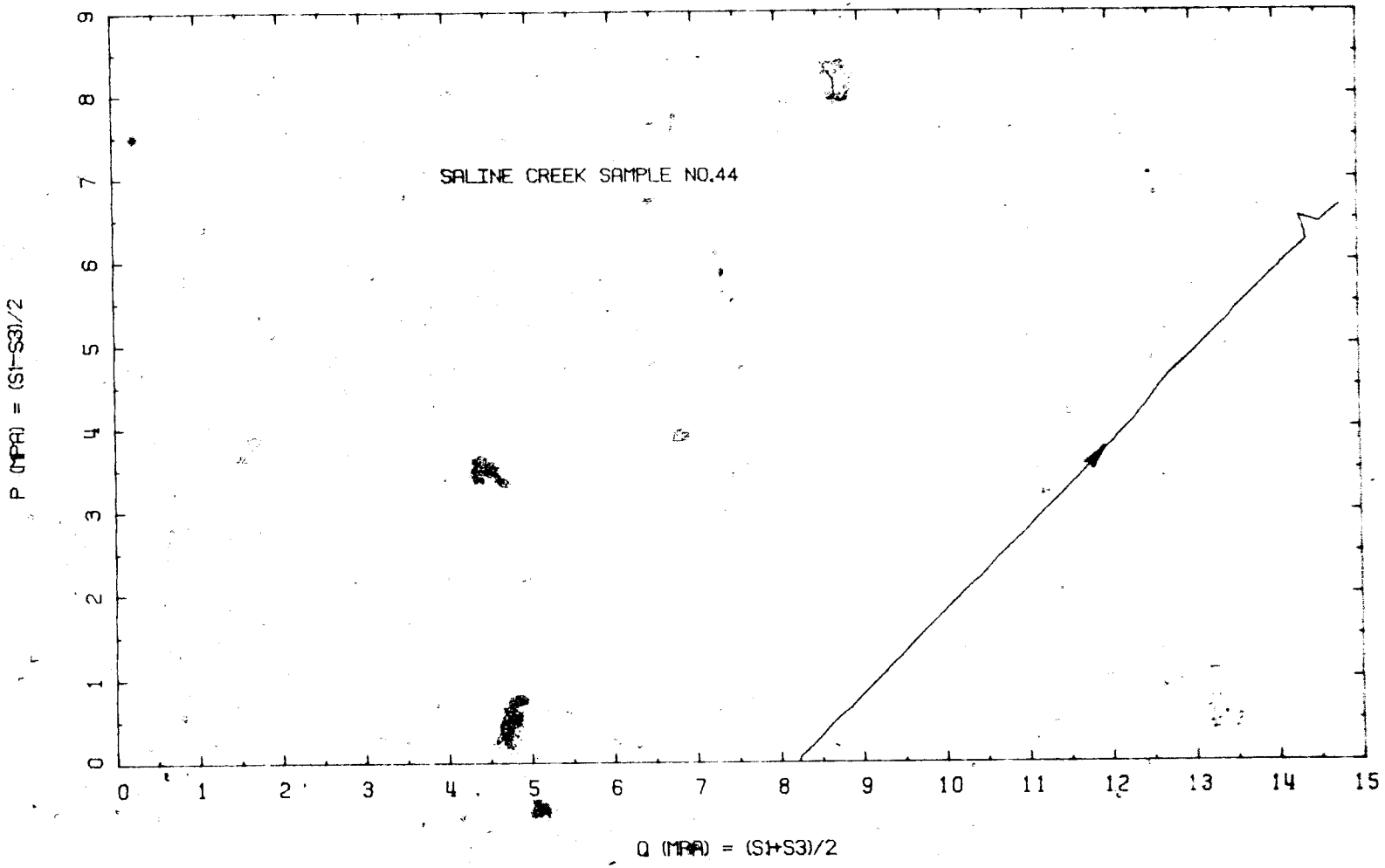

FIGURE 12.2 Triaxial Test 1054: Stress Path

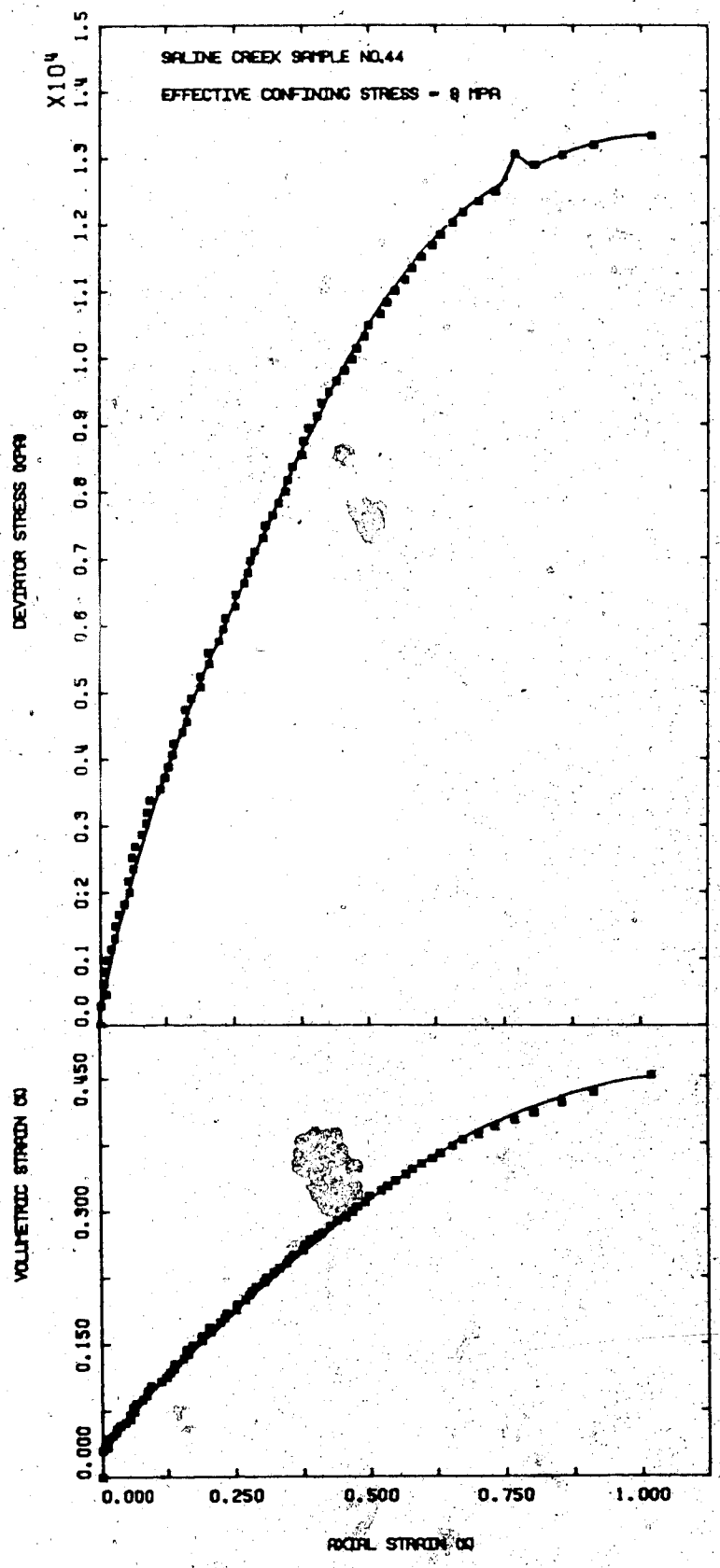

FIGURE E4.3 Triaxial Test TOS4: Deviator Stress Vs. Strain

TEST TOS 5

Drained Triaxial Compression of Saline Creek Sample No. 17
at 20°C and 8 MPa Effective Confining Stress

Procedural Details: Test TOS 5

1. Sample 17 was thawed and back saturated for 24 hours under 2 MPa back pressure and 10 MPa isotropic confining stress.
2. A drained triaxial compression test was performed with back pressure maintained constant at 2 MPa, lateral confining stress maintained constant at 10 MPa and temperature at 20°C. Vertical stress was increased at an average rate of 70 kPa per minute.

TEST TOS 5: SAMPLE DATA

Pretest Saline Creek Sample No. 17:

Dia.:	Ø	=	7.590 cm	w	=	0.035
Height:	H	=	15.300 cm	B	=	0.168
Area:	A	=	45.245 cm^2			
Volume:	V	=	692.25 ml	V_S	=	445.2 ml
Mass:	M	=	1419 g	V_V	=	247.0 ml
M_S:		=	1179.7 g	Dry Density	=	1.704 Mg/m^3

Density: = 2.050 Mg/m^3
Porosity: = 0.357
Void Ratio: = 0.555 g

Failed Sample No. 17 After Test TOS 5

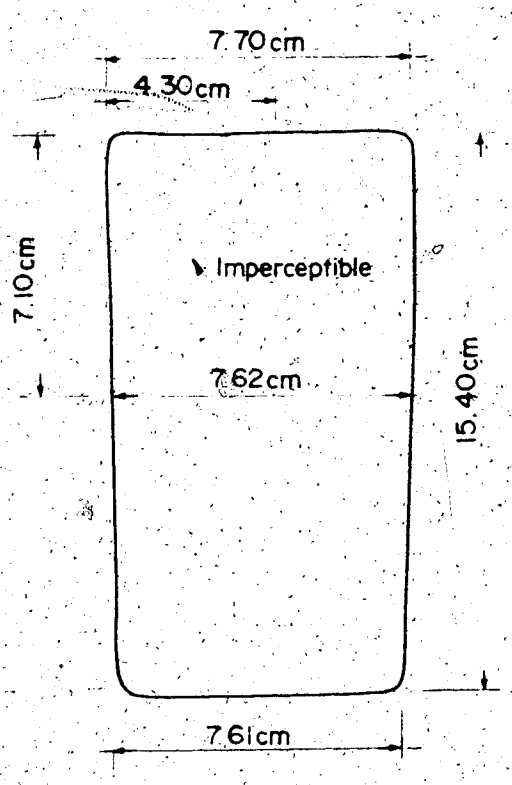

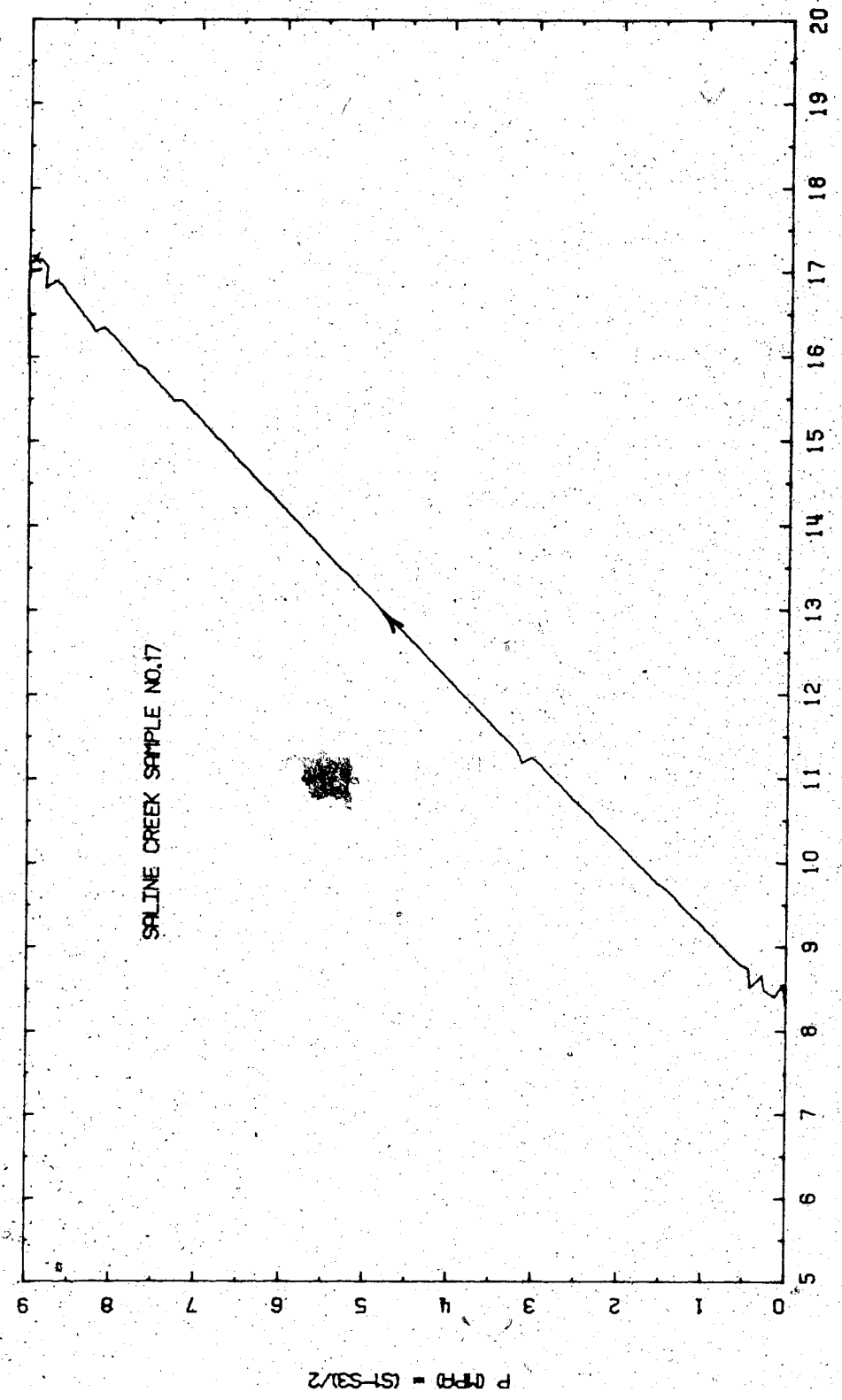

FIGURE E5.1 Triaxial Test TOS5: Stress Path

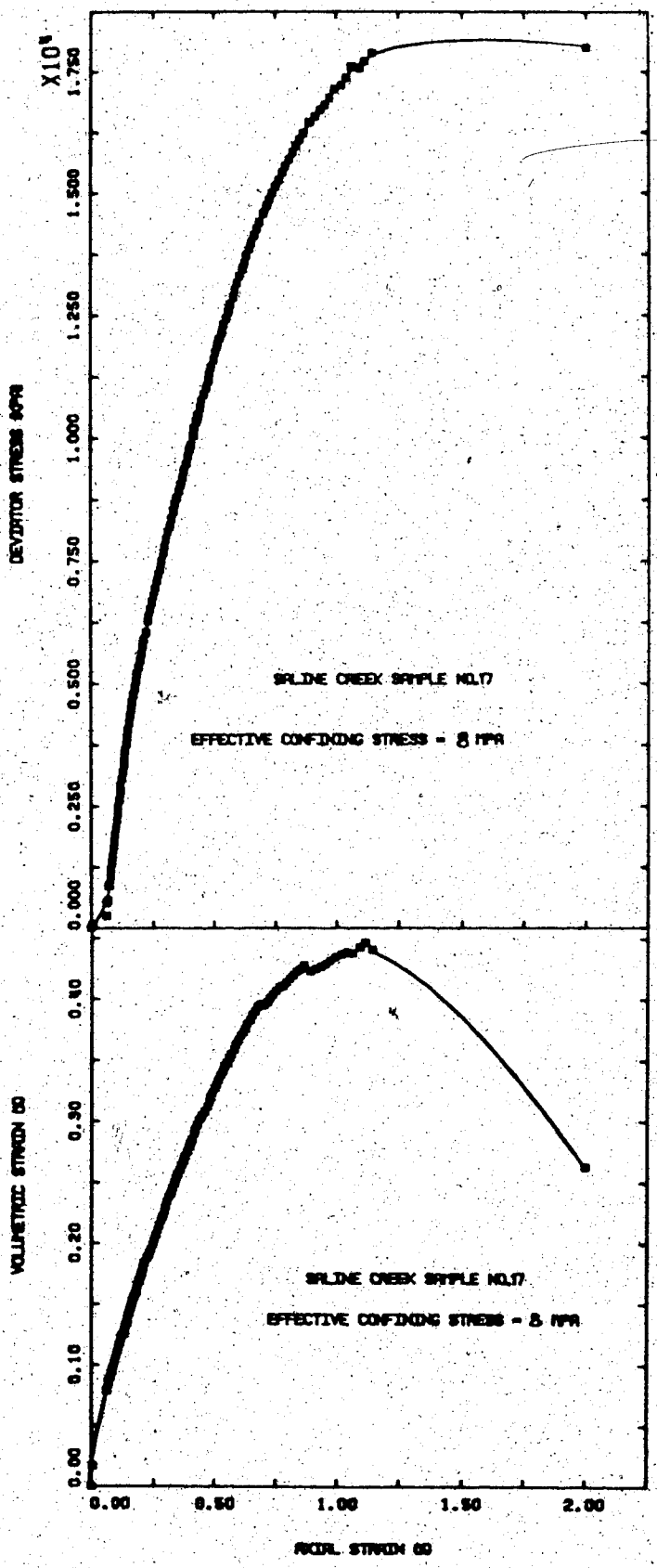

FIGURE E5.2 Triaxial Test TOS5: Deviator Stress Vs. Strain

TEST TOS 6

Drained Triaxial Compression of Saline Creek Sample No. 16 at 125°C Following Stress Path "F" (J1 Constant)

Procedural Details: Test TOS 6

1. Sample 16 was thawed and back saturated under 10 MPa back pressure and 14 MPa isotropic confining stress.
2. Heating of the apparatus and sample was started prior to complete thawing of the sample. The system was heated to 125°C; the volume of pore fluid expelled from the sample was monitored during heat.
3. Back pressure and isotropic confining stress were simultaneously increased to 12 MPa and 16 MPa respectively. The sample was allowed to consolidate overnight (i.e. for 17 hours).
4. A drained triaxial compression test was performed following stress path "F", i.e. J1 approximately constant:
   a) vertical stress was maintained constant at 16.3 MPa throughout the test.
   b) lateral confining stress was decreased in 250 kPa increments from 16 MPa to 10.4 MPa. Back pressure was decreased simultaneously in 50 - 75 kPa increments from 12 MPa to 650 kPa. The average deviatoric loading rate was 35 kPa per minute.
   c) vertical and volumetric deformations were monitored during the test.

TEST TOS 6: SAMPLE DATA

Pretest Saline Creek Sample No. 16:

Dia.:	Ø	=	7.600 cm	w	=	0.022	
Height:	H	=	15.107 cm	B	=	0.167	
Area:	A	=	45.365 cm^2				
Volume:	V	=	685.33 ml	V_S	=	461.2 ml	
Mass:	M	=	1453 g	V_V	=	224.1 ml	
M_S:		=	1222 g	Dry Density	=	1.783 Mg/m^3	

Density: = 2.120 Mg/m^3
Porosity: = 0.327
Void Ratio: = 0.486 g

Failed Sample No. 16 After Test TOS 6

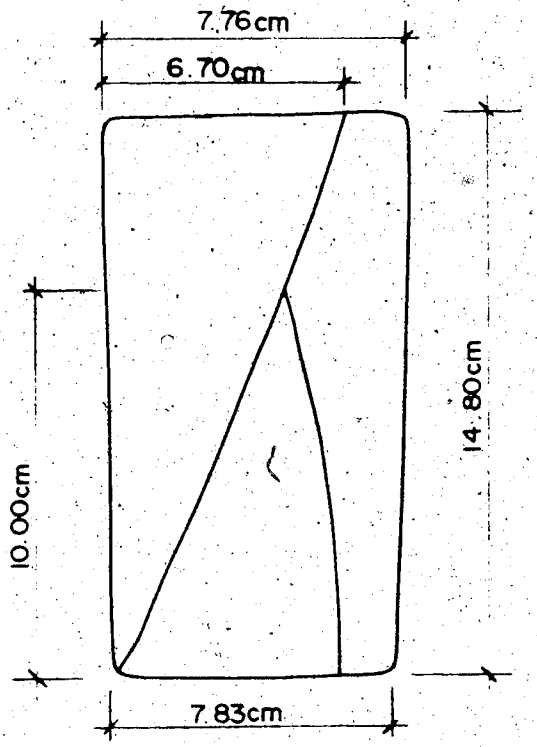

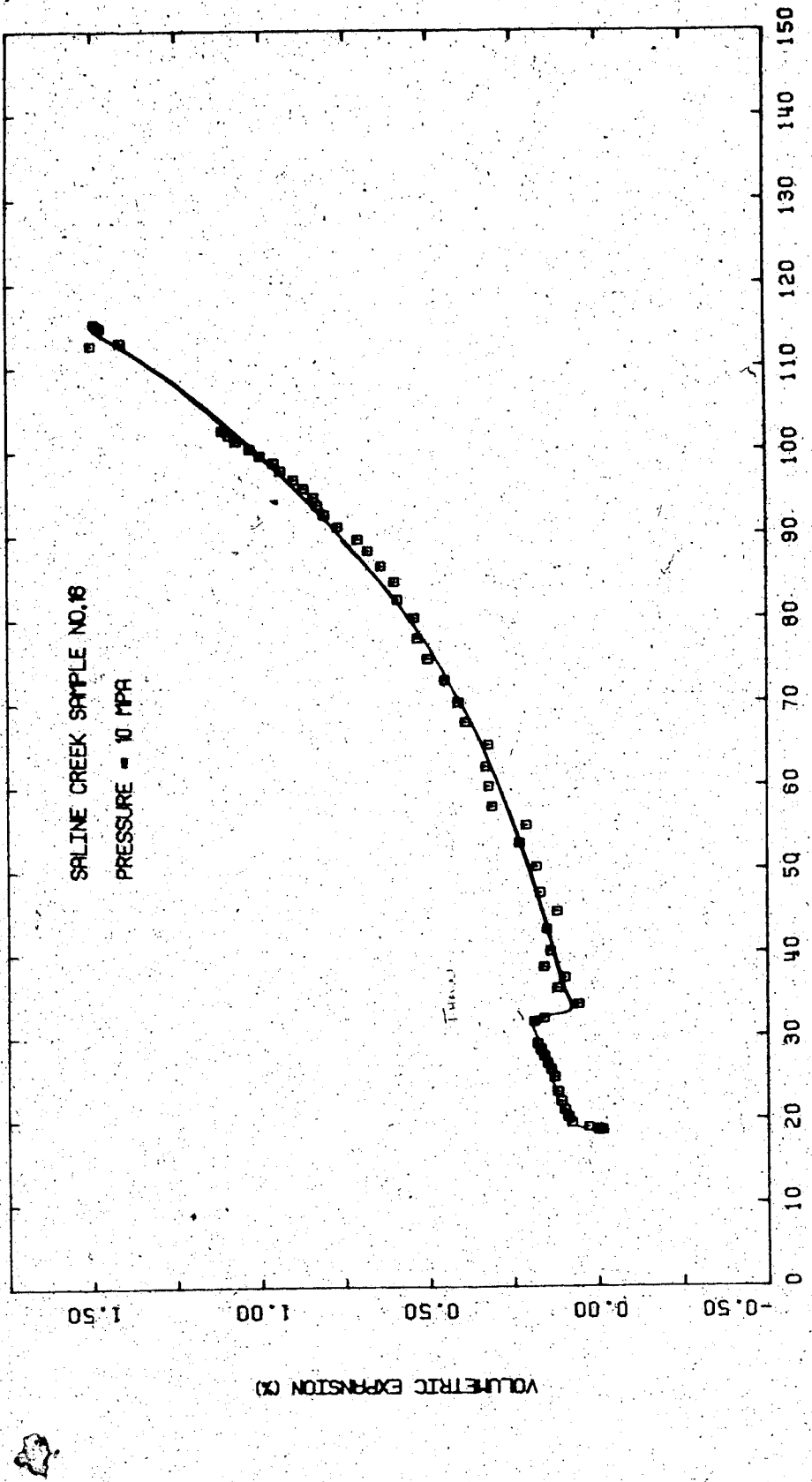

FIGURE E6.1 Triaxial Test TOS6: Drained Thermal Expansion

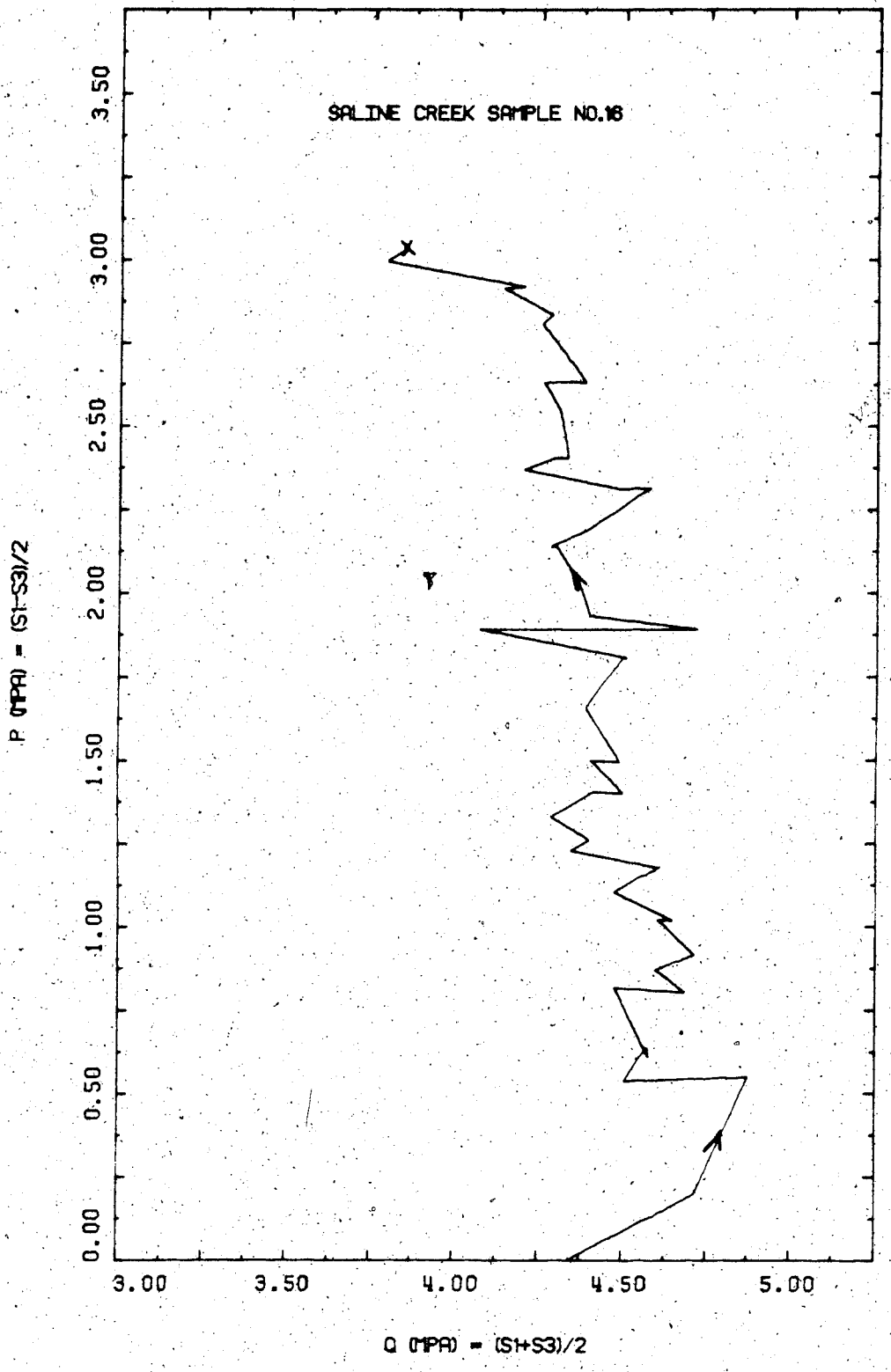

FIGURE E6.2 Triaxial Test TOS6: Stress Path

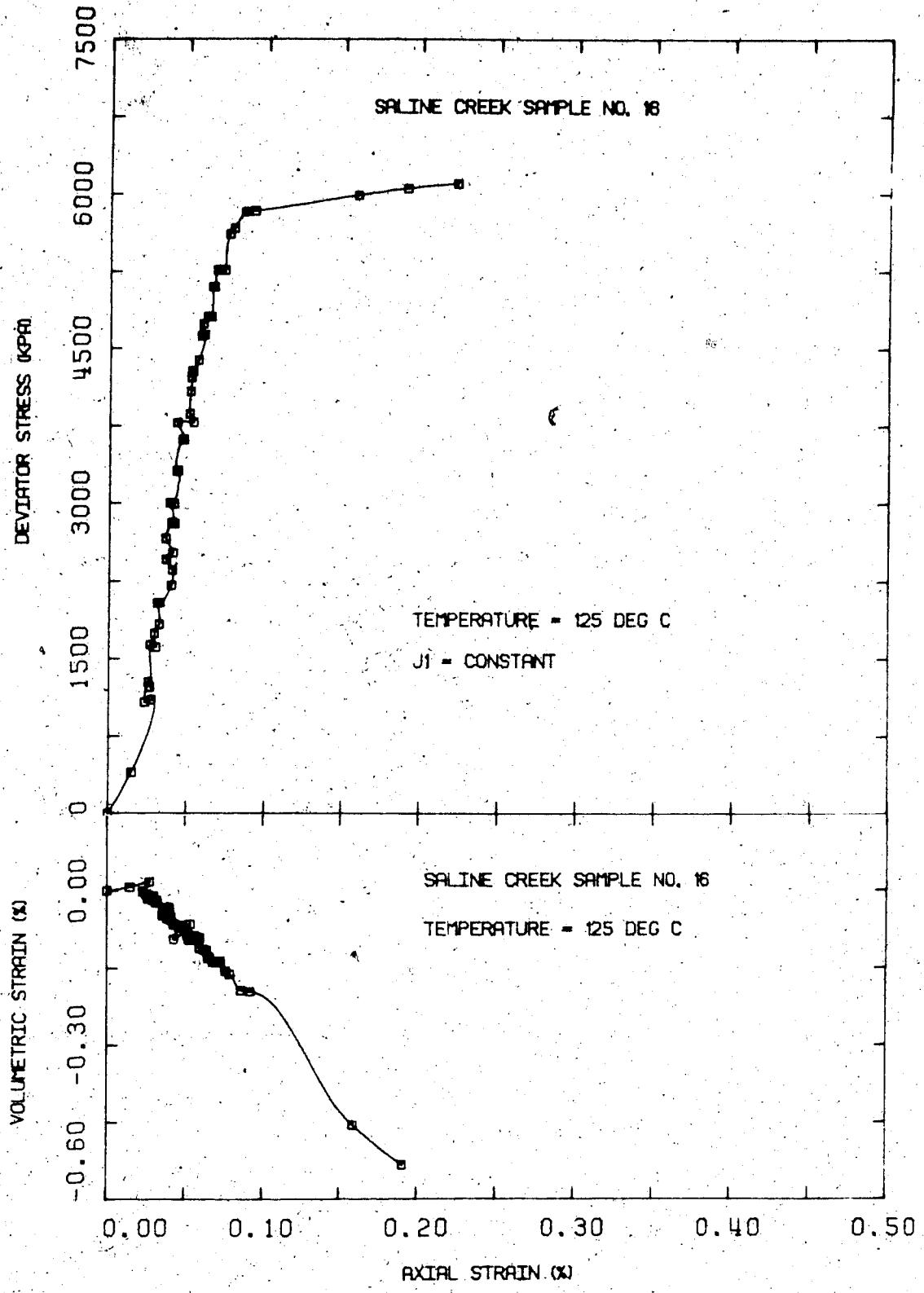

FIGURE E6.3 Triaxial Test TOS6: Deviator Stress Vs. Strain

TEST TOS 7

Drained Triaxial Compression of Saline Creek Sample No. 45 at 125°C and 4 MPa Effective Confining Stress

Procedural Details: Test TOS 7

1. Sample 45 was thawed and back saturated for 24 hours under 10 MPa back pressure and 14 MPa isotropic effective confining stre ss.
2. The apparatus and sample were heated to 125°C; the volume of pore fluid expelled from the sample was monitored during heating.
3. A drained triaxial compression test was performed:
   a) vertical stress was increased at an average rate of 70 kPa/minute;
   b) lateral confining stress was maintained constant at 14 MPa and the back pressure was held constant at 10 MPa;
   c) vertical deformation and volume change were monitored during deviatoric passive compression.

TEST TOS 7: SAMPLE DATA

Pretest Saline Creek Sample No. 45:

Dia.:	Ø	=	7.610 cm	w	=	0.022
Height:	H	=	15.430 cm	B	=	0.160
Area:	A	=	45.484 cm			
Volume:	V	=	701.82 ml	V_S	=	453.3 ml
Mass:	M	=	1420 g	V_V	=	248.5 ml
M_S:		=	1201 g	Dry Density	=	1.712 Mg/m^3

Density: = 2.023 Mg/m^3
Porosity: = 0.354
Void Ratio: = 0.548 g

Failed Sample No. 45 After Test TOS 7

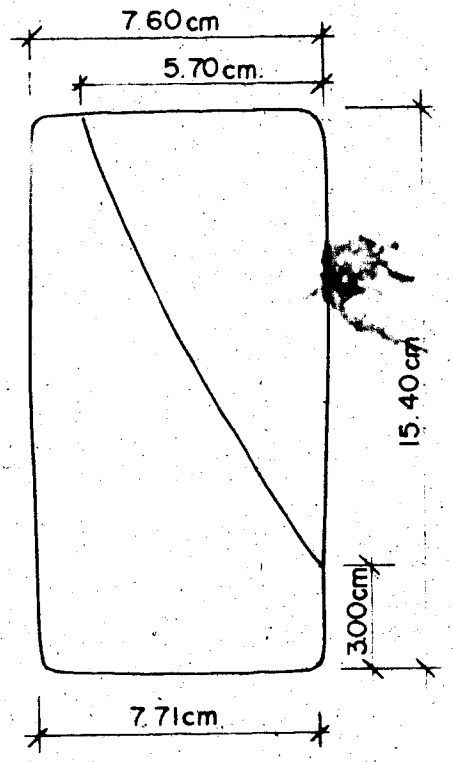

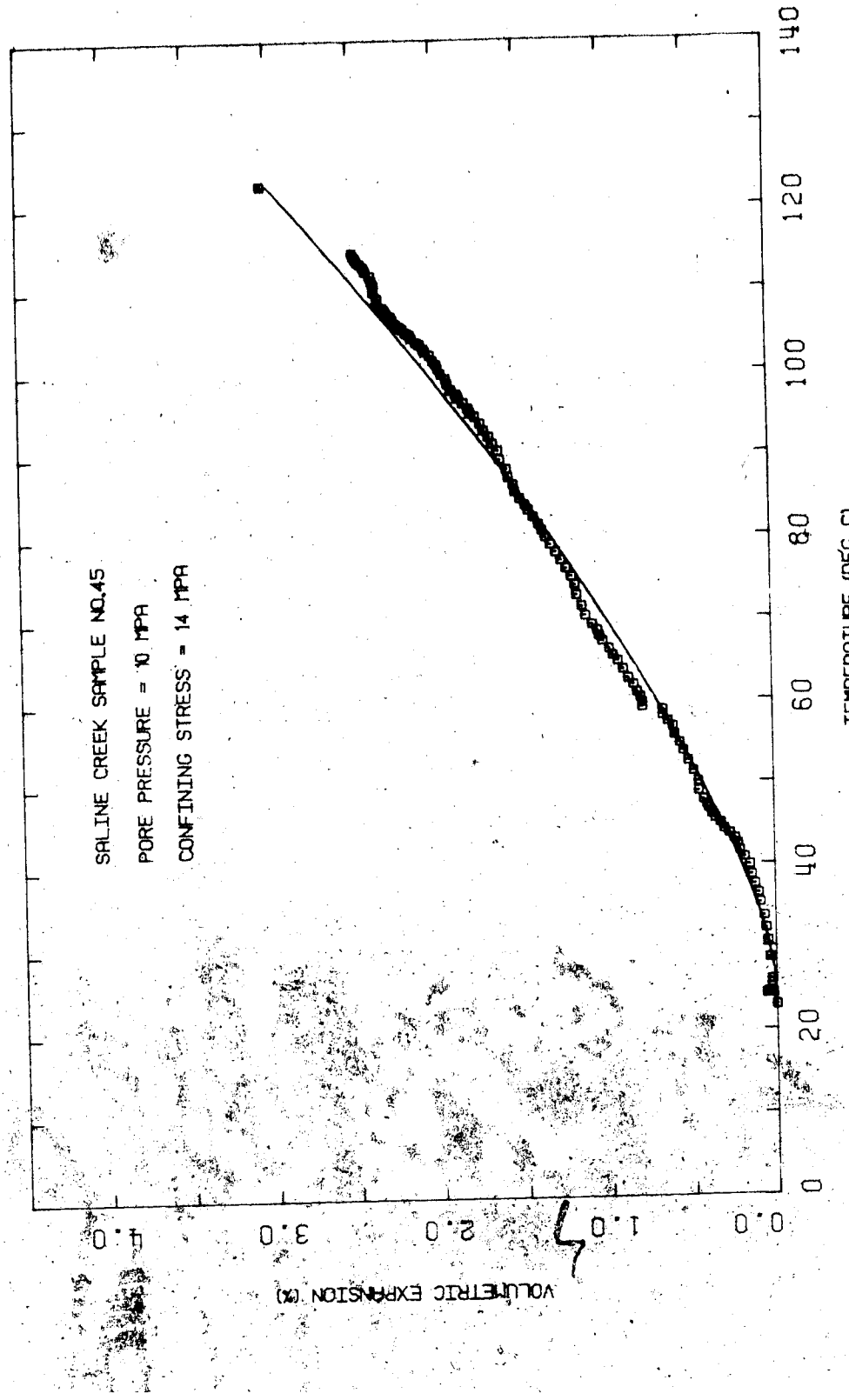

FIGURE 6/.1 Triaxial Test 105/: Drained Thermal Expansion

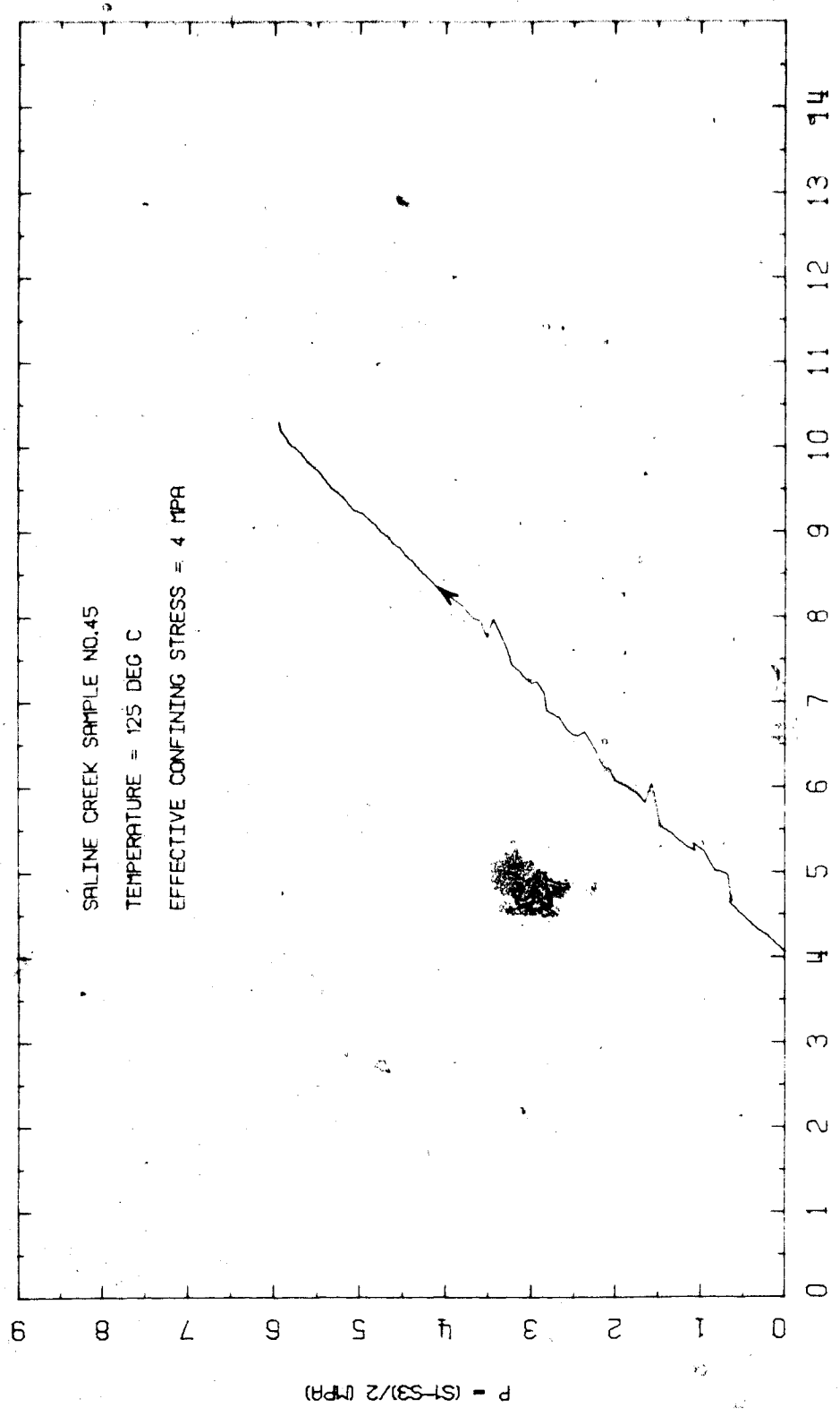

FIGURE E7.2 Triaxial Test TOS7: Stress Path

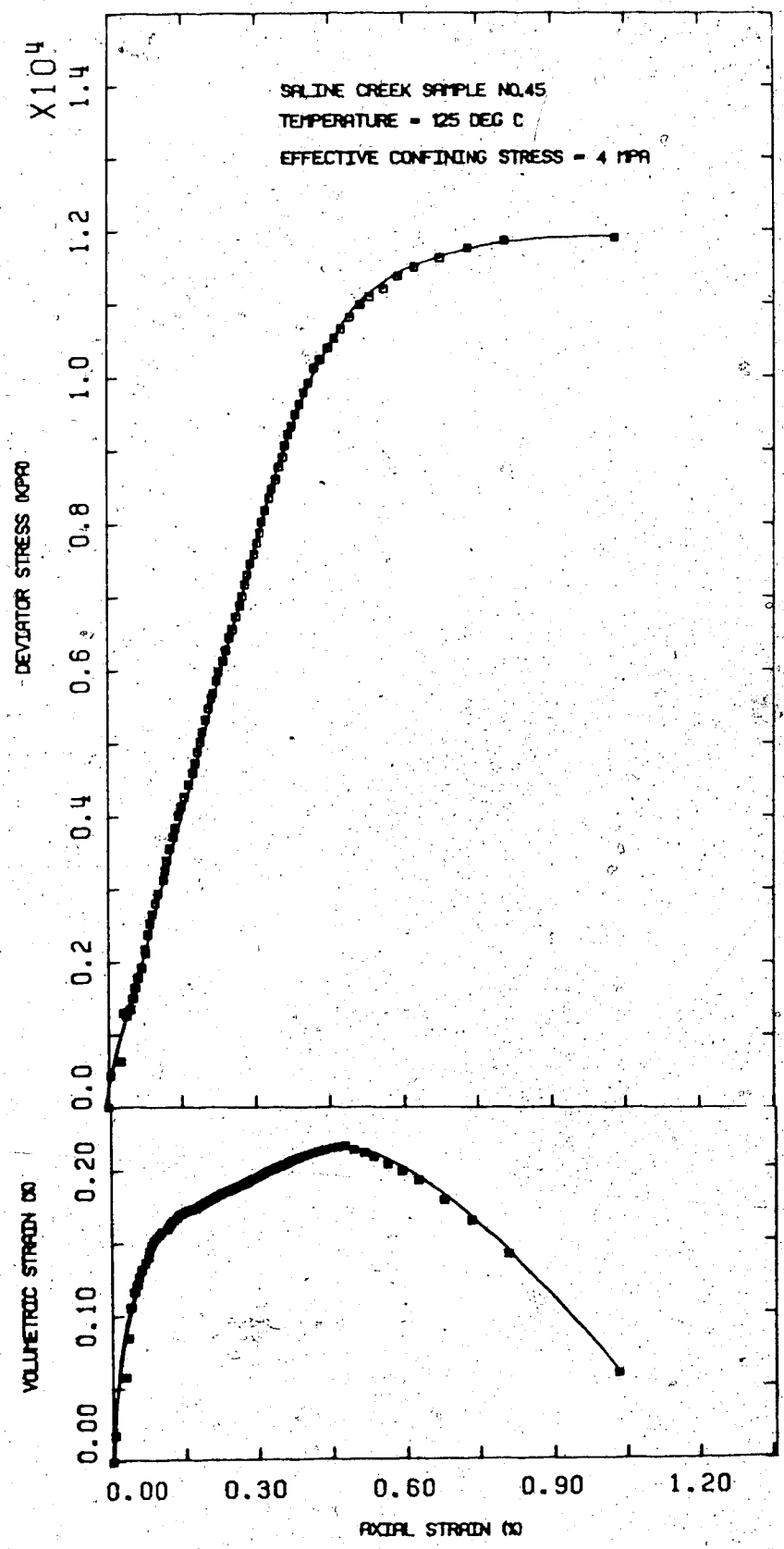

FIGURE E7.3 Triaxial Test TOS7: Deviator Stress Vs. Strain

TEST TOS 8

Undrained and Drained Isotropic Compression of Saline Creek Sample No. 28 at 220°C - O-Ring Seal Failure

Procedural Details: Test TOS 8

1. Sample 28 was thawed and back saturated for 21 hours under 10 MPa back pressure and 12 MPa effective confining stress.
2. The sample was heated to 220°C under drained conditions. Drained thermal expansion and the volume of pore fluid expelled from the sample were measured during heating up to 200°C. However, lateral deformation measurements on the sample are not considered reliable due to stiffness of the strain gauge clamp. A small amount of leakage of cell fluid past the O-ring seal at the base of the triaxial cell was noticed at this stage. Heating was discontinued.
3. A B-test was performed over a range of isotropic confining stress from 12 - 20.5 MPa. Volumetric strain was determined during undrained loading from internal vertical and lateral strain gauge measurements giving undrained compressibility. Again however, lateral deformation measurements were not reliable.
4. A drained isotropic compression test was started. However, severe leakage of cell fluid started during the first loading cycle. The test was discontinued.

TEST TOS 8: SAMPLE DATA

Pretest Saline Creek Sample No. 28:

Dia.:	Ø	= 7.433 cm	w	=	0.025
Height:	H	= 15.293 cm	B	=	0.170
Area:	A	= 45.393 cm^2			
Volume:	V	= 663.61 ml	V_S	=	428.8 ml
Mass:	M	= 1356 g	V_V	=	234.8 ml
M_S:		= 1136 g	Dry Density	=	1.712 Mg/m^3

Density: = 2.046 Mg/m^3
Porosity: = 0.354
Void Ratio: = 0.548 g

Failed Sample No. 28 After Test TOS 8

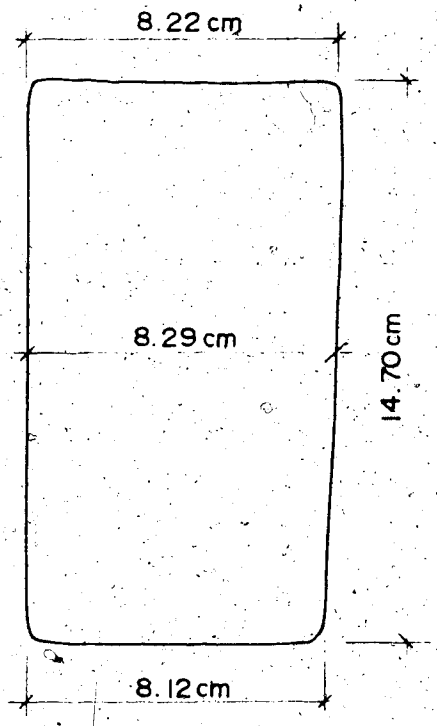

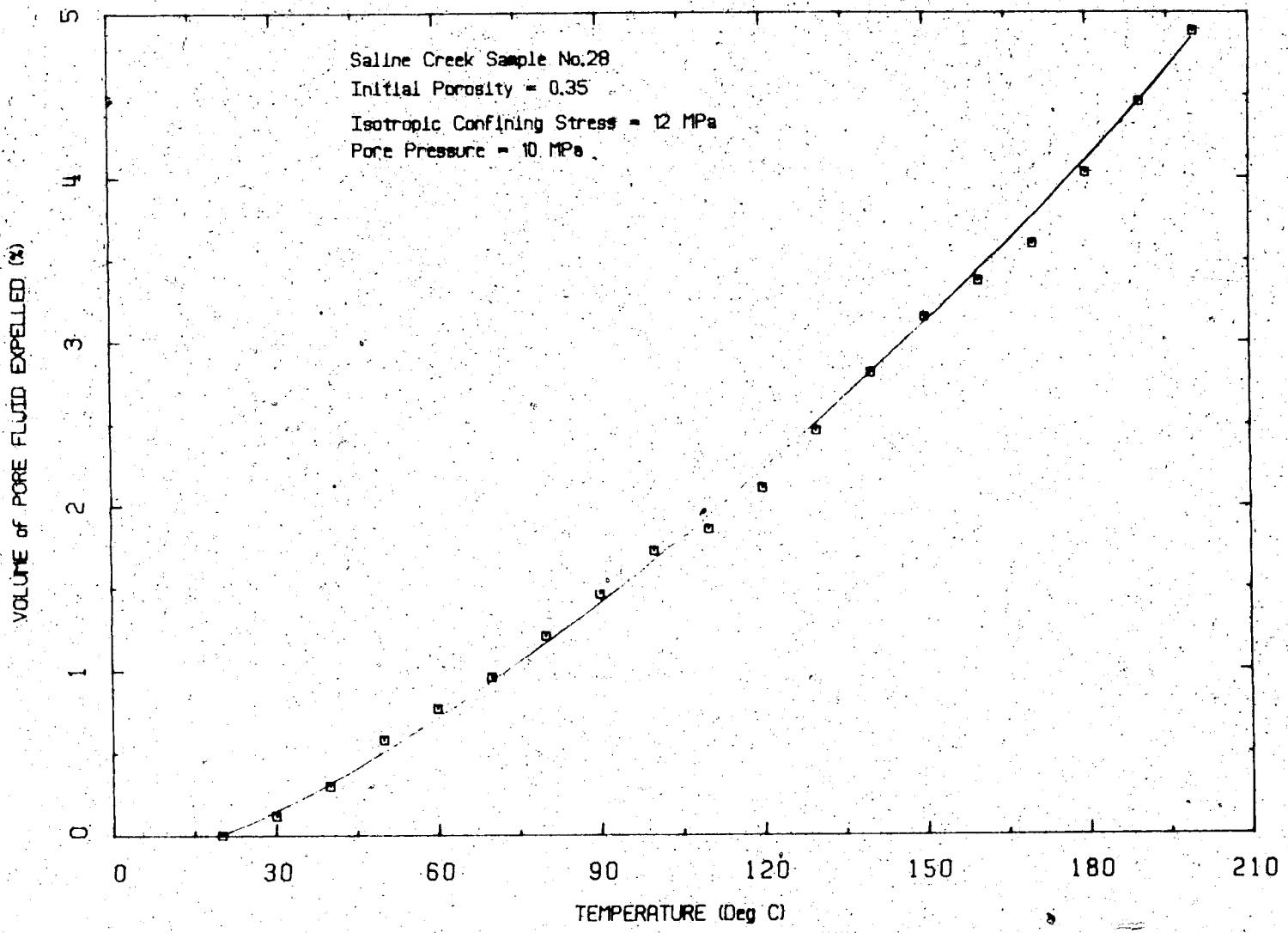

FIGURE 1.8.1 Triaxial Test TOS8: Volume of Pore Fluid Drained During Heating

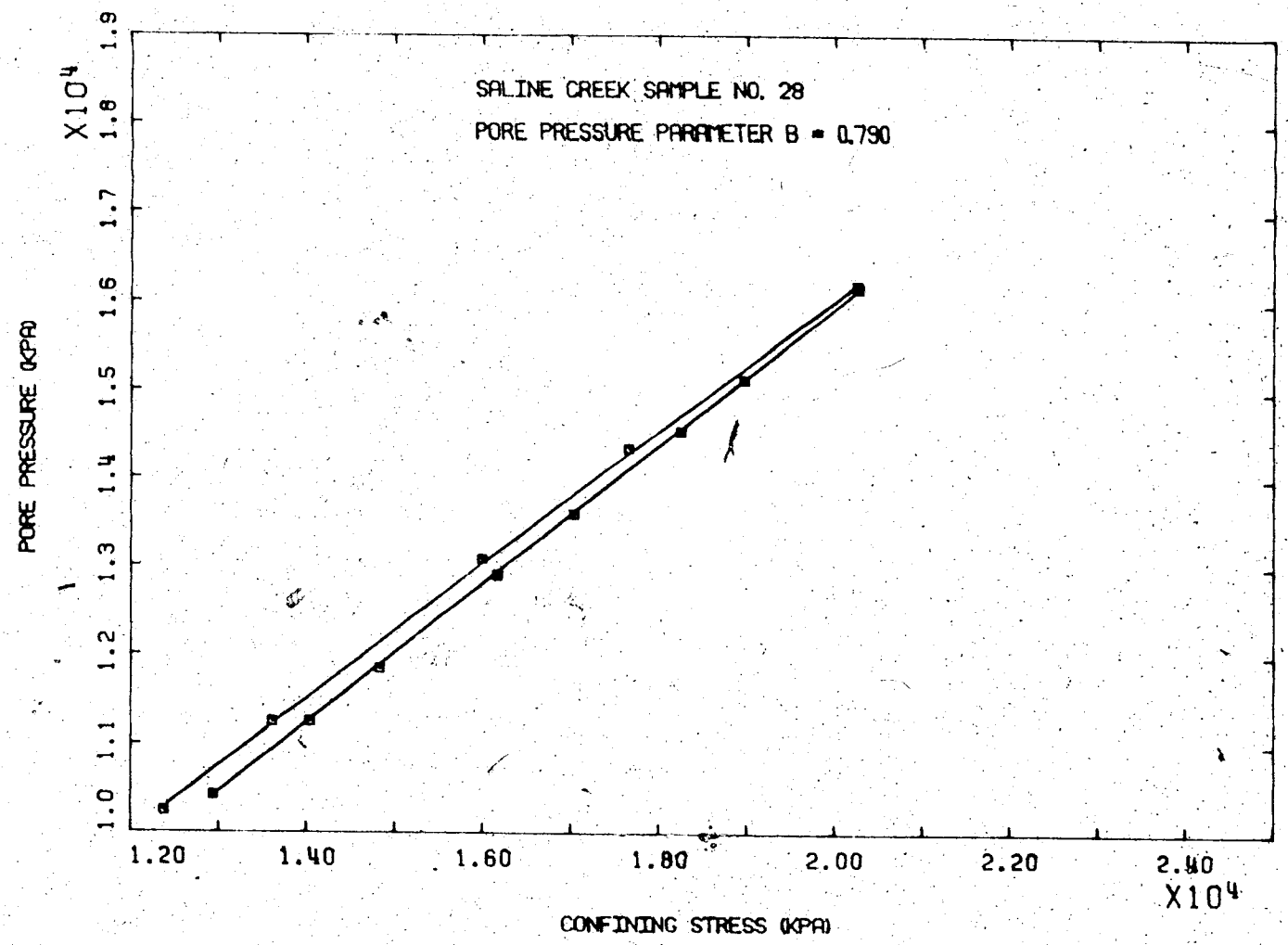

FIGURE 18.2 Triaxial Test 1058: B Test

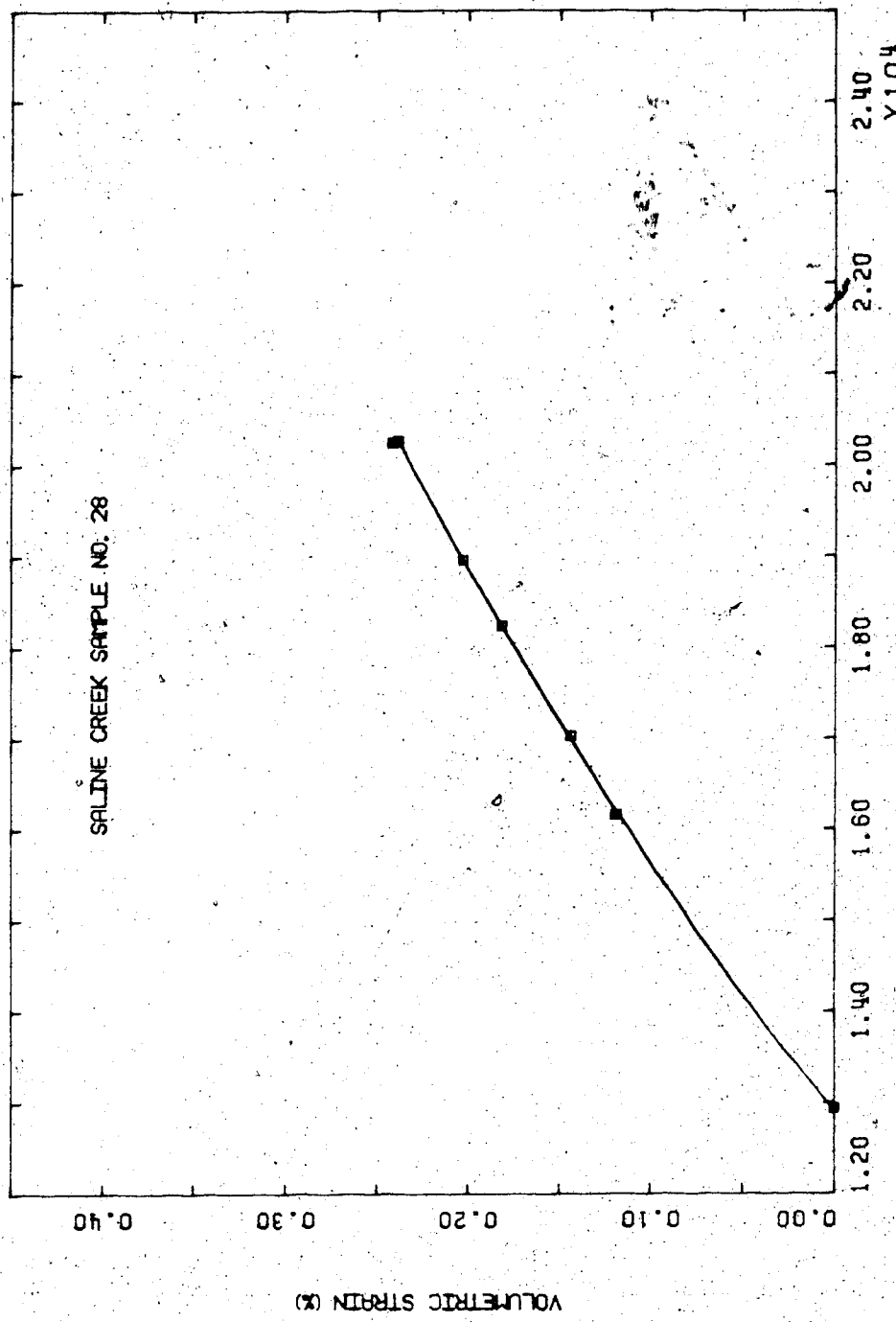

FIGURE E8.3 Triaxial Test TOS8: Undrained Compressibility

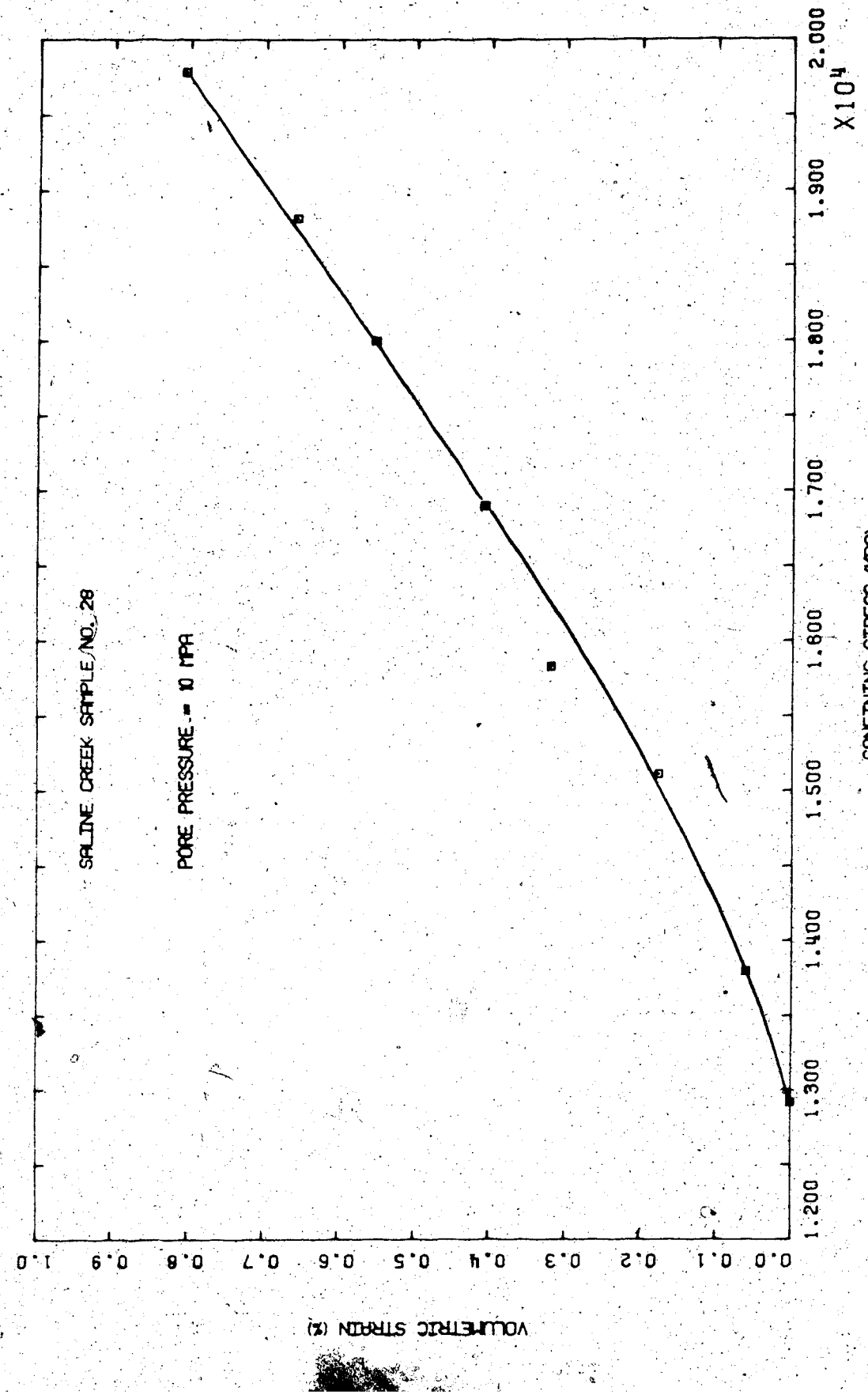

FIGURE 8.4 Triaxial Test TOS8: Drained Isotropic Compressibility

TEST TOS 9

Triaxial Test: Thermal Expansion of Saline Creek Sample No. 27 to 235°C Followed by Membrane Failure

Procedural Details: Test TOS 9

1. Sample 27 was thawed and back saturated for 24 hours under 10 MPa back pressure and 14 MPa isotropic confining stress.
2. The apparatus and sample were heated under drained conditions (i.e. constant back pressure) to 240°C. The silicone rubber triaxial membrane depolymerized during the night resulting in back pressure/confining pressure communication. Heated silicone oil cell fluid was injected through the sample under a differental pressure which was initially 4 MPa.

   The metal bellows interface in the volume change device was damaged.
3. The test was terminated.

TEST TOS 9: SAMPLE DATA

Pretest Saline Creek Sample No. 27:

Dia.:	Ø	=	7.610 cm	w	=	0.012
Height:	H	=	15.110 cm	B	=	0.171
Area:	A	=	45.484 cm^2			
Volume:	V	=	687.26 ml	V_S	=	455.8 ml
Mass:	M	=	1429 g	V_V	=	231.5 ml
M_S:		=	1208 g	Dry Density	=	1.757 Mg/m^3

Density: = 2.079 Mg/m^3
Porosity: = 0.337
Void Ratio: = 0.508 g

Sample 27 After Test TOS 9 Meltdown

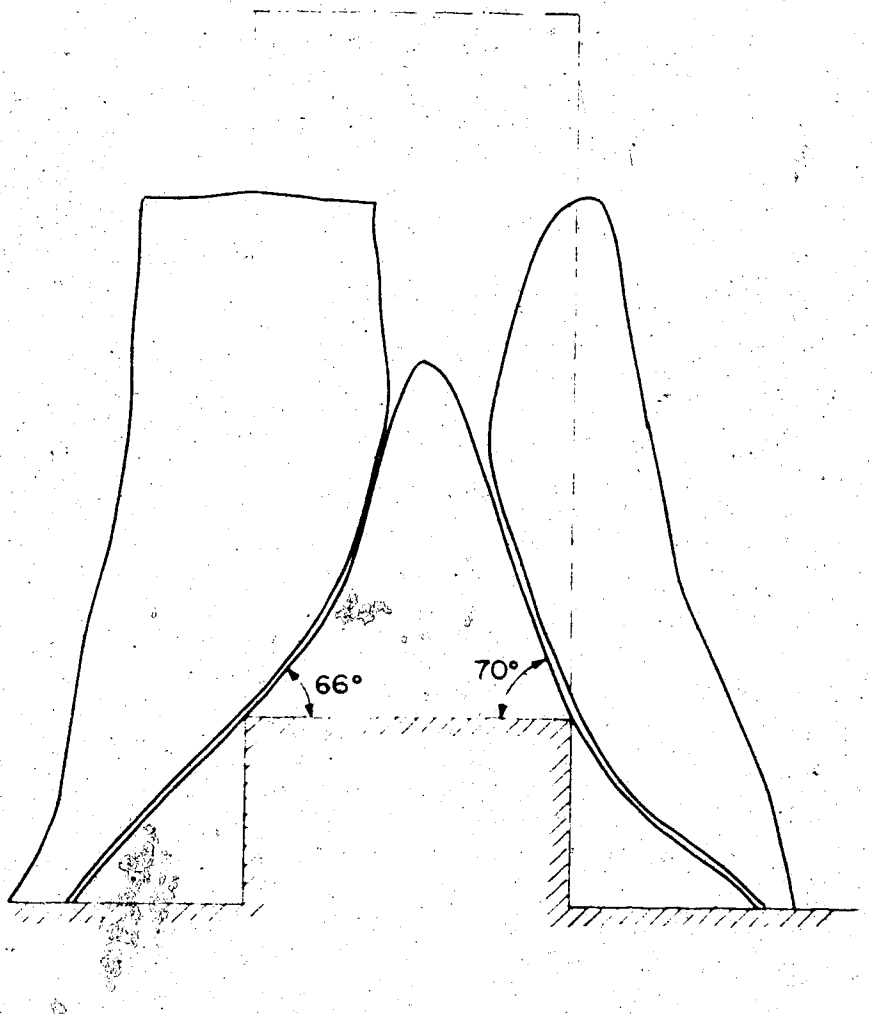

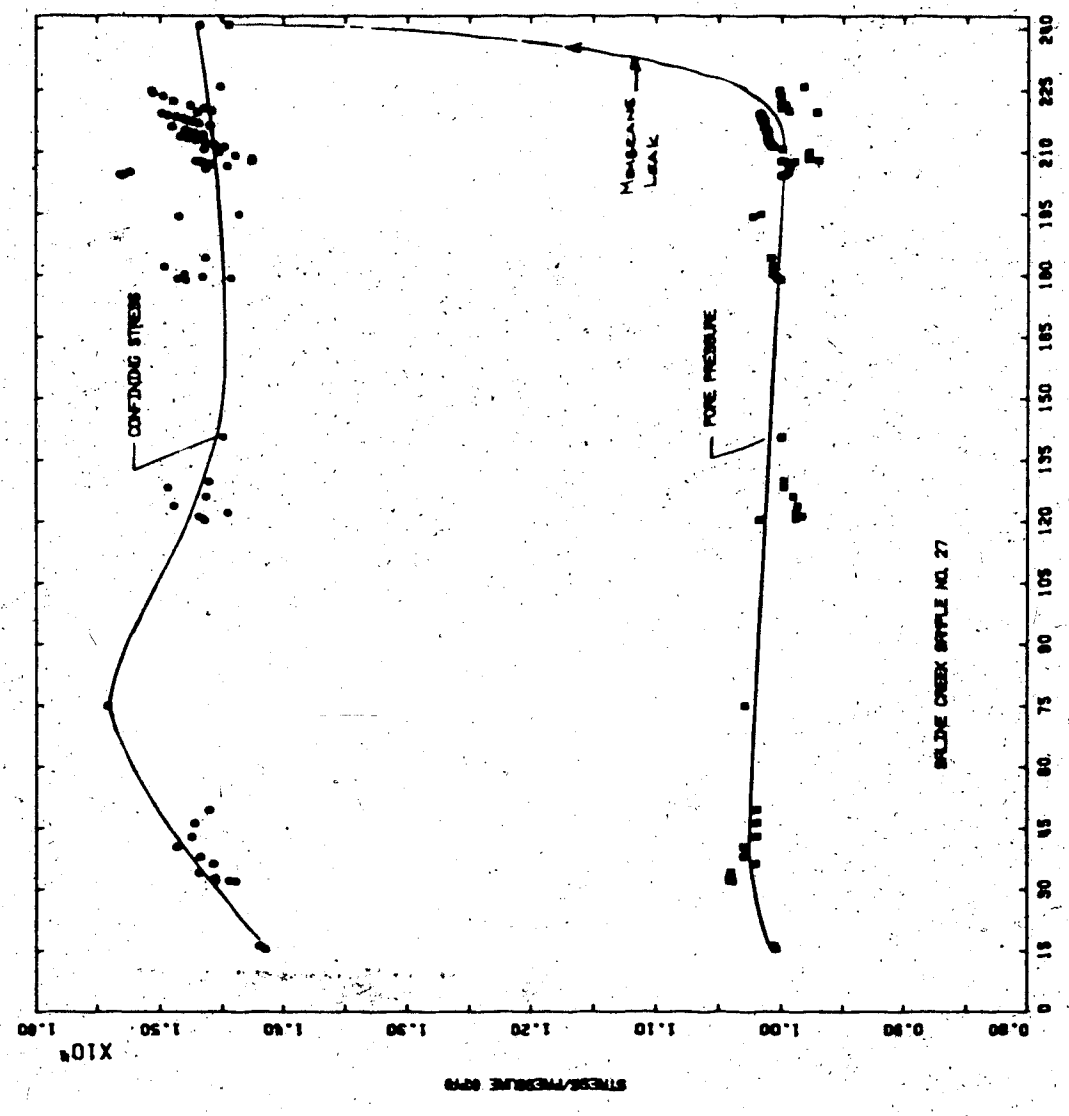

FIGURE E9.1 Triaxial Test TOS9: Confining Stress/Pore Pressure Vs. Temperature

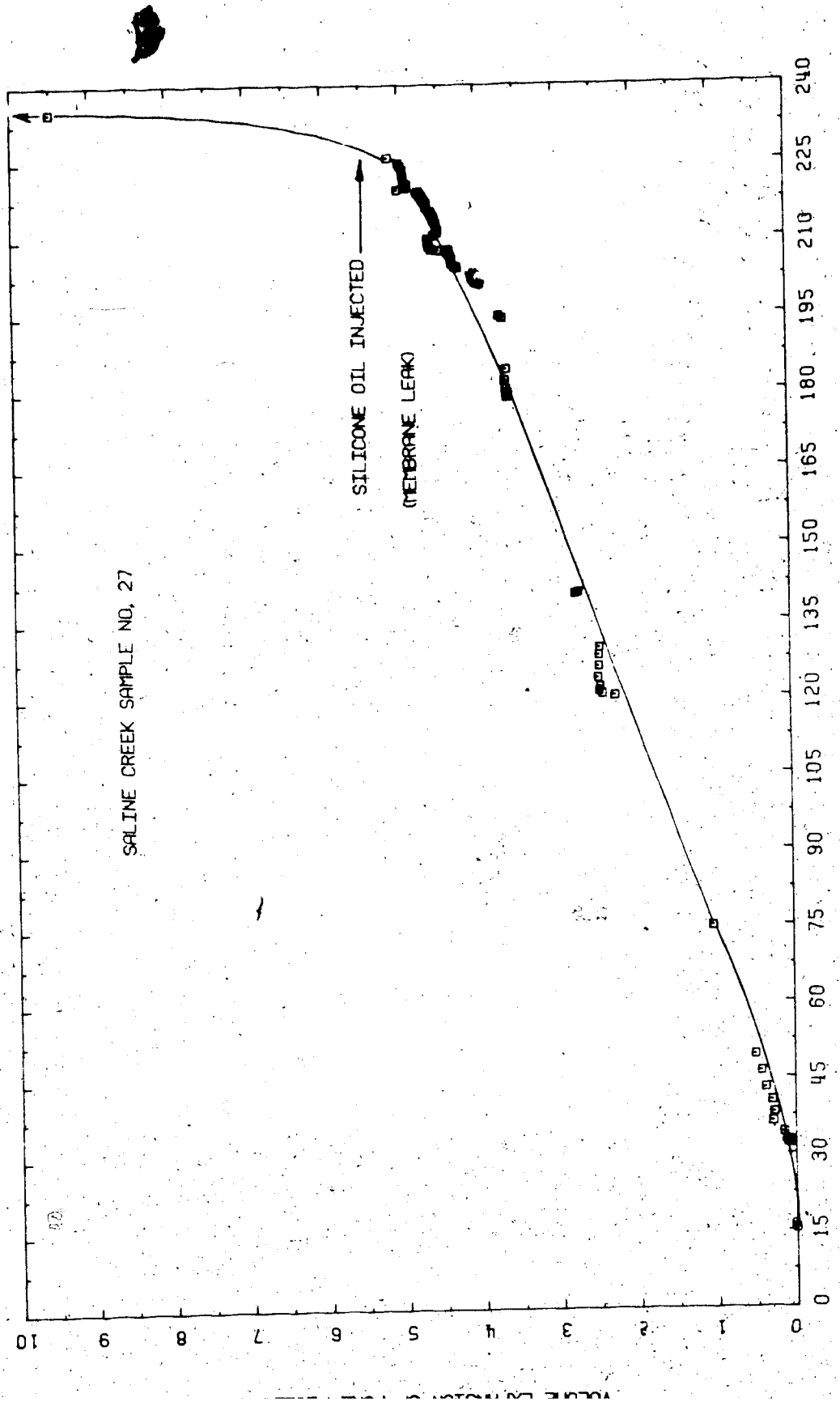

FIGURE E9.2 Triaxial Test T059: Thermal Expansion of Pore Fluids

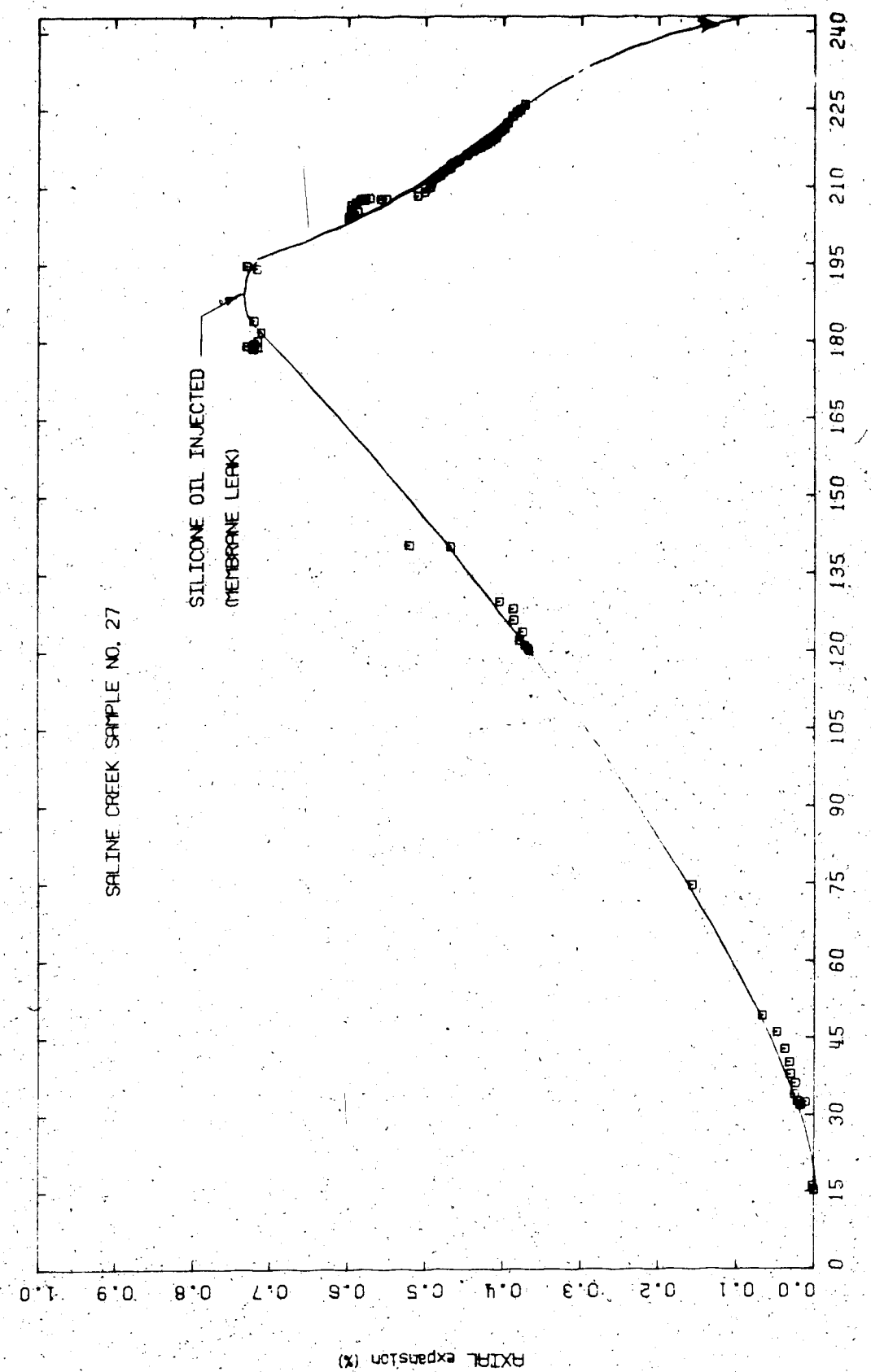

FIGURE 4.9.3 Triaxial Test T059: Vertical Thermal Expansion

TEST TOS 10

Pore Pressure Response to Undrained Heating and Undrained Triaxial Compression of Saline Creek Sample No. 20 at 200°C

Procedural Details: Test TOS 10

1. Sample 20 was thawed and back saturated for 21 hours under 10 MPa back pressure and 14 MPa isotropic confining stress.
2. Back pressure and isotropic confining stress were reduced simultaneously to 2 MPa and 6 MPa, respectively.
3. A B-test was performed over a range of confining stresses from 0 to 14 MPa to evaluate degree of saturation.
4. The back pressure and isotropic confining stress were set at 2 MPa and 6 MPa, respectively. Back pressure drainage valves were closed.
5. The apparatus and sample were heated slowly. Pore pressure response to undrained heating was monitored and confining stress was adjusted in an effort to maintain isotropic effective confining stress constant at about 4 MPa. The pressure limits of the apparatus were approached after a 25°C to 30°C temperature increase. Undrained heating was conducted in 8 heating cycles from 17.5°C to 200°C as shown in Table E2.
6. At the end of each heating cycle, the back pressure drainage valves were opened; back pressure and isotropic confining stress were reduced simultaneously to about 2-3

MPa respectively, always maintaining 4 MPa effective confining stress in the sample. Volume change (i.e. the volume of pore fluid expelled from the sample) was measured each time the drainage valves were opened.

7. Drainage valves were then reclosed and the next heating cycle started.
8. After undrained heating cycle No. 8 was completed, the back pressure was adjusted to 10 MPa and the isotropic confining stress was simultaneously adjusted to 14 MPa.
9. Back pressure drainage valves were closed. Vertical compression stress was increased at an average rate of 70 kPa per minute with lateral confining stress maintained constant and the temperature at 200°C.

Pore pressure and vertical deformation were monitored during the undrained triaxial compression test.

TABLE E-2

Test TOS 10: Summary of Undrained Heating Cycles

Heating Cycle	Temperature Range	ΔT (°C)	Δu (kPa)	$B = \frac{\Delta u}{\Delta T}$ (kPa/°C)	Average Effective Confining Stress (kPa)	$F = \frac{B}{\sigma_3}$ ($°C^{-1}$)
1	25 - 44	19	18760	980	3630	0.270
2	50 - 64	14	12300	880	3800	0.232
3	70 - 85	15	12400	825	3900	0.212
4	90 - 106	16	12600	790	3800	0.208
5	112 - 109	17	11900	700	3700	0.189
6	130 - 152	22	12900	590	4100	0.144
7	157 - 176	19	9500	500	4900	0.102
8	182 - 195	13	5900	450	4200	0.107

TEST TOS 10: SAMPLE DATA

Pretest Saline Creek Sample No. 20:

Dia.:	Ø	=	7.610 cm	w	=	0.026
Height:	H	=	15.170 cm	B	=	0.178
Area:	A	=	45.484 cm^2			
Volume:	V	=	690.00 ml	V_S	=	449.0 ml
Mass:	M	=	1432 g	V_V	=	241.5 ml
M_S:		=	1190 g	Dry Density	=	1.724 Mg/m^3

Density: = 2.076 Mg/m^3
Porosity: = 0.349
Void Ratio: = 0.536 g

Sample 27 After Test TOS 10

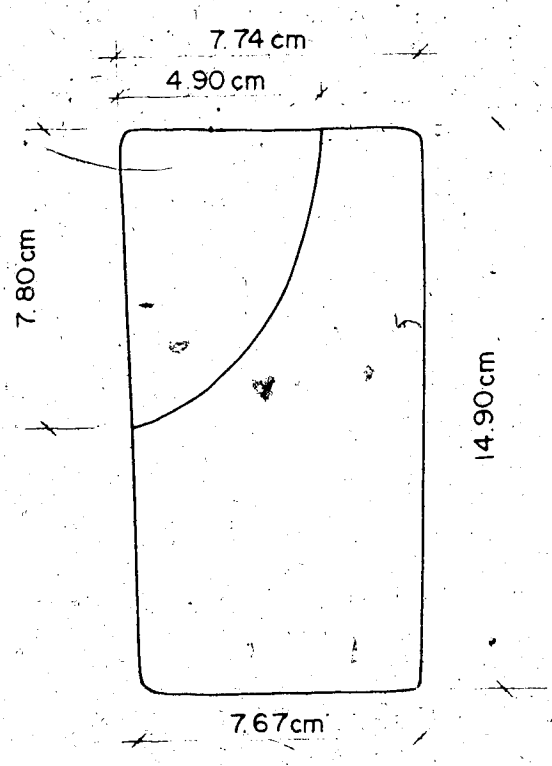

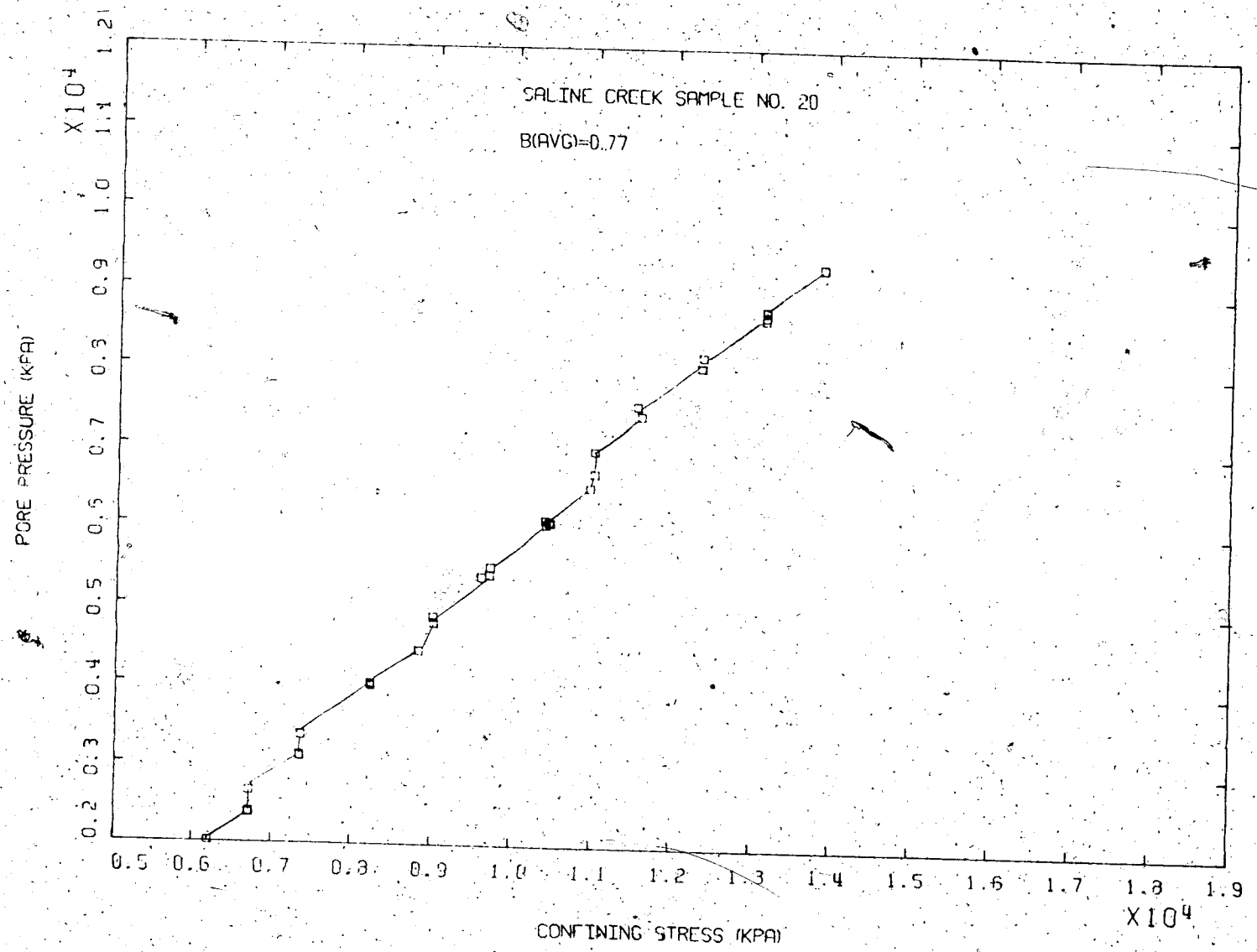

FIGURE E10.1 Triaxial Test TOS10: Modified B Test

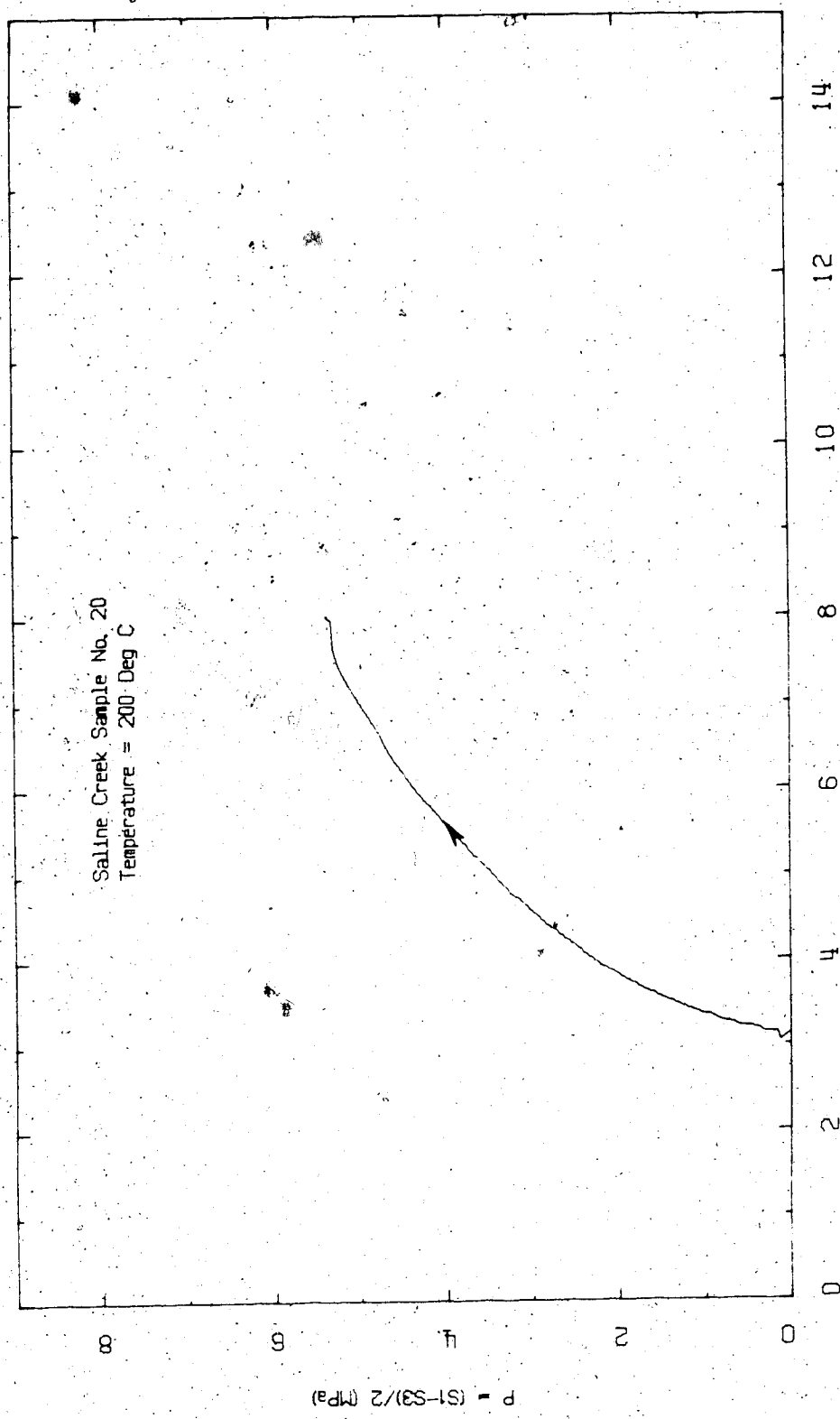

FIGURE E10.2 Triaxial Test TQS10: Effective Stress Path

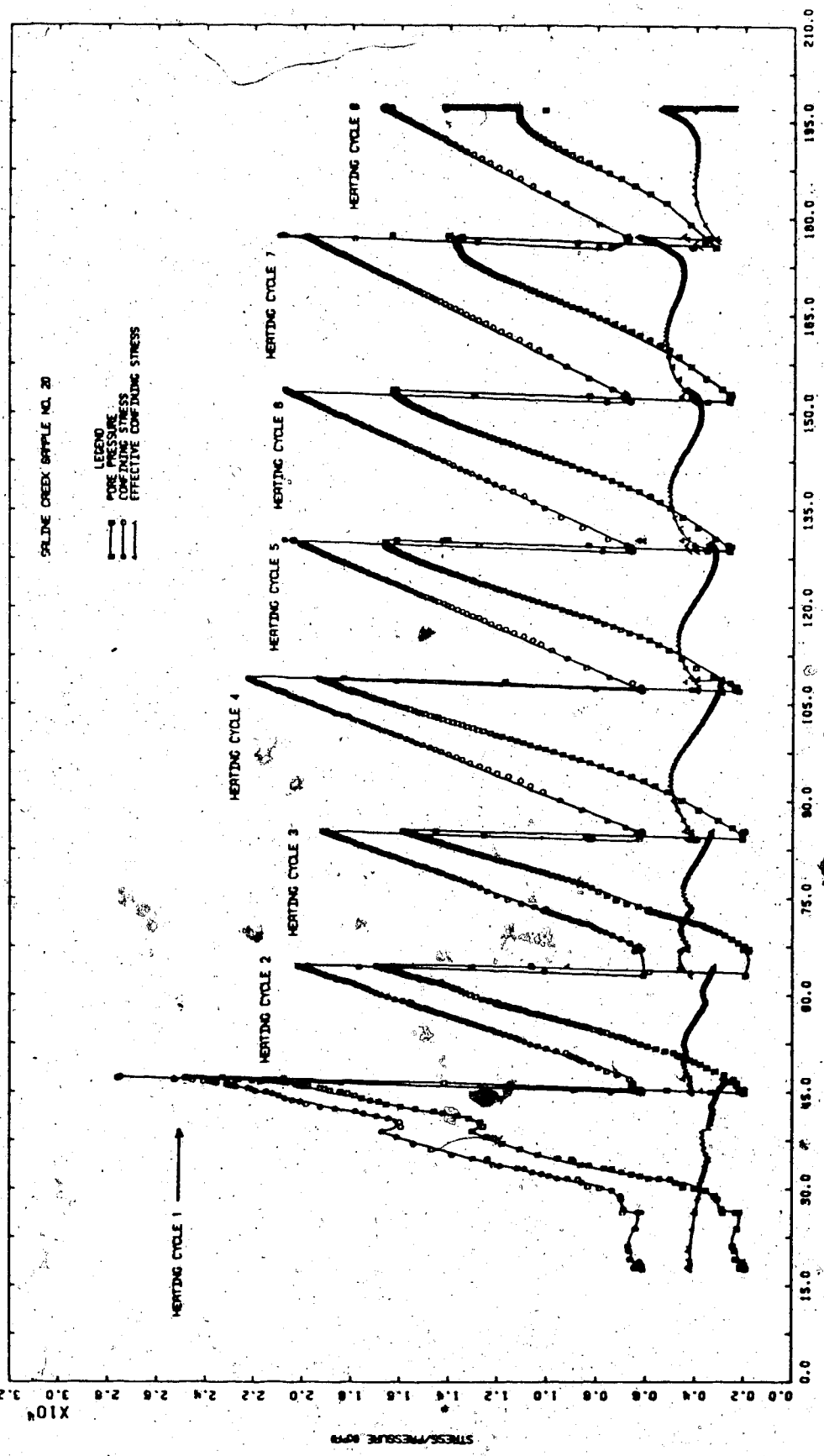

FIGURE E10.3 Triaxial Test TOS10: Pore Pressure and Confining Stress Changes With Temperature

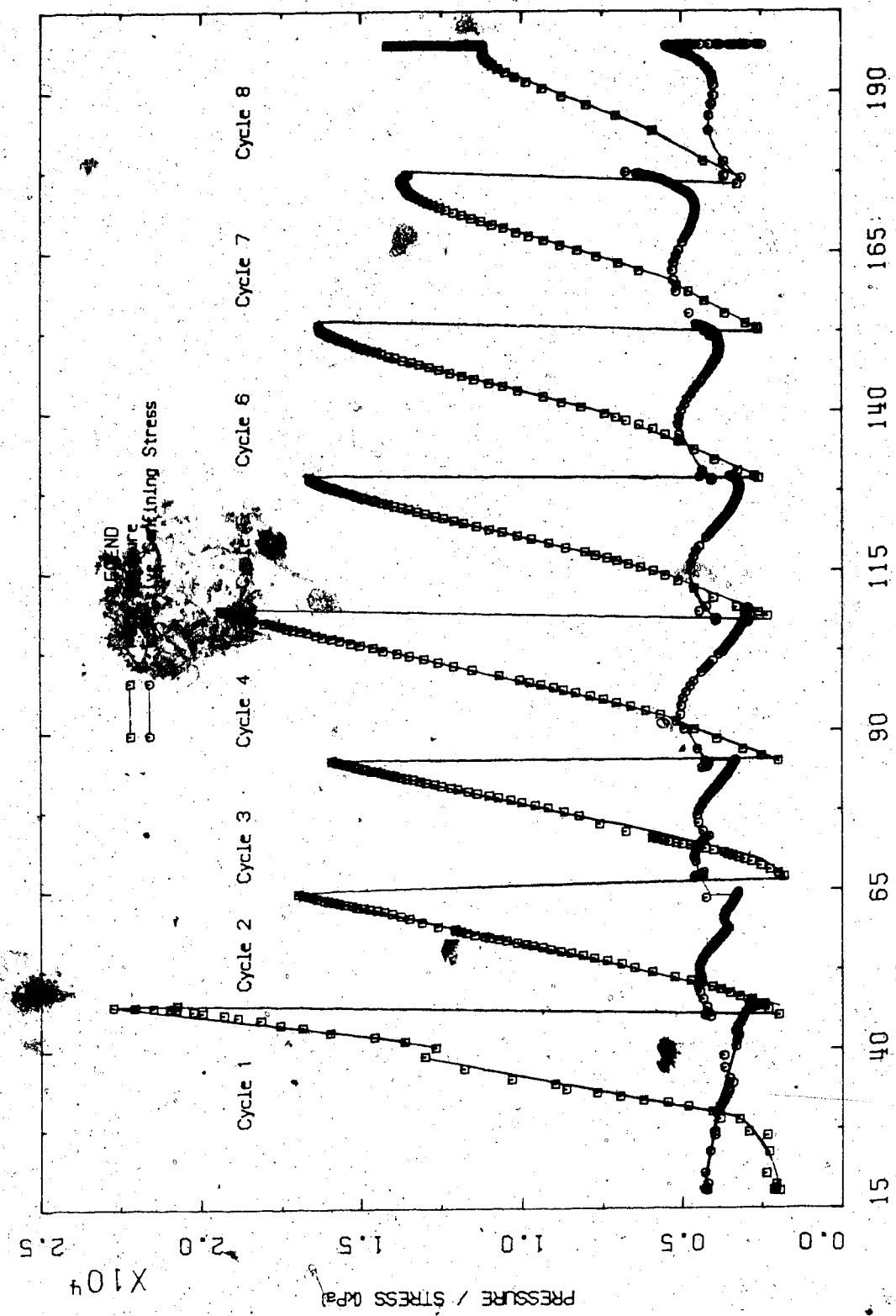

FIGURE E10.4 Triaxial Test TOS10: Pore Pressure Response to Undrained Heating

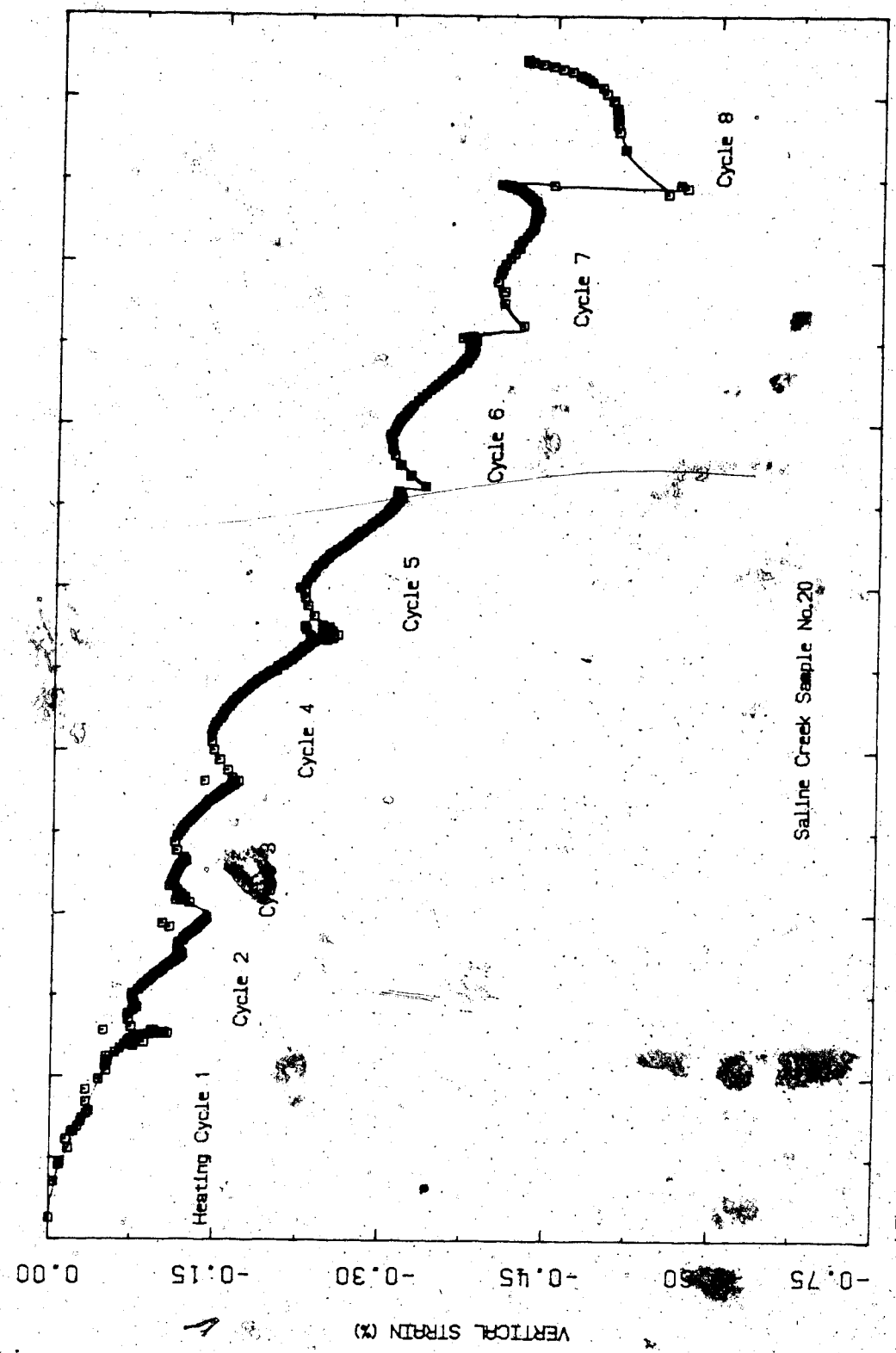

FIGURE E10.5 Triaxial Test TOS10: Vertical Strain During Heating

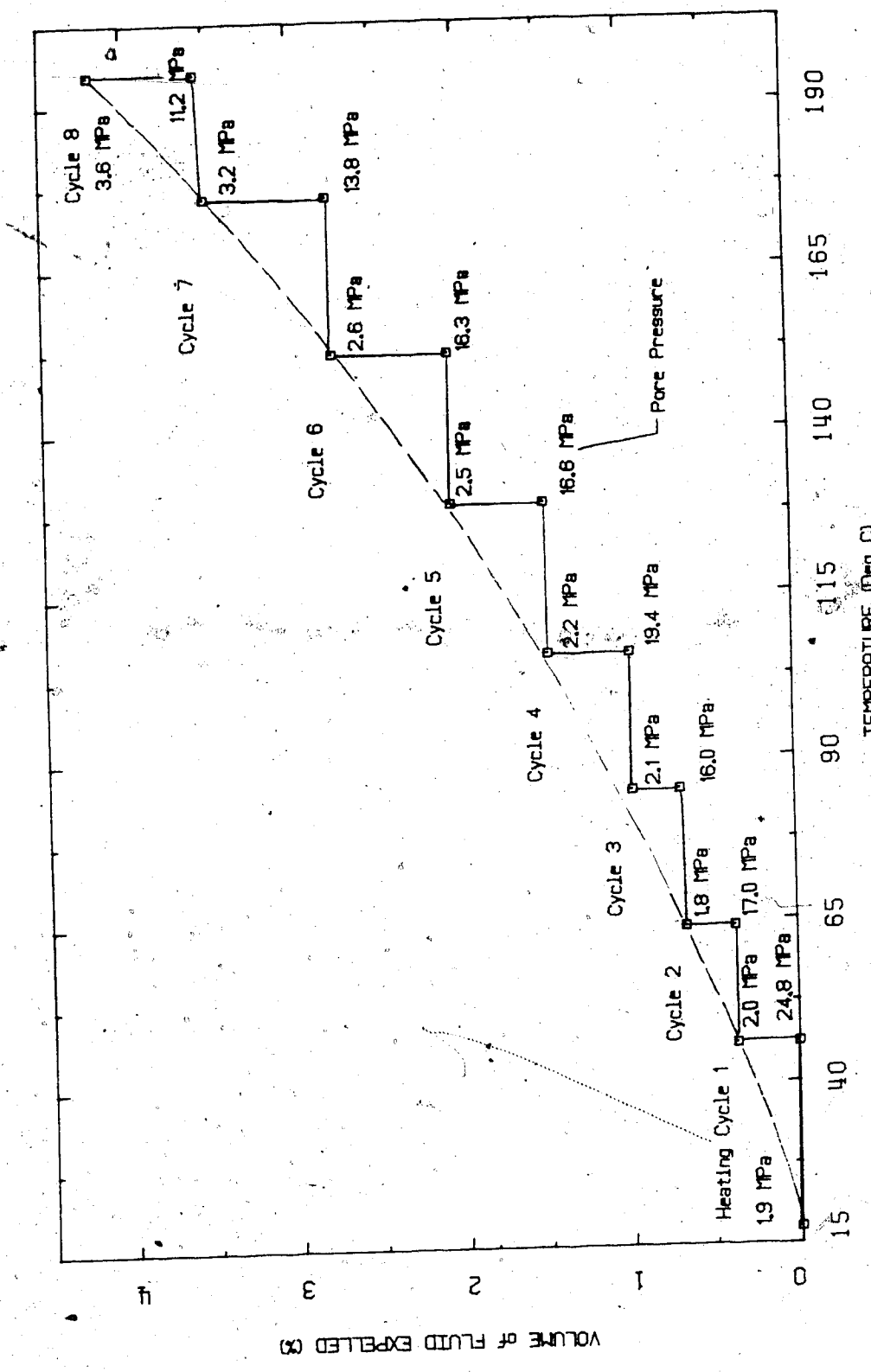

FIGURE E10.6 Triaxial Test TOS10: Volume of Fluid Expelled During Heating

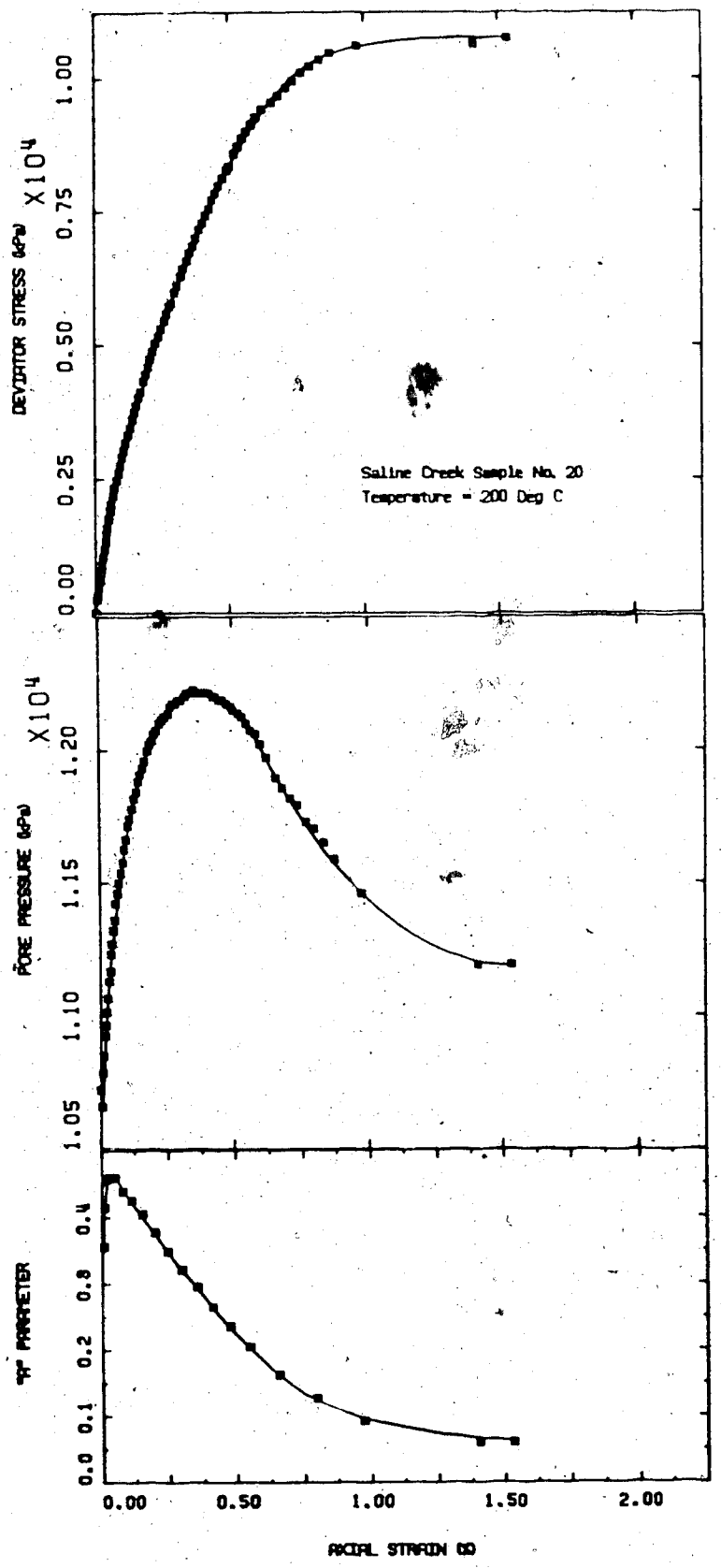

FIGURE E10.7 Triaxial Test TOS10: Deviator Stress and Undrained Pore Pressure Changes With

TEST TOS 11

Anisotropic Consolidation and Undrained Heating to Failure of Saline Creek Oil Sand Sample No. 22

Procedural Details: Test TOS 11

1. Sample 22 was thawed and back saturated for 22 hours under 10 MPa back pressure and 14 MPa isotropic confining stress.
2. Back pressure and confining stress were simultaneously reduced to 4 MPa and 8 MPa respectively.
3. A B-test was performed to evaluate degree of saturation over the range of confining stress 8 - 14.5 MPa.
4. Back pressure and isotropic confining stress were adjusted to 10 MPa and 14 MPa simultaneously.
5. Vertical compression stress was increased to 16 MPa. The sample was allowed to consolidate for approximately one hour under the ratio of horizontal to vertical effective stresses of 0.67.
6. Back pressure drainage valves were then closed. The apparatus and sample were heated slowly maintaining the vertical stress constant at 16 MPa and the horizontal stress constant at 14 MPa.

   Pore pressure and vertical (axial) strain were monitored during heating.
7. Heating was continued until shear failure (yielding) was observed at 101°C.

TEST TOS 11: SAMPLE DATA

Pretest Saline Creek Sample No. 22:

Dia.:	Ø	=	7.570 cm	w	=	0.025	
Height:	H	=	15.300 cm	B	=	0.185	
Area:	A	=	45.007 cm^2				
Volume:	V	=	688.60 ml	V_S	=	443.3 ml	
Mass:	M	=	1421 g	V_V	=	245.3 ml	
M_S:		=	1175 g	Dry Density	=	1.706 Mg/m^3	

Density: = 2.064 Mg/m^3
Porosity: = 0.356
Void Ratio: = 0.553 g

Sample 22 After Test TOS 11

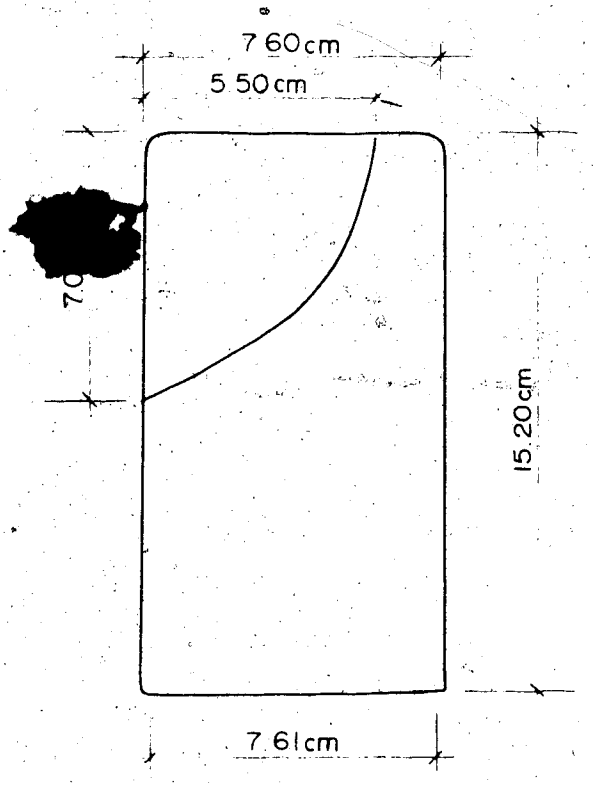

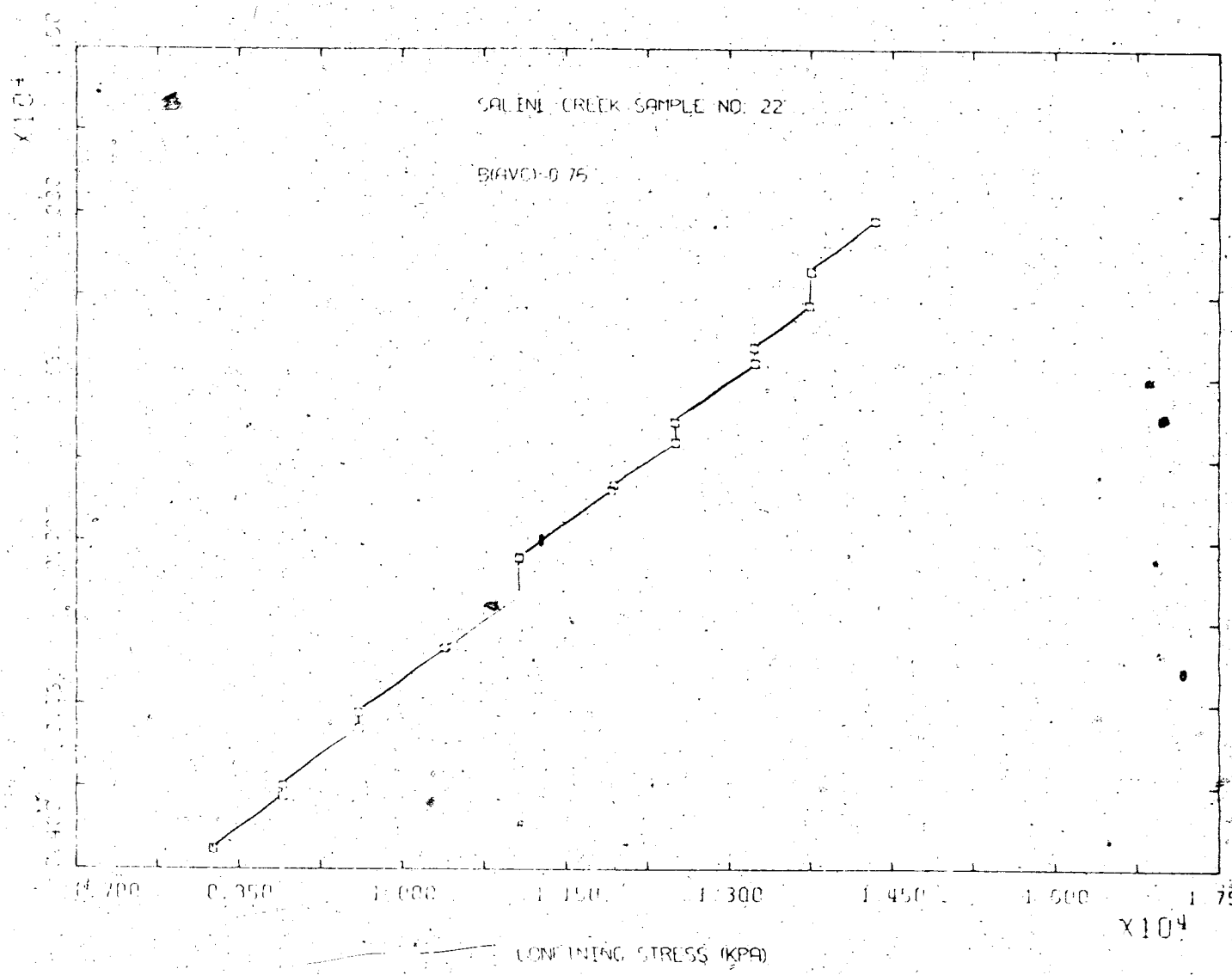

FIGURE 111.1 Triaxial Test TOS11: Modified B Test

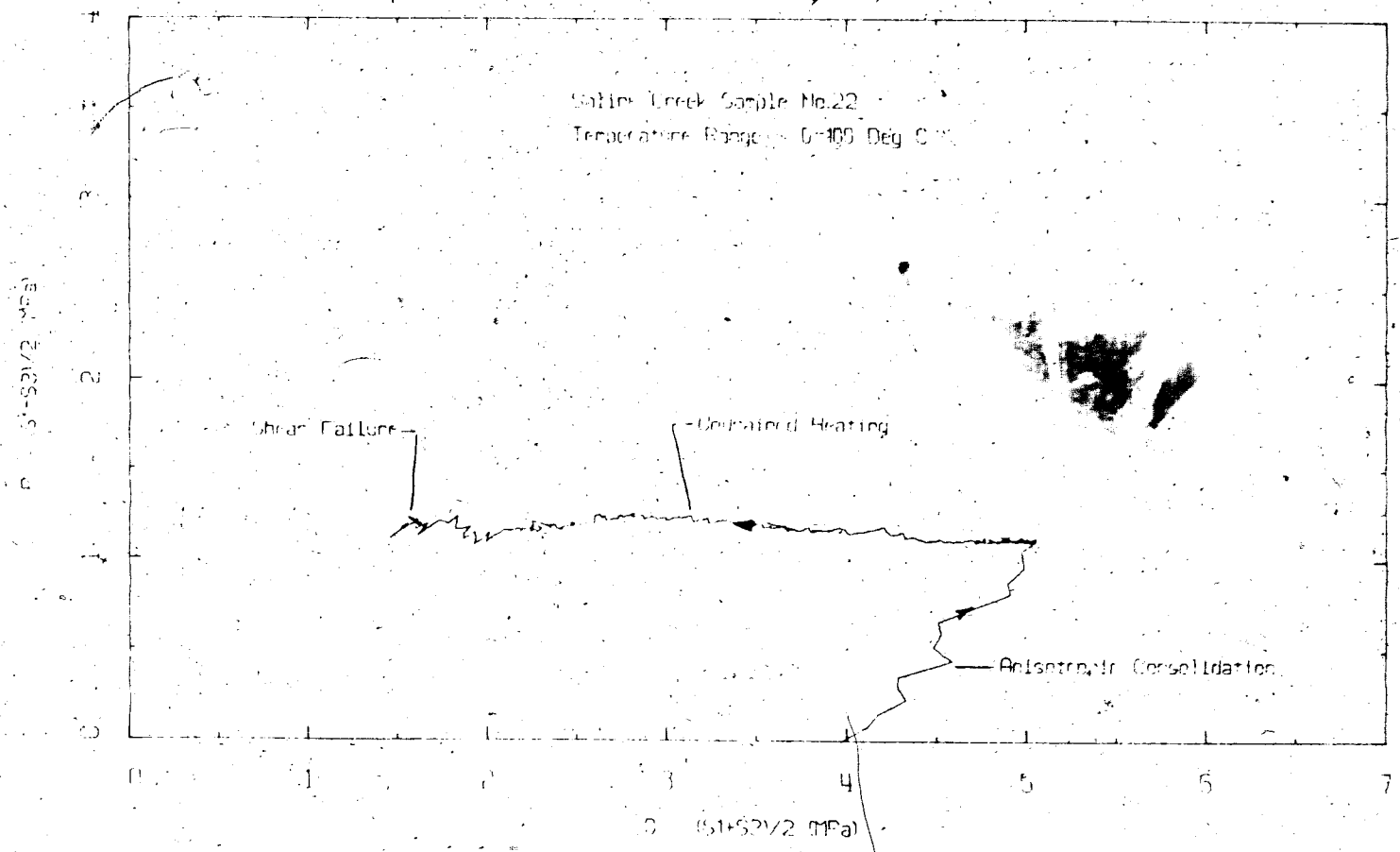

FIGURE E11.2 Triaxial Test TOS11: Stress Path

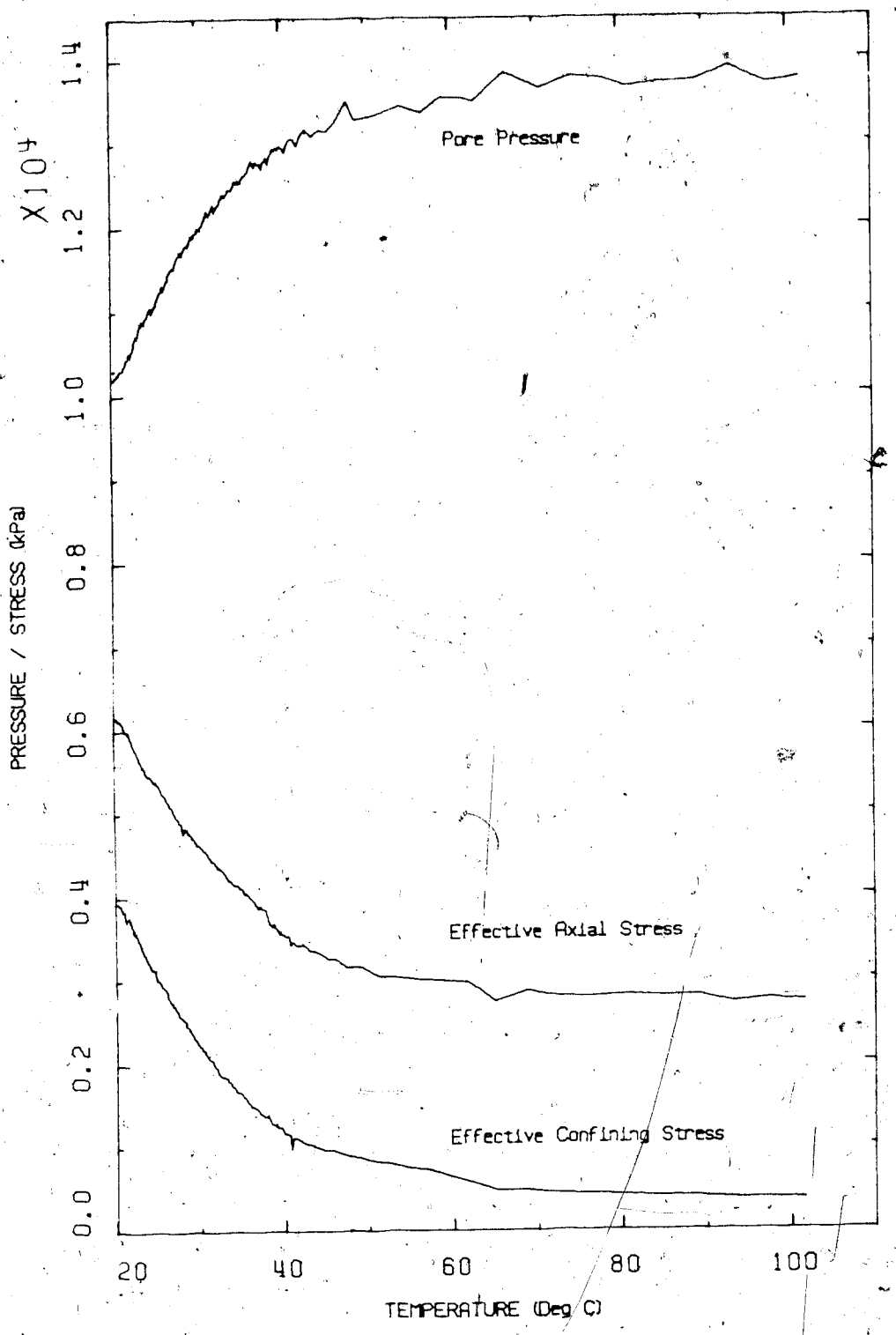

FIGURE E11.3 Triaxial Test TOS11: Pore Pressure and Effective Stress Changes During Undrained Heating

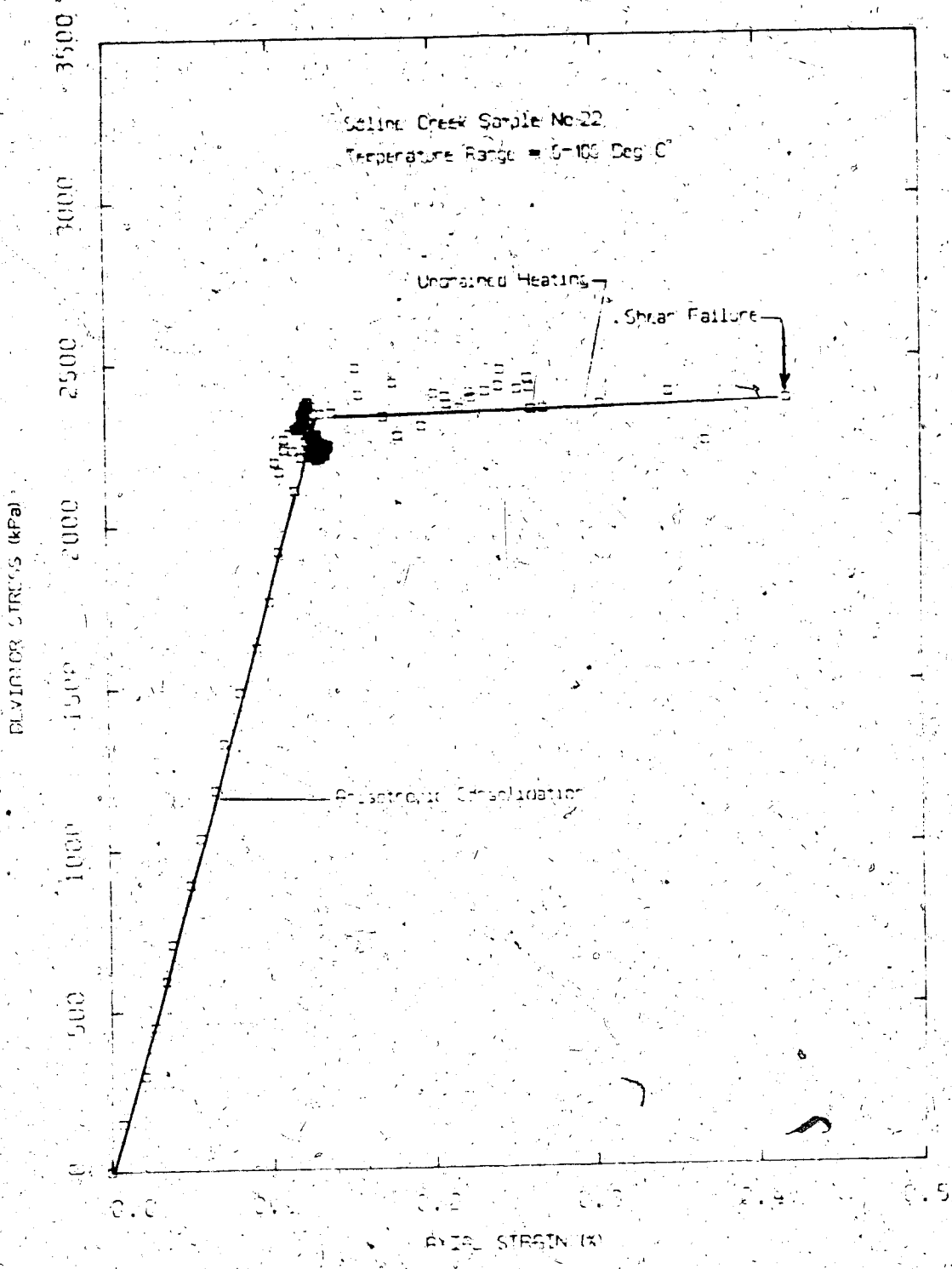

FIGURE E11.4 Triaxial Test TOS11: Deviator Stress Vs. Axial Strain

FIGURE E11.5 Triaxial Test TOS11: Pore Pressure Changes and Axial Strain During Undrained Heating

TEST TOS 12

Drained Isotropic Compression and Passive Triaxial Compression of Saline Creek Sample No. 29 at 200°C

Procedural Details: Test TOS 12

1. Sample 29 was thawed and back saturated for 22 hours under 10 MPa back pressure and 14 MPa isotropic confining stress.
2. The apparatus and sample were heated drained to 200°C and temperature allowed to stabilize for 16 hours. Vertical (axial) expansion was monitored during heating, however the volume change device was isolated during heating because of doubt about the durability of the triaxial membrane.
3. An isotropic compression test was performed over the effective stress range 4 - 17 MPa.
4. A drained passive triaxial compression test was also performed by increasing vertical stress at an average rate of 70 kPa/minute. Vertical deformation and volume change were monitored during the compression tests.

TEST TOS 12: SAMPLE DATA

Pretest Saline Creek Sample No. 29:

Dia.:	Ø	=	7.510 cm	w	=	0.010
Height:	H	=	14.837 cm	B	=	0.188
Area:	A	=	44.297 cm^2			
Volume:	V	=	657.23 ml	V_S	=	443.1 ml
Mass:	M	=	1375 g	V_V	=	224.1 ml
Mass Solids		=	1148 g	Dry Density	=	1.746 Mg/m^3

Density: = 2.092 Mg/m^3
Porosity: = 0.341
Void Ratio: = 0.517 g

Sample 29 After Test TOS 11

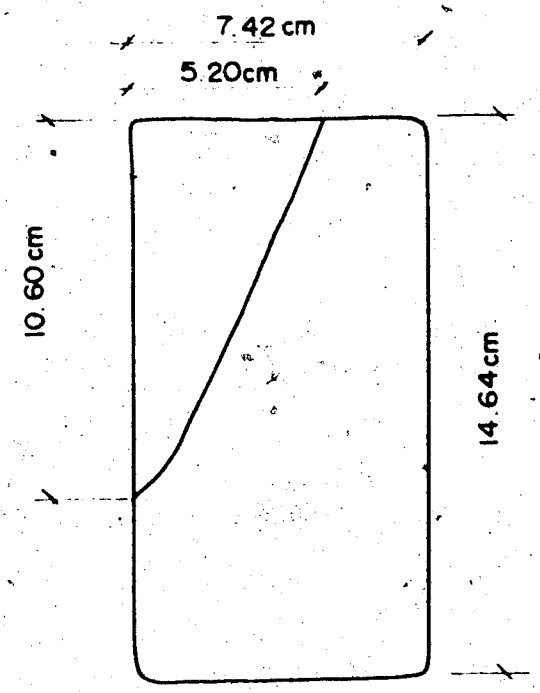

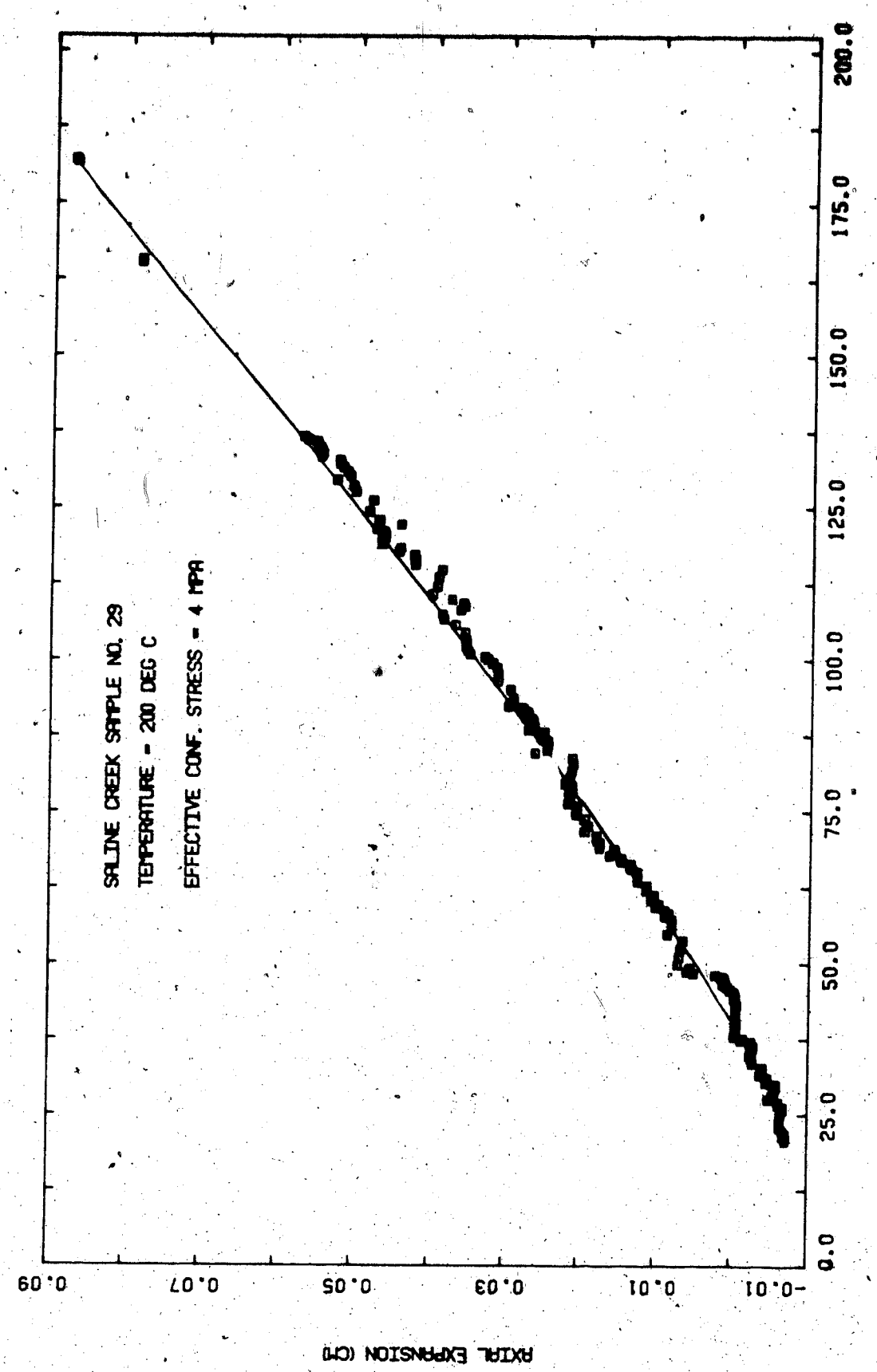

FIGURE E12.1 Triaxial Test TOS12: Axial Thermal Expansion

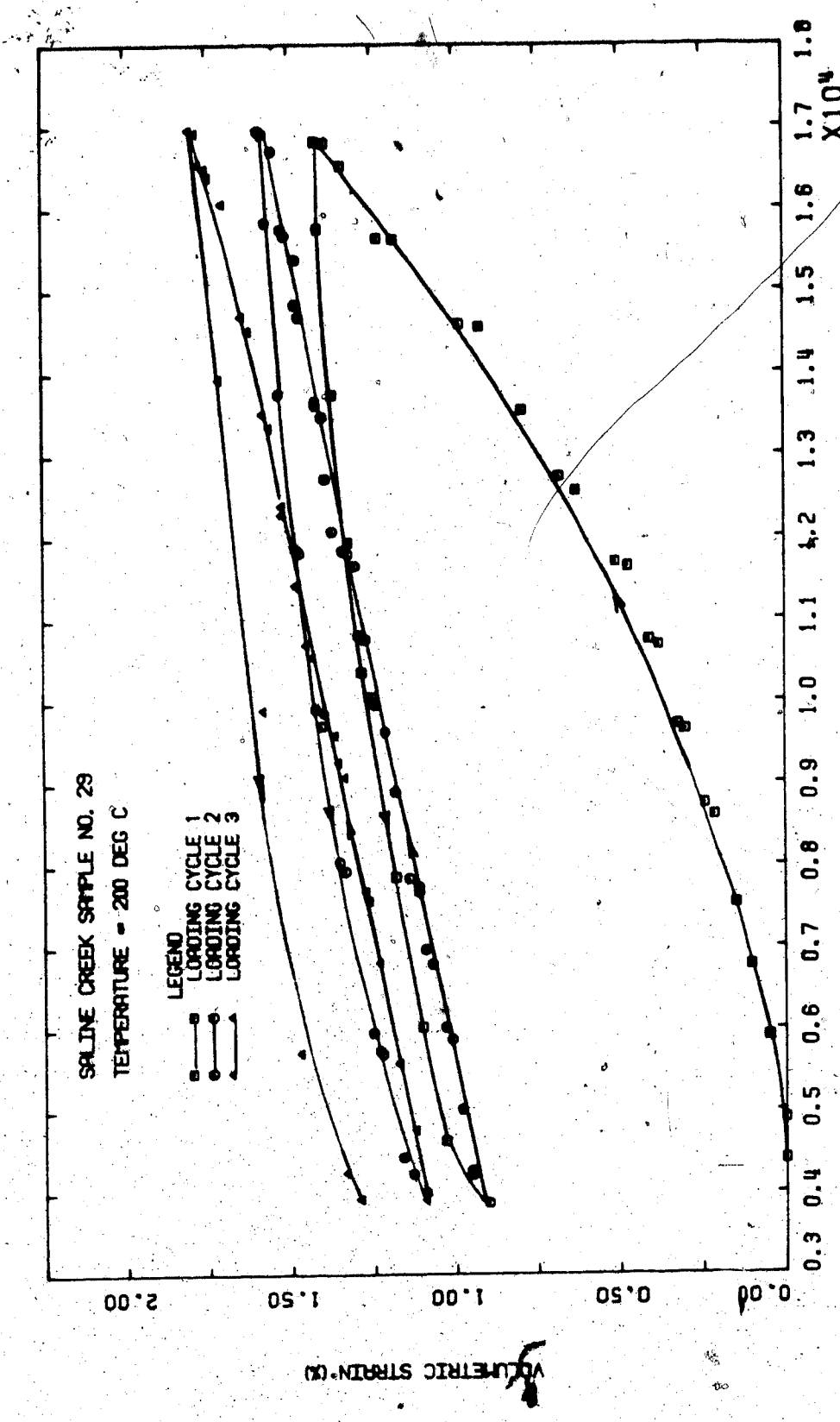

FIGURE E12.2 Triaxial Test TOS12: Drained Isotropic Compression

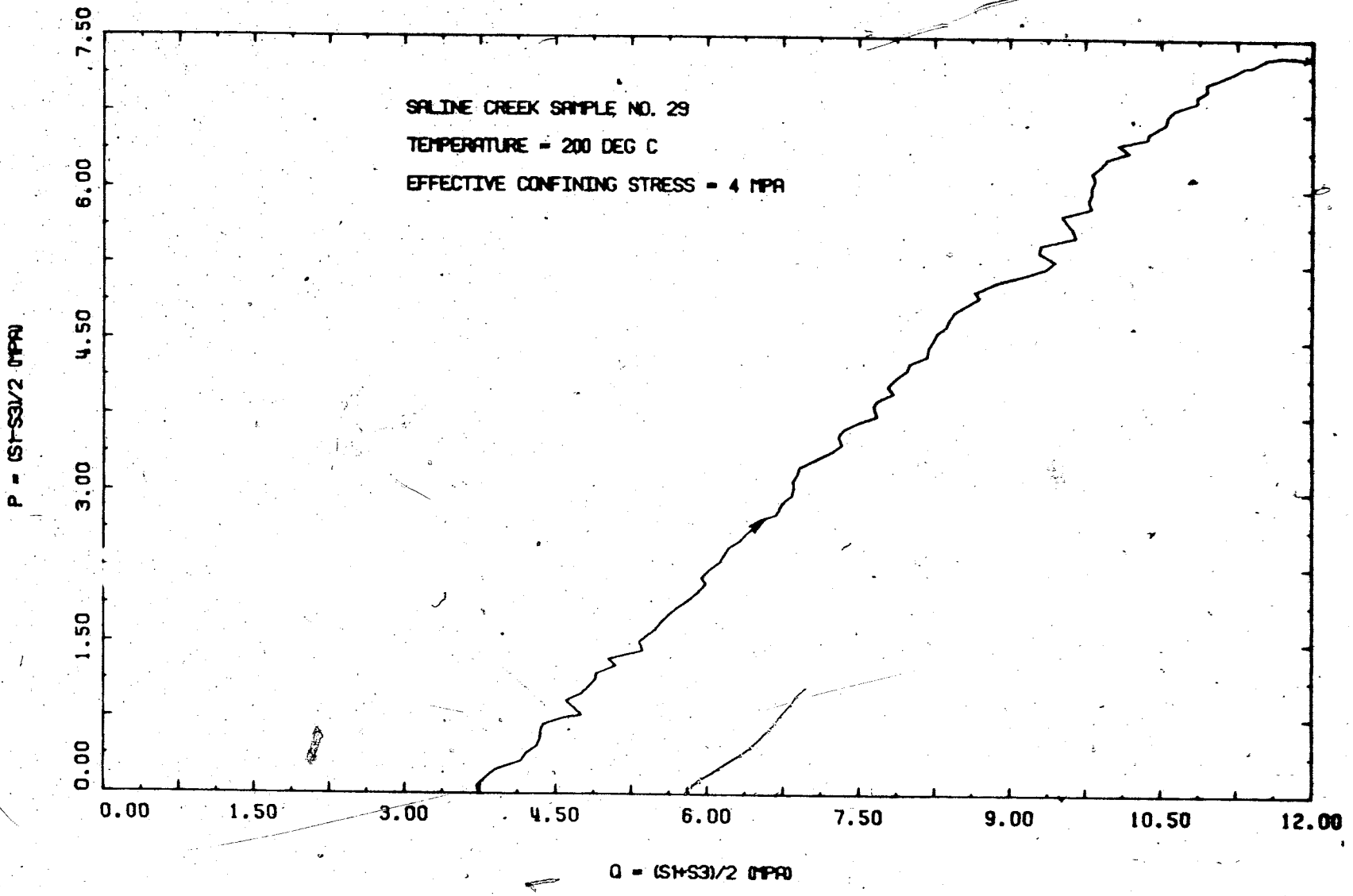

FIGURE 12.3 Triaxial Test TOS12: Stress Path

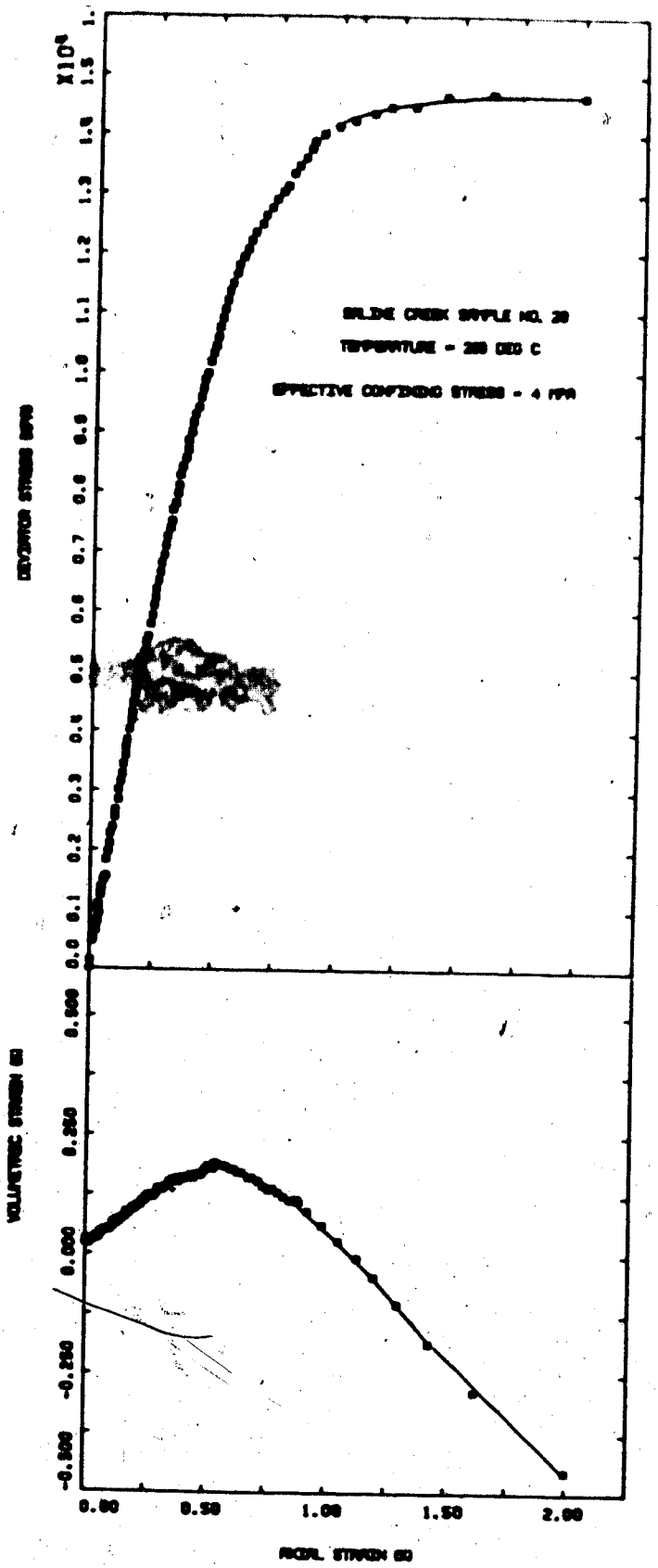

FIGURE E12.4 Triaxial Test TOS12: Deviator Stress Vs. Strain

TEST TOS 13

Thermal Expansion of Saline Creek Sample No. 26 - Membrane Meltdown at 240°C

Procedural Details: Test TOS 13

1. A fluorosilicone compound (Dow Corning RTV730) was applied as recommended by the manufacturer as a protective coating 3 mm thick over the surface of a silicone rubber membrane. It was anticipated that the fluorosilicone would inhibit chemical reaction between the silicone oil cell fluid and the silicone rubber membrane resulting in swelling and depolymerization of the rubber at temperatures above 200°C.
2. Saline Creek Sample 26 was thawed and back saturated under 10 MPa back pressure and 14 MPa isotropic confining stress.
3. The apparatus and sample were heated drained to 240°C at which temperature membrane meltdown occurred. The test was terminated.
4. Vertical (axial) expansion and volume change (i.e. volume of fluid expelled) were monitored during heating.

TEST TOS 13: SAMPLE DATA

Pretest Saline Creek Sample No. 26:

Dia.:	Ø	=	7.620 cm	w	=	0.036
Height:	H	=	15.300 cm	B	=	0.132
Area:	A	=	45.604 cm^2			
Volume:	V	=	697.74 ml	V_S	=	468.9 ml
Mass:	M	=	1451 g	V_V	=	228.6 ml
Mass Solids		=	1243 g	Dry Density	=	1.781 Mg/m^3

Density: = 2.080 Mg/m^3
Porosity: = 0.328 .
Void Ratio: = 0.488 g

Sample 26 After Test TOS 13

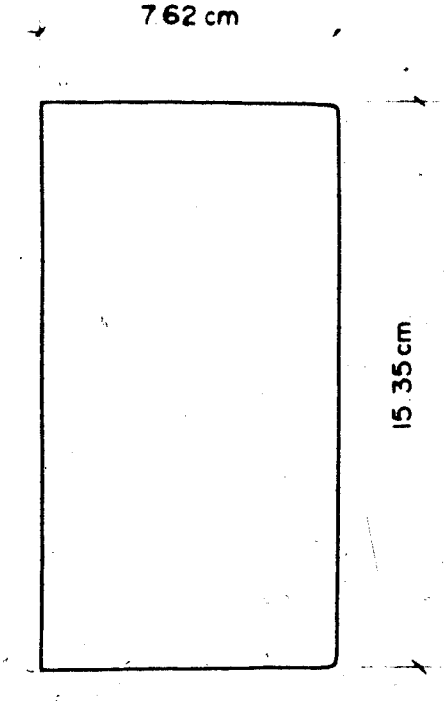

No Visible Deformation

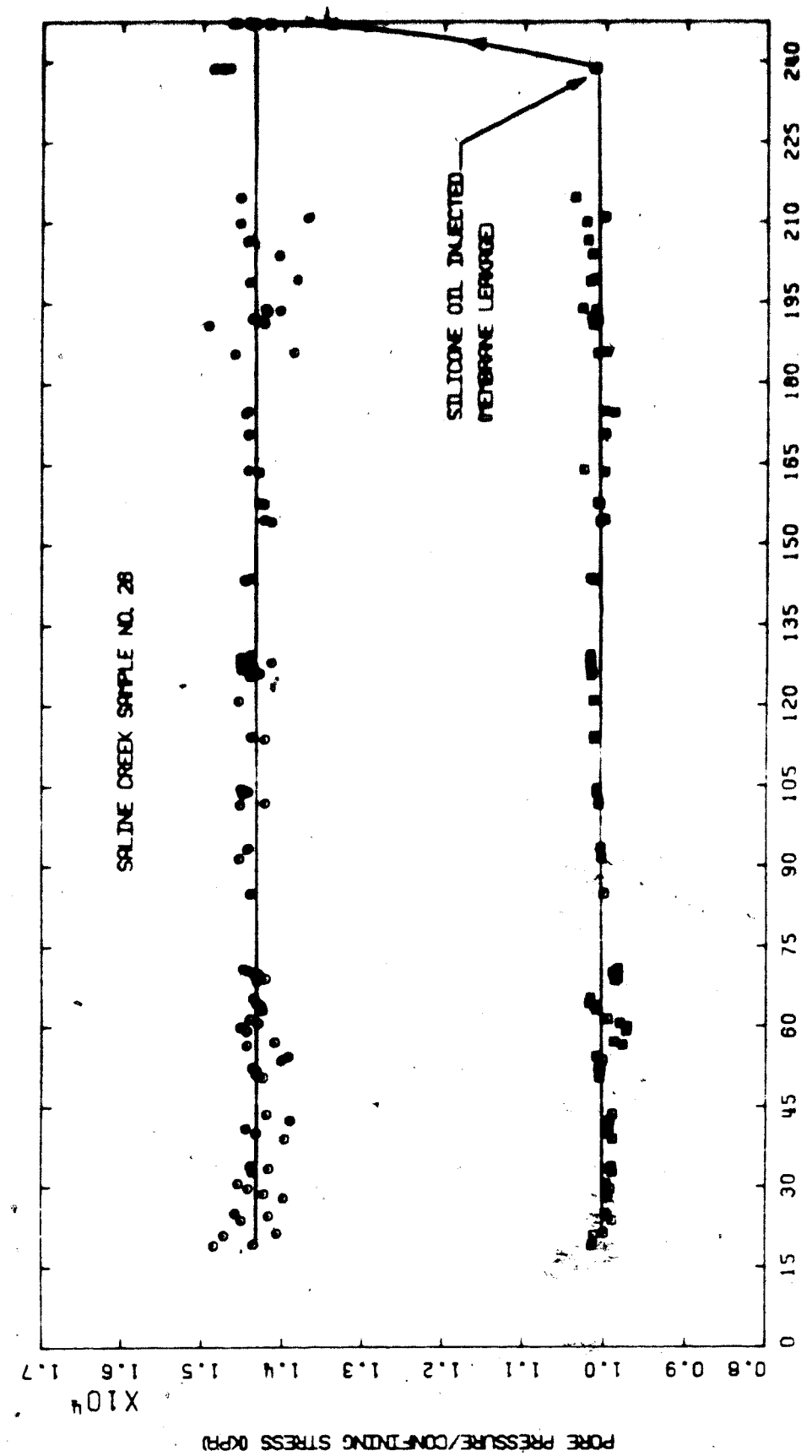

FIGURE 113.1 Triaxial Test TOS13: Pore Pressure and Confining Stress Vs. Temperature

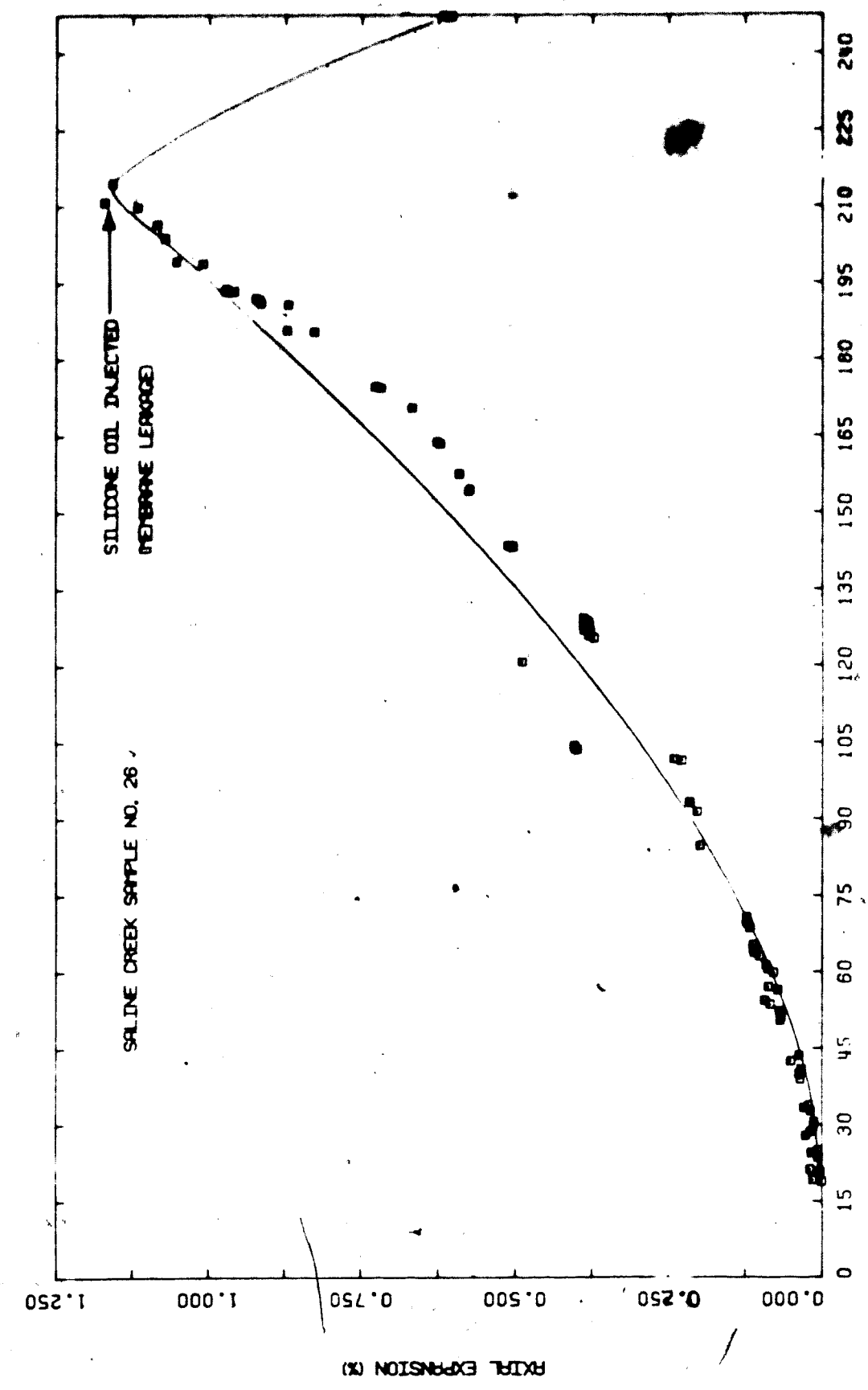

FIGURE E13.2 Triaxial Test TOS13: Axial Thermal Expansion

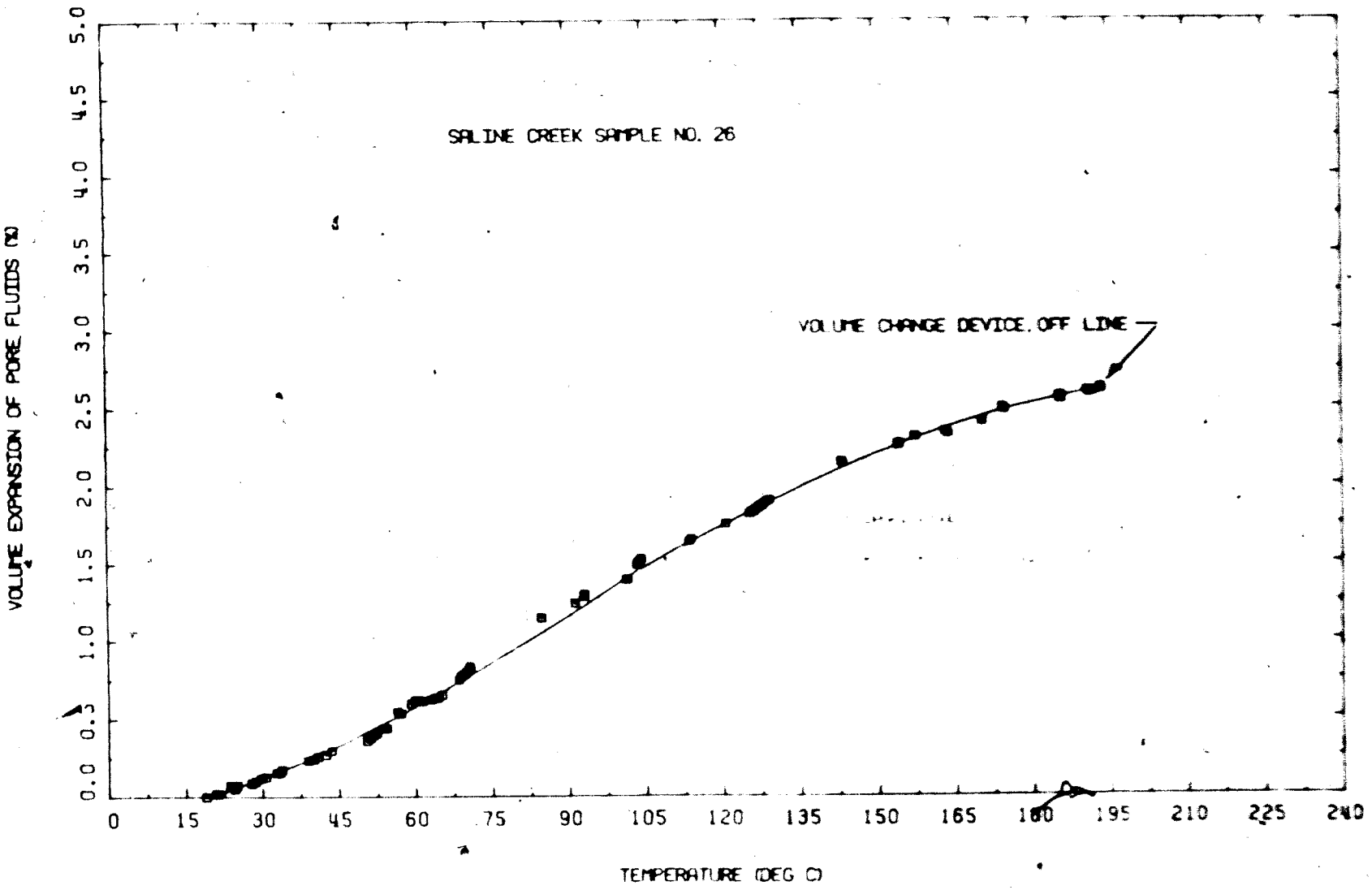

FIGURE E13.3 Triaxial Test 70513: Volume of Pore Fluid Expelled During Heating

TEST TOS 14

Multistage Triaxial Compression of Remoulded Saline Creek Oil Sand: Combined Samples 5, 7, and 8

Procedural Details: Test TOS 14

1. Pieces of Saline Creek samples 5, 7, and 8 were permitted to thaw, then remoulded and mixed by kneeding. The remoulded material was then placed in layers inside a steel split-ring cylindrical mould 7.58 cm in diameter. The material was compacted in 5 layers, each approximately 3 cm thick, using 30 blows per layer of a Modified Proctor compaction drop hammer. The compacted sample and mould were then placed in a freezer at -20°C for 48 hours.
2. The remoulded frozen oil sand sample was removed from the split-ring mould and mounted in the triaxial cell using procedures similar to those for undisturbed samples.
3. The sample was thawed and back saturated for 20 hours under a back pressure of 2 MPa and under 4 MPa isotropic confining stress.
4. A three stage, drained passive compression test was performed at room temperature with the back pressure maintained constant at 2 MPa. Vertical compressive stress was increased at an average rate of 55 kPa/minute. Three peak deviatoric stress levels were defined corresponding to effective confining stresses of 2 MPa, 4 MPa and 8 MPa.

5. After the triaxial compression test, the apparatus and sample were heated to test the durability of the rubber membrane, formed from a silicone elastomer (Dow Corning Sylgard 170). This rubber cures by an addition reaction when components A and B are mixed. The manufacturer had recommended this product as an alternate to silicone rubber. The membrane decomposed between 100°C and 120°C.

TEST TOS 14: SAMPLE DATA

Pretest Remoulded and Compacted Oil Sand Sample From Saline Creek Samples 5, 7 and 8:

Dia.:	Ø	=	7.576 cm	w	=	0.017
Height:	H	=	15.238 cm	B	=	0.187
Area:	A	=	45.079 cm^2			
Volume:	V	=	686.91 ml	V_S	=	398.3 ml
Mass:	M	=	1270 g	V_V	=	288.6 ml
Mass Solids		=	1055 g	Dry Density	=	1.537 Mg/m^3

Density: = 1.850 Mg/m^3
Porosity: = 0.418
Void Ratio: = 0.718 g

Remoulded Sample After Test TOS 14

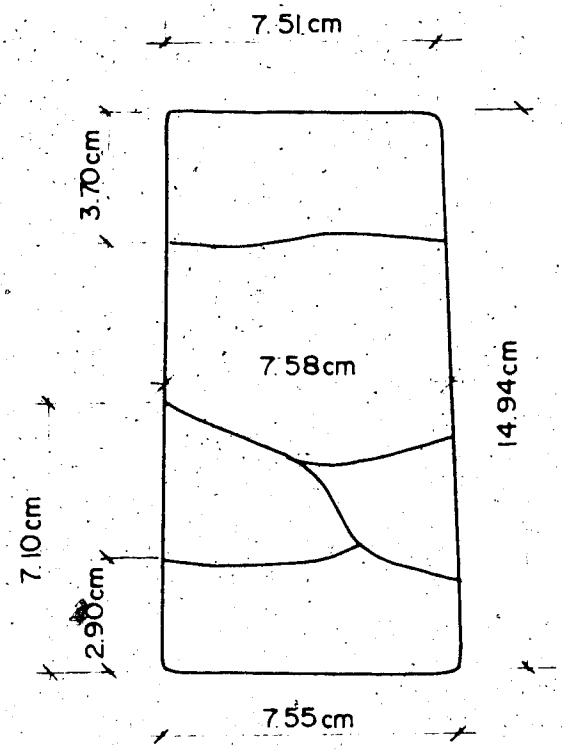

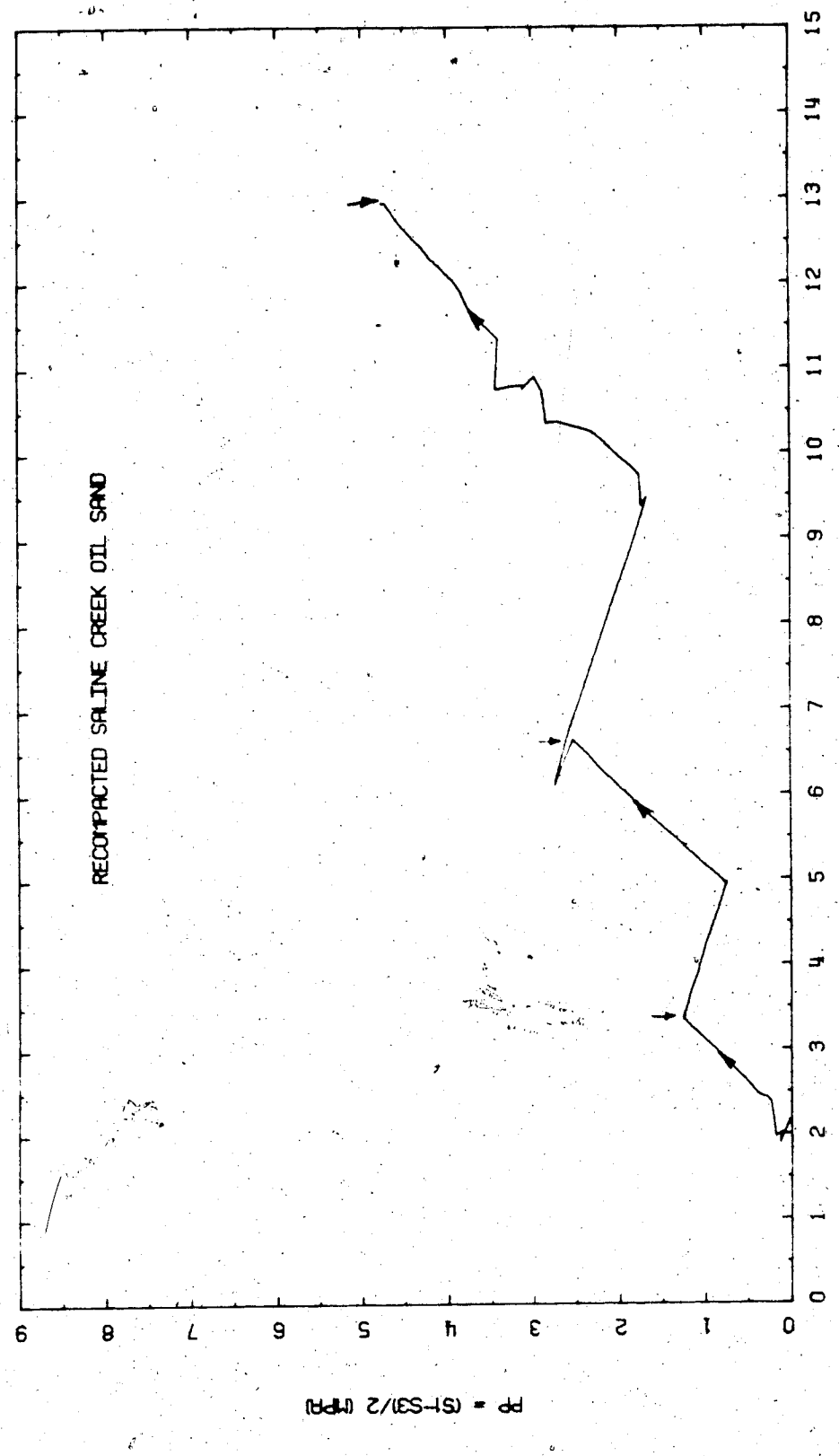

FIGURE E14.1 Triaxial Test TOS14: Three Stage Stress Path

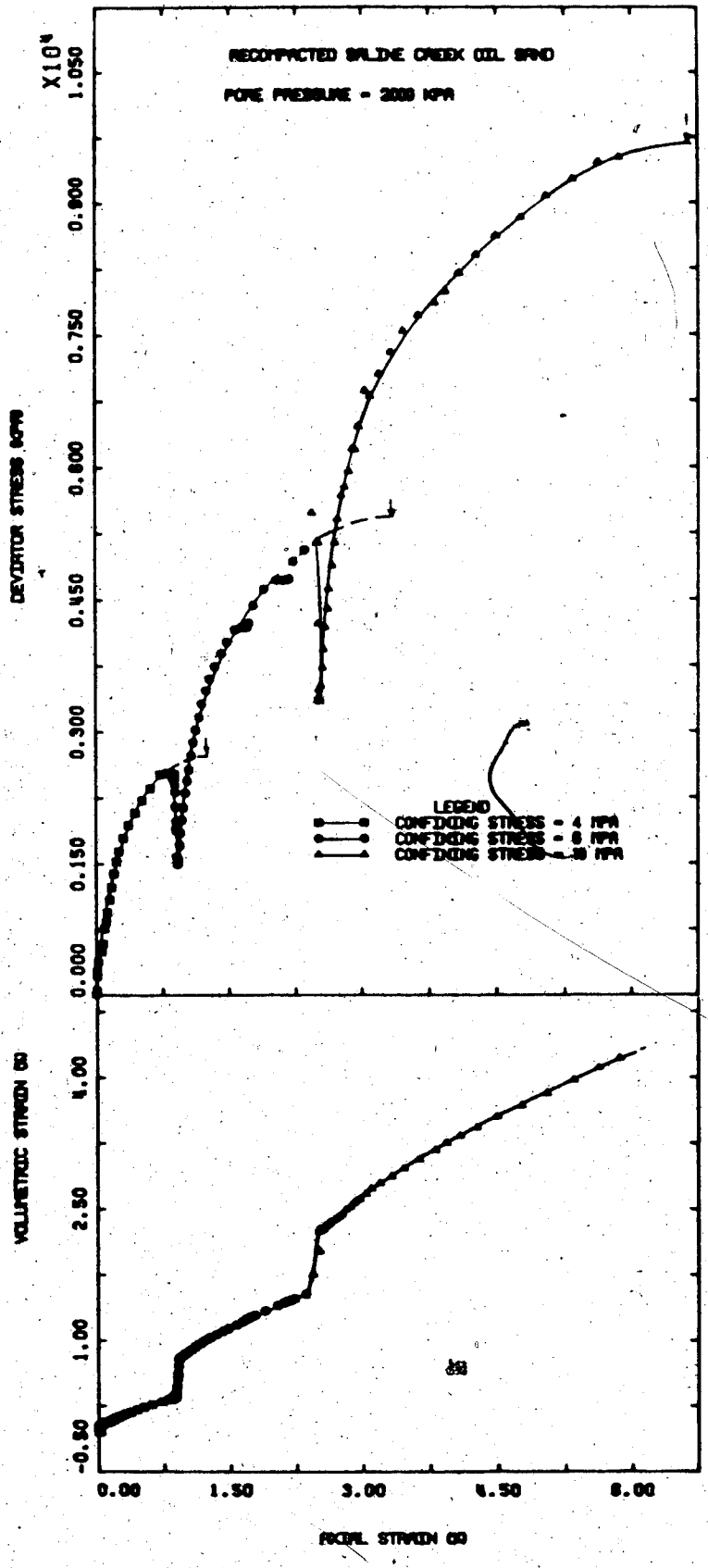

FIGURE E14.2 Triaxial Test TOS14: Deviator Stress Vs. Strain

TEST TOS 15

Isotropic Compression and Passive Triaxial Compression of Cold Lake Oil Sand Sample 12B at 200°C

Procedural Details: Test TOS 15

Note: Cold Lake oil sand sample 12B was a frozen core sample taken from the Clearwater Formation (depth 400 m) at Esso's Leming pilot project at Cold Lake in 1978.

1. Sample 12B was thawed and back saturated for 22 hours at 10 MPa back pressure and 14 MPa isotropic confining stress.
2. The apparatus and sample were heated to 200°C drained, i.e. at 10 MPa constant back pressure. Volume change (i.e. volume of pore fluid expelled) was monitored during heating.
3. The temperature was allowed to stabilize for 16 hours, then the sample was subjected to three cycles of isotropic compression over the effective stress range 4 - 17 MPa.
4. A drained triaxial passive compression test was performed by increasing vertical compressive stress at an average rate of 75 kPa/minute while maintaining the back pressure and horizontal confining stress constant at 10 MPa and 14 MPa respectively.
5. Pore pressure response to undrained heating was determined above 200°C. This was carried out, in part, to test the durability of a silicone rubber membrane coated with 4 to 5 mm of fluorosilicone (Dow Corning RTV730) rubber compound. The membrane depolymerized and began to leak at about 235°C. The test was terminated at 245°C.

TEST TOS 15: SAMPLE DATA

Pretest Cold Lake Oil Sand Sample 12B:

Dia.:	Ø	=	7.500 cm	w	=	0.056
Height:	H	=	15.000 cm	B	=	0.146
Area:	A	=	44.179 cm^2			
Volume:	V	=	662.68 ml	V_S	=	408.8 ml
Mass:	M	=	1302 g	V_V	=	253.9 ml
Mass Solids	=		1083 g	Dry Density	=	1.635 Mg/m^3

Density: = 1.965 Mg/m^3
Porosity: = 0.383
Void Ratio: = 0.621 g

Cold Lake Sample 12B After Test TOS 15

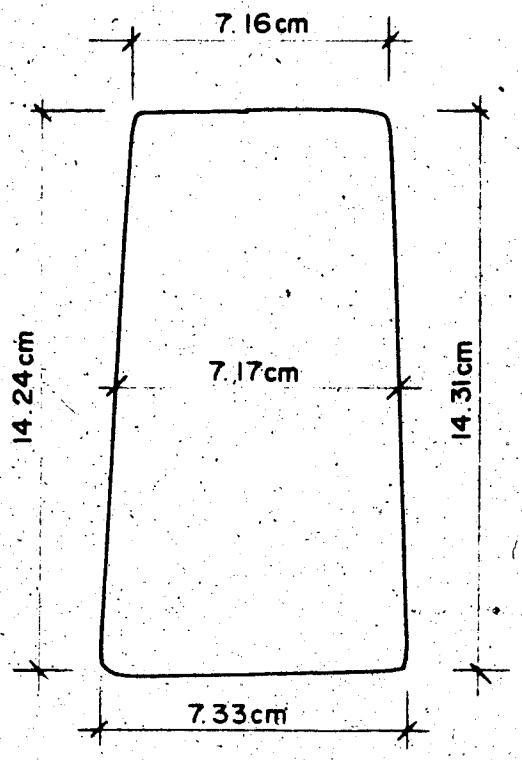

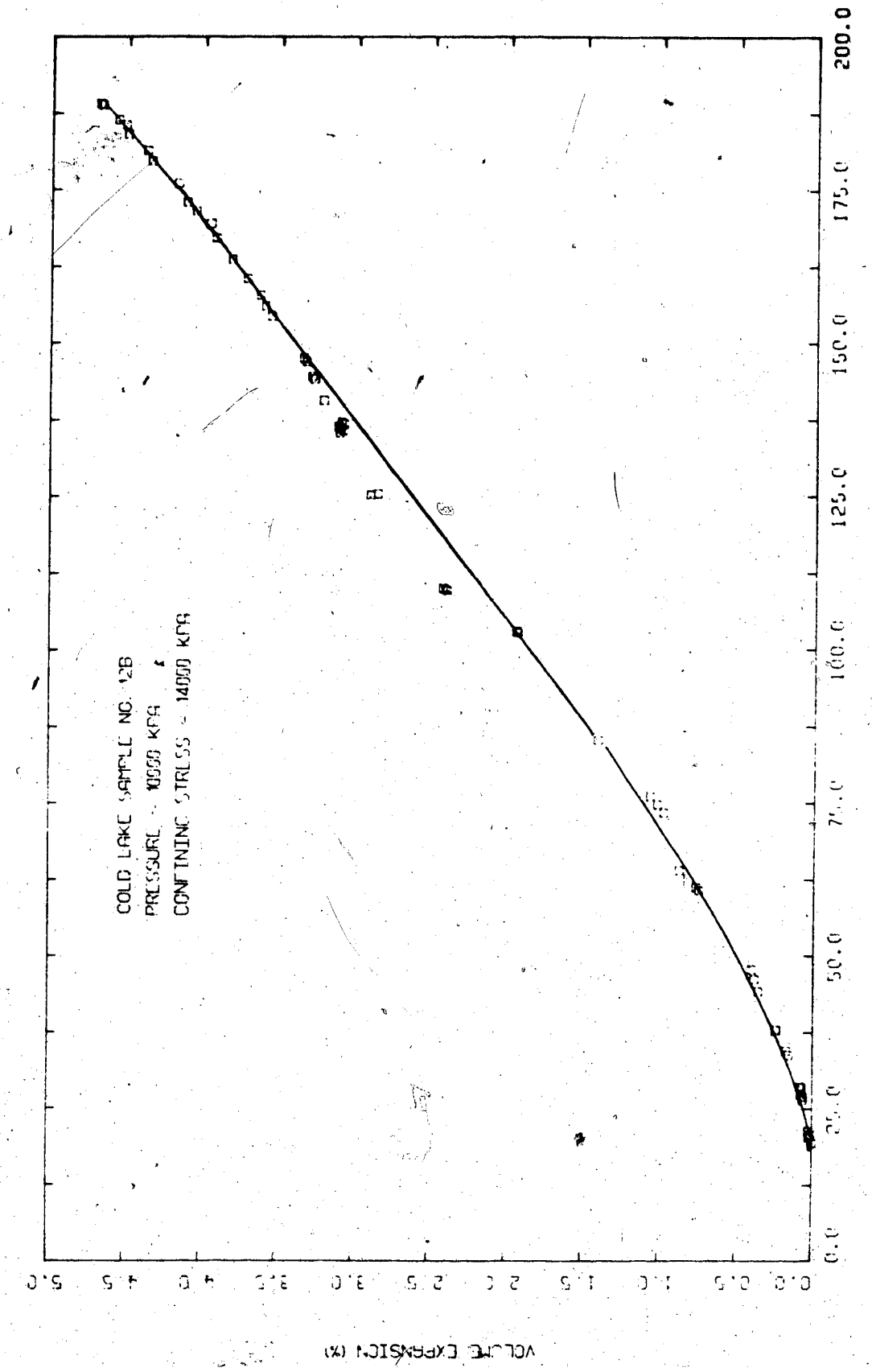

FIGURE E15.1 Triaxial Test TOS15: Volume of Pore Fluid Expelled During Heating

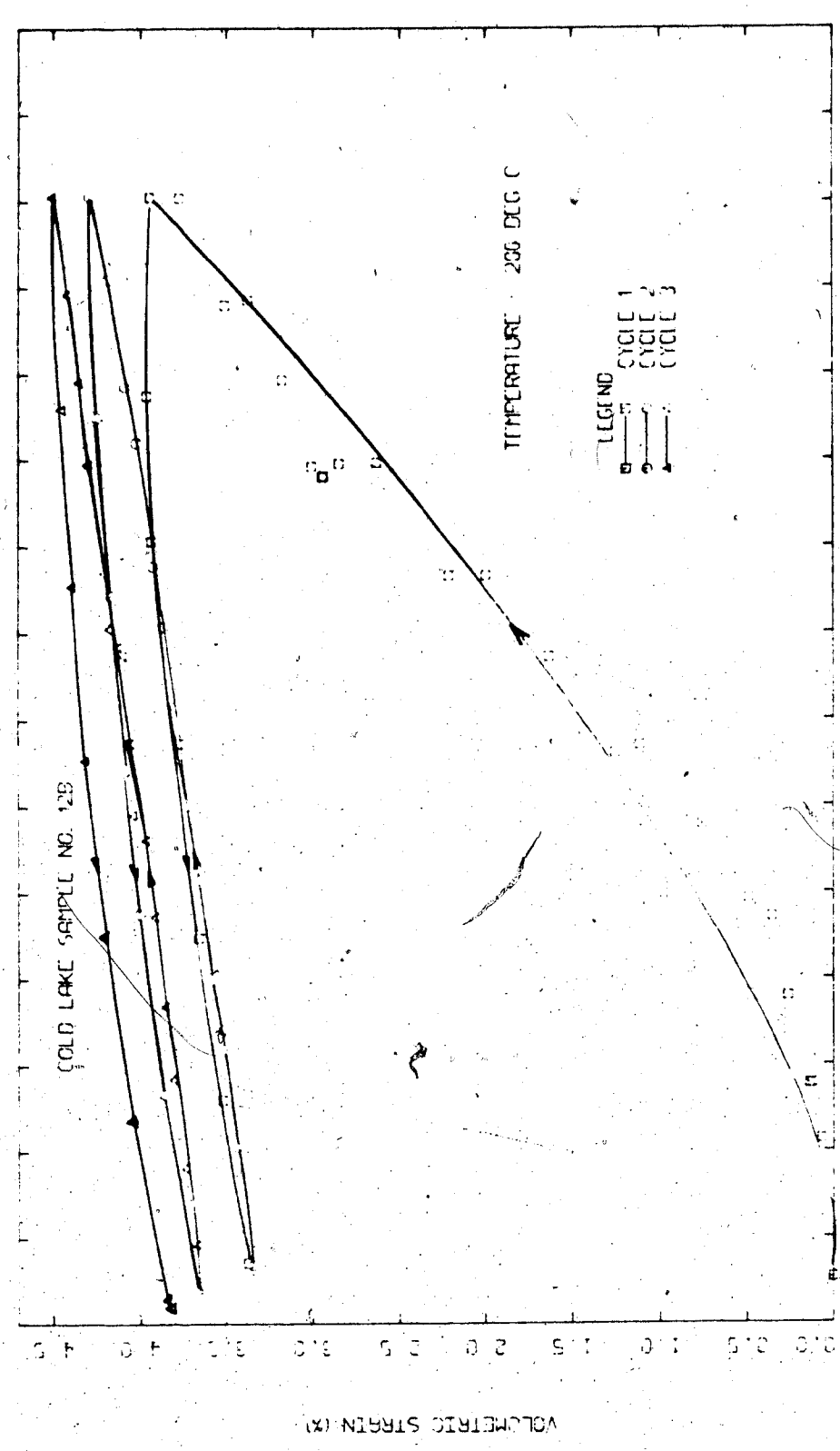

FIGURE E15.2 Triaxial Test TOS15: Drained Isotropic Compression

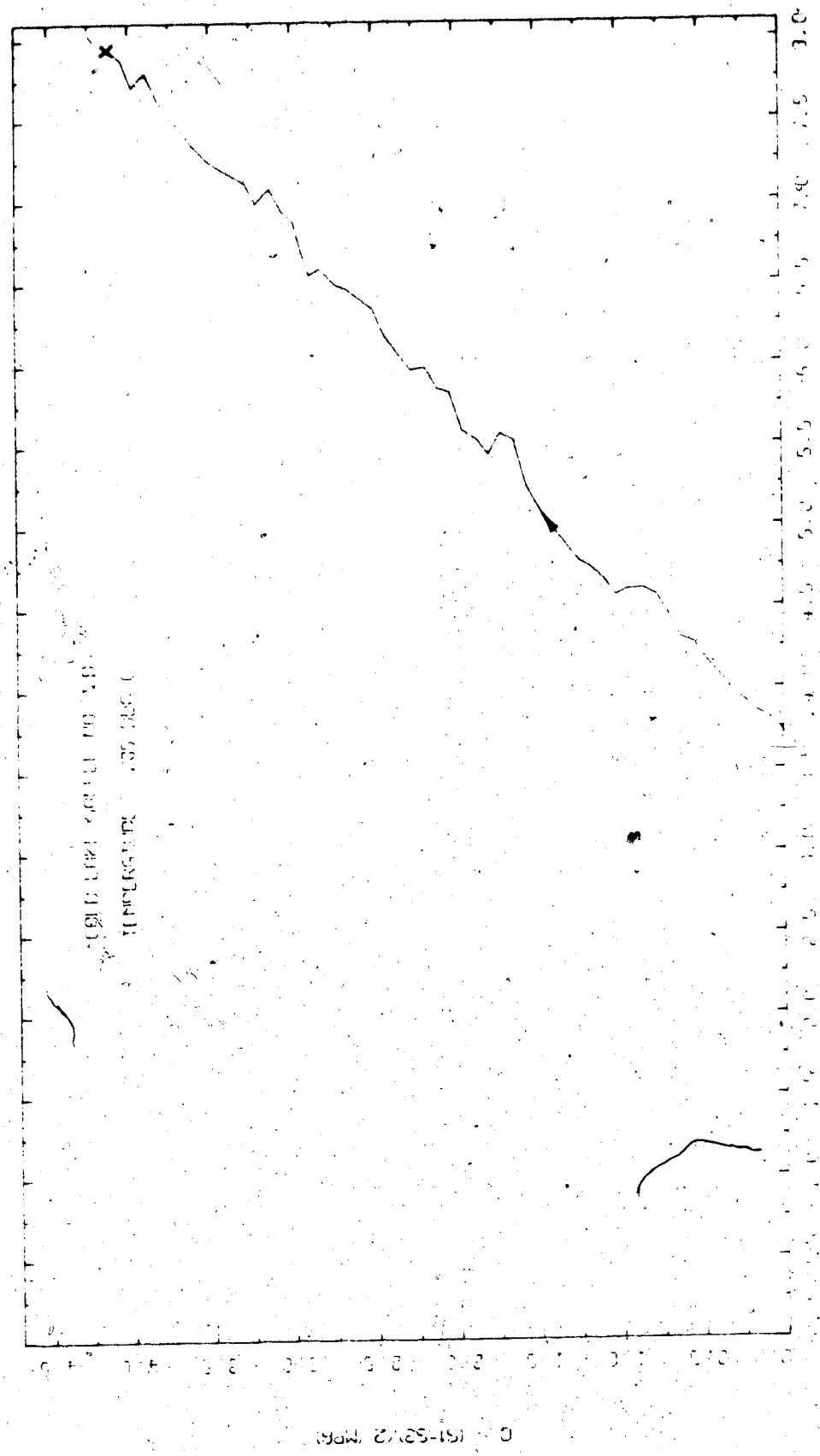

FIGURE E15.3 Triaxial Test TOS15: Stress Path

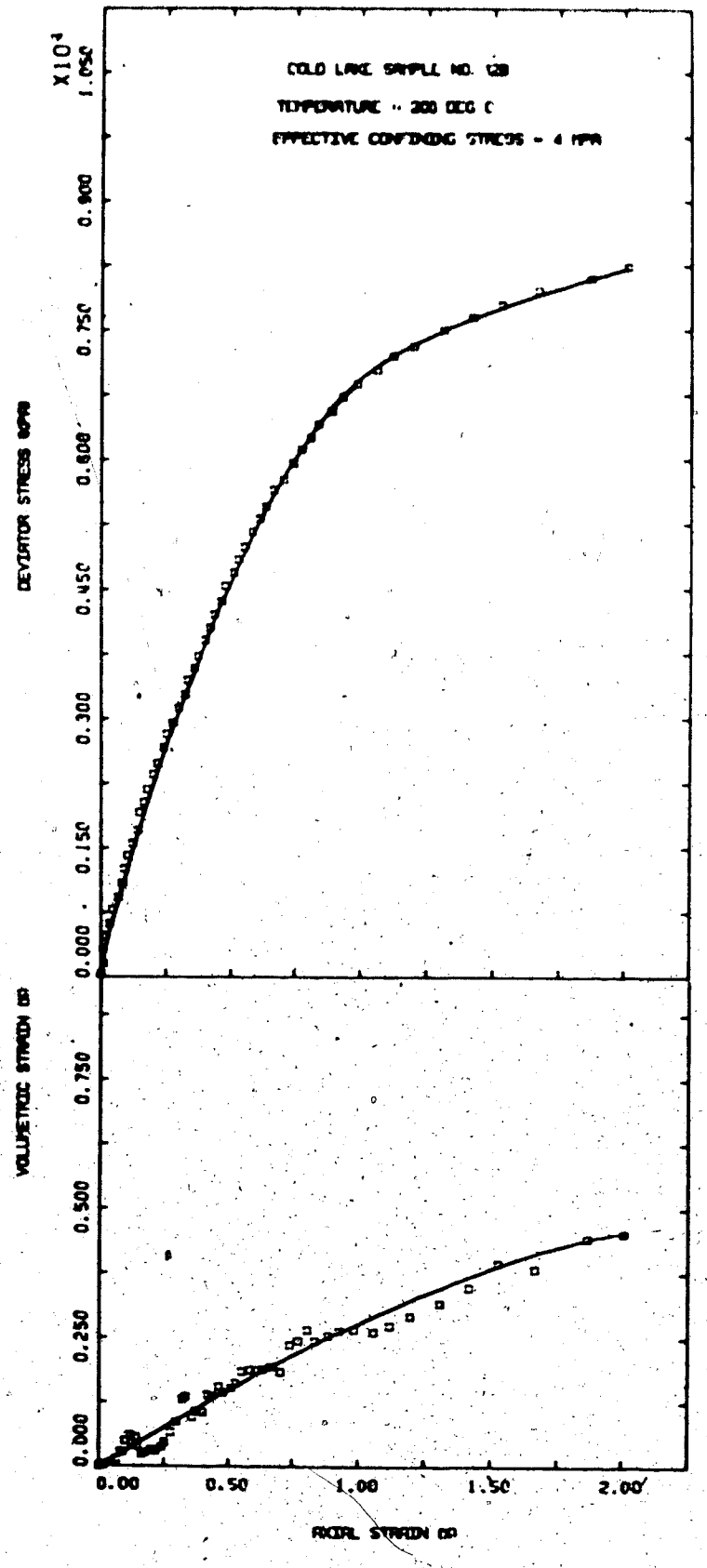

FIGURE E15.4 Triaxial Test TOS15: Deviator Stress Vs. Strain

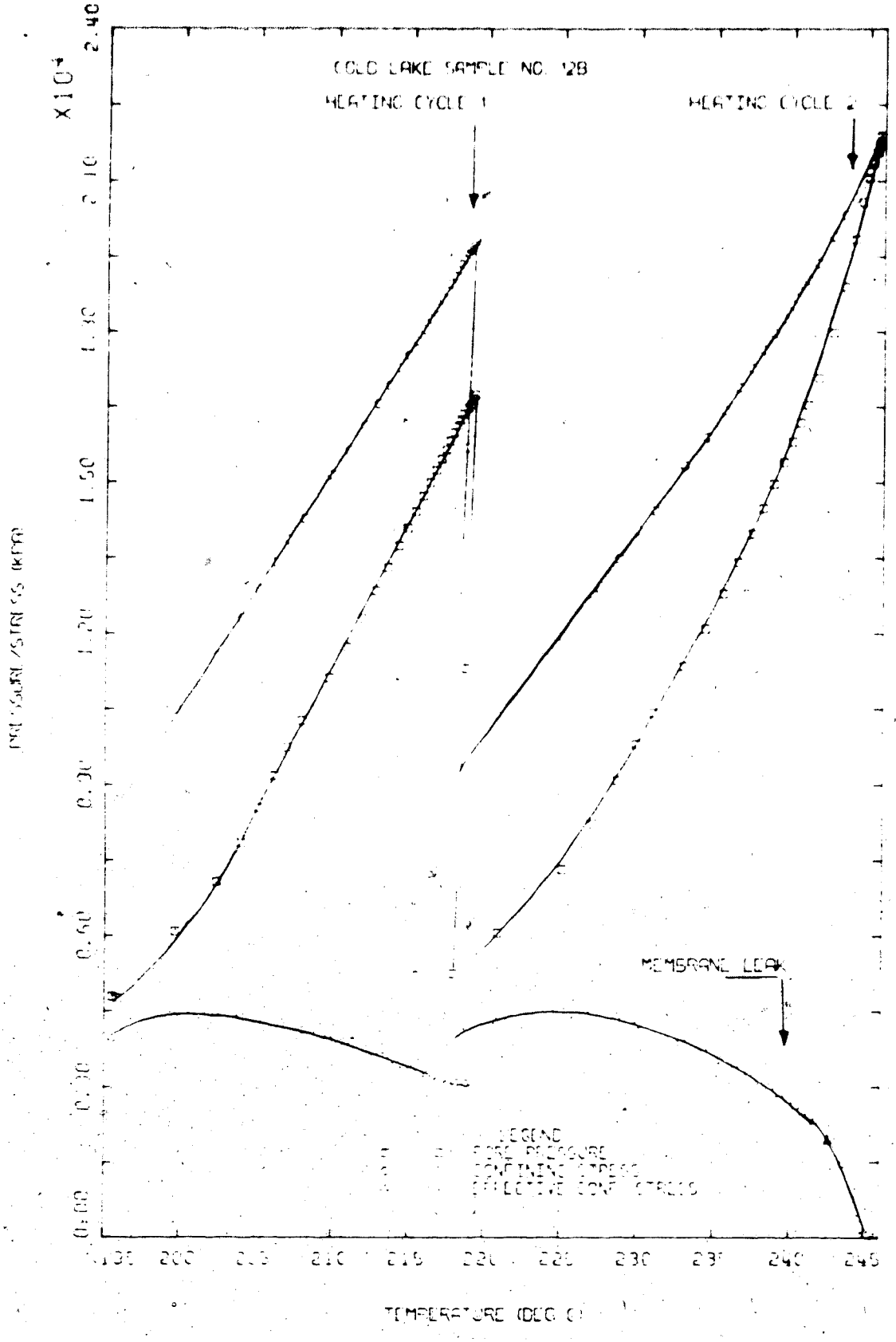

FIGURE E15.5 Triaxial Test TOS15: Pore Pressure Response to Undrained Heating

TEST TOS 16

Thermal Expansion of Saline Creek Oil Sand Sample No. 13

Procedural Details: Test TOS 16

1. Sample 13 was thawed and back saturated for 21 hours under 10 MPa back pressure and 14 MPa isotropic confining stress.
2. The apparatus and sample were heated drained, to 190°C at which point a leak developed in the rubber membrane. The test was terminated at this point.
   Vertical (axial) deformation and volume of fluid expelled from the sample were monitored during heating.

TEST 105 16: SAMPLE DATA

Protest Saline Creek Sample 15:

Dia.:	Ø	=	7.605 cm	w	= 0.130
Height:	H	=	15.235 cm	B	= 0.130
Area:	A	=	45.400 cm^2		
Volume:	V	=	691.68 ml	V_S	= 442.4 ml
Mass:	M	=	1420 g	V_V	= 248.8 ml
Mass Solids:			1174 g	Dry Density	= 1.697 M_g/m^3

Density: = 2.055 M_g/m^3
Porosity: = 0.358
Void Ratio: 0.558 g

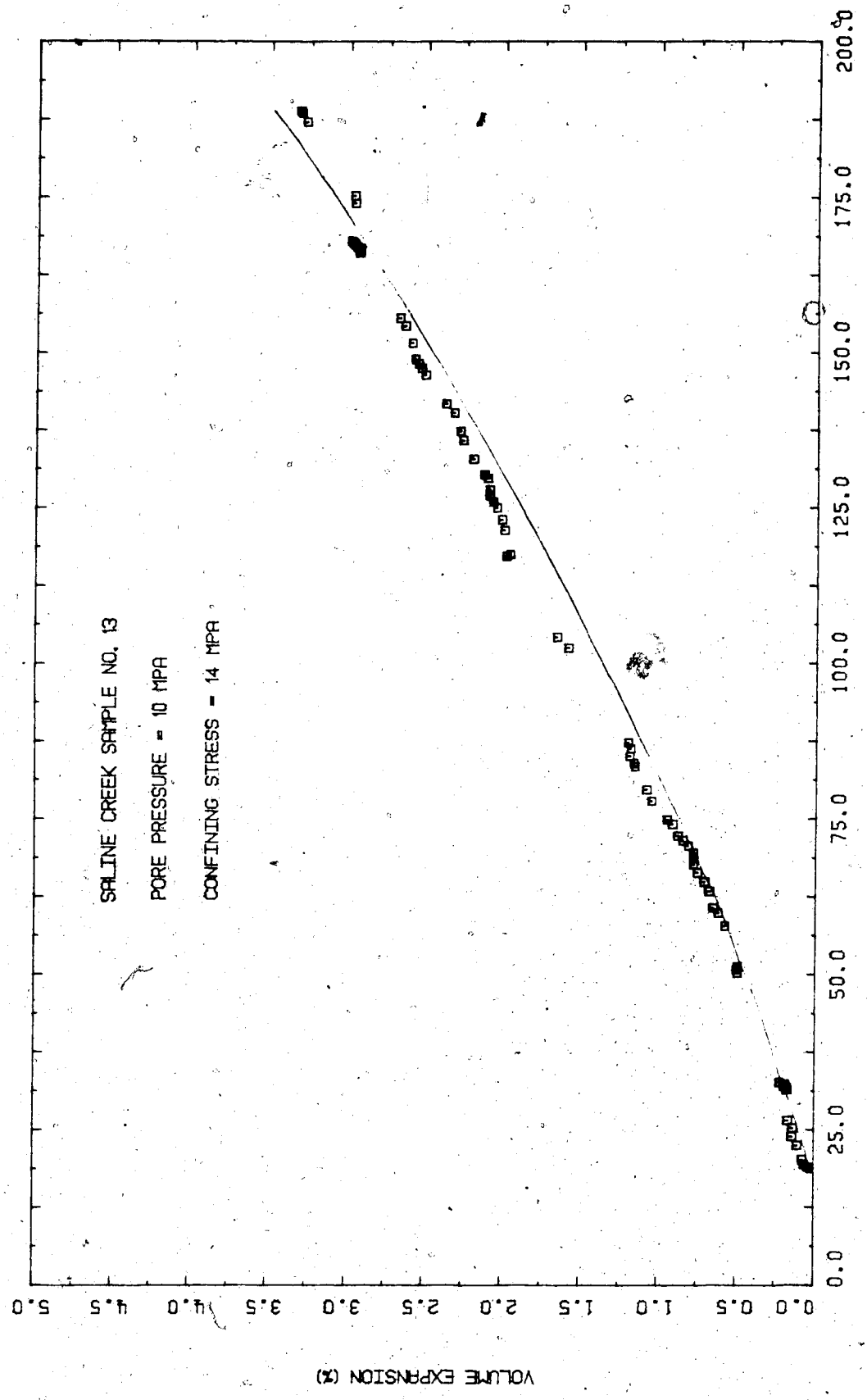

FIGURE E16.1 Triaxial Test TOS16: Volume of Pore Fluid Drained During Heating

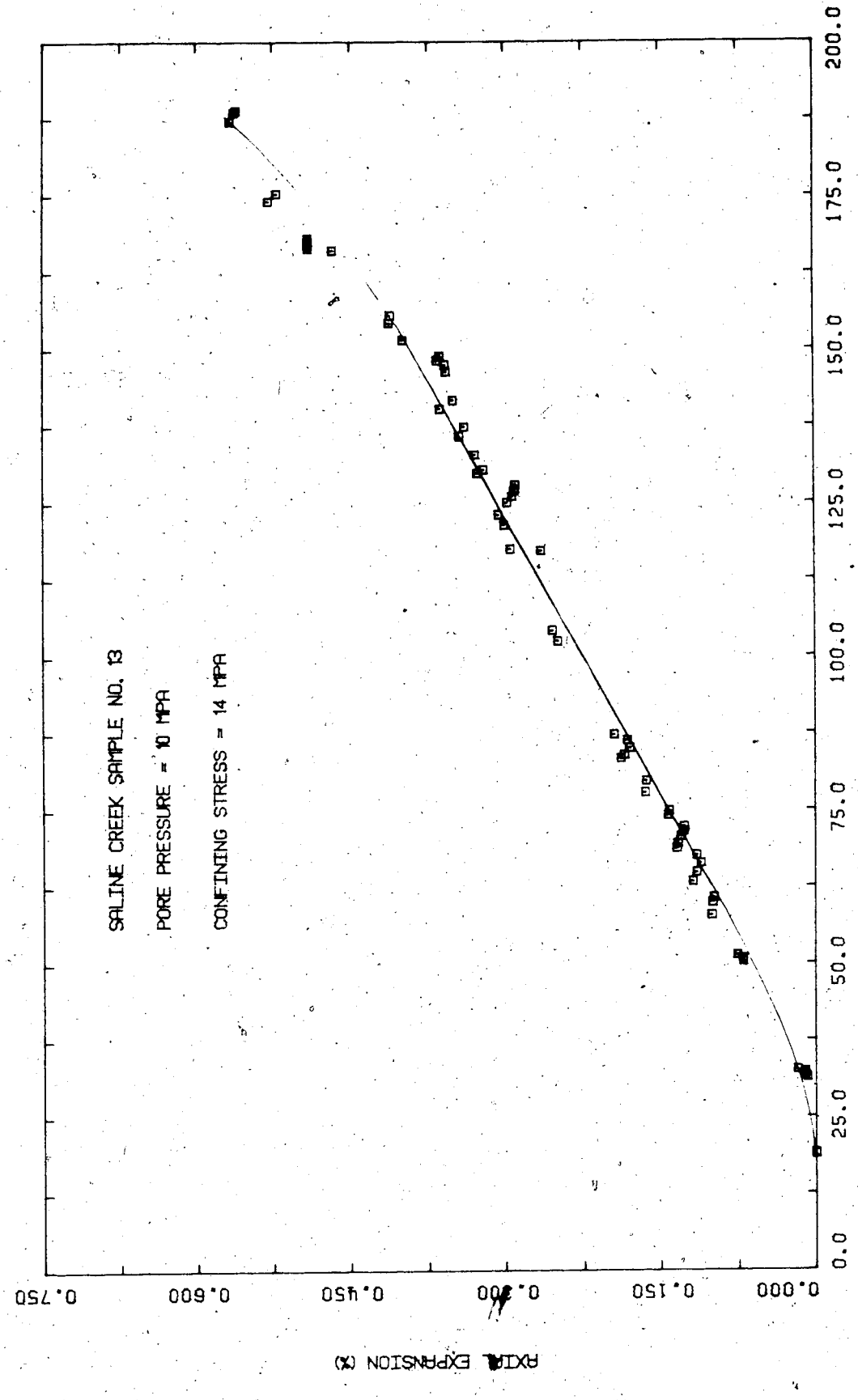

FIGURE E16.2 Triaxial Test TOS16: Vertical Thermal

TEST TOS 17

Drained Triaxial Passive Compression of Saline Creek Oil Sand Sample No. 23 at 200°C

Procedural Details: Test TOS 17

1. Sample 23 was thawed and back saturated for 18 hours under 10 MPa back pressure and 18 MPa isotropic confining stress.
2. The apparatus and sample were heated under drained conditions to 200°C. The volume of pore fluid expelled from the sample was monitored up to 180°C, however the volume change device was isolated overnight. The temperature was allowed to stabilize for 15 hours at 200°C.
3. A drained triaxial compression test was performed at 200°C. Vertical compressive stress was increased at an average rate of 65 kPa/minute while back pressure and confining stress were maintained constant at 10 MPa and 18 MPa respectively.
   Vertical (axial) deformation and volume change were monitored during triaxial compression.
4. A very small membrane leak developed near the peak deviatoric stress. The rate of leakage was measured and volume change readings corrected accordingly.

TEST TOS 17: SAMPLE DATA

Pretest Saline Creek Sample No. 23:

Dia.:	Ø	=	7.650 cm		w	=	0.020
Height:	H	=	15.042 cm		B	=	0.190
Area:	A	=	45.963 cm^2				
Volume:	V	=	691.36 ml		V_S	=	442.9 ml
Mass:	M	=	1420 g		V_V	=	248.5 ml
Mass Solids		=	1174 g	Dry Density		=	1.698 Mg/m^3

Density: = 2.054 Mg/m^3
Porosity: = 0.359
Void Ratio: = 0.560 g

Sample 23 After Test TOS 17

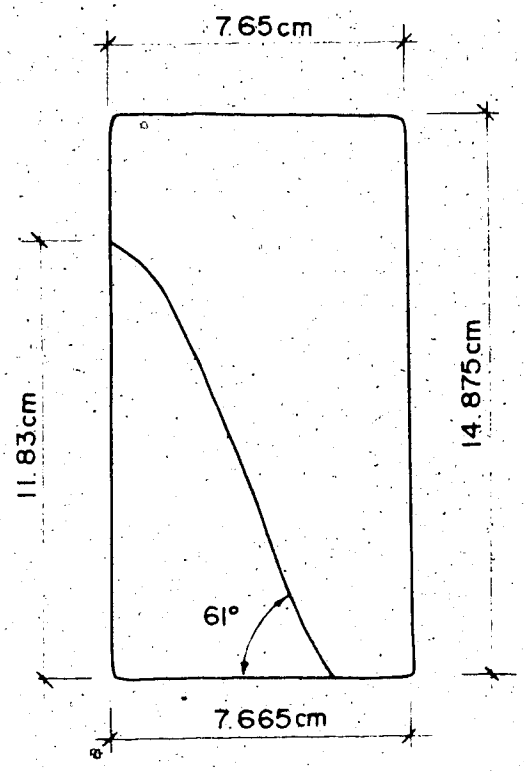

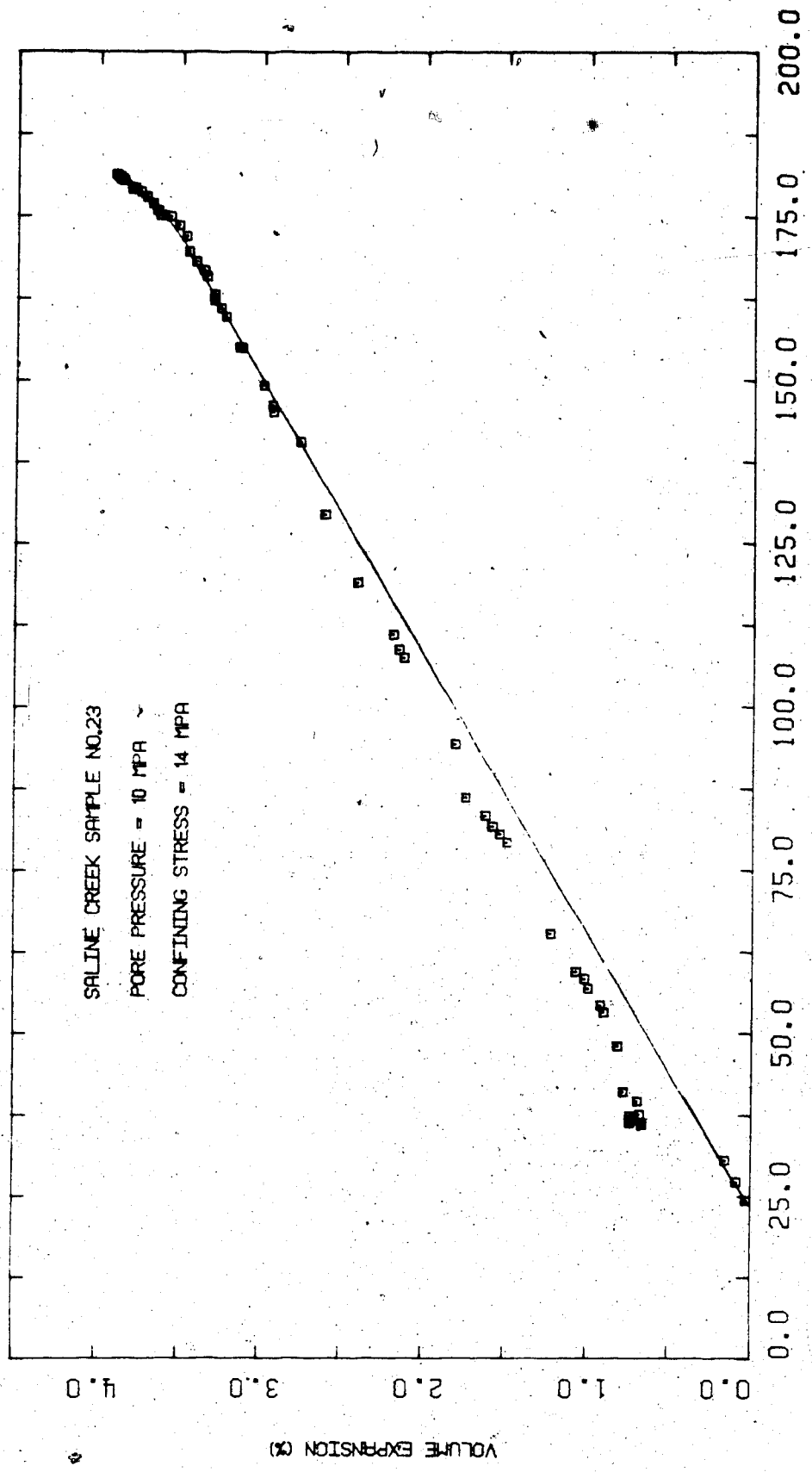

FIGURE E17.1 Triaxial Test TOS17: Volume of Pore Fluid Drained During Heating

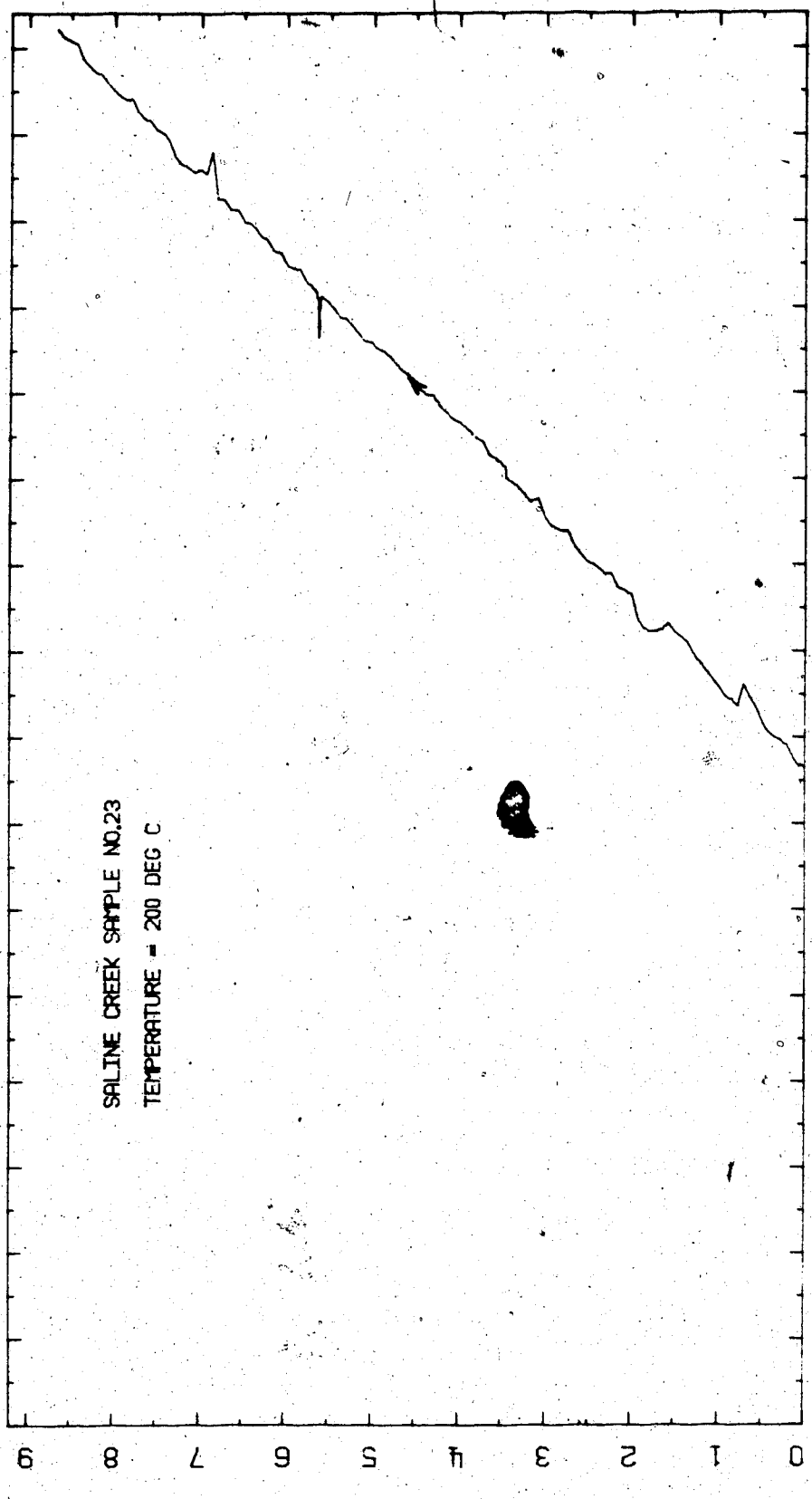

FIGURE E17.2 Triaxial Test TOS17: Stress Path

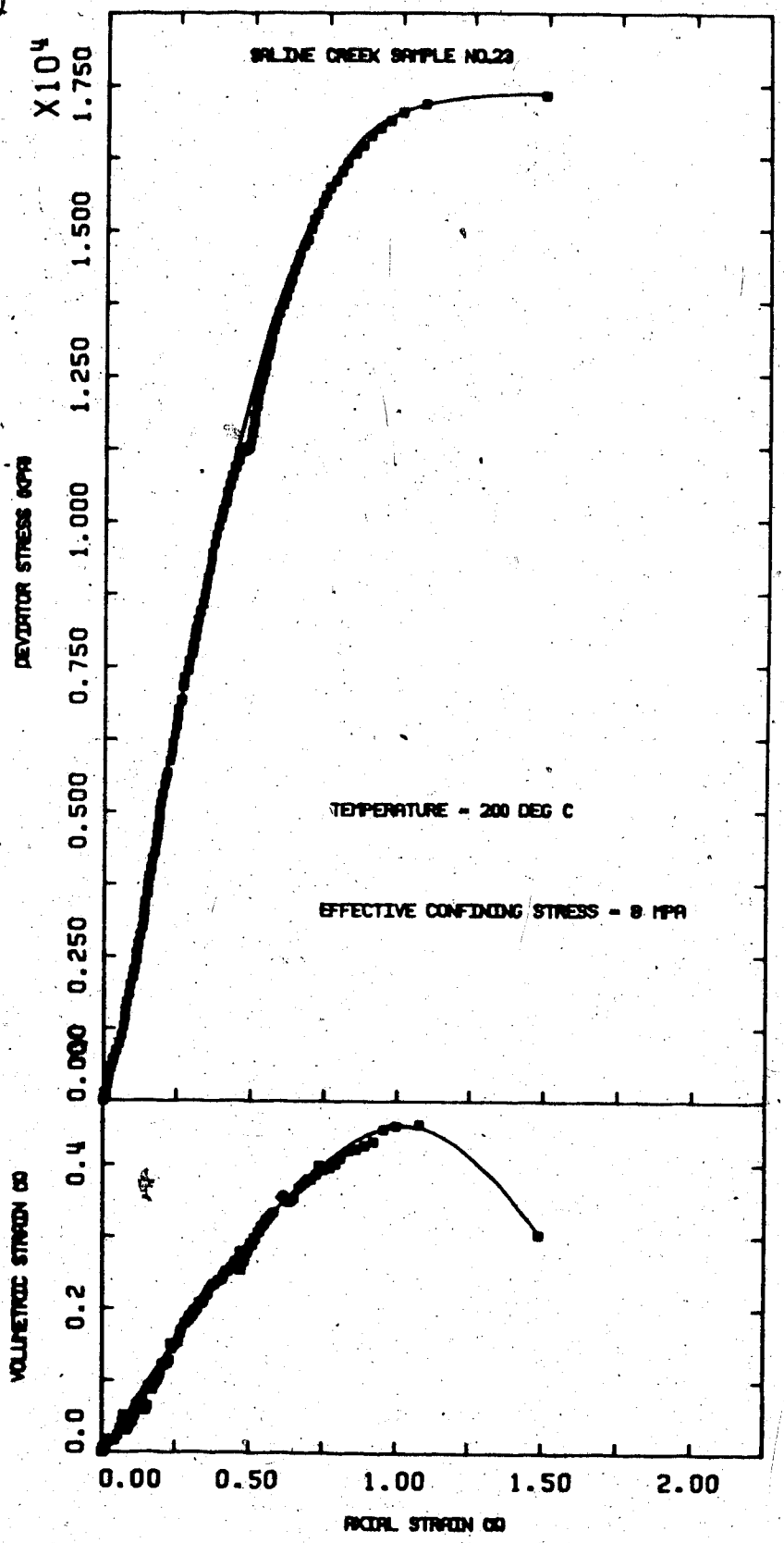

FIGURE E17.3 Triaxial Test TOS17: Deviator Stress Vs. Strain

TEST TOS 18

Drained Triaxial Compression of Saline Creek Oil Sand
Sample No. 24 at 200°C Following Stress Path"F" (J1 Constant)

Procedural Details: Test TOS 18

1. Sample 24 was thawed and back saturated for 19 hours under 10 MPa back pressure and 14 MPa isotropic confining stress.
2. The apparatus and sample were heated under drained conditions to 200°C. Volume of expelled pore fluid was monitored up to 180°C however, the volume change device was isolated overnight in case of membrane failure. The temperature was allowed to stabilize overnight (i.e. for 16 hours).
3. A drained triaxial compression test was performed following stress path "F" as follows:
   a) Back pressure and isotropic confining stress were increased simultaneously to 12 MPa and 16 MPa respectively.
   b) Vertical stress was maintained constant at 16 MPa during the test.
   c) Horizontal confining stress (i.e. cell pressure) was decreased in 250 kPa increments from 16 MPa to 10 MPa. Back pressure was decreased simultaneously from 12 MPa to 9.1 MPa.
   d) Vertical deformation and volume change were monitored during the test.

TEST TOS 18: SAMPLE DATA

Pretest Saline Creek Sample No. 24:

Dia.:	Ø	=	7.590 cm	w	=	0.035
Height:	H	=	15.143 cm	B	=	0.145
Area:	A	=	45.245 cm^2			
Volume:	V	=	685.15 ml	V_S	=	455.7 ml
Mass:	M	=	1425 g	V_V	=	229.4 ml
Mass Solids		=	1208 g	Dry Density	=	1.763 Mg/m^3

Density: = 2.080 Mg/m^3
Porosity: = 0.334
Void Ratio: = 0.502 g

Sample 24 After Test TOS 18

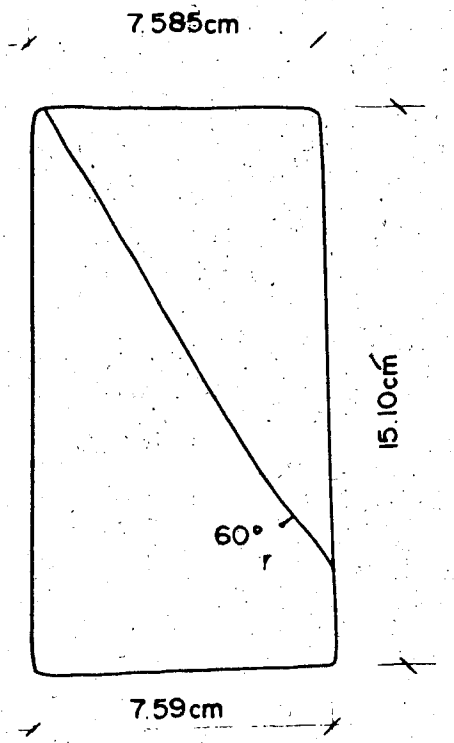

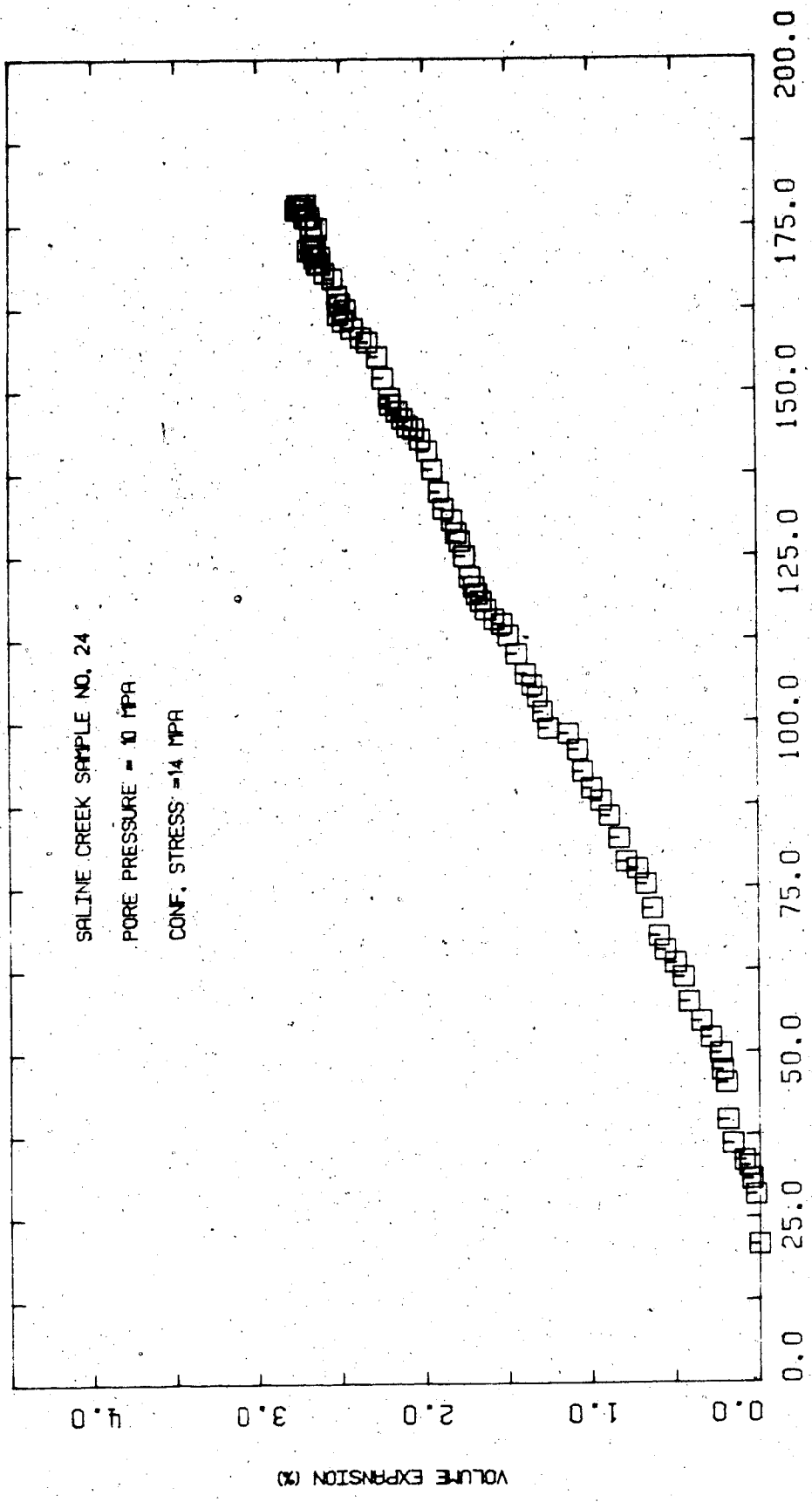

FIGURE E18.1 Triaxial Test TOS18: Volume of Pore Fluid Expelled During Heating

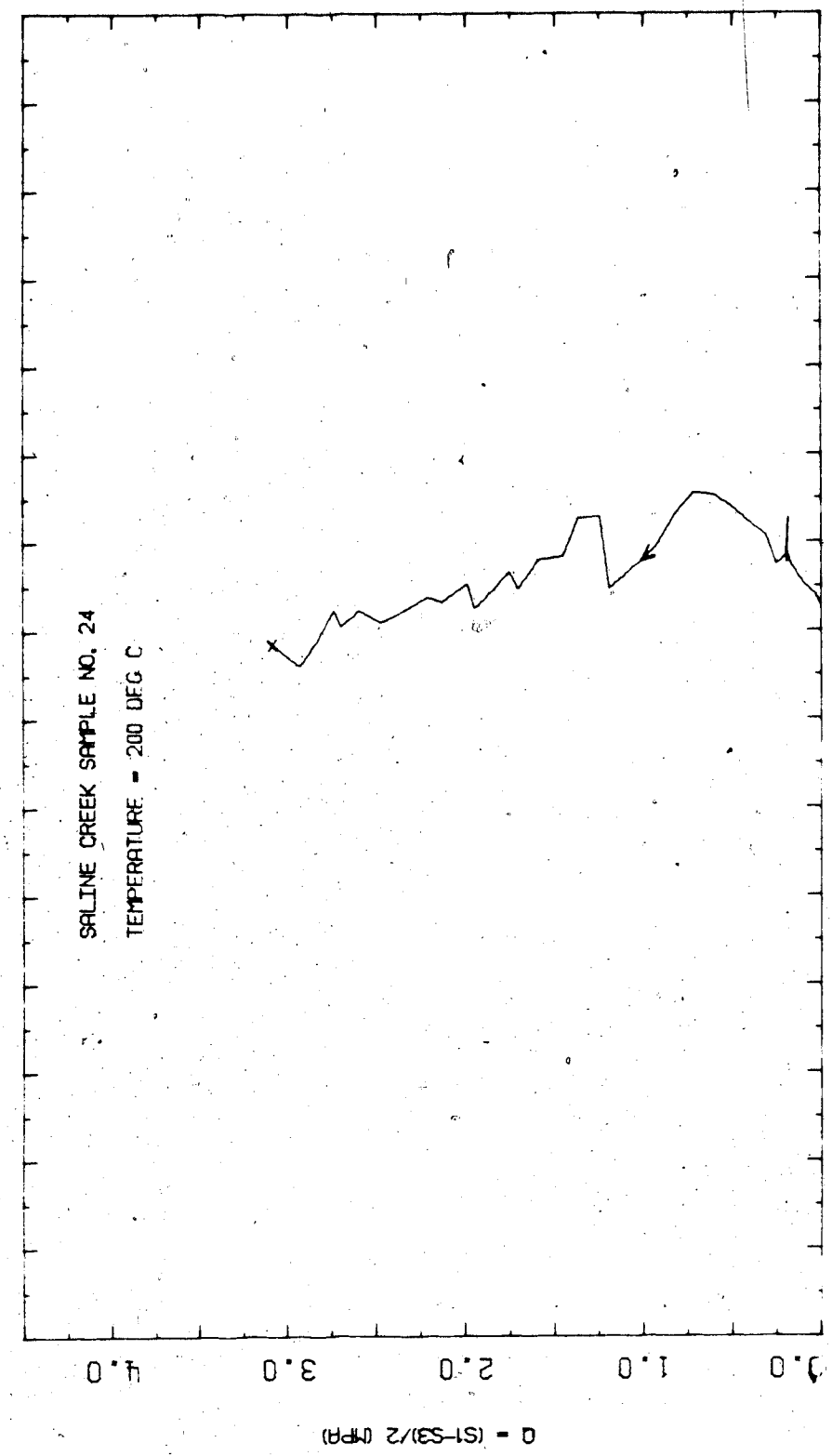

FIGURE 118.2 Triaxial Test TOS18: Stress Path

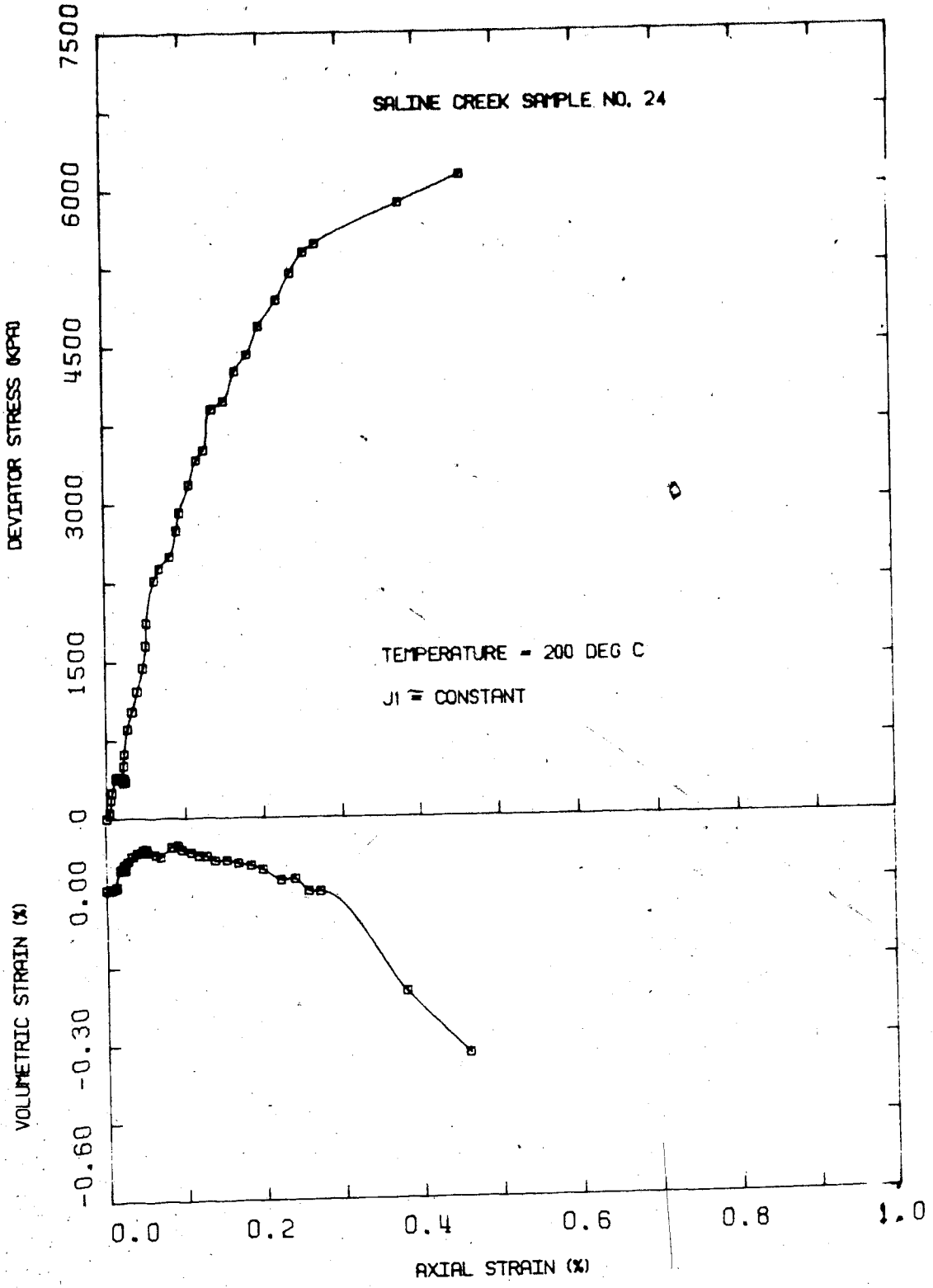

FIGURE E18.3 Triaxial Test TOS18: Deviator Stress Vs. Strain

TEST TOS 19

Drained Triaxial Isotropic and Passive Compression of Saline Creek Oil Sand Sample No. 19 at 125°C and 4 MPa Effective Confining Stress

Procedural Details: Test TOS 19

1. Sample 19 was thawed and back saturated for 23 hours under 10 MPa back pressure and 14 MPa isotropic confining stress.
2. The apparatus and sample were heated drained to 125°C. Volume of expelled pore fluid was monitored during heating.
3. Three cycles of drained isotropic compression and unloading were applied over the effective stress range 4 - 17 MPa. Back pressure was maintained constant at 10 MPa.
4. A drained triaxial passive compression test was performed. Vertical compressive stress was increased while horizontal confining stress and back pressure were maintained constant at 14 MPa and 10 MPa respectively.
   Vertical (axial) deformation and volume change were monitored during the test.

TEST NOS 19: SAMPLE DATA

Pretest Saline Creek Sample No. 19:

Dia.:	Ø	= 7.500 cm		w	= 0.15
Height:	H	= 15.050 cm		B	= 0.16
Area:	A	= 44.179 cm²			
Volume:	V	= 665.11 cm³		V_s	= 442.1 ml
Mass:	M	= 1385 g		V_v	= 223.0 ml
Mass Solids:		= 1172 g	Dry Density		= 1.762 Mg/m³

Density: = 2.264 Mg/m³
Porosity: = 0.335
Void Ratio: = 0.504

Sample 19 After Test Nos 19

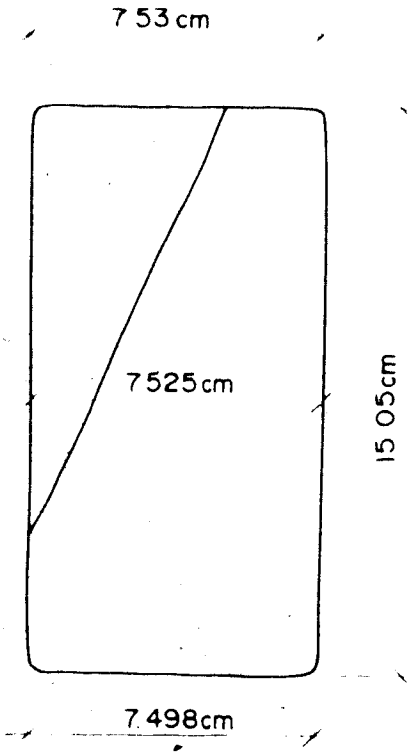

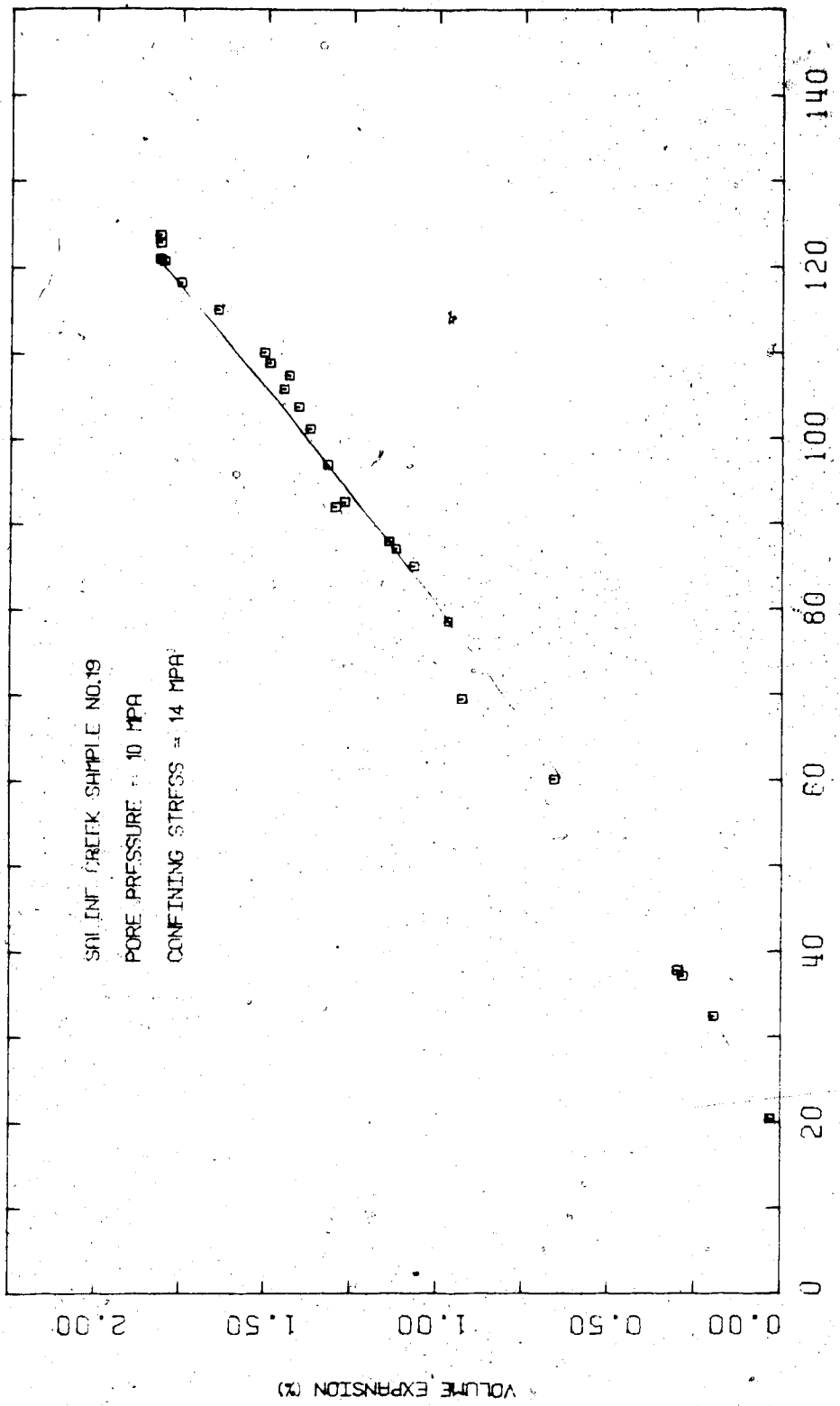

FIGURE E19.1 Triaxial Test TOS19: Volume of Pore Fluid Expelled During Heating

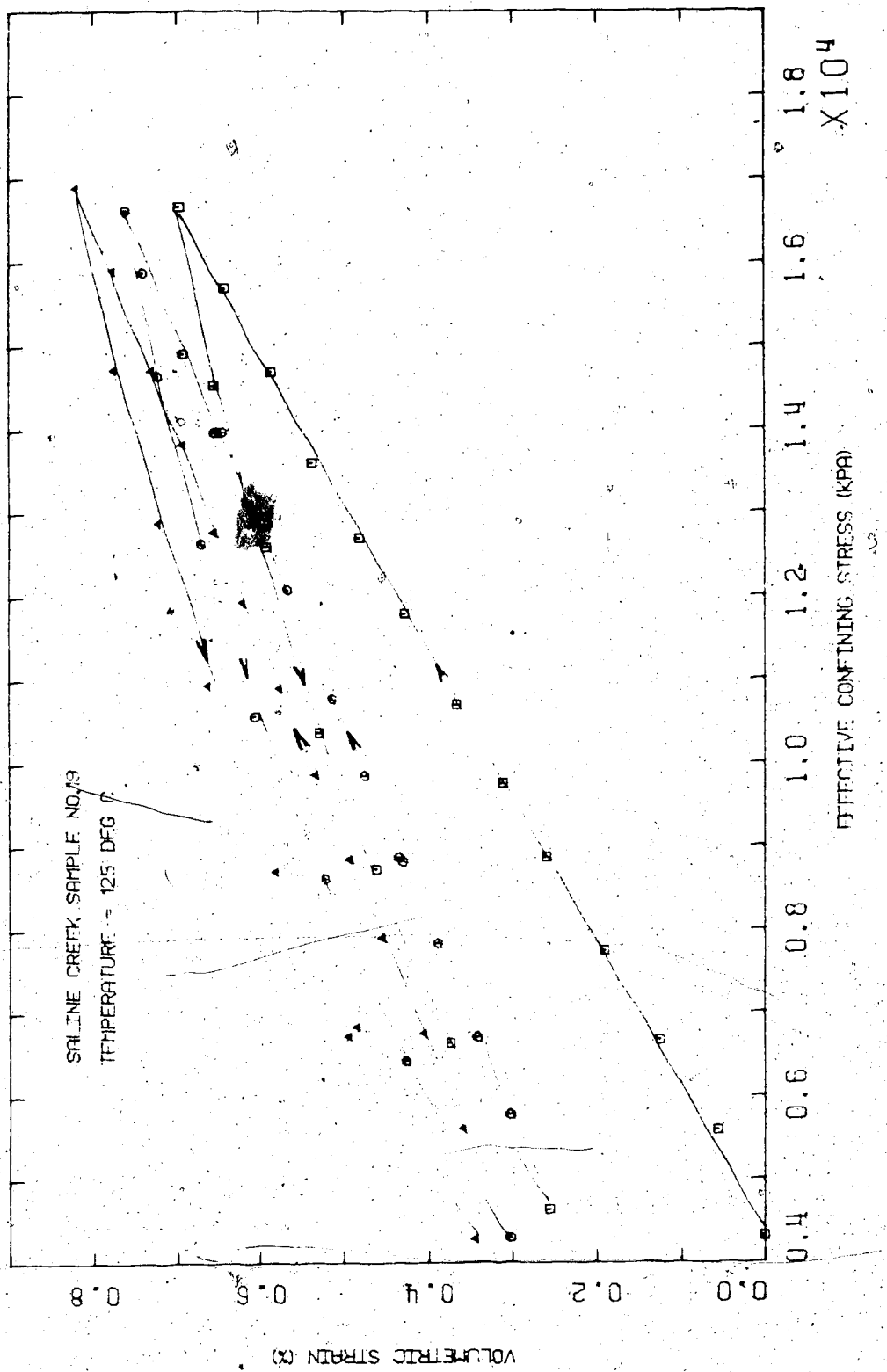

FIGURE E19.2 Triaxial Test TOS19: Drained Isotropic Compression

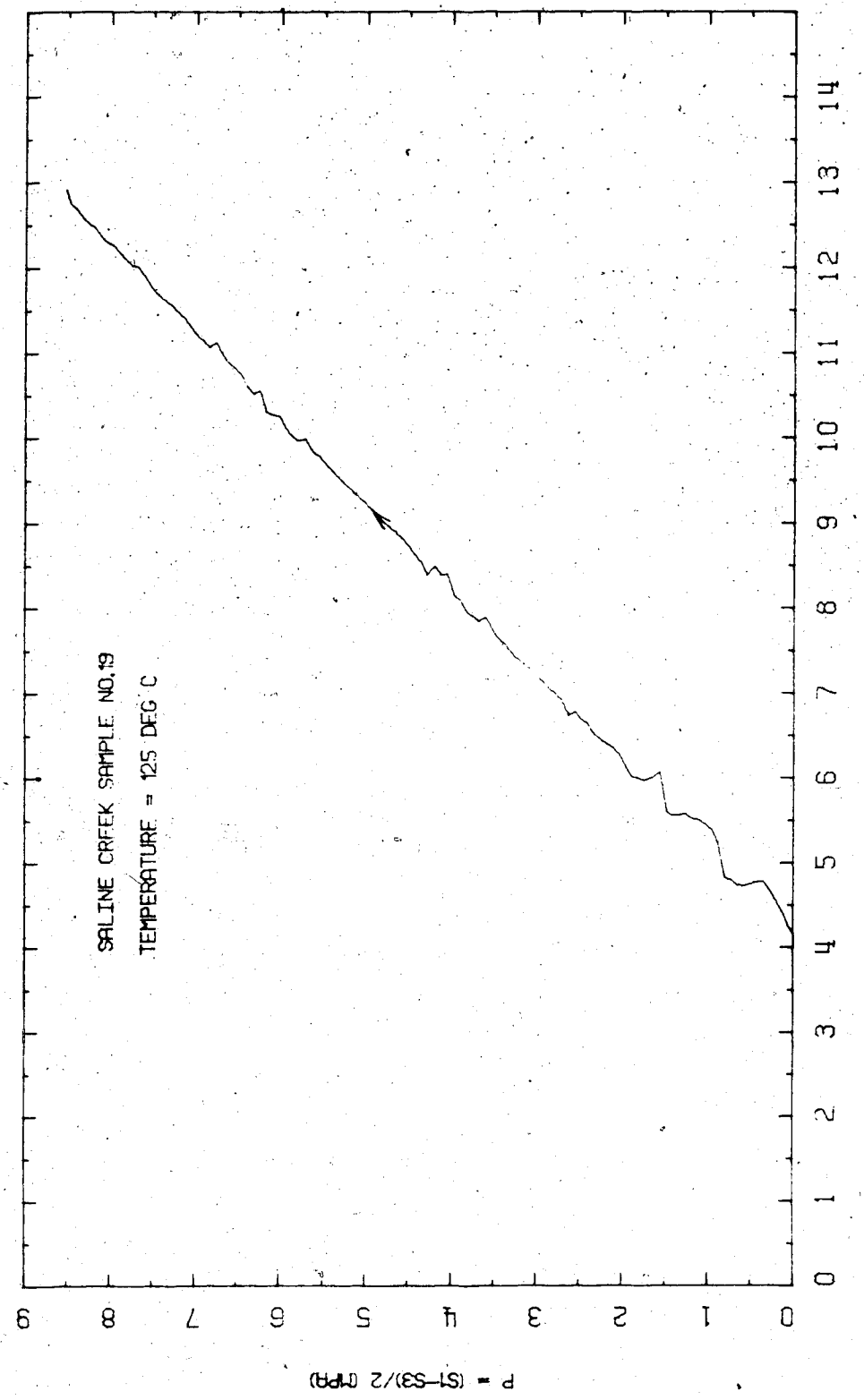

FIGURE E19.3 Triaxial Test TOS19: Stress Path

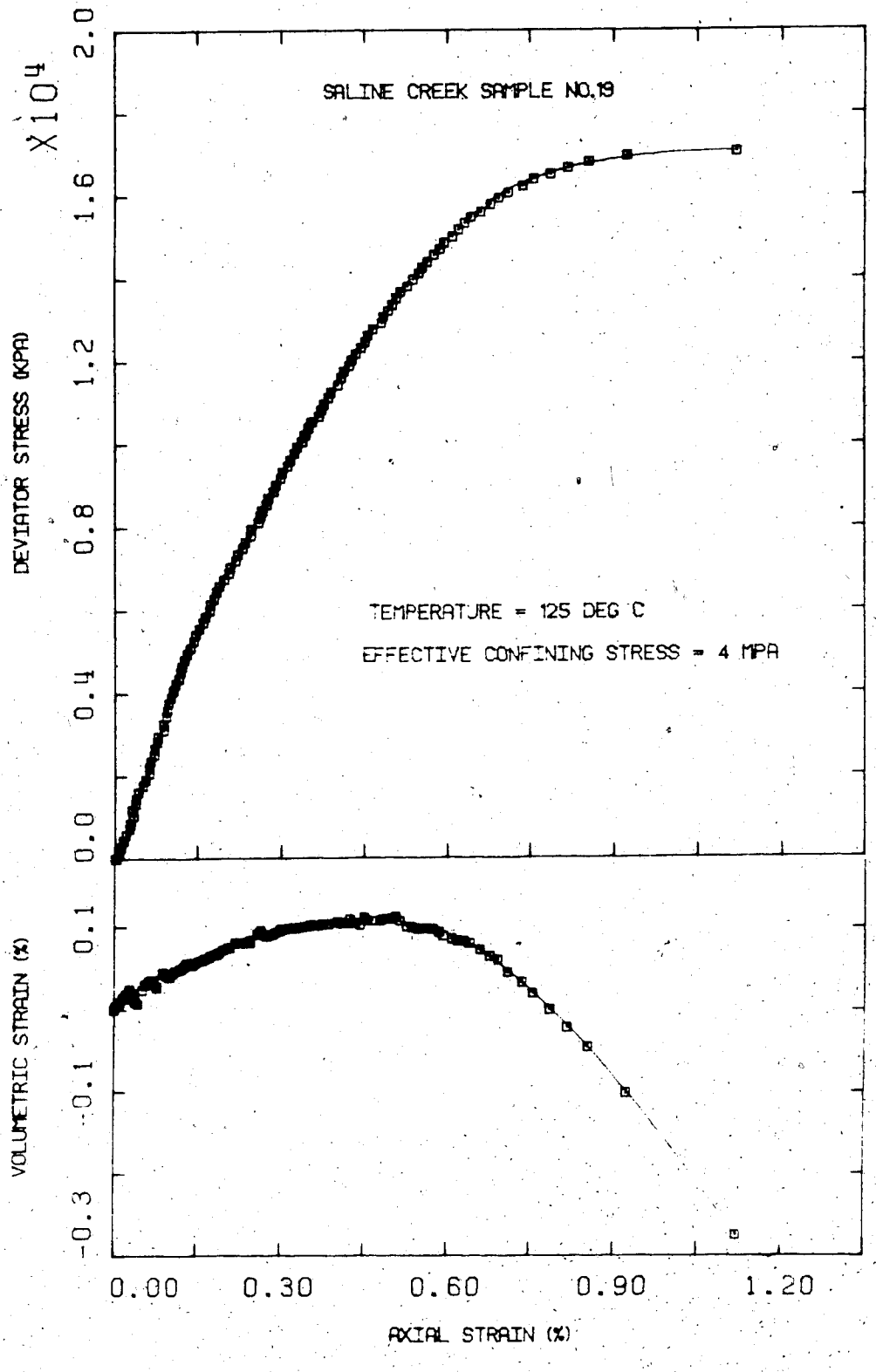

FIGURE E19.4 Triaxial Test TOS19: Deviator Stress Vs. Strain

TEST TOS 20

Unconfined Compression of Case Hardened Saline Creek Oil Sand Sample No. 2 Following Unsaturated Heating at 150°C

TEST TOS 20: SAMPLE DATA

Saline Creek Sample No. 20:

Before Heating:

Height:	=	15.13 cm
Diameter:	=	7.54 cm
Mass:	=	1332 g
Bulk Density:	=	1.972 Mg/m^3

Heating Procedure:

1. Sample confined under 15 kPa stress and vented radially and vertical, to atmospheric pressure.
2. Heating cycles:
   a) 4 hours at 65°C
   b) 24 hours at 105°C
   c) 88 hours at 150°C
   d) 36 hour cooldown at 20°C

Sample Dimensions After Heating and Cooldown:

Height:	=	14.75 cm
Diameter:	=	7.62 cm
Mass:	=	1259 g (i.e. 73 g of pore fluid vapourized)
Bulk Density:	=	1.872 g/cm^3

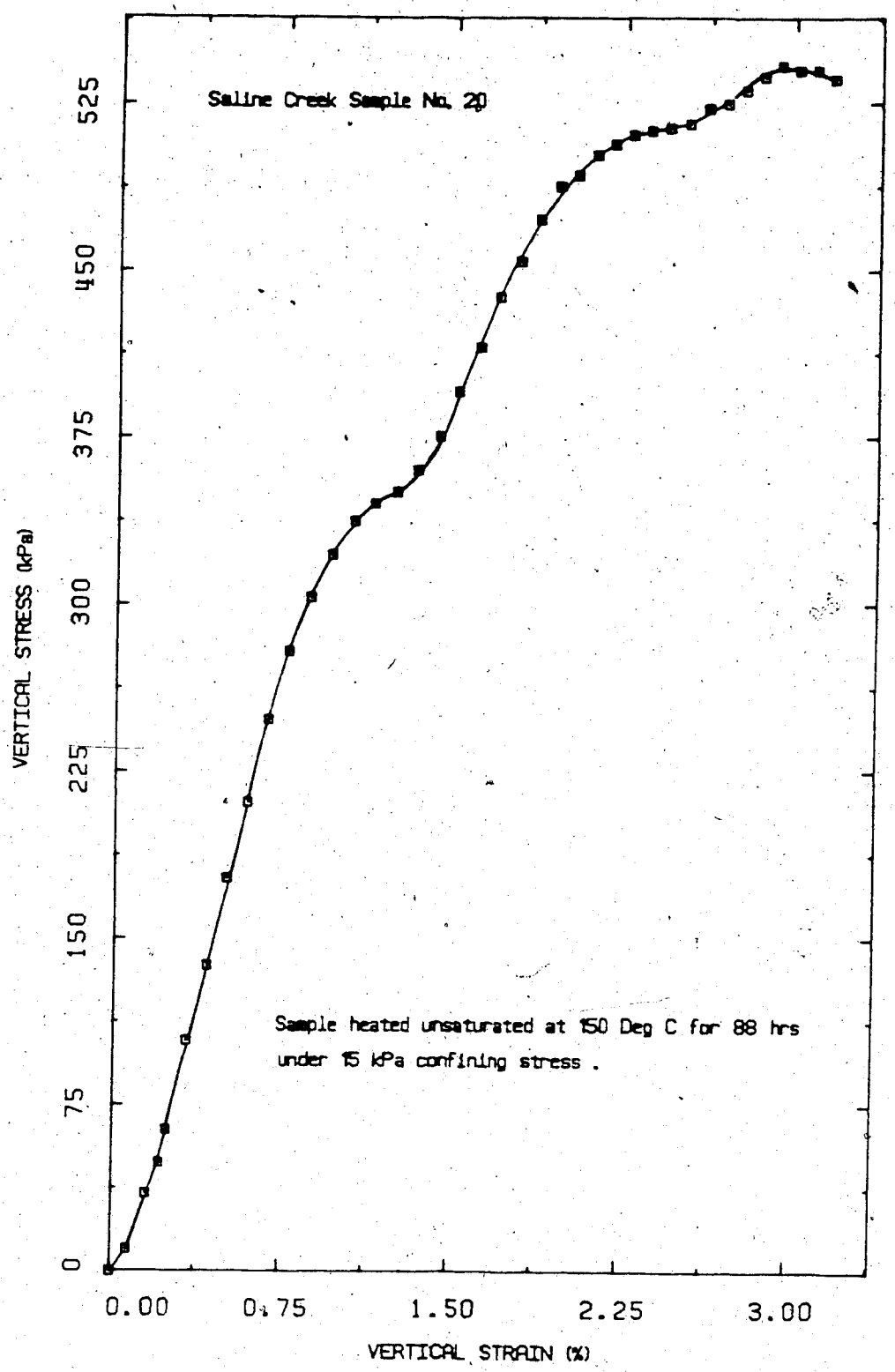

FIGURE E20.1 Unconfined Compression Test TOS20: Vertical Stress Vs. Strain

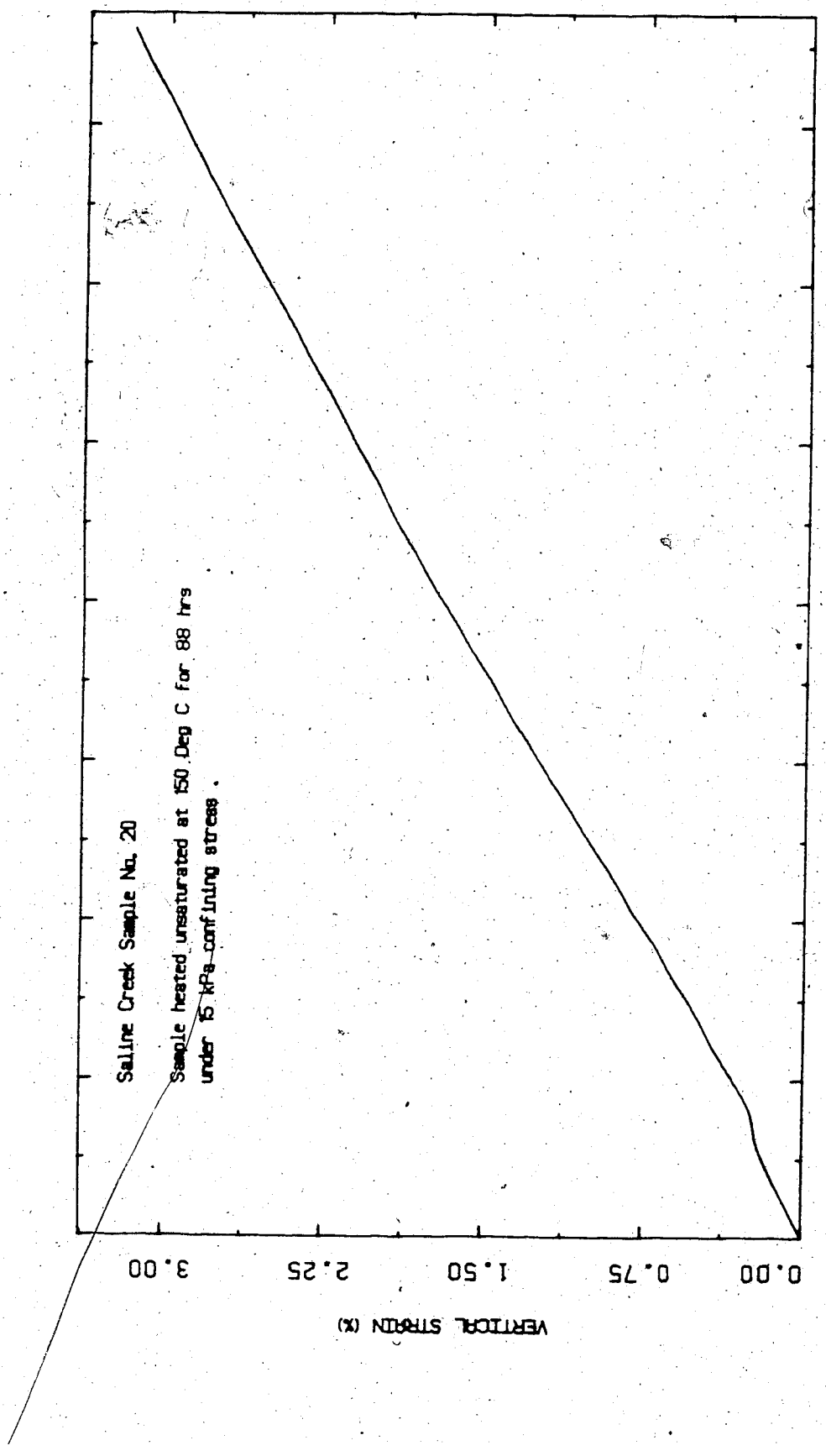

FIGURE E20.2 Unconfined Compression Test TOS20: Vertical Strain Rate

APPENDIX F

GRAIN SIZE ANALYSES

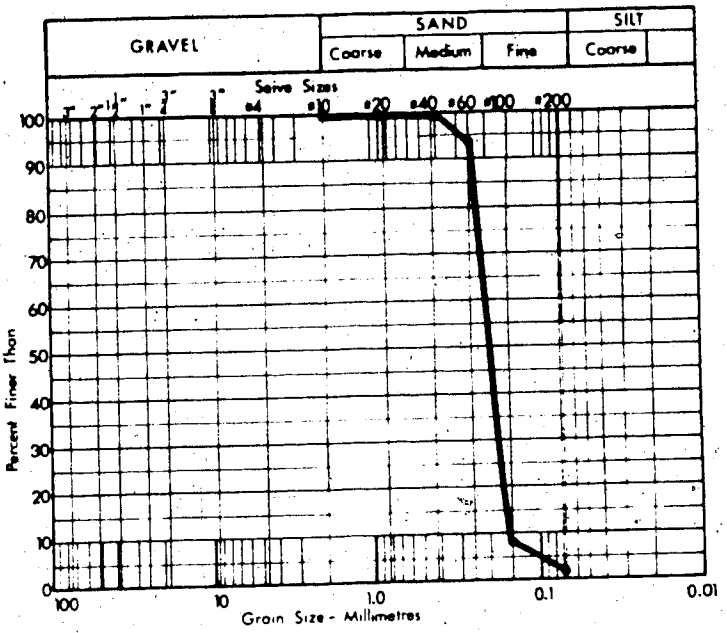

Before

$D_{10} = 0.16mm$
$D_{60} = 0.22mm$
$C_u = 1.4$

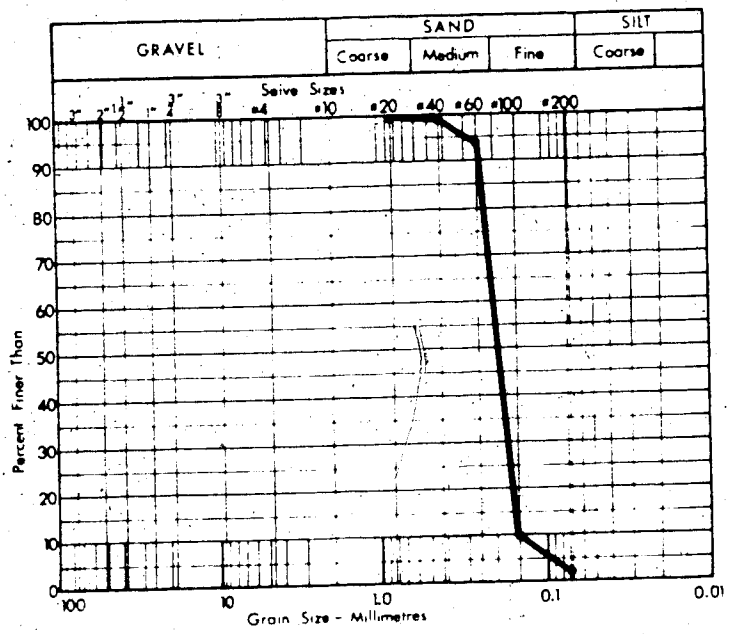

After

$D_{10} = 0.2mm$
$D_{60} = 0.3mm$
$C_u = 1.5$

FIGURE F1 Sample #41
Test COS 9

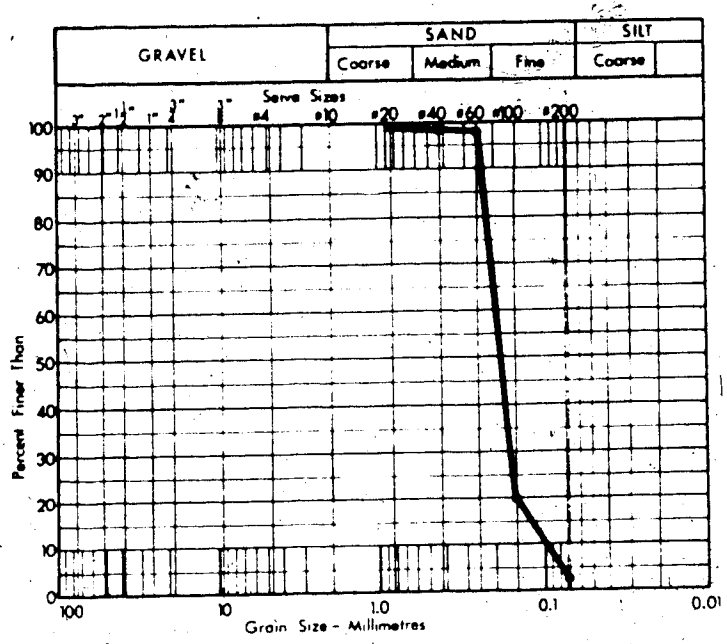

Before

$D_{10} = 0.1mm$
$D_{60} = 0.2mm$
$C_u = 2.0$

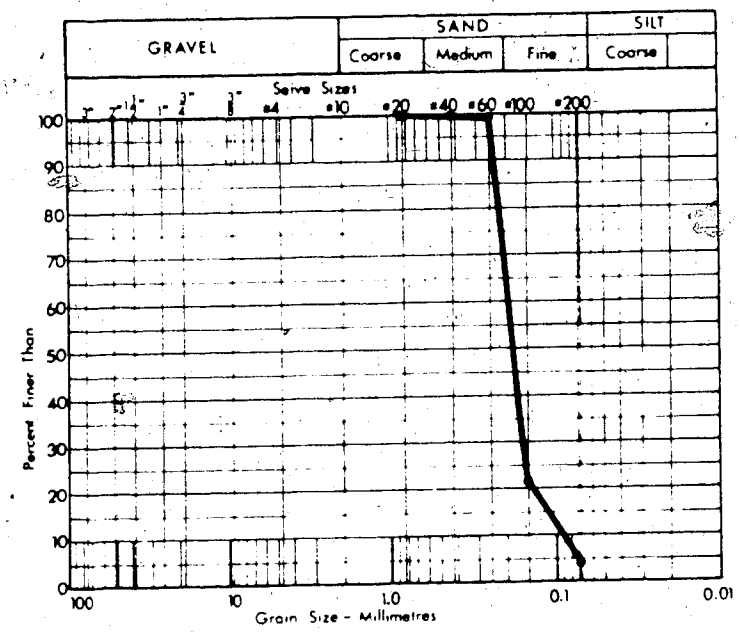

After (Top)

$D_{10} = 0.1mm$
$D_{60} = 0.2mm$
$C_u = 2.0$

FIGURE F2 Sample #36A
Test CPERM 4

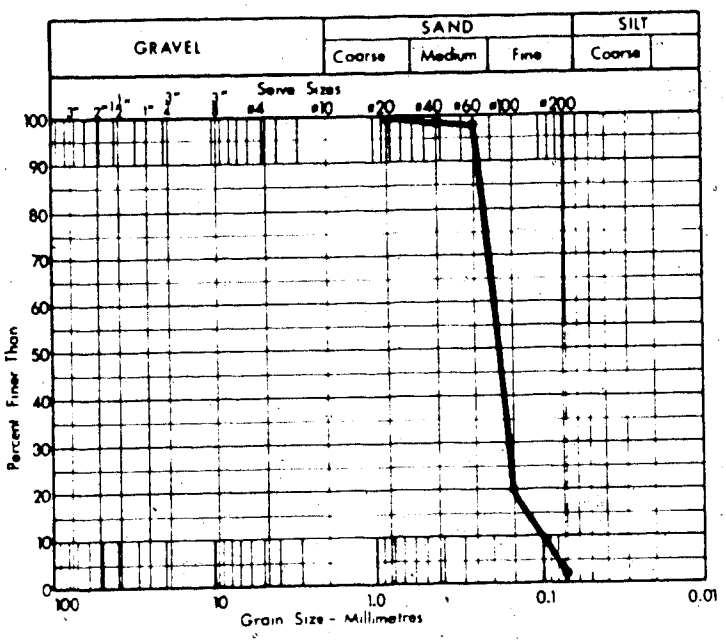

Before

D_{10} = 0.1mm
D_{60} = 0.2mm
C_u = 2.0

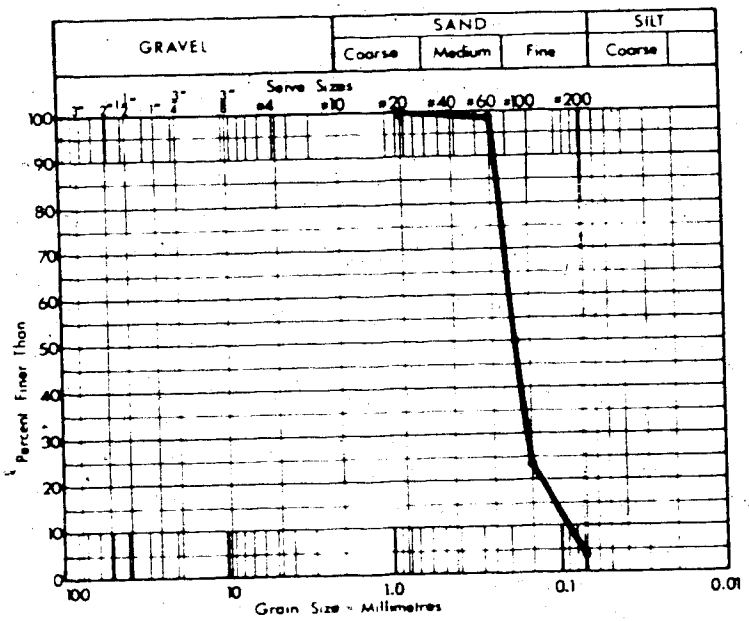

After (Bottom)

D_{10} = 0.09mm
D_{60} = 0.19mm
C_u = 2.1

FIGURE F3 Sample 36A
Test CPERM 4

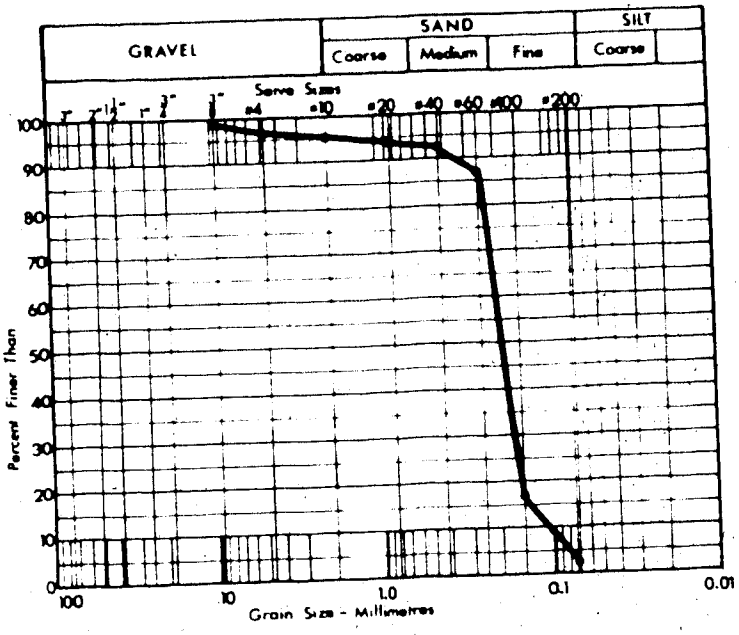

Before

D_{10} = 0.11mm
D_{60} = 0.22mm
C_u = 2.0

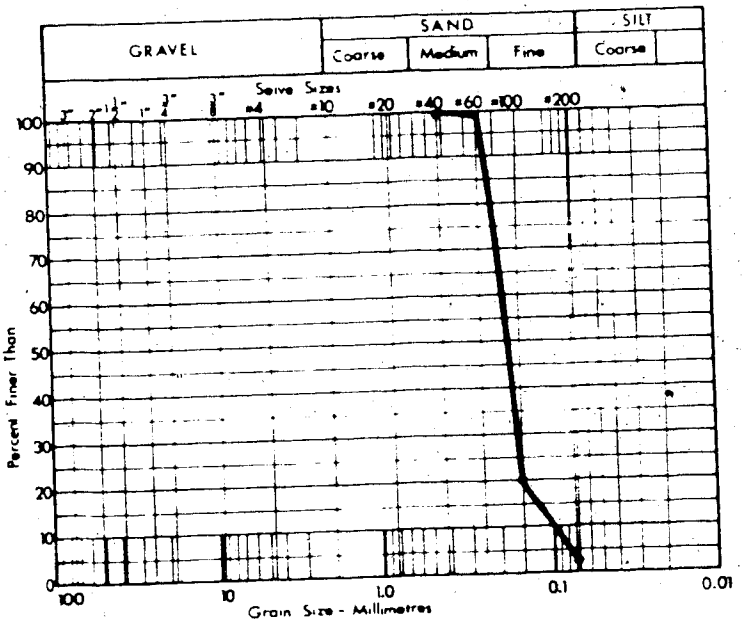

After (Top)

D_{10} = 0.1mm
D_{60} = 0.3mm
C_u = 3.0

FIGURE F4 Sample #31A
Test CPERM 5

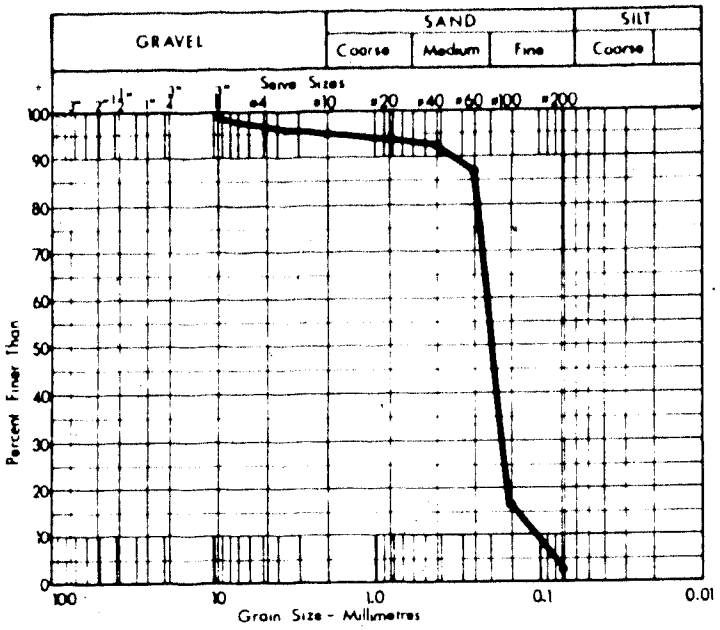

D_{10} = 0.11mm
D_{60} = 0.22mm
C_u = 2.0

Before

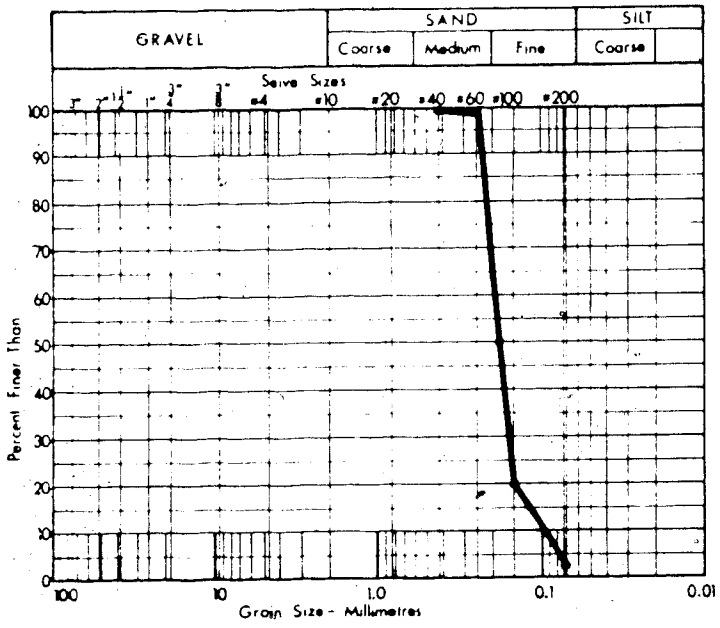

D_{10} = 0.1mm
D_{60} = 0.3mm
C_u = 3.0

After (Bottom Outside)

FIGURE F5 · Sample #31A
Test CPERM 5

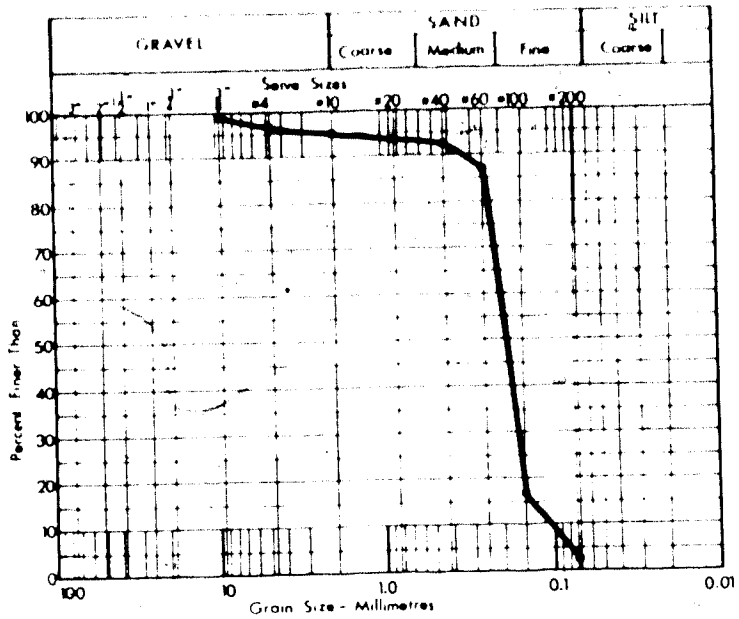

D_{10} = 0.11mm
D_{60} = 0.22mm
C_u = 2.0

Before

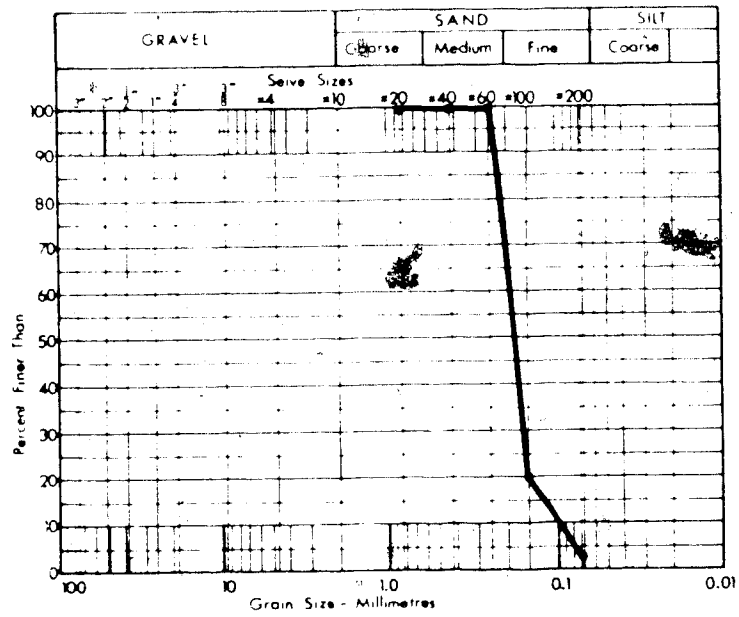

D_{10} = 0.1mm
D_{60} = 0.2mm
C_u = 2.0

After (Bottom Centre)

FIGURE F6 Sample #31A
Test CPERM 5

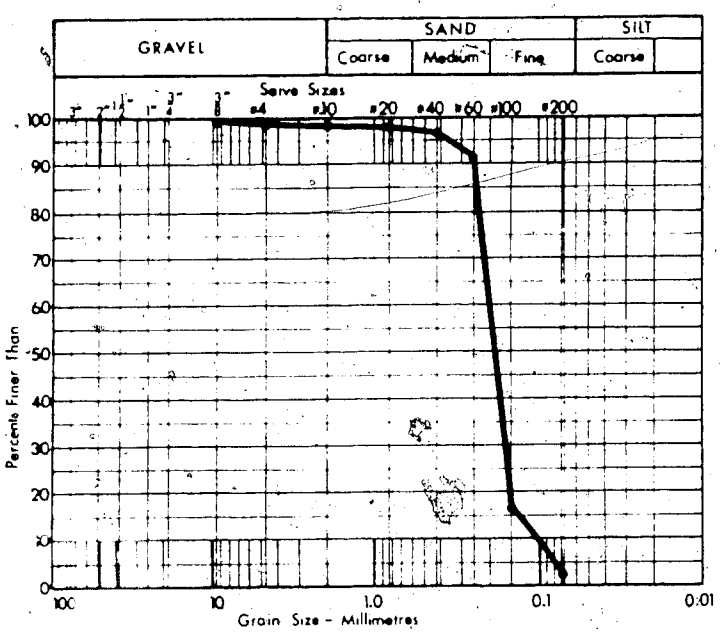

Before

D_{10} = 0.11mm
D_{60} = 0.21mm
C_u = 0.19

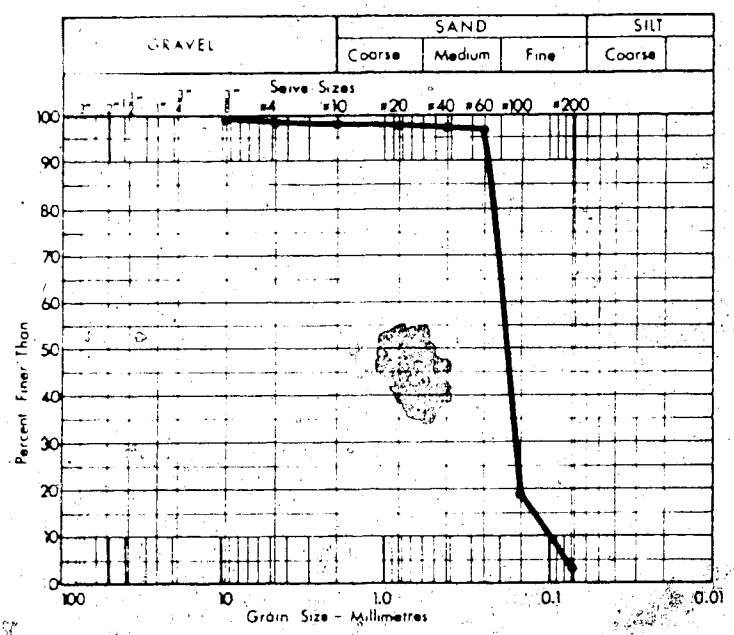

After

D_{10} = 0.1mm
D_{60} = 0.2mm
C_u = 2.0

FIGURE F7 Sample #31B
Test CPERM 6

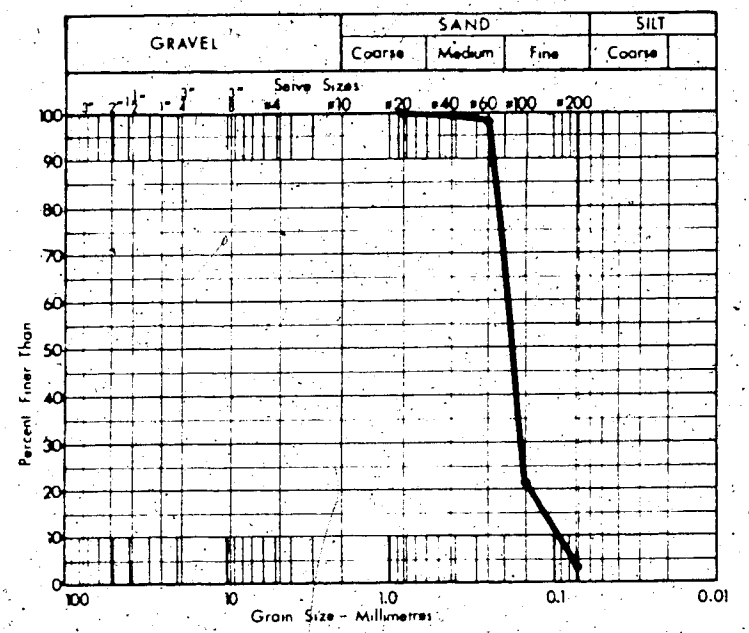

Before

D_{10} = 0.1mm
D_{60} = 0.2mm
C_u = 2.0

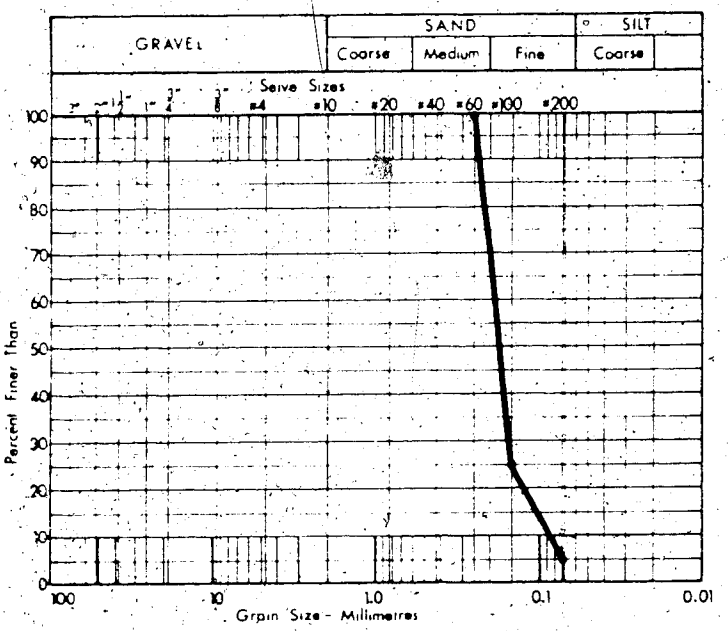

After

D_{10} = 0.09mm
D_{60} = 0.2mm
C_u = 2.2

FIGURE F8 Sample #36B
Test CPERM 19

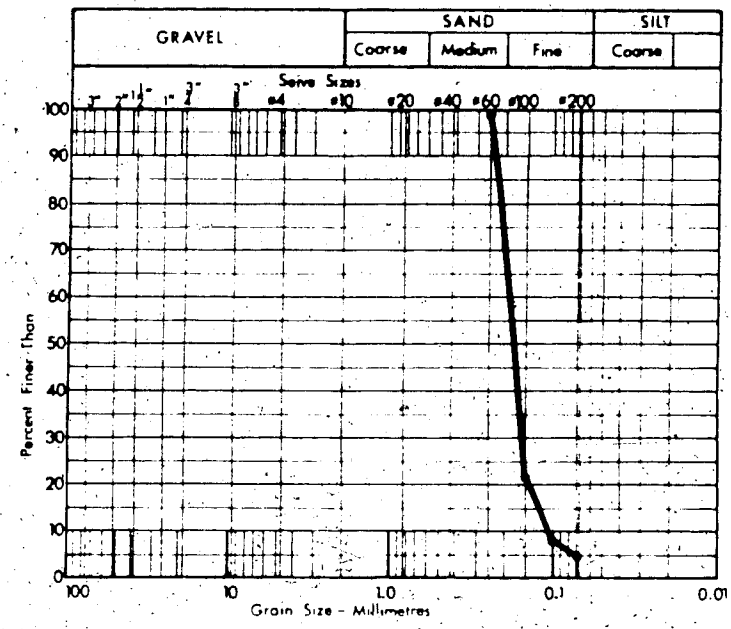

Before

D_{10}=0.11mm
D_{60}=0.2mm
C_u=1.8

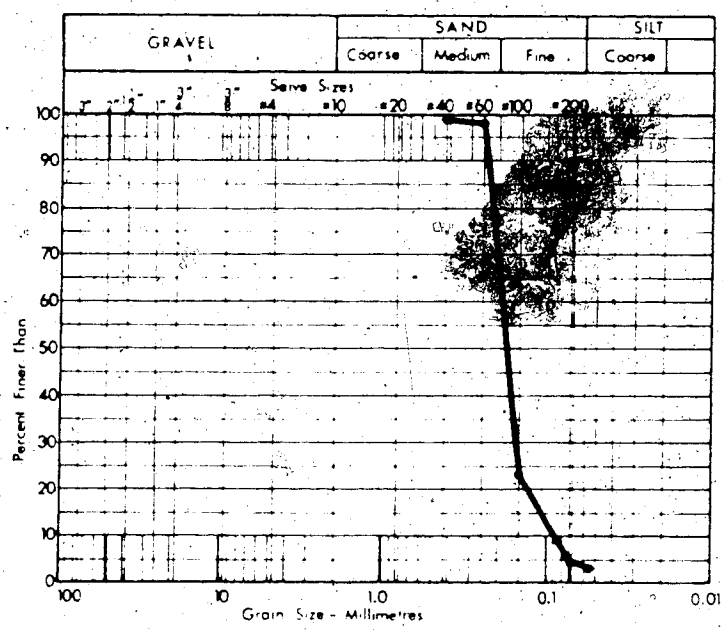

After

D_{10}=0.085mm
D_{60}=0.19mm
C_u=2.2

FIGURE F9 Sample #25
Test TOS 1

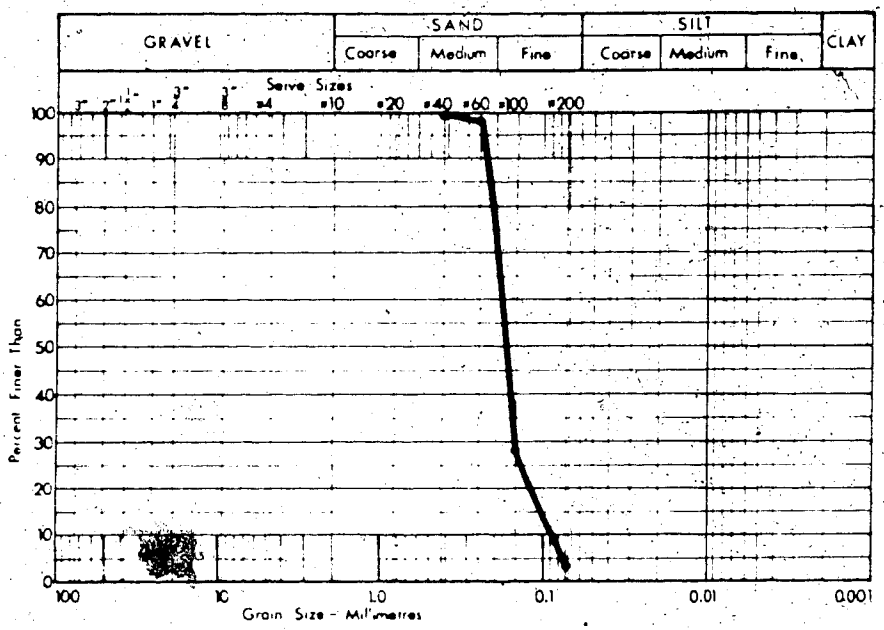

Before

D_{10}=0.09mm
D_{60}=0.19mm
C_u=2.1

FIGURE F10 Sample #33
Test TOS 2

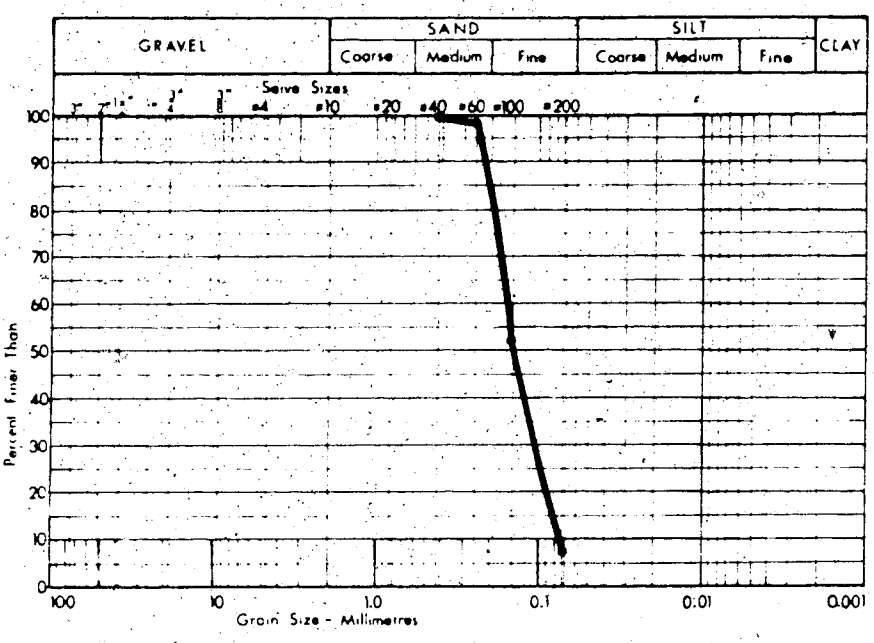

Before

$D_{10} = 0.078mm$
$D_{60} = 0.18mm$
$C_u = 2.3$

FIGURE F11 Sample #43
Test TOS 3

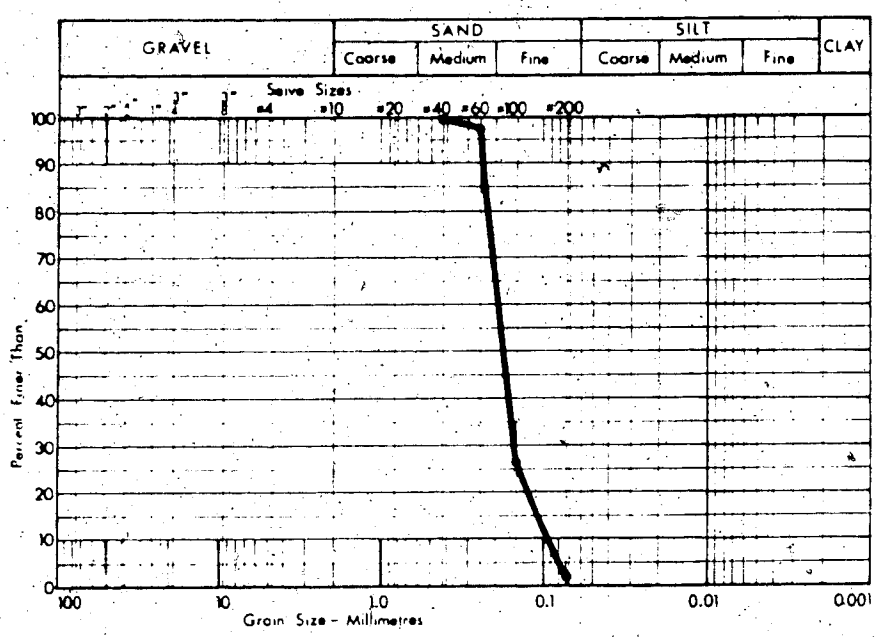

$D_{10} = 0.095\,mm$
$D_{60} = 0.19\,mm$
$C_u = 2.0$

Before

FIGURE F12 Sample #44
Test TOS 4

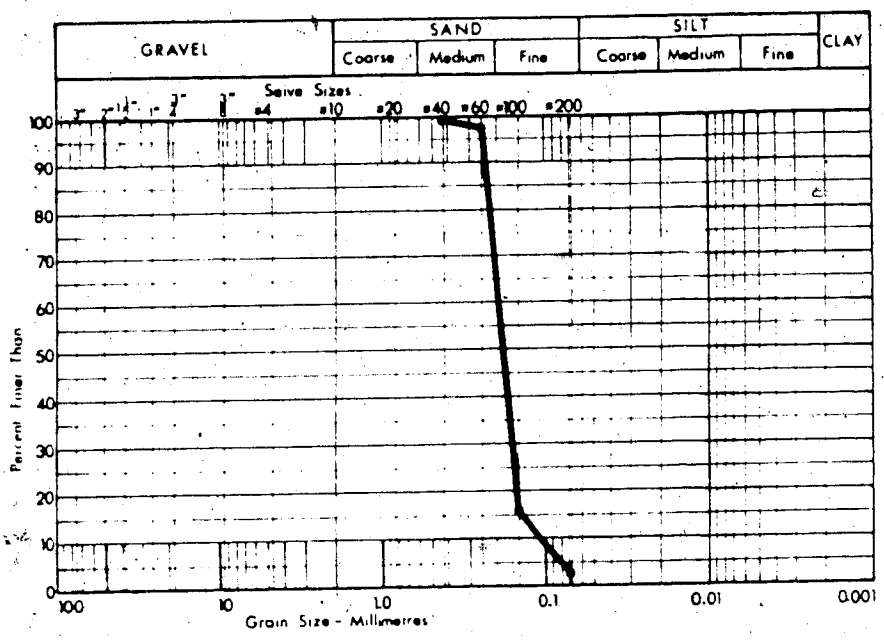

$D_{10} = 0.11mm$
$D_{60} = 0.2mm$
$C_u = 1.8$

Before

FIGURE F13 Sample #17
Test TOS 5

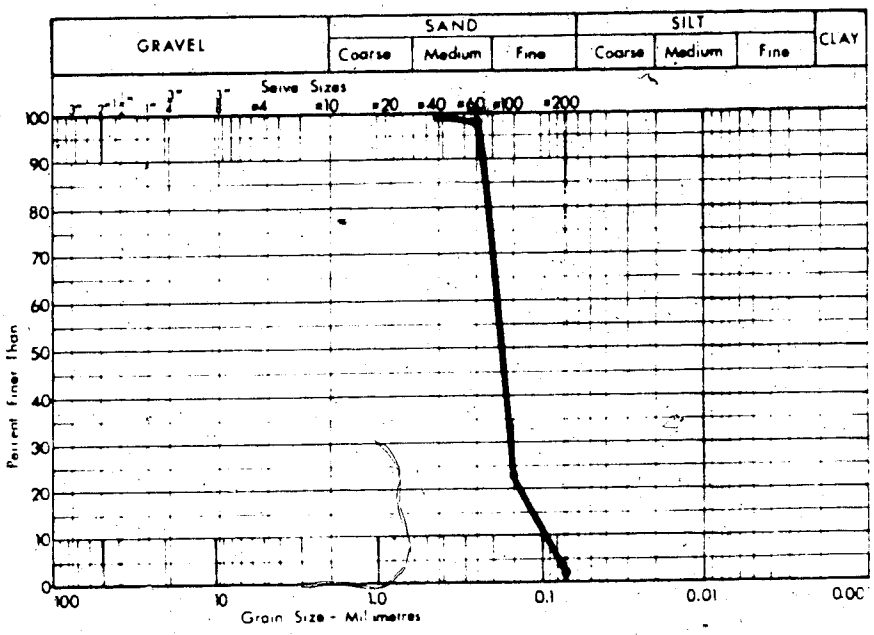

Before

D_{10} = 0.1mm
D_{60} = 0.2mm
C_u = 2.0

FIGURE F14 Sample #16
Test TOS 6

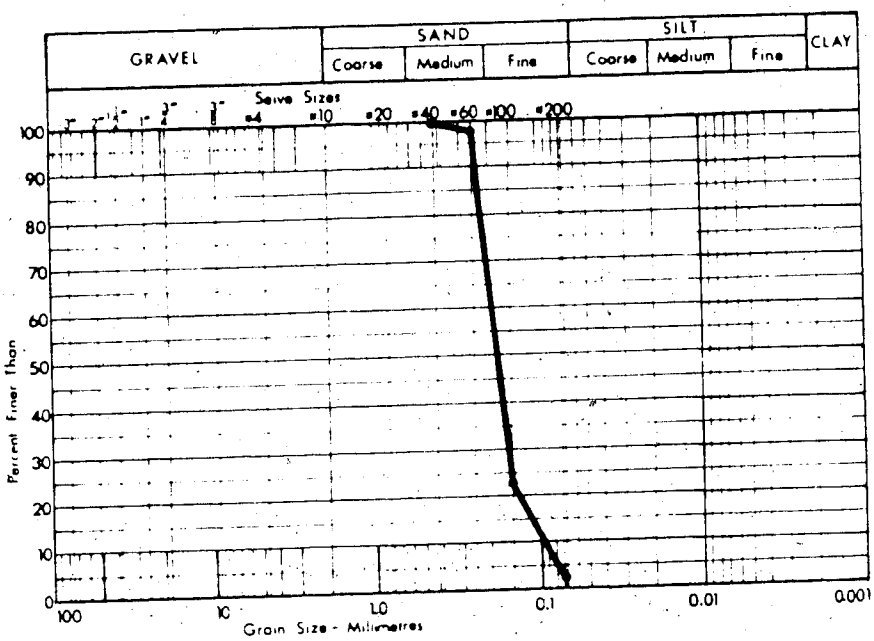

Before

$D_{10} = 0.1mm$
$D_{60} = 0.2mm$
$C_u = 2.0$

FIGURE F15 Sample #45
Test TOS 7

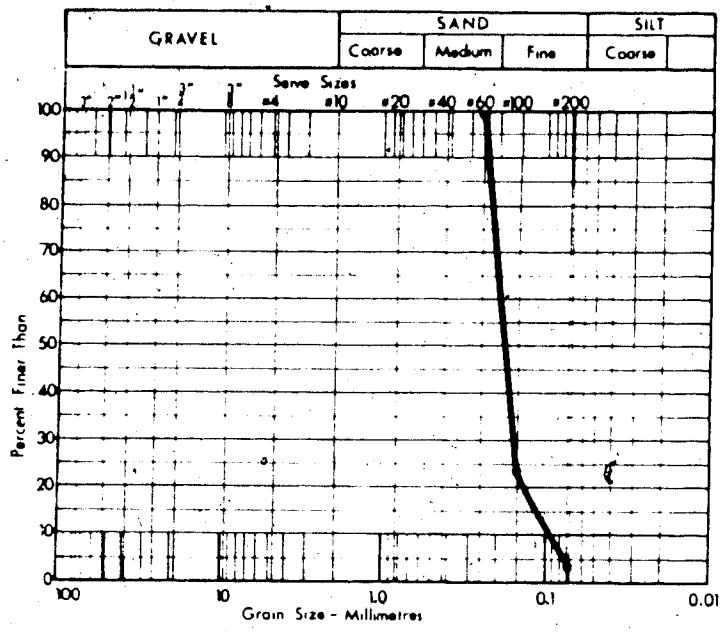

Before

$D_{10} = 0.09mm$
$D_{60} = 0.18mm$
$C_u = 2.0$

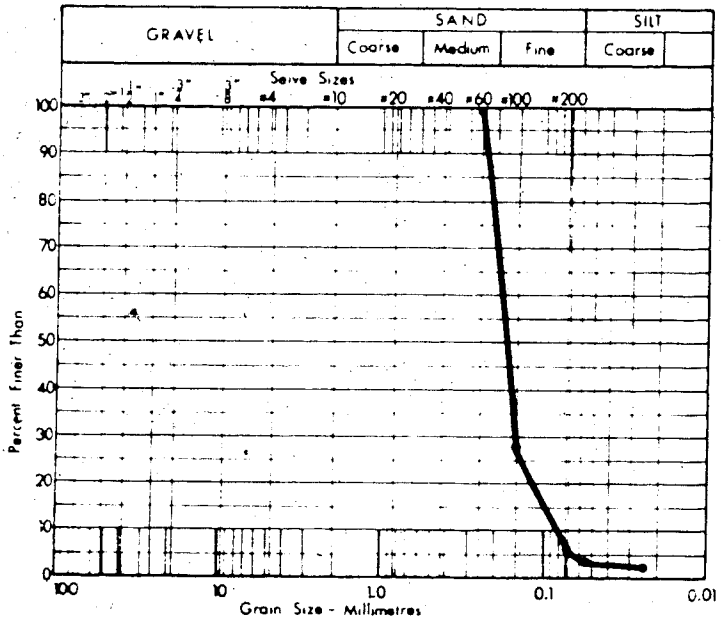

After

$D_{10} = 0.08mm$
$D_{60} = 0.19mm$
$C_u = 2.4$

FIGURE F16 Sample #20
Test TOS 10

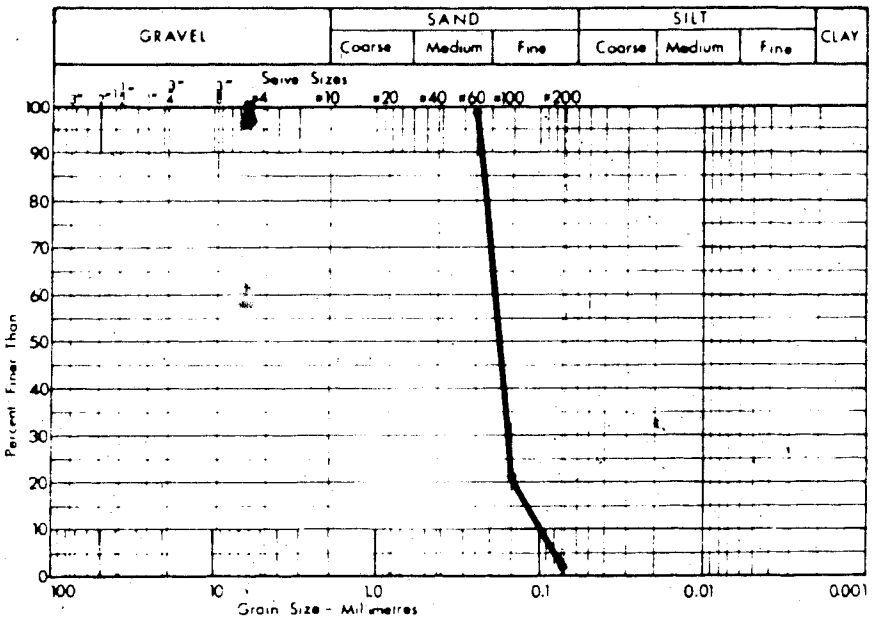

Before

$D_{10} = 0.1mm$
$D_{60} = 0.2mm$
$C_u = 2.0$

FIGURE F17 Sample #22
Test TUS 11

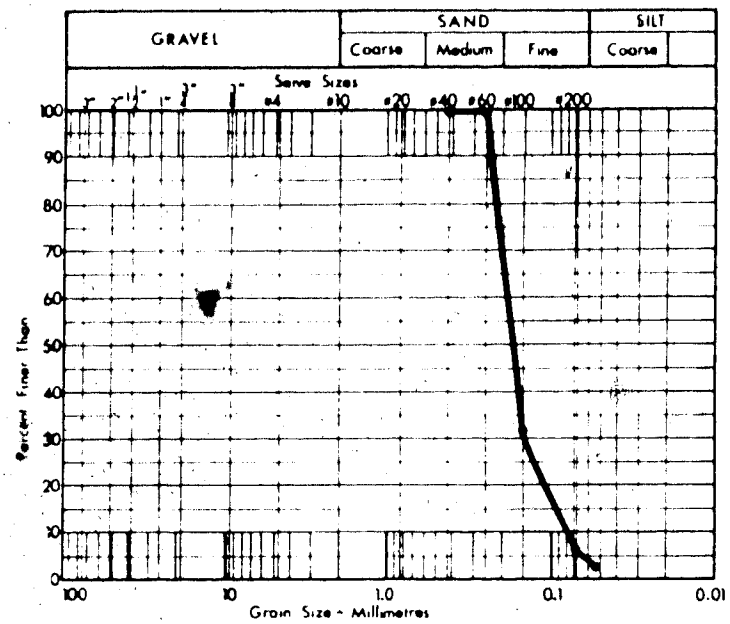

Before

D_{10} = 0.08mm
D_{60} = 0.19mm
C_u = 2.4

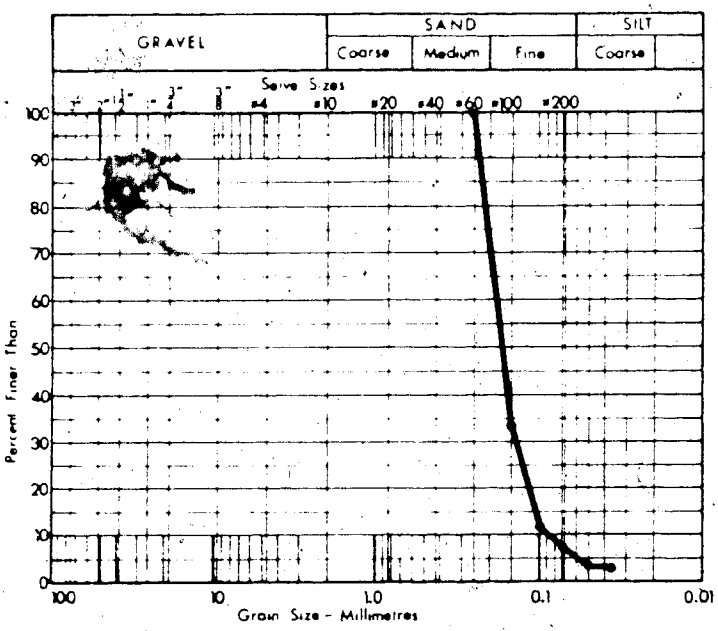

After

D_{10} = 0.09mm
D_{60} = 0.18mm
C_u = 2.0

FIGURE F18 Sample #29
Test TOS 12

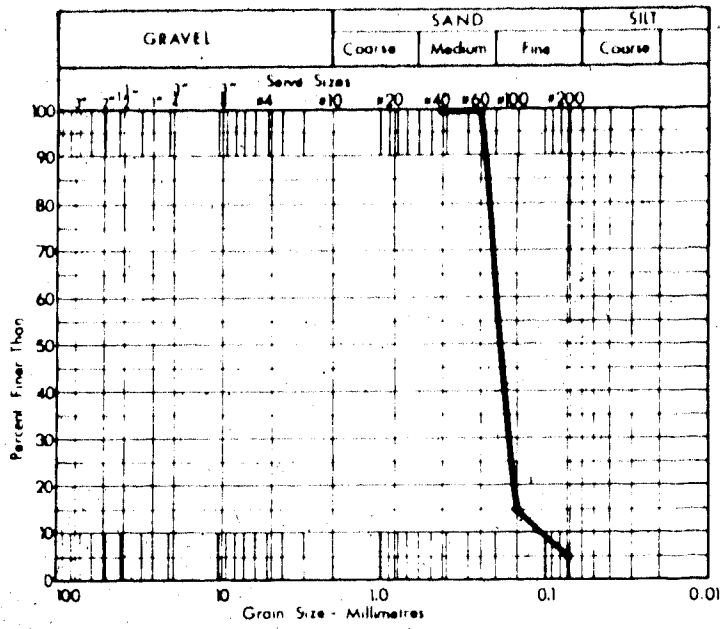

Before

$D_{10} = 0.1mm$
$D_{60} = 0.2mm$
$C_u = 2.0$

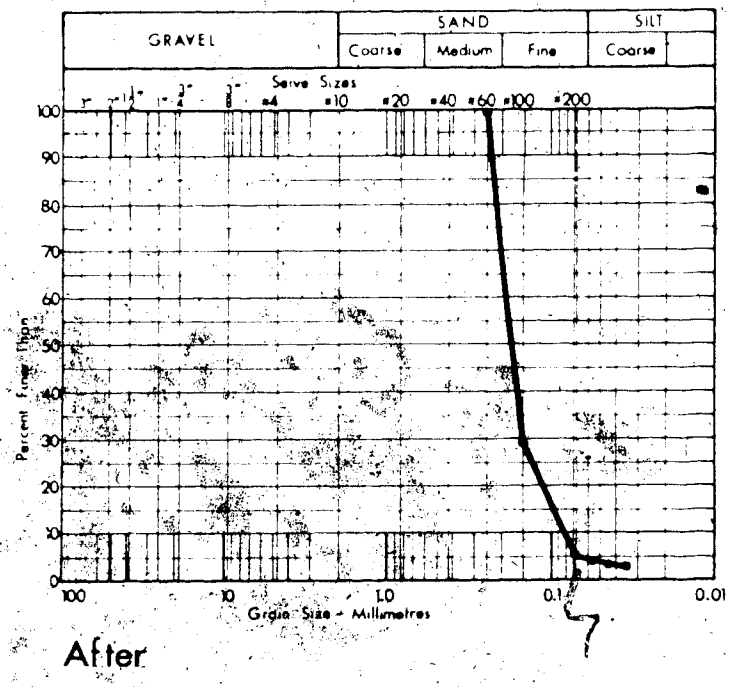

After

$D_{10} = 0.08mm$
$D_{60} = 0.19mm$
$C_u = 2.4$

FIGURE F19 Sample #5, 7, 8
Test TOS 14

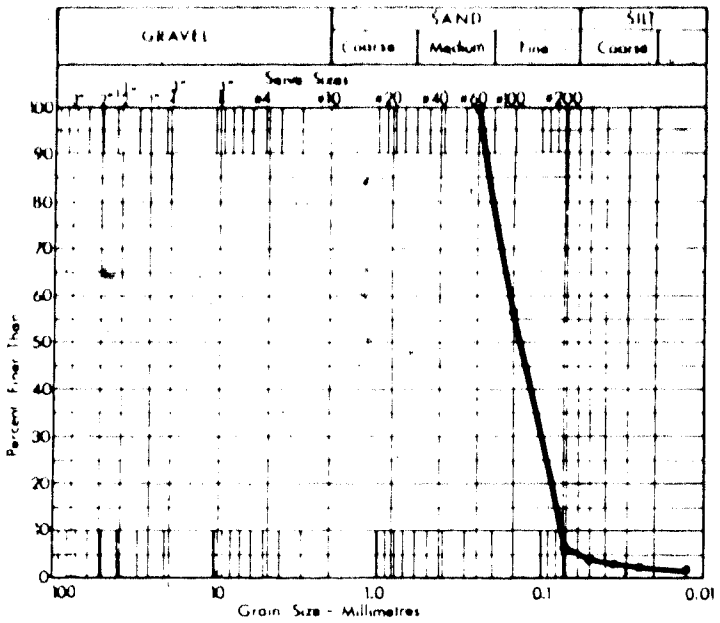

Before

D_{10} = 0.08mm
D_{60} = 0.17mm
C_u = 2.1

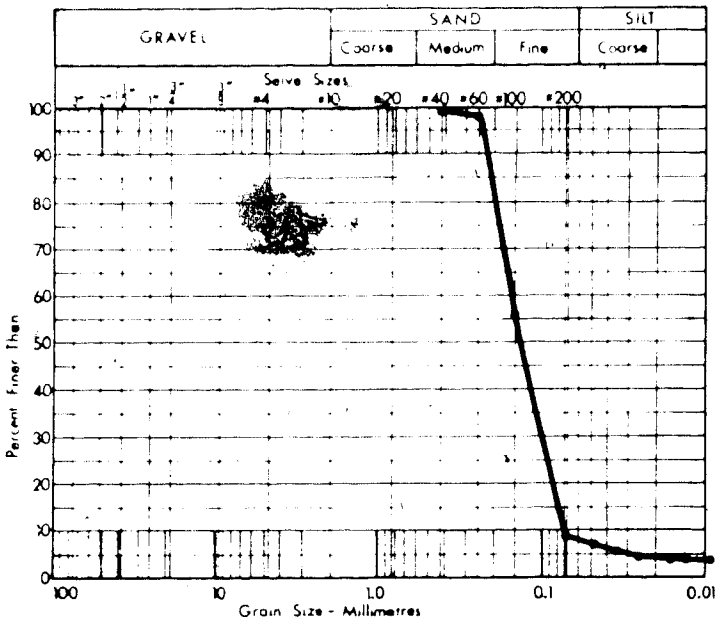

After

D_{10} = 0.07mm
D_{60} = 0.17mm
C_u = 2.4

FIGURE F23 Sample #23
Test TOS 17

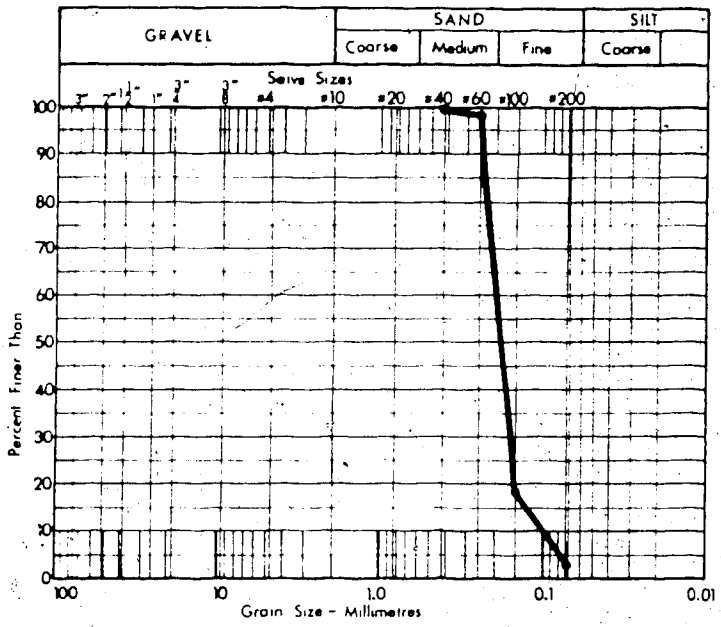

Before

$D_{10} = 0.1mm$
$D_{60} = 0.2mm$
$C_u = 2.0$

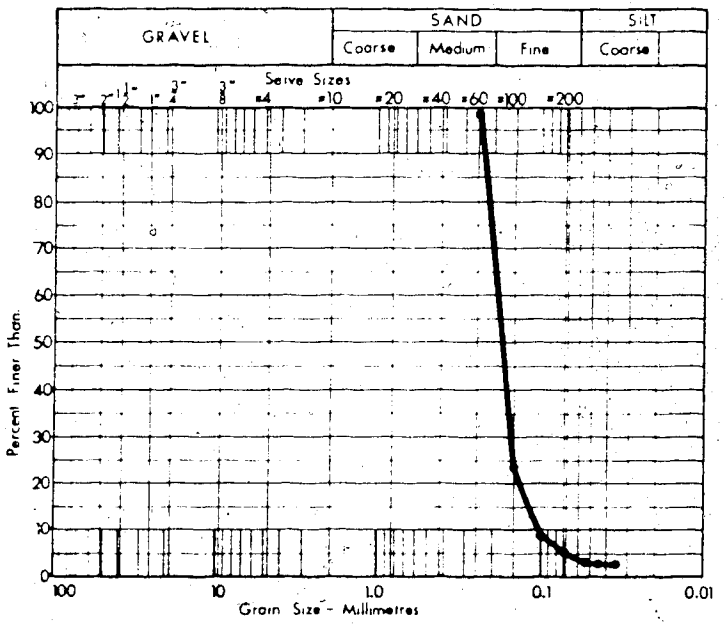

After

$D_{10} = 0.1mm$
$D_{60} = 0.2mm$
$C_u = 2.0$

FIGURE F21 Sample #24
Test TOS 18

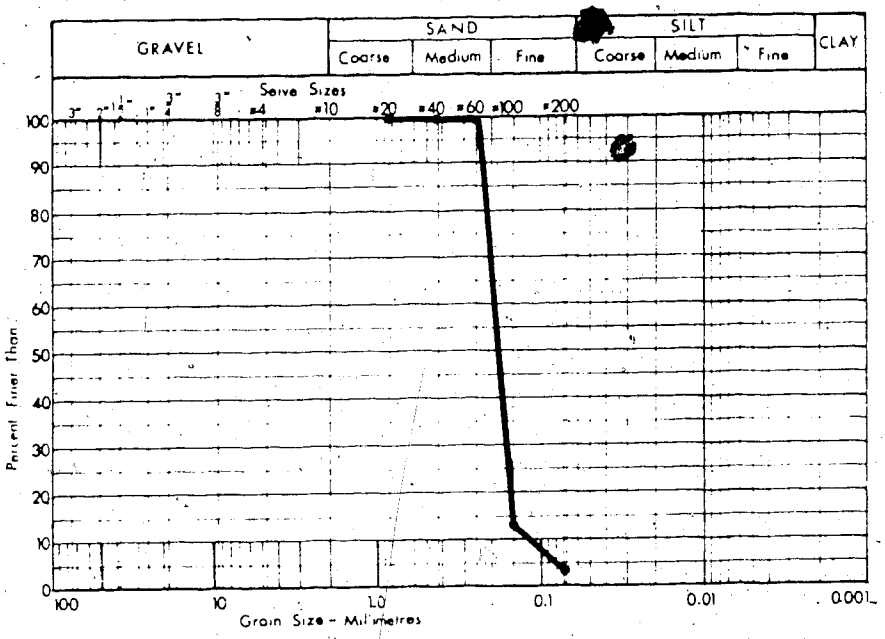

Before

$D_{10} = 0.12\,mm$
$D_{60} = 0.2\,mm$
$C_u = 1.7$

FIGURE F22 Sample #19
Test TOS 19

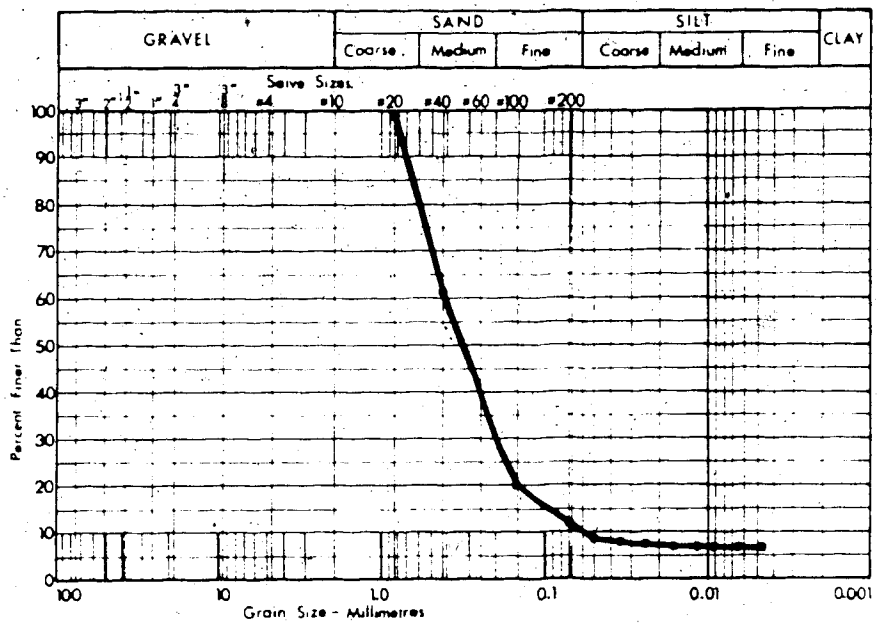

D_{10}=0.06mm
D_{60}=0.4mm
C_u=6.7

Before

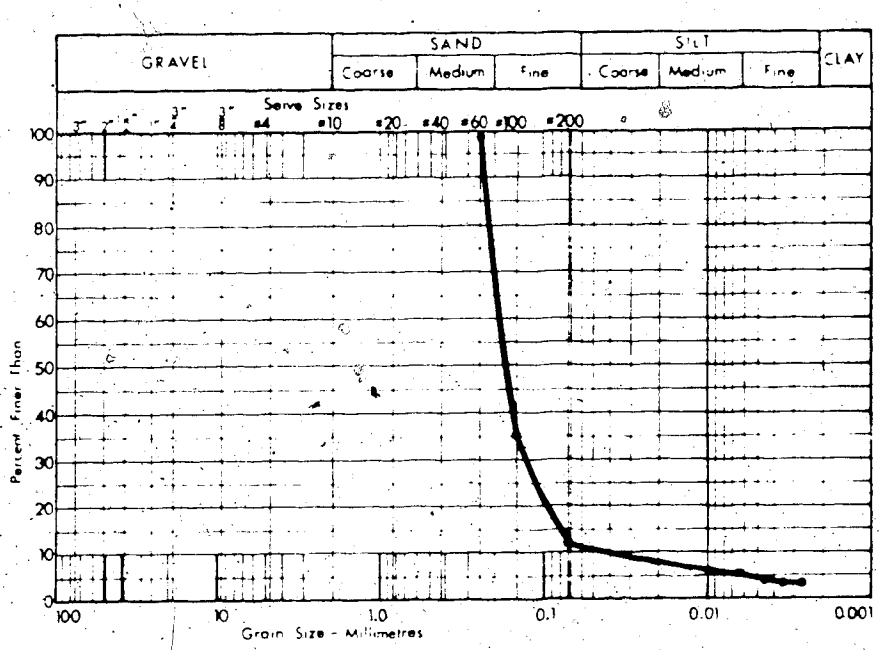

D_{10}=0.07mm
D_{60}=0.19mm
C_u=2.7

After

FIGURE F23 Sample #12B
Test TOS 15

APPENDIX G

SCANNING ELECTRON MICROPHOTOGRAPHS OF VARIOUS OIL SANDS BEFORE AND AFTER HEATING EXPERIMENTS

NOTES:

1. Scanning electron microphotographs of Athabasca and Cold Lake oil sand specimens presented in Appendix G were studied and photographed using a Cambridge Stereoscan electron microscope.

2. Mineral grain fabric and texture of seventeen oil sand specimens are included. Specimen preparation and study methods are described in section 3.9.2 of Volume I.

3. Mineralogic and textural alterations resulting from elevated pressures and temperatures were detected, however, these were relatively minor. Grain crushing is believed to contribute to loss of grain interlocking and reduced angle of shearing resistance.

PLATE G-1 Oven-dried McMurray Formation oil sand from the Suncor minesite.

PLATE G-2 Crystal overgrowth in McMurray Formation oil sand from the Suncor minesite.

PLATE G-3 Tension crack in "case-hardened" Athabasca bitumen between two sand grains (in oven-dried oil sand).

PLATE G-4 "Case-hardening" of bitumen due to unsaturated heating of Athabasca oil sand.

PLATE G-5 Oil-free McMurray Formation sand grains (loosely packed).

PLATE G-6 Oil-free McMurray Formation sand grains.

PLATE G-7 Oil-free Saline Creek sand grains (closely packed).

PLATE G-8 Intact oil-rich Saline Creek oil sand fabric.

PLATE G-9 Bitumen-coated Saline Creek sand grains.

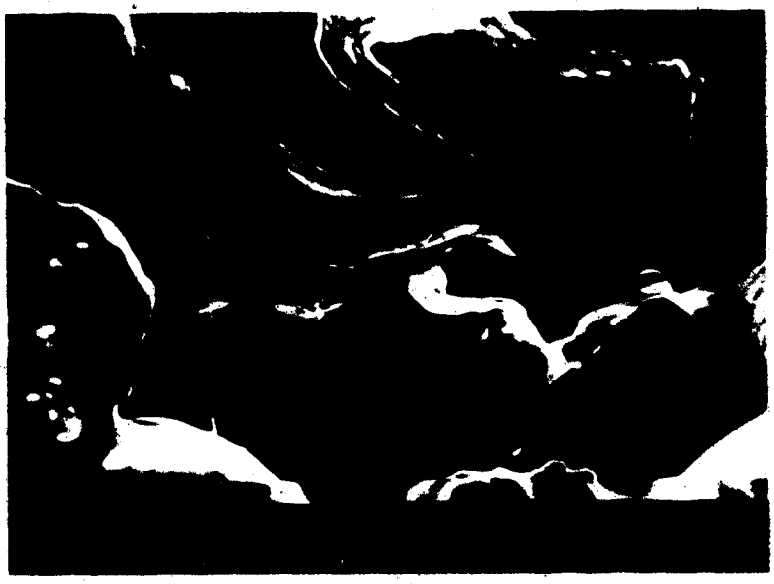

PLATE G-10 Rugose pore channel in Saline Creek oil sand.

PLATE G-11 Crystal overgrowth features in Saline Creek oil sand.

PLATE G-12 Saline Creek oil sand fabric following 100°C permeability test in which 10 percent of the bitumen was removed.

PLATE G-13 Saline Creek sand grain after 100°C permeability experiment.

PLATE G-14 Saline Creek oil sand fabric after 100°C permeability experiment.

PLATE G-15 Bitumen-coated Saline Creek sand grains after 100°C permeability experiment.

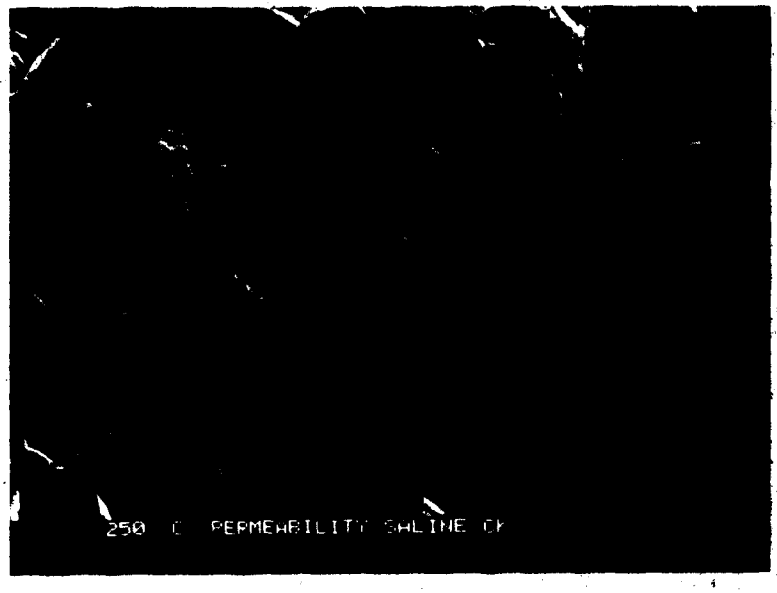

PLATE G-16 Saline Creek oil sand fabric following a 250°C permeability experiment.

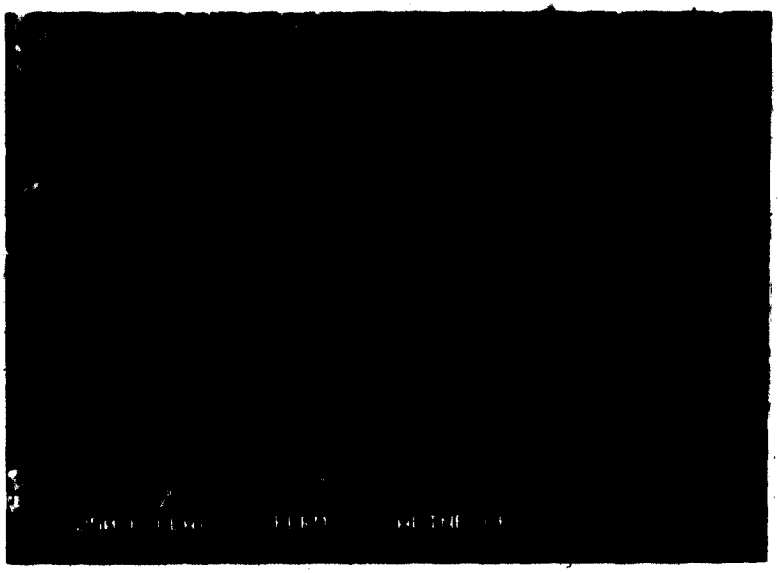

PLATE G-17 Clay particles in Saline Creek oil sand after a 250°C permeability experiment.

PLATE G-18 Clay particles in Saline Creek oil sand fabric (note the platy shape of the clay particles).

PLATE G-19 Saline Creek oil sand fabric after compression under 6 MPa confining stress and 300°C.

PLATE G-20 Bitumen-coated Saline Creek sand grains following 300°C compression test.

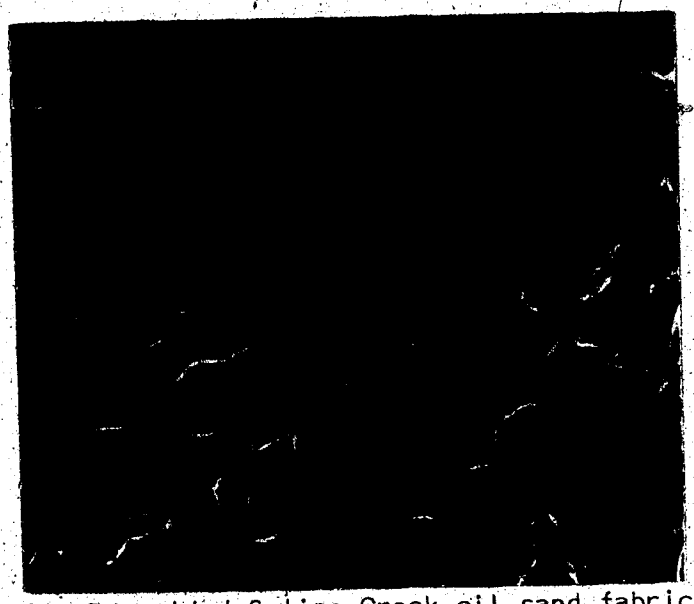

PLATE G-21 Remoulded Saline Creek oil sand fabric (note the clusters of "oil-bonded" grains).

PLATE G-22 Saline Creek oil sand fabric after triaxial compression under 8 MPa effective confining stress at 200°C.

PLATE G-23 Saline Creek oil sand fabric along the principal shear plane following triaxial compression at 200°C.

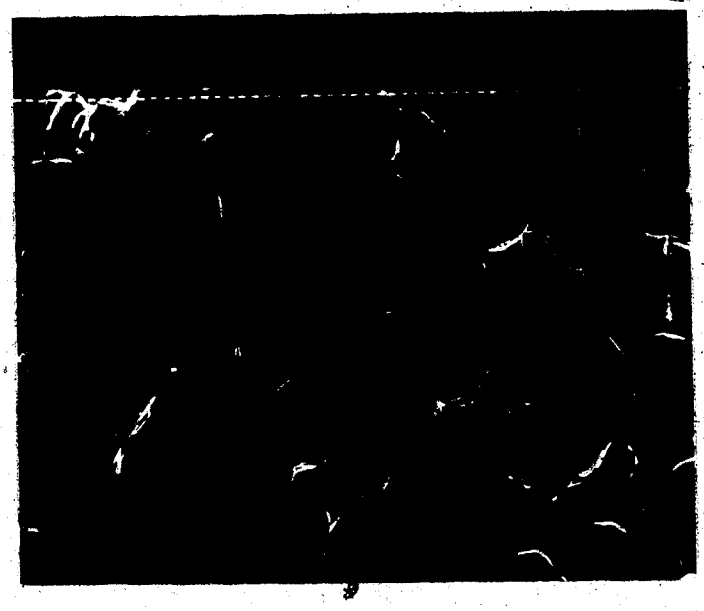

PLATE G-24 Saline Creek oil sand fabric after triaxial compression at 200°C (J-1 constant stress path).

PLATE G-25 Saline Creek oil sand-shear plane fabric after 200°C triaxial compression test.

PLATE G-26 Fabric of oil-rich Saline Creek oil sand after 125°C triaxial compression test.

PLATE G-27 Cold Lake oil sand fabric after triaxial compression under 4 MPa effective confining stress at 200°C.

APPENDIX H

X-RAY DIFFRACTION ANALYSES

APPENDIX H

LEGEND FOR SYMBOLS ON X-RAY DIFFRACTION TRACES

Q – Quartz

F – Feldspar

P – Pyrite (FeS_2)

B – Brookite (TiO_2)

A – Aluminium sample holder

K – Kaolinite

I – Illite

M – Montmorillonite

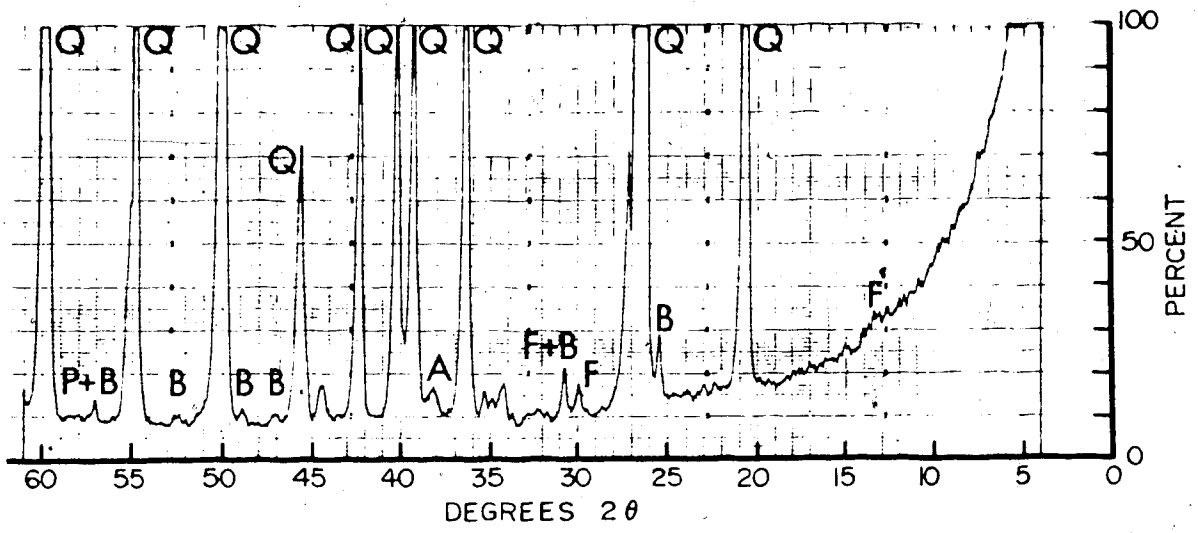

SAMPLE #20

TEST TOS 10 (BEFORE)

FIGURE H1

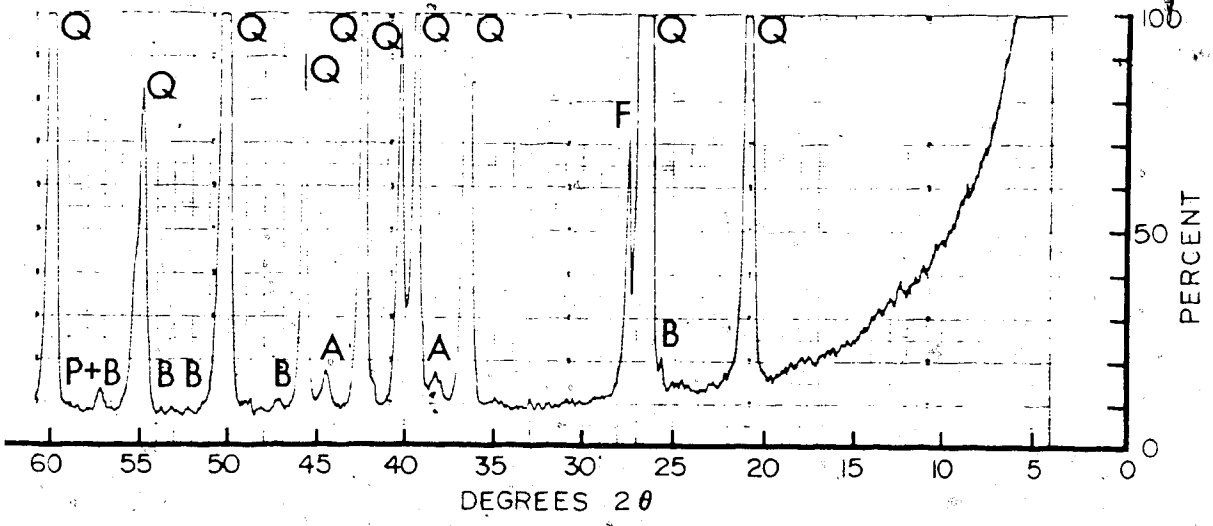

SAMPLE #20

TEST TOS 10 (AFTER)

FIGURE H2

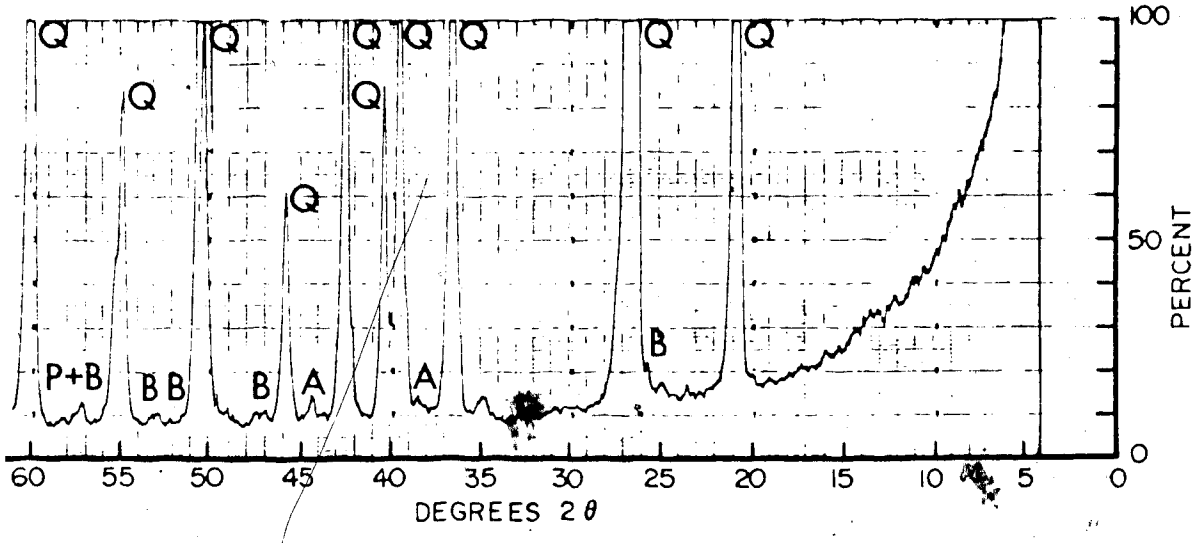

SAMPLE #31

TEST CPERM 5 & CPERM 6 (BEFORE)

FIGURE H3

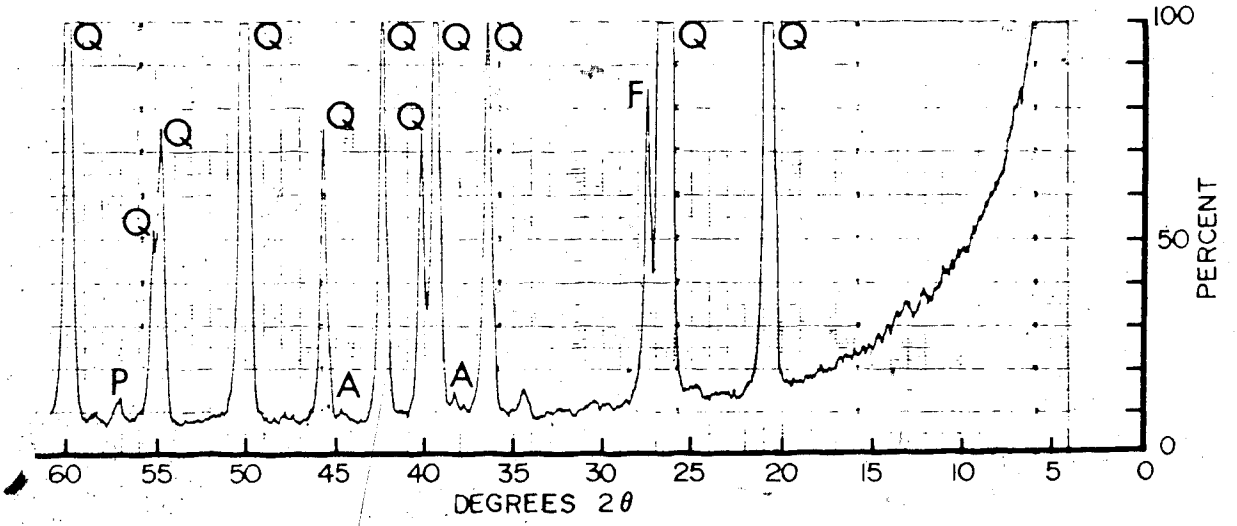

SAMPLE #31A

TEST CPERM 5 (AFTER)

FIGURE H4

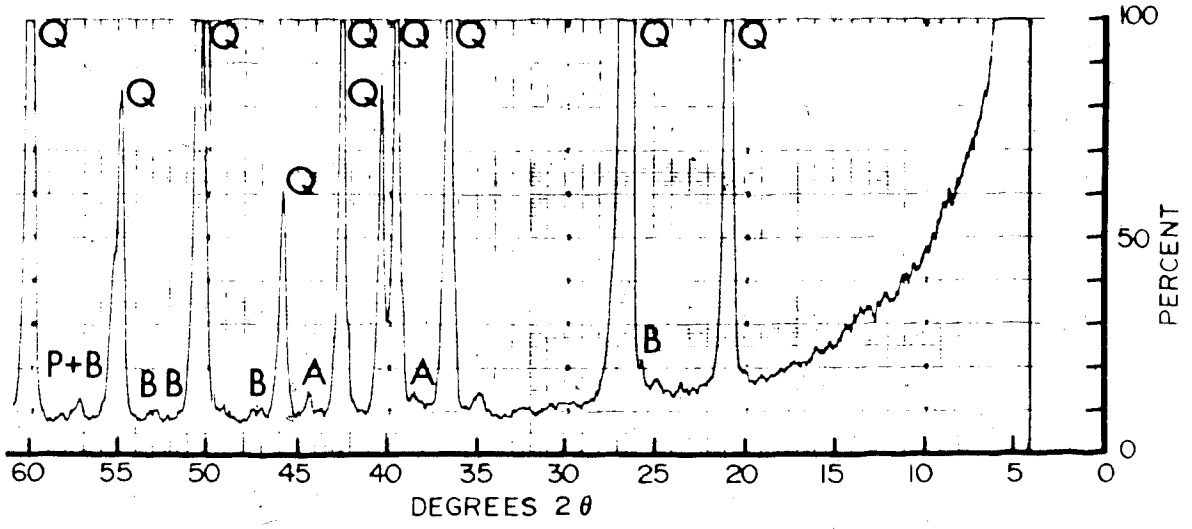

SAMPLE #31

TEST CPERM 5 & CPERM 6 (BEFORE)

FIGURE H3

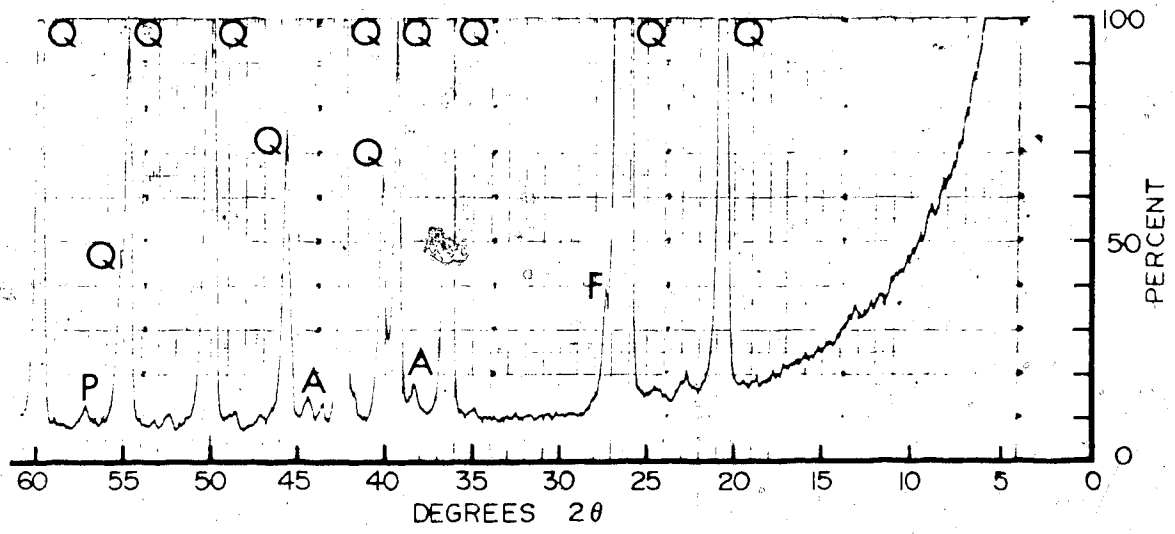

SAMPLE #31B

TEST CPERM 6 AFTER

FIGURE H5

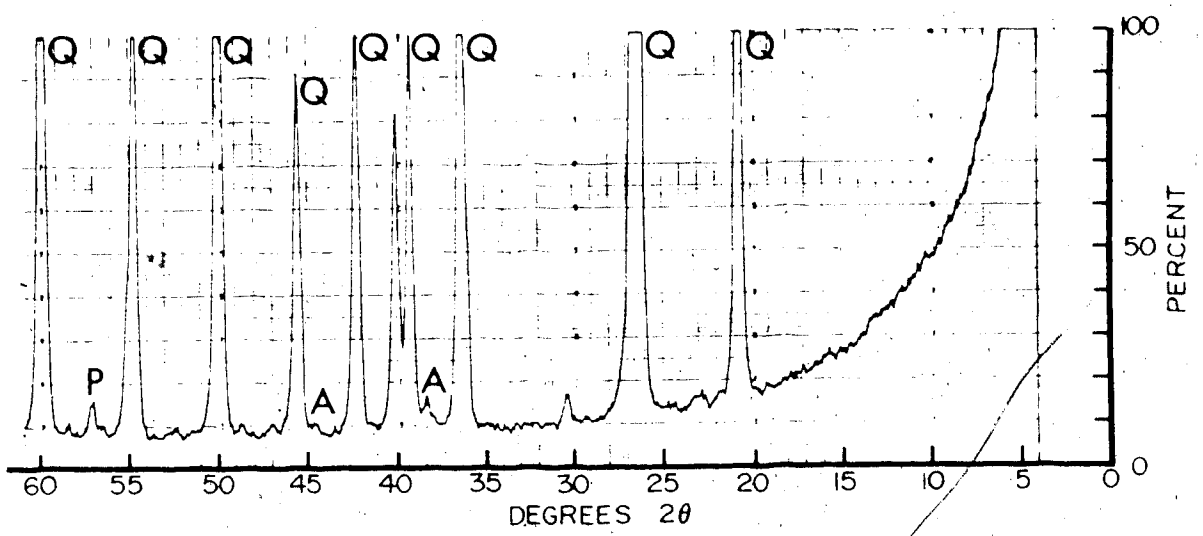

SAMPLE #41

TEST COS 9 (BEFORE)

FIGURE H6

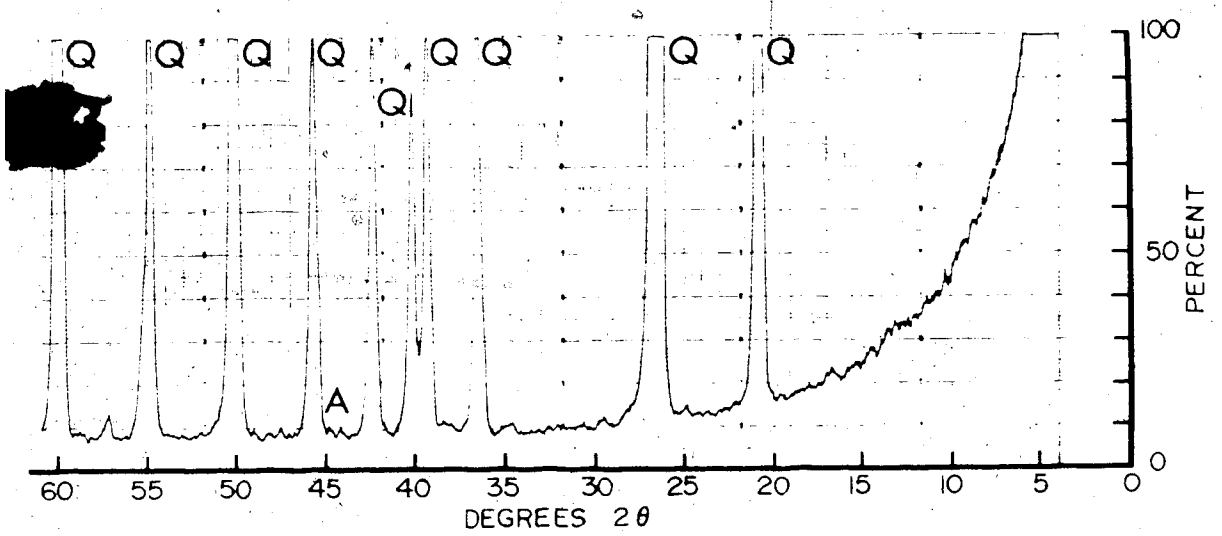

SAMPLE #41

TEST COS 9 (AFTER)

FIGURE H7

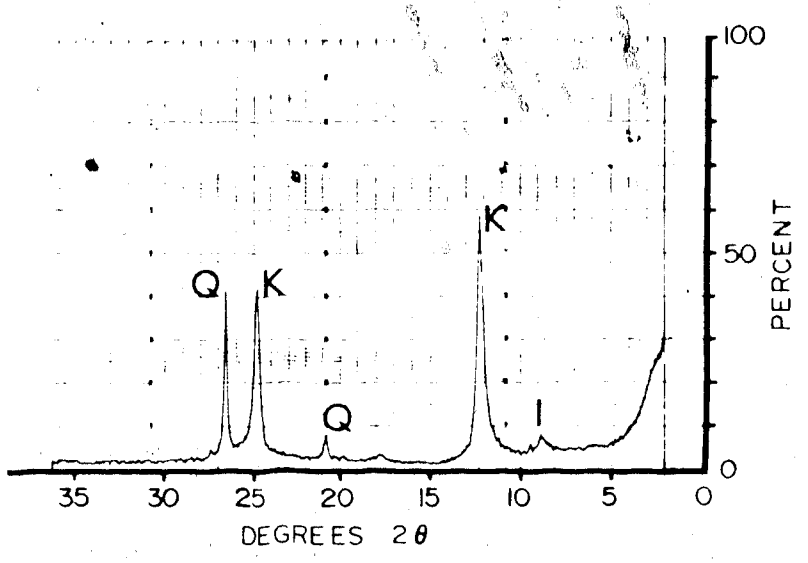

SAMPLE #20 (fines <2μm)

TEST TOS 10 (BEFORE)

FIGURE H8

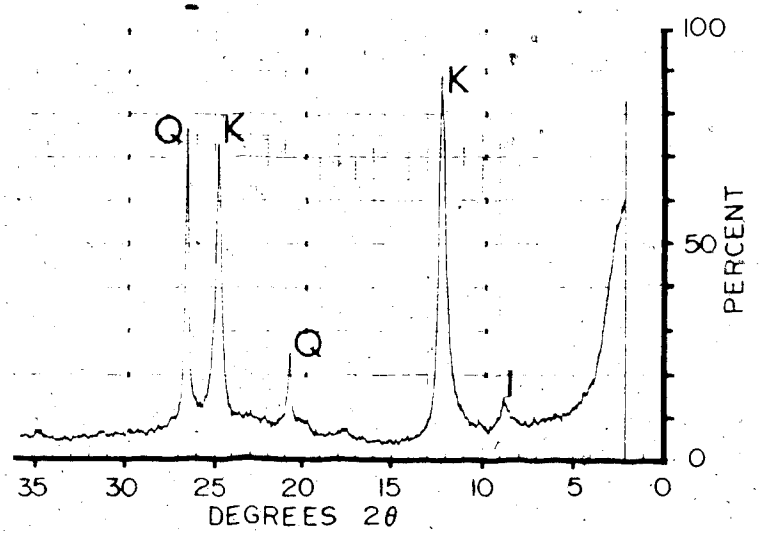

SAMPLE #20 (fines <2μm)

TEST TOS 10 (AFTER)

FIGURE H9

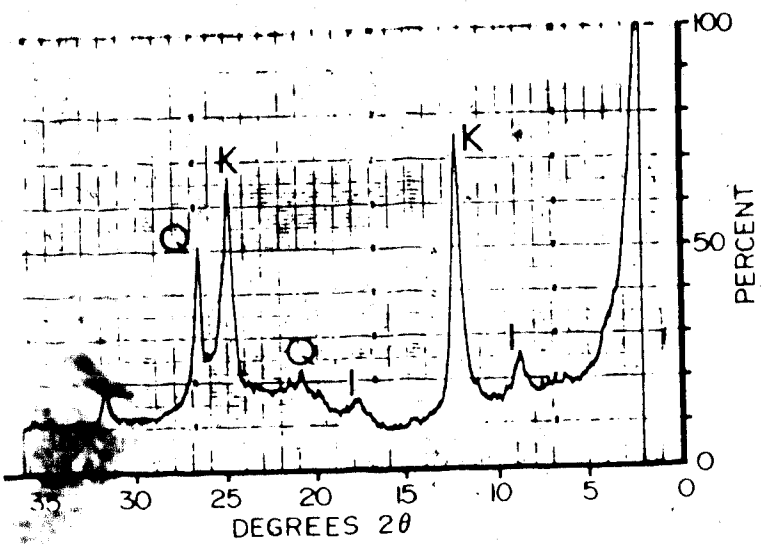

SAMPLE #31 (fines $< 2\mu m$)

TEST CPERM 5 & CPERM 6 (BEFORE)

FIGURE H10

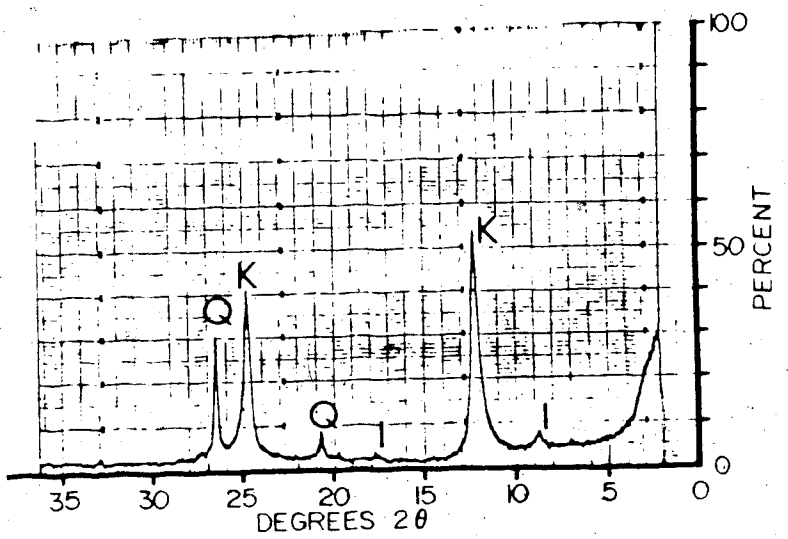

SAMPLE #31A (fines $< 2\mu m$)

TEST CPERM 5 (AFTER)

FIGURE H11

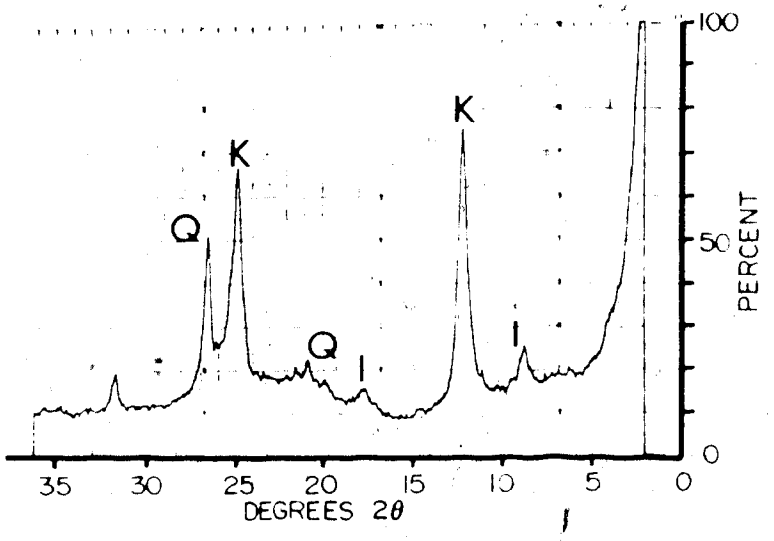

SAMPLE #31 (fines <2μm)

TEST CPERM 5 & CPERM 6 (BEFORE)

FIGURE H10

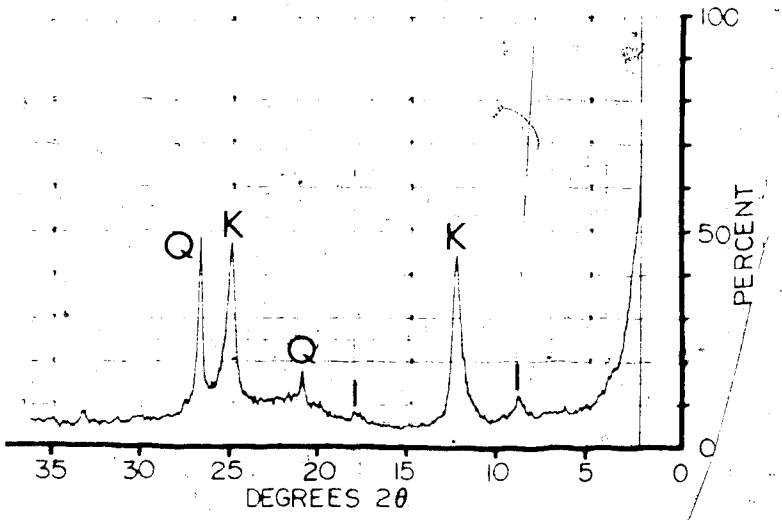

SAMPLE #31 (fines <2μm)

TEST CPERM 6 (AFTER)

FIGURE H12

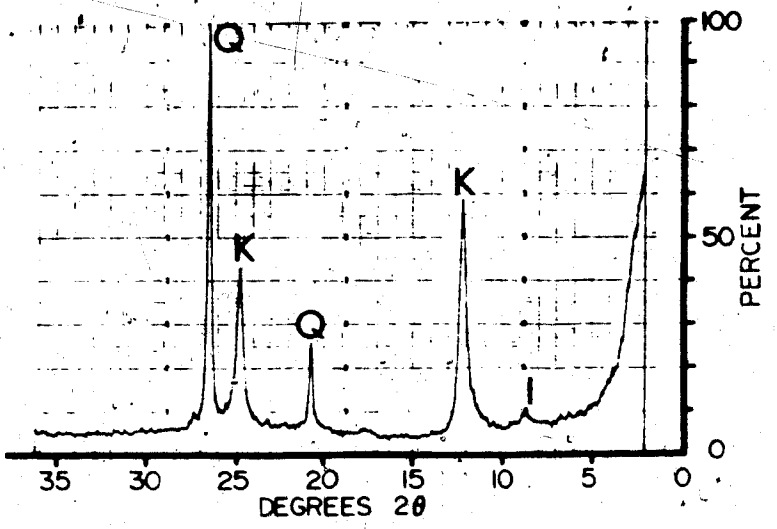

SAMPLE #41 (fines <2μm)

TEST COS 9 (BEFORE)

FIGURE H13

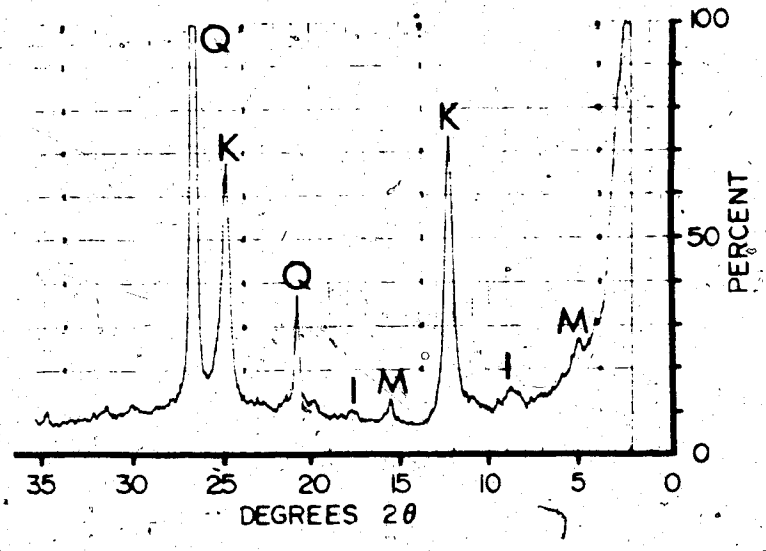

SAMPLE #41 (fines <2μm)

TEST COS 9 (AFTER)

FIGURE H14

APPENDIX I

VISCOSITY OF ATHABASCA BITUMEN AFTER UNSATURATED HEATING

Plate viscometer tests peformed in accordance with
ASTM D3570-77 Procedure B

TABLE 1-1: PLATE VISCOMETER TEST RESULTS FOR AN ATHABASCA BITUMEN SAMPLE HEATED AT 135°C AND 1 ATMOSPHERE FOR 24 HOURS

Plate Area (cm^2)	Film Thickness (μm)	Plate Disp. per Chart Div. (cm)	Chart Speed (cm/sec)	Chart Divs.(#)	Chart Disp. (cm)	Load (Grams)	Shearing Stress (Pascals)	Rate of Shear (sec^{-1})	Viscosity (Pa.s)
6.0	19.4	5×10^{-4}	2.82×10^{-2}	58.0	2.54	200	3.27×10^3	10.90×10^{-2}	0.3×10^5
6.0	19.4	5×10^{-4}	2.82×10^{-2}	29.0	1.27	250	4.09×10^3	16.60×10^{-2}	0.2×10^5
6.0	19.4	5×10^{-4}	2.82×10^{-2}	59.0	1.90	300	4.90×10^3	22.57×10^{-2}	0.2×10^5
6.0	19.4	5×10^{-4}	2.82×10^{-2}	52.0	1.27	350	5.72×10^3	29.76×10^{-2}	0.2×10^5
6.0	19.4	5×10^{-4}	2.82×10^{-2}	54.0	0.64	400	6.54×10^3	38.60×10^{-2}	0.2×10^5
6.0	19.4	5×10^{-4}	2.82×10^{-2}	42.0	0.64	450	7.36×10^3	47.68×10^{-2}	0.1×10^5

TABLE I-2: PLATE VISCOMETER TEST RESULTS FOR AN ATHABASCA BITUMEN SAMPLE REHEATED AT 150°C FOR 24 HOURS (AT 1 ATMOSPHERE)

Plate Area (cm^2)	Film Thickness (μm)	Plate Disp. per Chart Div. (cm)	Chart Speed (cm/sec)	Chart Divs.(#)	Chart Disp. (cm)	Load (Grams)	Shearing Stress (Pascals)	Rate of Shear (sec^{-1})	Viscosity (Pa.s)
6.0	31.4	5×10^{-4}	2.82×10^{-2}	27.0	2.54	500	4.90×10^{3}	4.77×10^{-2}	1.0×10^{5}
6.0	31.4	5×10^{-4}	2.82×10^{-2}	33.0	1.90	400	6.54×10^{3}	7.80×10^{-2}	0.8×10^{5}
6.0	31.4	5×10^{-4}	2.82×10^{-2}	58.0	2.54	500	8.18×10^{3}	10.25×10^{-2}	0.8×10^{5}
6.0	31.4	5×10^{-4}	2.82×10^{-2}	79.0	2.54	600	9.81×10^{3}	13.97×10^{-2}	0.7×10^{5}
6.0	31.4	5×10^{-4}	2.82×10^{-2}	76.0	1.90	700	11.45×10^{3}	17.96×10^{-2}	0.6×10^{5}
6.0	31.4	5×10^{-4}	2.82×10^{-2}	60.0	1.27	800	13.08×10^{3}	21.21×10^{-2}	0.6×10^{5}
6.0	31.4	5×10^{-4}	2.82×10^{-2}	77.0	1.27	900	14.72×10^{3}	27.22×10^{-2}	0.5×10^{5}
6.0	31.4	5×10^{-4}	2.82×10^{-2}	44.0	0.64	1000	16.35×10^{3}	30.87×10^{-2}	0.5×10^{5}

TABLE 1-3: PLATE VISCOMETER TEST RESULTS FOR AN ATHABASCA BITUMEN SAMPLE REHEATED AT 175°C FOR 24 HOURS (AT 1 ATMOSPHERE)

Plate Area (cm^2)	Film Thickness (mm)	Plate Disp. per Chart Div. (cm)	Chart Speed (cm/sec)	Chart Divs.(#)	Chart Disp. (cm)	Load (Grams)	Shearing Stress (Pascals)	Rate of Shear (sec^{-1})	Viscosity (Pa.s)
6.0	37.7	5×10^{-4}	2.82×10^{-2}	24.0	7.57	500	8.18×10^{5}	1.18×10^{-2}	6.9×10^{5}
6.0	37.7	5×10^{-4}	2.82×10^{-2}	27.0	4.44	700	11.45×10^{3}	2.27×10^{-2}	5.0×10^{5}
6.0	37.7	5×10^{-4}	2.82×10^{-2}	49.0	5.70	900	14.72×10^{3}	3.21×10^{-2}	4.6×10^{5}
6.0	37.7	5×10^{-4}	2.82×10^{-2}	81.0	8.32	1100	17.99×10^{3}	4.71×10^{-2}	3.8×10^{5}
6.0	37.7	5×10^{-4}	2.82×10^{-2}	80.0	4.42	1300	21.25×10^{3}	6.75×10^{-2}	3.1×10^{5}
6.0	37.7	5×10^{-4}	2.82×10^{-2}	85.0	5.16	1650	26.98×10^{3}	10.06×10^{-2}	2.7×10^{5}

APPENDIX J

COMPUTER CODES FOR ONE DIMENSIONAL HEAT CONSOLIDATION ANALYSES

LIST OF PARAMETERS

NN:	No. of Nodes
M:	No. of Time Steps
Z:	Height above base (m)
DZ:	Mesh spacing (m)
ZD:	Dimensionless Height Ratio
T:	Temperature (°C)
DT:	Temperature Increase (°C)
DTI:	Incremental Temperature Increase (°C)
DTA:	Average Temperature Increase for element (°C)
DTAI:	Average Incremental Temperature Increase (°C)
P:	Pore Fluid Pressure (kPa)
U:	Excess pore pressure (kPa)
BT:	Pore Pressure Parameter relating pore pressure with temperature
DU:	Pore pressure increase due to heating (kPa)
UDR:	Pore pressure dissipated (kPa)
SVO:	Initial Total Confining Stress (kPa)
SVEO:	Initial Effective Vertical Stress (kPa)
DELT:	Time Increment
ALPHAT:	Thermal Diffusivity (m^2/unit time)
CV:	Coefficient of 1-D Consolidation (m^2/unit time)
MV:	1-D Coefficient of volume compressibility (kPa^{-1})
ALPHAS:	Coefficient of Thermal Expansion of solid particles ($°C^{-1}$)
ALPHAF:	Coefficient of Thermal Expansion of solid pore fluids ($°C^{-1}$)
ALPHDR:	Drained Coefficient of Thermal Expansion of oil sand ($°C^{-1}$)
BETAS:	Compressibility of solid particles (kPa^{-1})
BETAF:	Compressibility of pore fluids (kPa^{-1})
POR:	Porosity
GAMF:	Density of pore fluid (kN/m^3)
GAMS:	Density of solid particles (kN/m^3)
GAM:	Density of oil sand (kN/m^3)
DM:	Total stress change due to density change (kPa)
HCR:	Dimensionless Heat Consolidation Ratio = (cv/)
RM:	Fluid/Mobility Ratio =
ALP:	Partially Drained Coefficient of Thermal Expansion ($°C^{-1}$)
DETA:	Dimensionless distance
DTAU:	Dimensionless time
RT:	Ratio of dimensionless time to dimensionless distance
OMEGA:	Weighting parameter
NPE:	Peclet Number

PROGRAM HC

```
$list hc on *print*
```

```
C*****************************************************************
C*                                                               *
C*                      PROGRAM HC                               *
C*                                                               *
C*     One dimensional heat consolidation of a deeply buried     *
C*     oil sand layer subjected to rapid , non-transient heating.*
C*     Mathematical solution of pore pressure dissipation with   *
C*     time using the solution presented by Taylor(1948).        *
C*     Taylor's solution was derived by the Separation of        *
C*     Variables technique ; pore pressure isochrones are        *
C*     characterized as sine wave functions .                    *
C*                                                               *
C*****************************************************************
C
C       Dimension Array Parameters
C
        DIMENSION ZD(32),TD(15),TV(15),DHT(10)
        DIMENSION U(32,15),DZ(32,15),HT(32,15)
C
C       Constant Parameters & Initial Conditions
C
        M=12
        N=31
        SVEO=6000.
        H=15.
        ALPHDR=3.6E-05
        MV=5.0E-07
        DO 3 K=1,1
        KK=K-1
        DT=200
        CV=1.08*(10**(DT/200))
        BT=1/(0.0016667+(DT/SVEO))
        UO=BT*DT
        HO=2*H*(1+MV*UO+ALPHDR*DT)
        DHO=100*((MV*UO)+(ALPHDR*DT))
C
C       Consolidation
C
        DO 2 J=1,M
        DO 1 I=1,N
        II=I-1
        JJ=J-1
        ZD(I)=II/(2*H)
        TD(J)=J*30
        TV(J)=CV*TD(J)/(H**2)
        F=3.14159/2
        U(I,J)=2*UO*(SIN(2*F*ZD(I))*EXP(-TV(J)*(F**2)))/F
        HT(1,J)=0.
        IF (I.EQ.1) GO TO 1
        DZ(I,J)=(1+MV*U(I,J)+ALPHDR*DT)
        HT(I,J)=HT(II,J)+DZ(I,J)
1       CONTINUE
        DHT(J)=100*(ALPHDR*DT)
2       CONTINUE
C
C       Printout
C
        WRITE(6,100) DT,UO
```

```
      100   FORMAT(//,'DT =',F5.1,/,'UO=',F10.2,//)
            DO 10 J=1,M
            WRITE(6,101)(U(I,J),ZD(I),I=1,N)
      101   FORMAT(G10.4,',',F10.3,',')
      10    CONTINUE
            WRITE(6,102) HO,DHO
      102   FORMAT(//,'HO=',F12.5,/,'DHO=',G10.3,//)
            WRITE(6,103) (TD(J),HT(N,J),DHT(J),J=1,M)
      103   FORMAT(F10.2,',',G10.4,',',G10.5,',')
      3     CONTINUE
            STOP
            END
End of file
$copy *1 *print*
```

PROGRAM HCD

```
$LIST hcd ON *PRINT*
      C*****************************************************************
      C*                                                               *
      C*                  ******************                           *
      C*                  * PROGRAM  HCD   *                           *
      C*                  ******************                           *
      C*     Semi Implicit Finite Difference Solution for              *
      C*    One Dimensional HEAT CONSOLIDATION of Oil Sand             *
      C*    Coupled with Transient Heating by Thermal Diffusion.       *
      C*_______________________________________________________________*
      C*                                                               *
      C*     Properties of the oil sand vary with temperature,         *
      C*    pressure,& effective stress . Variable parameters          *
      C*    include fluid mobility,porosity,bulk density,fluid         *
      C*    & solid densities . pore pressure response to              *
      C*    undrained heating & coefficient of consolidation .         *
      C*                                                               *
      C*    ASSUMPTIONS :                                              *
      C*                                                               *
      C*     1.Oil Saturation is assumed to be constant during         *
      C*     gravity drainage .                                        *
      C*     2.Total vertical stress varies with density of the        *
      C*     heated materials .                                        *
      C*     3.One-way drainage is assumed ; the top boundary of       *
      C*     the oil sand layer is a no-flow boundary.                 *
      C*     4.The top boundary of tne oil sand layer is assumed       *
      C*     to inhibit heat flow .                                    *
      C*     5.Properties of Saline Creek oil sand are used in         *
      C*     the analysis .                                            *
      C*_______________________________________________________________*
      C*                                                               *
      C*       CODED by J.G.Agar , July 1983                           *
      C*       All rights reserved by the author                       *
      C*                                                               *
      C*****************************************************************
      C
      C            ****************
      C            * MAIN PROGRAM *
      C            ****************
      C
      C
      C     Dimension Array Parameters
      C
            NN=32
            M=1441
            M1=721
            M2=361
      C      M3=92
            M4=181
            M5=61
      C      M6=11
            M7=11
            N=NN-1
            MM=M-1
            NI=NN-2
            REAL *4 MV
            COMMON /BLK1/ NN,M,N,MM,NI,DELT,ALPHAT,SVEO
            COMMON /BLK2/ DZ(35,3000),T(35,3000)
            COMMON /BLK3/ Z(35,3000),ZD(35,3000)
            COMMON /BLK4/ UDR(35,3000),U(35,3000)
```

```
119             GAMS=26.5/(1+ALPHAS*DT(I,J)+BETAS*U(I,JI))
120             GAM(I,J)=POR*GAMF+((1-POR)*GAMS)
121             DGAM=GAM(I,J)-21.0
122             DM(I,J)=DGAM*DZ(I,JI)
123             BT(I,J)=1/((1/BT(I,1))+(DT(I,J)/MAF*(SVEO-U(I,JI))))
124             DU(I,J)=BT(I,J)*DT(I,J)
125             CV(I,J)=CV(I,1)*(10**(DT(I,J)/200))
126       25    CONTINUE
127             CALL CONSOL(J,JJ,JI)
128             DO 20 I=2,N
129             JJ=J+1
130             JI=J-1
131             IJ=I+1
132             II=I-1
133             DZ(I,J)=DZ(I,1)*(1+(MV*U(I,J))+ALPHDR*DT(I,J))
134             Z(I,J)=Z(II,J)+DZ(I,J)
135             T(I,J)=T(I,1)+DT(I,J)
136             P(I,J)=P(I,1)+U(I,J)
137       20    CONTINUE
138       30    CONTINUE
139       C
140       C     Dimensionless Parameters
141       C
142             DO 50 J=2,M
143             DO 40 I=2,N
143.5           DH(I,J)=100*(Z(I,J)-Z(I,1))/Z(I,1)
143.51          IF(DT(I,J).LT..001) GO TO 41
143.58          ALP(I,J)=((MV*U(I,J))+(ALPHDR*DT(I,J)))/DT(I,J)
143.65          GO TO 42
143.72    41    ALP(I,J)=ALPHDR
144       42    ZD(I,J)=Z(I,J)/Z(N,J)
145             HCR(I,J)=(CV(I,J)/ALPHAT)/1000
146       40    CONTINUE
147       50    CONTINUE
148       C
149       C     Printout
150       C
151       C      PRINT 95
152       C95    FORMAT('  Depth  Temperature  Pressure  Time ',//)
153       C      WRITE(6,96) (Z(I,M7),T(I,M7),P(I,M7),M7,I=1,N)
154       C96    FORMAT(F7.4,2F11.3,I6)
155       C      WRITE(6,97) (Z(I,M5),T(I,M5),P(I,M5),M5,I=1,N)
156       C97    FORMAT(F7.4,2F11.3,I6)
157       C      WRITE(6,98) (Z(I,M2),T(I,M2),P(I,M2),M2,I=1,N)
158       C98    FORMAT(F7.4,2F11.3,I6)
159       C      WRITE(6,99) (Z(I,M),T(I,M),P(I,M),M,I=1,N)
160       C99    FORMAT(F7.4,2F11.3,I6)
161       C
162             PRINT 100
163       100   FORMAT(//2X,'Temperature vs. Depth & Time')
164             WRITE(6,101)(DT(I,M7),ZD(I,M7),I=1,N)
165       101   FORMAT(G10.3,',',G10.3,',')
166       C      WRITE(6,102)(DT(I,M6),ZD(I,M6),I=1,N)
167       C102   FORMAT(1X,G10.3,',',G10.3,',')
168             WRITE(6,103)(DT(I,M5),ZD(I,M5),I=1,N)
169       103   FORMAT(G10.3,',',G10.3,',')
170             WRITE(6,104)(DT(I,M4),ZD(I,M4),I=1,N)
171       104   FORMAT(1X,G10.3,',',G10.3,',')
172       C      WRITE(6,121)(DT(I,M3),ZD(I,M3),I=1,N)
173       C121   FORMAT(G10.3,',',G10.3,',')
```

```
174           WRITE(6,122)(DT(I,M2),ZD(I,M2),I=1,N)
175     122   FORMAT(1X,G10.3,',',G10.3,',')
176           WRITE(6,123)(DT(I,M1),ZD(I,M1),I=1,N)
177     123   FORMAT(G10.3,',',G10.3,',')
178           WRITE(6,124)(DT(I,M),ZD(I,M),I=1,N)
179     124   FORMAT(1X,G10.3,',',G10.3,',')
180     C
181           PRINT 105
182     105   FORMAT(//2X,'Pore Pressure vs. Depth & Time')
183           WRITE(6,106)(U(I,M7),ZD(I,M7),I=1,N)
184     106   FORMAT(G10.3,',',G10.3,',')
185     C      WRITE(6,107)(U(I,M6),ZD(I,M6),I=1,N)
186     C107   FORMAT(1X,G10.3,',',G10.3,',')
187           WRITE(6,108)(U(I,M5),ZD(I,M5),I=1,N)
188     108   FORMAT(G10.3,',',G10.3,',')
189           WRITE(6,109)(U(I,M4),ZD(I,M4),I=1,N)
190     109   FORMAT(1X,G10.3,',',G10.3,',')
191     C      WRITE(6,126)(U(I,M3),ZD(I,M3),I=1,N)
192     C126   FORMAT(G10.3,',',G10.3,',')
193           WRITE(6,127)(U(I,M2),ZD(I,M2),I=1,N)
194     127   FORMAT(1X,G10.3,',',G10.3,',')
195           WRITE(6,128)(U(I,M1),ZD(I,M1),I=1,N)
196     128   FORMAT(G10.3,',',G10.3,',')
197           WRITE(6,129)(U(I,M),ZD(I,M),I=1,N)
198     129   FORMAT(1X,G10.3,',',G10.3,',')
199     C
200           PRINT 115
201     115   FORMAT(//2X,'Thermal Expansion Coeff. vs. Depth&Time')
202           WRITE(6,116)(ALP(I,M7),ZD(I,M7),I=1,N)
203     116   FORMAT(G10.3,',',G10.3,',')
204     C      WRITE(6,117)(ALP(I,M6),ZD(I,M6),I=1,N)
205     C117   FORMAT(1X,G10.3,',',G10.3,',')
206           WRITE(6,118)(ALP(I,M5),ZD(I,M5),I=1,N)
207     118   FORMAT(G10.3,',',G10.3,',')
208           WRITE(6,119)(ALP(I,M4),ZD(I,M4),I=1,N)
209     119   FORMAT(1X,G10.3,',',G10.3,',')
210     C      WRITE(6,130)(ALP(I,M3),ZD(I,M3),I=1,N)
211     C130   FORMAT(G10.3,',',G10.3,',')
212           WRITE(6,131)(ALP(I,M2),ZD(I,M2),I=1,N)
213     131   FORMAT(1X,G10.3,',',G10.3,',')
214           WRITE(6,132)(ALP(I,M1),ZD(I,M1),I=1,N)
215     132   FORMAT(G10.3,',',G10.3,',')
216           WRITE(6,133)(ALP(I,M),ZD(I,M),I=1,N)
217     133   FORMAT(1X,G10.3,',',G10.3,',')
218     C
218.3         PRINT 135
218.6   135   FORMAT(//2X,'Vertical Expansion vs. Time')
219           WRITE(6,120) DH(N,M7),DH(N,M5),DH(N,M4),DH(N,M2),
220          &DH(N,M1),DH(N,M)
221     120   FORMAT(3G12.6,/,3G12.6,/)
222     C
223           STOP
224           END
225     C
226     C
227     C
228     C*************************************************************
229     C                                                            *
230     C                    SUBROUTINE TEMPD                        *
231     C     Determines temperature distribution with time in       *
```

```
C     oil sand due to 1-D thermal diffusion . The semi       *
C     implicit formulation yields a tridiagonal matrix       *
C     at each time step which is solved using                *
C     THOMAS' S ALGORITHM .                                  *
C                                                            *
C************************************************************
C
      SUBROUTINE TEMPD(J,JJ,JI)
C
      COMMON /BLK1/ NN,M,N,MM,NI,DELT,ALPHAT,SVEO
      COMMON /BLK2/ DZ(35,3000),T(35,3000)
      COMMON /BLK5/ DT(35,3000),DTI(35,3000)
      COMMON /BLK6/ DTA(35,3000),DTAI(35,3000)
      COMMON /BLK10/ A(35),B(35),C(35)
      COMMON /BLK11/ W(35),G(35)
C
      DO 1 I=2,N
      II=I-1
      IJ=I+1
      A(I)=-(ALPHAT*DELT)/(DZ(I,JI)**2)
      B(I)=1+(2*ALPHAT*DELT)/(DZ(I,JI)**2)
      C(I)=A(I)
      IF (I.GT.2) GO TO 2
      W(2)=C(2)/B(2)
      G(2)=(DT(2,JI)-A(2)*DT(1,JI))/B(2)
      GO TO 1
2     IF (I.EQ.N) GO TO 3
      W(I)=C(I)/(B(I)-A(I)*W(II))
      G(I)=(DT(I,JI)-A(I)*G(II))/(B(I)-A(I)*W(II))
      GO TO 1
3     G(N)=(DT(N,JI)-(2*A(N)*G(NI)))/(B(N)-(2*A(N)*W(NI)))
      DT(N,J)=G(N)
1     CONTINUE
      NII=N-2
      DO 4 I=1,NII
      IB=N-I
      IBJ=IB+1
      DT(IB,J)=G(IB)-W(IB)*DT(IBJ,J)
4     CONTINUE
      DO 5 I=2,N
      II=I-1
      DTI(I,J)=DT(I,J)-DT(I,JI)
      DTA(I,J)=(DT(I,J)+DT(II,J))/2
      DTAI(I,J)=(DTI(I,J)+DTI(II,J))/2
5     CONTINUE
      RETURN
      END
C
C
C************************************************************
C                                                            *
C                    SUBROUTINE CONSOL                       *
C     Determines pore pressure dissipation with time         *
C     in oil sand due to 1-D consolidation following each    *
C     transient heating increment .  The semi-implicit       *
C     formulation yields a tridiagonal matrix at each        *
C     time step which is solved using THOMAS'S ALGORITHM .   *
C                                                            *
C************************************************************
C
```

```
      SUBROUTINE CONSOL(J,JJ,JI)
C
      COMMON /BLK1/ NN,M,N,MM,NI,DELT,ALPHAT,SVEO
      COMMON /BLK2/ DZ(35,3000),T(35,3000)
      COMMON /BLK4/ UDR(35,3000),U(35,3000)
      COMMON /BLK5/ DT(35,3000),DTI(35,3000)
      COMMON /BLK6/ DTA(35,3000),DTAI(35,3000)
      COMMON /BLK8/ CV(35,3000),DM(35,3000)
      COMMON /BLK9/ BT(35,3000),DU(35,3000)
      COMMON /BLK12/ AA(35),BB(35),CC(35)
      COMMON /BLK13/ WW(35),GG(35),DGAM(35,3000)
      COMMON /BLK14/ DH(35,3000)
C
      DO 1 I=2,N
      II=I-1
      IJ=I+1
      IF (I.GT.2) GO TO 2
      AA(2)=-(CV(2,J)*DELT)/(DZ(I,1))
      BB(2)=1+(2*CV(2,J)*DELT/(DZ(I,1)))
      CC(2)=AA(2)
      WW(2)=CC(2)/BB(2)
      GG(2)=(U(2,JI)-AA(2)*U(1,JI))/BB(2)
      GO TO 1
    2 CVAVG=(CV(I,J)+CV(II,J))/2
      AA(I)=-(CVAVG*DELT)/(DZ(I,JI)**2)
      BB(I)=1+(2*CVAVG*DELT/(DZ(I,JI)**2))
      CC(I)=AA(I)
      IF (I.EQ.N) GO TO 3
      WW(I)=CC(I)/(BB(I)-AA(I)*WW(II))
      GG(I)=(U(I,JI)-AA(I)*GG(II))/(BB(I)-AA(I)*WW(II))
      GO TO 1
    3 GG(N)=(U(N,JI)-(2*AA(N)*GG(NI)))/(BB(N)-(2*AA(N)*WW(NI))
      UDR(N,J)=GG(N)
    1 CONTINUE
      NII=N-2
      DO 4 I=1,NII
      IB=N-I
      IBJ=IB+1
      UDR(IB,J)=GG(IB)-WW(IB)*UDR(IBJ,J)
    4 CONTINUE
      DO 5 I=2,N
      U(I,J)=DU(I,J)+UDR(I,J)+DM(I,J)
    5 CONTINUE
      RETURN
      END
End of file
$COPY *1 *PRINT*
```

PROGRAM HCCD

```
$LIST hccd ON *PRINT*
      C*****************************************************************
      C*                                                               *
      C*                  ******************                           *
      C*                  * PROGRAM  HCCD  *                           *
      C*                  ******************                           *
      C*     Semi Implicit Finite Difference Solution for              *
      C*    One Dimensional HEAT CONSOLIDATION of Oil Sand             *
      C*    Coupled with Transient Heating by both Thermal             *
      C*    CONVECTION & DIFFUSION.                                    *
      C*                                                               *
      C*                                                               *
      C*---------------------------------------------------------------*
      C*                                                               *
      C*     Properties of the oil sand vary with temperature,         *
      C*    pressure,& effective stress . Variable parameters          *
      C*    include fluid mobility,porosity,bulk density,fluid         *
      C*    & solid densities,pore pressure response to undrained      *
      C*    heating & coefficient of consolidation .                   *
      C*                                                               *
      C*    ASSUMPTIONS :                                              *
      C*                                                               *
      C*     1.Oil Saturation is assumed to be constant during         *
      C*     gravity drainage .                                        *
      C*     2.Total vertical stress varies only with density          *
      C*     changes of the heated material .                          *
      C*     3.One-way drainage is assumed : the top boundary of       *
      C*     the oil sand layer is a no-flow boundary.                 *
      C*     4.The top boundary of tne oil sand layer is assumed       *
      C*     to be a barrier to heat flow .                            *
      C*     5.Properties of Saline Creek oil sand are used in         *
      C*     the analysis .                                            *
      C*---------------------------------------------------------------*
      C*       CODED by J.G.Agar , July 1983                           *
      C*       All rights reserved by the author                       *
      C*                                                               *
      C*****************************************************************
      C
      C            ****************
      C            * MAIN PROGRAM *
      C            ****************
      C
      C
      C     Dimension Array Parameters
      C
      C-----------------------------------------------------------------
            NN=32
            M=1441
      C      M1=541
            M2=721
            M3=361
            M4=181
            M5=61
      C      M6=11
            M7=6
            N=NN-1
            MM=M-1
            NI=NN-2
            REAL *4 MV
            COMMON /BLK1/ NN,M,N,MM,NI,DELT,ALPHAT,SVEO
            COMMON /BLK2/ DZ(35,3000),T(35,3000)
```

```
      COMMON /BLK3/ Z(35,3000),ZD(35,3000)
      COMMON /BLK4/ UDR(35,3000),U(35,3000)
      COMMON /BLK5/ DT(35,3000),DTI(35,3000)
      COMMON /BLK6/ DTA(35,3000),DTAI(35,3000)
      COMMON /BLK7/ P(35,3000)
      COMMON /BLK8/ CV(35,3000),DM(35,3000)
      COMMON /BLK9/ BT(35,3000),DU(35,3000)
      COMMON /BLK10/ A(35),B(35),C(35)
      COMMON /BLK11/ W(100),G(100),RM(35,3000)
      COMMON /BLK12/ AA(35),BB(35),CC(35)
      COMMON /BLK13/ WW(100),GG(100),GAM(35,3000)
      COMMON /BLK14/ DH(35,3000)
C
C     Initial Conditions
C
      SVO=9000.
      SVEO=6000.
      DO 10 I=2,NN
      II=I-1
      DT(I,1)=0
      DTA(I,1)=0
      T(I,1)=5.0
      P(I,1)=3150.-(10*II)
      DZ(I,1)=1.0
      Z(I,1)=II*DZ(I,1)
      U(I,1)=0.
      CV(I,1)=1.08
      RM(I,1)=5.4E-07
      BT(I,1)=SVEO/10.
10    CONTINUE
C
C     Boundary Conditions
C
      DO 11 J=1,M
      Z(1,J)=0.
      T(1,J)=205.
      DT(1,J)=200.
      U(1,J)=1.
      P(1,J)=3150.
      CV(1,J)=10.8
      RM(1,J)=5.4E-06
11    CONTINUE
C
C     Constants
C
      AF=1.00
      DELT=1.0
      MV=5.0E-07
      ALPHDR=3.6E-05
      ALPHAT=6.0E-05
      ALPHAF=5.2E-04
      BETAS=5.0E-09
      ALPHAS=4.3E-05
C
C     Heat Consolidation Calculation
C
      DO 30 J=2,M
      JJ=J+1
      JI=J-1
      CALL TEMPC(J,JJ,JI)
```

```
119             DO 25 I=2,N
120             BETAF=4.0E-07*(10**(DTA(I,J)/200))
121             POR=0.33*(1+MV*U(I,JI)-(ALPHDR-ALPHAS)*DTA(I,J))
122             GAMF=9.85/(1+ALPHAF*DTA(I,J)-BETAF*U(I,J))
123             GAMS=26.5/(1+ALPHAS*DTA(I,J)+BETAS*U(I,J))
124             GAM(I,J)=POR*GAMF+((1-POR)*GAMS)
125             DGAM=GAM(I,J)-21.0
126             DM(I,J)=DGAM*DZ(I,JI)
127             BT(I,J)=1/((1/BT(I,1))+(DTAI(I,J)/(AF*(SVEO-U(I,JI)))))
128             DU(I,J)=BT(I,J)*DTAI(I,J)
129             CV(I,J)=CV(I,1)*(10**(DTA(I,J)/200))
130             RM(I,J)=CV(I,J)*MV
131     25      CONTINUE
132             CALL CONSOL(J,JJ,JI)
133             DO 20 I=2,N
134             JJ=J+1
135             JI=J-1
136             IJ=I+1
137             II=I-1
138             DZ(I,J)=DZ(I,1)*(1+(MV*U(I,J))+ALPHDR*DTA(I,J))
139             Z(I,J)=Z(II,J)+DZ(I,J)
140             T(I,J)=T(I,1)+DT(I,J)
141             P(I,J)=P(I,1)+U(I,J)
142     20      CONTINUE
143     30      CONTINUE
144     C
145     C       Dimensionless Parameters
146     C
147             DO 50 J=2,M
148             DO 40 I=1,N
148.5           DH(I,J)=100*(Z(N,J)-30)/30
149             ZD(I,J)=Z(I,J)/Z(N,J)
150     40      CONTINUE
151     50      CONTINUE
152     C
153     C       Printout
154     C
155     C        PRINT 95
156     C95      FORMAT('  Depth  Temperature  Pressure  Time ',//)
157     C        WRITE(6,96) (Z(I,M7),T(I,M7),P(I,M7),M7,I=1,N)
158     C96      FORMAT(F7.4,2F11.3,I6)
159     C        WRITE(6,97) (Z(I,M5),T(I,M5),P(I,M5),M5,I=1,N)
160     C97      FORMAT(F7.4,2F11.3,I6)
161     C        WRITE(6,98) (Z(I,M3),T(I,M3),P(I,M3),M3,I=1,N)
162     C98      FORMAT(F7.4,2F11.3,I6)
163     C        WRITE(6,99) (Z(I,M),T(I,M),P(I,M),M,I=1,N)
164     C99      FORMAT(F7.4,2F11.3,I6)
165     C
166             PRINT 100
167     100     FORMAT(//2X,'Temperature vs. Depth & Time')
168             WRITE(6,101)(DT(I,M7),ZD(I,M7),I=1,N)
169     101     FORMAT(G10.3,',',G10.3,',')
170     C        WRITE(6,102)(DT(I,M6),ZD(I,M6),I=1,N)
171     C102     FORMAT(1X,G10.3,',',G10.3,',')
172             WRITE(6,103)(DT(I,M5),ZD(I,M5),I=1,N)
173     103     FORMAT(G10.3,',',G10.3,',')
174             WRITE(6,104)(DT(I,M4),ZD(I,M4),I=1,N)
175     104     FORMAT(1X,G10.3,',',G10.3,',')
176             WRITE(6,121)(DT(I,M3),ZD(I,M3),I=1,N)
177     121     FORMAT(G10.3,',',G10.3,',')
```

```
      WRITE(6,122)(DT(I,M2),ZD(I,M2),I=1,N)
122   FORMAT(1X,G10.3,',',G10.3,',')
C      WRITE(6,123)(DT(I,M1),ZD(I,M1),I=1,N)
C123   FORMAT(G10.3,',',G10.3,',')
      WRITE(6,124)(DT(I,M),ZD(I,M),I=1,N)
124   FORMAT(1X,G10.3,',',G10.3,',')
C
      PRINT 105
105   FORMAT(//2X,'Pore Pressure vs. Depth & Time')
      WRITE(6,106)(U(I,M7),ZD(I,M7),I=1,N)
106   FORMAT(G10.3,',',G10.3,',')
C      WRITE(6,107)(U(I,M6),ZD(I,M6),I=1,N)
C107   FORMAT(1X,G10.3,',',G10.3,',')
      WRITE(6,108)(U(I,M5),ZD(I,M5),I=1,N)
108   FORMAT(G10.3,',',G10.3,',')
      WRITE(6,109)(U(I,M4),ZD(I,M4),I=1,N)
109   FORMAT(1X,G10.3,',',G10.3,',')
      WRITE(6,126)(U(I,M3),ZD(I,M3),I=1,N)
126   FORMAT(G10.3,',',G10.3,',')
      WRITE(6,127)(U(I,M2),ZD(I,M2),I=1,N)
127   FORMAT(1X,G10.3,',',G10.3,',')
C      WRITE(6,128)(U(I,M1),ZD(I,M1),I=1,N)
C128   FORMAT(G10.3,',',G10.3,',')
      WRITE(6,129)(U(I,M),ZD(I,M),I=1,N)
129   FORMAT(1X,G10.3,',',G10.3,',')
C
C
      WRITE(6,120) DH(N,M7),DH(N,M5),DH(N,M4),
     &DH(N,M3),DH(N,M2),DH(N,M)
120   FORMAT(3G12.6,/,3G12.6,/)
C
      STOP
      END
C
C
C
C*****************************************************************
C                                                               *
C                    SUBROUTINE TEMPC                           *
C     Determines temperature distribution with time in          *
C     oil sand due to 1-D thermal convection & diffusion .      *
C     The "TRUNCATION CANCELLATION PROCEDURE" (Laumbach,        *
C     1975) was used to formulate the semi-implicit             *
C     difference equations . Forward difference expressions     *
C     are used to approximate time derivatives & central        *
C     differences are used for spatial derivatives. Flow        *
C     velocity is described by Darcy's Law . A central          *
C     difference expression is used to approximate the          *
C     the velocity which varies nonlinearly in space &          *
C     time . Triadagonal matrices are inverted & solved         *
C     by Thomas's Algorithm.                                    *
C                                                               *
C*****************************************************************
C
      SUBROUTINE TEMPC(J,JJ,J1)
C
      COMMON /BLK1/ NN,M,N,MM,NI,DELT,ALPHAT,SVEO
      COMMON /BLK2/ DZ(35,3000),T(35,3000)
      COMMON /BLK3/ Z(35,3000),ZD(35,3000)
      COMMON /BLK5/ DT(35,3000),DTI(35,3000)
```

```
      COMMON /BLK6/ DTA(35,3000),DTAI(35,3000)
      COMMON /BLK10/ A(35),B(35),C(35)
      COMMON /BLK11/ W(100),G(100),RM(35,3000)
      COMMON /BLK4/ UDR(35,3000),U(35,3000)
      DOUBLE PRECISION NPE(35),DTAU(35),DETA(35)
      DOUBLE PRECISION RT(35),OMEGA(35),V(35)
      DIMENSION A1(35),B1(35),C1(35),DD(35)
C
      U(1,1)=5715.
      DO 1 I=2,N
      II=I-1
      IJ=I+1
      RMAV=(RM(IJ,JI)+RM(I,JI)+RM(II,JI))/3
      V(I)=RMAV*((U(IJ,JI)-U(II,JI))/(2*DZ(I,JI)))
      IF(V(I).EQ.0) V(I)=-1.0*RMAV/DZ(I,JI)
      IF(V(I).LT.-1.0) V(I)=-1.0
      IF(V(I).GT.1.0) V(I)=1.0
      DETA(I)=DZ(I,JI)/30
      DTAU(I)=(V(I)*DELT)/30
      RT(I)=V(I)*DELT/DZ(I,JI)
      OMEGA(I)=(0.3333)+((RT(I)**2)/6)
      IF(OMEGA(I).GT.0.5) OMEGA(I)=0.5
      NPE(I)=(V(I)*30)/(ALPHAT/6)
      A(I)=((OMEGA(I)/(2*DTAU(I)))-(1/(2*NPE(I)*(DETA(I)**2)))
     &-(1/(4*DETA(I))))
      B(I)=((1-OMEGA(I))/DTAU(I))+(1/(NPE(I)*DETA(I)**2))
      C(I)=(OMEGA(I)/(2*DTAU(I)))-(1/(2*NPE(I)*DETA(I)**2))
     &+(1/(4*DETA(I))))
      A1(I)=((OMEGA(I)/(2*DTAU(I)))+(1/(2*NPE(I)*(DETA(I)**2)))
     &+(1/(4*DETA(I))))
      B1(I)=((1-OMEGA(I))/DTAU(I))-(1/(NPE(I)*DETA(I)**2))
      C1(I)=(OMEGA(I)/(2*DTAU(I)))+(1/(2*NPE(I)*DETA(I)**2))
     &-(1/(4*DETA(I))))
      IF (I.GT.2) GO TO 2
      DD(2)=A1(2)*DT(1,JI)+B1(2)*DT(2,JI)+C1(2)*DT(3,JI)
      W(2)=C(2)/B(2)
      G(2)=(DD(2)-A(2)*DT(1,JI))/B(2)
      GO TO 1
2     IF (I.EQ.N) GO TO 3
      DD(I)=A1(I)*DT(II,JI)+B1(I)*DT(I,JI)+C1(I)*DT(IJ,JI)
      W(I)=C(I)/(B(I)-A(I)*W(II))
      G(I)=(DD(I)-A(I)*G(II))/(B(I)-A(I)*W(II))
      GO TO 1
3     DD(N)=((A1(N)+C1(N))*DT(NI,JI))+(B1(N)*DT(N,JI))
      G(N)=(DD(N)-((A(N)+C(N))*G(NI)))/(B(N)-((A(N)+C(N))*W(NI)))
      DT(N,J)=G(N)
1     CONTINUE
      NII=N-2
      DO 4 I=1,NII
      IB=N-I
      IBJ=IB+1
      DT(IB,J)=G(IB)-W(IB)*DT(IBJ,J)
4     CONTINUE
      DO 5 I=2,N
      II=I-1
      IF(DT(I,J).LT.0) DT(I,J)=-DT(I,J)
      IF(DT(I,J).GT.200) DT(I,J)=200.
      DTI(I,J)=DT(I,J)-DT(I,JI)
      DTA(I,J)=(DT(I,J)+DT(II,J))/2
      DTAI(I,J)=(DTI(I,J)+DTI(II,J))/2
```

```
      5     CONTINUE
            RETURN
            END
C
C
C*****************************************************************
C                                                                *
C                     SUBROUTINE CONSOL                          *
C     Determines pore pressure dissipation with time             *
C     in oil sand due to 1-D consolidation following each        *
C     transient heating increment . The semi-implicit            *
C     formulation yields a tridiagonal matrix at each            *
C     time step which is inverted & solved using                 *
C     "THOMAS'S ALGORITHM" .                                     *
C                                                                *
C*****************************************************************
C
      SUBROUTINE CONSOL(J,JJ,JI)
C
      COMMON /BLK1/ NN,M,N,MM,NI,DELT,ALPHAT,SVEO
      COMMON /BLK2/ DZ(35,3000),T(35,3000)
      COMMON /BLK4/ UDR(35,3000),U(35,3000)
      COMMON /BLK5/ DT(35,3000),DTI(35,3000)
      COMMON /BLK6/ DTA(35,3000),DTAI(35,3000)
      COMMON /BLK8/ CV(35,3000),DM(35,3000)
      COMMON /BLK9/ BT(35,3000),DU(35,3000)
      COMMON /BLK12/ AA(35),BB(35),CC(35)
      COMMON /BLK13/ WW(100),GG(100),DGAM(35,3000)
      COMMON /BLK14/ DH(35,3000)
C
      U(1,1)=0.
      DO 1 I=2,N
      II=I-1
      IJ=I+1
      IF (I.GT.2) GO TO 2
      AA(2)=-(CV(2,J)*DELT)/1.0
      BB(2)=1+(2*CV(2,J)*DELT/1.0)
      CC(2)=AA(2)
      WW(2)=CC(2)/BB(2)
      GG(2)=(U(2,JI)-AA(2)*U(1,JI))/BB(2)
      GO TO 1
    2 CVAVG=(CV(I,J)+CV(II,J))/2
      AA(I)=-(CVAVG*DELT)/(DZ(I,JI)**2)
      BB(I)=1+(2*CVAVG*DELT/(DZ(I,JI)**2))
      CC(I)=AA(I)
      IF (I.EQ.N) GO TO 3
      WW(I)=CC(I)/(BB(I)-AA(I)*WW(II))
      GG(I)=(U(I,JI)-AA(I)*GG(II))/(BB(I)-AA(I)*WW(II))
      GO TO 1
    3 GG(N)=(U(N,JI)-(2*AA(N)*GG(NI)))/(BB(N)-(2*AA(N)*WW(NI)))
      UDR(N,J)=GG(N)
    1 CONTINUE
      NII=N-2
      DO 4 I=1,NII
      IB=N-I
      IBJ=IB+1
      UDR(IB,J)=GG(IB)-WW(IB)*UDR(IBJ,J)
    4 CONTINUE
      DO 5 I=2,N
      U(I,J)=DU(I,J)+UDR(I,J)+DM(I,J)
```

```
      IF(U(I,J).LT.0) U(I,J)=-U(I,J)
    5 CONTINUE
      RETURN
      END
End of file
$COPY *1 *PRINT*
```

PROGRAM HCDR

```
$LIST hcdr ON *PRINT*
      C*****************************************************************
      C*                                                               *
      C*                  ******************                           *
      C*                  * PROGRAM  HCDR  *                           *
      C*                  ******************                           *
      C*     Semi Implicit Finite Difference Solution for              *
      C*    One Dimensional HEAT CONSOLIDATION of Oil Sand             *
      C*    Coupled with Transient Heating by Thermal Diffusion        *
      C*    in Radial Coordinates .                                    *
      C*_______________________________________________________________*
      C*                                                               *
      C*     Properties of the oil sand vary with temperature,         *
      C*    pressure,& effective stress . Variable parameters          *
      C*    include fluid mobility,porosity,bulk density,fluid         *
      C*    & solid densities , pore pressure response to              *
      C*    undrained heating & coefficient of consolidation .         *
      C*                                                               *
      C*    ASSUMPTIONS :                                              *
      C*                                                               *
      C*     1.Oil Saturation is assumed to be constant during         *
      C*     gravity drainage .                                        *
      C*     2.Total stress variation with density of the heated       *
      C*     material is not considered .                              *
      C*     3.One-way radial drainage is assumed ;                    *
      C*     4.The lateral boundaries are constant pressure/temp-      *
      C*     erature boundaries .                                      *
      C*     5.Properties of Saline Creek oil sand are used in         *
      C*     the analysis .                                            *
      C*_______________________________________________________________*
      C*       CODED by J.G.Agar , July 1983                           *
      C*       All rights reserved by the author                       *
      C*                                                               *
      C*****************************************************************
      C
      C            ****************
      C            * MAIN PROGRAM *
      C            ****************
      C
      C
      C     Dimension Array Parameters
      C
            NN=32
            M=1441
      C      M1=541
            M2=721
            M3=361
            M4=181
            M5=61
      *C     M6=11
            M7=6
            N=NN-1
            MM=M-1
            NI=NN-2
            REAL *4 MV
            COMMON /BLK1/ NN,M,N,MM,NI,DELT,ALPHAT,SVEO
            COMMON /BLK2/ DR(35,3000),T(35,3000)
            COMMON /BLK3/ R(35,3000),RD(35,3000)
            COMMON /BLK4/ UDR(35,3000),U(35,3000)
```

```
      COMMON /BLK5/ DT(35,3000),DTI(35,3000)
      COMMON /BLK6/ DTA(35,3000),DTAI(35,3000)
      COMMON /BLK7/ P(35,3000),HCR(35,3000)
      COMMON /BLK8/ CV(35,3000),DM(35,3000)
      COMMON /BLK9/ BT(35,3000),DU(35,3000)
      COMMON /BLK10/ A(35),B(35),C(35)
      COMMON /BLK11/ W(35),G(35)
      COMMON /BLK12/ AA(35),BB(35),CC(35)
      COMMON /BLK13/ WW(35),GG(35),GAM(35,3000)
      COMMON /BLK14/ ALP(35,3000)
C
C     Initial Conditions
C
      SVO=9000.
      SVEO=6000.
      DO 10 I=2,NN
      II=I-1
      DT(I,1)=0
      DTA(I,1)=0
      T(I,1)=5.0
      P(I,1)=3000.
      DR(I,1)=2.0
      R(I,1)=II*DR(I,1)
      U(I,1)=0.
      CV(I,1)=1.08
      BT(I,1)=SVEO/10.
10    CONTINUE
C
C     Boundary Conditions
C
      DO 11 J=1,M
      R(1,J)=0.
      RD(1,J)=0.
      T(1,J)=205.
      DT(1,J)=200.
      U(1,J)=0.
      P(1,J)=3000.
      CV(1,J)=10.8
11    CONTINUE
C
C     Constants
C
      AF=1.00
      DELT=5.0
      MV=5.0E-07
      ALPHDR=3.6E-05
      ALPHAT=6.0E-05
      ALPHAF=5.2E-04
      BETAS=5.0E-09
      ALPHAS=4.3E-05
C
C     Heat Consolidation Calculation
C
      DO 30 J=2,M
      JJ=J+1
      JI=J-1
      CALL TEMPD(J,JJ,JI)
      DO 25 I=2,N
      BETAF=4.0E-07*(10**(DT(I,J)/200))
      POR=0.33*(1+MV*U(I,JI)-(ALPHDR-ALPHAS)*DT(I,J))
```

```
      GAMF=9.85/(1+ALPHAF*DT(I,J)-BETAF*U(I,J))
      GAMS=26.5/(1+ALPHAS*DT(I,J)+BETAS*U(I,J))
      GAM(I,J)=POR*GAMF+((1-POR)*GAMS)
      DGAM=GAM(I,J)-21.0
      DM(I,J)=DGAM*1.0
      BT(I,J)=1/((1/BT(I,1))+(DTI(I,J)/(AF*(SVEO-U(I,JI)))))
      DU(I,J)=BT(I,J)*DTI(I,J)
      CV(I,J)=CV(I,1)*(10**(DT(I,J)/200))
25    CONTINUE
      CALL CONSOL(J,JJ,JI)
      DO 20 I=2,N
      JJ=J+1
      JI=J-1
      IJ=I+1
      II=I-1
      DR(I,J)=DR(I,1)*(1+(MV*U(I,J))+ALPHDR*DT(I,J))
      R(I,J)=R(II,J)+DR(I,J)
      T(I,J)=T(I,1)+DT(I,J)
      P(I,J)=P(I,1)+U(I,J)
20    CONTINUE
30    CONTINUE
C
C     Dimensionless Parameters
C
      DO 50 J=2,M
      DO 40 I=2,N
      IF(DT(I,J).LE.0.001)GO TO 41
      ALP(I,J)=((MV*U(I,J))+(ALPHDR*DT(I,J)))/DT(I,J)
      GO TO 42
41    ALP(I,J)=ALPHDR
42    RD(I,J)=R(I,J)/R(N,J)
      HCR(I,J)=(CV(I,J)/ALPHAT)/1000
40    CONTINUE
50    CONTINUE
C
C     Printout
C
C      PRINT 95
C95    FORMAT('  Radius  Temperature  Pressure  Time ',//)
C      WRITE(6,96) (R(I,M7),T(I,M7),P(I,M7),M7,I=1,N)
C96    FORMAT(F7.4,2F11.3,I6)
C      WRITE(6,97) (R(I,M5),T(I,M5),P(I,M5),M5,I=1,N)
C97    FORMAT(F7.4,2F11.3,I6)
C      WRITE(6,98) (R(I,M3),T(I,M3),P(I,M3),M3,I=1,N)
C98    FORMAT(F7.4,2F11.3,I6)
C      WRITE(6,99) (R(I,M),T(I,M),P(I,M),M,I=1,N)
C99    FORMAT(F7.4,2F11.3,I6)
C
      PRINT 100
100   FORMAT(//2X,'Temperature vs. Depth & Time')
      WRITE(6,101)(RD(I,M7),DT(I,M7),I=1,N)
101   FORMAT(G10.3,',',G10.3,',')
C      WRITE(6,102)(RD(I,M6),DT(I,M6),I=1,N)
C102   FORMAT(1X,G10.3,',',G10.3,',')
      WRITE(6,103)(RD(I,M5),DT(I,M5),I=1,N)
103   FORMAT(G10.3,',',G10.3,',')
      WRITE(6,104)(RD(I,M4),DT(I,M4),I=1,N)
104   FORMAT(1X,G10.3,',',G10.3,',')
      WRITE(6,121)(RD(I,M3),DT(I,M3),I=1,N)
121   FORMAT(G10.3,',',G10.3,',')
```

```
      WRITE(6,122)(RD(I,M2),DT(I,M2),I=1,N)
  122 FORMAT(1X,G10.3,',',G10.3,',')
C      WRITE(6,123)(RD(I,M1),DT(I,M1),I=1,N)
C123   FORMAT(G10.3,',',G10.3,',')
      WRITE(6,124)(RD(I,M),DT(I,M),I=1,N)
  124 FORMAT(1X,G10.3,',',G10.3,',')
C
      PRINT 105
  105 FORMAT(//2X,'Pore Pressure vs. Depth & Time')
      WRITE(6,106)(RD(I,M7),U(I,M7),I=1,N)
  106 FORMAT(G10.3,',',G10.3,',')
C      WRITE(6,107)(RD(I,M6),U(I,M6),I=1,N)
C107   FORMAT(1X,G10.3,',',G10.3,',')
      WRITE(6,108)(RD(I,M5),U(I,M5),I=1,N)
  108 FORMAT(G10.3,',',G10.3,',')
      WRITE(6,109)(RD(I,M4),U(I,M4),I=1,N)
  109 FORMAT(1X,G10.3,',',G10.3,',')
      WRITE(6,126)(RD(I,M3),U(I,M3),I=1,N)
  126 FORMAT(G10.3,',',G10.3,',')
      WRITE(6,127)(RD(I,M2),U(I,M2),I=1,N)
  127 FORMAT(1X,G10.3,',',G10.3,',')
C      WRITE(6,128)(RD(I,M1),U(I,M1),I=1,N)
C128   FORMAT(G10.3,',',G10.3,',')
      WRITE(6,129)(RD(I,M),U(I,M),I=1,N)
  129 FORMAT(1X,G10.3,',',G10.3,',')
C
      PRINT 115
  115 FORMAT(//2X,'Thermal Expansion Coeff. vs. Depth & Time')
      WRITE(6,116)(RD(I,M7),ALP(I,M7),I=1,N)
  116 FORMAT(G10.3,',',G10.3,',')
C      WRITE(6,117)(RD(I,M6),ALP(I,M6),I=1,N)
C117   FORMAT(1X,G10.3,',',G10.3,',')
      WRITE(6,118)(RD(I,M5),ALP(I,M5),I=1,N)
  118 FORMAT(G10.3,',',G10.3,',')
      WRITE(6,119)(RD(I,M4),ALP(I,M4),I=1,N)
  119 FORMAT(1X,G10.3,',',G10.3,',')
      WRITE(6,130)(RD(I,M3),ALP(I,M3),I=1,N)
  130 FORMAT(G10.3,',',G10.3,',')
      WRITE(6,131)(RD(I,M2),ALP(I,M2),I=1,N)
  131 FORMAT(1X,G10.3,',',G10.3,',')
C      WRITE(6,132)(RD(I,M1),ALP(I,M1),I=1,N)
C132   FORMAT(G10.3,',',G10.3,',')
      WRITE(6,133)(RD(I,M),ALP(I,M),I=1,N)
  133 FORMAT(1X,G10.3,',',G10.3,',')
C
      STOP
      END
C
C
C
C*************************************************************
C                                                            *
C                    SUBROUTINE TEMPD                        *
C     Determines temperature distribution with time in       *
C     oil sand due to 1-D thermal diffusion . The semi       *
C     implicit formulation yields a tridiagonal matrix       *
C     at each time step which is solved using                *
C     THOMAS'S ALGORITHM .                                   *
C                                                            *
C*************************************************************
```

```
      C
            SUBROUTINE TEMPD(J,JJ,JI)
      C
            COMMON /BLK1/ NN,M,N,MM,NI,DELT,ALPHAT,SVEO
            COMMON /BLK2/ DR(35,3000),T(35,3000)
            COMMON /BLK3/ R(35,3000),RD(35,3000)
            COMMON /BLK5/ DT(35,3000),DTI(35,3000)
            COMMON /BLK6/ DTA(35,3000),DTAI(35,3000)
            COMMON /BLK10/ A(35),B(35),C(35)
            COMMON /BLK11/ W(35),G(35)
      C
            NII=N-2
            DO 1 I=2,N
            II=I-1
            IJ=I+1
            A(I)=(ALPHAT*DELT)*((1/(2*R(I,JI)*DR(I,JI)))-(1/(DR(I,JI)
     &**2)))
            B(I)=1+(2*ALPHAT*DELT)/(DR(I,JI)**2)
            C(I)=(ALPHAT*DELT)*((-1/(2*R(I,JI)*DR(I,JI)))-(1/(DR(I,JI)
     &**2)))
            IF (I.GT.2) GO TO 2
            W(2)=C(2)/B(2)
            G(2)=(DT(2,JI)-A(2)*DT(1,JI))/B(2)
            GO TO 1
      2     IF (I.EQ.N) GO TO 3
            W(I)=C(I)/(B(I)-A(I)*W(II))
            G(I)=(DT(I,JI)-A(I)*G(II))/(B(I)-A(I)*W(II))
            GO TO 1
      3     G(N)=(DT(N,JI)-(2*A(N)*G(NI)))/(B(N)-(2*A(N)*W(NI)))
            DT(N,J)=G(N)
      1     CONTINUE
            DO 4 I=1,NII
            IB=N-I
            IBJ=IB+1
            DT(IB,J)=G(IB)-W(IB)*DT(IBJ,J)
      4     CONTINUE
            DO 5 I=2,N
            II=I-1
            DTI(I,J)=DT(I,J)-DT(I,JI)
            DTA(I,J)=(DT(I,J)+DT(II,J))/2
            DTAI(I,J)=(DTI(I,J)+DTI(II,J))/2
      5     CONTINUE
            RETURN
            END
      C
      C
      C*****************************************************************
      C                                                                *
      C                     SUBROUTINE CONSOL                          *
      C     Determines pore pressure dissipation with time             *
      C     in oil sand due to 1-D consolidation following each        *
      C     transient heating increment .  The semi-implicit           *
      C     formulation yields a tridiagonal matrix at each            *
      C     time step which is solved using THOMAS'S ALGORITHM .       *
      C                                                                *
      C*****************************************************************
      C
            SUBROUTINE CONSOL(J,JJ,JI)
      C
            COMMON /BLK1/ NN,M,N,MM,NI,DELT,ALPHAT,SVEO
```

```
295             COMMON /BLK2/ DR(35,3000),T(35,3000)
295.5           COMMON /BLK3/ R(35,3000),RD(35,3000)
296             COMMON /BLK4/ UDR(35,3000),U(35,3000)
297             COMMON /BLK5/ DT(35,3000),DTI(35,3000)
298             COMMON /BLK6/ DTA(35,3000),DTAI(35,3000)
299             COMMON /BLK8/ CV(35,3000),DM(35,3000)
300             COMMON /BLK9/ BT(35,3000),DU(35,3000)
301             COMMON /BLK12/ AA(35),BB(35),CC(35)
302             COMMON /BLK13/ WW(35),GG(35),DGAM(35,3000)
304       C
304.5           NII=N-2
305             DO 1 I=2,N
306             II=I-1
307             IJ=I+1
307.1           AA(I)=(CV(I,J)*DELT)*((1/(2*R(I,JI)*DR(I,JI)))
307.2          &-(1/(DR(I,JI)**2)))
307.3           BB(I)=1+(2*CV(I,J)*DELT/(DR(I,JI)**2))
307.4           CC(I)=(CV(I,J)*DELT)*(-(1/(2*R(I,JI)*DR(I,JI)))
307.5          &-(1/(DR(I,JI)**2)))
308             IF (I.GT.2) GO TO 2
312             WW(2)=CC(2)/BB(2)
313             GG(2)=(U(2,JI)-AA(2)*U(1,JI))/BB(2)
314             GO TO 1
319       2     IF (I.EQ.N) GO TO 3
320             WW(I)=CC(I)/(BB(I)-AA(I)*WW(II))
321             GG(I)=(U(I,JI)-AA(I)*GG(II))/(BB(I)-AA(I)*WW(II))
322             GO TO 1
323       3     GG(N)=(U(N,JI)-(2*AA(N)*GG(NI)))/(BB(N)-(2*AA(N)*WW(NI)))
324             UDR(N,J)=GG(N)
325       1     CONTINUE
327             DO 4 I=1,NII
328             IB=N-I
329             IBJ=IB+1
330             UDR(IB,J)=GG(IB)-WW(IB)*UDR(IBJ,J)
331       4     CONTINUE
332             DO 5 I=2,N
333             U(I,J)=DU(I,J)+UDR(I,J)+DM(I,J)
334       5     CONTINUE
335             RETURN
336             END
End of file
$COPY *1 *PRINT*
```

APPENDIX K

ONE DIMENSIONAL HEAT CONSOLIDATION OF OIL SAND: NUMERICAL SOLUTIONS

Influence of Temporal Discretization on Predicted Pore Pressures and Volumetric Strains

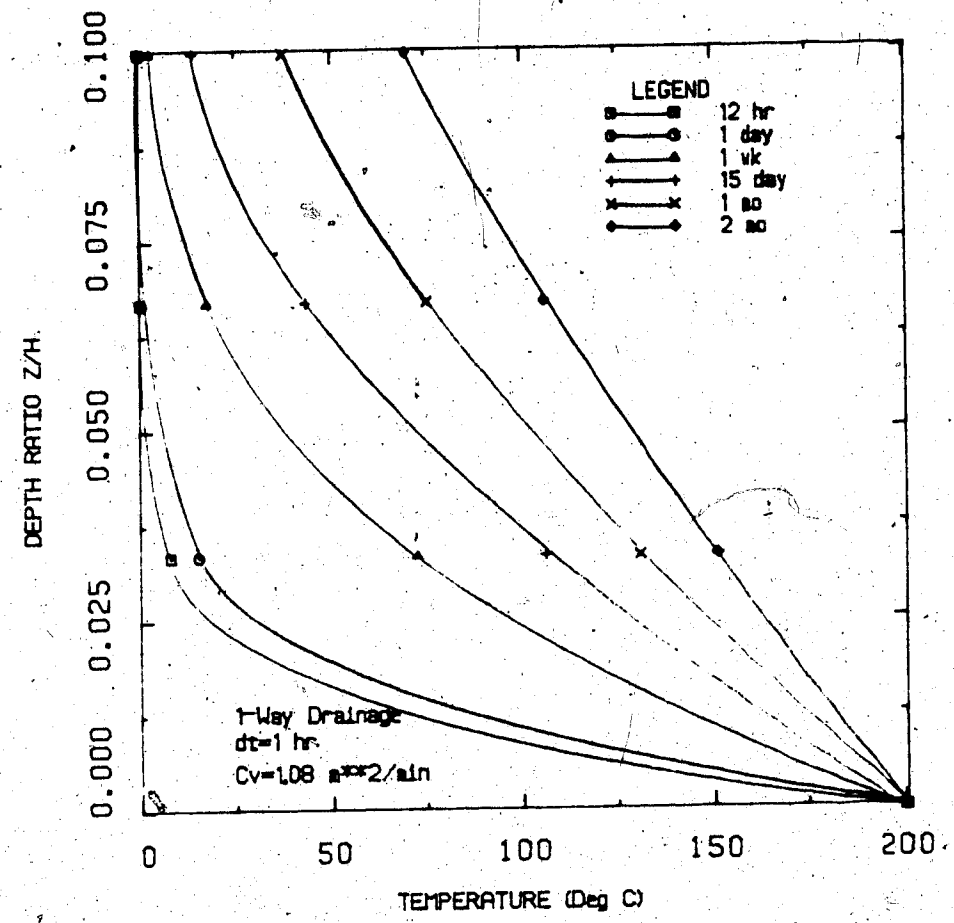

FIGURE K1.1 Transient Temperatures - One-Way Drainage (1 Hour Time Step)

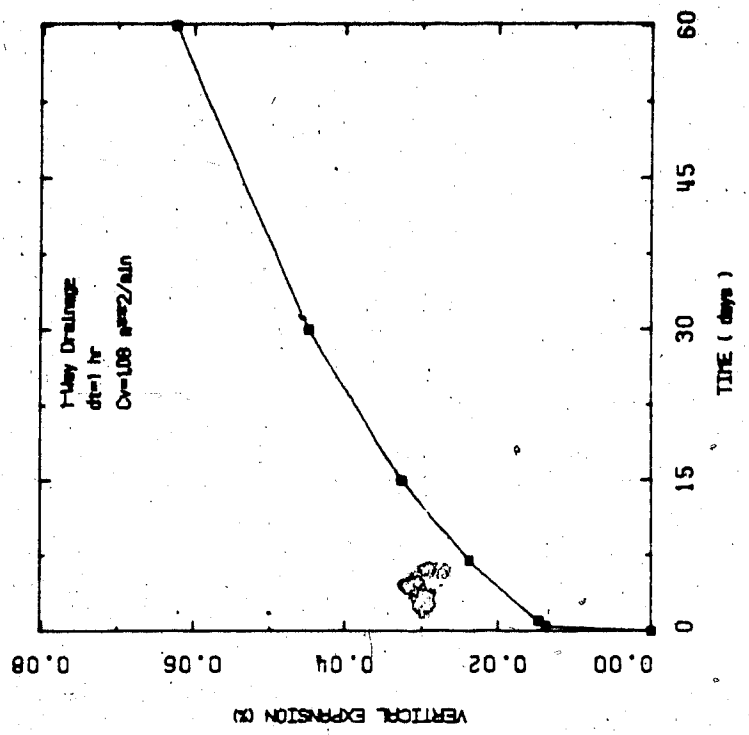

FIGURE K1.3 Transient Vertical Expansion - One-Way Drainage (1 Hour Time Step)

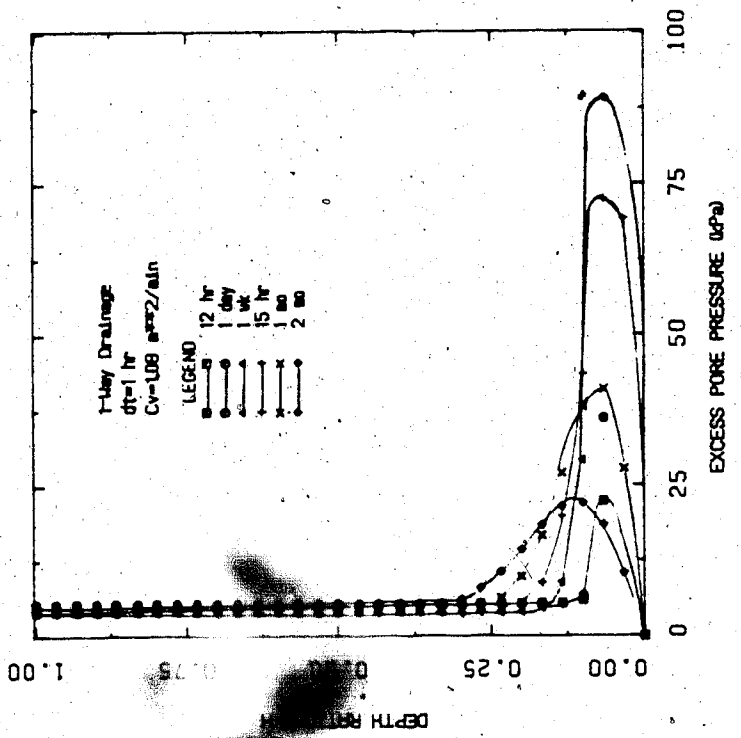

FIGURE K1.2 Transient Temperatures - One-Way Drainage (1 Hour Time Step)

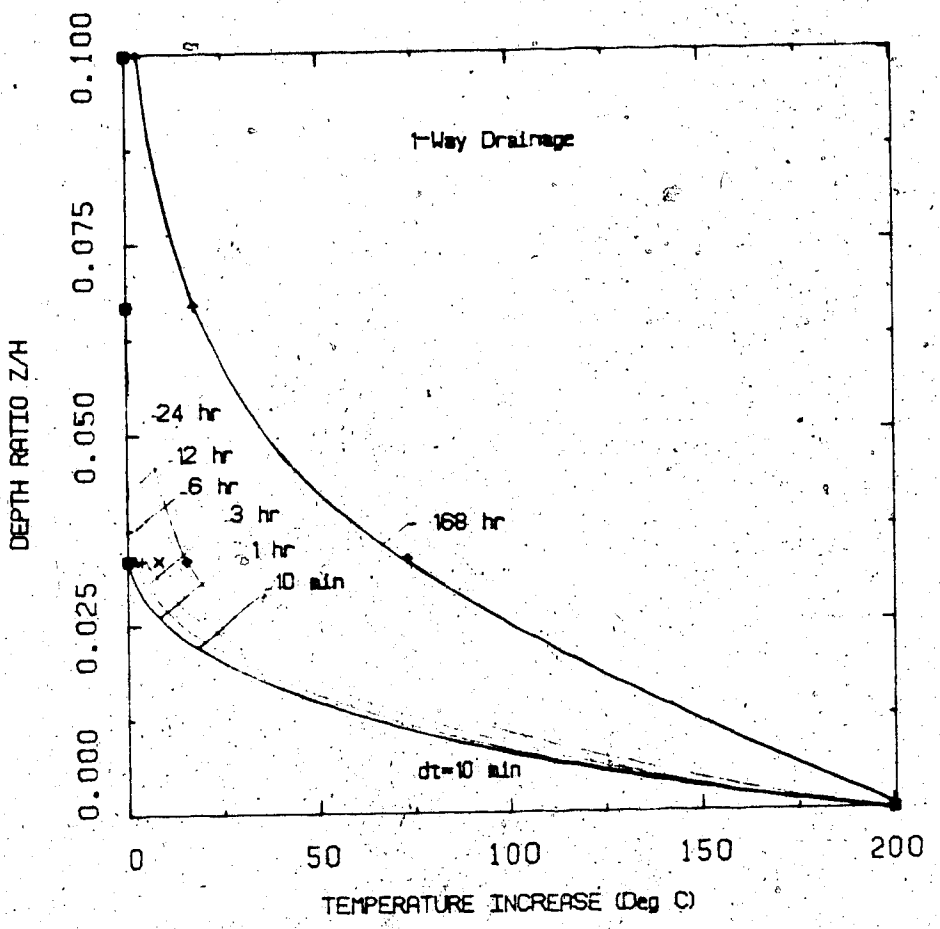

FIGURE 2.1 Transient Temperatures - One-way Drainage (10 Minute Time Step)

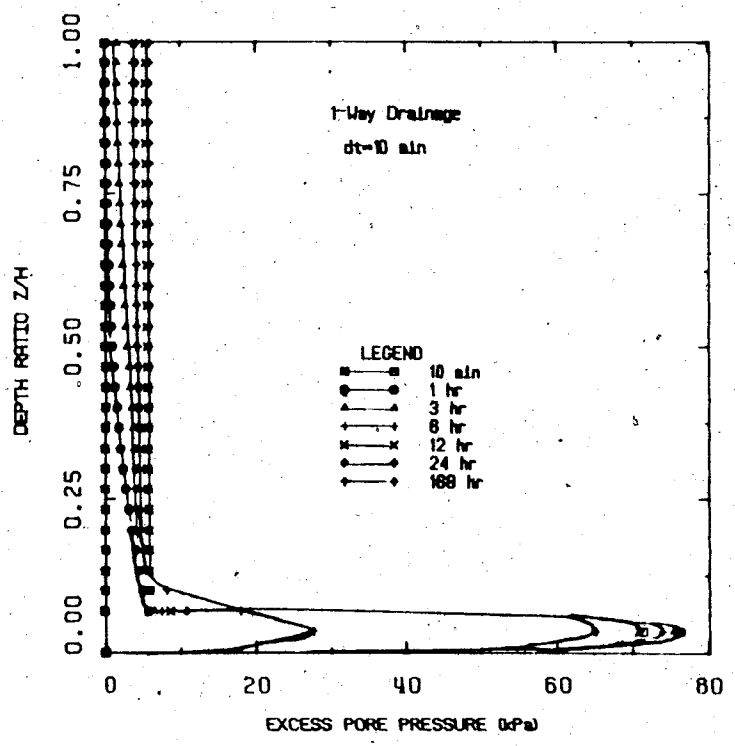

FIGURE K2.2 Transient Excess Pore Pressures-One-Way Drainage (10 Minute Time Step)

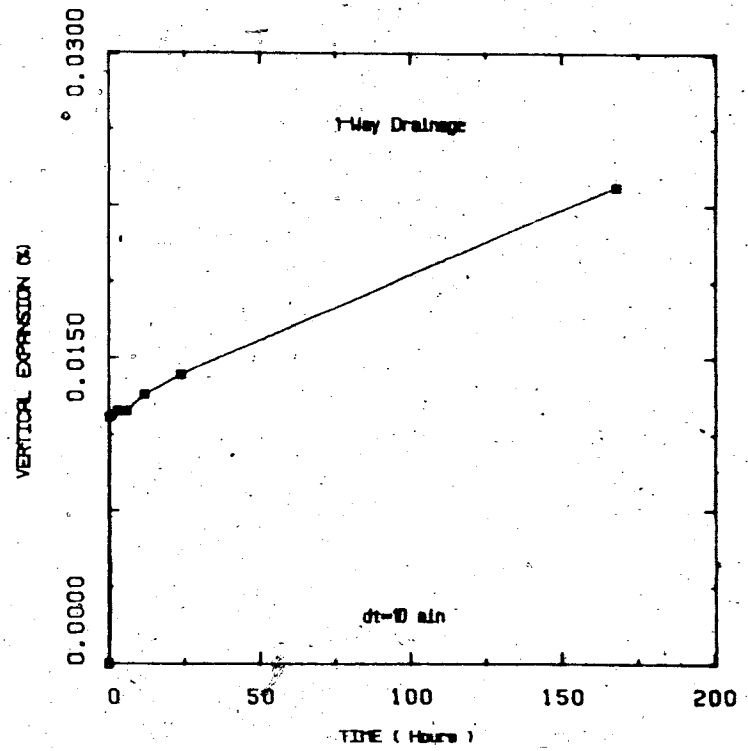

FIGURE K2.3 Transient Vertical Expansion - One-Way Drainage (10 Minute Time Step)

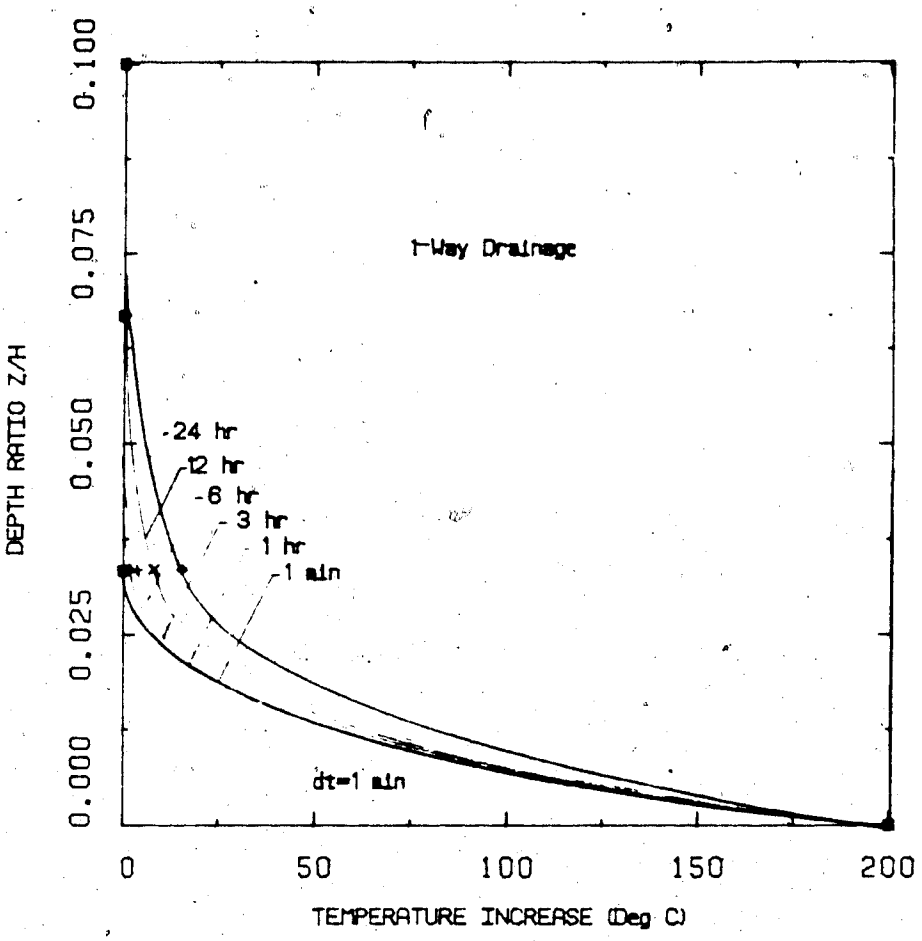

FIGURE A3.1 Transient Temperatures - One-Way Drainage (1 Minute Time Step)

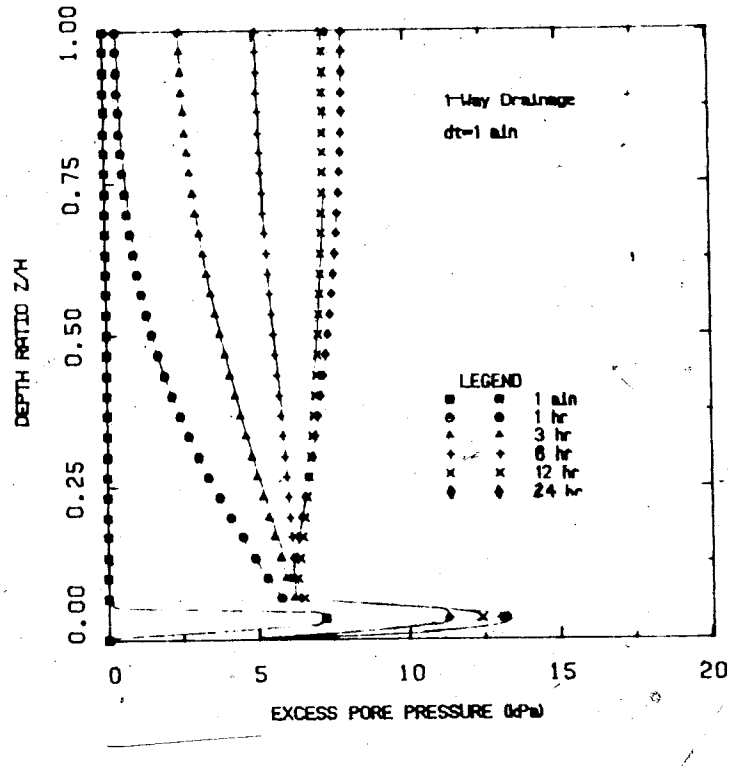

FIGURE K3.2 Transient Excess Pore Pressures-One-Way Drainage (1 Minute Time Step)

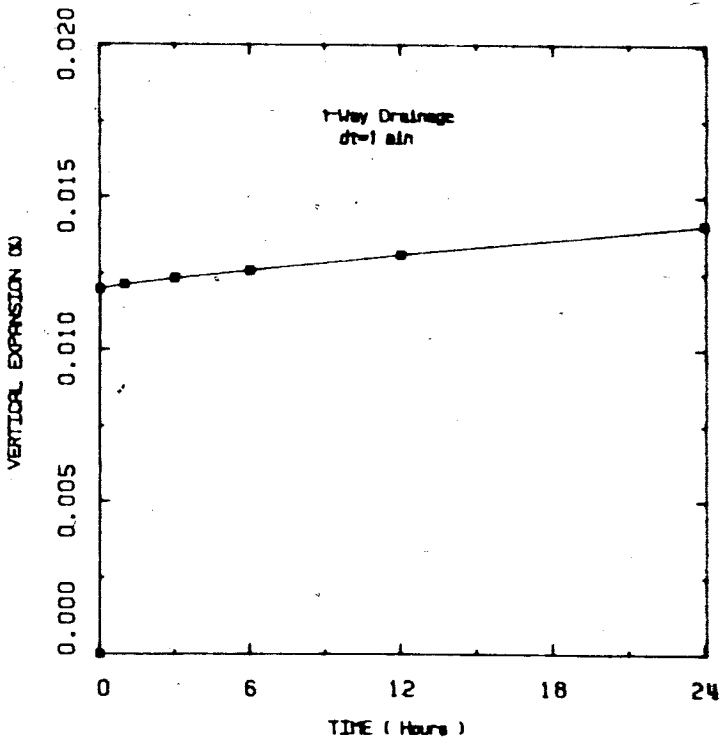

FIGURE K3.3. Transient Vertical Expansion - One-Way Drainage (1 Minute Time Step)

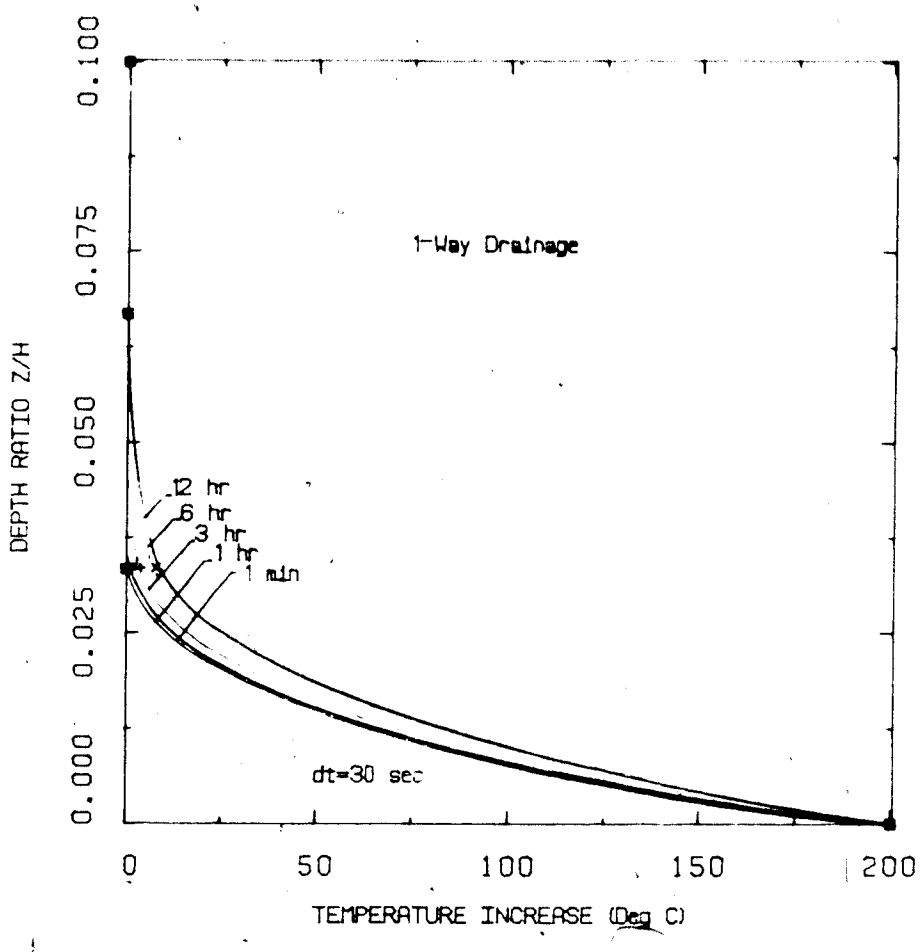

FIGURE K4.1 Transient Temperatures - One-Way Drainage (30 Second Time Step)

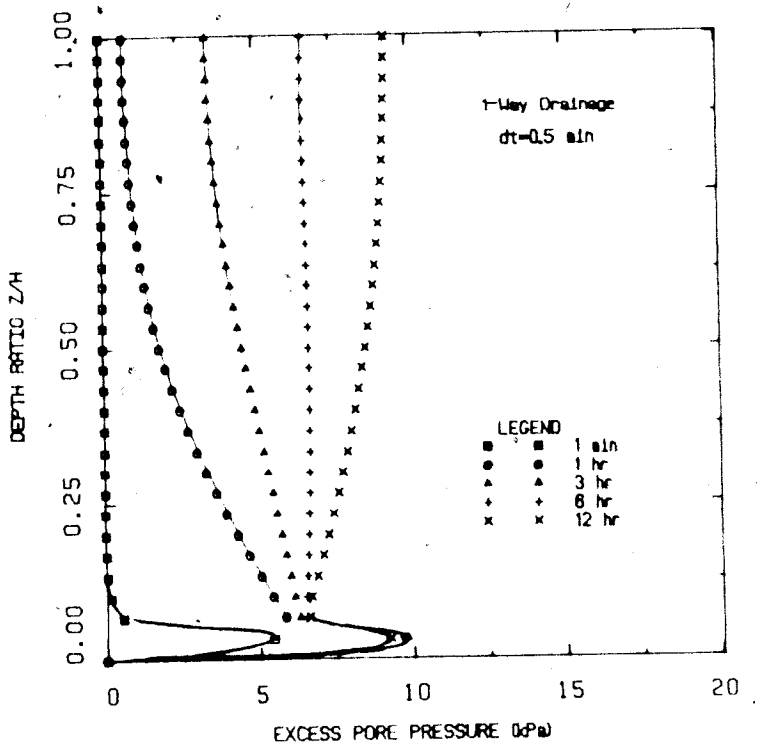

FIGURE K4.2 Transient Excess Pore Pressure-Time-
Way Drainage (30 Second Time Step)

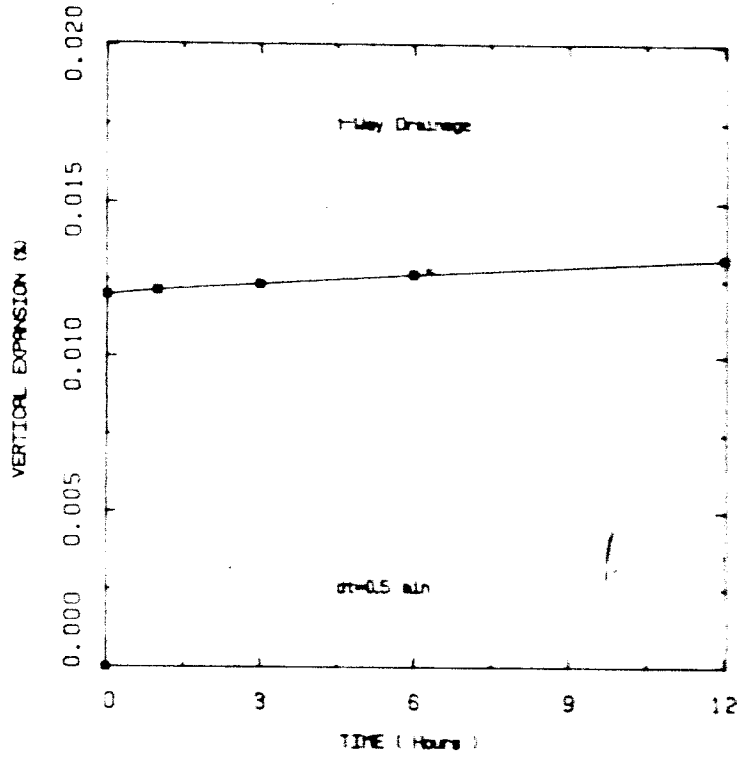

[illegible] K4.3 Transient Vertical Expansion - One-
Way Drainage (30 Second Time Step)

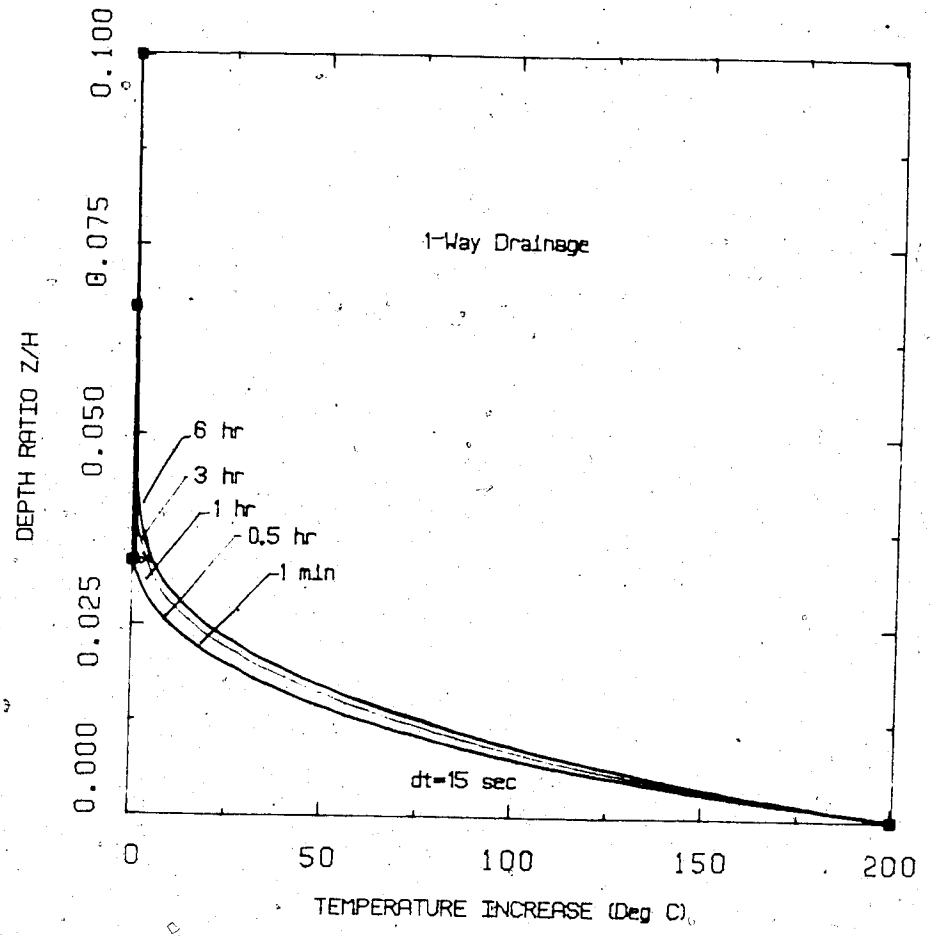

FIGURE K5.1 Transient Temperatures – One-Way Drainage (15 Second Time Step)

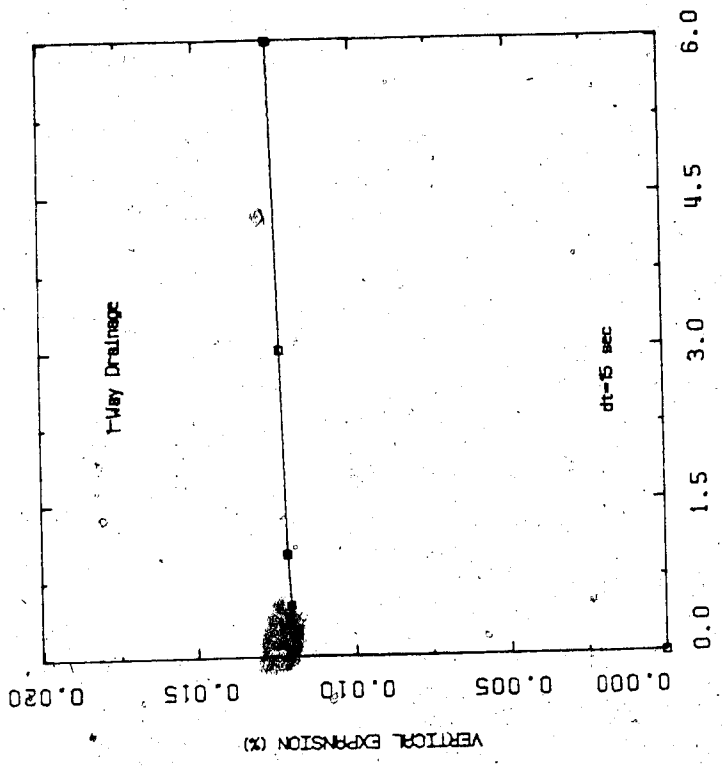

FIGURE K5.3 Transient Vertical Expansion - One-Way Drainage (15 Second Time Step)

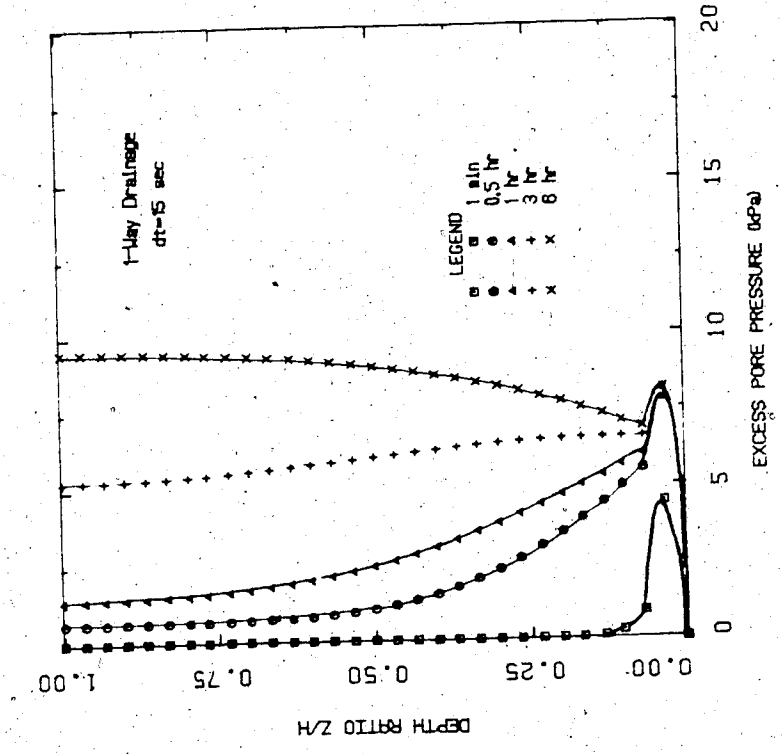

FIGURE K5.2 Transient Excess Pore Pressures-One-Way Drainage (15 Second Time Step)

Influence of Oil Sand Permeability on Predicted Pore Pressures and Volumetric Strains

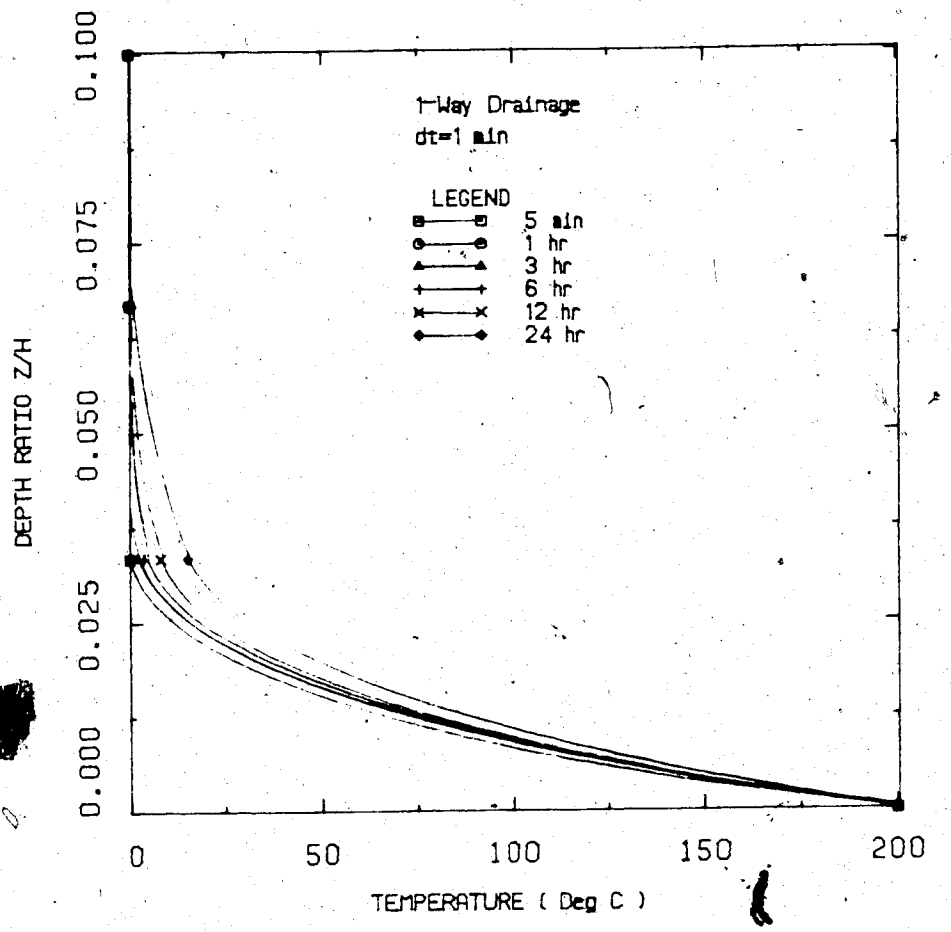

FIGURE K6 Transient Temperatures for One-way Drainage (1 Minute Time Step)

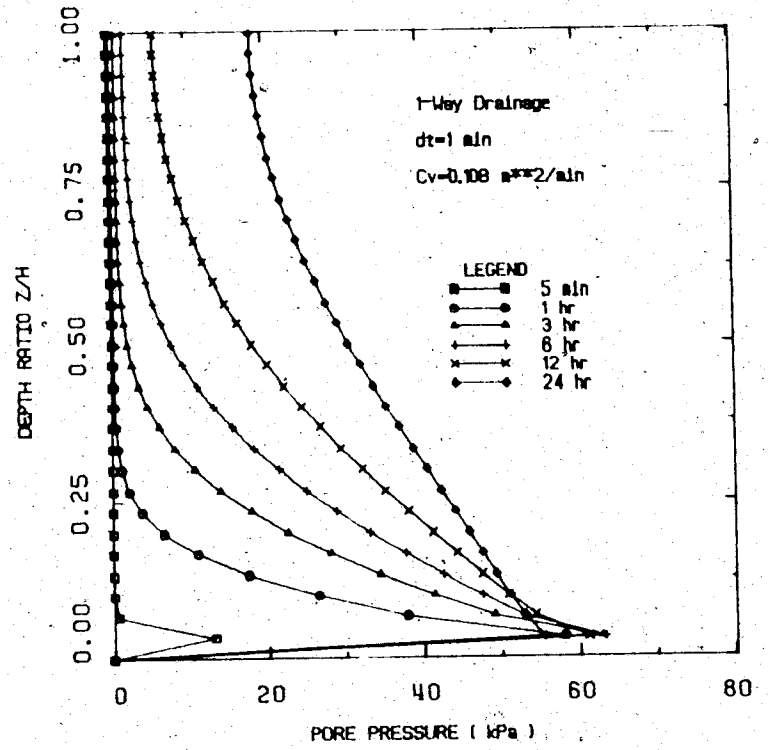

FIGURE K7.1 Transient Excess Pore Pressures (R_T = 1800)

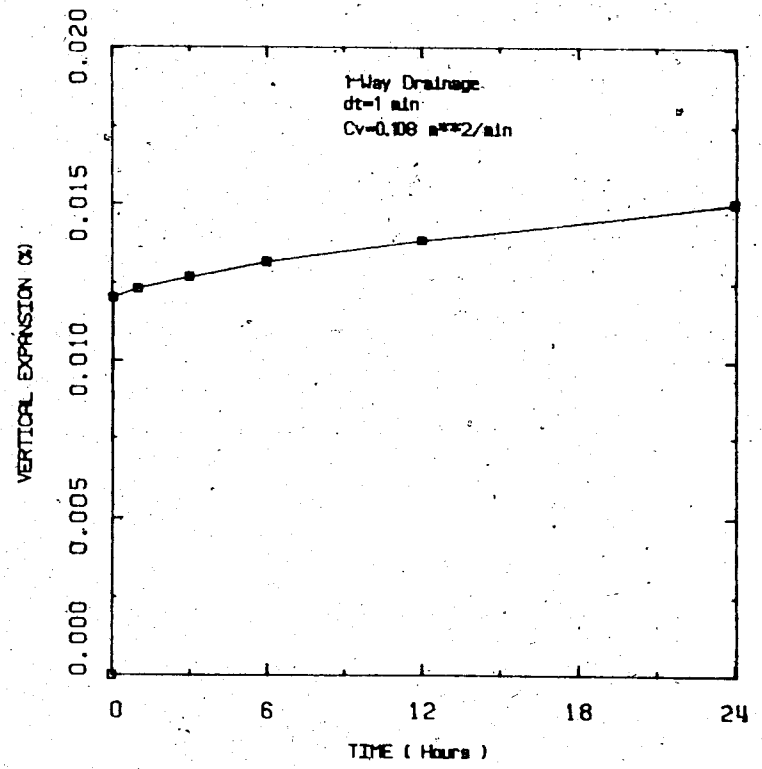

FIGURE K7.2 Transient Vertical Expansion (R_T = 1800)

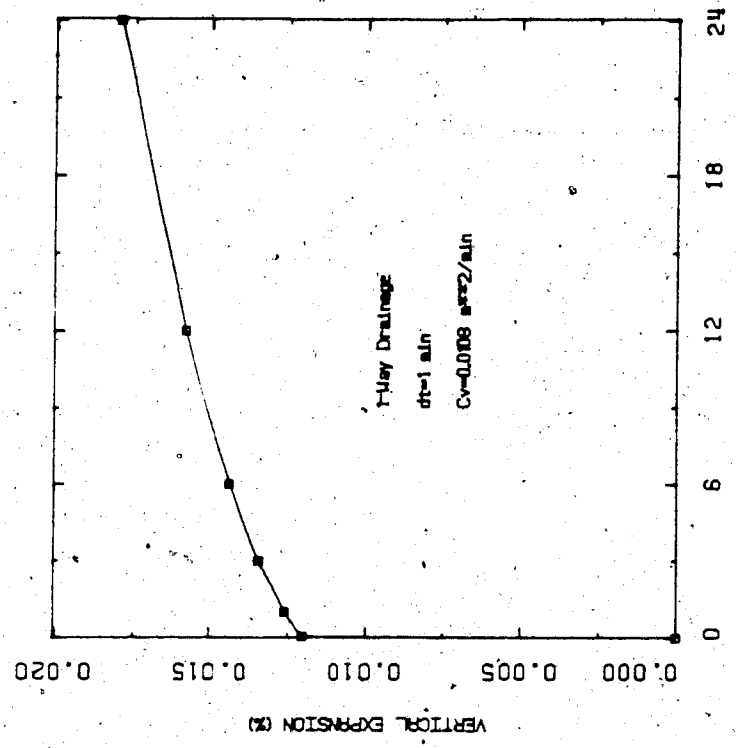

FIGURE K8.2 Transient Vertical Expansion (R_T = 180)

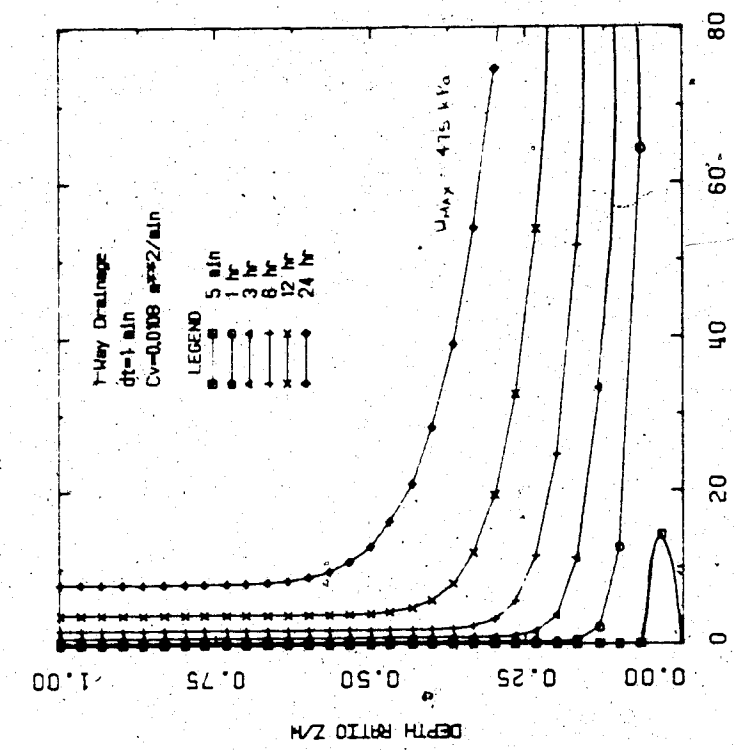

FIGURE K8.1 Transient Excess Pore Pressures (R_T = 180)

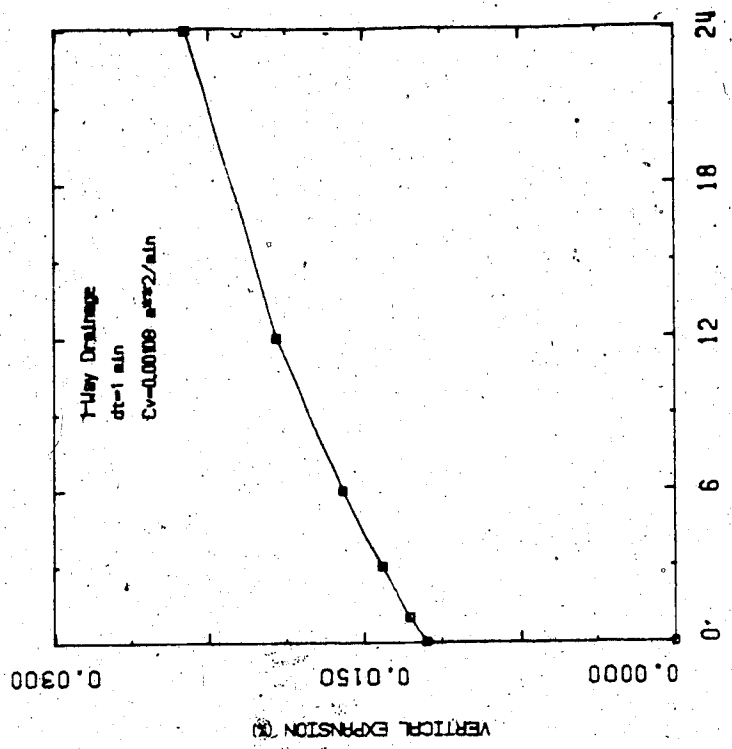

FIGURE K9.2 Transient Vertical Expansion (R_T = 18)

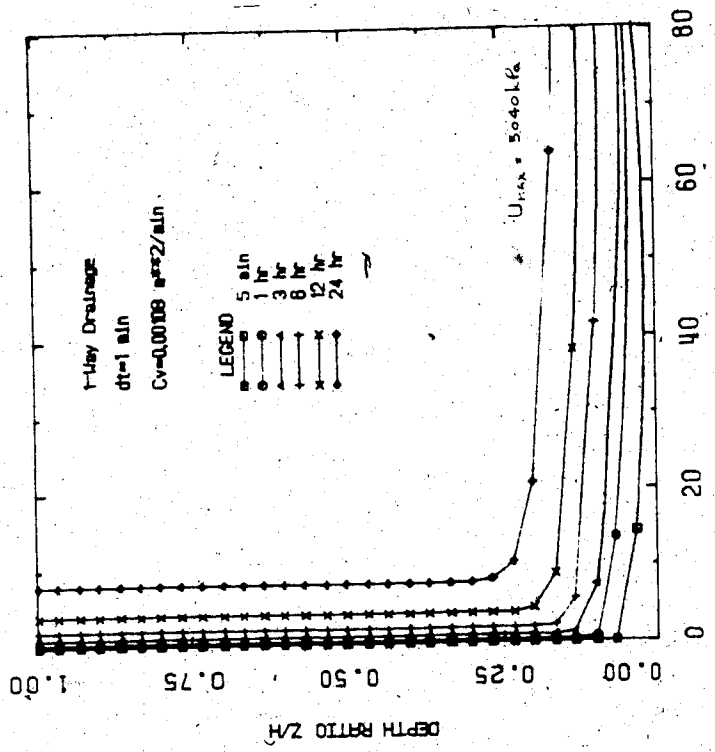

FIGURE K9.1 Transient Excess Pore Pressures (R_T = 18)

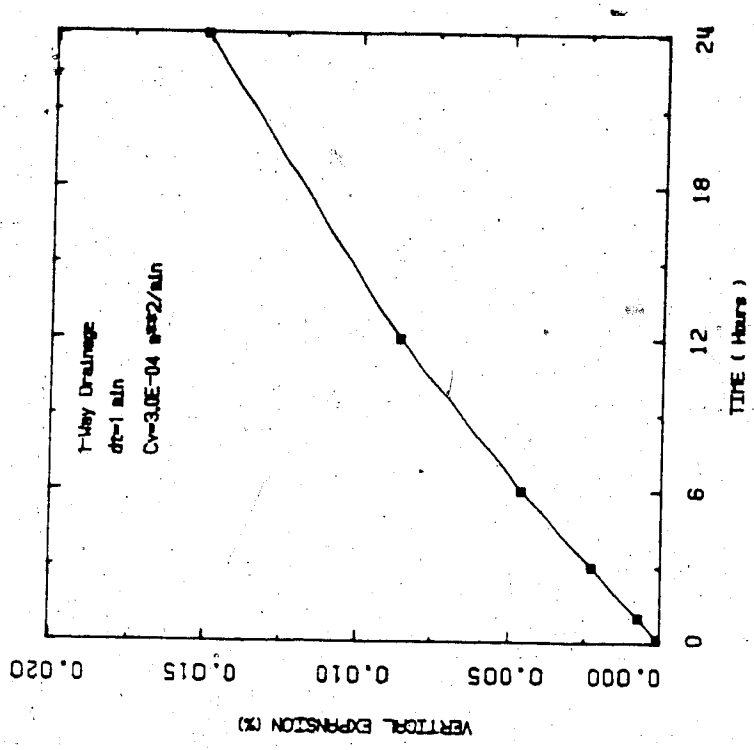

FIGURE K10.2 Transient Vertical Expansion (R_T = 5)

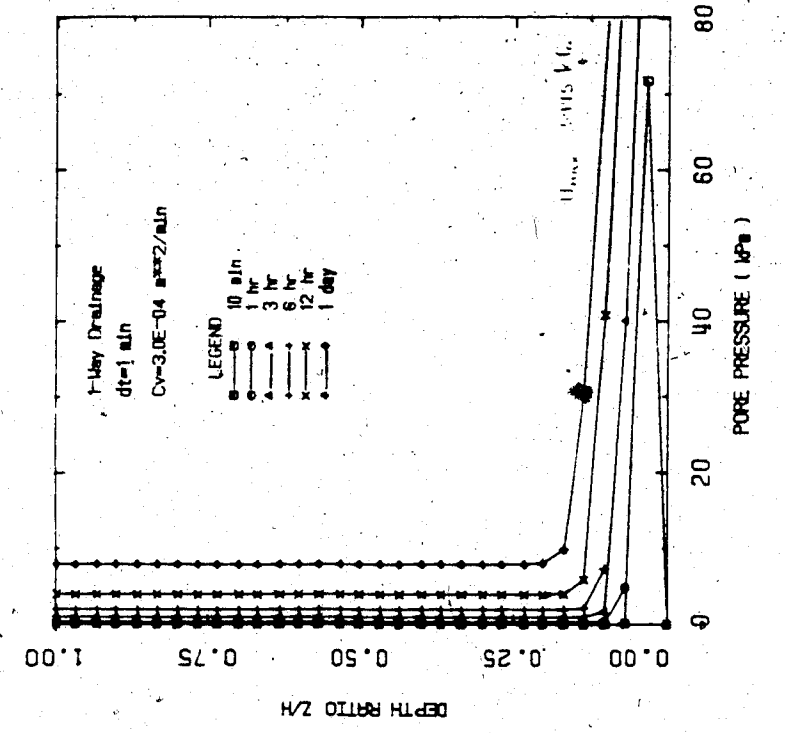

FIGURE K10.1 Transient Excess Pore Pressures (R_T = 5)

APPENDIX L

RESULTS OF THERMOELASTIC STRESS-STRAIN ANALYSES

Thermal Stress Changes and Deformations Adjacent to a Shaft in Oil Sand Assuming a Rigid Boundary Condition at the Production Zone

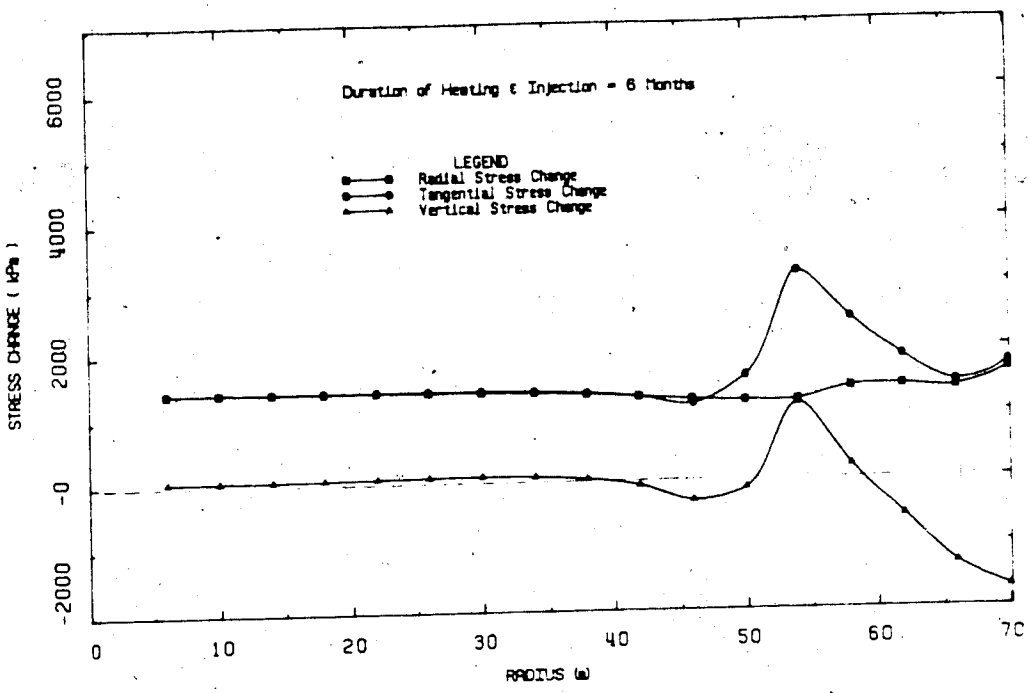

FIGURE L1.1 Stress Changes Around the Shaft After 6 Months of Steam Injection

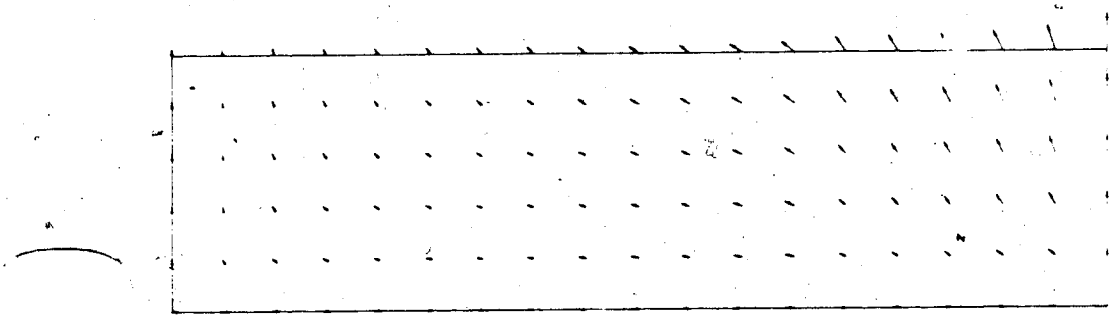

FIGURE L1.2 Deformations Around the Shaft After 6 Months of Steam Injection

DISPLACEMENT SCALE 1:100

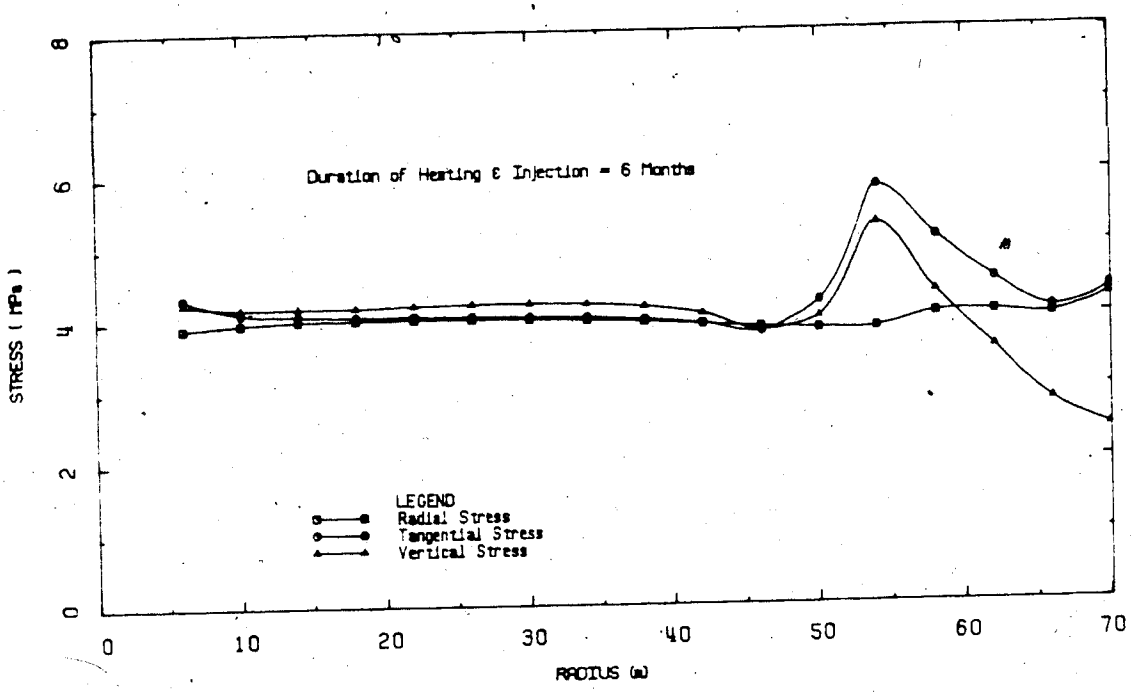

FIGURE L1.3 Effective Stresses Around the Shaft After 6 Months of Steam Injection

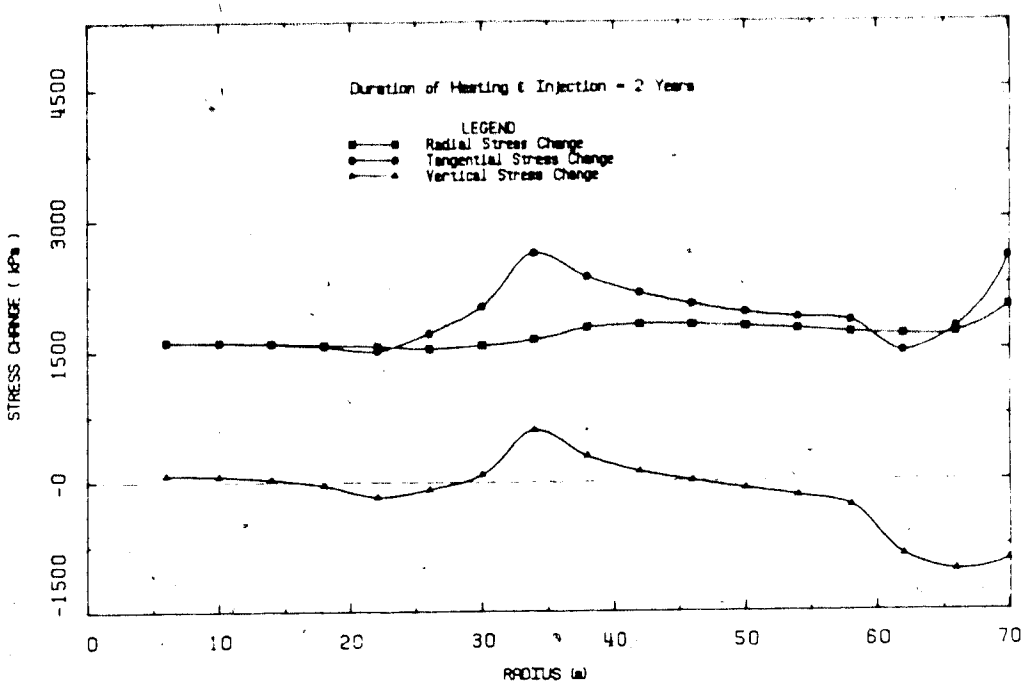

FIGURE L2.1 Stress Changes Around the Shaft After 2 Years of Steam Injection

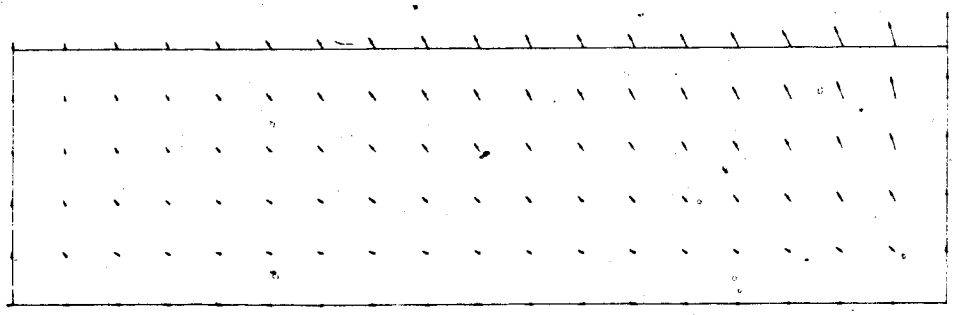

FIGURE L2.2 Deformations Around the Shaft After 2 Years of Steam Injection

DISPLACEMENT SCALE 1:100

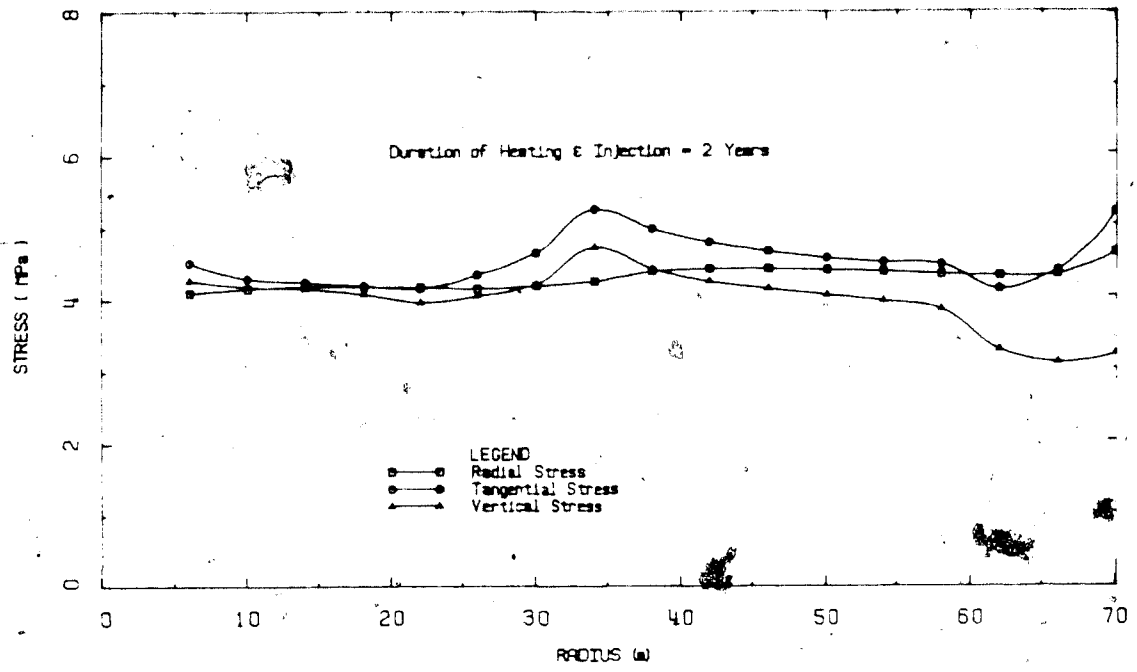

FIGURE 12.3 Effective Stresses Around the Shaft After 2 Years of Steam Injection

Stress Changes and Deformations Adjacent to a Shaft In Oil Sand Assuming a Constant Pressure Boundary Condition at the Production Zone

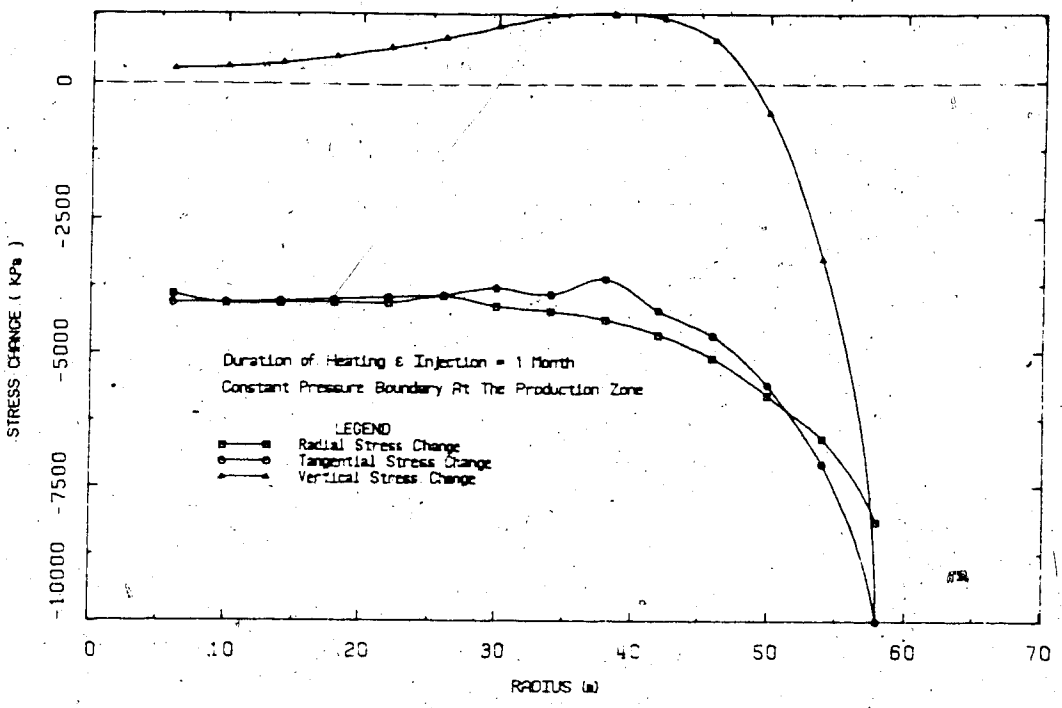

FIGURE L3.1 Stress Changes Around the Shaft After 1 Month of Steam Injection

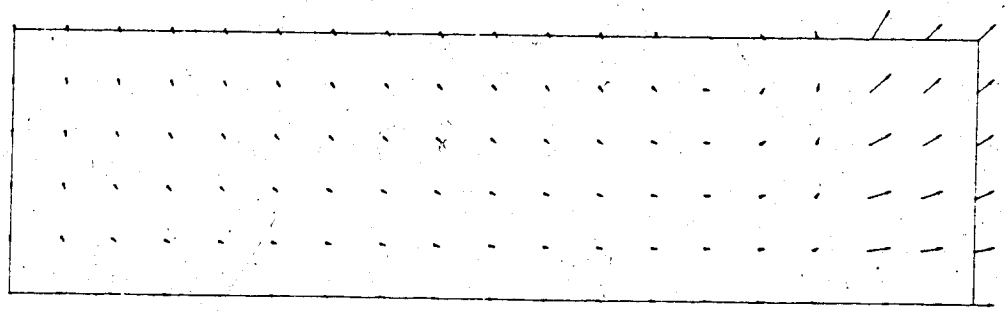

FIGURE L3.2 Deformations Around the Shaft After 1 Month of Steam Injection

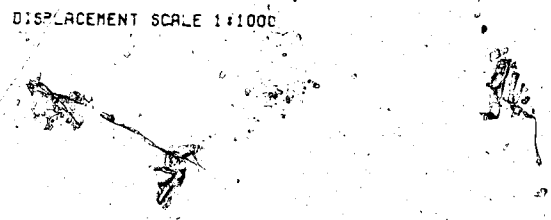

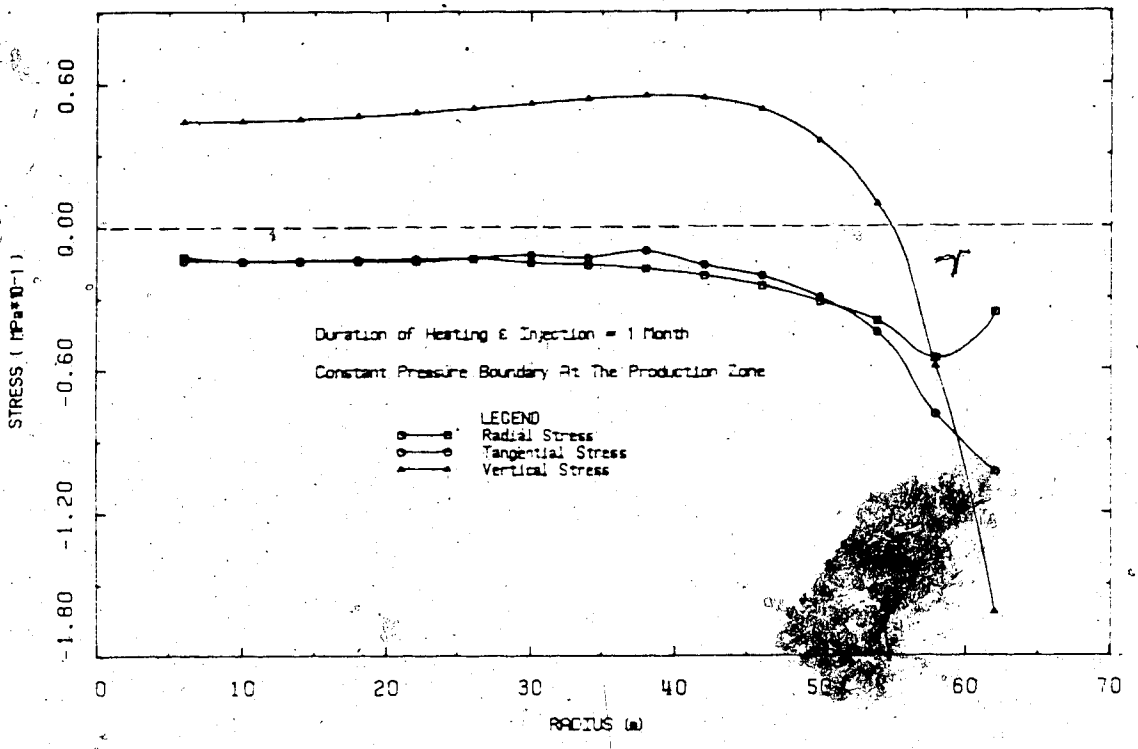

FIGURE L3.3 Effective Stresses Around the Shaft After 1 Month of Steam Injection

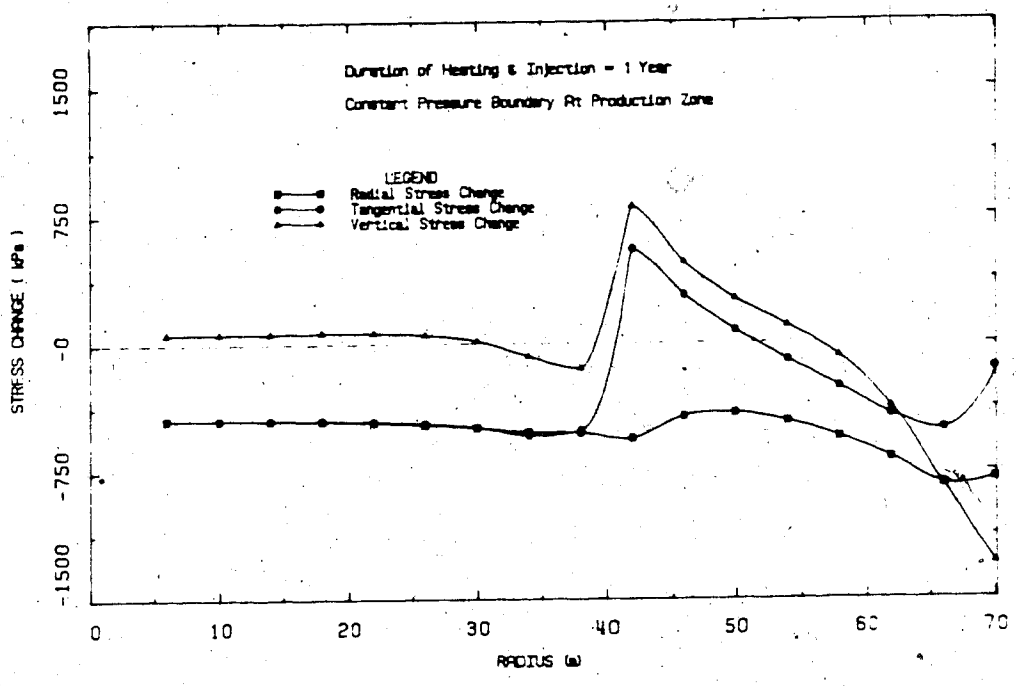

FIGURE L3.4 Stress Changes Around the Shaft After 1 Year of Steam Injection

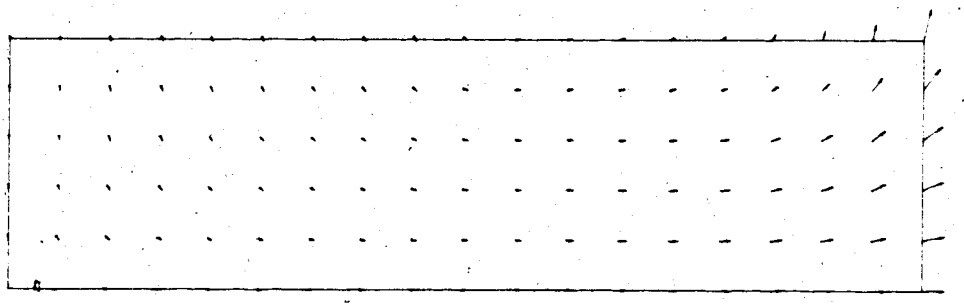

FIGURE L3.5 Deformations Around the Shaft After 1 Year of Steam Injection

DISPLACEMENT SCALE 1:100

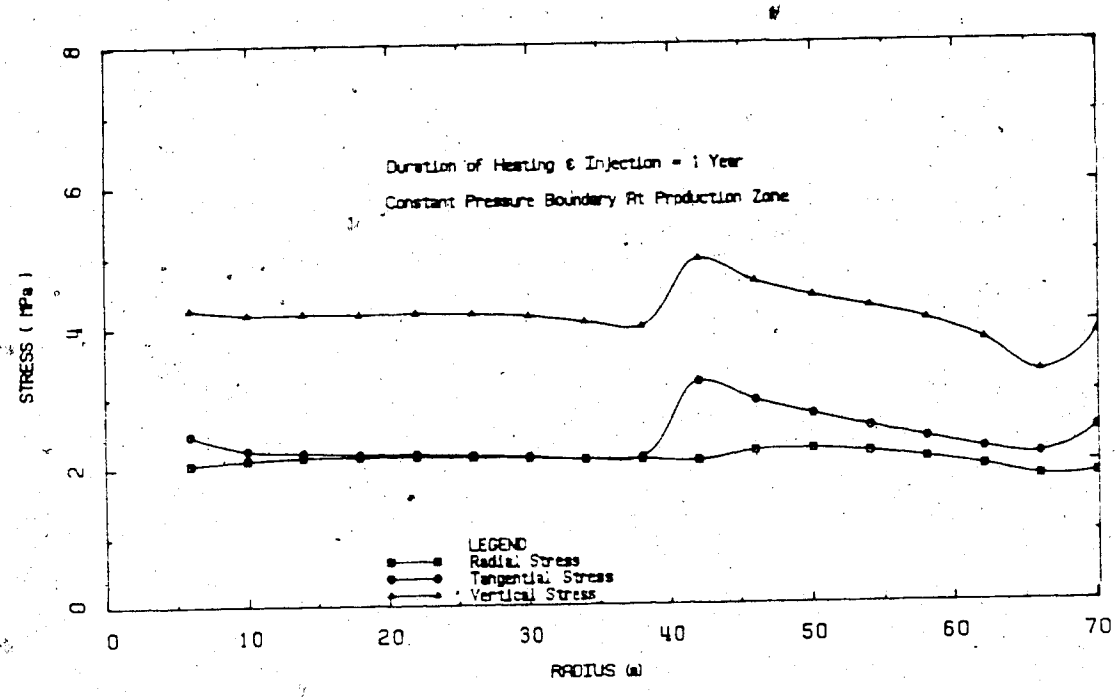

FIGURE L3.6 Effective Stresses Around the Shaft After 1 Year of Steam Injection

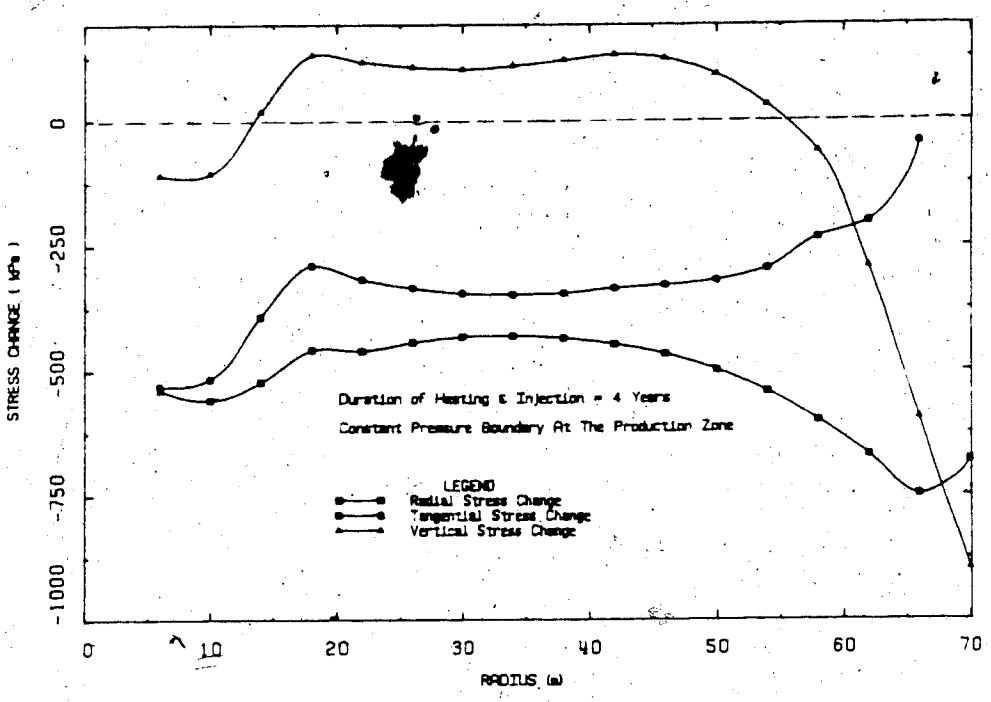

FIGURE L3.7 Stress Changes Around the Shaft After 4 Years of Steam Injection

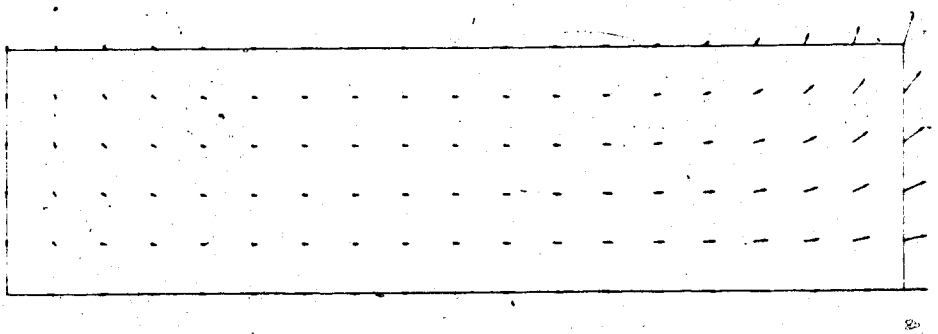

FIGURE L3.8 Deformations Around the Shaft After 4 Years of Steam Injection

DISPLACEMENT SCALE 1:100

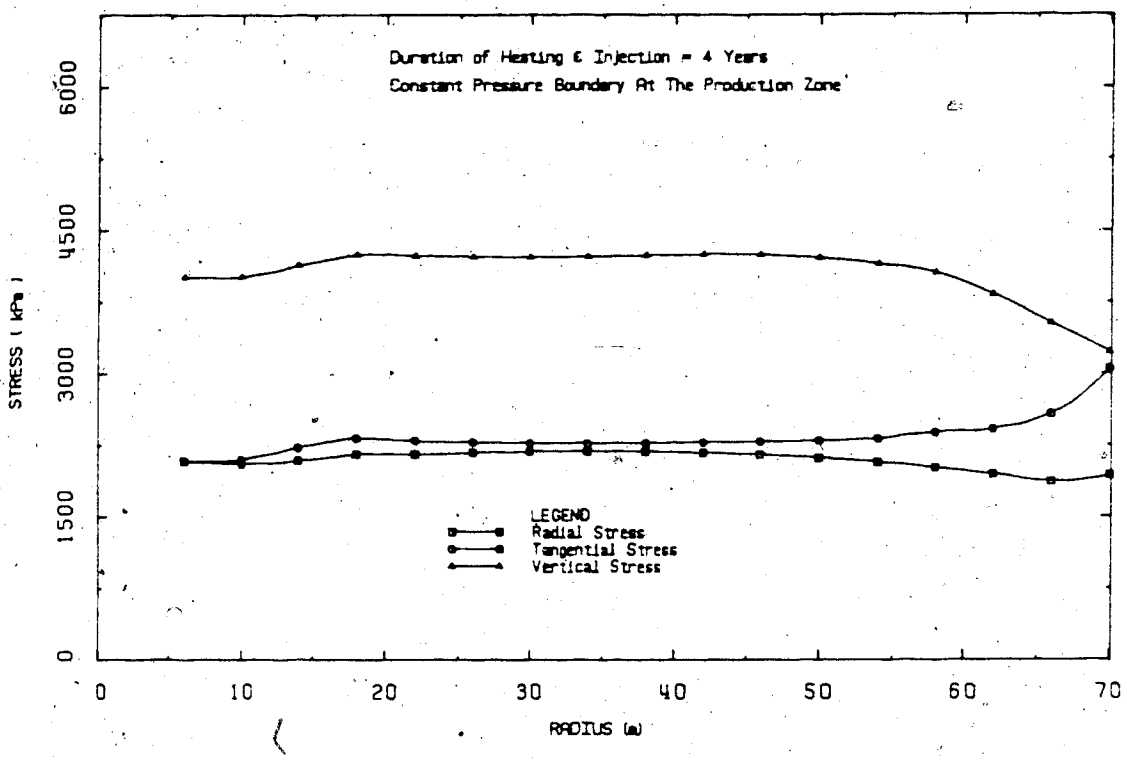

FIGURE L3.9 Effective Stresses Around the Shaft After 4 Years of Steam Injection

Thermal Stress Changes and Deformation Adjacent to a Shaft In Oil Sand Assuming a Compressible Boundary Condition at the Production Zone

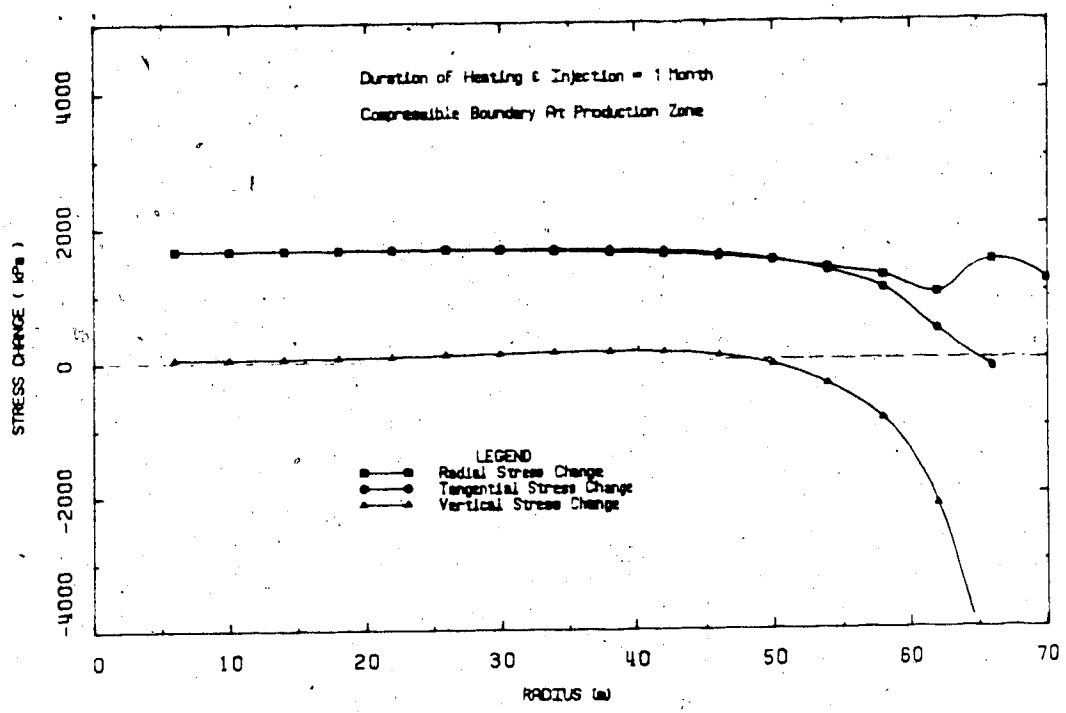

FIGURE L4.1 Stress Changes Around the Shaft After 1 Month of Steam Injection

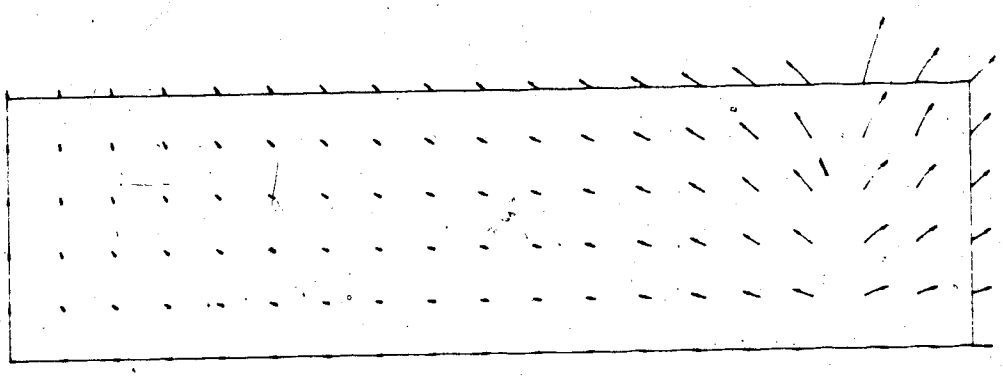

FIGURE L4.2 Deformations Around the Shaft After 1 Month of Steam Injection

DISPLACEMENT SCALE 1:100

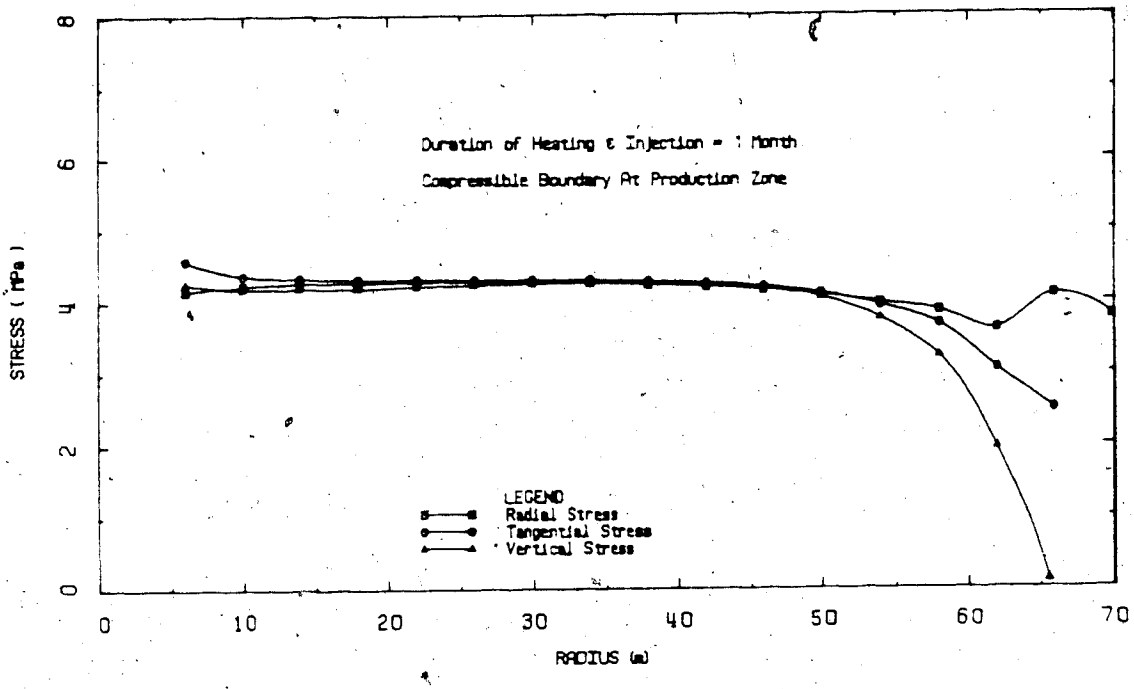

FIGURE 4.3 Effective Stresses Around the Shaft After 1 Month of Steam Injection

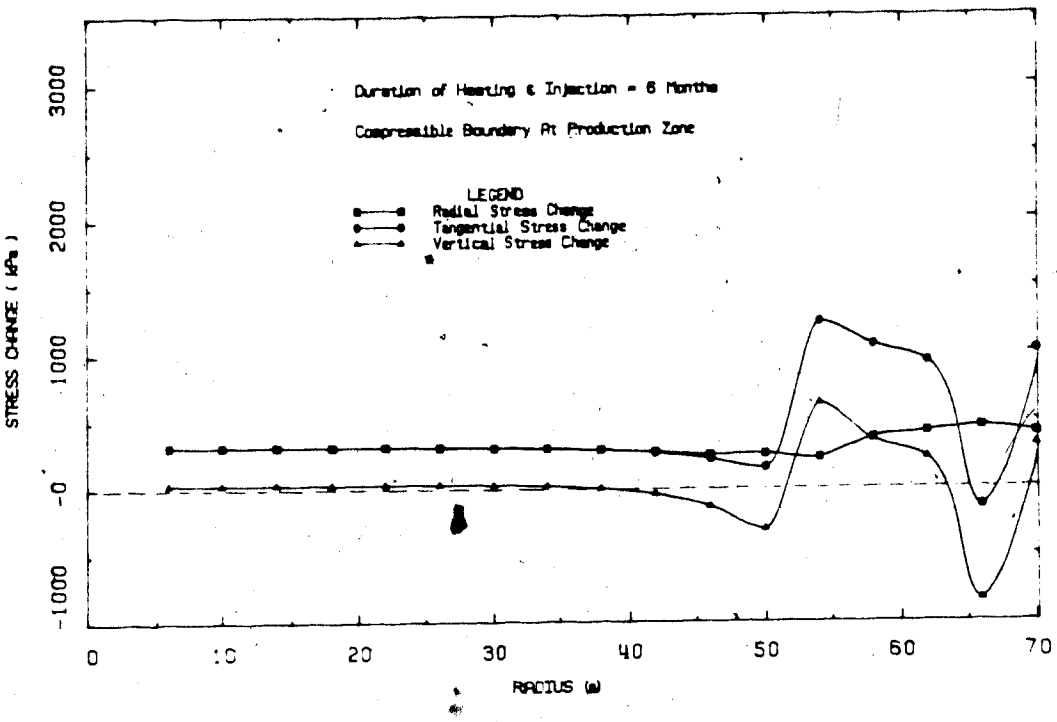

FIGURE L4.4 Stress Changes Around the Shaft After 6 Months of Steam Injection

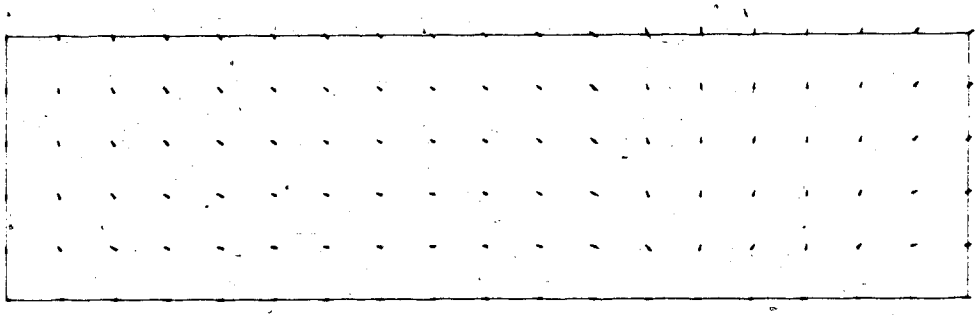

FIGURE L4.5 Deformations Around the Shaft After 6 Months of Steam Injection

DISPLACEMENT SCALE 1:100

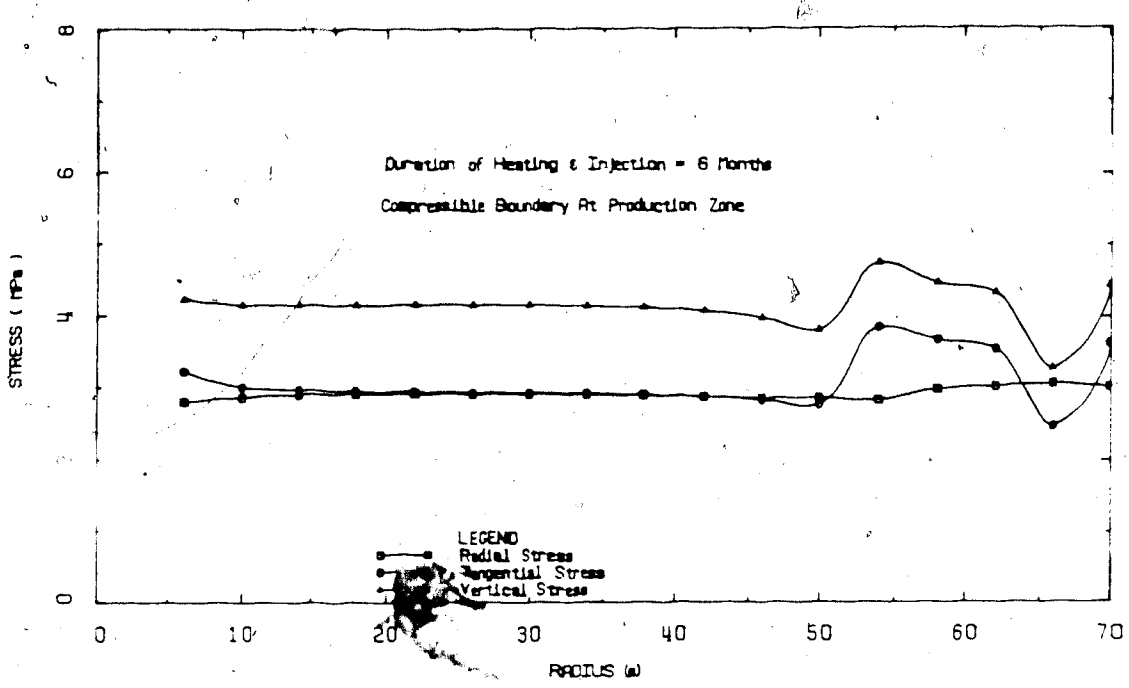

FIGURE 4.6 Effective Stresses Around the Shaft After 6 Months of Steam Injection

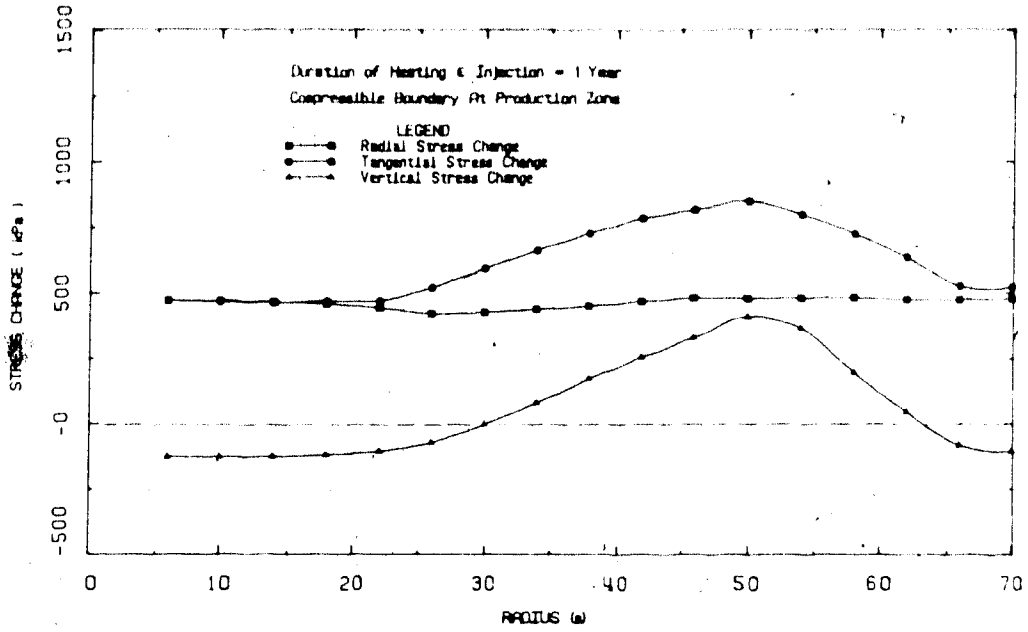

FIGURE L4.7 Stress Changes Around the Shaft After 1 Year of Steam Injection

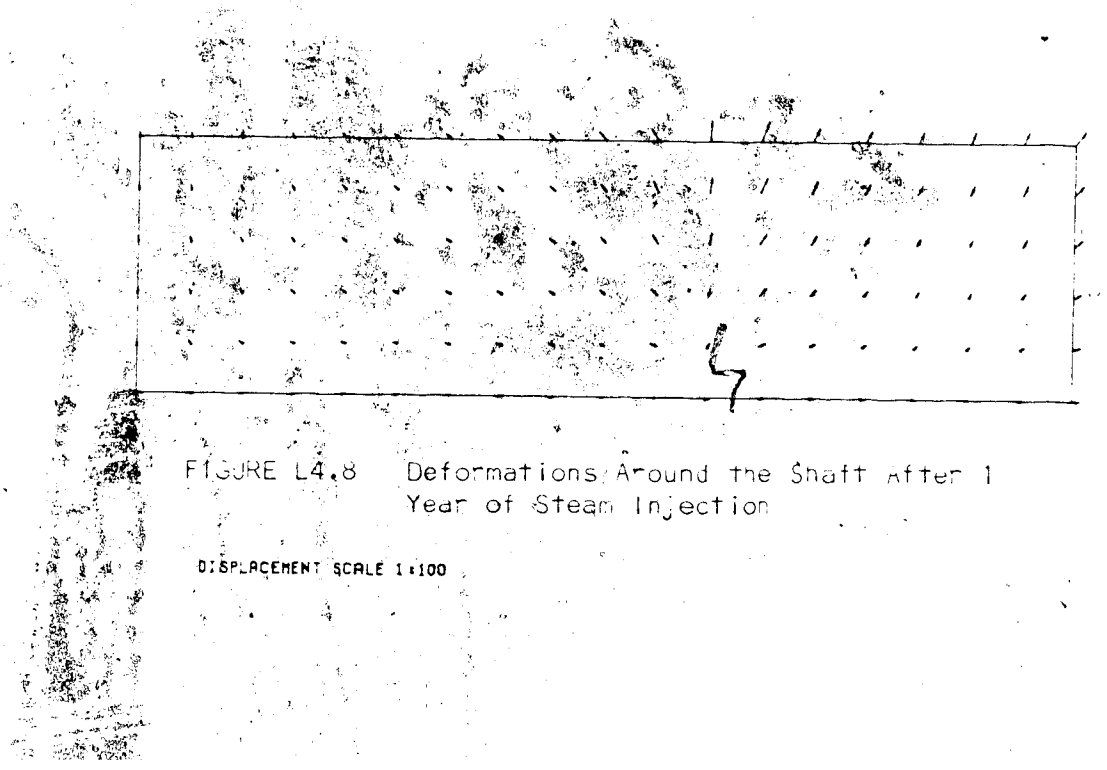

FIGURE L4.8 Deformations Around the Shaft After 1 Year of Steam Injection

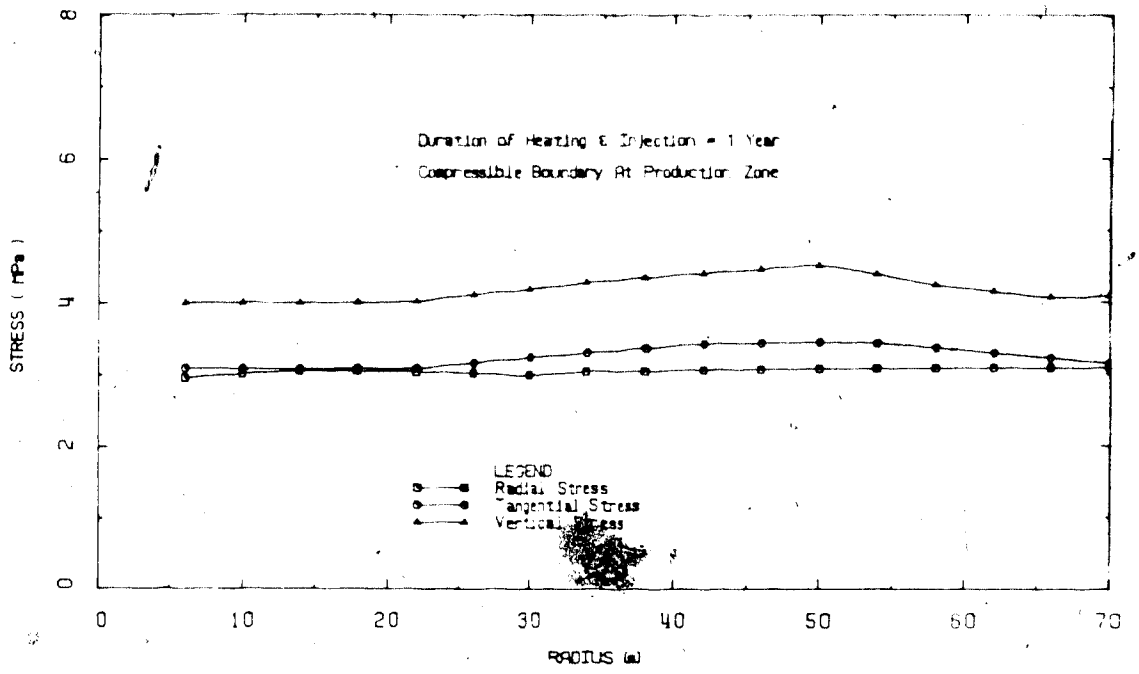

FIGURE 14.9 Effective Stresses Around the Shaft After 1 Year of Steam Injection

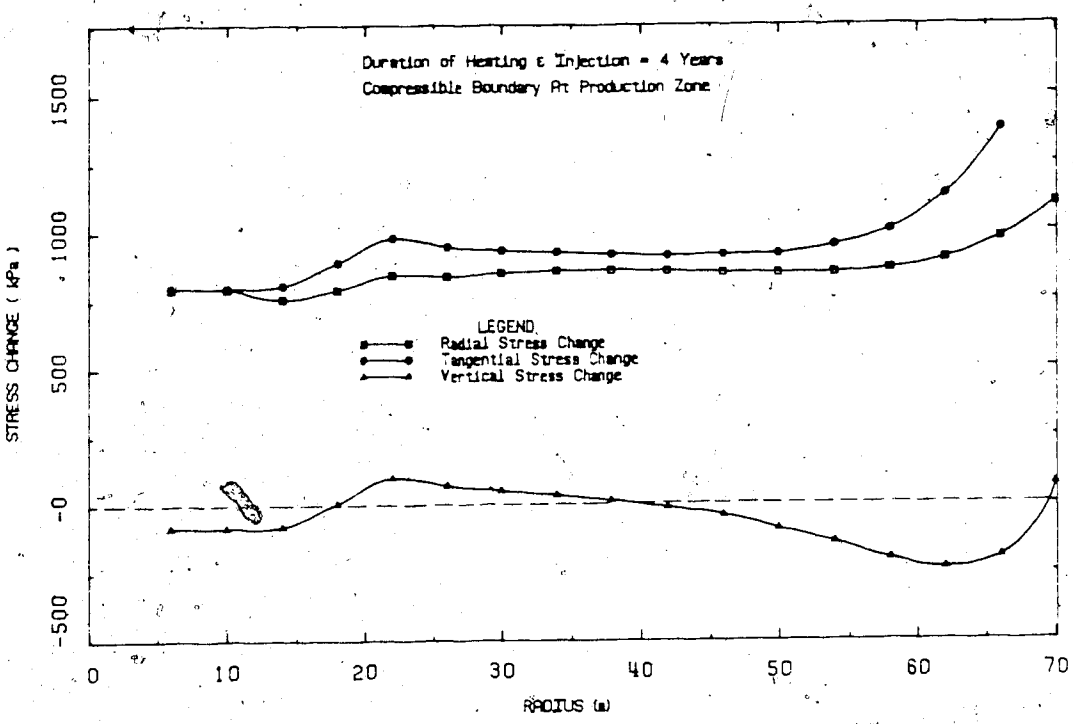

FIGURE L4.10 Stress Changes Around the Shaft After 4 Years of Steam Injection

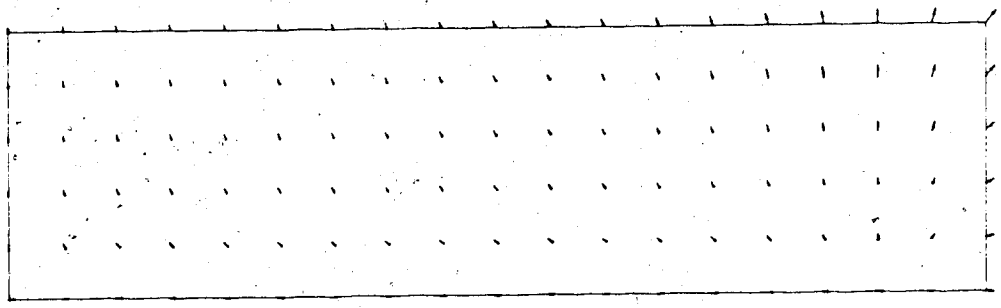

FIGURE L4.11 Deformations Around the Shaft After 4 Years of Steam Injection

DISPLACEMENT SCALE 1:100

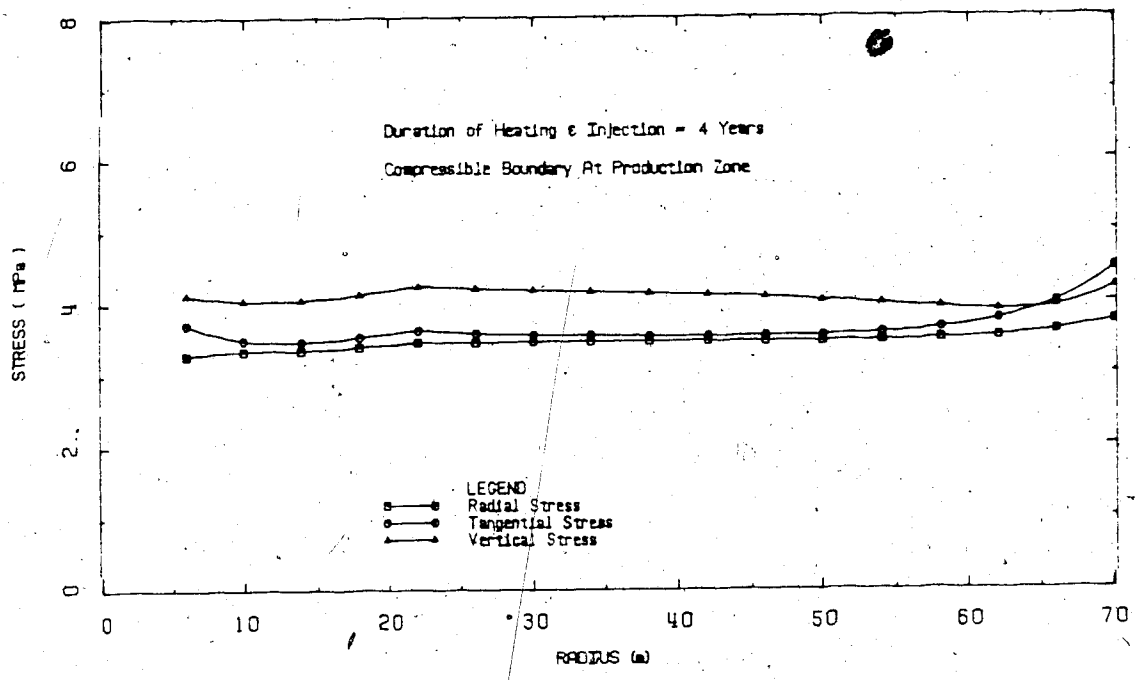

FIGURE L4.12 Effective Stresses Around the Shaft After 4 Years of Steam Injection

Drained Analyses

Thermal Stress Changes and Deformations Adjacent to a Shaft Assuming Drained Conditions

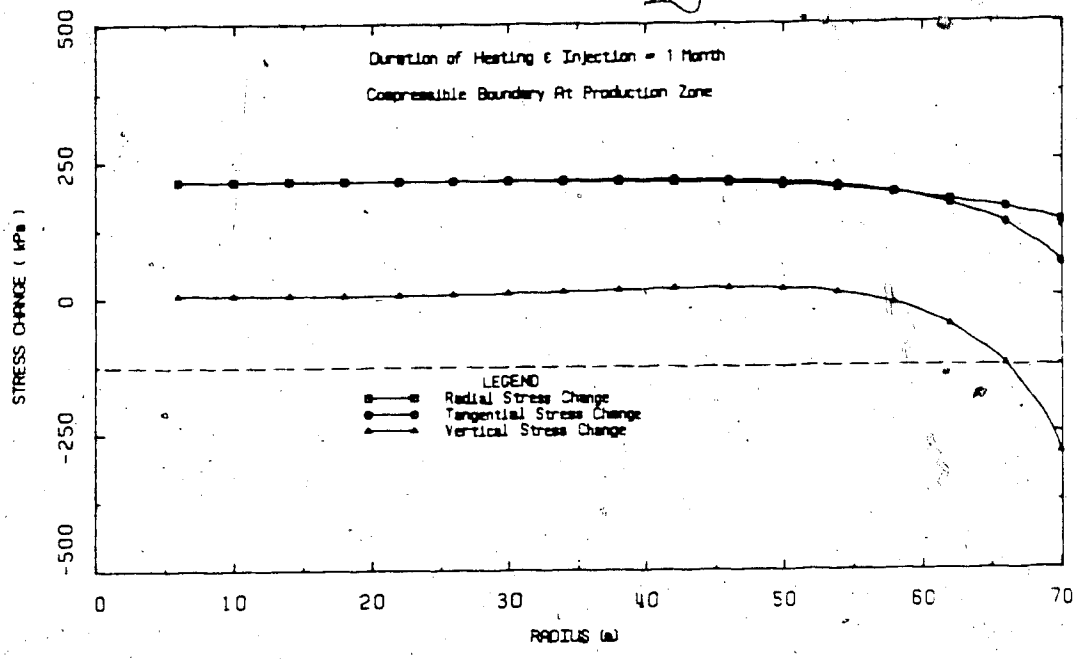

FIGURE L5.1 Stress Changes Around the Shaft After 1 Month of Drained Heating

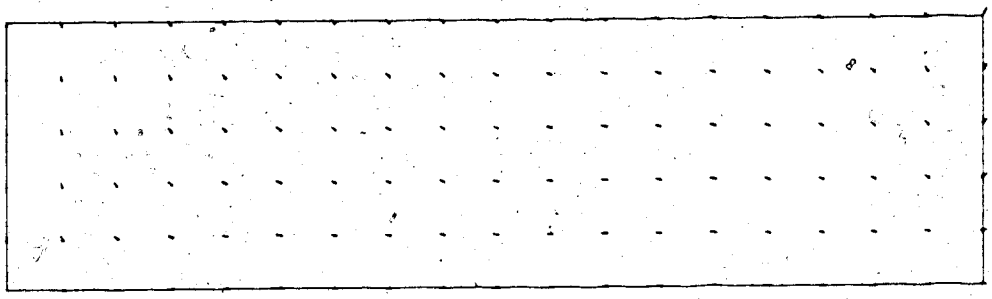

FIGURE L5.2 Deformations Around the Shaft After 1 Month of Drained Heating

DISPLACEMENT SCALE 1:100

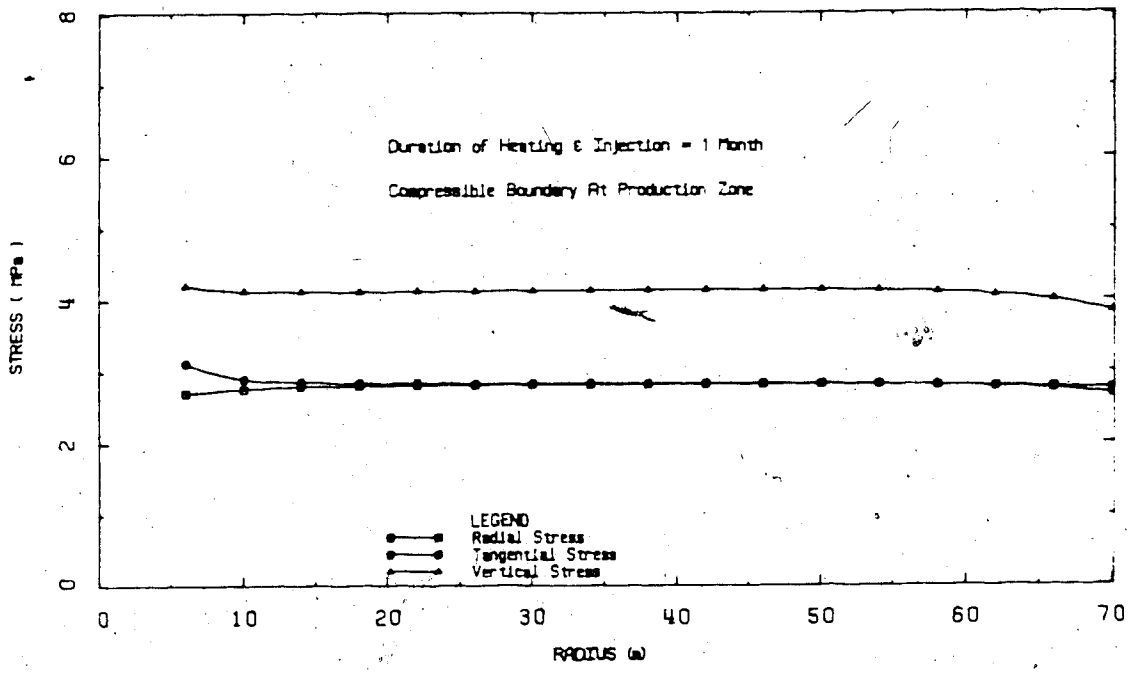

FIGURE L5.3 Effective Stresses Around the Shaft After 1 Month of Drained Heating

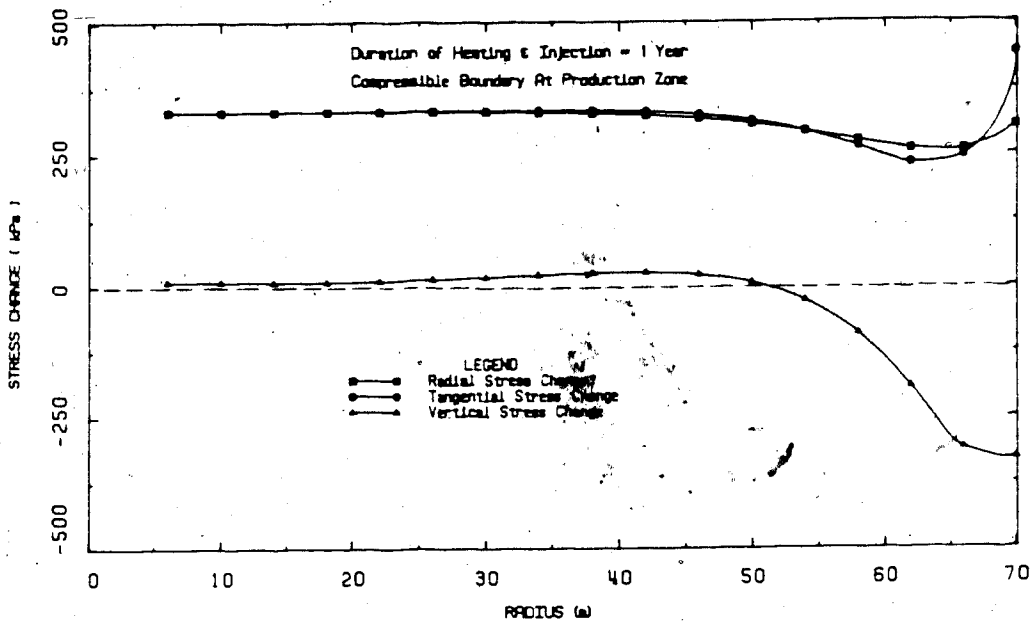

FIGURE L5.4 Stress Changes Around the Shaft After 1 Year of Drained Heating

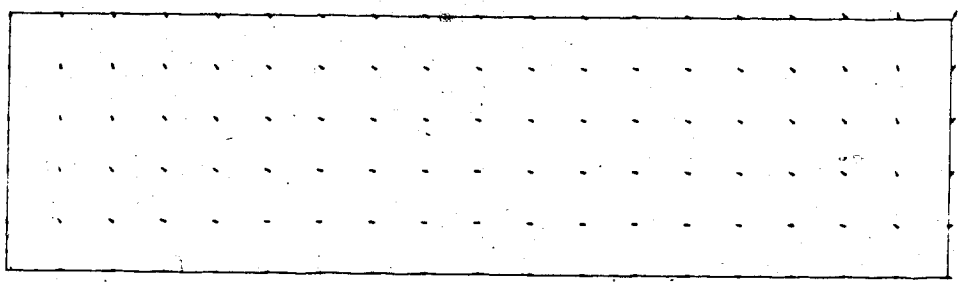

FIGURE L5.5 Deformations Around the Shaft After 1 Year of Drained Heating

DISPLACEMENT SCALE 1:100

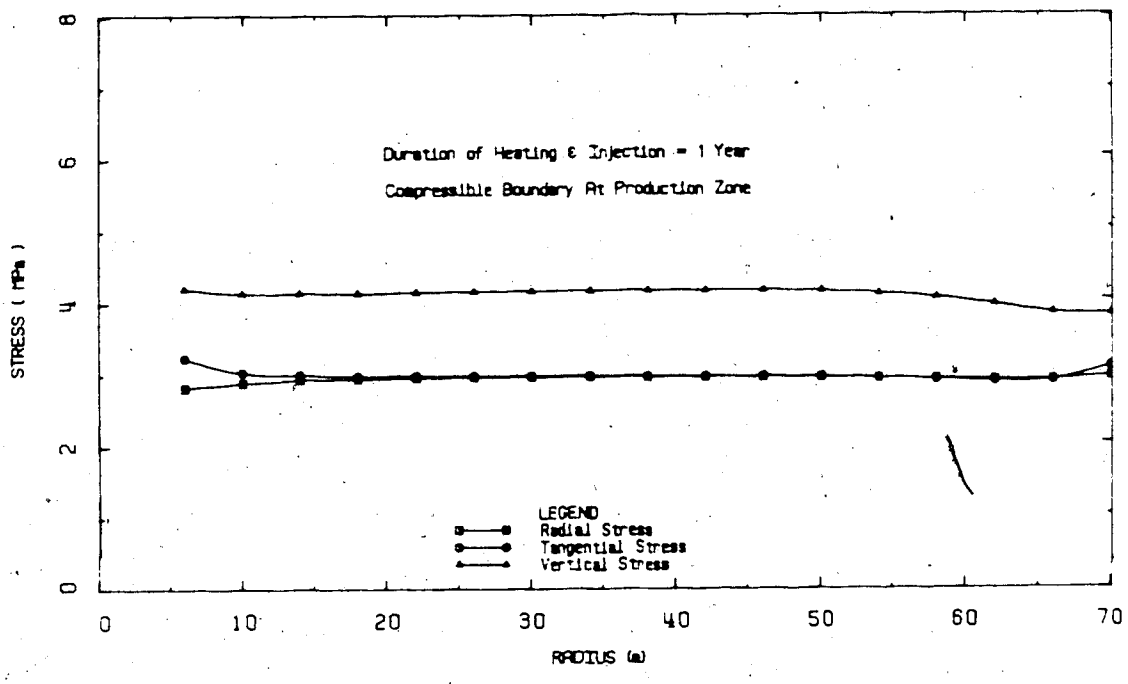

FIGURE L5.6 Effective Stresses Around the Shaft After 1 Year of Drained Heating

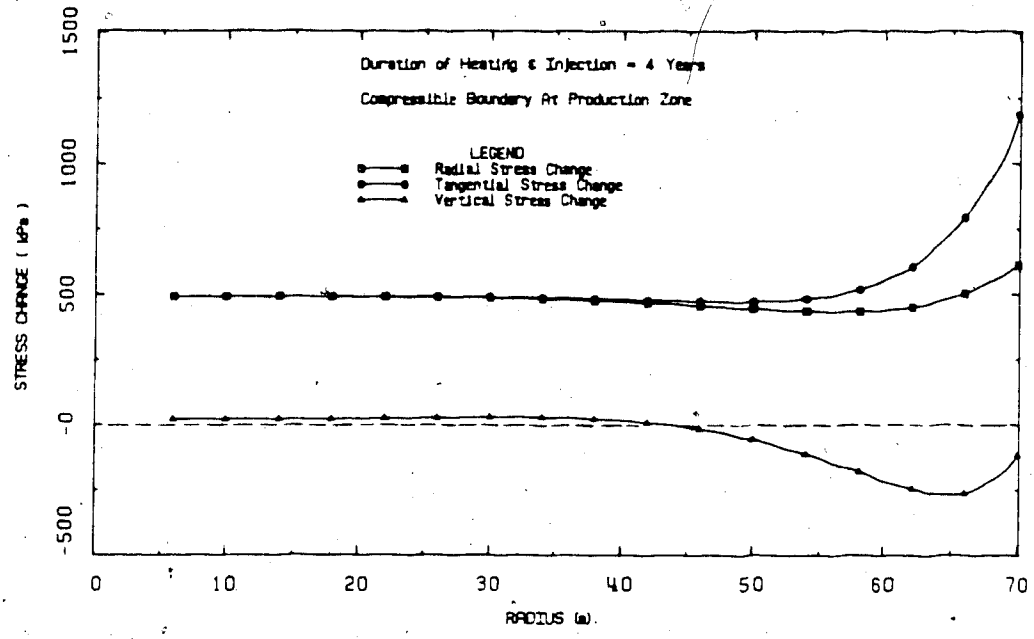

FIGURE L5.7 Stress Changes Around the Shaft After 4 Years of Drained Heating

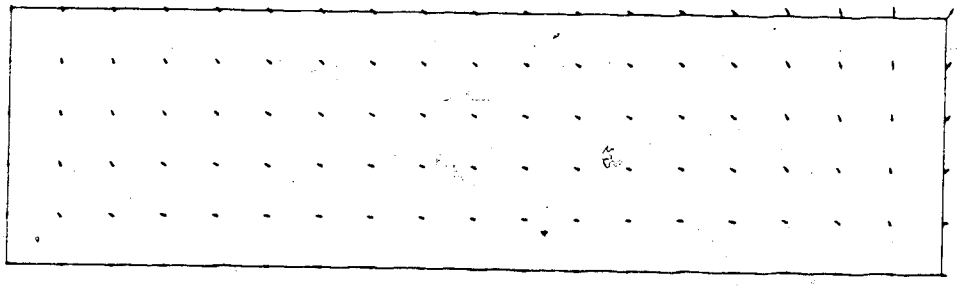

FIGURE L5.8 Deformations Around the Shaft After 4 Years of Drained Heating

DISPLACEMENT SCALE 1:100

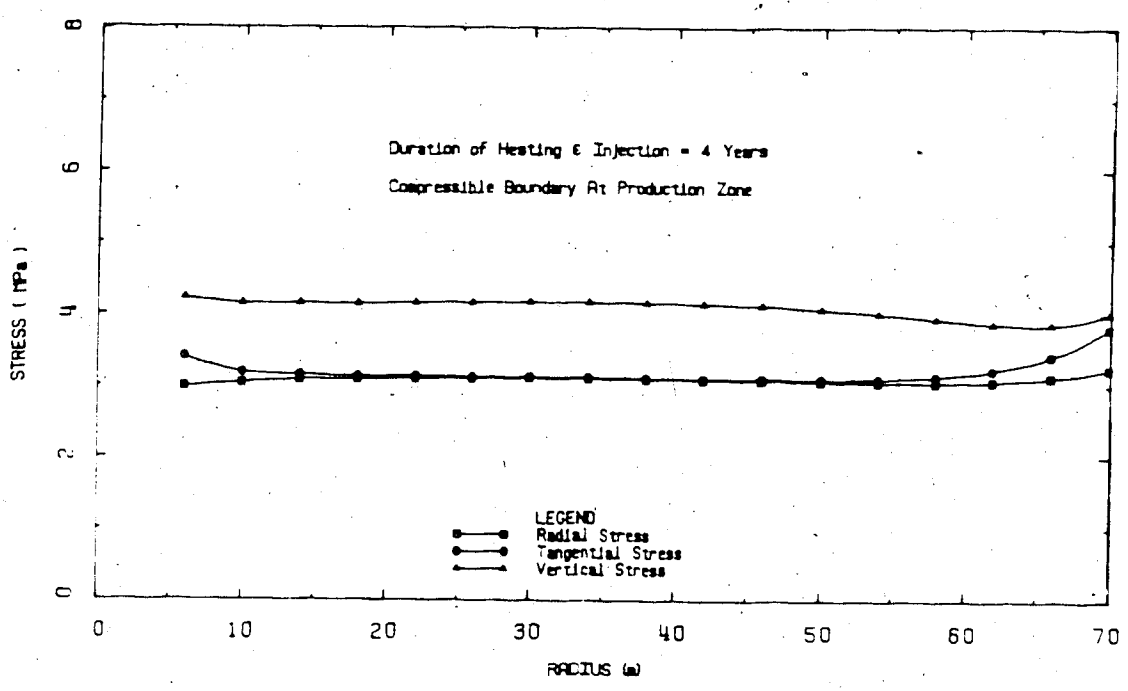

FIGURE L5.9 Effective Stresses Around the Shaft After 4 Years of Drained Heating

Undrained Analysis #1

Undrained Stress Changes and Deformations Using
Constant Undrained Thermoelastic Coefficients

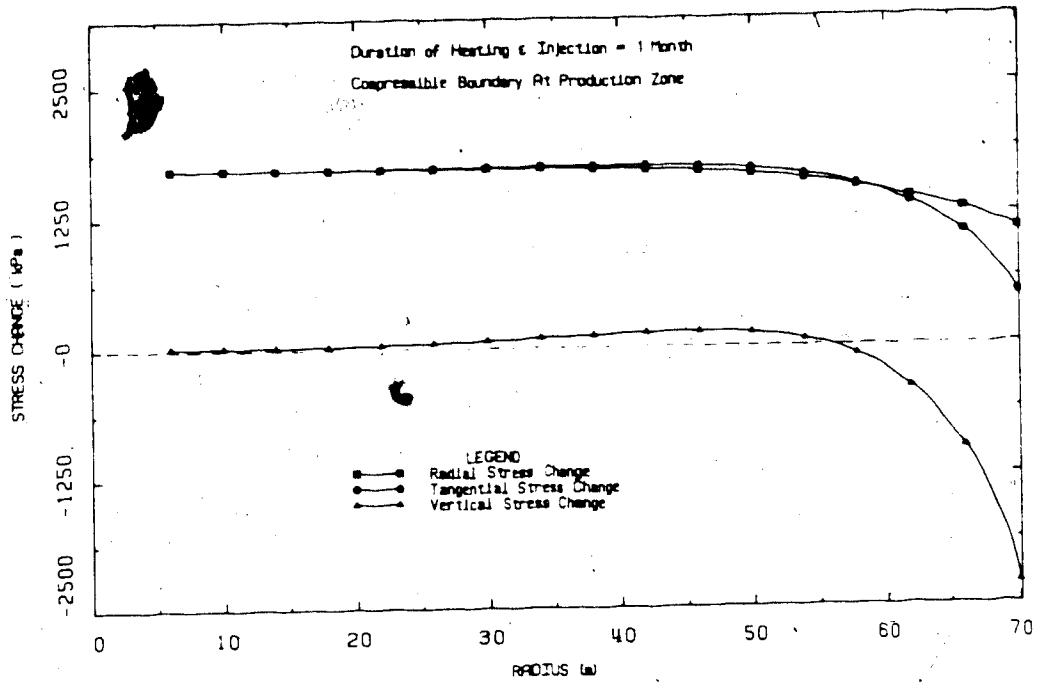

FIGURE L6.1 Stress Changes Around the Shaft After 1 Month of Undrained Heating (constant thermoelastic coefficients)

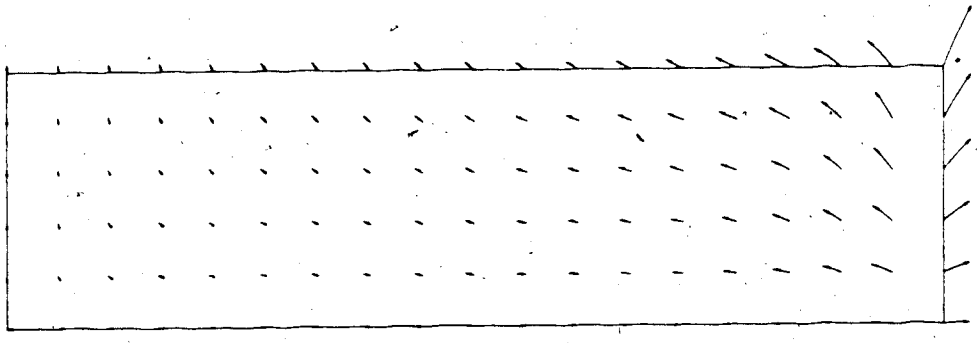

FIGURE L6.2 Deformations Around the Shaft After 1 Month of Undrained Heating (constant thermoelastic coefficients)

DISPLACEMENT SCALE 1:100

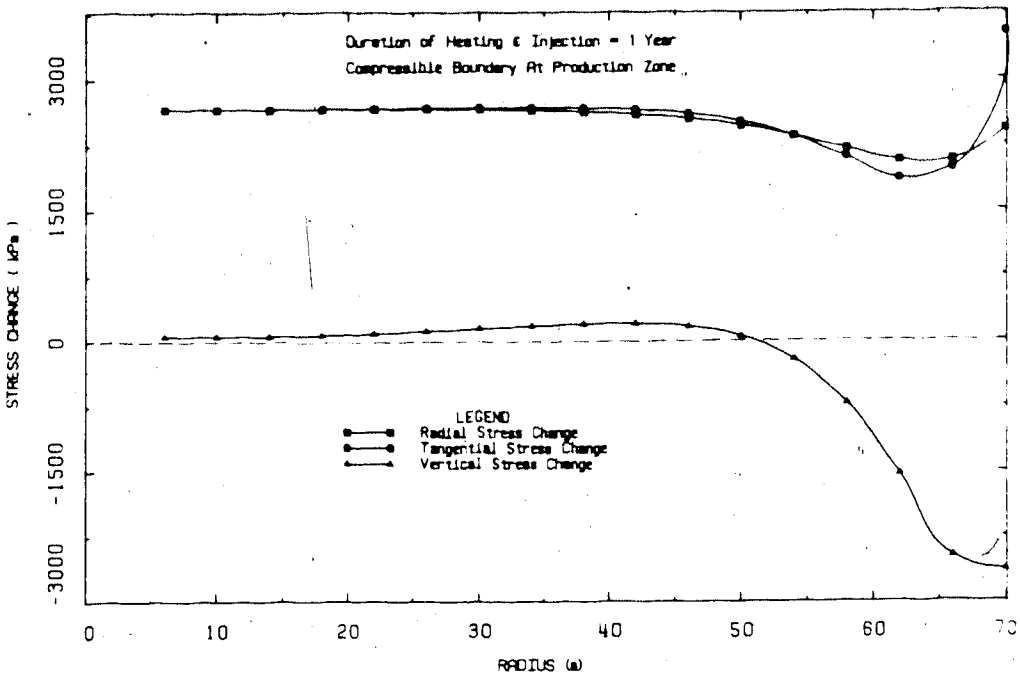

FIGURE L6.3 Stress Changes Around the Shaft After 1 Year of Undrained Heating (constant thermoelastic coefficients)

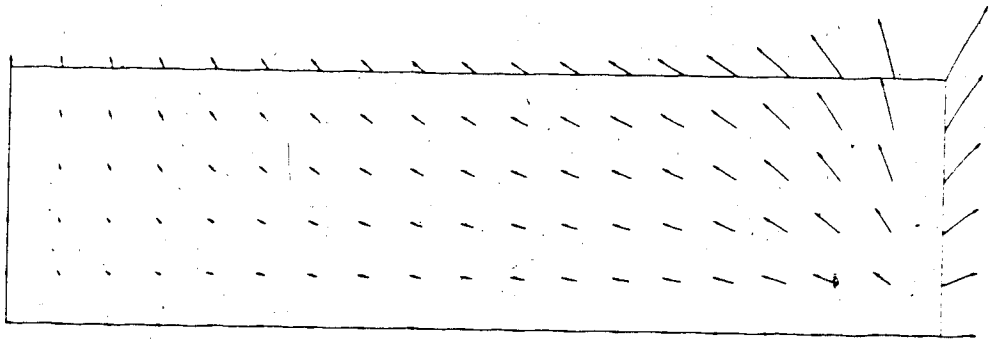

FIGURE L6.4 Deformations Around the Shaft After 1 Year of Undrained Heating (constant thermoelastic coefficients)

DISPLACEMENT SCALE 1:100

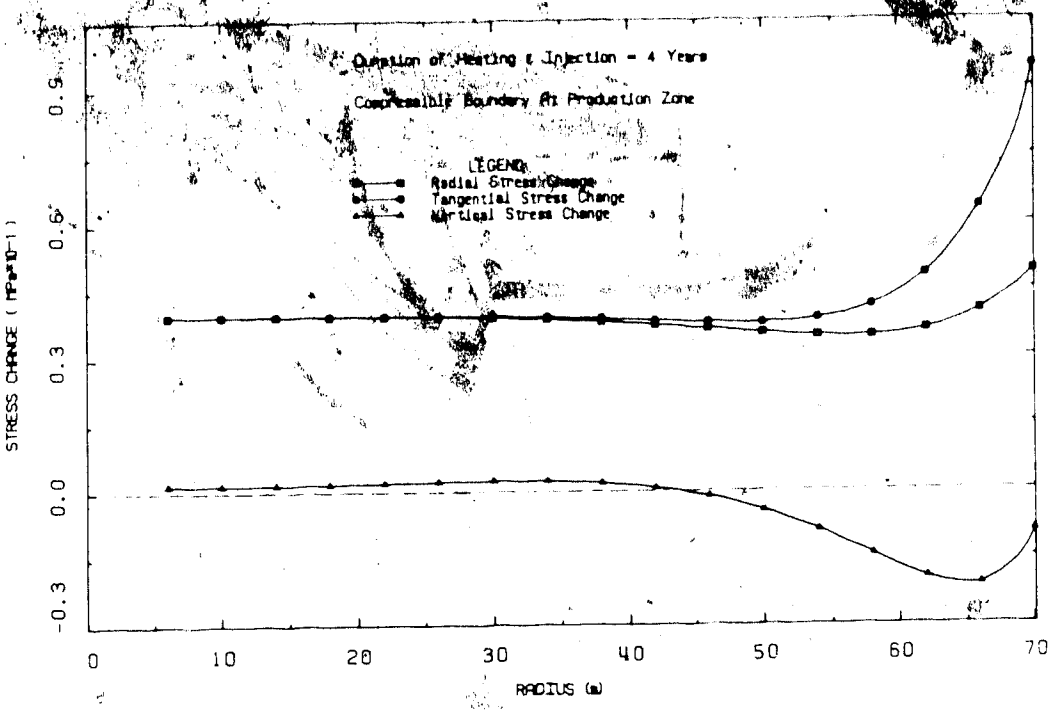

FIGURE L6.5 Stress Changes Around the Shaft After 4 Years of Undrained Heating (Constant thermoelastic coefficients)

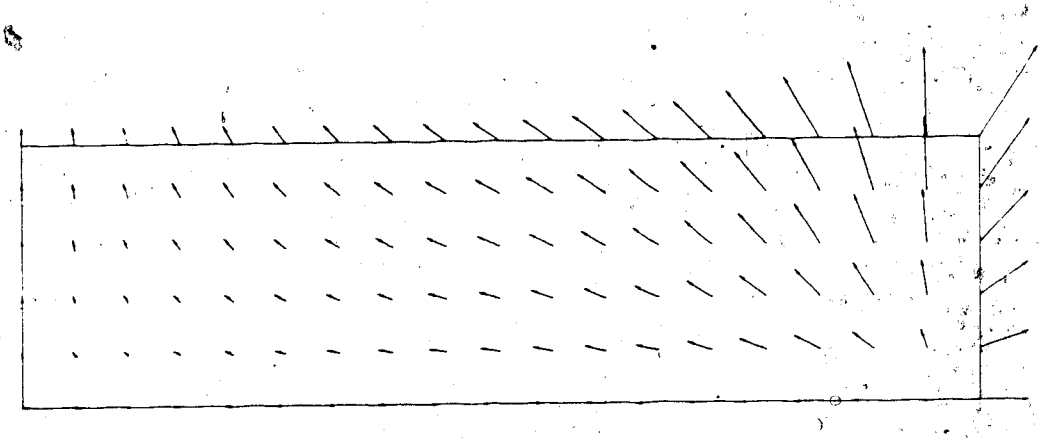

FIGURE L6.6 Deformations Around the Shaft After 4 Years of Undrained Heating (constant thermoleastic coefficients)

DISPLACEMENT SCALE 1:100

Undrained Analysis #2

Undrained Stress Changes and Deformations Determined Using Variable Thermoelastic Coefficients

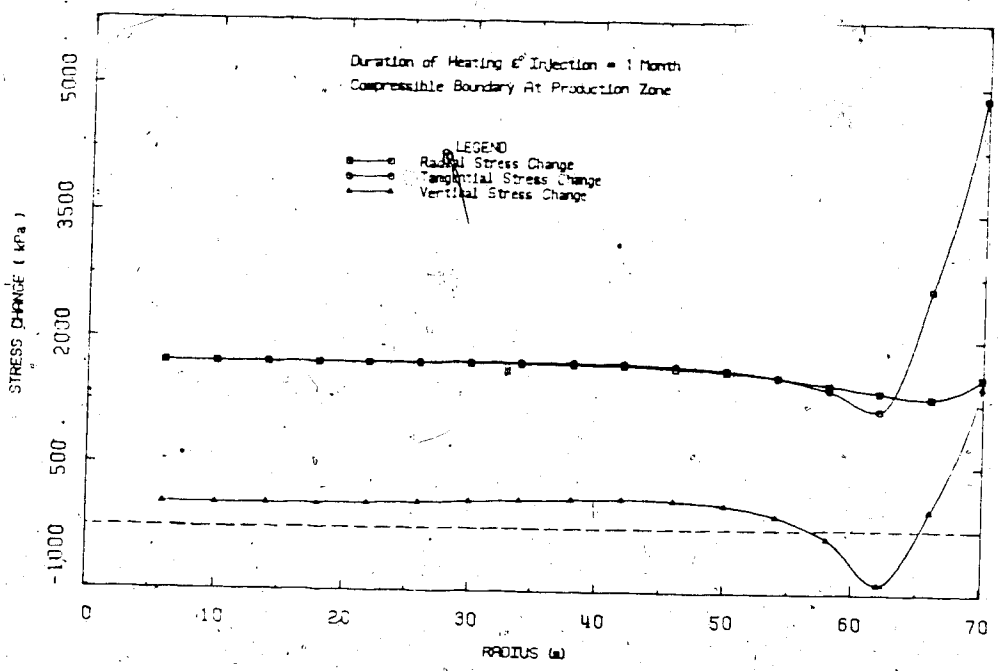

FIGURE L7.1 Stress Changes Around the Shaft After 1 Month of Transient Undrained Heating

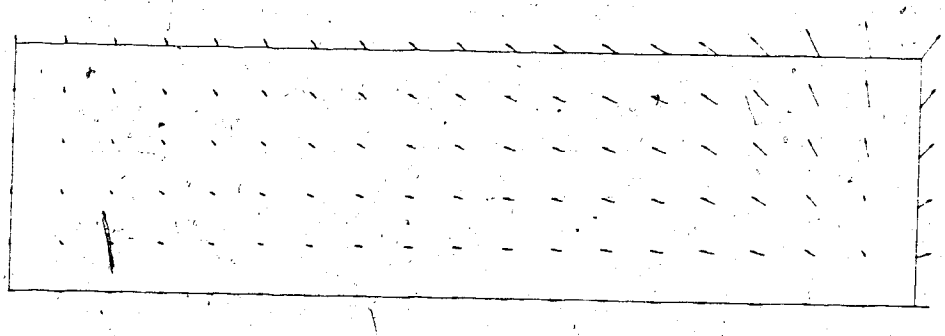

FIGURE L7.2 Deformations Around the Shaft After 1 Month of Transient Undrained Heating

DISPLACEMENT SCALE 1:100

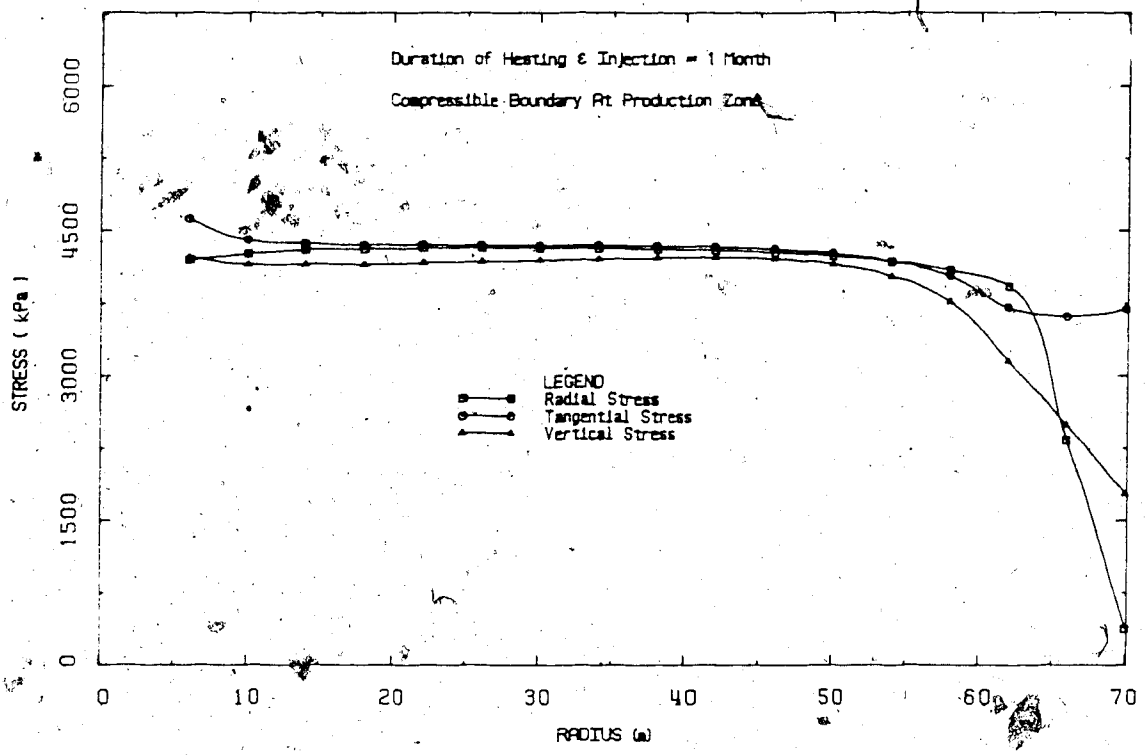

FIGURE L7.3 Effective Stresses Around the Shaft After 1 Month of Transient Undrained Heating

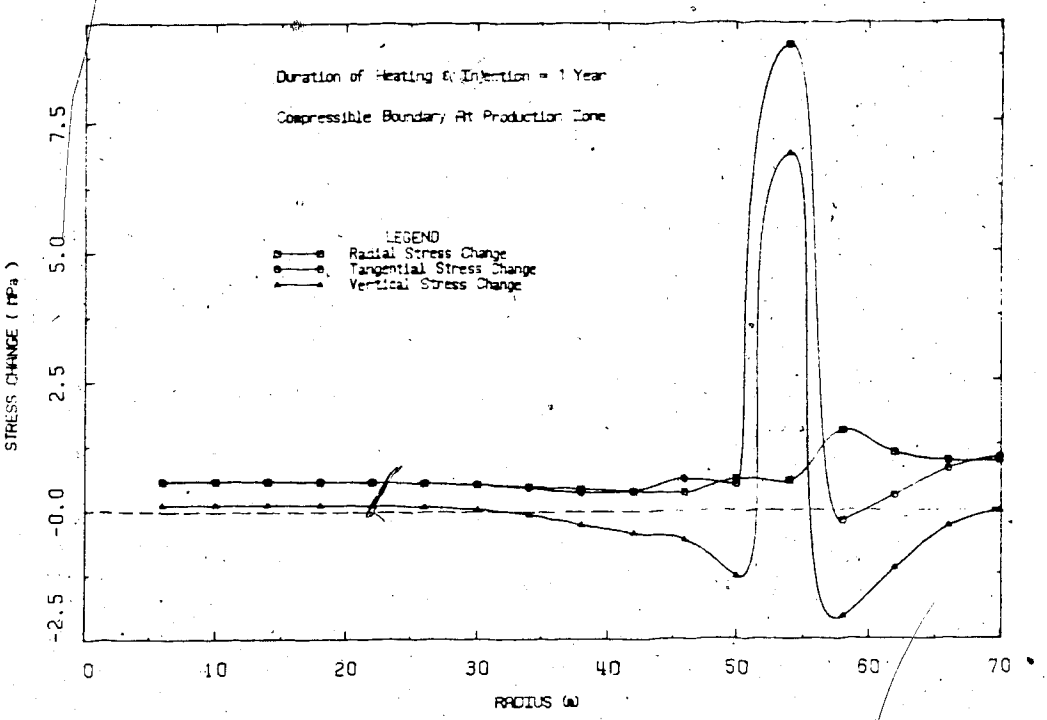

FIGURE L7.4 Stress Changes Around the Shaft After 1 Year of Transient Undrained Heating

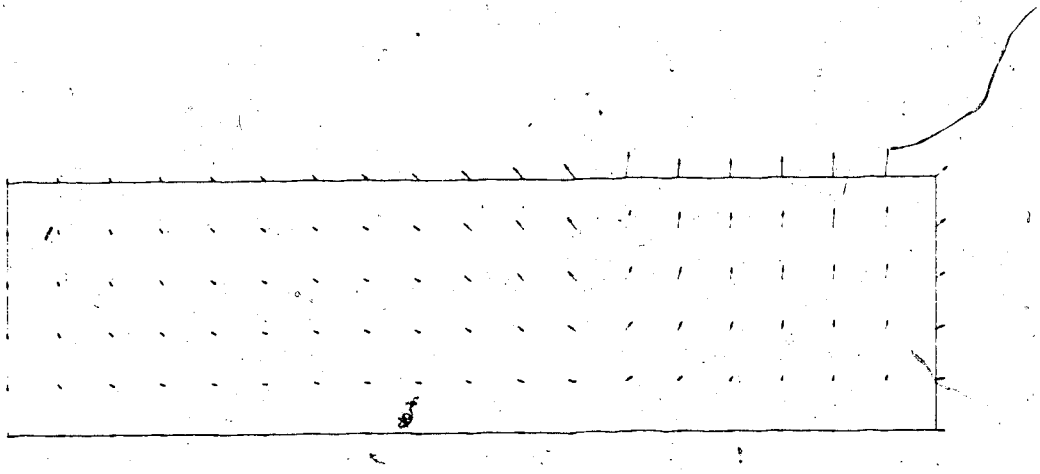

FIGURE L7.5 Deformations Around the Shaft After 1 Year of Transient Undrained Heating

DISPLACEMENT SCALE 1:100

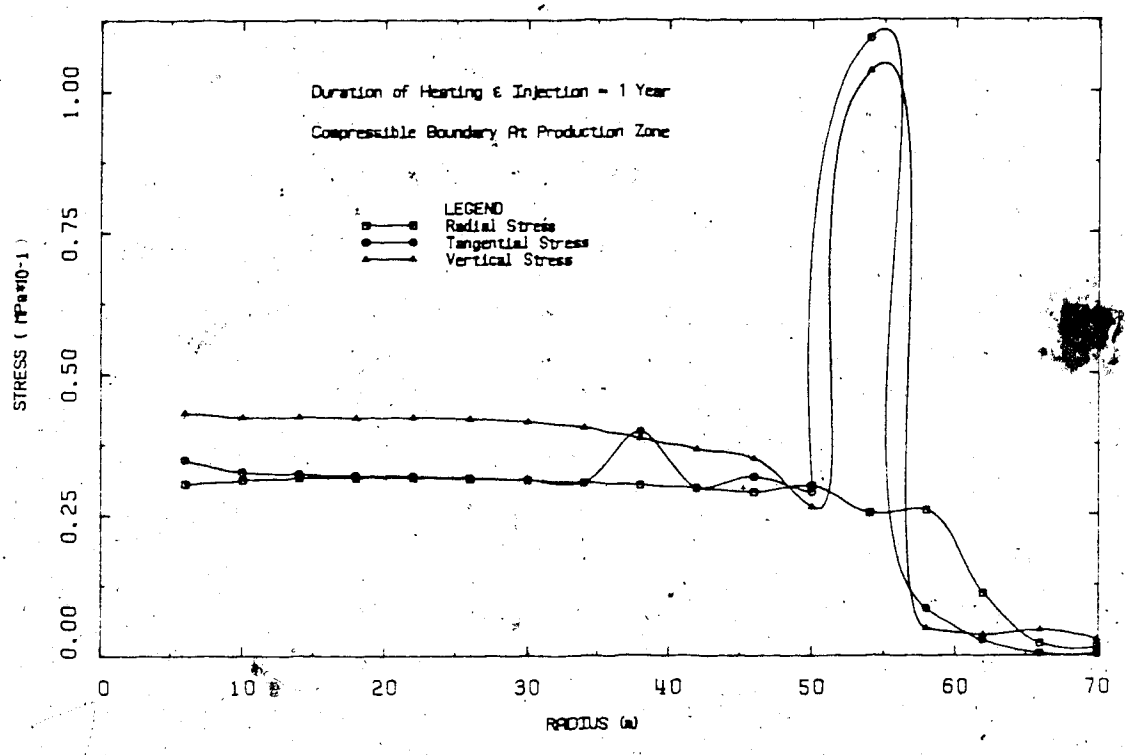

FIGURE L7.6 Effective Stress Around the Shaft After 1 Year of Transient Undrained Heating

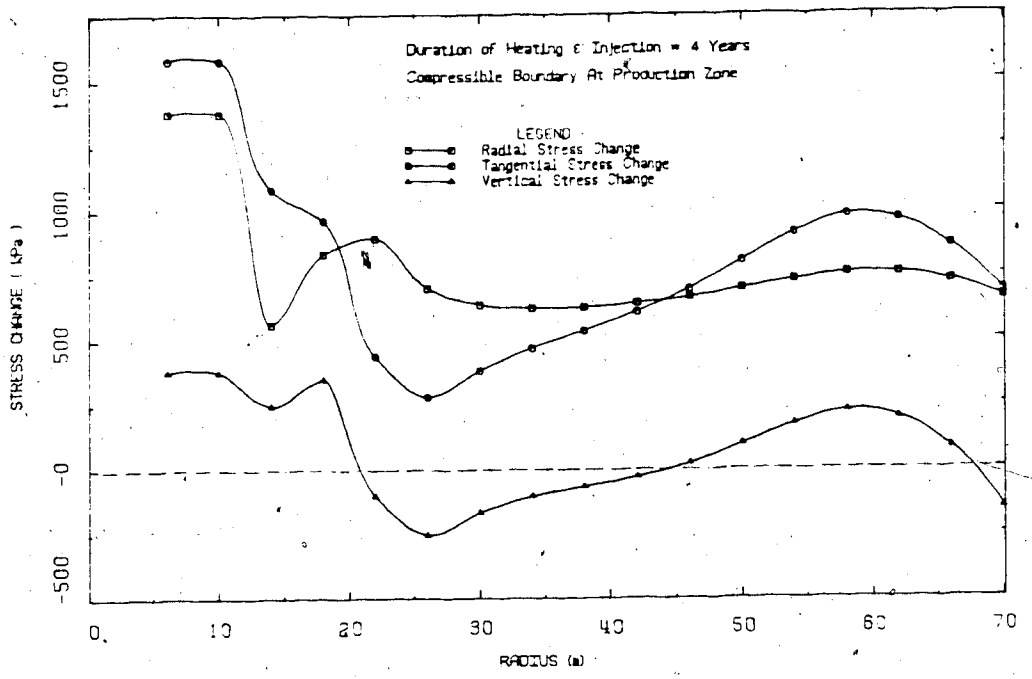

FIGURE L7.7 Stress Changes Around the Shaft After 4 Years of Transient Undrained Heating

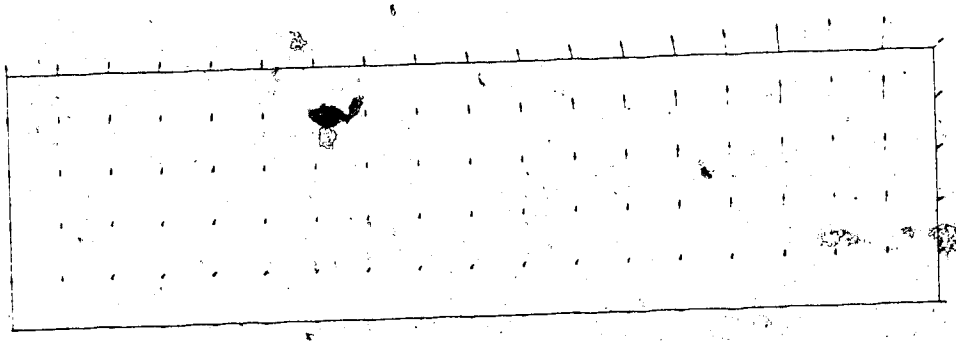

FIGURE L7.8 Deformations Around the Shaft After 4 Years of Transient Undrained Heating

DISPLACEMENT SCALE 1:100

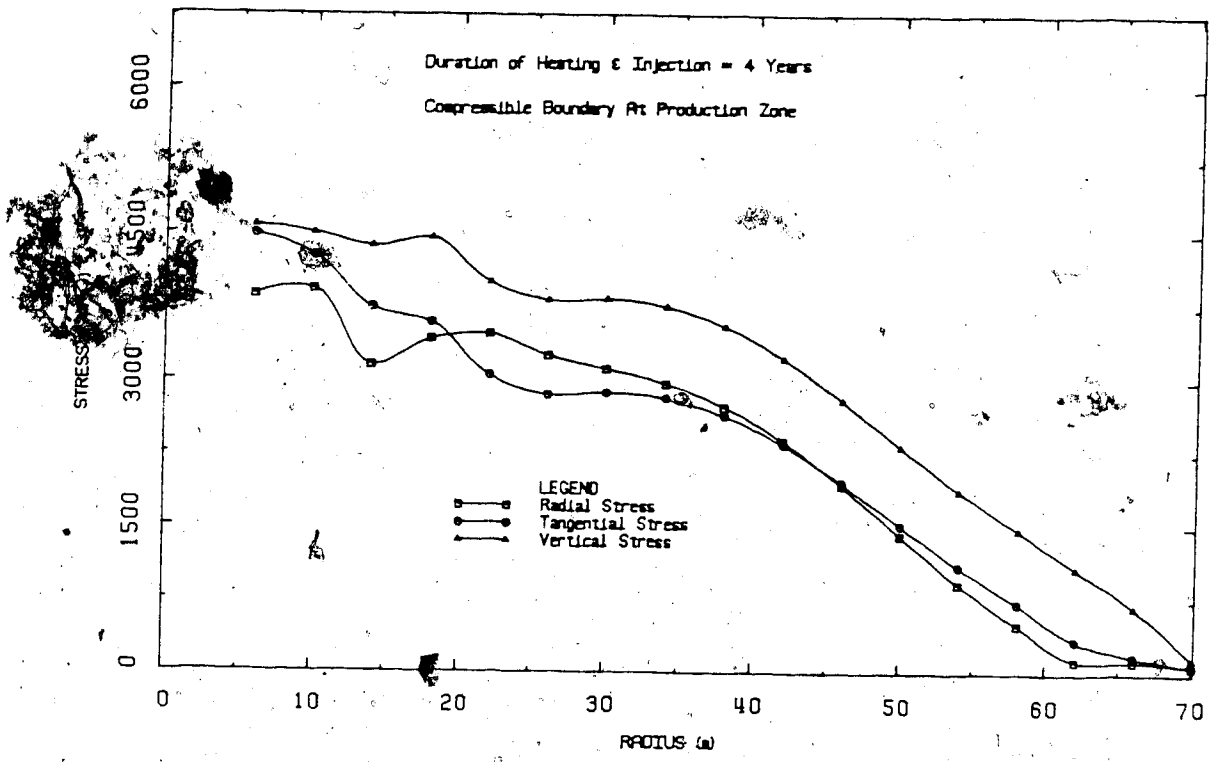

FIGURE L7.9 Effective Stresses Around the Shaft After 4 Years of Transient Undrained Heating

Thermal Stress Changes and Deformations Adjacent to a Shaft or Low Permeability Oil Sand

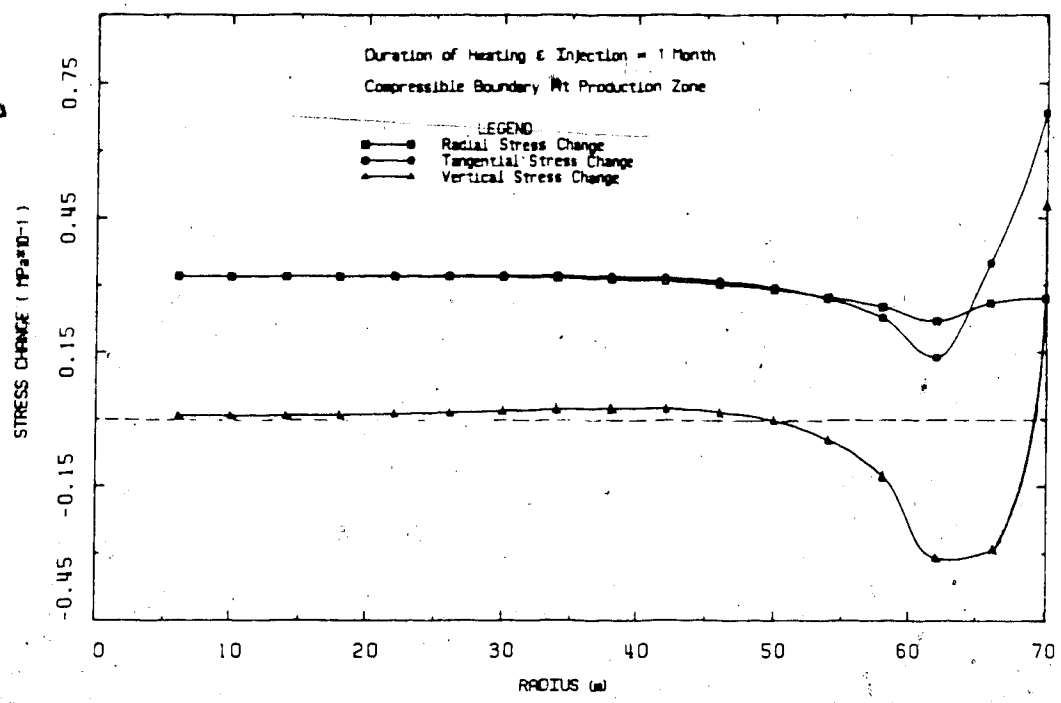

FIGURE L8.1 Stress Changes Around the Shaft After 1 Month of Steam Injection in Shale

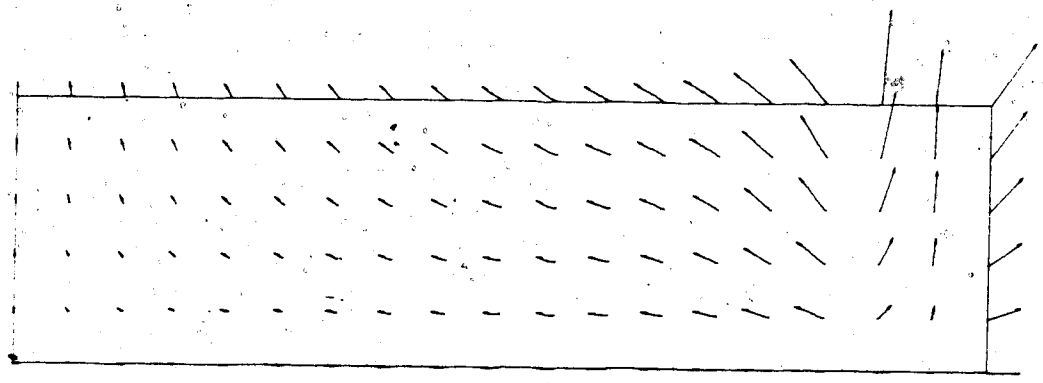

FIGURE L8.2 Deformations Around the Shaft After 1 Month of Steam Injection in Shale

DISPLACEMENT SCALE 1:100

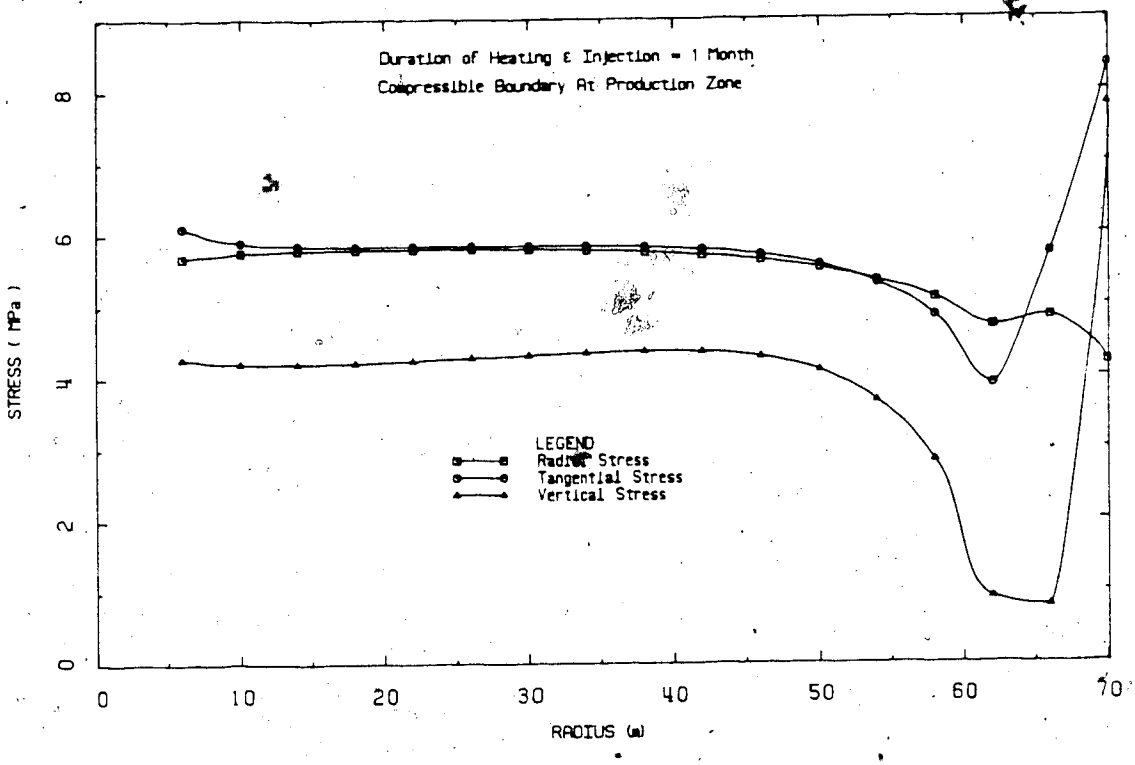

FIGURE L8.3 Effective Stresses Around the Shaft After 1 Month of Steam Injection in Shale

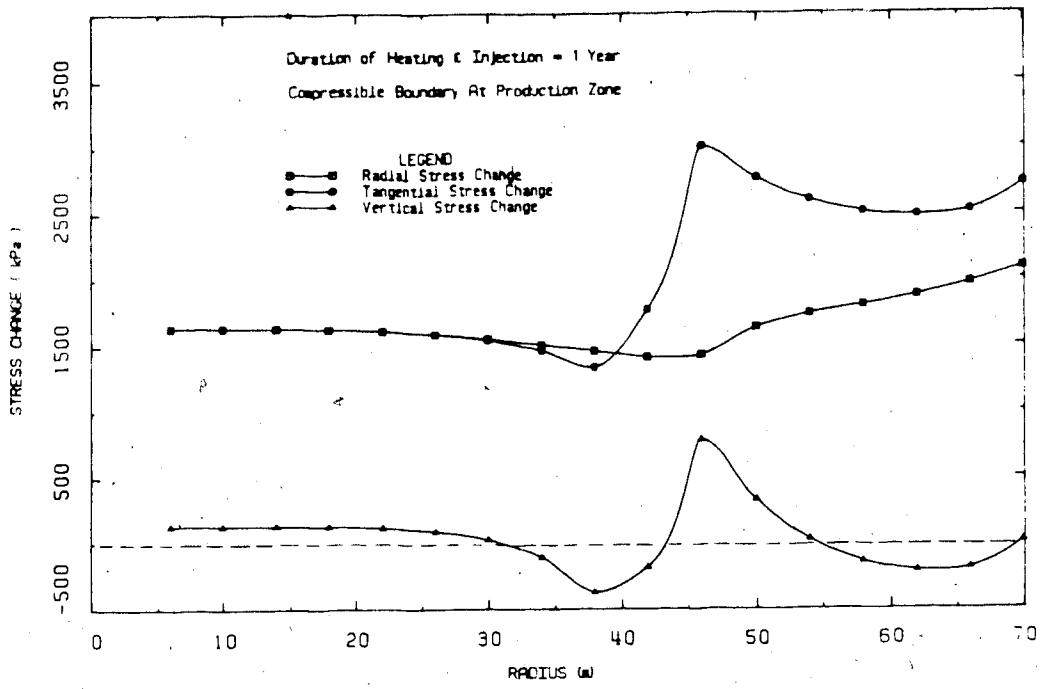

FIGURE L8.4 Stress Changes Around the Shaft After 1 Year of Steam Injection In Shale

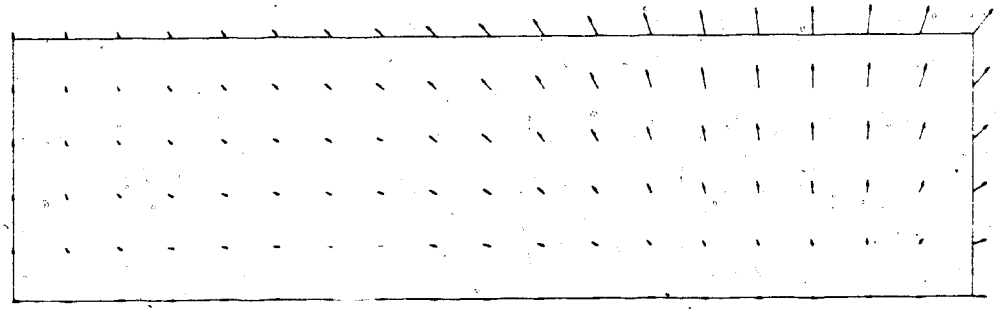

FIGURE L8.5 Deformations Around the Shaft After 1 Year of Steam Injection In Shale

DISPLACEMENT SCALE 1:100

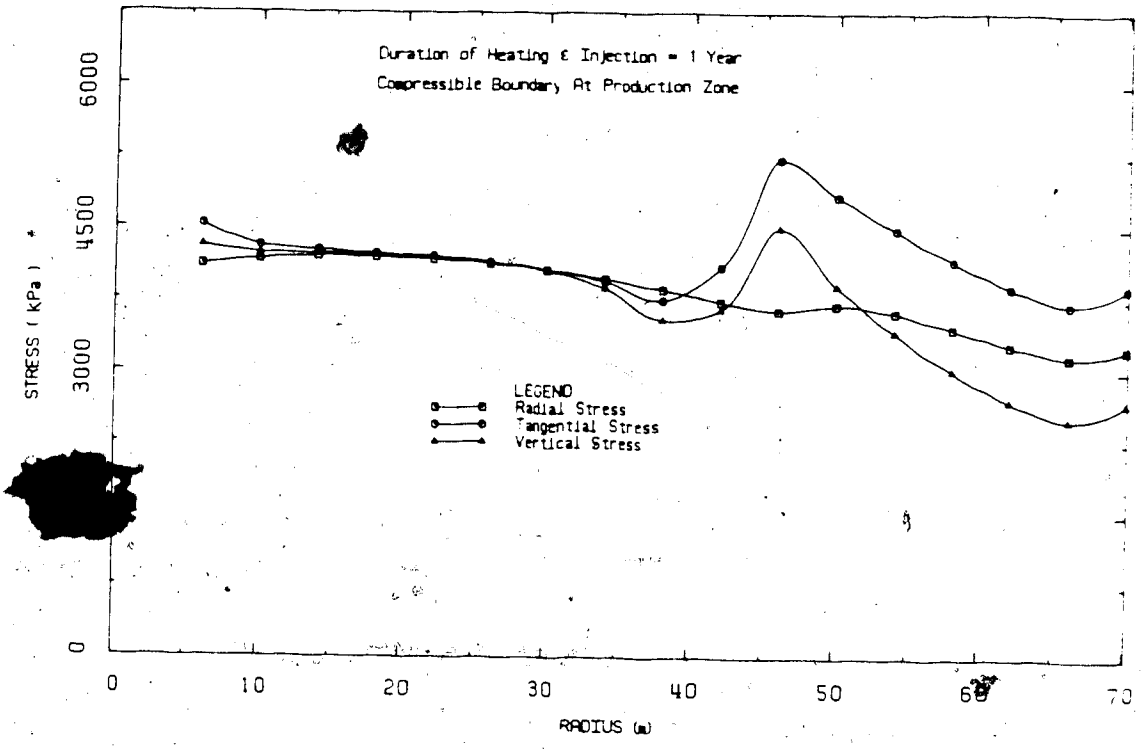

FIGURE L8.6 Effective Stresses Around the Shaft After 1 Year of Steam Injection in Shale

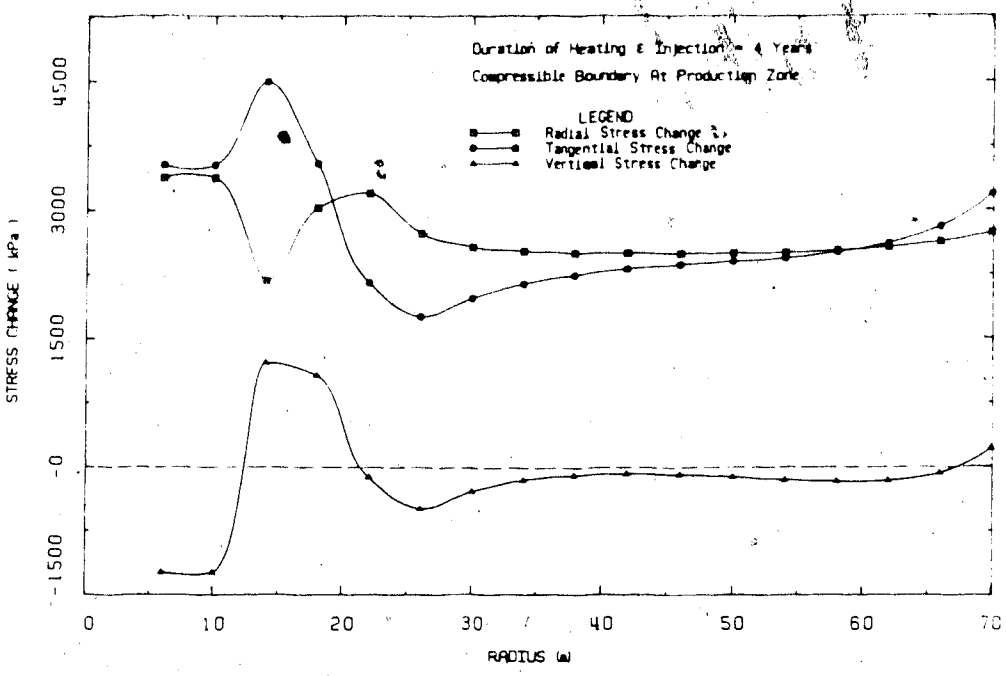

FIGURE L6.7 Stress Changes Around the Shaft After 4 Years of Steam Injection in Shale

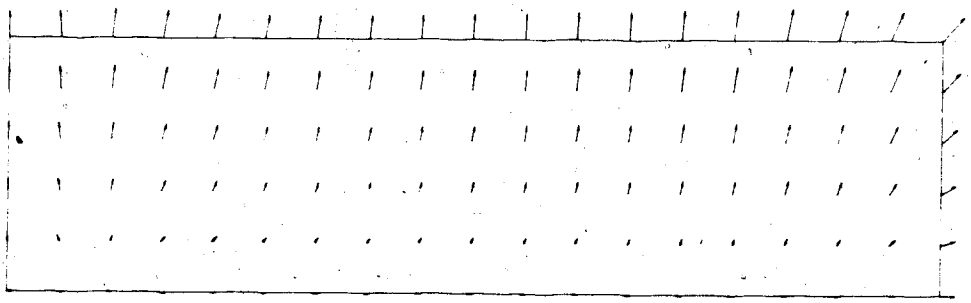

FIGURE L6.8 Stress Changes Around the Shaft After 4 Years of Steam Injection in Shale

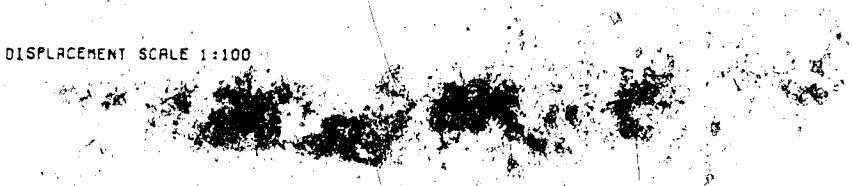

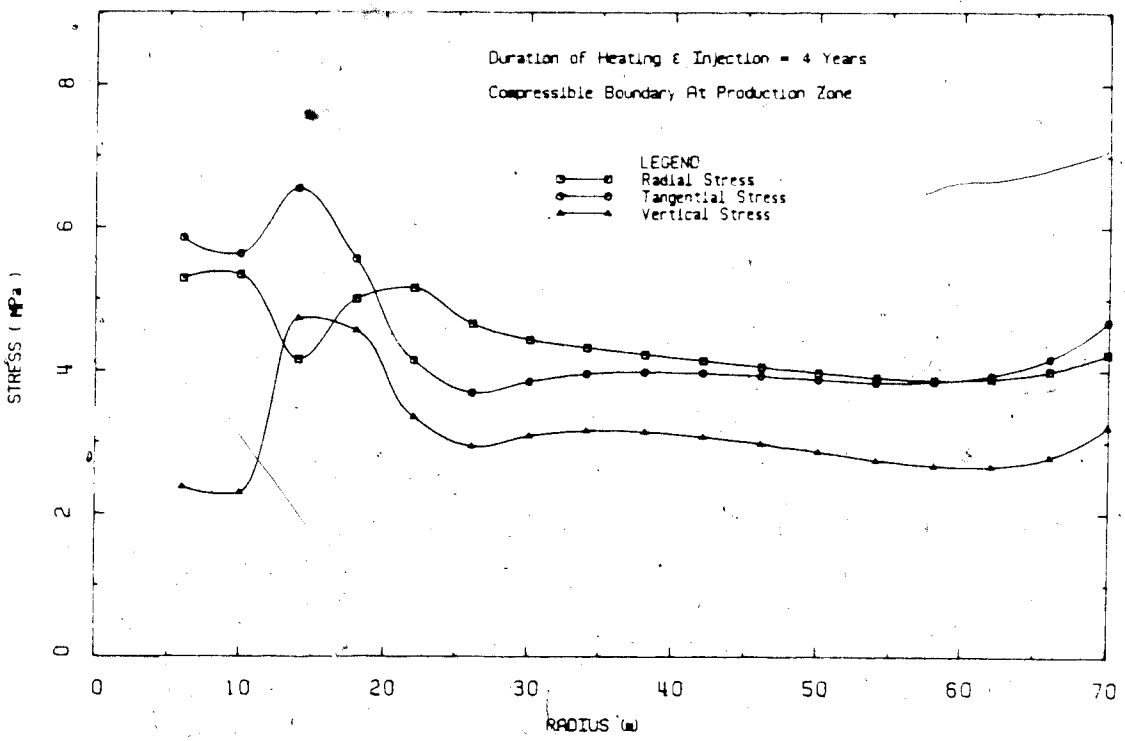

FIGURE L8.9 Stress Changes Around the Shaft After 4 Years of Steam Injection in Shale